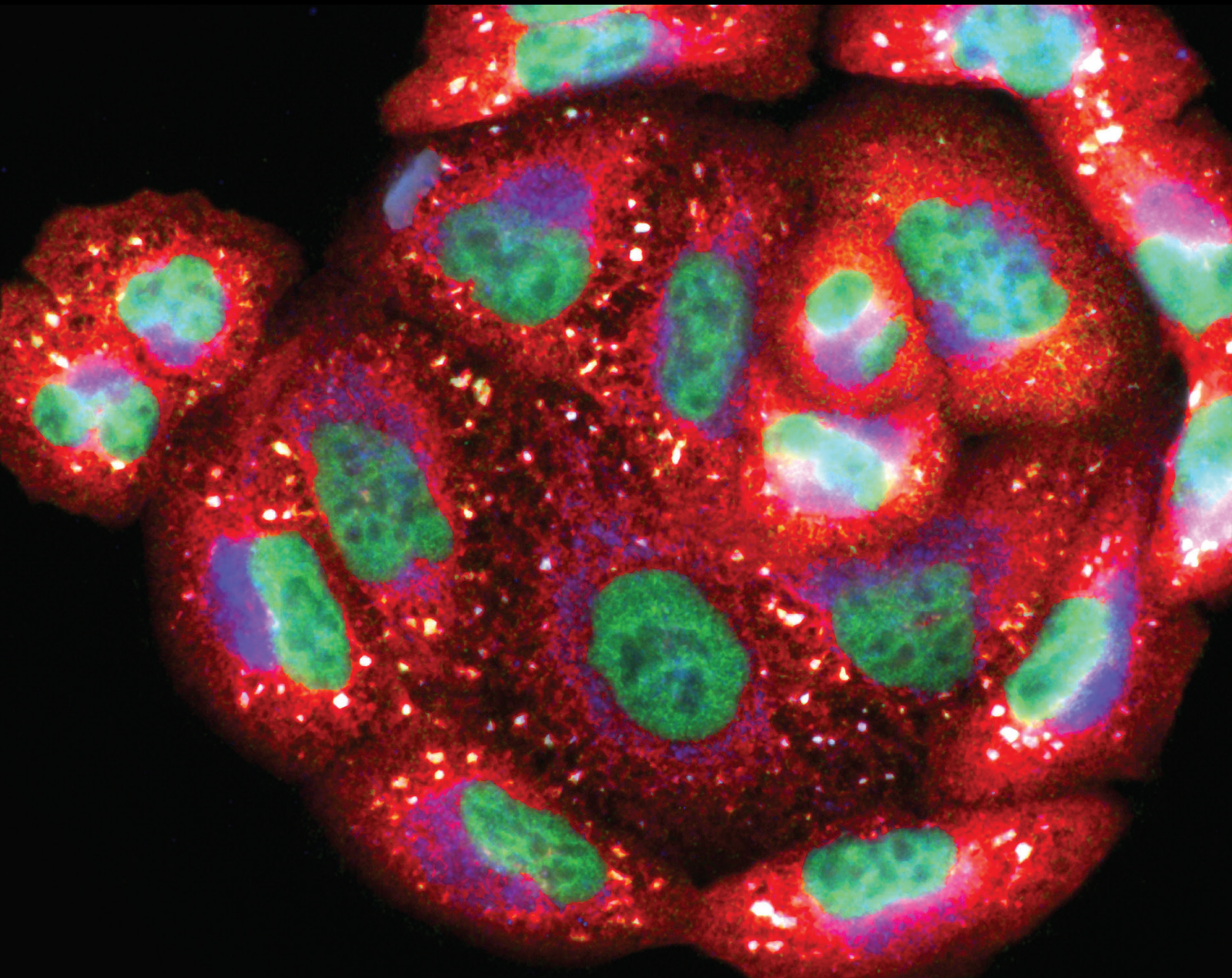


Oxidative Stress in Intervertebral Disc Degeneration and its Related Therapeutics

Lead Guest Editor: Sidong Yang

Guest Editors: Kaitao Lai, Ji Tu, and Wenyuan Ding





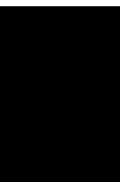
Oxidative Stress in Intervertebral Disc Degeneration and its Related Therapeutics

Oxidative Medicine and Cellular Longevity

Oxidative Stress in Intervertebral Disc Degeneration and its Related Therapeutics

Lead Guest Editor: Sidong Yang

Guest Editors: Kaitao Lai, Ji Tu, and Wenyuan Ding



Copyright © 2022 Hindawi Limited. All rights reserved.

This is a special issue published in "Oxidative Medicine and Cellular Longevity" All articles are open access articles distributed under the Creative Commons Attribution License, which permits unrestricted use, distribution, and reproduction in any medium, provided the original work is properly cited.

Chief Editor

Jeannette Vasquez-Vivar, USA

Associate Editors

Amjad Islam Aqib, Pakistan
Angel Catalá , Argentina
Cinzia Domenicotti , Italy
Janusz Gebicki , Australia
Aldrin V. Gomes , USA
Vladimir Jakovljevic , Serbia
Thomas Kietzmann , Finland
Juan C. Mayo , Spain
Ryuichi Morishita , Japan
Claudia Penna , Italy
Sachchida Nand Rai , India
Paola Rizzo , Italy
Mithun Sinha , USA
Daniele Vergara , Italy
Victor M. Victor , Spain

Academic Editors

Ammar AL-Farga , Saudi Arabia
Mohd Adnan , Saudi Arabia
Ivanov Alexander , Russia
Fabio Altieri , Italy
Daniel Dias Rufino Arcanjo , Brazil
Peter Backx, Canada
Amira Badr , Egypt
Damian Bailey, United Kingdom
Rengasamy Balakrishnan , Republic of Korea
Jiaolin Bao, China
Ji C. Bihl , USA
Hareram Birla, India
Abdelhakim Bouyahya, Morocco
Ralf Braun , Austria
Laura Bravo , Spain
Matt Brody , USA
Amadou Camara , USA
Marcio Carcho , Portugal
Peter Celec , Slovakia
Giselle Cerchiaro , Brazil
Arpita Chatterjee , USA
Shao-Yu Chen , USA
Yujie Chen, China
Deepak Chhangani , USA
Ferdinando Chiaradonna , Italy

Zhao Zhong Chong, USA
Fabio Ciccarone, Italy
Alin Ciobica , Romania
Ana Cipak Gasparovic , Croatia
Giuseppe Cirillo , Italy
Maria R. Ciriolo , Italy
Massimo Collino , Italy
Manuela Corte-Real , Portugal
Manuela Curcio, Italy
Domenico D'Arca , Italy
Francesca Danesi , Italy
Claudio De Lucia , USA
Damião De Sousa , Brazil
Enrico Desideri, Italy
Francesca Diomede , Italy
Raul Dominguez-Perles, Spain
Joël R. Drevet , France
Grégory Durand , France
Alessandra Durazzo , Italy
Javier Egea , Spain
Pablo A. Evelson , Argentina
Mohd Farhan, USA
Ioannis G. Fatouros , Greece
Gianna Ferretti , Italy
Swaran J. S. Flora , India
Maurizio Forte , Italy
Teresa I. Fortoul, Mexico
Anna Fracassi , USA
Rodrigo Franco , USA
Juan Gambini , Spain
Gerardo García-Rivas , Mexico
Husam Ghanim, USA
Jayeeta Ghose , USA
Rajeshwary Ghosh , USA
Lucia Gimeno-Mallench, Spain
Anna M. Giudetti , Italy
Daniela Giustarini , Italy
José Rodrigo Godoy, USA
Saeid Golbidi , Canada
Guohua Gong , China
Tilman Grune, Germany
Solomon Habtemariam , United Kingdom
Eva-Maria Hanschmann , Germany
Md Saquib Hasnain , India
Md Hassan , India


Tim Hofer , Norway
John D. Horowitz, Australia
Silvana Hrelia , Italy
Dragan Hrnčić, Serbia
Zebo Huang , China
Zhao Huang , China
Tarique Hussain , Pakistan
Stephan Immenschuh , Germany
Norsharina Ismail, Malaysia
Franco J. L. , Brazil
Sedat Kacar , USA
Andleeb Khan , Saudi Arabia
Kum Kum Khanna, Australia
Neelam Khaper , Canada
Ramoji Kosuru , USA
Demetrios Kouretas , Greece
Andrey V. Kozlov , Austria
Chan-Yen Kuo, Taiwan
Gaocai Li , China
Guoping Li , USA
Jin-Long Li , China
Qiangqiang Li , China
Xin-Feng Li , China
Jialiang Liang , China
Adam Lightfoot, United Kingdom
Christopher Horst Lillig , Germany
Paloma B. Liton , USA
Ana Lloret , Spain
Lorenzo Loffredo , Italy
Camilo López-Alarcón , Chile
Daniel Lopez-Malo , Spain
Massimo Lucarini , Italy
Hai-Chun Ma, China
Nageswara Madamanchi , USA
Kenneth Maiese , USA
Marco Malaguti , Italy
Steven McAnulty, USA
Antonio Desmond McCarthy , Argentina
Sonia Medina-Escudero , Spain
Pedro Mena , Italy
V́ctor M. Mendoza-Núñez , Mexico
Lidija Milkovic , Croatia
Alexandra Miller, USA
Sara Missaglia , Italy

Premysl Mladenka , Czech Republic
Sandra Moreno , Italy
Trevor A. Mori , Australia
Fabiana Morroni , Italy
Ange Mouithys-Mickalad, Belgium
Iordanis Mourouzis , Greece
Ryoji Nagai , Japan
Amit Kumar Nayak , India
Abderrahim Nemmar , United Arab Emirates
Xing Niu , China
Cristina Nocella, Italy
Susana Novella , Spain
Hassan Obied , Australia
Pál Pacher, USA
Pasquale Pagliaro , Italy
Dilipkumar Pal , India
Valentina Pallottini , Italy
Swapnil Pandey , USA
Mayur Parmar , USA
Vassilis Paschalis , Greece
Keshav Raj Paudel, Australia
Ilaria Peluso , Italy
Tiziana Persichini , Italy
Shazib Pervaiz , Singapore
Abdul Rehman Phull, Republic of Korea
Vincent Pialoux , France
Alessandro Poggi , Italy
Zsolt Radak , Hungary
Dario C. Ramirez , Argentina
Erika Ramos-Tovar , Mexico
Sid D. Ray , USA
Muneeb Rehman , Saudi Arabia
Hamid Reza Rezvani , France
Alessandra Ricelli, Italy
Francisco J. Romero , Spain
Joan Roselló-Catafau, Spain
Subhadeep Roy , India
Josep V. Rubert , The Netherlands
Sumbal Saba , Brazil
Kunihiro Sakuma, Japan
Gabriele Saretzki , United Kingdom
Luciano Saso , Italy
Nadja Schroder , Brazil



Anwen Shao , China
Iman Sherif, Egypt
Salah A Sheweita, Saudi Arabia
Xiaolei Shi, China
Manjari Singh, India
Giulia Sita , Italy
Ramachandran Srinivasan , India
Adrian Sturza , Romania
Kuo-hui Su , United Kingdom
Eisa Tahmasbpour Marzouni , Iran
Hailiang Tang, China
Carla Tatone , Italy
Shane Thomas , Australia
Carlo Gabriele Tocchetti , Italy
Angela Trovato Salinaro, Italy
Rosa Tundis , Italy
Kai Wang , China
Min-qi Wang , China
Natalie Ward , Australia
Grzegorz Wegrzyn, Poland
Philip Wenzel , Germany
Guangzhen Wu , China
Jianbo Xiao , Spain
Qiongming Xu , China
Liang-Jun Yan , USA
Guillermo Zalba , Spain
Jia Zhang , China
Junmin Zhang , China
Junli Zhao , USA
Chen-he Zhou , China
Yong Zhou , China
Mario Zoratti , Italy

Contents









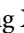
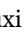
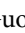


Corrigendum to “Salvianolic Acid B Protects Intervertebral Discs from Oxidative Stress-Induced Degeneration via Activation of the JAK2/STAT3 Signaling Pathway”

Shouqian Dai, Ting Liang, Xiu Shi, Zongping Luo , and Huilin Yang
Corrigendum (2 pages), Article ID 9874240, Volume 2022 (2022)




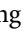






Programmed NP Cell Death Induced by Mitochondrial ROS in a One-Strike Loading Disc Degeneration Organ Culture Model

Bao-Liang Li, Xizhe Liu, Manman Gao, Fu Zhang, Xu Chen, Zhongyuan He, Jianmin Wang, Wei Tian, Dafu Chen , Zhiyu Zhou , and Shaoyu Liu
Research Article (17 pages), Article ID 5608133, Volume 2021 (2021)

Glycine-Serine-Threonine Metabolic Axis Delays Intervertebral Disc Degeneration through Antioxidant Effects: An Imaging and Metabonomics Study

Xiaolin Wu , Chang Liu , Shuai Yang , Nana Shen , Yan Wang , Youfu Zhu , Zhaoyang Guo , Shang-you Yang , Dongming Xing , Houxi Li , Zhu Guo , Bohua Chen , and Hongfei Xiang 
Research Article (33 pages), Article ID 5579736, Volume 2021 (2021)





TRPV1 Channel Activated by the PGE2/EP4 Pathway Mediates Spinal Hypersensitivity in a Mouse Model of Vertebral Endplate Degeneration

Sijing Liu , Qiong Wang , Ziyi Li , Lei Ma , Ting Li , Yukun Li , Na Wang , Chang Liu , Peng Xue , and Chuan Wang 
Research Article (16 pages), Article ID 9965737, Volume 2021 (2021)


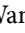






Tissue Renin-Angiotensin System (tRAS) Induce Intervertebral Disc Degeneration by Activating Oxidative Stress and Inflammatory Reaction

Kaiqiang Sun , Xiaofei Sun, Jingchuan Sun, Yan Jiang, Feng Lin, Fanqi Kong, Fudong Li, Jian Zhu, Le Huan, Bing Zheng, Yuan Wang, Weiguo Zou, Lu Gao , Ximing Xu , and Jiangang Shi 
Research Article (25 pages), Article ID 3225439, Volume 2021 (2021)

FAM134B-Mediated ER-phagy Upregulation Attenuates AGEs-Induced Apoptosis and Senescence in Human Nucleus Pulposus Cells

Rongjin Luo, Shuai Li, Gaocai Li, Saideng Lu , Weifeng Zhang, Hui Liu, Jie Lei, Liang Ma, Wencan Ke, Zhiwei Liao , Bingjin Wang, Yu Song, Kun Wang, Yukun Zhang , and Cao Yang 
Research Article (19 pages), Article ID 3843145, Volume 2021 (2021)




HIF-1 α -Mediated miR-623 Regulates Apoptosis and Inflammatory Responses of Nucleus Pulposus Induced by Oxidative Stress via Targeting TXNIP

Xiaogang Bao , Zhenhua Wang , Qi Jia , Sibao Shen , Likang Wu , Qi Jiang , Changwei Li , and Guohua Xu 
Research Article (17 pages), Article ID 6389568, Volume 2021 (2021)







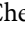





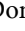



Deficiency of MIF Accentuates Overloaded Compression-Induced Nucleus Pulposus Cell Oxidative Damage via Depressing Mitophagy

Yiyang Wang , Yanzhu Hu , Haoming Wang , Ningyuan Liu , Lei Luo, Chen Zhao, Dandan Zhou , Hang Tong , Pei Li , and Qiang Zhou 
Research Article (19 pages), Article ID 6192498, Volume 2021 (2021)






Autophagic Degradation of Gasdermin D Protects against Nucleus Pulposus Cell Pyroptosis and Retards Intervertebral Disc Degeneration In Vivo

Zhiwei Liao , Suyun Li, Rong Liu, Xiaobo Feng, Yunsong Shi, Kun Wang, Shuai Li, Yukun Zhang, Xinghuo Wu , and Cao Yang 
Research Article (22 pages), Article ID 5584447, Volume 2021 (2021)





Exosomal MATN3 of Urine-Derived Stem Cells Ameliorates Intervertebral Disc Degeneration by Antisenescence Effects and Promotes NPC Proliferation and ECM Synthesis by Activating TGF- β

Zhu Guo , WeiLiang Su , RongYao Zhou , GuoQing Zhang , Shuai Yang , XiaoLin Wu , ChenSheng Qiu , WenBin Cong , Nana Shen , JianWei Guo , Chang Liu , Shang-You Yang , DongMing Xing , Yan Wang , BoHua Chen , and HongFei Xiang 
Research Article (18 pages), Article ID 5542241, Volume 2021 (2021)

Sodium Tanshinone IIA Sulfonate Ameliorates Injury-Induced Oxidative Stress and Intervertebral Disc Degeneration in Rats by Inhibiting p38 MAPK Signaling Pathway

Shouqian Dai , Xiu Shi , Rongqing Qin, Xing Zhang , Feng Xu , and Huilin Yang 
Research Article (12 pages), Article ID 5556122, Volume 2021 (2021)



Reactive Oxygen Species Mediate Low Back Pain by Upregulating Substance P in Intervertebral Disc Degeneration

Jiancheng Zheng , Jian Zhang, Xingkai Zhang, Zhiping Guo, Wenjian Wu , Zhe Chen , and Jitian Li 
Research Article (11 pages), Article ID 6681815, Volume 2021 (2021)



Ulinastatin Ameliorates IL-1 β -Induced Cell Dysfunction in Human Nucleus Pulposus Cells via Nrf2/NF- κ B Pathway

Xi Luo, Le Huan, Feng Lin, Fanqi Kong, Xiaofei Sun, Fudong Li, Jian Zhu, Jingchuan Sun, Ximing Xu, Kaiqiang Sun , Liwei Duan , and Jiangang Shi 
Research Article (21 pages), Article ID 5558687, Volume 2021 (2021)

Follistatin-Like 1 Attenuation Suppresses Intervertebral Disc Degeneration in Mice through Interacting with TNF- α and Smad Signaling Pathway






Shaoyi Wang, Jianlu Wei, Jie Shi, Qiting He, Xiacong Zhou, Ximei Gao , and Lei Cheng 
Research Article (13 pages), Article ID 6640751, Volume 2021 (2021)

The Role of Unfolded Protein Response in Human Intervertebral Disc Degeneration: Perk and IRE1- α as Two Potential Therapeutic Targets

Tianyong Wen , Peng Xue, Jinwei Ying, Shi Cheng, Yue Liu, and Dike Ruan 
Research Article (9 pages), Article ID 6492879, Volume 2021 (2021)



Contents

Research Progress on the Mechanism of Lumbarmultifidus Injury and Degeneration

Xianzheng Wang , Rui Jia , Jiaqi Li, Yibo Zhu, Huanan Liu , Weijian Wang , Yapeng Sun, Fei Zhang, Lei Guo, and Wei Zhang 






Review Article (9 pages), Article ID 6629037, Volume 2021 (2021)

Salvianolic Acid B Protects Intervertebral Discs from Oxidative Stress-Induced Degeneration via Activation of the JAK2/STAT3 Signaling Pathway

Shouqian Dai, Ting Liang, Xiu Shi, Zongping Luo , and Huilin Yang 




Research Article (13 pages), Article ID 6672978, Volume 2021 (2021)

Mechanosensitive Ion Channel Piezo1 Activated by Matrix Stiffness Regulates Oxidative Stress-Induced Senescence and Apoptosis in Human Intervertebral Disc Degeneration

Bingjin Wang , Wencan Ke, Kun Wang, Gaocai Li, Liang Ma, Saideng Lu, Qian Xiang , Zhiwei Liao, Rongjin Luo, Yu Song, Wenbin Hua, Xinghuo Wu, Yukun Zhang , Xianlin Zeng , and Cao Yang 


Research Article (13 pages), Article ID 8884922, Volume 2021 (2021)

Ferroportin-Dependent Iron Homeostasis Protects against Oxidative Stress-Induced Nucleus Pulposus Cell Ferroptosis and Ameliorates Intervertebral Disc Degeneration *In Vivo*

Saideng Lu, Yu Song, Rongjin Luo, Shuai Li, Gaocai Li, Kun Wang, Zhiwei Liao, Bingjin Wang, Wencan Ke, Qian Xiang , Chao Chen, Xinghuo Wu, Yukun Zhang, Li Ling , and Cao Yang 

Research Article (18 pages), Article ID 6670497, Volume 2021 (2021)

Long Noncoding RNA ANPODRT Overexpression Protects Nucleus Pulposus Cells from Oxidative Stress and Apoptosis by Activating Keap1-Nrf2 Signaling

Liang Kang, Yueyang Tian, Xing Guo, Xu Chu, and Yuan Xue 


Research Article (17 pages), Article ID 6645005, Volume 2021 (2021)

Tea Polyphenol Attenuates Oxidative Stress-Induced Degeneration of Intervertebral Discs by Regulating the Keap1/Nrf2/ARE Pathway

Dawei Song, Jun Ge, Yingjie Wang, Qi Yan, Cenhao Wu, Hao Yu, Ming Yang, Huilin Yang , and Jun Zou 


Research Article (13 pages), Article ID 6684147, Volume 2021 (2021)

Danshen Attenuates Intervertebral Disc Degeneration via Antioxidation in SD Rats

Rongqing Qin , Shouqian Dai , Xing Zhang , Hongpeng Liu, Bing Zhou, Pin Zhou, and Chuanliang Hu

Research Article (12 pages), Article ID 6660429, Volume 2020 (2020)

Allicin Attenuated Advanced Oxidation Protein Product-Induced Oxidative Stress and Mitochondrial Apoptosis in Human Nucleus Pulposus Cells

Qian Xiang, Zhangrong Cheng, Juntan Wang, Xiaobo Feng, Wenbin Hua, Rongjin Luo, Bingjin Wang, Zhiwei Liao, Liang Ma, Gaocai Li, Saideng Lu, Kun Wang, Yu Song, Shuai Li, Xinghuo Wu, Cao Yang, and Yukun Zhang 















Research Article (17 pages), Article ID 6685043, Volume 2020 (2020)

Overexpression of LMP-1 Decreases Apoptosis in Human Nucleus Pulposus Cells via Suppressing the NF- κ B Signaling Pathway

Yuan Liu , Wei Zhou , Fei-Fan Chen , Fei Xiao , Hai-Yang Zhu , Yun Zhou, and Guan-Cheng Guo 


Research Article (13 pages), Article ID 8189706, Volume 2020 (2020)

Exosomes Derived from Human Urine-Derived Stem Cells Inhibit Intervertebral Disc Degeneration by Ameliorating Endoplasmic Reticulum Stress

HongFei Xiang , WeiLiang Su , XiaoLin Wu , WuJun Chen , WenBin Cong , Shuai Yang , Chang Liu , ChenSheng Qiu , Shang-You Yang , Yan Wang , GuoQing Zhang , Zhu Guo , DongMing Xing , and BoHua Chen 

Research Article (21 pages), Article ID 6697577, Volume 2020 (2020)

Mitochondrial Dysfunction in Intervertebral Disc Degeneration: From Pathogenesis to Therapeutic Target

Danni Li, Fenghua Tao, and Lin Jin 

Review Article (13 pages), Article ID 8880320, Volume 2020 (2020)

Effect of Platelet-Rich Plasma on Intervertebral Disc Degeneration *In Vivo* and *In Vitro*: A Critical Review

Yvang Chang , Ming Yang , Song Ke , Yu Zhang , Gang Xu , and Zhonghai Li 

Review Article (10 pages), Article ID 8893819, Volume 2020 (2020)


Cell Senescence: A Nonnegligible Cell State under Survival Stress in Pathology of Intervertebral Disc Degeneration

Yuang Zhang, Biao Yang, Jingkai Wang, Feng Cheng, Kesi Shi, Liwei Ying, Chenggui Wang, Kaishun Xia, Xianpeng Huang, Zhe Gong, Chao Yu, Fangcai Li , Chengzhen Liang , and Qixin Chen 

Review Article (12 pages), Article ID 9503562, Volume 2020 (2020)

Corrigendum

Corrigendum to “Salvianolic Acid B Protects Intervertebral Discs from Oxidative Stress-Induced Degeneration via Activation of the JAK2/STAT3 Signaling Pathway”

Shouqian Dai,¹ Ting Liang,¹ Xiu Shi,² Zongping Luo ,¹ and Huilin Yang¹

¹Department of Orthopedics, The First Affiliated Hospital of Soochow University, Orthopedics Institute of Soochow University, Suzhou, Jiangsu, China

²Department of Obstetrics and Gynecology, The First Affiliated Hospital, Soochow University, Suzhou, Jiangsu, China

Correspondence should be addressed to Zongping Luo; zongping_luo@yahoo.com and Huilin Yang; suzhouspine@163.com

Received 2 February 2022; Accepted 2 February 2022; Published 23 February 2022

Copyright © 2022 Shouqian Dai et al. This is an open access article distributed under the Creative Commons Attribution License, which permits unrestricted use, distribution, and reproduction in any medium, provided the original work is properly cited.

In the article titled “Salvianolic Acid B Protects Intervertebral Discs from Oxidative Stress-Induced Degeneration via Activation of the JAK2/STAT3 Signaling Pathway” [1], there was an error in Section 3.3, and the following statement should be corrected:

“Figures 4(a)–4(d) demonstrate that in the H₂O₂ group, ROS and MDA levels were clearly less, and GSH and SOD2 levels significantly higher than those of the control group” should be corrected to

“Figures 4(a)–4(d) demonstrate that in the H₂O₂ group, ROS and MDA levels were clearly higher and GSH and SOD2 levels significantly lower than those of the control group.”

Additionally in Figure 2(d), the label for IDD was accidentally omitted during the typesetting process, and the corrected figure is as follows:

The authors confirm that this does not affect the results and conclusions of the article, and the editorial board agrees to the publication of a corrigendum.

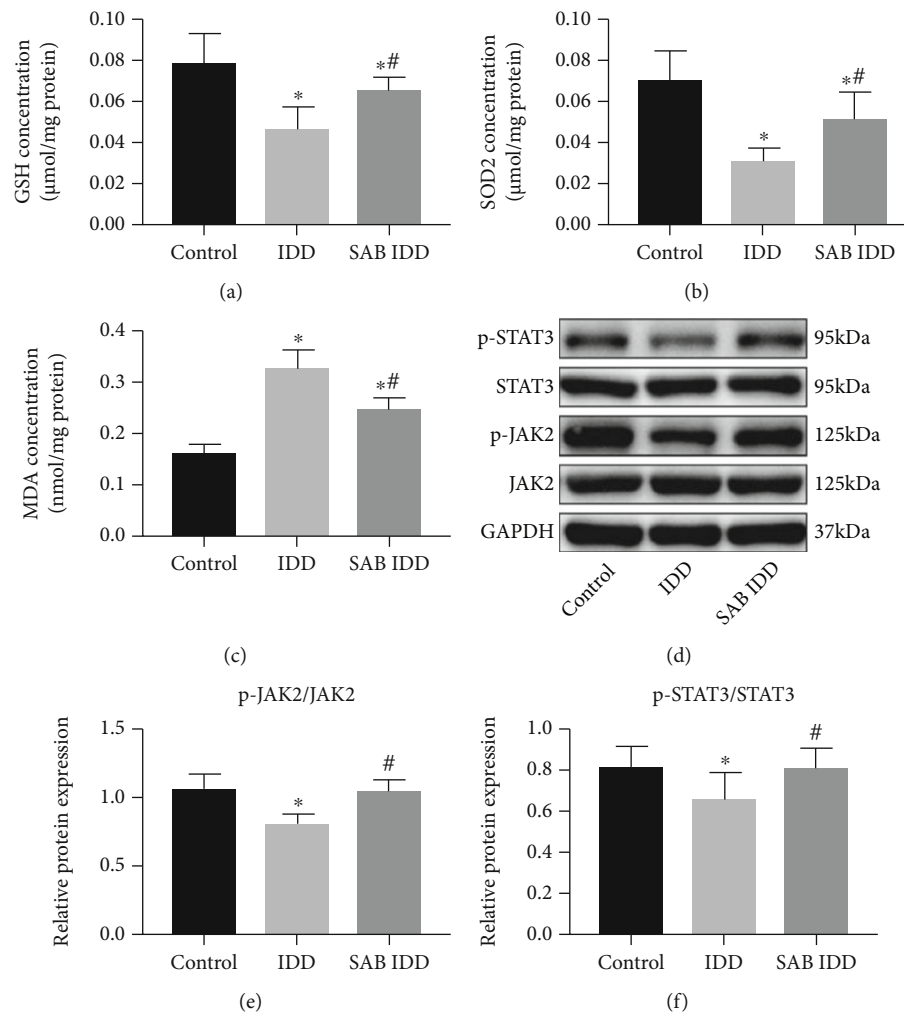




FIGURE 2: SAB reversed the effects on the antioxidant system induced by puncture injury in vivo that activated the JAK2/STAT3 signaling pathway. Animals were divided into three groups: control group, IDD group, or SAB group. Concentrations of (a) GSH, (b) SOD2, and (c) MDA were measured by assay kits. (d) Expression levels of phosphorylated and total JAK2 and STAT3 in IVDs were measured by Western blotting, and the relative ratios of (e) p-JAK2/JAK2 and (f) p-STAT3/STAT3 were calculated from gray-level values. * $P < 0.05$ compared with the control group; # $P < 0.05$ compared with the IDD group. SAB: salviaolic acid B; GSH: glutathione; SOD2: superoxide dismutase 2; MDA: malondialdehyde; GAPDH: glyceraldehyde-3-phosphate dehydrogenase; JAK2: Janus kinase 2; STAT3: signal transducer and activator of transcription 3.

References

- [1] S. Dai, T. Liang, X. Shi, Z. Luo, and H. Yang, "Salviaolic acid B protects intervertebral discs from oxidative stress-induced degeneration via activation of the JAK2/STAT3 signaling pathway," *Oxidative Medicine and Cellular Longevity*, vol. 2021, Article ID 6672978, 13 pages, 2021.

Research Article

Programmed NP Cell Death Induced by Mitochondrial ROS in a One-Strike Loading Disc Degeneration Organ Culture Model

Bao-Liang Li,^{1,2} Xizhe Liu,² Manman Gao,^{3,4} Fu Zhang,¹ Xu Chen,¹ Zhongyuan He,¹ Jianmin Wang,¹ Wei Tian,⁵ Dafu Chen ⁵, Zhiyu Zhou ^{1,2} and Shaoyu Liu^{1,2}

¹Innovation Platform of Regeneration and Repair of Spinal Cord and Nerve Injury, Department of Orthopaedic Surgery, The Seventh Affiliated Hospital, Sun Yat-sen University, Shenzhen 518107, China

²Guangdong Provincial Key Laboratory of Orthopedics and Traumatology, Orthopaedic Research Institute/Department of Spinal Surgery, The First Affiliated Hospital of Sun Yat-sen University, Guangzhou 510080, China

³Department of Sport Medicine, Inst Translat Med, The First Affiliated Hospital of Shenzhen University, Shenzhen Second People's Hospital, Shenzhen 518000, China

⁴Guangdong Key Laboratory for Biomedical Measurements and Ultrasound Imaging, School of Biomedical Engineering, Shenzhen University Health Science Center, Shenzhen 518060, China

⁵Laboratory of Bone Tissue Engineering, Beijing Laboratory of Biomedical Materials, Beijing Research Institute of Orthopaedics and Traumatology, Beijing Jishuitan Hospital, Beijing 100035, China

Correspondence should be addressed to Dafu Chen; chendafujst@126.com and Zhiyu Zhou; zhouzhy23@mail.sysu.edu.cn

Received 16 April 2021; Revised 17 July 2021; Accepted 2 August 2021; Published 1 September 2021

Academic Editor: Sidong Yang

Copyright © 2021 Bao-Liang Li et al. This is an open access article distributed under the Creative Commons Attribution License, which permits unrestricted use, distribution, and reproduction in any medium, provided the original work is properly cited.

Increasing evidence has indicated that mitochondrial reactive oxygen species (ROS) play critical roles in mechanical stress-induced lumbar degenerative disc disease (DDD). However, the detailed underlying pathological mechanism needs further investigation. In this study, we utilized a one-strike loading disc degeneration organ culture model to explore the responses of intervertebral discs (IVDs) to mechanical stress. IVDs were subjected to a strain of 40% of the disc height for one second and then cultured under physiological loading. Mitoquinone mesylate (MitoQ) or other inhibitors were injected into the IVDs. IVDs subjected to only physiological loading culture were used as controls. Mitochondrial membrane potential was significantly depressed immediately after mechanical stress ($P < 0.01$). The percentage of ROS-positive cells significantly increased in the first 12 hours after mechanical stress and then declined to a low level by 48 hours. Pretreatment with MitoQ or rotenone significantly decreased the proportion of ROS-positive cells ($P < 0.01$). Nucleus pulposus (NP) cell viability was sharply reduced at 12 hours after mechanical stress and reached a stable status by 48 hours. While the levels of necroptosis- and apoptosis-related markers were significantly increased at 12 hours after mechanical stress, no significant changes were observed at day 7. Pretreatment with MitoQ increased NP cell viability and alleviated the marker changes by 12 hours after mechanical stress. Elevated mitochondrial ROS levels were also related to extracellular matrix (ECM) degeneration signs, including catabolic marker upregulation, anabolic marker downregulation, increased glycosaminoglycan (GAG) loss, IVD dynamic compressive stiffness reduction, and morphological degradation changes at the early time points after mechanical stress. Pretreatment with MitoQ alleviated some of these degenerative changes by 12 hours after mechanical stress. These changes were eliminated by day 7. Taken together, our findings demonstrate that mitochondrial ROS act as important regulators of programmed NP cell death and ECM degeneration in IVDs at early time points after mechanical stress.

1. Introduction

Degenerative disc disease (DDD) is a chronic spinal disorder characterized by structural failure of the intervertebral

disc (IVD), increased proteolytic activity, nucleus pulposus (NP) cell death, and proinflammatory cytokine release [1, 2]. Lumbar DDD is one of the most common chronic degenerative diseases worldwide. It impacts forty percent of people

aged 40 years and affects more than eighty percent of the population aged 80 years, with nearly twenty percent of people with lumbar DDD showing a poor response to nonsurgical treatment [3]. Hence, there is an urgent need for a deep understanding of the underlying molecular mechanisms responsible for DDD for the sake of better management.

Nonphysiological mechanical stress (MS) is viewed as a significant risk factor for the development of lumbar DDD [4]. Excessive MS results in cell death and extracellular matrix (ECM) degradation, which leads to significant structural changes in IVDs [5]. Necroptosis and apoptosis are the two principal types of programmed cell death that have been implicated in lumbar DDD [6, 7]. Despite mounting evidence, the mechanisms underlying MS-induced DDD have not been fully elucidated.

Mitochondria are central cytoplasmic hubs essential for not only cellular metabolism but also various types of programmed cell death, including apoptosis and necroptosis, due to their production of reactive oxygen species (ROS) and other prodeath mediators [8]. Multiple complex mechanisms underlie MS-induced mitochondrial ROS production, including intracellular Ca^{2+} overload and cytoskeletal strain [9–11]. It was recently demonstrated that mechanical stimulation induces the endoplasmic reticulum Ca^{2+} releases and extracellular Ca^{2+} influx [12]. Excessive cytosolic Ca^{2+} elevations induce mitochondrial depolarization and ROS generation [13]. As the cytoskeleton interacts heavily with mitochondria, it is not surprising that cell strain results in mitochondrial strain and ROS generation. In addition, dissolution of the cytoskeleton by reagents prevents impact-induced ROS generation [9].

Several studies have emphasized the importance of mitochondrial ROS in NP cell mechanical injury. Excessive ROS generation activates multiple apoptosis pathways by causing damage to proteins, nucleic acids, lipids, membranes, and organelles. Mitochondrial-derived oxidative stress is thought to contribute to the necroptotic pathway at the receptor-interacting protein kinase 3 (RIPK3) or mixed-lineage kinase domain-like protein (MLKL) level [14]. A recent study has reported that mitochondrial ROS promote RIPK1 autophosphorylation on serine residue 161 (S161) and then recruit RIPK3 to further form a functional necrosome and that necrosomal RIPK3 enhances ROS production [8]. In recent years, a growing number of research articles have highlighted the critical role of mitochondrial ROS in the programmed death of NP cells, providing crucial novel insights into the progression of lumbar DDD [15]. For example, a study on isolated NP cells indicated that increased RIPK1 expression following compression-induced injury induces mitochondrial dysfunction and oxidative stress. However, how mitochondrial ROS affect NP cell viability in IVDs is still unclear.

Enhanced expression of catabolic markers such as matrix metalloproteases (MMPs) and a disintegrin and metalloproteinase with thrombospondin motif (ADAMTS) proteins and loss of glycosaminoglycan have been observed in NP tissue after MS. Interestingly, Nasto et al. reported that mitochondrial ROS induce MMP gene expression in NP cells in vitro, suggesting that mitochondrial ROS plays a pathological role in aging-related IVD degeneration [16]. Several

other reports have demonstrated that antioxidative therapy suppresses the gene expression of ECM-destructive enzymes in cartilage after MS [17]. Therefore, we hypothesized that MS-induced catabolic marker expression and ECM degeneration are partly mediated by mitochondrial ROS.

Several studies have shown that high-impact loading is a significant factor contributing to DDD [18–24]. Based on this finding, we successfully established a disc degeneration organ culture model via one-strike loading [24]. This model showed signs of early degeneration, including annulus fibrosus (AF) fissures, ECM degradation, glycosaminoglycan (GAG) release, and upregulated catabolic marker gene expression. Our one-strike loading model may not fully reveal the whole process of DDD development. Nevertheless, it is well suited for investigating the pathogenesis of MS-induced DDD at the early stage.

The objective of the present study was to investigate the occurrence of programmed cell death, ECM degeneration, and mitochondrial ROS production after MS in a one-strike loading model. More importantly, the correlations among MS, mitochondrial ROS, programmed cell death, and ECM degeneration were evaluated by measuring cellular reactions to help elucidate the molecular pathophysiology of DDD.

2. Materials and Methods

2.1. Isolation and Cultivation of IVDs. Tails from bovines were obtained from a local abattoir. As we used leftovers of the slaughterhouse, no approval of an ethical committee was required according to Chinese regulations. IVD isolation and cultivation were carried out as previously described on day 0 [19]. In brief, after dissecting the surrounding soft tissue, individual IVDs with endplates were resected with a band saw. The endplates were rinsed with phosphate-buffered saline (PBS) using an APEXPULSE Disposable Pulse Lavage system (Apex, Guangzhou, China). Then, the IVDs were washed with PBS containing 10% penicillin/streptomycin (Gibco, Waltham, MA) for 15 minutes on a shaking table. The IVDs were then incubated with Dulbecco's modified Eagle's medium (DMEM, Sigma-Aldrich, Munich, Germany) supplemented with 2% fetal calf serum (FCS), 1% penicillin/streptomycin, 1% ITS+1 (Sigma-Aldrich), 50 $\mu\text{g}/\text{ml}$ L-ascorbic acid (Sigma-Aldrich), and 0.1% Primocin (InvivoGen, San Diego, CA, USA) in a humidified (85%) atmosphere with 5% CO_2 at 37°C. All IVDs were cultured under physiological loading (0.02–0.2 MPa; 0.2 Hz; 1 hour/day) within a custom-designed bioreactor from day 1 (Figure 1(a)). The culture medium was replaced once a day after physiological loading. IVDs from the same tail were randomly assigned to different groups. IVDs subjected to only physiological loading culture were assigned to control (CON) groups.

2.2. Mechanical Stress. IVDs were subjected to MS using a custom-made universal mechanical tester in a custom-designed incubation chamber at room temperature on day 1 (Figure 1(a)). During the MS period, the IVDs were incubated in a culture medium to prevent dehydration. The IVDs were first subjected to a preload of 10 N for 3 minutes to

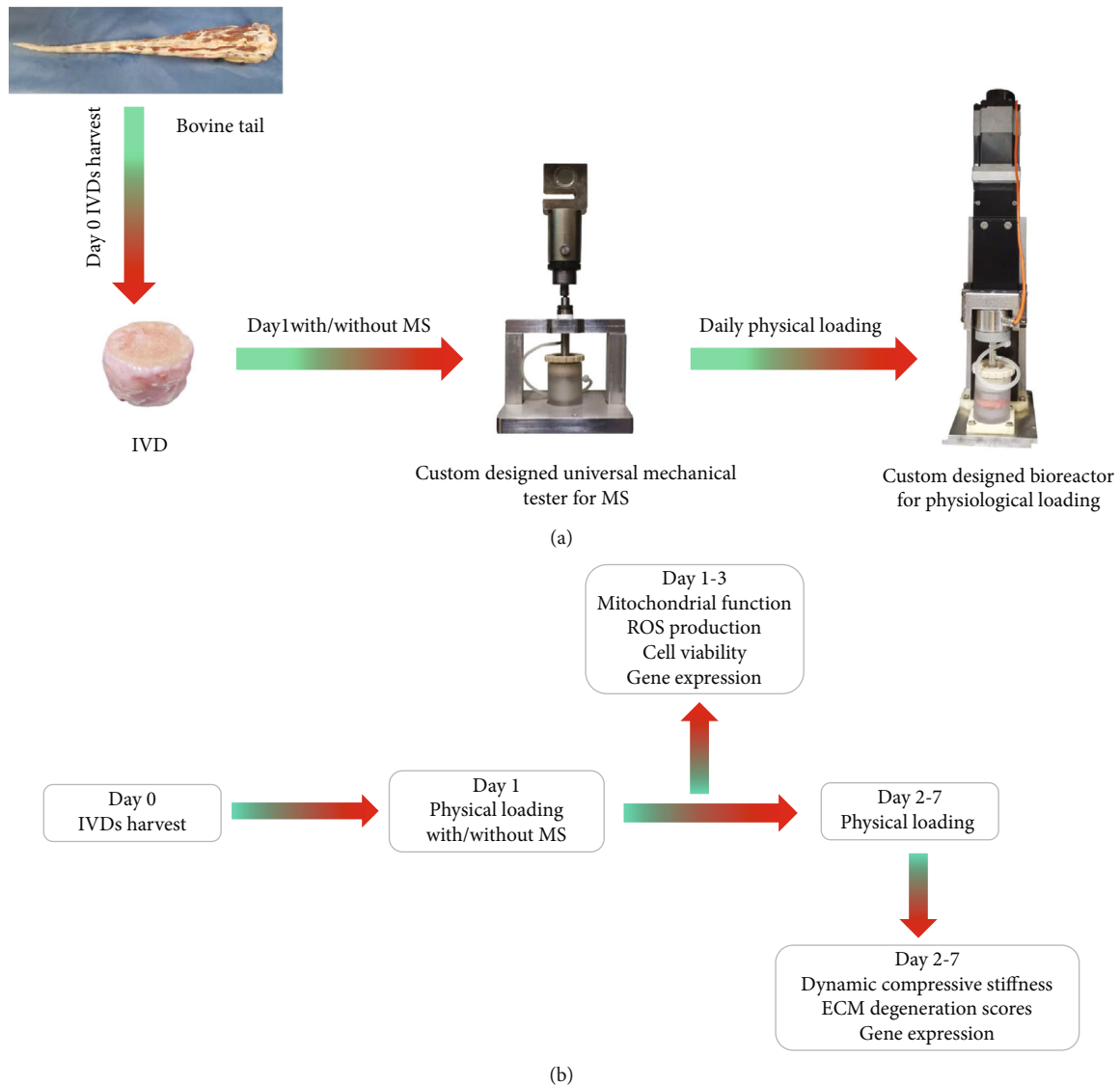


FIGURE 1: (a) Bioreactor and custom-designed chamber for physiological loading and the universal mechanical tester for MS on bovine IVDs. (b) Flow chart describing the study design.

prevent overhydration and to ensure reliable contact between the endplate, the incubation chamber, and the mechanical tester. MS injury was applied for one second with a strain of 40% of the disc height. Following MS injury, the IVDs were analyzed or incubated in a culture medium with daily physiological loading for another 1 to 7 days.

2.3. Dynamic Compressive Stiffness. The dynamic compressive stiffness was gauged by the custom-designed bioreactor at several time points: on day 1, day 2, and day 7 after overnight free-swelling culture [25]. The discs were first preloaded with 10% strain for 3 minutes and then loaded with 10 rounds of sinusoidal compression at 5–15% strain. Dynamic stress was determined by the following equation: $(F_{\max} - F_{\min})/S$. F_{\max} and F_{\min} represent the maximum and minimum forces achieved during one round, respectively, and S is the sectional area of the IVD. The dynamic compressive stiffness was gauged for every loading round,

and the average value from 10 rounds was calculated. The stiffness gauged on day 1 was used as a baseline for standardization.

2.4. Inhibitor Studies. For inhibitor studies, various reagents were dissolved in dimethyl sulfoxide (DMSO) and diluted in PBS. Then, 100 μl of PBS containing reagent was injected into the NP tissue with a 26-gauge needle during the middle of the dynamic loading cycle. To exclude potential interference, 100 μl of PBS containing 0.05% DMSO was injected into CON IVDs. After 2 hours of free-swelling recovery, the IVDs were subjected to a one-time MS injury. To distinguish between apoptosis and necroptosis, the RIPK1 inhibitor necrostatin-1 (Nec-1, 80 μM , MCE, NJ, USA) and the pan-caspase inhibitor N-benzyloxycarbonyl-Val-Ala-Asp-fluoromethylketone (Z-VAD-FMK, 50 μM , MCE) were used. The electron transport chain inhibitor rotenone (20 μM , Sigma-Aldrich) was used to inhibit mitochondrial ROS generation.

To verify the involvement of mitochondrial ROS in MS-induced programmed NP cell death and disc degeneration, the mitochondrial ROS scavenger mitquinone mesylate (MitoQ, 4 μ M, MCE) was used. MitoQ was mixed into the culture medium after daily medium renewal.

2.5. Cell Viability Assay. Cell viability was evaluated using calcein acetoxymethyl ester (calcein AM, eBioscience, Frankfurt, Germany) and propidium iodide (PI, MCE). In this system, green fluorescence indicates viable cells with intact membranes, green/red fluorescence indicates viable cells with compromised plasma membranes, and red fluorescence indicates dead cells [26]. For histological analysis, the AF and endplates were dissected with a scalpel. NP tissue was cut into slices (100 μ m) with a vibrating microtome (Leica VT1200S, Leica Microsystems, Germany). The NP tissue slices were incubated with a culture medium containing 1 μ g/ml calcein AM and 1 μ g/ml PI for one hour at 37°C. After washing with PBS, the slices were immediately viewed using an inverted confocal laser scanning microscope (Zeiss Confocal LSM 780, Carl Zeiss Jena GmbH, Jena, Germany), and one random image per disc was analyzed. The numbers of viable and dead cells were measured manually using ImageJ software (National Institutes of Health, USA).

2.6. Measurement of Mitochondrial Membrane Potential. Mitochondrial membrane potential was evaluated using 5,5',6,6'-tetrachloro-1,1',3,3'-tetraethylbenzimidazolocarbo-cyanine iodide (JC-1, MCE). In cells with normal mitochondria, JC-1 aggregates in mitochondria with a high red/green fluorescence intensity ratio. In cells with compromised mitochondria, JC-1 aggregates become JC-1 monomers, and the red/green fluorescence intensity ratio decreases. NP tissue slices were incubated with a culture medium containing 10 μ M JC-1 for one hour at 37°C. After washing with PBS, the slices were immediately viewed using an inverted confocal laser scanning microscope, and one random image per disc was analyzed. The JC-1 red fluorescence intensity was analyzed using ImageJ software.

2.7. ROS Detection. Intracellular ROS generation was detected using dihydroethidium (MCE). Dihydroethidium, which penetrates the plasma membrane quite easily, is converted into ethidium bromide by superoxide anions and intercalates into DNA in the nucleus, emitting marked red fluorescence. NP slices were incubated with a culture medium containing 10 μ M dihydroethidium and 1 μ g/ml calcein AM for one hour at 37°C. After washing with PBS, the slices were immediately viewed using an inverted confocal laser scanning microscope, and one random image per disc was analyzed. The numbers of viable cells and dihydroethidium-positive cells were manually measured using ImageJ software to calculate the proportion of dihydroethidium-positive cells.

2.8. RNA Extraction and Real-Time Quantitative Polymerase Chain Reaction (RT-qPCR). NP tissue was harvested on day 1 and day 7 for gene expression analysis. The cartilaginous endplates of each IVD were detached, and approximately 150 mg of NP tissue was collected. For RNA extraction, the tissue samples were digested with 2 mg/ml pronase for 1 hour

at 37°C, flash frozen, pulverized in liquid nitrogen, and homogenized using a TissueLyser [27]. Total RNA extraction was performed using TRI Reagent (Molecular Research Center, Cincinnati, OH, USA), and then, 400 ng of RNA was converted to cDNA using a SuperScript VILO cDNA Synthesis Kit (Life Technologies, Carlsbad, CA). RT-qPCR was performed using PowerUp SYBR Green Master Mix (Thermo Fisher Scientific, USA) on a Real-Time System (Bio-Rad). Each reaction mixture was 10 μ l and contained 2 μ l of 5 ng/ μ l cDNA, 5 μ l of 2x PowerUp SYBR Green Master Mix, 2 μ l of nuclease-free water, and 0.5 μ l each of 10 μ M forward and reverse primers. The following cycle conditions were applied: 50°C for 2 minutes and 95°C for 2 minutes followed by 44 cycles of 15 s at 95°C and 1 minute at 60°C. The specific primers used in this study were designed by using Primer 6.0 software (Applied Biosystems, Foster City, CA), and the sequences are provided in Table 1. Ribosomal protein lateral stalk subunit P0 (RPLP0) was used as a reference gene. The data were analyzed using the $2^{-\Delta\Delta Ct}$ algorithm.

2.9. Histology. NP tissues were fixed in 4% paraformaldehyde for 24 hours and dehydrated in graded sucrose solutions, after which 10 μ m thick sections were prepared. Immunofluorescence staining against CASPASE3 (1:400, Proteintech, China), BCL2 (1:200, Proteintech), BAX (1:400, Proteintech), MLKL (1:400, Invitrogen, CA, USA), MMP1 (1:200, Invitrogen), MMP3 (1:100, Proteintech), ADAMTS5 (1:200, Affinity, USA), and collagen II (1:200, Affinity) was performed. Briefly, the sections were permeabilized with 0.3% Triton X-100 for 30 minutes and then blocked with 5% bovine serum albumin and 0.1% Triton X-100 for 1 hour at room temperature. Subsequently, the sections were incubated with antibodies at 4°C overnight. The tissue sections were thoroughly washed with Tris-buffered saline with Tween-20 (TBST) and incubated with a Fluor-594-conjugated anti-rabbit secondary antibody (Jackson ImmunoResearch Inc., West Grove, PA, USA) at a 1:300 dilution for 1 hour at room temperature. Then, the sections were washed with TBST again, and the nuclei were counterstained with 4,6-diamidino-2-phenylindole (DAPI, Abcam, Germany) for 10 minutes.

Terminal deoxynucleotidyl transferase-mediated dUTP nick end labeling (TUNEL) was used to detect DNA fragmentation, which is known to be a characteristic of apoptosis. TUNEL staining was performed according to the instructions of a TUNEL Apoptosis Assay Kit (Dalian Meilun Biotech., Dalian, China), and the nuclei were counterstained with DAPI (Abcam) for 10 minutes. Images were visualized using an LSM 780 confocal microscope (Zeiss) with Zen Black software and analyzed using ImageJ.

After 0, 4, and 7 days of culture, IVDs were quickly fresh frozen, transected into 10 μ m thick sections and then fixed in 100% methanol. Safranin O (Sigma-Aldrich) and 0.02% Fast Green (Sigma-Aldrich) were used to show overall matrix organization, and Weigert's hematoxylin (Sigma-Aldrich) was used to show nuclear distribution. The stained sections were imaged with a digital pathology system (Kfbio, Ningbo, China). A semiquantitative scoring system was used to

TABLE 1: Primers used for RT-qPCR.

ADAMSTS4	F:5'-TACCGAGGGACTGAACTCCACATC-3' R:5'-GGAATGCCGCCATCTTGTCTATCT-3'
ADAMSTS5	F:5'-TGTGCGGTGATTGAAGACGATGG-3' R:5'-TGCTGGTGAGGATGGAAGACATTAAG-3'
BAX	F:5'-TTTGCTTCAGGGTTTCATCCAGGATC-3' R:5'-AGACACTCGCTCAGCTTCTTGGT-3'
BCL2	F:5'-TGTGGATGACCGAGTACCTGAAC-3' R:5'-GAGACAGCCAGGAGAAATCAAACAG-3'
CASPASE3	F:5'-CGCATATTCTACAGCACCTGGTTAC-3' R:5'-AGCATCTCACAAAGAGCCTGGAT-3'
CAT	F:5'-TCAACAGTGCCAACGATGACAATG-3' R:5'-GATGCGGGAGCCATATTCAGGAT-3'
COL2A1	F:5'-GAGCAGCAAGAGCAAGGACAAGA-3' R:5'-GCAGTGGTAGGTGATGTTCTGAGAG-3'
MLKL	F:5'-CAGACTTCCATCAGCCGACAACTA-3' R:5'-ATCTCCCAGAGGACAATTCCAAAGC-3'
MMP1	F:5'-CCAGACCTGTCAAGAGCAGATGT-3' R:5'-ATGAGCGTCTCCTCCGATACCT-3'
MMP3	F:5'-AACCTCCGATTCTGCTGTTGCTA-3' R:5'-GCTTGCGTATCACCTCCAGAGT-3'
MMP13	F:5'-AGACAAATGTGACCCTTCC-3' R:5'-ATAGGCGGCATCAATACG-3'
RIPK1	F:5'-CTCGCTTACCCTGGTGTGATGA-3' R:5'-TGATGGCAAGGAGGTGAATGGA-3'
RIPK3	F:5'-TCAAGCCCTCCAATGTCCTACTAGA-3' R:5'-ACTGTGAGCCTCCCTGAAATGTG-3'
RPLP0	F:5'-CACGCTGCTGAACATGCTGAAC-3' R:5'-AGGCACAGCTGGCAACATT-3'
SOD2	F:5'-TCTTCTGGACAAATCTGAGCCCTA-3' R:5'-TCCTGGTTAGAACAAGCAGCAATC-3'

determine the degree of degeneration [18]. The histological grading criteria were based mainly on cleft patterns found in the IVDs, with scores ranging from 0 to 9.

2.10. Measurement of Oxidized Glutathione (GSSG) and Total Glutathione. GSSG and total glutathione were measured using a GSH (reduced glutathione) and GSSG Assay Kit (Beyotime Biotechnology, China). Briefly, NP tissues were pulverized in liquid nitrogen, homogenized in a buffer according to the instructions, and then centrifuged. To measure GSSG, GSH was blocked prior to the reaction with GSH reductase and NADPH. To measure total glutathione (GSSG + GSH), the supernatant was added to a buffer containing

GSH reductase and NADPH. Five minutes later, dithionitrobenzoic acid (DTNB) was added, and the absorbance was measured at 412 nm.

2.11. Analysis of Released GAG. Cumulative release of GAG to the conditioned medium was measured using a modified 1,9-dimethylmethylene blue (DMMB) method [28]. The DMMB solution was prepared by dissolving 16 mg of DMMB (Sigma-Aldrich), 3.04 g of glycine (Sigma-Aldrich), and 2.37 g of NaCl in 1 L of distilled water (pH 3.0). Diluted conditioned medium (20 μ l) was mixed with 200 μ l of DMMB solution, and the absorbance was immediately measured at 535 nm. Serial dilutions of chondroitin 4-sulfate sodium salt (Aladdin, Shanghai, China) were used to generate the GAG standard reference curve.

2.12. Statistical Analysis. All statistical analyses were performed using SPSS 22.0 (IBM, Chicago, IL, USA). The Shapiro-Wilk normality test was performed to evaluate the normality of the data distribution. Comparisons between two groups were performed using Student's *t*-test for normally distributed data and Mann-Whitney *U*-tests for nonnormally distributed data. A difference was considered significant when the *P* value was <0.05.

3. Results

3.1. Presence of Mitochondrial ROS Accumulation and Mitochondrial Dysfunction in NP Cells after MS. Dihydroethidium staining was used to detect ROS production in NP cells at several time points after MS. MS significantly increased the ROS-positive cell proportion and remained at a stable high level over the first 12 hours (Figures 2(a) and 2(b)). Afterward, the proportion of ROS-positive cells decreased sharply and reached a low level by 48 hours. The proportion of ROS-positive cells remained stable in the physiological loading culture group. The mitochondrial electron transport inhibitor rotenone significantly reduced the proportion of ROS-positive cells immediately after MS (~78%, *P* < 0.01) (Figure 2(c)). The mitochondrial ROS scavenger MitoQ also significantly decreased the proportion of ROS-positive cells (~73%, *P* < 0.01).

JC-1 staining was used to monitor mitochondrial membrane potential in NP tissue immediately after MS. The NP cell mitochondrial membrane potential was significantly decreased in the MS group (Figures 2(d) and 2(e)). MitoQ pretreatment partially attenuated the depression of mitochondrial membrane potential. These results indicated that MS was able to directly induce mitochondrial dysfunction.

The GSSG/total glutathione ratio was calculated to further evaluate ROS levels in NP tissue. As shown in Figure 2(f), MS treatment increased the GSSG/total glutathione ratio, and this increase was alleviated by MitoQ pretreatment. In addition, RT-qPCR results showed that MitoQ significantly inhibited the mRNA expression of catalase (CAT) caused by MS (Figures 2(g) and 2(h)). These results demonstrated that the time-dependent ROS accumulation was mainly derived from the mitochondria after MS.

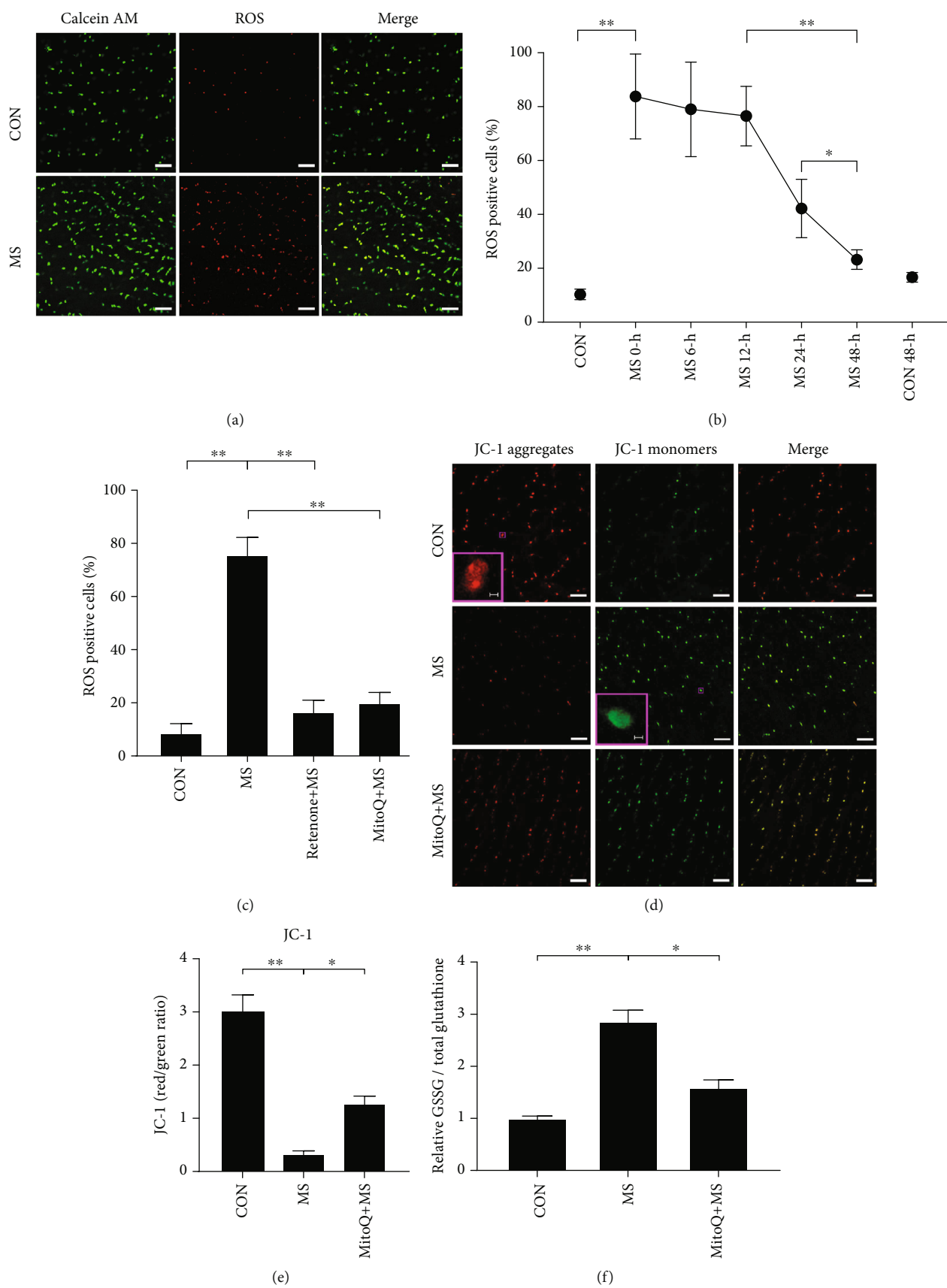


FIGURE 2: Continued.

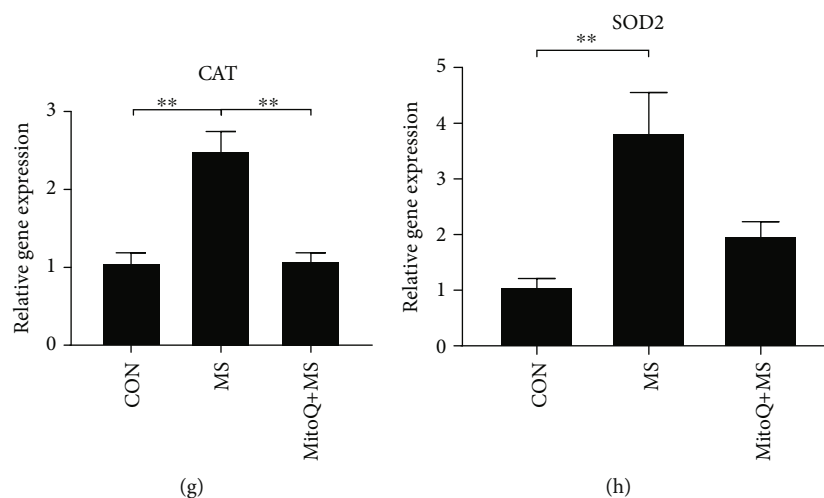


FIGURE 2: MS induced large-scale mitochondrial ROS generation and mitochondrial dysfunction. (a) Typical confocal images showing the viable cells (green) and ROS-positive cells (red) in the CON group and the MS group at 0 hours after MS. (b) Percentages of ROS-positive cells measured in the CON group and the MS group at different time points. (c) Rotenone and MitoQ pretreatment reduced the percentage of ROS-positive cells. (d) Typical confocal images of JC-1 staining showing the red fluorescence of JC-1 aggregates and the green signal of JC-1 monomers at 0 hours after MS. (e) Quantification of the mitochondrial membrane potential (ratio of red to green fluorescence) in the CON, MS, and MitoQ pretreatment groups. (f) The relative ratio of GSSG to total glutathione was measured at 12 hours after MS. (g, h) Quantification of SOD2 and CAT mRNA levels at 12 hours after MS. Scale bars, 50 μm and 5 μm (inset). The values are expressed as the means \pm SEMs. $n = 3$, * $P < 0.05$, and ** $P < 0.01$.

3.2. NP Cell Viability Change after MS. To explore the NP cell death mechanisms after MS, IVDs were cultivated and subsequently analyzed for cell viability at different time points. The application of MS to IVDs resulted in a dramatic time-dependent decrease in NP cell viability (Figures 3(a) and 3(b)). A small portion of NP cell death occurred immediately after MS, and cell viability remained stable during the first 12 hours ([CON vs. MS 0 hours]: 9.2%, $P < 0.01$; [MS 0 hours vs. MS 12 hours]: 1.9%, $P > 0.05$). More than 70% of NP cell death occurred within 12 to 48 hours after MS ([CON vs. MS 12 hours]: 11.1%, $P < 0.05$; [MS 12 hours vs. MS 48 hours]: 27.8%, $P < 0.01$). Cell viability reached a relatively stable status ([MS 48 hours vs. MS 72 hours]: 2.2%, $P > 0.05$) at 48 hours after MS application. Cell viability in the CON group remained stable at nearly 94% ([CON vs. CON 72 hours]: 1.8%, $P > 0.05$) after 72 hours in physiological loading culture. Thus, both the magnitude and the mechanism of cell death varied with time after MS.

The dramatic decrease in NP cell viability after 12 hours of MS suggested that, aside from necrosis that was directly caused by MS, programmed cell death was activated. For this reason, IVDs were pretreated with Z-VAD-FMK, Nec-1, or MitoQ for 2 hours and then subjected to MS. Cell viability analysis showed that inhibitor pretreatment significantly alleviated NP cell death (20% cell viability in the MitoQ group, $P < 0.05$; 15.82% cell viability in the Z-VAD-FMK group, $P < 0.05$; 13.12% cell viability in the Nec-1 group, $P < 0.05$) with respect to the MS group (Figure 3(c)).

3.3. Programmed Cell Death-Associated Marker Changes in NP Tissue after MS. We further investigated the relative changes in apoptosis indicator genes (CASPASE3, BCL2, and BAX) and necroptosis indicator genes (RIP1, RIP3, and MLKL) (Figures 4(a)–4(f)). The mRNA expression levels of

apoptosis and necroptosis genes were significantly increased at 12 hours after MS, and MitoQ pretreatment alleviated some of these changes (CASPASE3, RIP1, RIP3, and MLKL). In line with the mRNA expression results, the results of immunofluorescence staining showed that apoptosis (CASPASE3, BAX, and BAX/BCL2 ratio) and necroptosis (MLKL) were significantly increased at 12 hours after MS (Figures 4(g)–4(j) and 4(m)). MitoQ pretreatment significantly suppressed the expression of the programmed cell death-related markers MLKL, CASPASE3, and BAX and elevated the expression of BCL2. In addition, TUNEL staining indicated that MitoQ remarkably reversed the NP cell apoptosis caused by MS ($P < 0.01$) (Figures 4(k) and 4(l)).

To determine whether MS has a long-lasting impact on NP cell programmed death, the mRNA/protein levels of apoptosis and necroptosis genes and proteins were measured in the 7-day MS group. The levels of these markers were not significantly different between the 7-day MS group and the 7-day CON group (Figures 4(a)–4(j) and 4(m)). TUNEL staining indicated that there was no significant difference in the level of apoptosis between these two groups (Figures 4(k) and 4(l)).

3.4. Metabolic Dysregulation in NP Tissue after MS. NP tissue from both the MS group and the CON group was harvested for metabolic analysis at 12 hours and 7 days after MS. Compared with the CON group, the MS group exhibited upregulated catabolic gene (MMP1, MMP3, and ADAMTS5) expression levels and downregulated collagen type II alpha 1 (COL2A1) expression levels 12 hours after MS (Figures 5(a)–5(f)). The immunofluorescence staining results further confirmed the above changes (Figures 5(g)–5(j)). MitoQ pretreatment partly alleviated the MS-induced metabolic dysregulation.

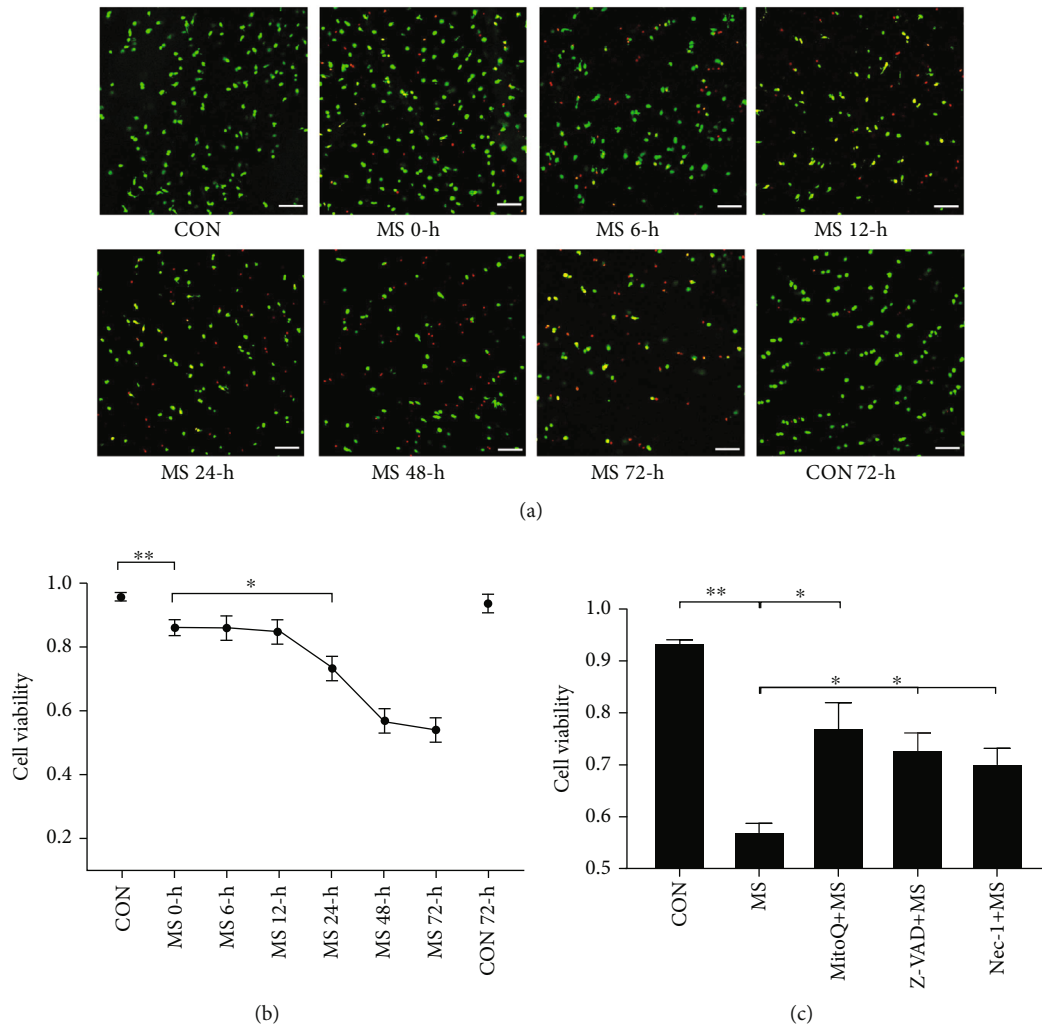


FIGURE 3: The time course of MS-induced NP cell death. (a) Typical confocal images showing the dead cells (red) and viable cells (green) after MS at different time points (0 hours, 6 hours, 12 hours, 24 hours, 48 hours, and 72 hours). Scale bars, 50 μm . (b) Quantification of the ratio of viable cells to total cells in the CON group and the MS group at different time points. (c) Quantification of the ratio of viable cells to total cells in the MitoQ, Nec-1, and Z-VAD pretreatment groups. Values are expressed as the means \pm SEM. $n = 3$, * $P < 0.05$, and ** $P < 0.01$.

To further investigate the extent of metabolic dysregulation, we analyzed cumulative GAG release using the DMMB method. The conditioned medium was collected daily after free-swelling culture. The value measured on day 1 was used as a baseline for normalization. MS significantly increased the cumulative GAG release on day 7. MitoQ pretreatment partially prevented GAG loss (Figure 5(k)).

3.5. Dynamic Compressive Stiffness and Morphology of IVDs. On the first day after MS, the changes in dynamic compressive stiffness did not significantly differ among the CON, MS, and MitoQ+MS groups (Figure 6(c)). Compared with those in the CON group, the IVDs in the MS group exhibited significantly lower stiffness on day 7, but this difference was attenuated by MitoQ (Figure 6(d)). These results indicated that MS reduced the stiffness of IVDs partly through mitochondrial ROS.

We then evaluated the morphology of IVDs by Safranin O/Fast Green and hematoxylin staining. Seven days after MS application, the MS group had significantly higher degenera-

tion scores than the CON group. Moreover, there were no significant differences in degeneration scores between day 4 and day 7 after MS application. In MitoQ-pretreated IVDs, the degeneration scores were significantly reduced (Figures 6(e) and 6(f)).

4. Discussion

MS has been identified as a significant risk factor for the onset and progression of DDD [27]. Numerous reports have suggested that sophisticated molecular cascades are involved in the pathophysiology of MS-induced DDD [29, 30]. In the current study, we attempted to address the interplay between mitochondrial ROS and DDD in an IVD organ culture model by using a custom-made universal mechanical tester. We obtained evidence that multiple modes of cell death are involved in MS-induced NP cell death, with mitochondrial ROS-orchestrated programmed cell death playing a critical role. Our data suggest that mitochondrial ROS are the primary sources of oxidants in IVDs after MS. In addition, we

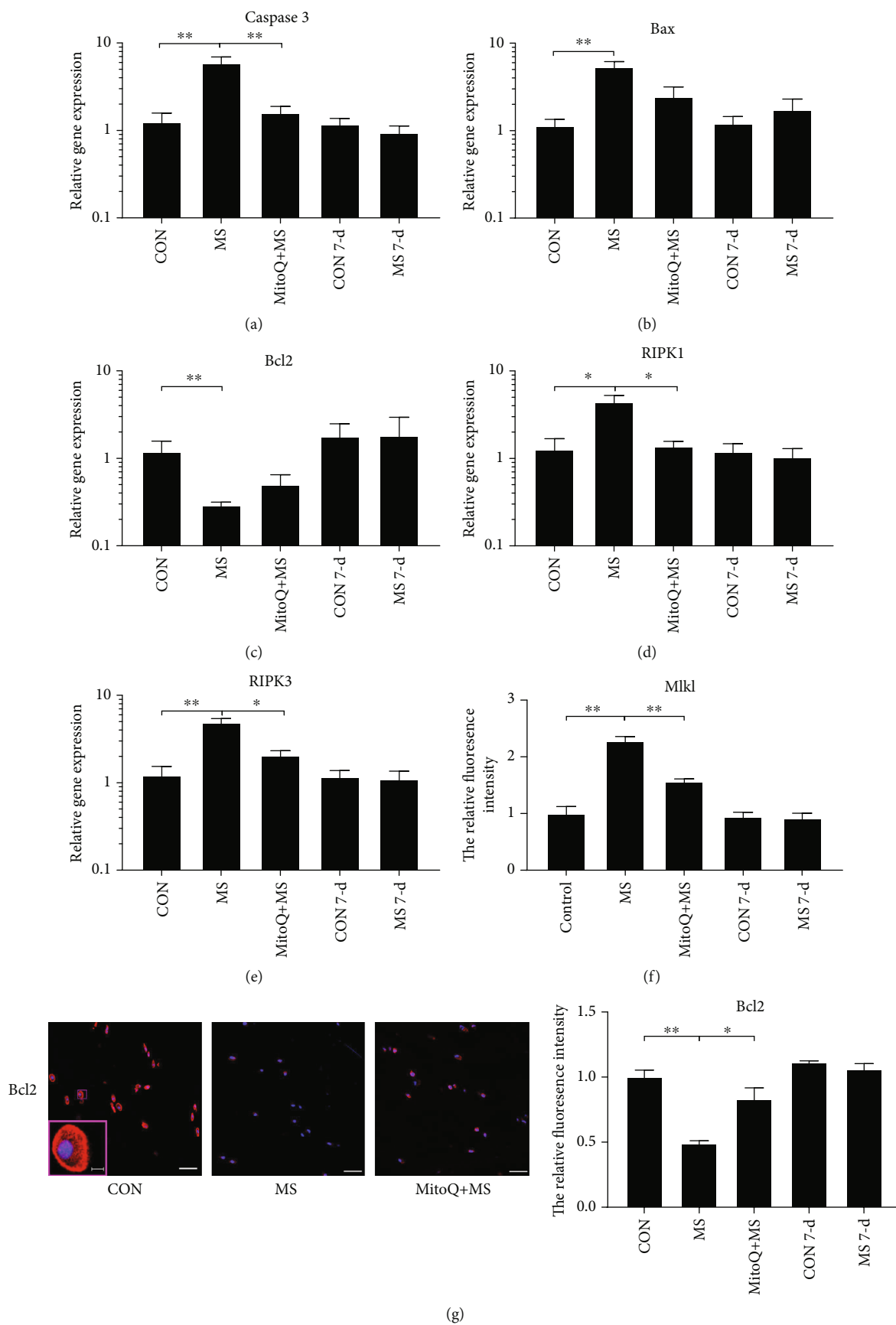
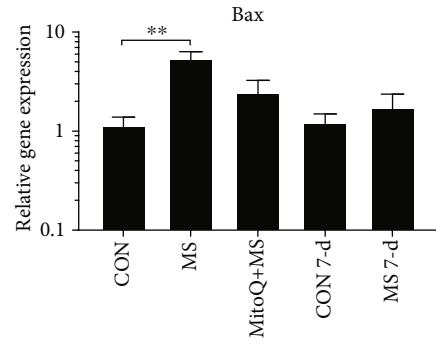
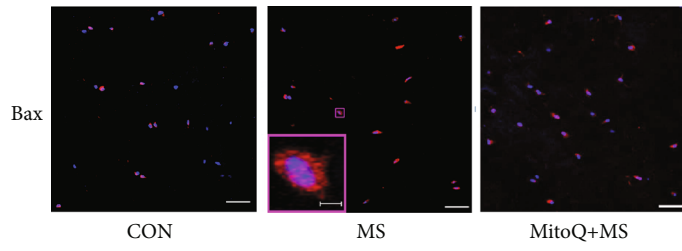
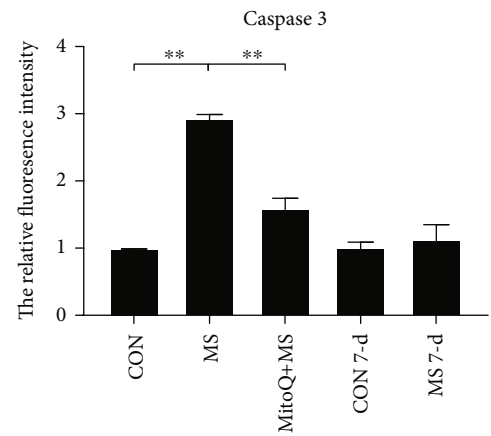
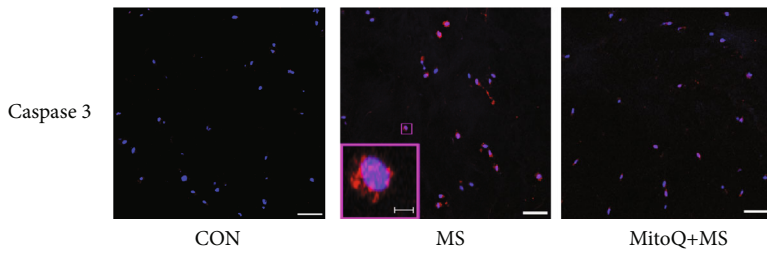


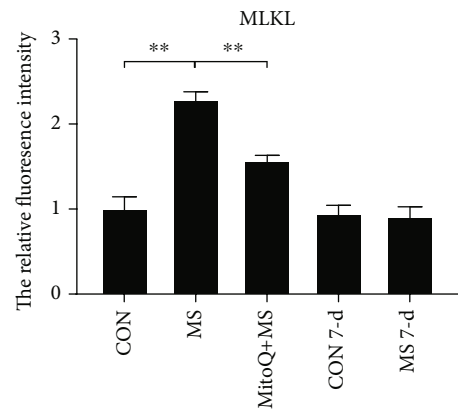
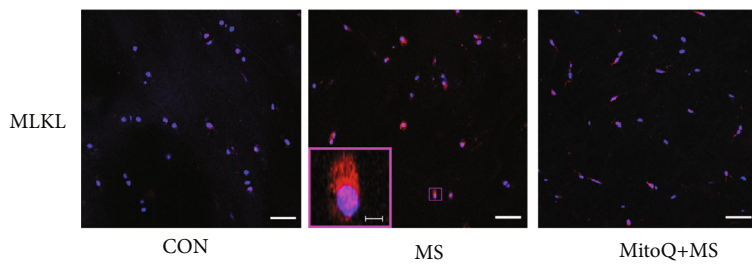
FIGURE 4: Continued.



(h)



(i)



(j)

FIGURE 4: Continued.

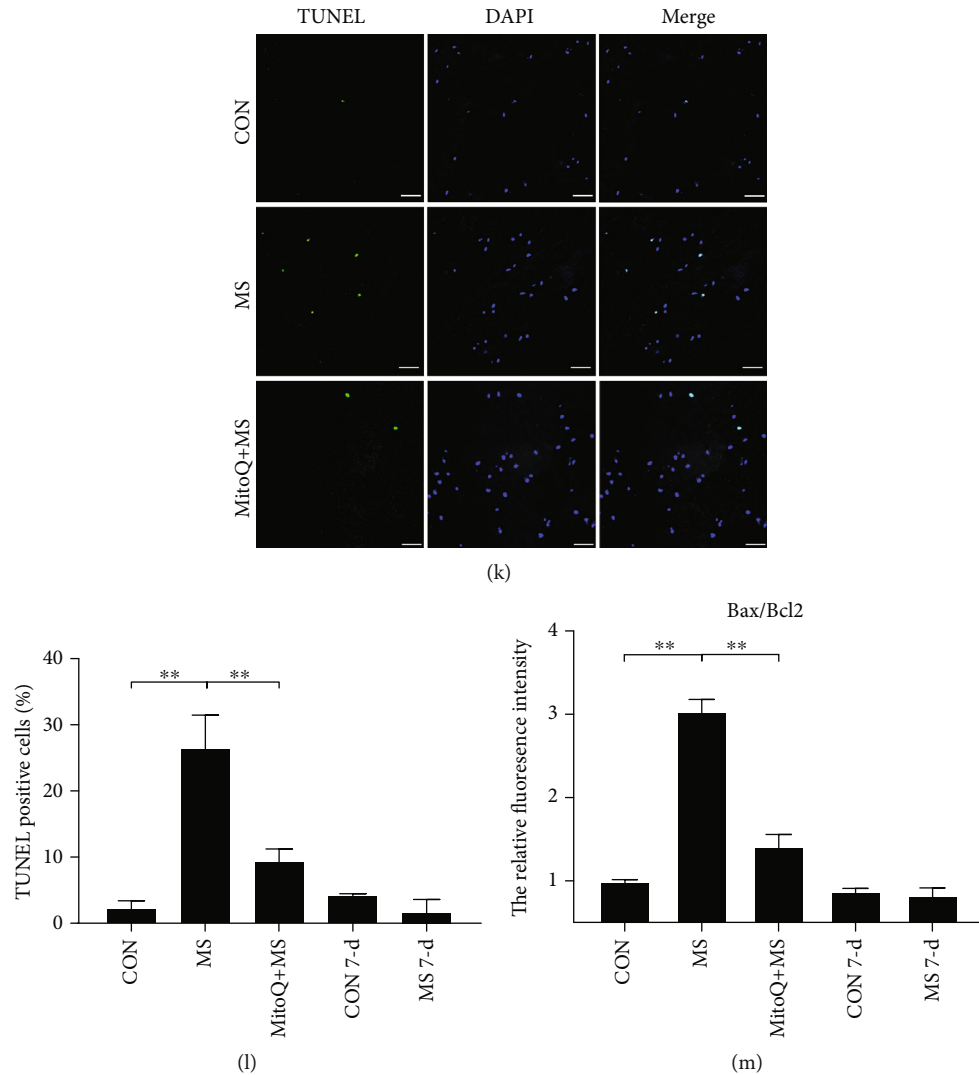


FIGURE 4: MS induced programmed NP cell death via mitochondrial ROS. (a–f) Necroptosis- and apoptosis-related gene expression in NP tissue was examined using RT-qPCR. The gene expression levels in the MS group and the MitoQ+MS group are expressed relative to those in the CON group at 12 hours after MS. The expression levels in the MS 7-day group were similar to those in the CON 7-day group. $n = 3$. (g–j) Necroptosis- and apoptosis-related markers in NP tissue were examined using immunohistochemical staining. Scale bars, 50 μm and 5 μm (inset). $n = 3$. (k, l) Apoptotic NP cells were examined using TUNEL staining, and the percentage of positive cells was quantified. Scale bars, 50 μm . $n = 3$. (m) Quantification analysis of the Bax/Bcl-2 immunohistochemical staining ratio. The data are expressed as the means \pm SEMs. * $P < 0.05$ and ** $P < 0.01$.

found that MS-induced ECM degeneration is mediated, at least in part, by mitochondrial ROS. Furthermore, we found that MS alters metabolic and programmed cell death-related marker expression levels at early time points.

ROS, as pleiotropic pathophysiological signaling agents, are generated from diverse intracellular sources, including cytosolic membrane NADPH oxidase, mitochondrial respiratory complexes, xanthine oxidase, and uncoupled nitric oxide synthase [31]. Accumulating evidence suggests that ROS play a crucial role in the onset and exacerbation of DDD [32]. Although a number of studies have suggested that mitochondrial-derived ROS participate in DDD, no studies have investigated the primary sources of ROS in NP cells after MS. MitoQ is a mitochondrial-targeted ROS scavenger that has been shown in numerous studies to alleviate oxida-

tive damage and decrease mitochondrial ROS levels [33]. We used MitoQ in our research to elucidate the importance of mitochondrial ROS in MS-induced cell death and ECM degradation. We also used rotenone to inhibit mitochondrial respiratory chain complex I. Rotenone pretreatment significantly and immediately inhibited ROS production after MS. In addition, the mitochondrial-targeted antioxidant MitoQ attenuated large-scale MS-induced ROS production. Thus, the data suggested that mitochondrial ROS were the main sources of oxidants in our model system. We also studied the time course of ROS generation. The proportion of ROS-positive cells reached a high level at the earliest observation time point. Long-term follow-up revealed that the proportion of positive cells remained stable from 0 to 12 hours but decreased sharply by 24 hours and reached a relatively low

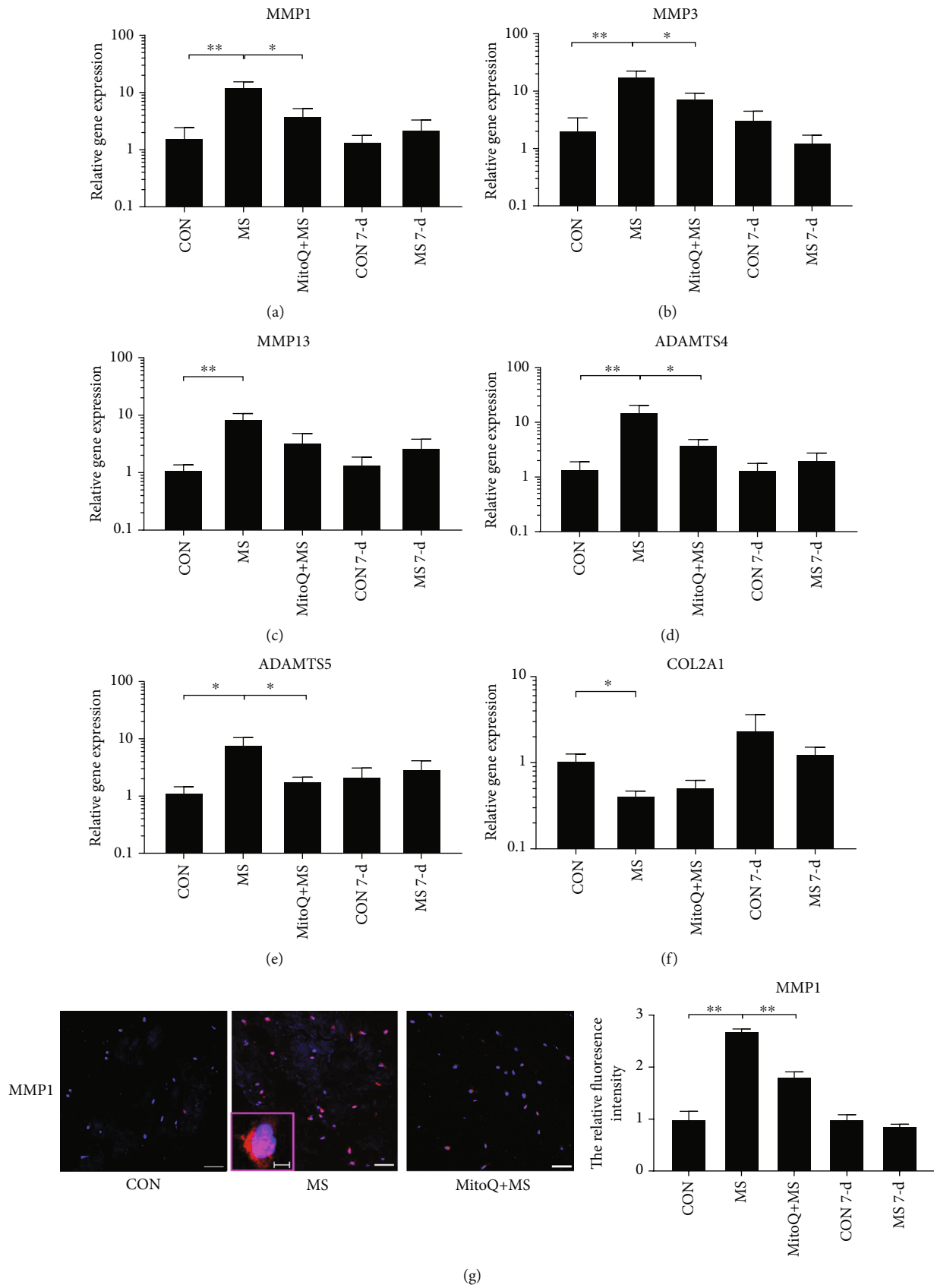


FIGURE 5: Continued.

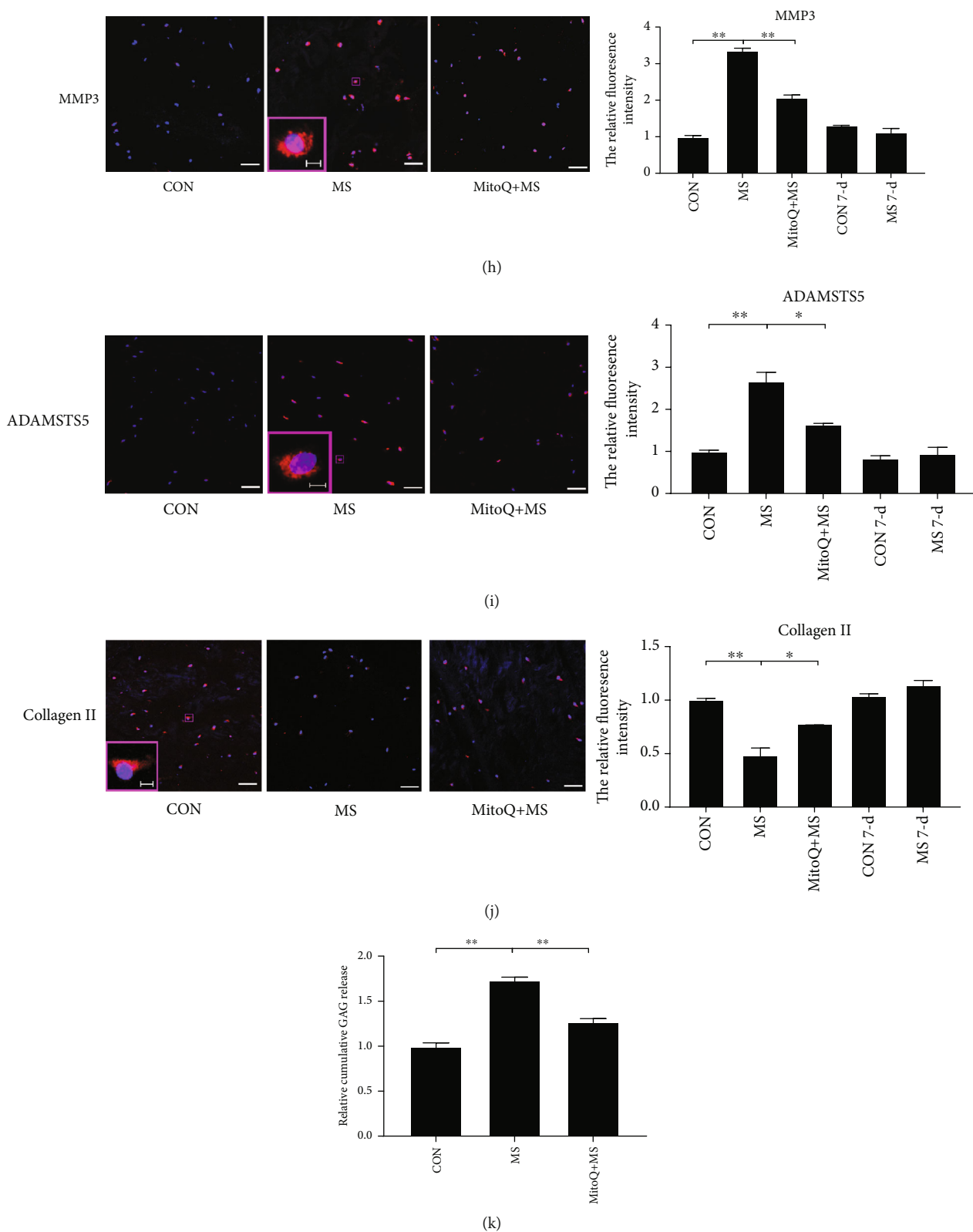


FIGURE 5: Mitochondrial ROS participated in MS-mediated metabolic dysregulation. Gene expression was analyzed by RT-qPCR for (a) MMP1, (b) MMP3, (c) MMP13, (d) ADAMTS4, (e) ADAMTS5, and (f) COL2A1. The gene expression levels in the MS group and the MitoQ+MS group are expressed relative to those in the CON group at 12 hours after MS. The expression levels in the MS 7-day group were similar to those in the CON 7-day group. The data are expressed as the means \pm SEMs. $n = 5$. (g-j) Anabolic-related markers and collagen II in NP tissue were examined using immunohistochemical staining. Scale bars, $50 \mu\text{m}$ and $5 \mu\text{m}$ (inset). $n = 3$. (k) Cumulative release of GAG into a culture medium. $n = 3$. The data are expressed as the means \pm SEMs. $*P < 0.05$ and $**P < 0.01$.

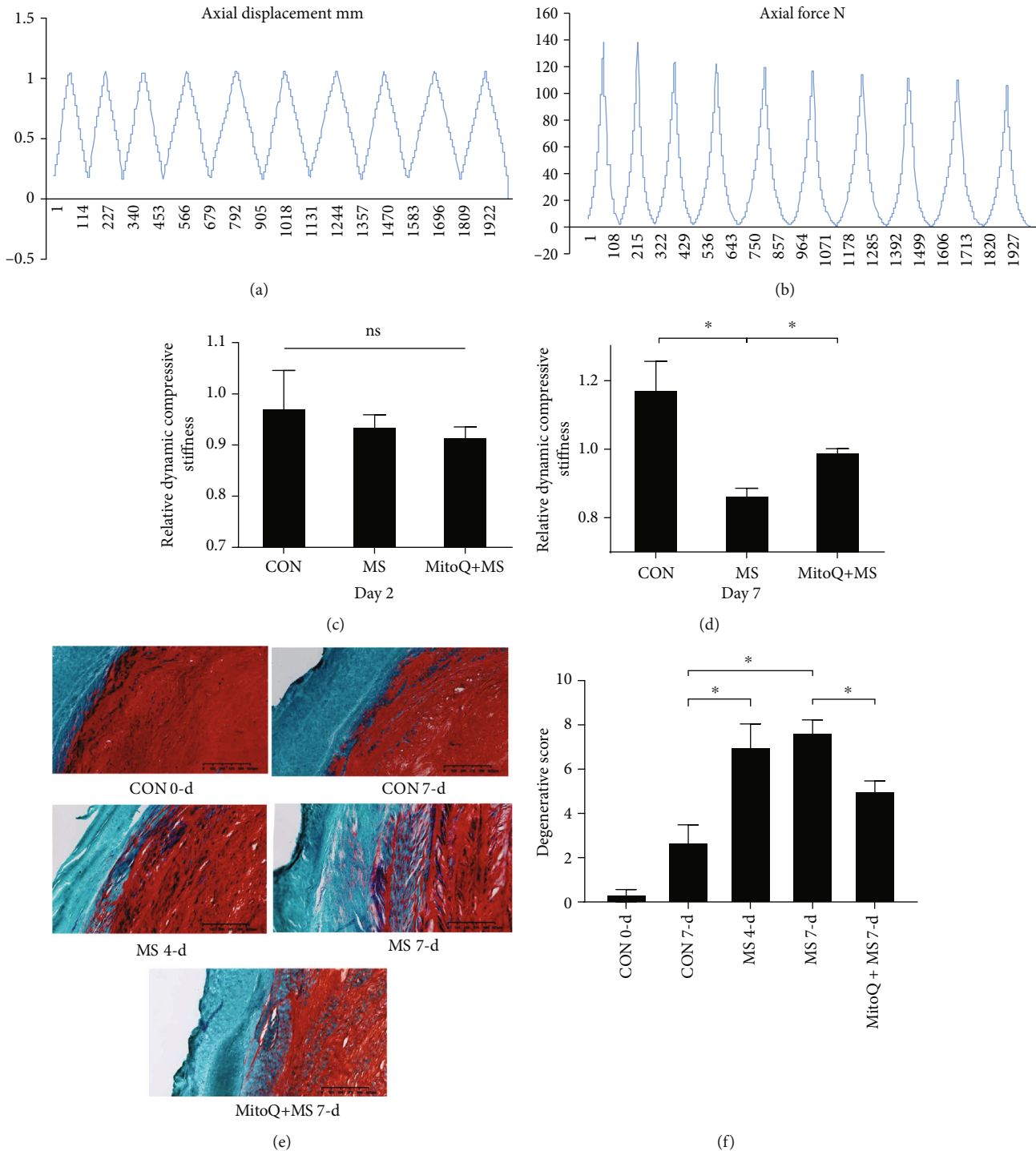


FIGURE 6: Mitochondrial ROS participated in MS-induced IVD dynamic compressive stiffness reduction and morphological degenerative changes. (a) Representative strain curves of the IVDs during stiffness gauging at a single time point. (b) Representative stress curves of the IVDs during stiffness gauging at a single time point. (c, d) Dynamic compressive stiffness measured on day 1 after overnight swelling (the day after dissection), on day 2 after overnight swelling (the day after MS), and on day 7 after overnight swelling recovery. The data were normalized to the levels on day 1 after overnight swelling. (e) The morphology of the IVDs was evaluated by Safranin O/Fast Green staining. Scale bars, 625 μm . (f) Degeneration scores based on Safranin O/Fast Green staining. The data are expressed as the means \pm SEMs. $n = 3$, * $P < 0.05$, and ** $P < 0.01$.

level at 48 hours after MS. These data indicate that ROS-related pathological changes may be limited to the early stage after MS.

In ex vivo studies using bovine IVD whole-organ culture models, MS has been found to reduce NP cell viability [34]. However, the NP cell death mode and time course have

remained largely unknown. Live/dead cell analysis of IVDs revealed that cell viability remained steady during the first 12 hours after MS, except that a few cells were lost immediately after MS, and that subsequent large-scale cell death occurred at 24 hours. The acute cell loss might have resulted from necrotic cell death induced by MS. The later occurrence of large-scale cell death suggested that, in addition to necrosis, programmed cell death was initiated.

In vitro experiments using a variety of cell culture compression apparatuses have shown that MS to NP cells induces apoptosis and necroptosis [15]. However, previous reports have focused mainly on short-term changes in the cell death mode, and there have been no reports about the long-term effects of MS on NP cells. To our knowledge, this is the first study to investigate the changes in programmed death after MS injury at early time points (12 hours) and long-term time points (7 days). In line with previous studies, our study demonstrated that necroptosis and apoptosis occurred in the IVD organ culture model in response to MS at early time points. However, necroptosis- and apoptosis-associated markers returned to normal levels by day 7 after force application. These data demonstrated that the influence of MS on NP cell viability was confined to a relatively short period.

The time course of NP cell death was consistent with the kinetics of mitochondrial ROS in this model, which peaked and then remained stable during the first 12 hours before decreasing to a relatively low level by 48 hours after MS. It is reasonable to suppose that mitochondrial ROS were partly responsible for the induction of necroptosis and apoptosis. In this study, MitoQ pretreatment significantly improved cell viability and partially restored necroptosis- and apoptosis-associated marker levels in the IVD model. Therefore, the results indicated that MS induced apoptosis and necroptosis via mitochondrial ROS in NP cells.

Similar to a number of previous studies, our study revealed that MS increased catabolic gene expression and ECM degeneration [35]. In the present study, using an ex vivo bovine IVD organ culture model, we found that MitoQ pretreatment attenuated the ECM degeneration and reduced catabolic marker expression. Based on the previously reported deleterious effects of ROS on the expression of catabolic markers and ECM integrity, these findings indicate that increased mitochondrial ROS levels are partly responsible for MS-induced degenerative changes in the disc NP region. As a previous study failed to provoke matrix degradation via catabolic molecules in bovine IVDs, further investigation is needed to explore the potential molecular mechanisms responsible for mitochondrial ROS-mediated NP tissue degeneration [36].

There were several limitations of our study. First, the ex vivo IVD organ model used in our study was subjected to acute compressive MS. Whether the research findings can be applied to complex physiological MS needs further investigation. Second, we confirmed that mitochondrial ROS are partly responsible for the induction of programmed NP cell death after MS, but we did not elucidate the precise molecular mechanisms. Third, the mitochondrial ROS elevation discussed in our study may represent only a small

proportion of the mitochondrial dysfunction mechanisms at play. More intricate mechanisms of mitochondrial dysfunction in DDD should be further investigated in future studies.

5. Conclusions

The data demonstrate that ROS induce programmed NP cell death and ECM degradation at early time points after MS. These accumulated ROS are derived mainly from mitochondria. These findings suggest that the use of mitochondrial-targeted antioxidants immediately after MS may be a promising method to prevent the onset or progression of DDD. Our results also provide novel insight into the pathological mechanism of DDD.

Data Availability

The data used to support the findings of this study are available from the corresponding author upon request.

Conflicts of Interest

The authors declare that they have no conflicts of interest.

Authors' Contributions

Bao-Liang Li, Xizhe Liu, and Manman Gao contributed equally to this work and should be regarded as co-first authors.

Acknowledgments

This study was funded by the National Key R&D Program of China (2017YFC1105000), the National Natural Science Foundation of China (81772400, 31900583, and 32071351), the Fundamental Research Funds for the Central Universities (19ykzd05), the Natural Science Foundation of Guangzhou City (201704030082, 201807010031, and 201604046028), the foundation of Shenzhen Committee for Science and Technology Innovation (JCYJ20190809142211354 and GJHZ20180929160004704), the Sanming Project of Medicine in Shenzhen (SZSM201911002), and the Beijing Municipal Health Commission (Grant Nos. BMHC-2019-9, BMHC-2018-4, and PXM2020_026275_000002).

References

- [1] Y. Huo, D. Yang, L. Ma, H. Wang, W. Ding, and S. Yang, "Oblique lumbar interbody fusion with stand-alone cages for the treatment of degenerative lumbar spondylolisthesis: a retrospective study with 1-year follow-up," *Pain Research & Management*, vol. 2020, article 9016219, pp. 1–6, 2020.
- [2] X. Guo, W. Ding, L. Liu, and S. Yang, "Intradiscal methylene blue injection for discogenic low back pain: a meta-analysis," *Pain Practice*, vol. 19, no. 1, pp. 118–129, 2019.
- [3] Medical Advisory S, "Artificial discs for lumbar and cervical degenerative disc disease - update: an evidence-based analysis," *Ontario Health Technology Assessment Series*, vol. 6, no. 10, pp. 1–98, 2006.

- [4] D. S. Schultz, A. G. Rodriguez, P. K. Hansma, and J. C. Lotz, "Mechanical profiling of intervertebral discs," *Journal of Biomechanics*, vol. 42, no. 8, pp. 1154–1157, 2009.
- [5] A. S. Issever, A. Walsh, Y. Lu, A. Burghardt, J. C. Lotz, and S. Majumdar, "Micro-computed tomography evaluation of trabecular bone structure on loaded mice tail vertebrae," *Spine (Phila Pa 1976)*, vol. 28, no. 2, pp. 123–128, 2003.
- [6] X. Bai, X. Guo, F. Zhang, L. Zheng, W. Ding, and S. Yang, "Resveratrol combined with 17 β -Estradiol prevents IL-1 β -induced apoptosis in human nucleus pulposus via the PI3K/AKT/Mtor and PI3K/AKT/GSK-3 β pathway," *Journal of Investigative Surgery*, vol. 34, no. 8, pp. 904–911, 2021.
- [7] H. Lin, L. Zhao, X. Ma et al., "Drp1 mediates compression-induced programmed necrosis of rat nucleus pulposus cells by promoting mitochondrial translocation of p53 and nuclear translocation of AIF," *Biochemical and Biophysical Research Communications*, vol. 487, no. 1, pp. 181–188, 2017.
- [8] Y. Zhang, S. S. Su, S. Zhao et al., "RIP1 autophosphorylation is promoted by mitochondrial ROS and is essential for RIP3 recruitment into necrosome," *Nature Communications*, vol. 8, no. 1, article 14329, 2017.
- [9] E. Sauter, J. A. Buckwalter, T. O. McKinley, and J. A. Martin, "Cytoskeletal dissolution blocks oxidant release and cell death in injured cartilage," *Journal of Orthopaedic Research*, vol. 30, no. 4, pp. 593–598, 2012.
- [10] C. A. Huser and M. E. Davies, "Calcium signaling leads to mitochondrial depolarization in impact-induced chondrocyte death in equine articular cartilage explants," *Arthritis and Rheumatism*, vol. 56, no. 7, pp. 2322–2334, 2007.
- [11] H. Lin, Y. Peng, J. Li et al., "Reactive Oxygen Species Regulate Endoplasmic Reticulum Stress and ER-Mitochondrial Ca²⁺ Crosstalk to Promote Programmed Necrosis of Rat Nucleus Pulposus Cells under Compression," *Oxidative Medicine and Cellular Longevity*, vol. 2021, Article ID 8810698, 20 pages, 2021.
- [12] L. Liu, H. Li, Y. Cui et al., "Calcium channel opening rather than the release of ATP causes the apoptosis of osteoblasts induced by overloaded mechanical stimulation," *Cellular Physiology and Biochemistry*, vol. 42, no. 2, pp. 441–454, 2017.
- [13] W. Goodwin, D. McCabe, E. Sauter et al., "Rotenone prevents impact-induced chondrocyte death," *Journal of Orthopaedic Research*, vol. 28, no. 8, pp. 1057–1063, 2010.
- [14] C. Moerke, F. Bleibaum, U. Kunzendorf, and S. Krautwald, "Combined knockout of RIPK3 and MLKL reveals unexpected outcome in tissue injury and inflammation," *Frontiers in Cell and Development Biology*, vol. 7, p. 19, 2019.
- [15] S. Chen, X. Lv, B. Hu et al., "Critical contribution of RIPK1 mediated mitochondrial dysfunction and oxidative stress to compression-induced rat nucleus pulposus cells necroptosis and apoptosis," *Apoptosis*, vol. 23, no. 5-6, pp. 299–313, 2018.
- [16] L. A. Nasto, A. R. Robinson, K. Ngo et al., "Mitochondrial-derived reactive oxygen species (ROS) play a causal role in aging-related intervertebral disc degeneration," *Journal of Orthopaedic Research*, vol. 31, no. 7, pp. 1150–1157, 2013.
- [17] M. Y. Ansari, N. Ahmad, S. Voleti, S. J. Wase, K. Novak, and T. M. Haqqi, "Mitochondrial dysfunction triggers catabolic response in chondrocytes via ROS mediated activation of JNK/AP1 pathway," *Journal of Cell Science*, vol. 133, no. 22, 2020.
- [18] B. Alkhatib, D. H. Rosenzweig, E. Krock et al., "Acute mechanical injury of the human intervertebral disc: link to degeneration and pain," *European Cells & Materials*, vol. 28, pp. 98–111, 2014.
- [19] S. Dudli, S. J. Ferguson, and D. Haschtman, "Severity and pattern of post-traumatic intervertebral disc degeneration depend on the type of injury," *The Spine Journal*, vol. 14, no. 7, pp. 1256–1264, 2014.
- [20] S. Dudli, D. Haschtman, and S. J. Ferguson, "Persistent degenerative changes in the intervertebral disc after burst fracture in an in vitro model mimicking physiological post-traumatic conditions," *European Spine Journal*, vol. 24, no. 9, pp. 1901–1908, 2015.
- [21] I. Sitte, A. Kathrein, K. Pfaller, F. Pedross, and S. Roberts, "Intervertebral disc cell death in the porcine and human injured cervical spine after trauma: a histological and ultrastructural study," *Spine (Phila Pa 1976)*, vol. 34, no. 2, pp. 131–140, 2009.
- [22] I. Sitte, A. Kathrein, M. Klosterhuber et al., "Morphological similarities after compression trauma of bovine and human intervertebral discs: do disc cells have a chance of surviving?," *Journal of Orthopaedic Research*, vol. 32, no. 9, pp. 1198–1207, 2014.
- [23] S. K. Tschoeke, M. Hellmuth, A. Hostmann et al., "Apoptosis of human intervertebral discs after trauma compares to degenerated discs involving both receptor-mediated and mitochondrial-dependent pathways," *Journal of Orthopaedic Research*, vol. 26, no. 7, pp. 999–1006, 2008.
- [24] Z. Zhou, S. Cui, J. Du et al., "One strike loading organ culture model to investigate the post-traumatic disc degenerative condition," *Journal of Orthopaedic Research*, vol. 26, pp. 141–150, 2021.
- [25] O. Goldmann, I. Sastalla, M. Wos-Oxley, M. Rohde, and E. Medina, "Streptococcus pyogenes induces oncosis in macrophages through the activation of an inflammatory programmed cell death pathway," *Cellular Microbiology*, vol. 11, no. 1, pp. 138–155, 2009.
- [26] S. Caprez, U. Menzel, Z. Li, S. Grad, M. Alini, and M. Peroglio, "Isolation of high-quality RNA from intervertebral disc tissue via pronase predigestion and tissue pulverization," *JOR Spine*, vol. 1, no. 2, article e1017, 2018.
- [27] F. Ding, Z. W. Shao, S. H. Yang, Q. Wu, F. Gao, and L. M. Xiong, "Role of mitochondrial pathway in compression-induced apoptosis of nucleus pulposus cells," *Apoptosis*, vol. 17, no. 6, pp. 579–590, 2012.
- [28] R. Farndale, D. Buttle, and A. Barrett, "Improved quantitation and discrimination of sulphated glycosaminoglycans by use of dimethylmethylene blue," *Biochimica et Biophysica Acta*, vol. 883, no. 2, pp. 173–177, 1986.
- [29] S. Yang, F. Zhang, J. Ma, and W. Ding, "Intervertebral disc ageing and degeneration: the antiapoptotic effect of oestrogen," *Ageing Research Reviews*, vol. 57, p. 100978, 2020.
- [30] W. Wang, Z. Guo, S. Yang, H. Wang, and W. Ding, "Upregulation of miR-199 attenuates TNF- α -induced human nucleus pulposus cell apoptosis by downregulating MAP3K5," *Biochemical and Biophysical Research Communications*, vol. 505, no. 3, pp. 917–924, 2018.
- [31] H. Sies and D. P. Jones, "Reactive oxygen species (ROS) as pleiotropic physiological signalling agents," *Nature Reviews. Molecular Cell Biology*, vol. 21, no. 7, pp. 363–383, 2020.
- [32] K. Li, Y. Li, J. Mi, L. Mao, X. Han, and J. Zhao, "Resveratrol protects against sodium nitroprusside induced nucleus pulposus cell apoptosis by scavenging ROS," *International Journal of Molecular Medicine*, vol. 41, no. 5, pp. 2485–2492, 2018.

- [33] J. Williamson, C. M. Hughes, J. N. Cobley, and G. W. Davison, "The mitochondria-targeted antioxidant MitoQ, attenuates exercise-induced mitochondrial DNA damage," *Redox Biology*, vol. 36, p. 101673, 2020.
- [34] Z. Li, Y. Gehlen, F. Heizmann et al., "Preclinical ex-vivo testing of anti-inflammatory drugs in a bovine intervertebral degenerative disc model," *Frontiers in Bioengineering and Biotechnology*, vol. 8, p. 583, 2020.
- [35] B. A. Walter, C. L. Korecki, D. Purmessur, P. J. Roughley, A. J. Michalek, and J. C. Iatridis, "Complex loading affects intervertebral disc mechanics and biology," *Osteoarthritis and Cartilage*, vol. 19, no. 8, pp. 1011–1018, 2011.
- [36] T. Furtwängler, S. C. Chan, G. Bahrenberg, P. J. Richards, and B. Gantenbein-Ritter, "Assessment of the matrix degenerative effects of MMP-3, ADAMTS-4, and HTRA1, injected into a bovine intervertebral disc organ culture model," *Spine*, vol. 38, no. 22, pp. E1377–E1387, 2013.

Research Article

Glycine-Serine-Threonine Metabolic Axis Delays Intervertebral Disc Degeneration through Antioxidant Effects: An Imaging and Metabonomics Study

Xiaolin Wu ¹, Chang Liu ¹, Shuai Yang ¹, Nana Shen ², Yan Wang ¹, Youfu Zhu ¹, Zhaoyang Guo ¹, Shang-you Yang ³, Dongming Xing ^{4,5}, Houxi Li ⁶, Zhu Guo ¹, Bohua Chen ¹ and Hongfei Xiang ¹

¹Department of Orthopedics, The Affiliated Hospital of Qingdao University, Qingdao, China 266003

²Department of Rehabilitation, The Affiliated Hospital of Qingdao University, Qingdao, China 266000

³School of Medicine-Wichita, University of Kansas, 929 N St. Francis Street, Wichita, KS, USA 67214

⁴Cancer Institute, The Qingdao University, Qingdao, China 266003

⁵School of Life Sciences, Tsinghua University, Beijing, China 100084

⁶Shandong First Medical University, Taian 271016, China

Correspondence should be addressed to Zhu Guo; guozhugz@126.com, Bohua Chen; bhchen@hotmail.com, and Hongfei Xiang; ymdx2004@vip.qq.com

Received 5 February 2021; Accepted 3 August 2021; Published 27 August 2021

Academic Editor: Jan Gebicki

Copyright © 2021 Xiaolin Wu et al. This is an open access article distributed under the Creative Commons Attribution License, which permits unrestricted use, distribution, and reproduction in any medium, provided the original work is properly cited.

Although intervertebral disc degeneration (IDD) can be described as different stages of change through biological methods, this long and complex process cannot be defined in stages by single or simple combination of biological techniques. Under the background of the development of nuclear magnetic resonance (NMR) technology and the emerging metabonomics, we based on animal models and expanded to the study of clinical human degeneration models. The characteristics of different stages of IDD were analyzed by omics. Omics imaging combined with histology, cytology, and proteomics was used for screening of the intervertebral disc (IVD) of research subjects. Furthermore, mass spectrometry nontargeted metabolomics was used to explore profile of metabolites at different stages of the IDD process, to determine differential metabolic pathways and metabolites. NMR spectroscopy was used to qualitatively and quantitatively identify markers of degeneration. NMR was combined with mass spectrometry metabolomics to explore metabolic pathways. Metabolic pathways were determined through protein molecular biology and histocytology of the different groups. Distinguishing advantages of magnetic resonance spectroscopy (MRS) for analysis of metabolites and effective reflection of structural integrity and water molecule metabolism through diffusion tensor imaging (DTI) were further used to verify the macrometabolism profile during degeneration. A corresponding model of *in vitro* metabolomics and *in vivo* omics imaging was established. The findings of this study show that a series of metabolic pathways associated with the glycine-serine-threonine (Gly-Ser-Thr) metabolic axis affects carbohydrate patterns and energy utilization efficiency and ultimately delays disc degeneration through antioxidant effects.

1. Introduction

Lumbar disc degeneration causes lumbar disc herniation, lumbar spinal stenosis, and other lumbar disc degeneration diseases [1]. Degenerative disc disease involves genetic, mechanical, immune, metabolic, and other complex physiological processes [2–4].

The intervertebral disc (IVD) is located between the vertebral bodies. It facilitates in intervertebral motion and distributes compressive load in adjacent vertebral bodies [5]. IVD consists of nucleus pulposus (NP), annulus fibrosus (AF), and endplates (EP) forming a relatively closed organ [6]. It is the largest hypovascular unit in the human body [7] and an immune-exempt organ [8]; therefore, its special

anatomical structure determines the pathophysiological specificity of IVD tissue [9]. The process and mode of degeneration of IVD are different from other tissues and organs. Loss of NP cells through degeneration and necrosis is the main feature of intervertebral disc degeneration (IDD). The extracellular matrix (ECM) component [10] and content of the type II collagen-based ECM secreted show significant changes during degeneration. ECM is the morphological maintenance structure. The live environment of NP cells and its metabolic regulation dominate the degeneration process.

Clinical diagnosis of IDD is mainly based on magnetic resonance imaging (MRI) as the first noninvasive examination. Degree of degeneration is defined by Pfirrmann grading, which is based on T₂WI images [11]. The overall shape and signal strength of the IVD are divided into five types. Clinical treatment of IDD is mostly involved decompression, fusion, and stabilization [12], and currently, there is no effective means to interfere with the degeneration process. The focus of studies on IDD is relatively fragmented, involving only limited proteins and factors, and cannot be used to systematically understand metabolism of related substances and their interaction mechanisms. The discovery of metabolomics in the 21st century [13] enables new understanding of a variety of biological functions. The easy-to-detect and easily identifiable properties of metabolites result in an effective bridge between molecular biology research and macroscopic cell behavior [14–16].

This study used mass spectrometry and nuclear magnetic resonance (NMR) metabolomics to explore metabolic characteristics of each process of IDD to understand the biological characteristics of the IVD. In addition, the findings of this study show the degeneration process from the level of material metabolism. The findings were verified through omics imaging, molecular biology, and histopathology thus establishing a complete metabolic profile. These findings showed the degenerative mechanism of antioxidant attenuation of the IVD.

2. Materials and Methods

2.1. Laboratory Animals and Ethics Statement. 48 healthy Sprague-Dawley (SD) rats were purchased from Shandong Jinan Animal Experiment and Breeding Center. The weight of animals ranged between 557 ± 31.5 g for males and 509 ± 26.3 g for females. Male rats were raised in different cages from female rats. Animals were maintained under suitable temperature and light control conditions (22 ± 2°C, 12 h light-dark cycle) and provided with rodent food and water *ad libitum*. All experimental procedures were approved by the Ethics Committee of Qingdao University (approval number: QDFY-19-012-03) and were implemented in accordance with relevant guidelines and regulations.

2.2. Handling and Grouping of Experimental Animals. Twenty-four 6-month-old healthy SD rats of the same strain were selected and were similar in size and weight. Three consecutive segments of intervertebral space were selected for ultrasound-guided puncture (the segment was Co3-6), with no intervention for grade I IVD, unidirectional puncture

with a fine puncture needle for grade II intervertebral disk, and multidirectional puncture with a thick puncture needle for grade III intervertebral disk. Three weeks later, 3.0T magnetic resonance imaging (MRI) T₂WI sequence and computed tomography (CT) scan confirmed establishment of the model.

2.3. Sources and Processing Methods of Human Samples. Selection criteria for experimental subjects were as follows: participants who presented with degenerative disease or acute injury of the lumbar spine that required IVD ectomy or discectomy and MRI can be performed at the corresponding time node before and after surgery were included in this study. Patients with tumors, infections, malformations, immune diseases, genetic diseases, metabolic diseases, and the young (<16 years) and elderly (>80 years) were excluded from the study. *In vitro* samples were obtained from 16- to 35-year-old patients with acute trauma. In this study, *in vivo* and *in vitro* experiments were performed after obtaining informed consent of patients and their families. All participants met ethical standards.

2.4. Data and Sample Acquisition Method. Image data was obtained by GE®3.0 T for preoperative MRI T₁WI, SAG-FSE-TSE, T₂WI, diffusion tensor imaging (DTI) and magnetic resonance spectroscopy (MRS). The corresponding relationship database of image data was established using patient information. Samples were collected by conventional surgical methods within 24 hours of injury or onset based on the preoperative MRI lesion responsibility segment. Samples were divided into four parts (for mass spectrometry, MRI, histopathology, cell culture, and molecular biology detection) and washed with distilled water. Samples were stored in vacuum packages and stored at low temperature.

2.5. Histopathological and Cellular Experiments. Paraffin-embedded sections: the attached tissue was separated from the spine, and tissues sections were fixed with 4% paraformaldehyde (Dalian Meilun Biological Co., Ltd., China) for 72 h. EDTA (Solarbio, China), NaOH (Shanghai Abel Chemical Company, China), and HCL (Tianjin Damao Reagent Company, China) were used to produce decalcification agent (pH 7.3-7.4) for decalcification. The decalcification agent was changed every week, for 4 weeks. After decalcification, paraffin-embedded sections of decalcified tissue (thickness 3-4 μm) were obtained.

2.5.1. HE Staining. To explore the tissue structure, the paraffin sections were stained using the HE kit (Solarbio). Paraffin sections were deparaffinized with xylene (Dalian Meilun Biological Co., Ltd., China) and washed with gradient ethanol (Dalian Meilun Biological Co., Ltd., China) and then rinsed with distilled water for hydration. Tissue sections were then stained with hematoxylin staining solution, differentiation solution, and eosin staining solution. After staining, gradient ethanol was used for dehydration, and then, tissues were treated with xylene:carbolic acid (3:1) to make them transparent and then sealed with neutral resin. Tissue sections were then observed under a light microscope.

2.5.2. Masson Staining. To explore distribution and content of collagen fibers in tissues, paraffinized sections were stained with the Masson kit (Solarbio). In summary, paraffin sections were deparaffinized with xylene (Dalian Meilun Biological Co., Ltd., China) and stained with Weigert iron hematoxylin. Fluid staining was used for acidic differentiation. Further, tissues were stained with Ponceau-magenta staining solution. Tissue sections were then washed with weak acid working solution and phosphomolybdic acid solution. Tissues were stained with aniline blue staining solution, rinsed with weak acid working solution, and dehydrated with 95% ethanol (Dalian Meilun Biological Co., Ltd., China). Xylene solution was added to make tissues transparent, and tissues were then sealed with neutral resin and observed under a light microscope.

2.5.3. Safranin O-Fast Green Staining. To assess the relative distribution of bone and cartilage in the tissue, paraffinized sections were stained with the Safranin O-Fast Green Kit (Solarbio). Paraffin sections were deparaffinized with xylene (Dalian Meilun Biological Co., Ltd., China). Weigert iron hematoxylin staining solution was then used for staining and acidic differentiation solution for differentiation. Fast green dye solution was used for dip dyeing, and tissues were washed with weak acid working solution. Tissues were dip-stained with Safranin O and dehydrated with gradient ethanol (Dalian Meilun Biological Co., Ltd., China). Xylene was used to make tissues transparent, and the film was mounted with neutral resin. Tissues were then observed under a light microscope.

2.5.4. Immunohistochemistry. Immunohistochemistry was used to evaluate the expression levels of MMP3/TIMP1 in tissues. Paraffin wax slices were baked overnight. Xylene (Dalian Meilun Biological Co., Ltd., China) was used for dewaxing, washed with gradient ethanol (Dalian Meilun Biological Co., Ltd., China), and TBST buffer was used for hydration. 3% hydrogen peroxide solution was added for blocking, and tissue sections were then washed with TBST solution. The slices were washed with TBST solution after antigen retrieval. Tissue slices were placed flat in the wet box, and the tissue boundary indicated with a hydrophobic pen, and then, 3% BSA solution was added. The blocking solution was aspirated, and primary antibody was added (MMP3/TIMP1 antibody purchased from Santa Cruz), and then, the mixture was incubated overnight at 4°C. Sections were warmed to room temperature and washed with TBST solution. Tissue sections were then incubated with secondary antibody at room temperature, and color was developed with diaminobenzidine (DAB) solution, under controlled reaction time. Tissues were then observed under a microscope. Hematoxylin solution was used for dyeing and counterstaining, and then, tissues were alkalized with alkalized water. Tissue sections were dehydrated with gradient ethanol (Dalian Meilun Biological Co., Ltd., China), and xylene was used to make sections transparent. The slide was mounted with neutral resin, and then, tissue sections were observed under a light microscope.

2.5.5. Cell Morphology and Cell Activity. AF and EP were separated from isolated IVD tissues. Primary NP cells were extracted from the NP tissue using the type II collagenase method. Cell culture flask containing NP cells was placed at 37°C, under 5% CO₂ incubator. The flask was taken out on days 1, 3, 5, and 7 for observation of cell morphology. The CCK-8 method was used to quantitatively analyze proliferation activity of NP cells at various levels. Cells were counted and seeded in a 96-well plate. Cells were then incubated in a 5% CO₂ incubator at 37°C, for 4 hours; 10% CCK-8 was added by changing the medium. After addition of CCK-8, cells were incubated for 2 h in the incubator, and the absorbance was determined at 450 nm using a microplate reader.

2.6. Western Blot (WB) Analysis. Western blot was used to detect degenerative factors in IVD samples. In summary, separation gel and concentrated gel were prepared, and samples were loaded according to the measured protein concentration. The application antibody product number information is TIMP1 (bs-0415R), TIMP2 (10396-H01H), TIMP3 (ab159704), MMP1 (bs-4597), MMP9 (sc-13520), MMP13 (310471-T40), MATN3 (ab106388), IL11 (ab76589), Aggrecan (bs-11655R), Collagen II (bs-11929R), and β -actin (bs-0061R). Samples were subjected at constant voltage 80 V electrophoresis. After entry of bromophenol blue dye in the separation gel, the constant voltage was changed to 100 V and electrophoresis was performed until the bromophenol blue dye reached the bottom of the separation gel. After cutting the glue, the membrane was transferred in a transfer box. PVDF membrane was sealed with skimmed milk powder, and primary antibody was added at 4°C overnight. After washing samples in the TBST shaker, secondary antibody was added to samples and incubated for 1 h. Liquid A and liquid B in the ECL kit were used to prepare a luminescent liquid 1:1. The liquid was added to the PVDF membrane and then placed on the Bio-Rad developing instrument for development. Expression of the target protein was observed, and images were obtained for analysis.

2.7. Routine Sequence Scanning and Pfirrmann Classification. A 3.0 T MRI machine (GE®-MR750, USA) was used to perform one-time detection of T₁WI, T₂WI, and other sequences after setting the relevant scanning parameters. Pfirrmann grading of the IVD was determined based on T₂WI.

2.8. DTI Detection Scan and ADC Value and FA Value Analysis. A 3.0 T MRI machine (GE®-MR750, USA) magnetic resonance imager was used to perform DWI imaging. Data were imported into PACS system to determine apparent diffusion coefficient (ADC) and partial anisotropy index (fractional anisotropy (FA)) of region of interest (ROI) related to the intervertebral disc nucleus pulposus.

2.9. NMR In Vivo¹H Spectrum Detection Scan and Data Processing. GE®3.0 T DISCOVERY MR750 was used to obtain the original data and which was then preprocessed with jMRUI_v6.0 beta to obtain MRS fitting spectrum. Peak calibration was performed on the final curve to obtain relevant compound information. Analysis of ¹H spectrum was

mainly the H atom signal distribution of characteristic groups. Distribution of the compound represented by each peak was assigned a compound name based on the identification of synchronous mass spectrometry. The assignment was determined by standard compound NMR spectrum database (https://sdb.sdb.aist.go.jp/sdb/cgi-bin/cre_index.cgi?+lang=eng). The assignment indicated the ^1H spectrum representative peaks of each level of IVD.

2.10. Nontargeted Metabonomics Analysis by High-Resolution Mass Spectrometry (HRMS). Ultrahigh-resolution performance liquid chromatography-Q-HF-X hybrid-high-resolution mass spectrometer detection (UHPLC-Q-HFX-HRMS): samples were washed and dried and then pretreated, extracted, and homogenized with a homogenizer and then sampled for testing. Mass spectrum platform was used for analysis of samples. Total ion chromatogram (TIC) was obtained from the raw data after noise reduction, baseline correction, peak alignment, data binning, peak standardization, and standardization.

Metabolite difference analysis: multivariate statistical analysis was performed using principal component analysis (PCA) and orthogonal partial least squares discriminant analysis (OPLS-DA) to identify labeled metabolites, and heat maps were generated. Permutation test and S-plot scatter plot were used to analyze significance of metabolite differences.

Metabolic pathway analysis and calibration: functional analysis was performed based on the differential metabolites. Related metabolic pathways were identified through enrichment analysis and topological structure. The five-level IVD groups were compared to draw statistical charts.

2.11. Bioinformatics Analysis. The microarray dataset of IDD was retrieved from the NCBI GEO database. Metabolic pathways of differentially expressed proteins were analyzed. Machine learning algorithms were used to further screen and determine the metabolic pathways of IDD. The ssGSEA tool was used to analyze the different subgroups of RNA-seq data. The proportion of each metabolic pathway was determined, and the correlation between metabolic pathways and specific genes was analyzed.

The ssGSEA tool was used to analyze RNA-seq data of different subgroups of patients to infer the relative proportions of 43 metabolic pathways. The “pheatmap” package was used to generate a heat map of metabolic pathways and compare distribution of metabolic pathways between the two groups. The “vioplot” package was used to determine the relative content of metabolic pathways, and the “corrplot” package was used to determine correlation coefficients between metabolic pathways and specific genes. $P < 0.05$ was considered as statistically significant.

2.12. NMR In Vitro ^1H Spectrum Sample Collection and Data Processing. NP tissue was lysed with RIPA and then ground. Tissue sample was resuspended in dichloromethane and methanol and then homogenized. Original data was obtained by computational analysis. Preprocessed data was based on the iconic lactate peak. The spectrum was aligned, and the full spectrum was labeled and integrated to obtain

the full spectrum peak data and peak shape distribution. After identification of the coupling situation of each peak, substance integration quantitative analysis was performed to obtain a compound prediction list.

2.13. Analysis of TOCSY Two-Dimensional NMR Spectra In Vitro. The “two-dimensional correlation spectrum” experiment was used to label the IVD qualitative IVD marker compounds. The original data was processed by Mestrenova 14.0.0 through spectral baseline correction, f_1 , f_2 phase correction, Fourier transform, window function, and zero function adjustment and signal suppression. After processing, the lactic acid (Lac) peak ($f_1 = 1.35$ ppm, $f_2 = 4.16$ ppm) was calibrated and a total correlation spectroscopy (TOCSY) spectrum generated. The newly identified compounds represented by each peak were then identified and assigned.

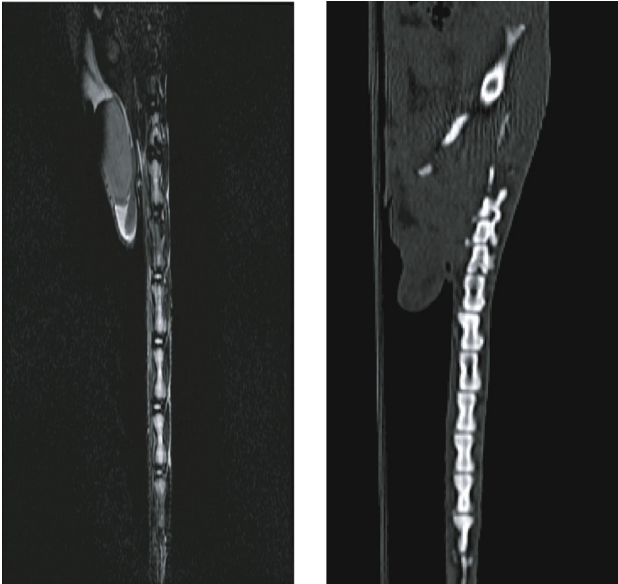
2.14. Statistical Analysis. Data obtained were analyzed based on their respective schemes and methods for intragroup difference statistics and between-group difference statistics. Quantitative data were represented as $X \pm S$ and parametric testing was done using a t -test. Nonparametric was represented as median and interquartile plotting rank sum test was used for nonparametric data. Multigroup analysis of quantitative data was performed using one-way analysis of variance followed by Kruskal-Wallis test. Correlation analysis was performed to compare expression in the different groups. $P < 0.05$ was considered as statistically significant.

3. Results

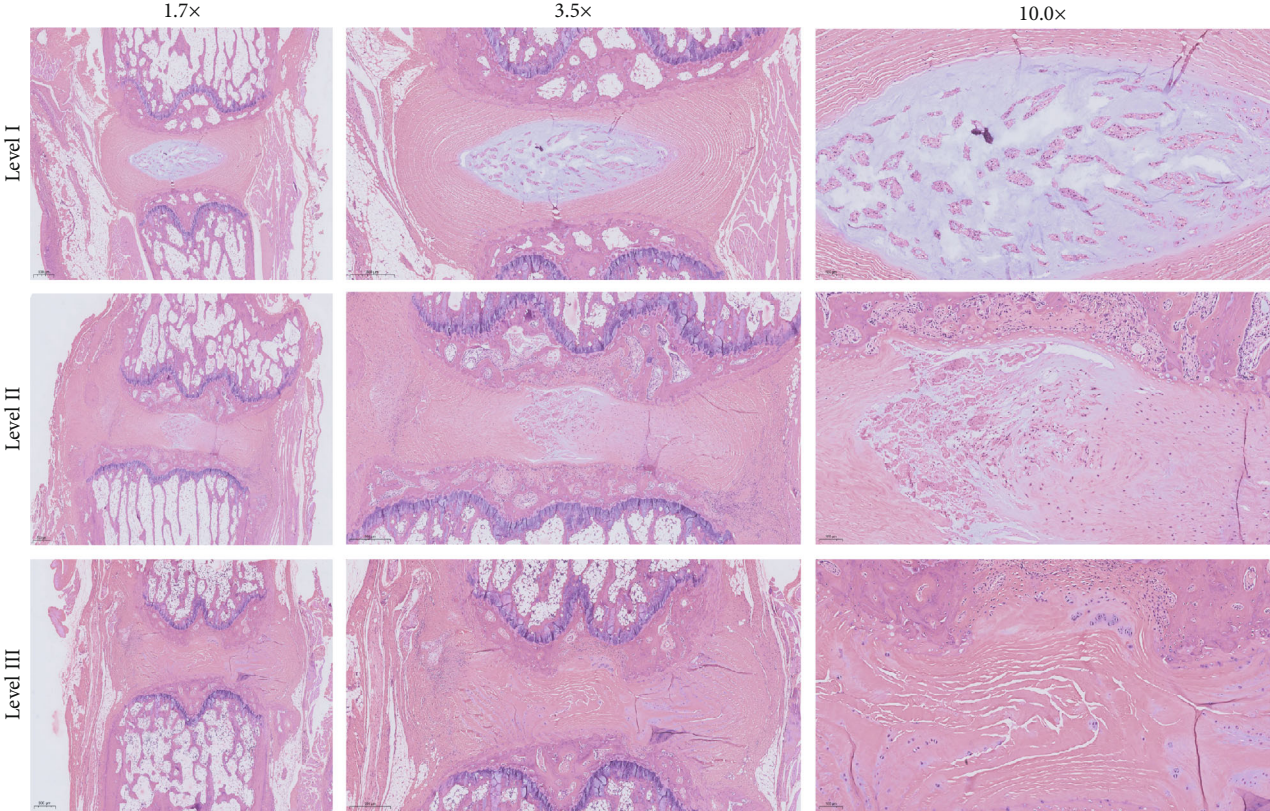
3.1. Establishment of the Rat IDD Model. Crawling posture of rats and the locking structure of the spinal joints hindered formation of the natural degeneration of the IVD. Disc puncture was performed to simulate natural degeneration. The principle was to destroy distribution of NP cells and the normal structure of the IVD. Three weeks after the puncture, MRI $T_2\text{WI}$ imaging showed that the model met the preset imaging conditions. In addition, CT showed significant differences in the height of the intervertebral space between models of different levels (Figure 1(a)).

Histopathological analysis showed significant differences in the macroscopic structure of the NP and AF and the relative microscopic morphology, coloring, and distribution of NP cells in the three-level IVDs in terms (Figure 1(b)). Furthermore, differences in morphology and distribution of collagen fibers and cartilage tissue were observed in the three-level IVDs (Figures 1(c) and 1(d)). Cell morphology and adherent growth state were different in the three-level IVDs. Proliferation activity was quantified by CCK-8 (Figure 1(e)).

Matrix metalloproteinase-1 (MMP-1) stained deeper in the NP-like cell with IDD (Figure 1(f)), and its expression was increased ($F = 884.1$, $P < 0.05$). Tissue inhibitor of metalloproteinase 1 (TIMP1) was light brown in the NP tissue (Figure 1(f)). TIMP1 expression increased with the level of IVDs; however, a decrease in the ratio of TIMP1 expression to MMP1 expression was observed ($F = 264.1$, $P < 0.05$).

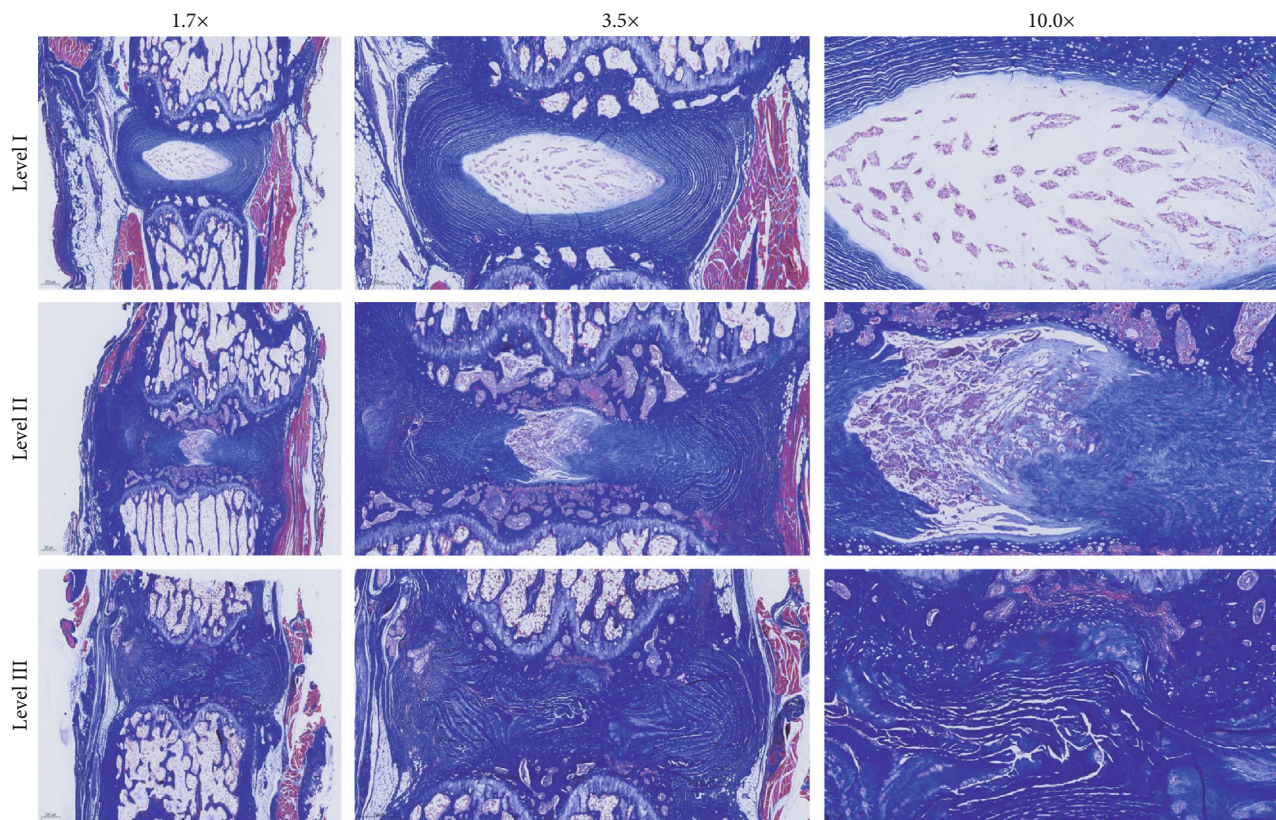


(a)

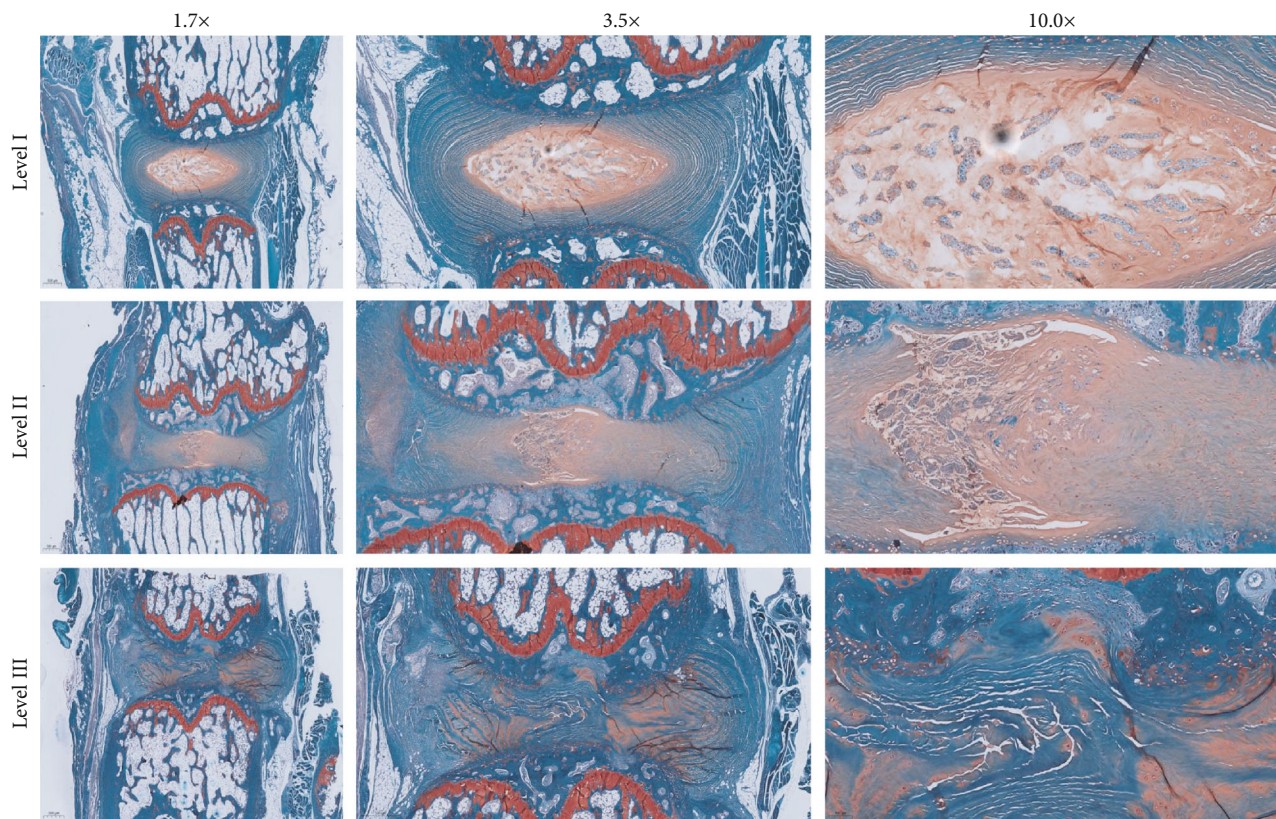


(b)

FIGURE 1: Continued.



(c)



(d)

FIGURE 1: Continued.

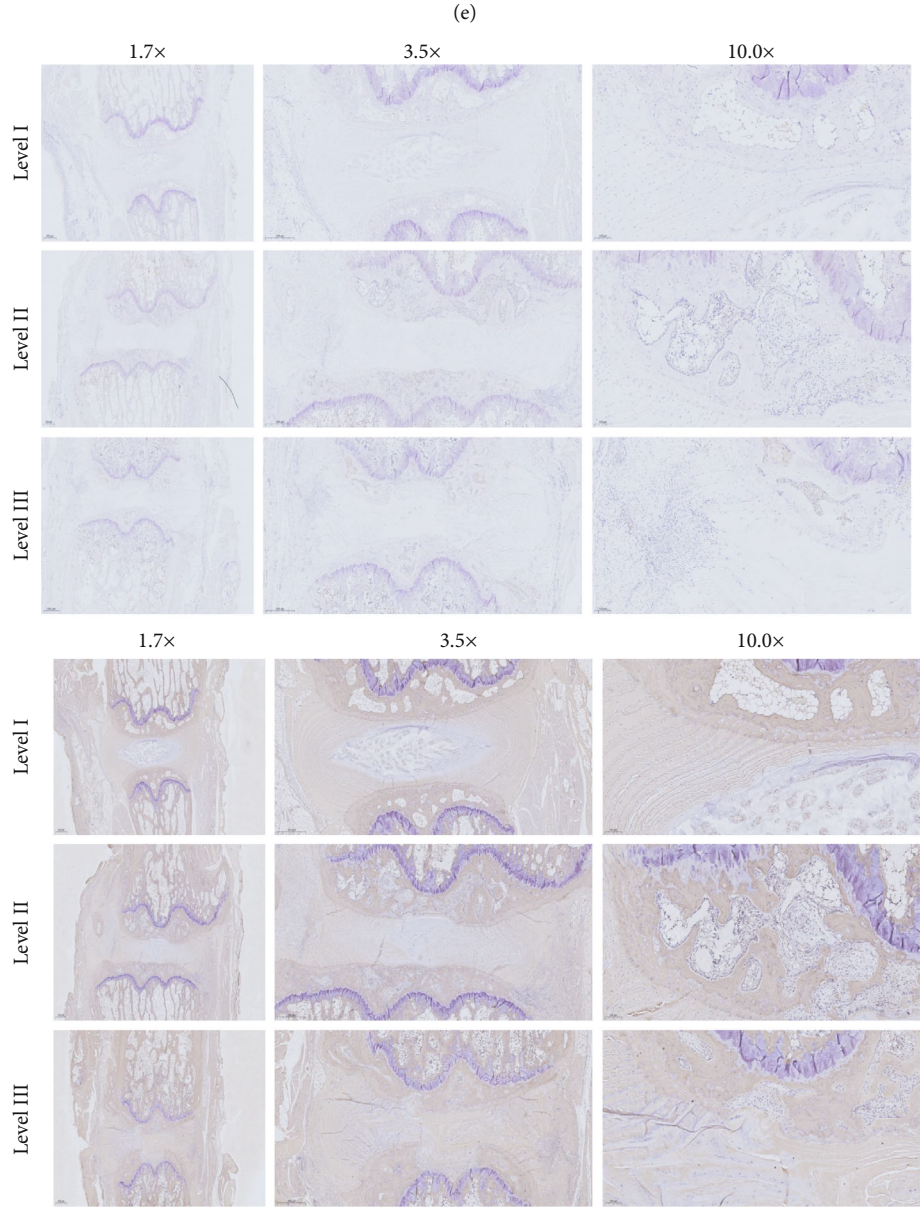
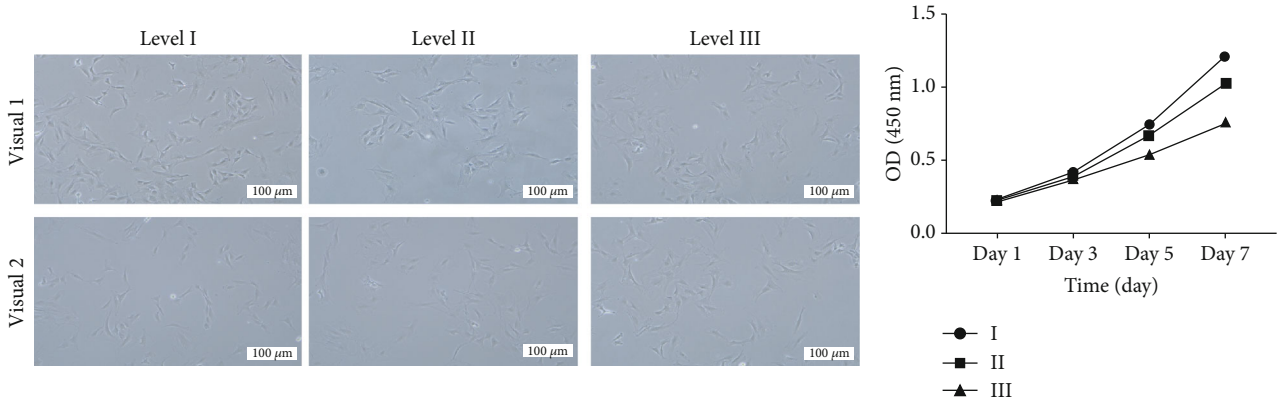
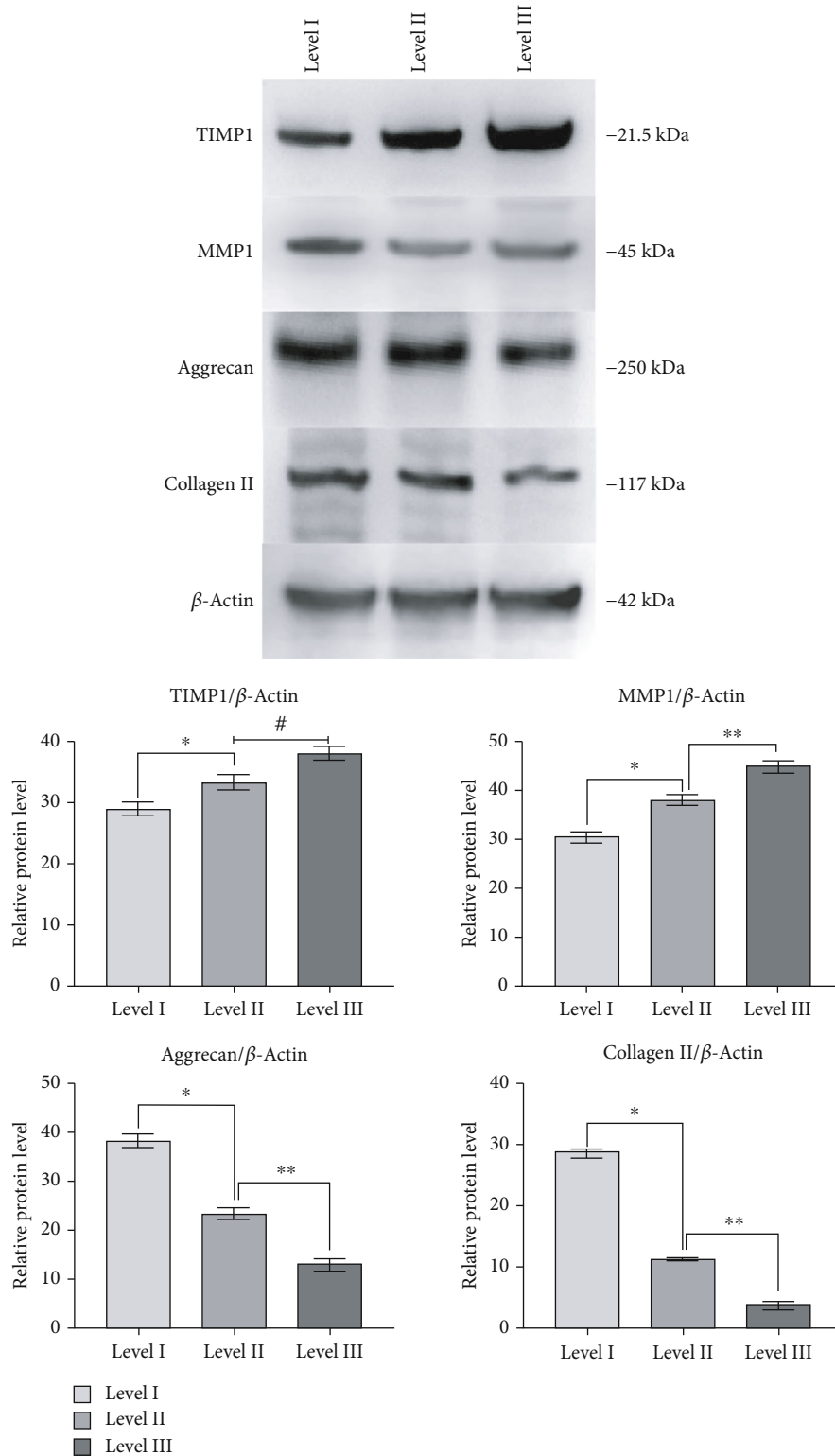
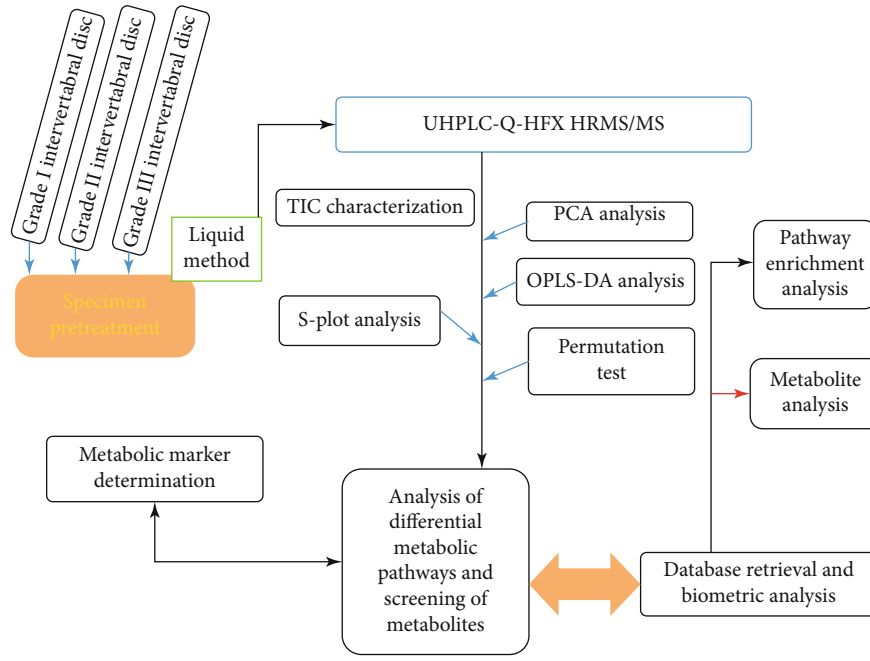


FIGURE 1: Continued.

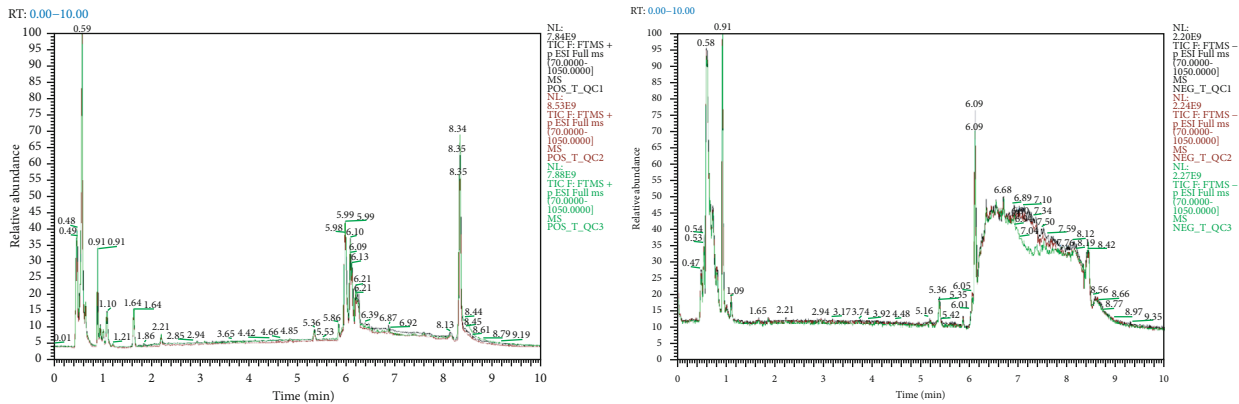


(g)

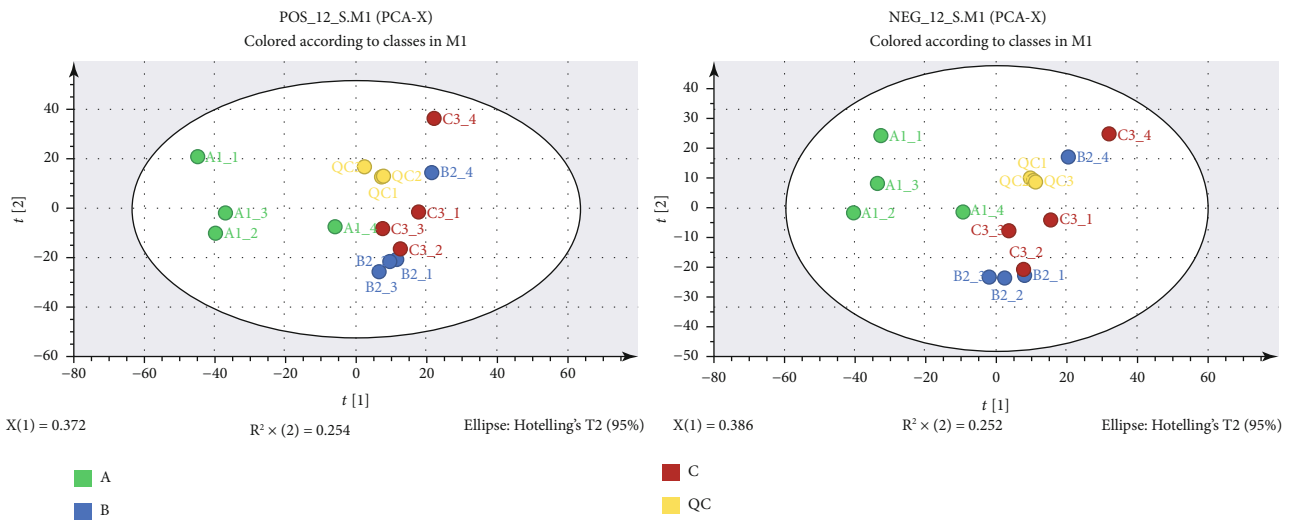
FIGURE 1: (a) MRI T₂WI imaging and CT scan imaging 3 weeks after inducing the puncture. (b) HE staining image of sagittal section. (c) Masson staining image of sagittal section. (d) Safranin O-fast green staining of sagittal section. (e) Light microscope image ① and cell growth line chart ② showing the morphological characteristics. (f) Immunohistochemistry of MMP1 ① and TIMP1 ②. (g) Western blot strip ① and grayscale images ② of TIMP1, MMP1, Aggrecan, and Collagen II.



(a)



(b)



(c)

FIGURE 2: Continued.

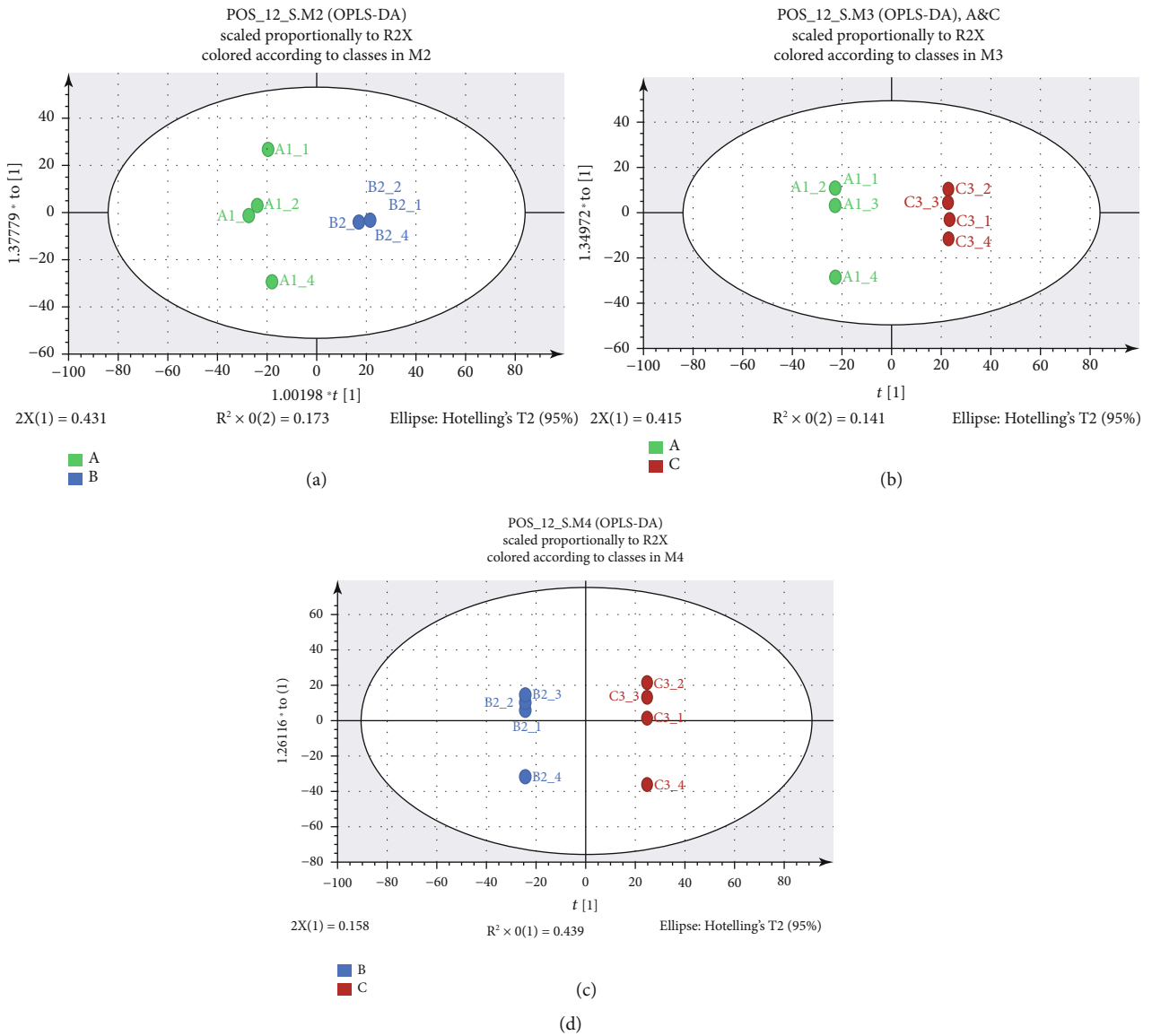


FIGURE 2: Continued.

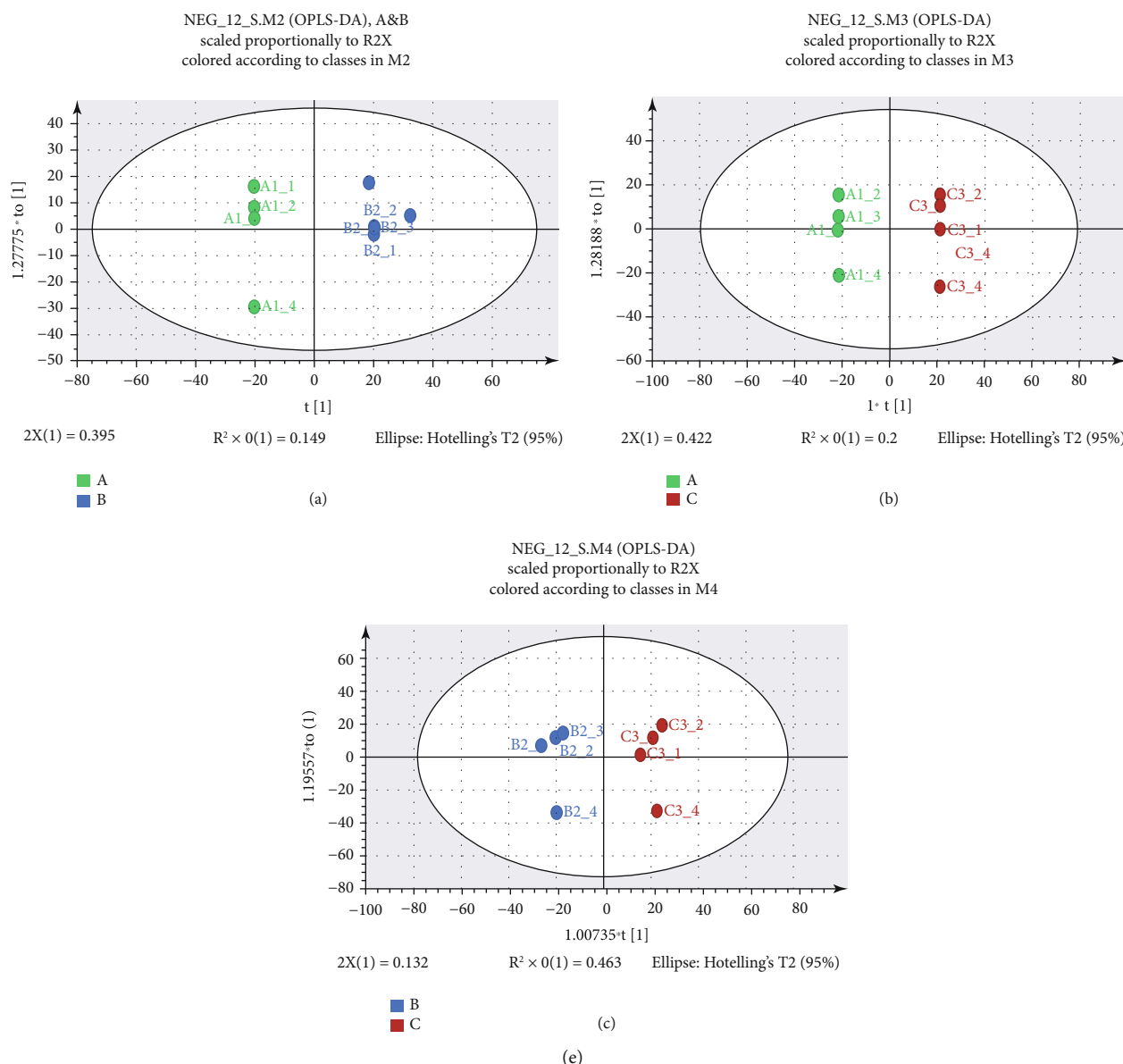


FIGURE 2: (a) Flowchart of metabolomics. (b) Total ion current (TIC) diagram. (c) Principal component analysis (PCA). QC: quality control group. (d) OPLS-DA diagram of each group in cation mode: (A) A/B group comparison, (B) A/C group comparison, and (C) B/C group comparison. (e) OPLS-DA diagram of each group in anion mode: (A) A/B group comparison, (B) A/C group comparison, (C) B/C group comparison.

WB results showed a decrease in the expression of structural characteristic proteins Aggrecan and Collagen II, whereas the expression of TIMP1 and MMP1 proteins related to ECM metabolism was higher (Figure 1(g)). Notably, the expression of MMP1 was higher compared with that of TIMP1.

3.2. Metabolomics of the Rat IDD Model. UHPLC-Q-HFX-HRMS was used to perform mass spectrometry metabolic analysis on rat IVD samples of different levels (Figure 2(a)). The superimposed spectra of the three groups of samples formed an overall picture of metabolites (Figure 2(b)). The total number of peaks in the cation mode of HRMS was 4505. Notably, 313 effective metabolites were identified. The

total number of peaks in the anion mode was 4430, resulting in identification of 226 metabolites (Figures 2(d) and 2(e)).

PCA was used to perform dimensionality reduction processing of data features. Analysis showed that the distribution ranges of groups B and C in PCA anion and cation mode were mostly overlapping, whereas the areas of group B and C were separated from the area of group A (Figure 2(c)). This finding implies that group A had unique independence, whereas groups B and C showed homogeneity in the metabolic data characteristics. OPLS-DA model operation was used to further distinguish the differences between groups to determine the sample attribution thus determining the relationship between disc grading and metabolite expression. OPLS-DA model under the anion

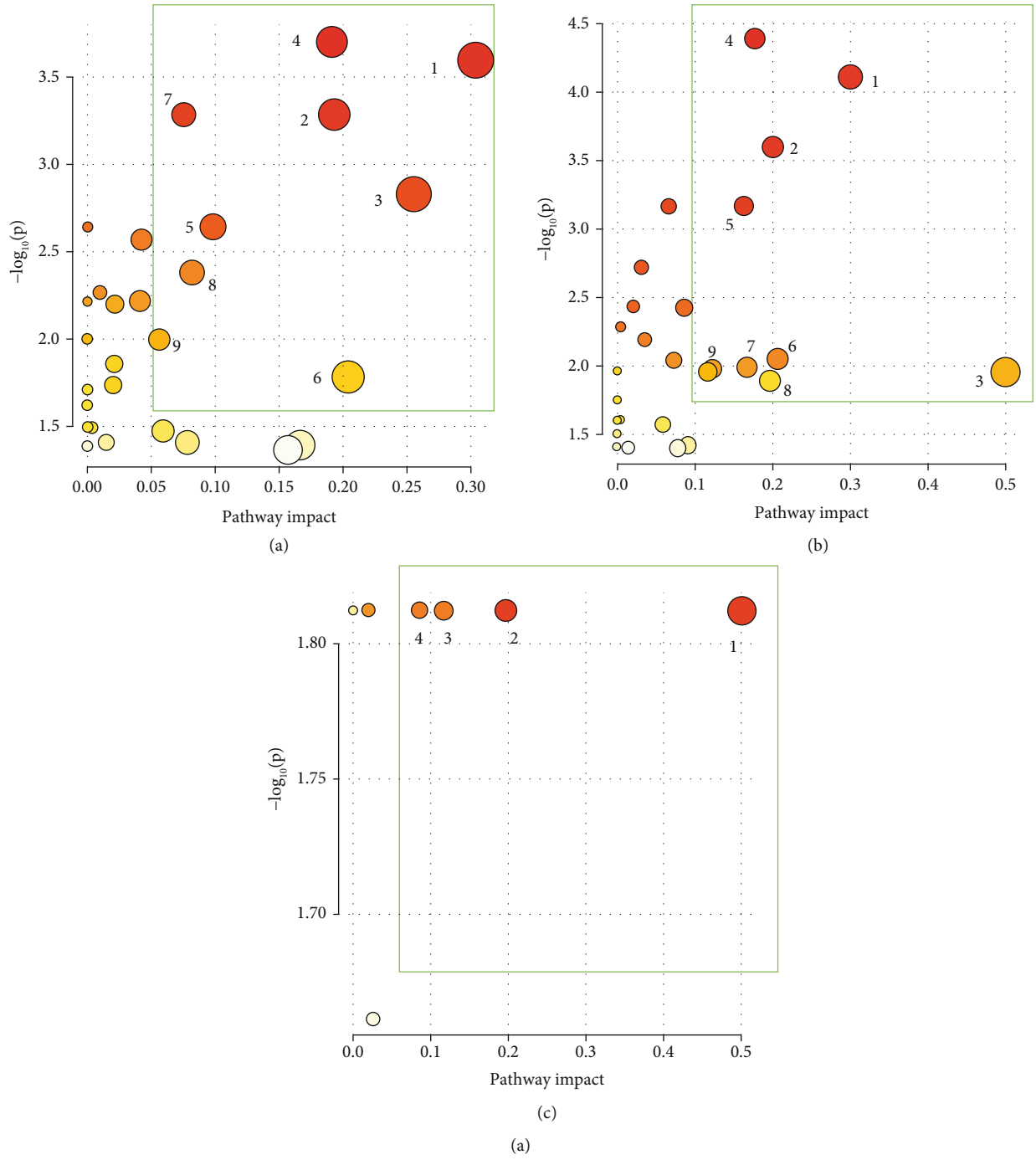


FIGURE 3: Continued.

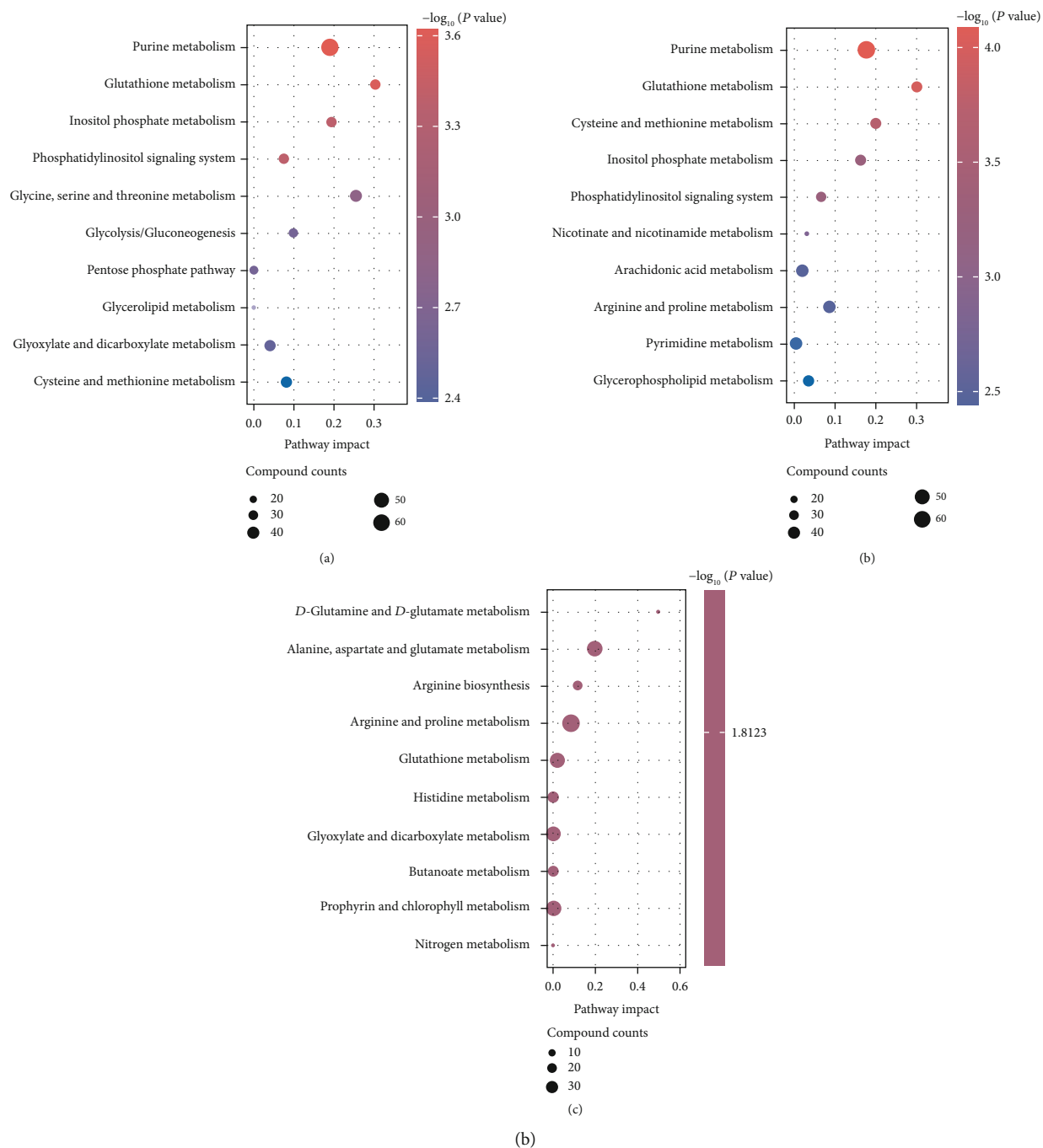


FIGURE 3: Continued.

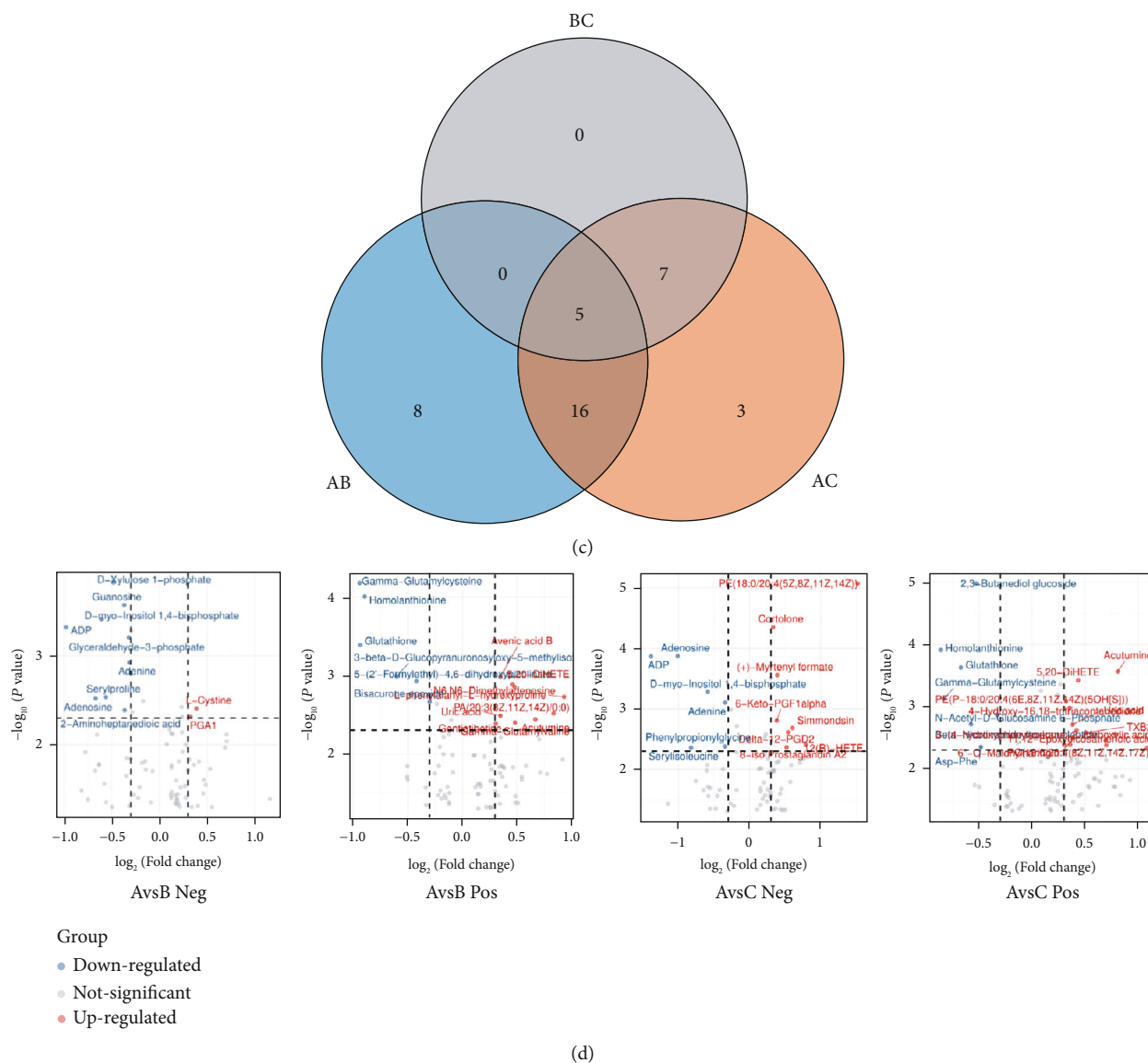


FIGURE 3: (a) Enrichment analysis of metabolic pathways in three groups of samples: (A) A&B group, (B) A&C group, and (C) B&C group. (b) Enrichment analysis of active metabolic pathways of three groups of samples: (A) A&B group, (B) A&C group, and (C) B&C group. (c) Venn diagram showing differences in metabolic pathways of the three groups of samples, A&B group, A&C group.

and cation mode showed differences in the three groups. However, significance of the differences needs further exploration. Permutation test was performed on OPLS-DA pairwise comparison model, and covariance and correlation coefficient of each variable were used to generate an S-plot. Analysis showed no significant difference between groups B and C.

3.3. Metabolic Pathway and Metabolite Analysis. Pathway enrichment analysis was performed using R software. A topological map of the metabolic pathway enrichment network of each comparison group was generated (Figure 3(a)). Metabolic pathways with significant differences were identified (Table 1). Main metabolic pathways before and after degeneration included ① glutathione

metabolism, ② glycine, serine, threonine metabolism, ③ inositol phosphate metabolism, ④ purine metabolism, ⑤ amino sugar and nucleotide sugar metabolism, ⑥ glycolysis/gluconeogenesis, ⑦ cysteine, methionine metabolism, ⑧ pentose phosphate pathway, and ⑨ alanine, aspartic acid, glutamate metabolism. Enrichment analysis of the above metabolic pathways based on the degree of activity (Figure 3(b)) was similar to the enrichment of differential metabolic pathways, implying that the consistency of pathway enrichment models was good. To explore the core degree of each metabolic pathway, a Venn diagram of the metabolic pathways in the early and late stages of IDD was constructed (Figure 3(c)). Analysis showed overlapping of more metabolites between group AB and group AC whereas group BC showed fewer overlapping. Group AB and group

TABLE 1: Differential metabolic pathway table of the three groups of samples.

Comparison group	Metabolic pathway
A group vs. B group	(1) Glutathione metabolism
	(2) Inositol phosphate metabolism
	(3) Glycine, serine, and threonine metabolism
	(4) Purine metabolism
	(5) Glycolysis/gluconeogenesis
	(6) Amino acid and nucleotide sugar metabolism
	(7) Phosphatidylinositol signaling system
	(8) Cysteine and methionine metabolism
	(9) Interconversion of pentose and glucuronic acid
A group vs. C group	(1) Glutathione metabolism
	(2) Cysteine and methionine metabolism
	(3) D-Glutamine and D-glutamate metabolism
	(4) Purine metabolism
	(5) Inositol phosphate metabolism
	(6) Glycine, serine, and threonine metabolism
	(7) Aminoacyl tRNA biosynthesis
	(8) Amino acid and nucleotide sugar metabolism
	(9) Alanine, aspartic acid, and glutamate metabolism
B group vs. C group	(1) D-Glutamine and D-glutamate metabolism
	(2) Alanine, aspartic acid, and glutamate metabolism
	(3) Arginine biosynthesis
	(4) Arginine and proline metabolism

AC were used to construct a volcano plot based on the degree of contribution (VIP) and metabolite analysis reliability (P value) (Figure 3(d)). The fold change was set at >2 times, P value < 0.05 to filter out differences in expressed metabolites. A total of 15 different metabolites were identified between group A and group B, which are implicated in 6 main metabolic pathways. A total of 19 different metabolites were identified between group A and group C, which are implicated in 6 main metabolic pathways.

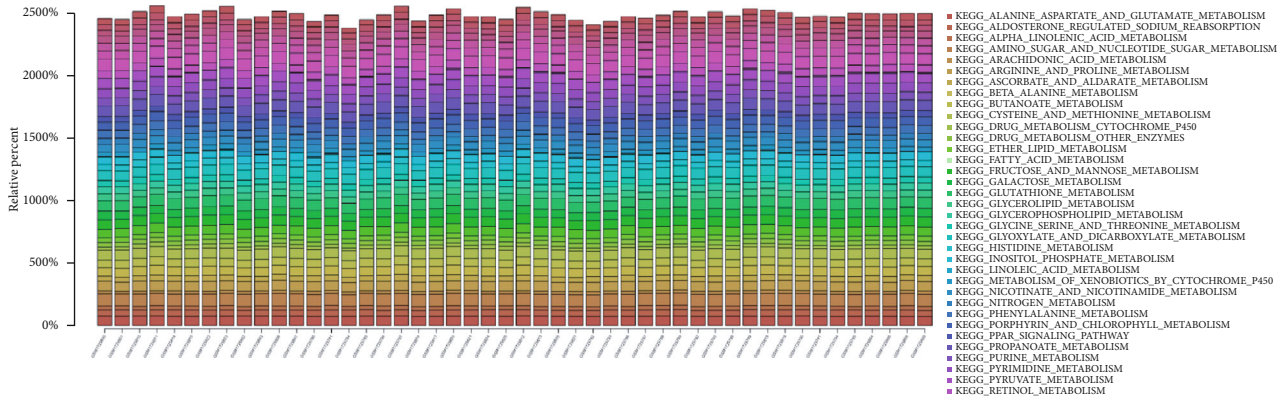
3.4. Biological Information Database Comparison. A total of 43 metabolic pathway subgroups in the 48 human samples of the GSE70362 dataset were retrieved from the NCBI GEO bioinformatics database. The expression of the 43 metabolic pathways was analyzed and summarized (Figure 4(a)). Functional enrichment analysis was used to compare the 43 differentially expressed metabolic pathways. A heat map was generated to show the expression of 43 metabolic pathways (Figure 4(b)). Analysis showed that the expressions of human and rat IVD material metabolism pathways were similar, and the metabolism mode was similar. The “corrplot” package was used to analyze the correlation coefficients of metabolic pathways and specific genes. Metabolites in each pathway were analyzed, and the core factors with significant differences were identified as the

significant factors of the pathway (Figure 4(c)). Gene Ontology (GO) function enrichment analysis was performed to explore the functions of metabolites in terms of the three biological characteristics of biological pathways: biological process (BP), cellular component (CC), and molecular function (MF) positioning and cellular processes. Analysis showed significant changes in the ratio of biological process including collagen catabolism, ECM synthesis, ECM decomposition, and collagen metabolism (Figure 4(d)). Analysis of the contribution degree of each path showed that the decomposition of collagen and ECM was the main source of the difference in IDD. This finding implies that cell function of ECM collagen and matrix membrane was mainly affected.

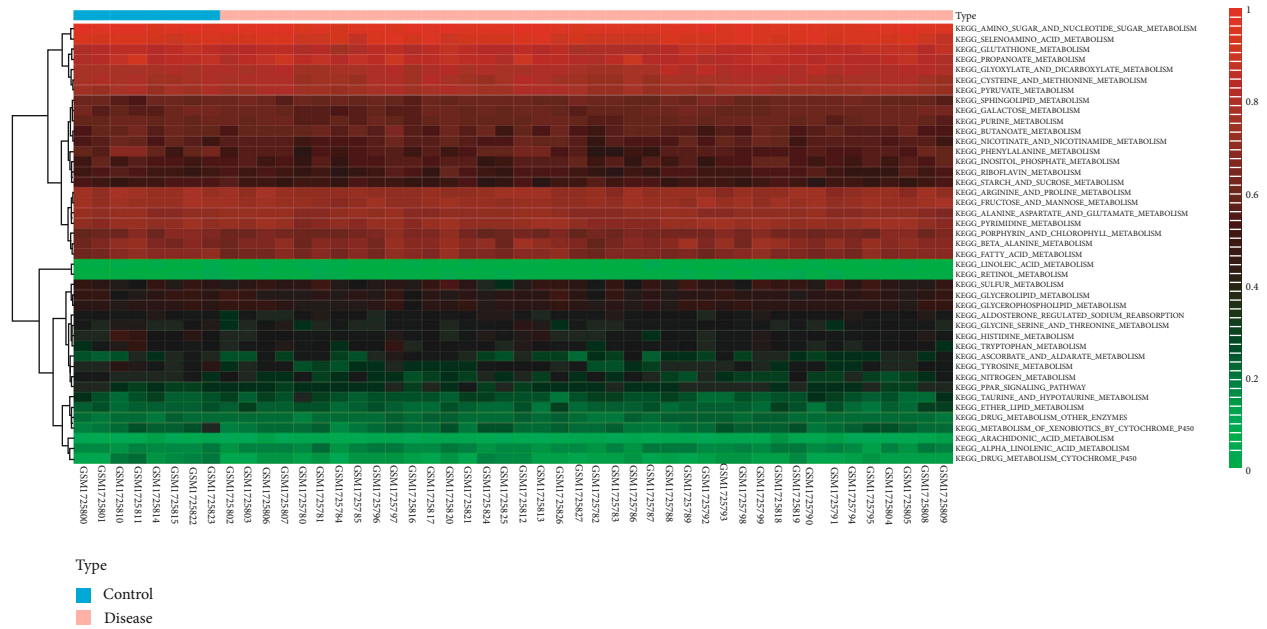
3.5. Mass Spectrometry Analysis of Human Samples. IVD of patients was analyzed by mass spectrometry metabolomics (Figure 5(a)). IVD was divided into five grades based on Pfirrmann classification. Information of isolated tissues that were screened and submitted is shown presented in Table 2. The TIC of substances obtained from analysis of the IVD samples of each level is shown in Figure 5(b). PCA showed that the samples of groups A and B were relatively close, and those of group C and group D were relatively similar (Figure 5(c)). Analysis using OPLS-DA model, permutation test, and S-plot load diagram showed that the five levels of human IVD can be divided into three metabolic stages.

Metabolic pathway enrichment analysis showed significant differences in metabolic pathways in the A-E group (Figure 5(d)). Notably, 11 types of amino acid metabolism pathways accounted for 36.7%, and 6 types of sugar metabolism pathways accounted for 20% of the total pathways. These findings show that amino acid and sugar metabolism were dominant. Furthermore, the most important common differential metabolic pathways between groups A and B and groups C and D included ① amino acid metabolism pathways: metabolism of glycine, serine, and threonine, metabolism of cysteine and methionine, acid biosynthesis, metabolism of arginine and proline; ② carbohydrate metabolism pathway: glycolysis/gluconeogenesis, galactose metabolism; and ③ small molecule, lipid metabolism pathway: taurine and hypotaurine metabolism, pyruvate metabolism, and inositol phosphate metabolism (Figure 5(e)). Further, the most important common differential metabolic pathways between groups C, D, and E included ① amino acid metabolism pathway: arginine and proline metabolism, glycine, serine, and threonine metabolism; ② sugar metabolism pathway: fructose and mannose metabolism; ③ small molecule and lipid metabolism pathway: inositol phosphate metabolism; and ④ nucleotide metabolism pathway: pyrimidine metabolism, purine metabolism, amino sugar, and nucleotide sugar metabolism.

Analysis of degeneration-related factors of these key pathways showed that metabolism of glycine-serine and threonine (MMP13, MATN3, TIMP2, and TIMP3) after the degeneration decreased expression of related molecules compared with the levels before degeneration (Figure 5(f)). In addition, metabolism in the late degeneration axis expression was significantly low. Analysis of galactose metabolism (ADAMTS1, TIMP1, MMP7, and MMP9) showed that ADAMTS1 reached

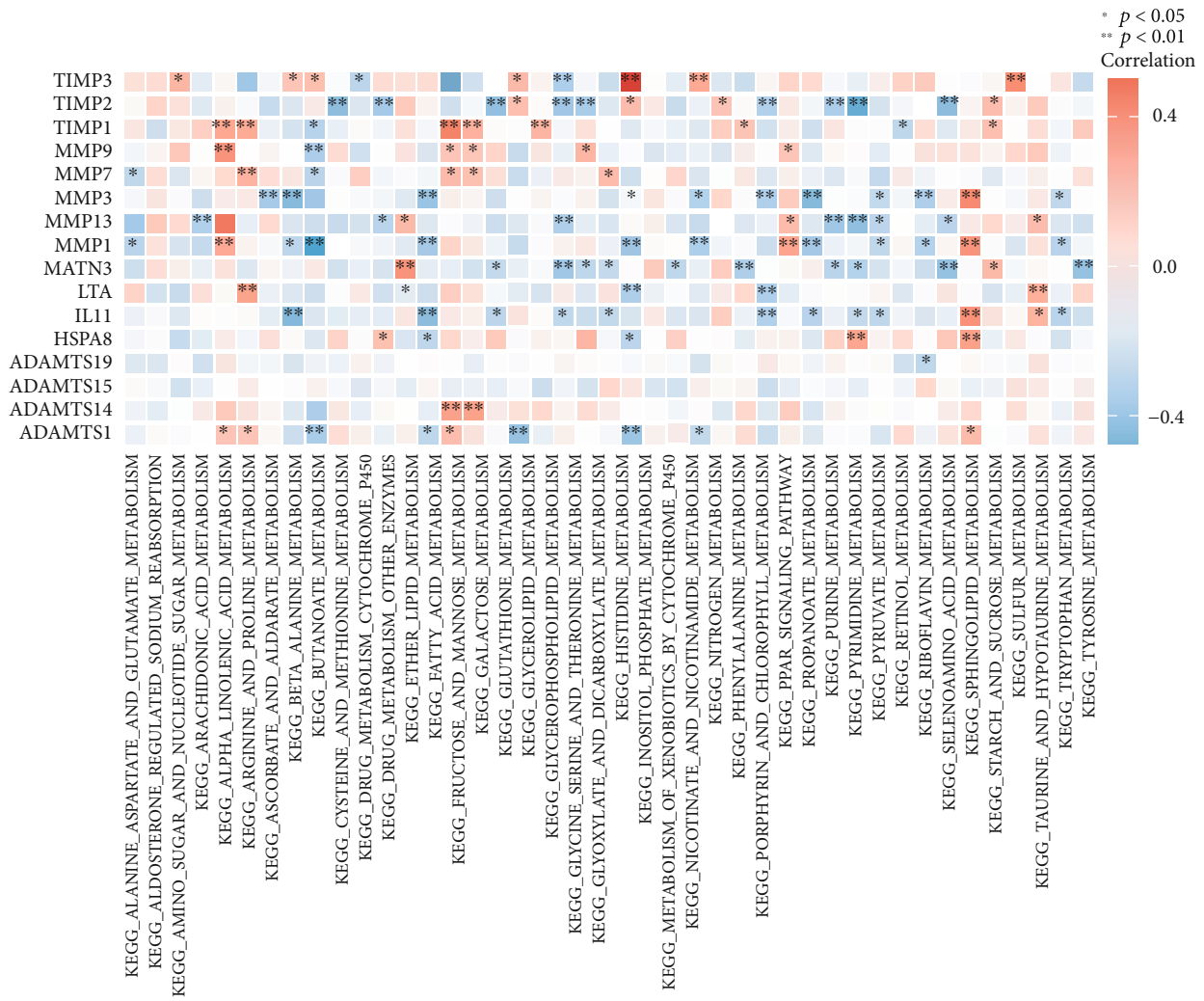


(a)

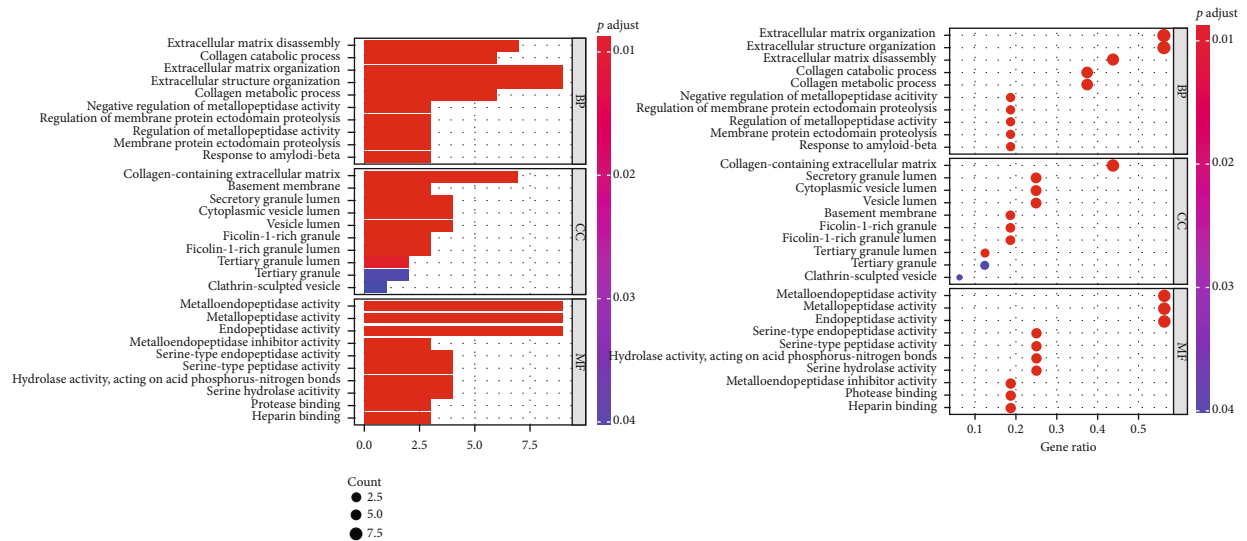


(b)

FIGURE 4: Continued.

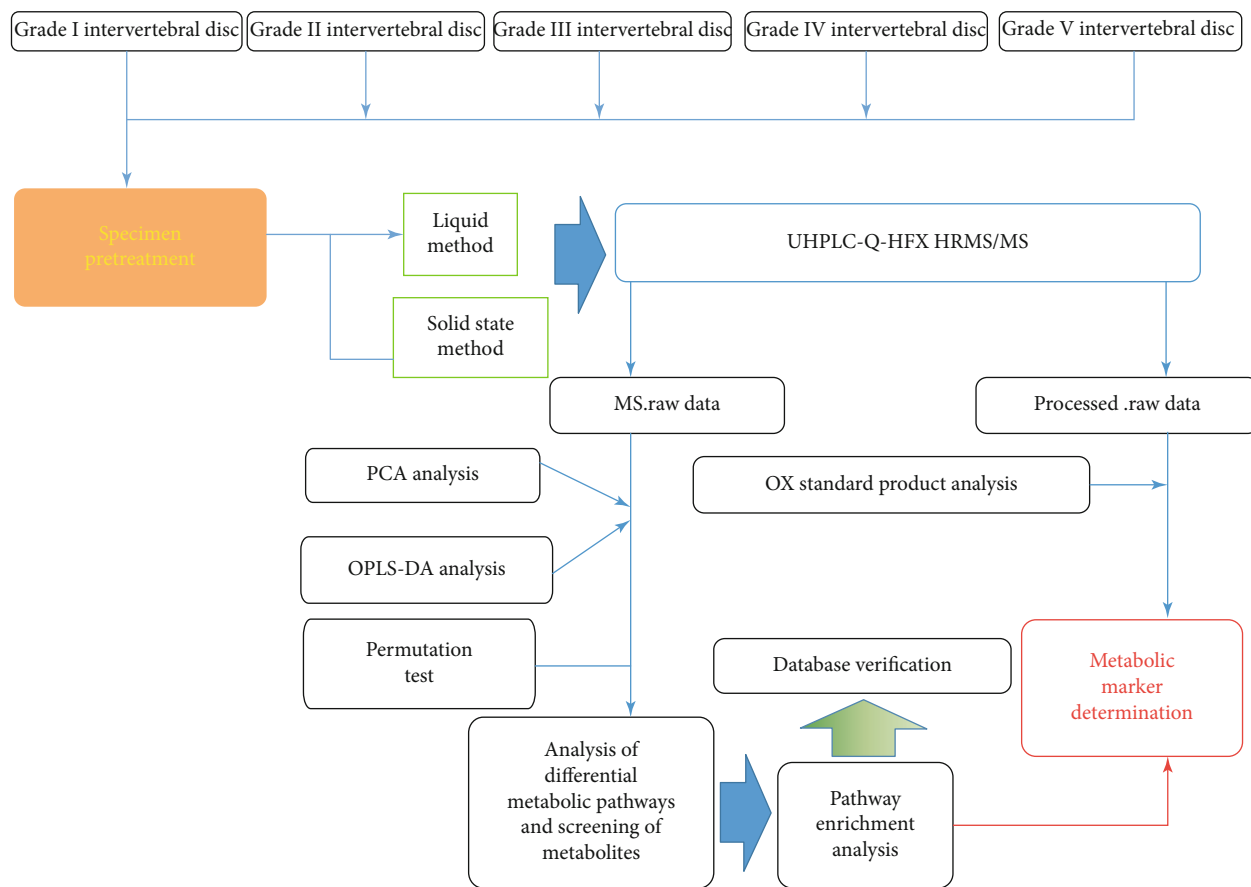


(c)



(d)

FIGURE 4: (a) Relative percentages of 43 metabolic pathway subgroups in 48 human samples. (b) Heat map of the expression of metabolic pathways differentially expressed in human IDD. (c) Heat map of the correlation between core genes and metabolic pathways, red color shows positive correlation and blue color shows negative correlation; * $P < 0.05$ and ** $P < 0.01$. (d) GO enrichment analysis bar scale chart, GO enrichment analysis load bubble chart.



(a)

FIGURE 5: Continued.

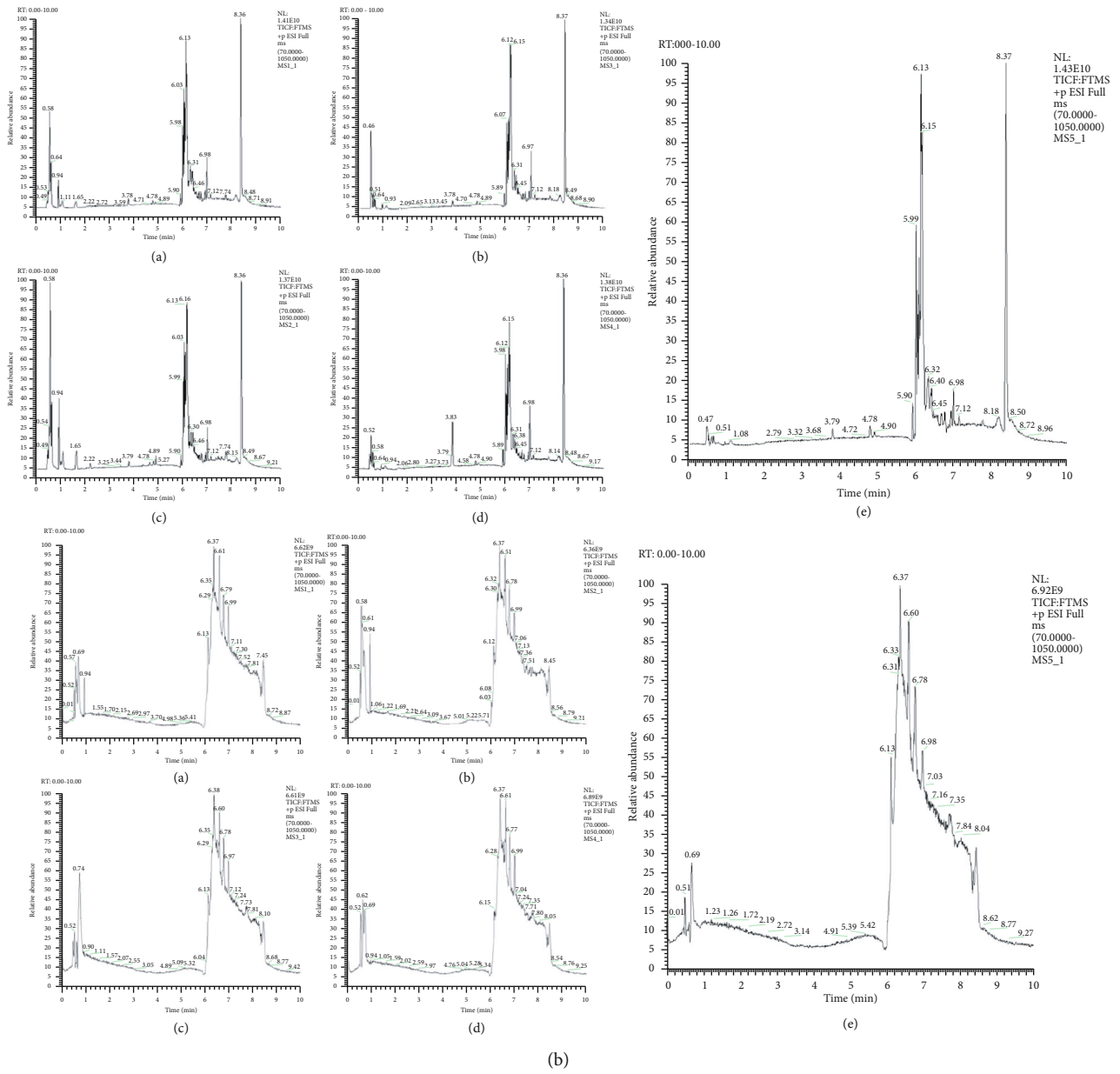
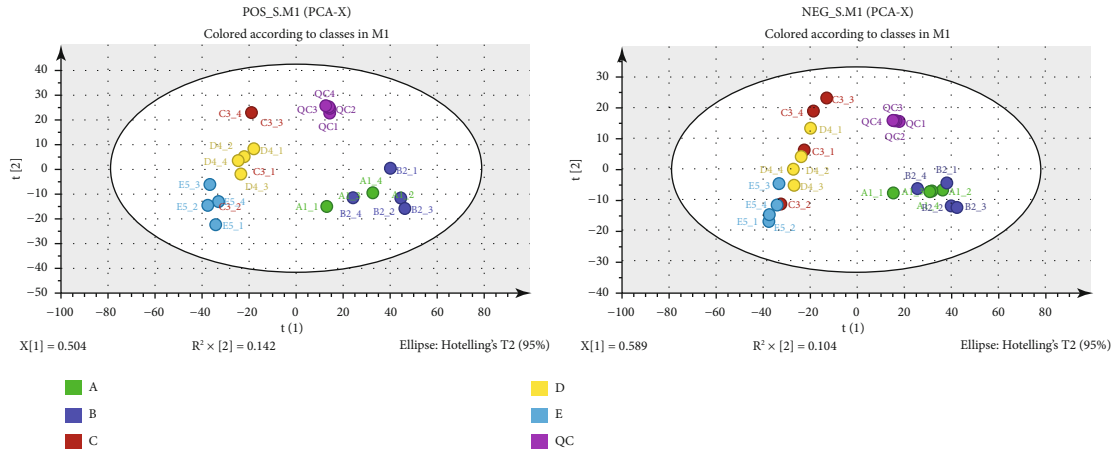
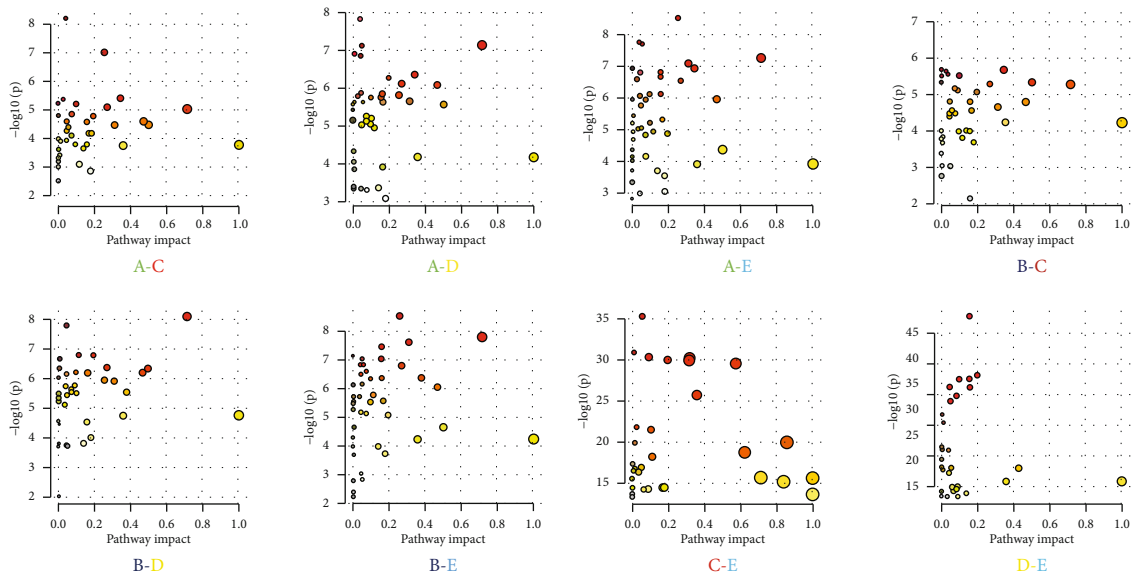


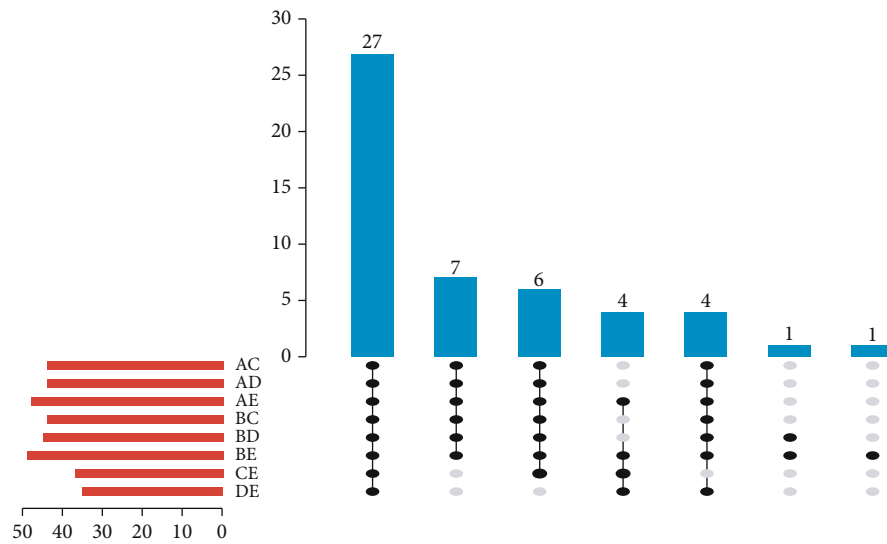
FIGURE 5: Continued.



(c)

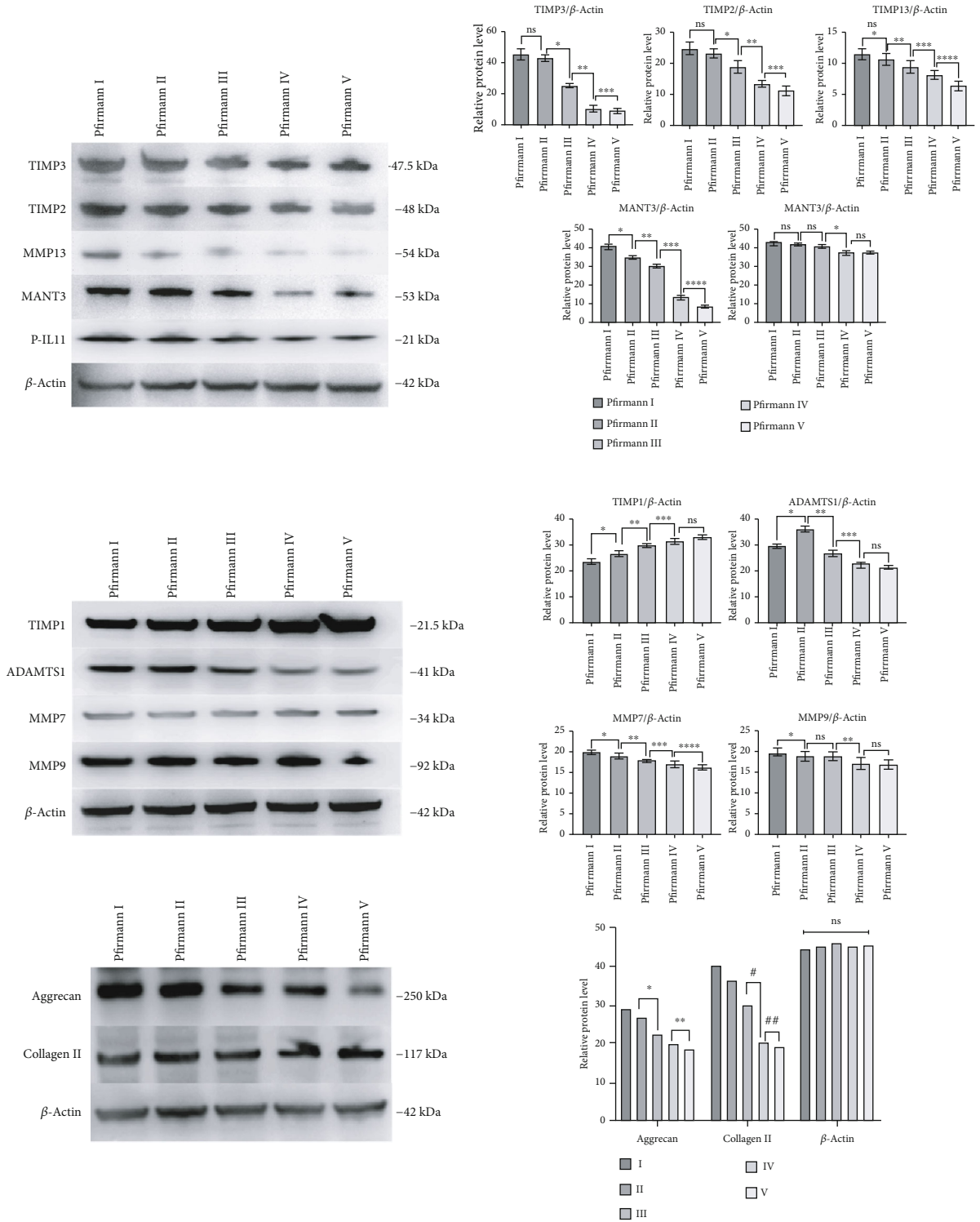


(d)



(e)

FIGURE 5: Continued.



(f)

FIGURE 5: (a) Mass spectrometry (UHPLC-Q-HFX HRMS) metabolomics flowchart. (b) Total ion current (TIC) diagram of human IVD. (c) Principal component analysis (PCA). (d) Differential metabolic pathway enrichment among groups. (e) Upset diagram of metabolic pathways of different substances in each group. (f) Western blot strip and grayscale map of degeneration factors related to key pathways ① glycine-serine-threonine, ② galactose, and ③ structural protein.

TABLE 2: General information of human IVD research subjects.

	Pfirrmann I	Pfirrmann II	Pfirrmann III	Pfirrmann IV	Pfirrmann V
GE 3.0T	28	32	64	121	137
SIEMENS 3.0T	14	22	52	65	72

its peak in grade II IVDs. Moreover, change in expression level of TIMP1, MMP7, and MMP9 was consistent with decomposition of ECM of IVDs. Expression levels of structural proteins (Collagen II and Aggrecan) decreased progressively throughout the degeneration process.

3.6. NMR Analysis of Human Samples. Distribution of compounds represented by each peak was identified through the attribution based on synchronous mass spectrometry identification. Representative peaks of the ^1H spectrum of each level of IVD were identified based on the attribution and data from the standard compound NMR spectrum database. The V-level disc was used as a representative sample (Figure 6(a)). Designated peaks of the ^1H spectrum of each graded IVD were manually integrated to determine the levels of metabolites for each peak. This was performed to determine the concentration of the substance in the unit magnetic field volume in the solution, and integral value of each substance was recorded and trend chart generated (Figure 6(b)). Notably, substances were not included in the statistics. Arrangement of the peaks of each spectrum is presented in Figure 6(c). One-dimensional ^1H spectroscopy produces a large amount of H signal overlap in the NMR system. Although it is used to accurately identify the types of amino acid residues, it is challenging to identify the spatial conformation of biopolymers such as proteins and proteoglycans. The “two-dimensional correlation spectrum” experiment was used to further determine types of polymer compounds by comparing with the clinical MRS (Figure 6(d)).

3.7. Verification of Human Imaging. Analysis of DTI imaging axial map of each level of the IVD showed that Pfirrmann I-V level represents gradual decrease of the high signal of water molecule activity (Figure 7(a)). ADC value and FA value of the IVD NP area were determined in the five levels (Figure 7(b)). Analysis showed that the ADC value of grade I-IV IVDs gradually decreased with degeneration of the disc ($F = 161.0$, $P < 0.01$). Notably, grade V IVDs were not detectable in DTI imaging. In grade V, ADC and FA values were not obtained, implying that the measured value range exceeded the high limit or cannot be imaged. This finding shows that the ADC value of degenerative IVDs gradually decreased, whereas the FA value increased with degeneration. Notably, analysis showed significant differences in ADC and FA values between groups ($F = 3810.0$, $P < 0.01$).

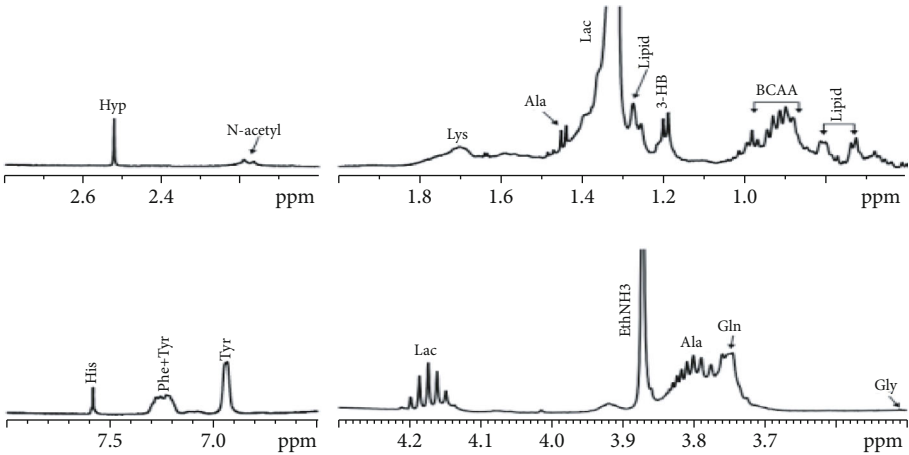
Pfirrmann grade IV disc spectrum peak identification was similar, from low field to high field (Figure 7(c)). The values are as follows: lactic acid (Lac) 1.33 ppm, alanine and propionate compounds (Ala) 1.36-1.64 ppm, N-acetyl resonance compound or collagen compound (N-Acetyl/PG) 2.02 ppm, glutamate and glutamine compound (Glu/Gln)

2.35 ppm-2.45 ppm, total choline compound (Cho) 3.02 ppm-3.20 ppm, muscle acid (Cr) 3.5 ppm, carbohydrates, and hydrocarbons and lipids (Carb) 3.6 ppm-4.7 ppm. The overall trend of levels of metabolites decreased with increase in degeneration intensity. Levels of metabolites in the grade V IVD were significantly low compared with other groups. N-Acetyl, Cho, Lac, Cr, Carb, N-Acetyl/Carb, N-Acetyl/Cr, Carb/Cr, N-Acetyl/Cho, and Carb/Cho were set based on peak imaging characteristics (Figure 7(d)). Absolute quantification of each value does not necessarily have a good trend under the conditions of NMR spectroscopy; therefore, the ratio of the integral value of each single peak was used to determine quantity of the spectrum material (Figure 7(e)).

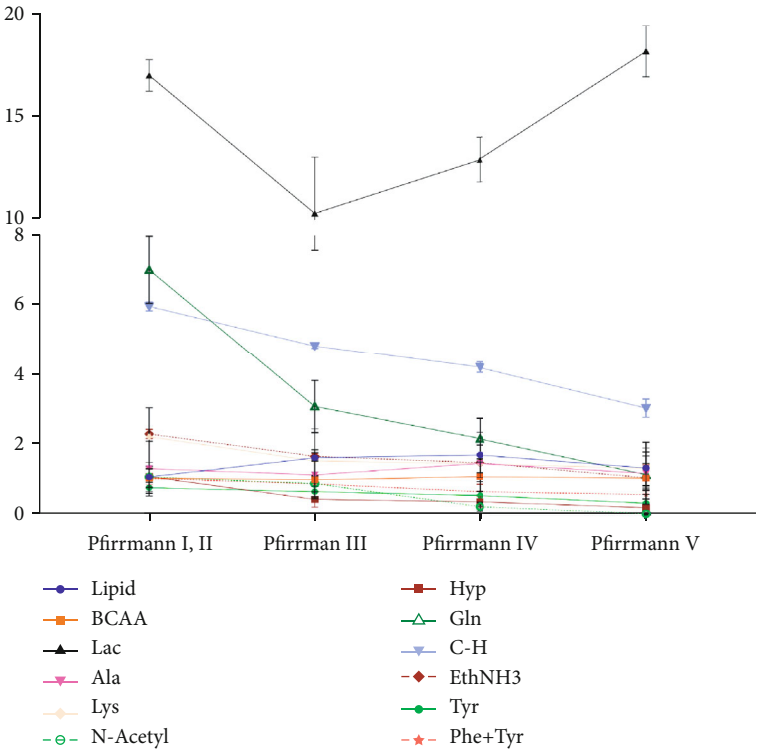
4. Discussion

Degeneration is a multistage physiological process with complex factors. IVDs at different degeneration stages are characterized by differences in morphology, pathology, and cell biology [17]. Clinically, IDD is divided into pre-, early, and late-stage degeneration [18]. The gold standard of IDD in the imaging field is Pfirrmann classification [17]. Microscopic analysis shows that many proteins and related degenerative factors are implicated in the degeneration process [19–22]. Interaction of these components further deteriorates degeneration. The three levels of degeneration process are relatively independent from each other. Advances in metabolomics provide a means to establish a systematic degeneration mode. In this study, rats and degenerative disc disease patients with high gene homology were used for metabolomics analysis. The overall picture of IDD was determined through imaging, histopathological analysis, and molecular biology methods.

Currently, MRI is the main method for noninvasive diagnosis of IDD [23]. Its principle is to collect proton relaxation signals in the body and construct a digital matrix to describe the spatial distribution characteristics of sample nuclei. MRI is used to visually observe morphological changes of the tissue structure [24]; however, due to the inevitable loss of the original characteristics of the information during the signal conversion process, it is challenging to generate the accurate profile within the tissue. Therefore, imaging is only useful for “appearance” stage. Advances in metabolomics allow immediate internal display of the organization of tissues [25]; however, its process is tedious and costly [26]; therefore, it is not widely used. This study used NMR metabolomics combined with mass spectrometry metabolomics to explore the metabolic profile of IVD and further performed quantitative and qualitative analysis of spectrograms to establish an *in vivo* metabolism model of noninvasive detection of degeneration.



(a)



(b)

FIGURE 6: Continued.

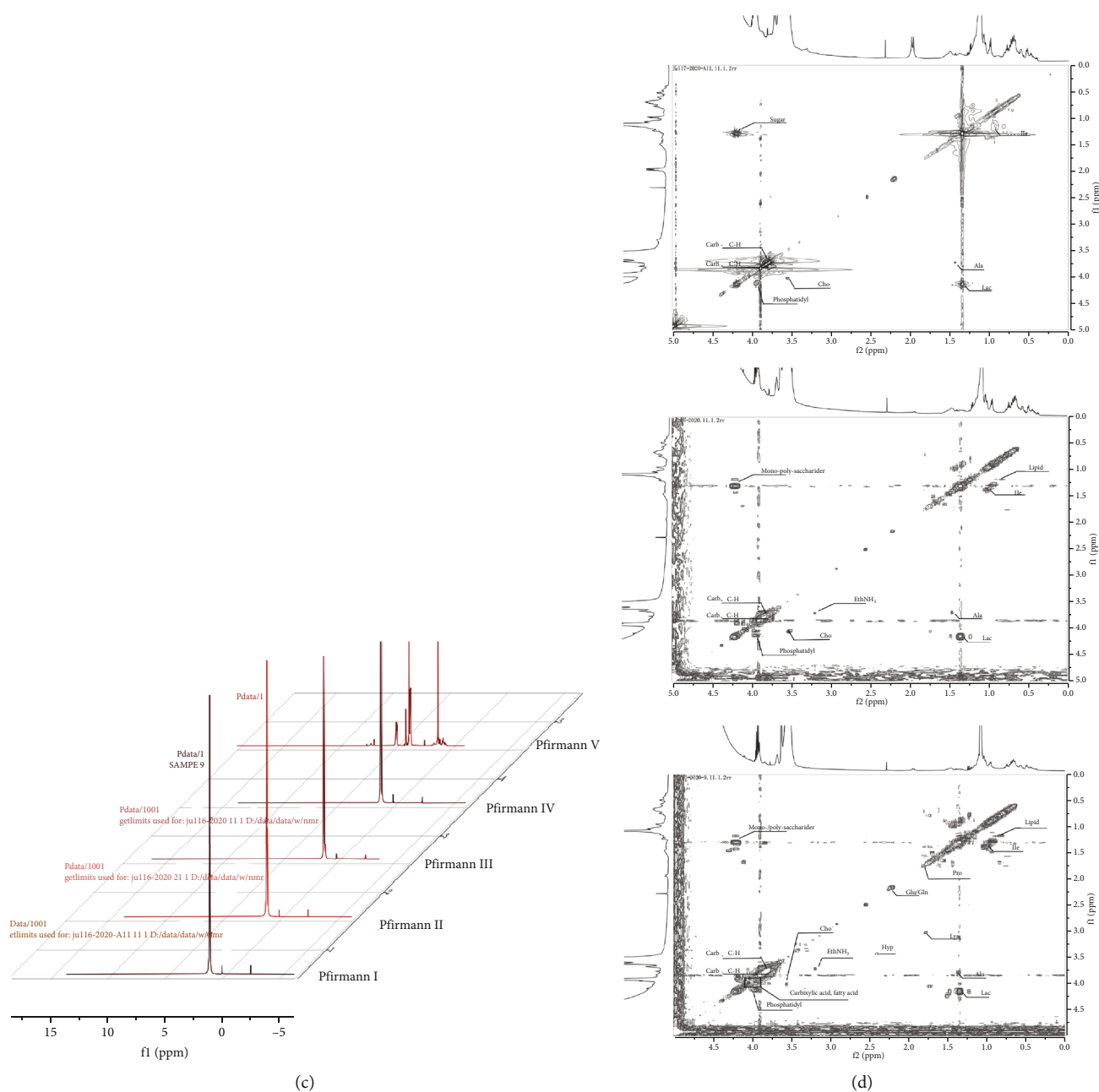
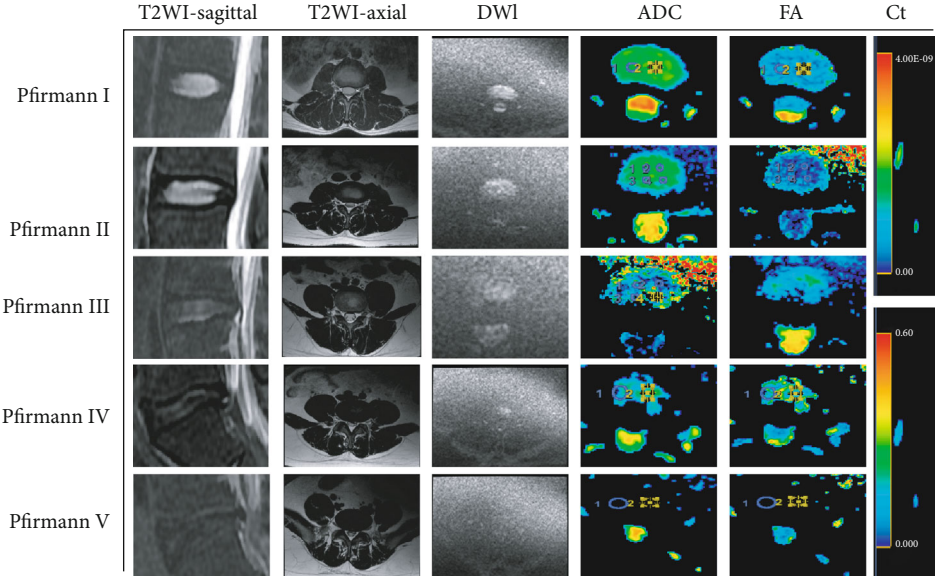


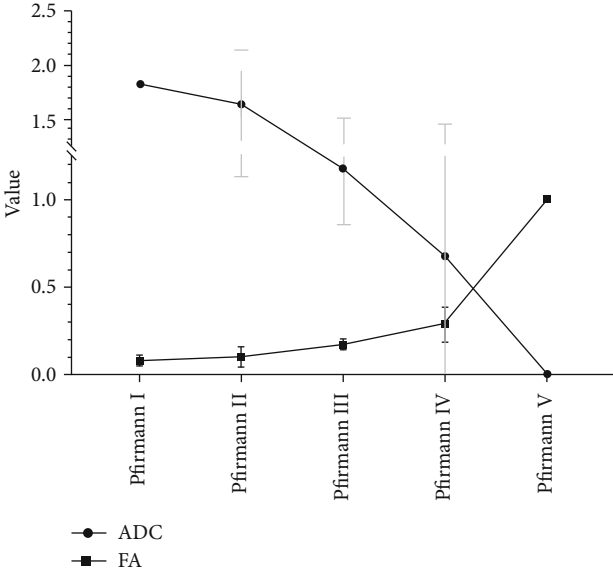
FIGURE 6: (a) Pfirrmann V grade disc NMR ^1H spectrum assignment. (b) Quantitative analysis chart of NMR ^1H spectrum of Pfirrmann I~V IVD. (c) Pfirrmann I~V grade IVD NMR ^1H spectrum peak line change arrangement diagram. (d) Two-dimensional TOCSY spectrum of Pfirrmann I ①, III ②, and V ③ disc.

Analysis showed that the main metabolic processes were carbohydrate and protein metabolism, mainly involving matrix components such as collagen and proteoglycans. Therefore, this study focuses on amino acid metabolism and sugar metabolism. Analysis of TIC, OPLS-DA, and the corresponding permutation test and S-PLOT load diagram showed that group A without intervention in the overall metabolic pattern of rat IVDs was significantly different from other groups. On the contrary, groups B and C showed similar trends in expression of metabolites. Therefore, the two stages before and after degeneration were explored.

The main different metabolic pathways before and after degeneration were mainly related to three types of biological activities including ① carbohydrate utilization (amino sugar and nucleotide sugar metabolism, pentose phosphate pathway, alanine metabolism, and glycolysis/gluconeogenesis pathway), ② antioxidant pathways (glutathione metabolism, cysteine, and methionine metabolism), and ③ structural protein synthesis and degradation (Gly-Ser-Thr metabolism) [27, 28]. Notably, most of the pathways revolved around the Gly-Ser-Thr metabolism axis [29, 30]. The Venn diagram of differential metabolic pathways showed that the

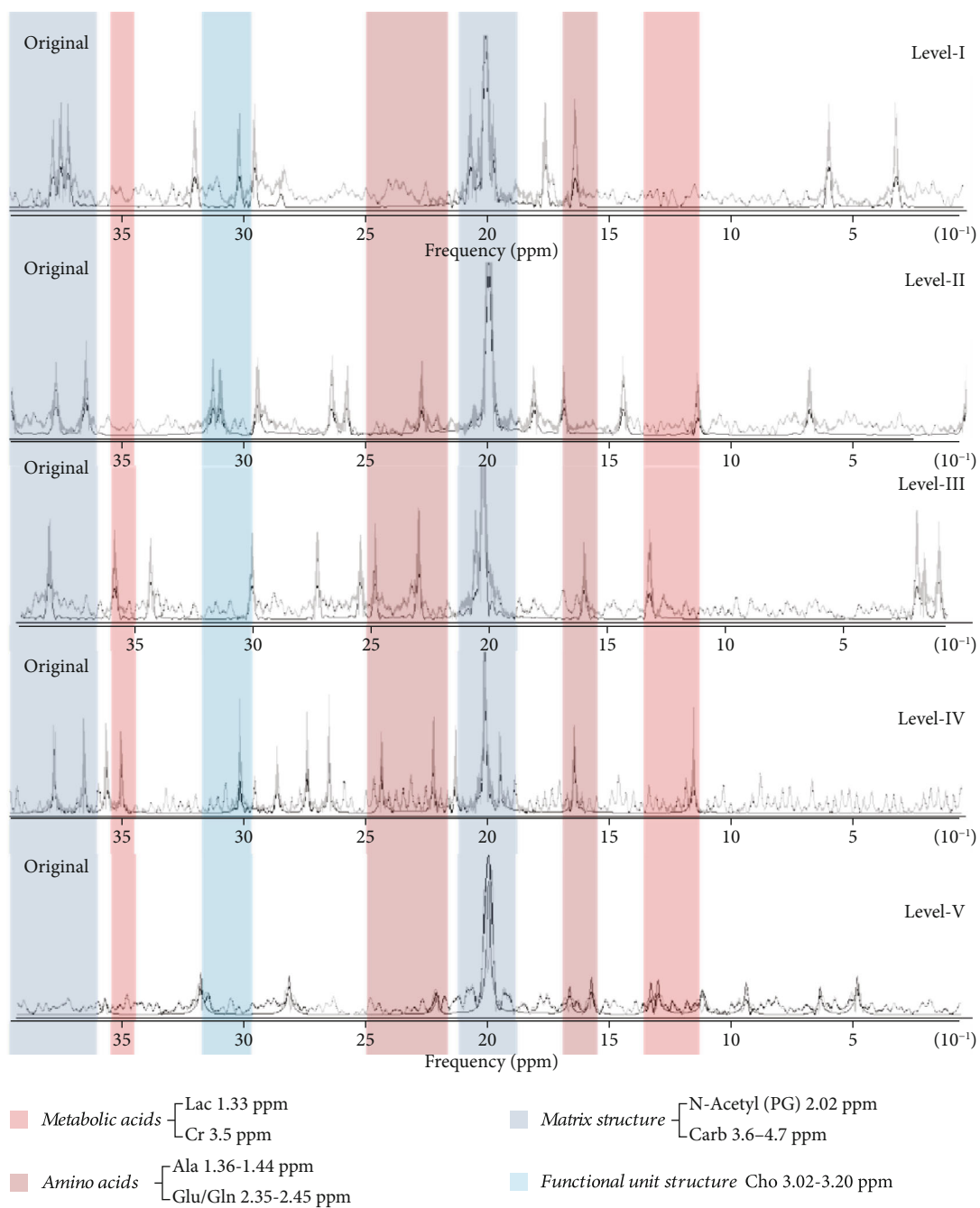


(a)



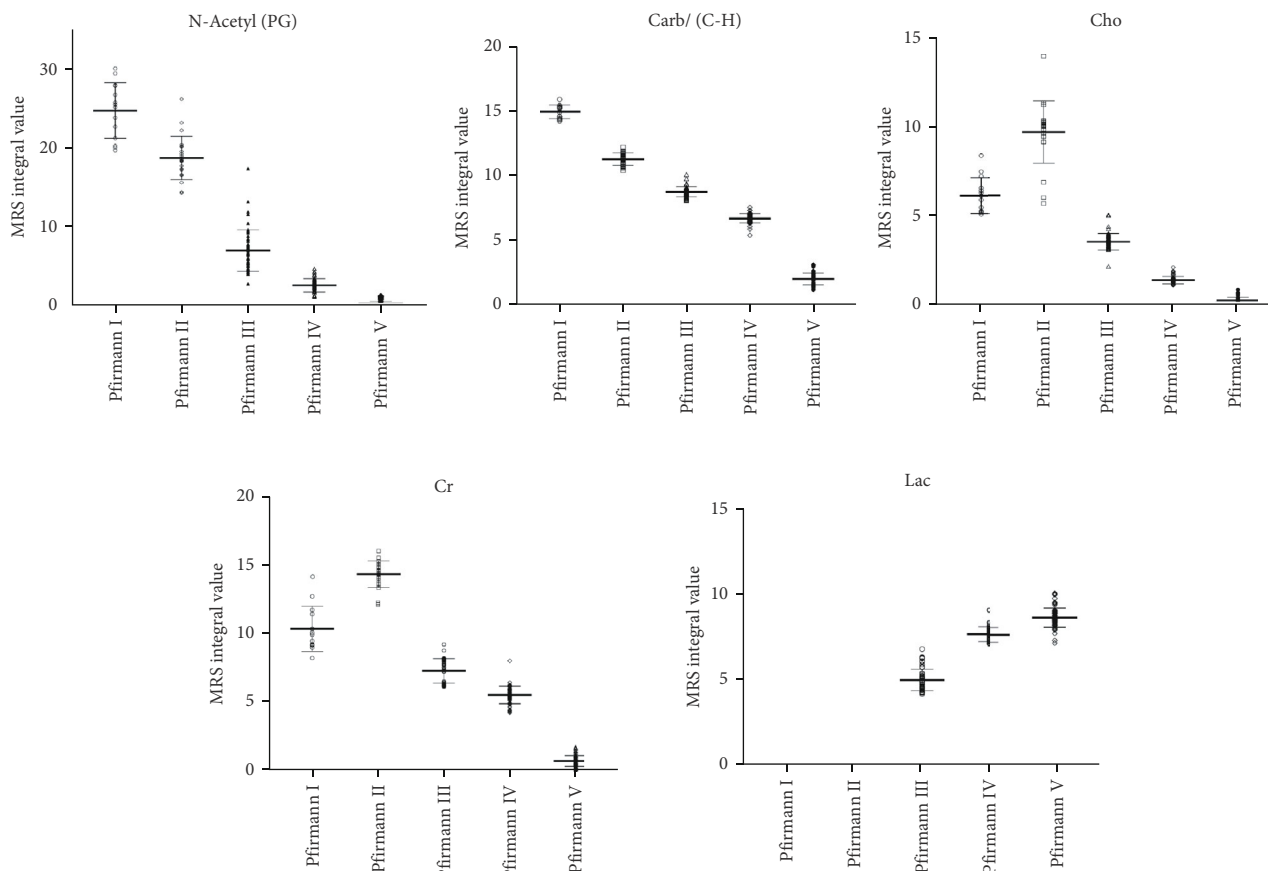
(b)

FIGURE 7: Continued.



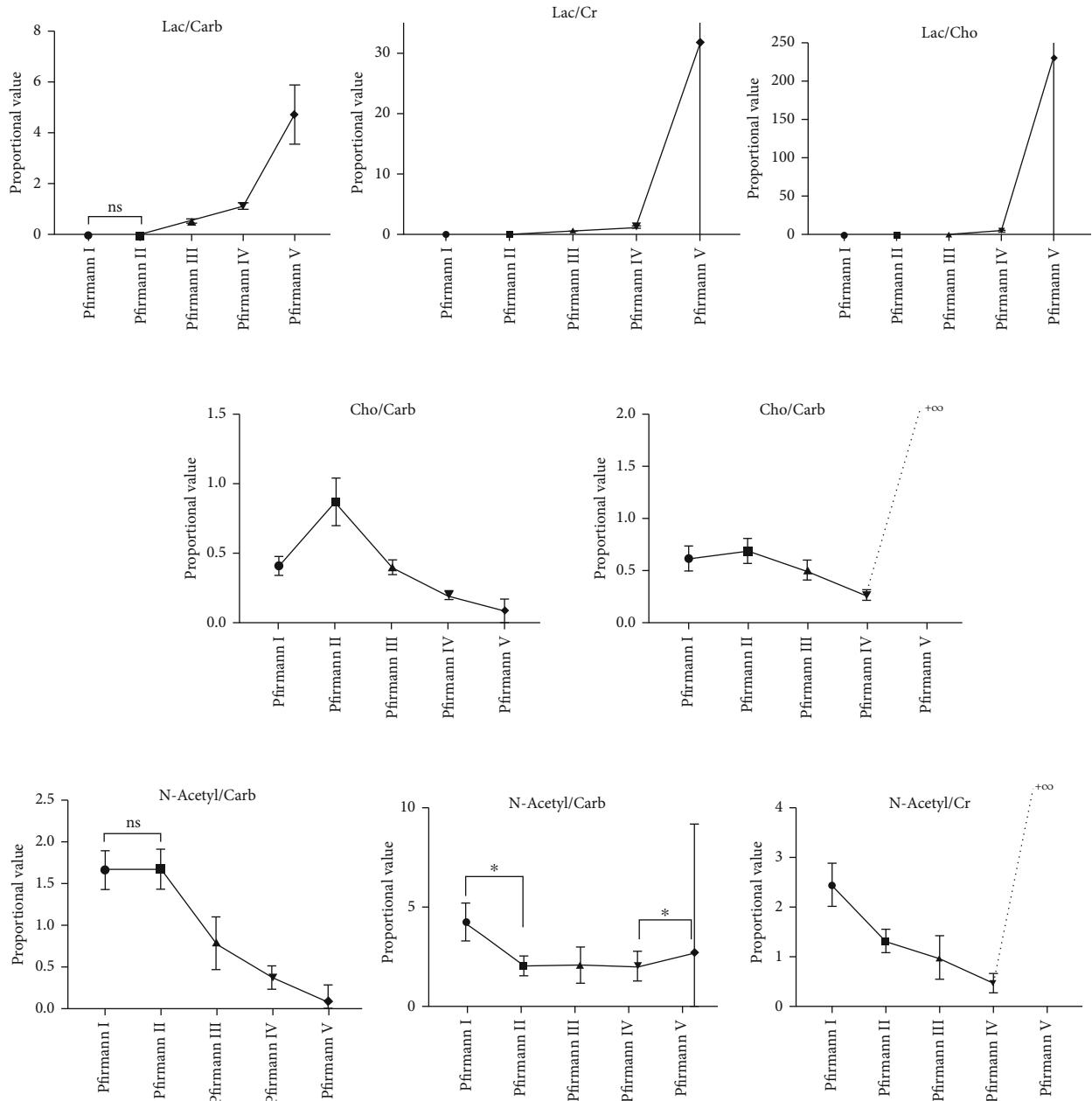
(c)

FIGURE 7: Continued.



(d)

FIGURE 7: Continued.



(e)

FIGURE 7: (a) DWI, ADC, and FA axis diagram of each grade of IVD. (b) Analysis of ADC value and FA value of Pfirrmann I-V IVD DTI imaging. (c) Identification and qualitative induction of MRS measurement peaks of Pfirrmann I-V IVDs *in vivo*. (d) Quantitative value statistics of five single peaks of MRS in each level of IVD. (e) Trend change graph of the integral value ratio of ① lactate, ② choline compound, and ③ N-acetyl resonance compound.

metabolism of Gly-Ser-Thr was different in intersection of AB and intersection of AC. This was attributed by the significant changes in the functional status of the Gly-Ser-Thr axis before and after degeneration [31].

Analysis of the difference in metabolites showed that marker metabolites in the predegeneration stage were mainly implicated in carbohydrate metabolism pathways including pentose phosphate pathway, glycolysis/xenogenesis, and amino sugar and nucleotide sugar metabolism and protein metabolism pathways including serine and thre-

onine metabolism, cysteine and methionine metabolism, and small molecule metabolism mainly inositol phosphate metabolism. In addition, marker metabolites in the late stage of degeneration were mainly involved in sugar metabolism pathways such as amino sugar and nucleotide sugar metabolism, proteoglycan structural metabolism, and tricarboxylic acid (TCA) cycle; protein metabolism pathways such as cysteine and methionine metabolism and serine and threonine metabolism; and small molecule metabolism including niacin and nicotinamide metabolism and PGI₂ metabolism.

Consistent with the findings on metabolic pathways, the main biological processes involved in rat IDD were energy metabolism [32], biological oxidation [33], and structural protein synthesis and decomposition [34]. Gly-Ser-Thr metabolic pathways are involved in biotransformation and metabolic activities during degeneration [35].

Cysteine plays a role regulating glutathione synthesis. Glutathione is an important antioxidant and oxygen free radical scavenger in the body. Methionine is involved in destruction of membrane lipids produced by oxidative free radicals through multiple channels of oxidation thus protecting membrane-containing structures such as cells and mitochondria [36]. Downregulation of cysteine and methionine metabolism during degeneration process leads to decline of the antioxidant function in the internal environment of the IVD [37]. Peroxidation of tissue membranes promotes degeneration of the IVD. Amino sugars and nucleotide sugars play important role in the process of carbohydrate conversion and energy utilization [38]. Notably, amino sugars and nucleotide sugars were downregulated during the degeneration process. Pentose phosphate pathway and glycolysis are involved in supply of energy and reducing equivalents important for antioxidant activity. These changes during degeneration indicate a transition from multimode coexistence of energy utilization in the IVD to a single mode of proteoglycan structural metabolism, implying that material disintegration of the NP tissue occurred in the later stage of degeneration. Furthermore, decline of the overall function of the energy utilization system may be the initiating factor leading to accumulation of Lac in the late stage of IDD. TCA cycle is the final metabolic pathway and metabolic hub of the three major nutrients [39]. Downregulation of TCA cycle in the later stage of degeneration implies that the metabolites of the IVD are depleted, which is attributed to apoptosis of NP cells and the decline in their secretory function. Further, the Gly-Ser-Thr metabolic axis was downregulated in the early and late stages of degeneration [35], implying that the functional state of the metabolic axis is negatively correlated with the degree of degeneration. It is speculated that antioxidants are produced through the Gly-Ser-Thr metabolic axis. The Gly-Ser-Thr metabolic axis may play a role in delaying degeneration of the IVD through regulation of carbohydrate conversion and energy utilization and ultimately through formation of antioxidant agents.

Although the rat genome is highly homologous to human genome and the metabolic pathways are similar, it cannot be inferred that the metabolic profiles of the two organisms are the same. Therefore, human metabolic pathway subgroups were retrieved from the NCBI GEO database and used for induction. A heat map on the correlation between core genes and metabolic pathways showed that main changes are changes in the metalloproteinase families [40, 41] and their tissue-specific inhibitory enzyme family-related factors. Moreover, Gene Ontology functional enrichment analysis showed that decomposition of collagen and ECM is the main source of disc degeneration differences [19, 42, 43]. Further analysis on key pathway degeneration-related factors showed that expression of metabolites involved in the Gly-Ser-Thr metabolic pathways [35]

(MMP13, MATN3, TIMP2, and TIMP3, IL-11) decreased after degeneration compared with before degeneration (I, level II \rightarrow level III). Notably, expression of metabolites involved in this metabolic axis was extremely low in the late stages of degeneration (levels IV, V). These findings show that the metabolic axis is consistent with the degeneration process, and its function declines with increase in degeneration progresses. IL-11 is an important factor of fibrosis [44], and high expression level causes fibrosis of NP tissue [45]. Metabolites involved in galactose metabolism included ADAMTS1, TIMP1, MMP7, and MMP9. ADAMTS1 participates in biological processes by hydrolyzing proteoglycans [46] and inhibiting angiogenesis [47]. It reaches its peak at level II discs and initiates proteoglycan production. The process of resolution and decline in expression in the later stage may be related to the vascular growth in the IVD in the late stage of degeneration. In addition, changes in levels of TIMP1, MMP7, and MMP9 [48] were consistent with increased decomposition of the ECM of the IVD, resulting in progressive decline of structural proteins (Collagen II and Aggrecan) throughout the degeneration process. Molecular biology analysis shows the stable relationship between macrobiological processes and metabolomics. The relationship between macrobiological processes and metabolomics provides an avenue to verify the phased expression trend of metabolic pathways.

NMR is an effective tool for mass spectrometry metabolomics due to its universality and high throughput for hydrogen-containing metabolites [49]. Advantages of the quantification function of NMR allow quantitative analysis of sample metabolites at various stages [50]. NMR ^1H spectrum identification and quantitative analysis showed that consistent with the mass spectrum metabolism findings, there was no significant change in the types of metabolites. Notably, Lac levels increased significantly with degeneration. Decrease in the level of phenylalanine, tyrosine, and other sugar metabolism regulating substances [51] with the degeneration of the IVD implied a decline in energy utilization efficiency and conversion of sugar utilization mode. Ethanolamine, EthNH_3 , is an intermediate metabolite of phospholipids [52], and its content decreases significantly with degeneration, implying that methionine has multiple pathways to prevent oxidation of membrane lipids by oxidative free radicals. Furthermore, levels of N-Acetyl decreased significantly with degeneration, indicating the process of dissolution of IVD structural substances. The presence of glycine residues in the final stage of degeneration indicates that the function of the Gly-Ser-Thr axis is effectively involved in the process of degeneration. However, ^1H spectrum has poor specificity in identifying compounds. In order to separate effective compound components from the overlapping peaks and peaks with small amplitude, TOCSY two-dimensional spectrum was used to transfer the magnetization vector using the direct coupled spin method [53] thus allowing observation of the same spin. Analysis of relevant signals between the indirectly connected nuclei in the system showed that the existing form of sugars changes from various types of sugars to monosaccharides/polysaccharides. These changes indicate that the types of

sugars available in the late stage of degeneration are reduced, and the corresponding metabolites result in reduction of carbohydrate metabolism pathways. In addition, glutamic acid/glutamine decreased in the initial stages then increased in the late stages of degeneration. Decrease in the early stage of degeneration results in inhibition of glutathione synthesis, which affects the antioxidant capacity of the Gly-Ser-Thr metabolism axis. On the other hand, the abnormal increase in the later period is related with accumulation of Lac. Increase in lactate is attributed to the decay process of the energy utilization system. In addition, increase in the types of amino acids in the other two-dimensional spectrum (such as alanine) indicated decomposition of the main structural proteins of the NP.

In vitro NMR ^1H spectrum and the TOCSY two-dimensional spectrum divide the stages of human IDD based on levels of amino acid residues and macromolecular compounds, highlighting the specificity of the metabolism process at different stages. The phase difference of metabolites can be explained by molecular biology regulation mechanism. Further studies should explore whether NMR analysis results are consistent with the corresponding MRS quantitative results and whether the macrobiological process can be explained by DTI.

Conventional NMR, DTI, and MRS were used to describe the classification of human IVDs from three levels including anatomical shape, water molecule pathophysiological behavior, and metabolic level adjustment. The process of degeneration was verified through metabolomics analysis.

T_2 WI-weighted images of the IVDs showed that the imaging features of the IVDs of each grade conformed to the Pfirrmann classification. In addition, imaging confirmed that there was no objection to the sorting of human IVD models. This study used functional nuclear magnetism to observe water metabolism based on morphological changes of T_2 WI [54]. Decrease in activity of the high signal of DTI water molecule resulted in changes in the corresponding ADC value and FA value. The ADC value shows that as the degeneration intensifies, the movement of water molecules in the NP is limited and the content decreases, indicating that large amounts of water-fixing groups are lost. Threonine, which contains a large amount of hydroxyl groups, is the key substance for water fixing. The FA value gradually increased with progression in degeneration, implying that the irregular structure and nondirectional distribution tissues that limit dispersion of water molecules increased. These findings indicate an increase in the fibrosis process of the NP tissue in the later stage of degeneration.

Qualitative analysis of NMR showed that the metabolites in the metabolic pool of the IVD were stable and the overall metabolic profile was consistent. Notably, lactate ratio represented accumulation of Lac in the unit structure substance, and its accumulation shows a decrease in energy utilization efficiency in the late stage of degeneration and that the sugar utilization pattern in mass spectrometry metabolomics was changed from the previous glycolysis. In addition, change in metabolites showed transformation from xenobiotics and pentose phosphate to fructose and mannose pathways in the late stages. N-Acetyl resonance compound is an

important identification peak of MRS. N-Acetyl/Carb is interpreted as the ratio of collagen content to carbohydrate and hydrocarbons. Carbohydrate content is a marker of matrix structure and carbohydrate metabolism of proteoglycans. The significant decrease in the ratio value indicates decrease of the collagen content in the structural material, which is consistent with the findings on the progressive fibrosis of the NP tissue. On the other hand, N-Acetyl/Cho represents the proportional relationship between the collagen content and the density of the IVD NP cells. The ratio of IDD showed significant decrease indicating that the unit number of cells matching ECM decreased with progress in degeneration. This implies that the proportion of NP cell apoptosis and degeneration increases, and its secretory function decreases. N-Acetyl/Cr represents the proportional relationship between collagen content and energy buffer mechanism, because Cr is an important substance for ATP buffering [55] and it mainly exists as an energy storage form. In the early stage of degeneration, the ratio is high. The downward trend and the abnormal increase in the end stage show the change in energy supply mode at the end of degeneration [56]. Furthermore, the peak of choline compound is used to measure the state of membrane phospholipids, reflecting the density of the NP cells of the IVD. The ratio of Pfirrmann I disc to Pfirrmann II disc in Cho/Carb increased gradually. However, the ratio decreased in Pfirrmann III of the IVD with the lowest value observed in Pfirrmann V disc. This change reflects increase in the ratio of degeneration and apoptosis of NP cells during the degeneration process. In addition, it indicates the decrease in activity of phospholipid synthesis and redox reactions of IVD cells. Therefore, there may be a period of active proliferation of NP cells before degeneration. *In vitro* metabolomics were linked with *in vivo* imaging mimics through spectrogram identification and spectral peak analysis. These findings were then confirmed through histopathological and molecular biology analysis.

5. Conclusion

In summary, this study described the relatively complete IDD through correlation analysis of rat and human metabolomics (mass spectrometry metabolomics and NMR metabolomics) combined with imaging, molecular biology, and histopathology verification. The findings of this study show tissue metabolism during degeneration. The findings showed that the process of IDD is closely related to the functional state of the Gly-Ser-Thr metabolic axis. Changes in carbohydrate utilization patterns around this metabolic axis and reduction of the antioxidant capacity of the IVD environment promote degeneration. The process eventually leads to disintegration of the annulus fibrosus and loss of water-fixing groups.

Data Availability

The datasets used and/or analyzed during the current study are available from the corresponding author on reasonable request.

Ethical Approval

This study was approved by the ethical committee of the Affiliated Hospital of Qingdao University. The study participants' data was coded for confidentiality and compliance with the Declaration of Helsinki.

Consent

Written informed consent was obtained from all the patients for publication of this research and any accompanying images.

Conflicts of Interest

The authors declare that there is no conflict of interest regarding the publication of this paper.

Authors' Contributions

Xiaolin Wu, Chang Liu, and Shuai Yang contributed to this work equally.

Acknowledgments

The authors thank Professor Bohua Chen for his helpful advice regarding researching unpublished literature. This work was supported by the National Natural Science Foundation of China (81802190 and 81772412), the Shandong Provincial Science Foundation of China (ZR2019BH084), the Young Taishan Scholars Program (tsqn201909190), the Qingdao Postdoctoral Applied Research Project (2020), the Shandong Higher Education Young Science and Technology Support Program (2020KJL005), and the National Key Research and Development Project (2019YFC0121404).

References











- [1] J.-A. Deane, A.-V. Pavlova, A. K. P. Lim, J. S. Gregory, R. M. Aspden, and A. H. McGregor, "Is intrinsic lumbar spine shape associated with lumbar disc degeneration? An exploratory study," *BMC Musculoskeletal Disorders*, vol. 21, no. 1, p. 433, 2020.
- [2] J. Clouet, M. Fusellier, A. Camus, C. le Visage, and J. Guicheux, "Intervertebral disc regeneration: from cell therapy to the development of novel bioinspired endogenous repair strategies," *Advanced Drug Delivery Reviews*, vol. 146, pp. 306–324, 2019.
- [3] M. Bashkuev, S. Reitmaier, and H. Schmidt, "Effect of disc degeneration on the mechanical behavior of the human lumbar spine: a probabilistic finite element study," *The Spine Journal*, vol. 18, no. 10, pp. 1910–1920, 2018.
- [4] Z. Liao, X. Wu, Y. Song et al., "Angiopoietin-like protein 8 expression and association with extracellular matrix metabolism and inflammation during intervertebral disc degeneration," *Journal of Cellular and Molecular Medicine*, vol. 23, no. 8, pp. 5737–5750, 2019.
- [5] W. Hua, Y. Zhang, X. Wu et al., "Icariin attenuates interleukin-1 β -induced inflammatory response in human nucleus pulposus cells," *Current Pharmaceutical Design*, vol. 23, no. 39, pp. 6071–6078, 2018.
- [6] B. Grignon and J. Roland, "Can the human intervertebral disc be compared to a diarthrodial joint?," *Surgical and Radiologic Anatomy*, vol. 22, no. 2, pp. 101–105, 2000.
- [7] Z. Sun, Z. H. Liu, Y. F. Chen et al., "Molecular immunotherapy might shed a light on the treatment strategies for disc degeneration and herniation," *Medical Hypotheses*, vol. 81, no. 3, pp. 477–480, 2013.
- [8] Z. Sun, B. Liu, and Z. J. Luo, "The immune privilege of the intervertebral disc: implications for intervertebral disc degeneration treatment," *International Journal of Medical Sciences*, vol. 17, no. 5, pp. 685–692, 2020.
- [9] X. Cheng, G. Zhang, L. Zhang et al., "Mesenchymal stem cells deliver exogenous miR-21 via exosomes to inhibit nucleus pulposus cell apoptosis and reduce intervertebral disc degeneration," *Journal of Cellular and Molecular Medicine*, vol. 22, no. 1, pp. 261–276, 2018.
- [10] L. D. Kozaci, A. Guner, G. Oktay, and G. Guner, "Alterations in biochemical components of extracellular matrix in intervertebral disc herniation: role of MMP-2 and TIMP-2 in type II collagen loss," *Cell Biochemistry and Function*, vol. 24, no. 5, pp. 431–436, 2006.
- [11] X. Liang, R. Xie, B. Hou et al., "Feasibility study for evaluating lumbar intervertebral disc degeneration using histogram analysis of T2* values," *European Spine Journal*, vol. 29, no. 10, pp. 2600–2608, 2020.
- [12] J. Fakhoury and T. J. Dowling, *Cervical Degenerative Disc Disease, in StatPearls*, StatPearls Publishing LLC, Treasure Island, FL, USA, 2020.
- [13] H. Tweeddale, L. Notley-McRobb, and T. Ferenci, "Effect of slow growth on metabolism of *Escherichia coli*, as revealed by global metabolite pool ("metabolome") analysis," *Journal of Bacteriology*, vol. 180, no. 19, pp. 5109–5116, 1998.
- [14] C. Franceschi, P. Garagnani, P. Parini, C. Giuliani, and A. Santoro, "Inflammaging: a new immune-metabolic viewpoint for age-related diseases," *Nature Reviews Endocrinology*, vol. 14, no. 10, pp. 576–590, 2018.
- [15] L. M. Seijo, N. Peled, D. Ajona et al., "Biomarkers in lung cancer screening: achievements, promises, and challenges," *Journal of Thoracic Oncology*, vol. 14, no. 3, pp. 343–357, 2019.
- [16] N. Shyh-Chang and H. H. Ng, "The metabolic programming of stem cells," *Genes & Development*, vol. 31, no. 4, pp. 336–346, 2017.
- [17] M. Teraguchi, N. Yoshimura, H. Hashizume et al., "Progression, incidence, and risk factors for intervertebral disc degeneration in a longitudinal population-based cohort: the Wakayama Spine Study," *Osteoarthritis and Cartilage*, vol. 25, no. 7, pp. 1122–1131, 2017.
- [18] P. Fan, X. Y. Yu, X. H. Xie et al., "Mitophagy is a protective response against oxidative damage in bone marrow mesenchymal stem cells," *Life Sciences*, vol. 229, pp. 36–45, 2019.
- [19] X. Cheng, L. Zhang, K. Zhang et al., "Circular RNA VMA21 protects against intervertebral disc degeneration through targeting miR-200c and X linked inhibitor-of-apoptosis protein," *Annals of the Rheumatic Diseases*, vol. 77, no. 5, pp. 770–779, 2018.
- [20] H. Choi, S. Tessier, E. S. Silagi et al., "A novel mouse model of intervertebral disc degeneration shows altered cell fate and matrix homeostasis," *Matrix Biology*, vol. 70, pp. 102–122, 2018.
- [21] L.-Y. Li, X.-L. Wu, R. J. Roman, F. Fan, C.-S. Qiu, and B.-H. Chen, "Diffusion-weighted 7.0T magnetic resonance

- imaging in assessment of intervertebral disc degeneration in rats," *Chinese Medical Journal*, vol. 131, no. 1, pp. 63–68, 2018.
- [22] K. Sun, X. Jing, J. Guo, X. Yao, and F. Guo, "Mitophagy in degenerative joint diseases," *Autophagy*, vol. 16, pp. 1–11, 2020.
- [23] R. C. da Costa, S. de Decker, M. J. Lewis, H. Volk, and The Canine Spinal Cord Injury Consortium (CANSORT-SCI), "Diagnostic imaging in intervertebral disc disease," *Frontiers in Veterinary Science*, vol. 7, article 588338, 2020.
- [24] J. Y. Kim and R. A. Gatenby, "Quantitative clinical imaging methods for monitoring intratumoral evolution," *Methods in Molecular Biology*, vol. 1513, pp. 61–81, 2017.
- [25] J. Rodríguez-Coira, M. Delgado-Dolset, D. Obeso et al., "Troubleshooting in large-scale LC-ToF-MS metabolomics analysis: solving complex issues in big cohorts," *Metabolites*, vol. 9, no. 11, p. 247, 2019.
- [26] E. Zubeldia-Varela, D. Barber, C. Barbas, M. Perez-Gordo, and D. Rojo, "Sample pre-treatment procedures for the omics analysis of human gut microbiota: turning points, tips and tricks for gene sequencing and metabolomics," *Journal of Pharmaceutical and Biomedical Analysis*, vol. 191, article 113592, 2020.
- [27] J. Southan, E. McHugh, H. Walker, and H. M. Ismail, "Metabolic signature of articular cartilage following mechanical injury: an integrated transcriptomics and metabolomics analysis," *Frontiers in Molecular Biosciences*, vol. 7, article 592905, 2020.
- [28] P. Zhang, W. Zhu, D. Wang et al., "A combined NMR- and HPLC-MS/MS-based metabolomics to evaluate the metabolic perturbations and subacute toxic effects of endosulfan on mice," *Environmental Science and Pollution Research International*, vol. 24, no. 23, pp. 18870–18880, 2017.
- [29] X. Ren, S. Ma, J. Wang et al., "Comparative effects of dexamethasone and bergenin on chronic bronchitis and their anti-inflammatory mechanisms based on NMR metabolomics," *Molecular BioSystems*, vol. 12, no. 6, pp. 1938–1947, 2016.
- [30] J. Gu, C. Ji, S. Yue et al., "Enantioselective effects of metalaxyl enantiomers in adolescent rat metabolic profiles using NMR-based metabolomics," *Environmental Science & Technology*, vol. 52, no. 9, pp. 5438–5447, 2018.
- [31] X. du, X. Zeng, K. Pan et al., "Metabolomics analysis of urine from healthy wild type mice exposed to ambient PM_{2.5}," *Science of The Total Environment*, vol. 714, article 136790, 2020.
- [32] E. B. de Sousa, G. C. dos Santos Junior, M. E. L. Duarte, V. Moura Neto, and D. P. Aguiar, "Metabolomics as a promising tool for early osteoarthritis diagnosis," *Brazilian Journal of Medical and Biological Research*, vol. 50, no. 11, article e6485, 2017.
- [33] X. Wang, N. Chen, Z. du et al., "Bioinformatics analysis integrating metabolomics of m6A RNA microarray in intervertebral disc degeneration," *Epigenomics*, vol. 12, no. 16, pp. 1419–1441, 2020.
- [34] A. Kuehne, J. Hildebrand, J. Soehle et al., "An integrative metabolomics and transcriptomics study to identify metabolic alterations in aged skin of humans in vivo," *BMC Genomics*, vol. 18, no. 1, p. 169, 2017.
- [35] M. A. Aon, M. Bernier, S. J. Mitchell et al., "Untangling determinants of enhanced health and lifespan through a multi-omics approach in mice," *Cell Metabolism*, vol. 32, no. 1, pp. 100–116.e4, 2020.
- [36] C. Ye, B. M. Sutter, Y. Wang, Z. Kuang, and B. P. Tu, "A metabolic function for phospholipid and histone methylation," *Molecular Cell*, vol. 66, no. 2, pp. 180–193.e8, 2017.
- [37] M. Sohail, R. B. H. Wills, M. C. Bowyer, and P. Pristijono, "Beneficial impact of exogenous arginine, cysteine and methionine on postharvest senescence of broccoli," *Food Chemistry*, vol. 338, p. 128055, 2021.
- [38] Y. Li, M. Zhao, W. Chen et al., "Comparative transcriptomic analysis reveals that multiple hormone signal transduction and carbohydrate metabolic pathways are affected by *Bacillus cereus* in *Nicotiana tabacum*," *Genomics*, vol. 112, no. 6, pp. 4254–4267, 2020.
- [39] J. Xu, Y. Zhai, L. Feng et al., "An optimized analytical method for cellular targeted quantification of primary metabolites in tricarboxylic acid cycle and glycolysis using gas chromatography-tandem mass spectrometry and its application in three kinds of hepatic cell lines," *Journal of Pharmaceutical and Biomedical Analysis*, vol. 171, pp. 171–179, 2019.
- [40] B. Tan, A. Jaulin, C. Bund et al., "Matrix metalloproteinase-11 promotes early mouse mammary gland tumor growth through metabolic reprogramming and increased IGF1/AKT/FoxO1 signaling pathway, enhanced ER stress and alteration in mitochondrial UPR," *Cancers*, vol. 12, no. 9, p. 2357, 2020.
- [41] P. J. Lu, G. Wang, X. D. Cai, P. Zhang, and H. K. Wang, "Sequencing analysis of matrix metalloproteinase 7-induced genetic changes in Schwann cells," *Neural Regeneration Research*, vol. 15, no. 11, pp. 2116–2122, 2020.
- [42] Y. Sun, X. Shi, X. Peng et al., "MicroRNA-181a exerts anti-inflammatory effects via inhibition of the ERK pathway in mice with intervertebral disc degeneration," *Journal of Cellular Physiology*, vol. 235, no. 3, pp. 2676–2686, 2020.
- [43] Y. Zhang, F. He, Z. Chen et al., "Melatonin modulates IL-1 β -induced extracellular matrix remodeling in human nucleus pulposus cells and attenuates rat intervertebral disc degeneration and inflammation," *Aging*, vol. 11, no. 22, pp. 10499–10512, 2019.
- [44] S. Schafer, S. Viswanathan, A. A. Widjaja et al., "IL-11 is a crucial determinant of cardiovascular fibrosis," *Nature*, vol. 552, no. 7683, pp. 110–115, 2017.
- [45] B. Corden, E. Adami, M. Sweeney, S. Schafer, and S. A. Cook, "IL-11 in cardiac and renal fibrosis: late to the party but a central player," *British Journal of Pharmacology*, vol. 177, no. 8, pp. 1695–1708, 2020.
- [46] C. M. Dancevic, D. R. McCulloch, and A. C. Ward, "The ADAMTS hyaluronanase family: biological insights from diverse species," *The Biochemical Journal*, vol. 473, no. 14, pp. 2011–2022, 2016.
- [47] J. Lambert, K. Makin, S. Akbareian et al., "ADAMTS-1 and syndecan-4 intersect in the regulation of cell migration and angiogenesis," *Journal of Cell Science*, vol. 133, no. 7, 2020.
- [48] A. C. Newby, "Metalloproteinase production from macrophages - a perfect storm leading to atherosclerotic plaque rupture and myocardial infarction," *Experimental Physiology*, vol. 101, no. 11, pp. 1327–1337, 2016.
- [49] A. M. Gil, P. G. de Pinho, M. S. Monteiro, and I. F. Duarte, "NMR metabolomics of renal cancer: an overview," *Bioanalysis*, vol. 7, no. 18, pp. 2361–2374, 2015.
- [50] A. Singh, R. K. Sharma, M. Chagtoo et al., "1H NMR metabolomics reveals association of high expression of inositol 1, 4, 5 trisphosphate receptor and metabolites in breast cancer patients," *PLoS One*, vol. 12, no. 1, article e0169330, 2017.

- [51] D. Demirbas, W. J. Brucker, and G. T. Berry, "Inborn errors of metabolism with hepatopathy: metabolism defects of galactose, fructose, and tyrosine," *Pediatric Clinics of North America*, vol. 65, no. 2, pp. 337–352, 2018.
- [52] Y. C. Lin, Y. C. Liu, and Y. Nakamura, "The choline/ethanolamine kinase family in Arabidopsis: essential role of CEK4 in phospholipid biosynthesis and embryo development," *Plant Cell*, vol. 27, no. 5, pp. 1497–1511, 2015.
- [53] A. B. Nielsen, M. R. Hansen, J. E. Andersen, and T. Vosegaard, "Single-spin vector analysis of strongly coupled nuclei in TOCSY NMR experiments," *The Journal of Chemical Physics*, vol. 151, no. 13, p. 134117, 2019.
- [54] P. A. Baltzer, D. M. Renz, K. H. Herrmann et al., "Diffusion-weighted imaging (DWI) in MR mammography (MRM): clinical comparison of echo planar imaging (EPI) and half-Fourier single-shot turbo spin echo (HASTE) diffusion techniques," *European Radiology*, vol. 19, no. 7, pp. 1612–1620, 2009.
- [55] M. M. Ommati, O. Farshad, V. Ghanbarinejad et al., "The nephroprotective role of carnosine against ifosfamide-induced renal injury and electrolytes imbalance is mediated via the regulation of mitochondrial function and alleviation of oxidative stress," *Drug Research*, vol. 70, no. 1, pp. 49–56, 2020.
- [56] S. Yang, F. Zhang, J. Ma, and W. Ding, "Intervertebral disc ageing and degeneration: the antiapoptotic effect of oestrogen," *Ageing Research Reviews*, vol. 57, p. 100978, 2020.

Research Article

TRPV1 Channel Activated by the PGE2/EP4 Pathway Mediates Spinal Hypersensitivity in a Mouse Model of Vertebral Endplate Degeneration

Sijing Liu ¹, Qiong Wang ², Ziyi Li ^{3,4}, Lei Ma ⁵, Ting Li ⁶, Yukun Li ^{3,4},
Na Wang ^{3,4}, Chang Liu ^{3,4}, Peng Xue ^{3,4} and Chuan Wang ²

¹Editorial Department of Hebei Medical University, Hebei Medical University, Shijiazhuang, Hebei 050017, China

²Department of Pharmacology, Hebei Medical University, Shijiazhuang, Hebei 050017, China

³Department of Endocrinology, The Third Hospital of Hebei Medical University, Shijiazhuang, Hebei 050051, China

⁴Key Orthopaedic Biomechanics Laboratory of Hebei Province, Shijiazhuang, Hebei 050051, China

⁵Department of Spine Surgery, The Third Hospital of Hebei Medical University, Shijiazhuang, Hebei 050051, China

⁶Institute of Biomedical Engineering, Chinese Academy of Medical Sciences and Peking Union Medical College, Tianjin 300020, China

Correspondence should be addressed to Peng Xue; hebmuxuepeng@163.com and Chuan Wang; wangchuan@hebm.u.edu.cn

Received 5 March 2021; Accepted 4 August 2021; Published 23 August 2021

Academic Editor: Kaitao Lai

Copyright © 2021 Sijing Liu et al. This is an open access article distributed under the Creative Commons Attribution License, which permits unrestricted use, distribution, and reproduction in any medium, provided the original work is properly cited.

Low back pain (LBP) is the primary cause of disability globally. There is a close relationship between Modic changes or endplate defects and LBP. Endplates undergo ossification and become highly porous during intervertebral disc (IVD) degeneration. In our study, we used a mouse model of vertebral endplate degeneration by lumbar spine instability (LSI) surgery. Safranin O and fast green staining and μ CT scan showed that LSI surgery led to endplate ossification and porosity, but the endplates in the sham group were cartilaginous and homogenous. Immunofluorescent staining demonstrated the innervation of calcitonin gene-related peptide- (CGRP-) positive nerve fibers in the porous endplate of LSI mice. Behavior test experiments showed an increased spinal hypersensitivity in LSI mice. Moreover, we found an increased cyclooxygenase 2 (COX2) expression and an elevated prostaglandin E2 (PGE2) concentration in the porous endplate of LSI mice. Immunofluorescent staining showed the colocalization of E-prostanoid 4 (EP4)/transient receptor potential vanilloid 1 (TRPV1) and CGRP in the nerve endings in the endplate and in the dorsal root ganglion (DRG) neurons, and western blotting analysis demonstrated that EP4 and TRPV1 expression significantly increased in the LSI group. Our patch clamp study further showed that LSI surgery significantly enhanced the current density of the TRPV1 channel in small-size DRG neurons. A selective EP4 receptor antagonist, L161982, reduced the spinal hypersensitivity of LSI mice by blocking the PGE2/EP4 pathway. In addition, TRPV1 current and neuronal excitability in DRG neurons were also significantly decreased by L161982 treatment. In summary, the PGE2/EP4 pathway in the porous endplate could activate the TRPV1 channel in DRG neurons to cause spinal hypersensitivity in LSI mice. L161982, a selective EP4 receptor antagonist, could turn down the TRPV1 current and decrease the neuronal excitability of DRG neurons to reduce spinal pain.

1. Introduction

Low back pain (LBP) is the primary cause for disability globally [1], with a 1-month prevalence of 23.2% [2]. Since LBP is generally a persistent symptom, about 2/3 of the patients with LBP complained about their pain-related symptoms

even after 12 months [3]. This persistent painful condition is associated with the development of multiple physical and psychosocial disabilities [4]. In 2017, a total of 577 million people experienced LBP, and more than 60 million healthy life years were lost worldwide, which resulted in a huge financial burden [5]. Unfortunately, we still do not understand the

natural course of LBP, and there is no effective therapeutic approach to modify this multicause induced disease.

To search the main cause of LBP, many research groups have been concentrating on the aneural [6, 7] intervertebral disc (IVD). Since there is only sporadic nerve ending existing in the outmost layer of the annulus, IVD as the main source for LBP remains debatable [8]. However, the endplate, which is rich in nerve endings in its ossified structure [7, 9], has been overlooked. In patients with LBP, researchers have detected signal changes in the degenerative endplates by magnetic resonance imaging (MRI) [10, 11]. Moreover, the close relationship between Modic changes or endplate defects and LBP has also been verified in some previous studies [12, 13].

Endplates undergo ossification and become highly porous during IVD degeneration [14–16], and more nerve innervation occurs in degenerative endplates than in healthy endplates [17]. It has been reported that osteoclasts generated porous endplates with calcitonin gene-related peptide (CGRP-) positive nerve ending innervation in the mice with lumbar spine instability (LSI) surgery [18]. As pain is generated by nociceptors, porous endplates with sensory nerve innervation should be the precondition for spinal pain in LSI mice.

Prostaglandin E2 (PGE2) is a lipid factor generated at the damaged region in diverse tissues, which could lead to inflammatory or neuropathic pain [19]. In the peripheral nerve system, PGE2 evokes primary sensory neurons, dorsal root ganglion (DRG), through its E-prostanoid (EP) receptors. There are 4 types of G protein-coupled EP receptors (including EP1, EP2, EP3, and EP4) mediating PGE2's function. In the previous studies, the EP4 receptor has been shown to participate in PGE2-induced inflammatory pain and sensory neuron excitability [20, 21]. In addition, selective EP4 receptor antagonists could relieve PGE2-induced inflammatory pain. For instance, it has been reported that some kinds of EP4 receptor antagonists could suppress inflammatory pain caused by carrageenan or by complete Freund's adjuvant [22–24].

The PGE2/EP4 pathway could activate a series of pain-related ion channels, such as transient receptor potential vanilloid 1 (TRPV1) [25]. TRPV1 is made up of four subunits. It is a nonselective, outwardly rectifying cation channel [26], which is distributed not only in the DRG neurons but also in the peripheral terminals [27]. Various factors could activate the TRPV1 channel, such as ligand binding [28], voltage [29], or temperature [30]. The TRPV1 channel is considered to be an aggregator of nocuous chemical, mechanical, or thermal stimuli and is demonstrated to be one of the most important ion channels participating in inflammatory or neuropathic pain [31, 32].

In this study, we found an elevated concentration of PGE2 in the porous endplate of LSI mice. This high-level PGE2 activated the TRPV1 channel in DRG neurons via its EP4 receptor in the CGRP⁺ sensory nerve, which causes spinal hypersensitivity. In particular, L161982, a selective EP4 receptor antagonist, turned down the TRPV1 current and decreased the neuronal excitability of DRG neurons to reduce spinal pain.

2. Materials and Methods

2.1. Mice and In Vivo Treatment. All animal experiments in this study were approved by the Local Committee of Animal Use and Protection of the Third Hospital of Hebei Medical University (Hebei, China). The C57BL/6J male mice were obtained from Shanghai SLAC Laboratory Animal Co. Ltd. (Shanghai, China). We anesthetized the 2-month-old mice with ketamine (at a dosage of 100 mg/kg) and xylazine (at a dosage of 10 mg/kg). For the spinous processes, supraspinous and interspinous ligaments of L3–L5 vertebrae were resected to create the LSI model that led to vertebral endplate degeneration. Correspondingly, the posterior paravertebral muscles of L3–L5 vertebrae were detached in the sham group. At 8 weeks after operation, LSI mice received vehicle or L161982 (5 mg/kg/d) (Tocris, U.S.) by intraperitoneal injection for 2 weeks. To overactivate the TRPV1 channel, LSI mice received capsaicin injection at caudal endplates of L4–L5. Specifically, 2 μ L capsaicin (2 mg/mL) was injected into the left part of caudal endplates of L4–L5 using borosilicate glass capillaries after drilling a hole at the left part of the endplate. The drilling holes were sealed with bone wax immediately after injection to prevent tracer leakage. After capsaicin injection, the wound was sutured, and a heating pad was used to protect mice during recovery from anesthesia. Using an overdose of isoflurane, we euthanized the animals at 4 or 8 weeks after sham or LSI operation or at 2 weeks after L161982 or vehicle treatment.

2.2. μ CT. Mice were euthanized by isoflurane and perfused by 10% buffered formalin. The L3–L5 lumbar spine was collected and examined by μ CT (voltage, 55 kVp; current, 181 μ A; 9.0 μ m per pixel) (Skyscan, 1176). Images were reconstructed by using NRecon v1.6 software (Skyscan). Quantitative analysis of the μ CT results was performed by using CTAn v1.9 software (Skyscan). Six consecutive images of the L4–L5 caudal endplates and L5 vertebrae (coronal view) were selected to show the 3-dimensional reconstruction results by using CTVol v2.0 software (Skyscan).

2.3. Histomorphometry and Immunofluorescence. The lumbar spine or DRG samples were dissected from mice and then were fixed in 10% buffered formalin (4°C, 24 h). The samples of the lumbar spine were decalcified by 0.5 M ethylenediamine tetraacetic acid at 4°C for 3 weeks, and the L2 DRGs were dehydrated by 30% sucrose at 4°C for 48 h. The spine samples were embedded in optimal cutting temperature compound (OCT) or paraffin. The DRG samples were embedded in OCT. We used the 4 μ m thick sections (lumbar spine) for safranin O and fast green staining. 40 μ m thick sections of the spine samples were used for nerve fiber-related immunostaining. 10 μ m thick sections of the spine or DRG sample were used for other immunostaining. For immunofluorescent staining, we incubated the sections (lumbar spine or DRG) with primary antibodies to CGRP (1:100, Abcam, U.S.), COX2 (1:100, Abcam, U.S.), EP4 (1:100, Abcam, U.S.), and TRPV1 (1:200, Abcam, U.S.) (4°C, overnight). Then, we incubated the sections (lumbar spine or DRG) with secondary antibodies (room

temperature, 1 h, avoiding light). The fluorescence or confocal microscopes were used to capture the images of spine or DRG samples. ImageJ software (National Institutes of Health, U.S.) was used for the quantitative analysis.

2.4. Behavioral Testing. Pressure tolerance was measured by the vocalization thresholds (as a nociceptive threshold) using a force gauge (Bioseb). Animals were gently restrained and received the pressure force by a sensor on their skin over the L4-L5 spine. A gradual increase in pressure force (50 g/s) was performed on the mice until the animals made an audible vocalization. To prevent tissue injury, the maximum force was limited to 500 g.

Spontaneous activity was measured by several indicators (including distance traveled, active time, and maximum speed) using the activity wheels (Bioseb). Animals were kept in the cages which are similar to their home cages, and the wheels of the device could be rotated by animals in both directions. The software of this device could record the real-time data of the animals' spontaneous activity.

The pain hypersensitivity in response to mechanical stimulation was measured by hind paw withdrawal frequency (PWF) using the von Frey test with 0.07 or 0.4 g filament (Stoelting). Animals were restrained in a transparent plastic cage, which was put on a metal mesh grid. The mid-plantar position of the animal's hind paw was stimulated by 0.07 or 0.4 g filament through the mesh grid. The filaments should be buckled by enough pressure, and the frequency of mechanical stimulus was 10 times at a 1 s interval. When the hind paw was withdrawn after the stimulation by von Frey filaments, it was recorded.

2.5. Quantitative Real-Time Polymerase Chain Reaction (qRT-PCR). The total RNA of the L4-L5 caudal endplate was extracted by using the TRIzol reagent (Tiangen, Beijing, China). We measured RNA purity by the absorbance of 260/280 nm. With the RevertAid™ First Strand cDNA Synthesis Kit (Thermo Fisher, U.S.), we reverse transcribed 1 μ g RNA into cDNA. Then, we performed qRT-PCR by using the SuperReal PreMix Plus (Tiangen, Beijing, China). Relative expression of target genes was analyzed by the $2^{-\Delta\Delta CT}$ method. The primers used in our study are listed in Table 1.

2.6. Enzyme-Linked Immunosorbent Assay (ELISA). The PGE2 Parameter Assay Kit purchased from R&D Systems (U.S.) was used to measure PGE2 concentrations in the L4-L5 endplates.

2.7. Western Blotting Analysis. We extracted the total protein of the L4-L5 caudal endplate by using RIPA lysis buffer (Beyotime, Shanghai, China). With 12% SDS-polyacrylamide gel electrophoresis, 20 μ g protein was resolved and then was transferred to polyvinylidene fluoride membranes (Millipore, U.S.). We blocked the membranes with 5% milk and incubated them with primary antibodies to EP4 (1:1000, Thermo Fisher, U.S.), TRPV1 (1:1000, Thermo Fisher, U.S.), and GAPDH (1:5000, Abcam, U.S.) (4°C, overnight). Then, we incubated the membranes with secondary antibodies (1:20,000, Rockland, U.S.) (37°C, 1 hour). Finally, with the

Odyssey infrared imaging system and ImageJ software (National Institutes of Health, U.S.), the integrated intensity of the protein band was detected and analyzed, respectively.

2.8. Electrophysiology. As previously described, we selected the small-diameter neurons ($C_m < 42$ pF) for whole-cell patch clamp recording [33].

2.9. Voltage Clamp Recording. Pipettes (3-4 M Ω) were filled with the following: KCl 140, MgCl₂ 1, CaCl₂ 0.5, EGTA 5, HEPES 10, and ATP 3 (in mM) (pH 7.4 with KOH). The bath solution for DRG neurons was as follows: NaCl 150, KCl 5, CaCl₂ 2.5, MgCl₂ 1, glucose 10, and HEPES 10 (in mM) (pH 7.4 with NaOH). TRPV1 currents were acquired via an Axopatch 200B amplifier (Molecular Devices) and low passed at 5 kHz. Cells were constantly held at -60 mV, and TRPV1 currents induced by 1 μ M capsaicin were recorded.

2.10. Current Clamp Recording. The pipette solution contained the following (in mM): KCl 140, EGTA 0.5, HEPES 5, and Mg-ATP 3 (pH 7.3 with KOH). The bath solution for DRG neurons was as follows (in mM): NaCl 140, KCl 3, MgCl₂ 2, CaCl₂ 2, and HEPES 10 (pH 7.3 with NaOH). Cells were examined for action potential firing with a series of 1 s current from 50 pA to 500 pA in 50 pA increments or with a linear ramp of current from 0 pA to 1000 pA (500 ms duration). -200 pA (200 ms) was injected to measure membrane input resistance (R_{in}).

2.11. Statistical Analysis. We conducted data analyses by using SPSS15.0 software. Data were shown as means \pm standard deviations. We used unpaired two-sample *t*-test to compare the means of two groups. We used one-way ANOVA with Bonferroni's post hoc test to compare the means of multiple groups. With the two-way ANOVA with repeated measures, we analyzed the effects of LSI surgery on animals' spinal hypersensitivity and movements at different time points. We established inclusion or exclusion criteria before each experiment and did not exclude any sample during data analysis. $p < 0.05$ was regarded as the statistical significance for all experiments.

3. Results

3.1. Sensory Innervation in the Porous Endplate in LSI Mice. To demonstrate the endplate porosity in LSI mice, we examined the L4-L5 caudal endplates after 4 and 8 weeks of surgery using histological staining and 3-dimensional μ CT. Safranin O and fast green staining results revealed that bone marrow cavities appeared in degenerative endplates in LSI mice, while the endplates in the sham group were cartilaginous and homogenous (Figure 1(a)). Moreover, the reconstruction of 3-dimensional μ CT also showed porous endplates in the LSI mice, while the microstructure of endplates was intact in the sham group (Figures 1(b) and 1(c)). However, LSI surgery did not influence the bone mass of the lumbar vertebra (Supplementary Figure 1A-E).

Immunofluorescent staining showed the innervation of CGRP⁺ nerve fibers in the porous endplate at 4 and 8 weeks

TABLE 1: The primer sequence for qRT-PCR.

Target gene	Forward primer	Reverse primer
COX2	CAGACAACATAAACTGCGCCTT	GATACACCTCTCCACCAATGACC
PGES	TTTCTGCTCTGCAGCACACT	GATTGTCTCCATGTCGTTGC
EP1	GACGATTCCGAAAGACCGCAG	CAACACCACCAACACCAGCAG
EP2	GATGGCAGAGGAGACGGAC	ACTGGCACTGGACTGGGTAGA
EP3	TGCTGGCTCTGGTGGTGAC	ACTCCTTCTCCTTTCCCATCTGTG
EP4	CTGGTGGTGTCTCATCTGCTC	AGGTGGTGTCTGCTTGGGTC
GAPDH	AATGTGTCCGTCGTGGATCTGA	AGTGTAGCCCAAGATGCCCTTC

after LSI surgery, but the CGRP⁺ nerve endings did not exist in homogenous endplates of sham surgery mice (Figures 1(d) and 1(e)).

3.2. Spinal Hypersensitivity Increased in LSI Mice. In the behavior test experiments, the vocalization threshold was recorded as an indicator of pressure tolerance. We found that LSI surgery significantly decreased the pressure tolerance at 4 and 8 weeks, as compared with the sham surgery mice (Figure 2(a)).

We further examined LSI surgery effects on animals' voluntary and spontaneous activity, including distance traveled, active time per 24 h, and maximum speed of movement. All three indicators decreased significantly in LSI mice rather than in the sham group at 4 and 8 weeks (Figures 2(b)–2(d)).

Finally, we performed the von Frey test to evaluate the mechanical hypersensitivity of the hind paw, which could indirectly reflect the severity of LBP. The PWF was increased significantly by LSI surgery at 4 and 8 weeks (Figures 2(e) and 2(f)).

3.3. PGE2 Concentration and EP4 Expression Increased in the Porous Endplate of LSI Mice. Since PGE2 is the cyclooxygenase 2 (COX2) product in the inflammatory environment, we examined COX2 expression, prostaglandin E synthase (PGES) expression, and PGE2 concentration in L4-L5 endplates at 8 weeks in the two groups. qRT-PCR and immunostaining showed an increase in COX-2 expression at 8 weeks in the LSI group relative to the sham group (Figures 3(a)–3(c)). Similarly, PGES mRNA and PGE2 concentration was significantly increased after 8 weeks of LSI surgery in qRT-PCR and ELISA, respectively, relative to the sham group (Figures 3(d) and 3(e)).

Since there were four types of EP receptors (EP1-EP4) mediating PGE2's functions, we used qRT-PCR to evaluate the change of the mRNA levels of these four types of EP receptors after LSI surgery. Interestingly, we found a 6-fold increase in EP4 expression and a 2-fold increase in EP2 expression in the LSI group relative to the sham group by qRT-PCR. But there was no significant difference in EP1 and EP3 expression between the LSI and sham groups (Figure 3(f)).

3.4. EP4/TRPV1 Expressed in CGRP⁺ Nerves in the Porous Endplate and in the CGRP⁺ Neuron of L2 DRG in LSI Mice, Respectively. Immunofluorescent staining showed that

EP4 expression existed in CGRP⁺ nerve fibers in degenerative endplates (Figure 4(a)). Moreover, there was also colocalization of TRPV1 and CGRP in the degenerative endplates, as examined by immunofluorescent staining (Figure 4(b)).

In a previous study, a retrograde tracing experiment was conducted in LSI mice. They found that Dil was significantly retrograded to L1-L2 DRG, especially to L2 DRG [18]. Therefore, we performed the costaining of EP4 and CGRP in L2 DRG. We found that the percentage of EP4⁺CGRP⁺/CGRP⁺ neurons was increased in the LSI group than in the sham group (Figures 4(c) and 4(d)). Meanwhile, we conducted the costaining of TRPV1 and CGRP in L2 DRG. The percentage of TRPV1⁺CGRP⁺/CGRP⁺ neurons was also increased in the LSI group (Figures 4(e) and 4(f)).

3.5. LSI Surgery Increased TRPV1 Channel Current Density in L2 DRG Neurons. Western blotting analysis showed that EP4 and TRPV1 expression increased in L2 DRG in LSI mice compared with the sham group (Figures 5(a) and 5(b)).

L2 DRG neurons were isolated from the mice at 8 weeks and then were cultured overnight. With the whole-cell patch clamp, we did the electrophysiological experiments in small-size neurons (Cm < 42 pF) taken from L2 DRGs [33]. The TRPV1 current amplitude (1 μ M capsaicin) increased significantly in LSI mice (Figures 5(c) and 5(d)). Furthermore, the proportion of capsaicin-responsive neurons also increased in LSI mice relative to the sham group (Figure 5(e)).

3.6. L161982, a Selective EP4 Receptor Antagonist, Reduced Spinal Hypersensitivity in LSI Mice. We used L161982, an EP4-receptor antagonist, to investigate the effects of blocking PGE2/EP4 signaling on spinal hypersensitivity. In pressure tolerance and spontaneous activity tests, L161982 treatment increased pressure tolerance and spontaneous activity of LSI mice compared to the vehicle group (Figures 6(a)–6(d)).

Similarly, the inhibitory effect of L161982 on hind paw mechanical hypersensitivity, as indicated by decreased PWF to 0.07 g or 0.4 g stimulation, was also demonstrated at 2 weeks after treatment (Figures 6(e) and 6(f)).

However, the EP4 receptor antagonist L161982 did not influence the endplate porosity of LSI mice (Supplementary Figure 1F, G).

Moreover, we injected capsaicin at the caudal endplate of L4-L5 of LSI mice to overactivate the TRPV1 channel. We

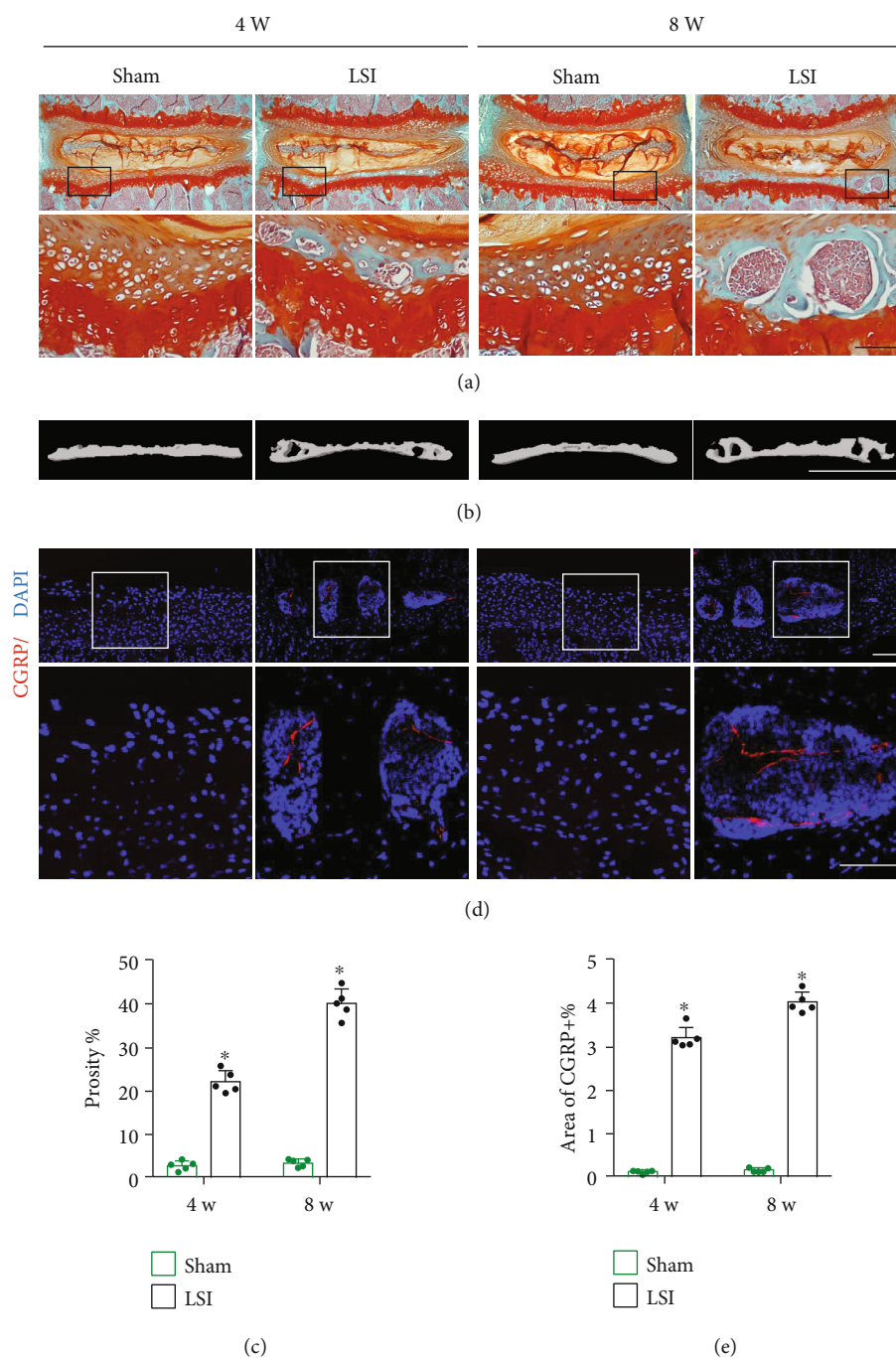


FIGURE 1: Sensory innervation in the porous endplate in LSI mice. (a) Representative images of safranin O and fast green staining of the proteoglycan (red) and bone marrow cavities (green) in the L4-L5 caudal endplates (coronal view) in the LSI or sham group. (b) Representative images of μ CT of the L4-L5 caudal endplates in the LSI or sham group. (c) Quantitative analysis of the percentage of endplate porosity examined by μ CT. (d) Representative images of immunostaining of CGRP (red) and DAPI (blue) in the L4-L5 caudal endplates (coronal view) in the LSI or sham group. (e) Quantitative analysis of the percentage of CGRP⁺ area in the L4-L5 caudal endplates. Scale bars, 50 μ m (a, d). Scale bars, 1 mm (b). * $p < 0.05$ vs. sham group at the corresponding time points. $n = 5$ per group (c, e).

found that TRPV1 overactivation increased spinal hypersensitivity based on the behavior test results. And the spinal hypersensitivity was obviously increased in the LSI+capsaicin+L161982 group, compared with the LSI+L161982 group (Supplementary Figure 2A-F).

3.7. L161982 Reduced TRPV1 Channel Current Density in L2 DRG Neurons. Western blotting analysis showed that EP4 and TRPV1 expression decreased in L2 DRG of mice with L161982 treatment relative to vehicle treatment (Figures 7(a) and 7(b)).

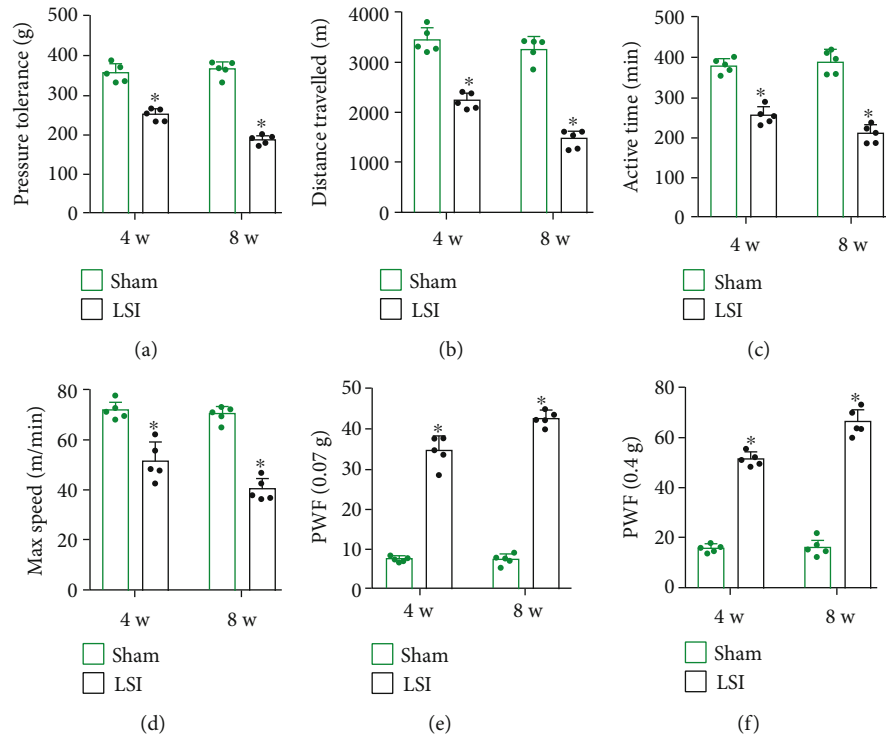


FIGURE 2: Spinal hypersensitivity increased in LSI mice. (a) Pressure tolerance was determined by a vocalization threshold in the LSI or sham group. (b–d) Voluntary and spontaneous activity was evaluated by three indicators including (b) distance traveled, (c) active time per 24 h, and (d) maximum speed of movement. (e, f) The PWF in response to the von Frey test in the LSI or sham group. * $p < 0.05$ vs. sham group at the corresponding time points. $n = 5$ per group.

The TRPV1 current amplitude ($1\mu\text{M}$ capsaicin) decreased significantly in LSI mice with L161982 treatment relative to vehicle treatment (Figures 7(c) and 7(d)).

In addition, the capsaicin-responsive neuron percentage decreased in the L161982 group compared to the vehicle group (Figure 7(e)).

We found that TRPV1 overactivation by capsaicin injection increased TRPV1 current measured with a patch clamp. And the TRPV1 current was obviously increased in the LSI +capsaicin+L161982 group, compared with the LSI +L161982 group (Supplementary Figure 3A, B).

3.8. L161982 Reduces the Excessive Neuronal Excitability of DRG Neurons Induced by LSI. To determine whether LSI surgery increases DRG neuronal excitability and whether PGE2/EP4/TRPV1 pathway activation is responsible for DRG neuron hyperexcitability of LSI mice, evoked action potentials (APs) were studied by current clamp recording.

With step current injection, LSI surgery increased AP firing frequency compared to the sham group, and the AP firing frequency could be reduced by L161982 treatment (Figures 8(a) and 8(b) and Table 2). The minimal depolarizing current that could evoke APs was significantly decreased after LSI operation, which could also be reversed by L161982 (Figure 8(c) and Table 2).

In addition, we evaluated the neuronal hyperexcitability by ramp current stimulation. LSI surgery significantly increased the firing of APs relative to the sham group, and the firing of APs was lowered by L161982 treatment

(Figures 8(d) and 8(e) and Table 2). The percentage of neurons which fired APs was also calculated under the simulation of ramp current injection. We found a higher responding rate in LSI mice compared with the sham group, and the responding rate was significantly lowered by L161982 treatment (Figure 8(f)).

4. Discussion

The IVD degeneration is regarded as one of the most common diseases causing LBP [34]. In recent decades, Modic changes, manifested as signal changes in endplates by MRI, have been demonstrated to be a specific cause of LBP [35]. Endplates undergo ossification and become porous during IVD degeneration, which leads to LBP [36, 37]. It has been reported that more nerve innervation occurs in degenerative endplates than in healthy endplates [17]. In our study, we used a mouse model of vertebral endplate degeneration by LSI surgery [14]. According to behavior test experiments, the pressure tolerance and spontaneous activity significantly decreased in LSI mice, whereas the hind paw mechanical hypersensitivity significantly increased in this model.

Consistent with the previous study [18], we demonstrated that CGRP⁺ nerves innervated in the porous endplate of LSI mice. It has been reported that CGRP could be generated from peripheral or central nerve fibers as the mechanical stimuli on skin [38]. CGRP receptors are demonstrated to be widely distributed in the pain-related pathway [39]. Acute or chronic nociception could promote sensory nerves

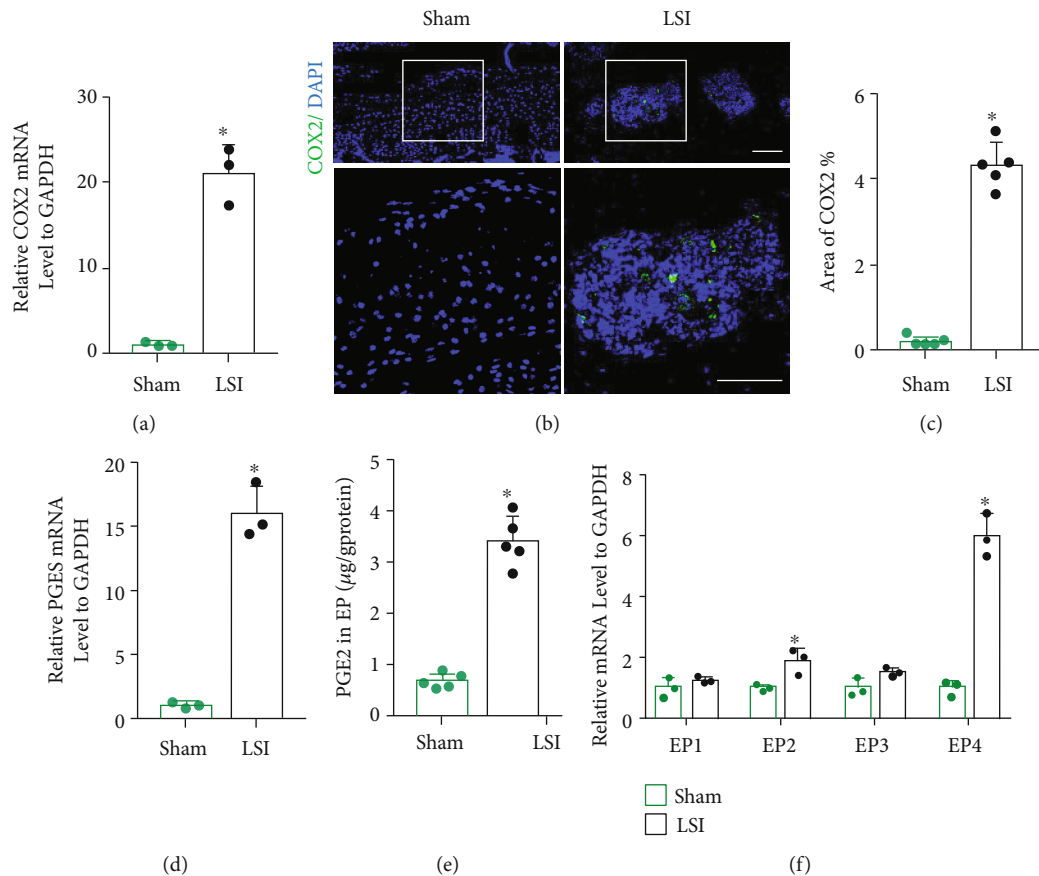


FIGURE 3: PGE2 concentration and EP4 expression increased in the porous endplate of LSI mice. (a) qRT-PCR analysis of COX-2 expression in L4-L5 caudal endplates in the LSI or sham group at 8 weeks. (b) Representative images of immunostaining of COX-2 (green) and DAPI (blue) in the L4-L5 caudal endplates in the LSI or sham group at 8 weeks. (c) Quantitative analysis of the percentage of COX-2⁺ area in endplates. (d) PGES expression by qRT-PCR in L4-L5 caudal endplates in the LSI or sham group at 8 weeks after surgery. (e) PGE2 concentration determined by ELISA analysis in L4-L5 caudal endplates in the LSI or sham group. (f) qRT-PCR analysis of EP1, EP2, EP3, and EP4 expression in L4-L5 caudal endplates in the LSI or sham group at 8 weeks after surgery. Scale bars, 50 μm (b). **p* < 0.05 vs. sham group. *n* = 3 per group (a, d, f); *n* = 5 per group (c, e).

or central terminals to generate more CGRP into the dorsal horn [40, 41]. Thus, the CGRP⁺ nerve innervated in the porous endplate, which was the precondition for spinal hypersensitivity in LSI mice.

In our study, we found that COX2 expression and PGE2 concentration were significantly increased in the porous endplate in LSI mice. Moreover, there was a 6-fold increase in EP4 expression and a 2-fold increase in EP2 expression in the endplate of LSI mice relative to sham mice, but there was no significant difference in EP1 and EP3 expression between the two groups. Thus, the PGE2/EP4 pathway might play a crucial role in spinal hypersensitivity of this animal model. When tissue was damaged, the inflammatory mediators, such as PGE2, were released at the local region or in the spinal cord [42]. PGE2 induces pain sensitization and leads to CGRP release in sensory nerves in vivo [43], as well as in cultured DRG neurons in vitro [44]. PGE2 displays functions via its G protein-coupled receptors (EP1–EP4) [45]. The EP4 receptor is coupled with G protein and activates adenylate cyclase, which enhances the intracellular activation of cAMP-dependent protein kinases (e.g., PKA) [46]. PGE2 has been reported to promote the capsaicin-

evoked CGRP generation by DRG neurons via its G protein-coupled EP receptor, EP4 receptor [21]. In our study, we demonstrated the colocalization of EP4 and CGRP in the nerve endings both in porous endplates and in the DRG neurons. Besides, we also found the colocalization of TRPV1 and CGRP in the nerve endings both in porous endplates and in the DRG neurons by immunofluorescent staining.

The crucial role of TRPV1 activation in spinal pain of LSI mice was also demonstrated in our present study. We found a higher expression of TRPV1 in L2 DRG which innervated in L4-L5 endplates of LSI mice. The upregulated expression of TRPV1 in L2 DRG correlated well with the increase in spinal hypersensitivity. Furthermore, the patch clamp results showed that LSI operation increased TRPV1 current density, suggesting that the functional TRPV1 expression was increased by LSI surgery. Thus, the increased current density of the TRPV1 channel might participate in LSI-induced spinal hypersensitivity.

TRPV1, a member of TRP ion channels, has been recognized as “a molecular gateway” to nociceptive sensation. TRPV1 was mainly distributed in the dorsal root ganglion,

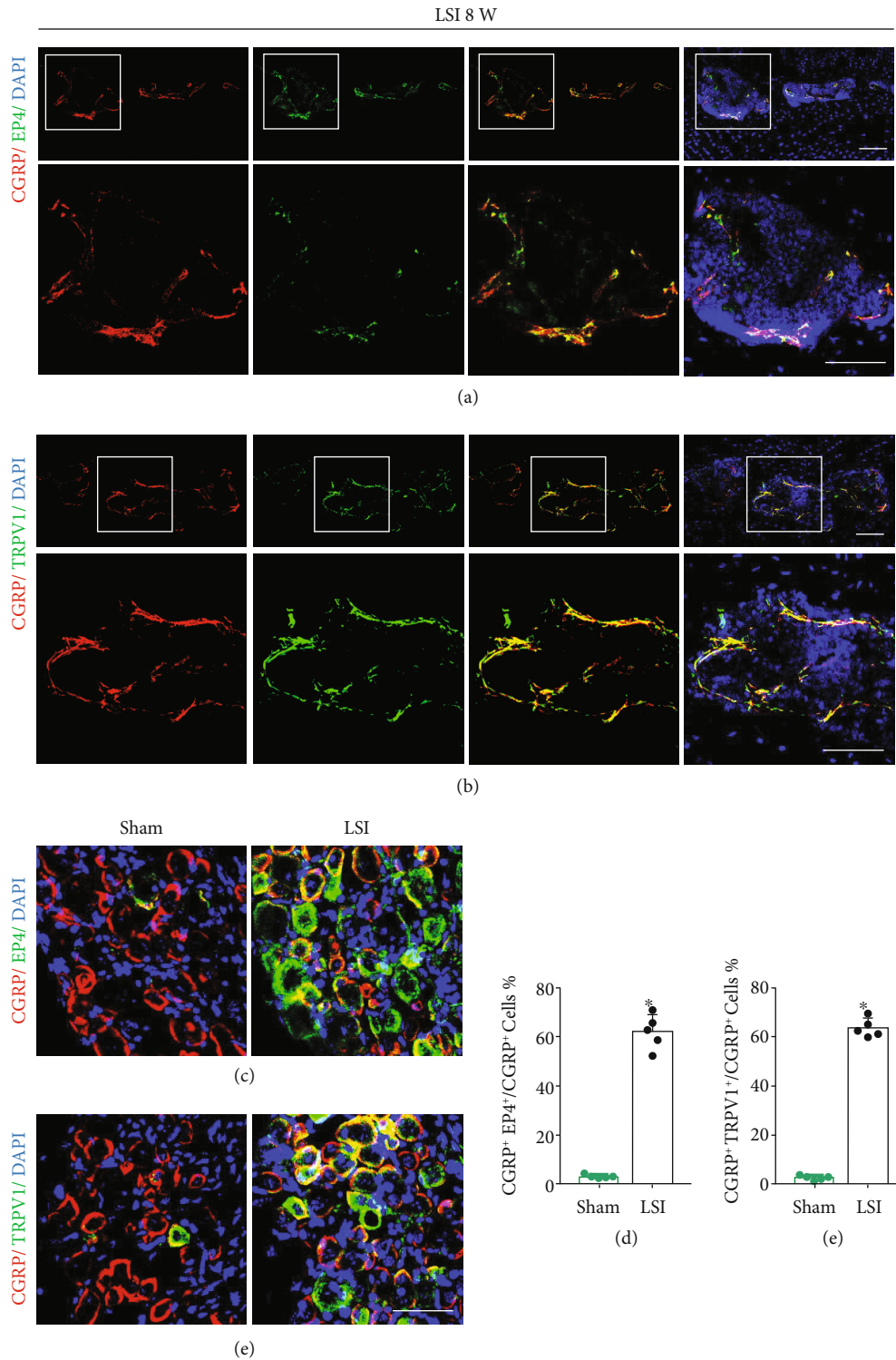


FIGURE 4: EP4 and TRPV1 expressed in CGRP⁺ nerves and in CGRP⁺ DRG neurons of LSI mice, respectively. (a) Representative images of the coimmunostaining of CGRP and EP4 in L4-L5 caudal endplates in the LSI or sham group at 8 weeks. (b) Representative images of the coimmunostaining of CGRP and TRPV1 in L4-L5 caudal endplates in the LSI or sham group at 8 weeks. (c) Representative images of the coimmunostaining of CGRP and EP4 in L2 DRGs in the LSI or sham group at 8 weeks. (d) The percentage of the EP4⁺CGRP⁺ area relative to the CGRP⁺ area in the LSI or sham group. (e) Representative images of the coimmunostaining of CGRP and TRPV1 in L2 DRGs in the LSI or sham group at 8 weeks. (f) The percentage of the TRPV1⁺CGRP⁺ area relative to the CGRP⁺ area in the LSI or sham group. Scale bars, 50 μ m (a, b, c, e). * $p < 0.05$ vs. sham group. $n = 5$ per group (d, f).

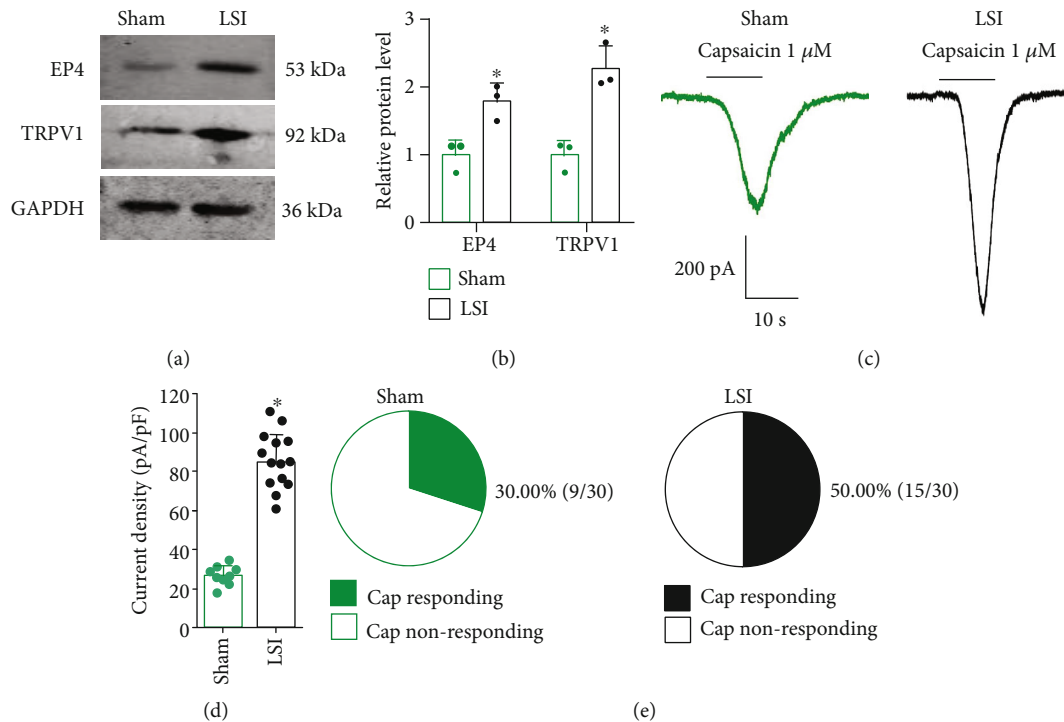


FIGURE 5: LSI surgery increased TRPV1 expression and TRPV1 channel current density in L2 DRG neurons. (a) Representative images of western blotting of EP4 and TRPV1 expression in L2 DRGs in the LSI or sham group at 8 weeks after surgery. (b) Quantitative analysis of EP4 and TRPV1 expression in L2 DRGs in the LSI or sham group at 8 weeks after surgery ($n = 3$ per group). (c) Representative traces of TRPV1 current induced by 1 μM capsaicin. (d) The TRPV1 current amplitude induced by 1 μM capsaicin increased significantly in LSI mice ($n = 9$ –15 cells per group). (e) The number of 1 μM capsaicin-responsive neurons was increased after LSI treatment ($n = 30$ cells per group). * $p < 0.05$ vs. sham group.

trigeminal ganglion, spinal cord, and peripheral nerve endings. In addition, TRPV1 was also found in some nonneural tissues such as the lung, gastrointestinal tract, and respiratory tract. In recent years, it has been found that TRPV1 is important in mediating hypersensitivity mediated by inflammation nocuous chemical, mechanical, or thermal stimuli in the airway, skin, gastrointestinal tract, and other organs [47–51]. There is less evidence about TRPV1-mediated hypersensitivity in a vertebral endplate degeneration model. However, in the arthritis model, whose pathogenesis is similar to the vertebral endplate degeneration model, the fact that TRPV1 is important in mediating hypersensitivity has been proven. Thermal hyperalgesia and osteoarthritic pain are associated with the activation of the TRPV1 channel [52]. TRPV1 may contribute to the pain hypersensitivity and inflammation of arthritis via an ERK-mediated pathway [53]. Polypeptide APHC3, a mode-selective TRPV1 antagonist, can significantly reverse mechanical hypersensitivity in the arthritis model [54]. The above evidence shows that TRPV1 is important in mediating hypersensitivity in degenerative osteoarthritis.

TRPV1 contributes to spinal hypersensitivity. Evidence proved that hypersensitivity induced by activation of spinal cord PAR2 receptors is mediated by TRPV1 receptors [55]. TRPV1 was functionally expressed in GABAergic spinal interneurons, and activation of spinal TRPV1 resulted in long-term depression of excitatory inputs and a reduction of inhibitory signaling to spinothalamic tract projection neu-

rons and eventually leads to central sensitization [56]. Evidence has demonstrated that blocking TRPV1 could relieve spinal hypersensitivity. The thermal and mechanical hypersensitivity in the spine can be relieved by the TRPV1 selective antagonist [57]. Intrathecal administration of the antisense oligonucleotide against TRPV1 reduced mechanical hypersensitivity in rats with spinal nerve ligation [58]. The hypersensitivity induced by lumbar 4 spinal nerve ligation in mice was completely reversed by the TRPV1 antagonist A-425619 [59]. The threshold against heat sensitivity in the L5 ipsilateral dorsal horn of the spinal cord was markedly prolonged in *Trpv1*^{-/-} mice than in WT mice [60]. Capsazepine, a TRPV1 blocker, could greatly inhibit thermal hypersensitivity in a spinally sensitized state [61]. AMG9810, the specific antagonist of TRPV1, could significantly attenuate the activation of bilateral spinal astrocytes and microglia [33]. The above evidence indicates that blocking TRPV1 could relieve spinal hypersensitivity.

Actually, there is a close relationship between the PGE2/EP4 pathway and TRPV1 channel. PGE2 has been shown to increase surface trafficking of EP4 and TRPV1 in vitro [62]. In a restraint stress rat model, overproduced PGE2 in injured nerves chronically increased EP4 and TRPV1 expression in primary sensory neurons, and EP4 antagonists relieved both inflammatory and neuropathic pain [25]. In our study, using behavior test experiments, we found that L161982, an EP4 receptor antagonist, relieved spinal hypersensitivity by blocking the PGE2/EP4 pathway

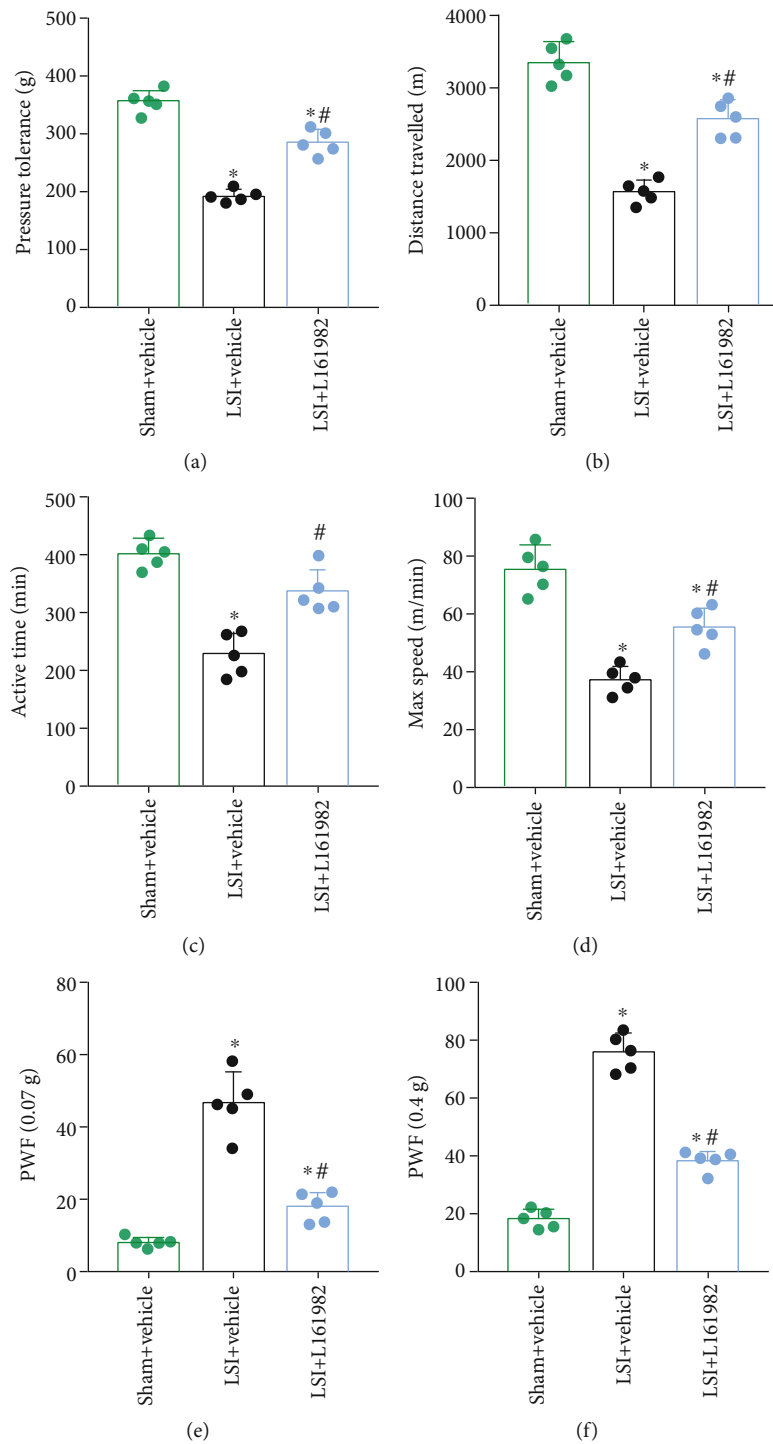


FIGURE 6: L161982 reduced spinal hypersensitivity of LSI mice. (a) Pressure tolerance was determined by a vocalization threshold at 2 weeks after L161982 or vehicle treatment. (b–d) Voluntary and spontaneous activity was evaluated by three indicators including (b) distance traveled, (c) active time per 24 h, and (d) maximum speed of movement. (e, f) The PWF in response to the von Frey test (0.07 g or 0.4 g) at 2 weeks after L161982 or vehicle treatment. * $p < 0.05$ vs. sham+vehicle group; # $p < 0.05$ vs. LSI+vehicle group. $n = 5$ per group.

in LSI mice. Furthermore, L161982 decreased the TRPV1 current density and the proportion of capsaicin-responsive neurons relative to L2 DRG neurons in LSI mice.

PGE2 acts on target cells through its receptors EP1, EP2, EP3, and EP4. Interactions of PGE2/EP4 and TRPV1 in pain hypersensitivity have been proven. PGE2 enhanced

capsaicin-induced currents in DRG neurons through EP4 [20] and EP4-PKA signaling cascades [63]. PGE2 potentiated pain evoked by the TRPV1 agonist [64]. The upregulation of TRPV1 in DRG neurons was suppressed by a selective COX2 inhibitor, suggesting that PGE2 stimulates TRPV1 synthesis in DRG neurons [65]. Furthermore,

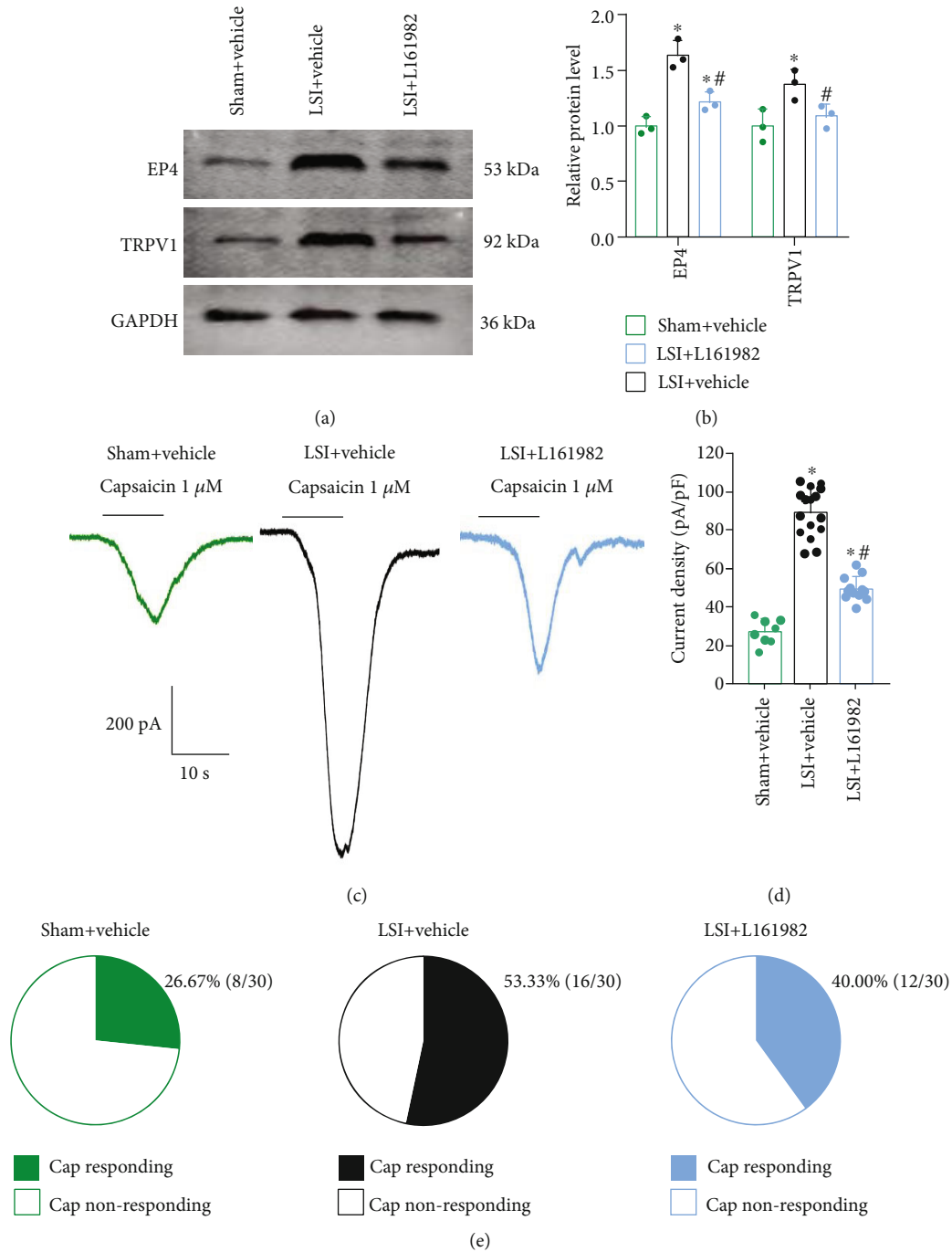


FIGURE 7: L161982 reduced TRPV1 expression and TRPV1 channel current density in L2 DRG neurons of LSI mice. (a) Representative images of western blotting of EP4 and TRPV1 expression in L2 DRGs at 2 weeks in the sham+vehicle, LSI+vehicle, and LSI+L161982 group. (b) Quantitative analysis of EP4 and TRPV1 expression in L2 DRGs at 2 weeks in the sham+vehicle, LSI+vehicle, and LSI+L161982 group ($n = 3$ per group). (c) Representative traces of TRPV1 current induced by 1 μM capsaicin ($n = 8-16$ cells per group). (d) Quantitative analysis of 1 μM capsaicin-induced current densities ($n = 8-16$ cells per group). (e) The percentage of the neurons in response to 1 μM capsaicin ($n = 30$ cells per group). * $p < 0.05$ vs. sham+vehicle group, # $p < 0.05$ vs. LSI+vehicle group.

PGE2-induced thermal hyperalgesia was abolished in TRPV1-knockout mice [63]. The above evidences suggest that functional interactions between PGE2/EP4 and TRPV1 are crucial to PGE2-induced nociceptor sensitization. A recent study has proven that PGE2/EP4 increased TRPV1 cell surface trafficking in DRG neurons via cAMP/PKA/ERK/MAPK sig-

naling pathways. Moreover, PGE2 induced TRPV1 externalization and enhances TRPV1 activity [62].

In our study, we showed that L2 DRG neurons exhibited an increased excitability in the LSI model. The hyperexcitability of DRG neurons was decreased by the inhibition of the PEG2/EP4 pathway with L161982. These results showed

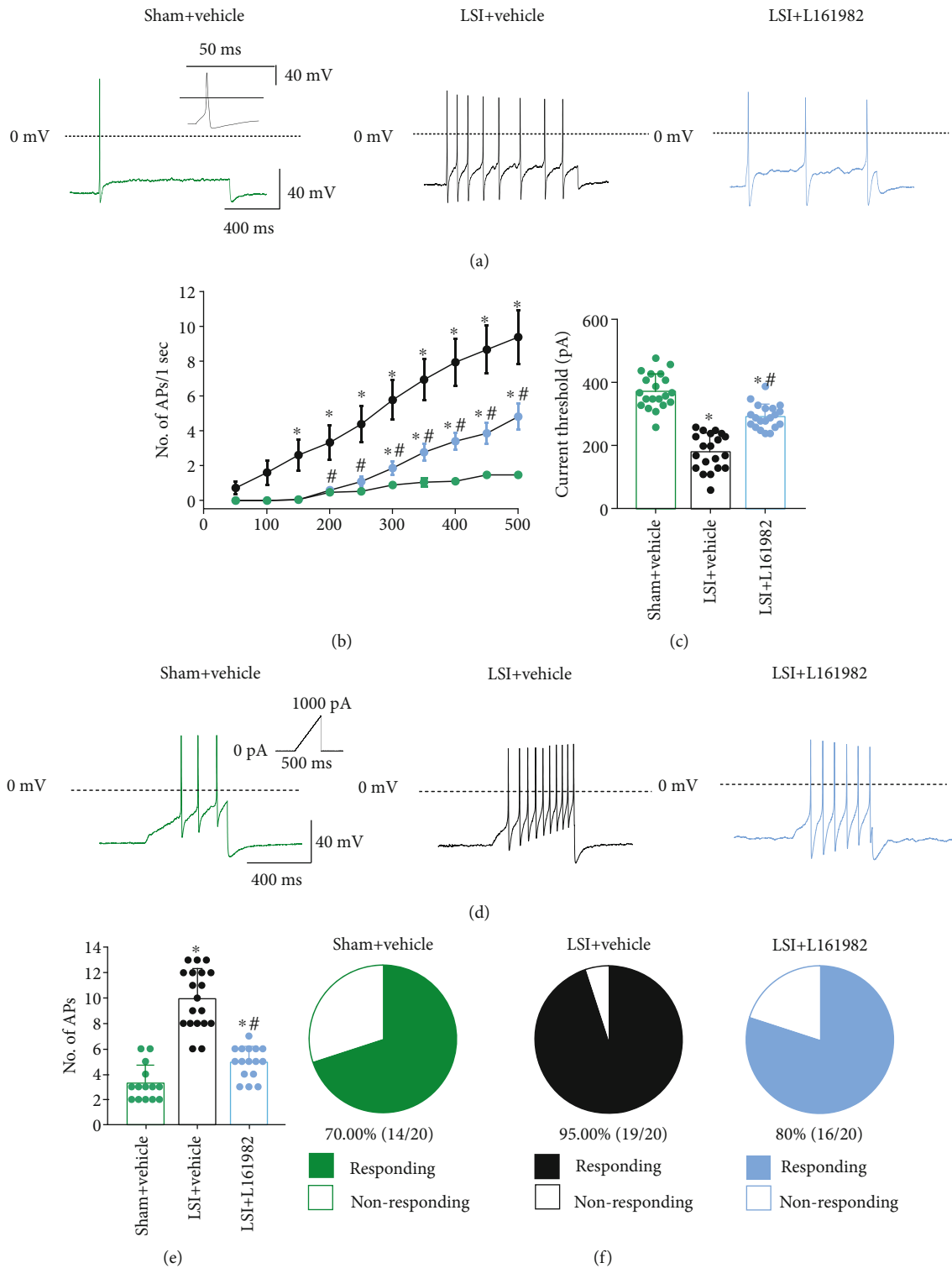


FIGURE 8: L161982 treatment attenuated LSI-induced increase in neuronal excitability. (a) AP firing traces in L2 DRG neurons to 1 s, 300 pA depolarizing current injection. (b) Quantitative analysis of APs induced by step current injection in the sham+vehicle, LSI+vehicle, and LSI+L161982 groups. (c) Current threshold for APs in the sham+vehicle, LSI+vehicle, and LSI+L161982 groups ($n = 20$ cells per group). (d) Current clamp recordings with ramp current stimulation starting from 0 pA to 1000 pA of 500 ms duration. (e) Quantitative analysis of APs induced by ramp current stimulation ($n = 14$ – 19 cells per group). (f) The percentage of the neurons in response to ramp current stimulation ($n = 20$ cells per group). * $p < 0.05$ vs. sham+vehicle group, # $p < 0.05$ vs. LSI+vehicle group.

TABLE 2: Summary of current clamp properties of DRG neurons.

Current clamp properties	Sham+vehicle			LSI+vehicle			LSI+L161982		
	Mean	SD	<i>n</i>	Mean	SD	<i>n</i>	Mean	SD	<i>n</i>
Input resistance (MΩ)	520.91	154.55	20	521.60	153.04	20	497.21	172.56	20
Capacitance (pF)	22.32	4.88	20	22.46	4.92	20	23.50	3.96	20
RMP (mV)	-59.00	7.57	20	-58.50	6.64	20	-58.65	7.39	20
AP amplitude (mV)	112.90	9.94	20	114.43	10.03	20	113.20	6.60	20
Threshold (pA, ramp protocol)	470.00	134.54	14	204.26*	81.77	19	351.38**	71.45	16

* $p < 0.05$ vs. sham+vehicle group, ** $p < 0.05$ vs. LSI+vehicle group.

that TRPV1 channel activated by the PEG2/EP4 pathway participated in the enhancement of the excitability of DRG neurons in LSI mice. It has been reported that the hyperexcitability of DRG neurons leads to central sensitization and chronic pain [66]. Therefore, the TRPV1 channel activated by the PEG2/EP4 pathway caused the hyperexcitability of DRG neurons, which could drive spinal pain.

In conclusion, the PGE2/EP4 pathway in the porous endplate could activate the TRPV1 channel in DRG neurons to cause spinal hypersensitivity in LSI mice. L161982, a selective EP4 receptor antagonist, could turn down the TRPV1 current and decrease the neuronal excitability in DRG neurons to reduce spinal pain.

Data Availability

The data used to support the findings of this study are available from the corresponding author upon request.

Conflicts of Interest

The authors declare that they have no conflicts of interest.

Authors' Contributions

Sijing Liu, Qiong Wang, and Ziyi Li contributed equally to the work.

Acknowledgments

This study was supported by the Basic Research Program for Beijing-Tianjin-Hebei Coordination (No. 19JCZDJC 65500[Z]), Osteoporosis Program for Young Doctors (No. GX20191107), Government Foundation to Train Clinical Talents and Leading Specialists (No. 361005), Medical Application Technology Program of Hebei Province (No. G2019008), Tianjin Outstanding Youth Fund Project (No. 20JCJC00230), and National Natural Science Foundation of China (No. 81971660).

Supplementary Materials

Supplementary Figure 1: the effects of LSI treatment on vertebra bone mass and L161982 treatment on endplate porosity. (A) Representative three-dimensional high-resolution μ CT images of the trabecular bone of the L5 vertebra (coronal view) at 8 weeks after sham or LSI surgery. (B–E) Quan-

titative analysis of the trabecular bone volume/total volume (BV/TV, B) and trabecular bone number (Tb.N, C), trabecular bone thickness (Tb.Th, D), and trabecular bone separation distribution (Tb.Sp, E) in the L5 vertebra determined by μ CT. * $p < 0.05$ vs. sham group. $n = 5$ per group. (F) Representative images of μ CT of the L4-L5 caudal endplates (coronal view) in the sham+vehicle, LSI+vehicle, or LSI+L161982 group. (G) Quantitative analysis of the percentage of endplate porosity examined by μ CT. * $p < 0.05$ vs. sham+vehicle group, ** $p < 0.05$ vs. LSI+vehicle group. $n = 5$ per group. Supplementary Figure 2: spinal hypersensitivity increased by TRPV1 overactivation. (A) Pressure tolerance was determined by the vocalization threshold in the LSI+vehicle, LSI+L161982, LSI+capsaicin, or LSI+L161982+capsaicin group. (B–D) Voluntary and spontaneous activity was evaluated by three indicators including (B) distance traveled, (C) active time per 24 h, and (D) maximum speed of movement. (E, F) The PWF in response to the von Frey test (0.07 g or 0.4 g) in the LSI+vehicle, LSI+L161982, LSI+capsaicin, or LSI+L161982+capsaicin group. * $p < 0.05$ vs. LSI+vehicle group, ** $p < 0.05$ vs. LSI+L161982 group, † $p < 0.05$ vs. LSI+capsaicin group. $n = 5$ per group. Supplementary Figure 3: TRPV1 channel current density in L2 DRG neurons by TRPV1 overactivation. (A) Representative traces of TRPV1 current induced by 1 μ M capsaicin. (B) Quantitative analysis of 1 μ M capsaicin-induced current densities ($n = 11-15$ cells per group). * $p < 0.05$ vs. LSI+vehicle group, ** $p < 0.05$ vs. LSI+L161982 group, † $p < 0.05$ vs. LSI+capsaicin group. (Supplementary Materials)

References

- [1] Global, regional, and national incidence, prevalence, and years lived with disability for 354 diseases and injuries for 195 countries and territories, “1990-2017: a systematic analysis for the Global Burden of Disease Study 2017,” *Lancet*, vol. 392, no. 10159, pp. 1789–1858, 2018.
- [2] D. Hoy, C. Bain, G. Williams et al., “A systematic review of the global prevalence of low back pain,” *Arthritis and Rheumatism*, vol. 64, no. 6, pp. 2028–2037, 2012.
- [3] R. D. Meucci, A. G. Fassa, and N. M. Faria, “Prevalence of chronic low back pain: systematic review,” *Revista de Saúde Pública*, vol. 49, 2015.
- [4] A. Onda and M. Kimura, “Reduction in anxiety during treatment with exercise and duloxetine is related to improvement of low back pain-related disability in patients with non-specific chronic low back pain,” *Fukushima Journal of Medical Science*, vol. 66, no. 3, pp. 148–155, 2020.





- [5] A. Wu, L. March, X. Zheng et al., "Global low back pain prevalence and years lived with disability from 1990 to 2017: estimates from the Global Burden of Disease Study 2017," *Annals of Translational Medicine*, vol. 8, no. 6, 2020.
- [6] I. K. Ashton, S. Roberts, D. C. Jaffray, J. M. Polak, and S. M. Eisenstein, "Neuropeptides in the human intervertebral disc," *Journal of Orthopaedic Research*, vol. 12, no. 2, pp. 186–192, 1994.
- [7] A. Fagan, R. Moore, B. Vernon Roberts, P. Blumbergs, and R. Fraser, "ISSLS prize winner: the innervation of the intervertebral disc: a quantitative analysis," *Spine (Phila Pa 1976)*, vol. 28, no. 23, pp. 2570–2576, 2003.
- [8] Y. Wang, T. Videman, and M. C. Battie, "Lumbar vertebral endplate lesions: prevalence, classification, and association with age," *Spine (Phila Pa 1976)*, vol. 37, no. 17, pp. 1432–1439, 2012.
- [9] M. F. Brown, M. V. J. Hukkanen, I. D. McCarthy et al., "Sensory and sympathetic innervation of the vertebral endplate in patients with degenerative disc disease," *Journal of Bone and Joint Surgery. British Volume (London)*, vol. 79-B, no. 1, pp. 147–153, 1997.
- [10] M. Brayda-Bruno, D. Albano, G. Cannella, F. Galbusera, and A. Zerbi, "Endplate lesions in the lumbar spine: a novel MRI-based classification scheme and epidemiology in low back pain patients," *European Spine Journal*, vol. 27, no. 11, pp. 2854–2861, 2018.
- [11] L. Chen, M. C. Battie, Y. Yuan, G. Yang, Z. Chen, and Y. Wang, "Lumbar vertebral endplate defects on magnetic resonance images: prevalence, distribution patterns, and associations with back pain," *The Spine Journal*, vol. 20, no. 3, pp. 352–360, 2020.
- [12] K. Luoma, T. Vehmas, L. Kerttula, M. Gronblad, and E. Rinne, "Chronic low back pain in relation to Modic changes, bony endplate lesions, and disc degeneration in a prospective MRI study," *European Spine Journal*, vol. 25, no. 9, pp. 2873–2881, 2016.
- [13] J. Järvinen, J. Karppinen, J. Niinimäki et al., "Association between changes in lumbar Modic changes and low back symptoms over a two-year period," *BMC Musculoskeletal Disorders*, vol. 16, no. 1, 2015.
- [14] Q. Bian, A. Jain, X. Xu et al., "Excessive Activation of TGF β by Spinal Instability Causes Vertebral Endplate Sclerosis," *Scientific Reports*, vol. 6, no. 1, 2016.
- [15] Q. Liu, Z. Yang, Y. Liu et al., "Cervical spinal instability causes vertebral microarchitecture change and vertebral endplate lesion in rats," *J Orthop Translat.*, vol. 24, pp. 209–217, 2020.
- [16] Y. Wang, T. Videman, and M. C. Battie, "ISSLS prize winner: lumbar vertebral endplate lesions: associations with disc degeneration and back pain history," *Spine (Phila Pa 1976)*, vol. 37, no. 17, pp. 1490–1496, 2012.
- [17] A. J. Fields, E. C. Liebenberg, and J. C. Lotz, "Innervation of pathologies in the lumbar vertebral end plate and intervertebral disc," *The Spine Journal*, vol. 14, no. 3, pp. 513–521, 2014.
- [18] S. Ni, Z. Ling, X. Wang et al., "Sensory innervation in porous endplates by netrin-1 from osteoclasts mediates PGE₂-induced spinal hypersensitivity in mice," *Nature Communications*, vol. 10, no. 1, p. 5643, 2019.
- [19] A. Kawabata, "Prostaglandin E₂ and pain—an update," *Biological & Pharmaceutical Bulletin*, vol. 34, no. 8, pp. 1170–1173, 2011.
- [20] C.-R. Lin, F. Amaya, L. Barrett et al., "Prostaglandin E₂ Receptor EP₄ contributes to inflammatory pain hypersensitivity," *The Journal of Pharmacology and Experimental Therapeutics*, vol. 319, no. 3, pp. 1096–1103, 2006.
- [21] M. D. Southall and M. R. Vasko, "Prostaglandin Receptor Subtypes, EP₃C and EP₄, Mediate the Prostaglandin E₂-induced cAMP Production and Sensitization of Sensory Neurons," *The Journal of Biological Chemistry*, vol. 276, no. 19, pp. 16083–16091, 2001.
- [22] J. Colucci, M. Boyd, C. Berthelette et al., "Discovery of 4-([1-[4-(trifluoromethyl)benzyl]-1H-indol-7-yl]carbonyl)amino)cyclopropyl]benzoic acid (MF-766), a highly potent and selective EP₄ antagonist for treating inflammatory pain," *Bioorganic & Medicinal Chemistry Letters*, vol. 20, no. 12, pp. 3760–3763, 2010.
- [23] K. Nakao, A. Murase, H. Ohshiro et al., "CJ-023,423, a novel, potent and selective prostaglandin EP₄ Receptor antagonist with antihyperalgesic properties," *The Journal of Pharmacology and Experimental Therapeutics*, vol. 322, no. 2, pp. 686–694, 2007.
- [24] A. Murase, T. Okumura, A. Sakakibara, H. Tonai-Kachi, K. Nakao, and J. Takada, "Effect of prostanoid EP₄ receptor antagonist, CJ-042,794, in rat models of pain and inflammation," *European Journal of Pharmacology*, vol. 580, no. 1–2, pp. 116–121, 2008.
- [25] W. Ma, L. Li, and S. Xing, "PGE₂/EP₄ receptor and TRPV1 channel are involved in repeated restraint stress-induced prolongation of sensitization pain evoked by subsequent PGE₂ challenge," *Brain Research*, vol. 1721, p. 146335, 2019.
- [26] S. Bevan, T. Quallo, and D. A. Andersson, "Trpv1," *Handbook of Experimental Pharmacology*, vol. 222, pp. 207–245, 2014.
- [27] S. Heber, C. I. Ciotu, G. Hartner et al., "TRPV1 antagonist BCTC inhibits pH 6.0-induced pain in human skin," *Pain*, vol. 161, no. 7, pp. 1532–1541, 2020.
- [28] K. Hui, B. Liu, and F. Qin, "Capsaicin activation of the pain receptor, VR1: multiple open states from both partial and full binding," *Biophysical Journal*, vol. 84, no. 5, pp. 2957–2968, 2003.
- [29] J. A. Matta and G. P. Ahern, "Voltage is a partial activator of rat thermosensitive TRP channels," *The Journal of Physiology*, vol. 585, no. 2, pp. 469–482, 2007.
- [30] J. Grandl, S. E. Kim, V. Uzzell et al., "Temperature-induced opening of TRPV1 ion channel is stabilized by the pore domain," *Nature Neuroscience*, vol. 13, no. 6, pp. 708–714, 2010.
- [31] C. Wang, L. Gu, Y. Ruan et al., "Pirt together with TRPV1 is involved in the regulation of neuropathic pain," *Neural Plasticity*, vol. 2018, Article ID 4861491, 10 pages, 2018.
- [32] C. Hanack, M. Moroni, W. C. Lima et al., "GABA blocks pathological but not acute TRPV1 pain signals," *Cell*, vol. 160, no. 4, pp. 759–770, 2015.
- [33] Q. Hu, Q. Wang, C. Wang et al., "TRPV1 channel contributes to the behavioral hypersensitivity in a rat model of complex regional pain syndrome type 1," *Frontiers in Pharmacology*, vol. 10, 2019.
- [34] Y. Chen, J. Bao, Q. Yan, C. Wu, H. Yang, and J. Zou, "Distribution of Modic changes in patients with low back pain and its related factors," *European Journal of Medical Research*, vol. 24, no. 1, p. 34, 2019.
- [35] M. T. Modic, P. M. Steinberg, J. S. Ross, T. J. Masaryk, and J. R. Carter, "Degenerative disk disease: assessment of changes in

- vertebral body marrow with MR imaging," *Radiology*, vol. 166, no. 1, pp. 193–199, 1988.
- [36] J. C. Lotz, A. J. Fields, and E. C. Liebenberg, "The role of the vertebral end plate in low back pain," *Global Spine Journal*, vol. 3, no. 3, pp. 153–163, 2013.
- [37] S. Dudli, A. J. Fields, D. Samartzis, J. Karppinen, and J. C. Lotz, "Pathobiology of Modic changes," *European Spine Journal*, vol. 25, no. 11, pp. 3723–3734, 2016.
- [38] S. K. Sauer, G. M. Bove, B. Averbeck, and P. W. Reeh, "Rat peripheral nerve components release calcitonin gene-related peptide and prostaglandin E₂ in response to noxious stimuli: evidence that nervi nervorum are nociceptors," *Neuroscience*, vol. 92, no. 1, pp. 319–325, 1999.
- [39] W. Ma, J. G. Chabot, K. J. Powell, K. Jhamandas, I. M. Dickerson, and R. Quirion, "Localization and modulation of calcitonin gene-related peptide-receptor component protein-immunoreactive cells in the rat central and peripheral nervous systems," *Neuroscience*, vol. 120, no. 3, pp. 677–694, 2003.
- [40] M. G. Buzzi, W. B. Carter, T. Shimizu, H. Heath 3rd, and M. A. Moskowitz, "Dihydroergotamine and sumatriptan attenuate levels of CGRP in plasma in rat superior sagittal sinus during electrical stimulation of the trigeminal ganglion," *Neuropharmacology*, vol. 30, no. 11, pp. 1193–1200, 1991.
- [41] C. R. Morton and W. D. Hutchison, "Morphine does not reduce the intraspinal release of calcitonin gene-related peptide in the cat," *Neuroscience Letters*, vol. 117, no. 3, pp. 319–324, 1990.
- [42] A. B. Malmberg and T. L. Yaksh, "Cyclooxygenase inhibition and the spinal release of prostaglandin E₂ and amino acids evoked by paw formalin injection: a microdialysis study in unanesthetized rats," *The Journal of Neuroscience*, vol. 15, no. 4, pp. 2768–2776, 1995.
- [43] L. Andreeva and H. P. Rang, "Effect of bradykinin and prostaglandins on the release of calcitonin gene-related peptide-like immunoreactivity from the rat spinal cord in vitro," *British Journal of Pharmacology*, vol. 108, no. 1, pp. 185–190, 1993.
- [44] M. R. Vasko, W. B. Campbell, and K. J. Waite, "Prostaglandin E₂ enhances bradykinin-stimulated release of neuropeptides from rat sensory neurons in culture," *The Journal of Neuroscience*, vol. 14, no. 8, pp. 4987–4997, 1994.
- [45] D. Shamir, S. Keila, and M. Weinreb, "A selective EP₄ receptor antagonist abrogates the stimulation of osteoblast recruitment from bone marrow stromal cells by prostaglandin E₂ in vivo and in vitro," *Bone*, vol. 34, no. 1, pp. 157–162, 2004.
- [46] S. Tumati, W. R. Roeske, T. W. Vanderah, and E. V. Varga, "Sustained morphine treatment augments prostaglandin E₂-evoked calcitonin gene-related peptide release from primary sensory neurons in a PKA-dependent manner," *European Journal of Pharmacology*, vol. 648, no. 1–3, pp. 95–101, 2010.
- [47] L. Y. Lee and Q. Gu, "Role of TRPV1 in inflammation-induced airway hypersensitivity," *Current Opinion in Pharmacology*, vol. 9, no. 3, pp. 243–249, 2009.
- [48] M. E. Barabas and C. L. Stucky, "TRPV1, but not TRPA1, in primary sensory neurons contributes to cutaneous incision-mediated hypersensitivity," *Molecular Pain*, vol. 9, p. 1744–8069-9-9, 2013.
- [49] S. Li and L. P. Duan, "Research progress in the relationship between TRPV1 and visceral hypersensitivity in functional gastrointestinal diseases," *Beijing Da Xue Xue Bao Yi Xue Ban*, vol. 43, no. 2, pp. 311–314, 2011.
- [50] Y. Wang, "The functional regulation of TRPV1 and its role in pain sensitization," *Neurochemical Research*, vol. 33, no. 10, pp. 2008–2012, 2008.
- [51] T. K. Lapointe and C. Altier, "The role of TRPA1 in visceral inflammation and pain," *Channels (Austin, Tex.)*, vol. 5, no. 6, pp. 525–529, 2011.
- [52] Y.-J. Sung, N. Sofoluke, M. Nkamany et al., "A novel inhibitor of active protein kinase G attenuates chronic inflammatory and osteoarthritic pain," *Pain*, vol. 158, no. 5, pp. 822–832, 2017.
- [53] Y. Chen, H. H. Willcockson, and J. G. Valtchanoff, "Vanilloid receptor TRPV1-mediated phosphorylation of ERK in murine adjuvant arthritis," *Osteoarthritis and Cartilage*, vol. 17, no. 2, pp. 244–251, 2009.
- [54] Y. A. Logashina, Y. A. Palikova, V. A. Palikov et al., "Anti-inflammatory and analgesic effects of TRPV1 polypeptide modulator APHC3 in models of osteo- and rheumatoid arthritis," *Mar Drugs*, vol. 19, no. 1, p. 39, 2021.
- [55] P. Mrozkova, D. Spicarova, and J. Palecek, "Hypersensitivity induced by activation of spinal cord PAR2 receptors is partially mediated by TRPV1 receptors," *PLoS One*, vol. 11, no. 10, p. e0163991, 2016.
- [56] Y. H. Kim, S. K. Back, A. J. Davies et al., "TRPV1 in GABAergic interneurons mediates neuropathic mechanical allodynia and disinhibition of the nociceptive circuitry in the spinal cord," *Neuron*, vol. 74, no. 4, pp. 640–647, 2012.
- [57] E. Uchytlova, D. Spicarova, and J. Palecek, "Hypersensitivity induced by intrathecal bradykinin administration is enhanced by N-oleoyldopamine (OLDA) and prevented by TRPV1 antagonist," *International Journal of Molecular Sciences*, vol. 22, no. 7, p. 3712, 2021.
- [58] T. Christoph, C. Gillen, J. Mika et al., "Antinociceptive effect of antisense oligonucleotides against the vanilloid receptor VR1/TRPV1," *Neurochemistry International*, vol. 50, no. 1, pp. 281–290, 2007.
- [59] D. Vilceanu, P. Honore, Q. H. Hogan, and C. L. Stucky, "Spinal nerve ligation in mouse upregulates TRPV1 heat function in injured IB4-positive nociceptors," *The Journal of Pain*, vol. 11, no. 6, pp. 588–599, 2010.
- [60] K. Baba, M. Kawasaki, H. Nishimura et al., "Heat hypersensitivity is attenuated with altered expression level of spinal astrocytes after sciatic nerve injury in TRPV1 knockout mice," *Neuroscience Research*, vol. 170, pp. 273–283, 2021.
- [61] M. M. Li, Y. Q. Yu, H. Fu, F. Xie, L. X. Xu, and J. Chen, "Extracellular signal-regulated kinases mediate melittin-induced hypersensitivity of spinal neurons to chemical and thermal but not mechanical stimuli," *Brain Research Bulletin*, vol. 77, no. 5, pp. 227–232, 2008.
- [62] W. Ma, B. St-Jacques, U. Rudakou, and Y. N. Kim, "Stimulating TRPV1 externalization and synthesis in dorsal root ganglion neurons contributes to PGE₂ potentiation of TRPV1 activity and nociceptor sensitization," *European Journal of Pain*, vol. 21, no. 4, pp. 575–593, 2017.
- [63] T. Moriyama, T. Higashi, K. Togashi et al., "Sensitization of TRPV1 by EP1 and IP reveals peripheral nociceptive mechanism of prostaglandins," *Molecular Pain*, vol. 1, 2005.
- [64] J. Sawynok, A. Reid, and J. Meisner, "Pain behaviors produced by capsaicin: influence of inflammatory mediators and nerve injury," *The Journal of Pain*, vol. 7, no. 2, pp. 134–141, 2006.

- [65] W. Ma, J. G. Chabot, F. Vercauteren, and R. Quirion, "Injured nerve-derived COX2/PGE2 contributes to the maintenance of neuropathic pain in aged rats," *Neurobiology of Aging*, vol. 31, no. 7, pp. 1227–1237, 2010.
- [66] J. M. Chung and K. Chung, "Importance of hyperexcitability of DRG neurons in neuropathic pain," *Pain Practice*, vol. 2, no. 2, pp. 87–97, 2002.

Research Article

Tissue Renin-Angiotensin System (tRAS) Induce Intervertebral Disc Degeneration by Activating Oxidative Stress and Inflammatory Reaction

Kaiqiang Sun ¹, Xiaofei Sun,¹ Jingchuan Sun,¹ Yan Jiang,² Feng Lin,¹ Fanqi Kong,¹ Fudong Li,¹ Jian Zhu,¹ Le Huan,¹ Bing Zheng,¹ Yuan Wang,¹ Weiguo Zou,³ Lu Gao ⁴, Ximing Xu ¹ and Jiangang Shi ¹

¹Department of Orthopedic Surgery, Changzheng Hospital, Navy Medical University (Second Military Medical University), No. 415 Fengyang Road, Shanghai 200003, China

²Department of Oral and Maxillofacial-Head Neck Oncology, Shanghai Jiao Tong University School of Medicine, Shanghai, China

³State Key Laboratory of Cell Biology, CAS Center for Excellence in Molecular Cell Sciences, Shanghai Institute of Biochemistry and Cell Biology, Chinese Academy of Sciences, University of Chinese Academy of Sciences, Shanghai 200031, China

⁴Department of Physiology, College of Basic Medical Sciences, Navy Medical University (Second Military Medical University), Shanghai 200433, China

Correspondence should be addressed to Lu Gao; roadgao@163.com, Ximing Xu; ming_89@126.com, and Jiangang Shi; shijiangangspine@163.com

Received 24 May 2021; Accepted 8 July 2021; Published 9 August 2021

Academic Editor: Sidong Yang

Copyright © 2021 Kaiqiang Sun et al. This is an open access article distributed under the Creative Commons Attribution License, which permits unrestricted use, distribution, and reproduction in any medium, provided the original work is properly cited.

Lumbar intervertebral disc degeneration (IDD) has been the major contributor to low back pain (LBP). IDD is an chronic inflammation process, with the activation of plentiful inflammation-related cytokines and ECM degradation-related enzymes. In the past few years, hypertension has been reported to correlate with LBP. In addition, the local tissue renin-angiotensin system (tRAS) has been identified in multiple tissues, including the spinal cord, skin, kidney, heart, and bone. Recently, tRAS has also been established in both bovine and human intervertebral disc tissues, especially in the degenerated disc tissue. However, the exact of tRAS and IDD remains unknown. In this present study, proteomic analysis, molecular biology analysis, and animal model were all used. Firstly, we revealed that tRAS was excessively activated in the human degenerated intervertebral disc tissue via proteomic analysis and molecular biology analysis. Then, in vitro experiment suggested that Ang II could decrease the cell viability of human NP cells and promote NP cell apoptosis, senescence, oxidative stress, and NLRP3 activation in human NP cells. In addition, Ang II could also trigger degeneration and fibrosis phenotype in human NP cells. Finally, the animal model demonstrated that the local activated ACE/Ang II axis in the NP tissue could accelerate IDD in aging spontaneously hypertensive rats (SHR). Collectively, the degenerated intervertebral disc tissue showed excessively activated tRAS, and local activated tRAS could induce NP cell senescence, apoptosis, oxidative stress, and inflammatory reaction to promote IDD. These biological effects of Ang II on human NP cells may provide novel insight into further treatment of IDD.

1. Introduction

Low back pain (LBP) has been the major contributor to hospitalization in patients with degenerative lumbar diseases, which brings enormous social and economic burdens for patients and their families worldwide [1]. Of the massive pathogenic factors, lumbar intervertebral disc degeneration

(IDD) has been the mostly studied. Anatomically, the normal intervertebral disc is consist of gel-like inner nucleus pulposus tissue (NP), surrounding annulus fibrosus tissue (AF), and cartilaginous endplates structure (EP), which connects adjacently superior and inferior vertebral bodies [2, 3]. In general, IDD is an age-related biological process. However, accumulating evidence has suggested that multifactorial

pathogenesis can initiate or accelerate IDD, such as repetitive mechanic load, infective diseases, trauma, and genetic predisposition. During the process of IDD, various pathological changes occur in the microenvironment of the NP tissue, such as cell apoptosis, cell senescence, inflammatory reaction, and oxidative stress, which will result in increased catabolic reaction and decreased synthetic reaction [4]. These abnormal biological processes will finally cause IDD-related diseases, such as spinal canal stenosis, adjacent segment degeneration (ASD), and spinal instability [4].

Clinical treatments have been well built based on the duration of symptoms, age, comorbidities, severity of IVD, compression of neural elements, and spinal stability. In early stage, patients with symptomatic IDD could be well controlled via medication therapy, such as vitamin B12 combined with nonsteroidal anti-inflammatory drugs [5]. However, surgical interventions are frequently recommended, especially for patients with serious neurological dysfunction [5]. Nevertheless, the long-term surgical effects could be ineffective, and the occurrence of ASD cannot be ignored [6]. In recent years, basic research therapy has attracted substantial interest. Various molecular treatments targeted at inhibiting the inflammatory responses and oxidative stress have been established, including gene therapy, growth factor therapy, and cell therapy [3, 5, 7]. However, due to the limitation of the exact mechanism of IDD and further clinical trials, these therapies above have not yet acquired satisfactory generalization. Thus, more work is still required to explore the potential mechanism of IDD.

Hypertension, as a common chronic disease, has been reported to be a risk factor for low back pain, and antihypertensive medication may attenuate this association [8, 9]. However, the potential mechanism of hypertension involved in IDD remains unknown. The regulatory effects of the renin-angiotensin system (RAS) on vasoconstriction, blood pressure, and electrolyte balance during hypertension have been well established. Ang II, as a key mediator in hypertension, is mainly produced from angiotensinogen (ATG) via angiotensin-converting enzyme (ACE) [10]. AT1 receptor (G protein-coupled receptor) is the main biological mediator of Ang II, and the binding of Ang II to AT1 will enhance the generation of ROS, the release of pro-inflammatory cytokines, and the accumulation of M1 macrophages [10, 11]. However, plentiful researches have suggested the circulatory homeostasis-independent biological effects of Ang II in multiple organs or tissues in the past decades. Li et al. ever reported that Ang II could induce mitochondrial oxidative stress and DNA damage in osteoblasts to accelerate the process of osteoporosis [12]. Ang II could also enhance the infiltration of inflammatory cells, such as macrophages, into local tissue, and cause tissue damage [13]. Andrew et al. previously demonstrated that macrophage Ang II receptor could trigger chronic neuropathic pain [14]. In addition, Ang II is also involved in degeneration-related diseases, such as osteoarthritis and Alzheimer's disease [10, 15, 16]. Therefore, a new term "Tissue Renin-Angiotensin System (tRAS)" has been proposed. Interestingly, Morimoto et al. firstly found tRAS components in the normal rat intervertebral disc tissue at both mRNA and protein levels [17]. Further, Li et al. con-

firmed the existence of tRAS components in the human disc tissue and found that within tRAS-positive disc samples, AGT, matrix-metalloproteinases 13/3 (MMP3/13), IL-1, and other inflammatory cytokines were highly expressed [18]. These results above indicated a potentially critical role of tRAS in IDD. However, the correlation between the activation of tRAS and the process of IDD and the exact molecular mechanisms of Ang II contributing to IDD have not yet been fully elucidated.

This present study is aimed at revealing (1) the correlation of activated tRAS and the degree of IDD in the human disc tissue, (2) the potential biological effects of Ang II on human NP cells and related pathological mechanisms in vitro, and (3) the long-term effects of local activated tRAS in the NP tissue on the process of IDD in vivo. The results will provide new information for future investigation of hypertension and IDD.

2. Methods and Materials

2.1. Acquisition of Patients' Samples. This study was approved by the ethic board of our institution, and the written informed consent was signed by all the participants enrolled in this study. Lumbar intervertebral disc tissue was acquired intraoperatively from twenty-two patients (mean age: 56 ± 12 years; range: 23-78 years) who accepted surgical fusion due to spine-related diseases (trauma and intervertebral disc herniation) in our institution. According to preoperative Pfirrmann grades on MRI, the disc tissue was divided into the nondegenerated group (grade II), moderately degenerated group (grade III), and severely degenerated group (grade IV). Disc tissue from ten patients including grade II (five cases) and grade IV (five cases) was used to perform TMT quantitative proteomic analysis. In addition, disc tissue from three patients (grade II) was used to isolate NP cells in vitro.

2.2. Experimental Protocols. Male WKY rats and SHR with age of 8 weeks (weighed 250-350 g) were obtained from Vital River Laboratory Animal Technology and kept in animal room with 12-h cycle of light and dark. All experiments were approved by the Animal Care and Use Committee of Navy Medical University.

2.3. Proteomic Analysis. The intervertebral disc tissue (nucleus pulposus as much as possible) was collected from ten patients (five cases with grade II and five cases with grade IV). The details of proteomic analysis have been described previously, with the experimental workflow in supplementary file (supplementary Figure 1) [19, 20]. Briefly, after collection of the disc sample, the proteins were extracted, alkylated, and digested. After SDS-PAGE separation, the proteins underwent tandem mass tag (TMT) labeling based on the instructions (Thermo Fisher Scientific, Waltham, MA, USA). Subsequently, the TMT-labeled samples underwent high pH reversed-phase peptide fractionation using kit (Thermo Fisher Scientific, Waltham, MA, USA), followed by LC-MS-MS data acquisition and bioinformatic analysis (GO and KEGG).

2.4. Acquisition and Culture of Human NP Cells. This method has been reported in our recent study [2]. Briefly, the collected intervertebral disc tissue was transported to laboratory using 0.9% sterile saline within two hours. Then, the tissue was washed 3 times using PBS (Servicebio, Wuhan, China) in super clean bench. Next, gel-like NP tissue was separated and digested using 0.25% Trypsin-EDTA (C0209-100 mL, Beyotime, Shanghai, China) for 30 minutes and 0.2% collagenase type II (Invitrogen, USA) for another 1 h at 37°C under a shaker (70 r/min). Finally, the isolated NP cells were resuspended in complete culture medium (Gibco; Thermo Fisher Scientific, Inc.) and cultured in a 37°C incubator. At the third, half of the culture medium will be replaced by complete medium. Five days after isolation, the spindle-shaped NP cells will move out and adhered at the bottom which we called passage 0. When the cell density reaches about 80%, the NP cells could be used further experiments.

2.5. Cell Viability Assay. After seeding in a 96-well plate (4×10^3 cells/well) for 24 hours, cells were incubated with Ang II (10^{-4} - 10^{-10} M) for another 24 hours. On the third day, 110 μ l CCK 8 detection solution (10 μ l CCK8 solution and 100 μ l DF-12 medium) was added into every single well and coincubated with NP cells for another 1 hour at 37°C. The absorbance of every well was measured with a wavelength of 450 nm on an absorbance microplate reader (Bio-Tek, USA).

2.6. Real-Time Quantitative PCR (Polymerase Chain Reaction). This method has been described in previous study [2]. After acquisition of mRNA from NP cells, total mRNA (100 ng/ μ L) was reversed using HiScript[®] III RT SuperMix for qPCR Kit (R323-01, Vazyme, Nanjing, China). Then, the acquired cDNA was quantified using SYBR qPCR Master Mix (Q711-02, Vazyme, Nanjing, China) on a ABI 7500 Real-Time PCR system (Applied Biosystems, Foster City, USA). GAPDH was used as the normalization, and all reactions were run for three times. Relative mRNA amount was quantified using the formula: $2^{-\Delta\Delta C_t}$. The primer sequences used are presented in Table 1.

2.7. Immunohistochemical Analysis. This method has been described previously [2]. Intervertebral disc samples were sectioned, embedded with paraffin, and deparaffinized, followed by blocking the endogenous peroxide using 3% hydrogen peroxide. Then, the sections were incubated in 5% blocking solution for 60 min and incubated with primary antibody against ACE (24743-1-AP, 1:500, Proteintech, China) overnight at the temperature of 4°C. Subsequently, HRP-conjugated secondary (GB23303, Servicebio, Wuhan, China) was used to binding primary antibody, followed by hematoxylin staining. Images were captured using light microscopy (Olympus, Japan).

2.8. Immunofluorescence Analysis. Our previous study also described this method in detailly [2]. After intervertebral disc sections or NP cells were well prepared, 0.1% Triton X-100 was employed to permeate samples for 5 min. Then, samples were blocked with 3-5% BSA for 60 min at 37°C. Then, the samples were incubated using primary antibody against

TABLE 1: Sequences of the primers for RT-qPCR.

Gene	Primer	Sequence
ACE	Forward	CTTGTACGGAAGCATCACC
	Reverse	GGCACATTTCGCAGGAAC
AT1	Forward	GCTGTCATCCACCGAAA
	Reverse	GGAACAAGAAGCCCAGAA
GAPDH	Forward	TGACCACAGTCCATGCCATC
	Reverse	GACGGACACATTGGGGGTAG

γ H2AX (GB111841, 1:200, Servicebio, Wuhan, China), aggrecan (GB11373, 1:500, Servicebio, Wuhan, China), collagen type II (GB14073, 1:500, Servicebio, Wuhan, China), iNOS (GB11119, 1:1000, Servicebio, Wuhan, China), collagen type I (GB11022, 1:500, Servicebio, Wuhan, China), NLRP3 (GB11300, 1:1000, Servicebio, Wuhan, China), CD206 (#24595, 1:800, Cell Signaling Technology, Inc. USA), MMP3 (GB11131, 1:500, Servicebio, Wuhan, China), AGT (ab108334, 1:200, Abcam, USA), Nrf2 (340675, 1:500, Zenbio, Chengdu, China), and p65 (GB11142, 1:200, Servicebio, Wuhan, China) at 4°C overnight. At the second day, samples were treated with fluorescence secondary antibody (GB22303, GB21301, Servicebio, Wuhan, China) for 1 h in the dark room. The nuclei were staining with DAPI solution (G1012-100ML, Servicebio, Wuhan, China). The fluorescence was detected using fluorescence microscope (Olympus, Japan).

2.9. Terminal Deoxynucleotidyl Transferase dUTP Nick-End Labeling (TUNEL) Assay. Our previous study also described this method detailly [2]. After intervertebral disc sections or NP cells were well prepared, 0.3% Triton X-100 was applied to permeating samples for 10 min. Then, the TUNEL detection solution was prepared with 5 μ l TDT enzyme and 45 μ l fluorescent labeling solution for each sample. After washing the sample twice using HBSS/PBS, the TUNEL detection solution was incubated with samples in a 37°C incubator for 60 min. Subsequently, the samples were again washed using HBSS/PBS for 3 times, followed by DAPI solution. Finally, TUNEL-positive cells were detected using fluorescence microscope (570 nm, Olympus, Japan).

2.10. Detection of Reactive Oxygen Species. Our previous study also described this method detailly [2]. Human NP cells were washed using PBS for 3 times, followed by staining with none-FBS cultural medium solved with 2,7-DHD (S0033S, Beyotime, Shanghai, China) for 20 mins. Then, the NP cells were again washed for 3 times in order to wash out remaining DCFH-DA. The level of ROS would be identified by fluorescence microscope (525 nm, Olympus, Japan).

2.11. Safranin O-Fast Green Staining. The rat caudal disc was fixed using 4% PFA for one day and decalcified using decalcifying fluid for 15-20 days. Then, the samples were embedded using paraffin. After dehydration, the samples were incubated with Safranin O Fast Green (G1053, Servicebio,

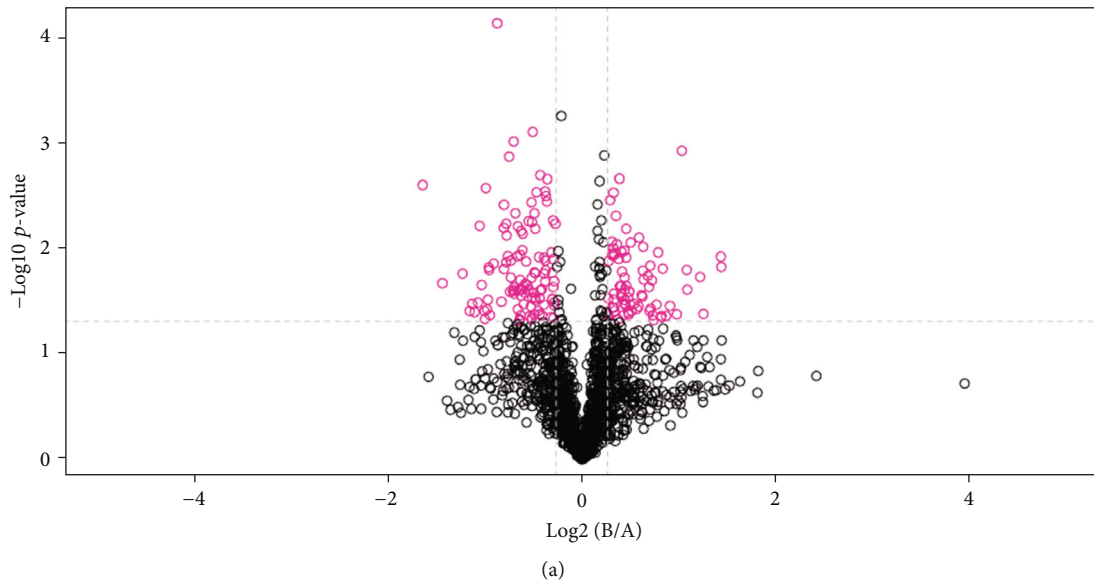
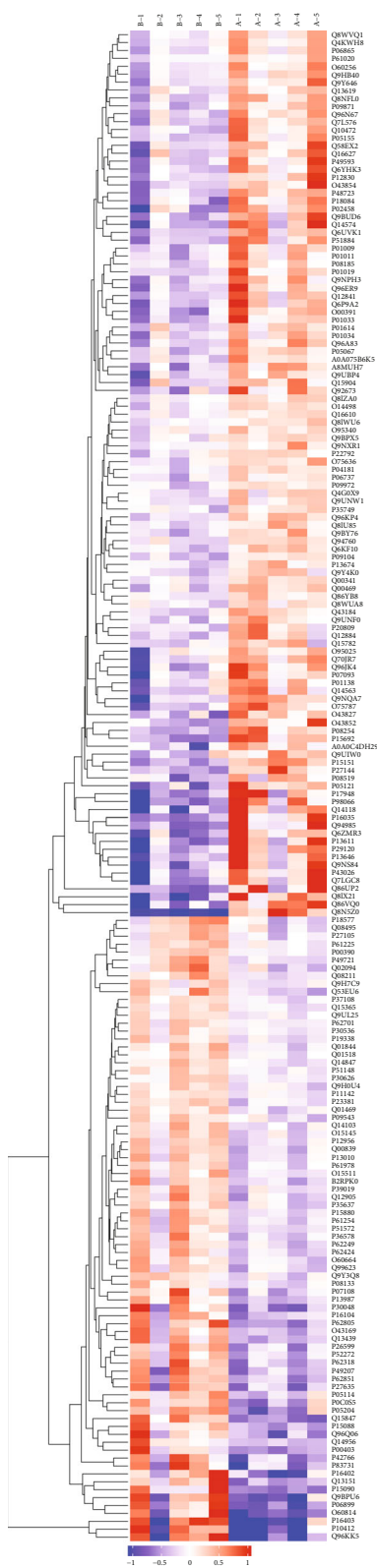
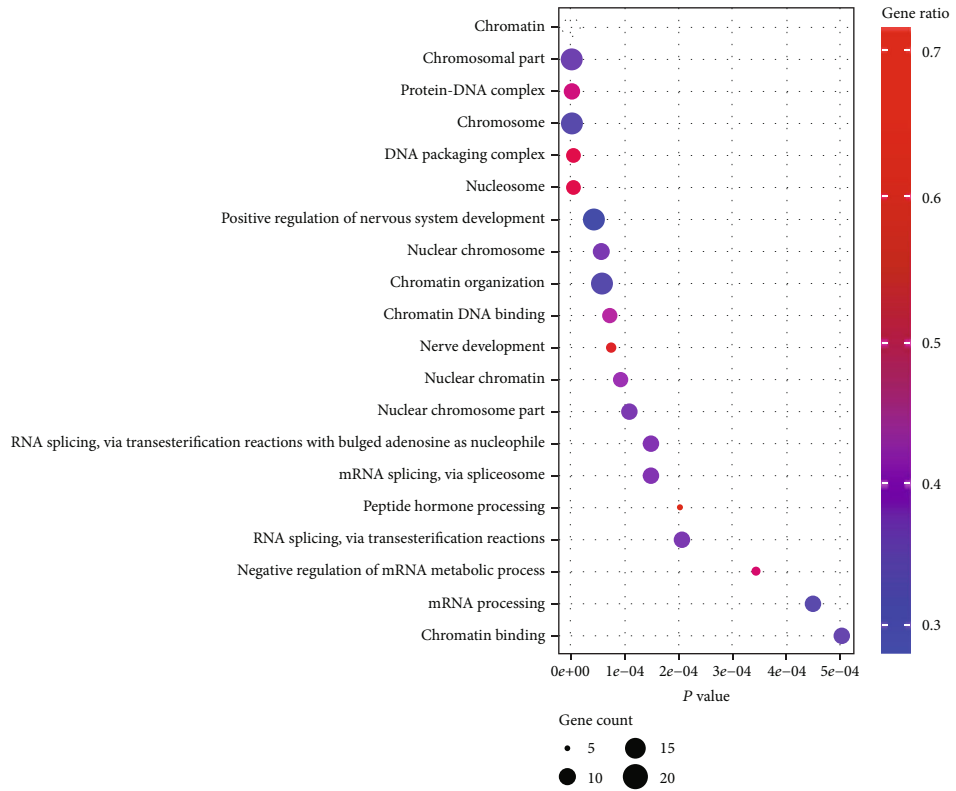


FIGURE 1: Continued.

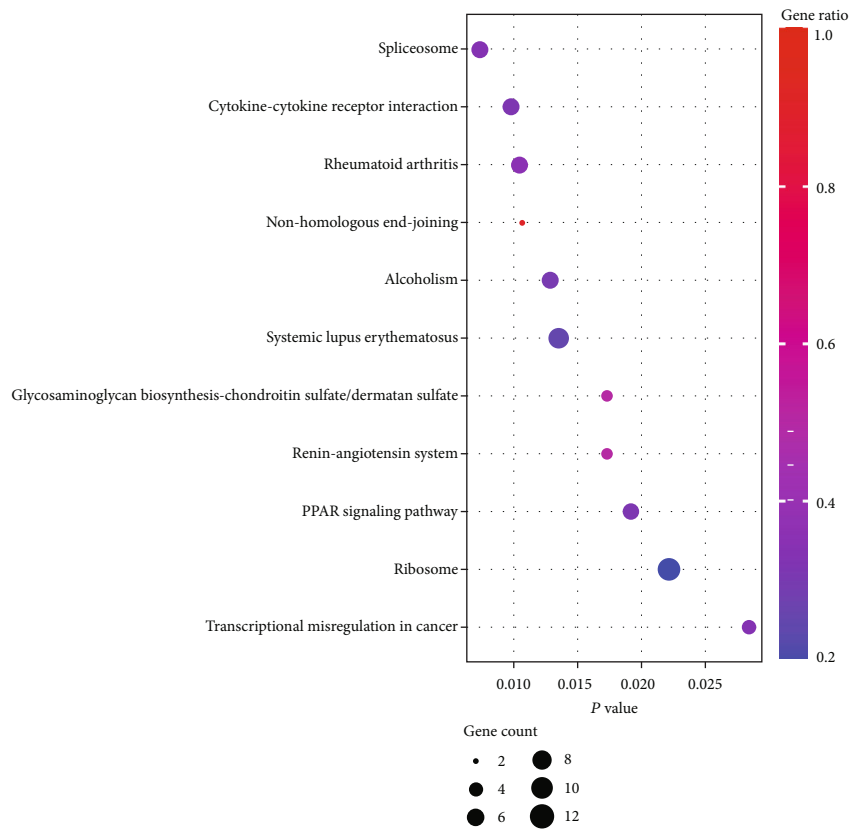


(b)

FIGURE 1: Continued.

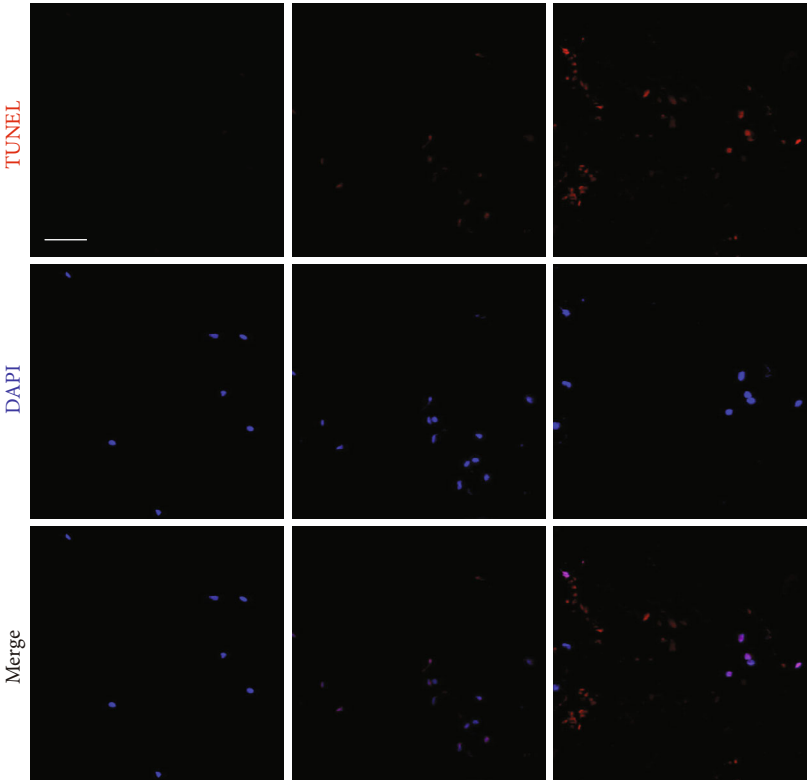


(c)

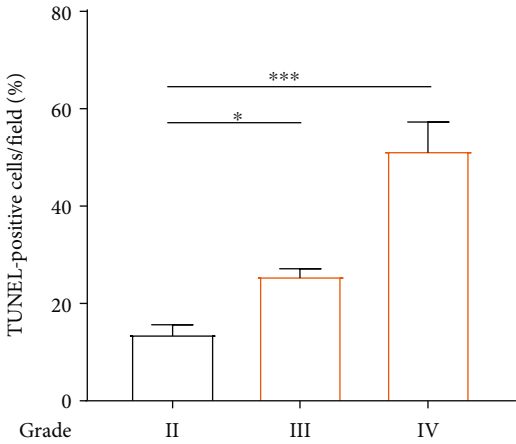


(d)

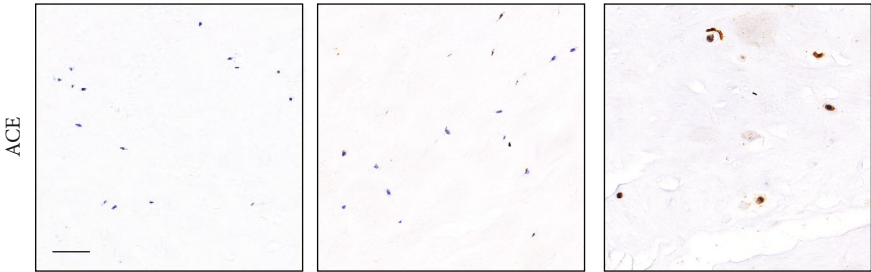
FIGURE 1: Continued.



(e)



(f)



(g)

FIGURE 1: Continued.

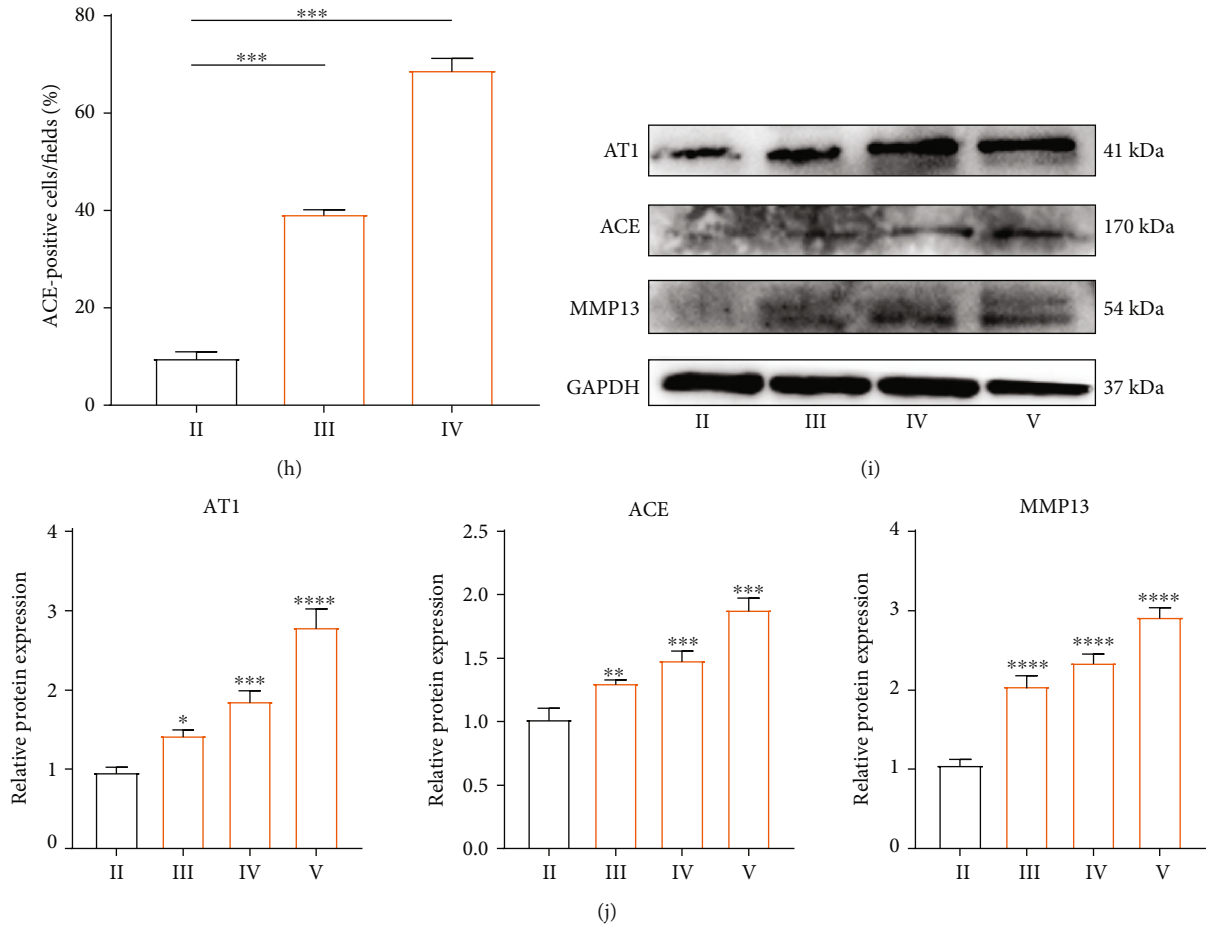


FIGURE 1: Activation of the tissue renin-angiotensin system (tRAS) in the human degenerated intervertebral disc tissue. (a) The volcano plot of the gene relative expression of NP tissue in the none-degenerated group compared to the severely degenerated group. Pink circles represented upexpressed proteins ($p < 0.05$), whereas black circles suggested proteins without expression differences between these two groups ($n = 5$). (b) The clustering analysis heat map. (c) Top 20 enriched GO terms. (d) Top ten enriched KEGG pathways. (e) TUNEL assay of the human NP tissue among grades II, III, and IV ($n = 3$). (f) Quantitative results of TUNEL-positive cells. (g) Immunohistochemical analysis of the expression of ACE in the human NP tissue among grades II, III, and IV ($n = 3$). (h) Quantitative results of ACE-positive cells. (i, j) Western blot results of the protein expression of tRAS components (ACE and AT1) and MMP13 in the human NP tissue ($n = 3$). Scale bar = 50 μm . * $p < 0.05$, ** $p < 0.01$, *** $p < 0.001$, **** $p < 0.0001$.

Wuhan, China). Typical images were randomly captured using light microscopy (Olympus, Japan).

2.12. Western Blot. Our recent study has described this method detailly [2]. The primary antibodies used in this present study included NOX2 (ab129068, 1:2000, Abcam, USA), AT1 (381666, 1:1000, Zenbio, Chengdu, China), ACE (24743-1-AP, 1:1000, proteintech, China), Bax (200958, 1:1000, Zenbio, Chengdu, China), MMP13 ((820098, 1:1000, Zenbio, Chengdu, China), C-caspase-3 (#9664, 1:1000, Cell Signaling Technology, Inc. USA), p53 (sc-393031, 1:500, Santa Cruz, Bio. Lnc, USA), Klotho (382164, 1:1000, Zenbio, Chengdu, China), Bcl2 (381702,, 1:1000, Zenbio, Chengdu, China), COX-2 (#12282, 1:1000, Cell Signaling Technology, Inc. USA), MMP-3 (380816, 1:1000, Zenbio, Chengdu, China), aggrecan (ab36861, 1 $\mu\text{g}/\text{mL}$, Abcam, USA), iNOS (#20609, 1:1000, Cell Signaling Technology, Inc. USA), Nrf2 (221102, 1:1000, Zenbio, Chengdu, China), HO-1 (#43966, 1:1000,

Cell Signaling Technology, Inc. USA), type II collagen (collagen II (1:1000, ab34712, Abcam), SOD1 (#37385, 1:1000, Cell Signaling Technology, Inc. USA), NLRP3 (381207, 1:1000, Zenbio, Chengdu, China), ASC (340097, 1:1000, Zenbio, Chengdu, China), and GAPDH (5174, 1:1000, Cell Signaling Technology, Inc. USA). The secondary antibodies were purchased from Zenbio (380172, 511103, Zenbio, Chengdu, China).

2.13. Enzyme-Linked Immunosorbent Assay. The secretory amount of IL-18, IL-1 β , and NO in supernatant of cultured human NP cells was detected using ELISA kit (ab215539, ab214025, Abcam, USA, and SD0621, Westang, China).

2.14. Assay of Mitochondrial Membrane Potential (MMP). Our previous study also described this method detailly [2]. After human NP cells were treated with Ang II, the prepared JC-1 staining fluid (Beyotime Biotechnology, Inc., Shanghai, China) was added into cells (1 mL/well) and incubated at

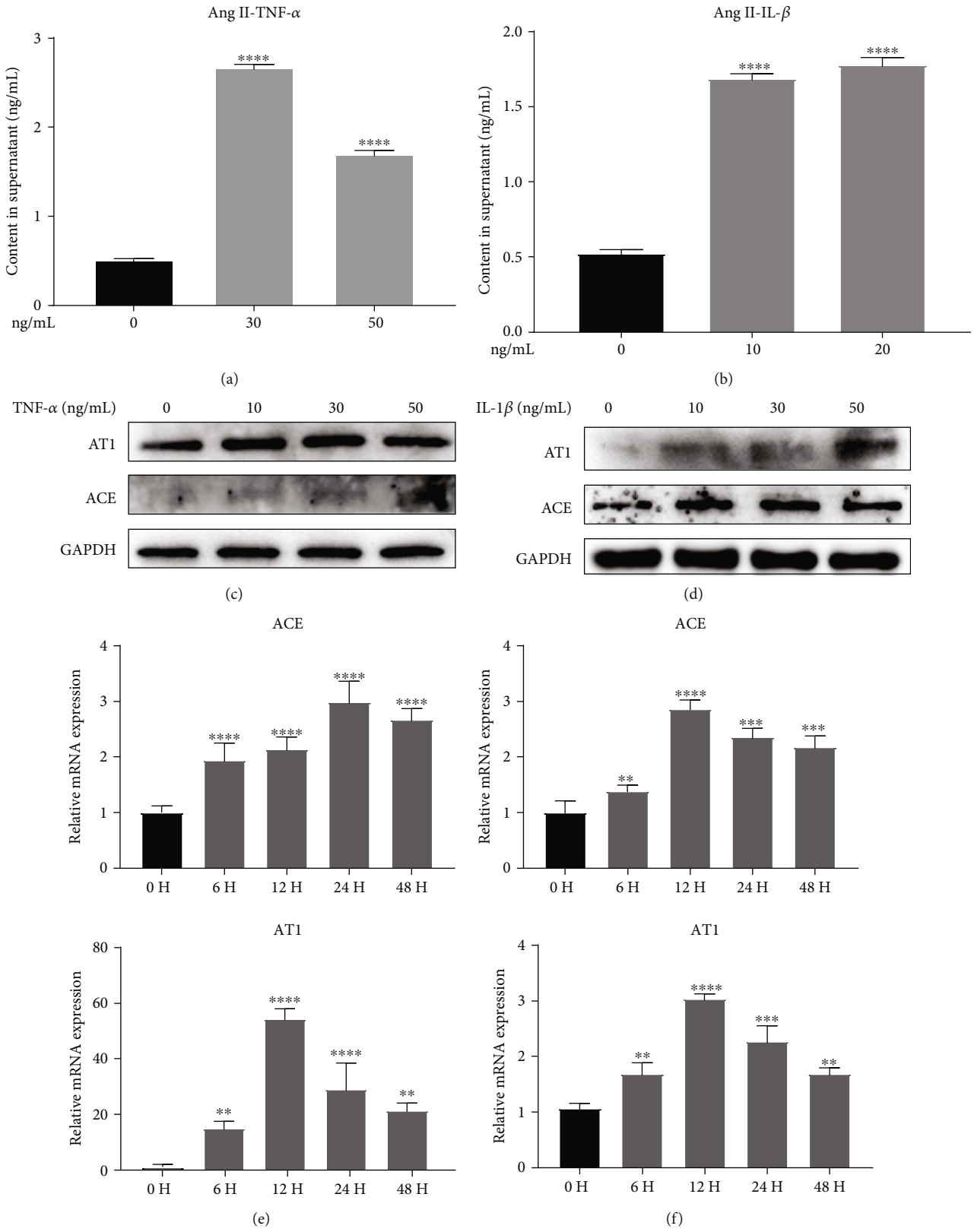


FIGURE 2: Inflammatory cytokines promoted the activation of tRAS in human nucleus pulposus cells in vitro. (a, b) Secretion amount of Ang II in supernatant of human NP cells induced by IL-1 β or TNF α was quantified by the ELISA assay ($n = 5$). (c, d) Western blot revealed the relative protein expression of tRAS components (ACE and AT1) in human NP cells induced by IL-1 β or TNF α ($n = 3$). (e, f) RT-qPCR quantified the relative mRNA expression tRAS components (ACE and AT1) in human NP cells induced by IL-1 β or TNF α in a time-change manner ($n = 3$). * $p < 0.05$, ** $p < 0.01$, *** $p < 0.001$, **** $p < 0.0001$.

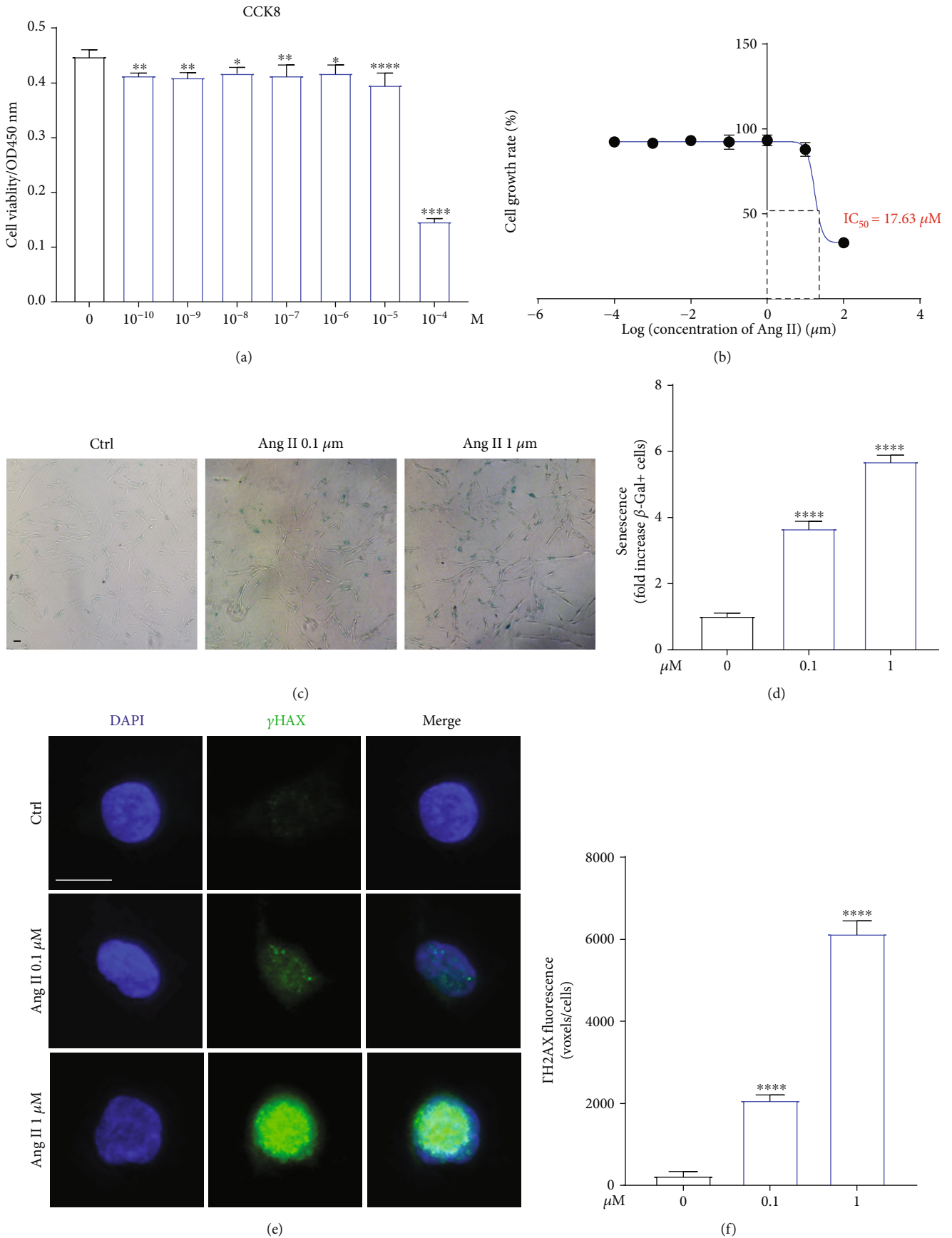


FIGURE 3: Continued.

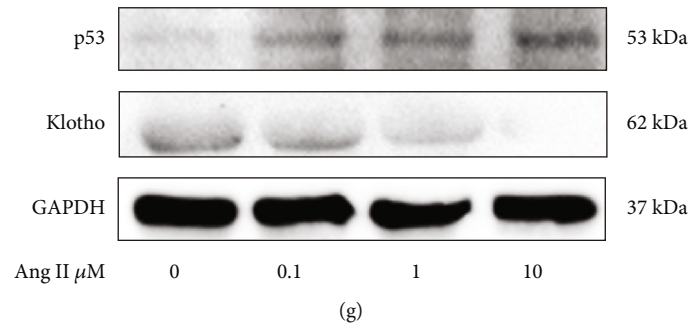


FIGURE 3: Angiotensin II triggered human NP cells senescence in a dose-dependent manner. (a) The SA- β -gal staining of human NP cells induced by Ang II ($n = 3$). (b) Quantitative results of SA- β -gal-positive NP cells in different groups ($n = 3$). (c) Immunofluorescence results for the expression of γ H2AX in human NP cells treated by Ang II ($n = 3$). Scale bar = 20 μ m. (d) The expression of γ H2AX was quantified as averaged fluorescent voxels/cell ($n = 3$). (e) The protein expression of senescence-related markers, p53, and Klotho in human NP cells induced by Ang II ($n = 3$). $p < 0.05$, ** $p < 0.01$, *** $p < 0.001$, **** $p < 0.0001$.

37°C for 20 min. After then, the NP cells were washed with buffer solution. Fluorescence microscope (Olympus, Japan) was used to analyze the MMP of NP cells.

2.15. Assay of Senescence-Associated β -Galactosidase (SA- β -gal) Activity. This method has been reported previously [21]. Firstly, SA- β -gal staining fixative was added to the treated cells and coincubated for 15 min. After washed by PBS, SA- β -gal work solution was added to cells drop by drop and incubated at 37°C overnight, covered by plastic wrap. The SA- β -gal staining image was acquired under a light microscope (Olympus, Japan).

3. Results

3.1. Activation of the Tissue-Renin-Angiotensin-System (tRAS) in the Human Degenerated Intervertebral Disc Tissue. This project was carried out using TMT Quantitative TMT-labeling LC-MS-MS, and totally, 1841 proteins were identified. With 1.2 less or more fold changes ($p < 0.05$) being screened by the criteria, there were 112 upregulated proteins and 79 downregulated proteins in none-degenerated group compared to the severely degenerated group (Figure 1(a)). The altered protein expression profile in these two groups was presented using hierarchical clustering (Figure 1(b)). The Kyoto Encyclopedia of Genes and Genome (KEGG) pathway enrichment analysis revealed the altered proteins with their important signal pathway, including renin-angiotensin system, glycosaminoglycan biosynthesis pathway, PPAR signaling pathway, alcoholism, and systemic lupus erythematosu (Figures 1(c) and 1(d)). Based on gene counts and gene ratio, we focused on RAS. In addition, AGT (P01019), the origin of Ang II, was found to be expressed higher in severely degenerated group, indicating increased activation of tRAS that may correlate with IDD.

We further confirmed the expression changes of tRAS components in the human NP tissue at the molecular level. Based on Pfirrmann grades on T2-weighted MRI, the human intervertebral disc tissue was divided into three groups: grade II, grade III, and grade IV, respectively ($n = 3$). As shown in Figure 1, the ratio of TUNEL-positive nucleus pulposus increased with Pfirrmann grades (Figures 1(e) and 1(f)). In

addition, the expression of ACE was also elevated with the increased degree of degeneration of disc (Figures 1(g) and 1(h)). Further, western blot analysis of the NP tissue of disc confirmed the increased tRAS components (AT1 and ACE) in degenerated disc (Figures 1(i) and 1(j)). These results above suggested the activation of tRAS in the human degenerated intervertebral disc tissue.

3.2. Inflammatory Cytokines Could Promote the Activation of RAS in Human Nucleus Pulposus Cells In Vitro. To further investigate the expression changes of tRAS components in nucleus pulposus, we stimulated human nucleus pulposus with inflammatory cytokines (TNF α and IL-1 β) in vitro, respectively. Firstly, human nucleus pulposus cells treated by either TNF α or IL-1 β secreted higher level of Ang II in supernatant (Figures 2(a) and 2(b) both $p < 0.05$). In addition, the results of western blot suggested that inflammatory cytokines could dose-dependently activate the expression of AT1 and ACE in NP cells (Figures 2(c) and 2(d)). RT-qPCR analysis also showed that inflammatory cytokines promoted the activation of tRAS in nucleus pulposus in a time-dependent manner, especially at 12-24 h following inflammatory stimulation (Figures 2(e) and 2(f)).

3.3. Angiotensin II Triggered Human NP Cell Senescence in a Dose-Dependent Manner. As shown in Figure 3, Ang II could decrease the cell viability of NP cells in a dose-dependent manner, with the IC₅₀ being 17.63 μ M (Figures 3(a) and 3(b)). SA- β -gal has been proposed as a marker of cell senescence [22]. After treated by Ang II (0, 0.1, and 1 μ M) for 24 h, the staining for SA- β -gal in human nucleus pulposus was significantly enhanced with increased concentrations (Figures 3(c) and 3(d)). In addition, before the occurrence of cell senescence, DNA damage will be firstly triggered, which has considered as presenescence responses to stress. Excessive accumulation of phosphorylated histone H2AX (γ H2AX) at the injured sites is the typical characteristic of DNA damage [23]. The immunofluorescence analysis demonstrated that Ang II increased the amount of γ H2AX distribution at nuclear DNA (Figures 3(e), 3(f), and 3(d)). Consistent with the results above, Ang II also increased the expression of proaging protein, p53, and decreased the

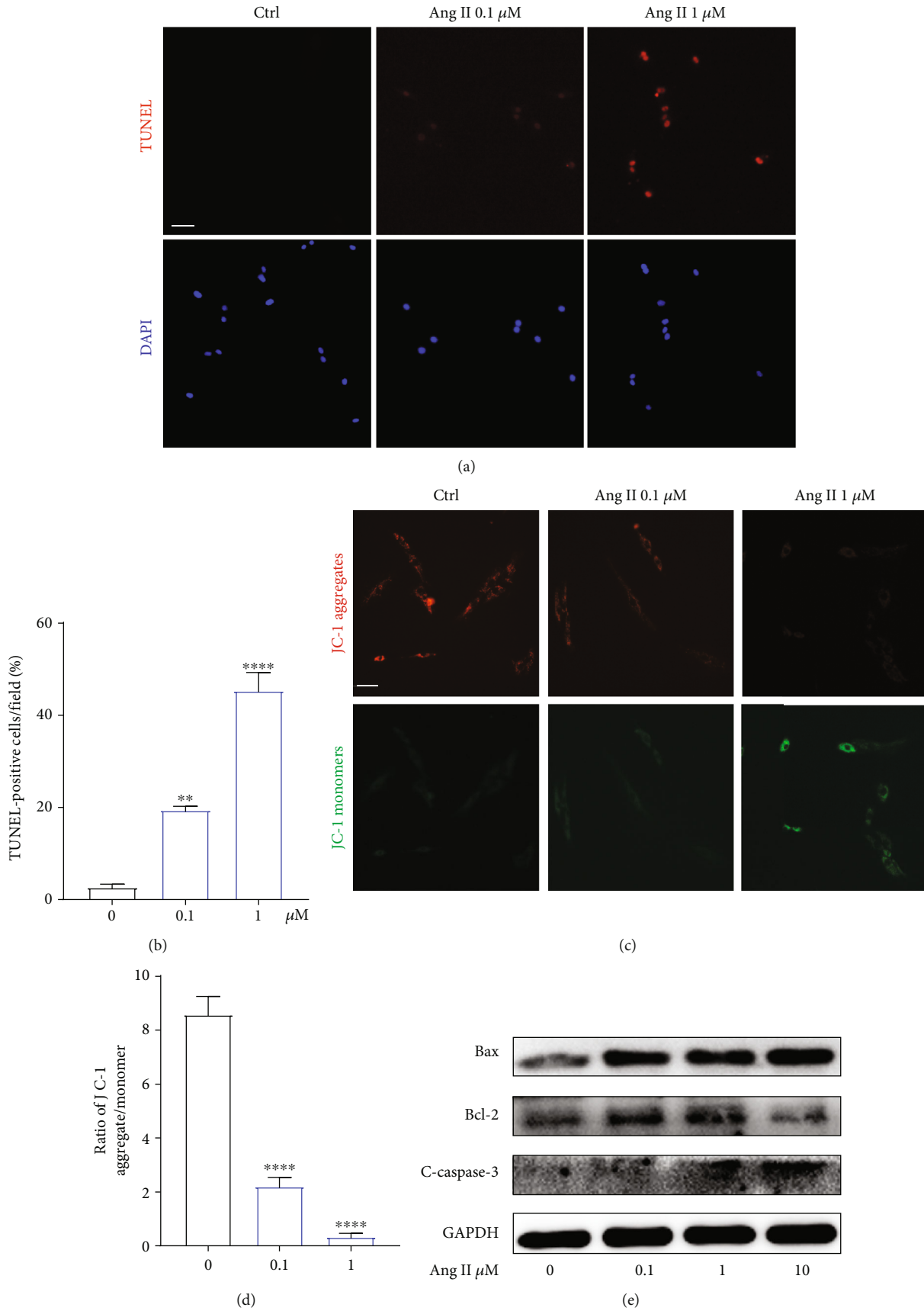


FIGURE 4: Continued.

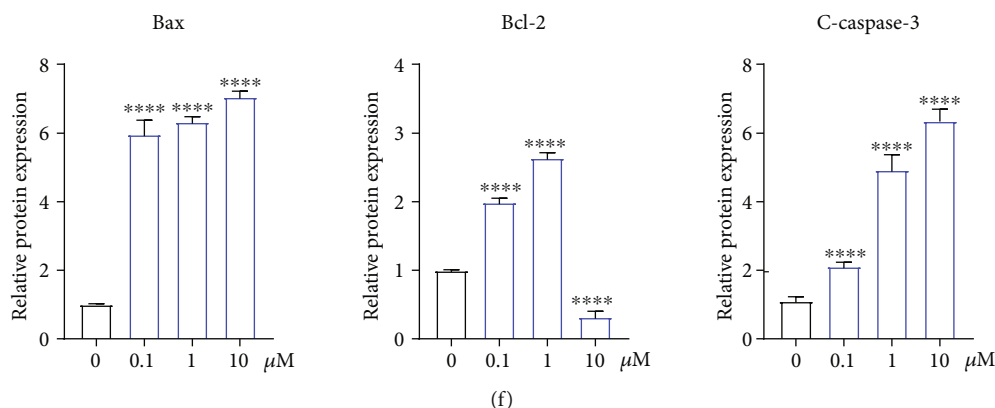


FIGURE 4: Angiotensin II decreased cell viability and induced apoptosis in human NP cells. (a) The effects of Ang II with different concentrations on human NP cells ($n = 5$). (b) The IC_{50} curve of Ang II for human NP cells. (c) Apoptotic human NP cells were presented using the TUNEL assay ($n = 3$). Scale bar = $50 \mu\text{m}$. (d) TUNEL-positive cells were quantified ($n = 3$). (e) The effect of Ang II on the mitochondrial membrane potential of NP cells was detected by JC-1 staining ($n = 3$). (f) The ratio of JC-1 aggregates (red) to monomers (green) was quantified ($n = 3$). Scale bar = $50 \mu\text{m}$. (g) The expression of apoptosis-related proteins was analyzed by western blot ($n = 3$). (h) The expression of apoptosis-related proteins was quantified ($n = 3$). $p < 0.05$, $**p < 0.01$, $***p < 0.001$, $****p < 0.0001$.

expression of antiaging protein, Klotho (Figure 3(g)). Taken together, Ang II could promote human NP cells senescence in vitro.

3.4. Angiotensin II Decreased Cell Viability and Induced Apoptosis in Human NP Cells. To further examine the biological effects of Ang II on human NP cells, we evaluated the change of NP cell viability after being exposed to Ang II. The TUNEL assay suggested the proapoptotic effect of Ang II on NP cells (Figures 4(a) and 4(b)). Mitochondrion plays a critical role in regulating cell apoptosis [24]. Therefore, we further evaluate the changes of mitochondrial membrane potential (MMP) and found that Ang II could also decrease MMP in a dose-dependent manner (Figures 4(c) and 4(d)). Proapoptosis markers, cleaved-caspase 3 and Bax, and antiapoptosis marker, Bcl-2, have been the vital components that are involve in the mitochondria-related pathway [25]. Our western blot results revealed that Ang II increased the expression of cleaved-caspase 3 and Bax and suppressed the expression of Bcl-2 (Figures 4(e) and 4(f)). The results above confirmed the suppressive effect of Ang II on cell viability and the promotive effects of Ang II on cell apoptosis.

3.5. Angiotensin II Induced Degeneration and Fibrosis Phenotype in Human NP Cells In Vitro. Decreased ECM (type II collagen and aggrecan) and elevated MMPs and type I collagen have been the typical features during IDD [7]. Therefore, in this present study, we evaluated the changes of these features. As shown by immunofluorescence analysis, human NP cells stimulated with Ang II expressed higher MMP 3 and lower aggrecan (Figures 5(a) and 5(b)). During the process of IDD, the gel-like NP tissue will possess fibrosis phenotype, with type II collagen being replaced by type I collagen [3, 7]. In addition, Ang II could promote tissue fibrosis [26, 27]. Thus, the expression of type I collagen was also evaluated, and the results suggested that Ang II significantly increased the expression of type I collagen (Figures 5(c) and

5(d)). Furthermore, consistent with the results of immunofluorescence analysis, western blot also confirmed that Ang II promoted degeneration and fibrosis phenotype in human NP cells in vitro (Figures 5(e) and 5(f)).

3.6. Angiotensin II Increased the ROS Level in Human NP Cells In Vitro. ROS level frequently indicates intracellular oxidative conditions. Previous studies have revealed that Ang II could induce the release of reactive oxygen species (ROS) in cardiovascular diseases [28]. During IDD, excessive production of intracellular ROS will accelerate NP cell damage and inflammatory response [2]. As a result, we examined the effect of Ang II on human NP cells and found that Ang II dose-dependently enhanced the intracellular ROS level (Figures 6(a) and 6(b)). As molecular level, western blot demonstrated the decreased antioxidative stress-related proteins (Nrf2, HO-1, and SOD1) and increased prooxidative stress-related protein, NOX 2, induced by Ang II (Figures 6(c) and 6(d)).

3.7. Angiotensin II Promoted the Activation of NLRP3 Inflammasome in Human NP Cells In Vitro. The NLR pyrin domain-containing 3 (NLRP3) inflammasome is the crucial source of inflammation-related cytokines, such as IL- 1β and IL-18 [29]. Notably, NLRP3 inflammasome has been indicated to involve in IDD recently [30, 31]. Therefore, we evaluated the activated effect of Ang II on NLRP3 inflammasome. As shown in the results, the ratio of NLRP3 inflammasome-positive NP cells was significantly increased by Ang II (Figure 7(a)). ELISA results revealed that Ang II also enhanced the secretion level of inflammatory cytokines, including IL-18, IL- 1β , and NO (Figure 7(b)). The upregulated expressions of NLRP3 inflammasome-related proteins (ASC and IL-18) and inflammation-related proteins (iNOS and COX2) also confirmed the promotive effect of Ang II on the activation of NLRP3 inflammasome in human NP cells in vitro (Figures 7(c) and 7(d)). In addition, macrophage has also participated in IDD, with M1 macrophage

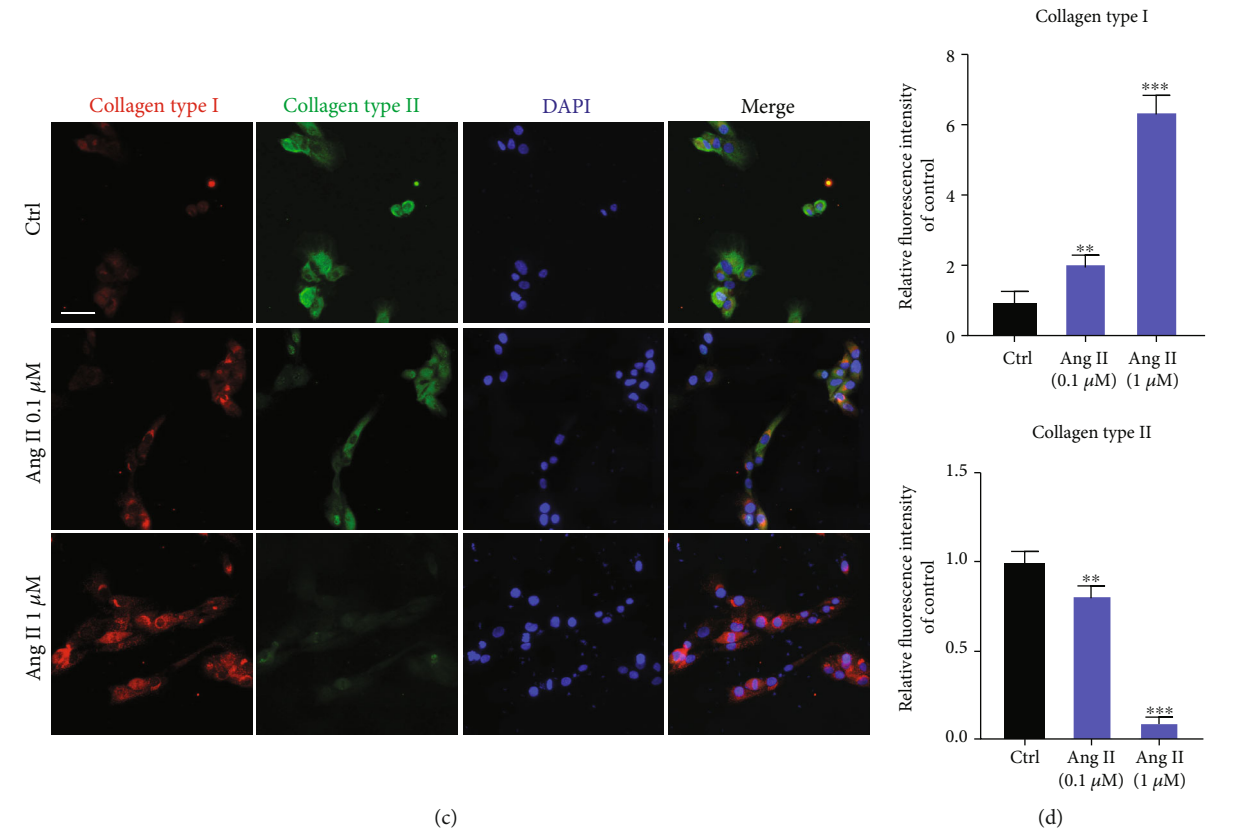
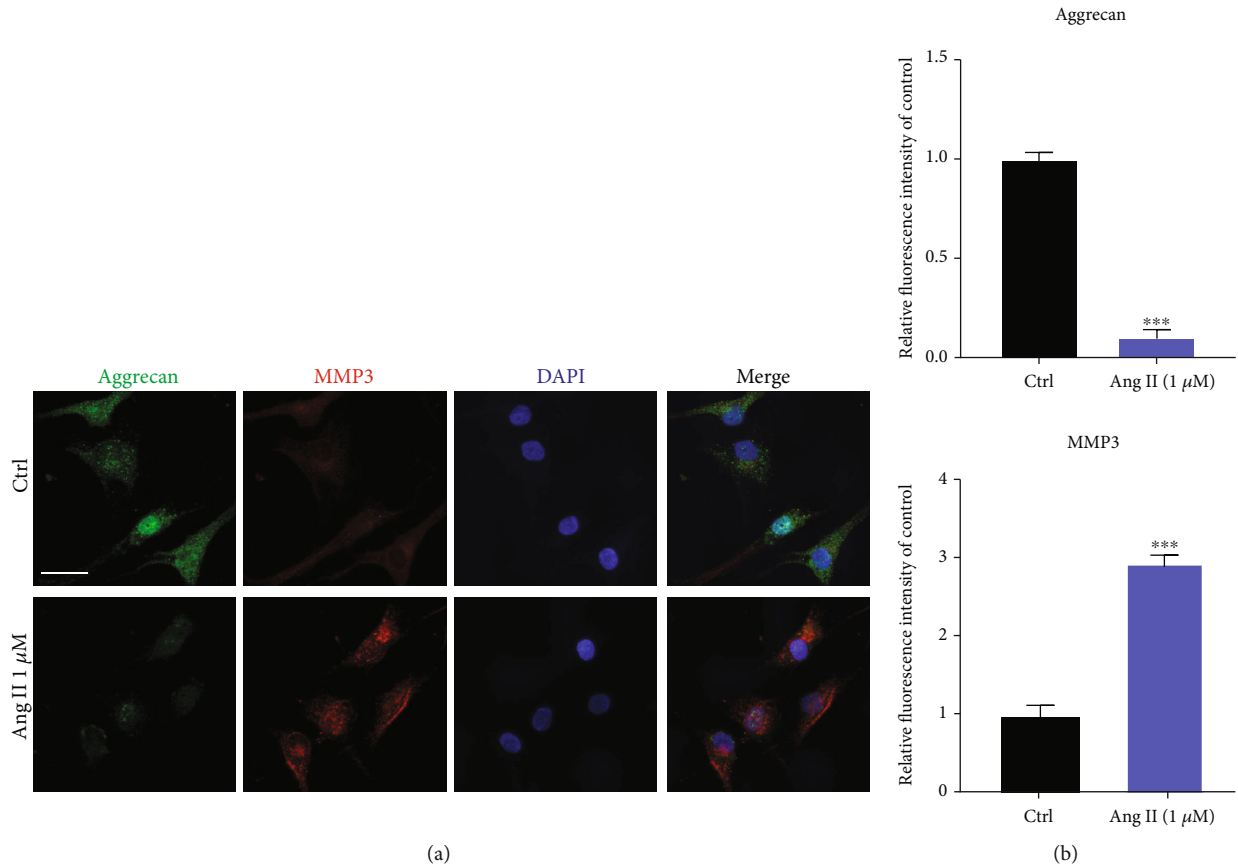


FIGURE 5: Continued.

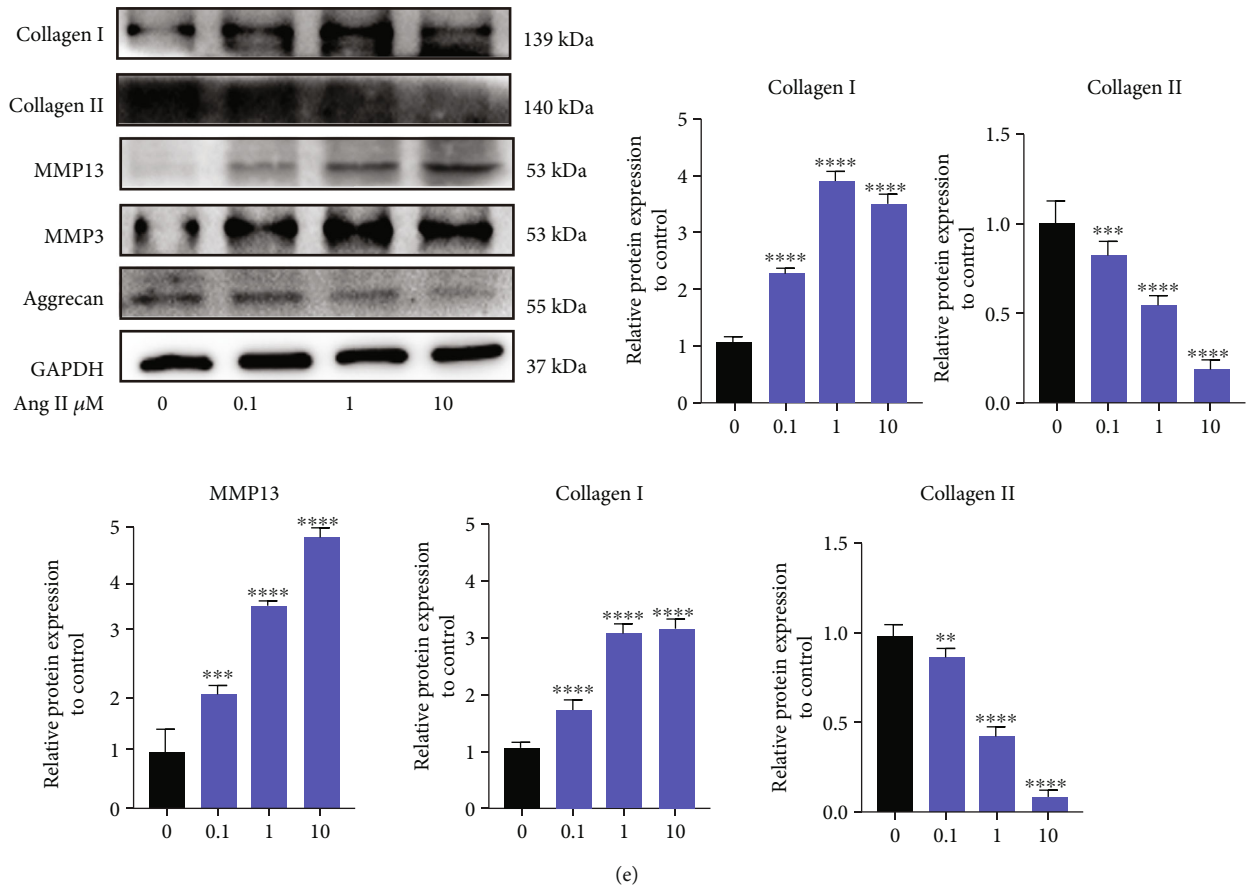


FIGURE 5: Angiotensin II induced degeneration and fibrosis phenotype in human NP cells in vitro. (a) Immunofluorescence results for the expression of aggrecan and MMP3 in human NP cells induced by Ang II. Scale bar = 50 μ m. (b) The relative expression of aggrecan and MMP3 was quantified ($n = 3$). (c) Immunofluorescence results for the expression of fibrosis-related proteins, collagen types I and II, in human NP cells induced by Ang II. Scale bar = 50 μ m. (d) Quantitative results for collagen types I and II were presented as graph ($n = 3$). (e, f) Western blot for the expression of IDD-related proteins in the human NP tissue ($n = 3$). $p < 0.05$, $**p < 0.01$, $***p < 0.001$, $****p < 0.0001$.

increasing in the degenerated disc tissue [32]. We also evaluated the effect of Ang II on macrophage polarization and found that Ang II could increase the expression of M1 markers, iNOS, IL-1 β , and TNF α and decrease the expression of M2 markers, CD 206, and YM1/2 (Supplementary Figure 2, A, B, and C). Collectively, we deduced that Ang II promoted the inflammatory reaction possibly via activating NLRP3 inflammasome and recruiting M1 macrophage in human NP cells.

3.8. Local Activated tRAS Existed in SHR Nucleus Pulposus Tissue In Vivo. Spontaneously hypertensive rats (SHR) is characterized by systematic activation of RAS, which has been widely used in RAS-related research [33]. To further confirm the biological effects of tRAS on IDD, we introduced SHR, with Wistar-Kyoto (WKY) rats being the control group. Firstly, we evaluated the change of blood pressure of SHR and WKY rats and found relatively higher SBP and DBP in SHR than those in WKY rats since the age of 3 M ($p < 0.05$) (Figures 7(a) and 7(b)). Then, we explored the local expression of tRAS components in the disc tissue. As indicated by western blot, HR with age of 6 and 12 months

showed higher expression of ACE and AT1 in the rat nucleus pulposus tissue compared to WKY rats (Figures 8(c) and 8(d)). Immunofluorescence analysis results also confirmed the higher local expression of AGT in SHR (12 months) NP cells than that in WKY rats, consistent with the results of proteomic analysis (Figures 8(e) and 8(f)). Collectively, systematic activation of RAS promoted the local activation of tRAS in SHR NP tissue in vivo. Interestingly, only the NP tissue was found positive cell that expressed ACE (Figure 7(a)). Collectively, SHR showed excessively activated tRAS in the intervertebral disc tissue, especially in the NP tissue.

3.9. Local Activated ACE/Ang II Accelerated Intervertebral Disc Degeneration in the Aging SHR Model. SHR and WKY rats with the age of 6 months and 12 months were used to evaluate the effect of local activated tRAS on IDD. As shown in Figure 9, SO-FG staining revealed that the NP tissue of SHR showed decreased proteoglycan content at both the age of 6 and 12 months (Figure 9(a)). Notably, at 12 months, the NP-AF boundary became not clear in SHR, with less NP tissue, compared to that in WKY rats (Figure 9(a)). Immunofluorescence analysis revealed that compared to WKY rats,

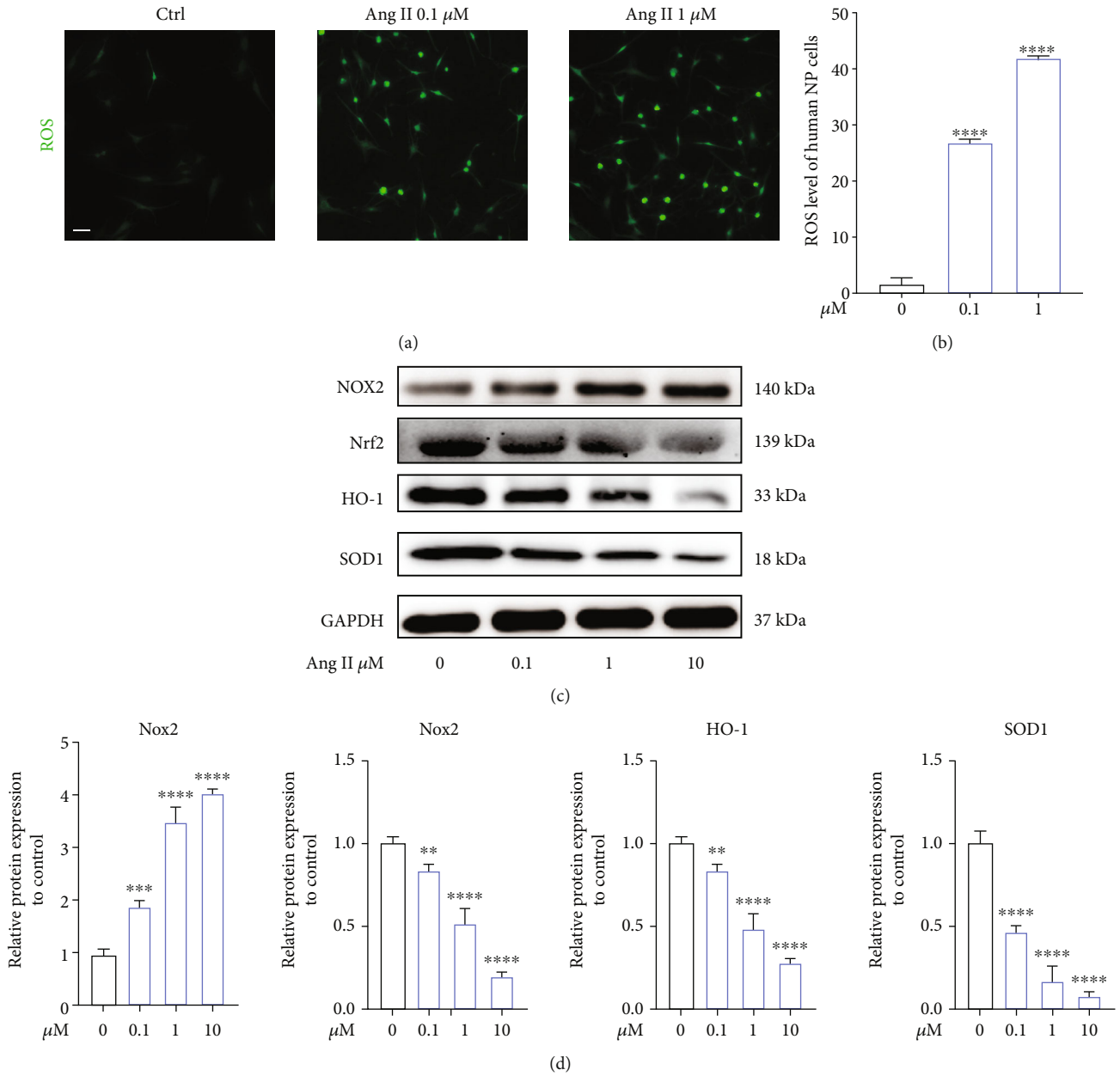


FIGURE 6: Angiotensin II increased the ROS level in human NP cells in vitro. (a) The level of intracellular ROS in human NP cells induced by Ang II. Scale bar = 50 μm . (b) The relative amount of intracellular ROS was quantified ($n = 3$). (c) Oxidative stress-related proteins were presented by western blot ($n = 3$). (d) The results of western blot were quantified as graphs ($n = 3$). $p < 0.05$, $**p < 0.01$, $***p < 0.001$, $****p < 0.0001$.

there was higher expression of MMP 3 and lower expression of collagen type II in SHR (Figure 9(b)). The TUNEL assay of THE disc tissue also suggested higher ratio of positive cells (Figures 9(c) and 9(d), $p < 0.05$). Nuclear tor erythroid 2-related factor-2 (Nrf2)/NF- κB signal cascade has been the critical pathway in IDD [2]. Therefore, we further examined the expression of these two proteins and found that at 12 months, SHR expressed higher protein level of p65 and lower protein level of Nrf2, compared to those in WKY rats (Figures 9(e) and 9(f), $p < 0.05$). Taken together, local activated ACE/Ang II could accelerate IDD in aging SHR, and Nrf2/NF- κB signal cascade could be involved.

4. Discussion

IDD is an chronic inflammation process, with plentiful activated inflammation-related cytokines (COX-2, iNOS, IL-1 β , TNF- α) and ECM degradation-related enzymes (MMP3/13, ADAMTS4/5/7) being excessively expressed [35]. Thus, strategies targeting at attenuating the inflammation response in IVD may prevent or postpone the onset of IDD. In the past few decades, increasing evidence has suggested that RAS shows its biological effects not just limited in the cardiovascular system. Various local tissue RAS (tRAS) have been identified in multiple tissues, including the brain, spinal cord,

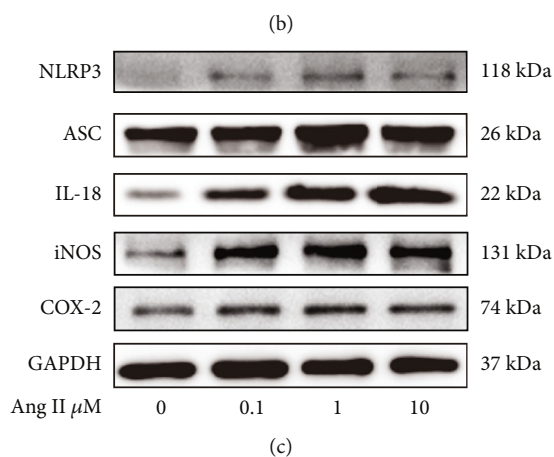
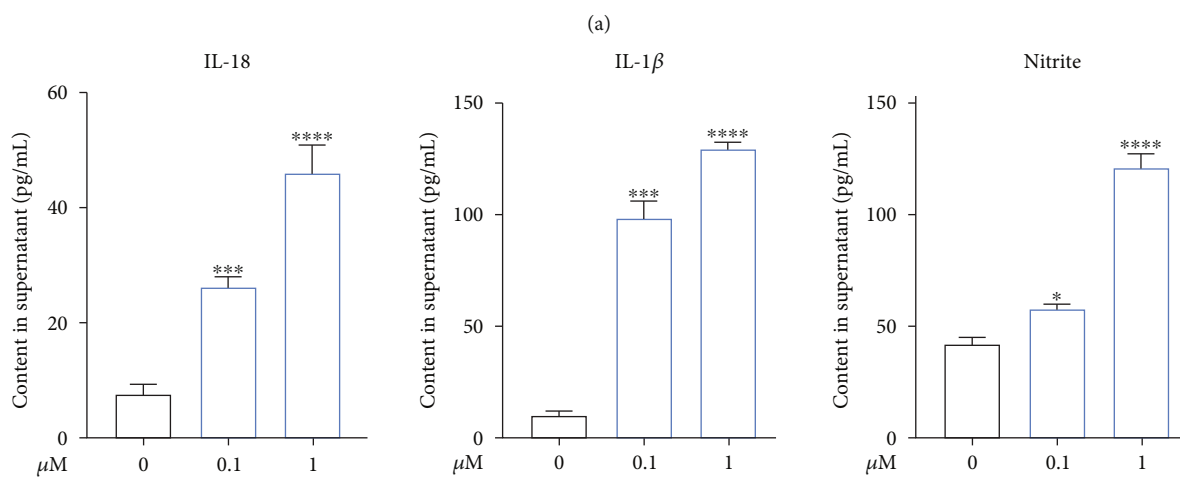
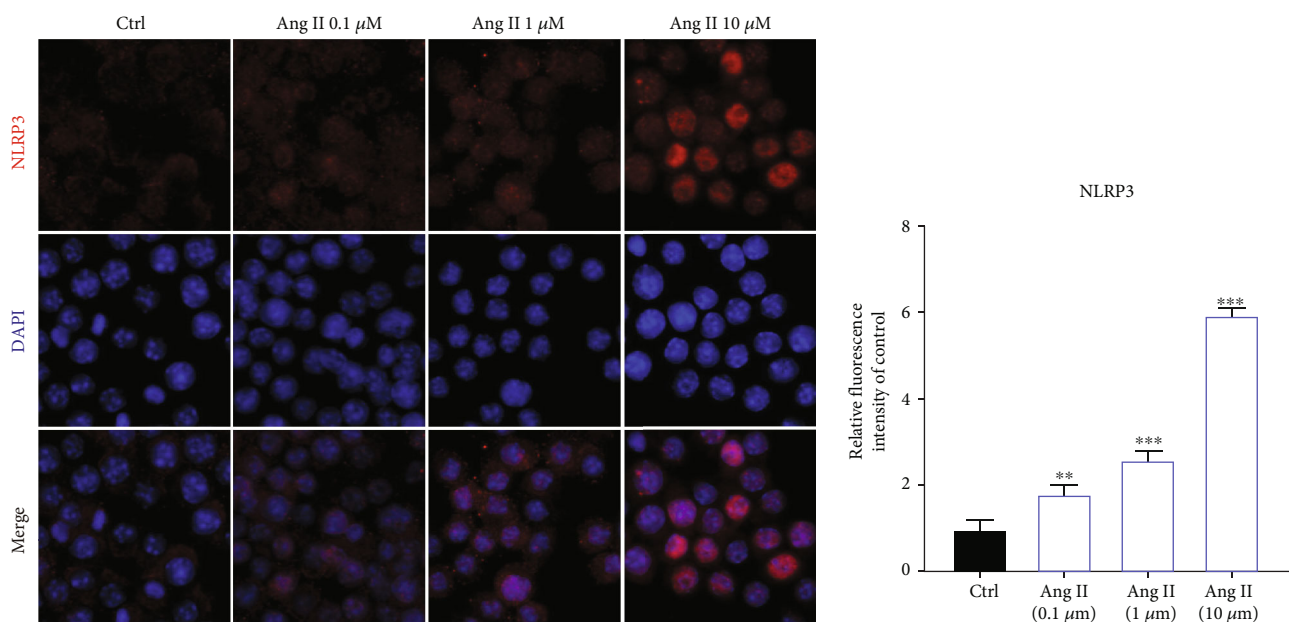


FIGURE 7: Continued.

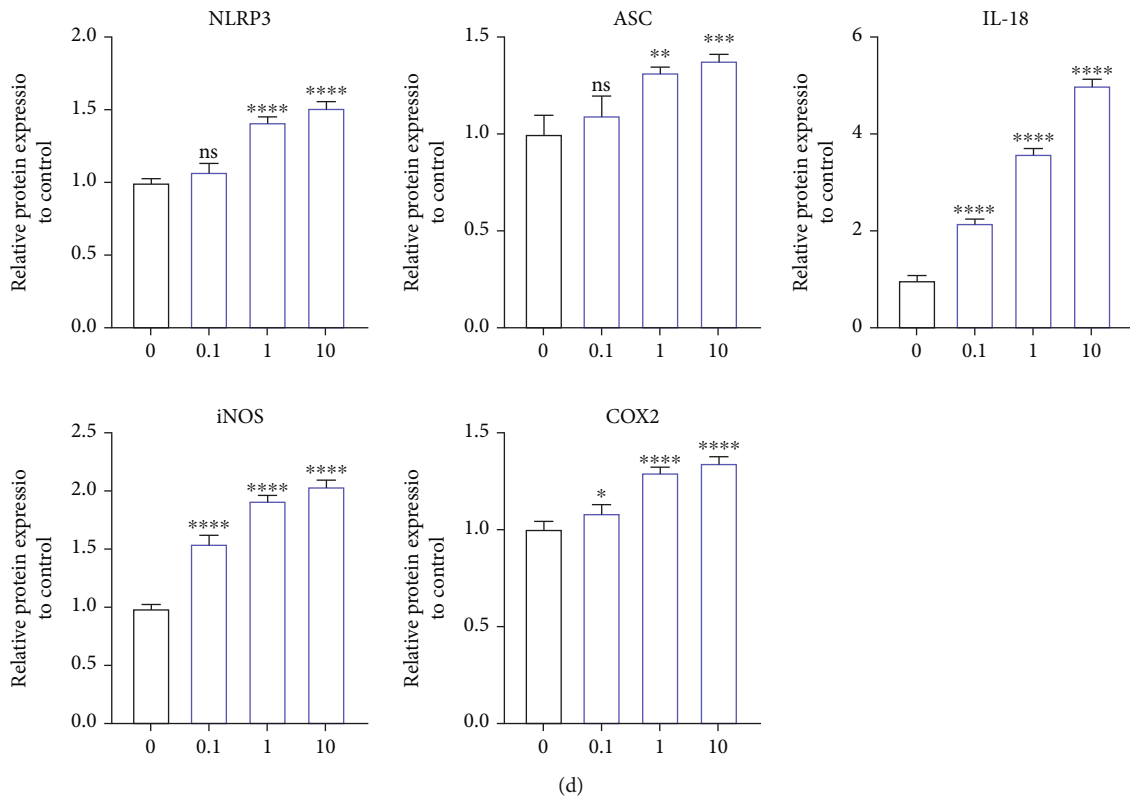


FIGURE 7: Angiotensin II promoted the activation of NLRP3 inflammasome in human NP cells in vitro. (a) Immunofluorescence results for the expression of NLRP3 in human NP cells induced by Ang II, $n = 3$. Scale bar = $50 \mu\text{m}$. (b) Ang II promoted the secretion of inflammation-related cytokines in human NP cells ($n = 3$). (c) The effects of Ang II on the expression of NLRP3 inflammasome-related proteins and inflammatory mediators in human NP cells ($n = 3$). (d) The results of western blot were quantified as graphs ($n = 3$). $p < 0.05$, ** $p < 0.01$, *** $p < 0.001$, **** $p < 0.0001$.

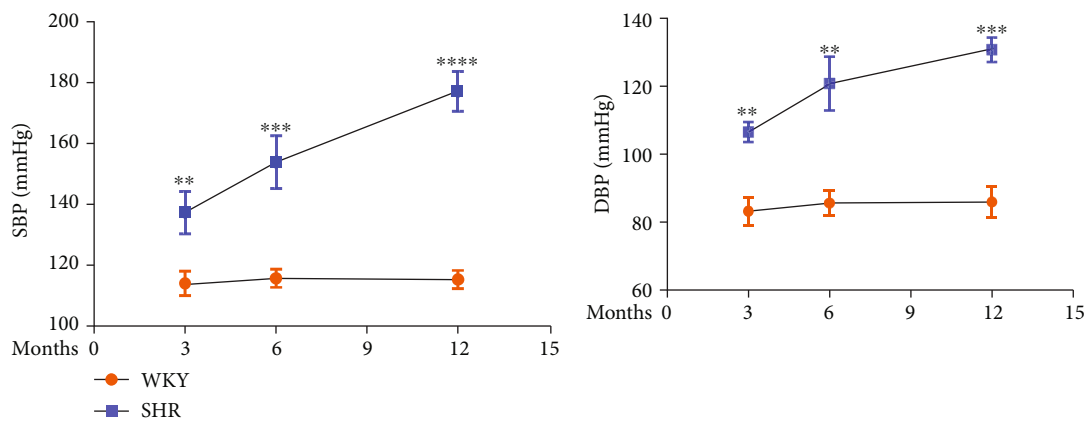
skin, kidney, heart, and bone, participating in inflammation, senescence, apoptosis, and fibrogenesis [16, 26, 36, 37]. In recent years, tRAS has also been established in both bovine and human intervertebral disc tissue, especially in the degenerated disc tissue [17, 18]. However, the exact of tRAS and IDD remains unknown.

In this present study, proteomic analysis, molecular biology analysis, and animal model were used, and the results revealed that (1) tRAS was activated in the human degenerated intervertebral disc tissue. (2) Ang II could decrease the cell viability of human NP cells, promote NP cell apoptosis, senescence, oxidative stress, and NLRP3 activation, and recruit M1 macrophage in human NP cells. (3) Ang II could trigger degeneration and fibrosis phenotype in human NP cells. (4) Local activated ACE/Ang II could accelerate IDD in aging SHR.

Cell senescence and apoptosis are two kinds of normal biological response to exogenous or endogenous stress and damage [38]. Human intervertebral disc tissue is the largest avascular tissue in the body, with high susceptibility to ischemia, hypoxia, and nutrient deprivation, and all these factors will trigger NP cell senescence and apoptosis [39]. NP cells have been the major cells that maintain the normal function of disc. Therefore, NP tissue and cells were used in this present study. We firstly evaluated the correlation between Ang II and IDD using the human intervertebral disc tissue. The

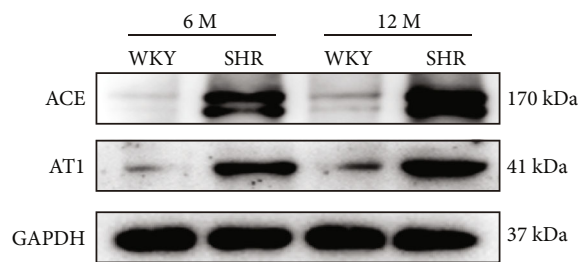
results found increased apoptotic rate of NP cells and expression of MMP13, as well as increased expression of tRAS components, such as ACE and AT1. The consistent changes above suggested a potentially close correlation between tRAS and IDD. In vitro experiment also confirmed the positive correlation between activated tRAS and IDD. SA- β -gal and p53 are the two typical senescence-related markers [40]. We found that Ang II increased the expression of SA- β -gal and p53 in human NP cells, as well as increased the amount of γ H2AX distribution over nuclear DNA. Klotho is a newly discovered antiaging gene, and deficiency in Klotho can result in senescence-like phenotypes [41]. Previous study also suggested an antagonistic relationship between Klotho and Ang II [37]. Therefore, we examined the expression of Klotho and found decreased expression of Klotho in Ang II-induced human NP cells. In addition, Ang II also caused increased ratio of apoptotic cells and decreased MMP in human NP cells. Taken together, local activated tRAS in the human disc tissue could trigger senescence and apoptosis to accelerate IDD.

Another major characteristic of IDD is excessive accumulation of MMPs and decreasing expression of aggrecan and type II collagen. In general, aggrecan and type II collagen have been the primary components in the intervertebral disc tissue, which are responsible for maintaining its high-water content feature. However, the abnormal expression of

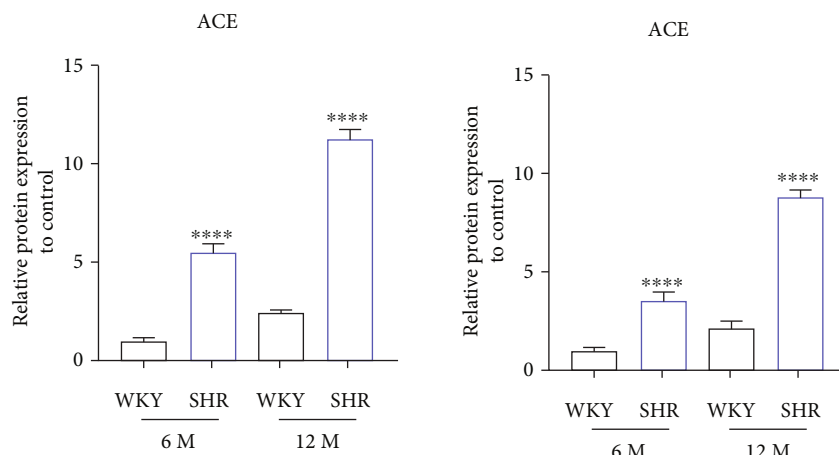


(a)

(b)



(c)



(d)

FIGURE 8: Continued.

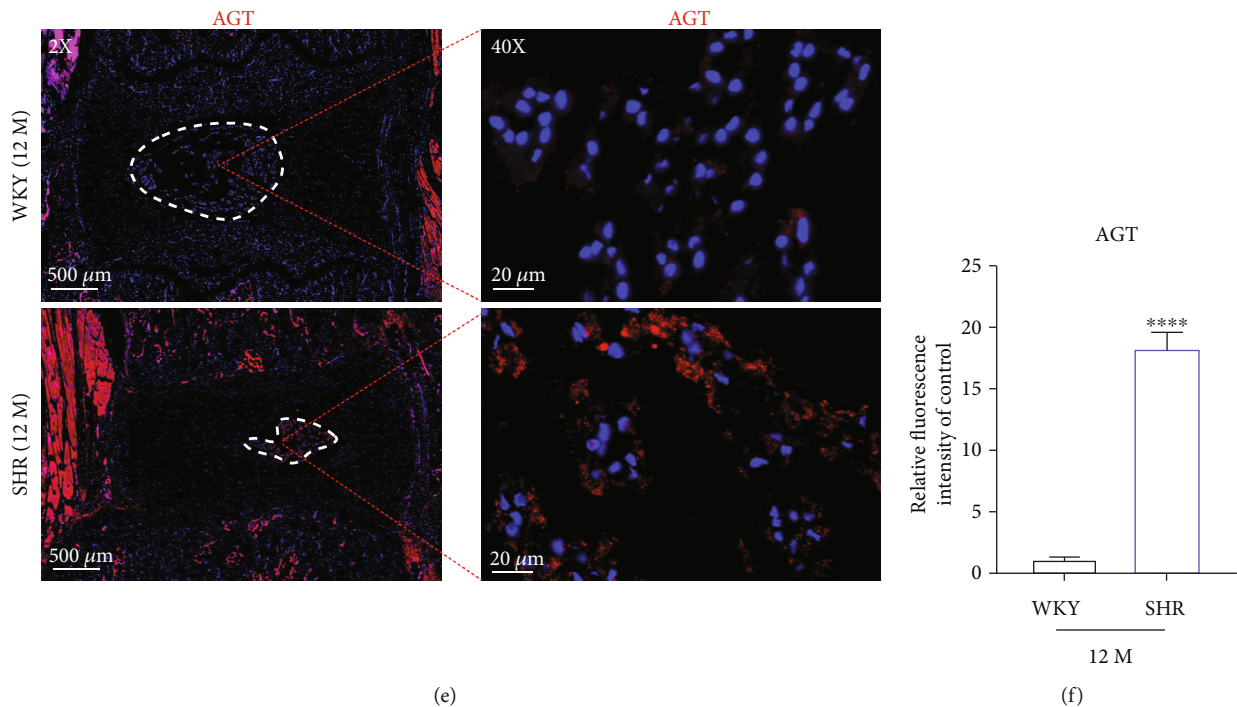


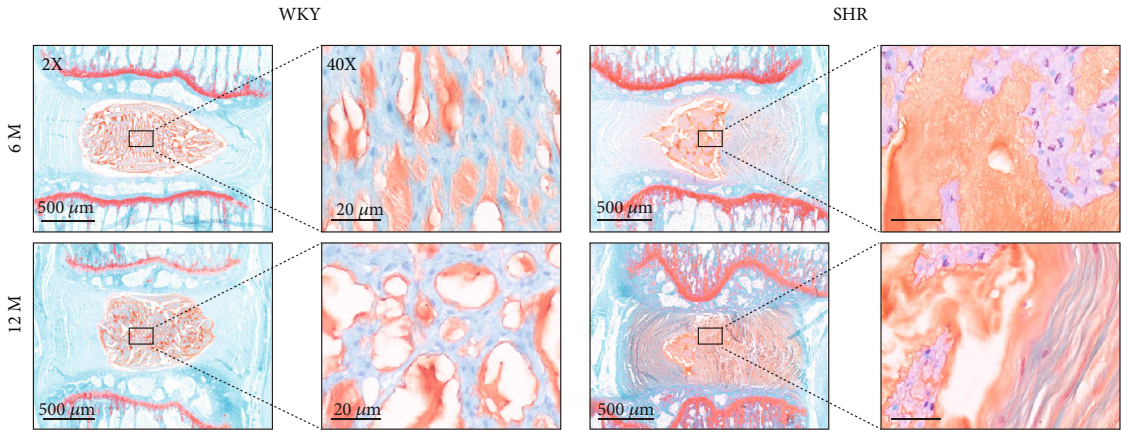
FIGURE 8: Systematic activation of RAS promoted the local expression of ACE in SHR nucleus pulposus tissue in vivo. (a, b) The blood pressure was measured with a noninvasive Tail-Cuff System Western (ALC-NIBP, Shanghai Alcott Biotech) at 3 M, 6 M, and 12 M, respectively, according to previous study [34]. (c) Western blot results for the expression of ACE and AT1 in the rat NP tissue at the age of 6 and 12 months, respectively ($n = 3$). (d) The results of western blot were quantified ($n = 3$). (e) Immunofluorescence results for the expression of AGT in the rat NP tissue at the age of 12 months ($n = 3$). (f) The results of immunofluorescence were quantified ($n = 3$). SBP: systolic blood pressure; DBP: diastolic blood pressure. $p < 0.05$, $**p < 0.01$, $***p < 0.001$, $****p < 0.0001$.

MMP3/13 will result in an imbalance between anabolism and catabolism of ECM and eventually the loss of intervertebral height [42]. In this present study, we also examined the effects of Ang II on MMPs and ECM. As shown in the results, Ang II increased the expression of MMP3/13 and decreased the expression of aggrecan and collagen type II. In addition, during IDD, the type II collagen will be gradually replaced by type I collagen [3, 7]. In fact, increasing studies have reported that Ang II induces tissue fibrosis [27, 43]. We also found that Ang II caused the increased expression of type I collagen in NP cells. The results above suggested that Ang II could induce degeneration and fibrosis phenotype in human NP cells in vitro.

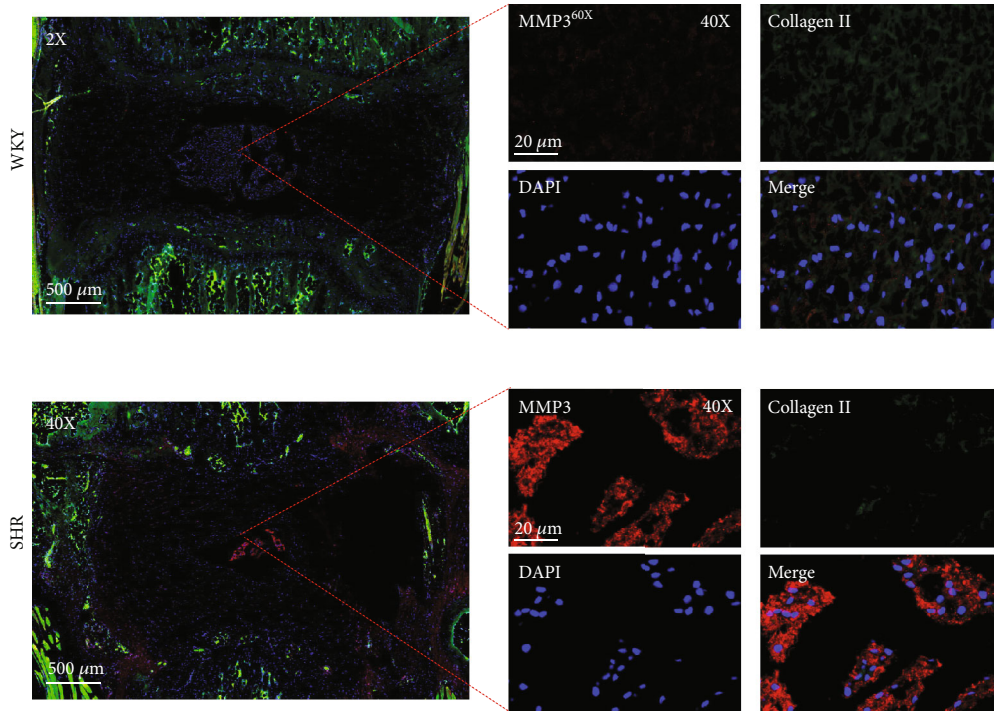
Oxidative stress and inflammation reaction have been the major causes to IDD. Excessive production of inflammatory cytokines and ROS will trigger or aggravate cell senescence, apoptosis, and ECM degradation to accelerate IDD [30]. In fact, the two biological progresses frequently cooccurred. Proinflammatory cytokines, such as IL-1 β , could enhance the level of intracellular ROS [44, 45]. Likely, high-level ROS also could increase the release of inflammatory factors [46]. Firstly, we found that Ang II dose-dependently enhanced intracellular ROS, as well as decreased the expression of Nrf2, HO-1, and SOD1. NLRP3, as one of the most studied inflammasomes, has been recently reported to participate in the inflammatory responses during IDD [47, 48]. In this present study, we found that Ang II activated the NLRP3 pathway, followed by increased production of proinflamma-

tory cytokines. In addition, the expression of inflammatory mediators, COX-2 and iNOS, were also enhanced. In addition, we also found that Ang II could induce macrophage M1 polarization. Previous studies have suggested that M1 macrophages could promote degenerative phenotypes in rat NP cells [49]. Furthermore, the mitochondrial pathway could implicate in the activation of NLRP3, and the generation of ROS and NLRP3 activation would be suppressed when mitochondrial activity was inhibited [50]. Therefore, combined the results above that Ang II could decrease MMP of mitochondrion, we deduced that Ang II could induce macrophage infiltration, inflammatory response, and oxidative stress and lead to mitochondrial dysfunction and NP cell injury. Damaged mitochondrion would further generate ROS. Subsequently, overproduction of ROS would trigger the activation of NLRP3 and the release of inflammatory cytokines. Thus, a vicious feedback among Ang II, mitochondrion, and NLRP3 will be established, accelerating NP cell injury. Agents targeting at these three points may facilitate to further treatment of IDD.

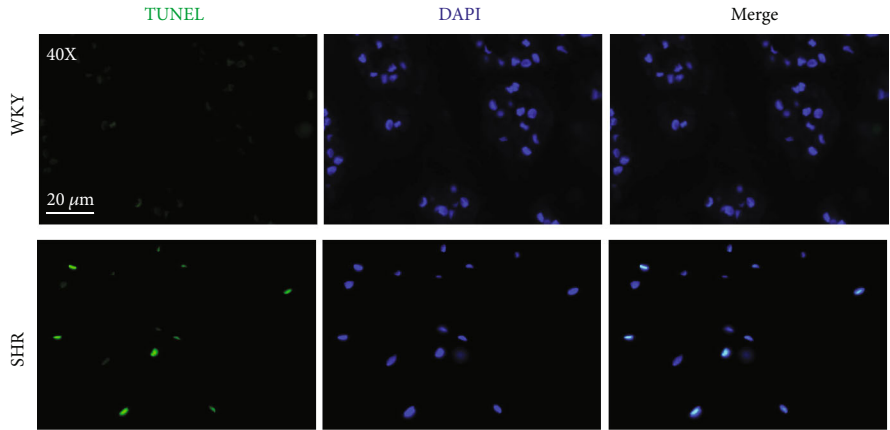
To further confirm the biological effects of tRAS on IDD, we introduced spontaneously hypertensive rats (SHR) which is characterized by systematic activation of RAS, with WKY rats as the control group [33, 34]. Firstly, we provided the evidence that local overactivated tRAS existed in the SHR NP tissue, but not in the AF tissue. Then, we found that aging SHR showed decreased proteoglycan content and reduced NP tissue compared to WKY rats. In addition, compared to



(a)



(b)



(c)

FIGURE 9: Continued.

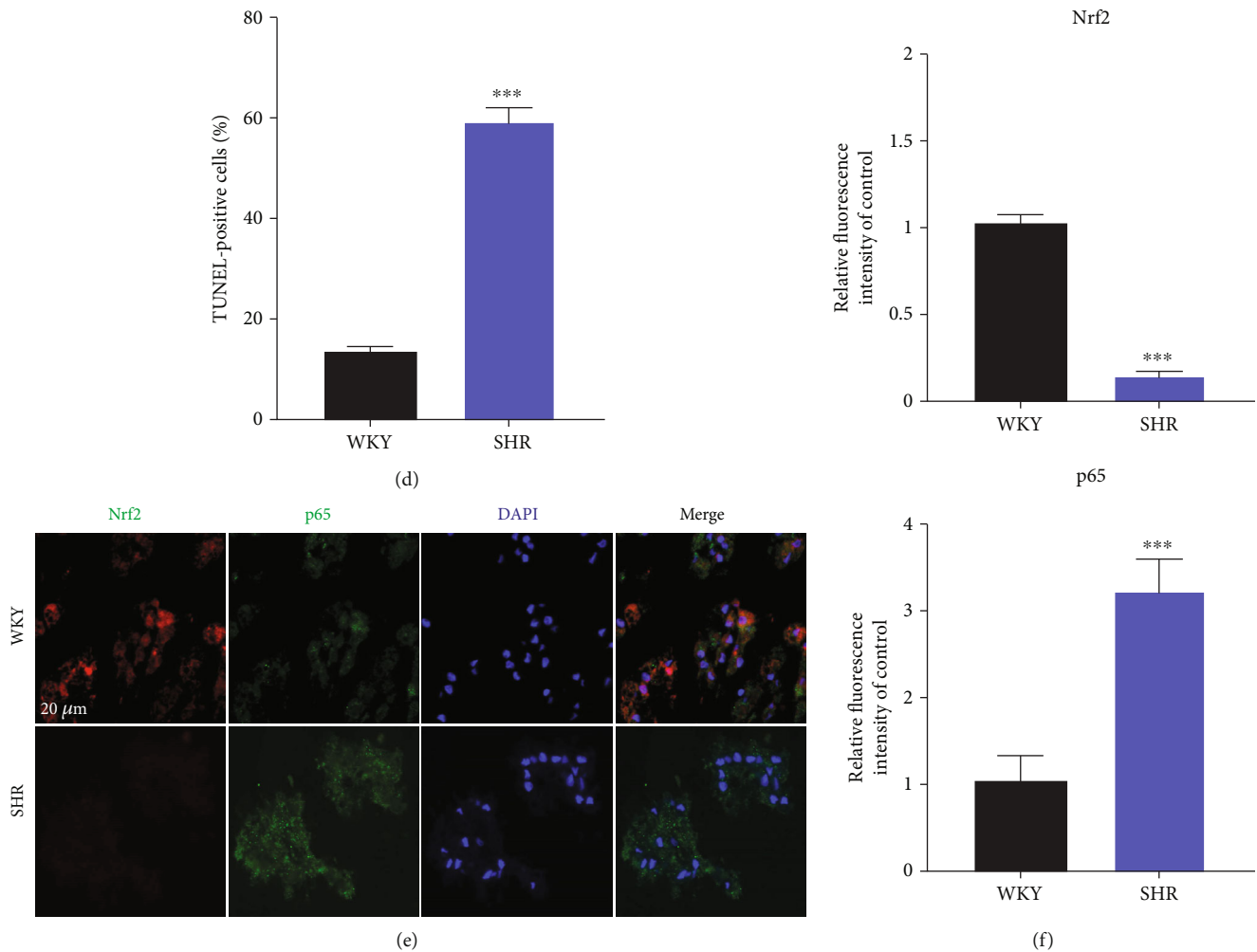


FIGURE 9: Local activated ACE/Ang II accelerated intervertebral disc degeneration in the aging SHR model. (a) SO-FG staining of intervertebral disc in the rat NP tissue at the age of 6 and 12 months, respectively ($n = 3$). (b) Immunofluorescence results for the expression of MMP3 and collagen II in the rat NP tissue at the age of 12 months ($n = 3$). (c, d) TUNEL staining and quantified results for apoptotic NP cells in the rat NP tissue at the age of 12 months, respectively ($n = 3$). (e, f) Immunofluorescence results for the expression of Nrf2 and p65 in the rat NP tissue at the age of 12 months ($n = 3$). $p < 0.05$, $**p < 0.01$, $***p < 0.001$, $****p < 0.0001$.

WKY rats, there were higher ratio of apoptotic cells, higher expression of MMP3, and lower expression of collagen I in the SHR NP tissue. The results were consistent with the results of in vitro experiments above, which suggested that SHR had higher susceptibility to IDD. Therefore, a potential correlation between hypertension and IDD may exist, which is consistent with previous clinical studies that hypertension was a risk factor to low back pain [9, 51]. In addition, treatment with RAS inhibitors has been shown anti-inflammatory effects in arthritis, a similar disease to IDD [52]. Therefore, tRAS may be a novel therapeutic target for IDD. In addition, we found that SHR at 12 months expressed higher protein level of p65 and lower protein level of Nrf2, which have been reported to correlate with oxidative stress and inflammation during IDD [2]. Taken together, local activated ACE/Ang II could accelerate IDD in aging SHR, and Nrf2/NF- κ B signal cascade could be involved. However, the further exact mechanism between tRAS and IDD remains to be identified.

Several limitations must be acknowledged. Firstly, the clinical sample size in this present study was still limited. However, to minimize the potential influence factors, we confirmed the correlation between tRAS and IDD from perspectives of proteomic analysis, western blot, and immunohistochemistry analysis. In addition, human NP cells induced by IL-1 β and TNF α also showed consistent results. Therefore, we could conclude that the activated tRAS exists in the human degenerated intervertebral disc tissue. Secondly, SHR has been reported to show overactivated systematic RAS. Although we have also confirmed the existence of activated tRAS in the SHR NP tissue, it will be better to examine the relationship between Ang II and IDD using animal models that specifically highly expressed Ang II gene. Thirdly, therapeutic experiments against the ACE/Ang II axis were not shown in this present study. In fact, we are now performing related experiments, and further outcomes will be presented in this journal if possible.

5. Conclusion

Degenerated intervertebral disc tissue showed excessively activated tRAS. Local activation of tRAS could induce NP cell senescence, apoptosis, oxidative stress, and inflammatory reaction to cause degeneration and fibrosis phenotype in human NP cells. These biological effects of Ang II on NP cells may be achieved via Nrf2/p65/NLRP3 pathway. The results will provide new information for future investigation of hypertension and IDD.

Data Availability

Data are available when required.

Conflicts of Interest

The authors declare that they have no conflicts of interest.

Authors' Contributions

Kaiqiang Sun, Xiaofei Sun, and Jingchuan Sun contributed equally to this study and should be considered as co-first authors.

Acknowledgments

The study is supported by the National Natural Science Foundation of China, Grant/Award Numbers: No. 81871828, No. 81802218, and No. 8210091000 (receive number).

Supplementary Materials

Supplementary Figure 1: illustration of the study workflow LC-MS/MS: liquid chromatography-tandem mass spectrometry. Supplementary Figure 2: Ang II promoted M1 polarization of RAW264.7. (a, b) Ang II increased the expression of M1 marker, iNOS, and decrease the expression of M2 marker, CD 206. (c) RT-qPCR revealed that Ang II increased the expression of M1 markers, IL-1 β and TNF α , and decrease the expression of M2 markers, CD 206 and YM1/2. Scale bar = 20 μ m. (*Supplementary Materials*)

References

- [1] S. Yang, F. Zhang, J. Ma, and W. Ding, "Intervertebral disc ageing and degeneration: the antiapoptotic effect of oestrogen," *Ageing Research Reviews*, vol. 57, p. 100978, 2020.
- [2] X. Luo, L. Huan, F. Lin et al., "Ulinastatin ameliorates IL-1 β -induced cell dysfunction in human nucleus pulposus cells via Nrf2/NF- κ B pathway," *Oxidative medicine and cellular longevity*, vol. 2021, 21 pages, 2021.
- [3] J. Dowdell, M. Erwin, T. Choma, A. Vaccaro, J. Iatridis, and S. K. Cho, "Intervertebral disk degeneration and repair," *Neurosurgery*, vol. 80, no. 3S, pp. S46-S54, 2017.
- [4] M. V. Risbud and I. M. Shapiro, "Role of cytokines in intervertebral disc degeneration: pain and disc content," *Nature reviews. Rheumatology*, vol. 10, no. 1, pp. 44-56, 2014.
- [5] P. Wilkens, I. B. Scheel, O. Grundnes, C. Hellum, and K. Storheim, "Effect of glucosamine on pain-related disability in patients with chronic low back pain and degenerative lumbar osteoarthritis: a randomized controlled trial," *JAMA*, vol. 304, no. 1, pp. 45-52, 2010.
- [6] C. Chen, T. Zhou, X. Sun et al., "Autologous fibroblasts induce fibrosis of the nucleus pulposus to maintain the stability of degenerative intervertebral discs," *Bone research*, vol. 8, no. 1, 2020.
- [7] P. Sampara, R. R. Banala, S. K. Vemuri, G. R. AV, and S. GPV, "Understanding the molecular biology of intervertebral disc degeneration and potential gene therapy strategies for regeneration: a review," *Gene therapy*, vol. 25, no. 2, pp. 67-82, 2018.
- [8] Y. H. Bae, J. S. Shin, J. Lee et al., "Association between hypertension and the prevalence of low back pain and osteoarthritis in Koreans: a cross-sectional study," *PloS one*, vol. 10, no. 9, article e0138790, 2015.
- [9] I. Heuch, I. Heuch, K. Hagen, and J. A. Zwart, "Does high blood pressure reduce the risk of chronic low back pain? The Nord-Trøndelag Health Study," *European journal of pain*, vol. 18, no. 4, pp. 590-598, 2014.
- [10] M. A. Sparks, S. D. Crowley, S. B. Gurley, M. Mirosou, and T. M. Coffman, "Classical renin-angiotensin system in kidney physiology," *Comprehensive Physiology*, vol. 4, no. 3, pp. 1201-1228, 2014.
- [11] P. Dandona, S. Dhindsa, H. Ghanim, and A. Chaudhuri, "Angiotensin II and inflammation: the effect of angiotensin-converting enzyme inhibition and angiotensin II receptor blockade," *Journal of human hypertension*, vol. 21, no. 1, pp. 20-27, 2007.
- [12] Y. Li, G. Shen, C. Yu et al., "Angiotensin II induces mitochondrial oxidative stress and mtDNA damage in osteoblasts by inhibiting SIRT1-FoxO3a-MnSOD pathway," *Biochemical and biophysical research communications*, vol. 455, no. 1-2, pp. 113-118, 2014.
- [13] S. Zhou, H. Lu, R. Chen et al., "Angiotensin II enhances the acetylation and release of HMGB1 in RAW264.7 macrophage," *Cell biology international*, vol. 42, no. 9, pp. 1160-1169, 2018.
- [14] A. J. Shepherd, A. D. Mickle, J. P. Golden et al., "Macrophage angiotensin II type 2 receptor triggers neuropathic pain," *Proceedings of the National Academy of Sciences of the United States of America*, vol. 115, no. 34, pp. E8057-E8066, 2018.
- [15] C. Mo, J. Ke, D. Zhao, and B. Zhang, "Role of the renin-angiotensin-aldosterone system in bone metabolism," *Journal of bone and mineral metabolism*, vol. 38, no. 6, pp. 772-779, 2020.
- [16] Y. Wang, J. Kou, H. Zhang et al., "The renin-angiotensin system in the synovium promotes periarticular osteopenia in a rat model of collagen-induced arthritis," *International immunopharmacology*, vol. 65, pp. 550-558, 2018.
- [17] R. Morimoto, K. Akeda, R. Iida et al., "Tissue renin-angiotensin system in the intervertebral disc," *Spine*, vol. 38, no. 3, pp. E129-E136, 2013.
- [18] Z. Li, L. Wystrach, A. Bernstein et al., "The tissue-renin-angiotensin-system of the human intervertebral disc," *European cells & materials*, vol. 40, pp. 115-132, 2020.
- [19] P. Li, X. Che, Y. Gao, and R. Zhang, "Proteomics and bioinformatics analysis of cartilage in post-traumatic osteoarthritis in a mini-pig model of anterior cruciate ligament repair," *Medical science monitor: international medical journal of experimental and clinical research*, vol. 26, article e920104, 2020.

- [20] D. Huang, Y. Wang, J. Lv et al., "Proteomic profiling analysis of postmenopausal osteoporosis and osteopenia identifies potential proteins associated with low bone mineral density," *PeerJ*, vol. 8, article e9009, 2020.
- [21] N. Tang, Y. Dong, C. Chen, and H. Zhao, "Anisodamine maintains the stability of intervertebral disc tissue by inhibiting the senescence of nucleus pulposus cells and degradation of extracellular matrix via interleukin-6/Janus kinases/signal transducer and activator of transcription 3 pathway," *Frontiers in pharmacology*, vol. 11, article 519172, 2020.
- [22] A. Biran, L. Zada, P. Abou Karam et al., "Quantitative identification of senescent cells in aging and disease," *Aging cell*, vol. 16, no. 4, pp. 661–671, 2017.
- [23] E. J. Novais, B. O. Diekman, I. M. Shapiro, and M. V. Risbud, "p16^{Ink4a} deletion in cells of the intervertebral disc affects their matrix homeostasis and senescence associated secretory phenotype without altering onset of senescence," *Matrix biology: journal of the International Society for Matrix Biology*, vol. 82, pp. 54–70, 2019.
- [24] X. Xu, C. Z. Di Wang, B. Gao et al., "Progerin accumulation in nucleus pulposus cells impairs mitochondrial function and induces intervertebral disc degeneration and therapeutic effects of sulforaphane," *Theranostics*, vol. 9, no. 8, pp. 2252–2267, 2019.
- [25] M. C. Maiuri, E. Zalckvar, A. Kimchi, and G. Kroemer, "Self-eating and self-killing: crosstalk between autophagy and apoptosis," *Nature reviews. Molecular cell biology*, vol. 8, no. 9, pp. 741–752, 2007.
- [26] S. E. Silva Ana Cristina and M. M. Teixeira, "ACE inhibition, ACE2 and angiotensin-(1-7) axis in kidney and cardiac inflammation and fibrosis," *Pharmacological research*, vol. 107, pp. 154–162, 2016.
- [27] J. Miao, J. Liu, J. Niu et al., "Wnt/ β -catenin/RAS signaling mediates age-related renal fibrosis and is associated with mitochondrial dysfunction," *Aging cell*, vol. 18, no. 5, p. e13004, 2019.
- [28] F. Zhang, Z. Dong, S. Gao, G. Chen, and D. Liu, "AT1R-mediated apoptosis of bone marrow mesenchymal stem cells is associated with mtROS production and mtDNA reduction," *Oxidative medicine and cellular longevity*, vol. 2019, 9 pages, 2019.
- [29] N. Kelley, D. Jeltema, Y. Duan, and Y. He, "The NLRP3 inflammasome: an overview of mechanisms of activation and regulation," *International journal of molecular sciences*, vol. 20, no. 13, p. 3328, 2019.
- [30] F. Chen, G. Jiang, H. Liu et al., "Melatonin alleviates intervertebral disc degeneration by disrupting the IL-1 β /NF- κ B-NLRP3 inflammasome positive feedback loop," *Bone research*, vol. 8, no. 1, 2020.
- [31] D. He, M. Zhou, Z. Bai, Y. Wen, J. Shen, and Z. Hu, "Propionibacterium acnes induces intervertebral disc degeneration by promoting nucleus pulposus cell pyroptosis via NLRP3-dependent pathway," *Biochemical and biophysical research communications*, vol. 526, no. 3, pp. 772–779, 2020.
- [32] K. R. Nakazawa, B. A. Walter, D. M. Laudier et al., "Accumulation and localization of macrophage phenotypes with human intervertebral disc degeneration," *The spine journal: official journal of the North American Spine Society*, vol. 18, no. 2, pp. 343–356, 2018.
- [33] F. Zhang, Y. Xu, Y. Pan et al., "Effects of angiotensin-(1-7) and angiotensin II on acetylcholine-induced vascular relaxation in spontaneously hypertensive rats," *Oxidative medicine and cellular longevity*, vol. 2019, 12 pages, 2019.
- [34] Y. Deng, X. Tan, M. L. Li, W. Z. Wang, and Y. K. Wang, "Angiotensin-converting enzyme 2 in the rostral ventrolateral medulla regulates cholinergic signaling and cardiovascular and sympathetic responses in hypertensive rats," *Neuroscience bulletin*, vol. 35, no. 1, pp. 67–78, 2019.
- [35] Y. Liu, Y. Qu, L. Liu et al., "PPAR- γ agonist pioglitazone protects against IL-17 induced intervertebral disc inflammation and degeneration via suppression of NF- κ B signaling pathway," *International immunopharmacology*, vol. 72, pp. 138–147, 2019.
- [36] J. D. Vadhan and R. C. Speth, "The role of the brain renin-angiotensin system (RAS) in mild traumatic brain injury (TBI)," *Pharmacology & therapeutics*, vol. 218, article 107684, 2021.
- [37] A. Romero, Á. San Hipólito-Luengo, L. A. Villalobos et al., "The angiotensin-(1-7)/Mas receptor axis protects from endothelial cell senescence via klotho and Nrf2 activation," *Aging Cell*, vol. 18, no. 3, article e12913, 2019.
- [38] C. Feng, Y. Zhang, M. Yang et al., "Oxygen-sensing Nox4 generates genotoxic ROS to induce premature senescence of nucleus pulposus cells through MAPK and NF- κ B pathways," *Oxidative medicine and cellular longevity*, vol. 2017, Article ID 7426458, 15 pages, 2017.
- [39] K. Sun, J. Zhu, J. Sun et al., "Neuropeptide Y prevents nucleus pulposus cells from cell apoptosis and IL-1 β -induced extracellular matrix degradation," *Cell cycle*, vol. 20, no. 10, pp. 960–977, 2021.
- [40] H. Zhu, B. Sun, L. Zhu, G. Zou, and Q. Shen, "N6-methyladenosine induced miR-34a-5p promotes TNF- α -induced nucleus pulposus cell senescence by targeting SIRT1," *Frontiers in cell and developmental biology*, vol. 9, article 642437, 2021.
- [41] Y. Xu and Z. Sun, "Molecular basis of Klotho: from gene to function in aging," *Endocrine reviews*, vol. 36, no. 2, pp. 174–193, 2015.
- [42] W. Ni, F. Zhang, L. Zheng et al., "Cyclin-dependent kinase 9 (CDK9) inhibitor atavaciclib suppresses intervertebral disk degeneration via the inhibition of the NF- κ B signaling pathway," *Frontiers in cell and developmental biology*, vol. 8, article 579658, 2020.
- [43] Q. Lu, Z. Ma, Y. Ding et al., "Circulating miR-103a-3p contributes to angiotensin II-induced renal inflammation and fibrosis via a SNRK/NF- κ B/p65 regulatory axis," *Nature communications*, vol. 10, no. 1, p. 2145, 2019.
- [44] J. Chen, J. Xuan, Y. T. Gu et al., "Celastrol reduces IL-1 β induced matrix catabolism, oxidative stress and inflammation in human nucleus pulposus cells and attenuates rat intervertebral disc degeneration in vivo," *Biomedicine & pharmacotherapy = Biomedecine & pharmacotherapie*, vol. 91, pp. 208–219, 2017.
- [45] Y. Liu, J. Lin, X. Wu et al., "Aspirin-mediated attenuation of intervertebral disc degeneration by ameliorating reactive oxygen species in vivo and in vitro," *Oxidative medicine and cellular longevity*, vol. 2019, 20 pages, 2019.
- [46] P. Tang, J. M. Gu, Z. A. Xie et al., "Honokiol alleviates the degeneration of intervertebral disc via suppressing the activation of TXNIP-NLRP3 inflammasome signal pathway," *Free radical biology & medicine*, vol. 120, pp. 368–379, 2018.
- [47] K. Zhao, R. An, Q. Xiang et al., "Acid-sensing ion channels regulate nucleus pulposus cell inflammation and pyroptosis

- via the NLRP3 inflammasome in intervertebral disc degeneration,” *Cell proliferation*, vol. 54, no. 1, p. e12941, 2021.
- [48] Z. H. Chen, S. H. Jin, M. Y. Wang et al., “Enhanced NLRP3, caspase-1, and IL-1 β levels in degenerate human intervertebral disc and their association with the grades of disc degeneration,” *Anatomical record*, vol. 298, no. 4, pp. 720–726, 2015.
- [49] L. Ni, Y. Zheng, T. Gong et al., “Proinflammatory macrophages promote degenerative phenotypes in rat nucleus pulposus cells partly through ERK and JNK signaling,” *Journal of cellular physiology*, vol. 234, no. 5, pp. 5362–5371, 2019.
- [50] W. Zhou, X. Liu, K. Cheng, X. Zhang, J. Lu, and R. Hu, “X-11-5-27, a daidzein derivative, inhibits NLRP3 inflammasome activity via promoting autophagy,” *Experimental cell research*, vol. 360, no. 2, pp. 320–327, 2017.
- [51] T. P. Bento, C. V. dos Santos Genebra, N. M. Maciel, G. P. Cornelio, S. F. Simeão, and A. de Vitta, “Low back pain and some associated factors: is there any difference between genders?,” *Brazilian journal of physical therapy*, vol. 24, no. 1, pp. 79–87, 2020.
- [52] Y. Wu, X. Lu, M. Li et al., “Renin-angiotensin system in osteoarthritis: a new potential therapy,” *International immunopharmacology*, vol. 75, article 105796, 2019.

Research Article

FAM134B-Mediated ER-phagy Upregulation Attenuates AGEs-Induced Apoptosis and Senescence in Human Nucleus Pulposus Cells

Rongjin Luo, Shuai Li, Gaocai Li, Saideng Lu , Weifeng Zhang, Hui Liu, Jie Lei, Liang Ma, Wencan Ke, Zhiwei Liao , Bingjin Wang, Yu Song, Kun Wang, Yukun Zhang , and Cao Yang 

Department of Orthopaedics, Union Hospital, Tongji Medical College, Huazhong University of Science and Technology, Wuhan 430022, China

Correspondence should be addressed to Cao Yang; caoyangunion@hust.edu.cn

Received 9 May 2021; Accepted 24 July 2021; Published 6 August 2021

Academic Editor: Wenyuan Ding

Copyright © 2021 Rongjin Luo et al. This is an open access article distributed under the Creative Commons Attribution License, which permits unrestricted use, distribution, and reproduction in any medium, provided the original work is properly cited.

Previous studies have established the pathogenic role of advanced glycation end products (AGEs) accumulation in intervertebral disc degeneration (IDD). Emerging evidence indicates that ER-phagy serves as a crucial cellular adaptive mechanism during stress conditions. This study is aimed at investigating the role of FAM134B-mediated ER-phagy in human nucleus pulposus (NP) cells upon AGEs treatment and exploring its regulatory mechanisms. We observed that AGEs treatment resulted in significantly increased apoptosis, senescence, and ROS accumulation in human NP cells; meanwhile, the enhanced apoptosis and senescence by AGEs treatment could be partially alleviated with the classic ROS scavenger NAC administration. Furthermore, we confirmed that FAM134B-mediated ER-phagy was activated under AGEs stimulation via ROS pathway. Importantly, it was also found that FAM134B overexpression could efficiently relieve intracellular ROS accumulation, apoptosis, and senescence upon AGEs treatment; conversely, FAM134B knockdown markedly resulted in opposite effects. In conclusion, our data demonstrate that FAM134B-mediated ER-phagy plays a vital role in AGEs-induced apoptosis and senescence through modulating cellular ROS accumulation, and targeting FAM134B-mediated ER-phagy could be a promising therapeutic strategy for IDD treatment.

1. Introduction

Intervertebral disc degeneration (IDD) and secondary spine pathological changes such as spinal instability, spinal stenosis, and disc herniation are considered as the leading causes of low back pain, resulting in a substantial burden on the global health care system [1]. Multiple factors have been verified to be associated with the pathogenesis of IDD, including genetic factors, mechanical overloading, nutrition loss, and inflammatory mediators [2–5]. Our previous studies have shown that advanced glycation end products (AGEs) could accumulate in the intervertebral disc with aging and drive

the apoptosis of nucleus pulposus (NP) cells and impede its metabolism balance via endoplasmic reticulum (ER) and mitochondria pathway [6–8]. However, the underlying mechanisms are still not fully elucidated.

NP cells are identified as the main cell type resident in the NP tissue, responsible for the synthesis and secretion of the extracellular matrix and maintaining its metabolic balance. The maintenance of an adequate number of functionally active NP cells is a prerequisite for the intervertebral disc to execute its normal physiological activities. It is widely recognized that the degenerated disc is characterized by a decreased number of NP cells and reduced function of resid-

ual NP cells [9]. The accumulation of AGEs in the NP during aging process could significantly damage the normal physiological functionalities of intracellular organelles like mitochondria and ER through reactive oxygen species (ROS) generation and calcium mobilization pathway and consequently lead to decreased function or death of NP cells [7, 8]. Although intracellular ROS dyshomeostasis under stress conditions has been well implicated in the pathogenesis of autophagy, senescence, and apoptosis of NP cells, the potential regulatory mechanisms are still not fully explained.

The ER is the central intracellular organelle that responsible for protein synthesis, maturation, and quality control. The protein-folding ability of ER is vulnerably susceptible to genetic and environmental stress, leading to accumulation of unfolded/misfolded proteins in the ER lumen, namely, ER stress, and sustained ER stress can initiate cellular self-destruction procedures [10, 11]. ER-phagy or reticulophagy is a special type of selective autophagy, whereby parts of the ER fragments are engulfed by autophagosomes through specific receptors and then delivered to lysosomal degradation, which in turn attempts to restore cellular energy levels and ER homeostasis [12]. Currently, multiple ER-phagy receptors have been identified in mammals, including FAM134B (RETREG1, reticulophagy regulator 1), RTN3L (reticulon 3 long isoform), SEC62 (SEC62 homolog), CCPG1 (cell-cycle progression gene 1), ATL3 (atlastin 3), and TEX264 (testis-expressed 264), the LIR (LC3-interacting region) domains of which directly recruit phagophores to facilitate ER-phagy [13–18]. FAM134B is the first identified ER-phagy receptor that involves in ER fragments and ER-resident protein clearance in mammalian cells; moreover, dysfunction of FAM134B has been reported to be involved in many diseases, including neuropathy, viral infection, osteoarthritis, and cancer [19–22]. Nevertheless, the role and mechanism of FAM134B and related ER-phagy in the initiation and progress of IDD has not been explored yet.

The purpose of our study was attempted to elucidate the relationship between FAM134B-mediated ER-phagy and apoptosis and senescence under AGEs stimulation. Our studies revealed that AGEs treatment could increase apoptosis, senescence, and FAM134B-mediated ER-phagy through ROS pathway in human NP cells; genetical knockdown and overexpression of FAM134B could increase and reduce cellular ROS generation, apoptosis, and senescence, respectively. Therefore, our findings provide a novel mechanistic insight into the pathogenesis of IDD.

2. Materials and Methods

2.1. Ethics Statement. Experimental ethics approval for the study was obtained from the Ethics Committee of Tongji Medical College, Huazhong University of Science and Technology (No. S341). Written informed consent was obtained from every donor participated in this study.

2.2. Cell Culture and Treatment. The primary human NP cells were isolated from relative undegenerated (Pfirrmann I or II) NP tissues that donated by 3 adolescent idiopathic scoliosis patients (2 males and 1 female, aged 16, 14, and 20

years old, respectively) undergoing spinal deformity correction surgery. The degenerated degree of the corresponding segment was determined by preoperative magnetic resonance imaging according to Pfirrmann classification [23]. Briefly, the freshly harvested human NP tissues were rinsed three times with phosphate buffer saline (PBS, Gibco, Grand Island, NY, USA), minced into 2–3 mm³ fragments, and enzymatically digested at 37°C for 8 h in Dulbecco's modified Eagle medium (DMEM/F12, Gibco) supplemented with 0.25 mg/mL type II collagenase (Invitrogen, Carlsbad, CA, USA). Then, the suspension was centrifuged, washed with PBS, and resuspended in DMEM/F12 with 15% fetal bovine serum (FBS; Gibco) and 1% penicillin/streptomycin (Sigma-Aldrich, St. Louis, MO, USA) at 37°C in 5% CO₂. The NP cell type was confirmed using fluorescently labeled antibody for NP cell markers as described previously [7]. Passage 2 and 3 NP cells were used in subsequent experiments.

In *in vitro* experiments, NP cells were treated with 200 µg/mL AGEs (Abcam, Cambridge, UK) for 0, 6, 12, 24, and 36 h or directly cocultured with AGEs in combination with ROS inhibitor N-acetyl-L-cysteine (NAC, 10 µM, Beyotime, Shanghai, China) for 36 h.

2.3. Western Blot Assay. After indicated intervention, cells were harvested using the corresponding protein extraction kit (Beyotime) to lyse and extract protein samples. Proteins were separated through 8–12% sodium dodecyl sulfate-(SDS-) polyacrylamide gel electrophoresis and transferred onto polyvinylidene difluoride (PVDF) membranes (Merck Millipore, Darmstadt, Germany). Next, after blocking with 5% nonfat milk at 25°C for 1 h, the membranes were incubated first with specific primary antibodies (1:500–1000) overnight at 4°C and then with the appropriate horseradish peroxidase- (HRP-) labeled secondary antibodies (1:2000; Proteintech). Then, membrane bands were visualized by the enhanced chemiluminescence system (Bio-Rad) and quantified with the ImageJ software. Primary antibodies against these molecules were used: p53 (10442-1-AP, Proteintech), p16 (ab151303, Abcam), cleaved caspase 3 (AF7021, Affinity Biosciences.), β-actin (66009-1-Ig, Proteintech), FAM134B (21537-1-AP, Proteintech), LC3 (14600-1-AP, Proteintech), and p62 (18420-1-AP, Proteintech).

2.4. Cell Proliferation Assay. Cell viability was illustrated using 5-ethynyl-2'-deoxyuridine (EdU) incorporation (C10310-3; Ribobio, Guangzhou, China) according to the manufacturer's instructions. Fluorescence images were captured using a fluorescence microscope (Olympus, BX53, Melville, NY, USA).

2.5. Cell Apoptosis Detection. Annexin V-FITC/PI Apoptosis Detection Kit (KeyGEN, Nanjing, China) was used to evaluate apoptosis as described previously [24]. Briefly, after washing with PBS, the cells were labeled with Annexin V-FITC (annexin V) and propidium iodide (PI). After double staining, apoptotic cells were detected via a flow cytometer (BD Biosciences, San Jose, CA, USA). Annexin V+/PI- (early apoptotic) cells and annexin V+/PI+ (late apoptotic) cells were counted.

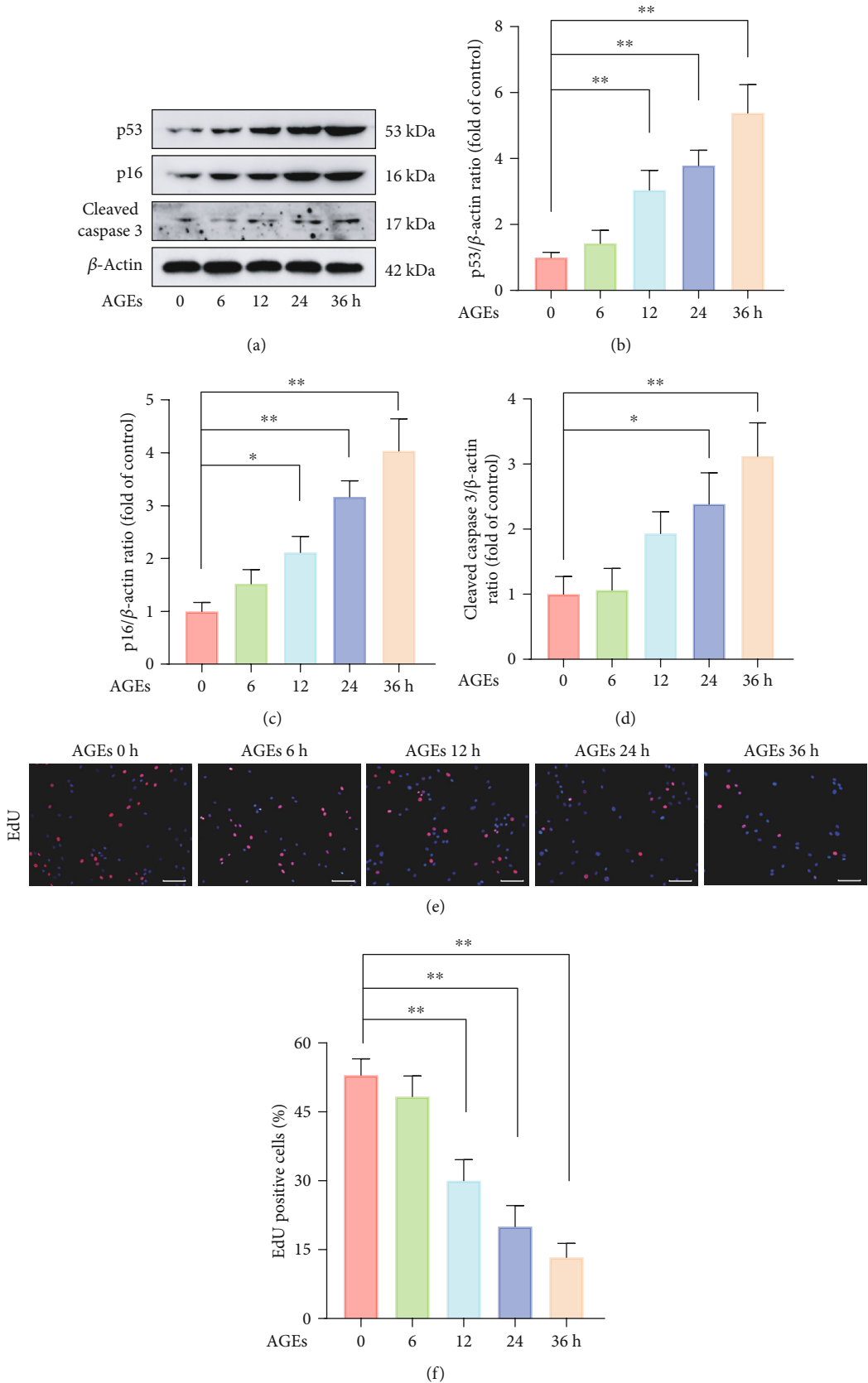
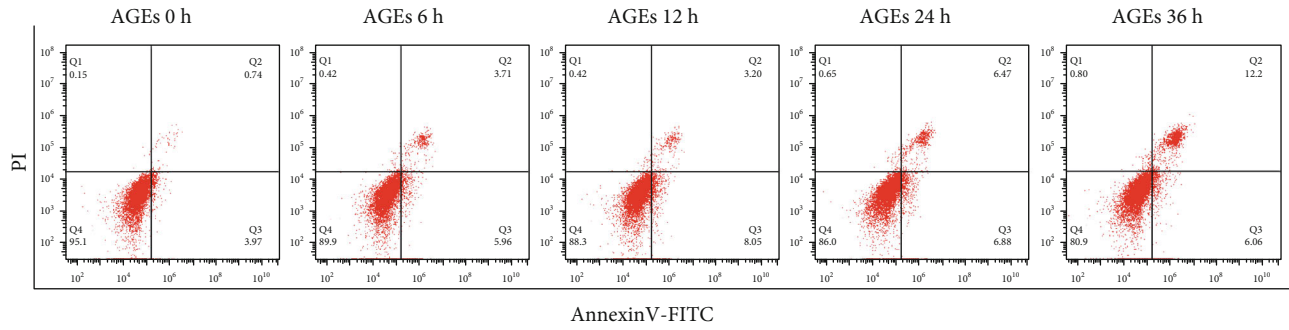
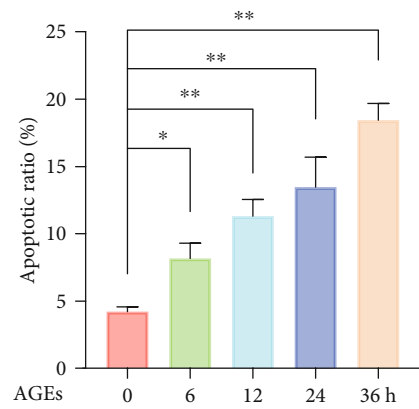


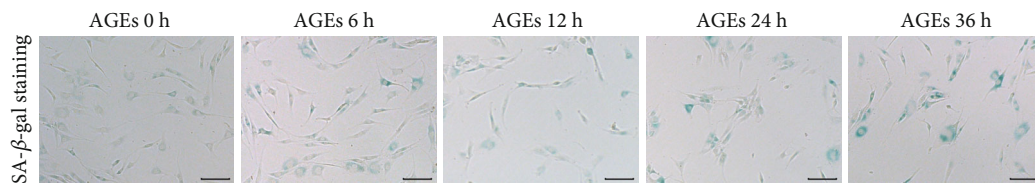
FIGURE 1: Continued.



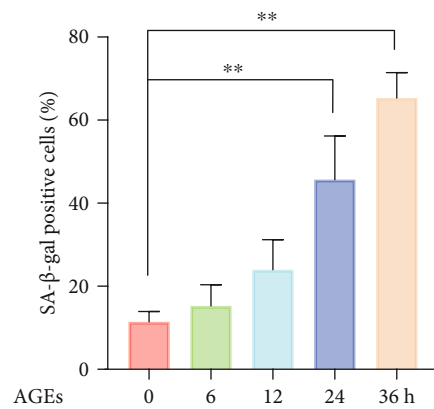
(g)



(h)

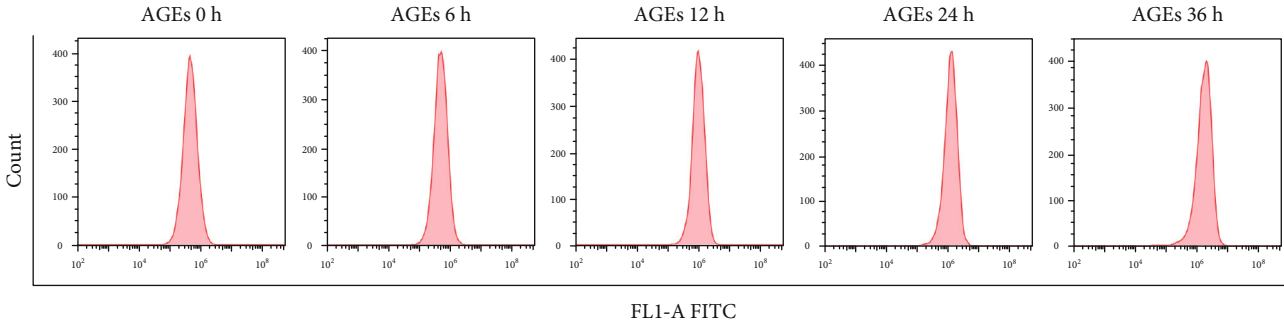


(i)

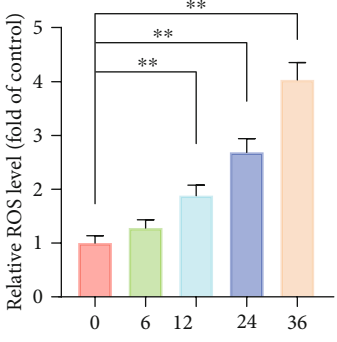


(j)

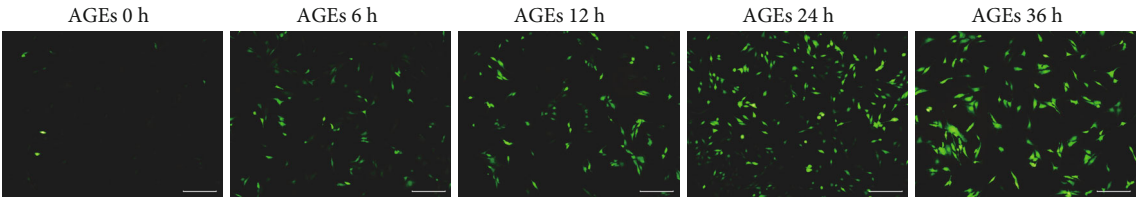
FIGURE 1: AGEs treatment promoted senescence and apoptosis in human NP cells. The human NP cells were exposed to 200 $\mu\text{g}/\text{mL}$ AGEs for different times (0, 6, 12, 24, and 36 h), and 0 h group served as the control. (a–d) Apoptosis and senescence-associated proteins p16, p53, and cleaved caspase 3 were measured using western blot assay, and relative band density was quantified. (e, f) Cell viability was determined using EdU staining combined with DAPI staining for the nuclei, and the positive cell ratio was quantitated, scale bar: 100 μm . (g, h) Representative dot plot images of flow cytometry analysis after labeled with Annexin V-FITC/PI double staining, both early and late apoptosis cells, were quantified. (i, j) Cell senescence was assessed by SA- β -gal staining; representative SA- β -gal staining images and positive cell ratio were illustrated, scale bar: 50 μm . Data are represented as mean \pm SD. ** $P < 0.01$, * $P < 0.05$.



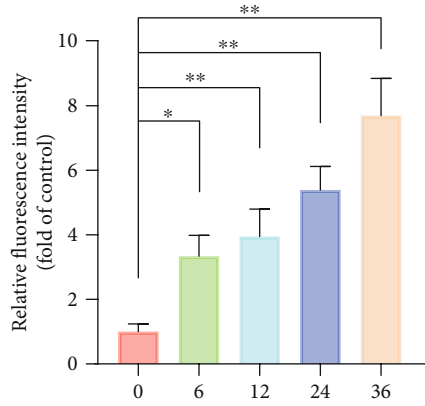
(a)



(b)

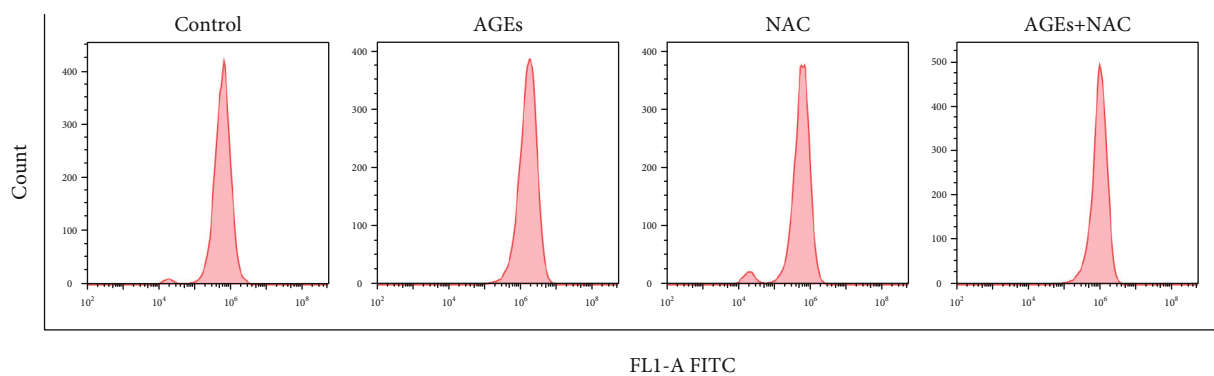


(c)

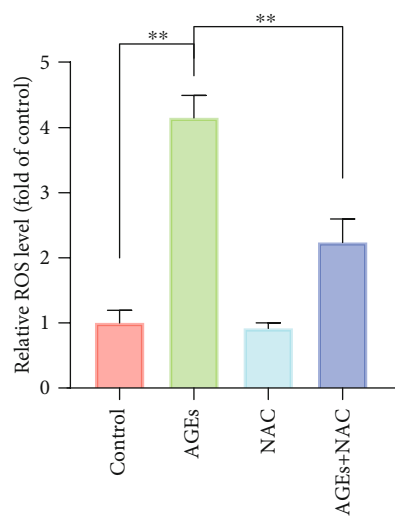


(d)

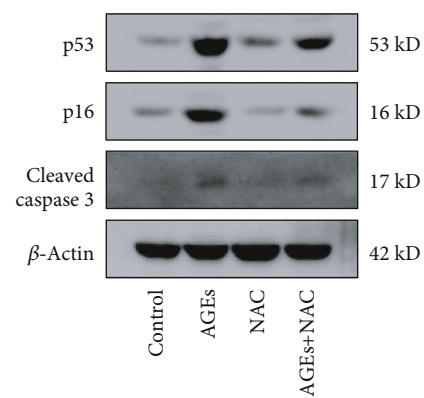
FIGURE 2: Continued.



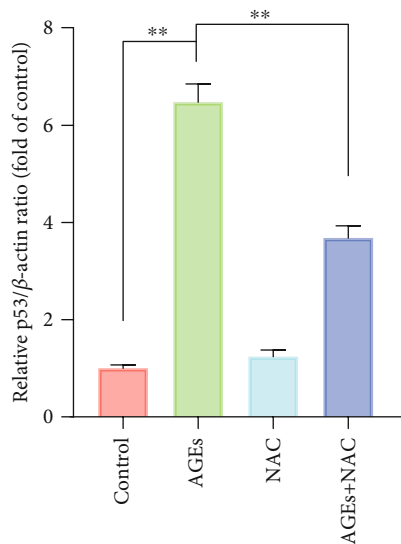
(e)



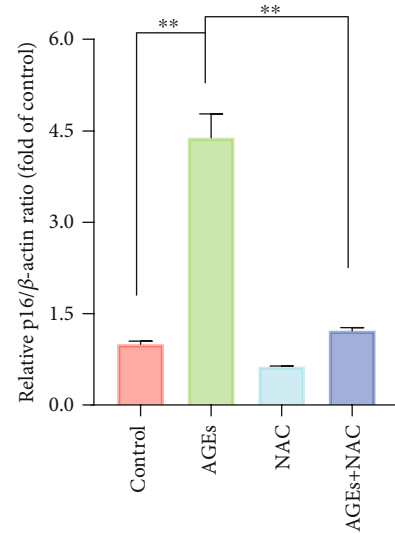
(f)



(g)



(h)



(i)

FIGURE 2: Continued.

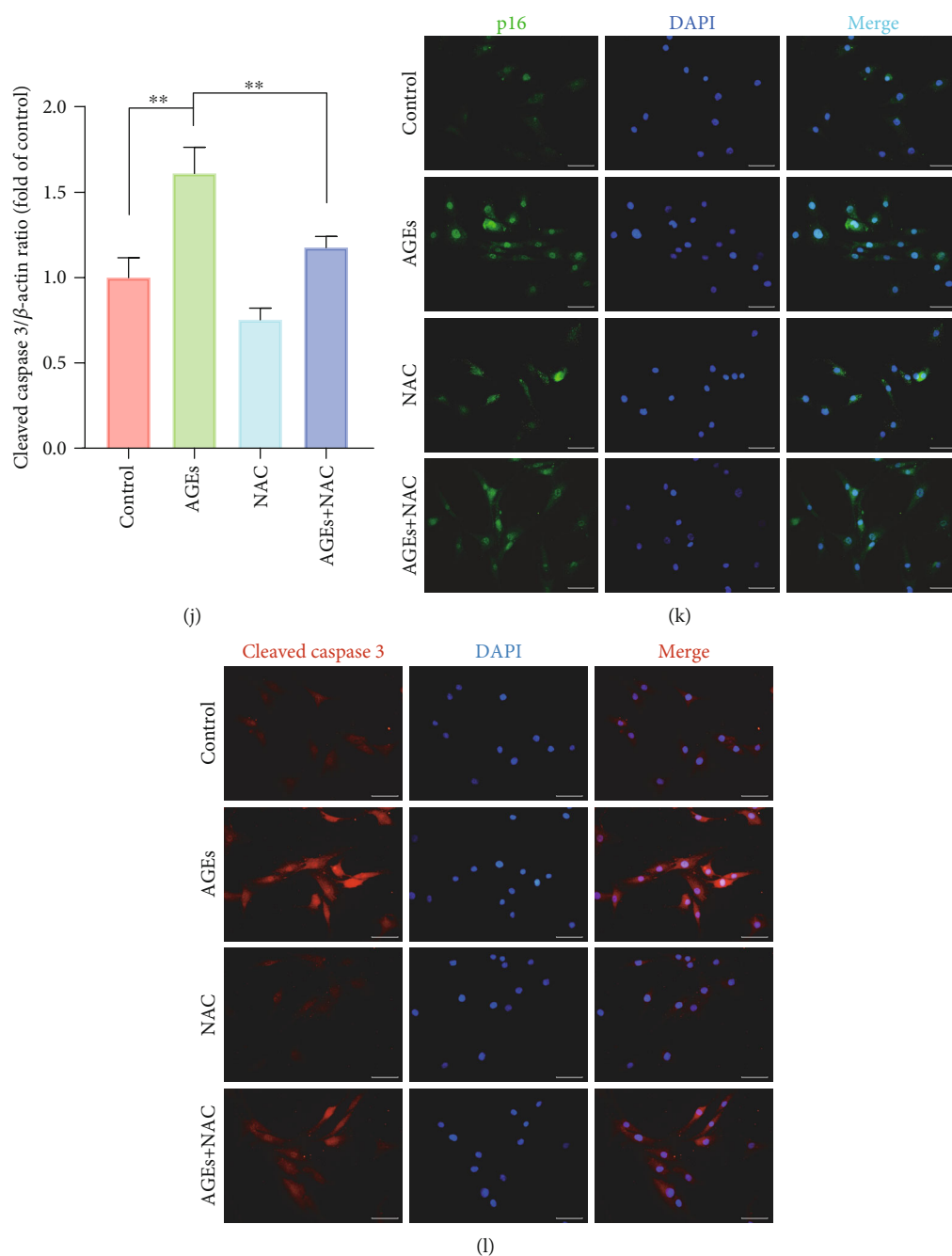


FIGURE 2: Intracellular ROS accumulation was involved in AGEs-induced senescence and apoptosis. The human NP cells were exposed to 200 $\mu\text{g}/\text{mL}$ AGEs for different times (0, 6, 12, 24, and 36 h) or directly cocultured with 200 $\mu\text{g}/\text{mL}$ AGEs and ROS inhibitor 10 μM NAC for 36 h. (a, b) The intracellular ROS levels were detected using the fluorescent probe DCFH-DA and measured by flow cytometry. (c, d) After labeled with DCFH-DA fluorescent probe, representative fluorescent images were acquired under a fluorescence microscope, scale bar: 100 μm . (g–j) Representative western blot bands of p16, p53, and cleaved caspase 3 and relative band density were quantified. (k, l) Representative images of immunofluorescence staining for p16 and cleaved caspase-3 in each group, with the relative fluorescence intensity quantified, scale bar: 50 μm . Data are represented as mean \pm SD. ** $P < 0.01$, * $P < 0.05$.

Terminal deoxynucleotidyl transferase-mediated dUTP nick end labeling (TUNEL) assay was also performed to assess apoptosis. Briefly, after the indicated treatment, cells were washed with PBS and processed with 4% paraformaldehyde for 20 min at 25°C, permeabilized with PBS-0.5% Triton X-100 for 10 min. Then, an in situ cell death detection kit (12156792910; Roche Applied Science, Basel, Switzerland)

was used for staining following the manufacturer's protocol. Fluorescence images were acquired through a fluorescence microscope (Olympus).

2.6. SA- β -gal Staining. SA- β -gal assay was performed to detect cell senescence. A SA- β -gal staining kit (Beyotime) was used to assess SA- β -gal activity according to the

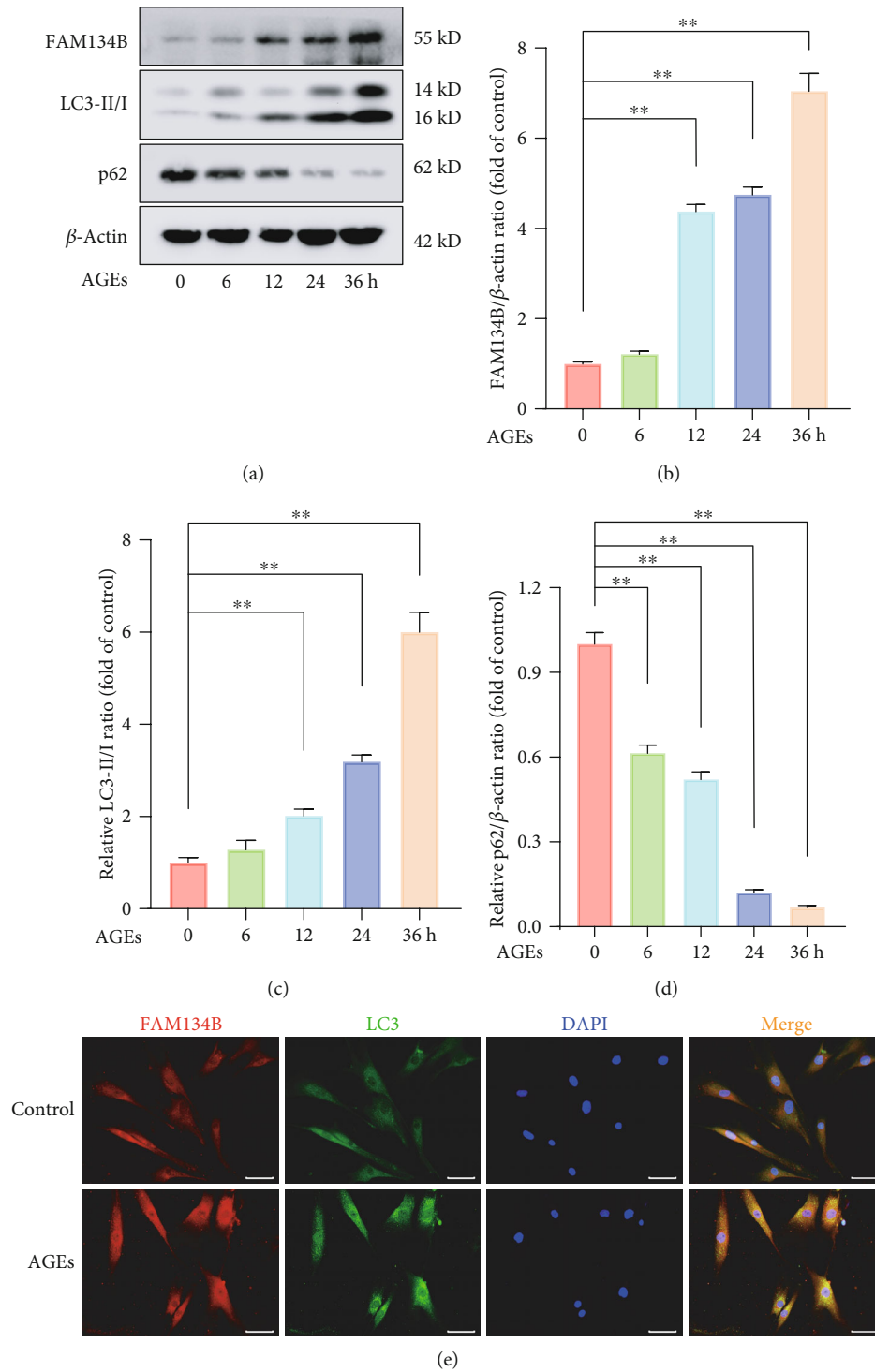


FIGURE 3: Continued.

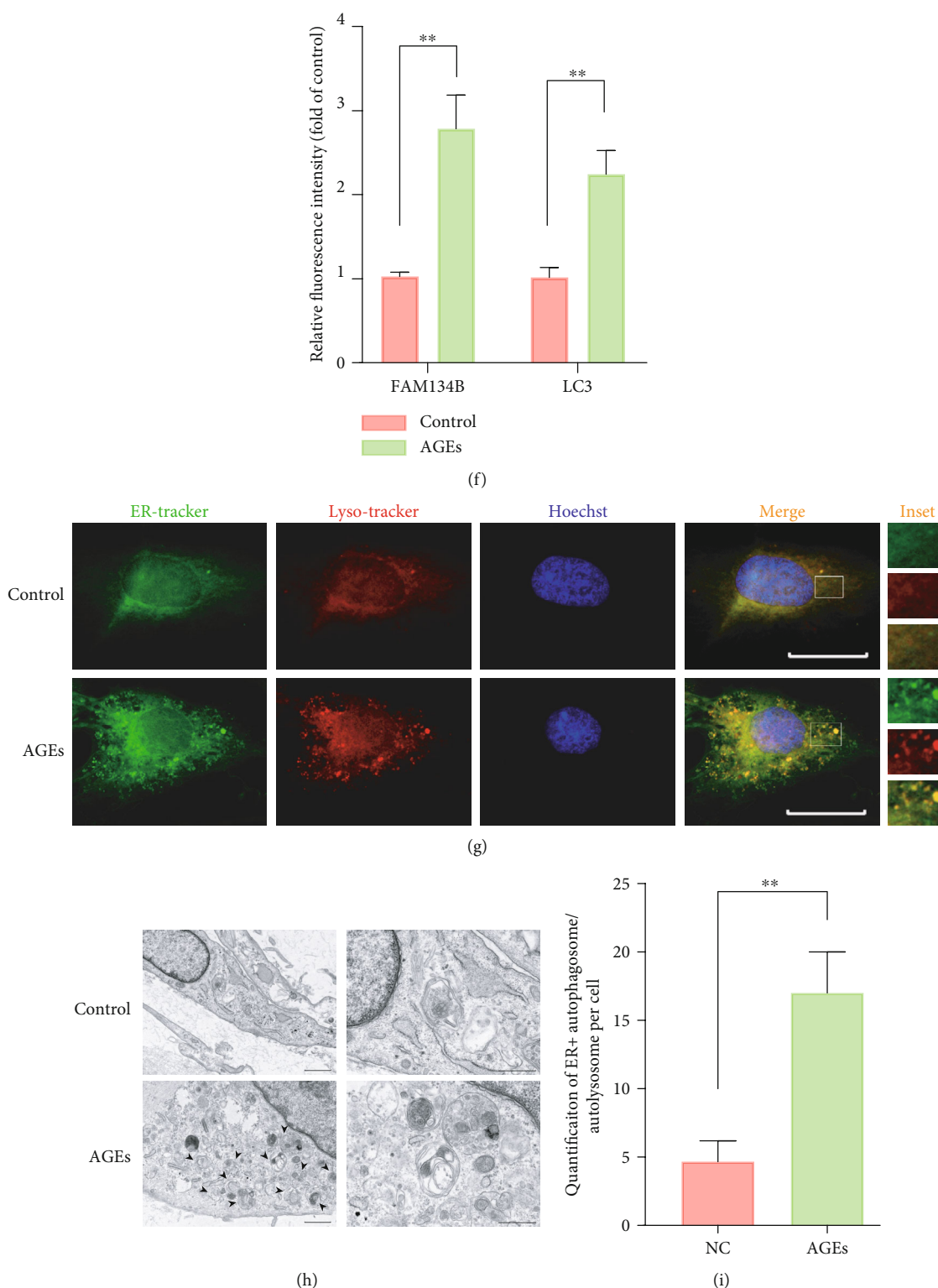


FIGURE 3: AGEs treatment upregulated FAM134B-mediated ER-phagy in human NP cells. (a–d) The human NP cells were exposed to 200 $\mu\text{g}/\text{mL}$ AGEs for different times (0, 6, 12, 24, and 36 h); ER-phagy-associated protein levels of FAM134B, LC3, and p62 were detected by western blot assay, and relative band density was quantified. (e, f) After treated with 200 $\mu\text{g}/\text{mL}$ AGEs for 36 h, relative protein expression of FAM134B and LC3 were assessed using immunofluorescence staining; representative images and relative intensity quantification were illustrated, scale bar: 50 μm . (g) ER and lysosome colocalization profile was detected by ER-tracker and Lyso-tracker staining. (h, i) Transmission electron microscopy results for ER positive autophagosomes/autolysosomes (as indicated by black arrow), scale bar: 1 μm and 500 nm. Data are represented as mean \pm SD. ** $P < 0.01$, * $P < 0.05$.

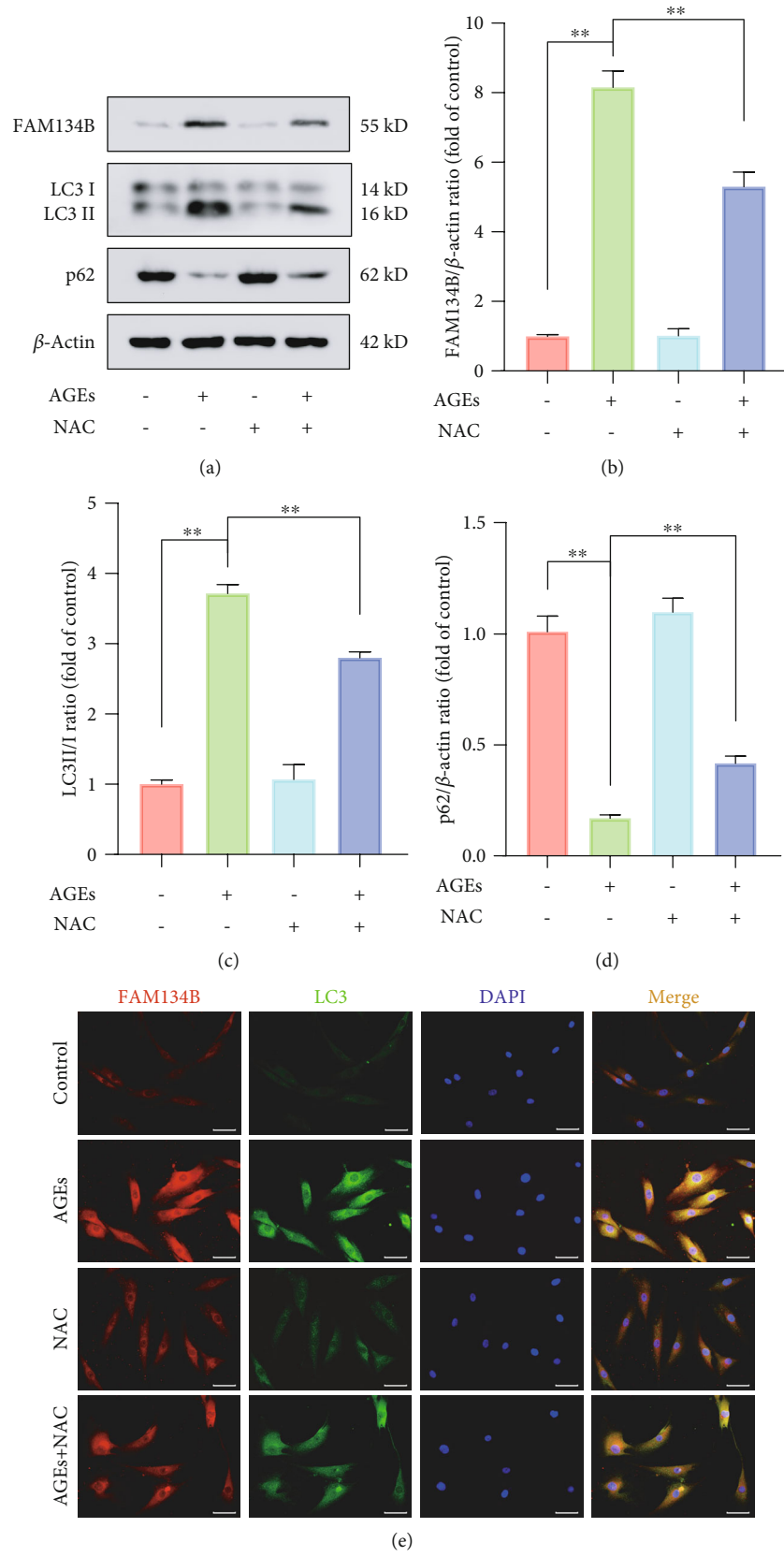


FIGURE 4: Continued.

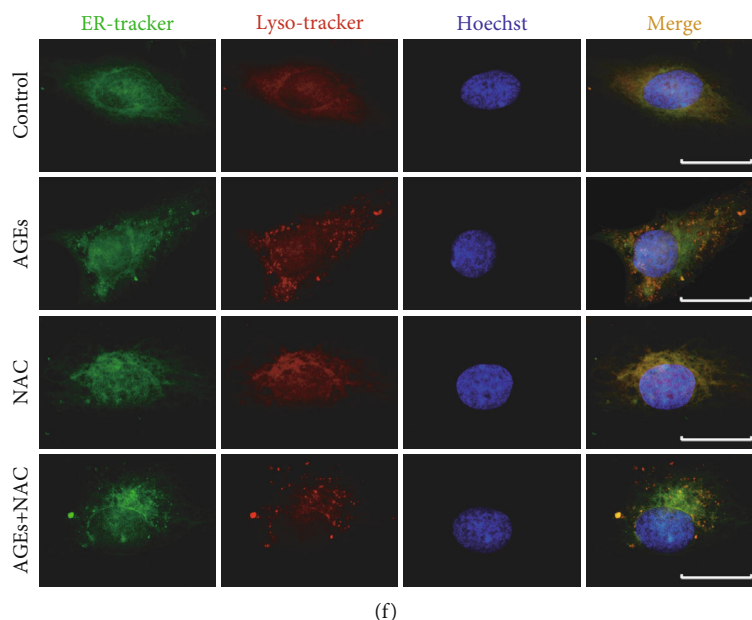


FIGURE 4: ROS inhibition partially attenuated AGEs-induced ER-phagy activation in human NP cells. The human NP cells were treated with 200 $\mu\text{g}/\text{mL}$ AGEs and 10 μM NAC for 36 h. (a–d) ER-phagy-associated protein levels of FAM134B, LC3, and p62 were detected by western blot assay, and the relative band density was quantified. (e) Representative fluorescent images of FAM134B and LC3 were evaluated, and cell nuclei were stained with DAPI. Scale bar: 50 μm . (f) ER and lysosome colocalization was labeled with ER-tracker and Lyso-tracker staining. Data are represented as mean \pm SD. ** $P < 0.01$, * $P < 0.05$.

manufacturer's instructions. A microscope was used to observe the cells, of which blue-colored cells were counted as SA- β -Gal-positive cells. SA- β -Gal activity was represented by the percentage of the number of blue cells and the total number of cells.

2.7. ROS Measurement. A ROS detection kit (Beyotime) was used to detect the intracellular ROS level according to instructions. Briefly, after indicated treatment, cells were incubated with 10 μM DCFH-DA (2,7-dichlorodihydrofluorescein diacetate dye) in culture media for 30 min. Then, cells were washed with PBS, trypsinized, resuspended in PBS supplemented with FBS, and analyzed for intracellular ROS production by flow cytometry or directly observe fluorescence signal using a fluorescence microscope (Olympus).

2.8. Lentivirus and siRNA Transfection. For lentivirus infection, the FAM134B overexpressing lentivirus was designed and constructed by GeneChem (Shanghai, China) using CV084 (Ubi-MCS-SV40-Neomycin) vector. The day before, human NP cells were seeded in 6-well plates at a density of 2×10^5 cells/mL; Then, the cells were infected with lenti-FAM134B or lentivector at a multiplicity of infection (MOI) of 20; transfection efficacy was detected by western blotting after cultured for 72 h. For siRNA-mediated knock-down, control-siRNA and FAM134B-siRNA were purchased from Qijing Biotechnology Co. (Wuhan, China); the corresponding target sequence for RNA interference was 5'-AGCTATCAAAGACCAGTTA. siRNAs were transfected using lipofectamine 2000 (Invitrogen) following the manufacturer's instructions. Cells knocked down for 48 h were followed by the indicated treatment.

2.9. Immunofluorescence. NP cells attached to slides were fixed with 4% paraformaldehyde for 20 min, washed three times with PBS, permeabilized with 0.5% Triton X-100 for 15 min, blocked with 2% bovine serum albumin (BSA) for 30 min, and then incubated overnight at 4°C with primary antibodies against p16 (1:100, Proteintech), cleaved caspase 3 (1:100, CST), FAM134B (1:100, Proteintech), and LC3 (1:100; Abconal, Wuhan, China). After washed three times with TBST, cells were incubated with CoraLite488 or Cora-Lite594 conjugated goat anti-rabbit/mouse IgG antibody (1:100, Proteintech) for 1 h and labeled with diamidino-2-phenylindole (DAPI; Beyotime) for 5 min and then observed images using a fluorescence microscope (Olympus).

2.10. ER-Tracker and Lyso-Tracker Staining. ER-tracker green (40763ES20, Yisheng Biotech, Shanghai, China) and Lyso-tracker red (40739ES50, Yisheng) dyes were used to identify ER-phagy. Briefly, human NP cells were mounted on glass coverslips in a 6-well plate. After the treatment, cells were stained with the recommended concentrations of ER-tracker, Lyso-tracker, and Hoechst 33342 (Beyotime) for 30 min at 37°C, washed three times with PBS, and then observed the fluorescence using a fluorescence microscope (Olympus).

2.11. Transmission Electron Microscopy. TEM was used to determine the status of ER positive autophagosome and autolysosome formation. Briefly, after the indicated treatment, NP cells were collected and fixed in a glutaraldehyde and sodium cacodylate solution for 2 h and then fixed with 1% OsO₄ for 1.5 h and then stained in 3% aqueous uranyl acetate for 1 h. After washing, specimens were dehydrated with graded ethanol series (50%, 70%, 80%, 90%, 95%),

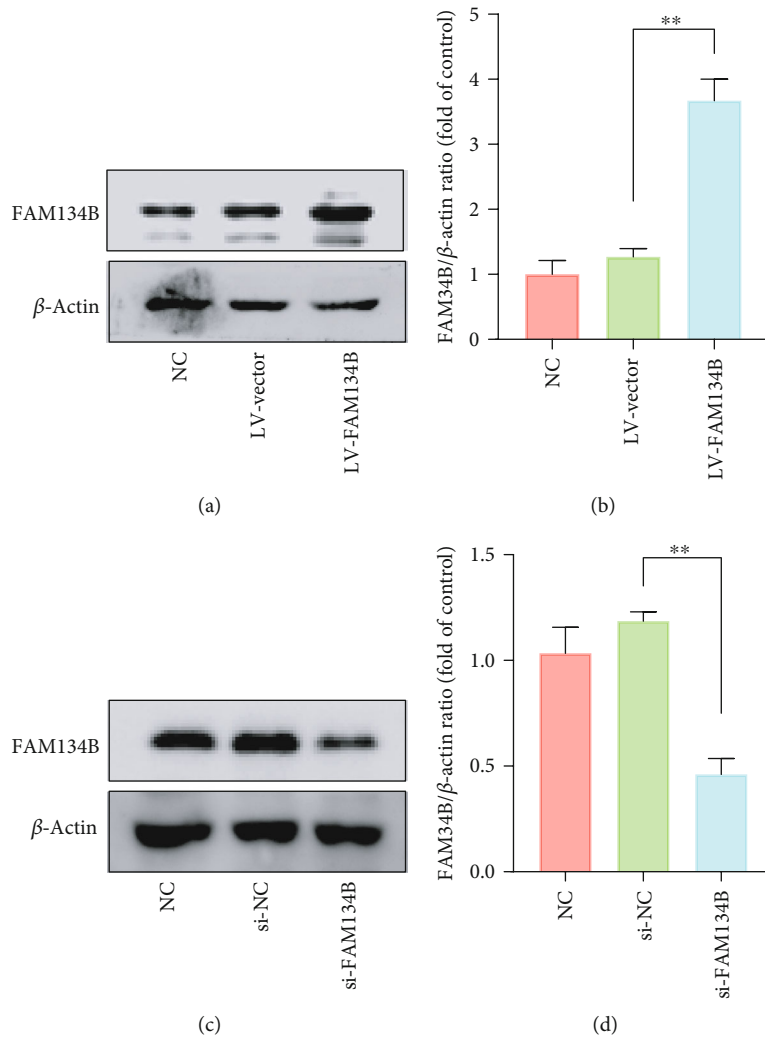
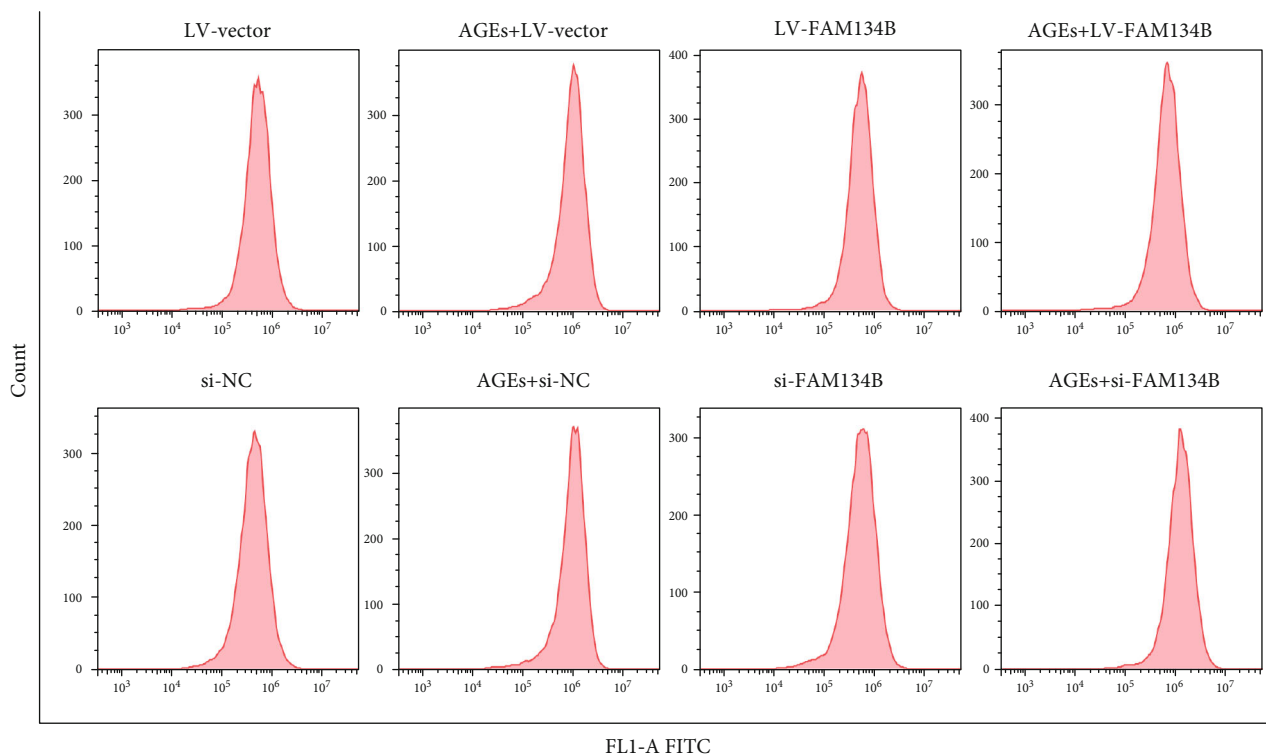
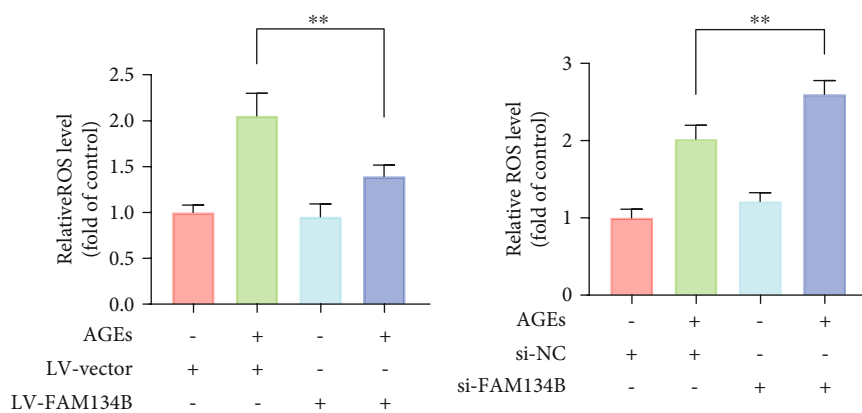


FIGURE 5: Continued.



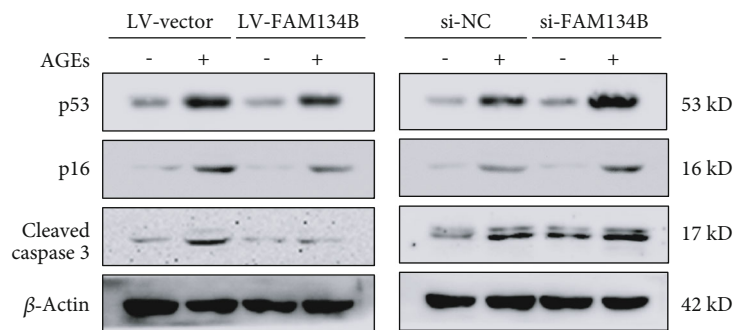
FLI-A FITC

(e)



(f)

(g)



(h)

FIGURE 5: Continued.

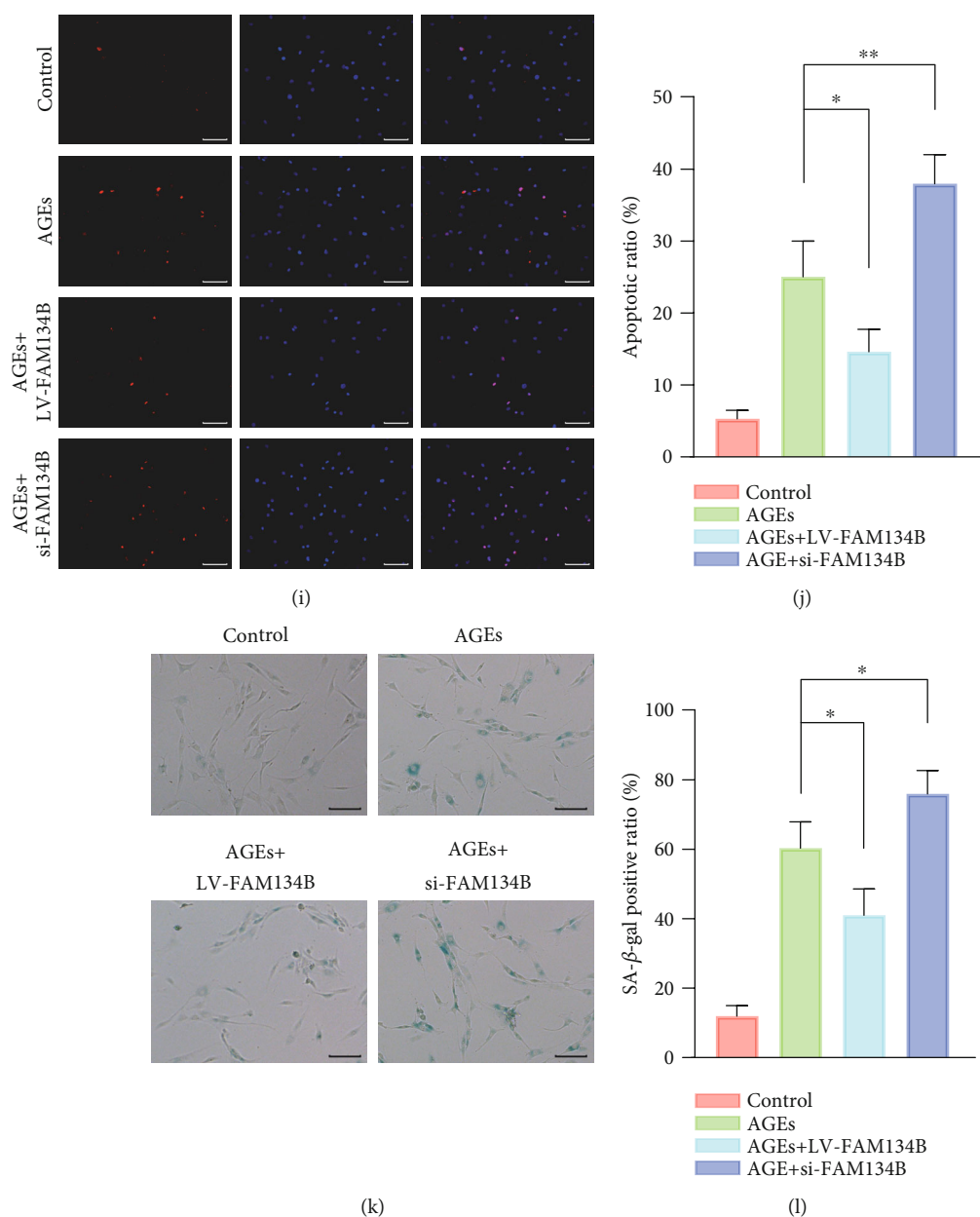


FIGURE 5: FAM134B-mediated ER-phagy regulated AGEs-induced intracellular ROS accumulation, apoptosis, and senescence in human NP cells. After lentivirus and siRNA transfection were separately conducted for 72 and 48 h, the human NP cells were cultured with 200 $\mu\text{g}/\text{mL}$ AGEs for 36 h. (a–d) FAM134B overexpression and knockdown efficacy were verified by western blot assay. (e–g) The intracellular ROS levels were probed using the fluorescent dye DCFH-DA and measured by flow cytometry. (h) Relative protein expression levels of the apoptotic and senescent associated proteins p53, p16, and cleaved caspase3 were evaluated using western blot assay. (i) Cell apoptosis was assessed by TUNEL staining; representative TUNEL immunofluorescent images and apoptotic ratio were quantitated, scale bar: 100 μm . (j) Representative SA- β -gal staining images and positive cell ratio were illustrated, scale bar: 50 μm . Data are represented as mean \pm SD. ** $P < 0.01$, * $P < 0.05$.

100%), followed by infiltrating and embedding in epoxy resin (SPI-Chem, #90529-77-4). Ultrathin sections were obtained and stained with saturated uranyl acetate–lead citrate and observed using a transmission electron microscope (Jeol, Tokyo, Japan).

2.12. Statistical Analysis. All data were presented as the mean \pm standard deviation of at least three independent experiments. Statistical analyses were performed using the

GraphPad Prism 8.0 software (La Jolla, CA, USA). Differences between groups were evaluated with Student's t -test or one-way ANOVA with post hoc analysis using the Tukey's test. $P < 0.05$ was considered statistically significant.

3. Results

3.1. AGEs Treatment Promoted Apoptosis and Senescence in Human NP Cells. To explore the impact of AGEs on the

apoptosis and senescence of human NP cells *in vitro*, a group of NP cells was exposed to AGEs (200 $\mu\text{g}/\text{mL}$) for different times (0, 6, 12, 24, and 36 h). Firstly, apoptosis and senescence-associated proteins p16, p53, and cleaved caspase 3 were determined using western blot assay, as shown in Figures 1(a)–1(d); compared to the control group, the protein expression of p16, p53, and cleaved caspase 3 in the AGEs-treated groups were significantly increased, especially in 24 and 36 h AGEs-treated groups. In addition, EdU staining was also used to assess the cell proliferation ability, as shown in Figures 1(e) and 1(f); the cell viability of human NP cells significantly decreased after AGEs treatment in a time-dependent manner. Moreover, we further employed Annexin V-PI double staining to determine the proapoptotic effects of AGEs on human NP cells, as shown in Figures 1(g) and 1(h); compared to the control group, a clearly higher apoptotic ratio in the AGEs-treated groups was observed. Senescent cells are often concomitant with larger size and higher SA- β -gal enzyme activity, as shown in Figures 1(i) and 1(j); the quantification of SA- β -gal positive cells in the AGEs-treated groups were robustly higher compared to that in the control group. Thus, our results showed that AGEs treatment could markedly promote apoptosis and senescence in human NP cells.

3.2. ROS Pathway Was Involved in AGEs-Induced Apoptosis and Senescence in Human NP Cells. Intracellular ROS homeostasis could rapidly change under stress circumstances and function as important messengers involved in cell survival and death. To investigate the relationship between ROS generation and AGEs, we exposed NP cells to AGEs (200 $\mu\text{g}/\text{mL}$) for different times (0, 6, 12, 24, and 36 h) and detected ROS levels using DCFH-DA Assay Kit. As the flow cytometry results shown in Figures 2(a) and 2(b), compared to the control group, AGEs treatment aroused significant time-dependent elevation of intracellular ROS levels and which were consistent with the observation that the AGEs treatment groups showed increased fluorescence intensity compared to the untreated group (Figures 2(c) and 2(d)). NAC is a classical ROS scavenger that reduced intracellular ROS accumulation, as expected, relative to the NAC deficient AGEs-treated group, the NAC existent AGEs-treated group showed clearly lower ROS levels (Figures 2(e) and 2(f)).

To further validate that ROS was involved in AGEs-induced apoptotic and senescent effects, NAC and AGEs were coadministered to human NP cells. As western blot results illustrated in Figures 2(g)–2(j), compared to the corresponding AGEs-treated alone group, protein expression levels of p53, p16, and cleaved caspase 3 were markedly declined in the AGEs plus NAC cotreated group. Similarly, as immunofluorescence results are shown in Figures 2(k) and 2(l). AGEs treatment significantly elevated p16 and cleaved caspase 3 fluorescence intensity relative to that in the control group, while these effects were markedly attenuated in the presence of NAC. Above all, these results suggested that high intracellular ROS level elicited by AGEs was closely associated with the apoptosis and senescence initiation.

3.3. FAM134B-Mediated ER-phagy Was Activated under AGEs Treatment in Human NP Cells. FAM134B-mediated

ER-phagy activation is an important regulatory mechanism to solve stress and maintain cellular homeostasis. To investigate the effects of AGEs on FAM134B-related ER-phagy, we exposed NP cells to AGEs (200 $\mu\text{g}/\text{mL}$) for different times (0, 6, 12, 24, and 36 h). FAM134B-related ER-phagy proteins FAM134B, LC3, and p62 were detected by western blot assay, as the results illustrated in Figures 3(a)–3(d); the protein expression profiles of FAM134B and LC3 were robustly upregulated in the AGEs-treated groups compared to that in the control group, along with downregulated autophagy substrate p62 protein levels, indicating the activation of ER-phagy. Meanwhile, as the FAM134B and LC3 fluorescence costaining results shown in Figures 3(e) and 3(f), both the fluorescence intensities of FAM134B and LC3 were significantly enhanced and combined with a higher extent of colocalization upon AGEs treatment. ER and lysosome could be specifically labelled by ER-tracker and Lyso-tracker, respectively; thus, colocalization with the fluorescent signals of ER-tracker green and Lyso-tracker red could be an effective method to determine the occurrence of ER-phagy. As shown in Figure 3(g), compared with the control group, the AGEs-treated group displayed an obvious ER clustering staining pattern, which was partially colocalized with the accumulation of lysosome staining. In addition, we also further monitored the formation of autophagosomes/autolysosomes containing ER fragments under TEM to confirm ER-phagy activation, as shown in Figures 3(h) and 3(i), we observed apparently increased number of autophagosomes/autolysosomes containing ER fragment formation in the AGEs-treated group compared to that in the control group, thereby confirming the occurrence of ER-phagy in human NP cells under AGEs exposition.

3.4. ROS Inhibition Partially Attenuated ER-phagy in Human NP Cells Subjected to AGEs Treatment. Since both intracellular ROS accumulation and ER-phagy activation upon AGEs treatment were observed, to further test their intrinsic relationship, the ER-phagy activation level under AGEs treatment was determined in the presence of NAC or not. As shown in Figures 4(a)–4(d), the ER-phagy-related protein expression levels were detected using western blot; compared to the corresponding AGEs-treated alone group, the protein expression levels of FAM134B and LC3 were markedly declined in the AGEs plus NAC co-treated group, whereas p62 protein level was slightly increased. Meanwhile, the enhanced fluorescence intensity of FAM134B and LC3 upon AGEs treatment were also significantly attenuated in the presence of NAC administration (Figure 4(c)). In addition, as shown in Figure 4(d), the elevated colocalization of ER and lysosome patterns under AGEs treatment were markedly decreased with NAC cotreatment. Therefore, our findings demonstrated that intracellular ROS accumulation plays a vital role in the process of FAM134B-mediated ER-phagy activation.

3.5. Modulation of FAM134B-Mediated ER-phagy Could Regulate Intracellular ROS Level, Apoptosis, and Senescence in AGEs-Treated Human NP Cells. It is classically recognized that FAM134B-mediated ER-phagy acts as an important

quality control mechanism in maintaining cellular homeostasis. We next investigated the influence of FAM134B-mediated ER-phagy activation or inhibition on intracellular ROS levels, apoptosis, and senescence by genetically upregulating and downregulating the FAM134B expression. As the western blot results demonstrated in Figures 5(a)–5(d), we efficiently achieved FAM134B overexpression and knockdown by lentiviral transduction and RNA interference, respectively. Subsequently, to determine whether ROS changes in response to FAM134B-mediated ER-phagy, we measured intracellular ROS levels using ROS-sensitive DCFH-DA dye. As the flow cytometry results illustrated in Figures 5(e)–5(g), the ROS level in the AGEs plus lenti-FAM134B group was significantly lower compared with that in the AGEs plus lentivector group, while FAM134B knockdown significantly increased intracellular ROS levels upon AGEs treatment than that noted in the blank knockdown group. Moreover, we next analyzed the effects of FAM134B-mediated ER-phagy on apoptosis and senescence under AGEs treatment. As shown in Figure 5(h), compared to the AGEs plus blank overexpression or knockdown group, FAM134B overexpression markedly attenuated the expression of the apoptotic and senescent associated proteins p53, p16, and cleaved caspase3, while FAM134B knockdown showed the opposite effects. Consistently, as the TUNEL and SA- β -gal staining results illustrated in Figures 5(i)–5(l), FAM134B overexpression could alleviate AGEs-induced apoptosis and senescence, while FAM134B suppression could exacerbate the proapoptotic and prosenescent effects of AGEs. Above all, our findings demonstrated that FAM134B-mediated ER-phagy activation could relieve intracellular ROS accumulation, apoptosis, and senescence in human NP cells upon AGEs treatment.

4. Discussion

Previous studies have shown that AGEs accumulation in the intervertebral disc along with aging plays a critical role in the pathogenesis of IDD [6–8], and emerging evidence indicates that ER-phagy could serve as a vital intracellular homeostatic regulatory mechanism that directly determines cell functionality and fate under various stress circumstances [19, 25]. However, the role of ER-phagy in AGEs-mediated IDD and its potential mechanisms require further exploration. In the present study, we revealed that FAM134-mediated ER-phagy was markedly activated upon AGEs treatment via ROS pathway in human NP cells, and genetical upregulation and inhibition of FAM134B-mediated ER-phagy could significantly decrease and increase intracellular ROS level, apoptosis, and senescence in NP cells subjected to AGEs stimuli, respectively.

The maintenance of healthy, active, and functional NP is an important prerequisite for the intervertebral disc to properly execute physiological function, which largely depends on the existence of adequate numbers of functionally active NP cells in the disc; thus, numerous studies investigating IDD mainly focus on exploring the underlying causes of abnormal quantity loss and functionality decline of NP cells. Age-related accumulation of AGEs in the intervertebral disc

impedes its extracellular matrix synthesis and turnover and ultimately impairs the biomechanical properties of the intervertebral disc and drives the development of IDD [26]. Song et al. found that AGEs accumulation in the disc could impede the anabolic and catabolic balance of NP cells via NLRP3-inflammasome pathway [6]. Furthermore, Song et al. and Luo et al. revealed that AGEs treatment could damage mitochondria redox balance via suppressing Sirt3 function and compromise ER function via disturbing calcium homeostasis and ultimately promote apoptosis [7, 8]. Consistently, we further explored the contribution of AGEs on NP cell apoptosis and senescence in the present study, and the results showed that AGEs treatment restrained cell proliferation, promoted cell apoptosis, and senescence in human NP cells.

ROS represents a group of unstable and highly reactive molecules such as superoxide anions, hydroxyl ions, and hydrogen peroxide, which mainly derived from aerobic metabolism. Physiological quantity of ROS is known to control cellular signal transduction and play roles in cell homeostasis, while excessive ROS produced under stress conditions appear to intervene with normal cell physiology and even lead to cell death [27]. Excessive ROS accumulation has been implicated in the pathogenesis of IVD degeneration [28, 29]. Furthermore, Xiang et al. and Kang et al. revealed that modulation of the cellular ROS level through antioxidant administration could efficiently mitigate oxidative stress-induced NP cell death [30, 31]. NAC, a ROS scavenger, was used to confirm the role of ROS in the proapoptotic and prosenescent effects of AGEs in the present study; as expected, we observed that the administration of NAC significantly attenuated AGEs-induced ROS burst, apoptosis, and senescence of NP cells.

ER-phagy, referred to the selective degradation of the ER by autophagy, is emerging as a critical regulator of cell homeostasis and function. Notably, the highly selective process is largely achieved through selective receptor that interact with autophagosome-associated LC3 and subsequently cargo ER fragments and ER-resident proteins for lysosomal degradation [32]. To date, six reticulophagy receptors have been identified in mammals: FAM134B, RTN3L, SEC62, CCPG1, ATL3, and TEX264, among which FAM134B was the first one to be identified. Although the intrinsic relationship between ER-phagy and classical macroautophagy is still not fully understood, several studies found that disruption of the interaction of FAM134B with LC3 by mutation or deletion of the LIR amino acid sequence failed to induce ER-phagy [17]. Moreover, the two major autophagy regulators, ATG5 and BECN1, are essential for ER fragmentation and degradation induced by FAM134B overexpression, suggesting that FAM134B-induced ER-phagy depends on the core macroautophagy machinery [33, 34]. ER-phagy is considered a stress-induced response mechanism to maintain cellular homeostasis and to promote cell survival; ER-phagy deflection has been validated to be associated with multiple human pathologies, including infectious, neurodegenerative diseases, aging, and cancer [35]. Indeed, in the present study, there are significantly increased autophagosomes containing layered membrane structures, and much more ER and lysosome colocalization clustering was observed upon AGEs

treatment, suggesting the occurrence of ER-phagy in NP cells under AGEs stimuli.

Furthermore, ER-phagy is emerging recognized as an alternative ER quality and quantity control regulatory mechanism via delivering excess ER fragments and ER-resident protein for lysosomal degradation, which is critical for cellular homeostasis and adaptation to variable environments. Strikingly, ER-phagy is substantially enhanced when encountering stress conditions such as starvation and contributes to resolve ER stress and reestablish ER homeostasis [16]. It is confirmed that FAM134B-mediated ER-phagy could restrict viral replication via eliminating ER-associated viral proteins, while suppression or knockdown of FAM134B could facilitate viral replication [36]. Additionally, a higher survival rate was observed in breast cancer patients with higher FAM134B expression [37]. Notably, the relationship between FAM134B-mediated ER-phagy and apoptosis is pretty complicated; ER-phagy could either act as a protective mechanism against apoptosis via restoring excessive ER stress [38, 39] or exhibit ER-phagy-dependent cell death via accelerating ER degradation and impairs ER homeostasis to trigger ER stress [21, 40]; these evidence may indicate the possibility that the adaptive capability of ER-phagy is limited; when encountered severe conditions overwhelming the regulatory capacity of ER-phagy, the protective ER-phagy may switch to facilitate cell death. Accordingly, we detected whether ER-phagy upregulation exerts a protective effect against AGEs stimuli in NP cells, and the results showed that the enhanced expression apoptotic and senescent associated proteins p53, p16, and cleaved caspase 3, and intracellular ROS levels were significantly decreased with FAM134B overexpression, indicating that FAM134B-mediated ER-phagy plays a critical protective role in defending AGEs-induced cell damage.

There are still several shortcomings in our study. Firstly, despite the facts that our research has suggested a crucial role of FAM134B-mediated ER-phagy activation in balancing intracellular ROS level and promoting cell survival, while the specific molecular mechanisms remain to be further studied. Moreover, we only focused on the typical ER-phagy receptor FAM134B in this study, whether other types of ER-phagy receptors are involved in this process was not explored. In addition, the current study lacks *in vivo* experimental and clinical validation.

Collectively, we demonstrated that FAM134B-mediated ER-phagy activation plays a crucial role in protecting against AGEs-induced intracellular ROS accumulation and cell injury in human NP cells, and targeting FAM134B-mediated ER-phagy may be a potentially effective therapeutic strategy for IDD.

Abbreviations

AGEs:	Advanced glycation end products
IDD:	Intervertebral disc degeneration
NP:	Nucleus pulposus
ROS:	Reactive oxygen species
ER:	Endoplasmic reticulum
FAM134B:	RETREG1, reticulophagy regulator 1

RTN3:	Reticulon 3 long isoform
SEC62:	SEC62 homolog
CCPG1:	Cell-cycle progression gene 1
ATL3:	Atlastin 3
TEX264:	Testis-expressed 264
EdU:	5-Ethynyl-2'-deoxyuridine
TUNEL:	Terminal deoxynucleotidyl transferase-mediated dUTP nick end labeling
NAC:	N-Acetyl-L-cysteine
SA- β -gal:	Senescence-associated β -galactosidase.

Data Availability

The data supporting the findings of this study are included in the article.

Conflicts of Interest

The authors declare no conflict of interest.

Authors' Contributions

Rongjin Luo and Shuai Li contributed equally to this work.

Acknowledgments

This study was supported by the National Key R&D Program of China (2018YFB1105700), the National Natural Science Foundation of China (81902261, 81772401), the Fundamental Research Funds for the Central Universities (2019kfyXMBZ063), and the Application Foundation and Advanced Program of Wuhan Science and Technology Bureau (2019020701011457).

References

- [1] G. B. D. Disease, I. Injury, and C. Prevalence, "Global, regional, and national incidence, prevalence, and years lived with disability for 328 diseases and injuries for 195 countries, 1990-2016: a systematic analysis for the Global Burden of Disease Study 2016," *The Lancet*, vol. 390, no. 10100, pp. 1211-1259, 2017.
- [2] J. E. Mayer, J. C. Iatridis, D. Chan, S. A. Qureshi, O. Gottesman, and A. C. Hecht, "Genetic polymorphisms associated with intervertebral disc degeneration," *The Spine Journal*, vol. 13, no. 3, pp. 299-317, 2013.
- [3] P. P. Vergroesen, I. Kingma, K. S. Emanuel et al., "Mechanics and biology in intervertebral disc degeneration: a vicious circle," *Osteoarthritis and Cartilage*, vol. 23, no. 7, pp. 1057-1070, 2015.
- [4] F. Wang, F. Cai, R. Shi, X. H. Wang, and X. T. Wu, "Aging and age related stresses: a senescence mechanism of intervertebral disc degeneration," *Osteoarthritis and Cartilage*, vol. 24, no. 3, pp. 398-408, 2016.
- [5] N. Feldman, A. Rotter-Maskowitz, and E. Okun, "DAMPs as mediators of sterile inflammation in aging-related pathologies," *Ageing Research Reviews*, vol. 24, Part A, pp. 29-39, 2015.
- [6] Y. Song, Y. Wang, Y. Zhang et al., "Advanced glycation end products regulate anabolic and catabolic activities via NLRP3-inflammasome activation in human nucleus pulposus

- cells,” *Journal of Cellular and Molecular Medicine*, vol. 21, no. 7, pp. 1373–1387, 2017.
- [7] Y. Song, S. Li, W. Geng et al., “Sirtuin 3-dependent mitochondrial redox homeostasis protects against AGEs- induced intervertebral disc degeneration,” *Redox Biology*, vol. 19, pp. 339–353, 2018.
- [8] R. Luo, Y. Song, Z. Liao et al., “Impaired calcium homeostasis via advanced glycation end products promotes apoptosis through endoplasmic reticulum stress in human nucleus pulposus cells and exacerbates intervertebral disc degeneration in rats,” *The FEBS Journal*, vol. 286, no. 21, pp. 4356–4373, 2019.
- [9] C. K. Kepler, R. K. Ponnappan, C. A. Tannoury, M. V. Risbud, and D. G. Anderson, “The molecular basis of intervertebral disc degeneration,” *The Spine Journal*, vol. 13, no. 3, pp. 318–330, 2013.
- [10] S. A. Oakes and F. R. Papa, “The role of endoplasmic reticulum stress in human pathology,” *Annual Review of Pathology*, vol. 10, no. 1, pp. 173–194, 2015.
- [11] J. Grootjans, A. Kaser, R. J. Kaufman, and R. S. Blumberg, “The unfolded protein response in immunity and inflammation,” *Nature Reviews Immunology*, vol. 16, no. 8, pp. 469–484, 2016.
- [12] M. Molinari, “ER-phagy: eating the factory,” *Molecular Cell*, vol. 78, no. 5, pp. 811–813, 2020.
- [13] E. Delorme-Axford, H. Popelka, and D. J. Klionsky, “TEX264 is a major receptor for mammalian reticulophagy,” *Autophagy*, vol. 15, no. 10, pp. 1677–1681, 2019.
- [14] T. M. Nthiga, B. K. Shrestha, T. Lamark, and T. Johansen, “CALCOCO1 is a soluble reticulophagy receptor,” *Autophagy*, vol. 16, no. 9, pp. 1729–1731, 2020.
- [15] M. D. Smith, M. E. Harley, A. J. Kemp et al., “CCPG1 is a non-canonical autophagy cargo receptor essential for ER-phagy and pancreatic ER proteostasis,” *Developmental Cell*, vol. 44, no. 2, pp. 217–232.e11, 2018.
- [16] F. Fumagalli, J. Noack, T. J. Bergmann et al., “Translocon component Sec62 acts in endoplasmic reticulum turnover during stress recovery,” *Nature Cell Biology*, vol. 18, no. 11, pp. 1173–1184, 2016.
- [17] A. Khaminets, T. Heinrich, M. Mari et al., “Regulation of endoplasmic reticulum turnover by selective autophagy,” *Nature*, vol. 522, no. 7556, pp. 354–358, 2015.
- [18] Y. Cui, S. Parashar, M. Zahoor et al., “A COPII subunit acts with an autophagy receptor to target endoplasmic reticulum for degradation,” *Science*, vol. 365, no. 6448, pp. 53–60, 2019.
- [19] J. Mo, J. Chen, and B. Zhang, “Critical roles of FAM134B in ER-phagy and diseases,” *Cell Death & Disease*, vol. 11, no. 11, p. 983, 2020.
- [20] L. Cinque, C. De Leonibus, M. Iavazzo et al., “MiT/TFE factors control ER-phagy via transcriptional regulation of FAM134B,” *The EMBO Journal*, vol. 39, no. 17, article e105696, 2020.
- [21] Y. Liao, B. Duan, Y. Zhang, X. Zhang, and B. Xia, “ER-phagy results in ER stress, UPR, and cell death,” *Journal of Biological Chemistry*, vol. 294, no. 52, pp. 20009–20023, 2019.
- [22] A. I. Chiramel, J. D. Dougherty, V. Nair, S. J. Robertson, and S. M. Best, “FAM134B, the selective autophagy receptor for endoplasmic reticulum turnover, inhibits replication of Ebola virus strains Makona and Mayinga,” *The Journal of Infectious Diseases*, vol. 214, Supplement 3, pp. S319–S325, 2016.
- [23] C. W. A. Pfirrmann, A. Metzendorf, M. Zanetti, J. Hodler, and N. Boos, “Magnetic resonance classification of lumbar intervertebral disc degeneration,” *Spine*, vol. 26, no. 17, pp. 1873–1878, 2001.
- [24] R. Luo, Z. Liao, Y. Song et al., “Berberine ameliorates oxidative stress-induced apoptosis by modulating ER stress and autophagy in human nucleus pulposus cells,” *Life Sciences*, vol. 228, pp. 85–97, 2019.
- [25] S. Zielke, S. Kardo, L. Zein et al., “ATF4 links ER stress with reticulophagy in glioblastoma cells,” *Autophagy*, pp. 1–17, 2020.
- [26] T. T. Tsai, N. Y. Ho, Y. T. Lin et al., “Advanced glycation end products in degenerative nucleus pulposus with diabetes,” *Journal of Orthopaedic Research*, vol. 32, no. 2, pp. 238–244, 2014.
- [27] F. Timóteo-Ferreira, D. Abreu, S. Mendes et al., “Redox imbalance in age-related ovarian dysfunction and perspectives for its prevention,” *Ageing Research Reviews*, vol. 68, article 101345, 2021.
- [28] G. Hou, H. Lu, M. Chen, H. Yao, and H. Zhao, “Oxidative stress participates in age-related changes in rat lumbar intervertebral discs,” *Archives of Gerontology and Geriatrics*, vol. 59, no. 3, pp. 665–669, 2014.
- [29] S. Lu, Y. Song, R. Luo et al., “Ferroportin-Dependent Iron Homeostasis Protects against Oxidative Stress- Induced Nucleus Pulposus Cell Ferroptosis and Ameliorates Intervertebral Disc Degeneration In Vivo,” *Oxidative Medicine and Cellular Longevity*, vol. 2021, Article ID 6670497, 18 pages, 2021.
- [30] L. Kang, Q. Xiang, S. Zhan et al., “Restoration of autophagic flux rescues oxidative damage and mitochondrial dysfunction to protect against intervertebral disc degeneration,” *Oxidative Medicine and Cellular Longevity*, vol. 2019, Article ID 7810320, 27 pages, 2019.
- [31] Q. Xiang, Z. Cheng, J. Wang et al., “Allicin attenuated advanced oxidation protein product-induced oxidative stress and mitochondrial apoptosis in human nucleus pulposus cells,” *Oxidative Medicine and Cellular Longevity*, vol. 2020, Article ID 6685043, 17 pages, 2020.
- [32] H. Chino and N. Mizushima, “ER-phagy: quality control and turnover of endoplasmic reticulum,” *Trends in Cell Biology*, vol. 30, no. 5, pp. 384–398, 2020.
- [33] P. Grumati, I. Dikic, and A. Stolz, “ER-phagy at a glance,” *Journal of Cell Science*, vol. 131, no. 17, 2018.
- [34] S. Song, J. Tan, Y. Miao, and Q. Zhang, “Crosstalk of ER stress-mediated autophagy and ER-phagy: involvement of UPR and the core autophagy machinery,” *Journal of Cellular Physiology*, vol. 233, no. 5, pp. 3867–3874, 2018.
- [35] I. Dikic and Z. Elazar, “Mechanism and medical implications of mammalian autophagy,” *Nature Reviews Molecular Cell Biology*, vol. 19, no. 6, pp. 349–364, 2018.
- [36] N. J. Lennemann and C. B. Coyne, “Dengue and Zika viruses subvert reticulophagy by NS2B3-mediated cleavage of FAM134B,” *Autophagy*, vol. 13, no. 2, pp. 322–332, 2017.
- [37] X. Dai, T. Hua, and T. Hong, “Integrated diagnostic network construction reveals a 4-gene panel and 5 cancer hallmarks driving breast cancer heterogeneity,” *Scientific Reports*, vol. 7, no. 1, article 6827, 2017.
- [38] Y. Liu, S. Wang, Z. Wang et al., “Dexmedetomidine alleviated endoplasmic reticulum stress via inducing ER-phagy in the spinal cord of neuropathic pain model,” *Frontiers in Neuroscience*, vol. 14, p. 90, 2020.

- [39] Z. Zhang, W. Gao, L. Zhou et al., “Repurposing brigatinib for the treatment of colorectal cancer based on inhibition of ER-phagy,” *Theranostics*, vol. 9, no. 17, pp. 4878–4892, 2019.
- [40] S. Jiang, Y. Lin, H. Yao et al., “The role of unfolded protein response and ER-phagy in quantum dots-induced nephrotoxicity: an in vitro and in vivo study,” *Archives of Toxicology*, vol. 92, no. 4, pp. 1421–1434, 2018.

Research Article

HIF-1 α -Mediated miR-623 Regulates Apoptosis and Inflammatory Responses of Nucleus Pulposus Induced by Oxidative Stress via Targeting TXNIP

Xiaogang Bao ¹, Zhenhua Wang ², Qi Jia ³, Sibao Shen ⁴, Likang Wu ⁵, Qi Jiang ⁶,
Changwei Li ⁷, and Guohua Xu ¹

¹Department of Orthopedic Surgery, Spine Center, Shanghai Changzheng Hospital, The Second Military Medical University, Shanghai, China

²Department of Laboratory Medicine, Shanghai Changzheng Hospital, The Second Military Medical University, Shanghai, China

³Department of Orthopedic Oncology, Spine Tumor Center, Shanghai Changzheng Hospital, The Second Military Medical University, Shanghai, China

⁴Hebei Key Laboratory of Active Components and Functions in Natural Products, College of Chemical Engineering, Hebei Normal University of Science and Technology, Qinhuangdao, 066600 Hebei, China

⁵School of Pharmaceutical Engineering & Life Science, Changzhou University, Changzhou, Zhejiang, China

⁶Department of Orthopedic Surgery, Changhai Hospital, The Second Military Medical University, Shanghai, China

⁷Shanghai Key Laboratory for the Prevention and Treatment of Bone and Joint Diseases with Integrated Chinese-Western Medicine, Shanghai Institute of Traumatology and Orthopedics, Rui Jin Hospital, Shanghai Jiao Tong University School of Medicine, Shanghai, China

Correspondence should be addressed to Changwei Li; lcw11876@rjh.com.cn and Guohua Xu; xuguohuamail@smmu.edu.cn

Received 21 April 2021; Accepted 14 July 2021; Published 3 August 2021

Academic Editor: Kaitao Lai

Copyright © 2021 Xiaogang Bao et al. This is an open access article distributed under the Creative Commons Attribution License, which permits unrestricted use, distribution, and reproduction in any medium, provided the original work is properly cited.

Excessive apoptosis and inflammatory responses of nucleus pulposus (NP) cells induced by oxidative stress contribute to intervertebral disc degeneration (IVDD). Though some microRNAs are associated with IVDD, the specific microRNA that can mediate apoptotic and inflammatory responses of NP cells induced by oxidative stress synchronously still needs further identification. Here, we find that microRNA-623 (miR-623) is downregulated in IVDD and its expression is regulated by hypoxia-inducible factor-1 α (HIF-1 α) under oxidative stress conditions. Mechanistically, HIF-1 α is observed to promote miR-623 expression by directly binding to its promoter region (−1,994/−1,987 bp). Functionally, miR-623 is found to work as an intermediary in alleviating apoptosis and inflammatory responses of NP cells induced by oxidative stress via regulating thioredoxin-interacting protein (TXNIP) expression by directly targeting its 3′-untranslated region (3′-UTR). Thus, on elucidating the expression and functional mechanisms of miR-623, our study suggests that miR-623 can be a valuable therapeutic target for treating oxidative stress-induced IVDD.

1. Introduction

Intervertebral disc degeneration (IVDD) is a common spinal disease, which is typically manifested by lower back pain and reduced lumbar spine support [1]. The intervertebral disc (IVD) has been elucidated to consist of three interrelated structures: the nucleus pulposus (NP), annulus fibrosus (AF), and cartilaginous endplate. As NP forms the inner core

of IVD, it has been shown to preserve high water content; thereby, allowing the vertebral disc to sustain forces of compression and torsion [2]. Many studies have shown that excessive apoptosis and inflammatory responses of NP cells trigger metabolic disorders, downregulate extracellular matrix (ECM) production, and abolish conventional homeostatic tissue remodeling, which eventually lead to IVDD [3, 4]. Thus, determining key molecular mechanisms of NP cells

that regulate apoptosis and inflammatory responses can significantly aid in managing IVDD.

Among many factors that can cause IVDD, accumulation of reactive oxygen species (ROS) has been reported to be one of them [5, 6]. Recent findings have proved the presence of oxidative stress and escalated concentrations of oxidation products in degenerated discs. Furthermore, reports have confirmed that oxidative stress and subsequent mitochondrial dysfunction play a role in facilitating intrinsic cellular apoptosis in NP cells [3]. Moreover, ROS has been shown to activate signaling pathways such as mitogen-activated protein kinases (MAPKs) and the nuclear factor kappa-light-chain-enhancer of activated B cells (NF- κ B) to promote expression of ECM proteases and proinflammatory genes, while inhibiting expression of ECM-related genes and anticatabolic genes [7]. Thus, establishing key molecular mechanisms of apoptosis and inflammatory responses in oxidative stress-induced NP cells can assist in effectively managing IVDD.

MicroRNAs (miRNAs) are 20–22 nucleotide long base sequences that can target 3'-untranslated regions (3'-UTR) of the target gene and thereby inhibit its expression. Increasing evidences have revealed the influence of miRNAs in IVDD such as mediating apoptosis and inflammatory responses of NP cells. miR-155 is a well-known miRNA that has been shown to play a crucial role in regulating apoptotic pathways. Compared to control NP cells, miR-155 expression has been reported to be significantly downregulated in IVDD and overexpression of miR-155 in NP cells has been shown to inhibit apoptosis by suppressing the expression of FAS-associated death domain protein (FADD) and caspase-3 [8]. Similarly, many studies have revealed the downregulation of miR-146a in IVDD. Regulated expression of miR-146a has been shown to significantly attenuate interleukin 1 β - (IL-1 β -) induced expression of tumor necrosis factor α (TNF- α), IL-6, matrix metalloproteinases (MMPs), and inducible nitric oxide synthase (iNOS) [9]. In addition, miR-145 overexpression has been demonstrated to attenuate apoptosis induced by oxidative stress and increase matrix synthesis in NP cells [10]. Thus, identifying the specific microRNAs that can mediate apoptotic and inflammatory responses of NP cells induced by oxidative stress may provide a potential therapeutic target for treating IVDD.

In the present study, we found that miR-623 was downregulated in IVDD and its expression was regulated by hypoxia-inducible factor 1 α (HIF-1 α) under oxidative stress conditions. Furthermore, miR-623 was observed to act as an intermediary in apoptosis and inflammatory responses of oxidative stress-induced NP cells by targeting thioredoxin-interacting protein (TXNIP) mRNA. Overall, our study proposes miR-623 as a potential therapeutic target for treating oxidative stress-induced IVDD.

2. Results

2.1. Oxidative Stress Downregulates miR-623 Expression in NP Cells. To identify the potential miRNAs that are involved in apoptosis and inflammatory responses of ROS-induced NP cells, we analyzed differentially expressed miRNAs in

control and degenerated NP tissues using microarray datasets (GSE63492 and GSE19943) that were obtained from the Gene Expression Omnibus (GEO) database. Analyses of both the datasets revealed seven miRNAs that were downregulated in degenerated NP tissues (Figure 1(a)). To determine the most evidently downregulated miRNA, we compared the expression of all seven miRNAs in each dataset. Results showed that miR-623 expression had the highest significant difference (Figures 1(b) and 1(c)). Furthermore, to confirm the database-oriented results, miR-623 expression was evaluated in degenerated NP tissues from patients with IVDD and in healthy NP tissues from patients with spinal tumor. Quantitative real-time PCR (qRT-PCR) analysis revealed that miR-623 expression was significantly downregulated in NP cells of IVDD tissues (Figure 1(d)). Further, we verified the dampened expression of miR-623 in degenerated NP tissues by RNA fluorescence in situ hybridization (RNA-FISH) analysis (Figure 1(e)).

On confirming the downregulated expression of miR-623 in IVDD, we then investigated whether miR-623 modulation was a response to ROS. Tert-butyl hydroperoxide (TBHP) was used as an exogenous ROS donor in previously published methodologies [11]. As shown in Figures 1(f)–1(h), stimulated primary NP cells with 100 μ M TBHP for 12 hours significantly induced NP cell apoptosis, as demonstrated by the decreased cell survival rate, decreased antiapoptotic regulator B-cell lymphoma 2 (BCL2) expression, and increased expression of BCL2-associated X (BAX). Meanwhile, miR-623 expression was found to be significantly dampened in the presence of 100 μ M TBHP stimulation for 12 hours (Figure 1(i)). Overall, our results demonstrated that miR-623 expression is downregulated in NP cells of IVDD which indicated that miR-623 might be involved in oxidative stress-induced apoptosis and inflammatory responses of NP cells.

2.2. miR-623 Attenuates Apoptosis of NP Cells Induced by Oxidative Stress. To determine the role of miR-623 in NP cell apoptosis induced by oxidative stress, primary human NP cells were transfected with the miR-623 mimic or inhibitor before being treated with TBHP. As illustrated in Figures 2(a)–2(c), fluorescence-activated cell sorting (FACS) analysis revealed that miR-623 overexpression restricts TBHP-induced apoptosis of NP cells. Consistently, Western blot analysis revealed that miR-623 overexpression significantly restores the expression of BAX, cleaved caspase 3, MMP13, BCL2, and collagen II, which were induced or reduced, on TBHP treatment (Figure 2(d)). Studies have shown that mitochondria are not only the main source for cellular ROS but also specifically susceptible to oxidative stress-related damage [12]. JC-1 staining revealed that miR-623 significantly alleviates TBHP-decreased mitochondrial membrane potential (Figures 2(e)–2(f)). This suggested that miR-623 overexpression may protect mitochondria from oxidative stress-related damage. Similarly, C11 fluorescent dye-mediated detection of the mitochondrial ROS level revealed that miR-623 overexpression markedly restricts ROS production in TBHP-induced NP cells (Figures 2(g) and 2(h)). In contrast to the ameliorated role of miR-623 overexpression in TBHP-induced apoptosis and ROS

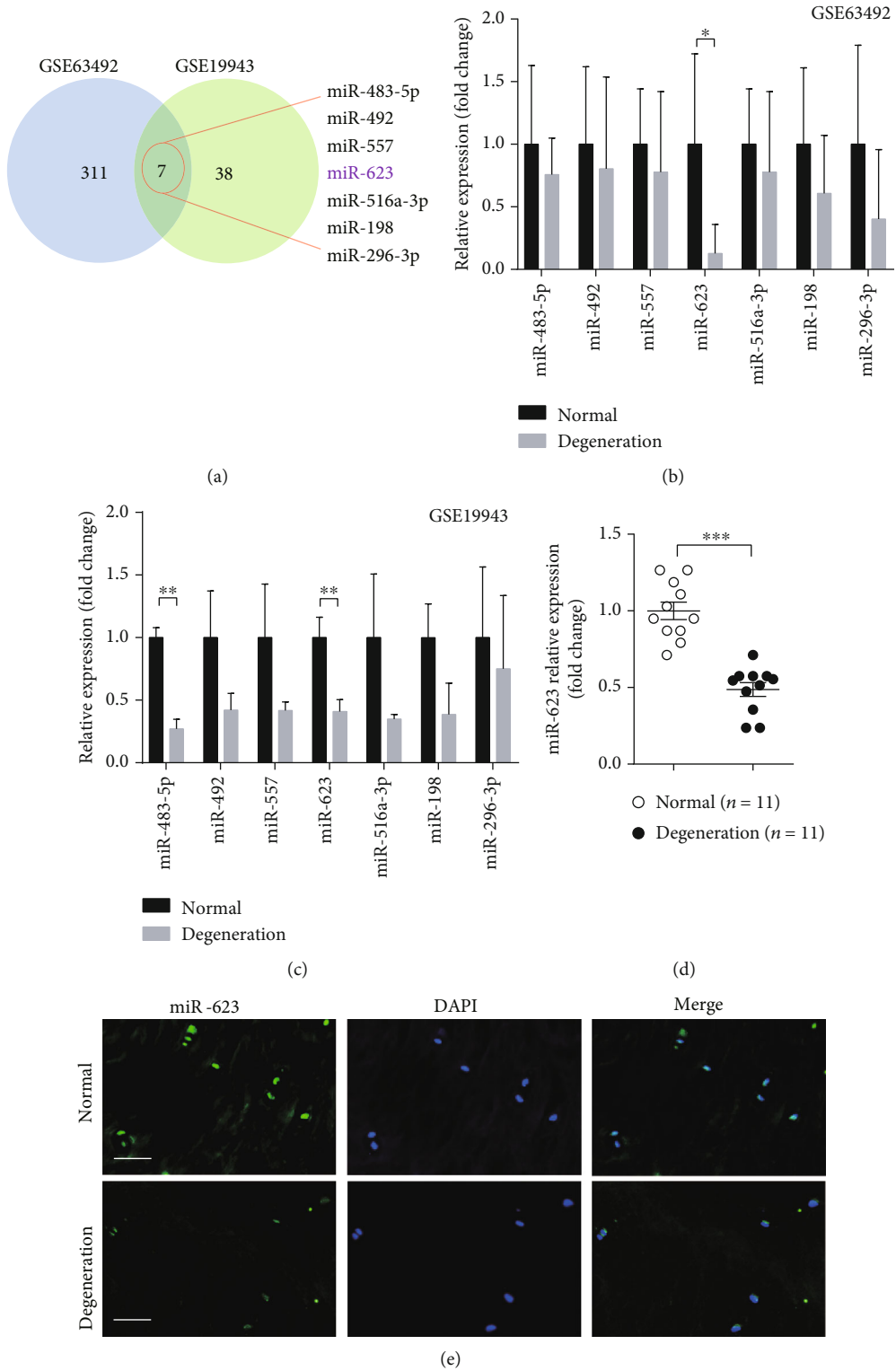


FIGURE 1: Continued.

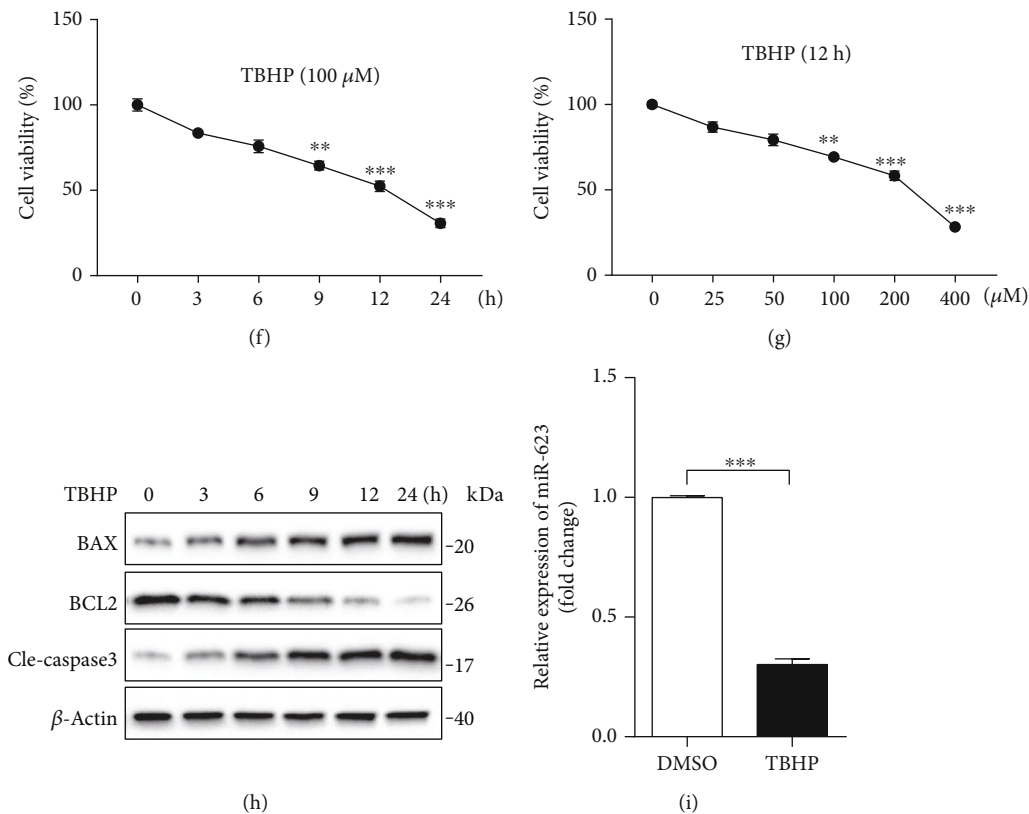


FIGURE 1: Oxidative stress dampens miR-623 expression in NP cells. (a) Differentially expressed miRNAs between normal and degenerated NP tissues were determined by analysis with microarray datasets of GSE63492 and GSE19943. Seven miRNAs were found to be downregulated in degenerated NP tissues both in the datasets of GSE63492 and GSE19943. (b) The fold change of relative mRNA expression of seven downregulated miRNAs (a) analyzed by the dataset of GSE63492 was shown as the column chart. (c) The fold change of relative mRNA expression of seven downregulated miRNAs (a) analyzed by the dataset of GSE19943 was shown as the column chart. (d) Quantification analysis of miR-623 mRNA expression in normal NP tissues ($n = 11$) and degenerated NP tissues ($n = 11$). (e) Immunostaining analysis of miR-623 mRNA expression in normal NP tissues and degenerated NP tissues. Scale bars represent $50 \mu\text{m}$. (f) The survival rate of NP cells incubated with $100 \mu\text{M}$ TBHP for different hours. (g) The survival rate of NP cells incubated with different doses of TBHP for 12 hours. (h) The protein of BAX, BCL2, and cleaved caspase-3 expression in NP cells induced by $100 \mu\text{M}$ TBHP for different hours. (i) Quantification analysis of miR-623 mRNA expression in NP cells with or without TBHP stimulation. * $P < 0.05$, ** $P < 0.01$, and *** $P < 0.001$. P values were analyzed by two-tailed t -tests in (b, c, d, and i) and one-way ANOVA in (f, g).

production, miR-623 inhibitor transfection significantly promoted the apoptosis and ROS production of NP cells induced by TBHP (Figures 2(i)–2(n)). Overall, these results demonstrated that miR-623 attenuates NP cell apoptosis induced by oxidative stress.

2.3. miR-623 Inhibits Inflammatory Responses of NP Cells Induced by Oxidative Stress. On elucidating the antiapoptotic role of miR-623, we further investigated whether miR-623 mediates inflammatory responses in oxidative stress-induced NP cells. Gain-of-function experiments revealed that on transfection of miR-623 mimic, expressions of inflammatory markers such as iNOS, IL-1 β , and IL-6 were significantly reduced in TBHP-treated NP cells (Figures 3(a)–3(d)). Conversely, loss-of-function experiments demonstrated that the miR-623 inhibitor significantly augmented the effect of TBHP on iNOS, IL-1 β , and IL-6 expression (Figures 3(e)–3(i)). Thus, these results demonstrated that miR-623 inhibits inflammatory responses in NP cells induced by oxidative stress.

2.4. miR-623 Attenuates TBHP-Induced Apoptosis and Inflammation by Targeting TXNIP mRNA. To identify the downstream targets of miR-623, bioinformatics analysis was performed using two miRNA databases, TargetScan and miRTarBase. Subsequently, 226 genes were selected for further investigation. On analyzing the microarray dataset, GSE34095, mRNA expressions of TXNIP, adaptor protein-1 complex subunit sigma-2 (AP1S2), WNT1-inducible-signaling pathway protein-1 (WISP1), basic leucine zipper and W-2 domain containing protein 1 (BZW1), and X-ray repair cross-complementing protein 5 (XRCC5) were found to be upregulated in IVDD among the selected 226 genes (Figures 4(a) and 4(b)). TXNIP has been reported as a key regulatory protein in oxidative stress-induced apoptosis and inflammatory responses [13]. Subsequently, we hypothesized that TXNIP might be the mRNA target of miR-623. To evaluate this hypothesis, we first compared the TXNIP expression level in normal IVDs and IVDD tissues. Results showed that TXNIP expression was upregulated in IVDD

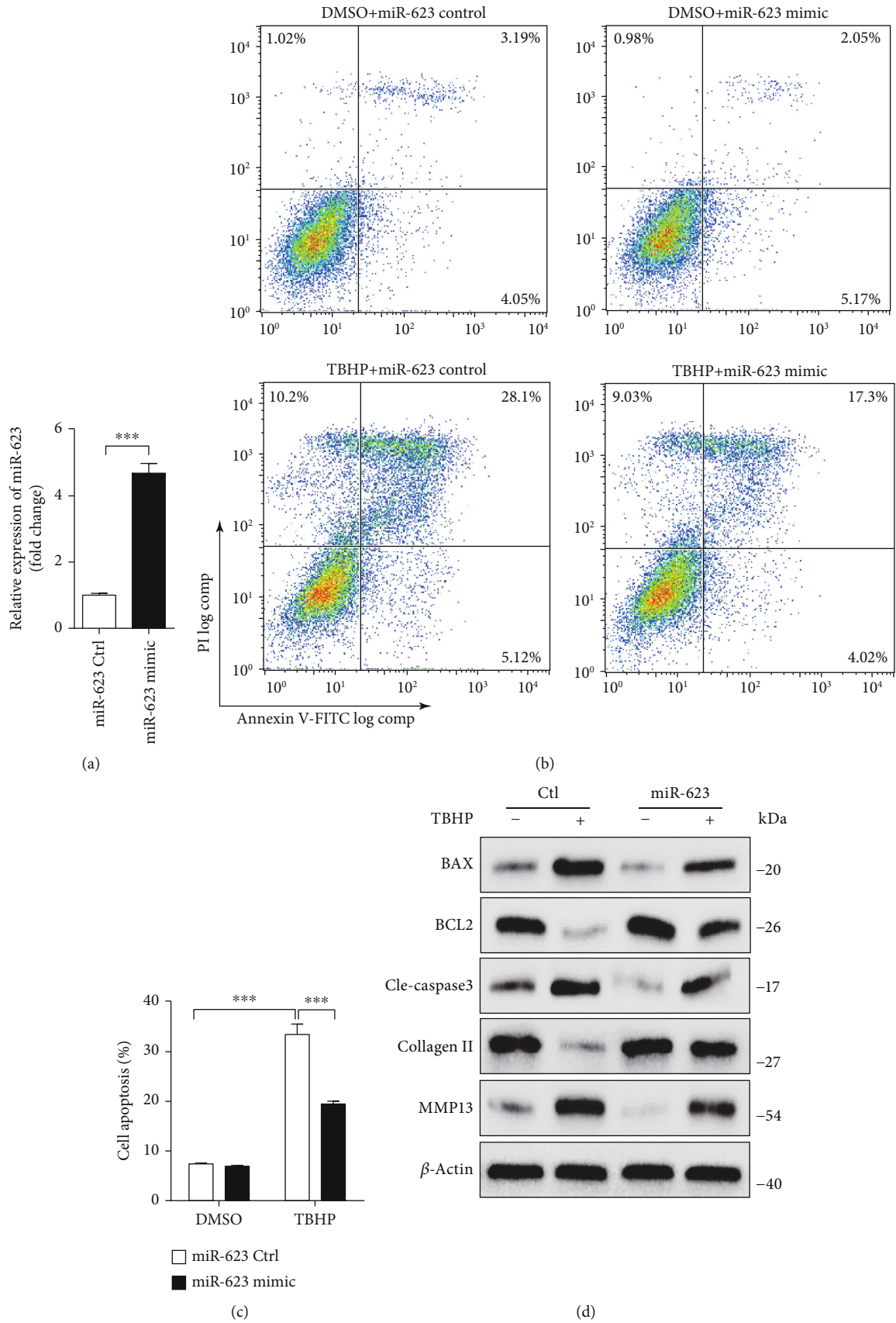


FIGURE 2: Continued.

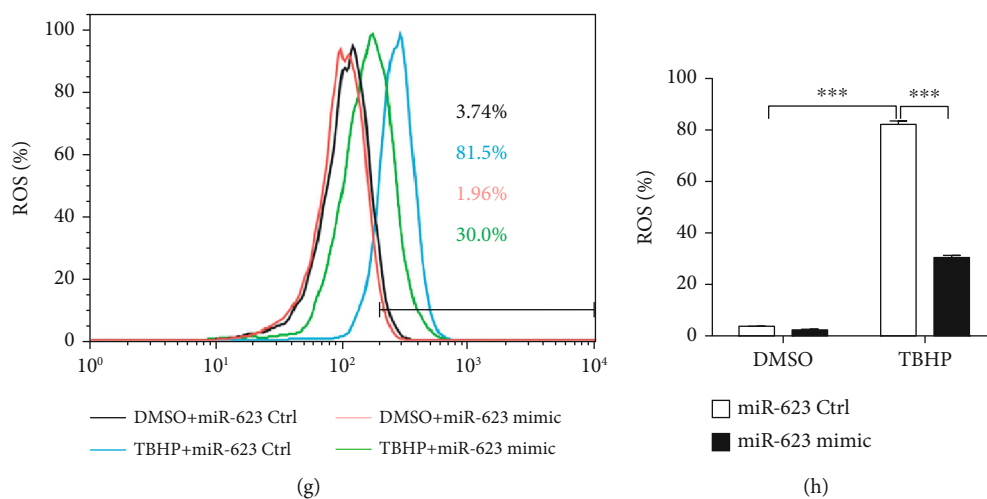
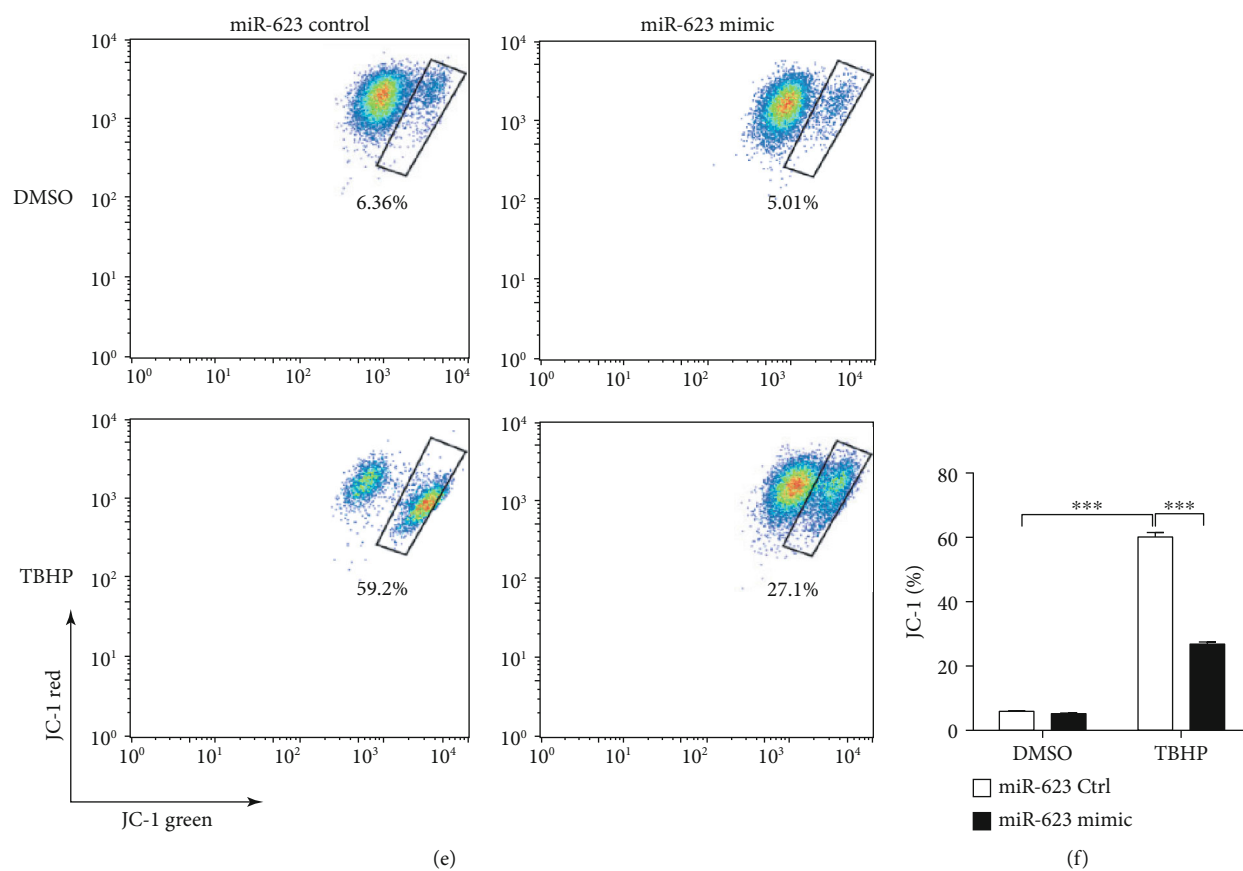


FIGURE 2: Continued.

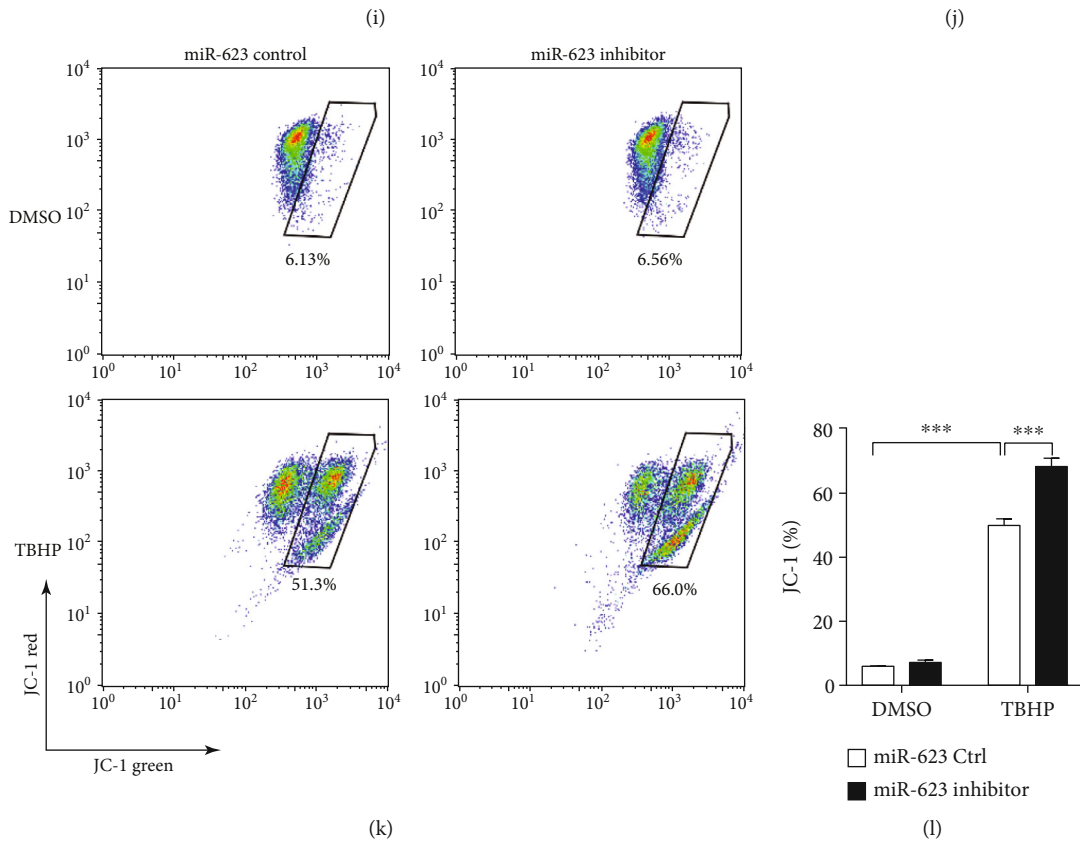
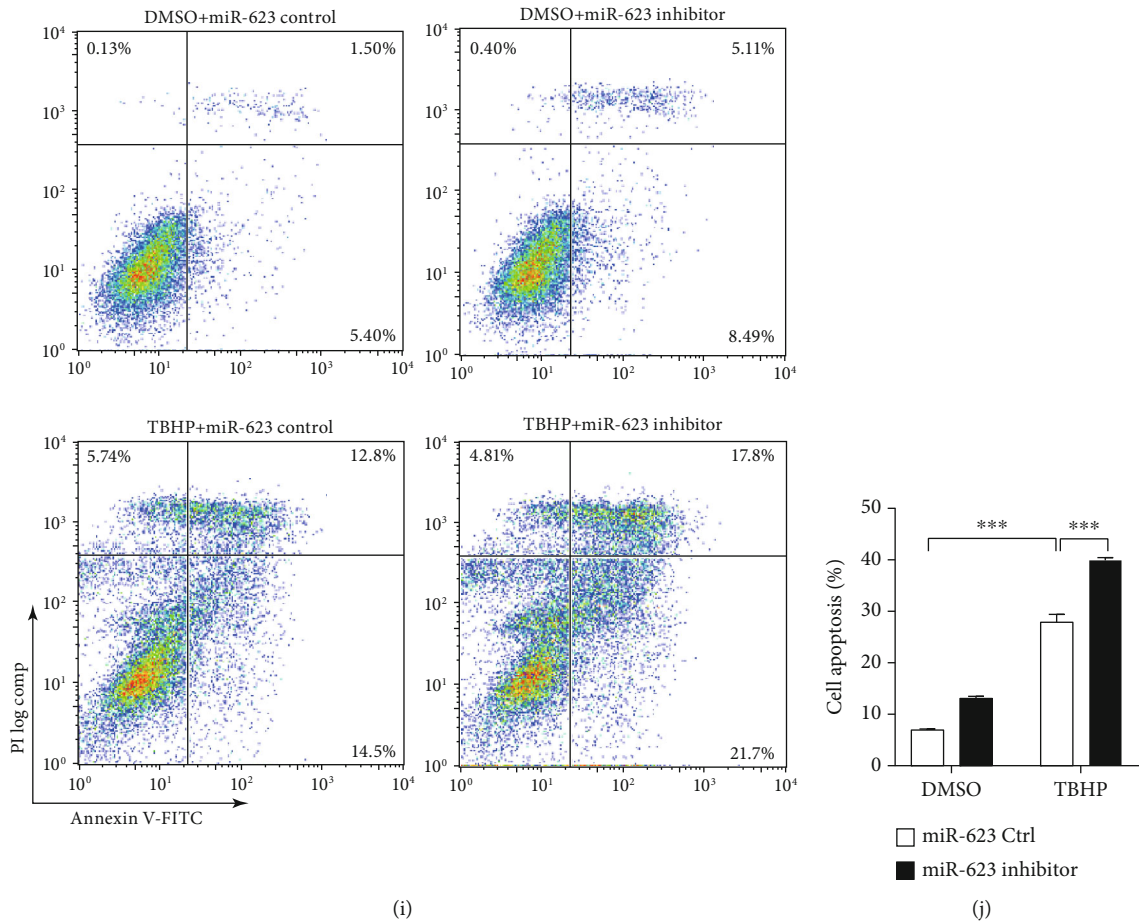


FIGURE 2: Continued.

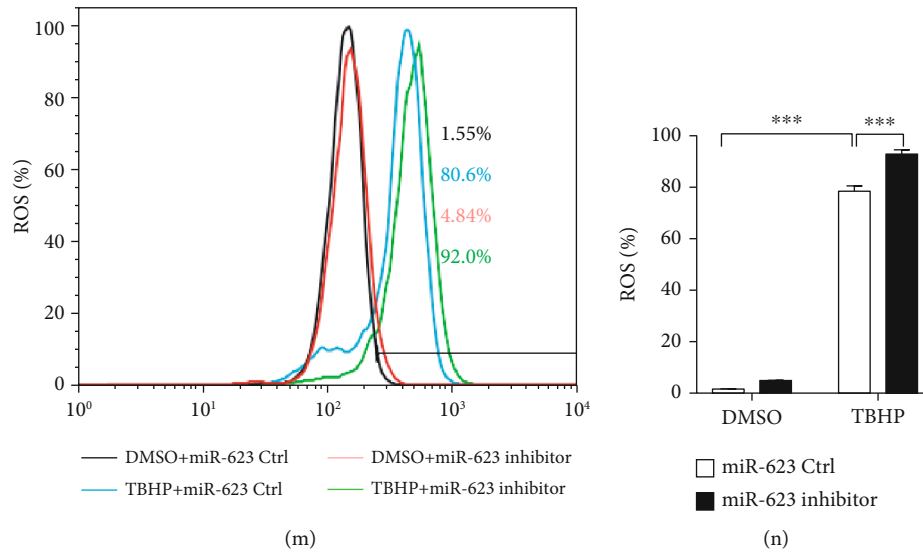


FIGURE 2: miR-623 decreases the apoptosis of NP cells induced by oxidative stress. (a) Quantification analysis of miR-623 mRNA expression in NP cells with or without miR-623 mimic transfection. (b) FACS analysis of NP cell apoptosis induced by TBHP with or without miR-623 mimic transfection. (c) The means of cell apoptosis in (b) were shown as the column chart. (d) Western blot analysis of BAX, BCL2, cleaved caspase-3, collagen II, and MMP13 expression in NP cells induced by TBHP with or without miR-623 mimic transfection. (e) FACS analysis of JC-1-positive cells induced by TBHP with or without miR-623 mimic transfection. (f) The means of JC-1-positive cells in (e) were shown as the column chart. (g) FACS analysis of ROS-positive cells induced by TBHP induced with or without miR-623 mimic transfection. (h) The means of ROS-positive cells in (g) were shown as the column chart. (i) FACS analysis of NP cell apoptosis induced by TBHP with or without miR-623 mimic transfection. (j) The means of cell apoptosis in (i) were shown as the column chart. (k) FACS analysis of JC-1-positive cells induced by TBHP with or without miR-623 mimic transfection. (l) The means of JC-1-positive cells in (k) were shown as the column chart. (m) FACS analysis of ROS-positive cells induced by TBHP induced with or without miR-623 mimic transfection. (n) The means of ROS-positive cells in (m) were shown as the column chart. *** $P < 0.001$. P values were analyzed by two-tailed t -tests in (a) and two-way ANOVA in (c, f, h, j, l, and n).

(Figure 4(c)). Further, the predicted binding sites of miR-623 on 3'-UTR of *TXNIP* were shown in Figure 4(d). To verify these putative binding sites, site-directed mutagenesis was performed (Figure 4(d)). 293T cells were transfected with wild-type (WT) or mutated 3'-UTR constructs of *TXNIP*, and luciferase activity was measured following cotransfection with miR-623. As shown in Figure 4(e), miR-623 mimic transfection was observed to inhibit luciferase reporter activity in WT-transfected cells and not in mutated *TXNIP*-transfected cells. This indicated that *TXNIP* mRNA was directly targeted by miR-623. Subsequently, qRT-PCR and immunoblotting analysis revealed that miR-623 overexpression significantly downregulates mRNA and protein expression levels of *TXNIP* in NP cells (Figures 4(f) and 4(g)). To further confirm whether *TXNIP* expression is regulated by TBHP via miR-623, NP cells were transfected with miR-623 mimic and treated with TBHP. As shown in Figure 5(a), TBHP was found to induce *TXNIP* expression, while miR-623 overexpression was observed to alleviate this effect.

To assess the role of *TXNIP* and miR-623 in TBHP-induced apoptosis and inflammation, we cotransfected NP cells with miR-623 mimic and *TXNIP*. Immunoblotting analysis showed that miR-623 inhibits TBHP-induced expression of proapoptotic proteins such as BAX, BCL2, and cleaved caspase-3; inflammatory mediators including IL-1 β , IL-6, and iNOS; and the majority of matrix degrading proteases such as MMP-13. In contrast, *TXNIP* was found to

enhance the expression of these proapoptotic proteins, inflammatory mediators, and matrix-degrading proteases (Figures 5(b)–5(e)). These results suggested that miR-623 attenuates TBHP-induced apoptosis and inflammation by targeting *TXNIP* mRNA.

2.5. miR-623 Expression Is Regulated by HIF-1 α under Oxidative Stress Conditions.

In IVDs, NP is an avascular tissue under the hypoxic environment. HIF is one of the vital factors that has been shown to directly mediate cellular responses to hypoxia [2]. In our previous study, we demonstrated the protective effect of HIF-1 α against apoptosis in NP cells [2]. In the present study, results revealed that HIF-1 α expression was significantly decreased in NP cells of IVDD tissue (Figure 6(a)). In addition, some studies have reported that oxidative stress inhibits HIF-1 α in NP cells [14], and our present study further reveals that oxidative stress mediates oxidative stress-induced NP cell apoptosis and inflammatory responses via miR-623 (Figure 3). Therefore, we hypothesized that HIF-1 α might be acting as an intermediary between oxidative stress and miR-623 expression in NP cells. To evaluate our hypothesis, we first detected miR-623 expression in oxidative stress-mediated NP cells with or without HIF-1 α overexpression. Results showed that HIF-1 α overexpression significantly restored miR-623 expression, which was downregulated by TBHP (Figures 6(b) and 6(c)). Consistent with miR-623 mimic-related results, HIF-1 α

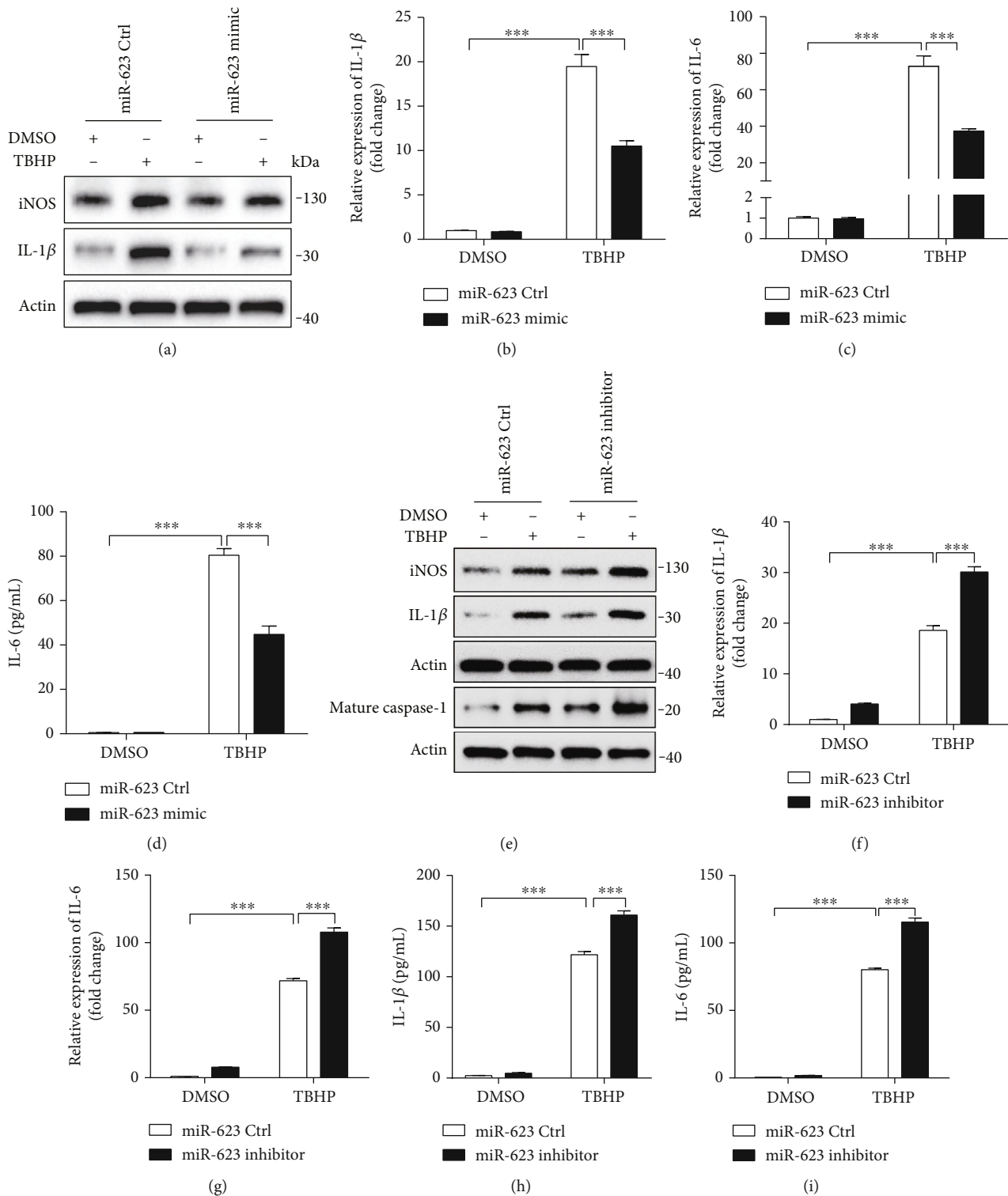


FIGURE 3: miR-623 inhibits the inflammatory responses of NP cells induced by oxidative stress. (a) Western blot analyses of IL-1 β and iNOS in NP cells induced by TBHP with or without miR-623 mimic transfection. (b, c) Quantification analysis of IL-1 β and IL-6 mRNA expression in NP cells induced by TBHP with or without miR-623 mimic transfection. (d) Quantification analysis of the secretion of IL-6 in culture medium of NP cells induced by TBHP with or without miR-623 mimic transfection. (e) Western blot analyses of IL-1 β , iNOS, and cleaved caspase-1 (C-caspase-1) in NP cells induced by TBHP with or without miR-623 inhibitor transfection. (f, g) Quantification analysis of IL-1 β and IL-6 mRNA expression in NP cells induced by TBHP with or without miR-623 inhibitor transfection. (h, i) Quantification analysis of the secretion of IL-1 β and IL-6 in culture medium of NP cells induced by TBHP with or without miR-623 inhibitor transfection. *** $P < 0.001$. P values were analyzed by two-way ANOVA.

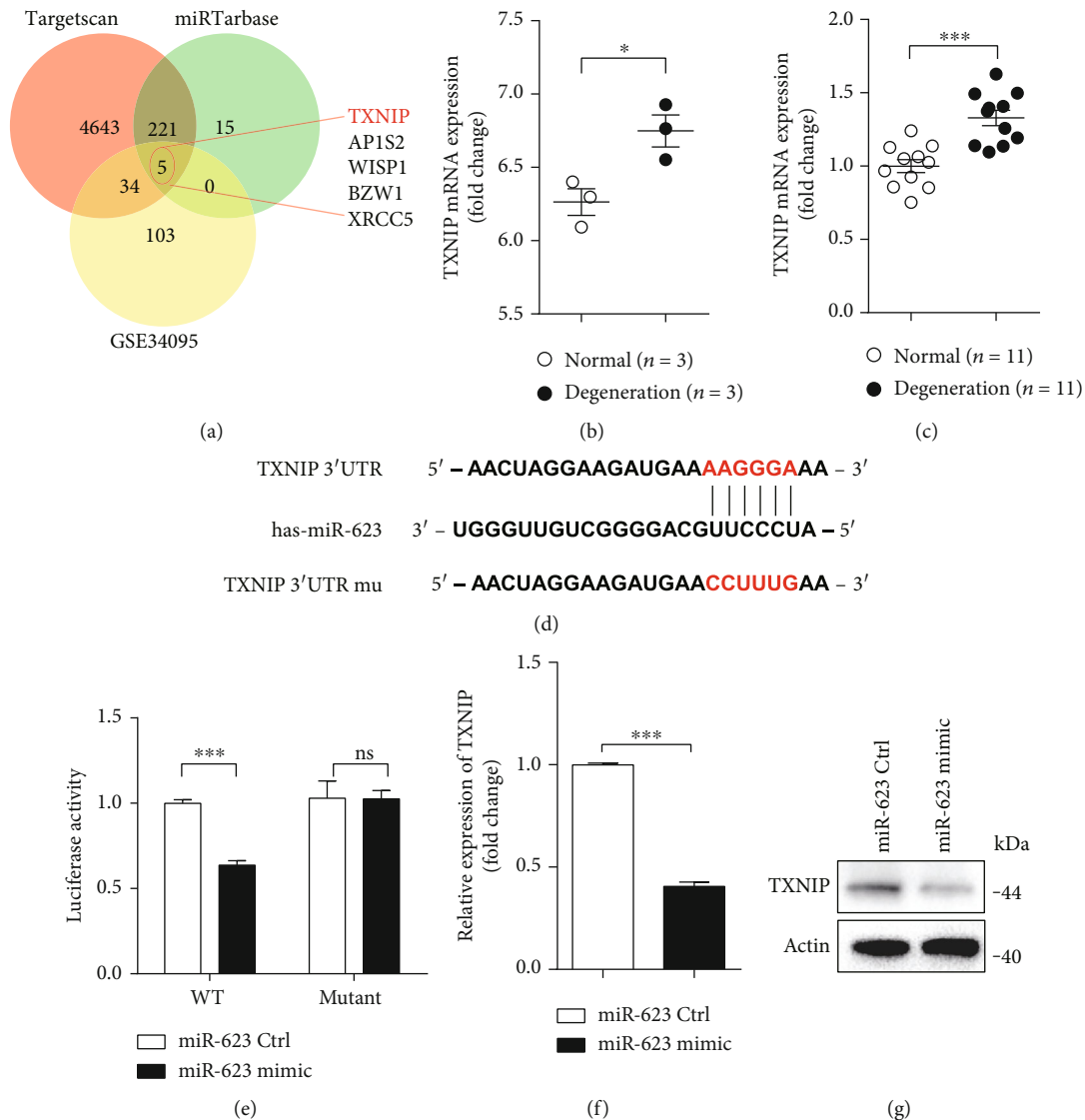


FIGURE 4: miR-623 inhibits TXNIP expression by targeting its 3'-UTR. (a) Bioinformatics analysis was performed to determine the predicted downstream targets of miR-623 with the dataset of TargetScan, miRTarBase, and GSE34095. (b) The fold change of relative mRNA expression of TXNIP analyzed by the dataset of GSE63492. (c) Quantification analysis of TXNIP mRNA expression in normal ($n = 11$) and degenerated ($n = 11$) NP tissues. (d) Schematic representation of the binding between miR-623 and the TXNIP 3'-UTR. (e) Relative luciferase activities were analyzed in 293T cells cotransfected with TXNIP 3'-UTR (wild-type or mutant) reporter plasmid and miR-623 mimics or miR-623 control. (f, g) qRT-PCR and Western blot analysis of TXNIP expression in NP cells transfected with miR-623 mimics or miR-623 control. * $P < 0.05$ and *** $P < 0.001$. P values were analyzed by two-tailed t -tests in (a, b, d, and e).

overexpression was found to markedly restore the expression of proapoptotic proteins (BAX and cleaved caspase-3), anti-apoptotic proteins (BCL2), and ECM metabolism-related proteins (MMP13 and collagen II), which were upregulated and downregulated, respectively, on TBHP treatment (Figure 6(d)).

HIF-1 α is a transcriptional factor that usually binds to the promoter region of target genes to facilitate their expression [15]. Thus, we investigated whether HIF-1 α mediates miR-623 expression by directly binding to its promoter region. A dual-luciferase reporter gene assay system was used to detect the promoter activity of miR-623 on HIF-1 α overexpression. Results showed that consistent with the mRNA expression of

HIF-1 α and miR-623, the promoter activity of miR-623 was found to be significantly augmented on HIF-1 α overexpression (Figure 6(e)). Further, we investigated the location of the hypoxia-reactive element (HRE) in the miR-623 promoter region. On analyzing the promoter sequence of human miR-623 using the JASPAR core database [16], we found one putative binding site for HIF-1 α at -1,994/-1,987 bp (CCAC GTGA) on its promoter region (Figure 6(f)). To further examine if the predicted binding site is an essential component for HIF-1 α -regulated miR-623 expression, we mutated the putative binding sites to TCCATCTA (Figure 6(f)). NP cells were then transfected with either WT or mutated constructs, and luciferase activity was measured following HIF-

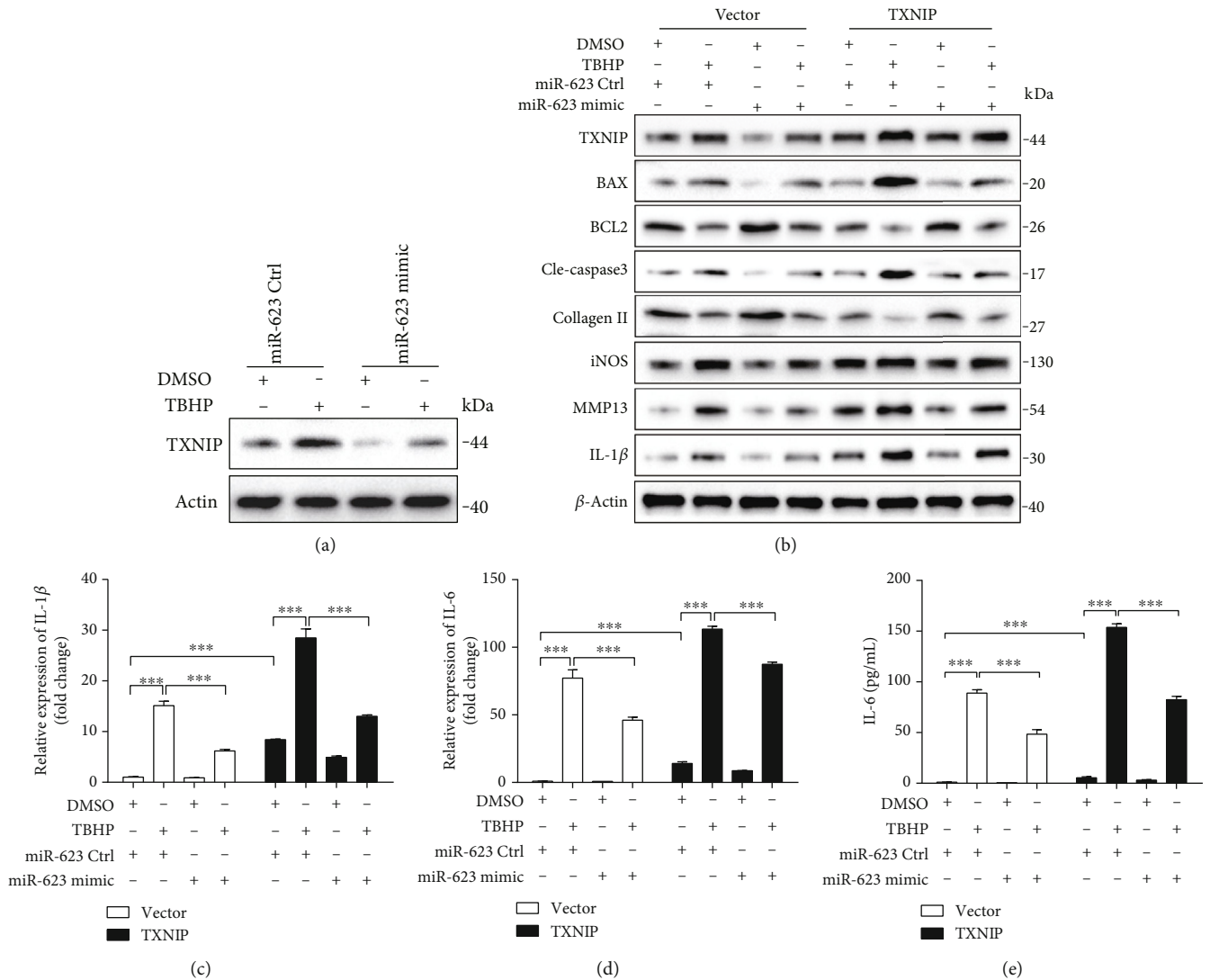


FIGURE 5: miR-623 attenuates TBHP-induced apoptosis and inflammation via TXNIP. (a) Western blot analysis of TXNIP expression in NP cells induced by TBHP with or without miR-623 mimic transfection. (b) Western blot analyses of TXNIP, BAX, BCL2, cleaved caspase-3, collagen II, iNOS, MMP13, and IL-1β in NP cells induced by TBHP with or without TXNIP overexpression and/or miR-623 mimic transfection. (c, d) Quantification analysis of IL-1β and IL-6 mRNA expression in NP cells induced by TBHP with or without TXNIP overexpression and/or miR-623 mimic transfection. (e) Quantification analysis of the secretion of IL-6 in culture medium of NP cells induced by TBHP with or without TXNIP overexpression and/or miR-623 mimic transfection. ****P* < 0.001. *P* values were analyzed by two-way ANOVA.

1α overexpression. Results revealed that compared to WT controls, mutation in the binding site reduced the promoter activity of miR-623 induced by HIF-1α overexpression (Figure 6(g)). Overall, these results demonstrated that miR-623 expression was regulated by HIF-1α under oxidative stress conditions.

3. Discussion

Excessive apoptosis and inflammatory responses in NP cells induced by oxidative stress can trigger metabolic disorders of NP tissues, obliterate the normal structure and physiological functions of IVD, and eventually lead to IVDD [17, 18]. Although many miRNAs have been associated with IVDD, the specific miRNAs that can co-mediate apoptosis and the

inflammatory response in oxidative stress-induced NP cells still need further identification. In this study, we found that miR-623 expression is downregulated in IVDD, which is regulated by HIF-1α under oxidative stress conditions. Furthermore, we demonstrated that miR-623 targets *TXNIP* mRNA and acts as an intermediary in apoptosis and inflammatory responses of oxidative stress-induced NP cells (Figure 6(h)). Thus, we proved miR-623 as an intermediary between oxidative stress and apoptosis and inflammatory responses of NP cells. Overall, on elucidating the expression and functional mechanisms of miR-623, our study suggests miR-623 as a therapeutic target for treating oxidative stress-induced IVDD.

IVDD has been reported to be typically instigated from the inner NP core, which has been shown to develop an

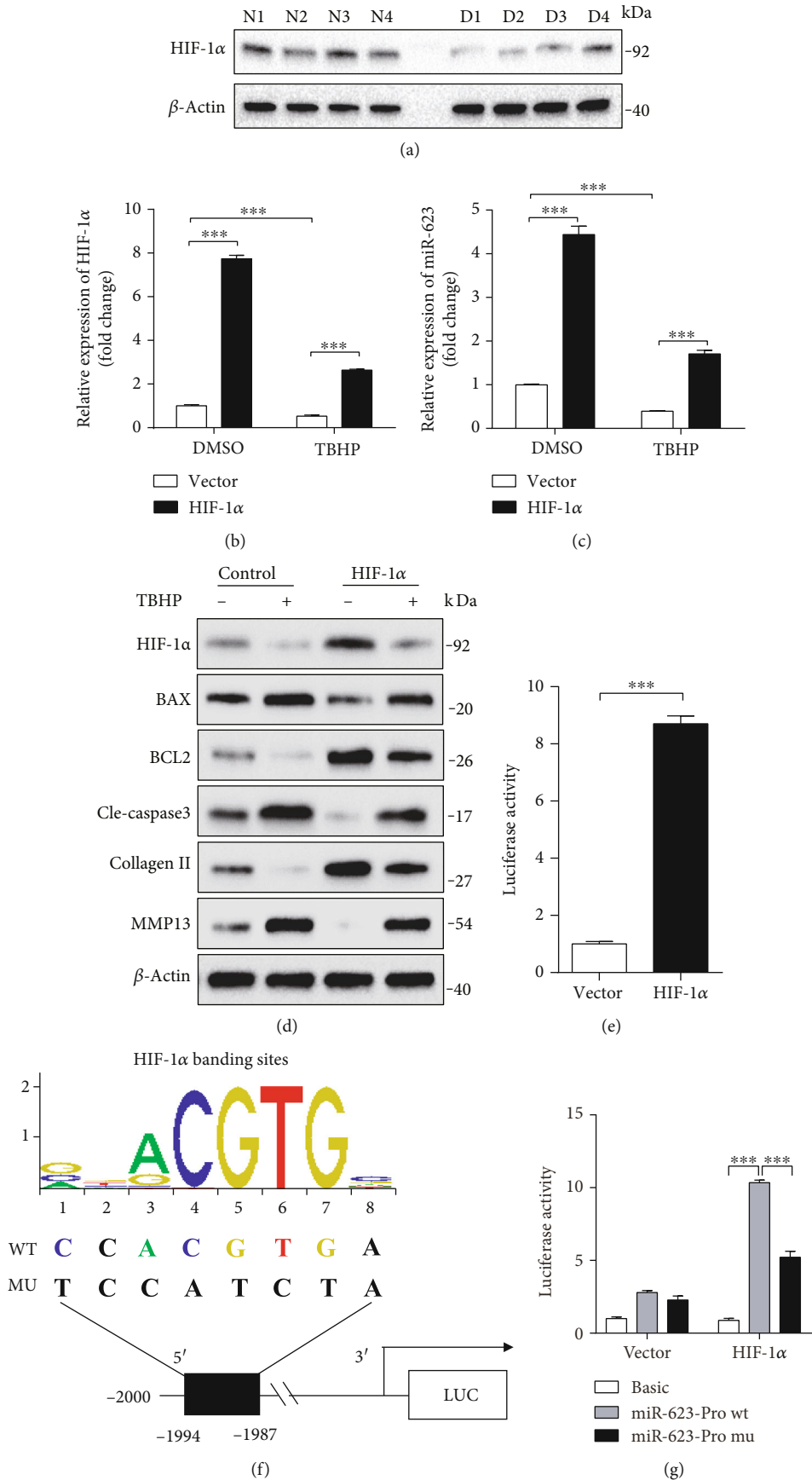


FIGURE 6: Continued.

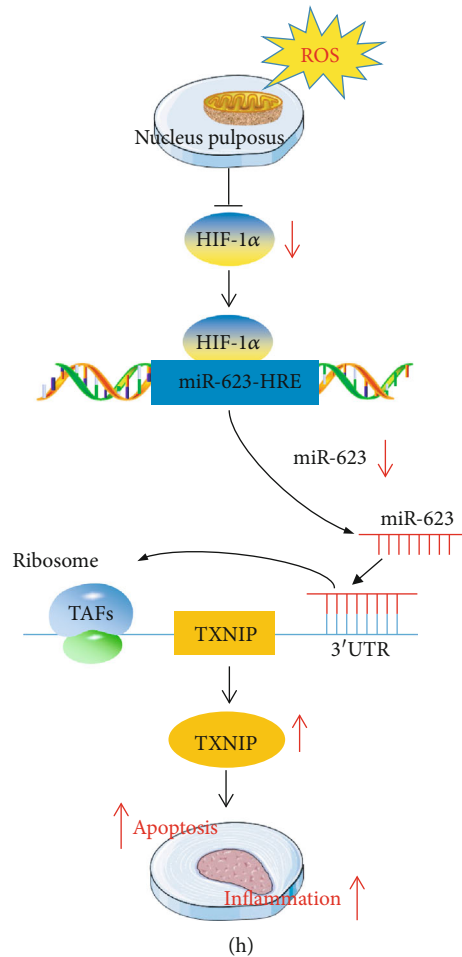


FIGURE 6: miR-623 expression is regulated by HIF-1 α under oxidative stress. (a) Western blot analysis of HIF-1 α expression in normal and degenerated NP tissues. (b, c) Quantification analysis of HIF-1 α and miR-623 expression in NP cells induced by TBHP with or without HIF-1 α overexpression. (d) Western blot analyses of HIF-1 α , BAX, BCL2, cleaved caspase-3, collagen II, and MMP13 in NP cells induced by TBHP with or without HIF-1 α overexpression. (e) miR-623 promoter activity induced by HIF-1 α overexpression. (f) The schematic of the WT and mutant miR-623 promoter constructs. (g) miR-623 promoter activity induced by HIF-1 α with or without putative HIF-1 α binding site mutation on the miR-623 promoter. (h) The schematic graph reflects the HIF-1 α -miR-623-TXNIP pathway in NP cell apoptosis and inflammatory responses induced by oxidative stress. Normally, NP is an avascular tissue under a hypoxic environment and expresses a high level of HIF-1 α . Under oxidative stress conditions, HIF-1 α expression is dampened and results in decreased nuclear translocation to bind to the hypoxia-reactive element on the miR-623 promoter, leading to decreased miR-623 transcription. The dampened miR-623 expression alleviates the inhibited effect miR-623 on TXNIP expression by targeting to its 3'-UTR, ultimately leading to increased apoptosis and inflammatory responses of NP cells and initiating the IVDD. *** $P < 0.001$. P values were analyzed by two-tailed t -tests in (e) and two-way ANOVA in (b, g).

altered cell phenotype with downregulated expression of proteoglycans and collagen II. Furthermore, studies have shown that such alterations can reduce pressure within the NP core and cause increased compressive stress towards the inner annulus, which has been demonstrated to trigger disc herniation [19]. Pathogenesis of IVDD has been shown to involve a complex signaling network and various effector molecules [20, 21]. Recent studies have reported that the onset and progression of IVDD is strictly associated with ROS and oxidative stress. Oxidative stress not only reinforces matrix degradation and inflammation but also promotes the decrease in the number of viable and functional cells in the IVD microenvironment. This has been observed to impair the mechanical function of IVDs and intensify the progres-

sion of IVDD [7]. Thus, evaluating oxidative stress-induced molecular mechanisms that mediate apoptosis and inflammatory responses in NP cells and finding an oxidative stress-targeted therapeutic strategy would provide a novel perspective in IVDD treatment. Our present study revealed that miR-623 expression was reduced in IVDD and regulated by HIF-1 α under oxidative stress conditions. Furthermore, we showed that miR-623 acted as an intermediary of apoptosis and inflammatory responses in oxidative stress-induced NP cells by directly targeting 3'-UTR of *TXNIP* mRNA.

TXNIP is a type of thioredoxin-interacting protein from the α -suppressor protein family and is expressed in a variety of cells and tissues. Besides functioning as an initial tumor suppressor protein [22], *TXNIP* has also been shown as a

key regulatory protein in oxidative stress-induced apoptosis and inflammatory responses [13]. Clusters of ROS have been demonstrated to promote nuclear translocation of TXNIP from cytoplasm and concurrently activate inflammation or apoptosis-related signaling molecules such as apoptosis signal-regulating kinase 1 (ASK1) and NACHT, LRR, and PYD domain-containing protein 3 (NLRP3) [23, 24]. Furthermore, upregulated expression of TXNIP has been shown to be accompanied by activation of inflammatory signals in IVDD [18]. In the present study, TXNIP expression was found to be upregulated in IVDD, which played a crucial role in apoptosis and inflammatory responses of oxidative stress-induced NP cells. Further, we found that miR-623 was a key regulator of TXNIP expression by directly targeting 3'-UTR of *TXNIP* mRNA.

In IVDs, NP is an avascular tissue under the hypoxic environment. As a cellular adaptation, alterations in the oxygen level have been reported to facilitate or inhibit HIF-1 α activation. This mechanism has been shown to promote expression of diverse homeostasis regulatory genes that mediate cell survival and accommodation [25]. In our earlier study, we show in NP-specific HIF-1 α -deficient mice that HIF-1 α plays a vital role in the survival of NP cells and ECM homeostasis. However, mechanisms by which HIF-1 α mediates cell survival are still not well elucidated [2]. In the present study, we found that HIF-1 α expression was downregulated in NP cells under oxidative stress conditions. We also demonstrated that HIF-1 α could mediate NP cell apoptosis induced by oxidative stress via miR-623. Moreover, we proved that HIF-1 α facilitated miR-623 expression by directly binding to the promoter region of miR-623 at -1,994/-1,987 bp.

Although these results are promising, we would like to point out some potential limitations of this study. First, the majority of the experiments were performed *in vitro*, which might not essentially complement the *in vivo* mechanisms. Second, the human NP cell culture was not monitored under conditions of hypoxia, which is physiologically relevant and may affect cell growth. Third, in the spine, one vertebra could be regarded a single oncologic compartment, as cartilaginous endplate and cartilaginous annulus fibrosus served as strong barriers to spinal tumor spread [26, 27]. And, all lesions of the cases selected showed well-defined anatomic compartment and the tumors did not invade the intervertebral disc. Moreover, the NP tissues from spinal tumor patients with Pfirrmann grades I and II were used in the present study, which showed no obvious degenerative phenotypes. All of which indicated that these NP tissues could be regarded as the normal controls. However, it is still necessary to determine that miR-623 expression in NP tissues were not affected by the spinal tumor microenvironment, as it has been reported that miR-623 is a tumor suppressor and its expression may change in tumor patients [28–30]. Finally, although the essential role of the HIF-1 α -miR-623-TXNIP pathway was observed in regulating apoptosis and inflammatory responses induced by oxidative stress in NP cells, it must be noted that the findings were collected from the experiment results within normal NP cells. Since there are degenerative cells in the degenerative disc, not normal cells, whether the

responses of these two kinds of cells to the same stimulus are consistent still needs further investigation.

In conclusion, this study demonstrated that HIF-1 α -induced miR-623 could regulate apoptosis and inflammation in TBHP-induced NP cells by targeting *TXNIP* mRNA. These findings improved our understandings of the mechanism involved in IVDD pathogenesis and might be a valuable resource to develop potentially effective therapeutic strategies against IVDD.

4. Materials and Methods

4.1. Bioinformatics Analysis. The miRNA expression profile datasets GSE63492 and GSE19943 were downloaded from the GEO database. The two-microarray expression data were compiled through Venn analysis, and the binding sites of HIF-1 α were predicted via the JASPAR database (http://jaspar.binf.ku.dk/cgi-bin/jaspar_db.pl). The sequence of the miR-623 promoter was founded in the UCSC database (<http://genome.ucsc.edu>). Meanwhile, the gene expression profile dataset GSE34095 was downloaded from the GEO database. The predicted targets of miR-623 and the upregulated gene expression of GSE34095 were compiled. The mRNA targets of miR-623 were predicted using two programs: TargetScan (<http://www.targetscan.org>), miRTarBase (<http://mirtarbase.mbc.nctu.edu.tw/php/download.php>).

4.2. Ethics Statement. All procedures were approved by the Ethics Committee of Shanghai Changzheng Hospital, Second Military Medical University, China (no. 2017SL040), and were carried out only after written informed consent had been obtained from all study participants and from the parents of subjects younger than 18 years of age.

4.3. NP Tissue Collection. Before the operation, the patients were examined via MRI and IVD degeneration was evaluated according to the classification system described by Pfirrmann et al. [31]. The degenerative NP tissues were obtained from 11 patients undergoing intervertebral disc discectomy in Changzheng Hospital, with Pfirrmann grades III and V. And the control NP tissues were obtained from 11 patients with spinal tumors undergoing total spondylectomy and reconstruction, with Pfirrmann grades I and II. Characteristics of the patients are summarized in Tables 1 and 2.

4.4. NP Cell Culture. NP cells were isolated from NP tissues of spinal tumor patients, with Pfirrmann grade I. NPCs were cultured in DMEM/F12 (HyClone) with 10% fetal bovine serum. Second-passage cells were used in all experiments. NPCs were treated with 100 μ M TBHP (Sigma, MO, USA) for 12 h to induce oxidative stress.

4.5. RNA FISH. In situ hybridization was performed to detect the expression of miR-623 in NP tissues by using specific probes. Blue fluorescence indicated cell nucleus and, green fluorescence indicated miR-623.

4.6. Analysis of Cell Apoptosis. Cell apoptosis was detected by Annexin V-PI flow cytometry assay. NPs were transfected with miRNA mimics or mimic control followed by TBHP

TABLE 1: Characteristics of the patients with disc degeneration.

Patient no.	Sex	Age	Diagnosis	Sample level	Disc of Pfirrmann grade
1	Female	17	Intervertebral disc herniation	L4-L5	V
2	Male	26	Intervertebral disc herniation	L4-L5	V
3	Female	65	Intervertebral disc herniation	L4-L5	III
4	Male	56	Intervertebral disc herniation	L4-L5	IV
5	Male	21	Intervertebral disc herniation	L5-S1	V
6	Female	32	Intervertebral disc herniation	L4-L5	IV
7	Female	64	Intervertebral disc herniation	L4-L5	IV
8	Female	62	Intervertebral disc herniation	L3-L4	IV
9	Male	74	Intervertebral disc herniation	L4-L5	V
10	Male	26	Intervertebral disc herniation	L3-L4	IV
11	Female	56	Intervertebral disc herniation	L4-L5	V

TABLE 2: Characteristics of the patients with spinal tumor.

Patient no.	Sex	Age	Diagnosis	Sample level	Disc of Pfirrmann grade
1	Female	34	L4 giant cell tumor	L4-5	I
2	Male	23	L3 osteosarcoma	L3-4	II
3	Male	25	C6 giant cell tumor	C6-7	I
4	Male	32	L1 chondrosarcoma	L1-2	I
5	Female	56	T12 Ewing's sarcoma	T12-L1	I
6	Female	45	L1 metastatic breast cancer	L1-2	I
7	Female	25	T11 metastatic renal cancer	T11-12	I
8	Male	43	T10 giant cell tumor	T10-11	II
9	Male	25	L4 metastatic lung cancer	L3-4	I
10	Female	36	T8 solitary plasmacytoma	T7-8	I
11	Male	43	C5 osteoblastoma	C4-5	I

treatment as indicated. Annexin V FITC Apop Dtec Kit I (BD, 556547) was used for assessing cell apoptosis according to the manufacturer's instructions.

4.7. RNA Isolation and qRT-PCR Analysis. Total RNA was extracted from NP tissues using TRIzol (TaKaRa). (Invitrogen Corporation, 15,596-018) according to the manufacturer's instructions. The PrimeScript™ RT Reagent Kit (Perfect Real Time, TaKaRa, RR037A) and SYBR Premix EX Taq™ (TaKaRa, RR820A) were used to detect and quantify miR-623, and RNU6/U6 was used as an internal control. For mRNA studies, The PrimeScript™ RT Master Mix (Perfect Real Time, TaKaRa, RR036A) was used to reverse transcript and RT-PCR was performed to detect HIF-1 α and TXNIP levels by using SYBR Premix EX Taq™ (TaKaRa, RR820A). GAPDH (glyceraldehyde-3-phosphate dehydrogenase) served as the reference gene. Relative expression was calculated using the comparative threshold cycle (Ct) method. Experiments were carried out in triplicate. A complete list of primers used was shown in Table 3.

4.8. Western Blotting. Protein concentration was determined by a BCA kit (KeyGen, KGP902). Protein extracts were then separated by electrophoresis in 10–12% polyacrylamide gels and were transferred to poly-vinylidene difluoride membranes (Millipore Sigma, IPVH00010). After blocking in 5%

skim milk (Biofroxx, 1172GR500), the membranes were incubated with the indicated primary antibodies (Bax: #2772, CST; Bcl2: #4223, CST; cle-caspase3: #9664, CST; TXNIP: #14715, CST; iNOS: #13120, CST; HIF-1 α : #36169, CST; IL-1 β : #12703, CST; Collagen II: ab34712, Abcam; MMP13: ab219620, Abcam; β -action: #4970, CST; and cleaved caspase-1: #4199, CST) at 4°C overnight, following by the corresponding horseradish peroxidase-conjugated secondary antibodies (anti-mouse IgG, HRP-linked antibody: #7076, CST; anti-rabbit IgG, HRP-linked antibody: #7074, CST). Signals were detected using chemiluminescent ECL reagent (Cytiva, RPN2235). Both the primary antibody and the second antibody were diluted in 1 : 1000.

4.9. Detection of the Mitochondrial Membrane Potential. The mitochondrial membrane potential was detected by a JC-1 kit (C2006; Beyotime, China) according to the manufacturer's instructions. Briefly, the NP cells were collected and resuspended in 1 mL of JC-1 staining buffer and then incubated in the dark at 37°C for 20 min, centrifuged for the collection of cell precipitation, washed with JC-1 staining buffer (1 \times) twice, 500 μ l JC-1 staining buffer (1 \times), and detected by flow cytometry.

4.10. ELISA. The supernatants of cell culture were collected for cytokine evaluation. Cytokine production was measured

TABLE 3: Primer sequences for real-time PCR.

Gene	Gene ID		Primer sequence(5'-3')
GAPDH	2597	Forward	TCCACTGGCGTCTTCACC
		Reverse	GGCAGAGATGATGACCCTTTT
IL-6	3569	Forward	ACTCACCTCTTCAGAACGAATTG
		Reverse	CCATCTTTGGAAGGTTTCAGGTTG
TXNIP	10628	Forward	TGTGTGAAGTTACTCGTGTCAAA
		Reverse	GCAGGTACTCCGAAGTCTGT
IL-1 β	3553	Forward	CGAATCTCCGACCACCACTAC
		Reverse	TCCATGGCCACAACAACCTG
HIF-1 α	3091	Forward	CCACTGCCACCACCTGATGAA
		Reverse	GTGAGGCTGTCCGACTTTGA
RNU6	26827	Forward	CTCGCTTCGGCAGCACAA
		Reverse	AACGCTTCACGAATTTGCGT
miR-623	693208	Forward	ATCCCTTGCAAGGGGCTGTTGGGT
		Reverse	AACGCTTCACGAATTTGCGT

by human IL-1 β and IL-6 Quantikine ELISA Kit (R&D Systems, DLB50 and D6050) according to the manufacturer's instructions.

4.11. Lipid ROS Assay. BODIPY-C11 dye (Thermo, D3861) was used to detect the lipid ROS level. Briefly, add BODIPY-C11 to the culture medium for the 5 μ M final concentration of BODIPY-C11. The culture was returned to the cell culture incubator for 20 min. Cells were collected in 1.5 mL tubes and washed twice with PBS. The amount of ROS within cells was determined by flow cytometry using the Beckman CyAn AOP.

4.12. Luciferase Reporter Assay. The promoter miR-623 luciferase reporter constructs containing the wild-type binding sites of HIF-1 α were amplified using the PCR method. The PCR products were cloned into the pGL3-report luciferase vector, immediately upstream of the luciferase gene. All the constructs containing promoter inserts were sequenced and verified.

The 3'-UTR-TXNIP luciferase reporter constructs containing the wild-type and mutant binding sites of miR-623 were amplified using the PCR method. The PCR products were cloned into the pMiR-report luciferase vector (Ambion, AM5795), immediately downstream of the luciferase gene. All the constructs containing 3'-UTR inserts were sequenced and verified.

Cells were cotransfected with reporter constructs, and the miRNA mimic and the β -gal plasmid were harvested 48 h after the transfection and lysed with reporter lysis buffer (Promega, E397A). The luciferase activities in the cellular extracts were determined using the dual-luciferase reporter assay system (Promega, E1910) according to the manufacturer's instructions. Data were represented as the fold induction after normalizing the luciferase activity of the tested sample to that of the corresponding control sample.

4.13. Statistical Analysis. All data representative of three independent experiments are present as mean \pm SEM. We

used two-tailed *t*-tests to determine significances between two groups. We did analyses of multiple groups by one- or two-way ANOVA with Bonferroni post-test of GraphPad prism version 5. For all statistical tests, we considered a *P* value < 0.05 to be statistically significant.

Data Availability

The data that support the findings of this study are available from the corresponding author upon reasonable request.

Conflicts of Interest

The authors declare no conflict of interest.

Authors' Contributions

Xiaogang Bao, Zhenhua Wang, and Qi Jia contributed equally to this work.

Acknowledgments

This work was sponsored by the National Natural Science Foundation of China (51802221) and Shanghai Youth Science and Technology Talent Sailing Program (20YF1449100).

References

- [1] Y. Lin, Y. Jiao, Y. Yuan et al., "Propionibacterium acnes induces intervertebral disc degeneration by promoting nucleus pulposus cell apoptosis via the TLR2/JNK/mitochondrial-mediated pathway," *Emerging Microbes & Infections*, vol. 7, no. 1, pp. 1–8, 2018.
- [2] Z. Liu, C. Li, X. Meng et al., "Hypoxia-inducible factor-1 α mediates aggrecan and collagen II expression via NOTCH1 signaling in nucleus pulposus cells during intervertebral disc degeneration," *Biochemical and Biophysical Research Communications*, vol. 488, no. 3, pp. 554–561, 2017.
- [3] L. Kang, S. Liu, J. Li, Y. Tian, Y. Xue, and X. Liu, "The mitochondria-targeted anti-oxidant MitoQ protects against

- intervertebral disc degeneration by ameliorating mitochondrial dysfunction and redox imbalance,” *Cell Proliferation*, vol. 53, no. 3, article e12779, 2020.
- [4] S. Wang, C. Liu, Z. Sun et al., “IL-1 β increases asporin expression via the NF- κ B p65 pathway in nucleus pulposus cells during intervertebral disc degeneration,” *Scientific Reports*, vol. 7, no. 1, p. 4112, 2017.
- [5] Y. Hu, L. Huang, M. Shen et al., “Pioglitazone protects compression-mediated apoptosis in nucleus pulposus mesenchymal stem cells by suppressing oxidative stress,” *Oxidative Medicine and Cellular Longevity*, vol. 2019, Article ID 4764071, 14 pages, 2019.
- [6] Y. Lin, G. Tang, Y. Jiao et al., “Propionibacterium acnes Induces Intervertebral Disc Degeneration by Promoting iNOS/NO and COX-2/PGE2 Activation via the ROS-Dependent NF- κ B Pathway,” *Oxidative Medicine and Cellular Longevity*, vol. 2018, 12 pages, 2018.
- [7] C. Feng, M. Yang, M. Lan et al., “ROS: crucial intermediators in the pathogenesis of intervertebral disc degeneration,” *Oxidative Medicine and Cellular Longevity*, vol. 2017, Article ID 5601593, 12 pages, 2017.
- [8] H. Q. Wang, X. D. Yu, Z. H. Liu et al., “Deregulated miR-155 promotes Fas-mediated apoptosis in human intervertebral disc degeneration by targeting FADD and caspase-3,” *The Journal of Pathology*, vol. 225, no. 2, pp. 232–242, 2011.
- [9] Y. Lee, C. Ahn, J. Han et al., “The nuclear RNase III Drosha initiates microRNA processing,” *Nature*, vol. 425, no. 6956, pp. 415–419, 2003.
- [10] J. Zhou, J. Sun, D. Z. Markova et al., “MicroRNA-145 overexpression attenuates apoptosis and increases matrix synthesis in nucleus pulposus cells,” *Life Sciences*, vol. 221, pp. 274–283, 2019.
- [11] Y. Chen, J. Lin, J. Chen et al., “Mfn2 is involved in intervertebral disc degeneration through autophagy modulation,” *Osteoarthritis and Cartilage*, vol. 28, no. 3, pp. 363–374, 2020.
- [12] H. M. Ni, J. A. Williams, and W. X. Ding, “Mitochondrial dynamics and mitochondrial quality control,” *Redox Biology*, vol. 4, pp. 6–13, 2015.
- [13] J. Zhou, Q. Yu, and W. J. Chng, “TXNIP (VDUP-1, TBP-2): a major redox regulator commonly suppressed in cancer by epigenetic mechanisms,” *The International Journal of Biochemistry & Cell Biology*, vol. 43, no. 12, pp. 1668–1673, 2011.
- [14] W. N. Xu, H. L. Zheng, R. Z. Yang et al., “Mitochondrial NDUFA4L2 attenuates the apoptosis of nucleus pulposus cells induced by oxidative stress via the inhibition of mitophagy,” *Experimental & Molecular Medicine*, vol. 51, no. 11, pp. 1–16, 2019.
- [15] H. Kang, K. Yang, L. Xiao et al., “Osteoblast hypoxia-inducible Factor-1 α pathway activation restrains osteoclastogenesis via the interleukin-33-microRNA-34a-notch1 pathway,” *Frontiers in Immunology*, vol. 8, p. 1312, 2017.
- [16] C. M. Tran, N. Fujita, B. L. Huang et al., “Hypoxia-inducible Factor (HIF)-1 α and CCN2 Form a Regulatory Circuit in Hypoxic Nucleus Pulposus Cells,” *The Journal of Biological Chemistry*, vol. 288, no. 18, pp. 12654–12666, 2013.
- [17] C. K. Kepler, R. K. Ponnappan, C. A. Tannoury, M. V. Risbud, and D. G. Anderson, “The molecular basis of intervertebral disc degeneration,” *The Spine Journal*, vol. 13, no. 3, pp. 318–330, 2013.
- [18] P. Tang, J. M. Gu, Z. A. Xie et al., “Honokiol alleviates the degeneration of intervertebral disc via suppressing the activation of TXNIP-NLRP3 inflammasome signal pathway,” *Free Radical Biology & Medicine*, vol. 120, pp. 368–379, 2018.
- [19] G. Pattappa, Z. Li, M. Peroglio, N. Wismer, M. Alini, and S. Grad, “Diversity of intervertebral disc cells: phenotype and function,” *Journal of Anatomy*, vol. 221, no. 6, pp. 480–496, 2012.
- [20] N. V. Vo, R. A. Hartman, P. R. Patil et al., “Molecular mechanisms of biological aging in intervertebral discs,” *Journal of Orthopaedic Research*, vol. 34, no. 8, pp. 1289–1306, 2016.
- [21] M. V. Risbud and I. M. Shapiro, “Role of cytokines in intervertebral disc degeneration: pain and disc content,” *Nature Reviews Rheumatology*, vol. 10, no. 1, pp. 44–56, 2014.
- [22] K. Nishizawa, H. Nishiyama, Y. Matsui et al., “Thioredoxin-interacting protein suppresses bladder carcinogenesis,” *Carcinogenesis*, vol. 32, no. 10, pp. 1459–1466, 2011.
- [23] O. Sandanger, T. Ranheim, L. E. Vinge et al., “The NLRP3 inflammasome is up-regulated in cardiac fibroblasts and mediates myocardial ischaemia-reperfusion injury,” *Cardiovascular Research*, vol. 99, no. 1, pp. 164–174, 2013.
- [24] R. Zhou, A. Tardivel, B. Thorens, I. Choi, and J. Tschopp, “Thioredoxin-interacting protein links oxidative stress to inflammasome activation,” *Nature Immunology*, vol. 11, no. 2, pp. 136–140, 2010.
- [25] W. J. Wu, X. K. Zhang, X. F. Zheng, Y. H. Yang, S. D. Jiang, and L. S. Jiang, “SHH-dependent knockout of HIF-1 alpha accelerates the degenerative process in mouse intervertebral disc,” *International Journal of Immunopathology and Pharmacology*, vol. 26, no. 3, pp. 601–609, 2013.
- [26] K. Tomita, N. Kawahara, H. Murakami, and S. Demura, “Total en bloc spondylectomy for spinal tumors: improvement of the technique and its associated basic background,” *Journal of Orthopaedic Science*, vol. 11, no. 1, pp. 3–12, 2006.
- [27] S. Kato, “Complications of thoracic spine surgery - their avoidance and management,” *Journal of Clinical Neuroscience*, vol. 81, pp. 12–17, 2020.
- [28] L. Jiang, W. Yang, W. Bian et al., “MicroRNA-623 targets cyclin D1 to inhibit cell proliferation and enhance the chemosensitivity of cells to 5-fluorouracil in gastric cancer,” *Oncology Research*, vol. 27, no. 1, pp. 19–27, 2018.
- [29] Q. Li, J. Liu, Y. Jia, T. Li, and M. Zhang, “miR-623 suppresses cell proliferation, migration and invasion through direct inhibition of XRCC5 in breast cancer,” *Aging (Albany NY)*, vol. 12, no. 11, pp. 10246–10258, 2020.
- [30] C. Wang, J. Wang, J. Zhang et al., “MicroRNA-623 inhibits tumor progression and is a predictor of poor prognosis of breast cancer,” *Oncology Letters*, vol. 20, no. 6, p. 386, 2020.
- [31] C. W. Pfirrmann, A. Metzdorf, M. Zanetti, J. Hodler, and N. Boos, “Magnetic resonance classification of lumbar intervertebral disc degeneration,” *Spine (Phila Pa 1976)*, vol. 26, no. 17, pp. 1873–1878, 2001.

Research Article

Deficiency of MIF Accentuates Overloaded Compression-Induced Nucleus Pulposus Cell Oxidative Damage via Depressing Mitophagy

Yiyang Wang ^{1,2}, Yanzhu Hu ^{1,2}, Haoming Wang ^{2,3}, Ningyuan Liu ^{1,2}, Lei Luo,¹
Chen Zhao,¹ Dandan Zhou ⁴, Hang Tong ⁵, Pei Li ^{1,2} and Qiang Zhou ^{1,2}

¹Department of Orthopedics, The Third Affiliated Hospital of Chongqing Medical University, Chongqing 401120, China

²Tissue Repairing and Biotechnology Research Center, The Third Affiliated Hospital of Chongqing Medical University, Chongqing 401120, China

³Department of Orthopedics, Three Gorges Central Hospital of Chongqing University, Chongqing 404000, China

⁴Department of Gastroenterology, The People's Hospital of Jiulongpo District, Chongqing 400050, China

⁵Department of Urology, The First Affiliated Hospital of Chongqing Medical University, Chongqing 400016, China

Correspondence should be addressed to Pei Li; lipei@hospital.cqmu.edu.cn and Qiang Zhou; zhouqiang@hospital.cqmu.edu.cn

Received 6 May 2021; Revised 4 June 2021; Accepted 11 June 2021; Published 2 July 2021

Academic Editor: Sidong Yang

Copyright © 2021 Yiyang Wang et al. This is an open access article distributed under the Creative Commons Attribution License, which permits unrestricted use, distribution, and reproduction in any medium, provided the original work is properly cited.

Established studies proved that mechanical compression loading had multiple effects on the biological behavior of the intervertebral disc (IVD). However, the regulating mechanism involved in this process remains unclear. The current study is aimed at exploring the potential bioregulators and signaling pathways involved in the compression-associated biological changes of nucleus pulposus (NP) cells. Tandem mass tag- (TMT-) based quantitative proteomics was exerted to analyze the differentially expressed proteins (DEPs) and signal pathways among the different groups of NP cells cultured under noncompression, low-compression (LC), and high-compression (HC) loading. Eight potential protective bioregulators for the NP cell survival under different compression loading were predicted by the proteomics, among which macrophage migration inhibitory factor (MIF) and oxidative stress-related pathways were selected for further evaluation, due to its similar function in regulating the fate of the cartilage endplate- (CEP-) derived cells. We found that deficiency of MIF accentuates the accumulation of ROS, mitochondrial dysfunction, and senescence of NP cells under overloaded mechanical compression. The potential molecular mechanism involved in this process is related to the mitophagy regulating role of MIF. Our findings provide a better understanding of the regulatory role of mechanical compression on the cellular fate commitment and matrix metabolism of NP, and the potential strategies for treating disc degenerative diseases via using MIF-regulating agents.

1. Introduction

Intervertebral disc (IVD) degeneration, which can result in low back pain (LBP), instability, and deformity of the spine, has been recognized as the leading cause of degenerative spine disease [1]. The human IVD consists of three compartments: nucleus pulposus (NP), annulus fibrosus (AF), and cartilage endplate (CEP), which connects the adjacent bony vertebral bodies. NP tissue is a type of gelatinous structure, containing collagen fibrils and proteoglycan molecules [2].

NP cell is responsible for the synthesis of the functional extracellular matrix (ECM) components (mainly aggrecan and collagen type II) in the core region of the disc, which firstly reveals apoptosis- and/or senescence-like changes during the process of IVD degeneration [2]. In the degenerative intervertebral disc, the senescent NP cells accumulate and result in weakened proliferation, compromised self-repair, increased organellar dysfunction, and enhanced breakdown of functional ECM [3, 4]. Hence, a potential strategy for treating IVD degeneration is to alleviate or retard the

apoptosis- and/or senescence-like changes of NP cells by regulating the potential signaling molecules or pathways involved in the degeneration process.

It is commonly held that the overloaded compressive force applied to the IVD is the leading cause of IVD degeneration [4–6]. The prior studies reported that the physiological intensity (0.35–0.75 MPa) of compression loading acted as an anabolic factor for the NP and AF cells, owing to the stimulation of proteoglycan synthesis. In contrast, excessive compression (≥ 1 MPa) aggravated the catabolic metabolism of proteoglycan of NP and AF cells [7, 8]. Noticeably, our previous studies also elucidated the function of graded compression loading in controlling NP cell survival and proved that overloaded mechanical compression markedly exacerbated degenerative changes of the NP [5, 6, 9, 10]. Although the molecular mechanism involved in the compression loading-associated biological behavior changes of NP cell remains unclear, most studies point that the overloaded compression-induced apoptotic and senescent changes of NP cell are related to the intracellular oxidative damage triggered by mechanosensing factors, such as the integrins and cadherins [5, 6, 11–13]. Therefore, it is meaningful to explore the potential bioregulators and signaling pathways involved in the compression-associated biological changes of NP cell.

Hence, in the present study, we used the human NP cells isolated from a surgical excisional IVD in a patient who suffered lumbar vertebral fracture (LVF) as the investigated subject. The NP cells, seeding in the methacrylamide-modified gelatin (GelMA) hydrogels, commonly used scaffolds for 3D cell culturing, were cultured in our self-developed compression loading bioreactor under the dynamic graded compression loading for 2 weeks, referring to our previous study [5]. After that, we analyzed the apoptosis- and senescence-like changes of the NP cells and determined 5% deformation of the hydrogel as the low-compression (LC) loading and 20% deformation of the hydrogel as the high-compression (HC) loading for the NP cells. We further used tandem mass tag- (TMT-) based quantitative proteomics to analyze the differentially expressed proteins (DEPs) among the different NP cells cultured under noncompression, LC, and HC loading compression. Analysis of the DEPs, Gene Ontology (GO), and Kyoto Encyclopedia of Genes and Genomes (KEGG) enrichment predicted eight potential protective bioregulators for the NP cell survival under overloaded compression, among which macrophage migration inhibitory factor (MIF) and oxidative stress-related pathways were further evaluated *in vivo* and *in vitro*, due to its similar function in regulating the fate of the human CEP-derived cells [14]. Moreover, the recombinant lentiviral vector construct containing MIF short hairpin RNA (shRNA) was used to establish the MIF knockout (MIF-KO) NP cells to further determine the protective function of MIF in NP cells that suffered overloaded compression.

2. Material and Methods

2.1. Source of the Human NP Sample. For the better homogeneity of the samples prepared for the proteomics analysis, the experimental NP samples in this study were obtained from a

32-year-old, female patient who suffered lumbar vertebral fracture (LVF) and admitted to the orthopedics department of our hospital. The patient received the discectomy surgery and donated the excisional IVD tissue for experimental research. The patient declared no documented medical history of LBP before suffering the LVF. The preoperative MRI scans of the patient revealed that the excisional IVD was graded in Pfirrmann II (normal or mild degeneration), according to the Pfirrmann classification system (Supplemental Figure 1) [15]. Informed consent was obtained from the patient, and the researching procedure complied with approval from the ethics committee of the Third Affiliated Hospital of Chongqing Medical University.

2.2. Isolation of the Primary Human NP Cells. The primary human NP cells were isolated as follows [5]. The NP tissue was carefully separated from the excisional IVD and washed by phosphate-buffered saline (PBS) five times in the tissue culture dishes (Jet Biofil, China). Then, the tissue was minced into flocculent pieces and digested in 0.2% type II collagenase (Sigma, USA) for 4 hours, following 0.25% trypsin (Gibco, USA) digestion for 30 minutes. The DMEM/F-12 medium (Gibco, USA) containing 10% fetal bovine serum (FBS, Gibco, USA) and 1% penicillin/streptomycin (Gibco, USA) was used to neutralize the digesting solution. The collected suspension was centrifuged at 1200 rpm for 8–10 minutes. Finally, the collected NP cells were resuspended by the completed culture medium and seeded into flasks (Jet Biofil, China), incubated at 37°C with 5% CO₂. Culturing media were replaced every four days.

2.3. GelMA Hydrogel Synthesis and Preparation. In brief, 10% (*w/v*) of gelatin from porcine skin (Sigma, USA) was dissolved in 1x PBS. The methacrylic anhydride (Aladdin, China) was added to the gelatin solution in a dropwise manner when the solution was heated to 60°C. The reaction was allowed to proceed for 4 hours at 60°C before being stopped using a 5x PBS dilution. The resulting solution was dialyzed against distilled water using a 12–14 kDa dialysis tubing (Thermo Fisher, USA) at 60°C for 5–7 days with two water changes per day. The solution was then stored at –20°C for 24 hours and lyophilized for 72 hours before use.

2.4. Establishment of the 3D NP Cell Culturing Network. The NP cells were encapsulated in GelMA hydrogel for 3D culturing and compression loading. The cell encapsulation procedure was performed according to our previous study [5]. In brief, the cells at passage II were trypsinized with 0.25% trypsin (Gibco, USA) for 2 minutes, and the collected cell suspension was then centrifuged at 1200 rpm for 5 minutes. The centrifuged cell pellets were then mixed with the GelMA hydrogel precursor (1×10^7 cells/mL). After that, the mixture suspension was pipette into a self-made mold (diameter = 1 cm, thickness = 0.5 cm) and exposed to the UV light (360 ± 5 nm, 850 mW) for about 1 minute at a distance of 8–10 cm to construct the 3D NP cell culturing network. The cell-encapsulated GelMA hydrogels were incubated in the dishes (Jet Biofil, China) for three days before the compression performing regime in the bioreactor.

2.5. Mechanical Compression Exerting Protocol. During the compression performing regime, the cell-encapsulated hydrogel was moved to the culturing chamber of our bioreactor and cultured for two weeks. Simultaneously, we set the pressure apparatus to provide intermittent compression load. Particularly, the cell-encapsulated GelMA hydrogel was exerted bionic compression (1.0 Hz, 4 hours/day) in the chamber at 0%, 5%, 10%, and 20% compressive deformation. The compression loading-treated cells used for the following tests were washed out from the hydrogel scaffold via type II collagenase (0.2%, Sigma, USA) digestion for 5 minutes at 37°C.

2.6. Senescence-Associated β -Galactosidase (SA- β -Gal) Staining. SA- β -Gal staining was usually used for detecting the cell senescence. Briefly, treated samples were fixed with paraformaldehyde (concentration = 0.2%) for 20 minutes at room temperature. The paraformaldehyde was removed from the cells, and then, the cells were stained with X-gal solution overnight at 37°C. The percentage of the senescent cells (green stained) was observed by optical microscopy (Olympus, Japan).

2.7. Live/Dead Assay. The cell viability was detected by the LIVE/DEAD Assay Kit (Invitrogen, USA). In brief, the samples were washed with PBS thrice and incubated with 1 mL of PBS containing 4 mM EthD-1 and 2 mM calcein AM for 30 minutes at 37°C. Then, the washed samples were observed and imaged via fluorescence microscopy (Leica, Germany).

2.8. Determination of Cell Apoptosis. The apoptosis of the NP cells was detected using flow cytometry-based Annexin V/PI double-staining. In brief, the cells were washed thrice with PBS and resuspended in 100 μ L binding buffer with 5 μ L Annexin V-FITC and 5 μ L PI for 30 minutes protected from light. The early apoptotic cells contained Annexin V+/PI-, the late apoptotic cells contained Annexin V+/PI+, and the normal cells contained Annexin V-/PI-. The early- and late-stage apoptotic cells were counted, and the results were expressed as a percentage of the total apoptotic cell count.

2.9. Protein Extraction and Western Blotting. After being ground in liquid nitrogen, the samples were lysed with RIPA lysis buffer containing 1% PMSF (Beyotime, China) for 30 minutes at 4°C. The lysates were centrifuged (12,000 rpm, 8 minutes) at 4°C. After determining protein concentration, the qualified protein samples spread in SDS-polyacrylamide gel electrophoresis and transferred to a PVDF membrane band by electroblotting. The PVDF membrane bands were then incubated with the primary antibodies (anti-nitrotyrosine (NT), anti-MIF, anti-LC3, anti-P62, anti-PINK1 (1 : 1000; Abcam, UK), anti-P53, anti-P21, anti-P16, anti-aggre-can, anti-collagen II, anti- β -actin (1 : 500; Proteintech, China), and anti-Parkin (1 : 1000; Cell Signaling, USA)) overnight at 4°C. After the bands were washed with Tris-Buffered Saline with Tween (TBST) thrice, they were then incubated with the fluorescent secondary antibody for 80 minutes. Being washed with TBST thrice, the intensity of the proteins was determined and analyzed by Image Lab software (Bio-Rad, USA).

2.10. TMT-Based Quantitative Proteomics. The TMT-based quantitative proteomics for this work was commissioned by Majorbio Bio-pharm Technology (Shanghai, China) for testing. In brief, we exerted mechanical compression to the NP cell-encapsulated hydrogels for two weeks using our self-developed bioreactor according to the compression performing regime. The treated samples were then divided into three groups based on the compressive deformation of the NP cell-encapsulated hydrogels: the control group—cultured in chambers but unloaded throughout, the LC loading group—loaded with 5% deformation, and the HC loading group—loaded with 20% deformation. Four copies of the samples (test pair $n = 3$, backup pair $n = 1$) were collected. After quick freezing in liquid nitrogen, the samples were stored in drikold and sent to the testing laboratory of Majorbio Bio-pharm Technology. After finishing the quality assessment, proteolysis, peptide labeling, peptide separation, Nano Liquid Chromatography-Mass Spectrometry/Mass Spectrometry (LC-MS/MS) analysis, and other steps of TMT proteomics, the analyzed data were uploaded on the online Majorbio Cloud Platform (<https://cloud.majorbio.com>). The thresholds of fold change (>1.2 or <0.83) and P value < 0.05 were used to identify DEPs. Annotation of all identified proteins was performed using GO (<http://www.blast2go.com/b2ghome>, <http://geneontology.org/>) and KEGG pathway (<http://www.genome.jp/kegg/>). DEPs were further used for GO and KEGG enrichment analysis.

2.11. Establishment of the Rat Tail IVD Compressed Model. All animal procedures were performed under the approval of the Animal Care and Use Committee at Chongqing Medical University. Twenty 12-week-old female Sprague-Dawley (SD) rats from 500 ± 5 g were used in the study. Radiographs were taken to confirm the rat tail IVD levels and heights under intraperitoneal anesthesia. Rat tail was then fixed with a self-developed compression loading apparatus between the 8th and 10th caudal vertebrae. An axial force from the distal side was exerted to produce a compression loading of 1.3 MPa, according to the previous study [16]. The rats were then divided into three groups based on the compression loading duration: the sham group—unloaded throughout, the 2 weeks group—loaded for 2 weeks, and the 4 weeks group—loaded for 4 weeks.

2.12. Histological Hematoxylin and Eosin (HE) Staining. The treated samples were harvested and fixed with 4% paraformaldehyde, embedded in paraffin, and then cut into 5 μ m per section. Then, the sections were stained with hematoxylin and eosin. The stained sections were observed and scanned under an optical microscope (Olympus, Japan).

2.13. Alcian Blue Staining. Alcian blue staining was used to detect the ECM glycosaminoglycan deposition. Briefly, each tissue section was incubated in 0.2% Alcian blue solution before rinsing with deionized water. Then, the stained sections were mounted and observed under an optical microscope (Olympus, Japan).

2.14. MIF Immunohistochemistry (IHC). After rehydration, tissue sections were blocked by goat serum, treated with

hyaluronidase (0.8%) for 20 minutes at 37°C, and then incubated with MIF antibody (1:100, Abcam, UK) for 60 minutes. After washing in PBS, biotinylated secondary antibody (1:100, Dako, Denmark) was applied for 30 minutes, washed in PBS, and treated with avidin-biotin complex reagents. Colour was developed using 3,3-diaminobenzidine reagents (Dako, Denmark), and the sections were counterstained with Harris's hematoxylin. The average optical density (AOD) of five randomly selected visual fields (per immunohistochemical slice) under high magnification (400x) was measured using the ImageJ analysis system.

2.15. NP Cell Transfection. For knockout of the endogenous MIF in NP cells, shRNA targeting MIF (MIF-shRNA (Santa Cruz Biotechnology, Dallas, TX, U.S.A.)) was transfected into cells by using a recombinant lentiviral vector (GeneChem, Shanghai, China). For transfection, cells were seeded into a 6-well plate (Jet Biofil, China), incubated for 24 h, and then transfected according to the manufacturer's instructions. In brief, the cells were transfected with lentivirus (multiplicity of infection = 50) for three days. After determining the efficacy of transfection by a fluorescent microscope, the transfected cells were subcultured and seeded in the hydrogels for the subsequent experiments.

2.16. Detection of Intracellular Reactive Oxygen Species (ROS) Content. Intracellular ROS content was detected by fluorescent DCFH-DA molecular probe staining (Beyotime, China). Briefly, 10 mg DCFH-DA molecular probes were added into a 1 mL basic medium without FBS to prepare the working solution. After that, the cells were incubated in a 6-well plate (Jet Biofil, China) with molecular probe working solution at 37°C for 20 minutes. Then, the cells were collected and the fluorescent intensity was determined by a flow cytometer under 488 nm excitation wavelength and 525 nm emission wavelength.

2.17. Determination of Mitochondrial Membrane Potential ($\Delta\Psi_m$). JC-1 fluorescent molecular probe staining (Beyotime, China) was performed to determine the cell $\Delta\Psi_m$, according to the manufacturer's protocol. In brief, after being washed with PBS thrice, 1 mL basic medium was added to each 6-well plate (Jet Biofil, China). Alive cells were immersed in 1 mL of prepared JC-1 molecular probe working solution and incubated for 30 minutes at 37°C. After being washed with precooled JC-1 1x washing buffer thrice, $\Delta\Psi_m$ was detected by laser scanning confocal microscopy (LSCM. Zeiss 780, Germany). The JC-1 molecular probes' fluorescence intensity ratio was then quantified by the ImageJ system.

2.18. Colocalization of Mitochondria and Autophagosomes. The intracellular mitophagy initiation was evaluated by the fluorescent colocalization of mitochondria and autophagosomes. NP cells were transiently transfected with GFP-LC3 (Beyotime, China). MitoTracker Red (Beyotime, China) was used to label the mitochondria in cells, which carries a thiol-reactive chloromethyl group that covalently binds to the reduced thiols that present mitochondrial matrix protein.

The numbers of total colocalizing GFP-LC3 puncta per cell (mitophagosomes) were counted using ImageJ.

2.19. Transmission Electron Microscopy (TEM) Observation. TEM is the most reliable approach for monitoring autophagy [17]. The NP cells were collected and immersed in 0.1 M sodium cacodylate buffer at room temperature for 12 hours. The ultrathin 50 nm sections were cut by using an ultramicrotome, stained with 2% (*w/v*) uranyl acetate and lead citrate, and then visualized and captured with a TEM machine (Hitachi, Japan).

2.20. Statistical Analysis. All data were analyzed using GraphPad Prism (version 6.0, GraphPad Software, USA) and presented as mean \pm standard deviation with $n = 3$. The thresholds of fold change (>1.2 or <0.83) and P value < 0.05 were used to identify DEPs. A two-tailed Student's t -test was used to assess the statistical significance of the measurement data (P value < 0.05).

3. Results

3.1. Effects of Graded Mechanical Compression on Cell Senescence, Viability, and ECM Synthesis of the Human NP Cells Cultured in a Bioreactor. Our previous studies evaluated that overloaded compressive force applied to IVD could lead to disc degeneration [5, 6, 9, 10], whereas proper physiological pressure is beneficial for maintaining the cell viability of NP [18]. Our previous studies verified that mechanical compression-induced hydrogel deformation could effectively imitate the in vivo loading situation of the NP cell or mesenchymal stem cell (MSC) [5, 19]. Thus, we cultured the NP cell-encapsulated GelMA hydrogels and imitated the in vivo compression situation using our self-developed compression loading bioreactor (Figure 1(a)). The SA- β -Gal staining was used to determine the degree of NP cell senescence in each group. The result revealed that the proportion of positive cell was significantly increased in the group that exerted HC loading ($\geq 10\%$ deformation), but not in the LC loading group ($\leq 5\%$ deformation) (Figures 1(b) and 1(c)). The result of the fluorescent Live/Dead staining also indicated that the death ratio of the NP cells was markedly enhanced by over 10% gel deformation (Figures 1(d) and 1(e)). However, LC loading did not increase the death ratio of the NP cells (Figures 1(d) and 1(e)). Flow cytometry was utilized to detect the cell apoptosis rate, and the result also indicated that apoptosis of the NP cell was significantly enhanced by HC loading, but not in the LC loading group (Figures 2(a) and 2(b)). Additionally, western blotting results revealed that the senescence-associated markers (P53, P21, and P16) were strongly overexpressed in NP cell that suffered HC loading, which was consistent with the results of SA- β -Gal staining (Figures 2(c) and 2(d)), whereas the synthesis of functional ECM components (aggrecan and collagen type II) was significantly inhibited by HC loading, but not in the LC loading group (Figures 2(c) and 2(d)).

3.2. DEPs and Pathways of the Human NP Cells That Exerted Graded Mechanical Compression Loading Were Analyzed by TMT-Based Quantitative Proteomics. For further analysis of

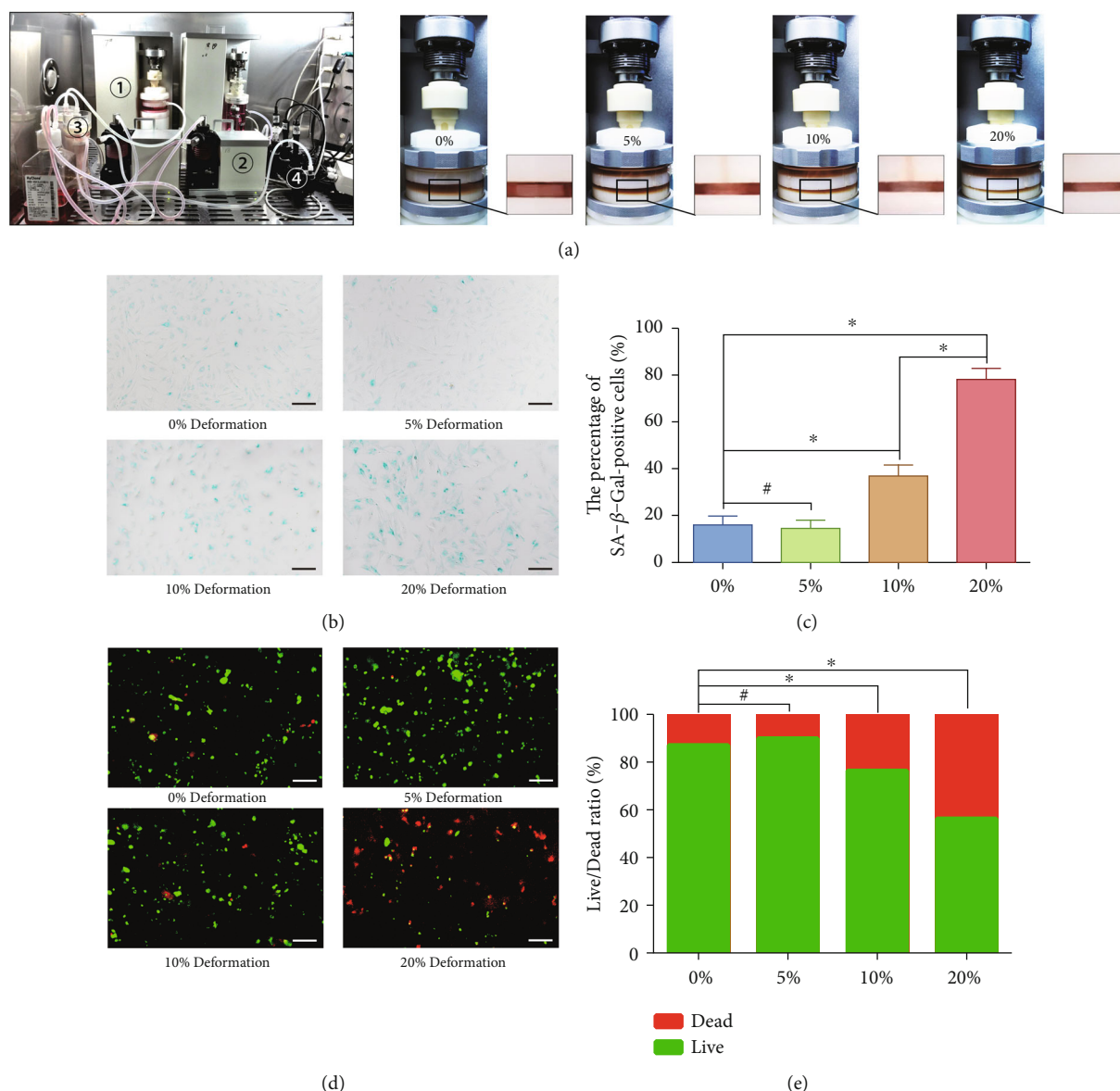


FIGURE 1: Effects of graded mechanical compression on cell senescence and viability of the human NP cells cultured in a bioreactor: (a) NP cell-encapsulated hydrogels cultured in chambers were dynamically compressed with 0%, 5%, 10%, and 20% deformation for 2 weeks, and the units of our self-developed bioreactor include (1) tissue culture chambers and compression loading application device; (2) substance exchanger peristaltic pumps; (3) medium container; and (4) pH, PO₂, and PCO₂ sensor. (b) The cell senescence degree of the NP cells that exerted graded compression loading was analyzed by SA-β-Gal staining (100x). (c) Statistic analysis of the SA-β-Gal positive rate of the NP cells that exerted graded compression loading. (d) The NP cell viability was analyzed by fluorescent Live/Dead staining (100x). (e) Statistic analysis of the cell Live/Dead rate of the NP cells that exerted graded compression loading. * $P < 0.05$. # $P > 0.05$. Scale bar = 100 μm.

the potential functional factors involved in the progress of compression-associated NP cell survival and senescence, the DEPs of the samples, respectively, that suffered nonloading (control), LC loading (5% deformation), and HC loading (20% deformation) were evaluated by TMT-based proteomics analysis (Figure 3). Among the 324 DEPs, 104 proteins were upregulated and 220 proteins were downregulated in the LC loading group compared with the control group (Figure 4(a), Supplemental Table 1). There were 427 overexpressed proteins and 377 underexpressed proteins in the HC loading group compared with the control group (Figure 4(a), Supplemental Table 2). Moreover, there were

1109 overexpressed proteins and 779 underexpressed proteins in the HC loading compression group compared with the LC loading group (Figure 4(a), Supplemental Table 3). Depending on the aforementioned experimental results, we speculated that the intersection of the overexpressed proteins in the LC loading group and the underexpressed proteins in the HC loading group might play as protective factors for NP cell survival. In contrast, the intersection of the underexpressed proteins in the LC loading group and the overexpressed proteins in the HC loading group might play as adverse factors for NP cell survival. Thus, we further analyzed the protein clusters and

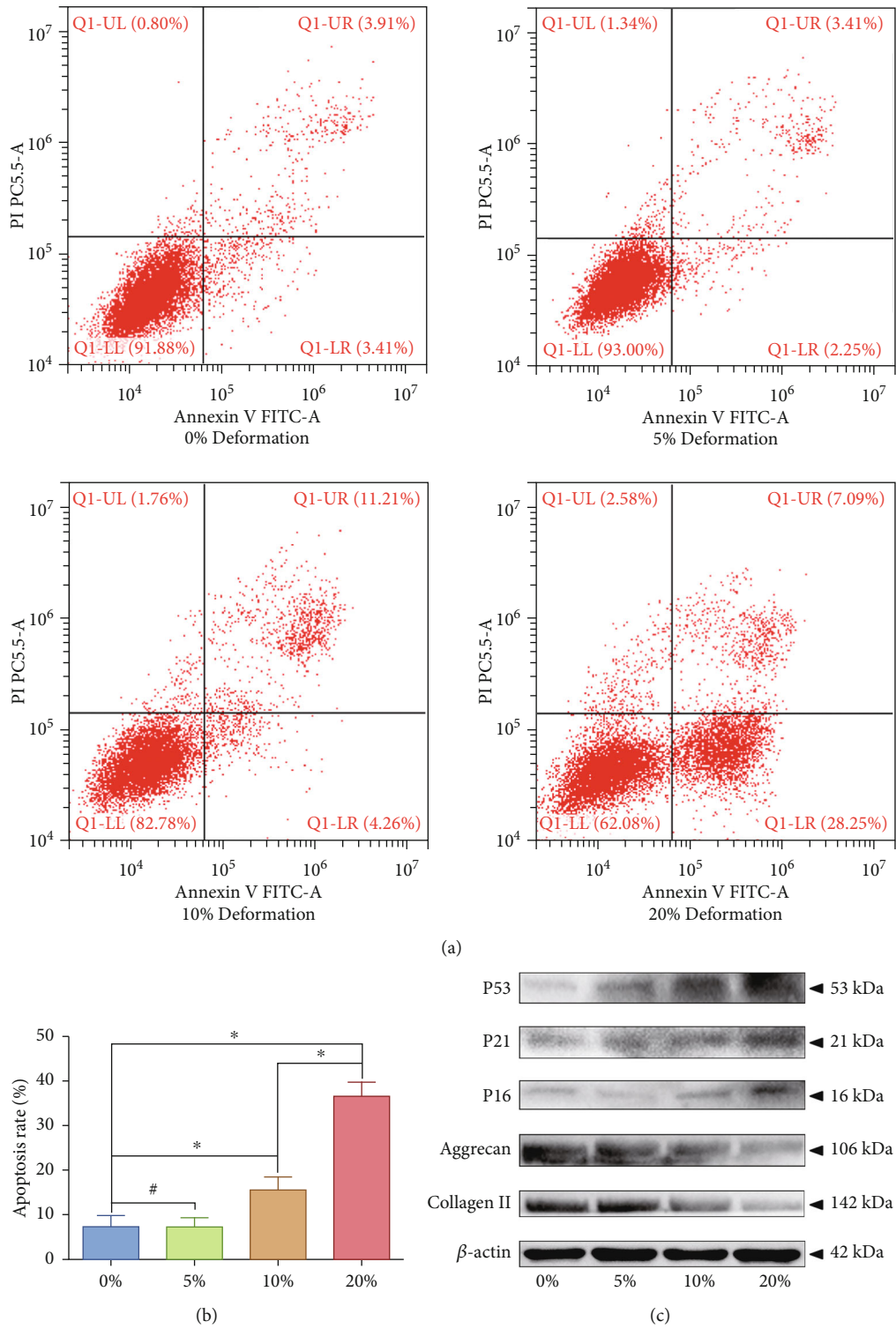


FIGURE 2: Continued.

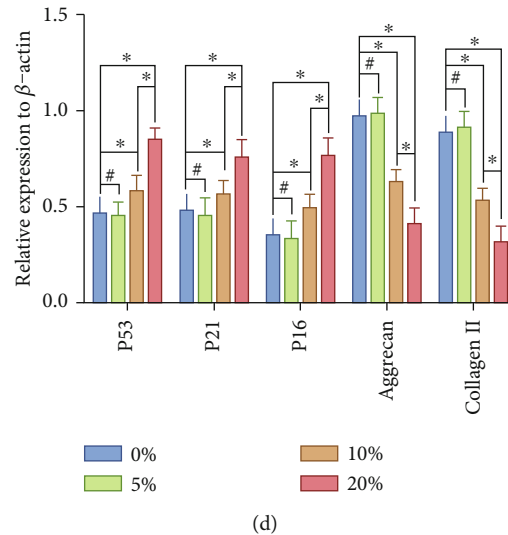


FIGURE 2: Effects of graded mechanical compression on cell apoptosis, senescence, and ECM homeostasis of the human NP cells cultured in a bioreactor: (a) the early- and late-apoptosis rate of the NP cells that exerted graded compression loading was analyzed by flow cytometry. (b) Statistic analysis of the apoptosis rate of the NP cells that exerted graded compression loading. (c) Western blotting analysis of the expression level senescence-associated markers (P53, P21, and P16) and main ECM functional components (aggrecan and collagen type II) of the NP cells that exerted graded compression loading. (d) Statistic analysis of the western blots of the NP cells that exerted graded compression loading. * $P < 0.05$. # $P > 0.05$.

predicted 8 potential protective factors and 3 potential adverse factors for NP cell survival (Figures 4(b) and 4(c)). Among the 8 potential protective factors, MIF was selected for further study due to its reported role in regulating the fate of the human CEP cells [14]. In addition, the GO and KEGG enrichment analysis indicated that compression loading affected the fate commitment of NP cell via regulating oxidative stress-associated pathways (ATP biosynthetic process and oxidative phosphorylation) (Figures 4(d) and 4(e)).

3.3. Effects of Overloaded Compression on Biological Behavior and MIF Expression of the Rat Tail NP Tissue. To further verify the relationship between the expression of MIF and compression loading-associated NP degeneration, we conducted a rat tail IVD overloaded compression model (Figure 5(a)) to detect the classification of IVD degeneration and MIF expression referring to the previous study [16]. The MRI T2-weighted image of the compressed rat tail IVD indicated that the NP tissue that revealed the sign of degeneration (darkened tissue signal) occurred under 2-week overloaded compression and deteriorated under 4-week overloaded compression (Figures 5(b) and 5(c)). Additionally, the morphology analysis by HE staining also showed moderate and severe degenerative signs (loss of NP and increase in waviness of the fibrocartilage lamellas of AF) of the compressed rat tail IVD in 2 weeks and 4 weeks according to the Masuda classification [20] (Figures 5(d) and 5(e)). The result of Alcian blue staining also revealed that the content of glycosaminoglycans was gradually declined by prolonging the duration of IVD compression (Figures 5(f) and 5(g)). Noticeably, the MIF expression was upregulated in the moderate degenerative NP that suffered 2-week compression but

downregulated in the severe degenerative NP that suffered 4-week compression (Figures 5(h) and 5(i)).

3.4. Deficiency of MIF Exacerbated Oxidative Stress-Induced Senescence of the Human NP Cell That Suffered Overloaded Compression. Based on the proteomics data, we further figured out the molecular mechanism involved in the MIF-related NP degenerative changes via analyzing the oxidative stress-associated biomarkers. The cells were transfected with lentiviral MIF-shRNA to knock out the endogenous MIF before the analysis of oxidative stress-associated biomarkers. The SA- β -Gal staining result indicated that MIF-KO did not affect the senescence rate of the NP cells, but HC loading significantly aggravated the senescence of NP cells (Figures 6(a) and 6(b)). However, MIF-KO further exacerbated the HC loading-induced senescence of NP cells (Figures 6(a) and 6(b)). Flow cytometry was then used to analyze the content of intracellular ROS in NP cells marked by DCFH-DA molecular probes, and the result revealed that knockout of MIF alone did not induce the accumulation of ROS. However, HC loading did increase the content of ROS in NP cells, and MIF-KO markedly exacerbated the ROS content of the HC loading-treated NP cells (Figures 6(c) and 6(d)). In addition, the western blot analysis revealed that the expression of MIF was markedly eliminated by MIF-KO, but the expression of senescence-associated markers (P53, P21, and P16) and oxidative stress-related marker (NT) was not affected by MIF-KO (Figures 6(e) and 6(f)). HC loading depressed the expression of MIF compared with the control group and markedly enhanced the P53, P21, P16, and NT expression. Similarly, knockout of MIF in HC loading-treated NP cells further aggravated the expression of senescence-related and oxidative stress-related markers (Figures 6(e) and 6(f)).

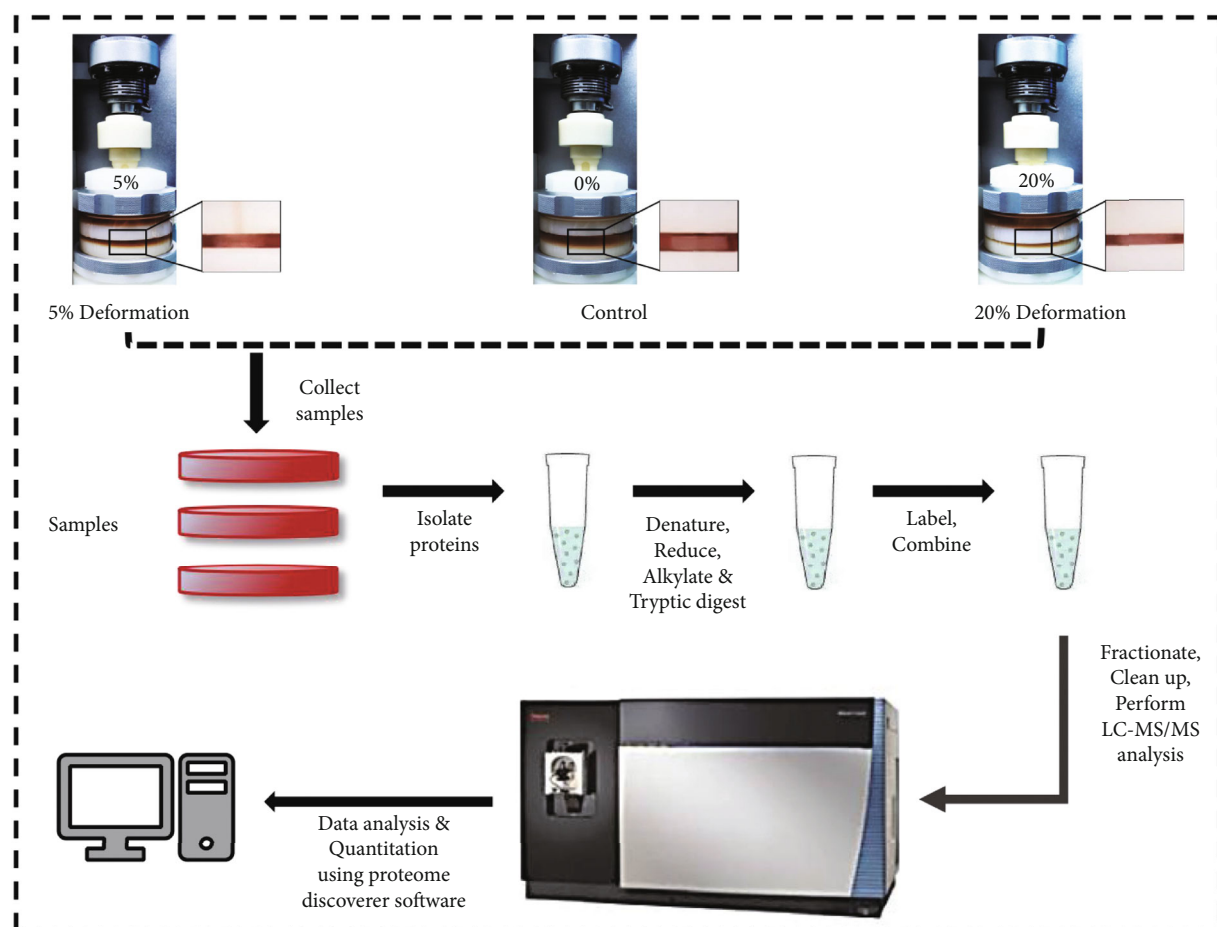


FIGURE 3: Schematic workflow of the TMT quantitative proteomics procedure: NP cell-encapsulated hydrogels cultured under dynamical compression with 0% (control), 5% (low-compression loading), and 20% deformation (high-compression loading) for 2 weeks, and protein extracts were labeled with 10-plex TMT reagent. Peptides were analyzed via LC-MS/MS, and the raw data for protein identification and relative quantification were analyzed by Proteome Discoverer.

3.5. Deficiency of MIF Accentuates Oxidative Stress-Induced Senescence of the NP Cell under Overloaded Compression via Depressing Mitophagy. As the major organelle for ATP biosynthetic process and oxidative phosphorylation, the mitochondrion is also the main ROS generating and attacking component of cells [21]. Our previous studies confirmed that mitophagy could alleviate the oxidative stress-induced senescence of NP cell via recycling the injured mitochondria [5, 22]. In terms of our prior studies and the present GO and KEGG enrichment analysis, we further observed the mitophagy-associated markers in the current study. The western blotting result indicated that both MIF-KO and treatment of HC loading could downregulate the expression of PINK1 and LC3II/I and upregulate the expression of Parkin and P62, which were symbols of the block of mitophagy (Figures 7(a) and 7(b)). Noticeably, knockout of MIF in HC loading-treated NP cells further exacerbated the restraint of mitophagy-related markers (Figures 7(a) and 7(b)). The JC-1 green/red fluorescence ratio is usually used for evaluating the state of the mitochondrion [5]. The JC-1 staining result indicated that knockout of MIF alone did not cause mitochondrial damage, but HC loading aggravated mitochondrial damage in NP cells (Figures 7(c) and 7(d)). Moreover, the

MIF-KO NP cells treated with HC loading had the highest JC-1 green/red fluorescence ratio, indicating that deficiency of MIF exacerbated accumulation of the damaged mitochondria induced by the HC loading (Figures 7(c) and 7(d)). To further investigate the mitophagy at various stages, NP cells were transfected with a plasmid encoding GFP-LC3 and incubated with MitoTracker Red to label autophagosomes and mitochondria, respectively. We found that mitochondria in the control group were filamentous and interconnected as a network. Exerting overloaded compression alone enhanced the formation of GFP-LC3 puncta, and a few were costained with mitochondria, which exhibited as short rods or spheres with the network breakdown (Figures 8(a) and 8(c)). Additionally, MIF-KO decreased the amount of colocalizing GFP-LC3 puncta significantly (Figures 8(a) and 8(c)). Furthermore, we observed the amount and morphology of the mitochondria and autophagosomes in the NP cells via TEM. As is shown in Figure 7(e), mitochondria of the NP cells in control and MIF-KO groups maintained the normal morphology and structure, whereas in the HC loading-treated NP cells, the mitochondria appeared shrunken with enhanced membrane density (Figure 8(b)). In addition, the HC loading-treated cell exhibited more autophagosomes,

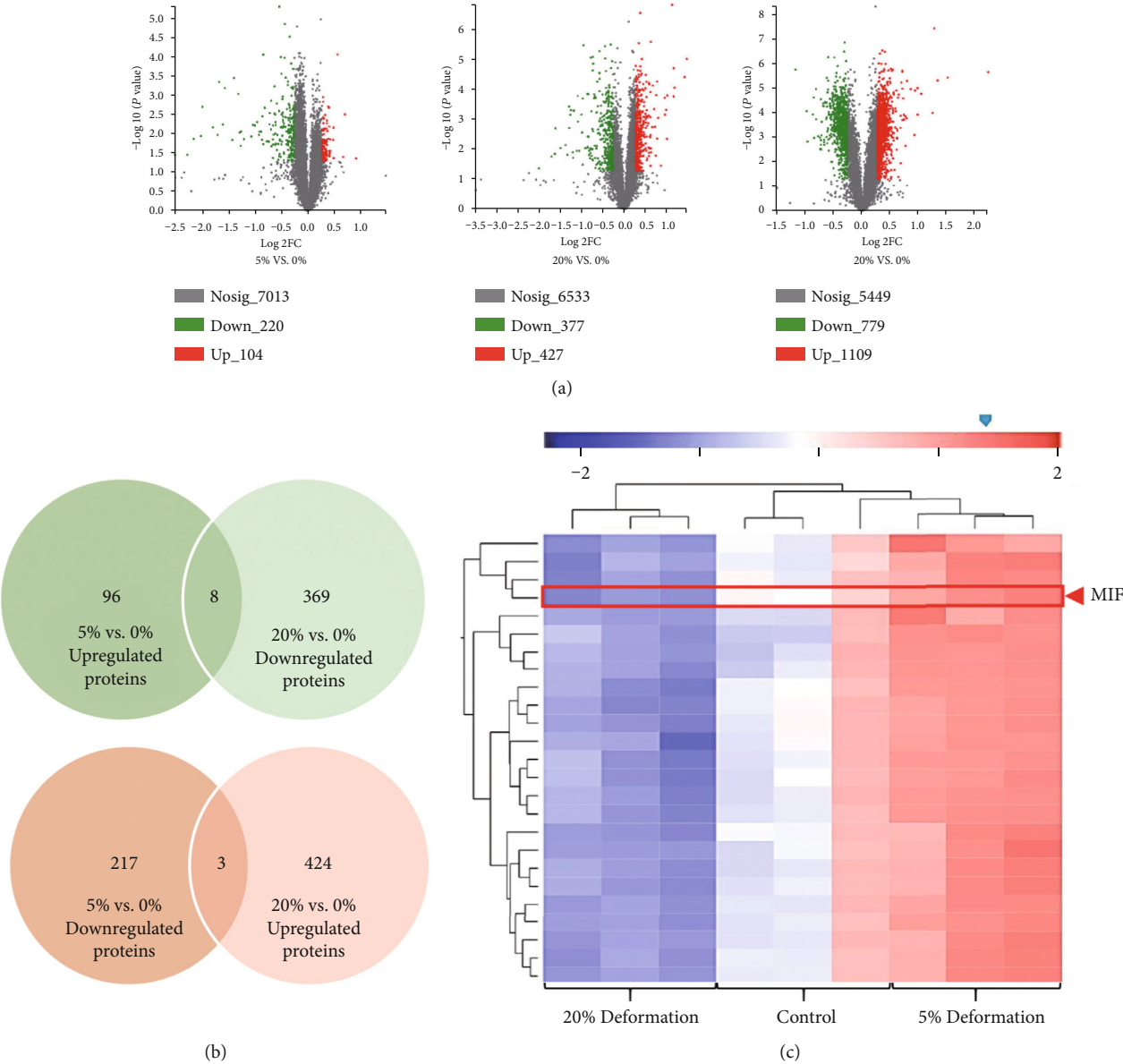


FIGURE 4: Continued.



FIGURE 4: TMT-based quantitative proteomics analyzed the differentially expressed proteins and pathways of the human NP cells that exerted graded mechanical compression loading: (a) the volcano plots revealed the DEPs of the NP cell-encapsulated hydrogels cultured under dynamical compression with 0% (control), 5% (low-compression loading), and 20% deformation (high-compression loading). (b) The Venn diagrams revealed the potential protective proteins (upregulated under low-compression loading but downregulated under high-compression loading) and adverse proteins (downregulated under low-compression loading but upregulated under high-compression loading) of the NP cells that suffered mechanical compression. (c) The heat map revealed part of the DEPs among the 0% (control), 5% (low-compression loading), and 20% deformation (high-compression loading) groups. (d) GO analysis of the DEPs between low-compression loading and high-compression loading groups revealed that the top enriched biological process was ATP biosynthetic process. (e) KEGG enrichment analysis of the DEPs between low-compression loading and high-compression loading groups revealed that the top enriched pathway was related to oxidative phosphorylation. ** $P < 0.01$ and *** $P < 0.001$.

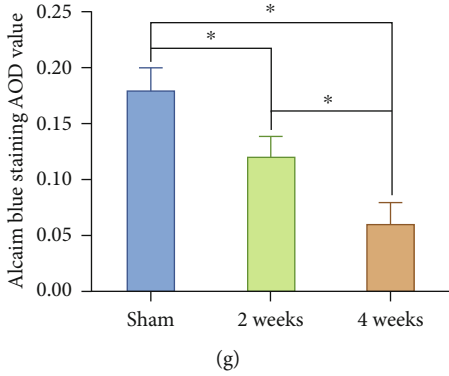
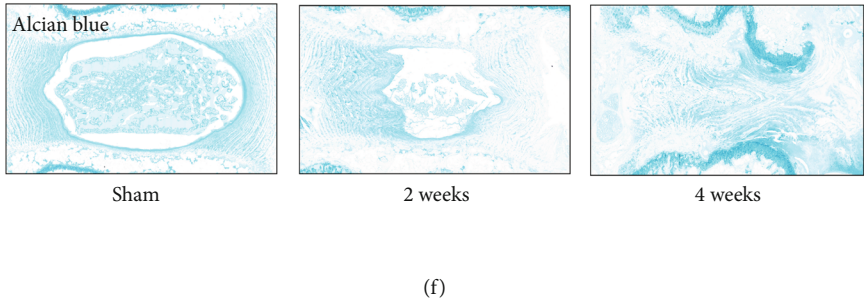
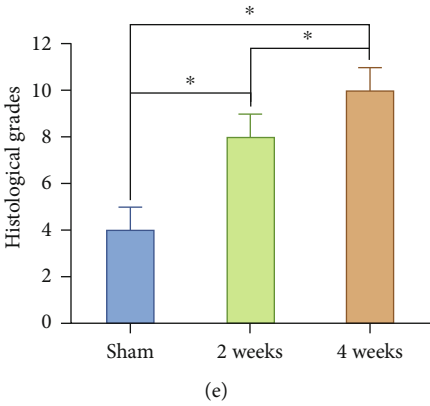
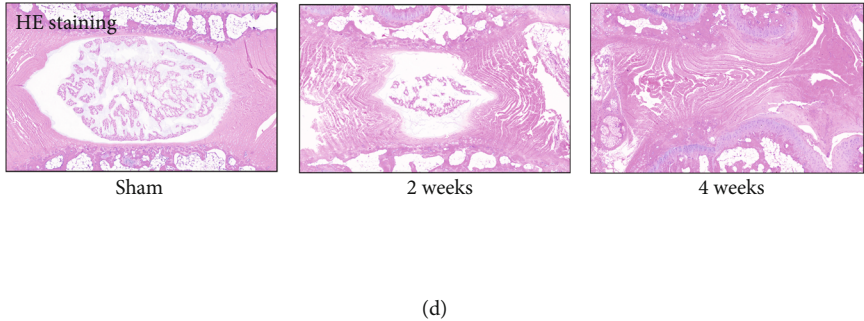
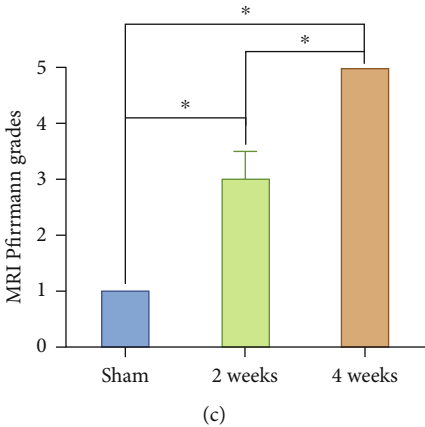
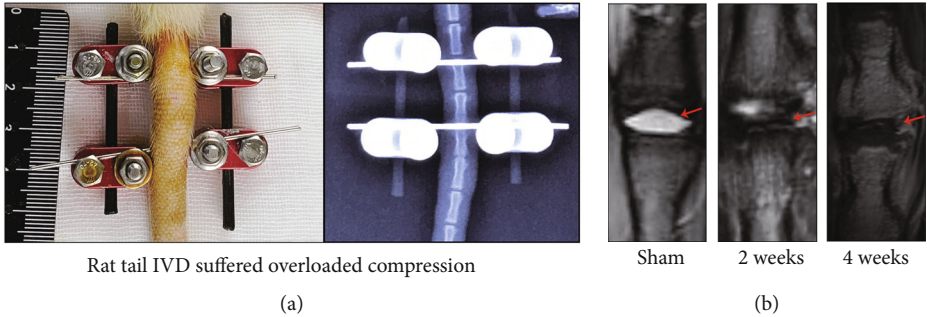


FIGURE 5: Continued.

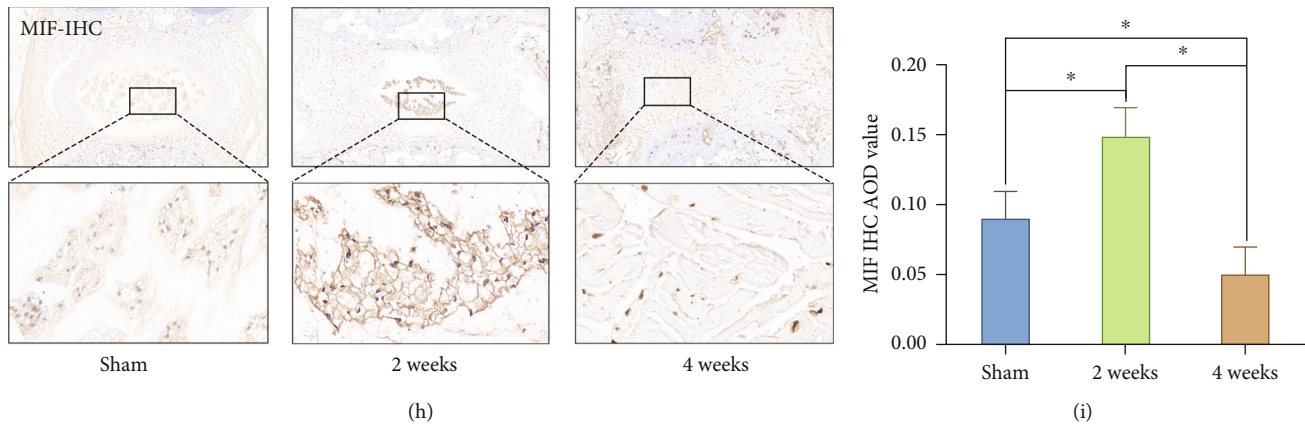


FIGURE 5: Effects of overloaded compression on biological behavior and MIF expression of the rat tail NP: (a) the close-up and X-ray views of the experimental rat tail IVD under the condition of overloaded compression. (b) The MRI image of the experimental rat tail IVD under the different duration of overloaded compression. (c) Statistic analysis of the MRI Pfirrmann grade changes of the experimental rat tail IVD under the different duration of overloaded compression. (d) The HE staining showed the histomorphological changes of the experimental rat tail IVD under the different duration of overloaded compression. (e) Statistic analysis of the Masuda degenerative score changes of the experimental rat tail IVD under the different duration of overloaded compression. (f) The Alcian blue staining showed the glycosaminoglycan content of the experimental rat tail IVD under the different duration of overloaded compression. (g) Statistic analysis of Alcian blue staining AOD value of the experimental rat tail IVD under the different duration of overloaded compression. (h) MIF IHC staining of the experimental rat tail IVD under the different duration of overloaded compression. (i) Statistic analysis of MIF IHC staining AOD value of the experimental rat tail IVD under the different duration of overloaded compression. * $P < 0.05$. # $P > 0.05$.

surrounding double-membrane mitochondrion-like segments, in its cytoplasm (Figure 8(b)). However, the MIF-KO NP cells treated with HC loading did not appear typical autophagosome in its cytoplasm (Figure 8(b)). Thus, the results above indicated that deficiency of MIF did retard the mitophagy of NP cells.

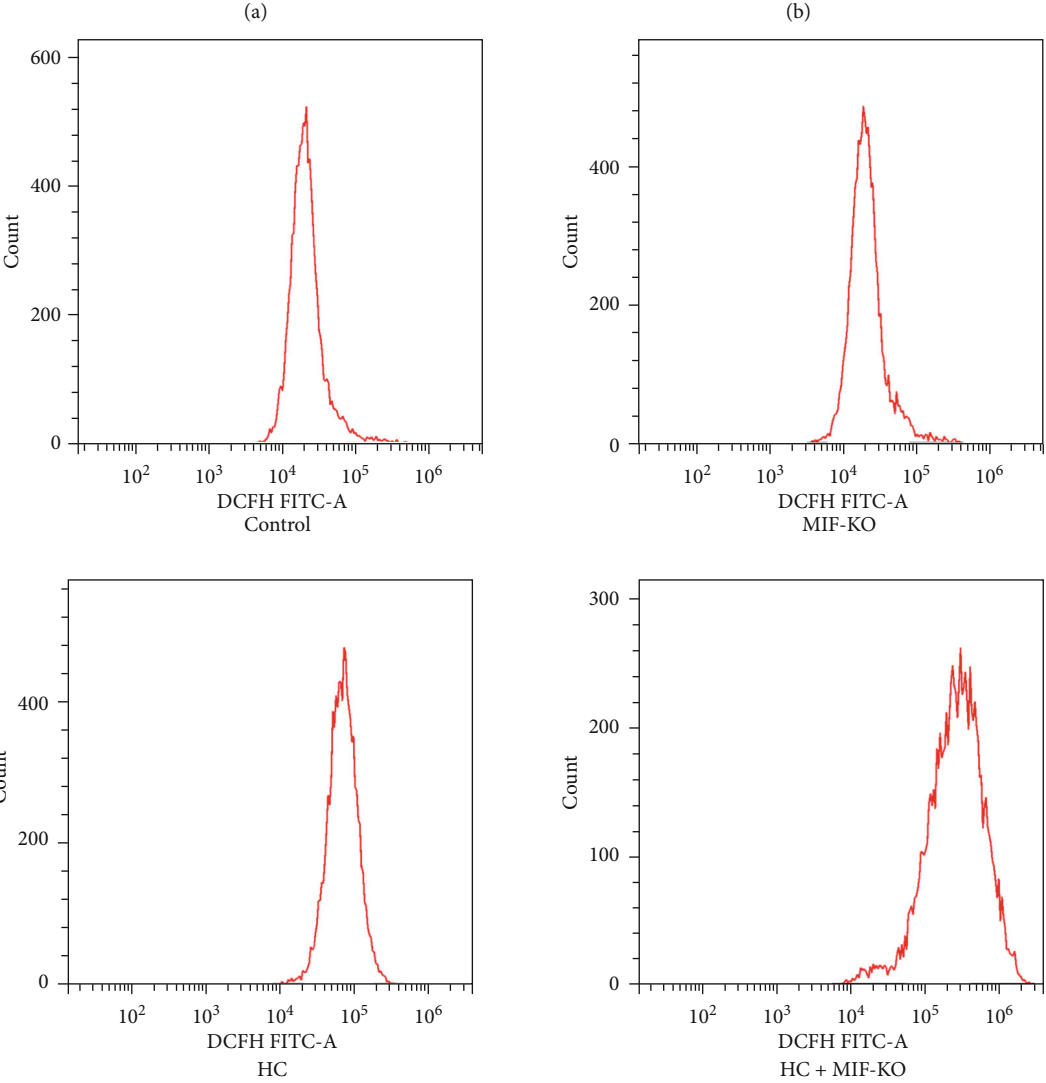
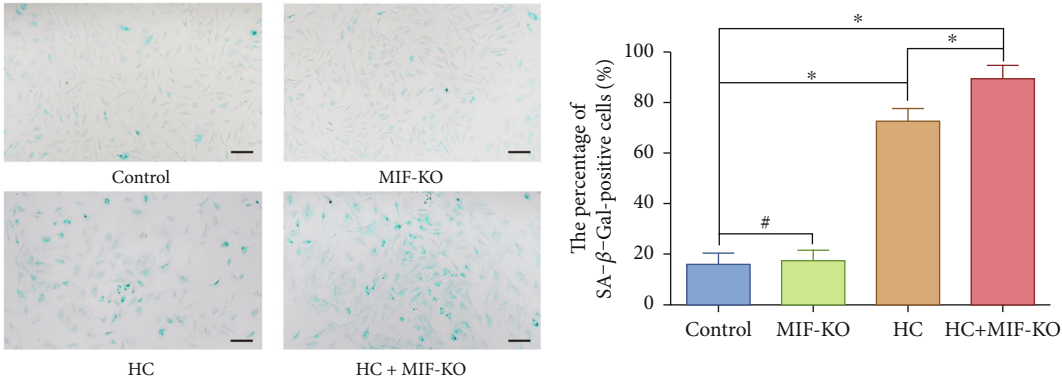
4. Discussion

Mass studies evaluated that the compressive force applied to the IVD played as a major regulator for the biological behavior of IVD cells, but the particular molecular mechanisms involved in this regulating process are still controversial. Our prior studies elucidated the biological responses of IVD cells to graded mechanical compression loading via establishing the compression-loaded perfusion culture models of IVD cell-encapsulated hydrogels and tissues [5, 6, 9, 10]. In the present study, we analyzed the apoptosis- and senescence-like changes of the human NP cells under graded dynamic compression loading and evaluated that LC loading did not lead to NP cell degenerative changes. In contrast, HC loading did cause cell apoptosis, senescence, and breakdown of ECM. For further exploration of potential regulators and molecular mechanisms involved in this process, we exerted TMT-based proteomics, a popular labeling proteomics method in identifying biomarkers and molecular mechanisms for several diseases.

Depending on the results of our current and prior studies, LC loading compression was beneficial for the NP cell survival and ECM homeostasis, whereas HC loading compression aggravated NP cell senescence, apoptosis, and breakdown of ECM [5, 6, 19]. Hence, we speculated that there might exist protective bioregulators that overexpressed

in NP cells under LC loading compression but lost their functions and underexpressed in NP cells that suffered HC loading compression. Based on this hypothesis, we analyzed the DEPs among the NP cells cultured under noncompression, LC, and HC loading compression and predicted eight proteins, which might play as potential protective factors for the NP cell survival under HC loading compression. Among the eight predicted proteins, MIF, a recognized hypoxic stress-associated regulator of innate immunity, was selected for further functional experiments due to its reported similar role in regulating the fate of the human CEP-derived cells [14]. Then, we tested the expression of MIF in both in vitro NP cell 3D-cultured hydrogels and in vivo rat tail IVD compressed models. The results revealed that the expression of MIF was markedly attenuated by HC loading in vitro and overloaded compression in vivo, which were consistent with the proteomics results.

MIF was first identified as a cytokine released from immune or nonimmune cells, including IVD and other types of cartilage cells, which can inhibit the random migration of macrophages and regulate chondroosteogenesis [14, 23, 24]. Despite its wide distribution, MIF secretion is closely related to multiple stresses, such as hypoxic, oxidative, and mechanical stresses [23–26]. MIF is thought as the downstream factor of hypoxia-inducible factor-1 (HIF-1), and the HIF-1 response of the cell is a kind of adaptive response that improves the chances of survival under hypoxic and/or oxidative stress by restoring oxidative homeostasis [25]. In the current study, the analysis of GO and KEGG enrichment also indicated that compression loading affected the fate commitment of NP cells via regulating the ATP biosynthetic process and oxidative phosphorylation. As the prominent organelle for ATP biosynthetic process and oxidative phosphorylation,



(c)
FIGURE 6: Continued.

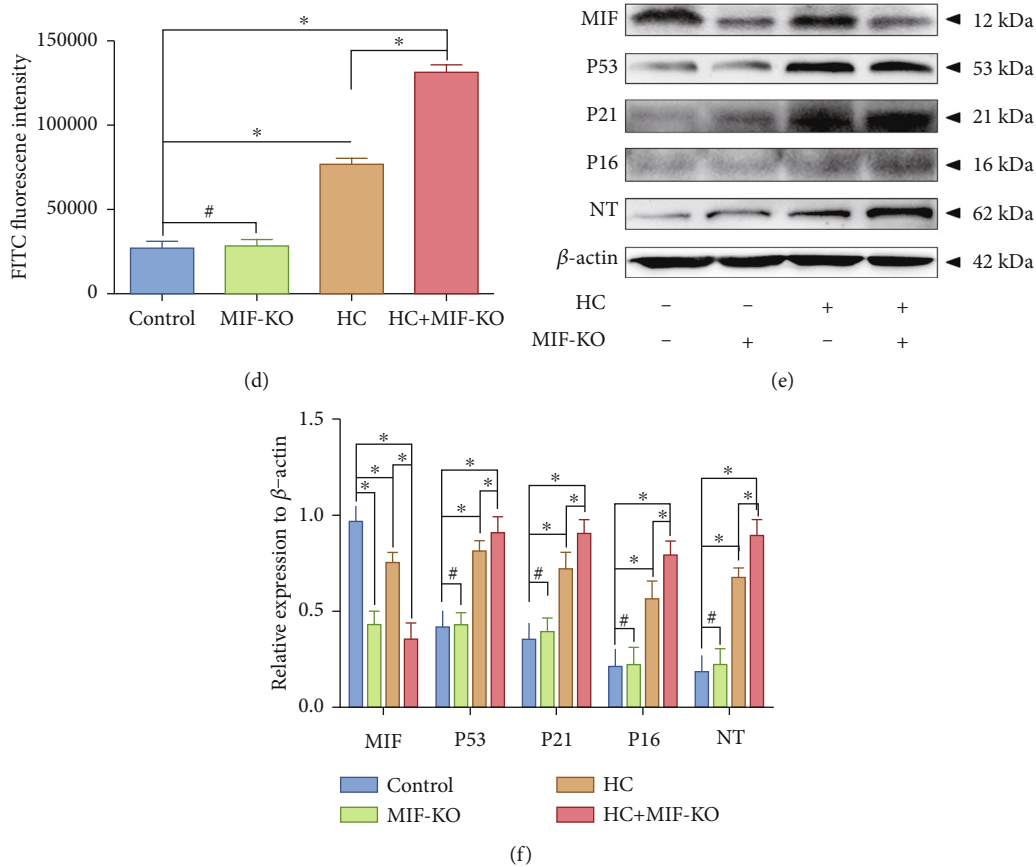


FIGURE 6: MIF-KO exacerbated oxidative stress-induced senescence of the NP cell that suffered overloaded compression: (a) after MIF-KO and high-compression loading treatment, the cell senescence degree of the NP cells was analyzed by SA- β -Gal staining (100x). (b) Statistic analysis of the SA- β -Gal-positive rate of the NP cells. (c) After MIF-KO and high-compression loading treatment, the ROS content of the NP cells was measured by flow cytometry following DCFH-DA staining. (d) Statistic analysis of the ROS content of the NP cells. (e) Western blotting analysis of the expression levels of MIF, oxidative stress biomarker NT, and senescence-associated markers (P53, P21, and P16) of the NP cells. (f) Statistic analysis of the western blots of the biomarkers. * $P < 0.05$. # $P > 0.05$. Scale bar = 100 μ m.

the mitochondrion is also the main targeting organelle for oxidative stress injury [21]. Noticeably, MIF was reported to play an essential role in regulating many repair/senescence-associated genes via activating autophagy or mitophagy, which is a critical antioxidative stress mechanism to restore intracellular oxygen homeostasis [25, 27]. Our previous studies have evaluated that overloaded compression could trigger oxidative stress-associated mitochondrial dysfunction and induce NP cell senescence, and mitophagy could alleviate oxidative stress-induced senescent changes of NP cell that suffered overloaded compression via clearance of damaged mitochondria. Therefore, we hypothesized that there might exist a relationship between compression-associated mitochondrial damage and mitophagy in NP cell.

The mitochondrion is an essential organelle with multiple functions in the maintenance of intracellular environment homeostasis, not only by regulating ATP production but also by regulating several signal cascades that control cell death, differentiation, and senescence [28]. Mitophagy, a particular form of macroautophagy, can specifically target mitochondria for degradation [29, 30]. In this process, a series of specific receptors or adaptors that mediated pathways were activated to recruit the autophagic machinery towards dam-

aged mitochondria, engulfed and digested by the autophagosomes [29, 30]. The aforementioned results of the current study indicated that HC loading could induce oxidative stress injury and senescence of the human NP cells. Simultaneously, HC loading aggravated mitochondrial dysfunction but retarded activity of mitophagy in NP cells. When we knock down the expression of MIF, the activity of mitophagy was further depressed, which substantially exacerbated the mitochondrial dysfunction, oxidative stress injury, and senescence of the NP cells under overloaded compression. Although mass studies confirmed the mitophagy regulating role of MIF in various types of cells, the specific regulating mechanisms involved in this process were still controversial [27]. The established researches identified and elucidated two signal pathways of mitophagy: ubiquitin- (Ub-) dependent and Ub-independent (receptor-mediated mitophagy) [31]. Some study holds that MIF induces mitophagy via BNIP3-mediated pathway, an Ub-independent manner of mitophagy [32], while some other holds that MIF is the regulator of PINK1/Parkin-mediated mitophagy, the most well-defined Ub-mediated pathway of mitophagy [33]. The results of our prior and current studies elucidated that overload compression-associated mitophagy was related to the

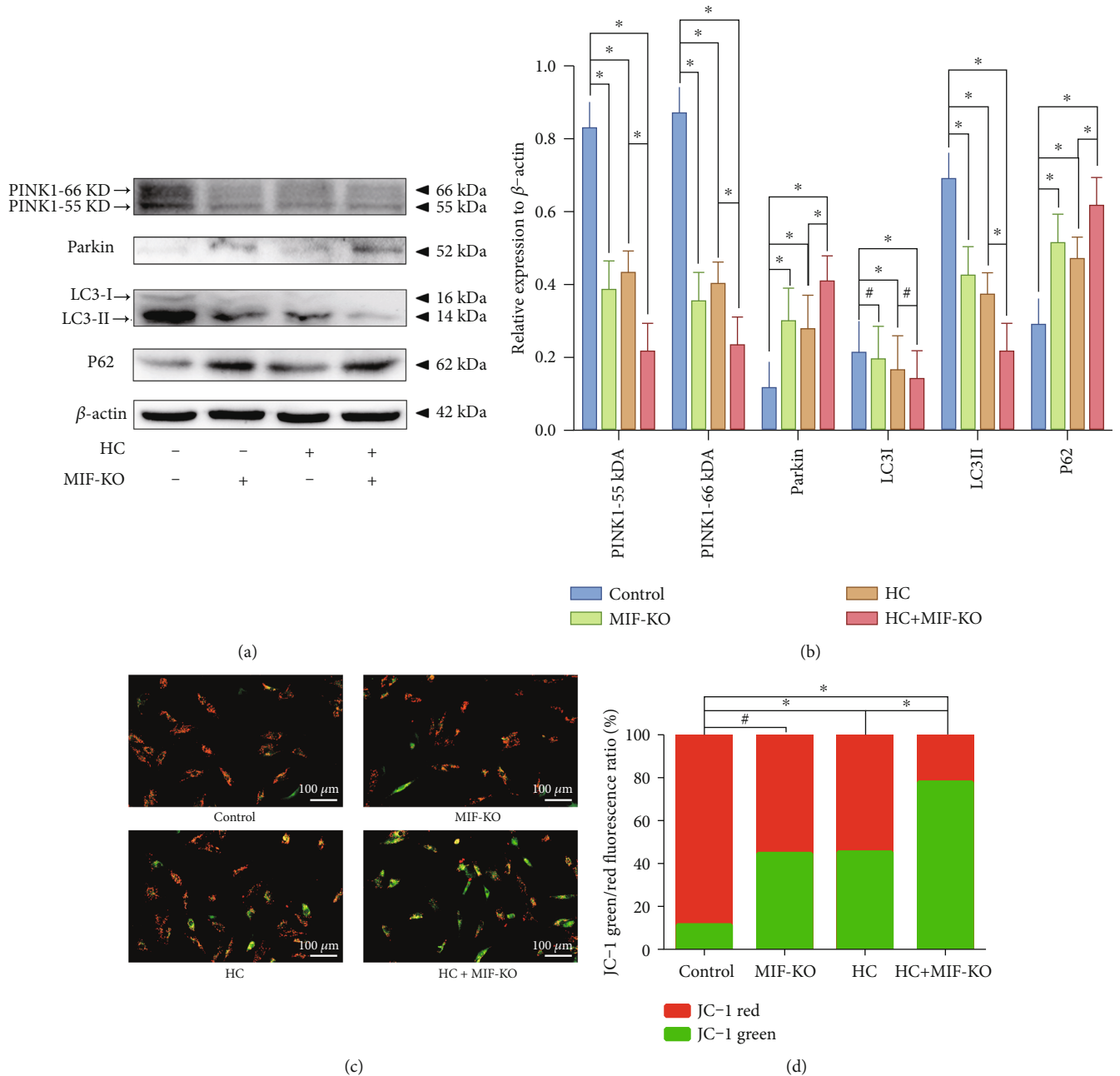


FIGURE 7: MIF-KO accentuates oxidative stress-induced senescence and mitochondrial dysfunction of the NP cell: (a) western blotting analysis of the expression levels of the mitophagy-related markers (PINK1, Parkin, LC3II/I, and P62) of the NP cells. (b) Statistic analysis of the western blots of the mitophagy-related biomarkers. (c) The mitochondrial membrane potential was observed and measured by fluorescence microscopy after JC-1 fluorescent molecular probe staining. (d) Statistic analysis of the JC-1 green/red fluorescence intensity ratio. * $P < 0.05$. # $P > 0.05$.

PINK1/Parkin-mediated macroautophagy [5]. Noticeably, the other series of studies also evaluated that MIF could protect cardiac cells against overload pressure-induced cardiac hypertrophy via activating Parkin-mediated macroautophagy or mitophagy [26, 34, 35]. Mitophagy-inducing signal cascades are relatively distinct but interconnected [31]. Importantly, mitophagy is dependent on the accumulation of ROS and damaged mitochondria [36]. Deficiency of mitophagy accumulates dysfunctional mitochondria that release

ROS into the cytosol and trigger oxidative stress injury [27, 31, 36]. Thus, this is because deficiency of MIF accentuates the oxidative stress damage and senescence of NP cells that suffered overloaded mechanical compression.

There were some limitations in the current study. First, the experimental NP cells in the current study were obtained from the same donor, due to the homogeneity of samples prepared for the proteomics analysis. The collection of clinical patients' IVD samples for the research is ongoing. We

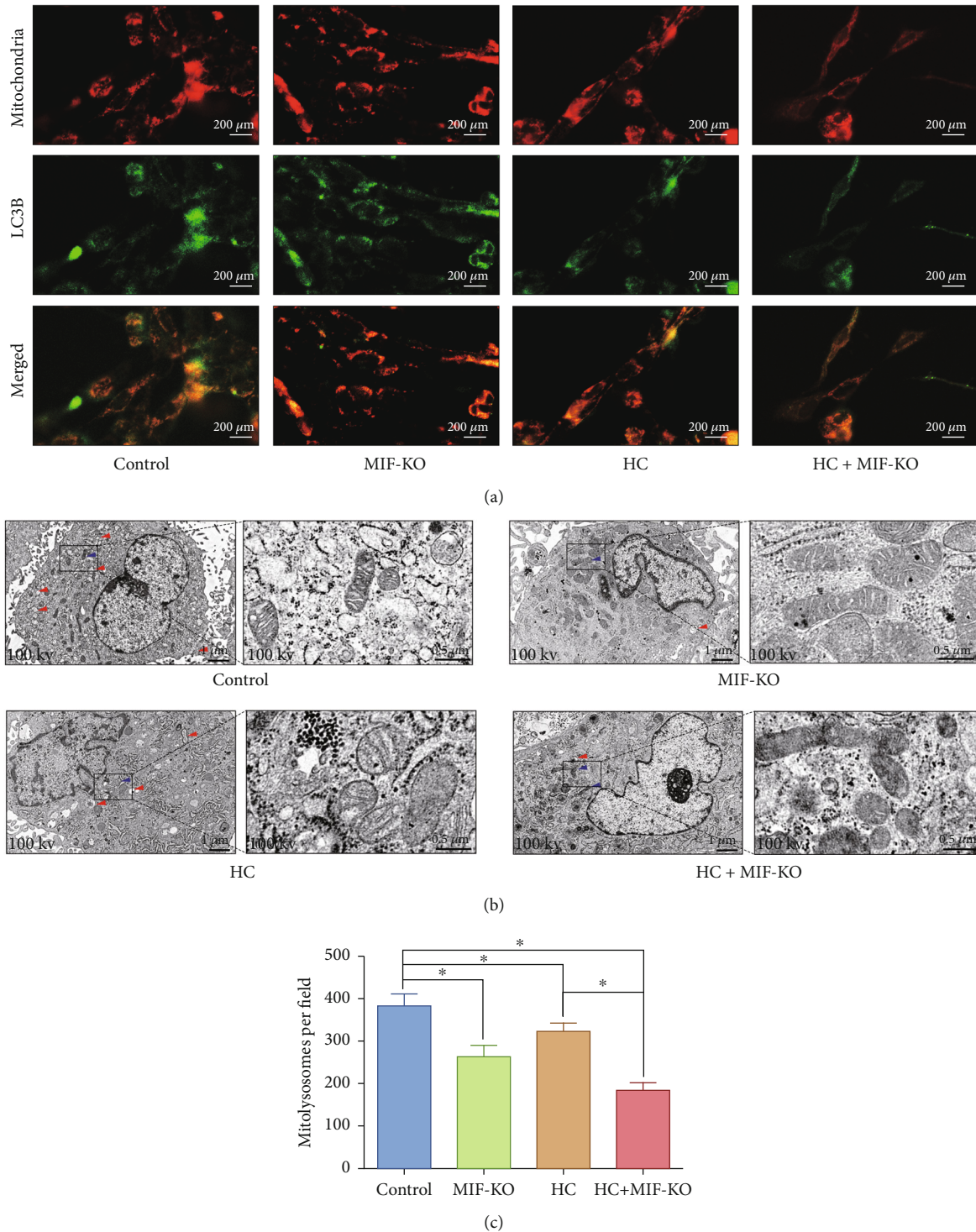


FIGURE 8: MIF-KO accentuates oxidative stress-induced senescence of the NP cell via depressing mitophagy: (a) mitophagy in NP cells was determined by observation of GFP-LC3 and MitoTracker Red colabeled autophagosomes and mitochondria. (b) The electron micrographs of mitochondria and autophagosomes were observed via TEM, and double-membrane profiles resembling pieces of digested mitochondria were found in some autophagosomes in the high-compression loading group. Blue arrows represent the autophagic vacuole ultrastructural morphology. Red arrows represent the mitochondrial electron micrographs. (c) Statistic analysis of the mitolysosomes per field under optical microscopy (400x). * $P < 0.05$. # $P > 0.05$.

have planned to carry out more advanced high-throughput sequencing, such as single-cell sequencing in future studies, which can conclude larger sample capacity and diminish

the deviation caused by individual differences. Second, the mechanism behind ROS-induced MIF release remains elusive, and the current study simply focused on its

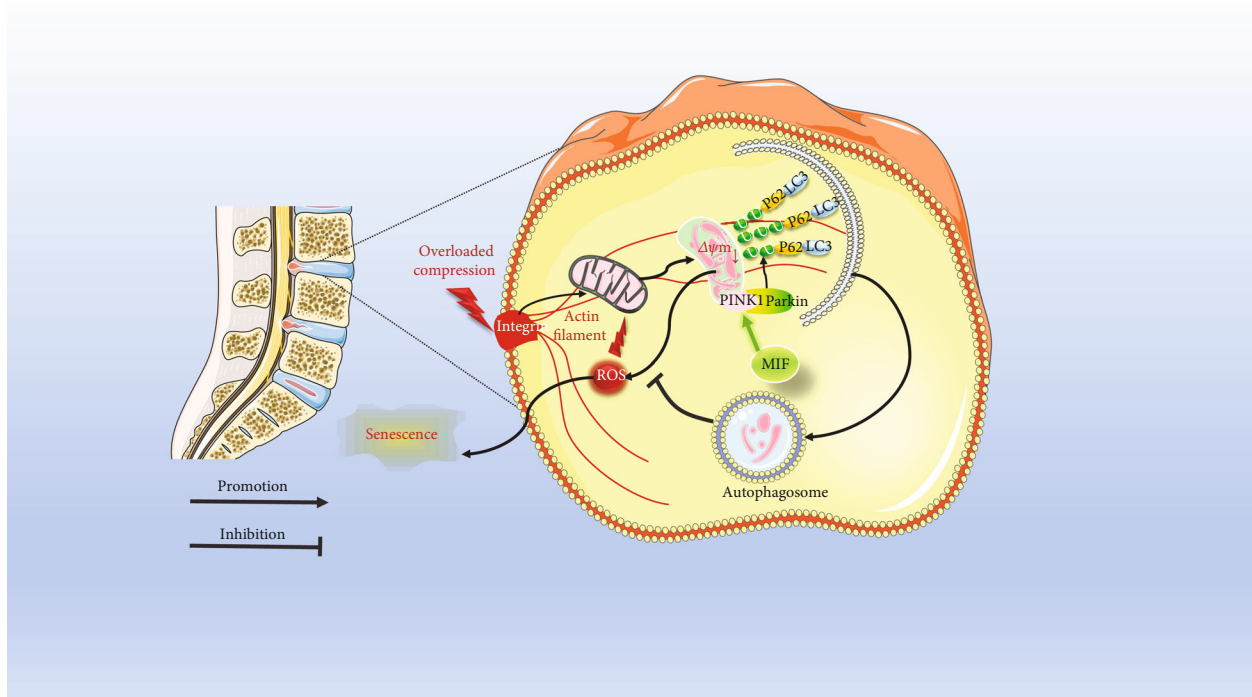


FIGURE 9: Schematic diagram shows the potential mechanism of MIF in regulating overloaded compression induced NP cell senescence: overloaded compression induces mitochondrial injury and triggers oxidative stress-associated senescence of NP cells. The deficiency of MIF depresses mitophagy in NP cells, which further exacerbates oxidative stress-associated senescence of the NP cells under overloaded compression.

autophagy-inducing role involved in the progress of mechanical compression-related disc degeneration. Hence, more researches on the MIF-associated biological changes in the pathomechanism of disc degeneration will be exerted in our further studies.

5. Conclusion

In conclusion, our study reveals that overloaded mechanical compression could induce oxidative stress, mitochondrial dysfunction, and degenerative changes in human NP cells. In contrast, proper physiological pressure is beneficial for maintaining cell viability and ECM homeostasis of the NP. Moreover, there exists a relationship between MIF expression and mechanical compression stress-associated biological changes of NP cells. The deficiency of MIF accentuates the accumulation of ROS, mitochondrial dysfunction, and senescence under overloaded mechanical compression. The potential molecular mechanism involved in this process is related to the mitophagy-inducing role of MIF (Figure 9). This work helps us better understand the regulating function of mechanical compression stress in the progress of disc degeneration and provides more substantial proofs for using MIF-alerting agents in treating disc degenerative diseases.

Data Availability

The data used to support the findings of this study are available from the corresponding authors upon request.

Conflicts of Interest

All authors declare no competing financial interests.

Authors' Contributions

Yiyang Wang and Yanzhu Hu were involved in the practical achievement of the experiments, contributed equally to this study, and should be regarded as co-first authors; Haoming Wang and Ningyuan Liu conducted the animal experiment; Lei Luo and Chen Zhao performed the surgery and collected the surgical sample; Yiyang Wang, Dandan Zhou, and Hang Tong collected, analyzed, and interpreted the data; Yiyang Wang drafted the manuscript; Qiang Zhou and Pei Li conceived and designed the study. All authors read and approved the final manuscript.

Acknowledgments

This work was supported by grants from the National Key R&D Program of China (No. 2018YFC1105803); Natural Science Foundation of China (No. 81772378 and No. 81974346); Natural Science Foundation of Chongqing, China (No. cstc2020jcyj-msxmX0148); Basic Research and Frontier Exploration Project of Yuzhong District, Chongqing, China (No. 20200121); Project of Innovative Science Research for Postgraduate of Chongqing Municipal Education Committee, Chongqing, China (CYB20168 and CYS20226); and Basic Research Incubation Project of the Third Affiliated

Hospital of Chongqing Medical University, Chongqing, China (No. KY20077).

Supplementary Materials

Supplementary Figure 1: preoperative MRI image of the patient's lumbar IVDs and the gross view of the separated NP tissues. Supplementary Table 1: annotation detail of the DEPs between the LC loading group and the control group. Supplementary Table 2: annotation detail of the DEPs between the HC loading group and the control group. Supplementary Table 3: annotation detail of the DEPs between the HC loading group and the LC loading group. (*Supplementary Materials*)

References

- [1] R. Buchbinder, M. van Tulder, B. Öberg et al., "Low back pain: a call for action," *Lancet*, vol. 391, no. 10137, pp. 2384–2388, 2018.
- [2] S. Roberts, "Disc morphology in health and disease," *Biochemical Society Transactions*, vol. 30, no. 6, pp. 864–869, 2002.
- [3] F. Zhang, X. Zhao, H. Shen, and C. Zhang, "Molecular mechanisms of cell death in intervertebral disc degeneration (review)," *International Journal of Molecular Medicine*, vol. 37, no. 6, pp. 1439–1448, 2016.
- [4] F. Wang, F. Cai, R. Shi, X. H. Wang, and X. T. Wu, "Aging and age related stresses: a senescence mechanism of intervertebral disc degeneration," *Osteoarthritis and Cartilage*, vol. 24, no. 3, pp. 398–408, 2016.
- [5] Y. Wang, H. Wang, Y. Zhuo et al., "SIRT1 alleviates high-magnitude compression-induced senescence in nucleus pulposus cells via PINK1-dependent mitophagy," *Aging*, vol. 12, no. 16, pp. 16126–16141, 2020.
- [6] P. Li, G. Hou, R. Zhang et al., "High-magnitude compression accelerates the premature senescence of nucleus pulposus cells via the p38 MAPK-ROS pathway," *Arthritis research & therapy*, vol. 19, no. 1, 2017.
- [7] C. Neidlinger-Wilke, K. Würtz, J. P. Urban et al., "Regulation of gene expression in intervertebral disc cells by low and high hydrostatic pressure," *European Spine Journal*, vol. 15, Supplement 3, pp. 372–378, 2006.
- [8] I. A. Stokes and J. C. Iatridis, "Mechanical conditions that accelerate intervertebral disc degeneration: overload versus immobilization," *Spine*, vol. 29, no. 23, pp. 2724–2732, 2004.
- [9] P. Li, Y. Gan, H. Wang et al., "Dynamic compression effects on immature nucleus pulposus: a study using a novel intelligent and mechanically active bioreactor," *International Journal of Medical Sciences*, vol. 13, no. 3, pp. 225–234, 2016.
- [10] P. Li, Y. Gan, H. Wang et al., "A substance exchanger-based bioreactor culture of pig discs for studying the immature nucleus pulposus," *Artificial organs*, vol. 41, no. 11, pp. E308–E319, 2017.
- [11] S. Yang, F. Zhang, J. Ma, and W. Ding, "Intervertebral disc ageing and degeneration: the antiapoptotic effect of oestrogen," *Ageing Research Reviews*, vol. 57, p. 100978, 2020.
- [12] L. Kang, S. Liu, J. Li, Y. Tian, Y. Xue, and X. Liu, "The mitochondria-targeted anti-oxidant MitoQ protects against intervertebral disc degeneration by ameliorating mitochondrial dysfunction and redox imbalance," *Cell proliferation*, vol. 53, no. 3, article e12779, 2020.
- [13] G. Hou, H. Zhao, H. Teng et al., "N-cadherin attenuates high glucose-induced nucleus pulposus cell senescence through regulation of the ROS/NF- κ B pathway," *Cellular Physiology and Biochemistry: International Journal of Experimental Cellular Physiology, Biochemistry, and Pharmacology*, vol. 47, no. 1, pp. 257–265, 2018.
- [14] Y. Yao, Q. Deng, W. Song et al., "MIF plays a key role in regulating tissue-specific chondro-osteogenic differentiation fate of human cartilage endplate stem cells under hypoxia," *Stem Cell Reports*, vol. 7, no. 2, pp. 249–262, 2016.
- [15] C. W. Pfirrmann, A. Metzdorf, M. Zanetti, J. Hodler, and N. Boos, "Magnetic resonance classification of lumbar intervertebral disc degeneration," *Spine*, vol. 26, no. 17, pp. 1873–1878, 2001.
- [16] H. Hirata, T. Yurube, K. Kakutani et al., "A rat tail temporary static compression model reproduces different stages of intervertebral disc degeneration with decreased notochordal cell phenotype," *Journal of Orthopaedic Research*, vol. 32, no. 3, pp. 455–463, 2014.
- [17] Y. Zhang, Y. Zhang, J. Tang et al., "Oxymatrine inhibits homocysteine-mediated autophagy via MIF/mTOR signaling in human umbilical vein endothelial cells," *Cellular Physiology and Biochemistry*, vol. 45, no. 5, pp. 1893–1903, 2018.
- [18] J. Zvicer and B. Obradovic, "Bioreactors with hydrostatic pressures imitating physiological environments in intervertebral discs," *Journal of Tissue Engineering and Regenerative Medicine*, vol. 12, no. 2, pp. 529–545, 2018.
- [19] Y. Gan, B. Tu, P. Li et al., "Low magnitude of compression enhances biosynthesis of mesenchymal stem cells towards nucleus pulposus cells via the TRPV4-dependent pathway," *Stem Cells International*, vol. 2018, Article ID 7061898, 12 pages, 2018.
- [20] K. Masuda, Y. Aota, C. Muehleman et al., "A novel rabbit model of mild, reproducible disc degeneration by an anulus needle puncture: correlation between the degree of disc injury and radiological and histological appearances of disc degeneration," *Spine*, vol. 30, no. 1, pp. 5–14, 2005.
- [21] C. Feng, M. Yang, M. Lan et al., "ROS: crucial intermediators in the pathogenesis of intervertebral disc degeneration," *Oxidative Medicine and Cellular Longevity*, vol. 2017, Article ID 5601593, 12 pages, 2017.
- [22] Y. Wang, J. Shen, Y. Chen et al., "PINK1 protects against oxidative stress induced senescence of human nucleus pulposus cells via regulating mitophagy," *Biochemical and Biophysical Research Communications*, vol. 504, no. 2, pp. 406–414, 2018.
- [23] C. Xiong, Y. Huang, H. Kang, T. Zhang, F. Xu, and X. Cai, "Macrophage inhibition factor-mediated CD74 signal modulate inflammation and matrix metabolism in the degenerated cartilage endplate chondrocytes by activating extracellular signal regulated kinase 1/2," *Spine*, vol. 42, no. 2, pp. E61–E70, 2017.
- [24] Y. Fujihara, A. Hikita, T. Takato, and K. Hoshi, "Roles of macrophage migration inhibitory factor in cartilage tissue engineering," *Journal of Cellular Physiology*, vol. 233, no. 2, pp. 1490–1499, 2018.
- [25] A. Maity and C. Koumenis, "HIF and MIF—a nifty way to delay senescence," *Genes & Development*, vol. 20, no. 24, pp. 3337–3341, 2006.
- [26] X. Xu, Y. Hua, S. Nair, R. Bucala, and J. Ren, "Macrophage migration inhibitory factor deletion exacerbates pressure overload-induced cardiac hypertrophy through mitigating autophagy," *Hypertension*, vol. 63, no. 3, pp. 490–499, 2014.

- [27] O. El Bounkari and J. Bernhagen, "MIF and autophagy: a novel link beyond "eating"," *Cell Research*, vol. 22, no. 6, pp. 950–953, 2012.
- [28] C. Correia-Melo, F. D. Marques, R. Anderson et al., "Mitochondria are required for pro-ageing features of the senescent phenotype," *The EMBO Journal*, vol. 35, no. 7, pp. 724–742, 2016.
- [29] Y. Kitagishi, N. Nakano, M. Ogino, M. Ichimura, A. Minami, and S. Matsuda, "PINK1 signaling in mitochondrial homeostasis and in aging (review)," *International Journal of Molecular Medicine*, vol. 39, no. 1, pp. 3–8, 2017.
- [30] A. Eiyama and K. Okamoto, "PINK1/Parkin-mediated mitophagy in mammalian cells," *Current Opinion in Cell Biology*, vol. 33, pp. 95–101, 2015.
- [31] J. Harris, N. Deen, S. Zamani, and M. A. Hasnat, "Mitophagy and the release of inflammatory cytokines," *Mitochondrion*, vol. 41, pp. 2–8, 2018.
- [32] Y. C. Lai, Y. C. Chuang, C. P. Chang, and T. M. Yeh, "Macrophage migration inhibitory factor has a permissive role in concanavalin A-induced cell death of human hepatoma cells through autophagy," *Cell Death & Disease*, vol. 6, no. 12, article e2008, 2015.
- [33] C. A. Smith, D. J. Tyrell, U. A. Kulkarni et al., "Macrophage migration inhibitory factor enhances influenza-associated mortality in mice," *JCI insight*, vol. 4, no. 13, 2019.
- [34] X. Xu, B. D. Pacheco, L. Leng, R. Bucala, and J. Ren, "Macrophage migration inhibitory factor plays a permissive role in the maintenance of cardiac contractile function under starvation through regulation of autophagy," *Cardiovascular Research*, vol. 99, no. 3, pp. 412–421, 2013.
- [35] X. Xu, J. Pang, Y. Chen, R. Bucala, Y. Zhang, and J. Ren, "Macrophage migration inhibitory factor (MIF) deficiency exacerbates aging-induced cardiac remodeling and dysfunction despite improved inflammation: role of autophagy regulation," *Scientific Reports*, vol. 6, no. 1, 2016.
- [36] N. D. Georgakopoulos, G. Wells, and M. Campanella, "The pharmacological regulation of cellular mitophagy," *Nature Chemical Biology*, vol. 13, no. 2, pp. 136–146, 2017.

Research Article

Autophagic Degradation of Gasdermin D Protects against Nucleus Pulposus Cell Pyroptosis and Retards Intervertebral Disc Degeneration In Vivo

Zhiwei Liao ¹, Suyun Li,¹ Rong Liu,² Xiaobo Feng,¹ Yunsong Shi,¹ Kun Wang,¹ Shuai Li,¹ Yukun Zhang,¹ Xinghuo Wu ¹, and Cao Yang ¹

¹Department of Orthopaedics, Union Hospital, Tongji Medical College, Huazhong University of Science and Technology, Wuhan 430022, China

²Department of Orthopaedic Surgery, Puren Hospital of Wuhan, Wuhan University of Science and Technology, Wuhan, China

Correspondence should be addressed to Xinghuo Wu; wuxinghuo@163.com and Cao Yang; caoyangunion@hust.edu.cn

Received 28 January 2021; Revised 5 May 2021; Accepted 19 May 2021; Published 21 June 2021

Academic Editor: Sidong Yang

Copyright © 2021 Zhiwei Liao et al. This is an open access article distributed under the Creative Commons Attribution License, which permits unrestricted use, distribution, and reproduction in any medium, provided the original work is properly cited.

Intervertebral disc degeneration (IDD) is the primary culprit of low back pain and renders heavy social burden worldwide. Pyroptosis is a newly discovered form of programmed cell death, which is also involved in nucleus pulposus (NP) cells during IDD progression. Moderate autophagy activity is critical for NP cell survival, but its relationship with pyroptosis remains unknown. This study is aimed at investigating the relationship between autophagy and pyroptotic cell death. The pyroptosis executor N-terminal domain of gasdermin D (GSDMD-N) and inflammation-related proteins were measured in lipopolysaccharide- (LPS-) treated human NP cells. Inhibition of autophagy by siRNA transfection and chemical drugs aggravated human NP cell pyroptosis. Importantly, we found that the autophagy-lysosome pathway and not the proteasome pathway mediated the degradation of GSDMD-N as lysosome dysfunction promoted the accumulation of cytoplasmic GSDMD-N. Besides, P62/SQSTM1 colocalized with GSDMD-N and mediated its degradation. The administration of the caspase-1 inhibitor VX-765 could reduce cell pyroptosis as confirmed in a rat disc IDD model *in vivo*, whereas ATG5 knockdown significantly accelerated the progression of IDD. In conclusion, our study indicated that autophagy protects against LPS-induced human NP cell pyroptosis via a P62/SQSTM1-mediated degradation mechanism and the inhibition of pyroptosis retards IDD progression *in vivo*. These findings deepen the understanding of IDD pathogenesis and hold implications in unraveling therapeutic targets for IDD treatment.

1. Introduction

Intervertebral disc degeneration (IDD) is considered as the primary pathological basis for painful spine diseases. Intervertebral disc (IVD) tissue mainly serves as an intervertebral junction and buffers mechanical pressure. This sandwich-like organ is composed of outer annulus fibrosus, inner nucleus pulposus (NP), and cartilaginous endplates at ends [1]. IDD is a common musculoskeletal degenerative disease characterized by chronic inflammation and progressive cell death [2, 3]. The death of resident NP cells accompanied by extracellular matrix metabolism disorder is closely related to IDD progression [4]. Different cell death pathways

(i.e., programmed cell death) could be involved in IDD and interact with each other to accelerate IDD progression [1]. Therefore, further investigation about the mechanisms of NP cell death is required and it may provide potential therapeutic targets for IDD treatment.

Pyroptosis is a form of regulated cell death initiated by inflammasomes and caspase activation, which induces pore formation on the plasma membrane and cell swelling or lysis [5]. Specifically, activation of inflammatory caspases induces the cleavage of gasdermin D (GSDMD), releasing the N-terminal domain (GSDMD-N), which leads to cell membrane perforation and lytic death [6, 7]. The inflammasome-mediated cell pyroptosis plays a critical role

in the pathogenesis of various diseases, including cancer, cardiovascular diseases, and osteoarthritis [8–10]. Previous studies have indicated that the sustained activation of inflammasomes exists during the progression of IDD [11, 12]; however, the role of NP cell pyroptosis in the pathogenesis of IDD remains unclear.

Autophagy is a conserved cellular mechanism that assists cells to adapt and protect themselves in response to stress [13]. Autophagy contributes to cellular quality control, including removing damaged proteins and organelles, which is closely associated with various forms of cell death [14, 15]. Several studies showed that autophagy limits the activation of inflammasomes and alleviates the secretion of inflammatory cytokines [16, 17]. It is reasonable to assume that autophagy regulates the activation of inflammasome and then affects the outcome of cell pyroptosis. However, the relationship between cell pyroptosis and autophagy is complicated. Based on our previous studies, autophagy activation protected NP cell against stress-induced cell death, whereas autophagy inhibition promotes cell apoptosis [18, 19]. Therefore, we assumed that reasonable autophagy activity is beneficial for NP cell survival and may play a role in regulating inflammasome activation and NP cell pyroptosis. The underlying mechanism of autophagy on regulating cell pyroptosis still needs to be investigated.

To test our hypothesis and elucidate the underlying mechanisms, we assessed the relationship between GSDMD-N and autophagy activation based on the detection of NP tissue specimens. We further treated NP cells with lipopolysaccharide (LPS) to establish the cell pyroptosis model and investigated the effects of autophagy intervention on NP cells *in vitro*, as well as in a puncture-induced rat IDD model *in vivo*. Our study revealed that autophagy inhibits the GSDMD-related NP cell pyroptosis and blocks GSDMD-N release via a P62-mediated degradative mechanism. Accordingly, this study helps to better understand the relationship between pyroptosis and autophagy during IDD and may provide a prospective strategy for IDD therapy.

2. Methods and Materials

2.1. Tissue Collection and Ethic Statement. Human NP tissues were obtained from patients that underwent intervertebral fusion surgery due to lumbar fracture or degenerative disc diseases. According to the magnetic resonance (MRI) images of patients, the IDD degree was assessed based on the Pfirrmann MRI-grade system [20]. Usually, Pfirrmann Grade I or II was considered as nondegenerative IVD (NC), and Pfirrmann Grade III, IV, or V belongs to degenerative discs (IDD). The tissue specimens were fixed in 4% formaldehyde and used for histological analysis or frozen stored for protein and RNA analysis. All experimental protocols including medical records, NP tissue collection, and cell interventions were approved by the Ethics Committee of Tongji Medical College, Huazhong University of Science and Technology.

2.2. Cell Culture. NP cells were isolated and cultured as previously described [21]. Briefly, NP tissues were cut into pieces

and enzymatically digested in 0.2% type II collagenase. After filtering and washing with phosphate-buffered saline (PBS), the suspension was centrifuged to collect the sediment. The isolated cells in precipitation were cultured in Dulbecco's modified Eagle medium containing 15% fetal bovine serum (Gibco, USA) and 1% penicillin/streptomycin. The culture medium was replaced twice a week, and cells from the second passage were prepared for use.

2.3. Western Blot. Cell lysates or milled tissues were treated with RIPA lysis buffer (Beyotime, China), and proteins were extracted. The proteins were separated by polyacrylamide gel electrophoresis (SDS-PAGE) and then transferred onto PVDF membranes. The membranes were blocked with 5% skim milk. The primary antibodies used were GSDMD (Proteintech, 1:5000), GSDMD-N (CST, 1:1000), caspase-1 (Proteintech, 1:1000), NLRP3 (Abcam, 1:1000), LC-3 (CST, 1:1000), Beclin-1 (Boster, 1:1000), P62 (Boster, 1:1000), COL2A1 (Proteintech, 1:6000), MMP3 (Proteintech, 1:4000), and GAPDH (Abcam, 1:10000). After incubation with horseradish peroxidase-conjugated secondary antibodies (Boster, China) and washed with Tris-buffered saline tween (TBST) buffer, the bands were visualized and detected using the enhanced chemiluminescence system. The band intensity value of proteins was calculated using ImageJ 1.52a (National Institutes of Health, USA) and normalized to GAPDH.

2.4. Evaluation of Cell Pyroptosis. Pyroptosis of NP cells was evaluated by extracellular lactate dehydrogenase (LDH) level and staining of caspase-1-related cell death. The activity of released LDH was assessed by LDH Activity Assay Kit (Boster, China). To evaluate the double-positive staining of caspase-1 and PI, the Caspase-1 Assay Kit (Immunochemistry Technologies, LCC, USA) was used to detect the caspase-1 activity and cell death. Cell detection and characterization were carried out using the FACSCalibur flow cytometer (BD Biosciences, USA), and data was analyzed by FlowJo X (Tree Star, USA).

2.5. Enzyme-Linked Immunosorbent Assay (ELISA). The NP cell supernatant was collected and centrifuged, and then, the contents of TNF- α , IL-1 β , and IL-6 were analyzed using the corresponding ELISA kit (Elabscience Biotechnology, China) according to the manufacturer's instructions. The experiment was performed in triplicates.

2.6. Immunoprecipitation. Cell lysates were treated with 50 mM Tris-HCl, 150 mM NaCl, 1 mM EDTA, and 1% NP-40 with protease inhibitor cocktail (Beyotime, China). The sample (500 μ g) at 4°C was added with 10 μ L of immunoprecipitation antibody (anti-P62, 1:100, Abcam) and incubated for 8 h at 4°C with magnetic beads (MCE, China). Then, the immunoprecipitates were separated by magnetic adsorption conducted with western blot assays.

2.7. Immunofluorescence Staining. NP cells were fixed with 4% paraformaldehyde and permeabilized with 0.2% Triton X-100. The slides were washed in PBS and blocked with blocking buffer (Beyotime, China) for 1 h. Then, the slides

were incubated with primary antibodies overnight. The primary antibodies used were GSDMD-N (CST, 1:100), P62 (CST, 1:200), and LC-3 (CST, 1:200). Nuclei were stained with DAPI (Beyotime, China) for 5 minutes. Images were captured under a fluorescence microscope (Olympus, BX53; Melville, NY). Fluorescence intensity analysis and colocalization analysis were performed by ImageJ 1.52a.

2.8. Transmission Electron Microscopy (TEM). NP cells were fixed in 2.5% glutaraldehyde for 8 h, then postfixed in 2% osmium tetroxide for 1 h, and stained with 2% uranyl acetate for 1 h. After dehydration in an ascending series of acetone, samples were embedded into Araldite. Samples were cut into ultrathin sections by a slicer (Leica, Germany) and then stained with toluidine blue. The sections were observed under a transmission electron microscope (Tecnai G2 20 TWIN, FEI, USA).

2.9. Knockdown Experiments. Knockdown of ATG5 or P62 in NP cells was carried out by transfection with small interfering RNA (siRNA). Target siRNA and scrambled siRNA (si-scr) were synthesized by RiboBio (Guangzhou, China): ATG5-siRNA sequence 5'-GCUAUAUCAGGAUGAG AUATT-3' and P62-siRNA sequence 5'-GUGUGAAUU UCCUGAAGAATT-3'. The siRNAs were transfected with Lipofectamine 2000 (Invitrogen) in NP cells according to the manufacturer's instructions. Transgenic efficacy in NP cells was detected using quantitative real-time polymerase chain reaction (qRT-PCR) at 48 h after transfection.

2.10. Quantitative Real-Time Polymerase Chain Reaction (qRT-PCR). Total RNA extracted with Trizol reagent (Invitrogen) from NP cells was reverse-transcribed and amplified by qRT-PCR according to the standard protocols. The qRT-PCR was performed to quantify GSDMD, ATG5, or P62 mRNA expression levels. The primer sequences were as follows: Homo GSDMD: forward 5'-GAGCCCAGTGC TCCAGAA-3', reverse 5'-TTGCATGATCTCCAGGT-3'; Homo ATG5: forward 5'-AAAGATGTGCTTCGAGATG TGTGGT-3', reverse 5'-GCAAATAGTATGGTTCTGCTT CCCT-3'; Homo P62: forward 5'-GGCTGATTGAGTCC CTCTCCCAGAT-3', reverse 5'-CGGCGGGGGATGCTTT GAATACTGG-3'; and Homo GAPDH: forward 5'-TCAA GAAGGTGGTGAAGCAGG-3', reverse 5'-TCAAAGGTG GAGGAGTGGGT-3'. GAPDH was used as an internal control for normalization.

2.11. Animal Experiments. Sprague-Dawley rats (SD, 2-month-old, male) purchased from Experimental Animal Center of Tongji Medical College, Huazhong University of Science and Technology, were used for animal experiments. A model of IDD was established by needle puncture as previously described [20, 22, 23]. Briefly, the rats were anaesthetized with 2% (*w/v*) pentobarbital (40 mg/kg). To set the disc degeneration model, the IVD of rats (Co 8/9) was punctured with a 20-gauge needle through the tail skin from the dorsal side. The needle was kept in the disc for 10 s to cause the injury. The length of the needle was predetermined to

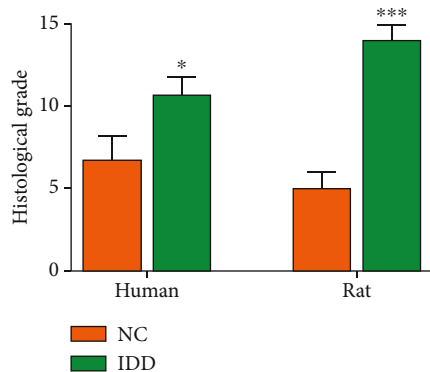
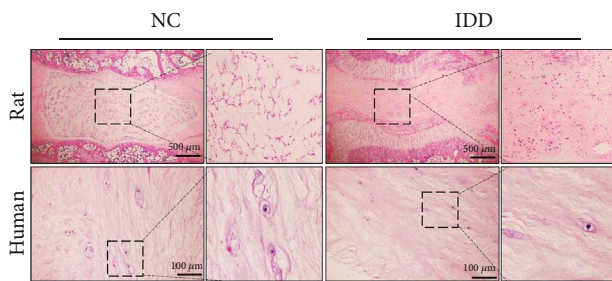
guarantee the puncture depth at approximately 4 mm. The rats were randomly divided into four groups: control group, the group with the puncture of a 33-gauge needle (Hamilton, Benade, Switzerland) as a sham group; IDD group, the group with a 20-gauge needle puncture to induce disc degeneration and with the injection of PBS (2 μ L) using a 33-gauge needle; si-ATG5 group, the group with a 20-gauge needle puncture and with injection of *in vivo* ATG5-siRNA (2 μ L, 20 μ mol/L, RiboBio, China) using a 33-gauge needle; and VX-765 group, the group with a 20-gauge needle puncture and with VX-765 (25 mg/kg) via oral gavage. The injection procedure was conducted biweekly whereas the oral gavage weekly.

2.12. Histological Analysis. The discs were harvested one month after the surgery. These samples were fixed in formaldehyde and then decalcified, dehydrated, and embedded in paraffin. The slides of each disc were stained with hematoxylin-eosin (HE), Alcian blue, and Masson staining. Histological grades of discs were evaluated based on the scoring scale [24]. This scale included 5 categories in assessing disc changes, with 0 points for a normal disc and 15 points for a severely degenerated disc. For immunohistochemistry analysis, the sections were deparaffinized and rehydrated. After blocking with 3% hydrogen peroxide for 10 min and 5% bovine serum albumin for 30 min successively, the sections were incubated with the primary antibodies for 8 h at 4°C. The sections were then incubated with an HRP-conjugated secondary antibody and counterstained with hematoxylin. The images of immunohistochemistry were captured, and the positive cells were analyzed using ImageJ 1.52a.

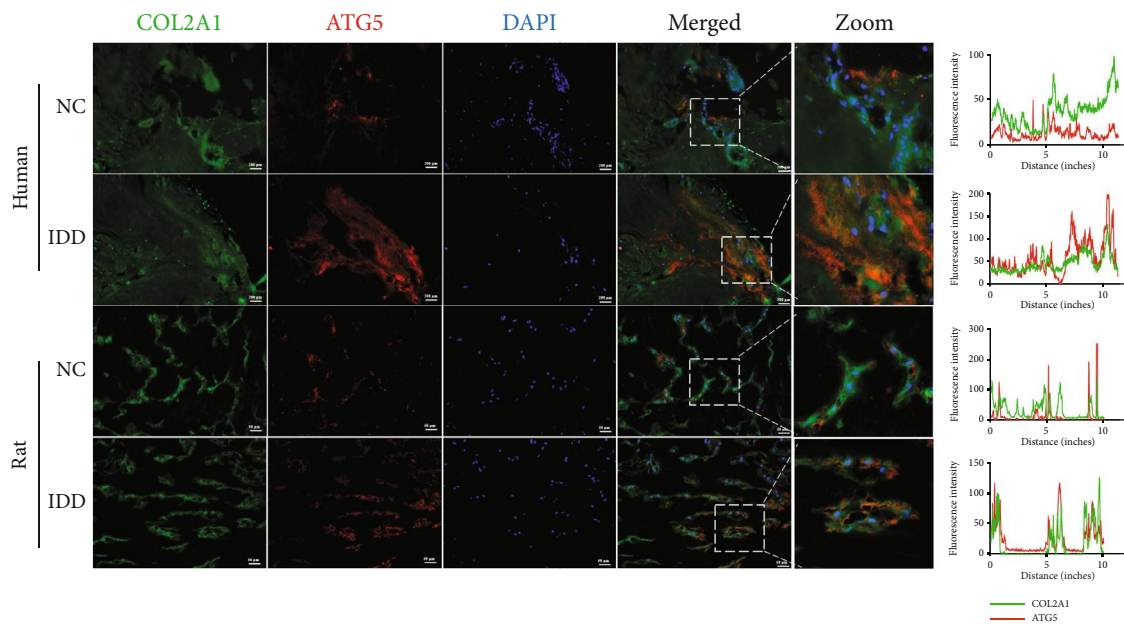
2.13. Statistical Analysis. Data are presented as means \pm standard deviation (SD). Student's *t*-test and one-way or two-way analysis of variance (ANOVA) with Tukey's *post hoc* test were performed to assess the differences of changes between groups. Statistical significance ($*P < 0.05$; $**P < 0.01$; $***P < 0.001$; $P > 0.05$, ns, no significant difference) was calculated using GraphPad Prism 8 (La Jolla, CA, USA).

3. Results

3.1. Detection of Autophagy and Pyroptosis Level in Human and Rat Intervertebral Discs. Histological staining was performed to assess the IDD degree of human and rat normal and degenerative discs. The corresponding histological grades based on tissue morphology and cellularity indicated a higher IDD score in both human and rat IDD groups (Figure 1(a)). The expression levels of autophagy-initiated protein ATG5, the pyroptosis executor GSDMD-N, and the extracellular matrix (ECM) component type II collagen (COL2A1) were detected by immunofluorescence staining (Figures 1(b) and 1(c)). The results showed that higher levels of ATG5 and GSDMD-N were found in degenerative disc tissues (Figures 1(d) and 1(e)). Moreover, protein levels of LC3, ATG5, GSDMD-N, COL2A1, and matrix degradative enzyme, MMP3, were measured by western blot in human IVD tissues (Figure 1(f)). The levels of LC3, ATG5, and GSDMD-N were all increased significantly in the IDD group



(a)



(b)

FIGURE 1: Continued.

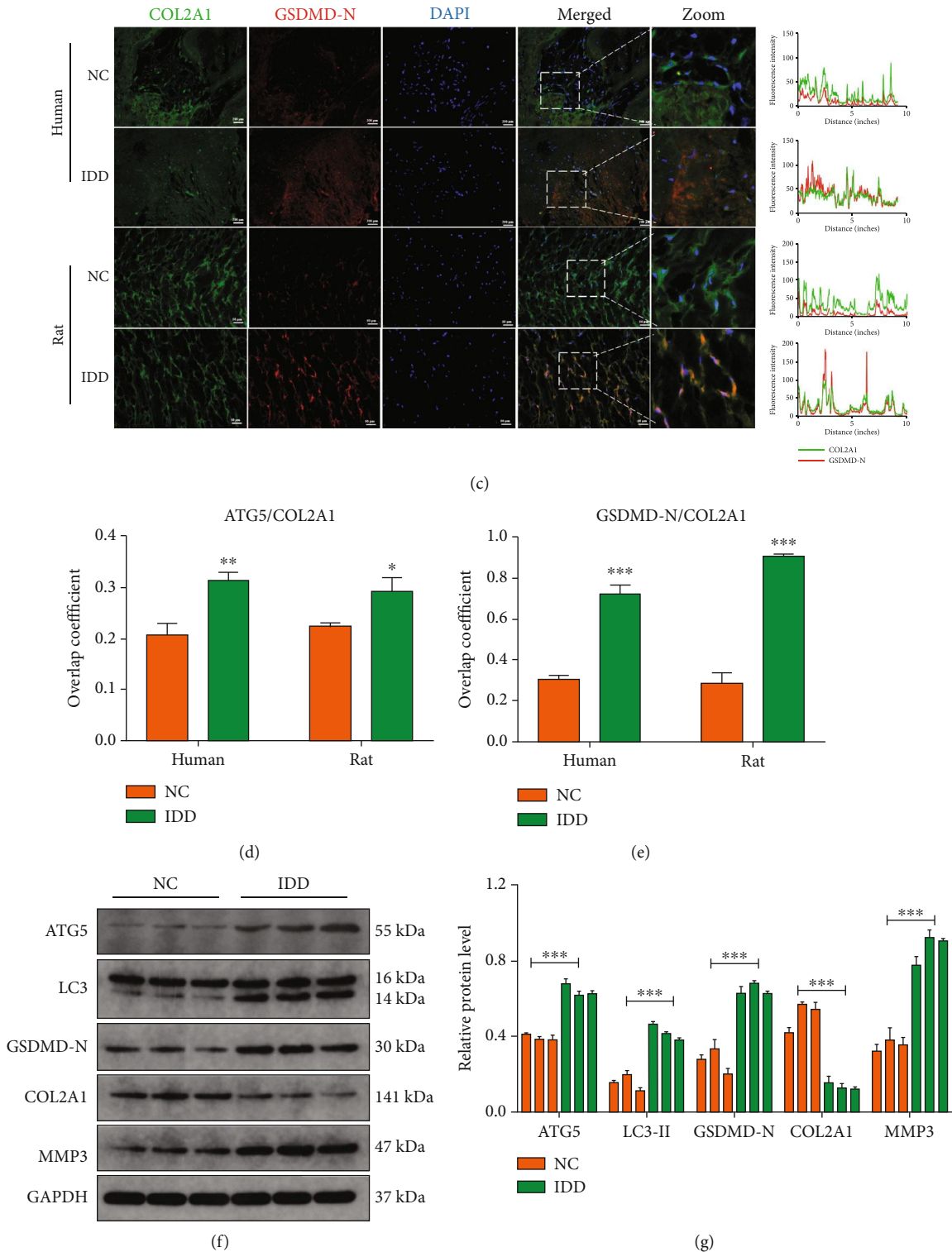


FIGURE 1: Histological staining results of human and rat intervertebral discs. (a) HE staining showed the morphology of rat discs and human NP tissues (upper panel), and histological grades were calculated based on HE staining (lower panel). (b) Immunofluorescence analysis of ATG5 (red) and type collagen II (green) in rat and human NP tissues. Corresponding fluorescence intensity analysis is listed in the right panel. Scale bar, 50 μ m. (c) Immunofluorescence analysis of GSDMD-N (red) and type collagen II (green) in rat and human NP tissues (left panel) and fluorescence intensity results (right panel). Overlap coefficient based on immunofluorescence results showed the colocalization relationship of (d) ATG5 and COL2A1 or (e) GSDMD-N and COL2A1. (f) Western blot analysis of ATG5, LC3, GSDMD-N, COL2A1, and MMP3 in human nondegenerative and degenerative NP tissues and (g) corresponding quantification of protein levels. NC: nondegenerative discs; IDD: degenerative discs. GAPDH was used as an internal control. Data were presented as the means \pm SD, $n = 3$. * $P < 0.05$, ** $P < 0.01$, and *** $P < 0.001$ vs. the NC group.

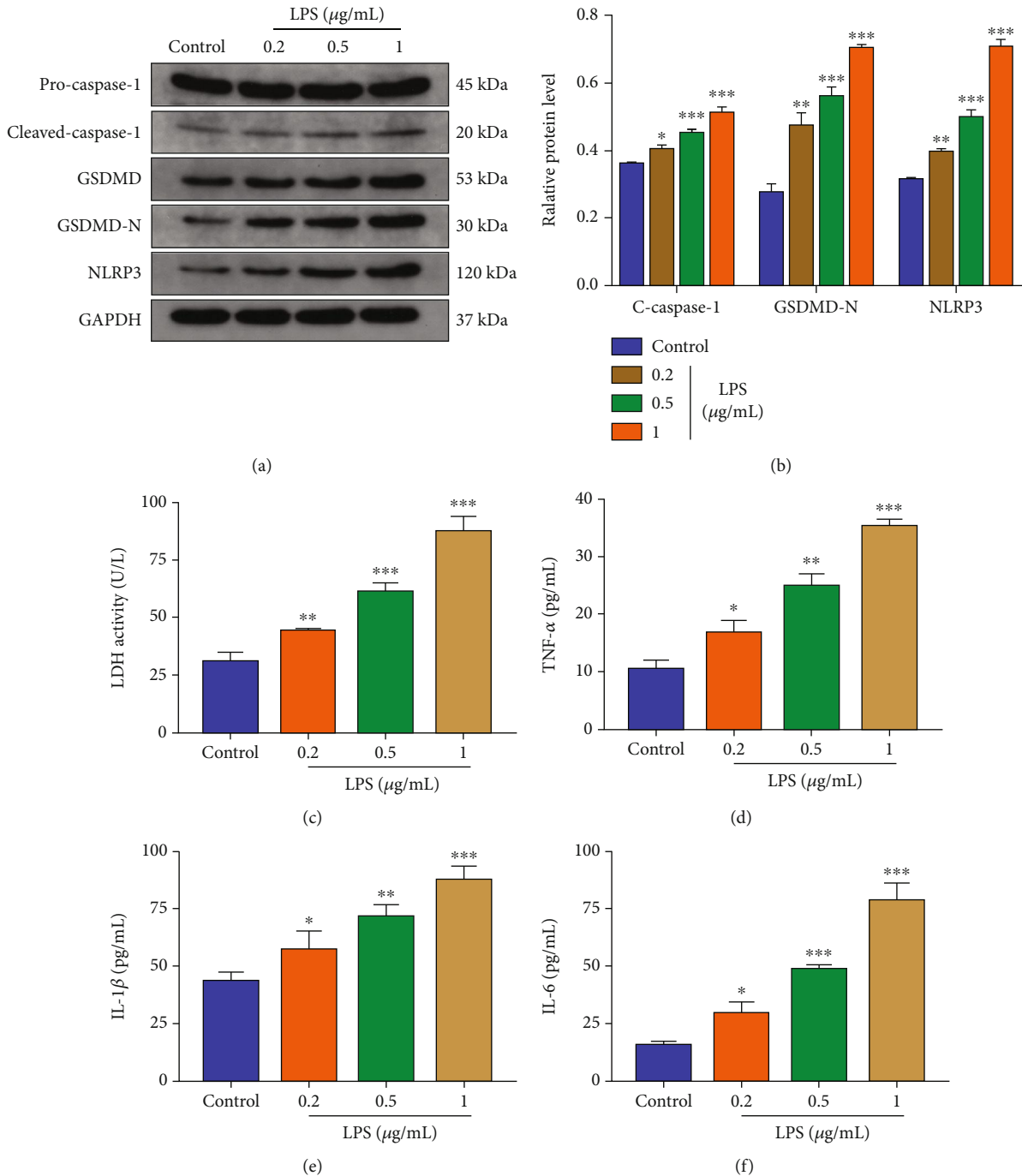


FIGURE 2: LPS induced NP cell pyroptosis in vitro in a dose-dependent manner. (a) Western blot analysis of pro-caspase-1, cleaved caspase-1, GSDMD, GSDMD-N, and NLRP3 in NP cells treated with LPS (0.2 µg/mL, 0.5 µg/mL, and 1 µg/mL) for 24 h. The control group was treated with equivalent solvent. (b) Quantification of cleaved caspase-1, GSDMD-N, and NLRP3 protein levels. GAPDH was used as an internal control. (c) Measurement of LDH activity in LPS-treated NP cells. ELISA analyzed the levels of secreted (d) TNF-α, (e) IL-1β, and (f) IL-6 in LPS-treated NP cells. Data were presented as the means ± SD, $n = 3$. * $P < 0.05$, ** $P < 0.01$, and *** $P < 0.001$ vs. the control group.

(Figure 1(g)). These results suggested that autophagy activity and pyroptosis levels were both increased in the degenerative disc tissues.

3.2. Evaluation of GSDMD-Mediated Pyroptosis in LPS-Treated NP Cells In Vitro. NP cells were treated with LPS, a typical pyroptotic phenotype inducer, and related proteins

of cell pyroptosis were evaluated (Figure 2(a)). The results indicated that LPS induced the expression of GSDMD-N, cleaved caspase-1 (c-caspase1), and NLRP3 in NP cells in a dose-dependent manner (Figure 2(b)). Besides, it was confirmed that GSDMD-N produced plasma membrane pores and extracellular LDH level was elevated simultaneously [6]. Extracellular LDH measured by an ELISA kit was

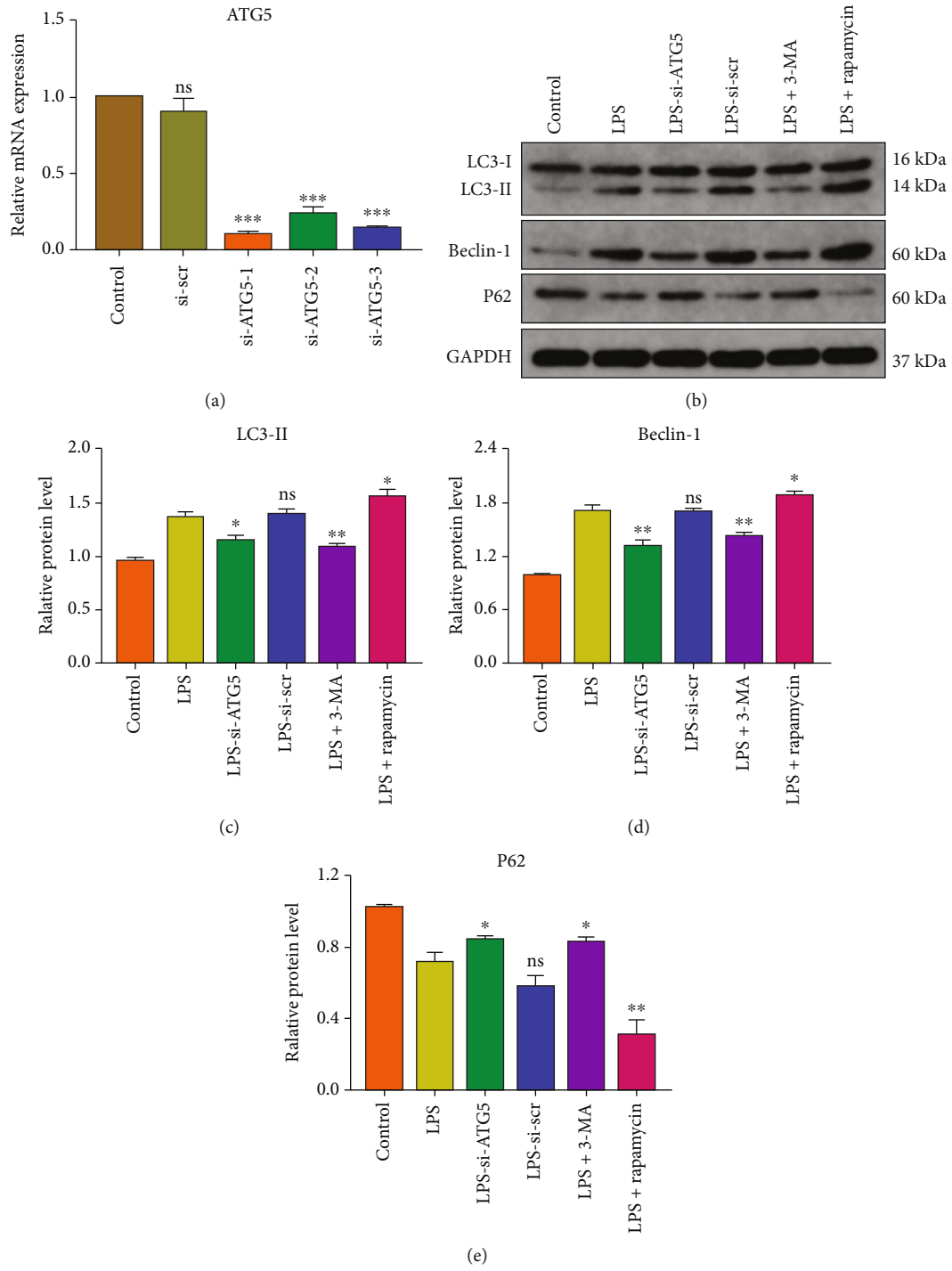


FIGURE 3: Continued.

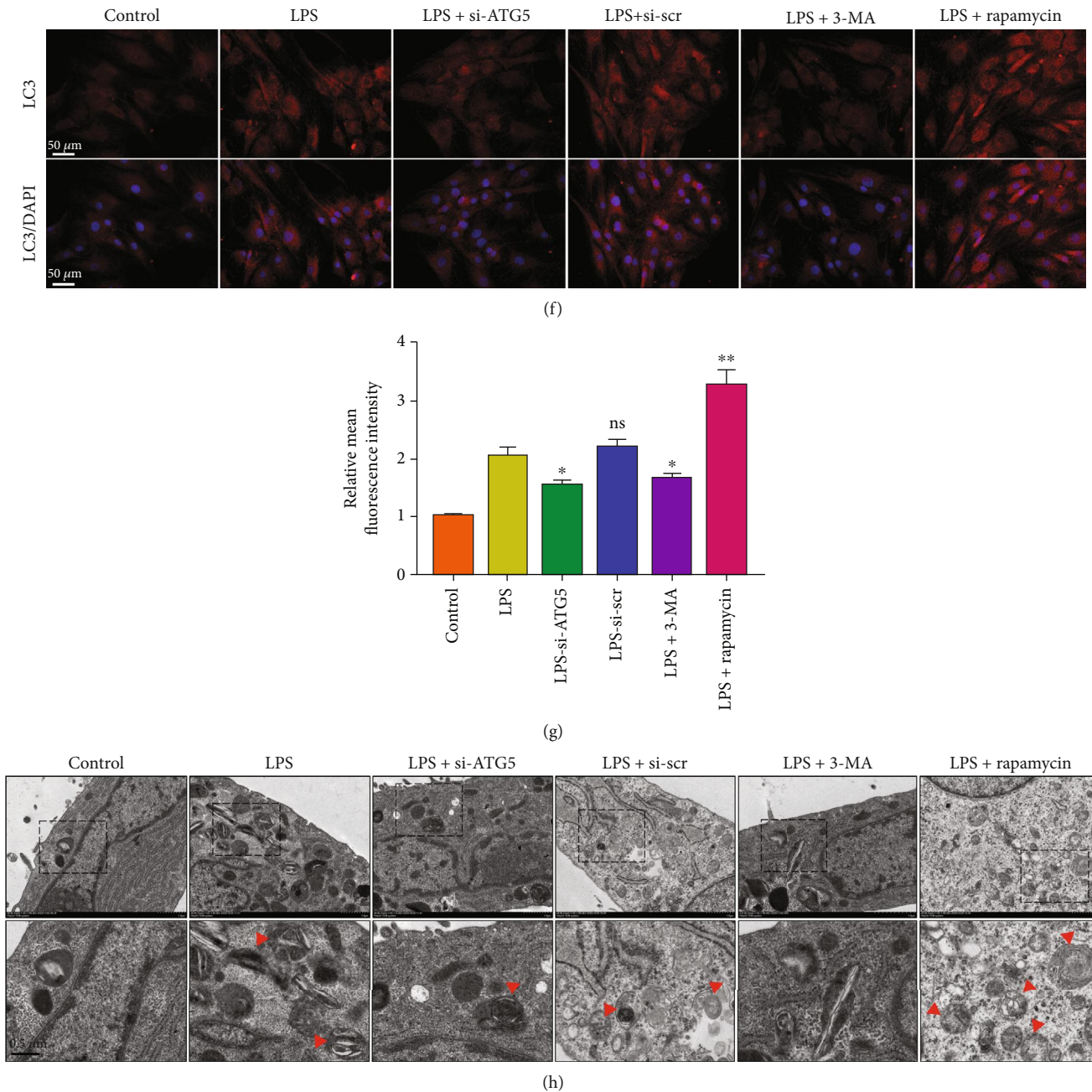


FIGURE 3: Detection of autophagy activity in NP cells in vitro. (a) The mRNA level of ATG5 in ATG5 siRNA-treated NP cells was analyzed by qRT-PCR. si-ATG5-1 was used in the following experiments. *** $P < 0.001$ vs. the control group; ns, $P > 0.05$, no significant difference. (b) Western blot analysis of LC3, Beclin-1, and P62. LPS-treated ($1 \mu\text{g}/\text{mL}$, 24 h) NP cells were cotreated with 3-MA (10 mM, 24 h) or rapamycin ($1 \mu\text{M}$, 24 h). Quantification of (c) LC3-II, (d) Beclin-1, and (e) P62 protein levels. GAPDH was used as an internal control. (f) Immunofluorescence analysis showed the expression level of LC3 and (g) relative mean fluorescence was calculated. Data were presented as the means \pm SD, $n = 3$. * $P < 0.05$ and ** $P < 0.01$ vs. the LPS group; ns, $P > 0.05$, no significant difference. (h) TEM images of NP cells indicated the number and morphology of autophagosomes (red arrowheads).

increased in LPS-treated NP cells (Figure 2(c)). The secretion of inflammatory cytokines TNF- α , IL-1 β , and IL-6 were also increased significantly upon LPS treatment (Figures 2(d)–2(f)). These results showed that LPS promoted the cleavage of GSDMD and induced the pyroptotic phenotype in NP cells in a dose-dependent manner.

3.3. Modulation of Autophagy Activity Affects the Outcome of Pyroptotic NP Cell Death. The effects of autophagy on NP cell pyroptosis were assessed by ATG5 knockdown to inhibit autophagosome formation. The knockdown efficiency was analyzed at the mRNA level (Figure 3(a)). The autophagy inhibitor 3-MA and autophagy inducer rapamycin were

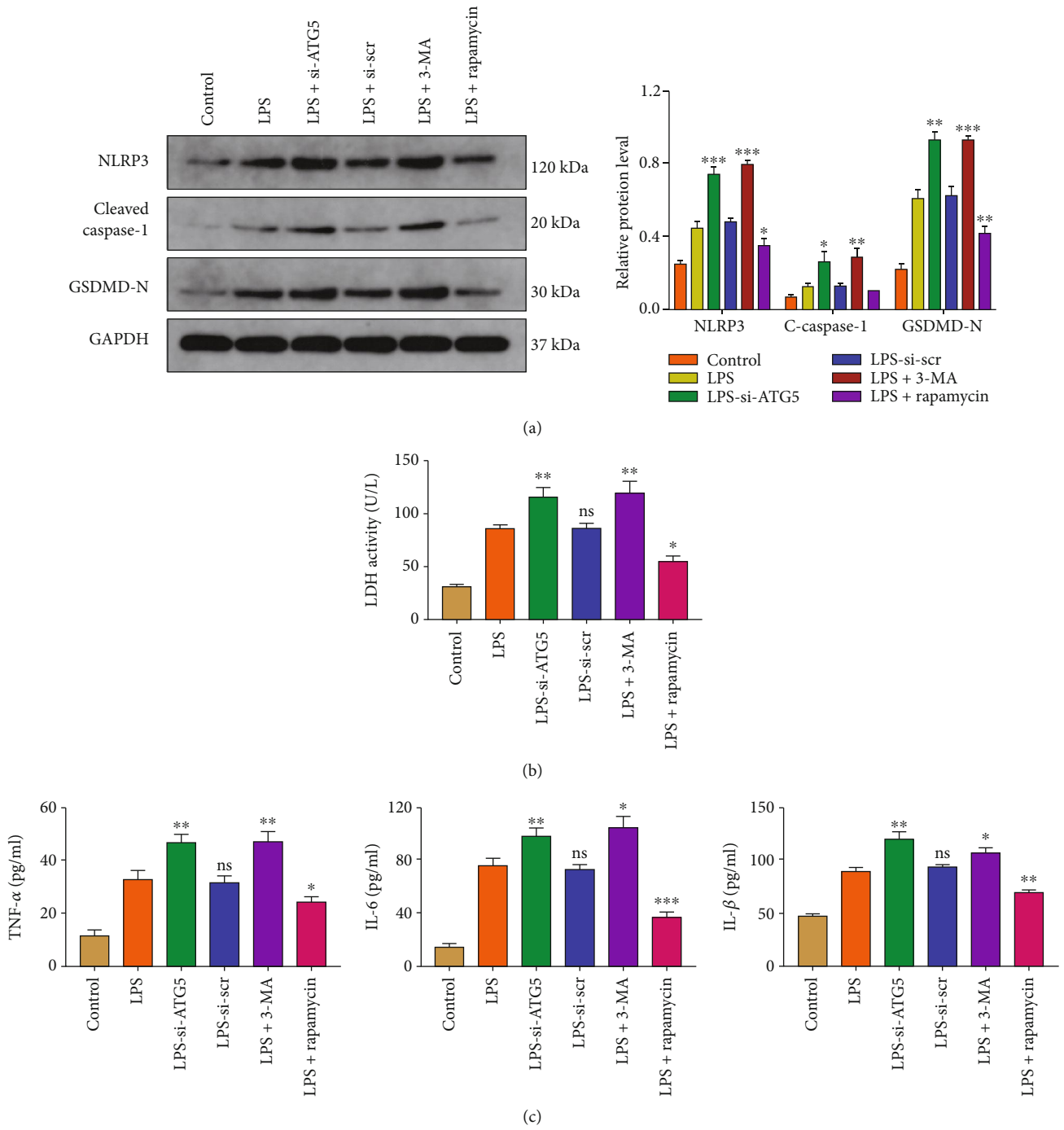
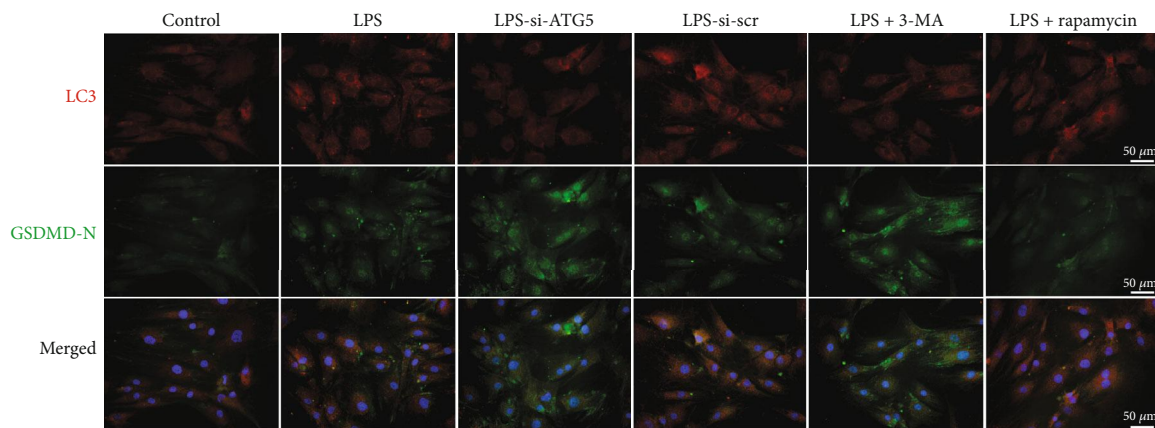
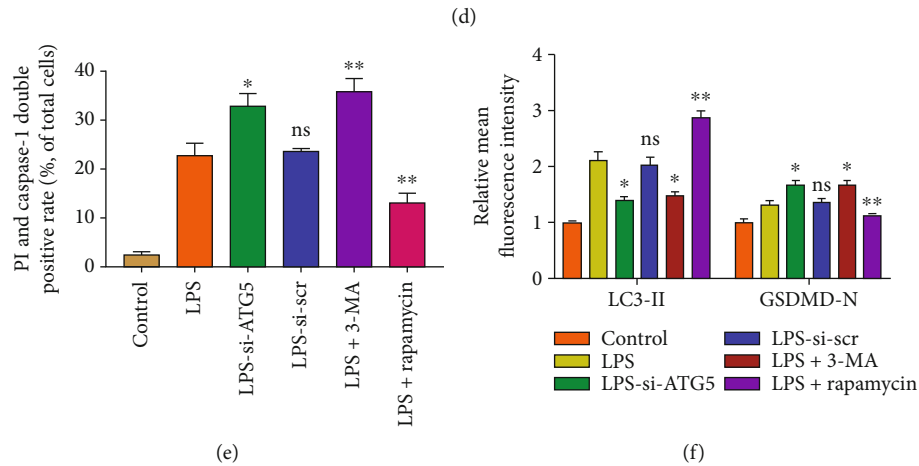
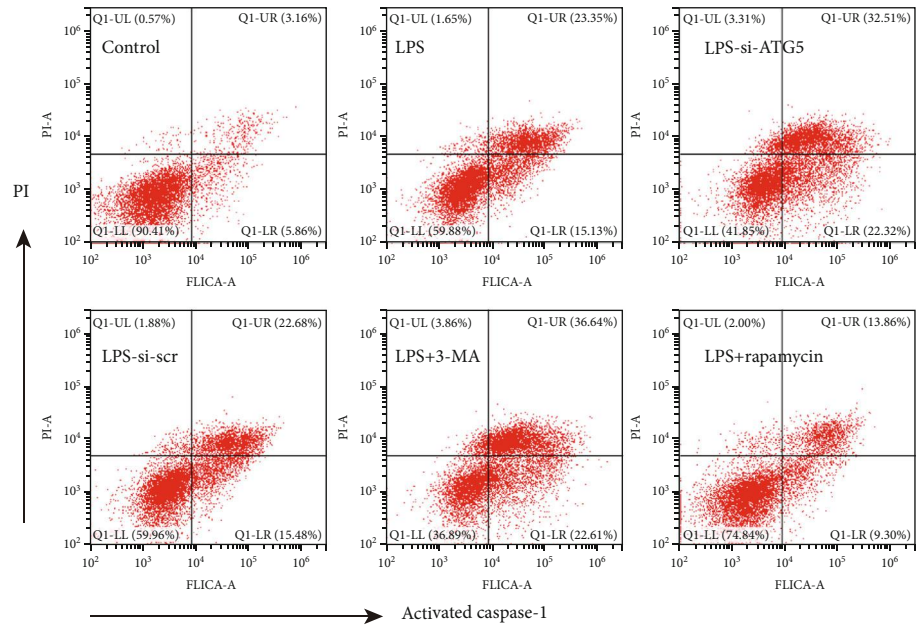


FIGURE 4: Continued.



(g)

FIGURE 4: Impaired autophagy activity aggravated LPS-induced NP cell pyroptosis in vitro. (a) Western blot analysis and quantification of NLRP3, cleaved caspase-1, and GSDMD-N protein levels. GAPDH was used as an internal control. (b) Measurement of extracellular LDH activity in NP cells. (c) ELISA analysis assessed the levels of secreted TNF- α , IL-1 β , and IL-6. (d) Flow cytometry analyzed the pyroptotic cells, which were double positive of activated caspase-1 and PI. (e) The rate of double-positive cells was calculated. (g) Double immunofluorescence analysis showed the expression level of LC3 (red) and GSDMD-N (green). Scale bar, 50 μ m. (f) The relative mean fluorescence in each group was calculated. Data were presented as the means \pm SD, $n = 3$. * $P < 0.05$, ** $P < 0.01$, and *** $P < 0.001$ vs. the corresponding LPS group; ns, $P > 0.05$, no significant difference.

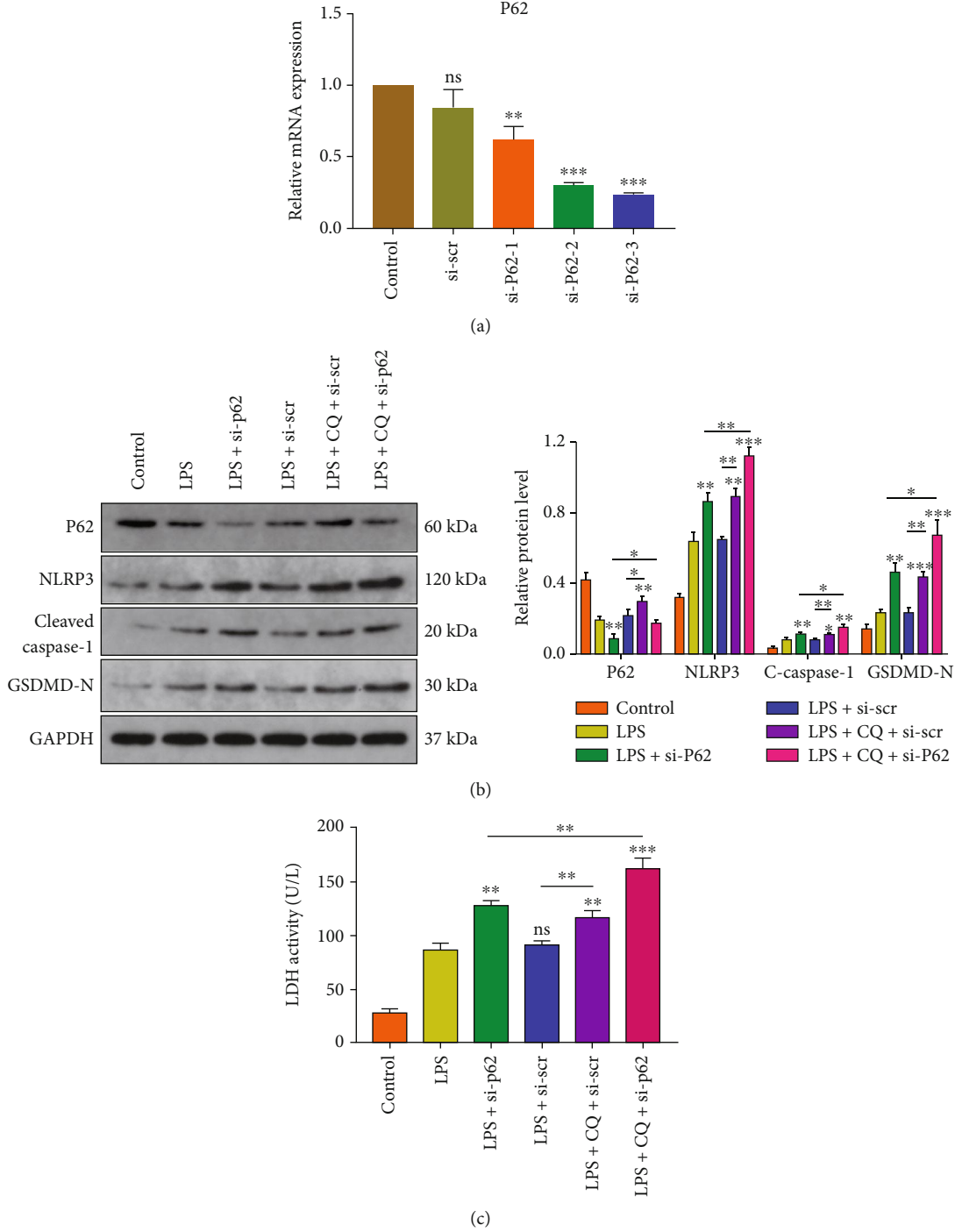
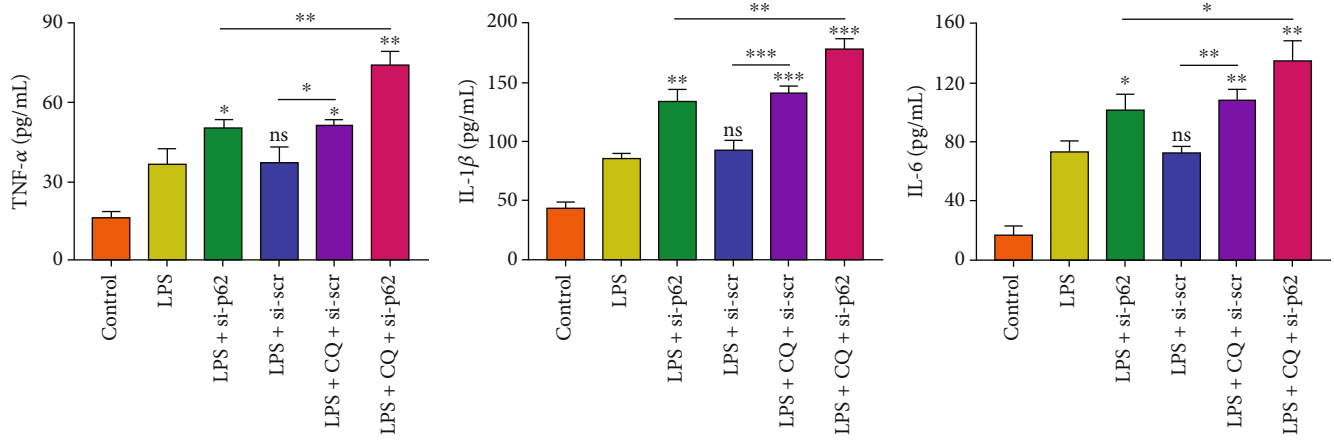
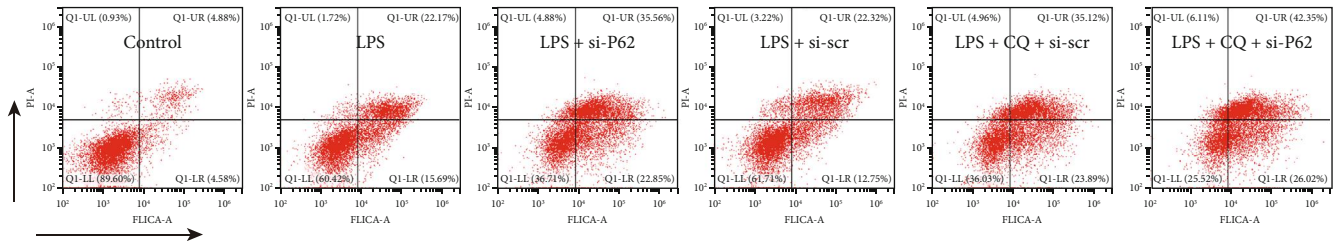


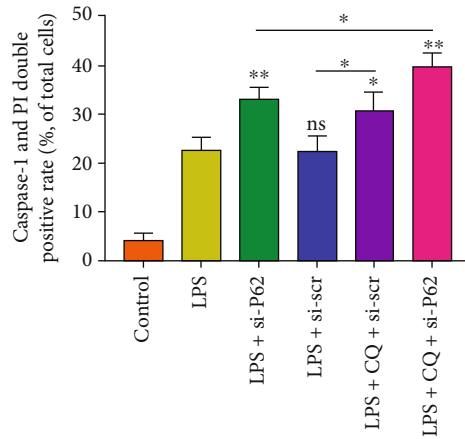
FIGURE 5: Continued.



(d)

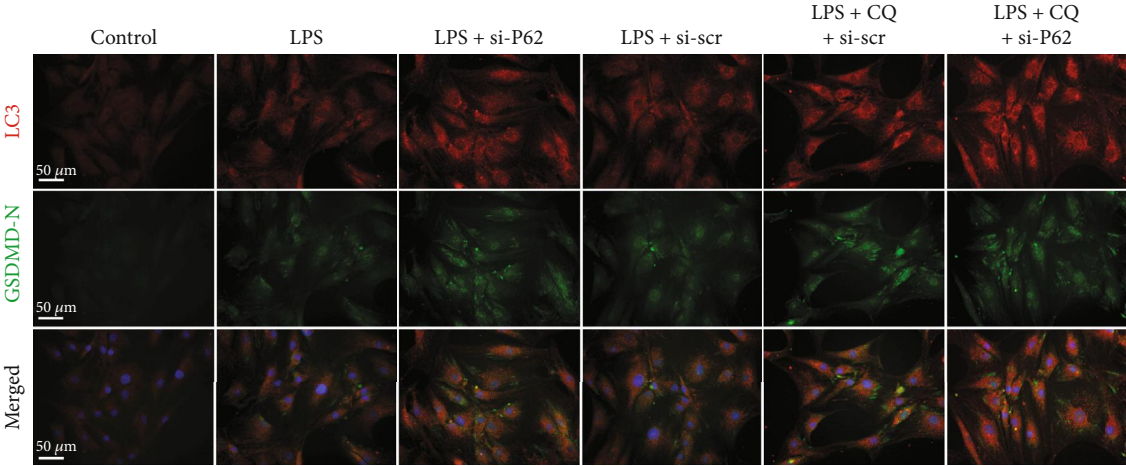


(e)

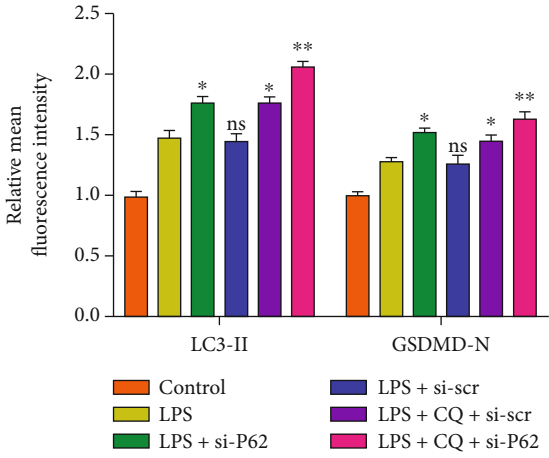


(f)

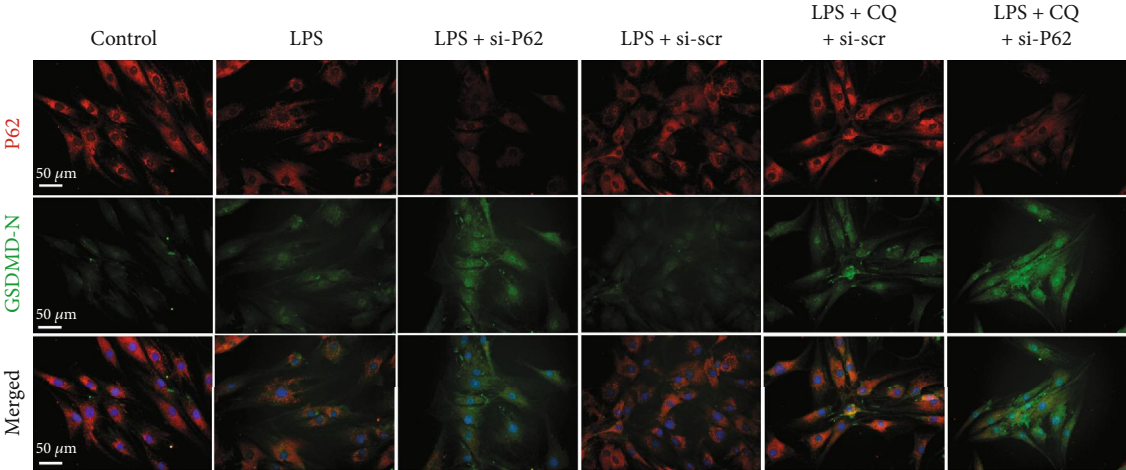
FIGURE 5: Continued.



(g)



(h)



(i)

FIGURE 5: Continued.

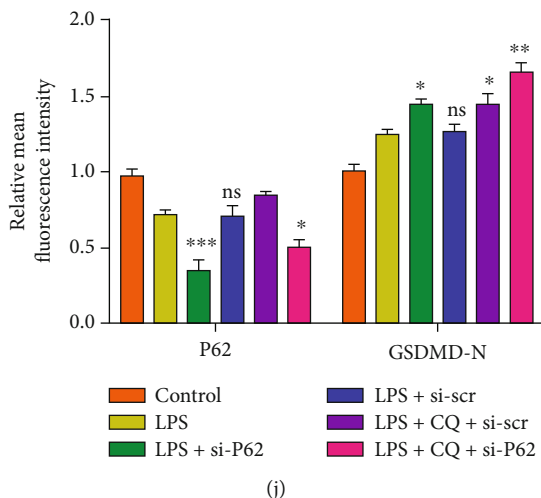


FIGURE 5: Dysfunction of the autophagy-lysosome pathway promoted the accumulation of cytoplasmic GSDMD-N. (a) The mRNA level of P62 was analyzed by qRT-PCR, and si-P62-3 was selected in the following experiments. $**P < 0.01$ and $***P < 0.001$ vs. the control group; ns, $P > 0.05$, no significant difference. (b) Western blot analysis and quantification of P62, NLRP3, cleaved caspase-1, and GSDMD-N. (c) Measurement of extracellular LDH activity. (d) ELISA analyzed the levels of secreted TNF- α , IL-1 β , and IL-6. (e) Flow cytometry analyzed the double-positive cell of activated caspase-1 and PI and (f) calculated the rate of double-positive cells. (g) Immunofluorescence analysis of LC3 (red) and GSDMD-N (green) and (h) the relative mean fluorescence in each group was calculated. (i) Immunofluorescence analysis of P62 (red) and GSDMD-N (green) and (j) the relative mean fluorescence in each group was calculated. Scale bar, 50 μ m. Data were presented as the means \pm SD, $n = 3$. $*P < 0.05$, $**P < 0.01$, and $***P < 0.001$ vs. the corresponding LPS group; ns, $P > 0.05$, no significant difference.

used, and the expression levels of autophagy markers LC3-II, Beclin-1, and P62 were assessed by western blotting (Figures 3(b)–3(e)). Immunofluorescence analysis of LC3-II also revealed the number of autophagosomes (Figures 3(f) and 3(g)). TEM images indicated the number and morphology of autophagosomes in different groups (Figure 3(h)). On the other hand, the expression levels of pyroptosis-associated proteins were measured in NP cells (Figure 4(a)). The GSDMD-N, NLRP3, and c-caspase1 expression levels were increased by ATG5 siRNA or 3-MA treatment but reduced by rapamycin treatment. These profiles were consistent with the activity of released LDH and the secretion of inflammatory cytokines (Figures 4(b) and 4(c)). To further assess the NP cell pyroptosis, the cell rates of activated caspase-1 and PI double-positive were analyzed by flow cytometry (Figures 4(d) and 4(e)). Besides, immunofluorescence analysis of GSDMD-N indicated the NP cell pyroptosis in different groups (Figures 4(f) and 4(g)). These results indicated that autophagy inhibition aggravated the LPS-induced NP cell pyroptosis, and autophagy activation ameliorated cell pyroptosis.

3.4. Autophagy Mediates NP Cell Pyroptosis via a Degradation Mechanism of GSDMD-N. The autophagy-lysosome degradation pathway is indispensable for controlling cellular protein quality [25]. Cytoplasmic damaged proteins are selected and mediated by specific receptors, such as P62/SQSTM1, which regulates selective degradation via autophagy [26]; however, the role of the autophagy-lysosome pathway in pyroptosis is still unclear. Knockdown of P62 was realized by siRNA, and the efficiency was analyzed accordingly (Figure 5(a)). Chloroquine (CQ) was used to

inhibit lysosome function in LPS-treated NP cells. Both si-P62 and CQ treatment increased the expression levels of NLRP3, c-caspase1, and GSDMD-N (Figure 5(b)), results that were in agreement with the activity of released LDH and the secretion of inflammatory cytokines (Figures 5(c) and 5(d)). The rate of pyroptotic cell death was higher in the si-P62 and CQ group than in the control group (Figure 5(e)). Moreover, cotreated si-P62 and CQ in NP cells showed a markedly higher cell pyroptosis rate (Figure 5(f)). Immunofluorescence analysis of LC3 and P62 reflected the dynamic changes of autophagy flux in NP cells (Figures 5(g) and 5(i)). Besides, impaired lysosome function significantly increased the level of cytoplasmic GSDMD-N (Figures 5(h) and 5(j)). These results indicated that autophagy regulated the degradation of GSDMD-N and blockage of the autophagy-lysosome pathway increased the accumulation of cellular GSDMD-N.

3.5. P62-Mediated Selective Degradation of GSDMD-N during NP Cell Pyroptosis. To further confirm the role of P62/SQSTM1 as an autophagy receptor in GSDMD-N degradation, immunoprecipitation analysis was performed to assess the integration of P62 and GSDMD-N (Figure 6(a)). Immunofluorescence results also indicated the colocalization between P62 and GSDMD-N (Figure 6(b)). The protein level of GSDMD-N in the si-ATG5 group was higher than in NP cells treating with si-scr (si-scr group), while the level of GSDMD mRNA was not significantly different between the two groups (Figure 6(c)). Colocalization analysis showed a decreased overlap coefficient in the si-ATG5 group, indicating that autophagy activity could influence the colocalization between P62 and GSDMD-N (Figure 6(d)). To further

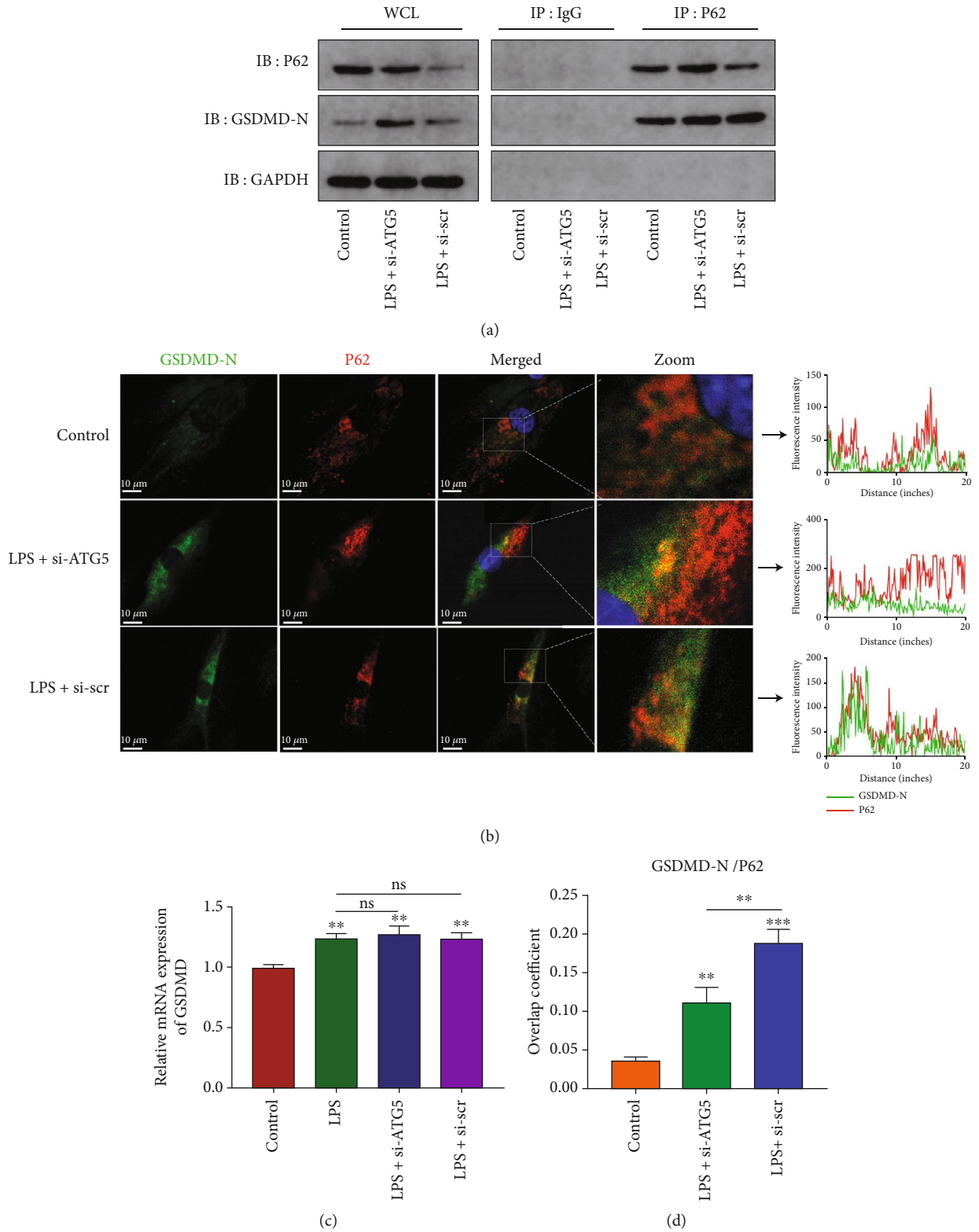


FIGURE 6: Continued.

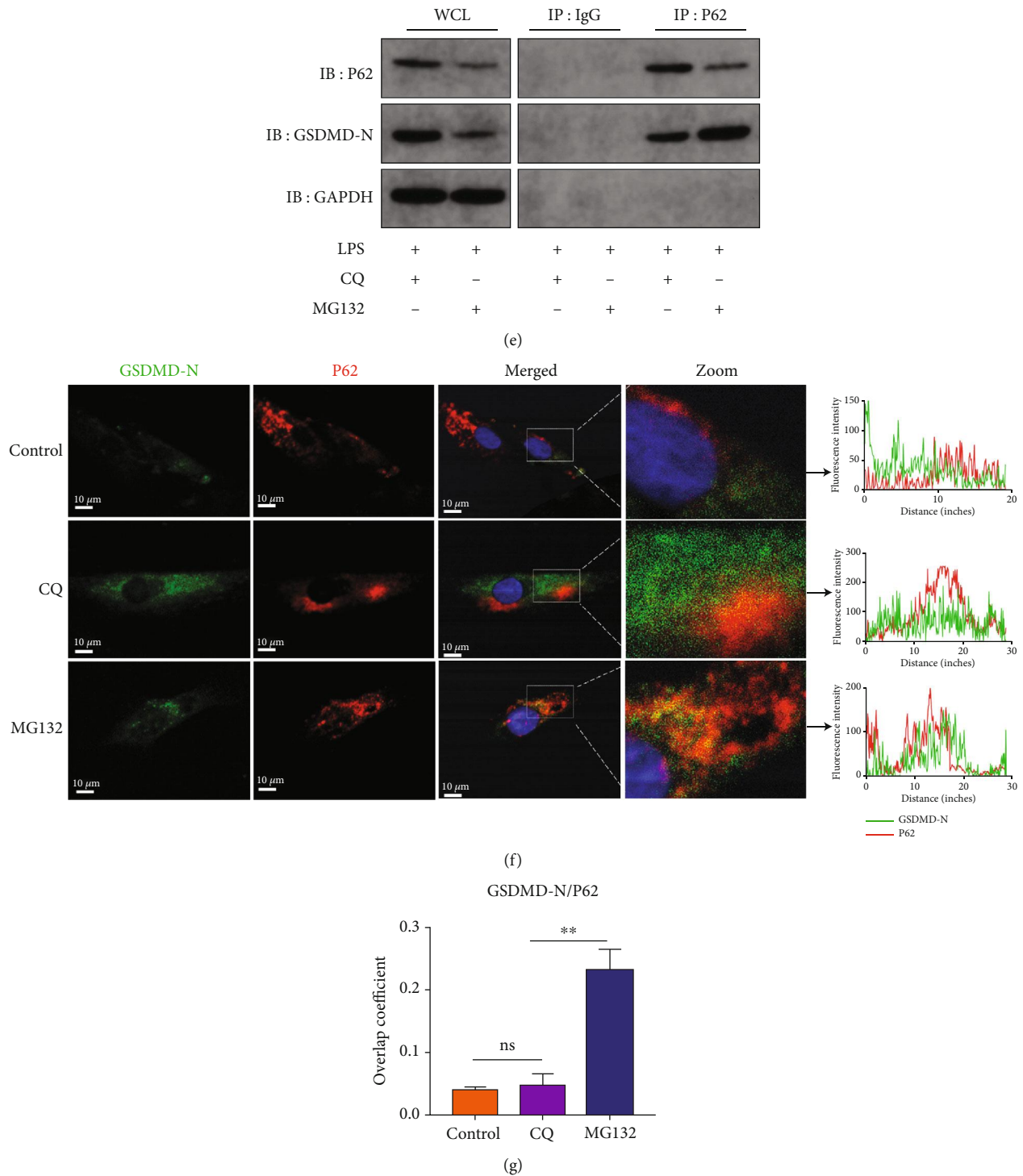
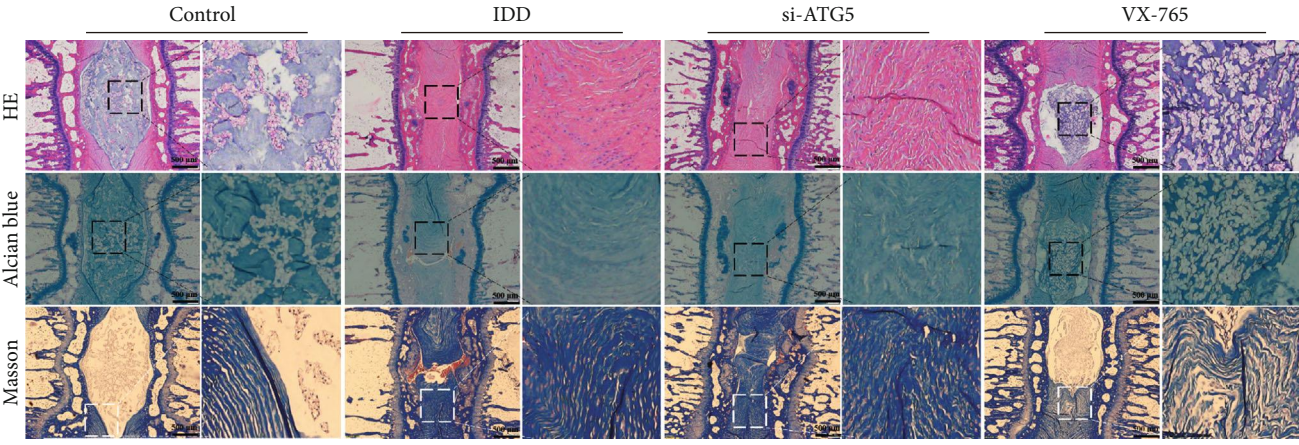
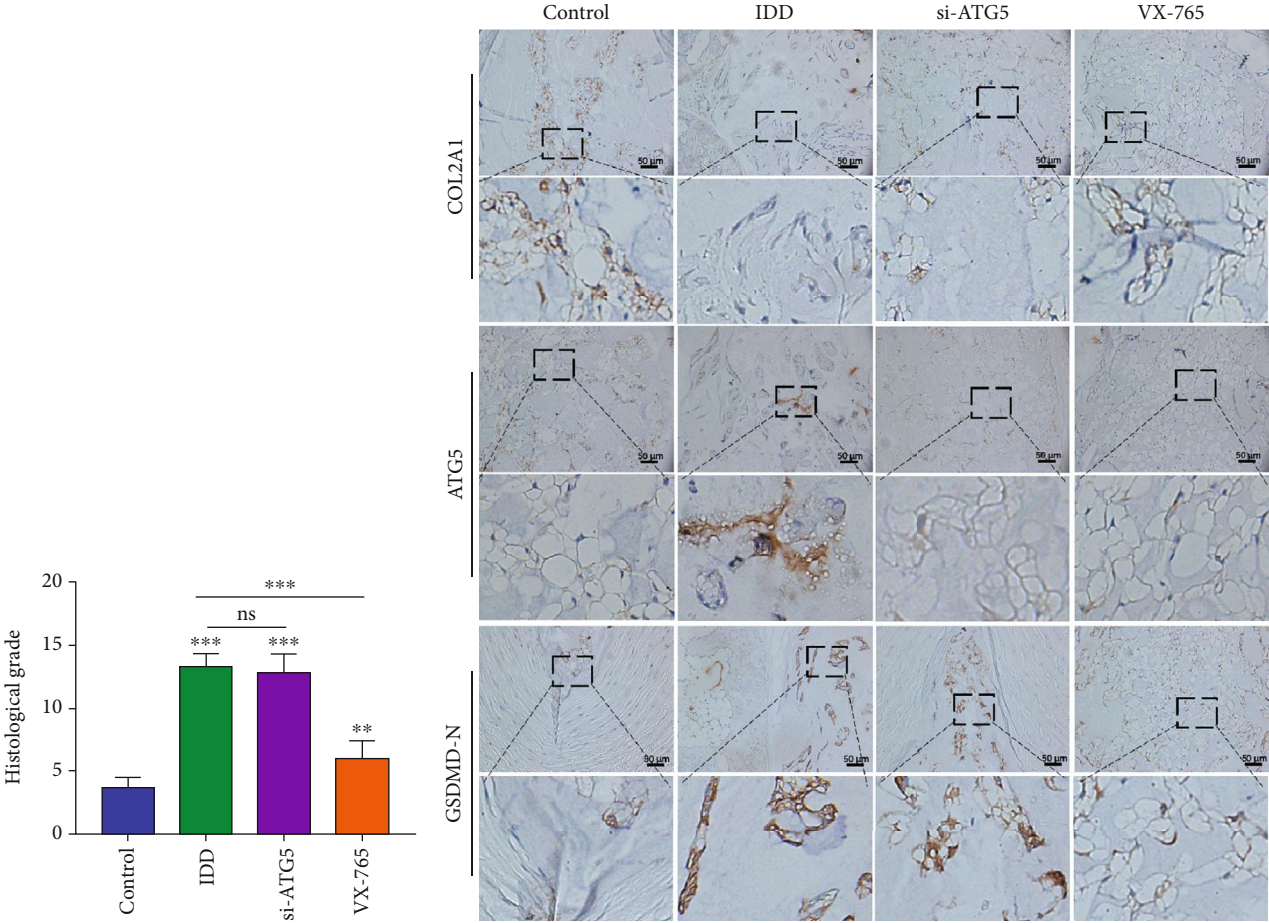


FIGURE 6: P62 mediated GSDMD-N degradation via an autophagy-lysosome pathway. (a) Immunoprecipitation for P62 was conducted to detect the integration of P62 and GSDMD-N. IgG was as a negative control. WCL: whole cell lysate. (b) Confocal images of GSDMD-N (green) and P62 (red) and fluorescence intensity results (right panel). (c) The mRNA level of GSDMD was analyzed by qRT-PCR. $**P < 0.01$ vs. the control group; ns, $P > 0.05$, no significant difference. (d) Overlap coefficient based on immunofluorescence images showed the colocalization relationship of GSDMD-N and P62. $**P < 0.01$ and $***P < 0.001$ vs. the control group. (e) Immunoprecipitation for P62 was conducted to detect the integration of P62 and GSDMD-N in CQ (20 μ M, 24 h) or MG132 (10 μ M, 24 h) treated NP cells under LPS stimulation. (f) Confocal images of GSDMD-N (green) and P62 (red) and fluorescence intensity measurement (right panel). (g) Overlap coefficient analyzed the colocalization of GSDMD-N and P62. $**P < 0.01$ vs. the CQ group. Data were presented as the means \pm SD, $n = 3$.



(a)



(c)

FIGURE 7: Continued.

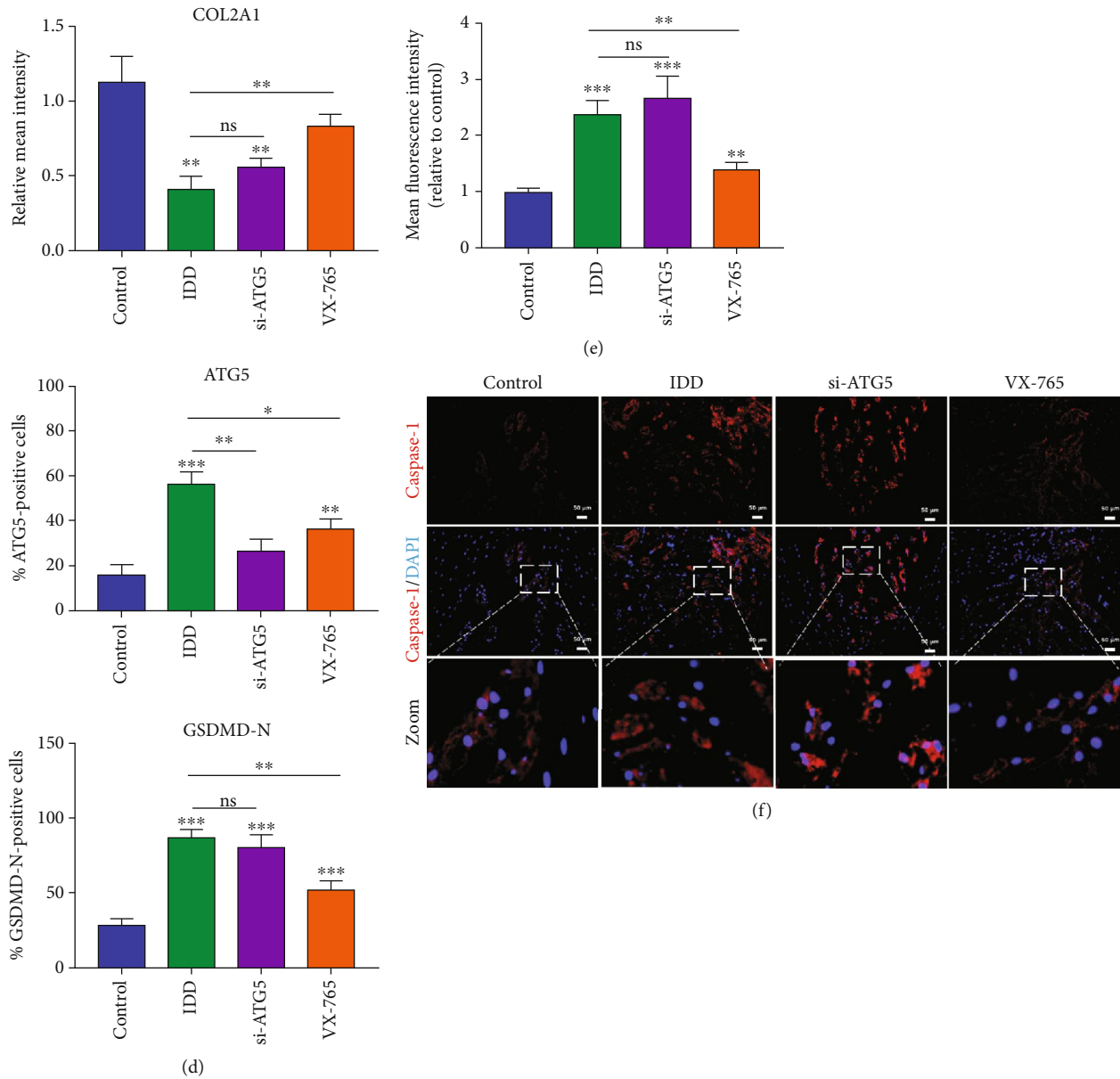


FIGURE 7: Administration of VX-765 ameliorated the progression of IDD in vivo. (a) Histological staining, including HE, Alcian blue, and Masson staining, showed the morphology of rat intervertebral disc. The IDD, si-ATG5, and VX-765 groups were treated with needle puncture, while the control group is an untreated group. (b) Histological grades were calculated based on the histological staining results. (c) Immunohistochemistry staining for COL2A1, ATG5, and GSDMD-N was conducted to evaluate the expression level of proteins in tissues. (d) Quantification of COL2A1, ATG5, and GSDMD-N in immunohistochemistry staining. (e) Immunofluorescence staining of caspase-1 and (f) quantification results of the caspase-1 mean fluorescence intensity. ** $P < 0.01$ and *** $P < 0.001$ vs. the control group; ns, $P > 0.05$, no significant difference. Data were presented as the means \pm SD, $n = 5$.

investigate the degradation mechanism of GSDMD-N, CQ (lysosome pathway inhibitor) and MG132 (proteasome pathway inhibitor) were used in LPS-treated NP cells. Immunoprecipitation and immunofluorescence analysis showed the colocalization between P62 and GSDMD-N in the CQ or MG132 group (Figures 6(e) and 6(f)). CQ-induced lysosome dysfunction resulted in the accumulation of cytoplasmic P62 and decreased the integration between P62 and GSDMD-N, while MG132 showed a nonsignificant effect (Figure 6(g)). These results demonstrated that autophagy regulates GSDMD-N protein levels in P62-mediated selective degrada-

tion, which depends on the functional lysosome pathway and not the proteasome pathway.

3.6. Administration of VX-765 Retards IDD Progression In Vivo. To further investigate the role of autophagy and pyroptosis in IDD, a rat disc IDD model was designed and conducted by needle puncture. VX-765, a caspase-1 inhibitor, which could efficiently decrease cell pyroptosis, was used in our animal model [27]. Degenerative NP tissues were marked by loss of ECM proteins and replaced by fibrous tissues. Alcian blue and Masson staining showed decreased contents

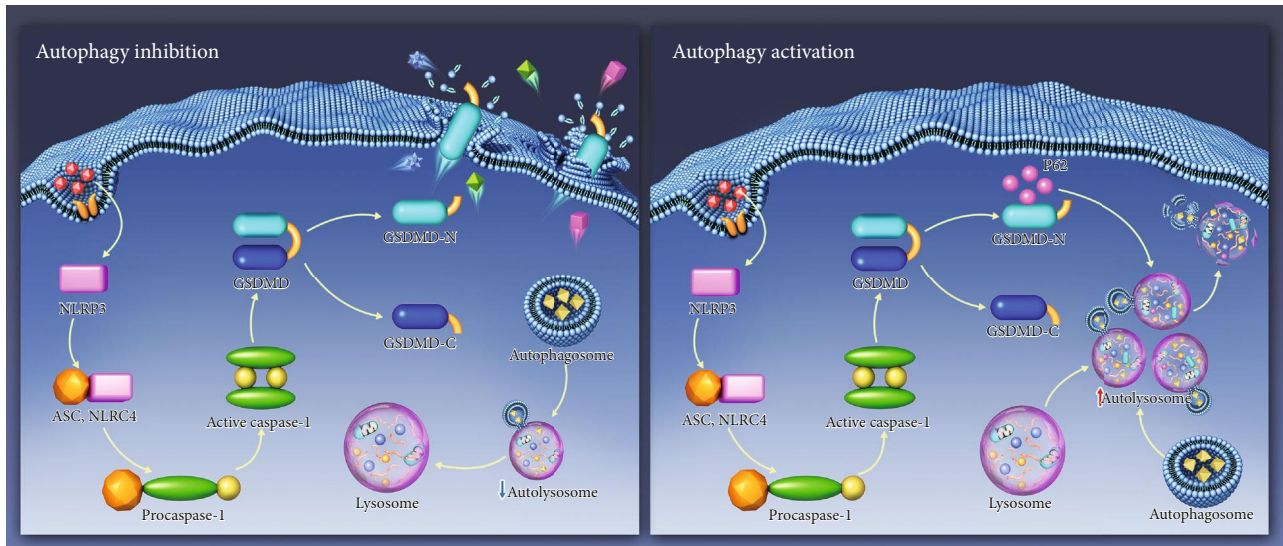


FIGURE 8: Schematic model illustrating the autophagy regulative mechanism of GSDMD-mediated pyroptosis. Autophagy inhibition promotes the accumulation of cytoplasmic GSDMD-N and elicits cell membrane perforation (a). Upon autophagy activation, P62 mediates the degradation of GSDMD-N in autolysosome and reduces the cell pyroptosis (b). NLRP3: NLR family PYRIN domain-containing 3; ASC: apoptosis-associated speck-like protein containing a CARD; NLRC4: NLR family CARD domain-containing protein 4; GSDMD: gasdermin D; GSDMD-N: N-terminal of gasdermin D; GSDMD-C: C-terminal of gasdermin D; P62: SQSTM1/sequestosome 1.

of aggrecan but increased fibrous tissues in the IDD and ATG5 knockdown groups (Figure 7(a)). The histological grade of the VX-765 group was markedly lower than that of the IDD group (Figure 7(b)), indicating a less degenerative profile. Immunohistochemistry results of COL2A1, ATG5, and GSDMD-N revealed that VX-765 treatment decreased GSDMD-N expression, while knockdown of ATG5 promoted the accumulation of GSDMD-N in NP tissues (Figures 7(c) and 7(d)). Immunofluorescence staining also showed that the level of caspase-1 was increased during IDD progression and that VX-765 significantly inhibited caspase-1 expression (Figures 7(e) and 7(f)). These results demonstrated that inhibition of autophagy activity aggravated cell pyroptosis and accelerated the IDD progression, while VX-765 treatment could retard IDD *in vivo*.

4. Discussion

Various types of programmed cell death contribute to the pathogenesis of IDD, including cell apoptosis, pyroptosis, and necroptosis [28]. In the present study, we revealed that impaired autophagy accelerates the pyroptotic NP cell death induced by LPS. Here, we presented the first evidence that P62-mediated autophagic degradation of the pyroptosis executor, GSDMD-N, serves as a regulatory mechanism of cell pyroptosis. Delivery of VX-765, the inhibitor of caspase-1, inhibits the activation of inflammasome and pyroptosis, thereby ameliorating the IDD progression *in vivo*. Our study suggests the important role of pyroptotic cell death during IDD and investigates the relationship between autophagy and pyroptosis (Figure 8). These results may provide a potential therapeutic target for IDD treatment.

Autophagy is a degrading intracellular mechanism that recycles organelles and proteins to maintain cellular homeo-

stasis [29]. Growing evidence has clarified the protective role of autophagy in IDD development, that activating autophagy could decrease the apoptotic rates of resident cells and promote matrix remodeling during IDD [30, 31]. Consistent with previous studies, our results showed increased expression of autophagy-related protein in degenerated discs [32]. Elevated basal autophagy might adjust resident cells to microenvironmental stress in degenerated discs; however, excessive or inappropriate stimuli could promote autophagic cell death [33]. Autophagy, closely interrelated with apoptosis, is considered as a double-edged sword in cell survival [34]. Indeed, autophagy has a controversial and complicated role in the progression of IDD. Based on the detection of autophagic markers in disc tissues, we found that autophagy levels increased during the progression of IDD. Intervention of autophagy accelerates the death of NP cells, indicating that autophagy is necessary for the survival of disc cells.

Recent researches indicated that pyroptotic death of resident cells in disc promotes the progression of IDD [35, 36]. In senescent or degenerated IVDs, a great deal of inflammatory cytokines or reactive oxygen species (ROS) accumulate, leading to the activation of NLRP3 inflammasome and caspase-1. Activated caspase-1 cleaves GSDMD to release GSDMD-N fragments, which ultimately results in membrane pore formation and cell death [37]. Silencing of GSDMD could inhibit the inflammatory response and reduce oxidative stress, which protect against stimulus-induced organ injury [38]. A previous study also showed that the progression of IDD was effectively retarded after delivering of the NLRP3 inflammasome inhibitor into the degenerated rat disc [35]. Consistent with their results, our study also demonstrated that administration of a caspase-1 inhibitor decreases GSDMD expression and significantly ameliorated IDD

in vivo. Therefore, the intervention of cell pyroptosis might be an effective therapeutic target in IDD.

Currently, the role of autophagy in pyroptotic cell death is still controversial. Several studies suggested that autophagy inhibits the inflammasome activation and indicated the protective effect of autophagy on cell pyroptosis [36, 39]. A research conducted by Bai et al. revealed that autophagy is activated during ROS-induced cell pyroptosis and autophagy inhibition could aggravate cell pyroptosis [36]. Since autophagosomes could degrade their contents enzymatically, it is reasonable to assume that autophagy activation removes some pyroptotic inducers or clears damaged organelles to reconstruct cellular homeostasis [39]. In the present study, we confirmed a direct connection and colocalization of LC3 and GSDMD-N. Moreover, GSDMD-N could be removed via P62-mediated autophagic degradation. P62 is incorporated into autophagosomes with GSDMD-N and then degraded by lysosomes, resulting in the efficient degradation of GSDMD-N. Other researchers also reported the conspirator role of autophagy in pyroptotic cell death [40, 41]. Wang et al. found that the accumulation of autophagy markers increased the occurrence of pyroptosis which was mainly associated with end-stage autophagy activation and lysosome instability and treatment of autophagy inhibitor reduced the cell pyroptosis [40]. Since autophagy is a diverse-stage activity and involves dynamic processes, a causal link between autophagy and pyroptosis remains unclear and controversial.

Indeed, inflammasome activation, including NLRP3 inflammasome, plays a critical role in pyroptotic cell death [42]. Several studies have indicated that autophagy activation reduces NLRP3 expression and decreases the production of cleaved caspase-1 [43, 44]. Houtman et al. reported a colocalization between NLRP3 and LC3-labeled structures, indicating a selective degradation mechanism of NLRP3 [45]. Besides, the mammalian target of rapamycin (mTOR) signaling pathway is always involved in autophagy activation. Intervention of autophagy could regulate NLRP3 activation via modulating the binding of mTOR and NLRP3 [43]. On the other hand, cell plasma membrane perforation is a symbol of pyroptotic cell death. The perforation of the plasma membrane leads to leakage of cellular contents and release of inflammatory cytokines [46]. Under autophagy activation, the lysosomes could serve as a membrane repair mechanism [47–49]. With a series of small GTPase activation, lysosomes fuse with the plasma membrane and release the degradation products via an exocytosis pathway [47], possibly repairing pyroptotic perforation and promoting cell survival.

Although our study provided enough evidence to elucidate the relationship between autophagy and pyroptosis during IDD progression, there still are several limitations in our research. First, we knock down the ATG5 expression with siRNA transfection, while utilization of ATG-knockout cells or animals may provide firmer evidence. Second, we focused on the autophagy receptor P62/SQSTM1 in the autophagic degradation of GSDMD-N. However, there may be more receptors mediating the autophagy activation and degradation mechanism. Moreover, GSDMD and GSDMD-N are important but not only participants in cell pyroptosis. More pyroptosis-related pathway should be investigated in IDD.

Therefore, further research and clinical studies on the role of autophagy and pyroptosis in IDD are required.

In conclusion, our study investigated the relationship between autophagy and cell pyroptosis in human NP cells. Our results clarified the detrimental role of pyroptosis in IDD and the protective role of autophagy in pyroptotic NP cell death. Importantly, our results demonstrated the regulatory role of the autophagy-lysosome pathway in pyroptosis, which may help identify novel therapeutic target for IDD treatment.

Data Availability

All datasets generated for this study are included in the article.

Conflicts of Interest

The authors declare no conflict of interest.

Authors' Contributions

Zhiwei Liao, Suyun Li, and Rong Liu contributed equally to this study and share first authorship. Xinghuo Wu and Cao Yang extensively reviewed and revised this manuscript. All authors have given approval to the final version of the manuscript.

Acknowledgments

This study was supported by the National Natural Science Foundation of China (Grant Nos. 81974349, 82072505, and 81772401), the National Key Research and Development Program of China (2018YFB1105700), and the Application Foundation and Advanced Program of Wuhan Science and Technology Bureau (2019020701011457).

References


- [1] G. J. Kerr, M. A. Veras, M. K. Kim, and C. A. Séguin, "Decoding the intervertebral disc: unravelling the complexities of cell phenotypes and pathways associated with degeneration and mechanotransduction," *Seminars in Cell & Developmental Biology*, vol. 62, pp. 94–103, 2017.
- [2] C. Cunha, A. J. Silva, P. Pereira, R. Vaz, R. M. Gonçalves, and M. A. Barbosa, "The inflammatory response in the regression of lumbar disc herniation," *Arthritis Research & Therapy*, vol. 20, no. 1, p. 251, 2018.
- [3] Z. I. Johnson, Z. R. Schoepflin, H. Choi, I. M. Shapiro, and M. V. Risbud, "Disc in flames: roles of TNF- α and IL-1 β in intervertebral disc degeneration," *European Cells & Materials*, vol. 30, pp. 104–117, 2015.
- [4] G. Tendulkar, T. Chen, S. Ehnert, H. P. Kaps, and A. K. Nüssler, "Intervertebral disc nucleus repair: hype or hope?," *International Journal of Molecular Sciences*, vol. 20, no. 15, p. 3622, 2019.
- [5] L. Vande Walle and M. Lamkanfi, "Pyroptosis," *Current Biology*, vol. 26, no. 13, pp. R568–R572, 2016.
- [6] P. Broz, P. Pelegrin, and F. Shao, "The gasdermins, a protein family executing cell death and inflammation," *Nature Reviews. Immunology*, vol. 20, no. 3, pp. 143–157, 2020.

- [7] E. A. Miao, J. V. Rajan, and A. Aderem, "Caspase-1-induced pyroptotic cell death," *Immunological Reviews*, vol. 243, no. 1, pp. 206–214, 2011.
- [8] X. Wu, G. Ren, R. Zhou, J. Ge, and F. H. Chen, "The role of Ca^{2+} in acid-sensing ion channel 1a-mediated chondrocyte pyroptosis in rat adjuvant arthritis," *Laboratory Investigation*, vol. 99, no. 4, pp. 499–513, 2019.
- [9] C. Zeng, R. Wang, and H. Tan, "Role of pyroptosis in cardiovascular diseases and its therapeutic implications," *International Journal of Biological Sciences*, vol. 15, no. 7, pp. 1345–1357, 2019.
- [10] Y. Zu, Y. Mu, Q. Li, S. T. Zhang, and H. J. Yan, "Icariin alleviates osteoarthritis by inhibiting NLRP3-mediated pyroptosis," *Journal of Orthopaedic Surgery and Research*, vol. 14, no. 1, p. 307, 2019.
- [11] Y. Song, Y. Wang, Y. Zhang et al., "Advanced glycation end products regulate anabolic and catabolic activities via NLRP3-inflammasome activation in human nucleus pulposus cells," *Journal of Cellular and Molecular Medicine*, vol. 21, no. 7, pp. 1373–1387, 2017.
- [12] P. Tang, J. M. Gu, Z. A. Xie et al., "Honokiol alleviates the degeneration of intervertebral disc via suppressing the activation of TXNIP-NLRP3 inflammasome signal pathway," *Free Radical Biology & Medicine*, vol. 120, pp. 368–379, 2018.
- [13] N. Mizushima and M. Komatsu, "Autophagy: renovation of cells and tissues," *Cell*, vol. 147, no. 4, pp. 728–741, 2011.
- [14] J. Doherty and E. H. Baehrecke, "Life, death and autophagy," *Nature Cell Biology*, vol. 20, no. 10, pp. 1110–1117, 2018.
- [15] F. Napoletano, O. Baron, P. Vandennebeele, B. Mollereau, and M. Fanto, "Intersections between regulated cell death and autophagy," *Trends in Cell Biology*, vol. 29, no. 4, pp. 323–338, 2019.
- [16] A. Claude-Taupin, B. Bissa, J. Jia, Y. Gu, and V. Deretic, "Role of autophagy in IL-1 β export and release from cells," *Seminars in Cell & Developmental Biology*, vol. 83, pp. 36–41, 2018.
- [17] M. Takahama, S. Akira, and T. Saitoh, "Autophagy limits activation of the inflammasomes," *Immunological Reviews*, vol. 281, no. 1, pp. 62–73, 2018.
- [18] S. Li, W. Hua, K. Wang et al., "Autophagy attenuates compression-induced apoptosis of human nucleus pulposus cells via MEK/ERK/NRF1/Atg7 signaling pathways during intervertebral disc degeneration," *Experimental Cell Research*, vol. 370, no. 1, pp. 87–97, 2018.
- [19] S. Zhan, K. Wang, Q. Xiang et al., "lncRNA HOTAIR upregulates autophagy to promote apoptosis and senescence of nucleus pulposus cells," *Journal of Cellular Physiology*, vol. 235, no. 3, pp. 2195–2208, 2019.
- [20] Z. Liao, R. Luo, G. Li et al., "Exosomes from mesenchymal stem cells modulate endoplasmic reticulum stress to protect against nucleus pulposus cell death and ameliorate intervertebral disc degeneration in vivo," *Theranostics*, vol. 9, no. 14, pp. 4084–4100, 2019.
- [21] X. Wu, Z. Liao, K. Wang et al., "Targeting the IL-1 β /IL-1Ra pathways for the aggregation of human islet amyloid polypeptide in an ex vivo organ culture system of the intervertebral disc," *Experimental & Molecular Medicine*, vol. 51, no. 9, pp. 1–16, 2019.
- [22] X. Wu, Y. Liu, X. Guo et al., "Prolactin inhibits the progression of intervertebral disc degeneration through inactivation of the NF- κ B pathway in rats," *Cell Death & Disease*, vol. 9, no. 2, p. 98, 2018.
- [23] Y. Liu, J. Lin, X. Wu et al., "Aspirin-mediated attenuation of intervertebral disc degeneration by ameliorating reactive oxygen species in vivo and in vitro," *Oxidative Medicine and Cellular Longevity*, vol. 2019, Article ID 7189854, 20 pages, 2019.
- [24] B. Han, K. Zhu, F. C. Li et al., "A simple disc degeneration model induced by percutaneous needle puncture in the rat tail," *Spine*, vol. 33, no. 18, pp. 1925–1934, 2008.
- [25] P. Luo, Z. Xu, G. Li et al., "HMGB1 represses the anti-cancer activity of sunitinib by governing TP53 autophagic degradation via its nucleus-to-cytoplasm transport," *Autophagy*, vol. 14, no. 12, pp. 2155–2170, 2018.
- [26] T. Lamark, S. Svenning, and T. Johansen, "Regulation of selective autophagy: the p62/SQSTM1 paradigm," *Essays in Biochemistry*, vol. 61, no. 6, pp. 609–624, 2017.
- [27] Z. Sun, M. Nyanzu, S. Yang et al., "VX765 Attenuates Pyroptosis and HMGB1/TLR4/NF- κ B Pathways to Improve Functional Outcomes in TBI Mice," *Oxidative Medicine and Cellular Longevity*, vol. 2020, Article ID 7879629, 21 pages, 2020.
- [28] C. Q. Zhao, L. S. Jiang, and L. Y. Dai, "Programmed cell death in intervertebral disc degeneration," *Apoptosis*, vol. 11, no. 12, pp. 2079–2088, 2006.
- [29] K. R. Parzych and D. J. Klionsky, "An overview of autophagy: morphology, mechanism, and regulation," *Antioxidants & Redox Signaling*, vol. 20, no. 3, pp. 460–473, 2014.
- [30] D. Chen, D. Xia, Z. Pan et al., "Metformin protects against apoptosis and senescence in nucleus pulposus cells and ameliorates disc degeneration in vivo," *Cell Death & Disease*, vol. 7, no. 10, article e2441, 2016.
- [31] Z. Zheng, Z. G. Wang, Y. Chen et al., "Spermidine promotes nucleus pulposus autophagy as a protective mechanism against apoptosis and ameliorates disc degeneration," *Journal of Cellular and Molecular Medicine*, vol. 22, no. 6, pp. 3086–3096, 2018.
- [32] J. Chen, J. J. Xie, M. Y. Jin et al., "Sirt6 overexpression suppresses senescence and apoptosis of nucleus pulposus cells by inducing autophagy in a model of intervertebral disc degeneration," *Cell Death & Disease*, vol. 9, no. 2, p. 56, 2018.
- [33] S. J. Zhang, W. Yang, C. Wang et al., "Autophagy: a double-edged sword in intervertebral disc degeneration," *Clinica Chimica Acta*, vol. 457, pp. 27–35, 2016.
- [34] S. Dang, Z. M. Yu, C. Y. Zhang et al., "Autophagy promotes apoptosis of mesenchymal stem cells under inflammatory microenvironment," *Stem Cell Research & Therapy*, vol. 6, no. 1, p. 247, 2015.
- [35] D. He, M. Zhou, Z. Bai, Y. Wen, J. Shen, and Z. Hu, "Propionibacterium acnes induces intervertebral disc degeneration by promoting nucleus pulposus cell pyroptosis via NLRP3-dependent pathway," *Biochemical and Biophysical Research Communications*, vol. 526, no. 3, pp. 772–779, 2020.
- [36] Z. Bai, W. Liu, D. He et al., "Protective effects of autophagy and NFE2L2 on reactive oxygen species-induced pyroptosis of human nucleus pulposus cells," *Aging (Albany NY)*, vol. 12, no. 8, article 103109, pp. 7534–7548, 2020.
- [37] L. Sborgi, S. Rühl, E. Mulvihill et al., "GSDMD membrane pore formation constitutes the mechanism of pyroptotic cell death," *The EMBO journal*, vol. 35, no. 16, pp. 1766–1778, 2016.
- [38] Y. Jia, R. Cui, C. Wang et al., "Metformin protects against intestinal ischemia-reperfusion injury and cell pyroptosis via TXNIP-NLRP3-GSDMD pathway," *Redox biology*, vol. 32, article 101534, 2020.

- [39] X. Wang, H. Li, W. Li et al., "The role of caspase-1/GSDMD-mediated pyroptosis in Taxol-induced cell death and a Taxol-resistant phenotype in nasopharyngeal carcinoma regulated by autophagy," *Cell Biology and Toxicology*, vol. 36, no. 5, pp. 437–457, 2020.
- [40] Y. Wang, X. Song, Z. Li et al., "MicroRNA-103 protects coronary artery endothelial cells against H₂O₂-induced oxidative stress via BNIP3-mediated end-stage autophagy and antipyr-optosis pathways," *Oxidative Medicine and Cellular Longevity*, vol. 2020, Article ID 8351342, 15 pages, 2020.
- [41] T. Qiu, P. Pei, X. Yao et al., "Taurine attenuates arsenic-induced pyroptosis and nonalcoholic steatohepatitis by inhibiting the autophagic-inflammasomal pathway," *Cell Death & Disease*, vol. 9, no. 10, p. 946, 2018.
- [42] D. Chauhan, L. Vande Walle, and M. Lamkanfi, "Therapeutic modulation of inflammasome pathways," *Immunological Reviews*, vol. 297, no. 1, pp. 123–138, 2020.
- [43] J. Cosin-Roger, S. Simmen, H. Melhem et al., "Hypoxia ameliorates intestinal inflammation through NLRP3/mTOR downregulation and autophagy activation," *Nature Communications*, vol. 8, no. 1, p. 98, 2017.
- [44] X. Han, S. Sun, Y. Sun et al., "Small molecule-driven NLRP3 inflammation inhibition via interplay between ubiquitination and autophagy: implications for Parkinson disease," *Autophagy*, vol. 15, no. 11, pp. 1860–1881, 2019.
- [45] J. Houtman, K. Freitag, N. Gimber, J. Schmoranzler, F. L. Heppner, and M. Jendrach, "Beclin1-driven autophagy modulates the inflammatory response of microglia via NLRP3," *The EMBO journal*, vol. 38, no. 4, 2019.
- [46] X. Liu, Z. Zhang, J. Ruan et al., "Inflammasome-activated gasdermin D causes pyroptosis by forming membrane pores," *Nature*, vol. 535, no. 7610, pp. 153–158, 2016.
- [47] X. Michelet, A. Tuli, H. Gan et al., "Lysosome-mediated plasma membrane repair is dependent on the small GTPase Arl8b and determines cell death type in *Mycobacterium tuberculosis* Infection," *Journal of immunology (Baltimore, Md: 1950)*, vol. 200, no. 9, pp. 3160–3169, 2018.
- [48] J. M. J. Tan, N. Mellouk, S. E. Osborne et al., "An ATG16L1-dependent pathway promotes plasma membrane repair and limits *Listeria monocytogenes* cell-to-cell spread," *Nature microbiology*, vol. 3, no. 12, pp. 1472–1485, 2018.
- [49] M. Radulovic, K. O. Schink, E. M. Wenzel et al., "ESCRT-mediated lysosome repair precedes lysophagy and promotes cell survival," *The EMBO journal*, vol. 37, no. 21, 2018.

Research Article

Exosomal MATN3 of Urine-Derived Stem Cells Ameliorates Intervertebral Disc Degeneration by Antisenescence Effects and Promotes NPC Proliferation and ECM Synthesis by Activating TGF- β

Zhu Guo ¹, WeiLiang Su ¹, RongYao Zhou ², GuoQing Zhang ¹, Shuai Yang ¹,
XiaoLin Wu ¹, ChenSheng Qiu ³, WenBin Cong ⁴, Nana Shen ⁵, JianWei Guo ¹,
Chang Liu ¹, Shang-You Yang ⁶, DongMing Xing ⁷, Yan Wang ¹, BoHua Chen ¹,
and HongFei Xiang ¹

¹Department of Orthopedics, The Affiliated Hospital of Qingdao University, Qingdao, China 266003

²Department of Orthopaedics, DongChangFu People's Hospital, Liaocheng, China 252000

³Department of Orthopedics, Qingdao Municipal Hospital, Qingdao, China 266011

⁴Radiology Department, The Affiliated Hospital of Qingdao University, Qingdao, China 266003

⁵Department of Rehabilitation, The Affiliated Hospital of Qingdao University, Qingdao, China 266003

⁶University of Kansas, School of Medicine-Wichita, 929 N St. Francis Street, Wichita, KS, USA 67230

⁷School of Life Sciences, Tsinghua University, Beijing, China 100084

Correspondence should be addressed to Yan Wang; sanwang1986@163.com, BoHua Chen; bhchen@hotmail.com, and HongFei Xiang; yndx2004@vip.qq.com

Received 5 February 2021; Revised 5 April 2021; Accepted 3 May 2021; Published 27 May 2021

Academic Editor: Sidong Yang

Copyright © 2021 Zhu Guo et al. This is an open access article distributed under the Creative Commons Attribution License, which permits unrestricted use, distribution, and reproduction in any medium, provided the original work is properly cited.

Objective. Low back pain (LBP) is one of the top three causes of disability in developed countries, and intervertebral disc degeneration (IDD) is a major contributor to LBP. In the process of IDD, there is a gradual decrease in nucleus pulposus cells (NPCs) and extracellular matrix (ECM). Exosomes are important exocrine mediators of stem cells that can act directly on cells for tissue repair and regeneration. In this study, we determined the antisenescence, cell proliferation promotion, and ECM modulation effects of human urine-derived stem cell (USC) exosomes (USC-exos) on degenerated intervertebral discs and explored the underlying mechanism. **Methods and Materials.** USCs were identified by multipotent differentiation and flow cytometry for mesenchymal stem cell- (MSC-) specific surface protein markers. USC-exos were isolated from the conditioned medium of USCs by ultracentrifugation and then analyzed by transmission electron microscopy (TEM), particle size analysis, and western blotting (WB) for exosome marker proteins. The effects of USC-exos on NPC proliferation and ECM synthesis were assessed by Cell Counting Kit-8 (CCK-8), WB, and immunofluorescence (IF) analyses. The protein differences between normal and degenerative intervertebral discs were mined, and the temporal and spatial variations in matrilin-3 (MATN3) content were determined by WB and IF in the intervertebral disc tissues. The candidate molecules that mediated the function of USC-exos were screened out and confirmed by multiple assays. Meanwhile, the mechanism underlying the candidate protein in USC-exos-induced cell proliferation and regulation of ECM synthesis promoting the activities of NPCs was explored. In addition, the effects of USC-exos on ameliorating intervertebral disc degeneration (IVD) in mice were examined by assessing computed tomography (CT), magnetic resonance imaging (MRI), and histological analyses. **Results.** The flow cytometry results showed that USCs were positive for CD29, CD44, and CD73, which are USC surface-specific markers, but negative for CD34 and CD45. In addition, USCs showed osteogenic, adipogenic, and chondrogenic differentiation potential. USC-exos exhibited a cup-shaped morphology, with a mean diameter of 49.7 ± 7.3 nm, and were positive for CD63 and TSG101 and negative for calnexin. USC-exos could promote NPC proliferation and ECM synthesis. The protein content of the matrilin family was significantly reduced in degenerative intervertebral discs, and the decrease in MATN3 was the most significant. USC-exos were

found to be rich in MATN3 protein, and exosomal MATN3 was required for USC-exos-induced promotion of NPC proliferation and ECM synthesis, as well as alleviation of intervertebral disc degeneration in IVD rats. In addition, the effects of MATN3 in USC-exos were demonstrated to be achieved by activating TGF- β , which elevated the phosphorylation level of SMAD and AKT. *Conclusions.* Our study suggests that reduced MATN3 can be considered a characteristic of intervertebral disc degeneration. USC-exos may represent a potentially effective agent for alleviating intervertebral disc degeneration by promoting NPC proliferation and ECM synthesis by transferring the MATN3 protein.

1. Introduction

Low back pain (LBP) is a very common problem experienced by most people at a certain time in their life, and it is among the top three causes of disability in developed countries [1–3]. The definite causes of low back pain remain unclear; however, intervertebral disc degeneration (IDD) has been documented to be a major contributor to LBP and is the pathological basis for spinal instability, disc herniation, and other spinal degenerative diseases, which cause a considerable burden to society and families and thus are the major global public health issues [4, 5].

In disc degeneration, the main pathological change is a gradual reduction in the total NPCs and extracellular matrix (ECM). NPCs are the main functional cells responsible for ECM synthesis. The homeostatic imbalance between anabolism and catabolism leads to the loss of collagen and proteoglycan [6, 7]. Collagen type II (COL2) and proteoglycan (predominantly aggrecan (ACAN)) are crucial ECMs for discs to maintain proper function, particularly for the nucleus pulposus [8, 9]. ACAN is a biological macromolecule formed by one or more glycosaminoglycan (GAG) chains covalently connected to a core protein. It is the main noncollagen component of the intervertebral disc. The glycosaminoglycans contained in ACAN are mainly chondroitin sulfate and keratan sulfate. The rich and unique molecular characteristics of intervertebral discs allow these structures to penetrate and withstand pressure. One of the reasons for the damage and degeneration of the intervertebral disc is the degradation and loss of ACAN. COL2 is one of the most important collagen components in intervertebral discs. COL2 is the main collagen in cartilage, accounting for more than 50% of the extracellular matrix of cartilage. COL2 is mainly expressed by chondrocytes and is abundantly present in the nucleus pulposus [10, 11]. In ECM, COL2 and ACAN are the two most representative components; therefore, this experiment measured the expression of COL2 and ACAN to illustrate ECM conditions. Determining the methods of rebalancing disordered COL2 and ACAN expression and increasing their synthesis is considered a key factor for slowing down or even reversing IVD damage.

Recently, increasing evidence has revealed that mesenchymal stem cells (MSCs) can release exosomes, which are specialized extracellular vesicles that could provide therapeutic benefits [12, 13]. Exosomes are membranous vesicles with a diameter of 50–200 nm, and they contain multiple cellular components, such as proteins, nucleic acids, and lipids. Exosomes act as a cell-free mediator and transfer particular cytokines into recipient cells to achieve their therapeutic paracrine effects in inhibiting senescence, modulating metabolism, and promoting regeneration [14]. Thus, stem cell exo-

somes may have potential applications as effective cell-free therapeutic agents [15].

However, MSCs have a limited source and cause certain trauma to the body, which limits their application. Human urine-derived stem cells are stem cells with multidifferentiation potential obtained from human urine. These cells have a wide range of sources, are convenient to obtain, present safe and noninvasive characteristics, do not violate ethics, and represent a better choice for obtaining exosomes [16–18]. MATN3 is a member of the matrilin protein family, and it is mainly distributed in cartilage cells and plays an important role in the synthesis of cartilage ECM. Variations or decreases in its content can lead to cartilage and intervertebral disc degeneration. In previous studies, we found that USC-exos are rich in this protein.

A number of studies have shown that USC transplantation is beneficial to degenerated intervertebral discs [12, 13]. Exosomes are exocrine vesicles of stem cells that play a paracrine role and deliver a variety of biological effectors of the parent cells. Exosomes that can be absorbed by recipient cells are involved in cellular communication, signaling pathway activation, and metabolism modulation and play an important role in MSC-based therapy. Exosomes are widely distributed and readily available and have no immunogenicity; therefore, they are ideal agents for the treatment of tissue repair and regeneration [19].

In the previous study [20], the team studied the effect of USC-exos on intervertebral disc degeneration by inhibiting the apoptosis of NPCs. We now further explored the promotion of cell proliferation and ECM modulatory effects of human urine-derived stem cell (USC) exosomes (USC-exos) on degenerated intervertebral discs in cell and rat models and explored the underlying mechanism.

2. Materials and Methods

2.1. Isolation and Culture of NPCs. The experimental scheme was approved by the Ethics Committee of the Affiliated Hospital of Qingdao University (approval number: QDFY-19-012-03). Nucleus pulposus cells were obtained from 6 patients with lumbar disc herniation, and they had an average age of 30 ± 4.8 . The clinical symptoms and physical examinations were consistent with the surgical indications. Before surgery, three experienced chief physicians of spine surgery and one chief physician of the imaging department evaluated their MRI, and the modified Pfirrmann scale of the lumbar intervertebral disc was grade 5. This finding indicated that the nucleus pulposus and the medial annular fiber showed low signal and the intervertebral disc was highly normal. After obtaining informed consent from the patients and their relatives and signing a donation agreement for the

study, disc tissue was obtained from patients undergoing posterior lumbar foraminal surgery. The fibrous annulus (AF) and cartilaginous endplate (CEP) were carefully removed from the specimens under a microscope. After rinsing with phosphate buffered saline (PBS) 3 times, the nucleus pulposus tissue was cut to approximately 1 mm³ in size and then digested in 0.2% type II collagenase (Gibco, Grand Island, NY, USA) for 3 h. After digestion, a 75 μ m filter was used to remove tissue residue, and then, the cell suspension was centrifuged at 800 r/min for 5-10 min. Dulbecco's modified Eagle medium/F12 (DMEM/F-12) containing 10% fetal bovine serum (FBS; Gibco, Grand Island, NY, USA) and 1% penicillin-streptomycin (Gibco, Grand Island, NY, USA) was used to resuspend the NPCs; subsequently, the cells were placed in a cell incubator at 37°C with 90% N₂, 5% CO₂, and 5% O₂ [21].

2.2. USC_s Extraction. The fresh sterile urine of 6 healthy male adults (mean age, 25.5 \pm 1.26) was collected under aseptic conditions. The obtained sample was centrifuged at 400 g for 10 min, the supernatant was discarded, and the cell precipitate was resuspended in phosphate buffer (PBS). The supernatant was carefully removed after centrifugation at 200 g for 10 min. The cell precipitates were resuspended in 4 ml DMEM/F-12 medium (HyClone, Utah, USA) composed of 10% FBS (Gibco, Australia), 1% penicillin-streptomycin, and RegM Singlequot growth factor additive (Lonza, Basel, Switzerland). The cells were then inoculated in 12-well plates precoated with gelatin and placed in an incubator at 37°C with 5% CO₂. The medium was changed every two days until the cell clone was formed and then replaced with RE/MC medium for further culture. The RE cell proliferation medium was 500 ml RE cell base medium supplemented with the RegM Single kit. The MC propagation medium includes 10% FBS and 1% Glutamax added to DMEM/F-12 medium (Gibco, Japan), 1% NEAA (Gibco, Grand Island, USA), 1% Pen/Strep (Gibco, Grand Island, USA), 5 ng/ml BFGF (Peprotech, Rocky Hill, USA), 5 ng/ml PDGF-Ab (Peprotech, Rocky Hill, USA), and 5 ng/ml EGF (Peprotech, Rocky Hill, USA). Re/MC medium is a 1:1 mixture of Re and MC medium. When the cell density reached approximately 70%-80%, passaging was carried out, and then, P2-4 generation cells were selected for subsequent experiments.

2.3. Flow Cytometric Analysis of Surface Markers of USC_s. After trypsin digestion, P3 USC_s in a good growth state were collected and then washed with PBS 3 times after centrifugation. A cell suspension with a final concentration of 1 \times 10⁶ /ml was prepared. Then, 100 μ l of cell suspension was added to 10 μ l of monoclonal antibody working solution for CD29, CD34, CD44, CD45, and CD73 (Santa Cruz Biotechnology, USA) and incubated for 1 hour at room temperature in the dark. The cells were washed for another 3 times and analyzed by flow cytometry.

2.4. Determination of the Multidirectional Differentiation Potential of USC_s. To evaluate the differentiation potential of human urine-derived stem cells, osteogenic, adipogenic,

and chondrogenic differentiation was performed according to the associated kit instructions. USC_s were inoculated into 6-well plates, and differentiation was induced when the cell fusion rate reached approximately 80%. Osteogenic induction differentiation medium (CYAGEN, China) was added and replaced every 3 days. After 21 days of induction, the USC_s were fixed with 4% paraformaldehyde and stained with Alizarin Red for observation. The kit contained 175 ml basal medium, 20 ml serum, 2 ml penicillin-streptomycin, 2 ml glutamine, 2 ml β -sodium glycerophosphate, 400 μ l ascorbic acid, and 20 μ l dexamethasone. For adipogenic induction differentiation, adipogenic induction differentiation medium A (Cyagen, China) was first added and then replaced with adipogenic induction differentiation medium B (Cyagen, China) 3 days later, and after 24 h, it was replaced with liquid A again, with this process alternated 3 times. Finally, 4% paraformaldehyde was used for fixation, and oil red O staining was used for observation. Adipogenesis induction differentiation medium A contained 175 ml basal medium, 20 ml fetal bovine serum, 2 ml penicillin-streptomycin, 2 ml glutamine, 400 μ l insulin, 200 μ l 3-isobutyl-1-methyl xanthine (IBMX), 200 μ l dexamethasone, and 200 μ l rosiglitazone. The adipogenic induction differentiation medium B contained 175 ml basal medium, 20 ml fetal bovine serum, 2 ml penicillin-streptomycin, 2 ml glutamine, and 400 μ l insulin. During chondroblast induction, the cells were first counted, and then 2.5 \times 10⁵ USC_s were collected. The supernatant was discarded after centrifugation in a 15 ml centrifuge tube at 150 g for 5 min, and then, 0.5 ml chondroblast induction medium was added and changed every 3 days. Approximately 21 days later, 4% paraformaldehyde was used for fixation, paraffin embedding was followed by sectioning, and allicin blue staining was used for observation. The chondroblast induction differentiation medium kit contained 194 ml basal medium, 600 μ l ascorbic acid, 20 μ l dexamethasone, 2 ml ITS+Supplement, 200 μ l sodium pyruvate, 200 μ l proline, and 2 ml factor- β 3 (TGF- β 3).

2.5. Exosome Extraction and Identification. When the cells grew to 70-75% confluence, the culture medium was removed and washed 3 times with PBS. Serum-free medium was added, and the culture was continued for 48 h. The culture medium was then collected, centrifuged at 4°C and 500 g for 10 min to remove residual cells, and centrifuged at 4°C and 2000 g for 20 min to remove cell debris. The impurities were further removed at 4°C and 10,000 g for 30 min, and the supernatant was retained and then filtered with a 0.22 μ m filter membrane to remove excess particles. The supernatant was centrifuged at 4°C and 100,000 g for 2 h, and the resulting precipitate was resuspended in PBS. The exosome morphology was observed by transmission electron microscopy (TEM) (JEM-1200EX, Japan). The number and size distribution of exosomes were analyzed using a NanoSight detector (Malvern, England) and NTA detection and analysis software. USC_s were cleaved to obtain their cleavage products, which were used as a negative control to conduct WB with USC-exos. Western blotting was used to detect the exosome markers CD63, TSG101, and calnexin.

2.6. Exosome Uptake of NPCs. P3 NPCs with good growth status were inoculated into 24-well plates for subsequent experiments after the cells adhered to the wall. First, GFP-lentivirus was transfected to observe the cell profile of NPCs. GFP virus and Lipofectamine 2000 (Thermo Fisher, Massachusetts, USA) were diluted with equal amounts of serum-free culture medium. The diluted GFP was mixed with Lipofectamine 2000 and kept at room temperature for 20 min. The mixture was added to the cell culture medium and transfected for approximately 3 h. Then, the exosomes were labeled with PKH26 (Sigma-Aldrich) fluorescent dye according to the operation instructions of the PKH26 fluorescent dye kit. The excess dye was neutralized with an equal volume of PBS containing 5% BSA. Finally, the supernatant was removed by centrifugation at 4°C for 70 min at 100,000 g and resuspended in 50 μ l PBS. The prepared USC-exos labeled with PKH26 were added to GFP-transfected NPCs and incubated in the dark for 12 h. After fixation with 4% paraformaldehyde for 20 min, the nuclei were stained with DAPI. The glycerin was sealed, and uptake was observed by laser confocal microscopy. The Leica Application Suite Advanced Fluorescence software was used to analyze the images in the later stage.

2.7. CCK-8 (Cell Counting Kit-8) Detects NPC Proliferation. NPCs were prepared into cell suspensions and counted and then seeded into 96-well plates, with 5×10^3 cells in each well and each group set up with 3 duplicate wells. PBS was added to the control group, and USC-exos, USC^{shMATN3}-exos, and USC^{conshRNA}-exos were added to the other groups. The cell-free wells were used as blank controls. After intervention, 10 μ l CCK-8 solution (Meilunbio, Dalian, China) was added on days 1, 3, 5, and 7 and then cultured in a cell incubator for approximately 3 h. A microplate reader (Molecular Devices, USA) was used to detect the absorbance at 450 nm, and then, the proliferation of NPCs was calculated based on the change in absorbance.

2.8. β -Galactosidase Staining to Detect Cell Senescence. NPCs with good P3 growth were inoculated into a 6-well plate and treated according to the experimental groups after the cells adhered to the wall. After the intervention, the instructions of the β -galactosidase staining kit (Beyotime, China) were followed for cell senescence detection. The specific steps were as follows. Staining fixative solution was added to fix the cells at room temperature for 15 minutes. After washing 3 times with PBS, the following was added to each well: 1 ml of 930 μ l β -galactosidase staining solution C, 10 μ l β -galactosidase staining solution A, 10 μ l β -galactosidase staining β -galactosidase staining working solution prepared from solution B, and 50 μ l X-Gal solution. The cells were incubated overnight at 37°C, and the senescence of NPCs was observed under an inverted phase contrast microscope.

2.9. Western Blot (WB) Analysis. After the intervention, the samples were collected and then lysed in RIPA lysis buffer (Solarbio, Beijing, China) containing 1 mM phenyl methyl-sulfonyl fluoride (PMSF) and protease inhibitors to extract proteins. The extracted protein was tested to determine its

TABLE 1: Primer sequences for quantitative real-time PCR.

Gene name	Primer sequences (5'-3')
MATN3	Forward (F) 5'-GGTGCAGGTGTTTGAAGAG-3'
	Reverse (R) 5'-TCCACTGTGAAGGCTTCGTC-3'
GAPDH	Forward (F) 5'-GGTATCGTGGAAGGACTC-3'
	Reverse (R) 5'-GTAGAGGCAGGGATGATG-3'

concentration using a BCA kit (Solarbio, Beijing, China). Then, the protein and loading buffer were mixed at a ratio of 4:1 (V/V) and boiled for 10 minutes. The proteins were separated by sodium dodecyl sulfate-polyacrylamide gel electrophoresis (SDS-PAGE) and then transferred to a polyvinylidene fluoride (PVDF) membrane. The PVDF membrane was blocked with 5% skimmed milk powder at room temperature and then incubated overnight at 4°C with primary antibodies against CD63, TSG101, calnexin, TGF- β 3, p-SMAD3, SMAD3, AKT, p-AKT, β -actin (all the above antibodies were purchased from Santa Cruz Biotechnology, USA), MATN3 (Bioss, Beijing, China), COL2 (Bioss, Beijing, China), and ACAN (Millipore, Massachusetts, USA). The membrane was incubated with a horseradish peroxidase- (HRP-) labeled secondary antibody (ABclonal, Wuhan, China) for 1 hour, and then, an ECL kit (Thermo Fisher Scientific, Rockville, MD, USA) was used for luminescence observation. The Image Lab software (Bio-Rad, Hercules, CA, USA) was used to take images and analyze them.

2.10. Transfection of MATN3 Lentivirus-shRNA. In the functional mechanism investigation, lentiviral shRNAs targeting MATN3 (shMATN3, sc106205V) (Santa Cruz Biotechnology, USA) and control shRNAs (Con shRNAs) were transfected before USC-exos treatment. In the feedback mechanism investigation, the overexpressed lentivirus of MATN3 (LV-MATN3) and the control lentiviral vectors (con-LV) were transfected. The lentivirus vectors were packaged by GeneChem (Shanghai, China). Transfection was conducted according to the manufacturer's instructions. Briefly, NPCs were plated into dishes 1 day before transfection. The next day, the NPCs were transfected with the lentivirus vectors at an MOI of 100 supplemented with 10 μ g/ml polybrene (Cyagen) for 24 h. The culture medium was replaced with fresh complete medium, and the cells were selected with 2.5 μ g/ml puromycin (Sigma) 72 h after transfection. Total RNA was harvested and subjected to qPCR analysis for efficiency. Forty-eight hours after transfection, the total RNA was harvested and subjected to qPCR analysis. Seventy-two hours after transfection, the total proteins were harvested and subjected to western blot analysis.

2.11. Quantitative Real-Time Polymerase Chain Reaction (qRT-PCR). Total RNA was extracted from the samples using TRIzol reagent (Invitrogen, Carlsbad, CA, USA). Then, the instructions of the reverse transcription kit for qRT-PCR were followed to reverse transcription and amplify related genes. GAPDH was used as an internal reference, and each sample was set with three auxiliary holes. The primer

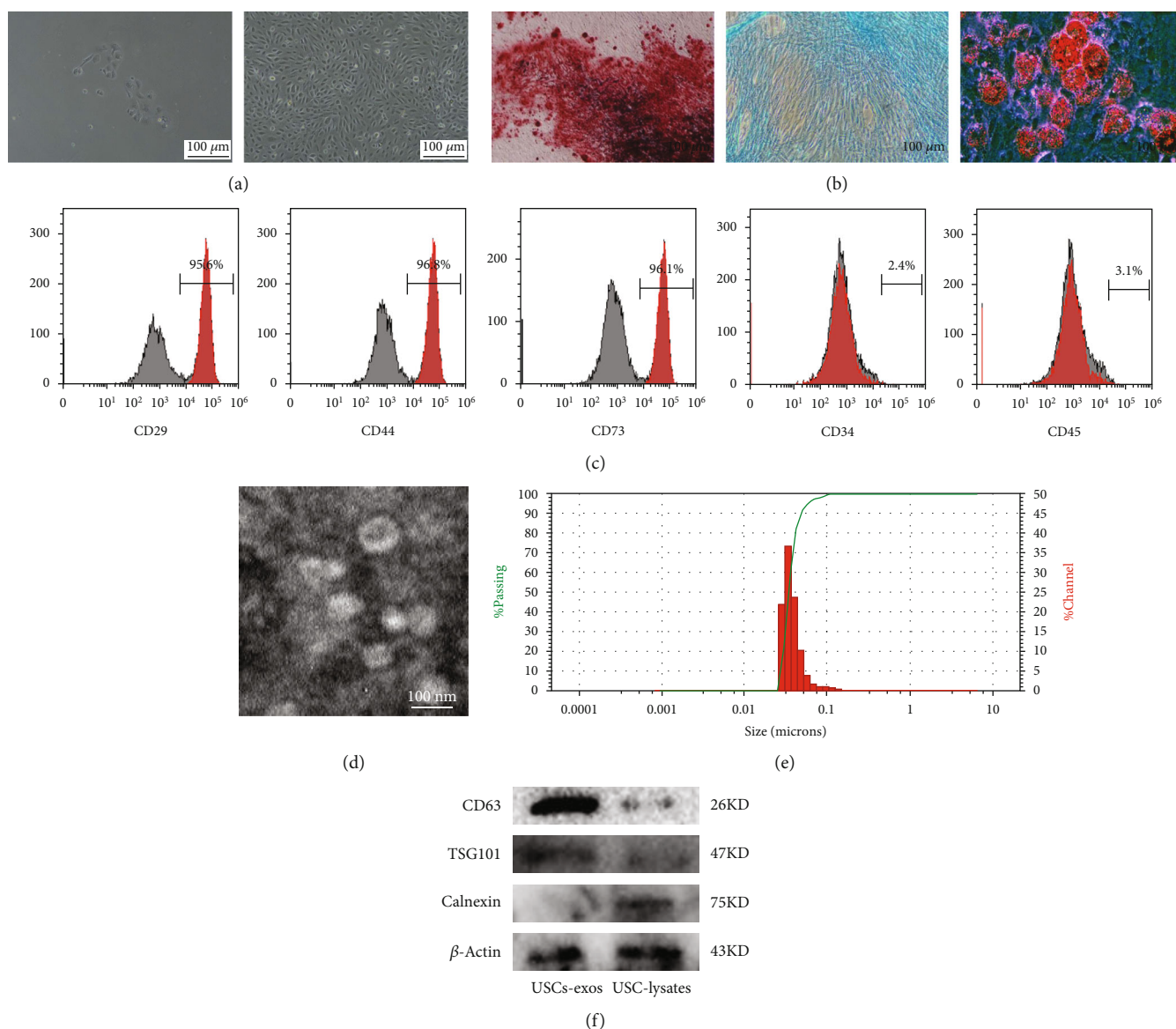


FIGURE 1: USC and USC-exos identification. (a) Morphological appearance of USCs under an optical microscope. USC colonies generally appeared at 7 to 10 days after the primary cell culture and exhibited cobblestone-like morphology under the light microscope. USCs could reach 90% confluence after 2-3 weeks of culture. (b) Multidirectional differentiation potential of USCs. After osteogenic induction, the formation of calcium nodules can be seen by staining with Alizarin Red, red-stained lipid droplets can be seen by staining with Oil Red O after the induction of fat formation, and accumulated glycosaminoglycans can be seen by staining with Alcian Blue after the induction of cartilage. (c) USC surface marker identification. USCs were positive for CD29, CD44, and CD73 but negative for CD34 and CD45. (d) TEM scanning of the USC-exos. (e) Particle size analysis of the USC-exos. (f) WB analysis of specific markers of USC-exos and USC-lysates.

sequences are shown in Table 1. The data obtained were analyzed using the $2^{-\Delta\Delta C_t}$ algorithm.

2.12. NPCs Immunofluorescence Test (IFT). P3 NPCs were used for cell counting, the cell concentration was adjusted to 1×10^5 , and a cell climbing sheet was inserted after the cells adhered to the wall. PBS was added to the control group, 100 μg/ml USC-exos was added to the USC-exos group, 100 μg/ml USC^{conshRNA-exos} was added to the USC^{conshRNA}-exos group, and 100 μg/ml USC^{shMATN3}-exos was added to the USC^{shMATN3}-exos group. After 7 days of intervention, the cells were fixed with 4% paraformaldehyde for 20 minutes at room temperature and blocked with 5% BSA for

30 minutes. Primary antibodies against COL2 (Bioss, Beijing, China) and ACAN (Santa Cruz Biotechnology, USA) were added and incubated overnight at 4°C. The next day, anti-mouse (Abcam, USA) and anti-rabbit (Abclonal, USA) fluorescent secondary antibodies were added separately under dark conditions. After incubation for 1 hour at room temperature, DAPI was added. After mounting in glycerol, the cells were observed under a laser confocal microscope (Nikon, Japan) to evaluate the expression of COL2 and ACAN.

2.13. Rat IDD Model Establishment and Intradisc Injection. Our group purchased 20 3-month-old Sprague Dawley (SD) rats for in vivo experiments. Among them, 5 rats were

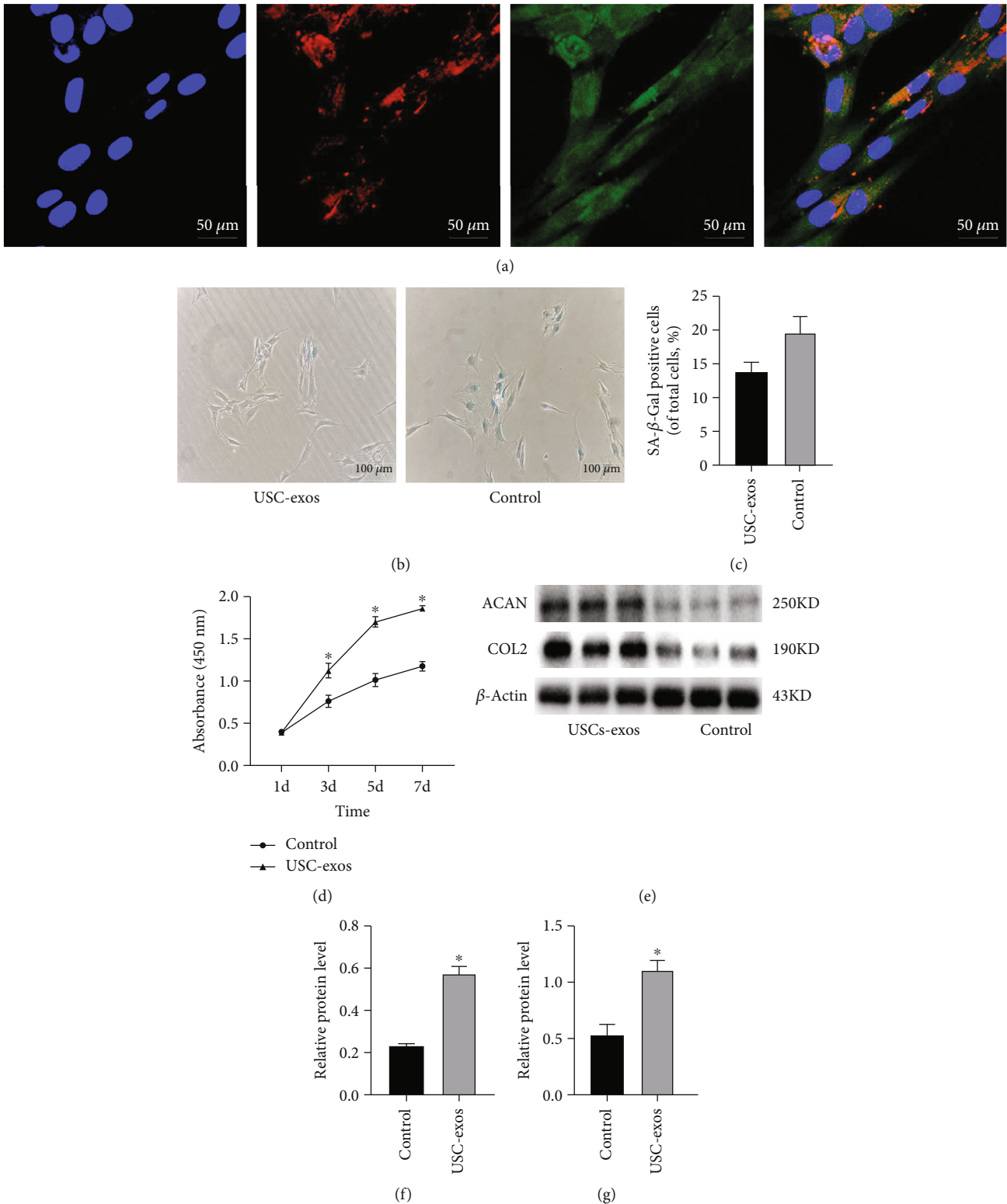


FIGURE 2: USC-exos resist senescence and promote NPC proliferation and ECM synthesis. (a) NPC uptake of USC-exos. NPCs were labeled by GFP. PKH26-labeled USC-exos were internalized to the perinuclear region of the NPCs after 3 h of incubation. (b) SA- β -Gal staining assay of NPCs induced by USC-exos and PBS. (c) SA- β -Gal staining assay showing the antisenesence effect of USC-exos. The multifield random counting method showed that the proportion of SA- β -Gal-positive NPCs in the USC-exos group was $13.8 \pm 1.4\%$, which was significantly lower than that in the control group ($19.6 \pm 2.4\%$). (d) CCK-8 assay showing NPC proliferation in response to USC-exos. The absorbance at 450 nm of the USCs group was markedly higher than that of the control group at 3, 5, and 7 d ($n = 3$, $*P < 0.05$). (e-g) WB analysis for NPC ECM synthesis. The expression of ACAN and COL2 was significantly increased when NPCs were stimulated with USC-exos (each group $n = 3$, $*P < 0.05$).

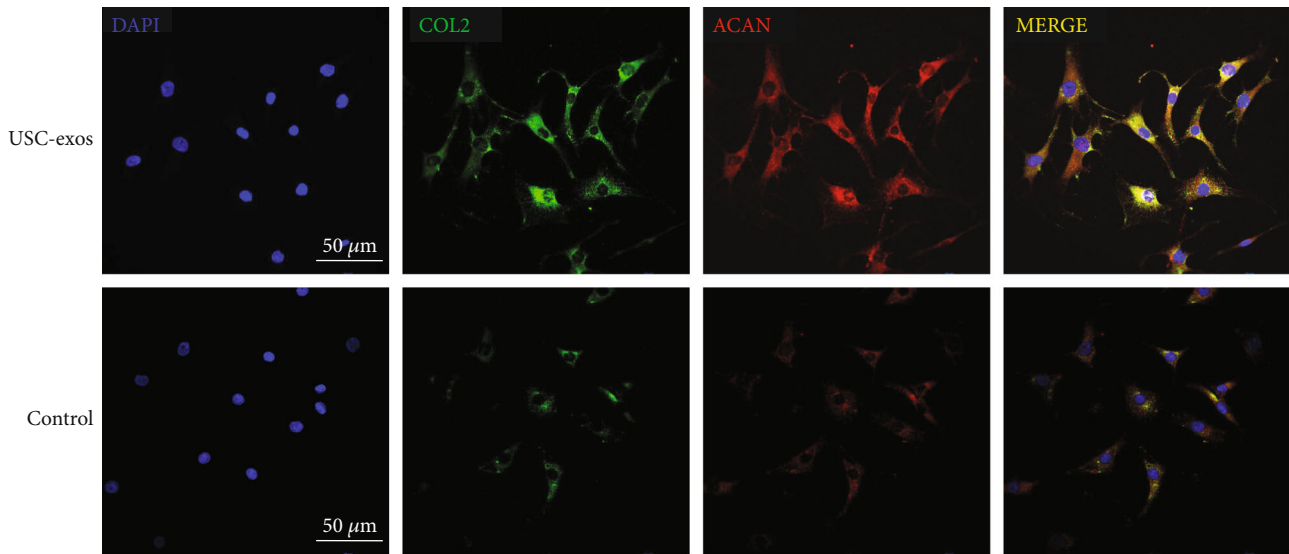


FIGURE 3: Immunofluorescence analysis of NPC ECM synthesis of COL2 and ACAN. Blue indicates DAPI, green indicates COL2, and red indicates ACAN. The expression of COL2 and ACAN was significantly increased when NPCs were induced by USC-exos.

regarded as the normal group without any treatment and the remaining 15 rats were regarded as the experimental group. Before the operation, the rats were anesthetized with 2% pentobarbital, and the three IVDs of each rat, namely, Co4/5, Co5/6, and Co6/7, were determined on the tail vertebrae by palpation with the aid of X-ray fluoroscopy [22]. A 20G fine needle (Hamilton, USA) was used to puncture the above three intervertebral discs, causing degeneration. Then, a 33G puncture needle (Hamilton, USA) was used to inject USC^{conshRNA}-exos (100 $\mu\text{g}/\text{ml}$) into Co4/5 cells, USC^{sh-MATN3}-exos (100 $\mu\text{g}/\text{ml}$) into Co5/6 cells, and PBS into Co6/7 cells (2 μl each). The first injection was performed 2 weeks after the puncture and repeated 4 weeks thereafter [23], and CT (GE, USA) and 3.0 MRI (GE, USA) were performed to observe the morphological appearance of the intervertebral discs in the 4th and 8th weeks. After 8 weeks, the rats were sacrificed, and intervertebral disc samples were collected for paraffin embedding and subsequent experiments. This experimental protocol was approved by the Animal Experiment Committee of Qingdao University.

2.14. Hematoxylin-Eosin (HE) Staining. The samples were decalcified and fixed in formaldehyde, dehydrated, embedded in paraffin, and sectioned. Then, a hematoxylin-eosin (HE) staining kit (Solarbio, Beijing, China) was used for HE staining. Specifically, paraffin sections were deparaffinized and hydrated stained with hematoxylin staining solution for 5-20 minutes and then treated with differentiation solution for 30 seconds. After washing with warm water, the sections were placed in eosin dye solution, washed again, and soaked, and they were then dehydrated, made transparent, mounted on film, sealed with neutral gum, and observed under a microscope.

2.15. Safranin O-Fast Green Staining. The sample was fixed with paraformaldehyde, decalcified, dehydrated, and then embedded in paraffin. Then, the Safranin O-Fast Green

Staining Kit (Solarbio, Beijing, China) was used for staining. Specifically, the sample was dewaxed in water, placed in freshly prepared Weigert's dye solution for 3-5 minutes, and then washed with water. Then, it was differentiated in acidic differentiation solution for 15 s, washed with distilled water for 10 min, dipped in the fast green staining solution for 5 min, and quickly washed with weak acid solution for 10-15 s to remove residual fast green. Then, it was placed in the Safranin O stain for 5 min, dehydrated in 95% ethanol and absolute ethanol, treated with xylene to make it transparent, and then sealed with optical resin for observations.

2.16. Tissue Immunofluorescence (IF) Staining. The samples were cut into frozen sections in advance for later use. Before staining, frozen sections were rewarmed at room temperature and then cleaned with TBST to remove residual optimal cutting temperature compound (OTC). After blocking with 3% BSA at room temperature for 1 hour, the MATN3 primary antibody (Bioss, Beijing, China) was added and incubated overnight at 4°C. After rewarming at room temperature for 30 minutes the next day, fluorescent secondary antibody was added, and the samples were incubated for 1 hour under dark conditions at room temperature. After DAPI was added, glycerol mount was used to observe the expression of MATN3 under a laser confocal microscope (Nikon, Japan) or stored at -20°C in the dark for subsequent observation.

2.17. Statistical Analysis. Each group of experiments was repeated at least three times. Continuous data are expressed as the mean \pm standard deviation (SD), and nonparametric data are expressed as the median and interquartile range. One-way analysis of variance (ANOVA) was used to compare the data between groups, and the parameters of parallel groups were compared by *t*-test. $P < 0.05$ indicates that the difference is statistically significant. All data were statistically analyzed using the SPSS 20.0 software (SPSS, Chicago, IL,

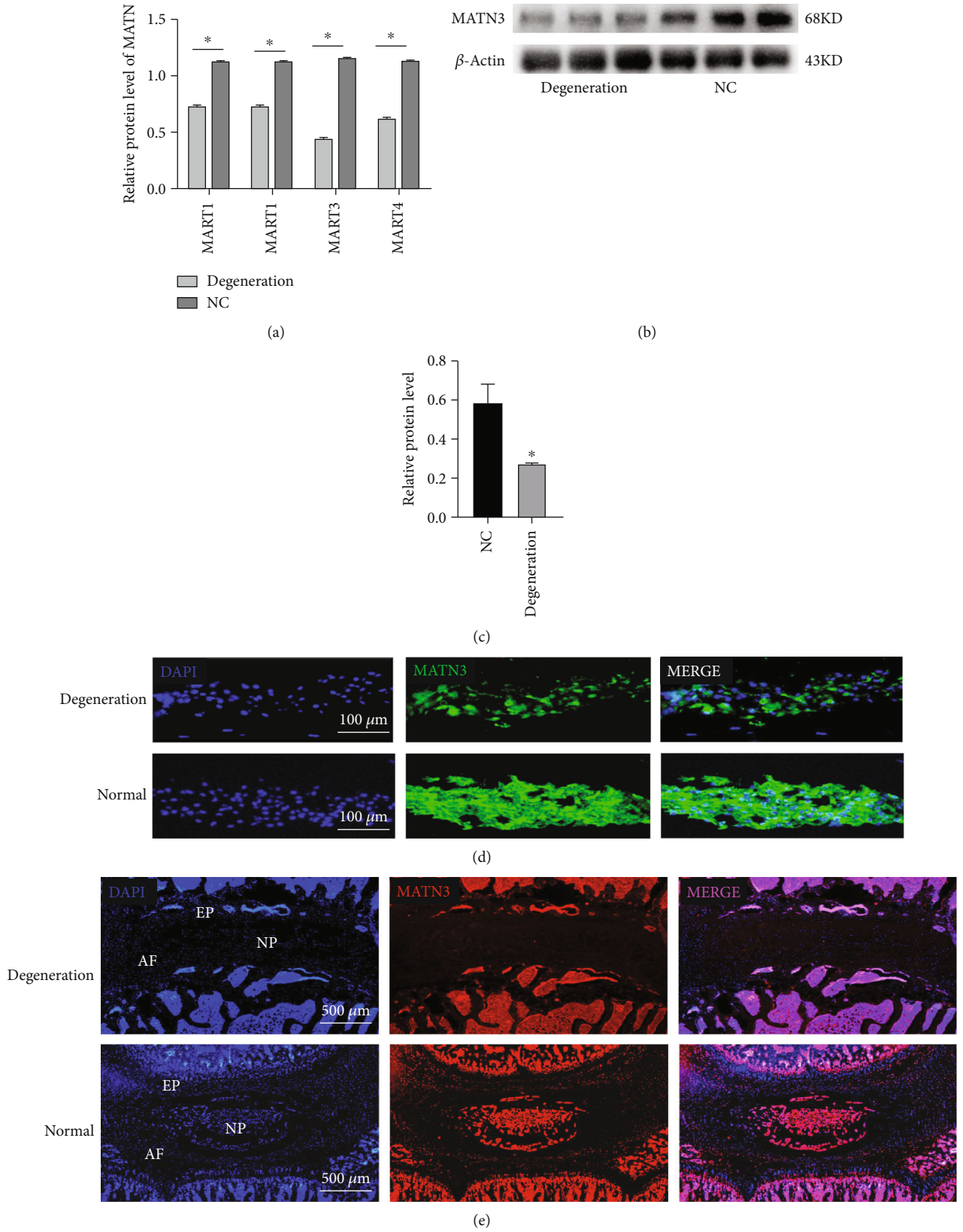


FIGURE 4: Continued.

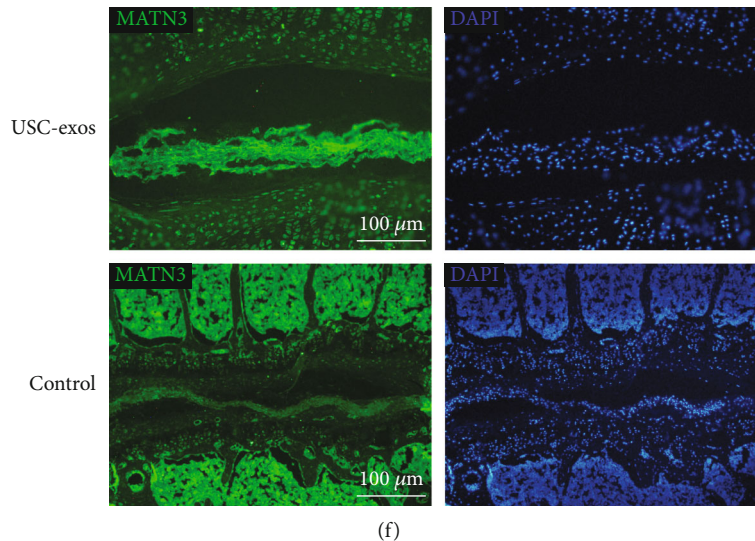


FIGURE 4: MATN3 was significantly decreased in the nucleus pulposus tissue of intervertebral discs. (a) Proteome analysis of the normal and degenerated discs of humans. The 4 matrilin family proteins were significantly decreased in the degenerated discs. MATN3 was the most differentially expressed ($n = 5$, $*P < 0.05$). (b, c) WB analysis of MATN3 expression in the normal and degenerated discs of humans. MATN3 significantly decreased in the degenerated discs ($n = 3$, $*P < 0.05$). (d) Immunofluorescence staining of human nucleus pulposus tissue for MATN3. Blue represents DAPI, and green represents MATN3. (e) Immunofluorescence image of intact rat IVDs for MATN3. (f) Exosome intervention in rat intervertebral discs was associated with the immunofluorescence results of degenerative intervertebral discs.

USA), and statistical graphs were drawn using GraphPad Prism 8 (GraphPad Software, USA).

3. Results

3.1. USC and USC-Exos Identification. USC colonies generally appeared 7 to 10 days after the primary cell culture and exhibited a cobblestone-like morphology under a light microscope. USCs had a relatively strong proliferation capacity and reached 90% confluence after 2-3 weeks of culture (Figure 1(a)). The characteristics of USCs were consistent with those described in a previous study [24].

Flow cytometry analysis showed that USCs were positive for USC surface markers CD29, CD44, and CD73 but negative for CD34 and CD45 (Figure 1(c)). USCs could differentiate into osteocytes, adipocytes, and chondrocytes when cultured in osteogenic, adipogenic, and chondrogenic conditioned culture media as previously reported [25] (Figure 1(b)). Therefore, the characteristics of USCs meet the criteria of multipotential differentiation as defined by MSCs.

USC-exos were obtained by ultrahigh-speed centrifugation. USC-exos were observed under a transmission electron microscope and showed a cup-shaped morphology with a diameter of approximately 50 nm (Figure 1(d)). The results of the particle size analysis showed that the diameter of USC-exos was 49.7 ± 7.3 nm (Figure 1(e)). WB showed that USC-exos were positive for CD63 and TSG101 but negative for calnexin (Figure 1(f)).

3.2. USC-Exos Resist Senescence and Promote NPC proliferation and ECM Synthesis. To assess the effects of USC-exos on NPCs function, we first determined the NPC

uptake of USC-exos. As shown in Figure 2(a), red fluorescent dye- (PKH26) labeled USC-exos were internalized into the perinuclear region of NPCs after 3 h of incubation. To determine the functional effects, USC-exos or an equal volume of PBS was added to the conditioned medium to culture NPCs for the indicated time.

A SA- β -Gal staining assay was utilized to examine the antisenescence effect of USC-exos, and the results showed that significantly less SA- β -Gal staining-positive NPCs were observed in the USC-exos group than that in the control group (Figure 2(b)). A CCK-8 analysis was performed to evaluate the effect of USC-exos on the proliferation of NPCs. The results revealed that the proliferation of NPCs was markedly promoted in response to USC-exos stimulation (Figure 2(d)).

To investigate the ECM modulation effect of USC-exos, NPCs were treated with USC-exos and PBS for 72 h. The results of western blot and immunofluorescent staining assays showed that NPCs of the USC-exos group had significantly elevated expression of COL2 and ACAN compared to the control (Figures 2(e), 2(f), and 3).

3.3. MATN3 Was Decreased Significantly in the Nucleus Pulposus Tissue of Intervertebral Disc. To investigate the potentially key proteins that lead to disc degeneration, a proteome analysis was applied in our previous study [26]. Further data mining was performed to compare the protein variation of normal and degenerated intervertebral discs, and we found that matrilin family proteins were significantly decreased in human degenerated intervertebral discs. The matrilin family has 4 members (MATN1, MATN2, MATN3, and MATN4), which are noncollagenous extracellular matrix proteins. Among them, MATN3 was the most differentially

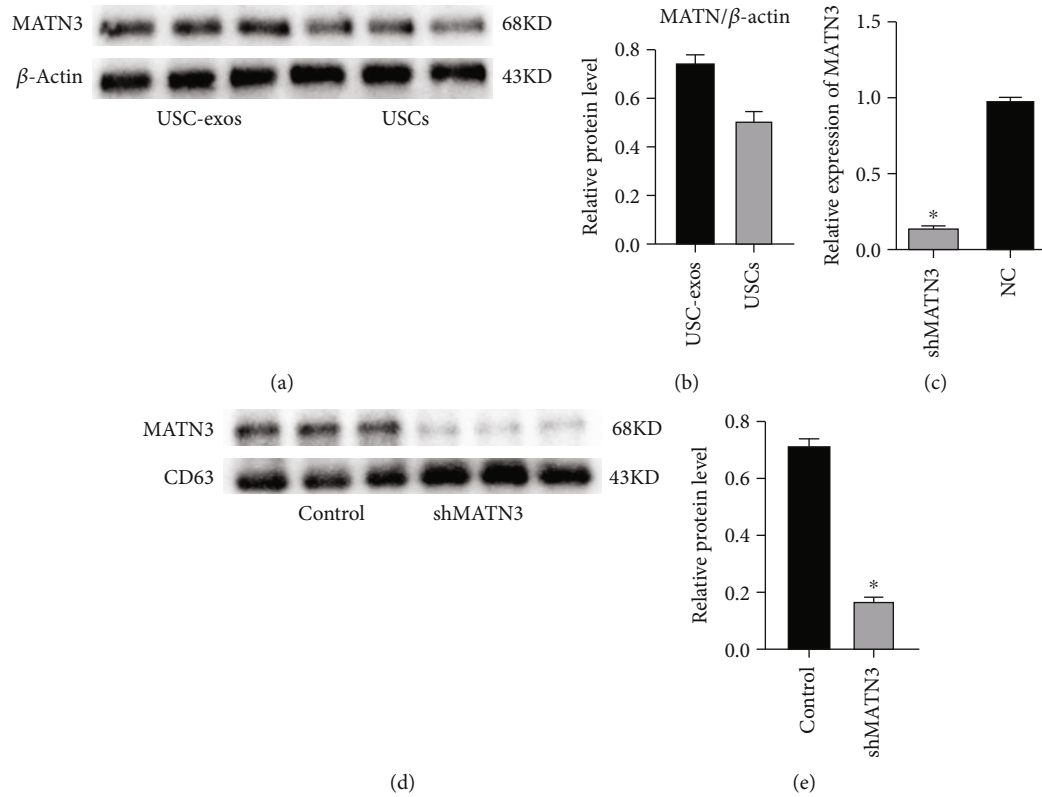


FIGURE 5: Identification of MATN3 in USC-exos and MATN3 knockdown in USCs. (a, b) WB analysis of MATN3 was rich in USC-exos ($n = 3$, $*P < 0.05$). (c) PCR analysis determined the silencing efficiency of shRNA-MATN3 to knockdown MATN3 expression in USCs ($n = 3$, $*P < 0.05$). (d, e) WB analysis of MATN3 knockdown in USC-exos ($n = 3$, $*P < 0.05$).

expressed (Figure 4(a)). The results of WB analysis and IF staining further confirmed the decrease in MATN3 in the degenerated human nucleus pulposus (Figures 4(b)–4(d)).

To reveal the variation of MATN3 throughout the degenerated intervertebral discs, normal and degenerated SD rat IVDs were detected for further IF staining. In normal rat IVDs, the nucleus pulposus (NP) and annulus fibrosus (AF) had a good morphological structure. MATN3 was widely distributed in the nucleus pulposus region and vertebral body and moderately distributed in the annulus fibrosus and endplate (EP). The number of MATN3-positive cells predominated in the NP and AF. However, in degenerated IVDs, the NP was unclear, and the structure of the AF was disordered. MATN3 was significantly reduced in both the nucleus pulposus and annulus fibrosus regions but not in the endplate region. Because of the partial ossification of the endplate in aged rats, there was a remarkable increase in MATN3 in endplate bone substances. However, there was no excessive expression of MATN3 in the endplates of young rats (Figure 4(e)). Immunofluorescence images of rat intervertebral discs treated with exosomes showed a significant increase in MATN3 content in the intervertebral discs, which in turn promoted extracellular matrix synthesis (Figure 4(f)).

3.4. Exosomal MATN3 in USCs Mediated the Antisenescence Activity and Proliferation and Promoted ECM Synthesis in NPCs. To investigate whether exosomal MATN3 of USCs mediates the effects, data mining was applied to previous

proteomic analyses of protein expression profiles in USC-exos and their parent USCs [25]. MATN3 was found to be rich in USC-exos, and our WB results also confirmed the enrichment (Figures 5(a) and 5(b)).

MATN3 shRNA was used to knockdown the expression of MATN3 in USCs, and the inhibitory efficiency of shMATN3 was examined by qRT-PCR (Figure 5(c)). USCs transfected with shMATN3 or control shRNA (Con shRNA) were used as parental cells to generate exosomes for downstream assays. The results of WB determined the downregulation of MATN3 in exosomes from MATN3-knockdown USCs (USC^{shMATN3}-exos) compared to the control exosomes from USCs transfected with Con shRNA (USC^{conshRNA}-exos) (Figures 5(d) and 5(e)).

Evidence has revealed that MATN3 can directly bind to a specific integrin, which promotes the dissociation and activation of TGF- β by changing the conformation of the TGF- β precursor complex [27]. Therefore, the activation of TGF- β and its downstream SMAD protein and proliferation-related AKT protein [28] was further investigated.

In the USC^{conMATN3}-exos group, the level of TGF- β and the extent of p-SMAD, COL2, and ACAN expression were significantly increased. However, in the USC^{shMATN3}-exos group, the promotive ability of USC-exos was markedly compromised when MATN3 expression in USC-exos was inhibited (Figure 6(a)). A SA- β -Gal staining assay showed that the antisenescence effect of USC-exos was mitigated, and it showed that SA- β -Gal staining-positive NPCs in

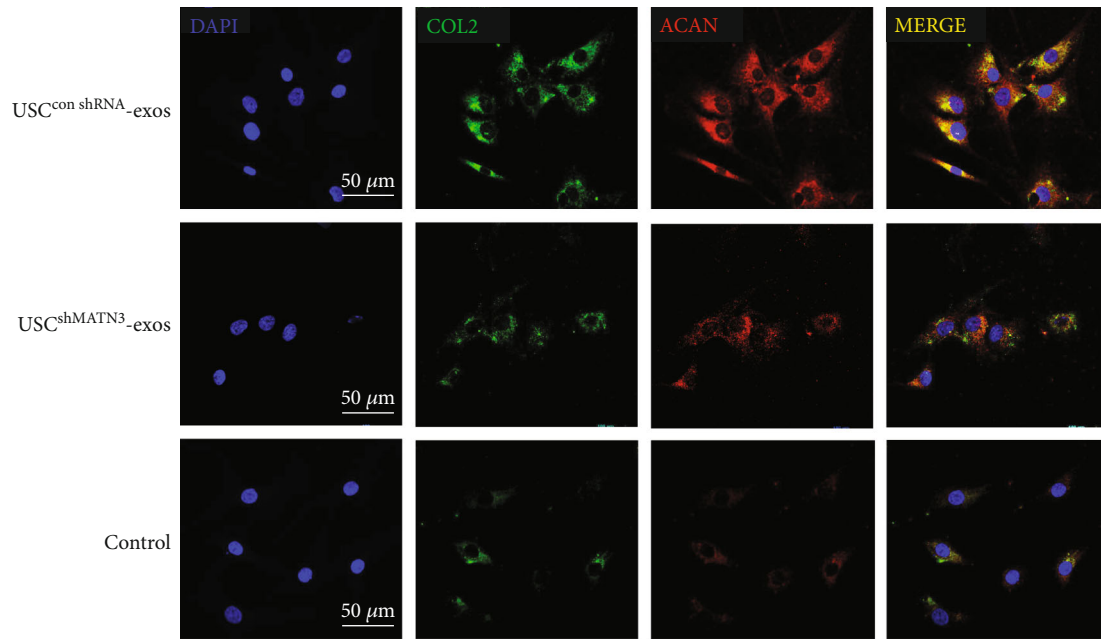


FIGURE 6: Immunofluorescence of NPC ECM synthesis for COL2 and ACAN. Blue indicates DAPI, green indicates COL2, and red indicates ACAN. The expression of COL2 and ACAN was significantly increased when NPCs were induced by USC^{con shRNA}-exos; however, the promotive effects were compromised when MATN3 was knocked down in USC^{shMATN3}-exos.

USC^{shMATN3}-exos group increased compared to those in the USC^{conMATN3}-exos group but was still lower than the control group (Figure 7(a)). The CCK-8 assay also showed a decreased ability of USC-exos to promote the proliferation of NPCs when MATN3 was knocked down.

In their parent USCs (Figure 7(b)), IF (Figure 8) indicated that the promotive effect of USC-exos on ECM synthesis was also suppressed once the MATN3 content was reduced in USC-exos.

Studies have reported that senescence and proliferation are associated with activating the PI3K-Akt pathway [29, 30]. Thus, we performed western blotting to detect the levels of Akt and p-Akt in NPCs following treatment with USC^{shMATN3}-exos, USC^{conshRNA}-exos, or an equal volume of PBS for 72 h. As shown in Figure 6(a), the ability of USC-exos to induce Akt phosphorylation was markedly compromised when MATN3 expression in USC-exos was inhibited. Collectively, our findings suggest that MATN3 is required for USC-exos-induced promotion of NPC proliferation and ECM synthesis.

4. Exosomal MATN3 Alleviates Intervertebral Disc Degeneration in the IVD Rat Model

To further verify the therapeutic effects of exosomal MATN3 of USC-exos, we applied USC^{conshRNA}-exos, USC^{shMATN3}-exos, and an equal volume of PBS to IVD rats. The degeneration grades of rat intervertebral discs were evaluated by CT and MRI examination at 4 and 8 weeks after the intradiscal intervention (Figures 9(a) and 9(d)–9(f)). Typical disc tissue could be seen in normal, undegenerated rat intervertebral discs (Figure 9(f)). The percent disc height index (%DHI) was measured according to the results of sagittal CT recon-

struction images (Figures 9(b) and 9(c)). A low %DHI indicates collapse or narrowing of the intervertebral space, which reflects the extent of degenerative changes. At 4 weeks and 8 weeks, the %DHI of the USC^{conshRNA}-exos group was higher than that of the USC^{conshRNA}-exos and PBS groups, and the %DHI of the USC^{shMATN3}-exos group was higher than that of the PBS group. Histological grade was analyzed according to HE and Safranin O-fast green staining (Figure 9(g)).

Meanwhile, the Pfirrmann grade was based on morphological changes of the intervertebral discs in MRI, and greater degeneration corresponded to a higher grade. The Pfirrmann grade of the USC^{conshRNA}-exos group was lower than that of the USC^{conshRNA}-exos and PBS groups, and the Pfirrmann grade of the USC^{shMATN3}-exos group was lower than that of the PBS group. In normal rats, however, there was no significant disc degeneration (Figure 9(a)).

To verify the radiographic results, further histological staining and immunohistochemical analysis were applied. As shown in Figure 9, the IVDs in the USC^{conshRNA}-exos group had higher disc heights, more ECM components, and more organized NP tissues than those in the USC^{shMATN3}-exos group and PBS group. However, the IVDs in the USC^{shMATN3}-exos group had a lower disc height, fewer ECM components, and more disorganized NP tissues than those in the USC^{conshRNA}-exos group but had a better morphological score than that of the PBS group. That is, compared to the PBS group, the intervertebral discs of the USC^{conshRNA}-exos group exhibited alleviated degeneration. However, in the USC^{shMATN3}-exos group, the ability to mitigate degeneration of the intervertebral disc was compromised when MATN3 was inhibited. Collectively, the radiographic results and morphological analyses indicated that full-ingredient USC-exos

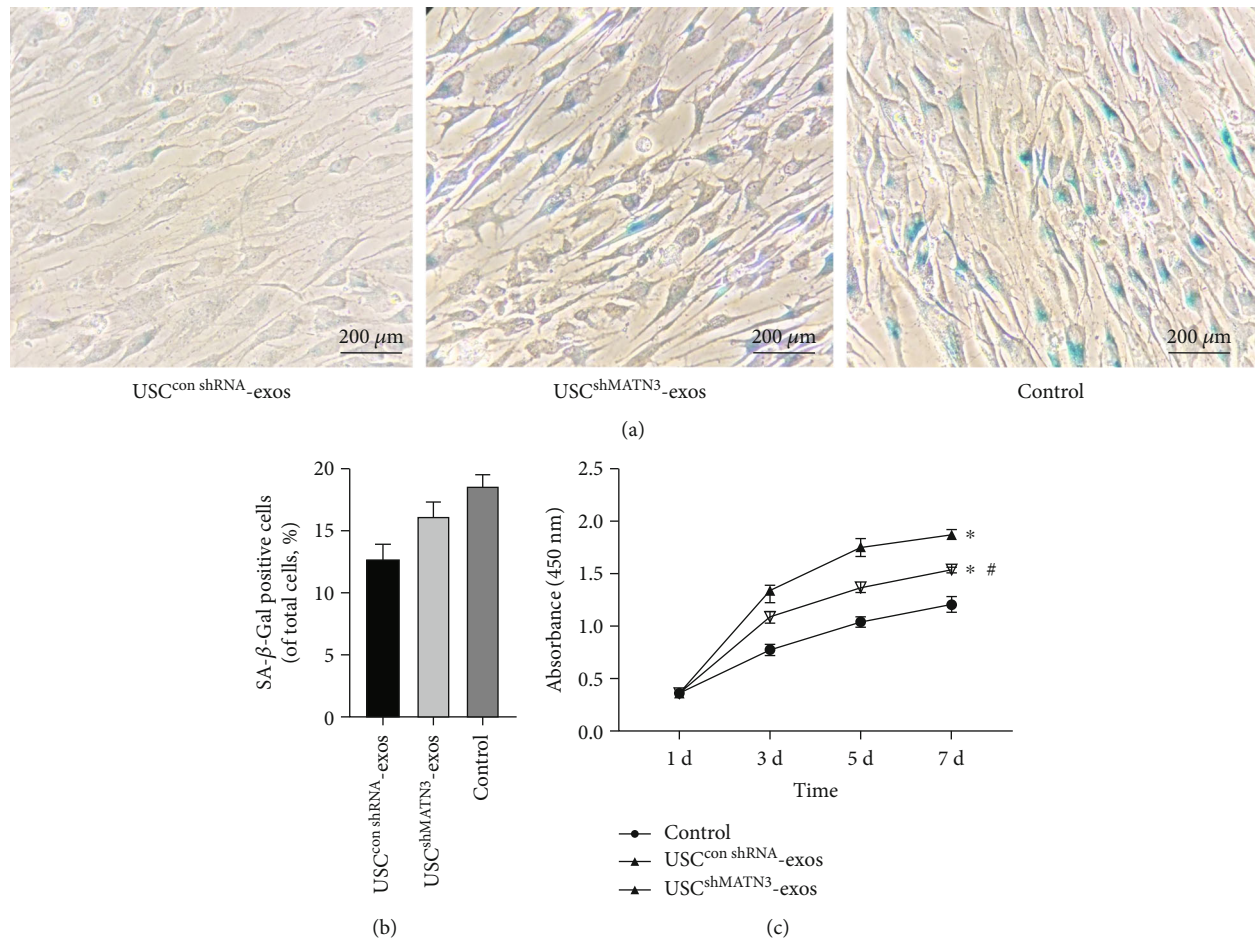


FIGURE 7: MATN3 of USC-exos mediated the antisenesence and proliferation promoting effects on NPCs. (a) SA-β-Gal staining assay of the NPCs induced by USC^{conMATN3}-exos, USC^{shMATN3}-exos, and PBS. (b) SA-β-Gal staining assay showing the antisenesence effect of USC-exos. Multifield random counting showed that the proportion of SA-β-Gal-positive NPCs in USC^{conMATN3}-exos and USC^{shMATN3}-exos groups was significantly lower than that in the control group. (c) CCK-8 analysis of NPCs proliferation stimulated with USC^{conMATN3}-exos, USC^{shMATN3}-exos, and PBS ($n = 3$ per group, $*P < 0.05$ vs. control, $\#P < 0.05$ vs. USC^{shMATN3}-exos).

with MATN3 could significantly ameliorate intervertebral disc degeneration, while the beneficial effect was attenuated when MATN3 was knocked down in USC-exos.

5. Discussion

The main causes for IDD have not been clarified. However, a consensus has been reached that a continuous decrease in NPCs and degradation of ECM are the pathological basis of IDD [7, 31]. Therefore, finding a method of maintaining the number of NPCs and promoting the synthesis of ECM are the keys to alleviating or even reversing IDD.

In this study, we demonstrated that the content of MATN3 was significantly reduced in degenerated intervertebral discs. MATN3 is a member of the matrilin family and a noncollagenous ECM protein that shares a common structure, including the von Willebrand factor A (WFA) domain, epidermal growth factor (EGF) domain, and C-terminal coiled-coil oligomerization domain [32]. MATN3 is a cartilage-specific protein that can assemble the chondrocyte ECM. As an ECM protein, matrilin-3 can cross-link with collagen fibrils and multiple proteoglycans, playing a critical

role in forming a fibrous matrix network [27]. In the past, MATN3 was found to be required for cartilage homeostasis [9]. Mutations in matrilin-3 in humans can cause many kinds of skeletal diseases, such as multiple epiphyseal dysplasia and early-onset osteoarthritis [33]. The polymorphisms in the MATN3 gene were previously tested, and they indicated a genetic association with IDD. Mutation of the MATN3 region leads to susceptibility to spinal disc degeneration [34]. Here, for the first time, we revealed the spatial and temporal variation in MATN3 in normal and degenerated intervertebral discs. The change in MATN3 was most significant in the NP tissue and moderate in the AF. The decrease in MATN3 in the IVD could be considered a characteristic of IDD.

With the development of exosome research, an increasing number of researchers are studying exosomes as a potential treatment for intervertebral disc degeneration. Stem cell-derived exosomes may offer cell-free therapies as an alternative to traditional stem cell therapies [35]. Intervertebral disc degeneration is usually accompanied by the apoptosis of nucleus pulposus cells and the loss of extracellular matrix. The accumulation of inflammatory factors and matrix-

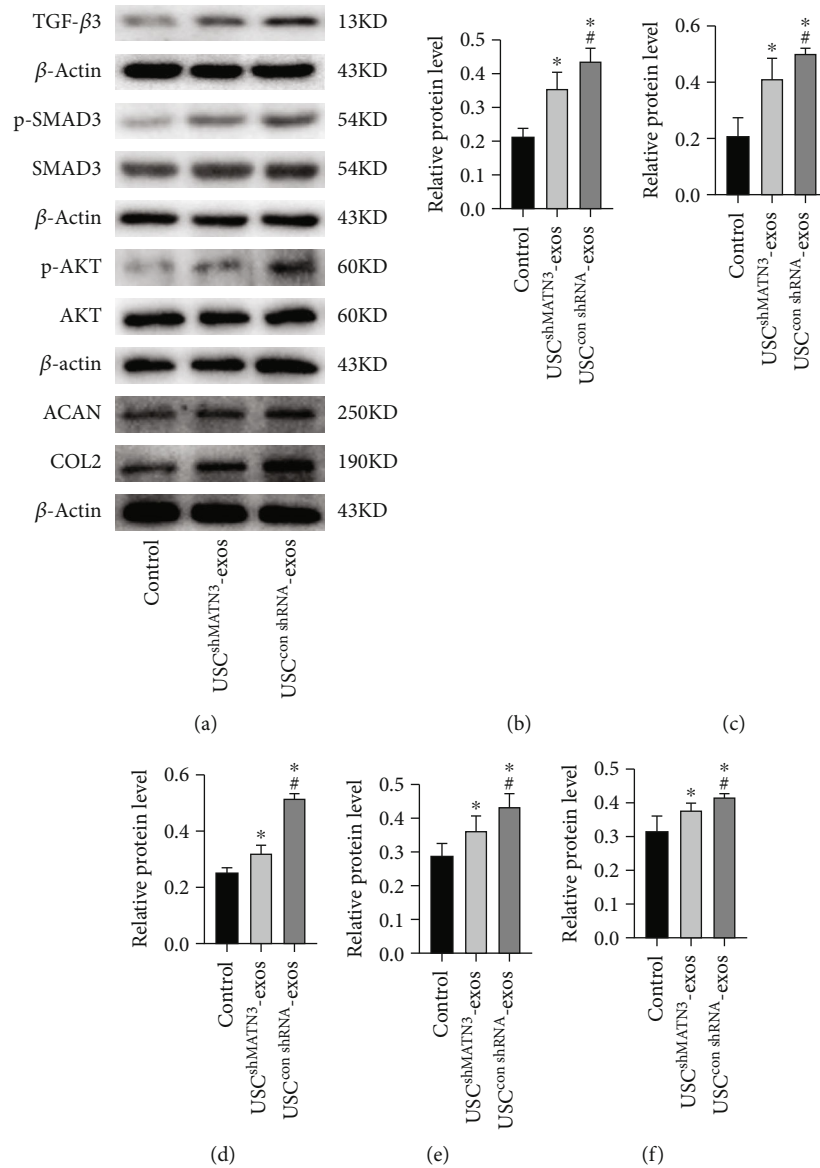


FIGURE 8: WB analysis of TGF- β canonical SMAD pathway and noncanonical pathway (AKT) activation ($n = 3$ per group; * $P < 0.05$ vs. control, # $P < 0.05$ vs. USC^{shMATN3}-exos).

degrading enzymes in intervertebral discs is an important reason for this phenomenon [36, 37]. In a study of degenerated and normal nucleus pulposus, Xia et al. [38] found that there were a variety of proteins related to the inflammatory response in intervertebral discs, most of which were expressed in degenerated intervertebral discs. The results showed that IL-1 β , iNOS, COX-2, IL-6, MMP3, MMP13, and other inflammatory cytokines and extracellular matrix-degrading enzymes were significantly reduced after the addition of stem cell-derived exosomes. These results suggest that stem cell-derived exosomes can reduce the inflammatory response of intervertebral discs and the degradation of extracellular matrix. At the present stage, most experiments have used MSCs; however, this research group uniquely chose USCs. USCs not only have MSC-related characteristics but also have a number of unique advantages. USCs are a population of cells isolated from

urine that have the biological properties and differentiation potential of stem cells. Although limited research has been performed on USCs, studies have confirmed that USCs can be induced to differentiate into osteoblasts, chondrocytes, smooth muscle cells, cardiomyocytes, urothelial cells, neural precursor cells, skeletal muscle cells, and adipocytes; moreover, after several generations of culture, the karyotype remains stable without tumorigenicity, the acquisition pathway is noninvasive and simple, and the culture system is stable [39–43]. Previous studies have found that the proliferation ability of stem cells is closely related to telomerase activity and telomere length. Compared with MSCs, USCs have higher telomerase activity and longer telomere sequences; therefore, they have stronger proliferation ability [44]. The above characteristics of USCs make them a better source for exosome extraction, and their application has very broad prospects.

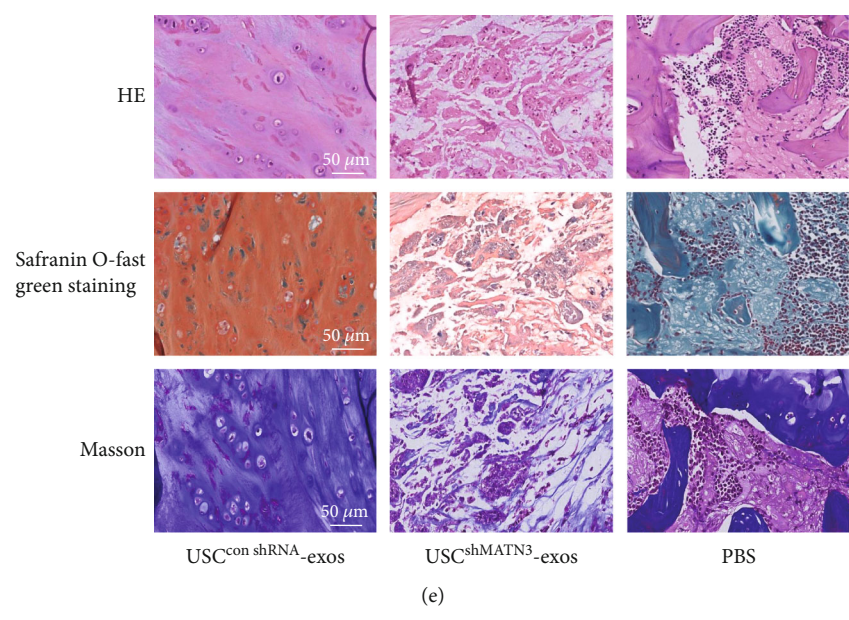
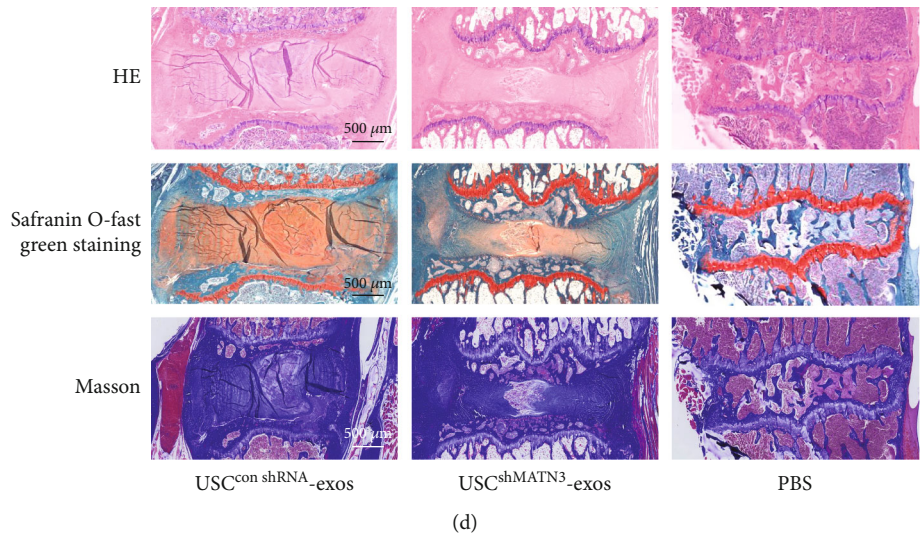
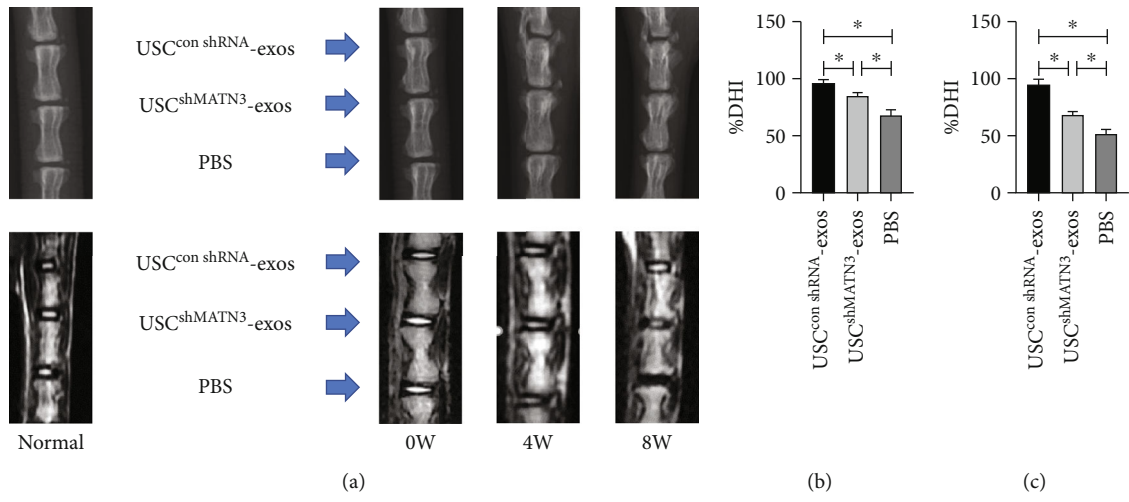


FIGURE 9: Continued.

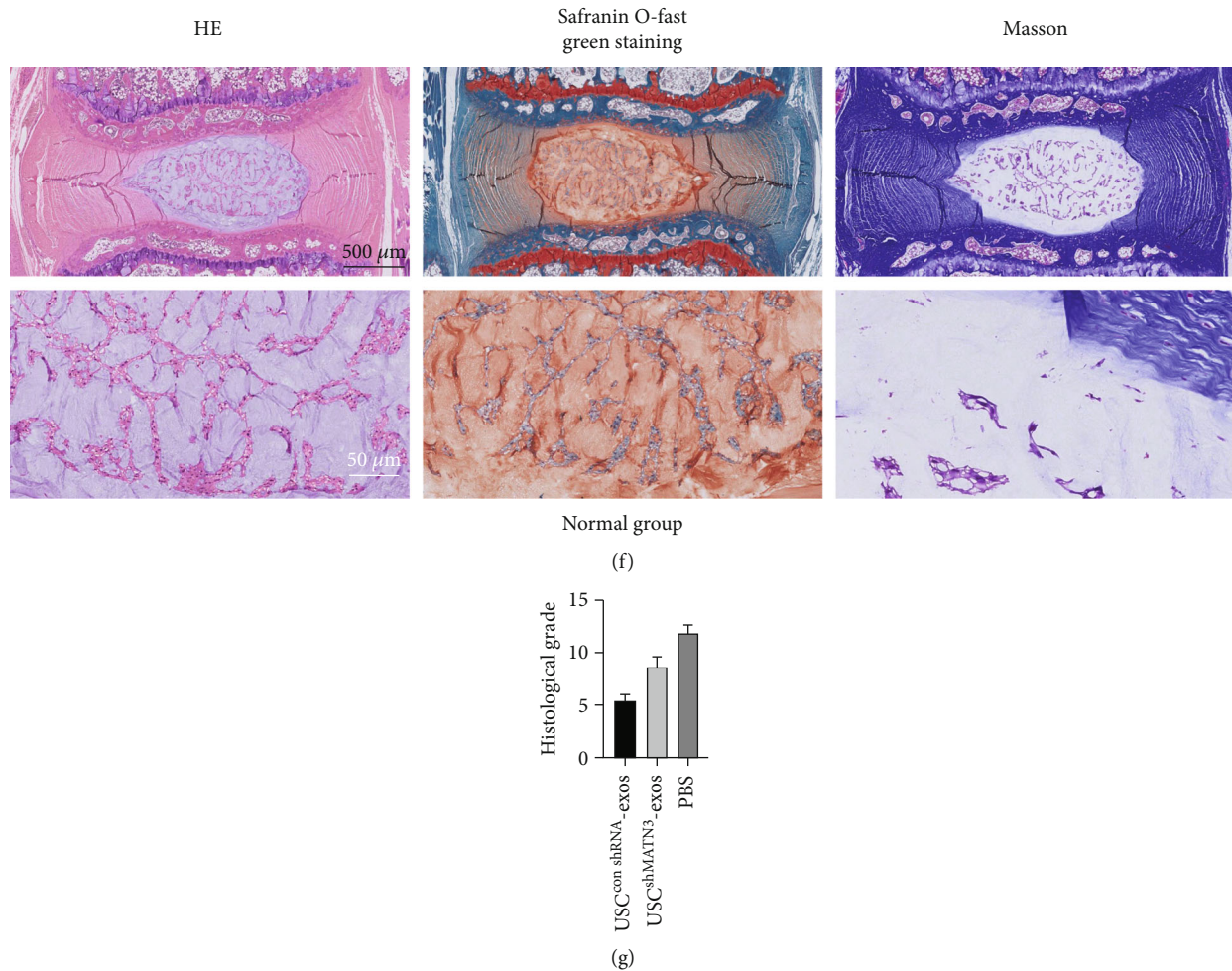


FIGURE 9: Exosomal MATN3 alleviates intervertebral disc degeneration in the IVD rat model. (a) CT and MRI images of normal rat intervertebral disc. CT and MR images of rat intervertebral discs treated with USC^{con shRNA}-exos, USC^{shMATN3}-exos, and PBS at 0, 4, and 8 weeks. (b, c) The change of percentage of disc height index (%DHI) was calculated based on CT measurements in each group, where (b) is the situation at 4 weeks and (c) is the situation at 8 weeks. Data are expressed as mean \pm SD. * means $P < 0.05$. (d) HE, Safranin O-fast green staining, and Masson of intact rat IVDs. (e) HE, Safranin O-fast green staining, and Masson of a partially enlarged NP of rat IVDs. (f) HE, Safranin O-fast green staining, and Masson of normal undegenerated rat intervertebral discs. (g) Histological grade was assessed by HE staining and Saffron O solid green staining. Data are expressed as mean \pm SD. * means $P < 0.05$.

In previous experiments, Lu et al. [45] used MSC-derived exosomes to intervene in NPCs, and the results showed that exosomes could stimulate the phenotypes of degenerated NPCs to restore undegenerated NPCs to increase the synthesis of extracellular matrix and achieve self-repair. Their studies suggest that exosomes may play a pivotal role in the endogenous repair of IVDs. In another study, Lu et al. [46] showed that MATN3 promoted the synthesis of COL2 and ACAN by promoting IL-1 α expression and inhibited the production of IL-1 β -induced catabolic matrix proteinases, thereby delaying intervertebral disc degeneration by reducing extracellular matrix degradation. In this study, our previous experiments showed that intervention with USC-exos could reduce the degradation of extracellular matrix and promote its synthesis, which delayed the effect of intervertebral disc degeneration. The presence of MATN3 in USC-exos was verified in subsequent experiments, suggesting that USC-exos may inhibit intervertebral disc degeneration through MATN3.

Studies have shown that exosomes can promote the proliferation of NPCs and the synthesis of extracellular matrix. Moreover, exosomes are complex and contain a large number of substances, which may be released in the presence of MATN3. Our results demonstrated that USC-exos could markedly promote NPC proliferation and ECM synthesis. The promotion of USC-exos was significantly reduced after siRNA was used. At the same time, the WB method was used to identify USC-exos, and the composition of MATN3 was confirmed. By mining the data of previous proteome analyses, we found that MATN3 was rich in USC-exos, which means that USC-exos could act as a vehicle to transfer the MATN3 protein. Due to the advantages of urine-derived stem cells, the source of exosomes was optimized in this study. Moreover, the role and mechanism of MATN3 in the treatment of intervertebral disc degeneration by USC-exos were verified, with the therapeutic effect achieved by regulating the TGF- β content. This study provides insights for

investigating exosome-based treatments for intervertebral disc degeneration.

Evidence has revealed that MATN3 can directly bind to specific integrins, which promotes the dissociation and activation of TGF- β by changing the conformation of the TGF- β precursor complex, thereby further affecting downstream gene activation [32]. Our results strongly suggested that MATN3 in USC-exos achieved the promotive function by activating TGF- β . TGF- β is a multifunctional cytokine that modulates cell fate and plasticity in a variety of tissues. The multiple cellular responses induced by TGF- β are mediated via the canonical SMAD pathway and noncanonical pathways, including the phosphatidylinositol 3'-kinase- (PI3K-) protein kinase B (AKT) pathway [28, 47]. TGF- β /SMAD pathway activation can promote the expression of COL2 and ACAN in the extracellular matrix of nucleus pulposus, and phosphorylation of AKT can promote antisenesence effects and cell proliferation [29, 30]. In the results, we demonstrated that exosomal MATN3 from USCs mediated the promotive effects. It is likely that MATN3 fulfilled its functions by activating the canonical SMAD pathway and noncanonical pathways (PI3K-AKT). We determined that MATN3 promoted the expression of TGF- β 3 and increased the phosphorylation level of SMD and AKT NPCs. Multiple further loss-of-function assays of MATN3 suggested that exosomal MATN3 of USCs mediated the antisenesence effect and promotive effects of NPCs on proliferation and ECM synthesis. Beyond that, we verified that MATN3 in USC-exos could ameliorate IVD in the IDD rat model. The ability of USC-exos to alleviate IDD was significantly compromised when MATN3 was knocked down. The radiographic and histological analysis results indicated that the USC-conshRNA-exos group exhibited a lower degree of IVD degeneration than the PBS group. However, in the USC^{sh-MATN3}-exos group, the promotive effects were suppressed when MATN3 was knocked down, which indicated that MATN3 in USC-exos mediated the beneficial effects on IDD.

In addition, no significant change was observed between the PBS injection discs and the no-intervention discs, indicating a negative effect of the puncture caused by 33-gauge fine needles on intervertebral disc degeneration.

6. Conclusions

MATN3 is not only a noncollagenous ECM protein but also a regulator that could assist in senescence and modulate NPC proliferation and ECM homeostasis. USC-exos may be a potential therapeutic agent for IDD by transferring the MATN3 protein.

Data Availability

The data analyzed in this research can be obtained from Zhu Guo, Yan Wang, BoHua Chen, and HongFei Xiang on reasonable request.

Ethical Approval

This study was approved by the ethical committee of Affiliated Hospital of Qingdao University. The study participants were required to give a written informed consent, and their data was coded for confidentiality and compliance with the Declaration of Helsinki.

Consent

Written informed consent was obtained from all the patients for publication of this research and any accompanying images.

Conflicts of Interest

The authors declare that they have no conflict of interest.

Authors' Contributions

Zhu Guo, Shuai Yang, RongYao Zhou, Yan Wang, BoHua Chen, and HongFei Xiang designed the study; Zhu Guo, WeiLiang Su, RongYao Zhou, HongFei Xiang, Chang Liu, Nana Shen, WenBin Cong, XiaoLin Wu, DongMing Xing, Yan Wang, Guoqing Zhang, JianWei Guo, Shang-You Yang, and ChenSheng Qiu enrolled the study participants and collected the data; Zhu Guo and WeiLiang Su analyzed the data; Zhu Guo, RongYao Zhou, Chang Liu, BoHua Chen, and HongFei Xiang interpreted the data and wrote the manuscript. All authors reviewed and approved the manuscript. Zhu Guo, WeiLiang Su, and Rong Yao Zhou contributed equally to this work.

Acknowledgments

This study was funded by the National Natural Science Foundation of China (81802190 and 81772412), Shandong Provincial Science Foundation, China (ZR2019BH084), Young Taishan Scholars Program (tsqn201909190), Qingdao Basic Applied Research Project (19-6-2-51-cg), and National Key Research and Development Project (2019YFC0121404).

References

- [1] C. Maher, M. Underwood, and R. Buchbinder, "Non-specific low back pain," *The Lancet*, vol. 389, no. 10070, pp. 736–747, 2017.
- [2] F. Balagué, A. F. Mannion, F. Pellisé, and C. Cedraschi, "Non-specific low back pain," *The Lancet*, vol. 379, no. 9814, pp. 482–491, 2012.
- [3] C. J. L. Murray, T. Vos, R. Lozano et al., "Disability-adjusted life years (DALYs) for 291 diseases and injuries in 21 regions, 1990–2010: a systematic analysis for the Global Burden of Disease Study 2010," *The Lancet*, vol. 380, no. 9859, pp. 2197–2223, 2012.
- [4] K. Luoma, H. Riihimäki, R. Luukkonen, R. Raininko, E. Viikari-Juntura, and A. Lamminen, "Low back pain in relation to lumbar disc degeneration," *Spine*, vol. 25, no. 4, pp. 487–492, 2000.

- [5] J. N. Katz, "Lumbar disc disorders and low-back pain: socioeconomic factors and consequences," *The Journal of Bone and Joint Surgery*, vol. 88, Supplement 2, pp. 21–24, 2006.
- [6] Z. Liao, R. Luo, G. Li et al., "Exosomes from mesenchymal stem cells modulate endoplasmic reticulum stress to protect against nucleus pulposus cell death and ameliorate intervertebral disc degeneration in vivo," *Theranostics*, vol. 9, no. 14, pp. 4084–4100, 2019.
- [7] F. Ding, Z. W. Shao, and L. M. Xiong, "Cell death in intervertebral disc degeneration," *Apoptosis*, vol. 18, no. 7, pp. 777–785, 2013.
- [8] C. L. Le Maitre, A. Pockert, D. J. Buttle, A. J. Freemont, and J. A. Hoyland, "Matrix synthesis and degradation in human intervertebral disc degeneration," *Biochemical Society Transactions*, vol. 35, Part 4, pp. 652–655, 2007.
- [9] N. V. Vo, R. A. Hartman, T. Yurube, L. J. Jacobs, G. A. Sowa, and J. D. Kang, "Expression and regulation of metalloproteinases and their inhibitors in intervertebral disc aging and degeneration," *The Spine Journal*, vol. 13, no. 3, pp. 331–341, 2013.
- [10] B. Zhang, W. Guo, C. Sun et al., "Dysregulated MiR-3150a-3p promotes lumbar intervertebral disc degeneration by targeting aggrecan," *Cellular Physiology and Biochemistry*, vol. 45, no. 6, pp. 2506–2515, 2018.
- [11] C. K. Kepler, R. K. Ponnappan, C. A. Tannoury, M. V. Risbud, and D. G. Anderson, "The molecular basis of intervertebral disc degeneration," *The Spine Journal*, vol. 13, no. 3, pp. 318–330, 2013.
- [12] H. Yang, J. Wu, J. Liu et al., "Transplanted mesenchymal stem cells with pure fibrinous gelatin-transforming growth factor- β 1 decrease rabbit intervertebral disc degeneration," *The Spine Journal*, vol. 10, no. 9, pp. 802–810, 2010.
- [13] D. C. Noriega, F. Ardura, R. Hernández-Ramajo et al., "Intervertebral disc repair by allogeneic mesenchymal bone marrow cells: a randomized controlled trial," *Transplantation*, vol. 101, no. 8, pp. 1945–1951, 2017.
- [14] S. Zhang, S. J. Chuah, R. C. Lai, J. H. P. Hui, S. K. Lim, and W. S. Toh, "MSC exosomes mediate cartilage repair by enhancing proliferation, attenuating apoptosis and modulating immune reactivity," *Biomaterials*, vol. 156, pp. 16–27, 2018.
- [15] D. G. Phinney and M. F. Pittenger, "Concise review: MSC-derived exosomes for cell-free therapy," *Stem Cells*, vol. 35, no. 4, pp. 851–858, 2017.
- [16] Y. Zhang, E. McNeill, H. Tian et al., "Urine derived cells are a potential source for urological tissue reconstruction," *The Journal of Urology*, vol. 180, no. 5, pp. 2226–2233, 2008.
- [17] X. Ji, M. Wang, F. Chen, and J. Zhou, "Urine-derived stem cells: the present and the future," *Stem Cells International*, vol. 2017, Article ID 4378947, 8 pages, 2017.
- [18] N. P. A. Manaph, M. Al-Hawwas, L. Bobrovskaya, P. T. Coates, and X.-F. Zhou, "Urine-derived cells for human cell therapy," *Stem Cell Research & Therapy*, vol. 9, no. 1, p. 189, 2018.
- [19] P. Wu, B. Zhang, H. Shi, H. Qian, and W. Xu, "MSC-exosome: a novel cell-free therapy for cutaneous regeneration," *Cytotherapy*, vol. 20, no. 3, pp. 291–301, 2018.
- [20] H. F. Xiang, W. L. Su, X. L. Wu et al., "Exosomes derived from human urine-derived stem cells inhibit intervertebral disc degeneration by ameliorating endoplasmic reticulum stress," *Oxidative Medicine and Cellular Longevity*, vol. 2020, Article ID 6697577, 21 pages, 2020.
- [21] L. Zheng, Y. Cao, S. Ni et al., "Ciliary parathyroid hormone signaling activates transforming growth factor- β to maintain intervertebral disc homeostasis during aging," *Bone Research*, vol. 6, no. 1, p. 21, 2018.
- [22] H. Zhang, F. La Marca, S. J. Hollister, S. A. Goldstein, and C.-Y. Lin, "Developing consistently reproducible intervertebral disc degeneration at rat caudal spine by using needle puncture," *Journal of Neurosurgery. Spine*, vol. 10, no. 6, pp. 522–530, 2009.
- [23] X. Cheng, G. Zhang, L. Zhang et al., "Mesenchymal stem cells deliver exogenous miR-21 via exosomes to inhibit nucleus pulposus cell apoptosis and reduce intervertebral disc degeneration," *Journal of Cellular and Molecular Medicine*, vol. 22, no. 1, pp. 261–276, 2018.
- [24] T. Zhou, C. Benda, S. Dunzinger et al., "Generation of human induced pluripotent stem cells from urine samples," *Nature Protocols*, vol. 7, no. 12, pp. 2080–2089, 2012.
- [25] C.-Y. Chen, S.-S. Rao, L. Ren et al., "Exosomal DMBT1 from human urine-derived stem cells facilitates diabetic wound repair by promoting angiogenesis," *Theranostics*, vol. 8, no. 6, pp. 1607–1623, 2018.
- [26] C. Qiu, X. Wu, J. Bian et al., "Differential proteomic analysis of fetal and geriatric lumbar nucleus pulposus: immunoinflammation and age-related intervertebral disc degeneration," *BMC Musculoskeletal Disorders*, vol. 21, no. 1, p. 339, 2020.
- [27] J. B. Vincourt, S. Etienne, L. Grossin et al., "Matrilin-3 switches from anti- to pro-anabolic upon integration to the extracellular matrix," *Matrix Biology*, vol. 31, no. 5, pp. 290–298, 2012.
- [28] A. Hamidi, J. Song, N. Thakur et al., "TGF- β promotes PI3K-AKT signaling and prostate cancer cell migration through the TRAF6-mediated ubiquitylation of p85 α ," *Science Signaling*, vol. 10, no. 486, 2017.
- [29] F. B. Feng and H. Y. Qiu, "Effects of Artesunate on chondrocyte proliferation, apoptosis and autophagy through the PI3K/AKT/mTOR signaling pathway in rat models with rheumatoid arthritis," *Biomedicine & Pharmacotherapy*, vol. 102, pp. 1209–1220, 2018.
- [30] C. Chai, L. J. Song, S. Y. Han, X. Q. Li, and M. Li, "Micro RNA-21 promotes glioma cell proliferation and inhibits senescence and apoptosis by targeting SPRY1 via the PTEN/PI3K/AKT signaling pathway," *CNS Neurosci Ther*, vol. 24, no. 5, pp. 369–380, 2018.
- [31] W. J. Wang, X. H. Yu, C. Wang et al., "MMPs and ADAMTSs in intervertebral disc degeneration," *Clinica Chimica Acta*, vol. 448, pp. 238–246, 2015.
- [32] O. Pullig, G. Weseloh, A. R. Klatt, R. Wagener, and B. Swoboda, "Matrilin-3 in human articular cartilage: increased expression in osteoarthritis," *Osteoarthritis and Cartilage*, vol. 10, no. 4, pp. 253–263, 2002.
- [33] K. L. Chapman, G. R. Mortier, K. Chapman, J. Loughlin, M. E. Grant, and M. D. Briggs, "Mutations in the region encoding the von Willebrand factor A domain of matrilin-3 are associated with multiple epiphyseal dysplasia," *Nature Genetics*, vol. 28, no. 4, pp. 393–396, 2001.
- [34] J. L. Min, I. Meulenbelt, N. Riyazi et al., "Association of matrilin-3 polymorphisms with spinal disc degeneration and osteoarthritis of the first carpometacarpal joint of the hand," *Annals of the Rheumatic Diseases*, vol. 65, no. 8, pp. 1060–1066, 2006.
- [35] S. Rani, A. E. Ryan, M. D. Griffin, and T. Ritter, "Mesenchymal stem cell-derived extracellular vesicles: toward cell-free

- therapeutic applications,” *Molecular Therapy*, vol. 23, no. 5, pp. 812–823, 2015.
- [36] T. Kadow, G. Sowa, N. Vo, and J. D. Kang, “Molecular basis of intervertebral disc degeneration and herniations: what are the important translational questions?,” *Clinical Orthopaedics and Related Research*, vol. 473, no. 6, pp. 1903–1912, 2015.
- [37] M. V. Risbud and I. M. Shapiro, “Role of cytokines in intervertebral disc degeneration: pain and disc content,” *Nature Reviews Rheumatology*, vol. 10, no. 1, pp. 44–56, 2014.
- [38] C. Xia, Z. Zeng, B. Fang et al., “Mesenchymal stem cell-derived exosomes ameliorate intervertebral disc degeneration via antioxidant and anti-inflammatory effects,” *Free Radical Biology & Medicine*, vol. 143, pp. 1–15, 2019.
- [39] J. Mulder, S. Sharmin, T. Chow et al., “Generation of infant- and pediatric-derived urinary induced pluripotent stem cells competent to form kidney organoids,” *Pediatric Research*, vol. 87, no. 4, pp. 647–655, 2020.
- [40] L. Wang, L. Wang, W. Huang et al., “Generation of integration-free neural progenitor cells from cells in human urine,” *Nature Methods*, vol. 10, no. 1, pp. 84–89, 2013.
- [41] H. Qin, C. Zhu, Z. An et al., “Silver nanoparticles promote osteogenic differentiation of human urine-derived stem cells at noncytotoxic concentrations,” *International Journal of Nanomedicine*, vol. 9, pp. 2469–2478, 2014.
- [42] G. Liu, R. A. Pareta, R. Wu et al., “Skeletal myogenic differentiation of urine-derived stem cells and angiogenesis using microbeads loaded with growth factors,” *Biomaterials*, vol. 34, no. 4, pp. 1311–1326, 2013.
- [43] S. Wu, Y. Liu, S. Bharadwaj, A. Atala, and Y. Zhang, “Human urine-derived stem cells seeded in a modified 3D porous small intestinal submucosa scaffold for urethral tissue engineering,” *Biomaterials*, vol. 32, no. 5, pp. 1317–1326, 2011.
- [44] D. Qin, T. Long, J. Deng, and Y. Zhang, “Urine-derived stem cells for potential use in bladder repair,” *Stem Cell Research & Therapy*, vol. 5, no. 3, p. 69, 2014.
- [45] K. Lu, H. Y. Li, K. Yang et al., “Exosomes as potential alternatives to stem cell therapy for intervertebral disc degeneration: in-vitro study on exosomes in interaction of nucleus pulposus cells and bone marrow mesenchymal stem cells,” *Stem Cell Research & Therapy*, vol. 8, no. 1, p. 108, 2017.
- [46] X. D. Lu, Y. R. Liu, and Z. Y. Zhang, “Matrilin-3 alleviates extracellular matrix degradation of nucleus pulposus cells via induction of IL-1 receptor antagonist,” *European Review for Medical and Pharmacological Sciences*, vol. 24, no. 10, pp. 5231–5241, 2020.
- [47] A. Goc, M. Choudhary, T. V. Byzova, and P. R. Somanath, “TGF β - and bleomycin-induced extracellular matrix synthesis is mediated through Akt and mammalian target of rapamycin (mTOR),” *Journal of Cellular Physiology*, vol. 226, no. 11, pp. 3004–3013, 2011.

Research Article

Sodium Tanshinone IIA Sulfonate Ameliorates Injury-Induced Oxidative Stress and Intervertebral Disc Degeneration in Rats by Inhibiting p38 MAPK Signaling Pathway

Shouqian Dai ^{1,2}, Xiu Shi ³, Rongqing Qin,^{4,5} Xing Zhang ^{4,5}, Feng Xu ², and Huilin Yang ¹

¹Orthopedic Institute, Department of Orthopedic Surgery, The First Affiliated Hospital, Soochow University, Suzhou, Jiangsu, China

²Department of Emergency Medicine, The First Affiliated Hospital, Soochow University, Suzhou, Jiangsu, China

³Department of Obstetrics and Gynecology, The First Affiliated Hospital, Soochow University, Suzhou, Jiangsu, China

⁴Department of Spinal Surgery, Gaoyou Hospital Affiliated Soochow University, Gaoyou, Jiangsu, China

⁵Department of Orthopedics, Gaoyou People's Hospital, Gaoyou, Jiangsu, China

Correspondence should be addressed to Feng Xu; sz_xf@suda.edu.cn and Huilin Yang; suzhouspine@163.com

Received 26 January 2021; Accepted 29 April 2021; Published 26 May 2021

Academic Editor: Wenyan Ding

Copyright © 2021 Shouqian Dai et al. This is an open access article distributed under the Creative Commons Attribution License, which permits unrestricted use, distribution, and reproduction in any medium, provided the original work is properly cited.

Objective. Sodium tanshinone IIA sulfonate (STS) is a water-soluble derivative of tanshinone IIA, a representative traditional Chinese medicine. The aim of the study was to investigate the capability of STS to reverse injury-induced intervertebral disc degeneration (IDD) and explore the potential mechanisms. **Methods.** Forty adult rats were randomly allocated into groups (control, IDD, STS10, and STS20). An IDD model was established by puncturing the Co8-9 disc using a needle. Rats in the STS groups were administered STS by daily intraperitoneal injection (10 or 20 mg/kg body weight) while rats in the control and IDD groups received the same quantity of normal saline. After four weeks, the entire spine from each rat was scanned for X-ray and MRI analysis. Each Co8-9 IVD underwent histological analysis (H&E, Safranin-O Fast green, and alcian blue staining). A tissue was analyzed by immunohistochemical (IHC) staining to determine the expression levels of collagen II (COL2), aggrecan, matrix metalloproteinase-3/13 (MMP-3/13), interleukin-1 β (IL-1 β), IL-6, and tumor necrosis factor- α (TNF- α). Levels of oxidative stress were measured using an ELISA while activity of the p38 MAPK pathway was assessed using Western blot analysis. **Results.** Compared with the control group, needle puncture significantly decreased IVD volume and T-2 weighted MR signal intensity, confirming disc degeneration. These alterations were significantly attenuated by treatment with 10 or 20 mg/kg STS. Lower COL2 and aggrecan and higher MMP-3/13, IL-1 β , IL-6, and TNF- α levels in the IDD group were substantially reversed by STS. In addition, treatment with STS increased antioxidative enzyme activity and decreased levels of oxidative stress induced by needle puncture. Furthermore, STS inhibited the p38 MAPK pathway in the rat model of IDD. **Conclusions.** STS ameliorated injury-induced intervertebral disc degeneration and displayed anti-inflammatory and antioxidative properties in a rat model of IDD, possibly via inhibition of the p38 MAPK signaling pathway.

1. Introduction

Intervertebral disc degeneration (IDD) is recognized as among the most common causes of lower back pain [1]. IDD is prevalent in both the middle-aged and elderly population, patients becoming increasingly younger over recent years. The condition has become an economic and healthcare

burden, requiring considerable medical resources and causing substantial economic pressures [2]. Risk factors for IDD include genetics, bacteria, and viruses [3], sex [4], obesity [5], smoking [6], aging [7], and mechanical loading [8]. Pathological changes in degenerated intervertebral discs (IVDs) include narrowing of the intervertebral space, dysfunction of nucleus pulposus cells (NPCs), degradation of the extracel-

lular matrix (ECM), rupture of the annulus fibrosus (AF), and calcification of the vertebral endplates [9]. However, the precise etiology and pathogenesis of IDD remain unclear. An increasing number of studies have concluded that IDD arises due to oxidative stress [10–12].

A previous research study demonstrated that oxidative stress at least partly leading to the structural failure of degenerated IVDs results from the excessive production of reactive oxygen species (ROS) [13]. A number of oxidative stress markers have been found and identified in degenerated human IVDs [14, 15]. ROS has been shown capable of promoting the progression of apoptosis in NPCs *in vitro* [11]. In addition, a number of external stimuli, including mechanical overloading, deprivation of nutrition, and inflammatory cytokines, can result in the accumulation of intracellular ROS [16, 17]. The observations above suggest that oxidative stress may be closely related to IDD.

The dried root of *Salvia miltiorrhiza* Bunge (Danshen) has multiple therapeutic properties relevant for a variety of cardiovascular diseases [18]. Sodium tanshinone IIA sulfonate (STS) is a water-soluble derivative of tanshinone IIA extracted from Danshen. Previous studies have demonstrated that STS has anti-inflammatory, antioxidative, and antiapoptotic properties [19–21]. However, until now, few studies have reported the effect of STS on an injury-induced rat model of IDD, the underlying mechanism of the possible protective actions of STS in IDD remaining largely unknown.

The present research employed an injury-induced rat model to ascertain the effect of STS on IDD. Previous evidence has shown that activation of the p38 MAPK signaling pathway is involved in oxidative stress [11, 22], and so this signaling pathway is a potential target for IDD in rats. The present study is the first to evaluate the effects of STS on oxidative stress and IDD in rats. Furthermore, the research explored the possible mechanism by which STS ameliorated the progression of IDD. The data demonstrated that STS ameliorated injury-induced oxidative stress and intervertebral disc degeneration in rats by inhibition of the p38 MAPK signaling pathway.

2. Materials and Methods

2.1. Reagents and Materials. STS (purity 99%) was obtained from Sigma-Aldrich Inc. (St. Louis, MO, USA). Enzyme-linked immunosorbent assay (ELISA) kits for superoxide dismutase (SOD, S0087), glutathione peroxidase (GSH-Px, S0056), catalase (CAT, P3541-100 ml), and malondialdehyde (MDA, S0131M) were acquired from Beyotime Biotechnology Co. Ltd. (Shanghai, China). All primary antibodies used in the study were purchased from Cell Signaling Technology, Inc. (MA, US), while secondary antibodies were from Beyotime Biotechnology Co. Ltd. (Shanghai, China). Sigma-Aldrich Inc. (St. Louis, MO, USA) supplied all other reagents.

2.2. Animals. Forty adult male Sprague-Dawley rats (weighing 270–320 g, 12 weeks of age) were purchased from the Animal Center at Soochow University (Suzhou, China). Animals were maintained within normal conditions and randomly allocated into four equal groups prior to surgery. All rats

received various treatments, as appropriate, for two weeks and then subjected to experimental surgery, as described below. All experimental procedures were approved by the Animal Care and Experiment Committee of Soochow University (2020 Approval No. ECSU-2020000108).

2.3. Grouping. The experimental rats were randomly divided into four groups (10 rats in each group) as follows: (1) control (sham) group; (2) IDD group; (3) STS10 group (IDD+STS 10 mg/kg body weight); and (4) STS20 group (IDD+STS 20 mg/kg body weight). Rats in the STS groups received daily intraperitoneal injections of STS (10 or 20 mg/kg body weight) while rats in the control and IDD groups were injected intraperitoneally with the same volume of normal saline until the end of the study, at which point the rats were sacrificed. The procedures used in the present study are detailed in a previously published study [23]. The therapeutic doses were selected from those established in another study [24].

2.4. Rat Model of IDD. Percutaneous needle puncture has been demonstrated to be an effective method of induction of disc degeneration [25]. Following acclimatization, animals were anesthetized by inhalation of 2% fluothane in oxygen/nitrous oxide. The surgical procedure was performed on the vertebrae in the tail, as described previously [26]. In the IDD and IDD+STS groups, the Co8-9 discs were punctured using a 20-gauge needle. Sham surgery was performed on rats in the control group. Following surgery, STS or normal saline was administered to each animal once per day for four consecutive weeks, after which their tails were scanned using X-rays and MRI while being anesthetized with isoflurane and the Co8-9 discs were harvested for subsequent experiments. All experimental steps complied with the Animal Research Reporting of In vivo Experiments (ARRIVE) guidelines.

2.5. Radiographic Analysis and Magnetic Resonance Imaging (MRI) Scanning. After four weeks of induction of IDD, each animal was scanned with X-rays and by MRI. X-ray images were obtained using a digital X-ray machine (Shimadzu, Japan) and stored digitally. Using a previously reported method [27], the disc height index (DHI) was calculated from the mean of measurements obtained from the anterior, middle, and posterior portions of the disc which was divided by the mean height of the adjacent vertebral body using ImageJ image analysis software. Changes in DHI were recorded as %DHI and normalized to the DHI of the preoperative IVD (%DHI = DHI postsurgery/DHI presurgery * 100).

T2 mapping of MRI signal intensity is commonly used to measure the degree of IDD. The procedure was conducted as previously described [28], in a 1.5T MRI scanner (GE, USA). Briefly, all rats were scanned and the T2 signal intensity of the Co8-9 discs was recorded. The ratio of T2 signal intensity of each injured disc to the control disc was recorded from analysis using ImageJ software. Therefore, normalized IVD intensity had values ranging from 0 to 1.

2.6. Histological Evaluation. All harvested IVDs were fixed in 10% formalin and embedded in paraffin. Five μm serial

sections were obtained from the midsagittal region and stained with hematoxylin and eosin (H&E), Safranin-O Fast green, and alcian blue in order that histological changes in the IVDs could be identified and assessed using a previously described scale, providing scores from 5 to 15 points, representing IVDs that were normal to severely degenerated [26].

2.7. Immunohistochemical (IHC) Analysis. The disc tissue of the Co8-9 IVDs was obtained from experimental rats, as described previously [29]. Immunohistochemical staining was performed on decalcified sections, as described previously [30]. Paraffin-embedded sections (5 μ m) were first subjected to H₂O₂ for fifteen minutes and then blocked in regular blocking solution for half an hour at 37°C. The sections were subsequently incubated with rabbit primary antibodies: ECM-associated proteins collagen II (COL2, 1:500) and aggrecan (1:500), matrix metalloproteinase-3 (MMP-3, 1:500), MMP-13 (1:500), and the inflammatory factors interleukin-1 β (IL-1 β , 1:500), IL-6 (1:500), and tumor necrosis factor- α (TNF- α , 1:500) or control rabbit IgG (1:200 in 5% BSA), respectively, overnight at 4°C. After washing three times, the sections were then incubated with diaminobenzidine- (DAB-) based peroxidase-conjugated goat anti-rabbit secondary antibody (1:200) for one hour at 37°C. All images were acquired with a light microscope (Olympus, Japan) at 40x magnification. IHC staining results were then analyzed semiquantitatively using a method described previously [30]. The number of positively stained cells and staining intensity were used in scoring; the two scores were multiplied together to reflect the degree of protein expression. Images from all sections were obtained and analyzed independently by two observers that were blinded to the experimental details.

2.8. Enzyme-Linked Immunosorbent Assays (ELISAs). Four common indicators of oxidative stress, SOD, GSH-Px, CAT, and MDA were quantified using the corresponding assay kit (Beyotime Biotechnology Co. Ltd., Shanghai, China) in accordance with the manufacturer's instructions. Briefly, the disc tissue was first lysed with 0.25% trypsin for 15 minutes and then centrifuged for 15 minutes at 4°C at 900 g. The supernatants and standards were added to cuvettes, and values of OD at 530 nm were recorded. The quantity of enzyme able to transform 1 mmol substrate in 1 minute was defined as 1 unit of enzyme activity. The activity of SOD, GSH-Px, CAT, and levels of MDA were calculated by reference to a standard curve.

2.9. Western Blot Analysis. Expression levels of p38 and p-p38 in the discs were measured using routine Western blot analysis. All disc tissues were homogenized using RIPA lysis buffer containing protease inhibitor to obtain a preparation of total protein. Equal quantities of protein were separated using routine sodium dodecyl sulfate polyacrylamide gel electrophoresis (SDS-PAGE), then transferred to polyvinylidene difluoride (PVDF) membranes. After blocking in 5% nonfat milk, the membranes were blotted with primary antibodies at 4°C overnight: p38 MAPK (1:1000), phosphorylated p38 MAPK (p-p38, 1:1000), and GAPDH (1:2000),

then an HRP-conjugated secondary antibody at 37°C for one hour. Protein bands were then visualized using an ECL imaging system. The signal intensity of each blot was analyzed using ImageJ software. Finally, the relative expression levels of p-p38 were normalized to those of p38.

2.10. Statistical Analysis. All experimental data are presented as the means \pm standard deviation (SD). One-way analysis of variance (ANOVA) was used to compare multiple groups after verification of normality with post hoc comparisons using a least-squares difference (LSD) method. *P* values of differences that were less than 0.05 were considered statistically significant.

3. Results

3.1. STS Reduces Narrowing of the IVD Space and Decreased T2-Weighted MRI Signal Intensity in a Rat Model of IDD. Analysis of the IVD space or height was conducted and recorded as the %DHI (ratio of DHI 4 weeks after surgery to before surgery). The T2-weighted MRI signals of IVDs reflect the extent of their degeneration. Representative X-ray and T2-weighted MRI images are displayed in Figures 1(a) and 1(c). By quantitative analysis, the height of the IVD space and the signal intensity of T2-weighted MRI in the IDD group were found to be significantly lower than those of the control group ($P < 0.01$). However, this decrease was substantially suppressed by treatment with 10 or 20 mg/kg STS ($P < 0.05$ and $P < 0.01$, respectively). These imaging data demonstrate that STS can ameliorate IDD.

3.2. STS Inhibits the Extent of IVD Degeneration in Injury-Induced IDD Rats. Normal IVDs in the control group consisted of round NPs, distributed evenly, and integrated among collagen lamellae, as displayed in Figure 2. Degenerated discs in the IDD groups exhibited NPs of significantly reduced size (including their complete disappearance), with a clearly blurred boundary between the NP and AF. Furthermore, disorganized inner collagen layers of the AF were bulging inward. However, four weeks' treatment with STS significantly rescued such disc degeneration in a dose-dependent manner. Semiquantitative analysis indicated that the histological scores of the IDD rats were significantly higher than those of control rats ($P < 0.01$, Figure 2). Histological scores were significantly lower in the STS10 and STS20 groups compared with the IDD group ($P < 0.05$ and $P < 0.01$, respectively). These findings demonstrated that STS ameliorates the histopathological degeneration of IVDs.

3.3. STS Inhibits the Degradation of COL2 and Aggrecan in the IDD Model. Compared with the control group, IDD rats exhibited ECM with significantly less COL2 and aggrecan expression levels, indicating that needle puncture induced significant degradation of COL2 and aggrecan ($P < 0.01$, Figure 3). This decrease was significantly restored by STS treatment compared with that of the IDD group. The results indicate that STS ameliorated IDD by inhibition of ECM degradation.

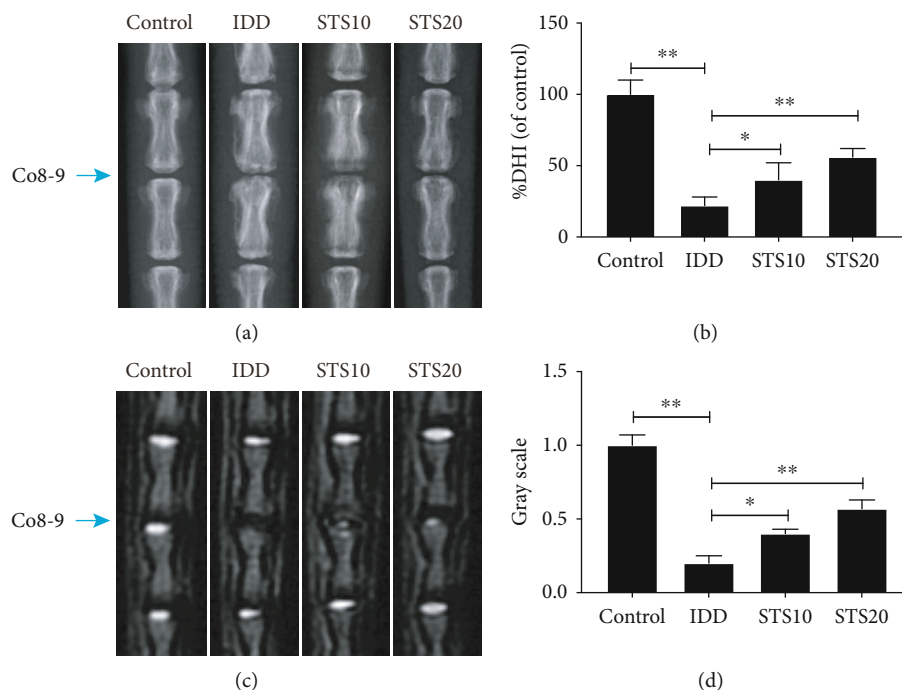


FIGURE 1: Imaging characteristics of IVDs in each group after 4 weeks. (a) Representative radiographic images of the Co8-9 discs in each group and (b) their semiquantitative analysis. (c) Representative images of T2-weighted MR in each group and (d) their semiquantitative analysis. The height of the IVD space and the signal intensity of T2-weighted MRI in the IDD group were found to be significantly lower than those of the control group. However, this decrease was substantially suppressed by treatment with 10 or 20 mg/kg STS. IDD: intervertebral disc degeneration; DHI: disc height index; STS10/20: 10/20 mg/kg sodium tanshinone IIA sulfonate; * $P < 0.05$ and ** $P < 0.01$ compared with the IDD group ($n = 10$ per group).

3.4. STS Inhibits the Protein Expression Levels of MMP-3 and MMP-13. MMPs (predominantly MMP-3 and MMP-13) have been proposed as the principal catabolic enzymes in degenerated IVDs [31]. As shown in Figure 4, IVDs in the control group displayed extremely little expression of either MMP-3 or MMP-13. Needle puncture in the IDD groups resulted in significant elevation of both MMP-3 and MMP-13 expressions in comparison with the control group ($P < 0.01$). Treatment with STS (10 and 20 mg/kg) resulted in a considerable decrease compared with the IDD group in a dose-dependent manner. These data suggest that STS ameliorates IDD via regulation of the activation of MMPs.

3.5. STS Suppresses the Expression Levels of Inflammatory Factors in the IDD Model. Analysis by IHC indicated that the expression levels of the inflammatory factors IL-1 β , IL-6, and TNF- α were significantly higher in the IDD group than in the control group ($P < 0.01$, Figure 4). However, treatment with 10 or 20 mg/kg STS significantly inhibited IL-1 β , IL-6, and TNF- α levels in comparison ($P < 0.05$, Figure 5). These data demonstrate that STS ameliorates IDD via inhibition of the production of inflammatory factors.

3.6. STS Regulates the Antioxidant System and Lipid Peroxidation. As depicted in Figures 6(a)–6(c), there was a considerable decline in SOD, GSH-Px, and CAT activity in rat IVDs in the IDD group compared with control rats ($P < 0.01$). Notably, treatment with STS upregulated the activity of these components of the enzymatic antioxidant

defense system in a dose-dependent manner. Moreover, the IVDs of IDD rats displayed a significantly higher MDA concentration compared with those of the control group (Figure 6(d), $P < 0.01$). However, treatment with STS (both 10 and 20 mg/kg) significantly reversed this difference. These results indicate that STS ameliorates IDD via the regulation of oxidative stress.

3.7. STS Regulates the p38 MAPK Signaling Pathway in the Rat Model of IDD. The p38 protein is known to transduce apoptotic or death signals in NPCs. Oxidative stress leads to activation and phosphorylation of the p38 signaling pathway [32, 33]. Western blot analysis demonstrated that protein expression levels of p-p38 MAPK in the IDD group were substantially higher than those in the control group ($P < 0.01$, Figure 7), indicating activation of the p38 pathway, while protein expression levels of GAPDH and p38 did not apparently change. Treatment with STS significantly downregulated p38 kinase phosphorylation compared with the IDD group, without influencing the total expression of p38 protein ($P < 0.05$, Figure 7). These data indicate that STS ameliorates IDD by inhibition of the p38 MAPK signaling pathway.

4. Discussion

IVD disease, the most common cause of lower back pain, is characterized by the progressive loss of ECM and a concomitant decrease in water content, changes in the structure of

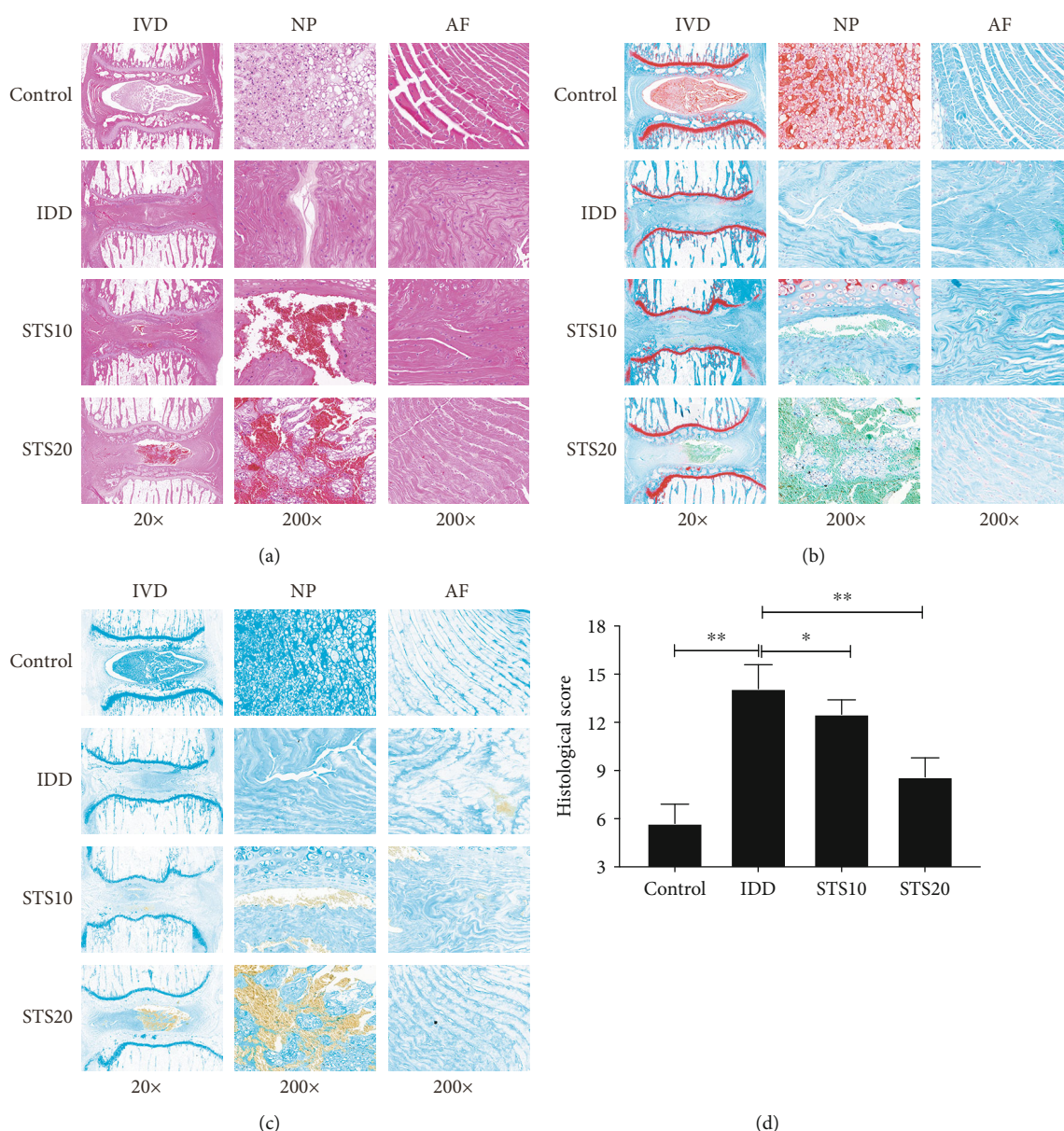


FIGURE 2: Histological analysis of IVDs in each group after 4 weeks. Representative histological images of IVDs stained with H&E (a), Safranin-O Fast green (b), and alcian blue (c) in each group. (d) Semiquantitative analysis of histological staining. Normal IVDs in the control group consisted of round NPs, distributed evenly, and integrated among collagen lamellae. Degenerated discs in the IDD groups exhibited NPs of significantly reduced size, with a clearly blurred boundary between the NP and AF. Four weeks' treatment with STS significantly rescued such disc degeneration in a dose-dependent manner. IVD: intervertebral disc degeneration; NP: nucleus pulposus; AF: annulus fibrosus; IDD: intervertebral disc degeneration; STS10/20: 10/20 mg/kg sodium tanshinone IIA sulfonate; * $P < 0.05$ and ** $P < 0.01$ compared with the IDD group ($n = 10$ per group).

the IVD, and disc dysfunction. The imbalance between anabolic and catabolic processes, leading to the upregulated production of MMPs and loss of collagen and proteoglycans, finally results in alterations to the mechanical properties of IVDs and their herniation. Current research has demonstrated that STS can preserve the water content and volume of an IVD, suppressing the excessive degradation of ECM-associated proteins and inhibition of injury-induced oxidative stress in a rat model of IDD. The results of the present study indicate that STS may be a novel therapeutic agent for IDD.

As a representative traditional medicine, tanshinone IIA displays multiple pharmacological functions, but its poor water solubility has greatly restricted its further development [34]. STS, a chemically modified form of Tan IIA, exhibits considerably increased water solubility [35], with multiple pharmacological properties, including being antioxidative, anti-inflammatory, anticancer, and antiapoptotic. In the present study, we first evaluated the effects of STS on the histopathological changes within a rat puncture model of IDD. The results of the present study indicate that STS can protect IVD height and water content by reducing and inhibiting the

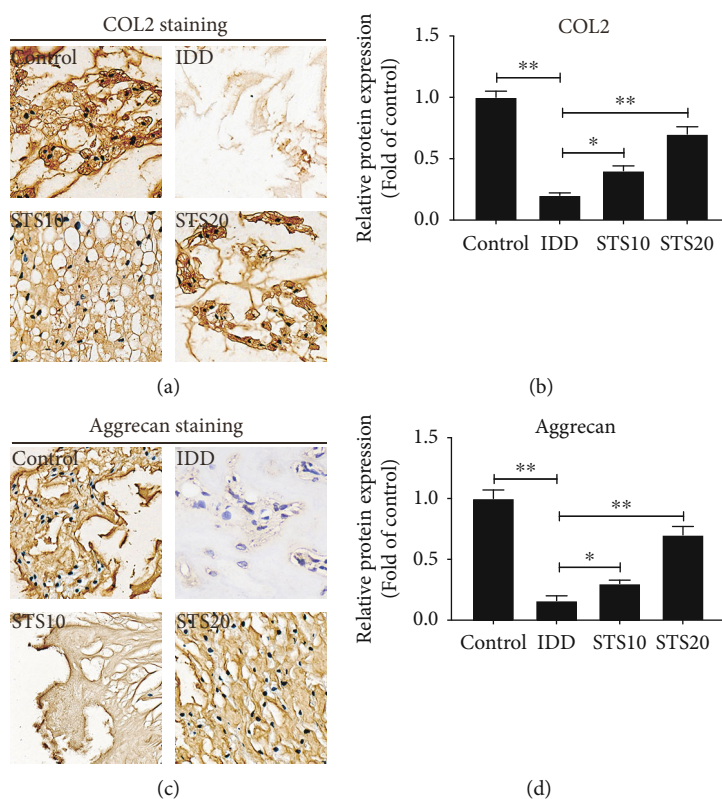


FIGURE 3: Immunohistochemical analysis of COL2 and aggrecan. (a) Representative IHC images of COL2 staining. (b) Semi-quantitative analysis of COL2. (c) Representative images of aggrecan staining. (d) Semi-quantitative analysis of aggrecan. Compared with the control group, IDD rats exhibited ECM with significantly less COL2 and aggrecan expression levels. This decrease was significantly restored by STS treatment indicating that STS ameliorated IDD by inhibition of ECM degradation. All images were acquired at 400x magnification. COL2: collagen II; IDD: intervertebral disc degeneration; STS10/20: 10/20 mg/kg sodium tanshinone IIA sulfonate; * $P < 0.05$ and ** $P < 0.01$ compared with the IDD group ($n = 10$ per group).

overproduction of MMP-3 and MMP-13, which are responsible for degradation of the ECM-associated proteins COL2 and aggrecan, thus suppressing the progression of IDD. The ECM of the NP primarily consists of three components: collagen, proteoglycans, and water, of which COL2 and aggrecan are the two principal components [36]. COL2 provides the elastic strength of an IVD while aggrecan maintains the water content of the NP. MMPs participate in the degradation of ECM components, including proteoglycans and collagen. An imbalance in the synthesis and catabolism of COL2 and aggrecan leads to the onset of IDD. Previous studies have indicated that MMP-3 and MMP-13 are initially upregulated in an injured AF or NP [37, 38]. IHC staining has demonstrated that the elevated production of MMPs correlates with the progression of IDD [39]. The findings of the present study reveal that STS reduces the degradation of COL2 and aggrecan through inhibition of MMP activity, ultimately ameliorating the progression of IDD.

It has been established that IDD is mediated by the excessive production of inflammatory cytokines secreted by different IVD cells, resulting in the apoptosis and autophagy of NPCs [40–42]. Oestrogen can decrease IVD cell apoptosis and inhibit IDD in multiple ways, including the inhibition of the inflammatory cytokines IL-1 β and TNF- α , reducing catabolism because of inhibition of matrix metalloprotein-

ases, decreasing oxidative damage [43]. Previous studies have revealed that inflammation is the key event during the progression of IDD [44]. Of the various proinflammatory mediators, IL-1 β , IL-6, and TNF- α are probably the most important. Increased expression levels of IL-1 and TNF have been observed in degenerated and herniated IVDs [9, 45]. In the present study, needle puncture was used to significantly increase the production of IL-1 β , IL-6, and TNF- α , demonstrating that environmental stressor injury can result in inflammatory events. Treatment with STS significantly reduced the indicators of inflammation in a rat model of IDD. It has been reported that STS can reduce the expression of the inflammatory cytokines IL-6 and TNF- α in a mouse model of atherosclerosis [46]. STS was also found to down-regulate the expression levels of IL-1 β , TGF- β , and TNF- α via the inhibition of NF- κ B phosphorylation in the nucleus [47, 48]. In addition, STS has been shown to suppress the release of IL-6 and TNF- α in a mouse model of sepsis [49].

Oxidative stress has been shown to be closely associated with the onset and progression of IDD. Oxidative stress is caused by the excessive accumulation of free radicals and ROS and can damage proteins and nucleic acids, leading to changes in cellular structure and function [50, 51]. The classical antioxidant system comprises the antioxidant enzymes SOD, CAT, GSH-Px, and lipoic acid [52]. As the

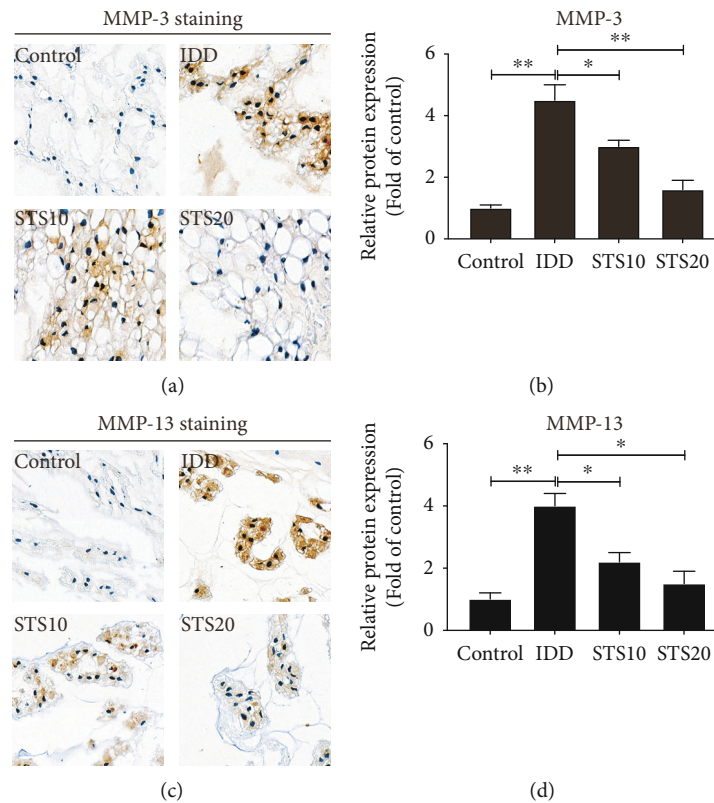


FIGURE 4: Immunohistochemical analysis of MMP-3 and MMP-13. (a) Representative IHC images of MMP-3 staining. (b) Semi-quantitative analysis of MMP-3. (c) Representative IHC images of MMP-13 staining. (d) Semi-quantitative analysis of MMP-13. Needle puncture in the IDD groups resulted in significant elevation of both MMP-3 and MMP-13 expressions in comparison with the control group. Treatment with STS resulted in a considerably decrease compared with the IDD group in a dose-dependent manner, indicating that STS ameliorates IDD via regulation of the activation of MMPs. All images were acquired at 400x magnification. MMP: matrix metalloproteinase; IDD: intervertebral disc degeneration; STS10/20: 10/20 mg/kg sodium tanshinone IIA sulfonate; * $P < 0.05$ and ** $P < 0.01$ compared with the IDD group ($n = 10$ per group).

predominant defensive enzyme in the antioxidative system, SOD catalyzes the disproportionation of superoxide anions, preventing tissue damage [53, 54]. CAT is an additional antioxidant enzyme, catalyzing H_2O_2 into H_2O and O_2 , thus balancing redox reactions [55]. GSH-Px is a powerful free radical scavenger that inhibits lipid peroxidation, while MDA concentration displays the extent of cell membrane lipid peroxidation [56]. Measurements of SOD, CAT, and GSH-Px allow the evaluation of the capability of cells to clear ROS, while MDA reflects the severity of an attack by ROS [57]. Thus, the levels of these indicators in IVDs reflect oxidative stress levels. In the present study, needle puncture, used to establish the model of IDD, resulted in a significant downregulation of SOD, CAT, and GSH-Px activity and increased MDA concentration, thus increasing oxidative stress levels. However, administration of 10 or 20 mg/kg STS inhibited injury-induced oxidative stress in a dose-dependent manner. A number of studies have reported the antioxidant capability of STS, for example, decreased MDA and GSH expression levels in a rat model of stroke [58]. STS was shown to inhibit the production of X-ray induced ROS [59] and ameliorated oxidative stress and lipid metabolism in isoproterenol-induced myocardial infarction [60]. Furthermore, STS suppressed the degree of cardiomyocyte

apoptosis via inhibition of phosphorylation of the oxidative stress-related protein JNK [24].

To explore the underlying mechanism by which STS inhibits oxidative stress and IDD, Western blot analysis was utilized to identify changes in pathway-associated protein expression. The p38 MAPK signaling pathway is a branch of the MAPK superfamily, mediating the regulation of various physiological and pathological processes such as inflammation, cell stress, growth, development, and apoptosis [22]. A previous study indicated that a number of signaling pathways and transcript factors including MAPKs, p53, NF- κ B, and Nrf2/HO-1 are involved in the regulation of oxidative stress [61]. The current study indicated that needle puncture resulted in the activation of the p38 signaling pathway in the IDD group, while STS ameliorated oxidative stress and IDD in a rat model through inhibition of p38 MAPK. Rannou et al. reported that mechanical overload causes the apoptosis of AF cells by p38 MAPK activation [33]. Blockade of p38 MAPK in cytokine-activated NPCs was shown to reduce the generation of cytokine factors associated with inflammation, pain, and matrix degradation [22]. These *in vitro* studies, in addition to observations in the present study, indicated that STS may reduce oxidative stress and IDD via inhibition of p38 MAPK activity.

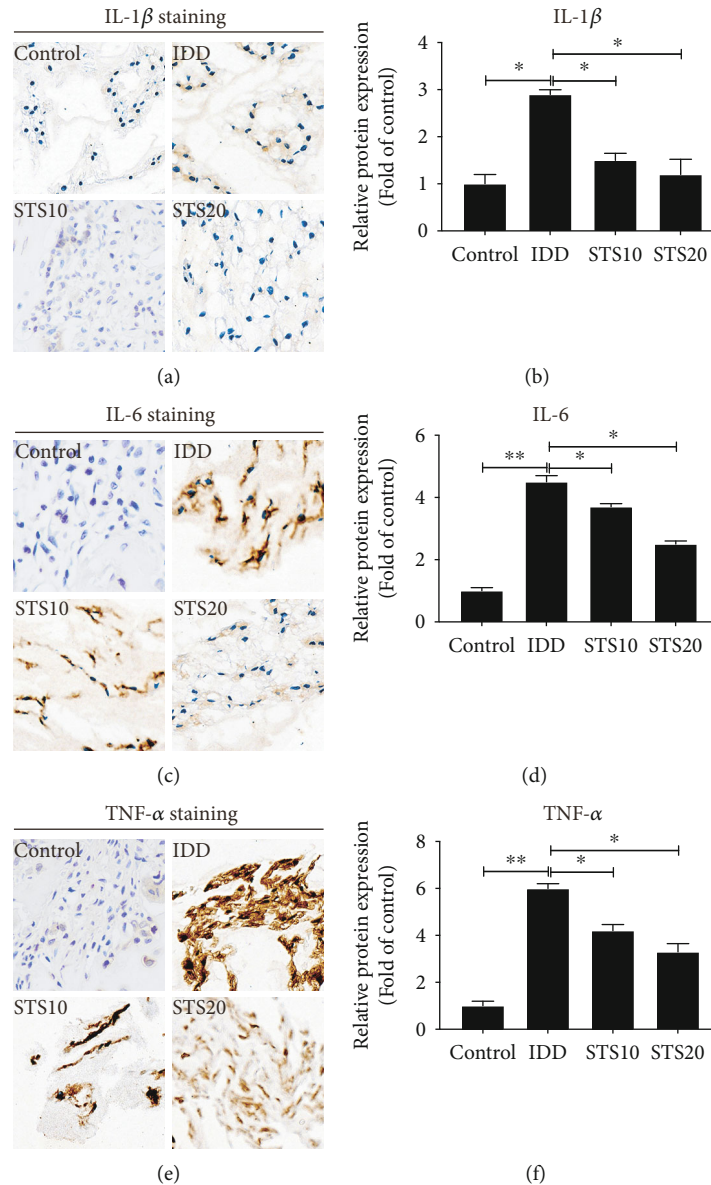


FIGURE 5: Immunohistochemical analysis of IL-1 β , IL-6 and TNF- α . (a) Representative IHC images of IL-1 β staining. (b) Semi-quantitative analysis of IL-1 β . (c) Representative IHC images of IL-6 staining. (d) Semi-quantitative analysis of IL-6. (e) Representative IHC images of TNF- α staining. (f) Semi-quantitative analysis of TNF- α . The expression levels of the inflammatory factors IL-1 β , IL-6, and TNF- α were significantly higher in the IDD group than in the control group. However, treatment with 10 or 20 mg/kg STS significantly inhibited IL-1 β , IL-6, and TNF- α levels in comparison, indicating that STS suppresses the expression levels of inflammatory factors in the IDD model. All images were acquired at 400x magnification. IL: interleukin; TNF: tumor necrosis factor; IDD: intervertebral disc degeneration; STS10/20: 10/20 mg/kg sodium tanshinone IIA sulfonate; * $P < 0.05$ and ** $P < 0.01$ compared with the IDD group ($n = 10$ per group).

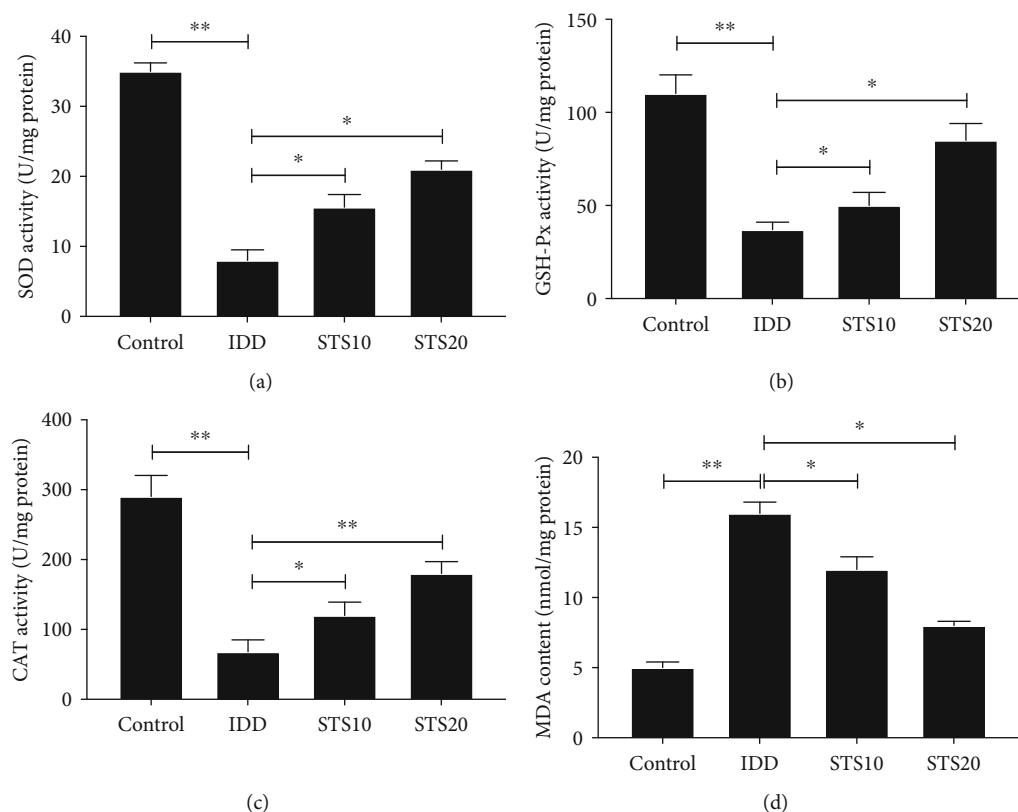


FIGURE 6: SOD, GSH-Px, CAT, and MDA contents in rat IVDs of each group. STS treatment increased the activity of (a) SOD, (b) GSH-Px, and (c) CAT that had been lowered by puncture injury and significantly decreased MDA levels (d) compared with the IDD group. These results demonstrated that STS regulates the antioxidant system and lipid peroxidation. SOD: superoxide dismutase; GSH-Px: glutathione peroxidase; CAT: catalase; MDA: malondialdehyde; IDD: intervertebral disc degeneration; STS10/20: 10/20 mg/kg sodium tanshinone IIA sulfonate; * $P < 0.05$ and ** $P < 0.01$ compared with the IDD group ($n = 10$ per group).

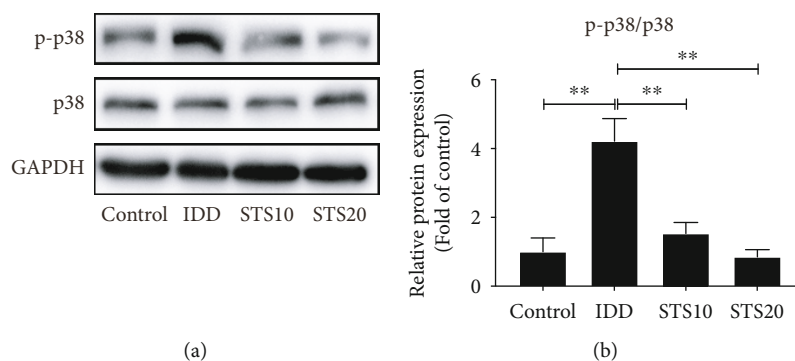


FIGURE 7: Western blot analysis of p38 and p-p38 protein expressions in each group. Activation of p-p38 MAPK was shown in IVDs of the IDD group (a). Overexpression of p-p38 in the IDD group was significantly inhibited by STS treatment (b). These data indicate that STS regulates the p38 MAPK signaling pathway in the model of IDD. GAPDH: glyceraldehyde-3-phosphate dehydrogenase; IDD: intervertebral disc degeneration; STS10/20: 10/20 mg/kg sodium tanshinone IIA sulfonate; * $P < 0.05$ and ** $P < 0.01$ compared with the IDD group ($n = 10$ per group).

There are a number of limitations to the study. Firstly, only animal experiments were used in the evaluation of the effect of STS on IDD. Cell experiments (especially human IVD cells) that investigate the use of a p38 MAPK inhibitor should be further conducted to obtain more convincing results. Secondly, STS receptors and downstream target genes were not explored. Thirdly, although STS exhibited profound anti-inflammatory and antioxidative effects in the present

animal study, the potential for treatment and possible complications of STS on human diseases require additional examination through clinical research.

5. Conclusion

The present study demonstrated that STS ameliorated injury-induced intervertebral disc degeneration, exerting

anti-inflammatory and antioxidative effects in a rat model of IDD, possibly by inhibition of the p38 MAPK signaling pathway.

Data Availability

No data were used to support this study.

Conflicts of Interest

The authors declare that they have no conflicts of interest.

Authors' Contributions

Shouqian Dai, Xiu Shi, and Rongqing Qin contributed equally to this work.

Acknowledgments

This project was funded by the Priority Academic Program Development of Jiangsu Higher Education Institutions (PAPD), Basic Research Program of Jiangsu Province (BK20180196), and Suzhou Science and Technology Project (SYS2020085).

References

- [1] L. Zhu, C. Yu, X. Zhang et al., "The treatment of intervertebral disc degeneration using Traditional Chinese Medicine," *Journal of Ethnopharmacology*, vol. 263, p. 113117, 2020.
- [2] A. Becker, H. Held, M. Redaelli et al., "Low back pain in primary care: costs of care and prediction of future health care utilization," *Spine*, vol. 35, no. 18, pp. 1714–1720, 2010.
- [3] F. M. Williams, M. Popham, P. N. Sambrook, A. F. Jones, T. D. Spector, and A. J. MacGregor, "Progression of lumbar disc degeneration over a decade: a heritability study," *Annals of the Rheumatic Diseases*, vol. 70, no. 7, pp. 1203–1207, 2011.
- [4] Y. X. Wang and J. F. Griffith, "Menopause causes vertebral endplate degeneration and decrease in nutrient diffusion to the intervertebral discs," *Medical Hypotheses*, vol. 77, no. 1, pp. 18–20, 2011.
- [5] D. Samartzis, J. Karppinen, D. Chan, K. D. Luk, and K. M. Cheung, "The association of lumbar intervertebral disc degeneration on magnetic resonance imaging with body mass index in overweight and obese adults: a population-based study," *Arthritis and Rheumatism*, vol. 64, no. 5, pp. 1488–1496, 2012.
- [6] S. Elmasry, S. Asfour, J. P. de Rivero Vaccari, and F. Travascio, "Effects of tobacco smoking on the degeneration of the intervertebral disc: a finite element study," *PLoS One*, vol. 10, no. 8, 2015.
- [7] K. Siemionow, H. An, K. Masuda, G. Andersson, and G. Cs-Szabo, "The effects of age, sex, ethnicity, and spinal level on the rate of intervertebral disc degeneration: a review of 1712 intervertebral discs," *Spine (Phila Pa 1976)*, vol. 36, no. 17, pp. 1333–1339, 2011.
- [8] L. Manchikanti, V. Singh, F. J. Falco, R. M. Benyamin, and J. A. Hirsch, "Epidemiology of low back pain in adults," *Neuromodulation*, vol. 17, Supplement 2, pp. 3–10, 2014.
- [9] C. L. Le Maitre, A. J. Freemont, and J. A. Hoyland, "The role of interleukin-1 in the pathogenesis of human intervertebral disc degeneration," *Arthritis Research & Therapy*, vol. 7, no. 4, pp. R732–R745, 2005.
- [10] S. Suzuki, N. Fujita, N. Hosogane et al., "Excessive reactive oxygen species are therapeutic targets for intervertebral disc degeneration," *Arthritis Research & Therapy*, vol. 17, no. 1, p. 316, 2015.
- [11] A. Dimozi, E. Mavrogenatou, A. Sklirou, and D. Kletsas, "Oxidative stress inhibits the proliferation, induces premature senescence and promotes a catabolic phenotype in human nucleus pulposus intervertebral disc cells," *European Cells & Materials*, vol. 30, pp. 89–103, 2015.
- [12] K. Schroder, "NADPH oxidases in bone homeostasis and osteoporosis," *Free Radical Biology & Medicine*, vol. 132, pp. 67–72, 2019.
- [13] D. Harman, "Aging: a theory based on free radical and radiation chemistry," *Journal of Gerontology*, vol. 11, no. 3, pp. 298–300, 1956.
- [14] A. G. Nerlich, B. E. Bachmeier, E. Schleicher, H. Rohrbach, G. Paesold, and N. Boos, "Immunomorphological analysis of RAGE receptor expression and NF- κ B activation in tissue samples from normal and degenerated intervertebral discs of various ages," *Annals of the New York Academy of Sciences*, vol. 1096, no. 1, pp. 239–248, 2007.
- [15] L. Poveda, M. Hottiger, N. Boos, and K. Wuertz, "Peroxy-nitrite induces gene expression in intervertebral disc cells," *Spine (Phila Pa 1976)*, vol. 34, no. 11, pp. 1127–1133, 2009.
- [16] X. Y. Cai, Y. Xia, S. H. Yang et al., "Ropivacaine- and bupivacaine-induced death of rabbit annulus fibrosus cells *in vitro*: involvement of the mitochondrial apoptotic pathway," *Osteoarthritis and Cartilage*, vol. 23, no. 10, pp. 1763–1775, 2015.
- [17] F. Ding, Z. W. Shao, S. H. Yang, Q. Wu, F. Gao, and L. M. Xiong, "Role of mitochondrial pathway in compression-induced apoptosis of nucleus pulposus cells," *Apoptosis*, vol. 17, no. 6, pp. 579–590, 2012.
- [18] Cheng TO, "Cardiovascular effects of Danshen," *International Journal of Cardiology*, vol. 121, no. 1, pp. 9–22, 2007.
- [19] D. Li, J. Wang, D. Sun et al., "Tanshinone IIA sulfonate protects against cigarette smoke-induced COPD and down-regulation of CFTR in mice," *Scientific Reports*, vol. 8, no. 1, p. 376, 2018.
- [20] R. Guan, J. Wang, Z. Li et al., "Sodium tanshinone IIA sulfonate decreases cigarette smoke-induced inflammation and oxidative stress via blocking the activation of MAPK/HIF-1 α signaling pathway," *Frontiers in Pharmacology*, vol. 9, p. 263, 2018.
- [21] J. Cheng, T. Chen, P. Li et al., "Sodium tanshinone IIA sulfonate prevents lipopolysaccharide-induced inflammation via suppressing nuclear factor- κ B signaling pathway in human umbilical vein endothelial cells," *Canadian Journal of Physiology and Pharmacology*, vol. 96, no. 1, pp. 26–31, 2018.
- [22] R. K. Studer, A. M. Aboka, L. G. Gilbertson et al., "p38 MAPK inhibition in nucleus pulposus cells: a potential target for treating intervertebral disc degeneration," *Spine (Phila Pa 1976)*, vol. 32, no. 25, pp. 2827–2833, 2007.
- [23] P. Kushwaha, V. Khedgikar, N. Ahmad et al., "A neoflavonoid dalsissoal isolated from heartwood of *Dalbergia sissoo* Roxb. has bone forming effects in mice model for osteoporosis," *European Journal of Pharmacology*, vol. 788, pp. 65–74, 2016.
- [24] R. Yang, A. Liu, X. Ma, L. Li, D. Su, and J. Liu, "Sodium tanshinone IIA sulfonate protects cardiomyocytes against oxidative

- stress-mediated apoptosis through inhibiting JNK activation,” *Journal of Cardiovascular Pharmacology*, vol. 51, no. 4, pp. 396–401, 2008.
- [25] L. Kang, Q. Xiang, S. Zhan et al., “Restoration of autophagic flux rescues oxidative damage and mitochondrial dysfunction to protect against intervertebral disc degeneration,” *Oxidative Medicine and Cellular Longevity*, vol. 2019, Article ID 7810320, 27 pages, 2019.
- [26] B. Han, K. Zhu, F. C. Li et al., “A simple disc degeneration model induced by percutaneous needle puncture in the rat tail,” *Spine (Phila Pa 1976)*, vol. 33, no. 18, pp. 1925–1934, 2008.
- [27] K. Masuda, Y. Aota, C. Muehleman et al., “A novel rabbit model of mild, reproducible disc degeneration by an annulus needle puncture: correlation between the degree of disc injury and radiological and histological appearances of disc degeneration,” *Spine (Phila Pa 1976)*, vol. 30, no. 1, pp. 5–14, 2005.
- [28] R. C. Lawrence, C. G. Helmick, F. C. Arnett et al., “Estimates of the prevalence of arthritis and selected musculoskeletal disorders in the United States,” *Arthritis and Rheumatism*, vol. 41, no. 5, pp. 778–799, 1998.
- [29] S. Dai, T. Liang, X. Shi, Z. Luo, and H. Yang, “Salvianolic acid B protects intervertebral discs from oxidative stress-induced degeneration via activation of the JAK2/STAT3 signaling pathway,” *Oxidative Medicine and Cellular Longevity*, vol. 2021, 2021.
- [30] J. J. Chen, J. F. Huang, W. X. Du, and P. J. Tong, “Expression and significance of MMP3 in synovium of knee joint at different stage in osteoarthritis patients,” *Asian Pacific Journal of Tropical Medicine*, vol. 7, no. 4, pp. 297–300, 2014.
- [31] N. V. Vo, R. A. Hartman, T. Yurube, L. J. Jacobs, G. A. Sowa, and J. D. Kang, “Expression and regulation of metalloproteinases and their inhibitors in intervertebral disc aging and degeneration,” *The Spine Journal*, vol. 13, no. 3, pp. 331–341, 2013.
- [32] P. M. van der Kraan and W. B. van den Berg, “Anabolic and destructive mediators in osteoarthritis,” *Current Opinion in Clinical Nutrition and Metabolic Care*, vol. 3, no. 3, pp. 205–211, 2000.
- [33] F. Rannou, T. S. Lee, R. H. Zhou et al., “Intervertebral disc degeneration: the role of the mitochondrial pathway in annulus fibrosus cell apoptosis induced by overload,” *The American Journal of Pathology*, vol. 164, no. 3, pp. 915–924, 2004.
- [34] Y. Zhang, P. Jiang, M. Ye, S. H. Kim, C. Jiang, and J. Lu, “Tanshinones: sources, pharmacokinetics and anti-cancer activities,” *International Journal of Molecular Sciences*, vol. 13, no. 12, pp. 13621–13666, 2012.
- [35] D. Tan, J. R. Wu, X. M. Zhang, S. Liu, and B. Zhang, “Sodium tanshinone II A sulfonate injection as adjuvant treatment for unstable angina pectoris: a meta-analysis of 17 randomized controlled trials,” *Chinese Journal of Integrative Medicine*, vol. 24, no. 2, pp. 156–160, 2018.
- [36] R. Hoogendoorn, B. Z. Doulabi, C. L. Huang, P. I. Wuisman, Bank RA, and M. N. Helder, “Molecular changes in the degenerated goat intervertebral disc,” *Spine*, vol. 33, no. 16, pp. 1714–1721, 2008.
- [37] J. J. Mac Lean, C. R. Lee, M. Alini, and J. C. Iatridis, “The effects of short-term load duration on anabolic and catabolic gene expression in the rat tail intervertebral disc,” *Journal of Orthopaedic Research*, vol. 23, no. 5, pp. 1120–1127, 2005.
- [38] Y. Matsui, M. Maeda, W. Nakagami, and H. Iwata, “The involvement of matrix metalloproteinases and inflammation in lumbar disc herniation,” *Spine (Phila Pa 1976)*, vol. 23, no. 8, pp. 863–868, 1998, discussion 868–869.
- [39] M. Kanemoto, S. Hukuda, Y. Komiya, A. Katsuura, and J. Nishioka, “Immunohistochemical study of matrix metalloproteinase-3 and tissue inhibitor of metalloproteinase-1 human intervertebral discs,” *Spine (Phila Pa 1976)*, vol. 21, no. 1, pp. 1–8, 1996.
- [40] C. K. Kepler, D. Z. Markova, A. S. Hilibrand et al., “Substance P stimulates production of inflammatory cytokines in human disc cells,” *Spine (Phila Pa 1976)*, vol. 38, no. 21, pp. E1291–E1299, 2013.
- [41] D. Purmessur, B. A. Walter, P. J. Roughley, D. M. Laudier, A. C. Hecht, and J. Iatridis, “A role for TNF α in intervertebral disc degeneration: a non-recoverable catabolic shift,” *Biochemical and Biophysical Research Communications*, vol. 433, no. 1, pp. 151–156, 2013.
- [42] C. Shen, J. Yan, L. S. Jiang, and L. Y. Dai, “Autophagy in rat annulus fibrosus cells: evidence and possible implications,” *Arthritis Research & Therapy*, vol. 13, no. 4, p. R132, 2011.
- [43] S. Yang, F. Zhang, J. Ma, and W. Ding, “Intervertebral disc ageing and degeneration: the antiapoptotic effect of oestrogen,” *Ageing Research Reviews*, vol. 57, p. 100978, 2020.
- [44] M. V. Risbud and I. M. Shapiro, “Role of cytokines in intervertebral disc degeneration: pain and disc content,” *Nature Reviews Rheumatology*, vol. 10, no. 1, pp. 44–56, 2014.
- [45] C. L. Le Maitre, J. A. Hoyland, and A. J. Freemont, “Catabolic cytokine expression in degenerate and herniated human intervertebral discs: IL-1 β and TNF α expression profile,” *Arthritis Research & Therapy*, vol. 9, no. 4, p. R77, 2007.
- [46] J. Zhu, Y. Xu, G. Ren et al., “Tanshinone IIA sodium sulfonate regulates antioxidant system, inflammation, and endothelial dysfunction in atherosclerosis by downregulation of CLIC1,” *European Journal of Pharmacology*, vol. 815, pp. 427–436, 2017.
- [47] P. Wu, Y. Du, Z. Xu et al., “Protective effects of sodium tanshinone IIA sulfonate on cardiac function after myocardial infarction in mice,” *American Journal of Translational Research*, vol. 11, no. 1, pp. 351–360, 2019.
- [48] B. Wei, W. W. Li, J. Ji, Q. H. Hu, and H. Ji, “The cardioprotective effect of sodium tanshinone IIA sulfonate and the optimizing of therapeutic time window in myocardial ischemia/reperfusion injury in rats,” *Atherosclerosis*, vol. 235, no. 2, pp. 318–327, 2014.
- [49] W. Zhu, Q. Lu, H. W. Chen, J. Feng, L. Wan, and D. X. Zhou, “Protective effect of sodium tanshinone IIA sulfonate on injury of small intestine in rats with sepsis and its mechanism,” *Chinese Journal of Integrative Medicine*, vol. 18, no. 7, pp. 496–501, 2012.
- [50] K. Apel and H. Hirt, “Reactive oxygen species: metabolism, oxidative stress, and signal transduction,” *Annual Review of Plant Biology*, vol. 55, no. 1, pp. 373–399, 2004.
- [51] R. Mittler, “Oxidative stress, antioxidants and stress tolerance,” *Trends in Plant Science*, vol. 7, no. 9, pp. 405–410, 2002.
- [52] Z. Y. Zhou, W. R. Zhao, J. Zhang, X. L. Chen, and J. Y. Tang, “Sodium tanshinone IIA sulfonate: a review of pharmacological activity and pharmacokinetics,” *Biomedicine & Pharmacotherapy*, vol. 118, p. 109362, 2019.
- [53] J. Medina and R. Moreno-Otero, “Pathophysiological basis for antioxidant therapy in chronic liver disease,” *Drugs*, vol. 65, no. 17, pp. 2445–2461, 2005.
- [54] O. R. Koch, G. Pani, S. Borrello et al., “Oxidative stress and antioxidant defenses in ethanol-induced cell injury,” *Molecular Aspects of Medicine*, vol. 25, no. 1–2, pp. 191–198, 2004.

- [55] X. Piao, Z. Liu, Y. Li et al., "Investigation of the effect for bisphenol A on oxidative stress in human hepatocytes and its interaction with catalase," *Spectrochimica Acta. Part A, Molecular and Biomolecular Spectroscopy*, vol. 221, p. 117149, 2019.
- [56] S. N. Patel, K. Pandya, G. J. Clark, M. C. Parikh, and C. A. Lau-Cam, "Comparison of taurine and pantoyltaurine as antioxidants _in vitro_ and in the central nervous system of diabetic rats," *Experimental and Toxicologic Pathology*, vol. 68, no. 2-3, pp. 103–112, 2016.
- [57] K. Oettl, V. Stadlbauer, F. Petter et al., "Oxidative damage of albumin in advanced liver disease," *Biochimica et Biophysica Acta*, vol. 1782, no. 7-8, pp. 469–473, 2008.
- [58] C. Qian, Y. Ren, and Y. Xia, "Sodium tanshinone IIA sulfonate attenuates hemorrhagic shock-induced organ damages by nuclear factor-kappa B pathway," *The Journal of Surgical Research*, vol. 209, pp. 145–152, 2017.
- [59] J. Gu, H. L. Li, H. Y. Wu et al., "Sodium tanshinone IIA sulfonate attenuates radiation-induced fibrosis damage in cardiac fibroblasts," *Journal of Asian Natural Products Research*, vol. 16, no. 9, pp. 941–952, 2014.
- [60] B. Wei, M. G. You, J. J. Ling et al., "Regulation of antioxidant system, lipids and fatty acid β -oxidation contributes to the cardioprotective effect of sodium tanshinone IIA sulphonate in isoproterenol-induced myocardial infarction in rats," *Atherosclerosis*, vol. 230, no. 1, pp. 148–156, 2013.
- [61] W. Luczaj, A. Gegotek, and E. Skrzydlewska, "Antioxidants and HNE in redox homeostasis," *Free Radical Biology & Medicine*, vol. 111, pp. 87–101, 2017.

Research Article

Reactive Oxygen Species Mediate Low Back Pain by Upregulating Substance P in Intervertebral Disc Degeneration

Jiancheng Zheng ^{1,2,3}, Jian Zhang,⁴ Xingkai Zhang,^{1,3} Zhiping Guo,² Wenjian Wu ^{1,3},
Zhe Chen ^{1,3} and Jitian Li ²

¹Department of Orthopaedics, Ruijin Hospital, Shanghai Jiaotong University School of Medicine, Shanghai 200025, China

²Henan Luoyang Orthopedic Hospital (Henan Provincial Orthopedic Hospital), Henan Provincial Orthopedic Institute, Zhengzhou 450000, China

³Shanghai Key Laboratory for Prevention and Treatment of Bone and Joint Diseases with Integrated Chinese-Western Medicine, Shanghai Institute of Traumatology and Orthopedics, Ruijin Hospital, Shanghai Jiaotong University School of Medicine, Shanghai 200025, China

⁴Department of Spine Surgery, Shenzhen Second People's Hospital, The First Affiliated Hospital of Shenzhen University, Shenzhen 518000, China

Correspondence should be addressed to Wenjian Wu; drwuwenjian@126.com, Zhe Chen; drchenzhe@live.com, and Jitian Li; jitianlee@hotmail.com

Received 18 December 2020; Revised 11 April 2021; Accepted 20 April 2021; Published 15 May 2021

Academic Editor: Wenyan Ding

Copyright © 2021 Jiancheng Zheng et al. This is an open access article distributed under the Creative Commons Attribution License, which permits unrestricted use, distribution, and reproduction in any medium, provided the original work is properly cited.

Reactive oxygen species (ROS) are thought to have a strong correlation with a number of intervertebral disc (IVD) diseases. Here, we aimed to determine whether ROS represent an etiology of low back pain (LBP) during IVD degeneration. Thirty degenerated intervertebral disc samples were obtained from patients, and ROS levels were quantified using dihydroethidium (DHE) staining. The results suggested a significant correlation between the ROS level and the severity of LBP. Subsequently, a puncture-induced LBP model was established in rats, and ROS levels significantly increased compared with those in the sham surgery group, accompanied with severe puncture-induced IVD degeneration. In addition, when ROS levels were increased by H₂O₂ administration or decreased by NAC treatment, the rats showed increased or decreased LBP, respectively. Based on this evidence, we further determined that stimulation with H₂O₂ in nucleus pulposus cells (NPCs) *in vivo* or *in vitro* resulted in upregulation of substance P (SP), a peptide thought to be involved in the synaptic transmission of pain, and that the severity of LBP decreased when SP levels were increased by exogenous SP administration or neutralized via aprepitant treatment in the IVDs of rats. In conclusion, ROS are primary inducers of LBP based on clinical and animal data, and the mechanism involves ROS stimulation of NPCs to secrete SP, which is a critical neurotransmitter peptide, to promote LBP in IVDs. Therefore, reducing the level of ROS with specific drugs and inhibiting SP may be alternative methods to treat LBP in the clinic.

1. Introduction

Low back pain (LBP) is a serious chronic disease that reduces quality of life and increases psychological burden in patients. Accordingly, approximately one-quarter of U.S. adults reported having LBP lasting at least 1 whole day in the past 3 months, and 7.6% reported at least 1 episode of severe acute low back pain within a 1-year period [1]. Unfortunately, most LBP is nonspecific, and it is difficult to find a specific

treatment due to the lack of a pathological or pathophysiological basis [2]. Therefore, only physical therapy or analgesic drugs can be used to relieve symptoms in patients.

There is no doubt that the intervertebral discs (IVDs) play a critical role in maintaining the stability of the whole spine, and abnormal anatomy or physiological dysfunction of IVDs leads to a series of spine-related diseases, especially LBP [3]. Degeneration of IVD was an independent etiology for LBP [4]. Also, etiologies of trauma, infection, and

immune dysregulation result in increased levels of inflammatory factors, upregulation of proalgesic factors, and promotion of nerve fiber growth in the IVDs, all of which lead to severe LBP [3]. Thus, maintaining IVD homeostasis is an important strategy for the treatment of LBP.

Reactive oxygen species (ROS) are products of biomarkers expressed in response to cellular damage or stimuli. Nucleus pulposus cells (NPCs) are the core of the IVDs, and they exhibit a remarkable increase in ROS levels after exposure to mechanical stress [5] or biochemical stimulation [6]. The generated ROS initiate a series of downstream cellular activities, such as apoptosis [7] and secretion of biochemical factors [8].

Until now, there has been no evidence concerning the pathological role of ROS in LBP. Thus, the first aim of this study was to elucidate the potential relationship between ROS and LBP. In addition, we wanted to investigate whether substance P (SP), a peptide in the IVDs that is responsible for LBP, participated in ROS-mediated LBP. The elimination of ROS in the IVDs could provide a promising therapeutic method for LBP in the future.

2. Method

2.1. Patients and Tissue Collection. The study was authorized by the Institutional Review Board of Ruijin Hospital, Shanghai Jiaotong University School of Medicine, and every participant signed an informed consent form. Thirty patients who underwent posterior lumbar discectomy at our hospital because of lumbar intervertebral disc degeneration were enrolled in this study between May 2020 and September 2020. All patients had LBP accompanied with or without sciatica for at least 6 months and failed to conservative treatment or physical therapy. If the patients had lumbar disc herniation associated with Modic changes, spondylolisthesis, or spinal instability, instrumented posterior lumbar interbody fusion was performed at the same time. The included patients ranged from 36 to 82 years of age, with an average age of 63.433 ± 12.560 years. Thirteen were male, and 17 were female. Three patients underwent surgery at the L3-L4 level, 17 patients underwent surgery at L4-L5, and 10 patients underwent surgery at L5-S1. To quantify the severity of LBP, Visual Analogue Scale (VAS), Oswestry Disability Index (ODI) [9], and Japanese Orthopaedic Association Back Pain Evaluation Questionnaire (JOABPEQ) [10] scores were recorded for all patients. The nucleus pulposus (NP) was obtained during surgery and frozen at -80°C for subsequent experiments.

2.2. LBP Model in Rats. All animal experiments in this study were approved by the Animal Care and Use Committee of Henan Provincial Orthopedic Institute, and we followed the protocols of the National Institutes of Health Guide for the Care and Use of Laboratory Animals (NIH Publications No. 8023, revised 1978). Based on a previous study [11], male rats weighing 250–300 g were anesthetized with 2.5% pentobarbital sodium, and then, the IVD of L4-5 was exposed using a transabdominal median approach. Subsequently, the IVD was penetrated vertically to reach the NP using an

18-gauge needle at a depth of 2 mm, and then, drugs were administered with a microsyringe. After that, the incision was sutured layer by layer with silk thread, and the animals were kept warm until they regained consciousness. For the behavioral study, seven groups were established: the sham-surgery group, puncture + saline group, puncture + NAC (N-acetyl-L-cysteine) group, puncture + H_2O_2 group, puncture + SP 0.1 μg group, puncture + SP 1 μg group, and puncture + aprepitant (an antagonist of the neurokinin 1 receptor, which blocks the effect of SP) group. To avoid bias, analgesic drugs and antibiotics were not used before or after the surgery. H_2O_2 was diluted in deionized water and administered at a concentration of 100 μM per disc after puncture. NAC (CAS No. 616-91-1, MedChemExpress, NJ, US) was administered at a concentration of 1 mM per disc after puncture. Substance P (cat No. 1156/5, R&D Inc., MN, US) was administered at a concentration of 0.1 μg or 1 μg per disc, and aprepitant (CAS No. 170729-80-3, MedChemExpress, NJ, US) was administered at a concentration of 1 mM per disc. For immunohistochemistry (IHC) and Western blot analysis about H_2O_2 -induced SP, the H_2O_2 was inoculated into rodent IVD with a 24-gauge needle, and the tissue was harvested 24 hours later.

2.3. Measurement of Mechanical and Cold Allodynia. LBP was quantified via the mechanical and/or cold paw/foot withdrawal threshold method following previous reports [11, 12]. For the mechanical threshold, the animals rested quietly for at least ten minutes to acclimate to the surrounding environment. Then, the calibrated Von Frey filaments (Stoelting, Wood Dale, IL, USA) were vertically stabbed into the plantar surface of the hind limb for 3 seconds. When the rats showed a positive reaction (a brisk movement with or without mouthing or biting of the hind limb), a smaller filament was used; otherwise, a larger filament was applied. Six tests were applied for each hind limb, and the reaction of the hind limb was recorded. To avoid the influence of anxiety on LBP, the stabbing motions were performed at an interval of at least two minutes, and if the animals showed any anxiety-related behavior, a longer rest time was necessary. The threshold of mechanical allodynia was then calculated according to the formula proposed by Chaplan et al. [13], and the average of the two hind limbs was considered the final score.

To assess cold allodynia, 100% acetone was used [14]. In brief, a drop of acetone was applied 2 mm below the plantar surface of the hind paw using a syringe because the evaporation of acetone would have a cooling effect on the surface of the hind paw and thus lead to cold hypersensitivity. Five tests were performed for each paw, and the rats with brisk movement with or without mouthing or biting of the hind limb were considered to have positive reactions. A two-minute interval was applied between each test. The threshold was calculated as the percentage of positive reactions in the ten tests.

2.4. Western Blot Analysis. After extraction, total proteins were separated by SDS-PAGE, transferred to polyvinylidene difluoride membranes (0.45 μm , Millipore, Bedford, MA, U.S.), and incubated with primary antibodies against SP

(cat.No.AF8094 TAC1/Substance P, Rabbit Polyclonal Antibody, Beyotime Biotechnology, Shanghai, China). Subsequently, the membranes were incubated with a horseradish peroxidase-conjugated secondary antibody, goat anti-rabbit IgG (cat. No. 7074, Cell Signaling Technology, MA, U.S.), at room temperature for 1 h, and the bands were visualized using chemiluminescence (Millipore, Bedford, MA, U.S.). B-actin (cat. No. BF0198, Affinity Biosciences LTD, U.S.) served as the internal control. The images were analyzed using a Fusion FX7 (Vilber Lourmat, Marne-la-Vallée, France) and analyzed with Image J software.

2.5. Real-Time Quantitative PCR. The Trizol reagent (Invitrogen, Life Technologies Corporation, CA, U.S.) was used to extract total RNA, and cDNA was synthesized from 1 μ g of total RNA using reverse transcriptase (TaKaRa, Shiga, Japan). An ABI 7500 Sequencing Detection System (Applied Biosystems, CA, U.S.) was used for qRT-PCR with the SYBR Premix Ex Tag Kit (TakaRa, Shiga, Japan). The cycling conditions were as follows: 40 cycles of denaturation at 95°C for 5 s and amplification at 60°C for 24 s. β -Actin served as a housekeeping gene, and all reactions were run in triplicate. The primer sequences (Sangon Biotech, Shanghai, China) used in this study were as follows: human β -actin: forward 5'-AGCCTCGCCTTTGCCGATCCG-3', reverse 5'-CATGCCGAGCCGTTGTGCGAC-3'; human substance P: forward 5'-GCAGAAGAAATAGGAGCCAATG-3', reverse 5'-CATAAAGAGCCTTTAACAGGGC-3'. The target gene expression level was normalized to the expression level of β -actin using the $2^{-\Delta\Delta C_t}$ method. All data were then normalized to the average of the control group.

2.6. Immunofluorescence. To quantify the ROS levels in the IVDs of patients, the samples were frozen at -20°C and sectioned at 5 μ m and then stained with dihydroethidium (DHE, cat No. GDP1018, Servicebio, Wuhan, China) according to the manufacturer's instructions. The IVDs of rats were fixed with 4% paraformaldehyde for 12 h and then were decalcified using 10% ethylenediaminetetraacetic acid (EDTA) for 1 month before routine embedding, sectioning, and deparaffinization. Then, the sections were stained with DHE (cat No. S0063, Beyotime Biotechnology, Shanghai, China) according to the manufacturer's instructions. All images were captured under a fluorescence microscope (Axio, Carl Zeiss, Oberkochen, Germany) and quantified with Image-Pro Plus software.

2.7. Immunohistochemistry (IHC). For IHC analysis, the human nucleus pulposus tissue was fixed with 4% paraformaldehyde for 12 h and then processed via routine paraffin embedding, sectioning, and deparaffinization. The IVDs from rats were fixed with 4% paraformaldehyde for 12 h and then were decalcified using 10% ethylenediaminetetraacetic acid (EDTA) for 1 month before sectioning. Subsequently, the sections were incubated with a TAC1/substance P rabbit polyclonal antibody (cat. no. AF8094, Beyotime Biotechnology Inc., Shanghai, China) at 4°C overnight. A specific IHC kit (cat. No. K5007, Agilent DAKO Inc., CA, US) was used for the whole process accord-

ing the manufacturer's protocol. Nuclei were counterstained with hemalum (cat. G1004, Servicebio Inc., China). The stained samples were observed and photographed under a microscope (Axio, Carl Zeiss, Oberkochen, Germany).

2.8. Statistical Analysis. The data are expressed as the mean \pm SD. For two-group analysis, a two-sided Student's *t* test was performed. Among three or more groups, one-way ANOVA with post hoc of Tukey's HSD test was used. Two-way ANOVA with post hoc Tukey's HSD test was performed for repeated measurements. GraphPad Prism (version 8) was used for statistical analysis, and $P < 0.05$ was considered significantly different.

3. Results

3.1. The Severity of LBP Showed a Correlation with ROS Levels in Human IVDs. To investigate the correlation between LBP and ROS, we performed DHE staining of IVDs from patients and quantified the ROS levels by measuring the mean density (Figure 1(a)). When all patients were classified into the mild (VAS \leq 3), moderate (VAS between 4 and 7), and severe (VAS \geq 8) LBP groups, there was a significant gradual increase in ROS levels among the three groups (as depicted in Figures 1(a) and 1(e)). Furthermore, there was a significant correlation between the ROS level and the VAS score ($Y = 0.08654 * X + 4.714$, $R^2 = 0.3926$, $P = 0.0002$) (as depicted in Figure 1(b)). In addition, a significant correlation was found between the ROS level and the ODI score ($Y = 0.1956 * X + 19.45$, $R^2 = 0.2221$, $P = 0.0086$), and a significant correlation was found between the ROS level and the JOA score ($Y = -0.1692 * X + 16.84$, $R^2 = 0.2297$, $P = 0.0074$) (as shown in Figures 1(c) and 1(d)). All of these data suggested that the severity of LBP showed a significantly correlation with the ROS level in human IVDs.

3.2. Increased Levels of ROS Determined the Severity of LBP in Rats. To verify the pathological role of ROS in LBP, we established an LBP model in rats according to a previous report [11]. An 18-gauge needle was used to puncture the IVD of L4-5 to induce discogenic LBP and severe intervertebral disc degeneration (Supplementary Figure 1). As depicted in Figure 2(a), the ROS level significantly increased after puncture, as measured by DHE staining. Furthermore, compared with the rats in the sham surgery group, the rats showed significant LBP starting on the 3rd day after puncture, indicating a decrease in the mechanical allodynia threshold and an increase in the cold allodynia threshold (as shown in Figures 2(b) and 2(c)). When H₂O₂ was injected into the IVD after puncture, the rats showed much more severe LBP than observed in the puncture + saline group, suggesting that ROS aggravated LBP in rats. In contrast, when NAC was injected into the IVD to decrease the ROS level, the LBP of the rats was relieved, showing an increase in the mechanical allodynia threshold and a decrease in the cold allodynia threshold compared with those of the puncture + saline group. Therefore, we believe that ROS represent the key factor mediating LBP in rats.

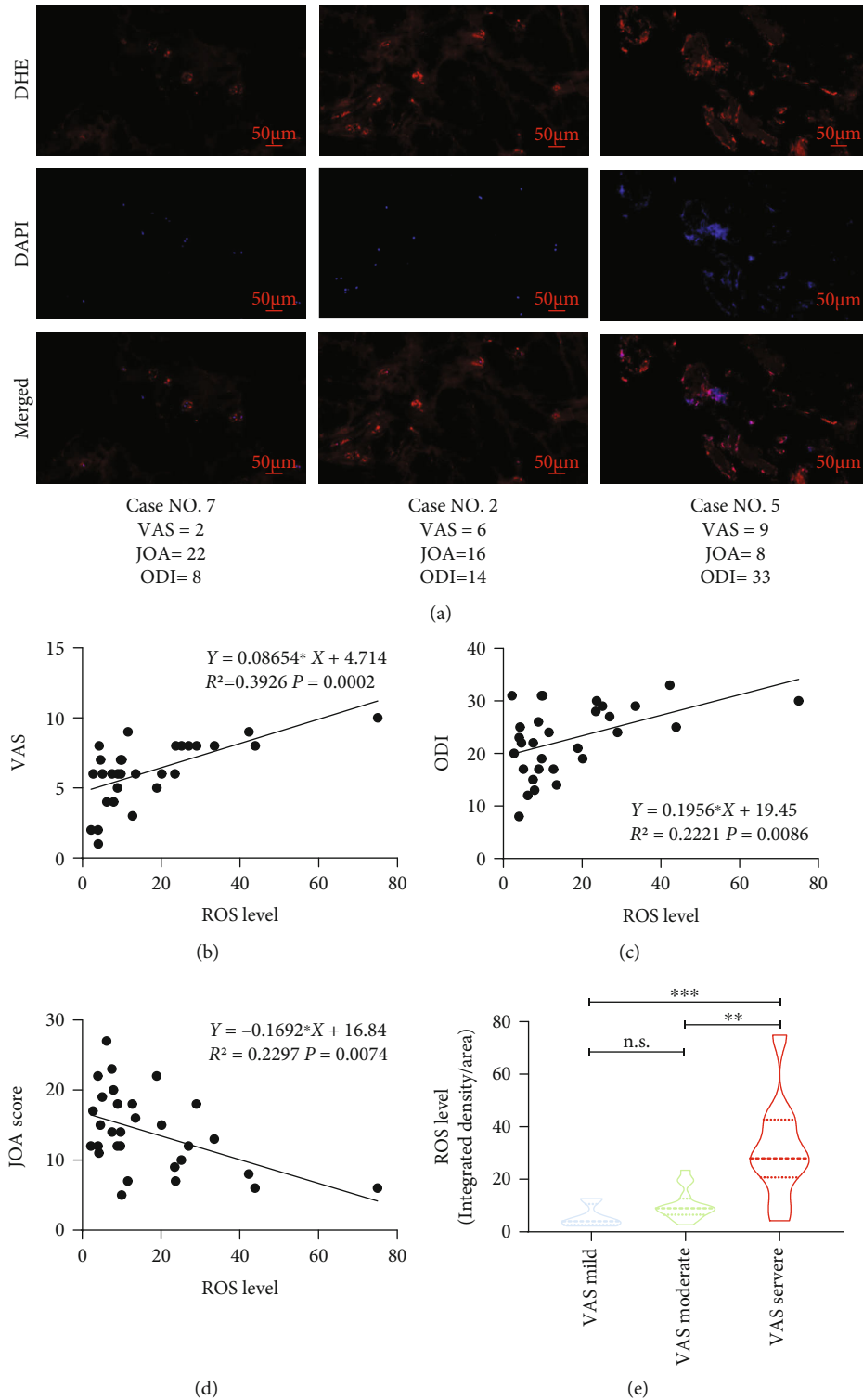


FIGURE 1: The severity of LBP showed a correlation with ROS levels in human IVDs. (a) DHE staining suggested a gradual increase in ROS levels along with more severe LBP in patients. (b, c) Linear regression analysis suggested a significant positive correlation between the ROS level in the NP and the VAS score or ODI score. (d) There was a significant negative correlation between the ROS level and the JOA score. (e) When the patients were classified as having mild, moderate, and severe LBP, the ROS levels were significantly gradually increased (** <0.01 and *** <0.001 when compared between different groups. The data are shown as the mean \pm SD. $n = 4$, $n = 16$, and $n = 10$ for the VAS mild, VAS moderate, and VAS severe groups, respectively. A linear regression model was used for correlation analysis. One-way ANOVA and Tukey's multiple comparison test were used for multiple group comparisons).

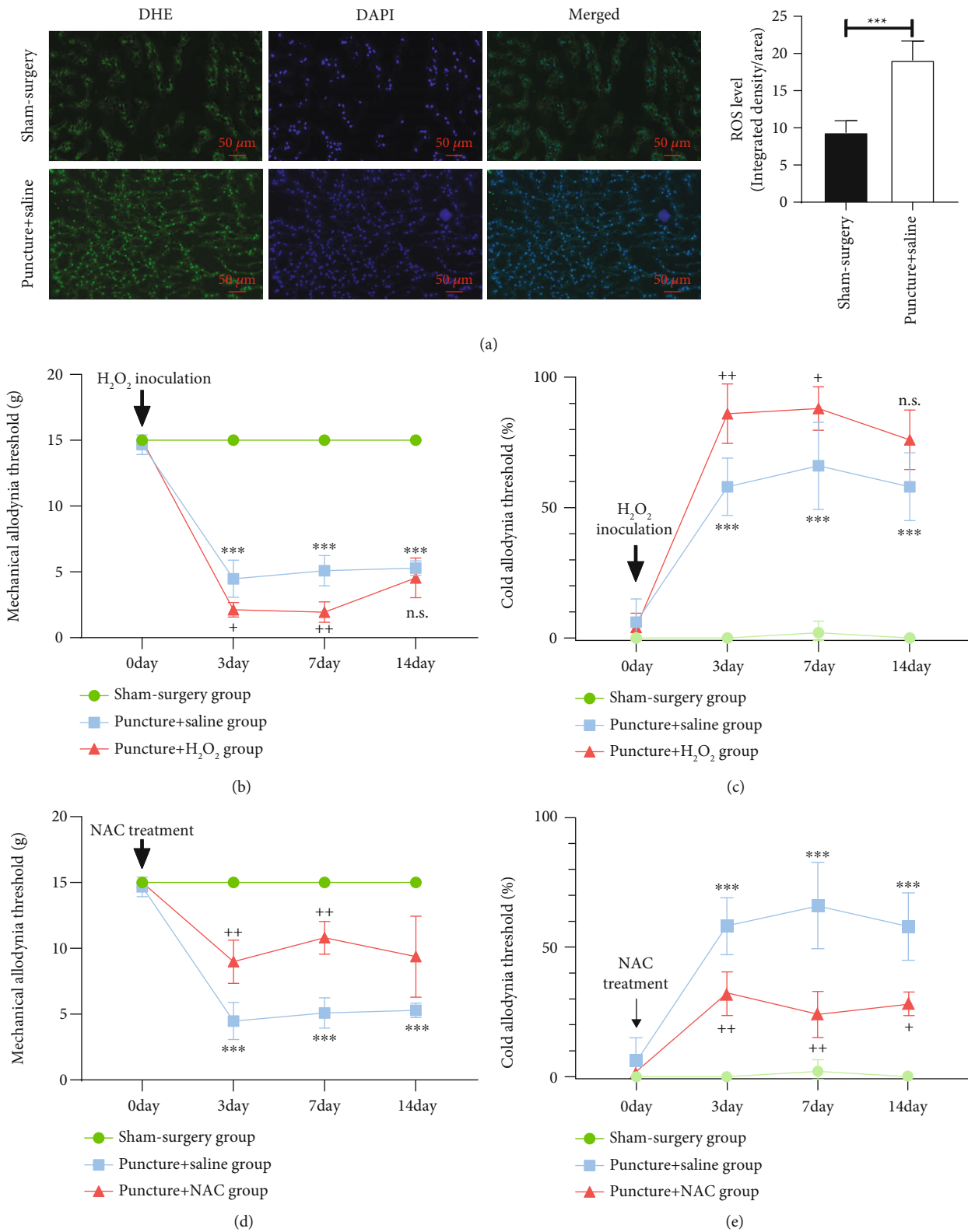


FIGURE 2: Continued.

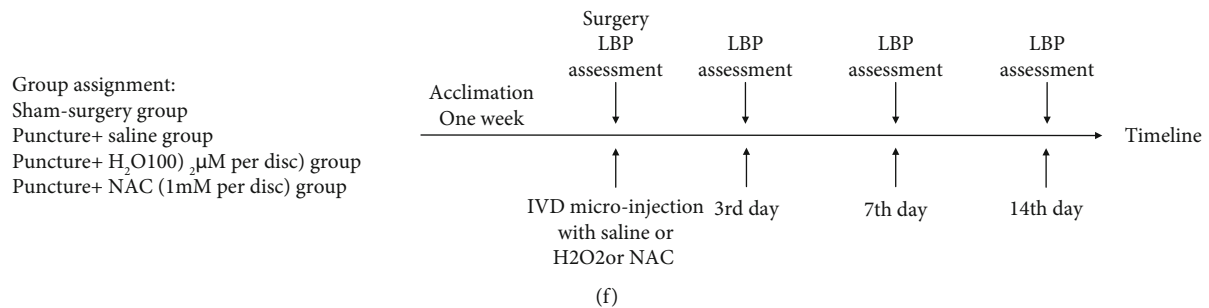


FIGURE 2: Increased ROS levels determined the severity of LBP in rats. (a) Immunofluorescence analysis of DHE suggested an increase in ROS after puncture of IVD with an 18-gauge needle. (b, c) Administration of H₂O₂ after puncture of IVDs resulted in much more severe LBP, indicating a decrease in the mechanical allodynia threshold and an increase in the cold allodynia threshold when compared with those of the puncture + saline group. (d, e) Administration of NAC (a classical antioxidant) significantly alleviated LBP in rats, suggesting an increase in the mechanical allodynia threshold and a decrease in the cold allodynia threshold compared with those of the puncture + saline group. (f) The timeline of drug delivery and behavioral testing for all groups (The data are shown as the mean \pm SD. $N = 3 \sim 5$ for each group. $*** < 0.001$ for comparisons between the sham surgery group and the puncture + saline group. $+ < 0.05$, $++ < 0.01$, and $+++ < 0.001$ for comparisons between the puncture + saline group and the puncture + H₂O₂ group or between the puncture + saline group and the puncture + NAC group. Two-way ANOVA and Tukey's multiple comparison test were used for statistical analysis).

3.3. ROS Induced LBP by Upregulating the Expression of SP in NPCs. It was suggested that SP, a peptide thought to be involved in the synaptic transmission of pain, could be secreted by NPC and play a critical role in discogenic LBP. Here, the relative gene expression of SP significantly increased when NPCs were cocultured with H₂O₂ in a dose-dependent manner, as shown in Figure 3(a). Furthermore, the NPCs had significantly upregulated expression of SP protein after stimulation with H₂O₂ in a dose-dependent manner (as shown in Figure 3(b)). When H₂O₂ was injected into the IVDs of rats, the rats showed excessive expression of SP (as shown in Figure 3(c)). IHC analysis verified the increase in SP in the IVDs and the degeneration of the IVDs (as shown in Figure 3(d)). Thus, ROS were able to induce NPCs to secrete SP in the IVDs.

3.4. The Expression of SP Showed a Correlation with LBP. To further confirm the pathological role of SP in LBP, we quantified the expression of SP in human IVDs. The expression of SP gradually increased with increasing severity of LBP, with a statistically significant dose-dependent response (as depicted in Figure 4(a)). Furthermore, direct injection of SP into the IVDs of rats at doses of 0.1 μ g and 1 μ g resulted in significant and marked LBP, with dose-dependent effects (as shown in Figure 4(b)). In contrast, when the biological effect of SP was inhibited by aprepitant, which is an antagonist of the SP receptor, LBP was significantly relieved (as shown in Figure 4(c)). Therefore, SP plays a critical role in mediating ROS-induced LBP.

4. Discussion

Here, we demonstrated that the ROS level in IVDs had a correlation with LBP based on clinical and animal studies. In addition, increased ROS levels resulted in significant upregulation of SP, which is a crucial factor in inducing LBP in IVDs. In contrast, elimination of ROS or inhibition of the

SP receptor induced remarkable relief of LBP in patients. Overall, we drew the reasonable conclusion that increased ROS levels acted as the trigger for LBP by upregulating SP in IVDs.

Multiple factors lead to an increase in ROS levels in IVDs. A previous study suggested that *Propionibacterium acnes*, an anaerobic low-virulence bacterium, easily infects IVDs and then induces a significant increase in ROS [15]. In addition, excessive mechanical loading results in mitochondrial dysfunction of NPCs and an increase in ROS levels [16]. Other factors, such as interleukin-1 β [17] or high glucose [18], were also responsible for increased ROS levels in IVDs. In this study, we determined that there was a remarkable increase in ROS levels in degenerated IVDs and that this change had a correlation with LBP in patients.

Although there are few reports clarifying the relationship between ROS and LBP, ROS are thought to be a key factor in inducing neuropathic pain or inflammatory pain. For example, control of ROS levels attenuated neuroexcitability and restrict bidirectional signaling between neurons, glia, and immune cells that creates and amplifies pain [19]. In osteoarthritis, treatment with ROS scavengers had obvious benefits for pronociceptive responses in rats [20]. Here, we further determined that ROS were the etiology of LBP. Linear regression analysis demonstrated that the concentration of ROS had a significant correlation with the severity of LBP, corresponding to an increase in VAS and ODI scores and a decrease in JOABPEQ scores. Animal data further validated this relationship: punctured discogenic lumbar IVDs had an increase in ROS levels, administration of H₂O₂ led to LBP degradation, and neutralization of ROS alleviated LBP in rats.

There was no previous report clarifying how ROS induce LBP. Here, our data suggested that SP maybe a key factor participating in ROS-induced LBP. Many studies have suggested that SP is an independent risk factor for LBP, because SP is a critical neurotransmitter peptide that promotes pain

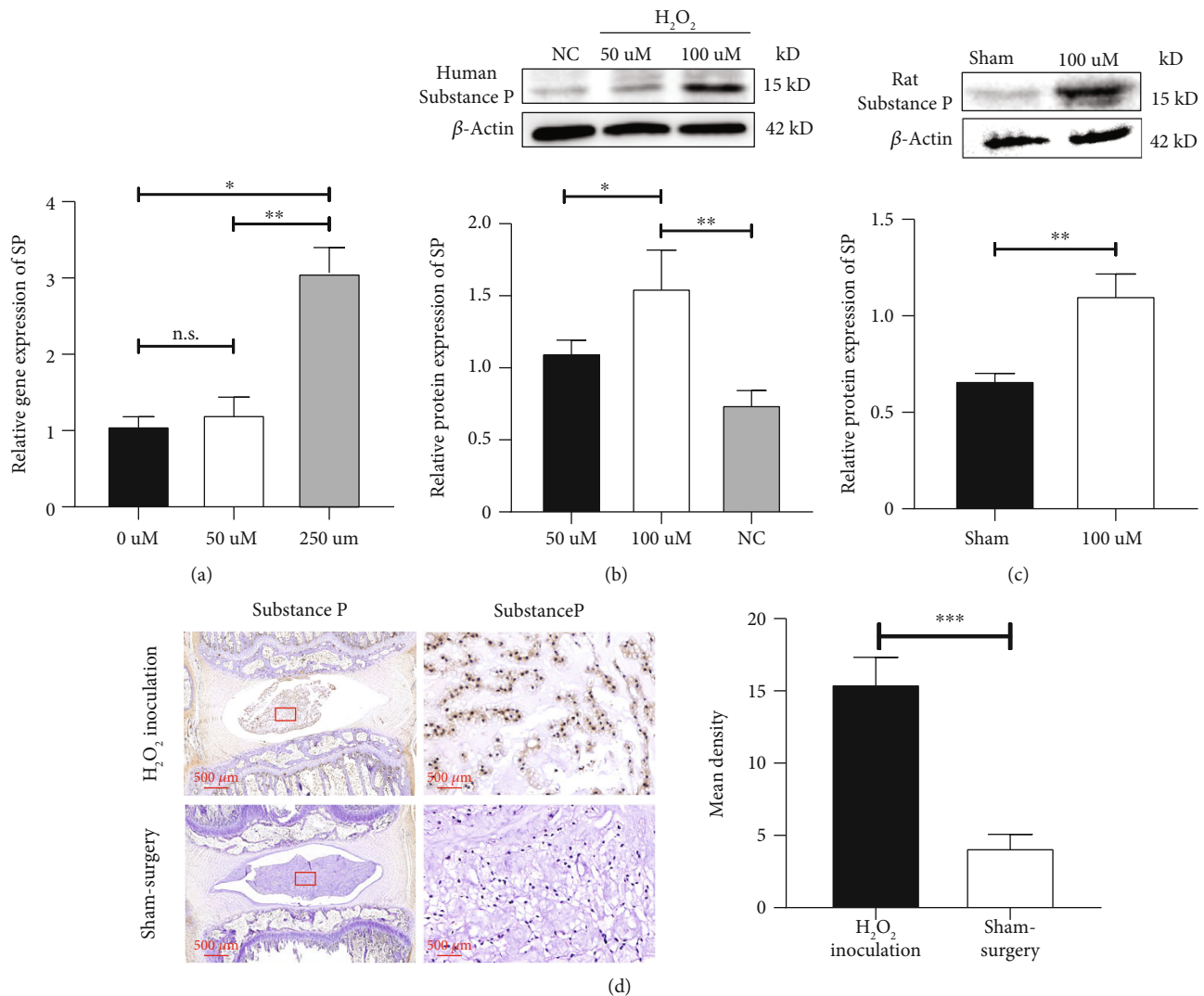


FIGURE 3: ROS significantly induced the expression of substance P. (a) H₂O₂ significantly induced the expression of the SP gene in NPCs in a dose-dependent manner with RT-PCR expression. (b) Western blot analysis also verified the increase in SP after stimulation with H₂O₂ in a dose-dependent manner. (c) Administration of H₂O₂ into the IVDs of rats resulted in significant upregulation of the SP protein. (d) IHC analysis suggested a remarkable increase in SP protein levels in the NP after administration of 100 μ M H₂O₂, while the expression of the SP protein in the sham surgery group was low (The data are shown as the mean \pm SD. $N = 3 \sim 5$ for each group. * <0.05 , ** <0.01 and *** <0.001 for comparisons between two or three groups. Student's t test was used for comparisons between two groups, ** while one-way ANOVA and Tukey's multiple comparison test were used for comparisons among three or more groups).

transmission in nerves. Previous histological finding suggested that nerve growth into IVD with expression of SP was a key factor in the pathogenesis of chronic low back pain [21, 22]. In addition, biochemical analysis of a discogenic IVD revealed the upregulation of SP when compared to the control specimens [23, 24]. In addition, bacteria-infected IVDs exhibited excessive secretion of SP, which then caused severe LBP in rats [11]. Besides the effect of causing discogenic LBP, SP also induced IVD degeneration by stimulating inflammatory mediators or catabolic factors [25, 26]. Thus, we believe that abundant SP secreted by NPCs triggers pain-related nerves in the NP and/or annulus fibrosus and then induces LBP, and targeting SP may be a key strategy to prevent LBP and IVD degeneration.

Here, we not only proved the close relationship between SP and LBP but also identified NPCs as the main source of SP after ROS stimulation. It has been reported that NPCs secrete SP when stimulated by *P. acnes* [11]. Additionally, metalloproteinase-3 (TIMP3) has been reported to regulate the secretion of SP in NPCs [27]. Previous study suggested that excessive ROS was a crucial factor for IVD degeneration by inducing inflammatory factors and these factors may be the trigger for production of SP [28].

However, there were still some limitations in this study. Firstly, the long-term therapeutic effectiveness of NAC or aprepitant treatment was not investigated in this study, and whether they were effective for chronic LBP

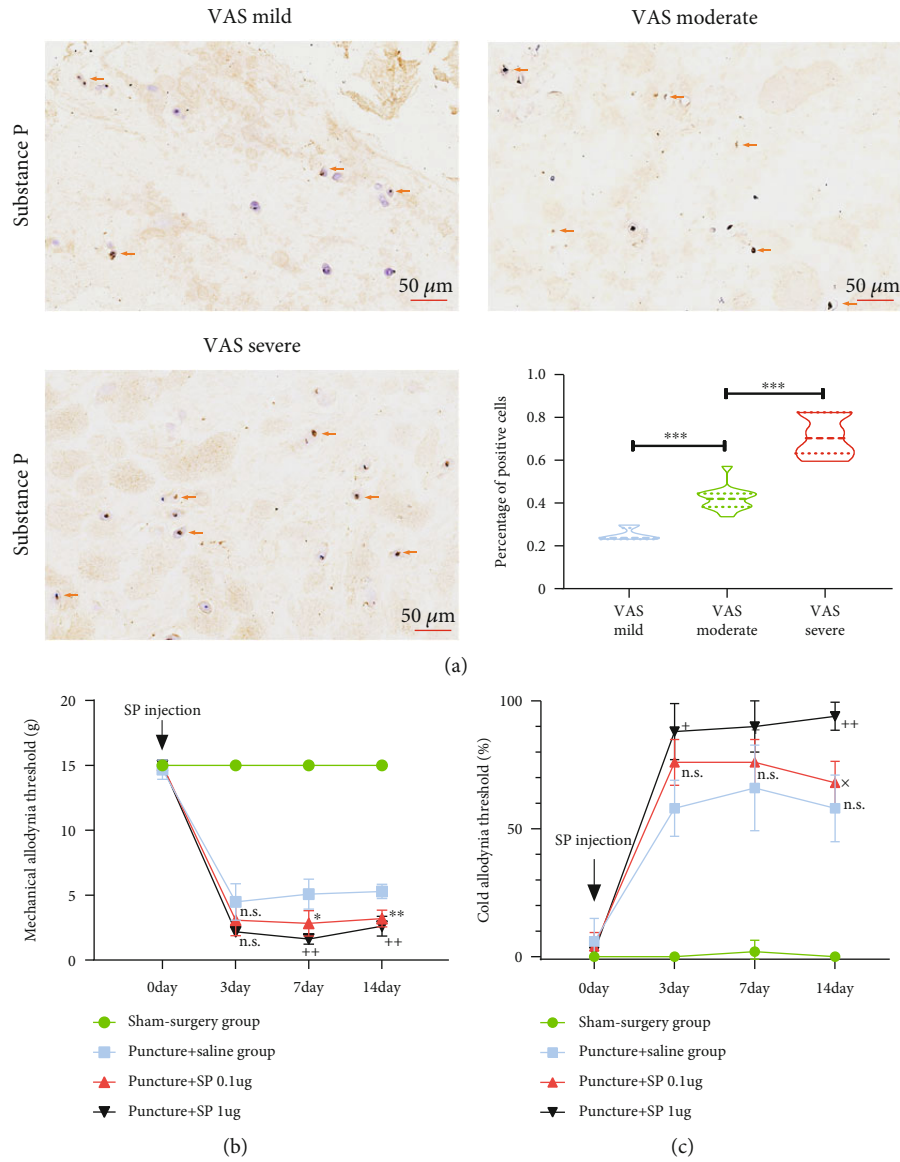


FIGURE 4: Continued.

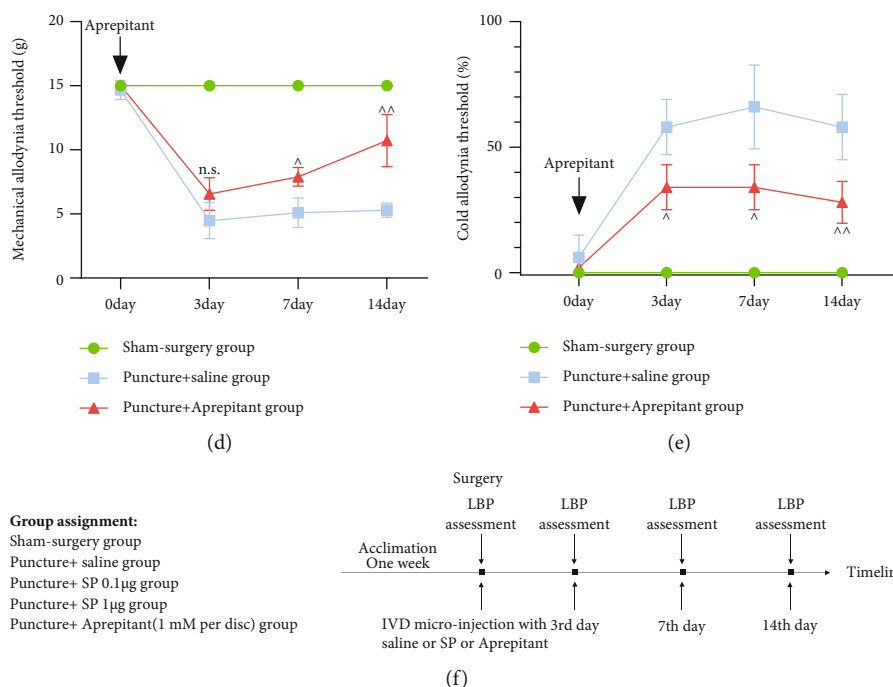


FIGURE 4: SP was the key factor mediating LBP. (a) IHC analysis suggested an increase of SP levels in human NP tissue, with a significant difference among the VAS mild, VAS moderate, and VAS severe groups. (b, c) Administration of SP into the IVDs of rats significantly induced LBP, indicating a decrease in the mechanical allodynia threshold and an increase in the cold allodynia threshold when compared with those of the puncture + saline group, with a dose-dependent response. (d, e) By contrast, administration of the SP receptor inhibitor of aprepitant significantly attenuated LBP in rats. (f) The timeline of drug delivery and behavioral testing for all groups (The data are shown as the mean \pm SD. The positive cell with SP was marked with red arrows. $n = 4$, $n = 16$, and $n = 10$ for the VAS mild, VAS moderate, and VAS severe groups, respectively. * <0.05 and ** <0.01 for comparisons between the puncture + SP 0.1 μg group and the puncture + saline group. + <0.05 and ++ <0.01 for comparisons between the puncture + SP 1 μg group and the puncture + saline group. \times <0.05 for comparisons between the puncture + SP 0.1 μg group and the puncture + SP 1 μg group. ^ <0.05 and ^^ <0.01 for comparisons between the puncture + aprepitant and the puncture + saline group. One-way or two-way ANOVA and Tukey's multiple comparison test were used for statistical analysis).

was still unclear. In addition, the small clinical sample is another limitation in this study and that may be the reason for the low R^2 value. Finally, the pathophysiological mechanism about how ROS regulating the production of SP is not clear in this study and more research is needed in the future.

In conclusion, ROS is a primary factor in the induction of LBP based on clinical and animal data, and the mechanism involves ROS-mediated stimulation of NPCs to secrete SP, which is a critical neurotransmitter peptide, to promote pain transmission within IVDs. Therefore, reducing the level of ROS with specific drugs may be an alternative method to treat LBP in the clinic.

Abbreviations

ROS: Reactive oxygen species
 LBP: Low back pain
 IVD: Intervertebral disc
 DHE: Dihydroethidium
 NPCs: Nucleus pulposus cells
 SP: Substance P.

Data Availability

The data that support the findings of this study are available from the corresponding author upon reasonable request.

Conflicts of Interest

The authors declare that there is no conflict of interest regarding the publication of this paper.

Authors' Contributions

Jiancheng Zheng and Jian Zhang contributed equally to this work.

Acknowledgments

This work was supported by grant from the fund of the Guangci Youth Plan of Ruijin Hospital (No. GCQN-2019-A09), the National Natural Science Fund of China (NSFC no. 81702188), the National Natural Science Fund of China (NSFC no. 82004397), and the Major Project of TCM

Research in Henan Province (Nos. 2019ZYZD02 and 2021ZYZD12). We also thank Pro Nicole R, from AJE, for editing the English text of a draft of this manuscript.

Supplementary Materials

The IVD of L4-5 had remarkable degeneration after an 18-gauge needle penetration. (a) The lateral X-ray examination demonstrated that an 18-gauge needle was penetrated into the IVD of L4-5 during the surgery (marked with red arrow). (b) Lateral X-ray examination figured out the punctured intervertebral disc height decreased when compared with sham-surgery animal after two weeks penetration (marked with red arrow). (c) The punctured IVD had decreased gray value at short T1 inversion-recovery (STIR) sequence of MRI after two weeks when compared with sham-surgery IVD (marked with red arrow). (d) Histological and immunohistochemical analysis suggested that the IVD in sham-surgery had normal appearance, indicating as aggrecan-rich, bulging nucleus pulposus with rare proliferated chondrocytes and no clefts, and organized annulus fibrosus as discrete fibrous lamellae, while the penetrated IVD had disappearance of notochordal cells and the numerous levels of proliferated chondrocytes in nucleus pulposus area and the disruption of endplates and annulus fibrosus due to the needle penetration. (*Supplementary Materials*)

References

- [1] R. Chou, A. Qaseem, V. Snow et al., "Diagnosis and treatment of low back pain: a joint clinical practice guideline from the American College of Physicians and the American Pain Society," *Annals of Internal Medicine*, vol. 147, no. 7, pp. 478–491, 2007.
- [2] F. Balague, A. F. Mannion, F. Pellise, and C. Cedraschi, "Non-specific low back pain," *Lancet*, vol. 379, no. 9814, pp. 482–491, 2012.
- [3] S. Pathak and T. Conermann, *Lumbosacral discogenic syndrome*, Stat Pearls, Treasure Island (FL), 2020.
- [4] F. J. Lyu, H. Cui, H. Pan, K. Mc Cheung, X. Cao, and J. C. Iatridis, "Painful intervertebral disc degeneration and inflammation: from laboratory evidence to clinical interventions," *Bone Research*, vol. 9, no. 1, p. 7, 2021.
- [5] P. Li, G. Hou, R. Zhang et al., "High-magnitude compression accelerates the premature senescence of nucleus pulposus cells via the p 38 MAPK-ROS pathway," *Arthritis Research & Therapy*, vol. 19, no. 1, p. 209, 2017.
- [6] X. Li, F. Lin, Y. Wu et al., "Resveratrol attenuates inflammation environment-induced nucleus pulposus cell senescence in vitro," *Bioscience reports*, vol. 39, no. 5, 2019.
- [7] Z. Li, J. Wang, X. Deng, D. Huang, Z. Shao, and K. Ma, "Compression stress induces nucleus pulposus cell autophagy by inhibition of the PI3K/AKT/mTOR pathway and activation of the JNK pathway," *Connective Tissue Research*, vol. 62, no. 3, pp. 337–349, 2021.
- [8] M. Y. Ansari, N. Ahmad, and T. M. Haqqi, "Oxidative stress and inflammation in osteoarthritis pathogenesis: role of polyphenols," *Biomedicine & pharmacotherapy*, vol. 129, p. 110452, 2020.
- [9] J. C. Fairbank, J. Couper, J. B. Davies, and J. P. O'Brien, "The Oswestry low back pain disability questionnaire," *Physiotherapy*, vol. 66, no. 8, pp. 271–273, 1980.
- [10] M. Fukui, K. Chiba, M. Kawakami et al., "JOA Back Pain Evaluation Questionnaire (JOABPEQ)/ JOA Cervical Myelopathy Evaluation Questionnaire (JOACMEQ) The report on the development of revised versions April 16, 2007: The Subcommittee of the Clinical Outcome Committee of the Japanese Orthopaedic Association on Low Back Pain and Cervical Myelopathy Evaluation," *Journal of orthopaedic science: official journal of the Japanese Orthopaedic Association*, vol. 14, no. 3, pp. 348–365, 2009.
- [11] Y. Jiao, Y. Yuan, Y. Lin et al., "Propionibacterium acnes induces discogenic low back pain via stimulating nucleus pulposus cells to secrete pro-algesic factor of IL-8/CINC-1 through TLR2-NF- κ B p65 pathway," *Journal of Molecular Medicine*, vol. 97, no. 1, pp. 25–35, 2019.
- [12] V. M. van Heeswijk, A. Thambyah, P. A. Robertson, and N. D. Broom, "Does an annular puncture influence the herniation path?: an in vitro mechanical and structural investigation," *Spine*, vol. 43, no. 7, pp. 467–476, 2018.
- [13] S. R. Chaplan, F. W. Bach, J. W. Pogrel, J. M. Chung, and T. L. Yaksh, "Quantitative assessment of tactile allodynia in the rat paw," *Journal of Neuroscience Methods*, vol. 53, no. 1, pp. 55–63, 1994.
- [14] J. Park, L. Zheng, G. Acosta et al., "Acrolein contributes to TRPA1 up-regulation in peripheral and central sensory hypersensitivity following spinal cord injury," *Journal of Neurochemistry*, vol. 135, no. 5, pp. 987–997, 2015.
- [15] Y. Lin, G. Tang, Y. Jiao et al., "Propionibacterium acnes induces intervertebral disc degeneration by promoting iNOS/NO and COX-2/PGE2 activation via the ROS-dependent NF- κ B pathway," *Oxidative Medicine and Cellular Longevity*, vol. 2018, Article ID 3692752, 12 pages, 2018.
- [16] L. Kang, S. Liu, J. Li, Y. Tian, Y. Xue, and X. Liu, "The mitochondria-targeted anti-oxidant MitoQ protects against intervertebral disc degeneration by ameliorating mitochondrial dysfunction and redox imbalance," *Cell Proliferation*, vol. 53, no. 3, article e12779, 2020.
- [17] Q. Liu, L. Jin, F. H. Shen, G. Balian, and X. J. Li, "Fullerol nanoparticles suppress inflammatory response and adipogenesis of vertebral bone marrow stromal cells—a potential novel treatment for intervertebral disc degeneration," *The spine journal: official journal of the North American Spine Society*, vol. 13, no. 11, pp. 1571–1580, 2013.
- [18] M. Yao, J. Zhang, Z. Li, S. Guo, X. Zhou, and W. Zhang, "Marin protects human nucleus pulposus cells against high glucose-induced injury and extracellular matrix degradation at least partly by inhibition of ROS/NF- κ B pathway," *International Immunopharmacology*, vol. 80, p. 106126, 2020.
- [19] P. M. Grace, A. D. Gaudet, V. Staikopoulos et al., "Nitroxidative signaling mechanisms in pathological pain," *Trends in Neurosciences*, vol. 39, no. 12, pp. 862–879, 2016.
- [20] K. N. Westlund, M. Y. Kochukov, Y. Lu, and T. A. McNearney, "Impact of central and peripheral TRPV1 and ROS levels on proinflammatory mediators and nociceptive behavior," *Molecular Pain*, vol. 6, 2010.
- [21] A. J. Freemont, T. E. Peacock, P. Goupille, J. A. Hoyland, J. O'Brien, and M. I. Jayson, "Nerve ingrowth into diseased intervertebral disc in chronic back pain," *Lancet*, vol. 350, no. 9072, pp. 178–181, 1997.

- [22] A. J. Freemont, A. Watkins, C. Le Maitre et al., "Nerve growth factor expression and innervation of the painful intervertebral disc," *The Journal of Pathology*, vol. 197, no. 3, pp. 286–292, 2002.
- [23] B. Peng, W. Wu, S. Hou, P. Li, C. Zhang, and Y. Yang, "The pathogenesis of discogenic low back pain," *The Journal of bone and joint surgery British volume*, vol. 87, pp. 62–67, 2005.
- [24] S. M. Richardson, P. Doyle, B. M. Minogue, K. Gnanalingham, and J. A. Hoyland, "Increased expression of matrix metalloproteinase-10, nerve growth factor and substance P in the painful degenerate intervertebral disc," *Arthritis Research & Therapy*, vol. 11, no. 4, p. R126, 2009.
- [25] J. D. Koerner, D. Z. Markova, G. D. Schroeder et al., "The effect of substance P on an intervertebral disc rat organ culture model," *Spine*, vol. 41, no. 24, pp. 1851–1859, 2016.
- [26] C. K. Kepler, D. Z. Markova, A. S. Hilibrand et al., "Substance P stimulates production of inflammatory cytokines in human disc cells," *Spine*, vol. 38, no. 21, pp. E1291–E1299, 2013.
- [27] M. He, J. Pang, H. Sun, G. Zheng, Y. Lin, and W. Ge, "Overexpression of TIMP3 inhibits discogenic pain by suppressing angiogenesis and the expression of substance P in nucleus pulposus," *Molecular Medicine Reports*, vol. 21, pp. 1163–1171, 2020.
- [28] S. Suzuki, N. Fujita, N. Hosogane et al., "Excessive reactive oxygen species are therapeutic targets for intervertebral disc degeneration," *Arthritis Research & Therapy*, vol. 17, no. 1, 2015.

Research Article

Ulinastatin Ameliorates IL-1 β -Induced Cell Dysfunction in Human Nucleus Pulposus Cells via Nrf2/NF- κ B Pathway

Xi Luo,¹ Le Huan,¹ Feng Lin,¹ Fanqi Kong,¹ Xiaofei Sun,¹ Fudong Li,¹ Jian Zhu,¹ Jingchuan Sun,¹ Ximing Xu,¹ Kaiqiang Sun ¹, Liwei Duan ² and Jiangang Shi ¹

¹Department of Orthopedic Surgery, Changzheng Hospital, Navy Medical University (Second Military Medical University), No. 415 Fengyang Road, Shanghai 200003, China

²Department of Emergency and Critical Care Medicine, Changzheng Hospital, Naval Medical University (Second Military Medical University), Shanghai 200433, China

Correspondence should be addressed to Kaiqiang Sun; 15721570551@163.com, Liwei Duan; 13262589308@163.com, and Jiangang Shi; shijiangangspine@163.com

Received 4 February 2021; Revised 5 April 2021; Accepted 9 April 2021; Published 22 April 2021

Academic Editor: Wenyuan Ding

Copyright © 2021 Xi Luo et al. This is an open access article distributed under the Creative Commons Attribution License, which permits unrestricted use, distribution, and reproduction in any medium, provided the original work is properly cited.

Low back pain (LBP) has been a wide public health concern worldwide. Among the pathogenic factors, intervertebral disc degeneration (IDD) has been one of the primary contributors to LBP. IDD correlates closely with inflammatory response and oxidative stress, involving a variety of inflammation-related cytokines, such as interleukin 1 beta (IL-1 β), which could result in local inflammatory environment. Ulinastatin (UTI) is a kind of acidic protein extracted from human urine, which inhibits the release of tumor necrosis factor alpha (TNF- α) and other inflammatory factors to protect organs from inflammatory damage. However, whether this protective effect of UTI on human nucleus pulposus (NP) exists, and how UTI affects the biological behaviors of human NP cells during IDD remain elusive. In this current study, we revealed that UTI could improve the viability of NP cells and promote the proliferation of NP cells. Additionally, UTI could protect human NP cells via ameliorating IL-1 β -induced apoptosis, inflammatory response, oxidative stress, and extracellular matrix (ECM) degradation. Molecular mechanism analysis suggested that the protective effect from UTI on IL-1 β -treated NP cells were through activating nuclear factor- (erythroid-derived 2-) like 2 (Nrf2)/heme oxygenase-1 (HO-1) signaling pathway and the suppression of NF- κ B signaling pathway. Therefore, UTI may be a promising therapeutic medicine to ameliorate IDD.

1. Introduction

Low back pain (LBP) has ranked as one of the major public concerns worldwide, with approximately 80% of the populations experiencing LBP in their lifetime [1]. Among various pathogenic contributors, intervertebral disc degeneration (IDD) has the mostly focused and studied [2].

Automatically, the intervertebral disc includes three main structures: the inner nucleus pulposus (NP), circumferential fibrocartilaginous annulus fibrosus (AF), and cartilaginous endplates (EP) that cap the NP and AF [3]. Under healthy condition, NP tissue is mainly composed of NP cells and extracellular matrix (ECM) (collagen type II and aggrecan) [4]. Plentiful studies have previously suggested that IDD is a pathological process which is closely related to inflamma-

tory responses and oxidative stress, and involves a variety of inflammation mediators such as interleukin 1 beta (IL-1 β) and tumor necrosis factor alpha (TNF- α) [5]. Furthermore, these inflammation cytokines will trigger the generation of a series of inflammatory factors, such as nitric oxide (NO) and prostaglandin E2 (PGE2), which can promote cell apoptosis, excessive inflammation reactions, and the generation of reactive oxygen species (ROS). Taken together, IDD will be initiated under the conditions above. Subsequently, these pathogenic changes may compromise the integrity of the intervertebral disc, cause abnormal distribution of mechanical load imposed on the spine, and consequently destroy the mechanical properties of the spine. At molecular level, nuclear tor-erythroid 2-related factor-2 (Nrf2) has been reported to process the role of antioxidant

and anti-inflammation in many degeneration-related diseases [6]. Previous studies have demonstrated that activated nuclear factor- (erythroid-derived 2-) like 2 (Nrf2)/heme oxygenase-1 (HO-1) signaling pathway showed inhibitory effect on NF- κ B in NP cells. Tang et al. have also suggested that the expression of Nrf2 elevated in human degenerative NP tissue and that knocking down Nrf2 aggravated IDD [7]. Therefore, agents targeting at reversing or enhancing the expression of Nrf2 may be beneficial in the treatment of IDD.

Ulinastatin (UTI) is a kind of acidic protein extracted from human urine, which is a highly effective protease inhibitor with the function of stabilizing cell membrane and lysosomal membrane [8]. In addition, UTI can inhibit the release of tumor TNF- α and other inflammatory factors, prevent the interaction between inflammatory mediators and leukocytes, and depress aggregation and activation of leukocyte. UTI is clinically used to inhibit systemic inflammatory reactions such as pancreatitis and acute circulatory failure, presenting a wide range of pharmacological effects and significant protective effects on the heart, lung, kidney, brain, and other organs [9]. Hua et al. have studied the effect of UTI on degenerated NP cells of rabbits and found that UTI could inhibit the expression of MMP-2, MMP-3, and iNOS [10]. However, whether this protective effect of UTI on human NP remains equally valid and how UTI affects the biological behaviors of human NP cells remain elusive.

The objective of the present study is to examine the biological effects of UTI on human NP cells and the underlying molecular mechanisms. The evidence provided by this study will be of great significance for the clinical application of UTI in the treatment of IDD.

2. Methods and Materials

2.1. Acquisition and Patient Samples. The experiment was approved by the ethics committee from Changzheng Hospital, and the signed informed consent was acquired from all patients. The NP cells were collected from 12 patients (male 5, female 7, mean age 45.00 ± 9.07 years) from January 2020 to January 2021. All patients accepted preoperative MRI of the lumbar spine, and the Pfirrmann grading system was used to assess the condition of the affected disc. According to Pfirrmann grade, patients were divided into nondegeneration group (Grade II) and degeneration group (Grade IV). The nondegeneration group consisted of 6 patients with idiopathic scoliosis or lumbar trauma who required lumbar surgery, and all 6 patients in degeneration group were treated due to IDD and associated compression of nerve roots at lumbar spine.

2.2. Human NP Cells Isolation, Culture, and Identification. This method has been reported previously [11, 12]. After separated from patients intraoperatively, NP tissue was immediately stored in 0.9% sodium chloride solution and then transported to super clean bench. Following being washed twice using aseptic PBS, NP tissue was isolated with Trypsin-EDTA (0.25%, Gibco, Invitrogen) for 20-30 minutes and collagenase type II (0.2%, Invitrogen, Carlsbad, CA,

USA) for another 3-4 h at 37°C combined with 0.1% of fetal bovine serum (FBS, Gibco; Thermo Fisher Scientific, Inc.) and 1% of a penicillin-streptomycin mix (Gibco; Thermo Fisher Scientific, Inc.). After isolation, NP cells were resuspended in DMEM/F12 with 20% of FBS and 1% penicillin-streptomycin solution and cultured at 37°C. Frequently, NP cells would move out of the fragment tissues after five days, which we could passage 0. When confluent to about 80%-90%, the cells were digested by Trypsin-EDTA for 2 minutes at 37°C. Next, cells were resuspended and replanted into 25 cm³ culture flasks with a proper density. Due to no obvious morphological changes of NP cells between initial cells (passage 1, P1) and following passage cells (P4), the low-passage (<4) cells were used for the following experiments. The phenotype of NP cells was validated by identifying the expression of type II collagen and aggrecan (Supplementary file 1).

2.3. Cell Viability Assay. In this section, cell Counting Kit-8 (CCK-8, Dojindo, Japan) was used. Briefly, the human NP cells were seeded in a 96-well plate with a density of $4 - 5 \times 10^3$ cells/well. After cell adhesion of 24 hours, cells were stimulated by various concentrations of UTI (0-5000 U/mL) were for 24 h at 37°C. Next, 10 μ L CCK-8 solution combined with 100 μ L of DF-12 was added into all tested well, and then, the cells were incubated at the temperature of 37°C for 1 h. The absorbance was measured (450 nm) on an absorbance microplate reader (Bio-Tek, USA).

2.4. Real Time Quantitative PCR (qRT-PCR). Total RNA was isolated from the human NP cells seeded in six-well plate with RNA extraction kit, and the concentration of mRNA was frequently 100 ng/ μ L (Magen, Inc. Guangzhou, China). Then, cDNA was reversed using HiScript[®] III RT SuperMix for qPCR Kit (R323-01, Vazyme, Nanjing, China), frequently with 2 μ L 5x III RT SuperMix, 1-2 μ L mRNA solution, and 6-7 μ L RNase-free ddH₂O. The expression at mRNA levels of anabolic and catabolic gene was then quantified by Real-time PCR with the SYBR qPCR Master Mix (Q711-02, Vazyme, Nanjing, China) on a ABI 7500 Real-Time PCR system (Applied Biosystems, Foster City, USA). The reaction conditions were designed as follows: one cycle at 95°C for 30 s (Step 1), followed by 40 cycles at 95°C for 10 s and at 60°C for 30 s (Step 2). GAPDH was used as the normalization, and all reactions were run for three times. The primer sequences used for qRT-PCR analysis are shown in Table 1.

2.5. Immunohistochemical Analysis. The methods have been reported previously [13]. Briefly, intervertebral disc sections were firstly embedded in paraffin. Then, the sections were deparaffinized, and the 3% hydrogen peroxide was used to block the endogenous peroxidase. Subsequently, after antigen retrieval using pepsin (Servicebio, Wuhan, China) in 5 mM HCl, the sections were incubated with 10% goat blocking serum for 20-30 min, then with primary antibody against IL-1 β (#12242, 1:100, Cell Signaling Technology, Inc. USA), p65 (#8242, 1:400, Cell Signaling Technology, Inc. USA), and Nrf2 (340675, Zenbio, Chengdu, China, 1:500) at 4°C overnight. Finally, HRP-conjugated secondary

TABLE 1: Sequence of primers for qRT-PCR.

Gene name		Sequence 5' to 3'
MMP-3	F	GATGCGCAAGCCCAGGTGTG
	R	GCCAATTTTCATGAGCAGCAACGA
MMP13	F	TCAGGAAACCAGGTCTGGAG
	R	T G A C G C G A A C A ATA C G G T TA
Collagen type II	F	AATTCGGACCTCGTCATCAG
	R	GCCTGGATAACCTCTGTG
Aggrecan	F	TGAGCGGCAGCACTTTGAC
	R	TGAGTACAGGAGGCTTGAGG
GAPDH	F	GCCGCTTCTTCTCGTGCAG
	R	AT G G AT C AT T G AT G G C G A C A A C AT

antibody (GB23302/23303, Servicebio, Wuhan, China) was added to the sections, and the sections were further counterstained using hematoxylin. Images were obtained using light microscopy (Olympus, Japan).

2.6. Western Blot (WB) Analysis. After different treatments, NP cells were lysed using ice-cold RIPA for 5 min, and the dissolved protein was quantified using the Protein Measurement Assay kit (PC0020, Solarbio Beijing, China). Sodium dodecyl sulphate polyacrylamide gel electrophoresis was carried out to separate the acquired proteins based on a 10% gel, and then, the separated proteins were transported onto a polyvinylidene fluoride (PVDF) membrane (EMD Millipore, Billerica, MA, USA). Blocking was carried out using nonfat milk dissolved in Tris-buffered saline-Tween (Invitrogen, San Diego, CA, USA) with the concentration of 5% for at least two hours, and the membranes were incubated with primary antibodies against: MMP-13 (820098; 54 kDa; Zenbio, Chengdu, China, 1:1000), type II collagen (Collagen II (1:1000, ab34712, Abcam), Aggrecan (ab36861, 1 µg/mL, Abcam, USA), PCAN (#13110, Cell Signaling Technology, Inc. USA, 1:1000), Bcl2 (381702, Zenbio, Chengdu, China, 1:1000), Bax (200958, Zenbio, Chengdu, China, 1:1000), C-caspase-3 (#9664, Cell Signaling Technology, Inc. USA, 1:1000), MMP-3 (380816; 60 kDa; Zenbio, Chengdu, China, 1:1000), NOX4 (ab109225, Abcam, USA, 1:2000), NOX2 ab129068, Abcam, USA, 1:2000), SOD1(#37385, Cell Signaling Technology, Inc. USA, 1:1000), TNF-α (#3707, Cell Signaling Technology, Inc. USA, 1:1000), IL-6 (#12153, Cell Signaling Technology, Inc. USA, 1:1000), iNOS (#20609, Cell Signaling Technology, Inc. USA, 1:1000), COX-2 (#12282, Cell Signaling Technology, Inc. USA, 1:1000), NF-κB p65 (D14E12, #8242, cell signaling technology, Inc., 3 Trask Lane Danvers, USA), p-p65 (Ser536; #3033, cell signaling technology, Inc., 3 Trask Lane Danvers, USA), Ik-Ba (380682, 35 kDa; Zenbio, Chengdu, China, 1:1,000), p-Ik-Ba (340776, 35 kDa; Zenbio, Chengdu, China, 1:1,000), Histon H3 (Histon H3 (250182, 15 kDa; Zenbio, Chengdu, China, 1:1,000), and GAPDH (5174, cell signaling technology, Inc., 3 Trask Lane Danvers, MA 01923) at 4°C for overnight. After washed using TBST for three times, the membranes were further incubated with the secondary antibodies (380172 and 511103, Zenbio, Chengdu, China,

1:5,000) for another 2 hours. The target protein bands were visualized using a Tanon Imaging System (version 5200, Tanon Science & Technology Co., Ltd., Shanghai, China).

2.7. TUNEL Assay. After fixed by paraformaldehyde (4%) for 30 mins, the disc samples were washed by PBS for 3-4 times. Then, NP cells were permeabilized using 0.3% Triton for 5-10 mins. Next, samples were incubated with fluorescein (FITC) Tunel Cell Apoptosis Detection Kit (G1501-100T, Servicebio, Wuhan, China) for 1 hour. Nuclear was subsequently stained with DAPI solution in the dark environment. Finally, images of apoptotic cells were acquired using fluorescence microscope (Olympus, Japan).

2.8. Hoechst Staining. After being treated by IL-1β (10 ng/mL) with or without UTI (100 U/mL) for 24h, the NP cells were incubated with 1 mL Hoechst 33342 solution for 20-30 minutes. The morphologic changes of the apoptotic cell nuclei could be detected by a fluorescence microscope (Olympus, Japan).

2.9. Evaluation of the Mitochondrial Membrane Potential. Mitochondrial membrane potential (MMP) could reveal the functional condition of mitochondrion. JC-1 Staining was performed via JC-1 Staining kit (Beyotime Biotechnology, Inc., Shanghai, China). Briefly, after treated with IL-1β (10 ng/mL) with/without UTI (100 U/mL) for 24h, NP cells were washed by cool PBS twice and were incubated with JC-1 staining fluid in 37°C for 2 hours. Then, the NP cells were washed with JC-1 dyeing buffer solution (1X) for two times, followed by adding 2 mL of cell complete medium. Finally, a fluorescence microscope (Olympus, Japan) was used to analyze the JC-1 staining of NP cells.

2.10. Analysis of Apoptosis by Flow Cytometry. The method has been reported previously [14]. Annexin V-FITC Apoptosis Detection Kit (C1062M, Beyotime Biotechnology, Inc., Shanghai, China) was used. Briefly, the NP cells in different groups (Control, IL-1β, IL-1β+UTI) were trypsinized (non-Ca²⁺), washed, and resuspended in 195 µL binding buffer at a density of 5.0 – 10.0 × 10⁴ cells/mL. Next, 5 µL of annexin V-FITC and 10 µL of a PI solution were added to the cells for 5-10 mins in the dark environment, whereas

the control group was stained with either annexin V-FITC or PI and, finally, examined via flow cytometry.

2.11. Enzyme-Linked Immunosorbent Assay. To obtain the conditioned media for cytokine array analysis, the NP cells were dealt with differently (Control, IL-1 β , IL-1 β L+UTI) for 24 without culture medium change. Then, the conditioned media were collected from each group and centrifuged (5000 rpm at 4°C for 15 minutes). The supernatants were stored at -80°C in separate until use and diluted with the appropriate standard diluents before measurement. Measurements for collagen-II, MMP-3/13, Aggrecan, MDA, SOD, TNF- α , IL-6, Nitrite, and PGE2 were performed on the supernatants with Enzyme-Linked Immunosorbent Assay (ELISA) kits (Westang, China). The optical density with a wavelength of 450 $_{OD}$ was tested.

2.12. Analysis of Reactive Oxygen Species (ROS). The method has been described previously [15]. After treatment, NP cells were washed for 2-3 times with PBS and then stained using FBS-free cultural medium with 2,7-dichlorodi-hydrofluorescein diacetate (DCFH-DA, 10 μ M, Beyotime, Shanghai, China) for 15 mins at 37°C. After that, the NP cells were once again washed for 3 times using FBS-free cultural medium. The reaction between ROS and DCFH-DA would generate dichlorofluorescein (DCFH), which could emit green fluorescence. The level of ROS was then observed by fluorescence microscope (Olympus, Japan).

2.13. Immunofluorescence Analysis. For aggrecan, type II collagen, MMP3, Ki-67, p65, and Nrf2 immunofluorescent staining, NP cells with different treatments were fixed using 4% PFA for 15-20 min and were permeated for another 5 min using 0.1% *v/v* Triton X-100. Cells were incubated with Aggrecan (GB11373, 1:500-1:1000, Servicebio, Wuhan, China), type II collagen (GB11021, 1:100-1:500, Servicebio, Wuhan, China), MMP3 (GB11131, 1:400-1:1600, Servicebio, Wuhan, China), Ki-67 (GB111141, 1:1200, Servicebio, Wuhan, China), NF- κ B p65 (D14E12, #8242, cell signaling technology, Inc., 3 Trask Lane Danvers, USA), and Nrf2 (340675, Zenbio, Chengdu, China, 1:100) diluted in 0.2% *w/v* bovine serum albumin- (BSA-) TBS for 1 h and then washed with PBS. Cells were incubated with DAPI solution (G1012-100ML, Servicebio, Wuhan, China) for visualization of nuclei and, then, incubated with FITC-conjugated goat anti-rabbit IgG (GB22303, Servicebio, Wuhan, China) and Cy3-conjugated goat anti-rabbit IgG (GB21301, Servicebio, Wuhan, China) for 30 mins in the dark environment. Fluorescence detection was performed by fluorescence microscope (Olympus, Japan).

2.14. Statistical Analysis. All experiments in this present study were performed for at least three times. The quantified data were presented as mean \pm standard deviation (S.D). Statistical analyses were carried out using GraphPad Prism 8 (GraphPad Software Inc; La Jolla, CA) for Windows adopting one-way analysis of variance (ANOVA), followed by the Student-Neuman-Keuls post hoc test to make the comparisons between groups. *p* values less than 0.05 or otherwise indicated a statistical difference.

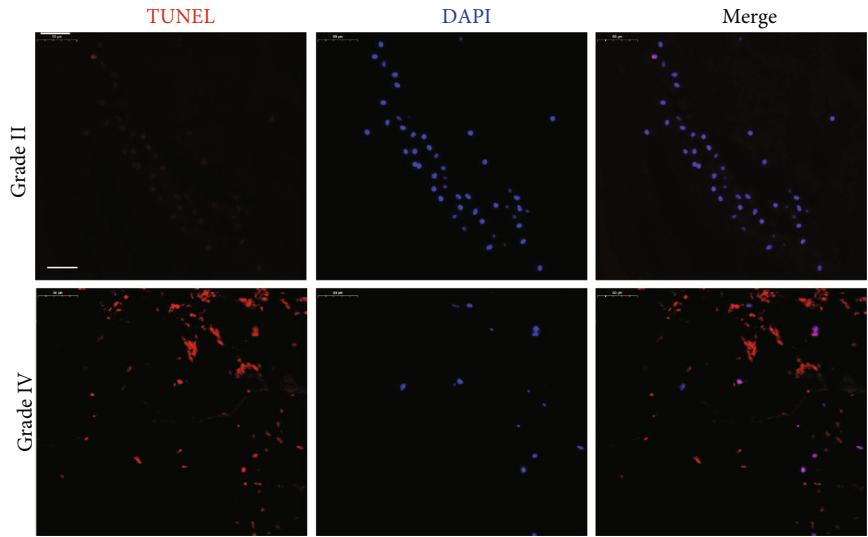
3. Result

3.1. Increased Expression of NF- κ B and Decreased Expression of Nrf2 in Degenerated Human Disc Tissue. Intervertebral disc tissue samples were divided into nondegenerated group (grade II, *n* = 6) and degenerated group (grade IV, *n* = 6) based on the classification system [16]. As shown in Figure 1, degenerated disc tissue had higher TUNEL-positive cell (Figure 1, A). In addition, Western blot analysis also suggested that intervertebral disc tissue sample of grade IV presented with typical features of IDD, including increased expression of MMP3 and decreased expression of type II collagen and aggrecan (Figures 1(b) and 1(c)). Furthermore, immunohistochemical analysis indicated that there were significantly higher ratio of IL-1 β -and NF- κ B-positive cells and lower ratio of Nrf2-positive cells in human NP tissue with degenerated intervertebral disc (Figures 1(e) and 1(f)). These results above showed that lower levels of Nrf2 may correlate with higher severity of IDD.

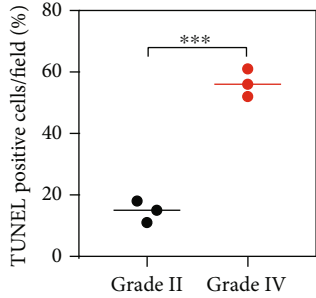
3.2. UTI Could Enhance the Cell Viability of NP Cells and Promote the Proliferative Ability of NP Cells. To determine the potential role of UTI on human NP cells, we firstly explored the cytotoxic effect of UTI on NP cells via a CCK-8 assay kit. As indicated in the results, UTI could significantly increase the cell viability of human NP cells without obvious cytotoxicity in vitro in a concentration below 4000 U/mL with the IC₅₀ of 6898 U/mL, which suggested the safety range of UTI was wide (Figures 2(a) and 2(b)). In addition, Western blot result suggested that UTI could also promote the expression of PCNA in NP cells in a concentration-dependent manner (Figures 2(c) and 2(d)). Immunofluorescence analysis for Ki-67, a marker of cell proliferation, also confirmed the promoting effect of UTI on the proliferative ability of human NP cells (Figures 2(e) and 2(f)).

3.3. UTI Could Protect Human NP Cells against Apoptosis Induced by IL-1 β . As indicated in Figure 1, the level of IL-1 β increased significantly in degenerated intervertebral disc (Figure 1(a)), and previous studies also reported that IL-1 β played a critical role in promoting IDD [17, 18]. Therefore, IL-1 β was used in its present study to established human NP injury model in vitro. We pretreated NP cells with UTI and then added IL-1 β to NP cells with for 24 h to investigate the biological effect of UTI on NP cells under IL-1 β condition. Western blot results uncovered that IL-1 β increased the apoptosis-related marker, Bax and cleaved-caspase 3, and suppressed the expression of antiapoptosis molecular, Bcl-2 (Figures 3(a) and 3(b)). However, this proapoptosis effect was reversed by UTI, as indicated by CCK-8 assay, Hoechst test, and flow cytometry analysis (Figures 3(c)-3(f)). In addition, western blot and analysis of MMP also confirmed the protective effect of UTI on IL-1 β -induced human NP cells (Figures 3(g)-3(j)). Collectively, these results above showed that UTI could protect human NP cells against IL-1 β -induced apoptosis.

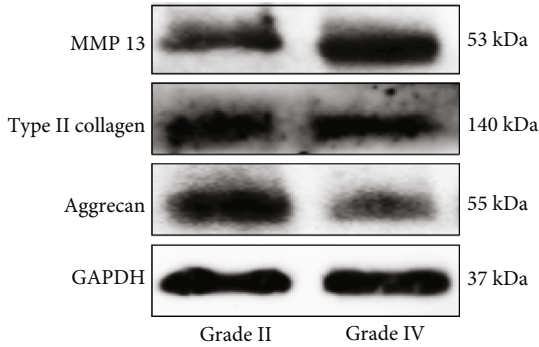
3.4. UTI Ameliorated ECM Degradation in IL-1 β -Induced Human NP Cells. The key feature of IDD is the



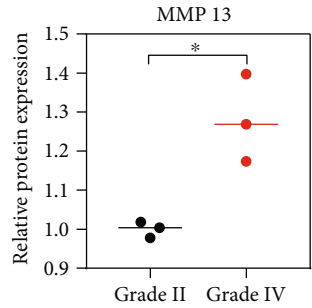
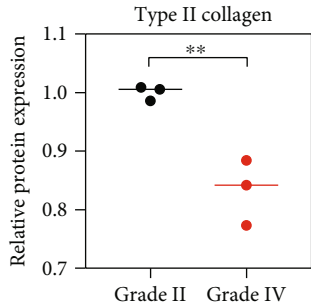
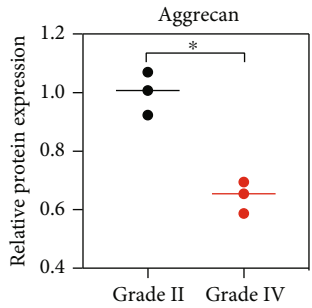
(a)



(b)



(c)



(d)

FIGURE 1: Continued.

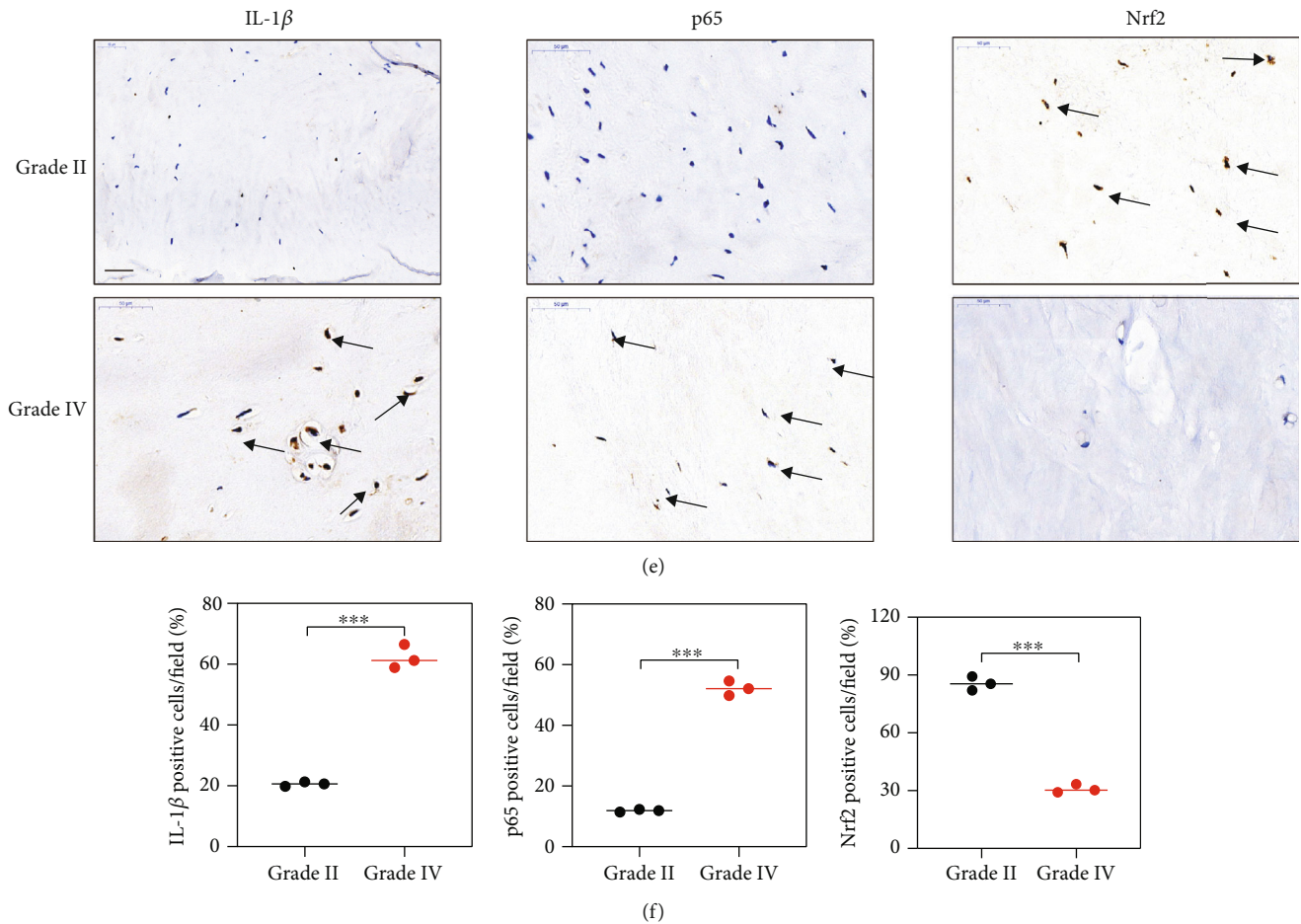


FIGURE 1: The protein expression of Nrf2 and p65 in human NP tissues. (a) The apoptotic NP cells (red) in intervertebral disc between Grade II and Grade IV were visualized via TUNEL staining and the nuclei were stained with DAPI. Scar bar = 300 μ m. (b) Three randomized versions were selected, and TUNEL staining-positive cells were quantified via the amount of red fluorescence. (c, d) Protein bands and quantification of expression levels of Aggrecan, Type II collagen, and MMP 13. Scar bar = 100 μ m. (e) Immunohistochemical results were used to examine the protein levels of IL-1 β , p65, and Nrf2 in the human NP tissue with Grade II and Grade IV. (f) Three versions were randomly selected, and the stained cells were quantified separately. * $p < 0.05$, ** $p < 0.01$, *** $p < 0.001$, **** $p < 0.0001$.

disequilibrium of ECM synthesis and degradation [19]. To explore the protective effect of UTI on IL-1 β -induced human NP injury, we then examined the change of ECM. As shown in Figure 4, immunofluorescence analysis for type II collagen and MMP3 suggested that IL-1 β stimulation obviously suppressed the synthesis of type II collagen in human NP cells but increased the production of MMP3 (Figure 4(a)). Nevertheless, these abnormal alterations in the ECM of NP cells induced by IL-1 β were significantly ameliorated by UTI (Figure 4(a)). Additionally, the results of qRT-PCR and Western blot also suggested the protective effect of UTI on IL-1 β -induced ECM degradation in human NP cells (Figures 4(b)–4(d)).

To explore the ECM change by phenotype, in addition to immunofluorescence analysis, we also examined the secretion of catabolic proteinases in IL-1 β -induced NP cells via ELISA, and the results revealed that pretreatment with UTI could also mitigate the increased expression of MMP3/13 induced by IL-1 β in a concentration-dependent dose and

that the protein expression of collagen type II and aggrecan were also improved by UTI, while NP cells were injured by IL-1 β (Figure 4(e)). Conclusively, UTI ameliorated IL-1 β -induced ECM degeneration in vitro.

3.5. UTI Improved Oxidative Stress Damage in Human NP Cells Induced by IL-1 β . ROS content frequently indicates intracellular oxidative conditions. As shown in Figure 5, IL-1 β increased the ROS level by more than 3-fold in NP cells (Figures 5(a) and 5(b)). However, after pretreatment with UTI, the increased ROS level induced by IL-1 β was ameliorated (Figures 5(a) and 5(b)). ELISA analysis also suggested the suppressive effect of UTI on IL-1 β -induced oxidative stress (Figure 5(c)). At the level of molecule, Western blot analysis suggested that prooxidative stress-related proteins, Nox2/4, were significantly increased by IL-1 β and that the expression of antioxidative stress-related protein, SOD1, was inhibited. Nevertheless, these effects were all reversed by UTI in a dose-dependent manner (Figures 5(d) and 5(e)).

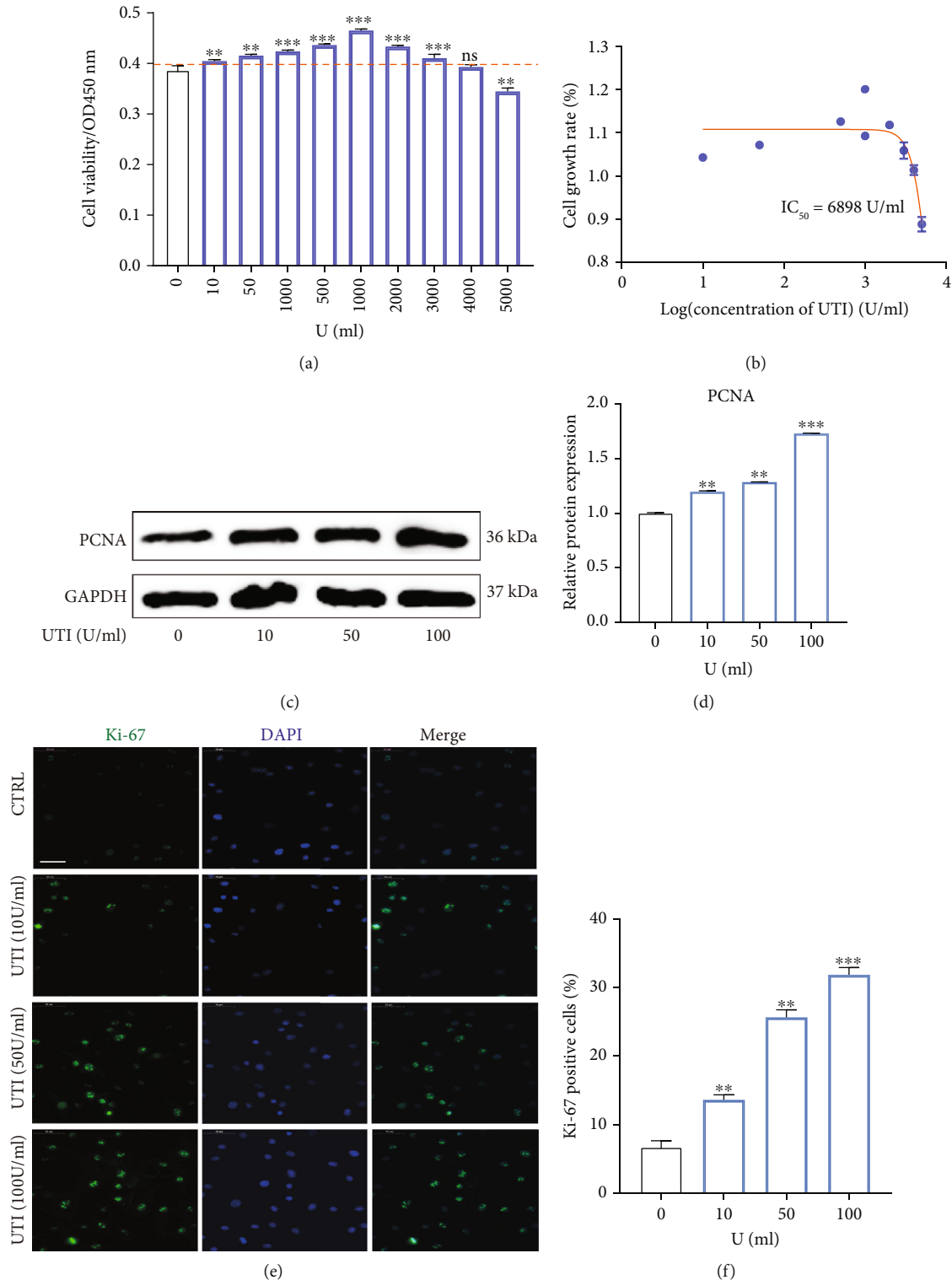


FIGURE 2: Effects of UTI on the proliferative ability in human NP cells. (a) The biological effect of UTI on the cell viability of NP cells ($n = 5$). (b) IC_{50} of UTI for human NP cells. (c, d) Protein bands and quantification of expression levels of PCNA ($n = 3$). (e, f) Expression of Ki-67 (green) was detected by the immunofluorescence. The ratios of cells with green fluorescence were calculated. Scar bar = $200 \mu\text{m}$. * $p < 0.05$, ** $p < 0.01$, *** $p < 0.001$, **** $p < 0.0001$.

3.6. UTI Exerted Anti-Inflammatory Effect via Regulated Inflammation-Related Mediators in Human NP Cells Induced by $IL-1\beta$. During IDD, excessive focal inflammatory

response will damage the normal biological function of NP cells in a positive-feedback manner, inhibiting the abnormal inflammatory microenvironment in disc tissue becomes a

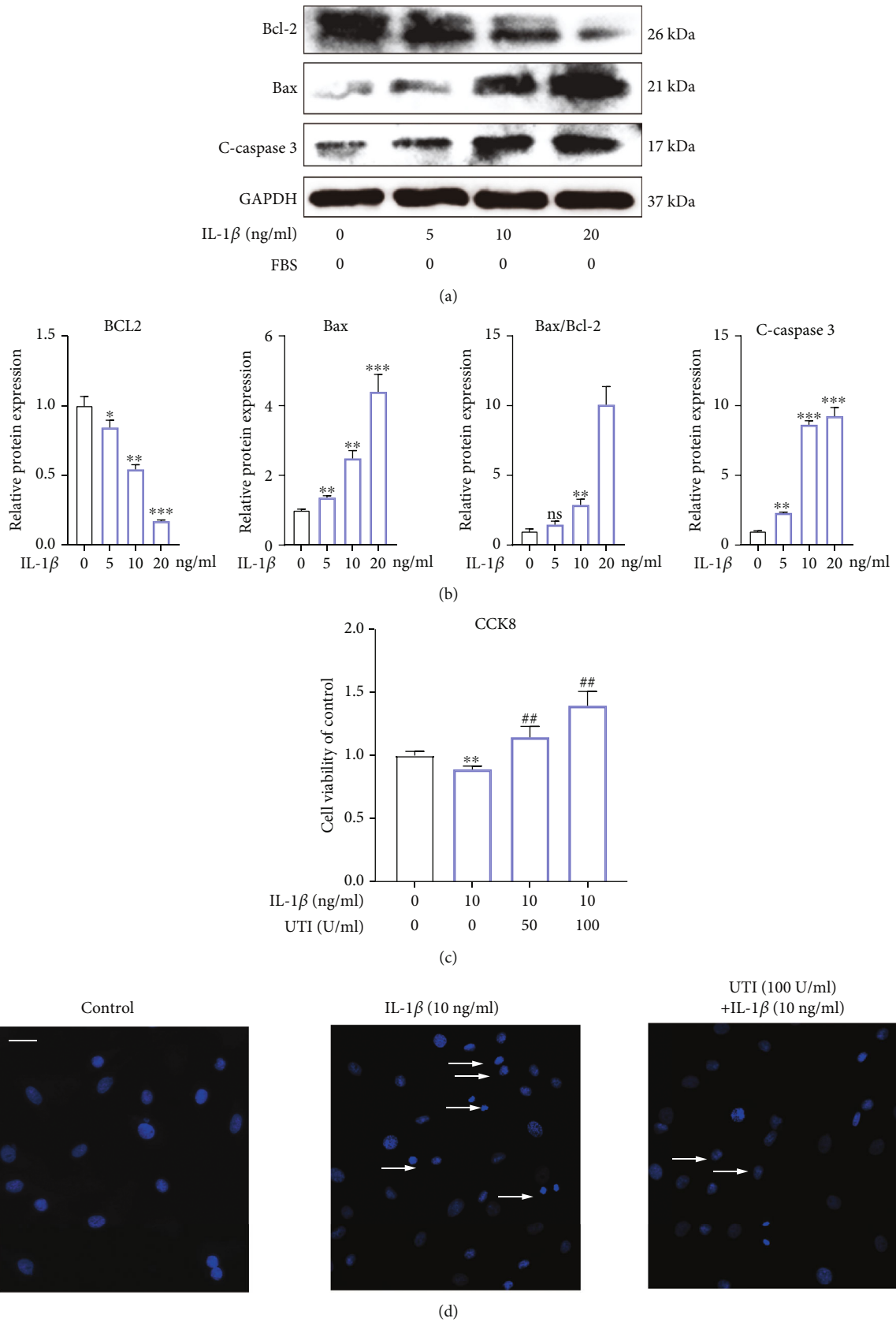
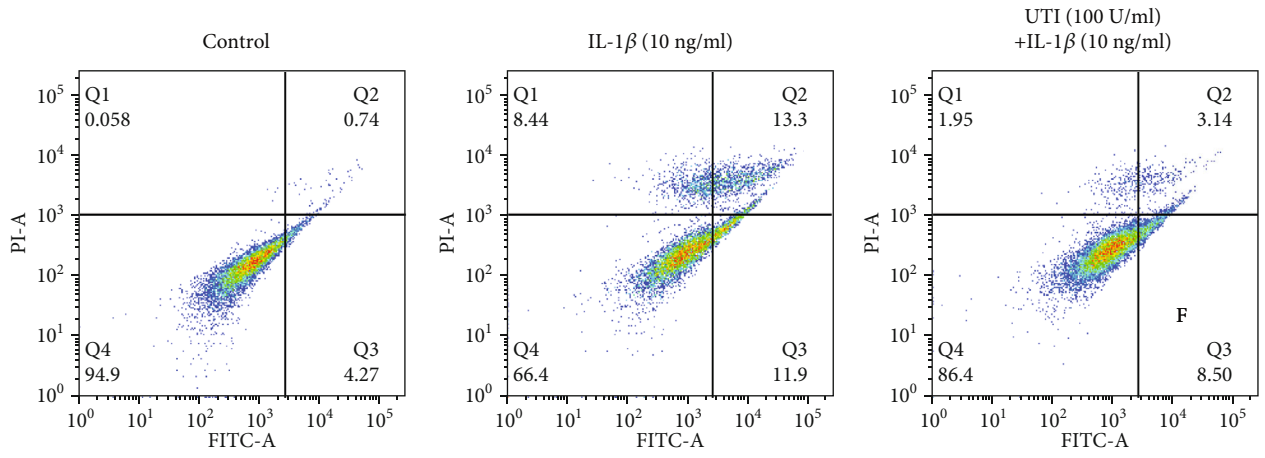
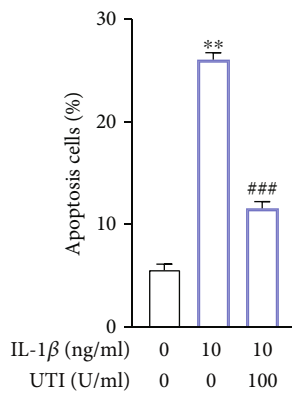


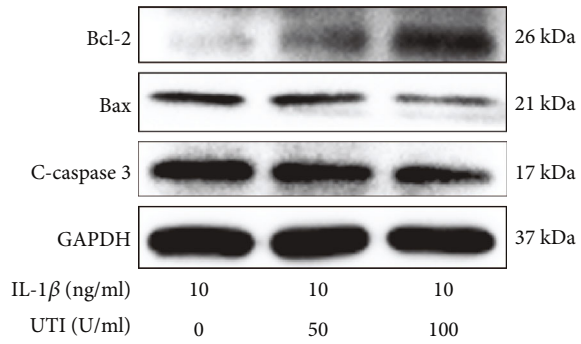
FIGURE 3: Continued.



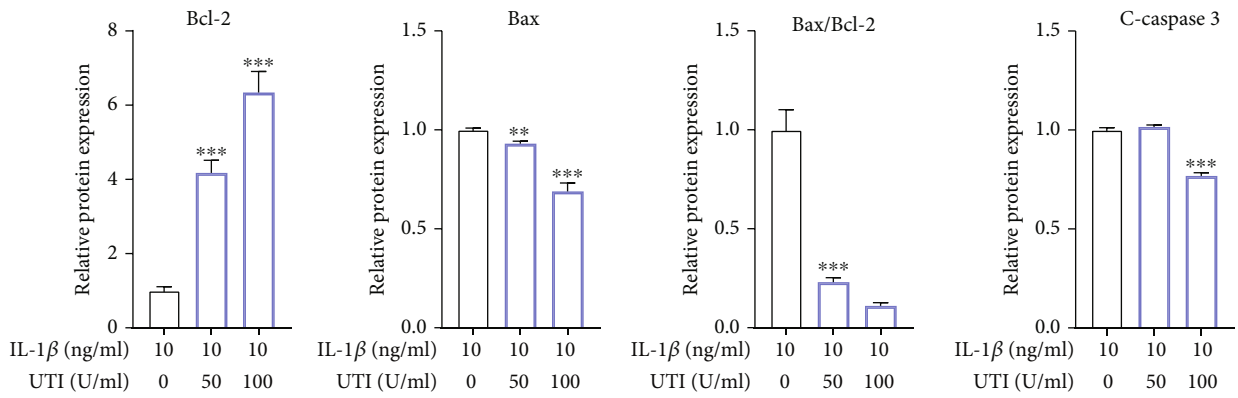
(e)



(f)



(g)



(h)

FIGURE 3: Continued.

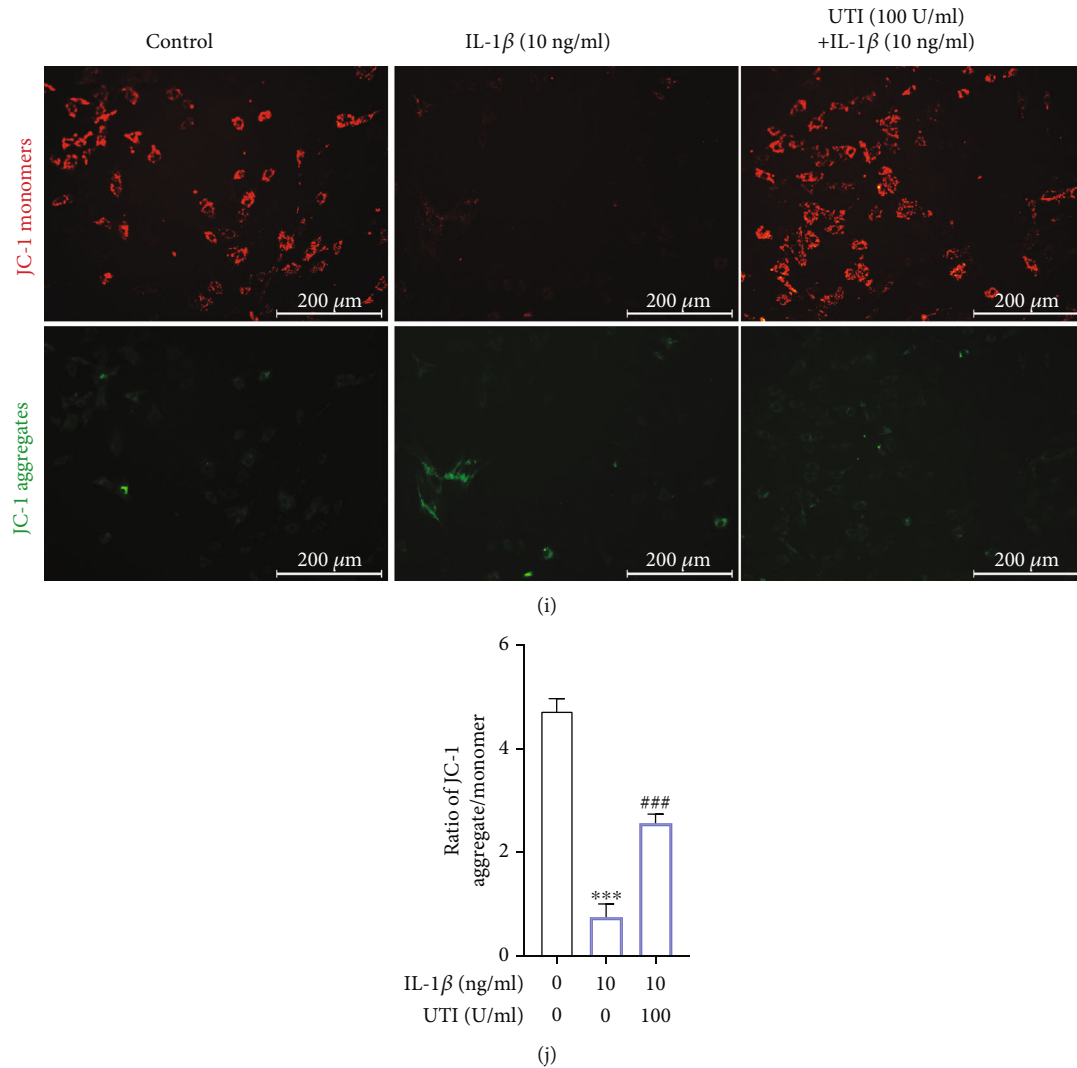


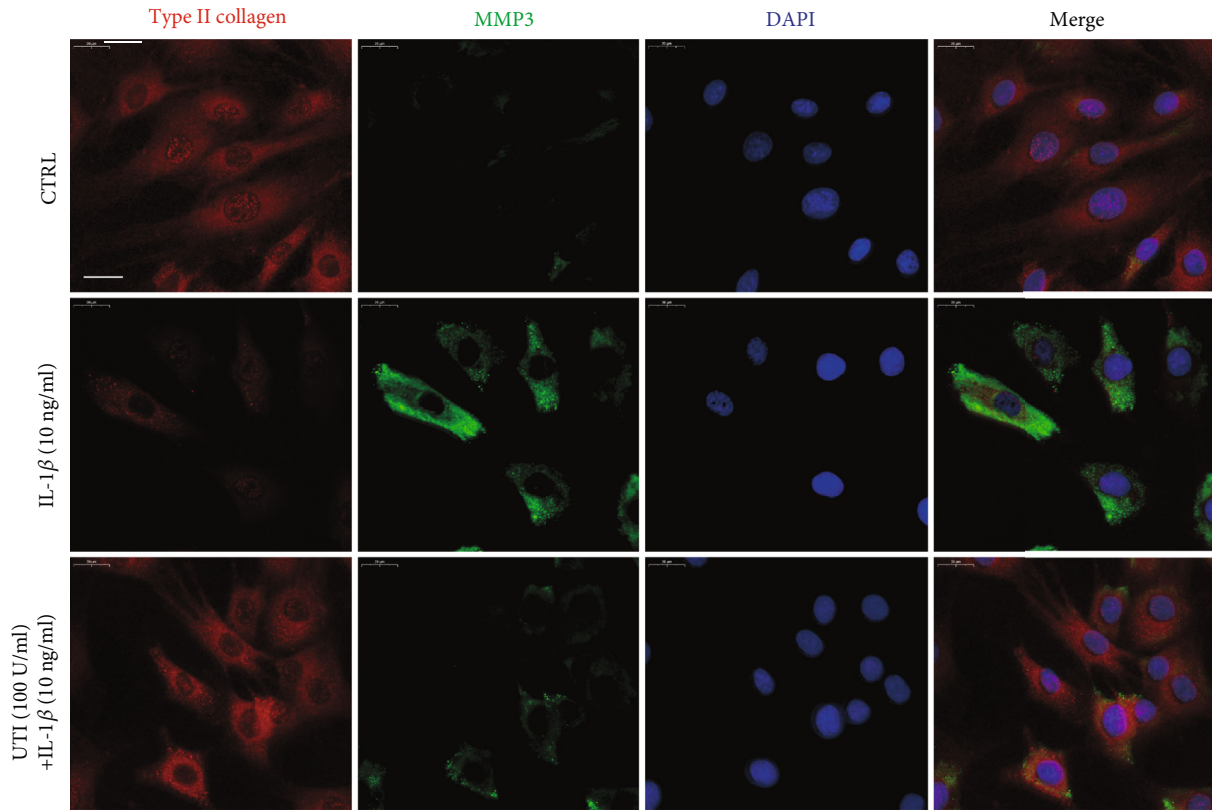
FIGURE 3: Biological effect of UTI on IL-1 β -induced apoptosis in human NP cells. (a, b) Protein bands and quantification of expression levels of Bcl-2, Bax, and cleaved caspase 3 in IL-1 β -induced NP cells. Bax/Bcl-2 ratios were calculated ($n = 3$). (c) Effect of UTI with indicated concentrations on cell viability of IL-1 β -induced NP cells ($n = 5$). (d) Hoechst staining was used to conduct analysis of the nuclear morphology. Scar bar = 100 μm . (e, f) The rates of apoptosis of human NP cells as determined by flow cytometry ($n = 3$). (g, h) Protein bands and quantification of expression levels of Bcl-2, Bax, and cleaved caspase 3 in IL-1 β -induced NP cells cotreated with UTI. Bax/Bcl-2 ratios were calculated ($n = 3$). (i, j) The JC-1 monomers (red) and JC-1 aggregates (green) were detected by the fluorescent probe JC-1, and the ratios of JC-1 aggregate/monomer were calculated. Scar bar = 200 μm . * $p < 0.05$, ** $p < 0.01$, *** $p < 0.001$, **** $p < 0.0001$. *indicated the comparison between group IL-1 β and group control. # $p < 0.05$, ## $p < 0.01$, ### $p < 0.001$, #### $p < 0.0001$. #indicated the comparison between group IL-1 β and group UTI+IL-1 β .

therapeutic target [20, 21]. Therefore, we further explored the impact of UTI on IL-1 β -induced inflammatory response. COX-2 and iNOS have been previously reported to be the two key inflammatory mediators during IDD. In this present study, we firstly examined the protein level of COX2 and iNOS in NP cells treated by L-1 β with or without UTI. As shown in Figure 6, UTI dramatically suppressed IL-1 β -induced expression of COX2 and iNOS as well as proinflammatory factors, IL-6 and TNF- α (Figures 6(a)–6(e)). In addition, The generation of endogenous of IL-6 and TNF- α during IL-1 β stimulation was also inhibited by UTI (Figures 6(f) and 6(g)). ELISA also demonstrated that UTI

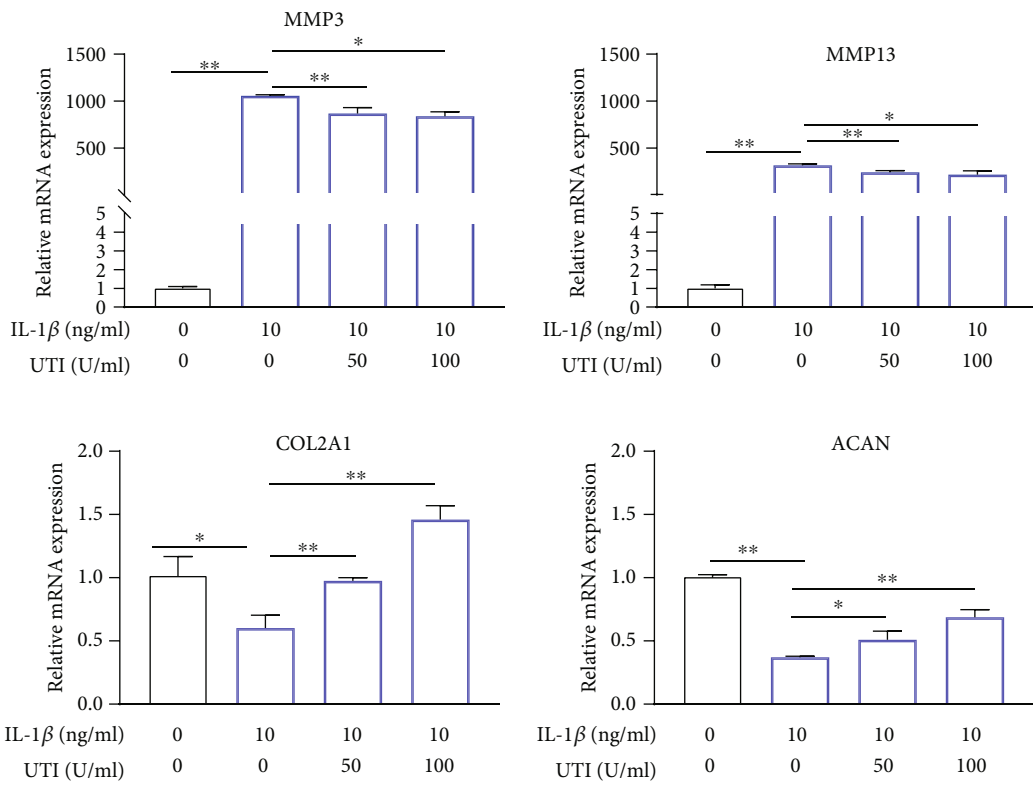
ameliorated the production of endogenous NO and PGE2 (Figures 6(h) and 6(i)).

These results indicated that UTI inhibited the IL-1 β -induced generation of inflammatory mediators and cytokines.

3.7. UTI Regulated IL-1 β -Induced NF- κ B Activation in NP Cells. NF- κ B pathway has been widely reported to be involved in the generation of inflammation response and oxidative stress during IDD [22–24]. As shown in Figure 7, without IL-1 β intervention, p65 was primarily distributed in the cytoplasm of NP cells, whereas the amount of p65



(a)



(b)

FIGURE 4: Continued.

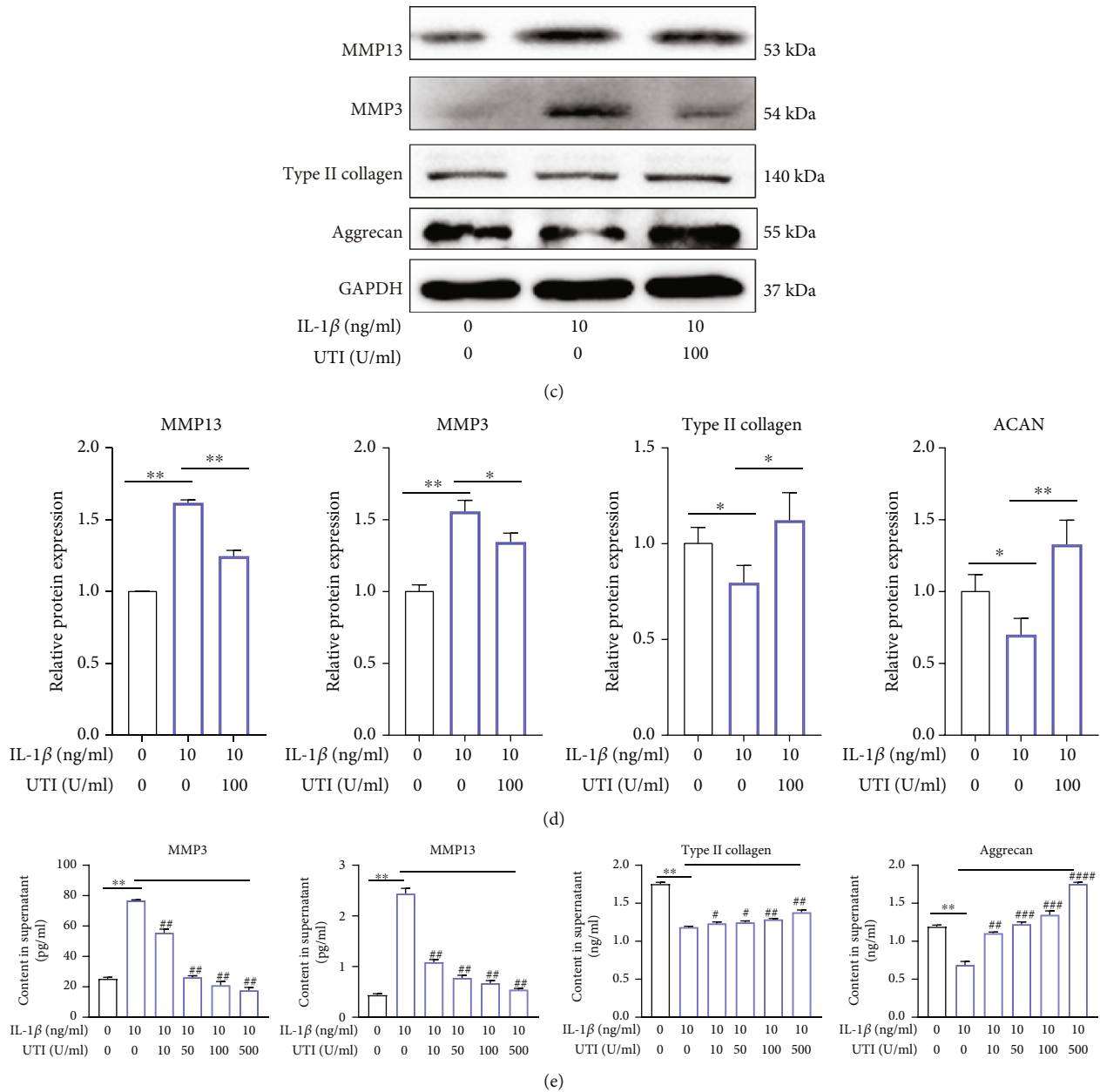


FIGURE 4: UTI ameliorated IL-1 β -induced ECM degradation in human NP cells. (a) The expression of MMP3 and type II collagen by the immunofluorescence. Scar bar = 50 μ m. (b) qRT-qPCR was used to evaluate the mRNA expression of MMP 3, MMP 13, ACAN, and COL2A1 ($n = 3$). (c, d) Protein bands and quantification of protein levels of MMP 13, MMP 3, type II collagen, and aggrecan. GAPDH as an internal control ($n = 3$). (e) IL-1 β -induced differential expression of MMP 13, MMP 3, type II collagen, and aggrecan were measured by ELISA cotreated with UTI in a dose-dependent manner in the cultural supernatant of NP cells ($n = 3$). * $p < 0.05$, ** $p < 0.01$, *** $p < 0.001$, **** $p < 0.0001$; # $p < 0.05$, ## $p < 0.01$, ### $p < 0.001$, #### $p < 0.0001$. The comparison among groups has been marked in figure.

was elevated dramatically in the nuclei and was reduced in the cytoplasm following IL-1 β treatment. This phenomenon suggested that IL-1 β treatment dramatically increased the nuclear translocation of p65. However, this effect was suppressed by UTI (Figures 7(a) and 7(b)). Additionally, Western blot analysis also confirmed the suppressive effect of UTI on IL-1 β -triggered nuclear translocation of p65 (Figures 7(c) and 7(d)). In general, NF- κ B exists as an inactive condition in the cytoplasm due to its interaction with I κ B family proteins which suppress the nuclear trans-

location of NF- κ B. Once stimulated, the phosphorylated IKK- β activates I κ B- α which becomes phosphorylated and ensuing degraded, and thus, NF- κ B will be released and translocate into cell nucleus [25]. Therefore, we also explored the change of I κ B- α and found that IL-1 β intervention markedly promoted the phosphorylation and degradation of I κ B α in the cytoplasm. The increased amount of p65 in the cytoplasm of the NP cells treated by UTI also confirmed the suppression of IL-1 β -activated nuclear translocation of p65 (Figures 7(e) and 7(f)).

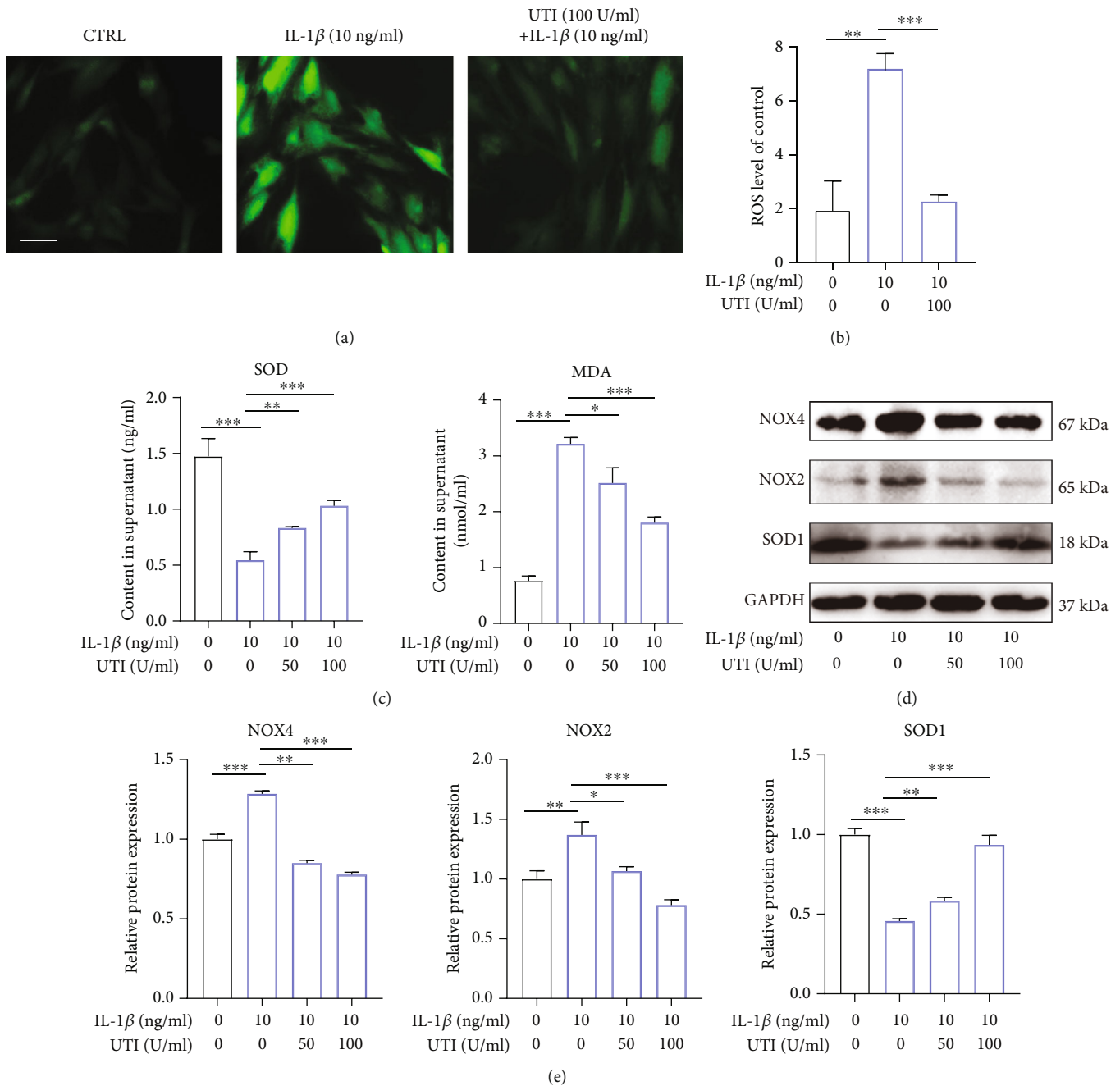


FIGURE 5: Effect of UTI on IL-1 β -induced oxidative stress in human NP cells. (a) The distribution of ROS (green) was detected by the immunofluorescence in human NP cells treated with IL-1 β or cotreated with IL-1 β and UTI. Scar bar = 100 μ m. (b) The fluorescence strength of ROS (green) was quantified by Image J ($n = 3$). (c) IL-1 β -induced differential levels of SOD and MDA were assessed by ELISA with UTI in a dose-dependent manner in human NP cells ($n = 5$). (d, e) Protein bands and quantification of protein levels of NOX4, NOX2, and SOD1 ($n = 3$). * $p < 0.05$, ** $p < 0.01$, *** $p < 0.001$, **** $p < 0.0001$.

In conclusion, UTI inhibited the IL-1 β -induced activation of NF- κ B by inhibiting I κ B α phosphorylation in the cytoplasm and thus suppressed the amount of p65 translocation into the nuclei of the NP cells.

3.8. UTI Regulated IL-1 β -Induced Apoptosis, Inflammation Response, and Oxidative Stress via Nrf2/NF- κ B Signaling Pathways in Human NP Cells. As presented, Western blot

results suggested that IL-1 β suppressed the amount of Nrf2 in the nucleus and HO-1 in cytoplasm of human NP cells, whereas these effects were ameliorated by UTI (Figures 8(a) and 8(b)). Notably, no obvious difference was observed between normal cultured NP cells and IL-1 β -treated NP cells in terms of the expression level of Nrf2 and HO-1, although NP cells with IL-1 β seem to express higher level of these two proteins (Figures 8(a) and 8(b)). Furthermore,

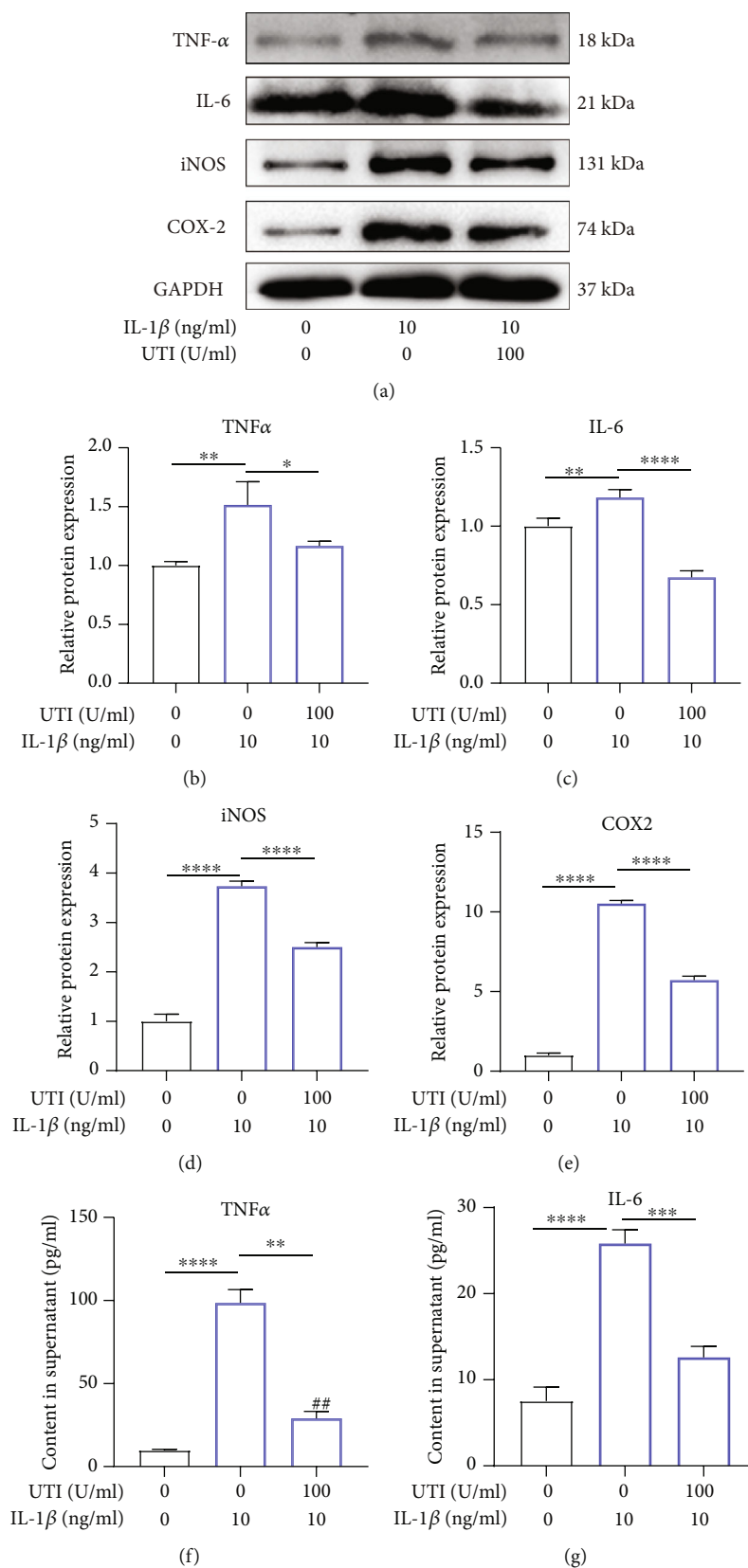


FIGURE 6: Continued.

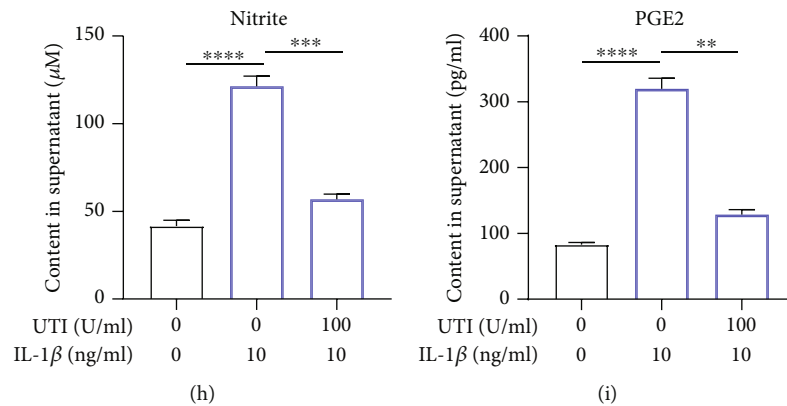


FIGURE 6: Impact of UTI on IL-1 β -induced expression of inflammatory factors in human NP cells. (a–e) Protein bands and quantification of protein expression of TNF- α , iNOS, IL-6, and COX-2. GAPDH as an internal control ($n = 3$). (f–i) Differential expression of TNF- α , IL-6, Nitrite, and PGE2 were quantified by ELISA assay ($n = 5$). * $p < 0.05$, ** $p < 0.01$, *** $p < 0.001$, **** $p < 0.0001$.

immunofluorescence analysis for Nrf2 demonstrated that UTI enhanced the nuclear translocation of Nrf2, which was consistent with the results of WB (Figure 8(c)).

To further explore the potential association between Nrf2 and pathological features of human NP cells induced by IL-1 β , we used small interfering RNA for Nrf2 (siRNA-Nrf2) to establish the knockdown model of Nrf2 in NP cells. As shown in Figure 8, siRNA-Nrf2 evidently inhibited the expression of Nrf2, suggesting the successful establishment of Nrf2 knockdown (Figure 8(d)). However, following knockdown of Nrf2, the amount of p65 in nucleus of NP cells was negatively increased during stimulation by IL-1 β with or without UTI (Figure 8(d)). What is more, the expression of SOD1 was decreased, whereas the expression of iNOS, COX2, and c-caspase3 was increased after pretransfection with siRNA-Nrf2 (Figures 8(e) and 8(f)). Taken together, the Nrf2 pathway was involved in UTI-mediated NF- κ B signaling suppression, and subsequent regulation of apoptosis, inflammation response, and oxidative stress in human NP cells treated with IL-1 β .

4. Discussion

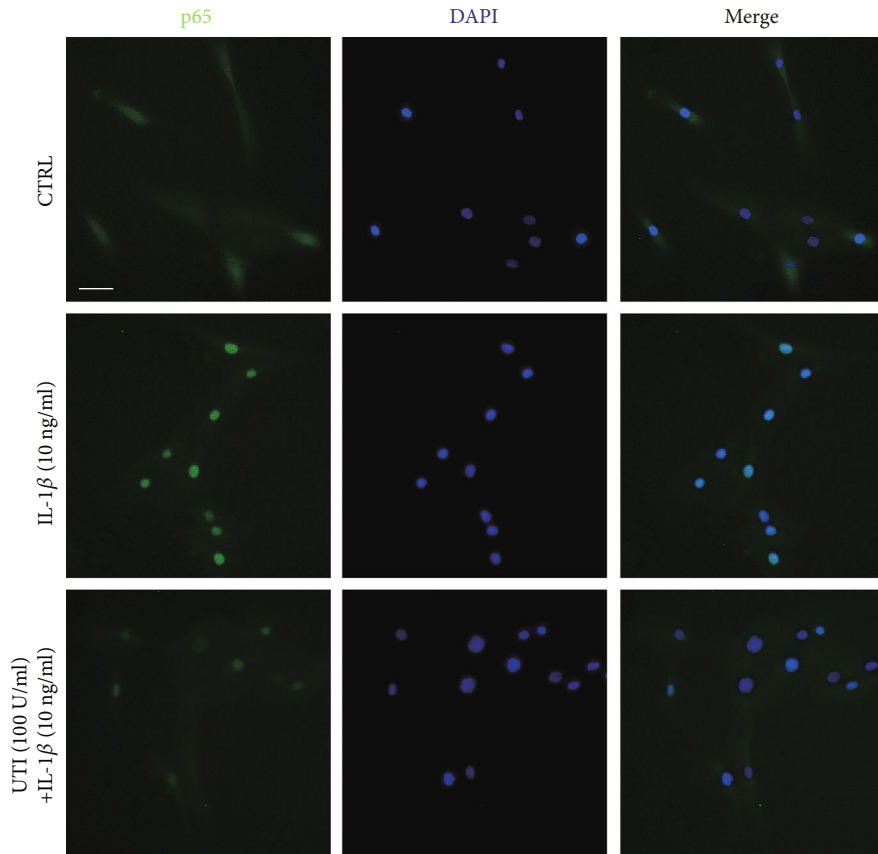
In the context of the fourth industrial revolution, the proportion of static work in human labor is increasing, and the spine is under an unprecedented state of continuous fatigue. According to the epidemiological survey, more than 80% of the population worldwide would suffer from LBP in their lifetime [3]. As a major cause of LBP, IDD has been a multifactorial disease with typical features of ECM degradation and an increasing reduction in the number of NP cells. Thus, delaying the ECM degradation and reducing the cell apoptosis become the critical aims in the treatment of IDD.

An increasing number of studies have suggested excessive inflammatory response and oxidative stress may be the major causes of IDD [26]. Accumulating the production of local inflammatory mediators, such as IL-1 β , could trigger NP cell injury [27]. In addition, injured NP cells could further produce proinflammatory and oxidative stress-related cytokines which further exacerbate the progression of IDD via a malignant positive feedback loop [28]. Therefore, genetic or phar-

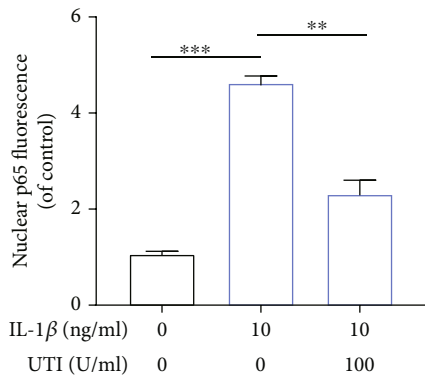
macologic interventions targeting at the inflammatory mechanisms and ECM degradation may be a novel strategy for treating IDD. IL-1 β is reported to correlate closely with multiple pathological process of IDD [29]. Therefore, in this present study, we established IDD model in vitro using IL-1 β , and the results suggested the protective role of UTI in IL-1 β -induced cell apoptosis, inflammation response, oxidative stress, and ECM degradation via Nrf2/NF- κ B pathway in human NP cells.

One of the major characteristics of IDD is decreasing number of NP cells [29]. Accumulating studies have shown that cell apoptosis played a vital role in reducing NP cells [30, 31]. Firstly, we evaluated the biological effect of UTI on the proliferative ability of NP cells induced by IL-1 β . As demonstrated in the results, UTI elevated the cell viability and proliferative ability of NP cells. On the other hand, we also explored the effect of UTI on NP cell apoptosis. Apoptosis is mainly triggered by two classical pathways: death receptors pathway and mitochondria pathway. In fact, the intrinsic pathway is frequently coregulated by Bcl-2 and Bax [32]. The ratio of Bax/Bcl-2 can be used to estimate level of apoptosis. As indicated by the results, IL-1 β aggravated the apoptosis of NP cells, whereas this damaging effect was improved by UTI. Further results of CCK-8 assay, Hoechst test, flow cytometry analysis, and analysis of MMP also confirmed the protective effect of UTI on NP cells. Taken together, the results above suggested that UTI has proproliferative and antiapoptotic effects on NP cells stimulated by IL-1 β and that the antiapoptotic effect may, at least partly, be attributed to the suppression of the mitochondrial apoptosis pathway.

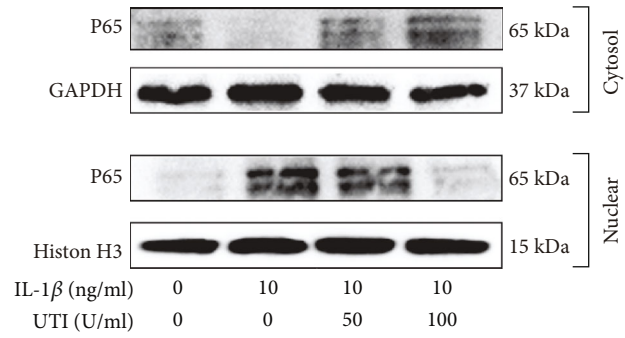
During the process of IDD, increasing MMPs, and decreasing type II collagen and aggrecan can be another two typical features of degenerated disc. Under normal condition, the type II collagen and aggrecan constitute the highly hydrated nature of the NP, which can help keep disc height [33]. However, abnormal generation of matrix-degrading enzymes (MMPs and ADAMTs) due to various factors will result in ECM degradation. In addition, excessive accumulation of inflammatory mediators can further increase the expression of MMPs and ADAMTs, accelerating the



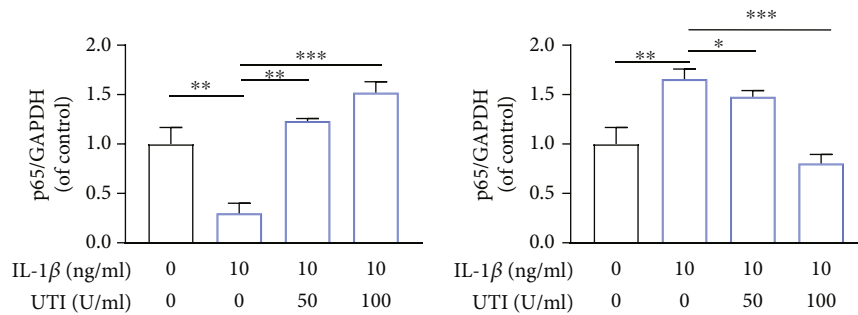
(a)



(b)



(c)



(d)

FIGURE 7: Continued.

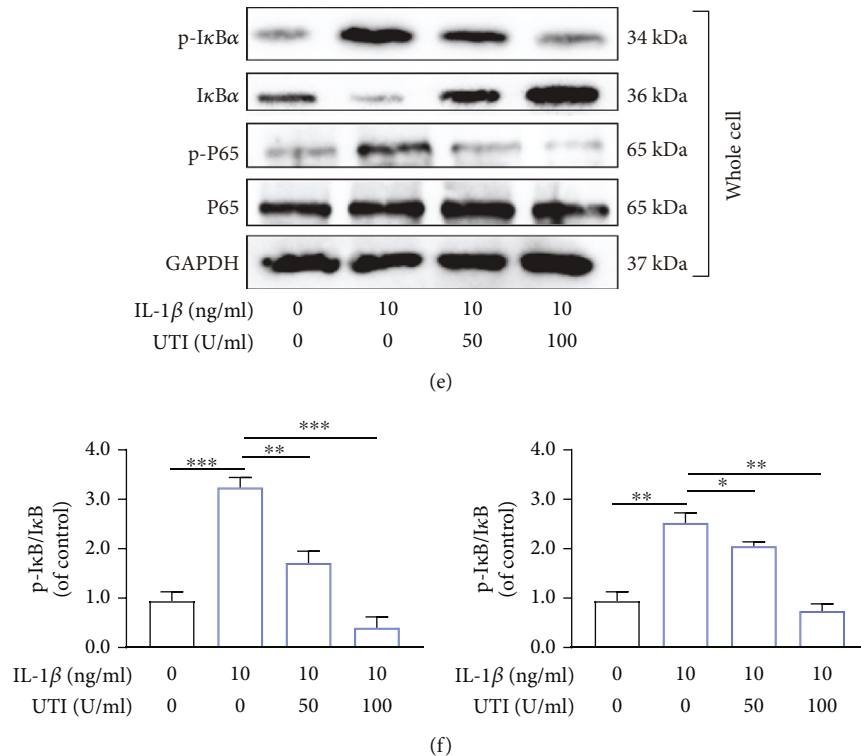


FIGURE 7: Effects of UTI on the activation of NF- κ B pathway induced by IL-1 β in human NP cells. (a, b) The nuclei translocation of p65 in different groups was visualized. Intensity of nuclear p65 fluorescence was quantified ($n = 3$). Scar bar = 200 μ m. (c, d) Differential expressions of p65 in cytoplasm and in nucleus were visualized and quantified by WB, respectively ($n = 3$). (e, f) Protein levels of I κ B α , p65, and their phosphorylated forms were analyzed by WB in different groups ($n = 3$). * $p < 0.05$, ** $p < 0.01$, *** $p < 0.001$, **** $p < 0.0001$.

progression of IDD [34]. Following, we stimulated NP cells with IL-1 β , and the NP cells showed increased expression of MMP3/13 and decreased expression of type II collagen and aggrecan. Nevertheless, administration of UTI suppressed these abnormal changes, indicating the suppressive effect of UTI on IL-1 β -induced ECM degradation.

Abnormally, increasing proinflammatory mediators, such as IL-6, can also accelerate IDD [34, 35]. We also assessed the potential effect of UTI on the IL-1 β -induced inflammatory response and found that the increased levels of IL-6 and TNF- α induced by IL-1 β were inhibited by UTI, as demonstrated by Western blot analysis and ELISA results. In addition, the proinflammatory mediators, iNOS and COX-2, were also negatively regulated by UTI. On the other hand, overproduction of ROS due to environmental stress or inflammation was also a critical factor contributing to IDD [36]. In our study, IL-1 β caused increased levels of ROS, MDA, and NOX2/4 but decreased level of SOD, whereas UTI mitigated these changes. Collectively, UTI showed a protective effect on IL-1 β -treated NP cells by suppressing the excessive activation of inflammatory responses and oxidative stress.

Increasing studies have proved that activated NF- κ B pathway is associated with the progression of IDD and, widely, involved in the proapoptotic effect, inflammatory response, oxidative stress, and the production of ECM-degradation proteinases [37–39]. IL-1 β stimulation can activate I κ B α , which subsequently facilitates the nuclear

translocation of p65. The activated NF- κ B pathway will further promote the generation of proinflammatory molecules (COX-2 and iNOS), which could result in the ECM degradation [18, 40]. Suppressing the activation of NF- κ B pathway has been considered as a promising therapeutic insight against IDD. A recent study by Yi et al. revealed that inhibiting NF- κ B pathway could decrease apoptosis and inflammation response in injured NP cells [22]. In this present study, we found that UTI could suppress the nuclear translocation of p65 and reduce the cell apoptosis and abnormal generation of inflammatory mediators, cytokines, and MMPs. Although not all of those effects of p65 are direct, UTI, at least partly, protects NP cells against apoptosis and the inflammatory response by suppressing NF- κ B pathway.

According to this current study, oxidative stress injury frequently occurs with inflammatory response during IDD. The results above also suggested the inhibitory effect of UTI on the level of oxidative stress. Previous studies have revealed that Nrf2/HO-1 pathway plays a key role in anti-inflammation, antioxidation, and reducing mitochondrial damage [41, 42]. Tang et al. ever reported that activating Nrf2 could suppress the NF- κ B signaling pathway and ameliorate the progression of osteoarthritis (OA) [43]. Dawei song found that theophylline could activate Keap1/Nrf2/ARE pathway to exert effects of antioxidation and slow down the IDD [44]. Cuadrado et al. also revealed that the deficiency of Nrf2 can lead to the enhancement of NF- κ B activity and cytokine production [45]. However, whether Nrf2/HO-1

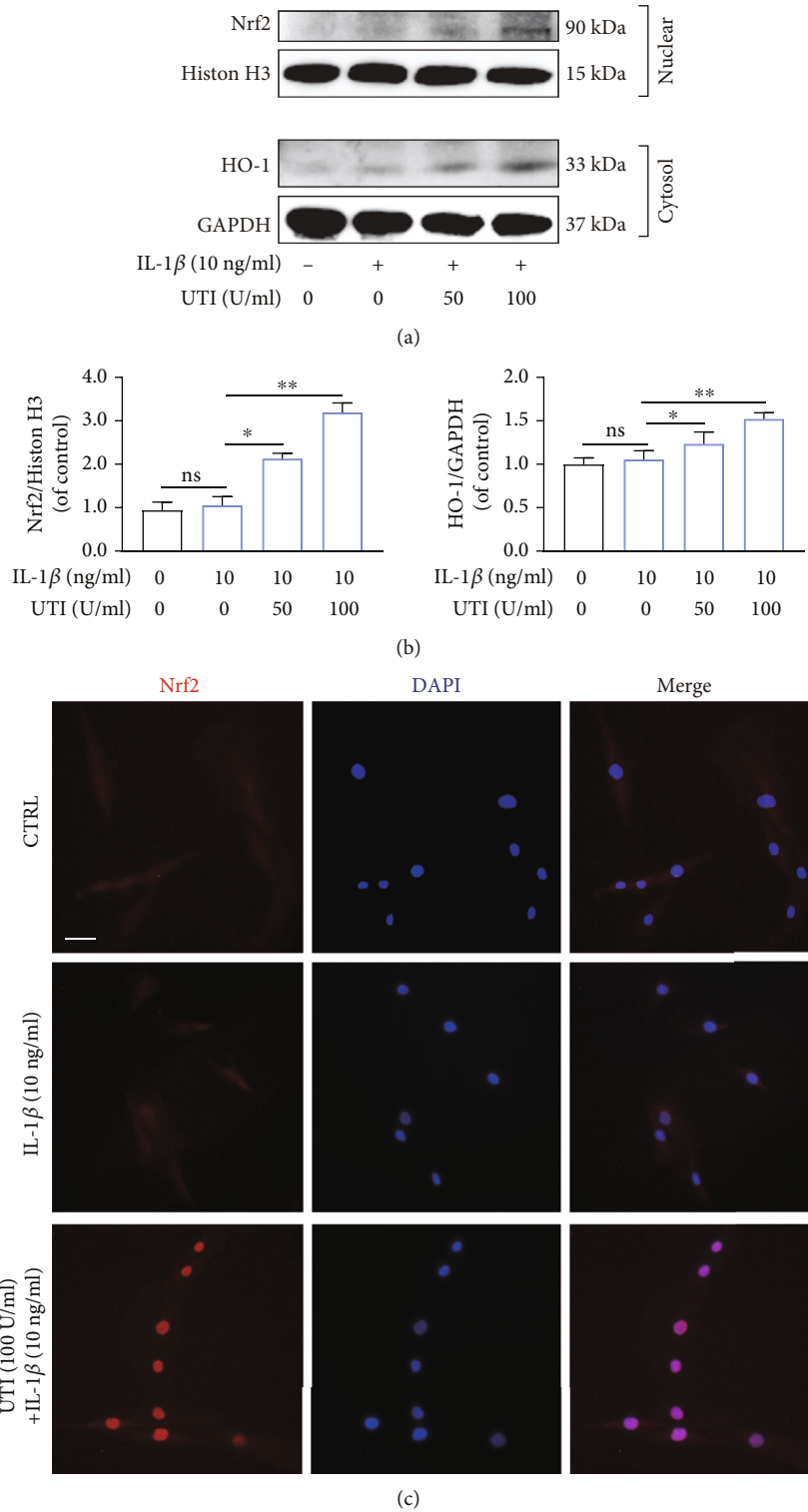


FIGURE 8: Continued.

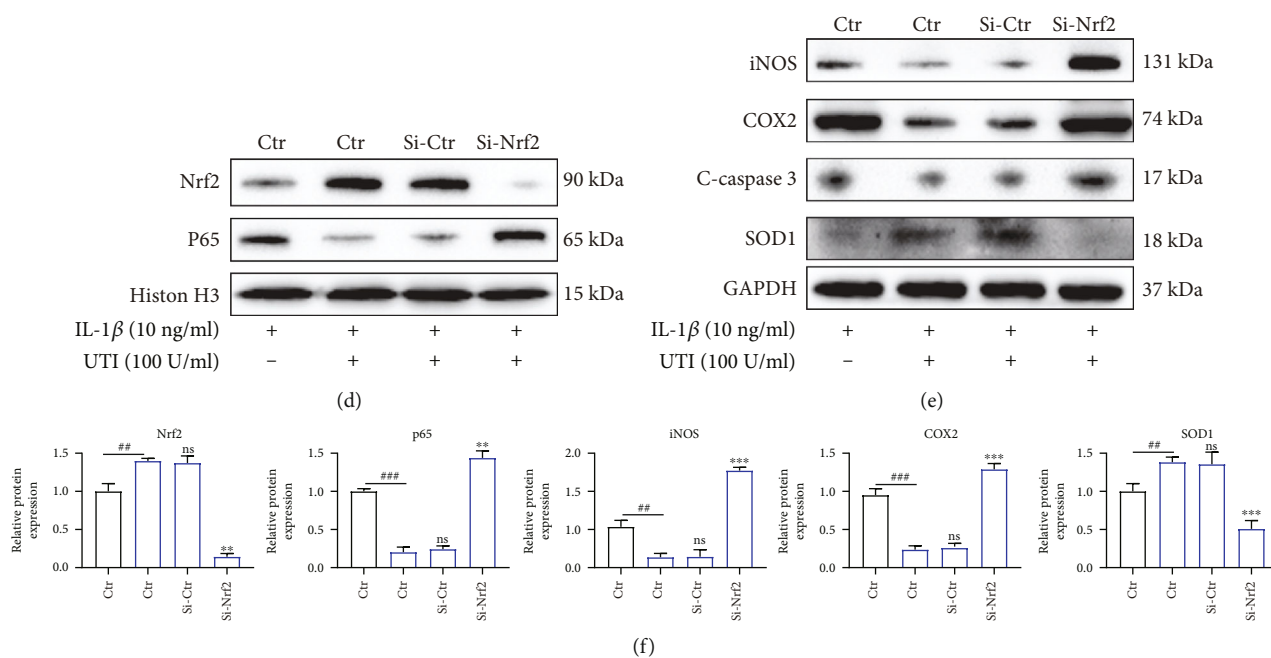


FIGURE 8: Effects of UTI on Nrf2/HO-1 pathway in human NP cells induced by IL-1 β . (a, b) Expression at protein level of Nrf2 in nucleus and HO-1 in cytoplasm were analyzed and quantified ($n = 3$). (c) The nuclear translocation of Nrf2 was visualized via immunofluorescence. Scar bar = 200 μm . (d, e) After knockdown of Nrf2, the protein amount of Nrf2 and p65 in nucleus and iNOS, COX2, c-caspase3, and SOD1 in cytoplasm in NP cells were presented by WB ($n = 3$). (f) Quantification of WB results of Nrf2, p65, iNOS, COX2, c-caspase3, and SOD1. * $p < 0.05$, ** $p < 0.01$, *** $p < 0.001$, **** $p < 0.0001$.

pathway is also associated with the protective effect of UTI on NP cells remains elusive. In this present study, we also found the decreasing expression of Nrf2 in degenerated disc tissue. In addition, we used siRNA-Nrf2 to knock down the expression of Nrf2, and the results demonstrated that suppressed Nrf2 aggravated the cell apoptosis, oxidative stress, and inflammation reactions. Interestingly, the suppression of Nrf2 also led to the activation of NF- κ B pathway. Taken together, UTI may exert antiapoptotic, anti-inflammatory, and antioxidative function via activating the Nrf2/HO-1 axis and suppressing the NF- κ B pathway in IL-1 β -treated human NP cells.

In conclusion, this current study uncovered that UTI could protect human NP cells against IL-1 β stimulation by inhibiting apoptosis, inflammatory response, oxidative stress, and ECM degradation in human NP cells. In addition, the protective effect of UTI on IL-1 β -treated NP cells was accomplished by activating the Nrf2/HO-1 signaling axis and suppressing NF- κ B signaling pathway. Therefore, UTI may be potential therapeutic medicine to delay the progression of IDD. However, further work needs to be done, such as in vivo experiment, before it can be known whether UTI is efficacious as a reliable treatment for IDD.

Data Availability

Data is available on request.

Conflicts of Interest

The authors have declared no conflict of interest.

Authors' Contributions

Kaiqiang Sun, Liwei Duan, and Jiangang Shi conceived and designed the experiments. Xi Luo, Le Huan, and Feng Lin performed the experiments and wrote the original manuscript. Fanqi Kong, Xiaofei Sun, and Jian Zhu analyzed the data, and Fudong Li and Jingchuan Sun prepared the figures. Ximing Xu revised the manuscript. All authors reviewed the manuscript. Xi Luo, Le Huan, and Feng Lin contributed equally to this study and should be considered as cofirst authors.

Acknowledgments

We would like to thank Professor Weizhong Wang and Professor Yangkai Wang from Navy Medical University for their experimental platform and useful suggestions on my research. The study is supported by the National Natural Science Foundation of China, Grant/Award Numbers: No. 81871828, No. 81702218.

Supplementary Materials

The human NP cell phenotype was confirmed by identifying the expression of type II collagen and aggrecan. Immunofluorescence analysis for collagen type II and toluidine blue staining for aggrecan were used in this present study. The results were shown in Supplementary Figure 1. Supplementary Figure 1: culture and identification of human nucleus pulposus (NP) cells. (a) The human NP cells of passage 1 and 4 under light microscope. Scar bar = 400 μm . (b)

Immunofluorescence analysis for collagen type II of NP cells of passage 1 and 4. (c) Toluidine blue staining for aggrecan of NP cells of passage 1 and 4. Scar bar = 200 μm . (Supplementary Materials)

References

- [1] S. Yang, F. Zhang, J. Ma, and W. Ding, "Intervertebral disc ageing and degeneration: the antiapoptotic effect of oestrogen," *Ageing research reviews*, vol. 57, p. 100978, 2020.
- [2] B. Peng, W. Wu, S. Hou, P. Li, C. Zhang, and Y. Yang, "The pathogenesis of discogenic low back pain," *The Journal of bone and joint surgery. British volume*, vol. 87, no. 1, pp. 62–67, 2005.
- [3] P. J. Roughley, "Biology of intervertebral disc aging and degeneration: involvement of the extracellular matrix," *Spine*, vol. 29, no. 23, pp. 2691–2699, 2004.
- [4] J. Dowdell, M. Erwin, T. Choma, A. Vaccaro, J. Iatridis, and S. K. Cho, "Intervertebral disk degeneration and repair," *Neurosurgery*, vol. 80, no. 3S, pp. S46–S54, 2017.
- [5] K. Wang, T. Chen, X. Ying et al., "Ligustilide alleviated IL-1 β induced apoptosis and extracellular matrix degradation of nucleus pulposus cells and attenuates intervertebral disc degeneration _in vivo_," *International immunopharmacology*, vol. 69, pp. 398–407, 2019.
- [6] J.-F. Huang, X.-Q. Zheng, J.-L. Lin et al., "Sinapic acid inhibits IL-1 β -induced apoptosis and catabolism in nucleus pulposus cells and ameliorates intervertebral disk degeneration," *Journal of inflammation research*, vol. Volume 13, pp. 883–895, 2020.
- [7] Z. Tang, B. Hu, F. Zang, J. Wang, X. Zhang, and H. Chen, "Nrf2 drives oxidative stress-induced autophagy in nucleus pulposus cells via a Keap1/Nrf2/p62 feedback loop to protect intervertebral disc from degeneration," *Cell death & disease*, vol. 10, no. 7, p. 510, 2019.
- [8] K. Inoue and H. Takano, "Urinary trypsin inhibitor as a therapeutic option for endotoxin-related inflammatory disorders," *Expert Opinion on Investigational Drugs*, vol. 19, no. 4, pp. 513–520, 2010.
- [9] Y. U. N.-H. E. E. SUNG, M. A. L.-S. O. O. N. SHIN, I. L.-G. Y. U. KO et al., "Ulinastatin suppresses lipopolysaccharide-induced prostaglandin E2 synthesis and nitric oxide production through the downregulation of nuclear factor- κB in BV2 mouse microglial cells," *International journal of molecular medicine*, vol. 31, no. 5, pp. 1030–1036, 2013.
- [10] G. Hua, Z. Haiping, H. Baorong, and H. Dingjun, "Effect of ulinastatin on the expression of iNOS, MMP-2, and MMP-3 in degenerated nucleus pulposus cells of rabbits," *Connective tissue research*, vol. 54, no. 1, pp. 29–33, 2013.
- [11] J. Jia, L. Nie, and Y. Liu, "Butyrate alleviates inflammatory response and NF- κB activation in human degenerated intervertebral disc tissues," *International immunopharmacology*, vol. 78, p. 106004, 2020.
- [12] Y. Zhang, Y. Zhao, J. Li et al., "Interleukin-9 promotes TNF- α and PGE2 release in human degenerated intervertebral disc tissues," *Spine*, vol. 41, no. 21, pp. 1631–1640, 2016.
- [13] J. Wang, J. Hu, X. Chen et al., "BRD4 inhibition regulates MAPK, NF- κB signals, and autophagy to suppress MMP-13 expression in diabetic intervertebral disc degeneration," *FASEB journal: official publication of the Federation of American Societies for Experimental Biology*, vol. 33, no. 10, pp. 11555–11566, 2019.
- [14] J. Wu, S. Liu, H. Meng et al., "Neuropeptide Y enhances proliferation and prevents apoptosis in rat bone marrow stromal cells in association with activation of the Wnt/ β -catenin pathway in vitro," *Stem cell research*, vol. 21, pp. 74–84, 2017.
- [15] R. He, M. Cui, H. Lin et al., "Melatonin resists oxidative stress-induced apoptosis in nucleus pulposus cells," *Life sciences*, vol. 199, pp. 122–130, 2018.
- [16] C. W. A. Pfirrmann, A. Metzendorf, M. Zanetti, J. Hodler, and N. Boos, "Magnetic resonance classification of lumbar intervertebral disc degeneration," *Spine*, vol. 26, no. 17, pp. 1873–1878, 2001.
- [17] L. Wang, Y. Yao, R. He et al., "Methane ameliorates spinal cord ischemia-reperfusion injury in rats: antioxidant, anti-inflammatory and anti-apoptotic activity mediated by Nrf2 activation," *Free radical biology & medicine*, vol. 103, pp. 69–86, 2017.
- [18] J. Lin, J. Chen, Z. Zhang et al., "Luteoloside inhibits IL-1 β -induced apoptosis and catabolism in nucleus pulposus cells and ameliorates intervertebral disk degeneration," *Frontiers in pharmacology*, vol. 10, 2019.
- [19] Z. Li, X. Chen, D. Xu, S. Li, M. T. V. Chan, and W. K. K. Wu, "Circular RNAs in nucleus pulposus cell function and intervertebral disc degeneration," *Cell proliferation*, vol. 52, no. 6, p. e12704, 2019.
- [20] D. Chen, D. Xia, Z. Pan et al., "Metformin protects against apoptosis and senescence in nucleus pulposus cells and ameliorates disc degeneration _in vivo_," *Cell death & disease*, vol. 7, no. 10, p. e2441, 2016.
- [21] K. Zhao, R. An, Q. Xiang et al., "Acid-sensing ion channels regulate nucleus pulposus cell inflammation and pyroptosis via the NLRP3 inflammasome in intervertebral disc degeneration," *Cell proliferation*, vol. 54, no. 1, p. e12941, 2021.
- [22] W. Yi, Y. Wen, F. Tan et al., "Impact of NF- κB pathway on the apoptosis-inflammation-autophagy crosstalk in human degenerative nucleus pulposus cells," *Ageing*, vol. 11, no. 17, pp. 7294–7306, 2019.
- [23] L. Zou, H. Lei, J. Shen et al., "HO-1 induced autophagy protects against IL-1 β -mediated apoptosis in human nucleus pulposus cells by inhibiting NF- κB ," *Ageing*, vol. 12, no. 3, pp. 2440–2452, 2020.
- [24] Q. Xiang, Z. Cheng, J. Wang et al., "Allicin attenuated advanced oxidation protein product-induced oxidative stress and mitochondrial apoptosis in human nucleus pulposus cells," *Oxidative medicine and cellular longevity*, vol. 2020, Article ID 6685043, 2020.
- [25] J. DiDonato, F. Mercurio, C. Rosette et al., "Mapping of the inducible I κ B phosphorylation sites that signal its ubiquitination and degradation," *Molecular and cellular biology*, vol. 16, no. 4, pp. 1295–1304, 1996.
- [26] C. Le Maitre, J. Hoyland, and A. J. Freemont, "Catabolic cytokine expression in degenerate and herniated human intervertebral discs: IL-1 β and TNF α expression profile," *Arthritis research & therapy*, vol. 9, no. 4, 2007.
- [27] P. Andrade, G. Hoogland, M. A. Garcia, H. W. Steinbusch, M. A. Daemen, and V. Visser-Vandewalle, "Elevated IL-1 β and IL-6 levels in lumbar herniated discs in patients with sciatic pain," *European spine journal*, vol. 22, no. 4, pp. 714–720, 2013.
- [28] S. R. Sloan, C. Wipplinger, S. Kirnaz et al., "Combined nucleus pulposus augmentation and annulus fibrosus repair prevents

- acute intervertebral disc degeneration after discectomy,” *Science translational medicine*, vol. 12, no. 534, p. eaay2380, 2020.
- [29] F. Chen, G. Jiang, H. Liu et al., “Melatonin alleviates intervertebral disc degeneration by disrupting the IL-1 β /NF- κ B-NLRP3 inflammasome positive feedback loop,” *Bone research*, vol. 8, no. 1, 2020.
- [30] K. Wei, J. Dai, Z. Wang et al., “Oxymatrine suppresses IL-1 β -induced degradation of the nucleus pulposus cell and extracellular matrix through the TLR4/NF- κ B signaling pathway,” *Experimental biology and medicine (Maywood, N.J.)*, vol. 245, no. 6, pp. 532–541, 2020.
- [31] M. N. Barcellona, J. E. Speer, B. V. Fearing et al., “Control of adhesive ligand density for modulation of nucleus pulposus cell phenotype,” *Biomaterials*, vol. 250, p. 120057, 2020.
- [32] M. C. Maiuri, E. Zalckvar, A. Kimchi, and G. Kroemer, “Self-eating and self-killing: crosstalk between autophagy and apoptosis,” *Nature reviews. Molecular cell biology*, vol. 8, no. 9, pp. 741–752, 2007.
- [33] D. Purmessur, M. C. Cornejo, S. K. Cho, A. C. Hecht, and J. C. Iatridis, “Notochordal cell-derived therapeutic strategies for discogenic back pain,” *Global spine journal*, vol. 3, no. 3, pp. 201–217, 2013.
- [34] M. V. Risbud and I. M. Shapiro, “Role of cytokines in intervertebral disc degeneration: pain and disc content,” *Nature reviews. Rheumatology*, vol. 10, no. 1, pp. 44–56, 2014.
- [35] A. Sharma, “The Role of Adipokines in Intervertebral Disc Degeneration,” *Medical sciences (Basel, Switzerland)*, vol. 6, 2018.
- [36] C. Feng, M. Yang, M. Lan et al., “ROS: crucial intermediators in the pathogenesis of intervertebral disc degeneration,” *Oxidative medicine and cellular longevity*, vol. 2017, Article ID 5601593, 2017.
- [37] L. Kang, J. Hu, Y. Weng, J. Jia, and Y. Zhang, “Sirtuin 6 prevents matrix degradation through inhibition of the NF- κ B pathway in intervertebral disc degeneration,” *Experimental cell research*, vol. 352, no. 2, pp. 322–332, 2017.
- [38] Z. Li, X. Wang, H. Pan et al., “Resistin promotes CCL4 expression through toll-like receptor-4 and activation of the p38-MAPK and NF- κ B signaling pathways: implications for intervertebral disc degeneration,” *Osteoarthritis and cartilage*, vol. 25, no. 2, pp. 341–350, 2017.
- [39] H. Wang, P. He, H. Pan et al., “Circular RNA circ-4099 is induced by TNF- α and regulates ECM synthesis by blocking miR-616-5p inhibition of Sox9 in intervertebral disc degeneration,” *Experimental & molecular medicine*, vol. 50, no. 4, pp. 1–14, 2018.
- [40] L. Lu, J. Hu, Q. Wu et al., “Berberine prevents human nucleus pulposus cells from IL-1 β -induced extracellular matrix degradation and apoptosis by inhibiting the NF- κ B pathway,” *International journal of molecular medicine*, vol. 43, no. 4, pp. 1679–1686, 2019.
- [41] T. W. Kensler, N. Wakabayashi, and S. Biswal, “Cell survival responses to environmental stresses via the Keap1-Nrf2-ARE pathway,” *Annual review of pharmacology and toxicology*, vol. 47, no. 1, pp. 89–116, 2007.
- [42] J. D. Wardyn, A. H. Ponsford, and C. M. Sanderson, “Dissecting molecular cross-talk between Nrf2 and NF- κ B response pathways,” *Biochemical Society transactions*, vol. 43, no. 4, pp. 621–626, 2015.
- [43] Q. Tang, Z. Feng, M. Tong et al., “Piceatannol inhibits the IL-1 β -induced inflammatory response in human osteoarthritic chondrocytes and ameliorates osteoarthritis in mice by activating Nrf2,” *Food & function*, vol. 8, no. 11, pp. 3926–3937, 2017.
- [44] D. Song, J. Ge, Y. Wang et al., “Tea polyphenol attenuates oxidative stress-induced degeneration of intervertebral discs by regulating the Keap1/Nrf2/ARE pathway,” *Oxidative medicine and cellular longevity*, vol. 2021, Article ID 6684147, 2021.
- [45] A. Cuadrado, Z. Martín-Moldes, J. Ye, and I. Lastres-Becker, “Transcription factors NRF2 and NF- κ B are coordinated effectors of the Rho family, GTP-binding protein RAC1 during inflammation,” *The Journal of biological chemistry*, vol. 289, no. 22, pp. 15244–15258, 2014.

Research Article

Follistatin-Like 1 Attenuation Suppresses Intervertebral Disc Degeneration in Mice through Interacting with TNF- α and Smad Signaling Pathway

Shaoyi Wang,^{1,2} Jianlu Wei,¹ Jie Shi,^{1,2} Qiting He,^{1,2} Xiaocong Zhou,³ Ximei Gao ,^{4,5} and Lei Cheng ¹

¹Department of Orthopedic, Qilu Hospital, Cheeloo College of Medicine of Shandong University, Jinan, China

²Cheeloo College of Medicine, Shandong University, Jinan, China

³Shandong Qianfoshan Hospital, Cheeloo College of Medicine, Shandong University, Jinan, China

⁴Department of International Medicine, Qilu Hospital of Shandong University, Jinan, China

⁵Nursing Theory & Practice Innovation Research Center of Shandong University, Jinan, China

Correspondence should be addressed to Ximei Gao; gximei@126.com and Lei Cheng; chenglei@email.sdu.edu.cn

Received 10 October 2020; Revised 23 November 2020; Accepted 23 March 2021; Published 12 April 2021

Academic Editor: Sidong Yang

Copyright © 2021 Shaoyi Wang et al. This is an open access article distributed under the Creative Commons Attribution License, which permits unrestricted use, distribution, and reproduction in any medium, provided the original work is properly cited.

Background. Inflammation plays an important role in intervertebral disc degeneration (IDD). The protein follistatin-like 1 (FSTL1) plays a proinflammatory role in a variety of inflammatory diseases. **Objectives.** The purpose of this study was to investigate whether IDD could be delayed by inhibiting FSTL-1 expression. **Methods.** We established a puncture-induced IDD model in wild-type and FSTL-1^{+/−} mice and collected intervertebral discs (IVDs) from the mice. Safranin O staining was used to detect cartilage loss of IVD tissue, and HE staining was used to detect morphological changes of IVD tissue. We measured the expression of FSTL-1 and related inflammatory indicators in IVD tissues by immunohistochemical staining, real-time PCR, and Western blotting. **Results.** In the age-induced model of IDD, the level of FSTL-1 increased with the exacerbation of degeneration. In the puncture-induced IDD model, FSTL-1-knockdown mice showed a reduced degree of degeneration compared with that of wild-type mice. Further experiments showed that FSTL-1 knockdown also significantly reduced the level of related inflammatory factors in IVD. In vitro experiments showed that FSTL-1 knockdown significantly reduced TNF- α -induced inflammation. Specifically, the expression levels of the inflammatory factors COX-2, iNOS, MMP-13, and ADAMTS-5 were reduced. Knockdown of FSTL-1 attenuated inflammation by inhibiting the expression of P-Smad1/5/8, P-Erk1/2, and P-P65. **Conclusion.** Knockdown of FSTL-1 attenuated inflammation by inhibiting the TNF- α response and Smad pathway activity and ultimately delayed IDD.

1. Introduction

Intervertebral disc degeneration (IDD) is the most common cause of low back pain and lumbar disc herniation (LDH) and has become an important public health issue, posing a serious burden on countries, society, and families [1–3]. Inflammation and oxidative stress are thought to play important roles in disc degeneration [4, 5]. Most previous studies showed that IDD was a passive process: the local homeostasis of intervertebral disc (IVD) tissues was destroyed, the biomechanical relationship of normal lumbar vertebrae was changed, and the number of local inflammatory cells and the

secretion and synthesis of related inflammatory factors were altered [4, 6–11]. The significantly high expression of inflammatory factors is an important characteristic of the inflammatory microenvironment of the degenerative nucleus pulposus. Therefore, it is critical to block the effects of inflammatory factors in IDD, inhibit the inflammatory response caused by these factors, and delay the degeneration of nucleus pulposus cells to reduce the clinical symptoms of patients.

TNF- α is a member of the tumor necrosis factor superfamily. As a powerful inflammatory cytokine, TNF- α plays an important role in the inflammatory response to

degenerative diseases [12–14]. Studies have shown that the expression level of TNF- α is positively correlated with the degree of disc degeneration [15]. TNF- α levels in IVDs are associated with clinical symptoms of low back pain in patients [16]. On the one hand, TNF- α can exacerbate the inflammatory response by promoting the secretion of inflammatory factors such as COX-2 (cyclooxygenase-2), iNOS (inducible nitric oxide synthase), and IL-1 β (interleukin-1 β); on the other hand, TNF- α can accelerate matrix destruction by promoting the secretion of matrix-degrading enzymes such as matrix metalloproteinase- (MMP-) 13 and a disintegrin and metalloproteinase with thrombospondin motifs- (ADAMTS-) 5 [17, 18]. The NF- κ B and Erk signaling pathways are key pathways that facilitates the function of TNF- α , and their role in disc degeneration has been extensively studied [12, 19, 20]. Therefore, finding a cytokine that can specifically inhibit TNF- α to reduce the inflammatory response is worth exploring.

The protein follistatin-like 1 (FSTL1), also known as transforming growth factor-stimulated clone 36 (TSC-36) or follistatin-related protein (FRP), is a soluble secreted extracellular glycoprotein that plays an important role in many kinds of tissue degeneration and autoimmune diseases [21, 22]. Studies have shown that FSTL1 can alleviate the occurrence of inflammatory pulmonary fibrosis, suggesting that FSTL1 may be closely related to the occurrence of inflammation [23]. Further studies have reported that FSTL1 regulates the secretion of inflammatory factors such as interleukin- α , TNF- α , and ADAMTS and participates in the immune inflammatory response in tissues in many systemic autoimmune diseases, including systemic lupus erythematosus, ulcerative colitis, rheumatoid arthritis, and Sjogren's syndrome [24, 25]. In rheumatoid arthritis and osteoarthritis, FSTL1 exacerbates inflammation by increasing the expression of inflammatory factors and promoting synovial proliferation by activating the NF- κ B signaling pathway [25]. In many previous studies, FSTL1 can activate P-Smad1/5/8 by binding to the BMP4 receptor, causing an inflammatory response and cell damage [26, 27]. Thus, we hypothesized that FSTL1 plays a similar role in IDD.

Herein, we specifically reduced the expression of FSTL-1 to observe the degree of disc inflammation and degeneration. Additionally, we examined the role of FSTL-1, as well as the involved pathways.

2. Methods

2.1. Mice. All animal studies were performed in accordance with institutional guidelines and approved by the Laboratory Animal Centre of Qilu Hospital of Shandong University. Male 8- to 12-week-old FSTL-1-knockdown (FSTL-1+/-) mice (Jackson Laboratories, USA) and 2-, 4-, and 9-month-old C57/BL6 wild-type (WT) mice (Qilu College of Medicine, Shandong University) were used for our experiments. All experimental animals were genotyped before use.

2.2. Primary Cell Isolation and Culture. We selected 2-month-old FSTL-1+/- and WT male mice to extract nucleus pulposus cells. The entire thoracolumbar spine was

completely separated. The nucleus pulposus and annulus fibrosus were carefully separated under the microscope. Then, the cells were washed with sterile phosphate-buffered saline (PBS) 3 times and digested with 0.25% trypsin (Sigma, St. Louis, USA) for 30 minutes and 0.2% type II collagenase (Sigma, St. Louis, USA) for 4 hours. The nucleus pulposus cells were cultured in DMEM/F12 (HyClone, Logan, USA) supplemented with 10% foetal bovine serum (FBS; Gibco, USA), 100 U/ml penicillin, and 0.1 mg/ml streptomycin (HyClone, USA) and incubated in standard conditions (37°C, 5% CO₂) for experiments. The culture medium was replaced every 3 days. When the nucleus pulposus cells were almost 80% confluent, the cells were subcultured at a ratio of 1 : 3. Cells up to five generations old were used in all in vitro experiments. And all experiments were performed with two repeating holes.

2.3. Cell Treatments. To examine the effect of FSTL-1 on IVD inflammation, mouse nucleus pulposus cells were divided into the WT group and the FSTL-1+/- group. And the two groups were stimulated with TNF- α (10 ng/ml) [6, 20]. The cells were harvested for real-time PCR (RT-PCR) after stimulation for 8 hours and harvested for Western blot analysis after stimulation for 48 hours [20]. Protein samples were stored at -20°, and RNA samples were stored at -80° and analyzed within 1 week.

2.4. Mouse Model of Puncture-Induced Disc Degeneration. Eight- to twelve-week-old FSTL-1+/- and C57/BL6 WT mice were used in this study. The 15 mice were divided into three groups (FSTL-1+/- group, WT group, and the control group). The mice were anesthetized with pentobarbital. X-ray (Siemens, Germany) radiography was used to locate the L5 and L6 discs which to be punctured. A 0.5 cm incision was made at the site of the puncture disc. After disinfection, the discs needed to be exposed were exposed posterolateral under a microscope. The disc was inserted about 0.5 mm with a 29G needle and moved out after 2 seconds [20, 28]. Puncture was performed in the FSTL-1+/- group and WT group. The control group only exposed the intervertebral disc. All the mice were housed under normal conditions. The mice were fed in a cage and rubbed with iodine every day. Biting incisions were avoided.

2.5. Immunohistochemistry (IHC). At 1 week after puncture, mouse disc tissues at the site of the previous puncture (L5 and L6) were harvested and fixed with 4% paraformaldehyde for 48 hours and then decalcified with 10% ethylenediaminetetraacetic acid (EDTA) for 14 days. The IVDs were then made into 5 μ m paraffin sections. The sections were treated with 0.125% trypsin (ZSGB-Bio, Beijing, China) for 30 minutes at 37°C for antigen repair, 3% hydrogen peroxide for 20 minutes at room temperature to eliminate endogenous peroxidase activity, and 20% goat serum (ZSGB-Bio, Beijing, China) for 20 minutes to block the nonspecific protein binding sites. Then, the sections were incubated with goat anti-FSTL-1 (1 : 200, Abcam, USA), rabbit anti-COX-2 (1 : 200, Abcam, USA), rabbit anti-ADAMTS-5 (1 : 200, Abcam, USA), and rabbit anti-MMP-13 (1 : 200, Abcam, USA) at

TABLE 1: Real-time PCR primers.

Target	Forward primers, 5' -3'	Reverse primers, 5' -3'
FSTL-1	TTATGATGGGCACrGCAAAGAA	ACTGCCTTTAGAGAACCAGCC
ADAMTS-5	GCATTGACGCATCCAAACCC	CGTGGTAGGTCCAGCAAACAGTTAC
iNOS	ACAGGAGGGGTAAAGCTGC	TTGTCTCCAAGGGACCAGG
β -Actin	CCTCATGAAGATCCTGACCG	ACCGCTCATTGCCGATAGTG
MMP-13	ACTTTGTTGCCAATTCCAGG	TTTGAACACGGGGAAGAC
COX2	TCCCTTGGGTGTCAAAGGTA	TGGCCCTCGCTTATGATCTG

4°C overnight. The next day, the sections were incubated with mouse anti-goat immunoglobulin- (IgG-) horseradish peroxidase (HRP) (1 : 200, Jackson ImmunoResearch, USA) or goat anti-rabbit IgG-HRP secondary antibody (1 : 200, Jackson ImmunoResearch, USA) at 37°C for 1 hour. The results were observed with an IX71-SIF microscope (Olympus, Tokyo, Japan). Brown particles were considered positive, and the relative area of brown particles was used for the Image-Pro Plus 6.0 software (Media Cybernetics, Inc., USA) analysis.

Safranin O/Fast Green staining was performed with a modified Safranin O/Fast Green FCF cartilage stain kit (Solarbio, Beijing, China) according to the manufacturer's instructions.

2.6. Immunofluorescence Staining. After treatment with 10 ng/ml TNF- α for 48 h, nucleus pulposus cells were fixed with 4% formaldehyde for 15 minutes, permeabilized in 0.2% Triton-X 100 for 15 minutes, and blocked in 1% BSA for 30 minutes. Then, the cells were incubated with rabbit anti-ADAMTS-5 (1 : 400, Abcam, USA) and rabbit anti-COX-2 (1 : 400, Abcam, USA) primary antibodies overnight. The next day, the cells were incubated with fluorescently labelled goat anti IgG (1 : 200, ZSGB-BIO, China) for 1 hour. The results were observed by a microscope (Olympus IX51, Japan). Green fluorescence is considered positive. The Image-Pro Plus 6.0 software (Media Cybernetics, Inc., USA) was used for quantitative analysis of pictures.

2.7. Total Protein Extraction and Western Blotting. The nucleus pulposus tissue harvested from mice and nucleus pulposus cells were washed with sterile PBS 3 times and placed in RIPA lysis buffer (Millipore, Billerica, MA, USA) supplemented with 5% PMSF (a protease inhibitor) on ice for 40 minutes. After centrifugation at 12,000 rpm for 15 minutes at 4°C, the supernatant was retained. A BCA protein assay kit (Biotechnology Co, Beijing, China) was used to measure the protein concentration according to the manufacturer's instructions. Equal amounts of proteins were resolved on 10% SDS-polyacrylamide gels and transferred to a polyvinylidene difluoride (PVDF) membrane (Millipore, USA). After being blocked in Tris-buffered saline with Tween-20 (TBST) with 5% milk powder, the blots were incubated with goat anti-FSTL-1 (1 : 1,000, Abcam, USA), rabbit anti-COX-2 (1 : 1,000, Abcam, USA), rabbit anti-ADAMTS-5 (1 : 1,000, Abcam, USA), rabbit anti-MMP-13 (1 : 1,000, Abcam, USA), rabbit anti-iNOS (1 : 1,000, Abcam, USA), rabbit anti-P-smad2/3 (1 : 1,000, CST, USA), rabbit anti-P-

smad1/5/8 (1 : 1,000, CST, USA), rabbit anti-P-Erk1/2 (1 : 1,000, CST, USA), rabbit anti-P-P65 (1 : 1,000, CST, USA), and rabbit anti-GAPDH-HRP (1 : 5,000, Protein-Tech, USA) primary antibodies overnight at 4°C. GAPDH was used to ensure equal protein loading. After being incubated with goat anti-rabbit IgG-HRP (1 : 3,000, Jackson ImmunoResearch, USA) or mouse anti-goat IgG-HRP secondary antibody (1 : 3,000, Jackson ImmunoResearch, USA) for 1 hour at room temperature, the blots were visualized using a chemiluminescence system (Amersham Imager 600, GE Amersham USA), and grey value analysis was used with the ImageJ software (National Institutes of Health, USA).

2.8. RNA Extraction and Real-Time PCR. Mouse nucleus pulposus tissues (2-3 mg) and nucleus pulposus cells were treated with TNF- α and lysed with TRIzol reagent (Takara Bio, Japan). A total of 1 μ g of RNA was used for reverse transcription by a cDNA synthesis kit (GeneCopoeia, Inc., USA). RT-PCR was performed in 10 μ l of SYBR Green PCR matrix mix (Toyobo, Japan) on a thermal cycler (Bio-Rad, Hercules, USA). Cycle parameters were as follows: 95°C for 1 min, 40 cycles (95°C for 15 s, 60°C for 15 s, and 72°C for 45 s), and 72°C for 5 min. The RT-PCR results were calculated using the $2^{-\Delta\Delta C_t}$ method. The primers (FSTL-1, COX-2, MMP-13, ADAMTS-5, β -actin, and iNOS) were designed based on published sequences of these genes and listed in Table 1 [29, 30].

2.9. Statistical Analyses. GraphPad Prism 7 (GraphPad Software Inc., San Diego, CA, USA) and Statistical Package for Social Sciences version 25.0 were used for statistical analyses, including one-way analysis of variance (ANOVA) and *t*-tests. The data are expressed as the mean value \pm standard deviation (SD), and *P* < 0.05 was considered significant.

3. Results

3.1. FSTL-1 Was Expressed in the Nucleus Pulposus of Mice and Was Increased with Age. To verify the role of FSTL-1 in mouse IVDs, we measured the expression of FSTL-1 in the IVDs of mice during ageing. The IHC results demonstrated that the level of FSTL-1 in IVDs was elevated in the 9-month-old group compared with the 4-month-old group (Figure 1(a)). The positive expression area and intensity of FSTL-1 in the 9-month-old group were significantly higher than those in the 4-month-old group (Figure 1(b)). We extracted the IVD tissue from mice in the two groups and

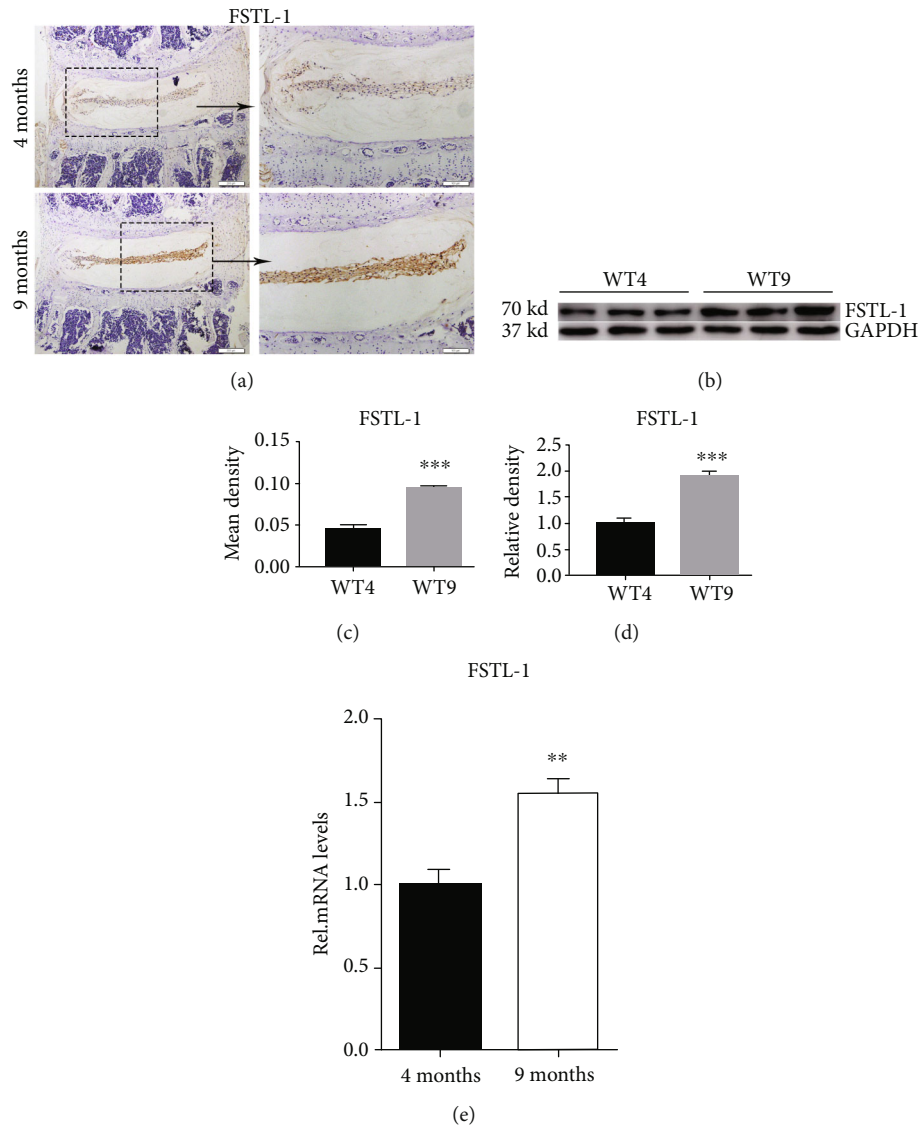


FIGURE 1: FSTL-1 was expressed in the nucleus pulposus of mice and was increased with age. (a) The expression of FSTL-1 in mouse disc tissues was determined by immunohistochemical staining. (b) Quantitative analysis of the FSTL-1-positive area in disc tissues of 4-month-old and 9-month-old mice by immunohistochemical staining. (c) Western blot analysis of the expression of FSTL-1 in mouse disc tissues. The transcript level of PGRN was measured by RT-PCR. (d) Western blot grey value analysis of FSTL-1 in the disc tissues of 4-month-old and 9-month-old mice. (e) The RNA level of FSTL-1 in 4-month-old and 9-month-old mice was assayed by RT-PCR. Magnification $\times 200$, $\times 400$. Scale bar = 200 μm , 100 μm . The values are the mean \pm SD of at least 3 independent experiments; ** $P < 0.01$, *** $P < 0.001$.

performed Western blot analysis. As shown in Figures 1(c) and 1(d), the Western blot results showed that the protein expression of FSTL-1 in the 9-month-old group was higher than that in the 4-month-old group. The RT-PCR results also indicated that the transcription level of FSTL-1 in the 9-month group was higher than that in the 4-month group. These results indicated that the expression of FSTL-1 increased with age in the mouse IVD. FSTL-1 is involved in IDD in mice.

3.2. FSTL-1-Knockdown Mice Exhibited Reduced Cartilage Degeneration and Disc Degeneration. To determine the role of endogenous FSTL-1 in IDD, we used 8- to 12-week-old FSTL-1 $^{+/-}$ and C57/BL6 WT mice to establish a model of

IDD by acupuncture. After 7 days, we harvested the IVD tissue and prepared paraffin sections. The Safranin O staining results showed that IVD inflammation caused cartilage loss, but knockdown of FSTL-1 alleviated the loss of cartilage (Figures 2(a) and 2(b)). As shown in Figure 2(c), HE staining showed that inflammation accelerated the loss of disc height and caused the annulus to be disorganized in the IVD, and knockdown of FSTL-1 alleviated this structural degeneration. These results suggest that a reduction in FSTL-1 may alleviate disc degeneration.

3.3. FSTL-1-Knockdown Mice Had Reduced Levels of Inflammatory Cytokines in the IVDs. Inflammation is thought to play an important role in IDD. FSTL-1 plays a

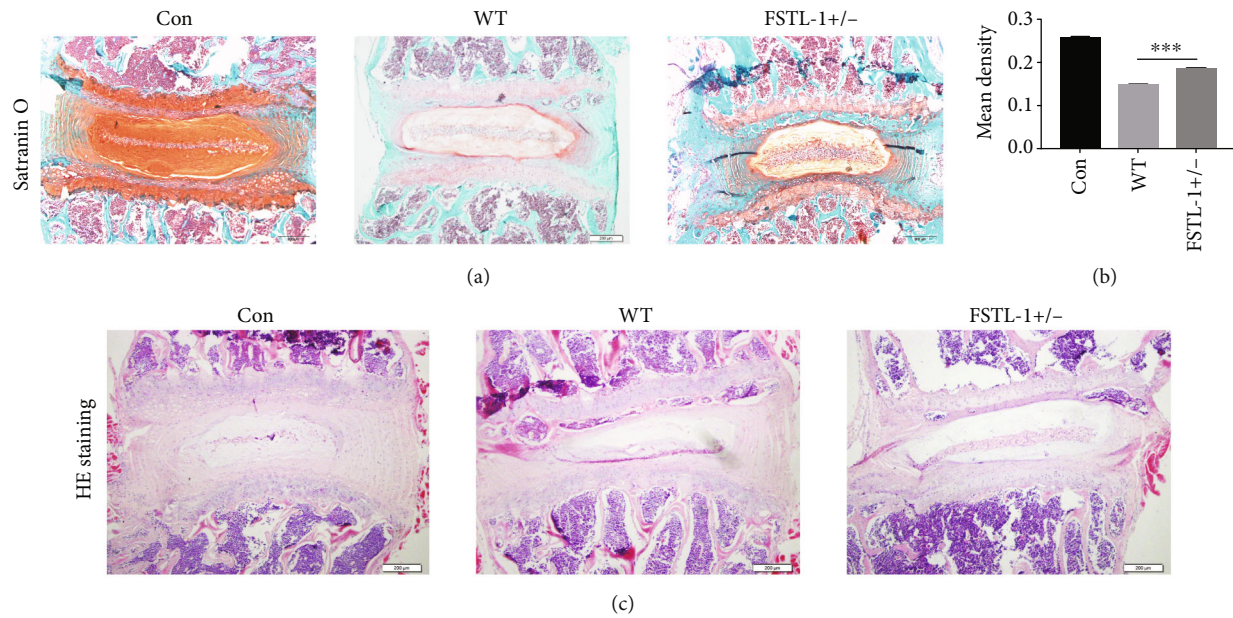


FIGURE 2: FSTL-1-knockdown mice expressed a lower level of cartilage degeneration and suppressed disc degeneration. (a) Safranin O staining of IVD tissues in the different groups. CON: normal discs. WT: degenerative discs of WT mice. FSTL-1^{+/-}: degenerative discs of FSTL-1-knockdown mice. Magnification $\times 200$. Scale bar = $200 \mu\text{m}$. (b) Quantitative analysis of the cartilage area based on Safranin O staining. (c) Representative image of HE staining of IVDs in the different groups. Magnification $\times 200$. Scale bar = $200 \mu\text{m}$. *** $P < 0.001$.

proinflammatory role in a variety of inflammatory diseases. Therefore, we first hypothesized that FSTL-1 knockdown probably reduced inflammatory cytokines, alleviating IDD. Therefore, we established a mouse model of puncture-induced disc degeneration and analysed IVD tissues from FSTL-1^{+/-} and C57/BL6 WT mice after 7 days. Immunohistochemical staining showed that COX2, MMP-13, and ADAMTS-5 were expressed in the IVD during IDD, while the expression of these inflammatory factors was decreased after FSTL-1 was knocked down (Figures 3(a) and 3(b)). We further extracted the total proteins in the IVD tissue and performed Western blotting. As shown in Figures 4(a)–4(e), compared with that of the WT group, the expression of inflammatory cytokines (iNOS, COX-2, MMP-13, and ADAMTS-5) in the FSTL-1^{+/-} group was decreased, and the difference was statistically significant. The RT-PCR results also showed that knockdown of FSTL-1 reduced the transcription level of inflammatory factors (iNOS, COX-2, MMP-13, and ADAMTS-5) in the IVD. These results suggest that knockdown of FSTL-1 can reduce the inflammatory response and delay disc degeneration.

3.4. Knockdown of FSTL-1 Reduced TNF- α -Induced Inflammatory Cytokines In Vitro. To further examine the role of FSTL-1, we extracted nucleus pulposus cells from FSTL-1^{+/-} and C57/BL6 WT mice for in vitro experiments. Total protein was extracted after 48 hours of stimulation with 10 ng/ml TNF- α , and Western blotting was performed to measure the expression of COX-2, MMP-13, ADAMTS-5, and iNOS. As shown in Figures 5(a)–5(e), knockdown of FSTL-1 reduced TNF- α -induced inflammatory cytokines (COX-2, MMP-13, ADAMTS-5 and iNOS). Then, we extracted the total RNA and performed RT-PCR to verify

the transcription levels of these inflammatory cytokines after 6 hours of stimulation with TNF- α . As shown in Figures 5(f)–5(i), compared with those of the WT group, the transcription levels of COX-2, MMP-13, ADAMTS-5, and iNOS were significantly decreased in the FSTL-1^{+/-} group. After 48 hours of TNF- α stimulation, immunofluorescence staining of COX-2 and ADAMTS-5 was performed. As shown in Figures 5(j)–5(m), the expression of COX-2 and ADAMTS-5 was markedly downregulated in the FSTL-1^{+/-} group. In summary, knockdown of FSTL-1 can reduce TNF- α -induced downstream inflammatory molecules, thereby reducing the degree of the inflammatory response.

3.5. Knockdown of FSTL-1 Reduced the TNF- α -Mediated Inflammatory Response by Inhibiting the Expression of P-Smad1/5/8, P-P65, and P-Erk1/2. To further investigate the mechanism by which FSTL-1 knockdown inhibited the inflammatory response, TNF- α was used to generate an inflammatory environment in vitro, and the phosphorylation levels of corresponding pathway proteins were measured. Our results showed that the expression levels of P-Smad1/5/8, P-P65, and P-Erk1/2 could be reduced by knockdown of FSTL-1 (Figures 6(b)–6(d)). There was no significant change in P-Smad2/3 (Figure 6(a)).

4. Discussion

FSTL1, also known as FRP, is a secreted glycoprotein that is involved in various pathological and physiological processes, such as immune regulation, growth factors, cell proliferation, and differentiation, as well as the development of the central nervous system, orthopedic system, and respiratory system [22, 23, 31–40]. In the context of the inflammatory response,

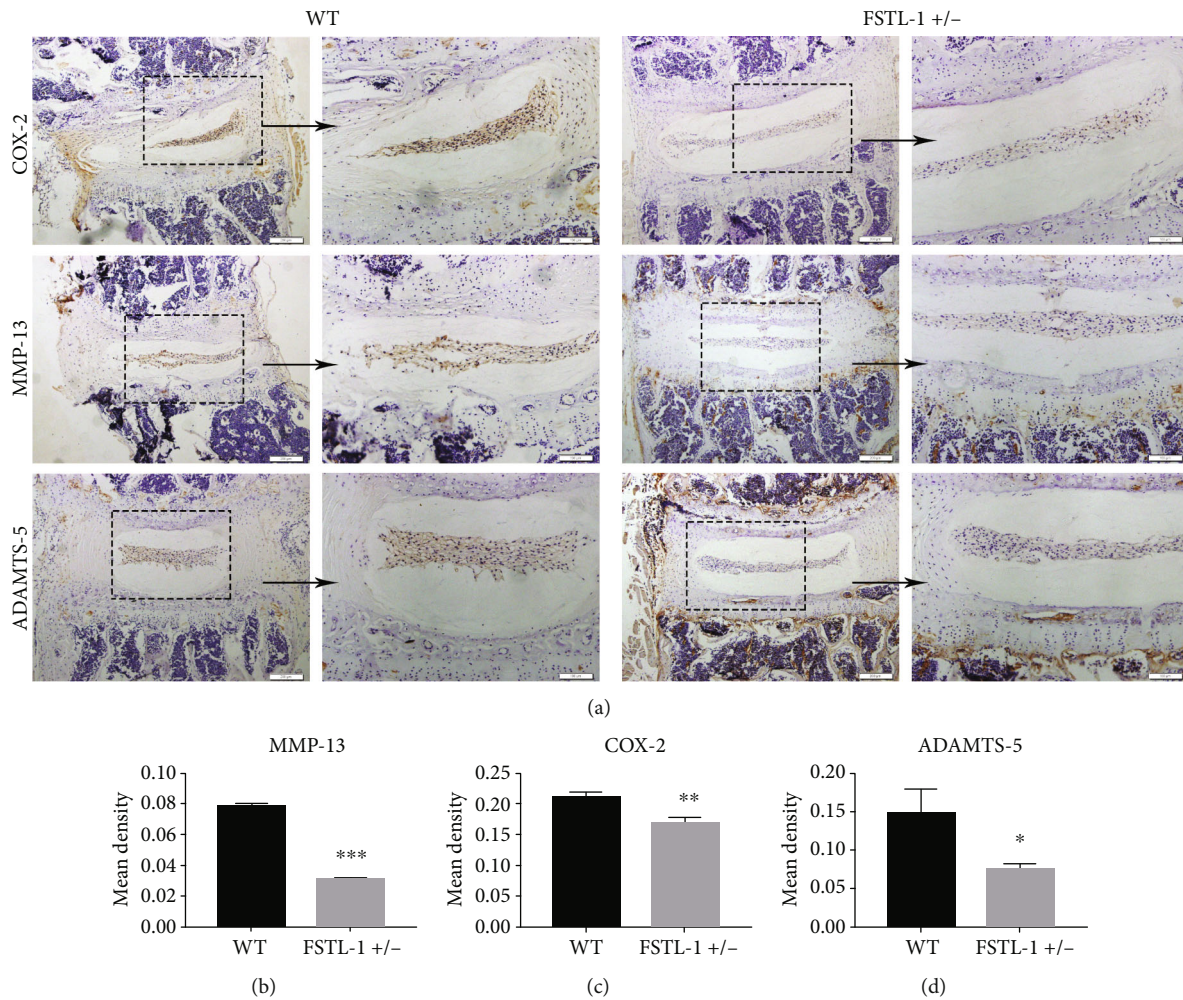


FIGURE 3: FSTL-1-knockdown mice had reduced levels of inflammatory cytokines in the IVDs. (a) Immunohistochemical staining of COX-2, MMP-13, and ADAMTS-5 in the degenerative discs of WT and FSTL-1^{+/-} mice. Magnification $\times 200$, $\times 400$. Scale bar = 200 μm , 100 μm . (b–d) Quantitative analysis of the positive areas of COX-2, MMP-13, and ADAMTS-5 in WT and FSTL-1^{+/-} mice by immunohistochemical staining. The values are the mean \pm SD of at least 3 independent experiments; * $P < 0.05$, ** $P < 0.01$, *** $P < 0.001$.

FSTL-1 has been reported to play both anti-inflammatory and proinflammatory roles [26]. In an ischemia/reperfusion-induced myocardial injury model, systemic or intracoronary injection of FSTL1 reduced the expression of inflammatory cytokines such as TNF- α and IL-6, thereby improving cardiac hypertrophy and dysfunction [27]. In a mouse arthritis model, FSTL-1 significantly reduced the expression of IL-6 and MMP-13, thereby reducing joint destruction and synovial inflammation [41, 42].

In contrast to the few reported anti-inflammatory effects of FSTL-1, a large number of studies have shown that FSTL-1 promotes inflammation by stimulating the release of inflammatory factors [43, 44]. Cluterr et al. showed that the upregulation of FSTL-1 resulted in significant paw swelling and upregulation of the IFN receptor, which could be neutralized by downregulating FSTL-1 [45]. In addition, Miyamae et al. transfected FSTL-1 into fibroblasts and macrophages and showed that FSTL-1 promoted the production of inflammatory cytokines, including IL-1 β , TNF- α , and IL-6 [46]. Another study showed that when synoviocytes from the synovial tissues of patients with osteoarthritis were exposed

to recombinant FSTL-1 protein, the levels of some inflammatory factors, such as TNF- α , IL-6, and IL-1 β , were significantly increased, and the activation of the NF- κ B signaling pathway was also significantly upregulated [25]. FSTL-1 has also been reported to promote the transcription of NLRP3 and procaspase-1 and promote the secretion of IL-1 β by macrophages [47]. It has been shown that oxidized low-density lipoprotein (oxLDL) increased the production and secretion of the inflammatory cytokines TLR4, IL-6, IL-8, and ICAM-1 in a model of endothelial cell injury induced by oxLDL, while the levels of these molecules completely decreased when FSTL-1 was depleted [48]. In conclusion, FSTL-1 can upregulate the expression of proinflammatory factors and promote the inflammatory response.

In summary, FSTL-1 plays a role in promoting the inflammatory response in a variety of inflammatory diseases. The upregulation of FSTL-1 at the gene or protein level can promote the release of inflammatory factors such as IL-1 β , TNF- α , COX-2, MMP-13, and IL-6. Inflammation is considered an important cause of disc degeneration. Inflammatory factors can cause inflammatory responses and accelerate disc

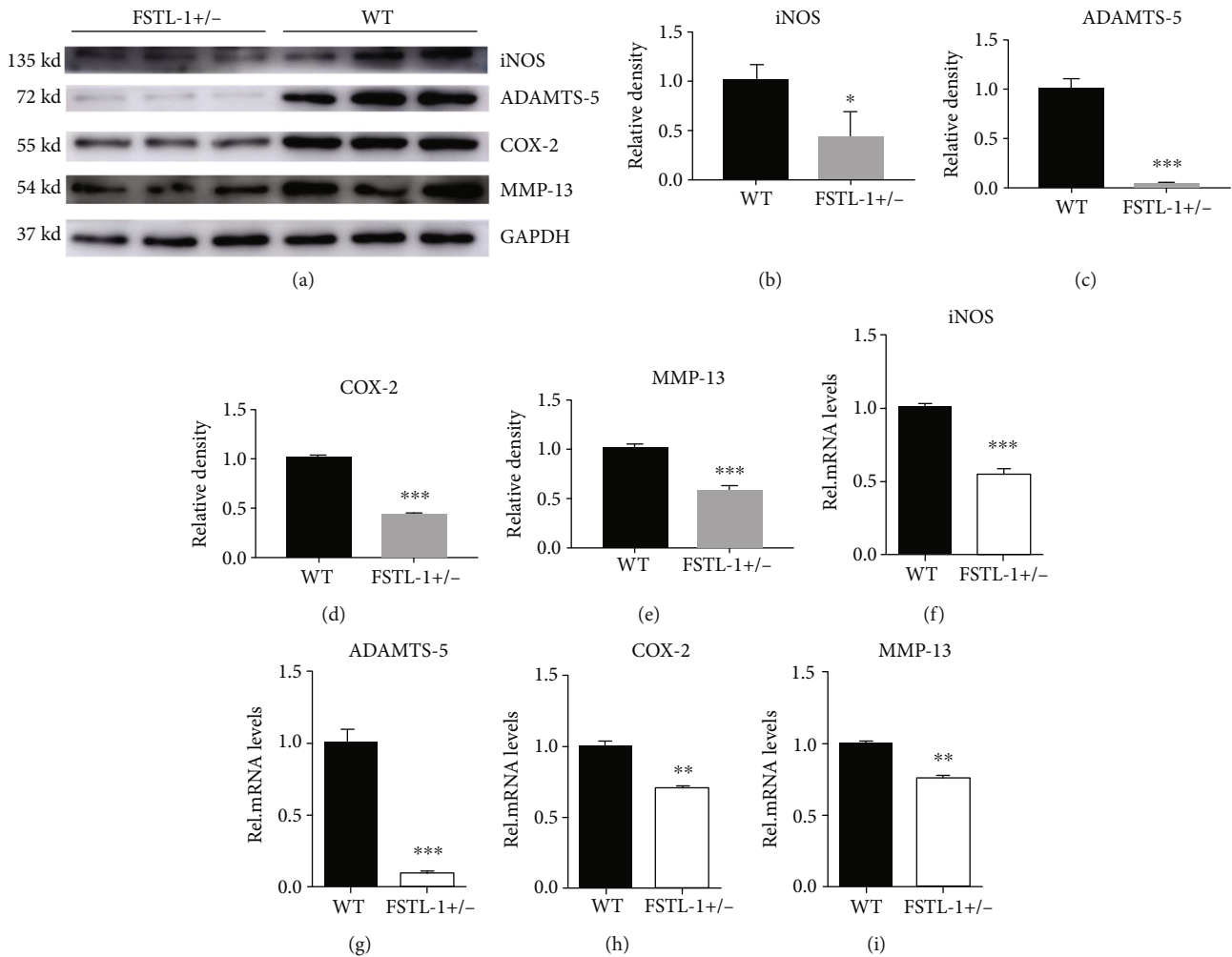


FIGURE 4: FSTL-1-knockdown mice had reduced levels of inflammatory cytokines in the IVDs. (a) The protein levels of iNOS, COX-2, MMP-13, and ADAMTS-5 in the disc tissues after puncture in WT and FSTL-1+/- mice. (b-e) Relative density of iNOS, COX-2, MMP-13, and ADAMTS-5 by Western blotting. (f-i) mRNA levels of iNOS, COX-2, MMP-13, and ADAMTS-5 in disc tissues after puncture in WT and FSTL-1+/- mice. The values are the mean \pm SD of at least 3 independent experiments; * $P < 0.05$, ** $P < 0.01$, *** $P < 0.001$.

destruction by inducing nucleus pulposus cell apoptosis and matrix degradation [20, 30]. Therefore, we hypothesized that FSTL-1 plays an important role in disc inflammation. We observed increased levels of FSTL-1 in degenerated IVDs in humans and rats. In vitro, recombinant FSTL-1 increased inflammatory factor levels through the Erk1/2, JNK, and NF- κ B pathways [16]. Although FSTL-1 can promote inflammation, our original aim was to suppress inflammation and delay disc degeneration. To further investigate whether FSTL-1 can be a target for the treatment of IDD, we will suppress FSTL-1 and observe the degree of disc degeneration.

Previous studies have shown that ageing is an important factor in disc degeneration [30, 49]. In this study, we used longitudinal analysis to evaluate the changes in FSTL-1 in the IVD. We extracted the disc tissues of sex-matched mice of different ages and measured the expression of FSTL-1. The level of FSTL-1 in the disc tissue of 9-month-old mice was significantly higher than that of 4-month-old mice. This finding also indicates an increased level of FSTL-1 in the degenerated discs.

FSTL-1 gene-knockout (KO) mouse pups die of respiratory failure soon after birth [50]. Therefore, in this study, we used FSTL-1+/- mice. We constructed a model of puncture-induced disc degeneration, which resulted in inflammatory degeneration of IVDs. We observed that when we inhibited the expression of FSTL-1, the morphology of the mouse disc was repaired, and cartilage degeneration was alleviated. This finding suggests that FSTL-1 knockdown can protect chondrocytes and cartilage matrix. Cartilage oligomeric matrix protein (COMP) and type-2 collagen degradation of matrix proteins is an important change in IDD [17, 51-55]. MMP-13 and ADAMTS-5 have been reported to be involved in the degradation of disc matrix, exacerbating disc degeneration [20, 56, 57]. In our study, after the expression of FSTL-1 was knocked down, the expression levels of both MMP-13 and ADAMTS-5 were decreased. On the other hand, inflammatory factors such as COX-2, iNOS, and TNF- α can stimulate the inflammatory response, thus exacerbating the local inflammatory microenvironment, causing metabolic dysfunction of local cells, and ultimately exacerbating the degeneration of IVDs. We observed that FSTL-1

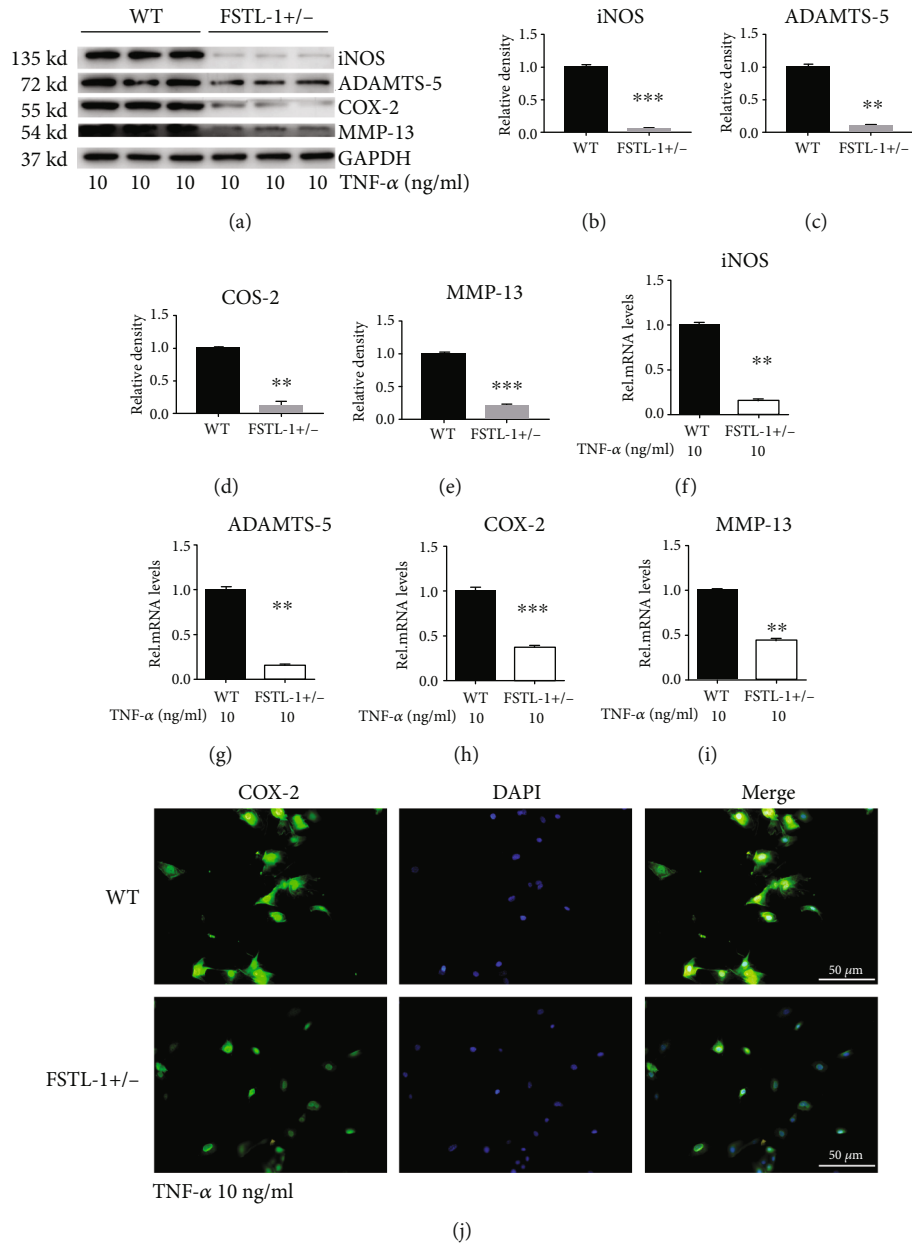


FIGURE 5: Continued.

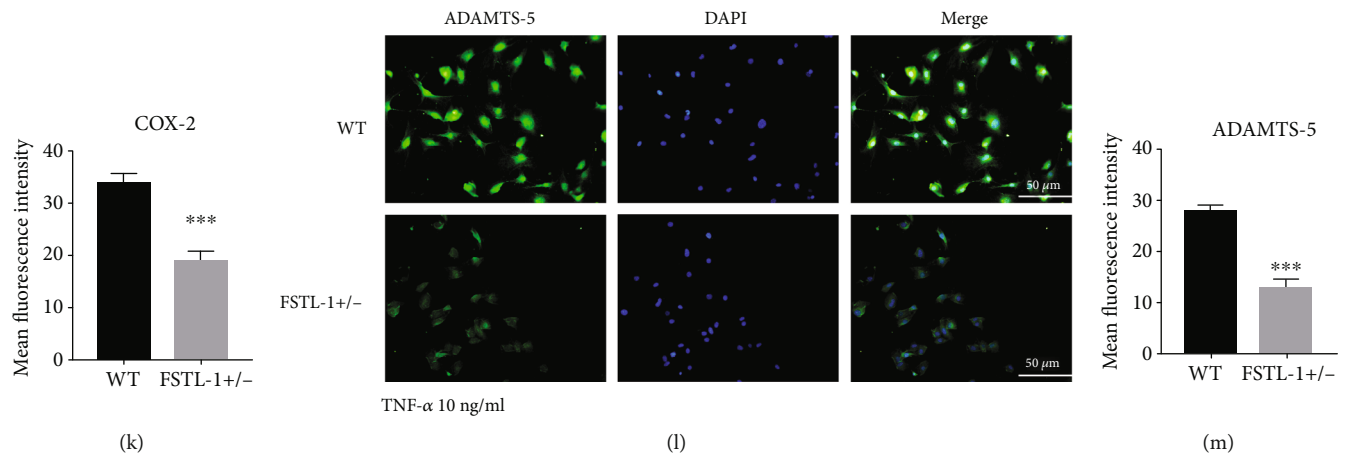


FIGURE 5: Knockdown of FSTL-1 reduced TNF- α -induced inflammatory cytokines in vitro. (a–e) Western blot and grey value analysis of iNOS, COX-2, MMP-13, and ADAMTS-5 in nucleus pulposus cells from WT and FSTL-1 $^{-/-}$ mice after stimulation with 10 ng/ml TNF- α . (f–i) The mRNA levels of iNOS, COX-2, MMP-13, and ADAMTS-5 in nucleus pulposus cells from WT and FSTL-1 $^{-/-}$ mice after stimulation with 10 ng/ml TNF- α were determined by RT-PCR. (j, l) The expression of COX-2 and ADAMTS-5 in nucleus pulposus cells after stimulation with 10 ng/ml TNF- α was detected by immunofluorescence analysis. Scale bar = 50 μ m. (k, m) Analysis of the mean fluorescence intensity of COX-2 and ADAMTS-5 according to the immunofluorescence results. The values are the mean \pm SD of at least 3 independent experiments; ** $P < 0.01$, *** $P < 0.001$.

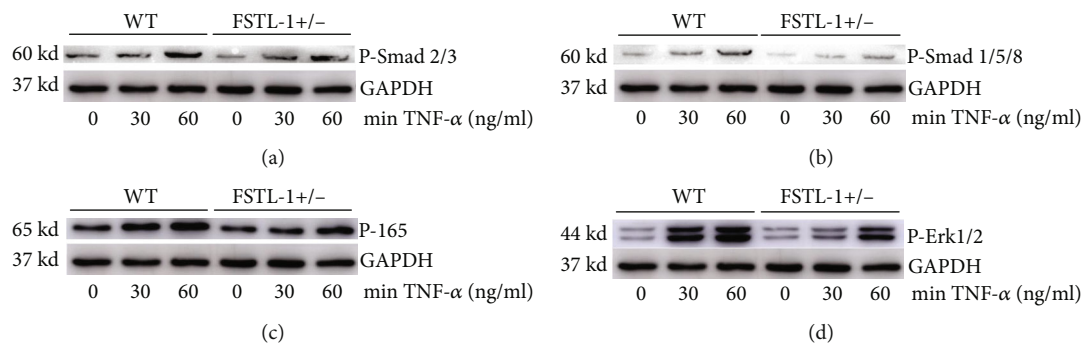


FIGURE 6: Knockdown of FSTL-1 can reduce the TNF- α -mediated inflammatory response by inhibiting the expression of P-Smad1/5/8, P-P65, and P-Erk1/2. (a–d) Western blot analysis of P-Smad2/3, P-Smad1/5/8, P-P65, and P-Erk1/2 in nucleus pulposus cells at different time points after stimulation with 10 ng/ml TNF- α in WT and FSTL-1 $^{-/-}$ mice.

knockdown could effectively reduce the expression of these inflammatory factors. In summary, knockdown of FSTL-1 can delay disc degeneration by inhibiting both the degradation of the disc matrix and the expression of inflammatory factors.

TNF- α , a potent inflammatory cytokine, is highly associated with the development and degeneration of IVDs [15]. On the one hand, TNF- α can exacerbate the structural destruction of IVD tissue and increase the inflammatory bone absorption of adjacent vertebral bodies by inducing the expression of inflammatory factors [58]. On the other hand, TNF- α can upregulate IVD matrix-degrading enzymes such as ADAMTS-5 and MMP-13 through the NF- κ B signaling pathway, affecting the metabolic homeostasis of IVD cells and resulting in protein denaturation and necrosis [17, 56]. Therefore, how to effectively inhibit the effect of TNF- α in IDD is still a hot research area. In vitro, TNF- α was used to stimulate nucleus pulposus cells from two different sources, WT mice and FSTL-1 $^{-/-}$ mice. Our results showed that FSTL-1 knockdown reduced the protein and transcript levels

of major inflammatory factors, such as COX-2, iNOS, MMP-13, and ADAMTS-5, induced by TNF- α stimulation. In summary, knockdown of FSTL-1 can suppresses the TNF- α -mediated inflammatory response, reduce the release of inflammatory factors, and reduce the production of matrix metalloproteinases, thereby delaying the degeneration of IVDs.

Oxidative stress is also an important cause in disc degeneration [59]. In the process of oxidative stress, the mitochondria will produce excessive ROS, which can directly damage nucleus pulposus cells, interfere with the synthesis of cell matrix, and increase the expression of MMP [60]. TNF- α can promotes oxidative stress in a variety of disease processes [61, 62]. In intervertebral discs, TNF- α can induce oxidative stress in human NP cells, specifically by promoting mitochondrial swelling, lowering membrane potential, and increasing ROS levels [6]. Therefore, knockdown of FSTL-1 may not only reduce the inflammatory effect of TNF- α but also inhibit the effect of TNF- α on oxidative stress.

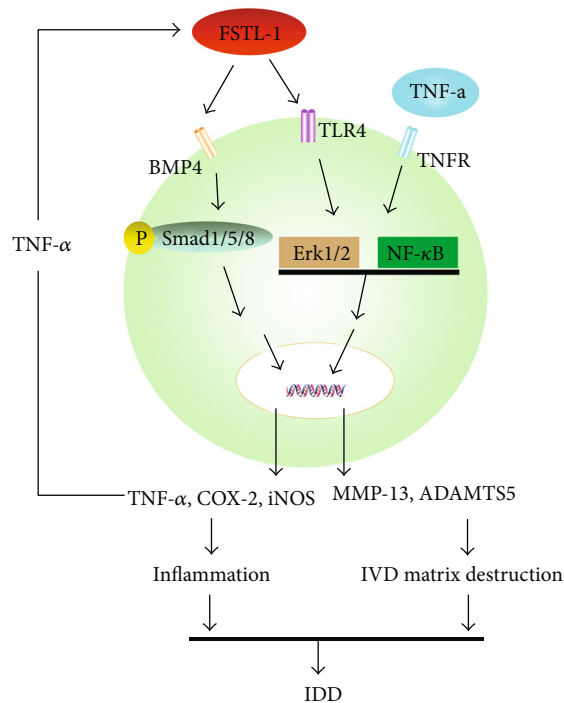


FIGURE 7: Schematic model of the proposed signaling pathways of the effect of FSTL-1 in IDD.

In osteoarthritis and disc degeneration, TNF- α can activate the NF- κ B and Erk pathways by binding specifically to TNF receptors, resulting in inflammatory changes and cartilage degeneration [30, 63]. In previous studies, FSTL-1 was reported to promote inflammatory responses through the NF- κ B and Erk pathways by specifically binding to TLR4 [16, 22, 25, 48]. After knockdown of FSTL-1, we found that the common pathway of FSTL-1 and TNF- α was also inhibited. We hypothesized that the NF- κ B and Erk pathways were also inhibited when FSTL-1 was knocked down, weakening the inflammatory effect of TNF- α . This may explain why knockdown of FSTL-1 attenuated the TNF- α -mediated inflammatory response. In addition, FSTL-1 can activate P-Smad1/5/8 by binding to the BMP4 receptor, causing an inflammatory response and cell damage [26, 27, 64]. Therefore, in our study, we measured the expression levels of two key P-Smad proteins. Consistent with previous reports, the expression level of P-Smad1/5/8 decreased after FSTL-1 was knocked down, while the expression level of P-Smad2/3 did not change significantly. This finding indicated that P-Smad1/5/8 was involved in the inflammatory response mediated by FSTL-1. In summary, knockdown of FSTL-1 suppressed the effect of TNF- α by inhibiting the activity of the NF- κ B and Erk pathways; on the other hand, knockdown of FSTL-1 attenuated the proinflammatory effect by inhibiting the activity of P-Smad1/5/8 (Figure 7).

5. Conclusion

Knockdown of FSTL-1 can reduce inflammation in the IVD by reducing TNF- α -mediated inflammation and Smad signaling pathway, protecting cartilage, and thus delaying

degeneration of the IVD in mice. FSTL-1 could be a potential target for the treatment of IDD.

Abbreviations

FSTL-1:	Follistatin-like 1
IDD:	Intervertebral disc degeneration
TNF- α :	Tumor necrosis factor α
IVD:	Intervertebral disc
MMP-13:	Matrix metalloproteinase 13
ADAMTS-5:	Disintegrin and metalloproteinase with thrombospondin motifs-5
iNOS:	Inducible nitric oxide synthase
COX-2:	Cyclooxygenase-2
IL-1 β :	Interleukin-1 β .

Data Availability

The datasets used and/or analyzed of this study are available from authors on reasonable request.

Ethical Approval

This study was approved by the Ethics Committee of Animal Medicine in Qilu Hospital of Shandong University (Jinan) and conducted according to the relevant guidelines.

Conflicts of Interest

The authors declare that they have no competing interests.

Authors' Contributions

Study concept and design were conceived by Ximei Gao and Lei Cheng. Acquisition of data was done by Shaoyi Wang and Jianlu Wei. Analysis and interpretation of data were done by Shaoyi Wang and Jie Shi. Statistical analysis was done by Shaoyi Wang, Qiting He, and Jianlu Wei. Drafting of the manuscript was done by Shaoyi Wang and Xiacong Zhou. All authors read and approved the final manuscript. Shaoyi Wang and Jianlu Wei contributed equally in this work.

Acknowledgments

The study was supported by the Qilu Hospital of Shandong University Clinical Practical New Technology Fund (2019-8), Department of Science and Technology of Shandong Province (2019GSF108029), China Postdoctoral Foundation (2019M651064), Natural Science Foundation of Shandong Province (ZR2019BH071), and National Natural Science Foundation of China Youth Program (81900804) in the role of design of the study, collection, analysis data, and writing manuscript.

References

- [1] B. Pennicooke, Y. Moriguchi, I. Hussain, L. Bonssar, and R. Härtl, "Biological treatment approaches for degenerative disc disease: a review of clinical trials and future directions," *Cureus*, vol. 8, no. 11, article e892, 2016.



- [2] Y. Liu, J. Lin, X. Wu et al., "In vivo aspirin-mediated attenuation of intervertebral disc degeneration by ameliorating reactive oxygen species," *Oxidative Medicine and Cellular Longevity*, vol. 2019, 20 pages, 2019.
- [3] S. Yang, F. Zhang, J. Ma, and W. Ding, "Intervertebral disc ageing and degeneration: the antiapoptotic effect of oestrogen," *Ageing Research Reviews*, vol. 57, p. 100978, 2020.
- [4] C. Feng, H. Liu, M. Yang, Y. Zhang, B. Huang, and Y. Zhou, "Disc cell senescence in intervertebral disc degeneration: causes and molecular pathways," *Cell cycle*, vol. 15, no. 13, pp. 1674–1684, 2016.
- [5] C. Feng, M. Yang, M. Lan et al., "ROS: crucial intermediators in the pathogenesis of intervertebral disc degeneration," *Oxidative Medicine and Cellular Longevity*, vol. 2017, 12 pages, 2017.
- [6] Y. Zhao, C. Qiu, W. Wang et al., "Cortistatin protects against intervertebral disc degeneration through targeting mitochondrial ROS-dependent NLRP3 inflammasome activation," *Theranostics*, vol. 10, no. 15, pp. 7015–7033, 2020.
- [7] Y. Zhang, Y. Zhao, J. Li et al., "Interleukin-9 promotes TNF- α and PGE2 release in human degenerated intervertebral disc tissues," *Spine*, vol. 41, no. 21, pp. 1631–1640, 2016.
- [8] Z. Yao, L. Nie, Y. Zhao et al., "Salubrinal suppresses IL-17-induced upregulation of MMP-13 and extracellular matrix degradation through the NF- κ B pathway in human nucleus pulposus cells," *Inflammation*, vol. 39, no. 6, pp. 1997–2007, 2016.
- [9] J. Li, L. Nie, Y. Zhao et al., "IL-17 mediates inflammatory reactions via p38/c-Fos and JNK/c-Jun activation in an AP-1-dependent manner in human nucleus pulposus cells," *Journal of Translational Medicine*, vol. 14, no. 1, p. 77, 2016.
- [10] Y. Liu, J. du, P. Peng et al., "Regulation of the inflammatory cycle by a controllable release hydrogel for eliminating postoperative inflammation after discectomy," *Bioactive materials*, vol. 6, no. 1, pp. 146–157, 2021.
- [11] Z. Chen, Y. Han, C. Deng et al., "Inflammation-dependent downregulation of miR-194-5p contributes to human intervertebral disc degeneration by targeting CUL4A and CUL4B," *Journal of Cellular Physiology*, vol. 234, no. 11, pp. 19977–19989, 2019.
- [12] Y. Zhao, B. Liu, Q. Tian, J. Wei, B. Richbrough, and C. Liu, "Progranulin protects against osteoarthritis through interacting with TNF- α and β -catenin signalling," *Annals of the Rheumatic Diseases*, vol. 74, no. 12, pp. 2244–2253, 2015.
- [13] N. Costa, T. Veiga Iriyoda, A. Kallaur et al., "Influence of insulin resistance and TNF- α on the inflammatory process, oxidative stress, and disease activity in patients with rheumatoid arthritis," *Oxidative Medicine and Cellular Longevity*, vol. 2016, 9 pages, 2016.
- [14] R. Fischer and O. Maier, "Interrelation of oxidative stress and inflammation in neurodegenerative disease: role of TNF," *Oxidative Medicine and Cellular Longevity*, vol. 2015, 18 pages, 2015.
- [15] C. Wang, X. Yu, Y. Yan et al., "Tumor necrosis factor- α : a key contributor to intervertebral disc degeneration," *Acta Biochimica et Biophysica Sinica*, vol. 49, no. 1, pp. 1–13, 2016.
- [16] Y. Liu, J. Wei, Y. Zhao et al., "Follistatin-like protein 1 promotes inflammatory reactions in nucleus pulposus cells by interacting with the MAPK and NF κ B signaling pathways," *Oncotarget*, vol. 8, no. 26, pp. 43023–43034, 2017.
- [17] Y. Lai, X. Bai, Y. Zhao et al., "ADAMTS-7 forms a positive feedback loop with TNF- α in the pathogenesis of osteoarthritis," *Annals of the Rheumatic Diseases*, vol. 73, no. 8, pp. 1575–1584, 2014.
- [18] S. Wang, W. Zhang, Y. Zhang et al., "IL-17A enhances ADAMTS-7 expression through regulation of TNF- α in human nucleus pulposus cells," *Journal of Molecular Histology*, vol. 46, no. 6, pp. 475–483, 2015.
- [19] W. Tang, Y. Lu, Q. Tian et al., "The growth factor progranulin binds to TNF receptors and is therapeutic against inflammatory arthritis in mice," *Science*, vol. 332, no. 6028, pp. 478–484, 2011.
- [20] S. Wang, J. Wei, Y. Fan et al., "Progranulin is positively associated with intervertebral disc degeneration by interaction with IL-10 and IL-17 through TNF pathways," *Inflammation*, vol. 41, no. 5, pp. 1852–1863, 2018.
- [21] M. Lau, K. Ng, T. Wong et al., "FSTL1 promotes metastasis and chemoresistance in esophageal squamous cell carcinoma through NF κ B-BMP signaling cross-talk," *Cancer Research*, vol. 77, no. 21, pp. 5886–5899, 2017.
- [22] K. Wei, V. Serpooshan, C. Hurtado et al., "Epicardial FSTL1 reconstitution regenerates the adult mammalian heart," *Nature*, vol. 525, no. 7570, pp. 479–485, 2015.
- [23] Y. Dong, Y. Geng, L. Li et al., "Blocking follistatin-like 1 attenuates bleomycin-induced pulmonary fibrosis in mice," *The Journal of Experimental Medicine*, vol. 212, no. 2, pp. 235–252, 2015.
- [24] P. Hu, C. Ma, F. Sun, W. Chen, and L. Wu, "Follistatin-like protein 1 (FSTL1) promotes chondrocyte expression of matrix metalloproteinase and inflammatory factors via the NF- κ B pathway," *Journal of Cellular and Molecular Medicine*, vol. 23, no. 3, pp. 2230–2237, 2019.
- [25] S. Ni, K. Miao, X. Zhou et al., "The involvement of follistatin-like protein 1 in osteoarthritis by elevating NF- κ B-mediated inflammatory cytokines and enhancing fibroblast like synovio-cyte proliferation," *Arthritis Research & Therapy*, vol. 17, no. 1, 2015.
- [26] W. Li, M. Alahdal, Z. Deng et al., "Molecular functions of FSTL1 in the osteoarthritis," *International Immunopharmacology*, vol. 83, p. 106465, 2020.
- [27] Y. Ogura, N. Ouchi, K. Ohashi et al., "Therapeutic impact of follistatin-like 1 on myocardial ischemic injury in preclinical models," *Circulation*, vol. 126, no. 14, pp. 1728–1738, 2012.
- [28] F. Yang, V. Leung, K. Luk, D. Chan, and K. Cheung, "Injury-induced sequential transformation of notochordal nucleus pulposus to chondrogenic and fibrocartilaginous phenotype in the mouse," *The Journal of Pathology*, vol. 218, no. 1, pp. 113–121, 2009.
- [29] M. Liu, R. Liu, H. Wu et al., "Radix puerariae extracts ameliorate paraquat-induced pulmonary fibrosis by attenuating follistatin-like 1 and nuclear factor erythroid 2p45-related factor-2 signalling pathways through downregulation of miRNA-21 expression," *BMC Complementary and Alternative Medicine*, vol. 16, p. 11, 2016.
- [30] Y. Zhao, Q. Tian, B. Liu et al., "Progranulin knockout accelerates intervertebral disc degeneration in aging mice," *Scientific Reports*, vol. 5, no. 1, p. 9102, 2015.
- [31] M. Sylva, V. Li, A. Buffing et al., "The BMP antagonist follistatin-like 1 is required for skeletal and lung organogenesis," *PLoS One*, vol. 6, no. 8, article e22616, 2011.

- [32] Y. Yang, J. Liu, H. Mao, Y. Hu, Y. Yan, and C. Zhao, "The expression pattern of *_follistatin-like 1_* in mouse central nervous system development," *Gene expression patterns: GEP*, vol. 9, no. 7, pp. 532–540, 2009.
- [33] M. Shimano, N. Ouchi, K. Nakamura et al., "Cardiac myocyte follistatin-like 1 functions to attenuate hypertrophy following pressure overload," *Proceedings of the National Academy of Sciences of the United States of America*, vol. 108, no. 43, pp. E899–E906, 2011.
- [34] N. Fan, H. Sun, Y. Wang et al., "Follistatin-like 1: a potential mediator of inflammation in obesity," *Mediators of Inflammation*, vol. 2013, 12 pages, 2013.
- [35] D. Adams, B. Larman, and L. Oxburgh, "Developmental expression of mouse *_follistatin-like 1_* (*_Fstl1_*): dynamic regulation during organogenesis of the kidney and lung," *Gene expression patterns*, vol. 7, no. 4, pp. 491–500, 2007.
- [36] S. Maruyama, K. Nakamura, K. Papanicolaou et al., "Follistatin-like 1 promotes cardiac fibroblast activation and protects the heart from rupture," *EMBO Molecular Medicine*, vol. 8, no. 8, pp. 949–966, 2016.
- [37] D. Wilson, A. Marinov, H. Blair et al., "Follistatin-like protein 1 is a mesenchyme-derived inflammatory protein and may represent a biomarker for systemic-onset juvenile rheumatoid arthritis," *Arthritis and Rheumatism*, vol. 62, no. 8, pp. 2510–2516, 2010.
- [38] B. Elsadek, A. Abdelghany, M. Abd El-Aziz et al., "Validation of the diagnostic and prognostic values of ADAMTS5 and FSTL1 in osteoarthritis rat model," *Cartilage*, vol. 1947603519852405, 2019.
- [39] Y. Wang, D. Li, N. Xu et al., "Follistatin-like protein 1: a serum biochemical marker reflecting the severity of joint damage in patients with osteoarthritis," *Arthritis Research & Therapy*, vol. 13, no. 6, p. R193, 2011.
- [40] G. Ponti, K. Obernier, and A. Alvarez-Buylla, "Lineage progression from stem cells to new neurons in the adult brain ventricular-subventricular zone," *Cell cycle*, vol. 12, no. 11, pp. 1649–1650, 2013.
- [41] M. Tanaka, S. Ozaki, F. Osakada, K. Mori, M. Okubo, and K. Nakao, "Cloning of follistatin-related protein as a novel autoantigen in systemic rheumatic diseases," *International Immunology*, vol. 10, no. 9, pp. 1305–1314, 1998.
- [42] D. Kawabata, M. Tanaka, T. Fujii et al., "Ameliorative effects of follistatin-related protein/TSC-36/FSTL1 on joint inflammation in a mouse model of arthritis," *Arthritis and Rheumatism*, vol. 50, no. 2, pp. 660–668, 2004.
- [43] M. Gorelik, N. Fall, M. Altaye et al., "Follistatin-like protein 1 and the ferritin/erythrocyte sedimentation rate ratio are potential biomarkers for dysregulated gene expression and macrophage activation syndrome in systemic juvenile idiopathic arthritis," *The Journal of Rheumatology*, vol. 40, no. 7, pp. 1191–1199, 2013.
- [44] Y. Chaly, A. Marinov, L. Oxburgh, D. Bushnell, and R. Hirsch, "FSTL1 promotes arthritis in mice by enhancing inflammatory cytokine/chemokine expression," *Arthritis and Rheumatism*, vol. 64, no. 4, pp. 1082–1088, 2012.
- [45] S. Clutter, D. Wilson, A. Marinov, and R. Hirsch, "Follistatin-like protein 1 promotes arthritis by up-regulating IFN-gamma," *Journal of immunology*, vol. 182, no. 1, pp. 234–239, 2009.
- [46] T. Miyamae, A. Marinov, D. Sowders et al., "Follistatin-like protein-1 is a novel proinflammatory molecule," *Journal of immunology*, vol. 177, no. 7, pp. 4758–4762, 2006.
- [47] Y. Chaly, Y. Fu, A. Marinov et al., "Follistatin-like protein 1 enhances NLRP3 inflammasome-mediated IL-1 β secretion from monocytes and macrophages," *European Journal of Immunology*, vol. 44, no. 5, pp. 1467–1479, 2014.
- [48] J. Guo, W. Liang, J. Li, and J. Long, "Knockdown of FSTL1 inhibits oxLDL-induced inflammation responses through the TLR4/MyD88/NF- κ B and MAPK pathway," *Biochemical and Biophysical Research Communications*, vol. 478, no. 4, pp. 1528–1533, 2016.
- [49] M. Lotz and R. Loeser, "Effects of aging on articular cartilage homeostasis," *Bone*, vol. 51, no. 2, pp. 241–248, 2012.
- [50] Y. Geng, Y. Dong, M. Yu et al., "Follistatin-like 1 (*Fstl1*) is a bone morphogenetic protein (BMP) 4 signaling antagonist in controlling mouse lung development," *Proceedings of the National Academy of Sciences of the United States of America*, vol. 108, no. 17, pp. 7058–7063, 2011.
- [51] J. Li, L. Cheng, Y. Zhao et al., "ADAMTS-7 exhibits elevated expression in cartilage of osteonecrosis of femoral head and has a positive correlation with TNF- α and NF- κ B P65," *Mediators of Inflammation*, vol. 2015, 10 pages, 2015.
- [52] S. Fukuta, K. Miyamoto, K. Suzuki et al., "Abundance of calpain and aggrecan-cleavage products of calpain in degenerated human intervertebral discs," *Osteoarthritis and Cartilage*, vol. 19, no. 10, pp. 1254–1262, 2011.
- [53] S. Gu, X. Li, J. Hamilton et al., "MicroRNA-146a reduces IL-1 dependent inflammatory responses in the intervertebral disc," *Gene*, vol. 555, no. 2, pp. 80–87, 2015.
- [54] J. Wei, W. Fu, A. Hettinghouse, W. He, K. Lipson, and C. Liu, "Role of ADAMTS-12 in protecting against inflammatory arthritis in mice by interacting with and inactivating proinflammatory connective tissue growth factor," *Arthritis & rheumatology*, vol. 70, no. 11, pp. 1745–1756, 2018.
- [55] J. Wei, W. Fu, Y. Ding et al., "Progranulin derivative Atsttrin protects against early osteoarthritis in mouse and rat models," *Arthritis Research & Therapy*, vol. 19, no. 1, p. 280, 2017.
- [56] H. Ding, J. Wei, Y. Zhao, Y. Liu, L. Liu, and L. Cheng, "Progranulin derived engineered protein Atsttrin suppresses TNF- α mediated inflammation in intervertebral disc degenerative disease," *Oncotarget*, vol. 8, no. 65, pp. 109692–109702, 2017.
- [57] H. Li, D. Wang, Y. Yuan, and J. Min, "New insights on the MMP-13 regulatory network in the pathogenesis of early osteoarthritis," *Arthritis Research & Therapy*, vol. 19, no. 1, p. 248, 2017.
- [58] Y. Zhao, Q. Tian, S. Frenkel, and C. Liu, "The promotion of bone healing by progranulin, a downstream molecule of BMP-2, through interacting with TNF/TNFR signaling," *Bio-materials*, vol. 34, no. 27, pp. 6412–6421, 2013.
- [59] J. Chen, B. Ni, B. Li, Y. Yang, S. Jiang, and L. Jiang, "The responses of autophagy and apoptosis to oxidative stress in nucleus pulposus cells: implications for disc degeneration," *Cellular Physiology and Biochemistry: International Journal of Experimental Cellular Physiology, Biochemistry, and Pharmacology*, vol. 34, no. 4, pp. 1175–1189, 2014.
- [60] H. Zhang, X. Kong, J. Kang et al., "Oxidative stress induces parallel autophagy and mitochondria dysfunction in human glioma U251 cells," *Toxicological sciences: an official journal of the Society of Toxicology*, vol. 110, no. 2, pp. 376–388, 2009.
- [61] S. Wang, B. Sarriá, R. Mateos, L. Goya, and L. Bravo-Clemente, "TNF- α -induced oxidative stress and endothelial dysfunction in EA.hy926 cells is prevented by mate and green coffee extracts, 5-caffeoylquinic acid and its microbial metabolite,

- dihydrocaffeic acid,” *International Journal of Food Sciences and Nutrition*, vol. 70, no. 3, pp. 267–284, 2019.
- [62] M. Cunningham, A. Jayaram, E. Deer et al., “Tumor necrosis factor alpha (TNF- α) blockade improves natural killer cell (NK) activation, hypertension, and mitochondrial oxidative stress in a preclinical rat model of preeclampsia,” *Hypertension in Pregnancy*, pp. 1–6, 2020.
- [63] Y. Han, M. Si, Y. Zhao et al., “Progranulin protects against osteonecrosis of the femoral head by activating ERK1/2 pathway,” *Inflammation*, vol. 40, no. 3, pp. 946–955, 2017.
- [64] W. Chen, J. Xia, P. Hu et al., “Follistatin-like 1 protects cardiomyoblasts from injury induced by sodium nitroprusside through modulating Akt and Smad1/5/9 signaling,” *Biochemical and Biophysical Research Communications*, vol. 469, no. 3, pp. 418–423, 2016.

Research Article

The Role of Unfolded Protein Response in Human Intervertebral Disc Degeneration: Perk and IRE1- α as Two Potential Therapeutic Targets

Tianyong Wen ¹, Peng Xue,² Jinwei Ying,¹ Shi Cheng,¹ Yue Liu,¹ and Dike Ruan ¹

¹Department of Orthopedic Surgery, Sixth Medical Center, Chinese PLA General Hospital, Beijing, China

²Institute of Stomatology, First Medical Center, Chinese PLA General Hospital, Beijing, China

Correspondence should be addressed to Dike Ruan; ruandikengh@163.com

Received 9 July 2020; Revised 4 February 2021; Accepted 27 February 2021; Published 25 March 2021

Academic Editor: Wenyan Ding

Copyright © 2021 Tianyong Wen et al. This is an open access article distributed under the Creative Commons Attribution License, which permits unrestricted use, distribution, and reproduction in any medium, provided the original work is properly cited.

Inflammation plays a key role in intervertebral disc degeneration (IDD). The association between inflammation and endoplasmic reticulum (ER) stress has been observed in many diseases. However, whether ER stress plays an important role in IDD remains unclear. Therefore, this study is aimed at investigating the expression of ER stress in IDD and at exploring the underlying mechanisms of IDD, ER stress, and inflammation. The expression of ER stress was activated in nucleus pulposus cells from patients who had IDD (D-NPCs) compared with patients without IDD (N-NPCs); and both the proliferation and synthesis capacity were decreased by inducer tunicamycin (Tm) and proinflammatory cytokines. Pretreatment of NPCs with 4-phenyl butyric acid (4-PBA) prevented the inflammatory cytokine-induced upregulation of unfolded protein response- (UPR-) related proteins and recovered cell synthetic ability. Furthermore, proinflammatory cytokine treatment significantly upregulated the expression of inositol-requiring protein 1 (IRE1- α) and protein kinase RNA-like ER kinase (PERK), but not activating transcription factor 6 (ATF6). Finally, knockdown of IRE1- α and PERK also restored the biological activity of NPCs. Our findings identified that IRE1- α and PERK might be the potential targets for IDD treatment, which may help illustrate the underlying mechanism of ER stress in IDD.

1. Introduction

Low back pain (LBP) is a common disease, which may result in patients' disability and cause great economic burden to society [1]. Intervertebral disc degeneration (IDD) has been verified as a key factor for LBP [2]. Intervertebral disc (IVD) maintains homeostasis in physiological condition and degeneration can be triggered by several risk factors, such as abnormal mechanical stress, nutrient deficient, and aberrant inflammatory condition [3].

More importantly, inflammation is also considered an important contribution to IDD [4]. Inflammatory cytokines are significantly associated with the progression of IDD [5–7]. Furthermore, nucleus pulposus cells (NPCs) play an important role in maintaining nucleus pulposus (NP) tissue homeostasis, thereby facilitating the maintenance of spine biomechanics [8].

Therefore, the inflammatory microenvironment of IDD may have influence on the biological behaviors of NPCs.

The endoplasmic reticulum (ER) is responsible for folding and maturation of secreted and membrane proteins. Accumulation misfolded or unfolded proteins can compromise ER stress [9]. Restoring the normal function of ER can be achieved by the unfolded protein response (UPR), which involves three pathways—protein kinase RNA-like ER kinase (PERK), inositol-requiring protein 1 (IRE1- α), and activating transcription factor 6 (ATF6) [10]. Our previous studies demonstrated that chronic inflammation could lead to impairment of ER function, prolongation of ER stress, and defective osteogenic differentiation of PDLSCs [11]. However, there are rare studies reporting the role of ER stress and UPR in biological activity of human NPCs under inflammatory conditions in IDD.

TABLE 1: Details of samples and patients.

Case no.	Diagnosis	Disc level	Pfirrmann's grade	Gender	Age
1	Disc herniation	L4-5	II	M	33
2	Disc herniation	L4-5	IV	M	52
3	Disc herniation	L4-5	V	F	34
4	Disc herniation	L4-5, L5-S1	V	M	22
5	Vertebral fracture	L3-4	II	F	43
6	Disc herniation	L4-5	IV	M	17
7	Lumbar stenosis	L3-4	IV	M	50
8	Disc herniation	L4-5	II	M	28
9	Scoliosis	L1-2	I	F	21

In this study, we used two prominent proinflammatory cytokines (IL-1 β and TNF- α) involved in IDD, aiming to mimic the inflammatory microenvironment. We isolated human nondegenerated NPCs (N-NPCs) and degenerated NPCs (D-NPCs) and observed the ER stress responses from both morphology and molecular biology level. We also tested the effects of IL-1 β and TNF- α treatment on ER stress responses as well as biological activity potential.

2. Materials and Methods

2.1. Specimen Selection. Human NP tissues were obtained from 9 patients who underwent posterior discectomy for lumbar degenerative disease or other lumbar diseases (spine fracture, scoliosis, etc.). The details of all samples and patients are shown in Table 1. The NP tissues were sterilely stored in PBS solution. All surgical treatments were performed at the sixth medical center of PLA General Hospital (Navy General Hospital) from January 2016 to June 2017.

MRI was performed in all patients before surgery, and the degree of disc degeneration was assessed according to Pfirrmann's grading system based on T2-weighted MRI images [12]. Degenerated NPCs (D-NPCs) were isolated from the intervertebral disc classified as grade IV-V, while nondegenerated NPCs (N-NPCs) were isolated from the intervertebral disc classified as grade I-II.

The present study was approved by the medical ethics committee of PLA General Hospital (Navy General Hospital). Specific informed consent was obtained in all cases.

2.2. Cell Isolation and Culture. NP cells were isolated as described by Chelberg et al. [13]. Briefly, NP tissues were digested with 0.1% type II collagenase (Sigma-Aldrich, USA) in a serum-free medium overnight at 37°C with 5% CO₂. The cells were cultured in a culture medium composed of DMEM/F12 (HyClone, USA) and 10% FBS for 7-10 days until confluent. To preserve the NPCs phenotype, primary cells were used when comparing expression levels in N-NPCs and D-NPCs, and the 1st and 2nd passages for other experiments.

ER stress response was triggered by 500 ng/ml tunicamycin (Tm) in DMEM containing 10% FBS for 12 hours. Our previous study showed that tunicamycin is more effective than thapsigargin (Peng Xue et al., Cell Death and Differentiation. 2016); thus, we chose TM as an ERs inducer. We

tested the basal activation of the ER stress response by detection the main sensors (GRP78, CHOP, IRE-1 α , PERK, and ATF6) on mRNA and protein levels.

A concentration of 5 ng/ml TNF- α and 1 ng/ml IL-1 β was determined to efficiently simulate inflammatory microenvironment, and N-NPCs were treated with IL-1 β and TNF- α in DMEM containing 10% FBS for 12 hrs. In another group, N-NPCs were pretreated by inhibitor 4-PBA (5 mmol/l) for 24 hrs, then treated with IL-1 β and TNF- α as above. All Tm, 4-PBA, IL-1 β , and TNF- α were purchased from Sigma-Aldrich, USA.

2.3. Transfection with Small Interfering RNA (siRNA). To inhibit target genes expression, cells were transfected with PERK, IRE1, and ATF6 siRNA (Cell Signaling Technology, USA) conjugated with Lipofectamine 3000 (Invitrogen, USA) for 6 hrs. The cells were incubated at 37°C in an incubator for 24-48 h before further assay.

2.4. Transmission Electron Microscope (TEM). After fixing in 4% glutaraldehyde and 4% paraformaldehyde (Sigma, both fix at Transives were diluted in phosphate buffered saline, pH7.2) for one night, the NP tissue was postfixed in 2% osmium tetroxide and block-stained with 2% uranyl acetate, then dehydrated in a graded ethanol series, and embedded in situ in a LX-812 resin (Ladd Research Industries Inc., USA). Ultrathin sections were observed by a FEI Tecnai G12 Spirit BioTwin transmission electron microscope (FEI Company, USA) with an accelerating voltage of 100 kV. The digital images were captured by a CCD camera (Olympus-SIS, Germany).

2.5. Immunohistochemical (IHC) Analysis. The fragment of NP tissue was fixed in paraformaldehyde (4%), and paraffin sections (4 μ m thick) were prepared. IHC was performed using the Histostain Plus kit (Origin Technologies, China) with the anti-PERK, IRE1- α , and ATF6 antibody (Abcam, 1:500) at 4°C overnight. The sections were treated with 1% hyaluronidase for 60 min at 37°C (IRE1- α only), 0.25 units/ml protease-free chondroitinase ABC in 0.1 mol/l Tris acetate, 0.3% Triton for 30 min, and 3% H₂O₂ for 15 min at room temperature. The primary antibodies were diluted in goat serum and incubated overnight at 4°C. The primary antibodies were all rabbit anti-human against

IRE1- α (monoclonal IgG 1/50; Cell Signaling Technology), PERK (monoclonal IgG 1/100; Cell Signaling Technology), and ATF6 (polyclonal IgG 1/100; Abcam). Detection was conducted using a DAB Horseradish Peroxidase Color Development kit (Origin Technologies, China).

2.6. Cell Proliferation. Cell proliferation of the 1st passage (P1) of N-NPCs, cells treated by TM, or inflammatory cytokines were evaluated using CCK-8 (Dojindo Laboratories, Japan). Briefly, 10 μ l of CCK-8 solution was added to each well of a 96-well plate containing 5000 cells. After incubating the plate at 37°C for 4 hrs, absorbance at 450 nm was measured using a microplate absorbance reader (Bio-Rad, USA). Cell proliferation was tested on days 1 to 7.

2.7. Quantification of mRNA and RT-PCR. The total RNA of every sample was extracted using the RNeasy mini kit (Qiagen GmbH, Germany) and converted to cDNA using Prime Script RT Master Mix (Takara Bio, Japan). RT-PCR was performed on real-time PCR (ABI PRISM 7000, USA), using the SYBR Green Master Mix reagent (Applied Biosystems, USA). The specific primers used for ER stress genes are shown in Table 2. GAPDH expression was used to normalize the expression of all genes. The relative expression levels of each gene were determined using the $2^{-\Delta\Delta Ct}$ method.

2.8. Western Blotting. Total protein of every sample was extracted using the radioimmunoprecipitation assay lysis buffer (Beyotime Institute of Biotechnology, China). Each sample was subjected to SDS-PAGE on a 10% gel and transferred to PVDF membranes. The membranes were blocked with 5% nonfat dry milk for 1 h at room temperature and then incubated with anti- β -actin (1/2000; Abcam), anti-grp78 (1/1000; Abcam), anti-PERK (1/1000; Cell Signaling Technology), anti-ATF6 (1:1000), anti-IRE1- α (1/1000; Cell Signaling Technology), anti-CHOP (1/1000; Abcam), anti-ColII (1/1000; Abcam), anti-Agg (1/1000; Abcam), and anti-Sox9 (1/1000; Abcam), at 4°C overnight. Then the membranes were incubated with the appropriate HRP-conjugated secondary antibody (1/2000) for 1 hr at room temperature, and signals were visualized using an enhanced chemiluminescence kit. Bands were detected and assessed through densitometric analysis.

2.9. Statistical Analysis. All quantitative data were presented as means \pm standard deviation. The histological and western blot data are described qualitatively and shown as images. The values between the two groups were calculated by independent two-tailed unpaired Student's *t*-test, and the values between multiple comparisons were assessed with analysis of variance (ANOVA) with the Bonferroni correction. All statistical analyses were performed using Graph Pad Prism 5.0 (GraphPad Software, USA), and *P*-values less than 0.05 were considered statistically significant.

3. Results

3.1. Activation of ER Stress and UPR Target Genes in D-NPCs Isolated from Degenerative Microenvironment. We isolated D-NPCs and N-NPCs. To investigate whether ER stress

TABLE 2: Sequences of primers used in real-time RT-PCR.

Gene	Primer sequences(5'-3')
PERK	Forward: GTCCGGAACCAGACGATGAG Reverse: GGCTGGATGACACCAAGGAA
ATF6	Forward: CGGAGTATTTTGTCCGCCTG Reverse: GCTGCTTCCAATTGCAGCTC
IRE1- α	Forward: CCTAGTCAGTTCTGCGTCCG Reverse: TTCCATCCAGCGTTGACACA
GRP78	Forward: TCAAGTCTTGTCCGTTCAAGG Reverse: AAATAAGCCTCAGCGTTTCTT
CHOP	Forward: CAAGAGTCTCTGTTTCAGATGA Reverse: TCTGTTTCCGTTTCTGTTTC

was induced in D-NPCs, we used TEM analysis to observe the endoplasmic reticulum. Our results showed that more dilated and abundant ER were observed in D-NPCs (Figure 1(a)). Next, validation by RT-PCR was performed for the representatives of the UPR target genes *PERK* (also called *EIF2AK3*), *GRP78* (*HSPA5/B*), and *CHOP* (*DDIT3*). The results of PCR indicated that the expression of UPR target genes was increased in D-NPCs compared to N-NPCs. Furthermore, we looked at whether the expression of UPR target genes was reflected in protein production by western blotting assay. The results shown in Figure 1(c) indicate that the UPR target genes expressions were upregulated in D-NPCs, indicating that degeneration may induce ER stress and subsequently produce UPR in NPCs.

3.2. UPR Activation Leads to the Decreased Biological Activity of NPCs. Since the chronic inflammation activates UPR response as well as impairs the biological activity of NPCs in IDD, we want to know whether activated UPR also leads to the impaired biological activity of NPCs. Then, we treated NPCs with UPR inducer, tunicamycin (Tm) for 12 hrs. The greatest increase of expression was observed in *GRP78*, *IRE1- α* , and *CHOP*, and increased expression was also noted with *PERK* and *ATF6* (Figure 2(a)). Western blot also indicated that the three main branches of UPR, PERK, IRE1- α , and ATF6 expression significantly increased, as well as *GRP78* and *CHOP* (Figure 2(b)). As to proliferation capacity assay, similar growth tendencies were observed in both groups. According to the OD values, a continuous increase was observed from days 1 to 7, and a little decrease was formed at day 5 in the TM group. However, a significant higher proliferation capacity was found in the control group at the last 3 time points (Figure 2(c)).

Our previous study showed defective biological activity of D-NPCs [14]. To know whether activated ER stress results in synthetic impairment of NPCs, we tested the biological activity of N-NPCs treated by Tm for 12 hrs. Increased UPR may contribute to a decrease in Aggrecan (Agg), Collagen II (Col2), and Sox9 after 24 hrs of induction (Figure 2(d)). These results indicate that strong responsiveness to acute ER stress could be observed in NPCs, which could have an influence on biological activity.

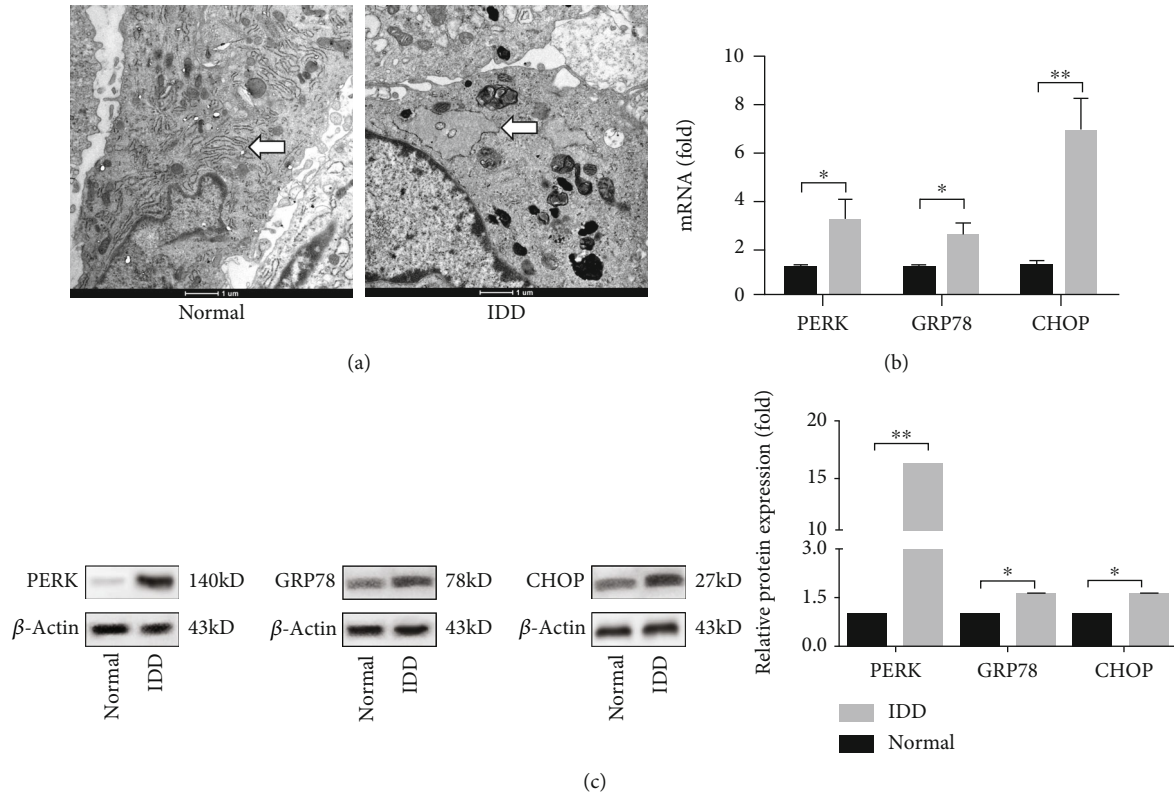


FIGURE 1: Activation of the UPR target genes in degenerated NPCs. (a) Transmission electron microscopy (TEM) images of endoplasmic reticulum (ER) in N-NPCs and D-NPCs. The morphology of ERs was showed with white arrows. The results showed more dilated and abundant ERs in D-NPCs. (b) The expressions of the UPR target genes (PERK, GRP78, and CHOP) in N-NPCs and D-NPCs were determined by real-time PCR. The results were normalized to GAPDH mRNA expression. (c) Western blot analysis showed the protein levels of PERK, GRP78, and CHOP in N-NPCs and D-NPCs. β -Actin was used as an internal control. The representative results were from three independent experiments. The error bars represent the SD from the mean values. * $P < 0.05$, ** $P < 0.01$.

3.3. Inflammation Triggers UPR and Impairs Biological Activity of NPCs. To know whether inflammatory stimulation induces UPR in NPCs, we used IL-1 β and TNF- α , which were found highly expressed in NPCs in IDD patients [14], to treat N-NPCs and observe the UPR in the cells. However, after the 12 hrs stimulation of IL-1 β and TNF- α synergistically, our results showed that the expressions of GRP78, PERK, IRE1- α , and CHOP were increased. Then, we pre-treated NPCs with an UPR inhibitor 4-PBA for 24 hrs, while GRP78, PERK, IRE1- α , and CHOP of D-NPCs were decreased after the 4-PBA treatment, but the expression of ATF6 was similar in all the three groups (Figure 3(a)). The western blot had similar results, indicating that PERK and IRE1- α expression in the inflammatory response are upregulated in D-NPCs; however, the ATF6 expression was similar (Figure 3(b)).

Regarding the proliferation capacity, similar growth tendencies were observed in all the three groups. A continuous increase was observed from days 1 to 7, which was similar with the CCK8 results of the TM-treated group (Figure 2(c)). However, a slightly higher proliferation capacity was found in IL-1 β , TNF- α , and 4-PBA groups at the last 2 time points (Figure 3(c)).

Next, IL-1 β and TNF- α were used to treat NPCs synergistically in biological activity. Western blot showed that

Agg, Col2, and Sox9 were decreased. However, the biological activity of N-NPCs was rescued after 4-PBA treatment, since the synthetic marker proteins were recovered (Figure 3(d)).

Taken together, these results indicate that the ER stress response is not globally or fully activated in the inflammatory environment of NPCs.

3.4. UPR Activation Regulates Biological Activity of NPCs through PERK and IRE1- α Pathways. The basal activation status of the three main branches of UPR was monitored in D-NPCs. The presence of PERK, IRE1- α , and ATF6 was determined by immunohistochemical (IHC) in nondegenerated and degenerated NP tissues. The presence of PERK and IRE1- α was determined by IHC in D-NPCs, whereas ATF6 was similar in both N-NPCs and D-NPCs (Figure 4(a)).

In order to know whether impaired biological activity of NPCs is affected by PERK and IRE1- α pathway in chronic inflammatory microenvironment, we used siRNAs to knockdown three sensors of ER stress, respectively, and observed the biological activity of N-NPCs. The results showed decreased expressions of PERK, IRE1- α , and ATF6 by real-time PCR (Figure 4(b)). We found that the synthesis proteins of Agg, Col2, and Sox9 were significantly increased in PERK and IRE1- α siRNA-transfected D-NPCs, respectively, compared with the controlled group caused by IL-1 β

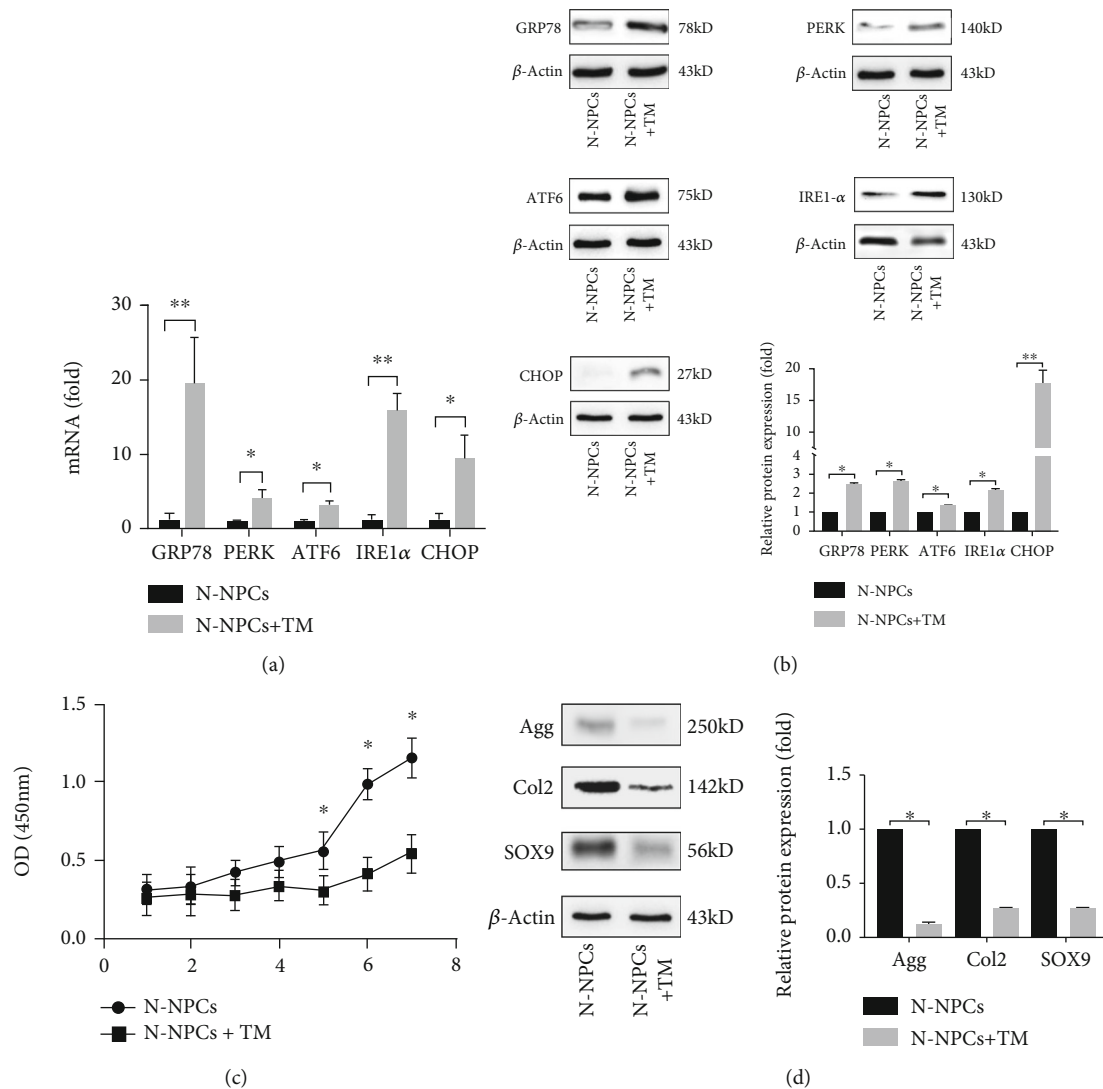


FIGURE 2: UPR activation leads to the decreased biological activity of NPCs. The expression of UPR genes in NPCs treated by Tm was analyzed by real-time PCR (a) and western blot (b). (c) Cell proliferation was evaluated by the CCK-8 assay at days 1 to 7 after TM treatment. (d) The expression of Agg, Col2, and SOX9 following the exposure of NPCs to Tm was confirmed by western blot. β -Actin was used as an internal control. The representative results were from three independent experiments. The error bars represent the SD from the mean values. * $P < 0.05$, ** $P < 0.01$.

and TNF- α treatment. However, the biological activity of NPCs was not rescued after the transfection with ATF6 siRNA (Figure 4(c)).

As described above, we demonstrate that ER stress regulates biological activity of NPCs through PERK and IRE1- α pathway.

4. Discussion

In this study, we uncovered a previously unrecognized link between the UPR pathway and IDD. For the first time, we report that inflammatory factors activate the UPR sensors (PERK, IRE1- α) and then impair the biological activity of NP cells, as summarized in the Graphical Abstract. According to our data, when the two pathways were blocked, the cell function can be recovered. The results indicated PERK

and IRE1- α may be the important mediators of UPR and IDD.

IDD is a degenerative status of spine with aging, which mainly starts from nucleus pulposus. Loss of NPCs and decrease of protein synthesis could result in the degradation of ECM and break the homeostasis in IVD [15], which would cause discogenic low back pain, disc herniation, etc. Despite the increasing prevalence of IDD-related diseases and consequently high economic burden, both conservative and surgical treatments mainly focus on the relief of pain and reconstruction of stability, not on the etiology of degeneration. Current studies explore new strategies for restoring the function and homeostasis of degenerated discs via inhibition of inflammation, prevention of premature aging, and improvement of the ECM content [2].

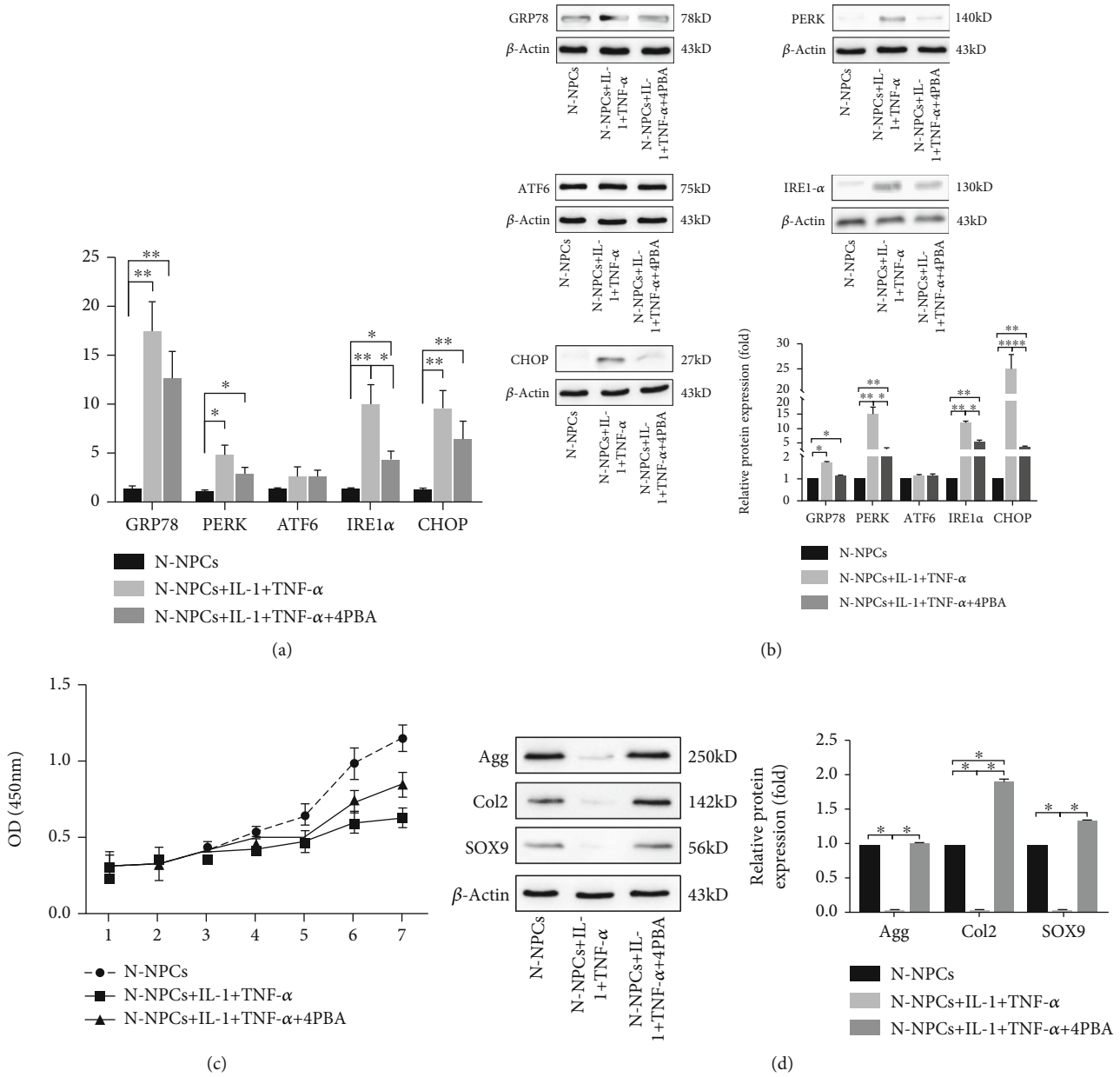


FIGURE 3: Inflammation triggers UPR and impairs biological activity of NPCs. The expression of UPR gene in NPCs treated by IL-1 and TNF-α synergistically without/with 4-PBA was analyzed by real-time PCR (a) and western blot (b). (c) Cell proliferation was evaluated by the CCK-8 assay at days 1 to 7 after IL-1 and TNF-α synergistically without/with 4-PBA treatment. (d) The expression of Agg, Col2, and SOX9 following the exposure of NPCs to IL-1 and TNF-α synergistically without/with 4-PBA was confirmed by western blot analysis. β-Actin was used as an internal control. The representative results were from three independent experiments. The error bars represent the SD from the mean values. **P* < 0.05, ***P* < 0.01.

Increasing attention has been paid on the research of inflammatory reactions in NPCs, though several factors have been found to play a key role in degeneration of NPCs [16, 17]. ER stress is an identified subcellular pathological process, which has been found participating in many chronic inflammatory diseases (such as rheumatoid arthritis and diabetes) [18, 19]. The UPR is a following response to ER stress, serving to compromise the stress that results from the presence of misfolded proteins in an attempt to restore homeostasis. It is activated via three pathways: PERK, IRE1-α, and ATF6 [20]. Therefore, we speculated that there may be a relationship between IDD and UPR. Similar with IDD which begins with cell degeneration, osteoarthritis (OA) is a progressive disease of the joints resulting in the degeneration of articular cartilage. Some studies showed the expression of some UPR genes had been investigated in OA chondrocytes. A study showed that chondrocytes from human OA cartilage displayed ER stress and that ER stress and apoptosis were increased during the progression of OA. The authors found XBP1 mRNA splicing, which represented a protective ER stress response, increased in moderate OA cartilage, but not in mild or severe cartilage [21]. However, one research

relationship between IDD and UPR. Similar with IDD which begins with cell degeneration, osteoarthritis (OA) is a progressive disease of the joints resulting in the degeneration of articular cartilage. Some studies showed the expression of some UPR genes had been investigated in OA chondrocytes. A study showed that chondrocytes from human OA cartilage displayed ER stress and that ER stress and apoptosis were increased during the progression of OA. The authors found XBP1 mRNA splicing, which represented a protective ER stress response, increased in moderate OA cartilage, but not in mild or severe cartilage [21]. However, one research

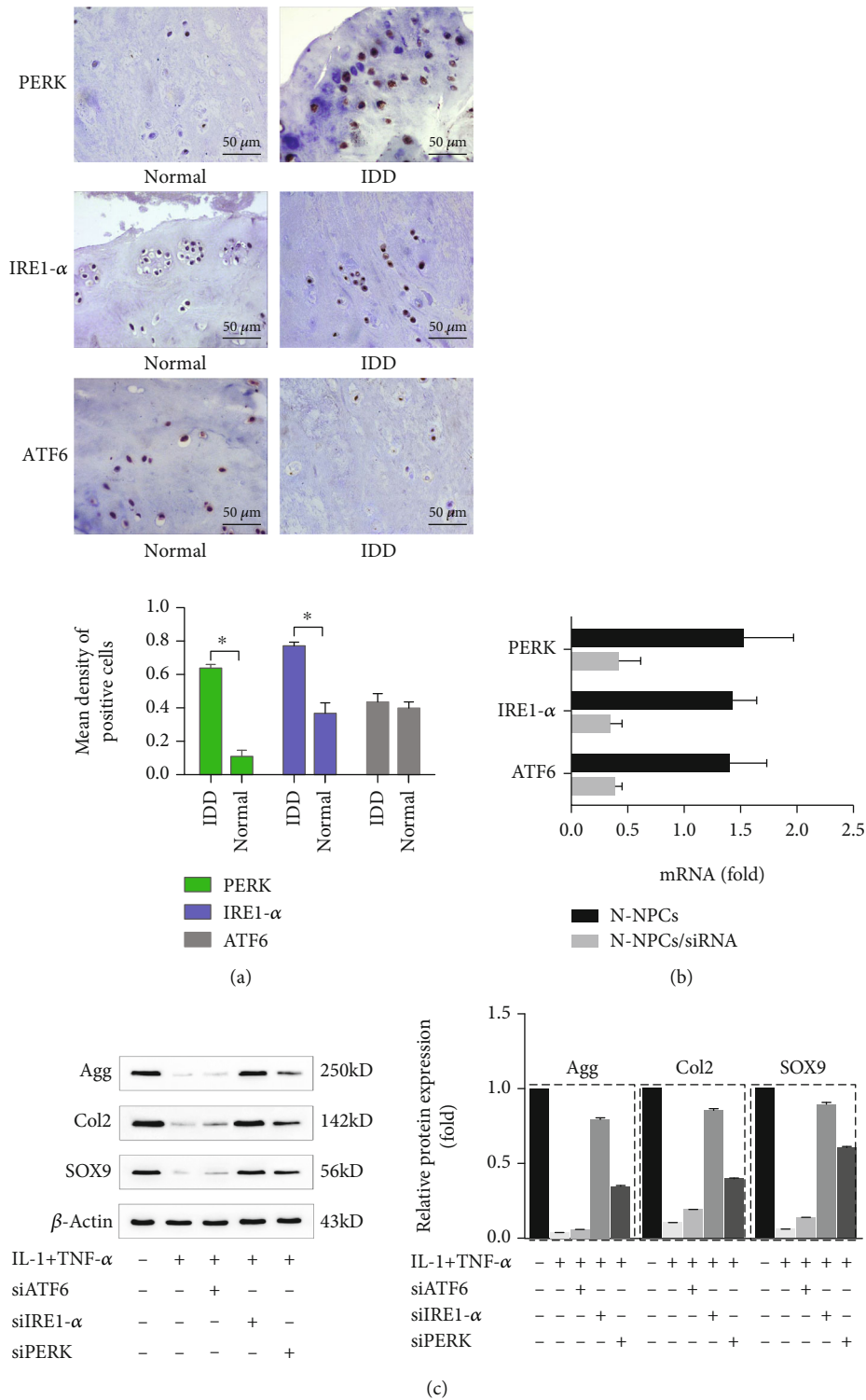


FIGURE 4: UPR activation regulated the synthesis of NPCs through the PERK and IRE1- α pathways. (a) The expression of PERK, ATF6, and IRE1- α proteins in degenerated and nondegenerated NP tissues was detected by IHC. Representative images are presented at the indicated magnifications. Scale bar, 50 μ m. Compared with the controlled group, the presence of PERK and IRE1- α was significantly increased in degenerated tissues, whereas ATF6 was similar. (b) The expression of ATF6, IRE1- α , and PERK was downregulated after being transfected with PERK, ATF6, and IRE1- α siRNA as assayed by real-time PCR. (c) The expression of Agg, Col2, and SOX9 was significantly increased after knockdown of PERK and IRE1- α than ATF6 as assessed by western blot. β -Actin was used as an internal control. The representative results were from three independent experiments. The error bars represent the SD from the mean values.

demonstrated that the level of ER stress is not significantly increased in OA chondrocytes [22]. But in their results, downregulating PERK expression increased COL1a1 and suppressed COL2a1 expression which impacted ECM of cartilage. Another study reported the intracellular accumulation of AGE-induced chondrocytes apoptosis via ER stress [23]. However, few investigations have identified the relationship between ER stress and the degeneration of NPCs. A study reported disc cell apoptosis mediated simultaneously by ER and mitochondria played a potent role in IDD, but no more further molecular results about UPR were presented [24]. In our present research, we found the level of ER stress in D-NPCs is obviously higher than N-NPCs. The morphology of ER also showed more dilated and abundant in D-NPCs by TEM. Then, we activated the ER stress and found the proliferation and synthesis of NPCs all declined. These findings indicate the ER stress may participate in the process of IDD.

IL-1 β and TNF- α are the classical primary proinflammatory cytokines of IDD; and their progression plays a role in the inhibition of anabolic process and proliferation required for IVD maintenance [16, 25, 26]. In this study, we combined IL-1 β and TNF- α to stimulate the inflammatory status in vitro and also demonstrated that IL-1 β and TNF- α inhibited the NPCs proliferation and synthesis. Meanwhile, the UPR was activated. When the ER stress inhibitor 4-PBA was added to the proinflammatory factor-treated cells, the biological activity partially recovered. These evidences further illustrated the inflammatory environment induced IDD via ER stress.

The results of RT-PCR and Western blot indicated that (1) the signaling pathways of UPR had been activated partially and (2) the mRNA and protein level of IRE1- α and PERK are significantly higher than the controlled group, which were consistent with the IHC in the IDD tissues from patients. All those findings indicated that IL-1 β and TNF- α affected the biological activity of NPCs through the PERK and IRE1- α pathways. To confirm this opinion, we used the gene-silencing technique to block the UPR pathway separately and found the silence of PERK and IRE1- α caused the upregulation of synthesis activity, especially the silence of IRE1- α . These results accorded with another research of OA [22]. However, as reported in other diseases, PERK and IRE1- α played dual roles depending on whether they were activated by physiological factors or by ER stress, and the cellular responses were different depending on the stimulating factors [27, 28].

In conclusion, we found the ER stress was activated in degenerated IDD. The cell biological activity of NPCs can be partly preserved by the block of the two UPR pathways when treated by TNF- α and IL-1, which indicated inflammation may induce IDD by the PERK and IRE1- α pathways. Our study identifies the two pathways as the potential target for molecular therapeutics of IDD.

Data Availability

All data generated or analyzed during this study are included in this article.

Conflicts of Interest

The authors declare that they have no conflicts of interest.

Authors' Contributions

Tianyong Wen and Peng Xue were involved in the practical achievement of the experiments and contributed equally to this study; Yue Liu conducted qRT-PCR and western blot assays; Tianyong Wen, Jinwei Ying, and Shi Cheng collected, analyzed, and interpreted the data; Tianyong Wen and Peng Xue drafted the manuscript. Tianyong Wen and Dike Ruan conceived and designed the study. All authors read and approved the final manuscript.

Acknowledgments

This work was supported by the National Science Foundation of China (No. 81472121, No. 81700968) and the NGH Innovation Incubator Fund (CXPY201402).

References

- [1] D. I. Rubin, "Epidemiology and risk factors for spine pain," *Neurologic Clinics*, vol. 25, no. 2, pp. 353–371, 2007.
- [2] D. Sakai and S. Grad, "Advancing the cellular and molecular therapy for intervertebral disc disease," *Advanced Drug Delivery Reviews*, vol. 84, pp. 159–171, 2015.
- [3] F. Wang, F. Cai, R. Shi, X. H. Wang, and X. T. Wu, "Aging and age related stresses: a senescence mechanism of intervertebral disc degeneration," *Osteoarthritis and Cartilage*, vol. 24, no. 3, pp. 398–408, 2016.
- [4] M. V. Risbud and I. M. Shapiro, "Role of cytokines in intervertebral disc degeneration: pain and disc content," *Nature Reviews Rheumatology*, vol. 10, no. 1, pp. 44–56, 2014.
- [5] R. Maidhof, T. Jacobsen, A. Papatheodorou, and N. O. Chahine, "Inflammation induces irreversible biophysical changes in isolated nucleus pulposus cells," *PLoS One*, vol. 9, no. 6, article e99621, 2014.
- [6] C. A. Seguin, M. Bojarski, R. M. Pilliar, P. J. Roughley, and R. A. Kandel, "Differential regulation of matrix degrading enzymes in a TNF α -induced model of nucleus pulposus tissue degeneration," *Matrix Biology*, vol. 25, no. 7, pp. 409–418, 2006.
- [7] J. Wang, D. Markova, D. G. Anderson, Z. Zheng, I. M. Shapiro, and M. V. Risbud, "TNF- α and IL-1 β Promote a Disintegrin-like and Metalloprotease with Thrombospondin Type I Motif-5-mediated Aggrecan Degradation through Syndecan-4 in Intervertebral Disc," *The Journal of Biological Chemistry*, vol. 286, no. 46, pp. 39738–39749, 2011.
- [8] G. D. O'Connell, E. J. Vresilovic, and D. M. Elliott, "Human intervertebral disc internal strain in compression: the effect of disc region, loading position, and degeneration," *Journal of Orthopaedic Research*, vol. 29, no. 4, pp. 547–555, 2011.
- [9] S. W. Kang and R. S. Hegde, "Lighting up the stressed ER," *Cell*, vol. 135, no. 5, pp. 787–789, 2008.
- [10] P. Walter and D. Ron, "The unfolded protein response: from stress pathway to homeostatic regulation," *Science*, vol. 334, no. 6059, pp. 1081–1086, 2011.
- [11] P. Xue, B. Li, Y. An et al., "Decreased MORF leads to prolonged endoplasmic reticulum stress in periodontitis-

- associated chronic inflammation," *Cell Death and Differentiation*, vol. 23, no. 11, pp. 1862–1872, 2016.
- [12] I. Castro-Mateos, R. Hua, J. M. Pozo, A. Lazary, and A. F. Frangi, "Intervertebral disc classification by its degree of degeneration from T2-weighted magnetic resonance images," *European Spine Journal*, vol. 25, no. 9, pp. 2721–2727, 2016.
- [13] M. K. Chelberg, G. M. Banks, D. F. Geiger, and T. R. Oegema Jr., "Identification of heterogeneous cell populations in normal human intervertebral disc," *Journal of Anatomy*, vol. 186, pp. 43–53, 1995.
- [14] W. Li, T. Liu, L. Wu et al., "Blocking the function of inflammatory cytokines and mediators by using IL-10 and TGF- β : a potential biological immunotherapy for intervertebral disc degeneration in a beagle model," *International Journal of Molecular Sciences*, vol. 15, no. 10, pp. 17270–17283, 2014.
- [15] F. Ding, Z. W. Shao, and L. M. Xiong, "Cell death in intervertebral disc degeneration," *Apoptosis*, vol. 18, no. 7, pp. 777–785, 2013.
- [16] 1025 Walnut Street, Suite 511 College Building, Philadelphia, PA 19107, USA, Z. I. Johnson, Z. R. Schoepflin, H. Choi, I. M. Shapiro, and M. V. Risbud, "Disc in flames: roles of TNF- α and IL-1 β in intervertebral disc degeneration," *European cells & materials*, vol. 30, pp. 104–117, 2015.
- [17] P. Patil, L. J. Niedernhofer, P. D. Robbins, J. Lee, G. Sowa, and N. Vo, "Cellular senescence in intervertebral disc aging and degeneration," *Current molecular biology reports*, vol. 4, no. 4, pp. 180–190, 2018.
- [18] M. Flamment, E. Hajdich, P. Ferre, and F. Fougere, "New insights into ER stress-induced insulin resistance," *Trends in Endocrinology and Metabolism*, vol. 23, no. 8, pp. 381–390, 2012.
- [19] Q. Qiu, Z. Zheng, L. Chang et al., "Toll-like receptor-mediated IRE1 α activation as a therapeutic target for inflammatory arthritis," *The EMBO Journal*, vol. 32, no. 18, pp. 2477–2490, 2013.
- [20] M. Wang and R. J. Kaufman, "Protein misfolding in the endoplasmic reticulum as a conduit to human disease," *Nature*, vol. 529, no. 7586, pp. 326–335, 2016.
- [21] K. Takada, J. Hirose, K. Senba et al., "Enhanced apoptotic and reduced protective response in chondrocytes following endoplasmic reticulum stress in osteoarthritic cartilage," *International Journal of Experimental Pathology*, vol. 92, no. 4, pp. 232–242, 2011.
- [22] Y. H. Li, G. Tardif, D. Hum et al., "The unfolded protein response genes in human osteoarthritic chondrocytes: PERK emerges as a potential therapeutic target," *Arthritis Research & Therapy*, vol. 18, no. 1, p. 172, 2016.
- [23] S. Yamabe, J. Hirose, Y. Uehara et al., "Intracellular accumulation of advanced glycation end products induces apoptosis via endoplasmic reticulum stress in chondrocytes," *The FEBS Journal*, vol. 280, no. 7, pp. 1617–1629, 2013.
- [24] C. Q. Zhao, Y. H. Zhang, S. D. Jiang, L. S. Jiang, and L. Y. Dai, "Both endoplasmic reticulum and mitochondria are involved in disc cell apoptosis and intervertebral disc degeneration in rats," *Age (Dordrecht, Netherlands)*, vol. 32, no. 2, pp. 161–177, 2010.
- [25] K. L. Phillips, K. Cullen, N. Chiverton et al., "Potential roles of cytokines and chemokines in human intervertebral disc degeneration: interleukin-1 is a master regulator of catabolic processes," *Osteoarthritis and Cartilage*, vol. 23, no. 7, pp. 1165–1177, 2015.
- [26] D. Purmessur, B. A. Walter, P. J. Roughley, D. M. Laudier, A. C. Hecht, and J. Iatridis, "A role for TNF α in intervertebral disc degeneration: a non-recoverable catabolic shift," *Biochemical and Biophysical Research Communications*, vol. 433, no. 1, pp. 151–156, 2013.
- [27] C. Duran-Aniotz, V. H. Cornejo, S. Espinoza et al., "IRE1 signaling exacerbates Alzheimer's disease pathogenesis," *Acta Neuropathologica*, vol. 134, no. 3, article 1694, pp. 489–506, 2017.
- [28] E. Karali, S. Bellou, D. Stellas, A. Klinakis, C. Murphy, and T. Fotsis, "VEGF signals through ATF6 and PERK to promote endothelial cell survival and angiogenesis in the absence of ER stress," *Molecular Cell*, vol. 54, no. 4, pp. 559–572, 2014.

Review Article

Research Progress on the Mechanism of Lumbar Multifidus Injury and Degeneration

Xianzheng Wang ¹, Rui Jia ², Jiaqi Li,¹ Yibo Zhu,³ Huanan Liu ¹, Weijian Wang ¹,
Yapeng Sun,¹ Fei Zhang,¹ Lei Guo,¹ and Wei Zhang ¹

¹Department of Spinal Surgery, The Third Hospital of Hebei Medical University, Shijiazhuang, 050000 Hebei Province, China

²Department of Reproductive Medicine, The Second Hospital of Hebei Medical University, China

³School of Chemical Engineering, The University of Queensland, Australia

Correspondence should be addressed to Wei Zhang; zworthopedics@163.com

Received 6 October 2020; Revised 26 January 2021; Accepted 9 February 2021; Published 27 February 2021

Academic Editor: Daniele Vergara

Copyright © 2021 Xianzheng Wang et al. This is an open access article distributed under the Creative Commons Attribution License, which permits unrestricted use, distribution, and reproduction in any medium, provided the original work is properly cited.

This review summarizes recent research progress in the clinical features, image manifestations, and pathological mechanism of multifidus injury. After a brief introduction to the fiber classification, innervation, blood supply, and multifidus function, some factors of multifidus injury, consisting of denervation, intraoperative incision selection and traction, and lumbar degenerative disease are overviewed. In addition, the clinical index of multifidus injury including myoglobin, creatine kinase, IL-6, C-reactive protein, the cross-sectional area of multifidus, the degree of fat infiltration, and intraoperative biopsy are summarized. Furthermore, we recommend that patients with chronic low back pain should take the long-term exercise of lumbodorsal muscles. Finally, some remaining issues, including external fixation and the imaging quantitative evaluation criteria of multifidus, need to be further explored in the future.

1. Introduction

All around the globe, 65-85% of the population suffer from low back pain, which is highly related to lumbar degenerative disease [1, 2]. The recurrent low back pain not only brings the loss of productivity and working time but also increases the economic burden borne by the whole society [3]. Studies showed that most patients with lumbar degenerative disease had atrophy of multifidus muscle and fat infiltration [4, 5].

Multifidus is the only paraspinal lumbar muscle innervated by a single nerve root [6], which plays an important role in maintaining the stability of the spine [7]. Multifidus injury often occurs in patients with chronic low back pain, lumbar disc herniation, and scoliosis and lumbar surgery [8-10]. Multifidus injury is often manifested as atrophy and steatosis in imaging and increases inflammatory reaction [11]. In the development of lumbar degenerative diseases, the protection and treatment of multifidus need more interventions.

In this study, we try to review the anatomical structure and function of multifidus, the clinical manifestations, imaging findings, pathological mechanism, and research progress of multifidus injury; discuss the risk factors; list the clinical detection methods of multifidus injury; explore the mechanism of oxidative stress that induced multifidus injury; and finally, we summarized the recovery methods of multifidus injury, which may play a positive role in clinical work.

2. Anatomy and Function of Multifidus

Multifidus is the deep internal back muscle. It is composed of multiple muscle bundles and fills the groove on both sides of the spinous process. It is close to the innermost side of the spine and has the largest attachment area in the paravertebral muscle. The lumbar multifidus is wrapped in the muscle sheath formed by the superficial and middle layers of the thoracolumbar fascia. The Longissimus muscle, spinous

process, and lamina are on the outside, medial side, and the ventral side of the multifidus.

The multifidus muscle originates from the sacrum and the posterior superior iliac spine, the mastoid process of the lumbar spine, the transverse process of the thoracic vertebrae, and the articular process of C4-C7. It attaches to all the spinous processes of the upper vertebrae. Rosatelli et al. [12] found that L1-L4 multifidus could be divided into three layers: shallow and middle and deep layer. L5 multifidus was divided into two layers, shallow layer and deep layer. The superficial multifidus started from the L1-L5 spinous process and moved outward and downward. L1 multifidus stopped at L5, S1 mastoid, and posterior superior iliac spine; L2 multifidus stops at S1 mastoid and posterior superior iliac spine; L3 multifidus stops at S1-S3 dorsal side; L4 multifidus stops at the dorsal side of S2-S4; L5 multifidus stops at the dorsal side of S3-S4. The medial multifidus starts from the L1-L4 spinous process and ends at the L4, L5, S1 mastoid, and dorsal side of S2. The deep multifidus starts from the L1-L5 lamina and ends at the L3-S1 mastoid and sacrum.

Multifidus muscle fibers are classified as type I fibers (slow-twitch fibers), type IIa fiber (fast-twitch fiber), and type IIX fiber (fast-twitch glycolytic) [13, 14]. Type I fiber has slow contraction speed and small contraction strength, but its antifatigue ability makes it work for a long time. It possesses low ATPase activity, low maximal velocity, higher mitochondrial content, and more significant oxidative enzyme complement than the type II fiber. The aerobic capacity of type I fiber is higher than that of type II fiber. Type II fiber has short contraction latency, fast contraction speed, strong contraction, and weak force fatigue resistance. Type II fibers are endowed with higher ATPase activities and contain enzymes, which support the regeneration of ATP through anaerobic mechanisms. The size of type II muscle fiber decreased significantly with the increase of adult age, while type I muscle fiber was the opposite [15]. In the elderly, type II muscle fiber size is significantly smaller than that of young people [16]. Some studies have shown that the lumbar dorsal multifidus muscles consist of 54%–70% type I fibers and 23.6%–52.54% type II fibers [17]. The atrophy of type I fibers in the multifidus muscle can be explained by muscle fibers chronic stretch due to pain-induced spasm. Moreover, the atrophy of type II fibers was often attributed to low activity level [18].

The lumbosacral multifidus is innervated by the dorsal root of the lumbar nerve [19], which divides from the spinal nerve [20, 21] and passes through a bone fiber ring to the medial edge of the intertransverse muscles, and is divided into the medial and lateral branch. The medial branch runs backward and downward at the lateral side of the lower vertebrae, passes through the bone fiber tube, reaches the dorsal side of the lamina, and then enters the multifidus muscle. However, due to the small anatomic structure and lack of elasticity, the stenosis of for a man can oppress the lumbar nerve and cause low back pain.

The lumbosacral multifidus is supplied by the dorsal branch of the lumbar artery [22] and the lateral iliac artery. From both sides of the abdominal aorta, the lumbar artery crosses the anterior and lateral sides of the lumbar vertebral

body and accompanies the lumbar vein. It divides the dorsal branch at the medial edge of the psoas major to supply the multifidus and other dorsal muscles [23].

In paravertebral muscles, multifidus is the primary source of maintaining lumbar stability [24]. The superficial multifidus muscle crosses multiple segments, moves outward and downward from the L1-L5 spinous process, prevents the vertebral body from rotatory dislocation, and maintains lumbar physiological lordosis. The deep multifidus muscle crosses few segments and is close to the central axis, which can increase lumbar segmental tension and reduces the movement between lumbar segments [25]. Some scholars believe that when the body's centre of gravity suddenly loses balance, the multifidus will be activated in advance and contract ahead of time enhancing the stability of the lumbar spine sequence, which is called feedforward control [26, 27]. Due to the short length, large cross-sectional area, and the short reaction time of multifidus, the risk of lumbar instability can be reduced (Figure 1).

3. Factors of Multifidus Injury

3.1. Denervation. Lumbar degenerative diseases are often related to nerve injury, and most of the electromyography shows potential denervated changes. In the experiment, the multifidus muscle of pig atrophied rapidly after nerve root injury [28]. There are a lot of pathological changes in denervated multifidus: reduced diameter of muscle fiber [29] and cross-sectional area of muscle bundle [30], dissolved muscle fiber mitochondria [31], and disordered transverse tubular system. As the number of mitochondria decreased, the sodium-potassium pump activity decreased, the energy supply of the tricarboxylic acid cycle decreased, and muscle strength weakened. Also, the absence of proprioceptor in multifidus will lead to the interruption of feedforward reflex and a further decrease of spinal stability. Some scholars have pointed out [32] that asymmetric multifidus atrophy will break the biomechanical balance of the spine and cause spinal degeneration. Fortunately, Cha et al. [33] pointed out that patients with preoperative denervation of the multifidus had reinnervation of the multifidus during a 12-month follow-up after bone graft fusion, which meant that nerve recovery after the operation was possible.

3.2. Intraoperative Incision Selection and Traction. During the posterior lumbar surgery exposure process, it is inevitable that paravertebral muscles will be stripped and damaged [34]. Postoperative lumbar MRI shows that paravertebral muscles have different degrees of injury [35], accompanied by low back pain and dysfunction [36]. However, minimally invasive surgical methods can significantly reduce paravertebral muscle atrophy. Studies have shown that the paramedian approach is used to separate the multifidus and the longissimus muscle in the posterior lumbar approach. The postoperative multifidus atrophy is 4.8%, significantly less than the posterior median approach (20.7%) [37].

Posterior lumbar interbody fusion is an important cause of multifidus muscle injury and atrophy in posterior lumbar surgery [38]. Fusion and fixation of the posterior lumbar

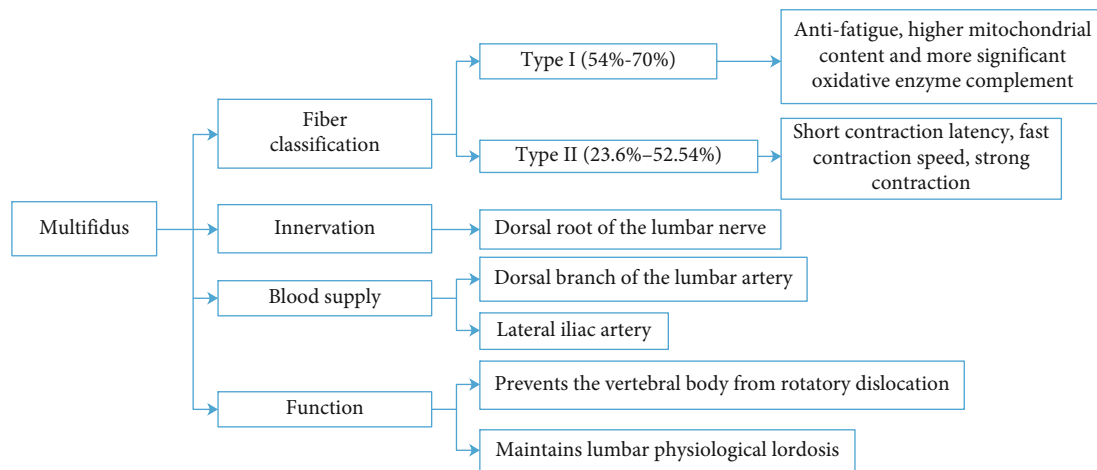


FIGURE 1: Anatomy and function of multifidus.

spine usually requires extensive anatomy and forced traction of the paravertebral muscles, which may seriously damage the structure and function of the muscles. Denervation and abandonment may be important factors of multifidus atrophy [38]. The underlying pathophysiology of muscle injury may involve mechanical and ischemic mechanisms. On the other hand, surgical related stress may trigger some protective responses in the injured paraspinal muscles. After the contraction of multifidus, the expression of heat shock protein 70 and malondialdehyde was significantly increased. Through the study of multifidus samples, Lu et al. found that the decrease of heat shock protein 70 in muscle cells after the long-term contraction resulted from severe muscle injury [39].

Kawaguchi et al. [40] pointed out that the traction of paravertebral muscles or excessive pressure on the lumbodorsal muscles during the operation will induce the injury and bleeding, and the length of the traction time also affects the degree of atrophy. Some researchers [41] suggest that the operator should perform a 5-minute stretch release every hour to avoid severe muscle injury after surgery. However, direct intraoperative injury is not the only factor for multifidus atrophy. Motosuneya et al. [42] found that although the lumbodorsal muscles of patients in the anterior lumbar interbody fusion group did not undergo surgical trauma, paravertebral muscle atrophy still occurred after surgery. It is pointed out that the use of external fixation such as waist supporter after operation leads to decreased activity of the operative segment, which is the main cause of paravertebral muscle injury in patients with anterior lumbar interbody fusion.

3.3. Lumbar Degenerative Disease. Lumbar degenerative disease is one of the causes of multifidus injury [43]. After multifidus injury, the biomechanical balance of the spine is disturbed. The frequent displacement between segments will accelerate the degeneration of the spine, which will lead to further injury of paraspinal muscles. Furthermore, if no effective intervention is taken, a vicious circle will be formed. Faur et al.'s study showed a significant correlation between

lumbar disc degeneration and fat atrophy of multifidus, and at the level of L5/S1, the percentage of multifidus atrophy was higher than other segments [30]. The causes of lumbar degenerative disease leading to multifidus atrophy can be divided into two aspects: (1) compression caused by lateral recess stenosis [44], intervertebral disc herniation, long-term local ischemia, and nerve damage leading to denervated atrophy [45]. (2) The sinuvertebral nerve compressed unilaterally causes low back pain [46], and the reduced exercise of the affected side leads to disuse atrophy of multifidus muscle. Wan et al. [47] found that the multifidus on the affected side of patients with chronic low back pain was significantly atrophied compared with the healthy side. On the contrary, Ranger et al. [48] believed a negative correlation between multifidus atrophy and chronic low back pain after 12 months of follow-up, which means the relationship between paravertebral muscles and chronic low back pain still needs to be confirmed by a higher quality cohort study.

Chronic low back pain is one of the most common and costly medical problems; very few treatments have proved effective [49, 50]. However, very few treatments have proved effective. Among the 291 diseases studied, lower back pain in Western Europe was ranked as the highest disability burden, according to the Agten et al.'s study [51]. Rahmani et al.'s study showed that pain intensity and disability index were significantly correlated with muscle size, and the multifidus muscle size of 15-18 years old male adolescents with low back pain was lower than that of healthy people [37].

4. Oxidative Stress and Inflammation of Multifidus

Oxidative stress and inflammation are two molecular mechanisms of multifidus injury and atrophy after posterior lumbar surgery (Figure 2). The molecular mechanism of muscle injury is very complex [52]. Up to now, the cellular or molecular mechanism of multifidus injury is not completely clear.

The inflammatory reaction of multifidus muscle is mostly related to IL-1 β , tumor necrosis factor, and IL-10. According to one hypothesis, increased expression of proinflammatory

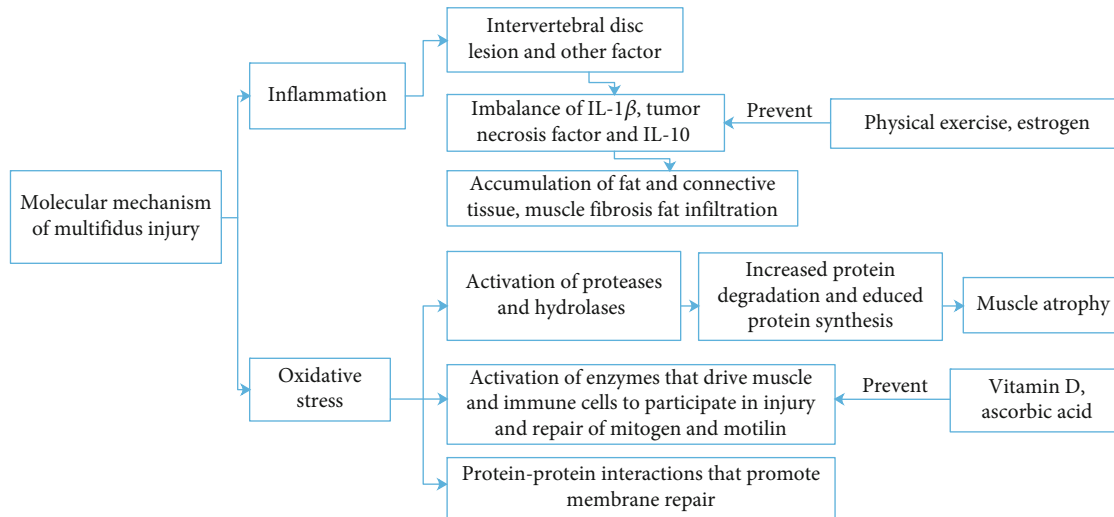


FIGURE 2: Molecular mechanism of multifidus injury. IL: interleukin.

cytokine and tumor necrosis factor- α (TNF- α) is associated with muscle atrophy. TNF- α affects myoblast differentiation and fiber degradation. TNF- α expression increased with intervertebral disc injury and affect axon conduction. Hodges et al. found that after intervertebral disc lesion, muscle fibrosis appeared and the TNF- α expression in muscle is increased [53].

James et al. [54] conducted a case-control study on mice and found that the levels of IL-1, tumor necrosis factor, IL-10, adiponectin, and leptin were lower in the sports group. The results indicated that intervertebral disc degeneration could lead to the imbalance of active inflammatory pathways in multifidus. In addition, these changes are related to the severity of intervertebral disc degeneration and can be prevented by physical exercise.

Recent animal studies [55] have found that local inflammatory dysfunction is a new mechanism to explain fat and connective tissue accumulation in multifidus muscle during disc degeneration and injury. James examined whether there were differences in the expression of inflammatory genes in multifidus between individuals with low and high intramuscular fat content to test whether there was a similar mechanism in humans. It was found that the expression of TNF in multifidus was higher in the participants with a higher degree of fat infiltration. These results support the hypothesis that intervertebral disc degeneration is associated with maladjustment of local spinous muscle inflammation.

Evidence showed that estrogen has strong antioxidant activity, which may maintain membrane stability and limit creatine kinase leakage from damaged muscles [56]. In Yang et al.'s study, estrogen protects intervertebral disc cells from apoptosis by inhibiting inflammatory cytokines IL-1 β and TNF- α [57].

For the oxidative stress process, skeletal muscle pathology is mainly attributed to muscle cell membrane damage. The injury is often related to the unregulated influx of calcium through membrane lesions, which includes (1) activation of proteases and hydrolases that cause muscle injury, (2) activation of enzymes that drive muscle and immune cells

to participate in injury and repair of mitogen and motilin, and (3) protein-protein interactions that promote membrane repair. At present, there is no specific cellular or molecular mechanism of multifidus injury [58]. In addition, the accumulation of free radicals caused by damage stimulation can also activate the proteolytic systems, thus, resulting in the increased protein degradation and reduced protein synthesis, which eventually lead to muscle atrophy [59].

Histochemical and pathological analysis of patients with idiopathic scoliosis showed necrosis, fibrosis, and fatty degeneration of paravertebral muscle. Compared with the control group, severe muscle injury and oxidative stress were increased in patients, and abnormal myogenesis was observed. The increased oxidative stress reaction can lead to muscle apoptosis and dysmyogenesis, which may be related to the pathological changes of idiopathic scoliosis and participate in the development and idiopathic scoliosis [60].

Dzik et al. [61] studied the changes in antioxidant enzyme activity and vitamin D receptor in paravertebral muscles with different serum vitamin D concentrations. Superoxide dismutase and glutathione peroxidase activities in the vitamin D deficiency group were significantly higher than those in the supplemented group. In vitamin D supplemented participants, lipid and protein-free radical damage markers were weakened, and the patients with high serum vitamin D concentration had stronger antioxidant capacity.

In another study [62], researchers found that vitamin D deficiency causes muscle atrophy. Vitamin D deficiency is associated with increased oxidative stress, muscle atrophy, and decreased mitochondrial function in multifidus muscle, leading to worse recovery after surgery in patients with vitamin D deficiency.

Ascorbic acid may protect multifidus muscle after operation. Tang et al. assessed the inflammation, steatosis, and fibrosis of muscle by quantitative real-time polymerase chain reaction, histological, and immunohistochemical analysis. It was found that the marker genes and scores of fibrosis and steatosis in the ascorbic acid group were significantly lower than those in the control group at 14 and 28 days after

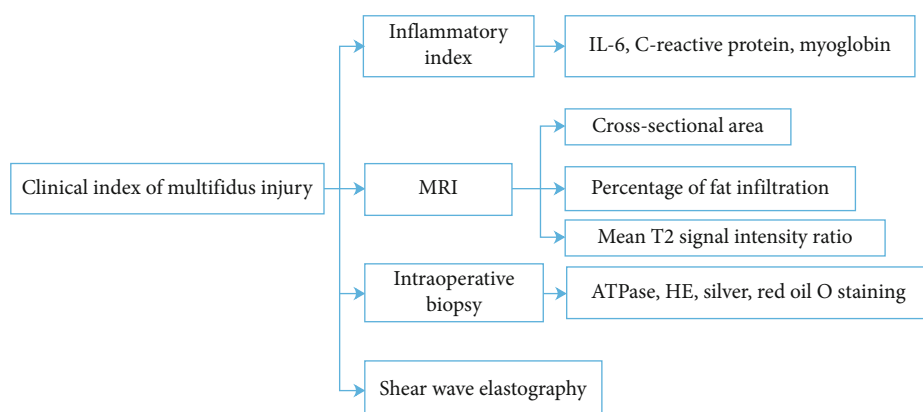


FIGURE 3: Clinical index of multifidus injury. IL: interleukin; HE: hematoxylin-eosin staining.

operation. It was suggested that ascorbic acid could reduce the oxidative stress and inflammatory reaction of multifidus muscle after operation [63].

Severe muscle degeneration, inflammation, and decreased blood vessels are commonly observed in biopsies of people with lumbar lesions compared to normative data. Active muscle degeneration suggests that muscle tissue change is more complex than simple atrophy [64].

5. Clinical Index of Multifidus Injury (Figure 3)

5.1. Inflammatory Index. Linzer et al. [11] chose myoglobin and creatine kinase levels as muscle injury indicators and IL-6 and C-reactive protein as systemic inflammatory indicators. In muscle injury-related research, all indexes were detected before and 1, 3, and 7 days after operation.

5.2. MRI. After lumbar spine surgery, MRI showed that most of the patients had fat infiltration in different degrees, and the cross-sectional area of paravertebral muscle was also decreased compared with that before operation. In Wu et al.'s study, the mean T2 signal intensity ratio of MRI increased one year after surgery [65]. The ratio of fat infiltration rate of cross-sectional area is a common index of multifidus injury. Also, Urrutia et al. [66] pointed out in the imaging study that single segment fat infiltration detection and cross-section cannot represent the degeneration of the whole lumbar spine, and multisegmental paravertebral muscle evaluation should be adopted in the study of spinal degeneration. As for multifidus fatty evaluation, Li et al. developed a measurement system for automatic segmentation of multifidus and erector spinae in MRI images based on the deep neural network [67], and Shahidi et al. used custom-written MATLAB software and two-term Gaussian model to calculate fat signal fraction [4], which avoid human factors on the calculation of fat infiltration rate.

5.3. Intraoperative Biopsy [68]. For intraoperative biopsy [69], the atrophic muscles were observed on preoperative imaging. During the operation, tissue scissors and other instruments are used to take atrophic muscles out, and the biopsy should be sent to the laboratory for the frozen section of atomized liquid immediately. HE staining [70] can be used

to observe the regularity of muscle fiber arrangement, the clarity of muscle transverse striation, and granulation tissue infiltration. After silver staining [71], the number of branches of nerve endings and the number of muscle fibers innervated by nerves could be observed. The distribution and type of muscle fibers can be observed by ATPase staining [72], and the content and distribution of lipid in tissues can be estimated by red oil O staining [73]. Wajchenberg et al. [74] detected the fat content of the samples, which can quantitatively compare the differences between the samples.

However, there is no accepted histopathological reference value in paraspinal muscle biopsy. Zimmermann et al. used histological staining and respiratory chain enzyme biochemical analysis methods to analyze biopsy of multifidus muscle in 20 healthy subjects. It was found that the staining showed incomplete myopathy characteristics, such as increased fiber size variability, type 1 hypertrophy, intramuscular fibrosis, and fat tissue replacement. The positive rate of acid phosphatase reaction was 35%, and the changes in mitochondria were obvious. According to Zimmermann et al., it is easy to be misunderstood as myopathy due to the increased variability of morphological details. The incomplete myopathy characteristics of complex I, cytochrome c oxidase, and citrate synthase and the decrease of oxidase activity should consider as normal changes when analyzing paravertebral muscles [75].

5.4. Other. In addition, shear wave elastography can evaluate muscle stiffness noninvasively [76]. Ultrasonic muscle quantification can detect the degree of muscle atrophy [77]. Airaksinen et al. evaluated lumbar muscle density by computed tomography [78].

6. Recovery of Multifidus Function

Multifidus is an important factor to maintain spinal stability. The rest after paravertebral muscle fatigue can make the activity of paravertebral muscle decrease gradually [79]. The damaged multifidus can be repaired and activated in various ways. Clinicians should guide the choice of patients' recovery mode through professional knowledge [80]. Freeman et al. [81] found that the degree of multifidus atrophy and fat infiltration decreased in patients with one-year continuous multifidus exercise. Kliziene et al. [82] found that

after eight months of core stability training, such as sit-ups, spinal bridging, and leg kick, the cross-sectional area of multifidus muscle increased by 22%. In the prospective randomized controlled study of Mannion et al. [15, 83], the isometric muscle strength, endurance, and fatigue resistance of the lumbar and dorsal muscles were significantly enhanced in patients undergoing rehabilitation exercise than those before treatment. Some experts believe that the increase of length and cross-sectional area of muscle fibers can make more nerve innervation needed after muscle training. Subsequently, new endplates will appear in large numbers to reinnervate the damaged muscles.

Besides, back stretching can improve the blood flow of lumbar muscles and effectively relieve the lower back pain related to muscle ischemia [84]. Kumamoto et al. studied the changes of oxyhemoglobin and electromyography in standing stretching exercise and found that standing stretching can improve hemodynamic performance, but excessive exercise will lead to a decrease of hemodynamic changes. Though patients with muscle ischemia should be more cautious when doing such exercises [85]. Besides that, based on taking protective measures, older adults can also benefit from exercise [86], and the inflammatory indexes of low back pain patients will decrease after exercise [87].

7. Summary

Multifidus is an indispensable link to maintain spinal stability. The long-term damage of chronic lumbar degenerative diseases and the direct damage of lumbar surgery are the main causes of multifidus injury. Oxidative stress and inflammation are two molecular mechanisms of multifidus injury and atrophy after posterior lumbar surgery. Minimally invasive spinal surgery is effective in protecting the postoperative function of multifidus muscle. To avoid further atrophy of multifidus and progressive degeneration of the lumbar spine, patients after lumbar surgery and patients with chronic low back pain should actively carry out long-term rehabilitation exercise of the lumbar muscles. At present, there are still some problems that need to be further studied. Such as how to avoid the disuse atrophy of paravertebral muscles as far as possible in the use of external fixation such as waist supporter after lumbar surgery, and the imaging quantitative evaluation criteria of multifidus atrophy need further research and discussion. Monitoring oxidative stress and vitamin D receptor protein content may help to further study the mechanism of vitamin D in the muscle recovery process.

Conflicts of Interest

The authors declare that there is no conflict of interest regarding the publication of this paper.

Authors' Contributions

Xianzheng Wang, Rui Jia, and Jiaqi Li contributed equally to this work.

References

- [1] C. J. Murray, C. Atkinson, K. Bhalla et al., "The state of US health, 1990-2010: burden of diseases, injuries, and risk factors," *JAMA*, vol. 310, no. 6, pp. 591-608, 2013.
- [2] G. B. Andersson, "Epidemiological features of chronic low-back pain," *The Lancet*, vol. 354, no. 9178, pp. 581-585, 1999.
- [3] A. L. Asher, C. J. Devin, K. R. Archer et al., "An analysis from the quality outcomes database, part 2. Predictive model for return to work after elective surgery for lumbar degenerative disease," *Journal of Neurosurgery Spine*, vol. 27, no. 4, pp. 370-381, 2017.
- [4] B. Shahidi, C. L. Parra, D. B. Berry et al., "Contribution of lumbar spine pathology and age to paraspinal muscle size and fatty infiltration," *Spine (Phila Pa 1976)*, vol. 42, no. 8, pp. 616-623, 2017.
- [5] P. W. Hodges and L. Danneels, "Changes in structure and function of the back muscles in low back pain: different time points, observations, and mechanisms," *The Journal of Orthopaedic and Sports Physical Therapy*, vol. 49, no. 6, pp. 464-476, 2019.
- [6] M. Farshad, C. Gerber, N. A. Farshad-Amacker, T. J. Dietrich, V. Laufer-Molnar, and K. Min, "Asymmetry of the multifidus muscle in lumbar radicular nerve compression," *Skeletal Radiology*, vol. 43, no. 1, pp. 49-53, 2014.
- [7] J. M. Martuscello, J. L. Nuzzo, C. D. Ashley, B. I. Campbell, J. J. Orriola, and J. M. Mayer, "Systematic review of core muscle activity during physical fitness exercises," *Journal of Strength and Conditioning Research*, vol. 27, no. 6, pp. 1684-1698, 2013.
- [8] L. Kalichman, E. Carmeli, and E. Been, "The association between imaging parameters of the paraspinal muscles, spinal degeneration, and low back pain," *BioMed Research International*, vol. 2017, Article ID 2562957, 14 pages, 2017.
- [9] X. Y. Sun, C. Kong, T. T. Zhang et al., "Correlation between multifidus muscle atrophy, spinopelvic parameters, and severity of deformity in patients with adult degenerative scoliosis: the parallelogram effect of LMA on the diagonal through the apical vertebra," *Journal of Orthopaedic Surgery and Research*, vol. 14, no. 1, p. 276, 2019.
- [10] A. Palpan Flores, P. García Feijoo, and A. Isla Guerrero, "Paraspinal muscle atrophy after posterior lumbar surgery with and without pedicle screw fixation with the classic technique," *Neurocirugia (Asturias, Spain)*, vol. 30, no. 2, pp. 69-76, 2019.
- [11] P. Linzer, M. Filip, F. Šámal et al., "Comparison of biochemical markers of muscle damage and inflammatory response between the open discectomy, microsurgical discectomy, and microsurgical discectomy using tubular retractor," *Journal of Neurological Surgery Part A: Central European Neurosurgery*, vol. 76, no. 5, pp. 384-391, 2015.
- [12] A. L. Rosatelli, K. Ravichandiran, and A. M. Agur, "Three-dimensional study of the musculotendinous architecture of lumbar multifidus and its functional implications," *Clinical Anatomy*, vol. 21, no. 6, pp. 539-546, 2008.
- [13] W. J. Evans and J. Lexell, "Human aging, muscle mass, and fiber type composition," *The Journals of Gerontology Series A, Biological Sciences and Medical Sciences*, vol. 50A, pp. 11-16, 1995.
- [14] S. Ciciliot, A. C. Rossi, K. A. Dyar, B. Blaauw, and S. Schiaffino, "Muscle type and fiber type specificity in muscle wasting," *The International Journal of Biochemistry & Cell Biology*, vol. 45, no. 10, pp. 2191-2199, 2013.



- [15] A. F. Mannion, S. Taimela, M. Müntener, and J. Dvorak, "Active therapy for chronic low back pain part 1. Effects on back muscle activation, fatigability, and strength," *Spine (Phila Pa 1976)*, vol. 26, no. 8, pp. 897–908, 2001.
- [16] R. Nilwik, T. Snijders, M. Leenders et al., "The decline in skeletal muscle mass with aging is mainly attributed to a reduction in type II muscle fiber size," *Experimental Gerontology*, vol. 48, no. 5, pp. 492–498, 2013.
- [17] B. Cagnie, F. Dhooge, C. Schumacher et al., "Fiber typing of the erector spinae and multifidus muscles in healthy controls and back pain patients: a systematic literature review," *Journal of Manipulative and Physiological Therapeutics*, vol. 38, no. 9, pp. 653–663, 2015.
- [18] J. K. Ng, C. A. Richardson, V. Kippers, and M. Parnianpour, "Relationship between muscle fiber composition and functional capacity of back muscles in healthy subjects and patients with back pain," *The Journal of Orthopaedic and Sports Physical Therapy*, vol. 27, no. 6, pp. 389–402, 1998.
- [19] K. Yaltirik, B. O. GÜdü, Y. Işık, Ç. Altunok, U. Tipi, and B. Atalay, "Volumetric muscle measurements indicate significant muscle degeneration in single-level disc herniation patients," *World Neurosurgery*, vol. 116, pp. e500–e504, 2018.
- [20] L. Leng, L. Liu, and D. Si, "Morphological anatomy of thoracolumbar nerve roots and dorsal root ganglia," *European Journal of Orthopaedic Surgery & Traumatology: Orthopedie Traumatologie*, vol. 28, no. 2, pp. 171–176, 2018.
- [21] G. Silav, M. Arslan, A. Comert et al., "Relationship of dorsal root ganglion to intervertebral foramen in lumbar region: an anatomical study and review of literature," *Journal of Neurosurgical Sciences*, vol. 60, no. 3, pp. 339–344, 2016.
- [22] Y. Tatara, H. Nasu, M. Tsutsumi, and K. Akita, "Origins, courses, and distributions of the lumbar arterial branches in relation to the spinal nerves: an anatomical study," *Spine (Phila Pa 1976)*, vol. 44, pp. E808–e814, 2019.
- [23] S. Caglar, H. Dolgun, H. C. Ugur et al., "Extraforaminal lumbar arterial anatomy," *Surgical Neurology*, vol. 61, no. 1, pp. 29–33, 2004.
- [24] H. J. Wilke, S. Wolf, L. E. Claes, M. Arand, and A. Wiesend, "Stability increase of the lumbar spine with different muscle groups. A biomechanical in vitro study," *Spine (Phila Pa 1976)*, vol. 20, no. 2, pp. 192–197, 1995.
- [25] L. A. Danneels, G. G. Vanderstraeten, D. C. Cambier, E. E. Witvrouw, and H. J. De Cuyper, "CT imaging of trunk muscles in chronic low back pain patients and healthy control subjects," *European Spine Journal*, vol. 9, no. 4, pp. 266–272, 2000.
- [26] J. Cholewicki, A. P. Simons, and A. Radebold, "Effects of external trunk loads on lumbar spine stability," *Journal of Biomechanics*, vol. 33, no. 11, pp. 1377–1385, 2000.
- [27] J. Cholewicki and S. M. McGill, "Mechanical stability of the in vivo lumbar spine: implications for injury and chronic low back pain," *Clinical Biomechanics*, vol. 11, no. 1, pp. 1–15, 1996.
- [28] P. Hodges, A. K. Holm, T. Hansson, and S. Holm, "Rapid atrophy of the lumbar multifidus follows experimental disc or nerve root injury," *Spine (Phila Pa 1976)*, vol. 31, no. 25, pp. 2926–2933, 2006.
- [29] D. Goubert, J. V. Oosterwijck, M. Meeus, and L. Danneels, "Structural changes of lumbar muscles in non-specific low back pain: a systematic review," *Pain Physician*, vol. 19, no. 7, pp. E985–e1000, 2016.
- [30] C. Faur, J. M. Patrascu, H. Haragus, and B. Anglitoiu, "Correlation between multifidus fatty atrophy and lumbar disc degeneration in low back pain," *BMC Musculoskeletal Disorders*, vol. 20, no. 1, p. 414, 2019.
- [31] M. B. Delisle, M. Laroche, H. Dupont, P. Rochaix, and J. L. Rumeau, "Morphological analyses of paraspinal muscles: comparison of progressive lumbar kyphosis (camptocormia) and narrowing of lumbar canal by disc protrusions," *Neuromuscular Disorders*, vol. 3, no. 5–6, pp. 579–582, 1993.
- [32] E. E. Ozcan-Eksi, I. Yagci, H. Erkal, and S. Demir-Deviren, "Paraspinal muscle denervation and balance impairment in lumbar spinal stenosis," *Muscle & Nerve*, vol. 53, no. 3, pp. 422–430, 2016.
- [33] J.-R. Cha, Y.-C. Kim, W.-K. Yoon et al., "The recovery of damaged paraspinal muscles by posterior surgical treatment for patients with lumbar degenerative diseases and its clinical consequence," *Journal of Back and Musculoskeletal Rehabilitation*, vol. 30, no. 4, pp. 801–809, 2017.
- [34] T. Tsutsumimoto, M. Shimogata, H. Ohta, and H. Misawa, "Mini-open versus conventional open posterior lumbar interbody fusion for the treatment of lumbar degenerative spondylolisthesis: comparison of paraspinal muscle damage and slip reduction," *Spine (Phila Pa 1976)*, vol. 34, no. 18, pp. 1923–1928, 2009.
- [35] R. Tandon, V. Kiyawat, and N. Kumar, "Clinical correlation between muscle damage and Oswestry disability index score after open lumbar surgery: does open surgery reduces functional ability?," *Asian Spine Journal*, vol. 12, no. 3, pp. 518–523, 2018.
- [36] J. Gu, F. Guan, L. Zhu et al., "Risk factors of postoperative low back pain for lumbar spine disease," *World Neurosurgery*, vol. 94, pp. 248–254, 2016.
- [37] N. Rahmani, A. Kiani, M. A. Mohseni-Bandpei, and I. Abdollahi, "Multifidus muscle size in adolescents with and without back pain using ultrasonography," *Journal of Bodywork and Movement Therapies*, vol. 22, no. 1, pp. 147–151, 2018.
- [38] Z. J. Hu, X. Q. Fang, Z. J. Zhou, J. Y. Wang, F. D. Zhao, and S. W. Fan, "Effect and possible mechanism of muscle-splitting approach on multifidus muscle injury and atrophy after posterior lumbar spine surgery," *The Journal of Bone and Joint Surgery-American Volume*, vol. 95, no. 24, pp. e192–e1-9, 2013.
- [39] K. Lu, C. L. Liang, C. L. Cho et al., "Oxidative stress and heat shock protein response in human paraspinal muscles during retraction," *Journal of Neurosurgery*, vol. 97, no. 1, pp. 75–81, 2002.
- [40] Y. Kawaguchi, S. Yabuki, J. Styf et al., "Back muscle injury after posterior lumbar spine surgery. Topographic evaluation of intramuscular pressure and blood flow in the porcine back muscle during surgery," *Spine (Phila Pa 1976)*, vol. 21, no. 22, pp. 2683–2688, 1996.
- [41] R. Gejo, H. Matsui, Y. Kawaguchi, H. Ishihara, and H. Tsuji, "Serial changes in trunk muscle performance after posterior lumbar surgery," *Spine (Phila Pa 1976)*, vol. 24, no. 10, pp. 1023–1028, 1999.
- [42] T. Motosuneya, T. Asazuma, T. Tsuji, H. Watanabe, Y. Nakayama, and K. Nemoto, "Postoperative change of the cross-sectional area of back musculature after 5 surgical procedures as assessed by magnetic resonance imaging," *Journal of Spinal Disorders & Techniques*, vol. 19, no. 5, pp. 318–322, 2006.

- [43] B. Colakoglu and D. Alis, "Evaluation of lumbar multifidus muscle in patients with lumbar disc herniation: are complex quantitative MRI measurements needed?," *The Journal of International Medical Research*, vol. 47, no. 8, pp. 3590–3600, 2019.
- [44] R. Izzo, T. Popolizio, P. D'Aprile, and M. Muto, "Spinal pain," *European Journal of Radiology*, vol. 84, no. 5, pp. 746–756, 2015.
- [45] A. Pezolato, E. E. de Vasconcelos, H. L. A. Defino, and M. H. Nogueira-Barbosa, "Fat infiltration in the lumbar multifidus and erector spinae muscles in subjects with sway-back posture," *European Spine Journal*, vol. 21, no. 11, pp. 2158–2164, 2012.
- [46] P. P. Raj, "Intervertebral disc: anatomy-physiology-pathophysiology-treatment," *Pain Practice*, vol. 8, no. 1, pp. 18–44, 2008.
- [47] Q. Wan, C. Lin, X. Li, W. Zeng, and C. Ma, "MRI assessment of paraspinal muscles in patients with acute and chronic unilateral low back pain," *The British Journal of Radiology*, vol. 88, no. 1053, pp. 20140546–20140546, 2015.
- [48] T. A. Ranger, F. M. Cicuttini, T. S. Jensen et al., "Are the size and composition of the paraspinal muscles associated with low back pain? A systematic review," *The Spine Journal*, vol. 17, no. 11, pp. 1729–1748, 2017.
- [49] D. Hoy, P. Brooks, F. Blyth, and R. Buchbinder, "The epidemiology of low back pain," *Best Practice & Research Clinical Rheumatology*, vol. 24, no. 6, pp. 769–781, 2010.
- [50] M. Russo, K. Deckers, S. Eldabe et al., "Muscle control and non-specific chronic low back pain," *Neuromodulation: Technology at the Neural Interface*, vol. 21, no. 1, pp. 1–9, 2018.
- [51] A. Agten, S. Stevens, J. Verbrugghe, A. Timmermans, and F. Vandenabeele, "Biopsy samples from the erector spinae of persons with nonspecific chronic low back pain display a decrease in glycolytic muscle fibers," *The Spine Journal*, vol. 20, no. 2, pp. 199–206, 2020.
- [52] P. Bonaldo and M. Sandri, "Cellular and molecular mechanisms of muscle atrophy," *Disease Models & Mechanisms*, vol. 6, pp. 25–39, 2012.
- [53] P. W. Hodges, G. James, L. Blomster et al., "Can proinflammatory cytokine gene expression explain multifidus muscle fiber changes after an intervertebral disc lesion?," *Spine (Phila Pa 1976)*, vol. 39, no. 13, pp. 1010–1017, 2014.
- [54] G. James, M. Millemcamps, L. S. Stone, and P. W. Hodges, "Dysregulation of the inflammatory mediators in the multifidus muscle after spontaneous intervertebral disc degeneration SPARC-null mice is ameliorated by physical activity," *Spine (Phila Pa 1976)*, vol. 43, no. 20, pp. E1184–E1194, 2018.
- [55] G. James, X. Chen, A. Diwan, and P. W. Hodges, "Fat infiltration in the multifidus muscle is related to inflammatory cytokine expression in the muscle and epidural adipose tissue in individuals undergoing surgery for intervertebral disc herniation," *European Spine Journal*, 2020.
- [56] P. M. Tiidus, "Estrogen and gender effects on muscle damage, inflammation, and oxidative stress," *Canadian Journal of Applied Physiology*, vol. 25, no. 4, pp. 274–287, 2000.
- [57] S. Yang, F. Zhang, J. Ma, and W. Ding, "Intervertebral disc ageing and degeneration: the antiapoptotic effect of oestrogen," *Ageing Research Reviews*, vol. 57, article 100978, 2020.
- [58] J. G. Tidball, "Mechanisms of muscle injury, repair, and regeneration," *Comprehensive Physiology*, vol. 1, pp. 2029–2062, 2011.
- [59] L. Dalla Libera, B. Ravara, V. Gobbo et al., "A transient antioxidant stress response accompanies the onset of disuse atrophy in human skeletal muscle," *Journal of Applied Physiology*, vol. 107, no. 2, pp. 549–557, 2009.
- [60] J. Li, M. Tang, G. Yang, L. Wang, Q. Gao, and H. Zhang, "Muscle injury associated elevated oxidative stress and abnormal myogenesis in patients with idiopathic scoliosis," *International Journal of Biological Sciences*, vol. 15, no. 12, pp. 2584–2595, 2019.
- [61] K. Dzik, W. Skrobot, D. J. Flis et al., "Vitamin D supplementation attenuates oxidative stress in paraspinal skeletal muscles in patients with low back pain," *European Journal of Applied Physiology*, vol. 118, no. 1, pp. 143–151, 2018.
- [62] K. P. Dzik, W. Skrobot, K. B. Kaczor et al., "Vitamin D deficiency is associated with muscle atrophy and reduced mitochondrial function in patients with chronic low back pain," *Oxidative Medicine and Cellular Longevity*, vol. 2019, Article ID 6835341, 11 pages, 2019.
- [63] P. Tang, R. Zhu, Y. Gu et al., "Ascorbic acid attenuates multifidus muscles injury and atrophy after posterior lumbar spine surgery by suppressing inflammation and oxidative stress in a rat model," *Spine (Phila Pa 1976)*, vol. 43, no. 21, pp. E1249–E1259, 2018.
- [64] B. Shahidi, J. C. Hubbard, M. C. Gibbons et al., "Lumbar multifidus muscle degenerates in individuals with chronic degenerative lumbar spine pathology," *Journal of Orthopaedic Research*, vol. 35, no. 12, pp. 2700–2706, 2017.
- [65] J. Wu, C. Zhang, K. Lu, C. Li, and Y. Zhou, "A novel inextensible endoscopic tube versus traditional extensible retractor system in single-level minimally invasive transforaminal lumbar interbody fusion: a prospective observation study," *Pain Physician*, vol. 22, no. 6, pp. E587–E599, 2019.
- [66] J. Urrutia, P. Besa, D. Lobos, M. Andia, C. Arrieta, and S. Uribe, "Is a single-level measurement of paraspinal muscle fat infiltration and cross-sectional area representative of the entire lumbar spine?," *Skeletal Radiology*, vol. 47, no. 7, pp. 939–945, 2018.
- [67] H. Li, H. Luo, and Y. Liu, "Paraspinal muscle segmentation based on deep neural network," *Sensors (Basel, Switzerland)*, vol. 19, no. 12, p. 2650, 2019.
- [68] A. Agten, J. Verbrugghe, S. Stevens et al., "Feasibility, accuracy and safety of a percutaneous fine-needle biopsy technique to obtain qualitative muscle samples of the lumbar multifidus and erector spinae muscle in persons with low back pain," *Journal of Anatomy*, vol. 233, no. 4, pp. 542–551, 2018.
- [69] M. Mattila, M. Hurme, H. Alaranta et al., "The multifidus muscle in patients with lumbar disc herniation. A histochemical and morphometric analysis of intraoperative biopsies," *Spine (Phila Pa 1976)*, vol. 11, no. 7, pp. 732–738, 1986.
- [70] W. P. Zhao, Y. Kawaguchi, H. Matsui, M. Kanamori, and T. Kimura, "Histochemistry and morphology of the multifidus muscle in lumbar disc herniation: comparative study between diseased and normal sides," *Spine (Phila Pa 1976)*, vol. 25, no. 17, pp. 2191–2199, 2000.
- [71] E. Segura-Anaya, R. Flores-Miranda, A. Martínez-Gómez, and M. A. R. Dent, "A novel histochemical method of simultaneous detection by a single- or double- immunofluorescence and Bielschowsky's silver staining in teased rat sciatic nerves," *Journal of Neuroscience Methods*, vol. 304, pp. 46–51, 2018.
- [72] C. S. Hintz, E. F. Coyle, K. K. Kaiser, M. M. Chi, and O. H. Lowry, "Comparison of muscle fiber typing by quantitative enzyme assays and by myosin ATPase staining," *The Journal*

- of Histochemistry and Cytochemistry : Official Journal of the Histochemistry Society*, vol. 32, no. 6, pp. 655–660, 1984.
- [73] R. Koopman, G. Schaart, and M. K. Hesselink, “Optimisation of oil red O staining permits combination with immunofluorescence and automated quantification of lipids,” *Histochemistry and Cell Biology*, vol. 116, no. 1, pp. 63–68, 2001.
- [74] M. Wajchenberg, N. Astur, E. A. Fernandes et al., “Assessment of fatty infiltration of the multifidus muscle in patients with adolescent idiopathic scoliosis through evaluation by magnetic resonance imaging compared with histological analysis: a diagnostic accuracy study,” *Journal of Pediatric Orthopaedics. Part B*, vol. 28, no. 4, pp. 362–367, 2019.
- [75] C. Zimmermann, R. Kalepu, M. Ponfick et al., “Histological characterization and biochemical analysis of paraspinal muscles in neuromuscularly healthy subjects,” *Muscle & Nerve*, vol. 52, no. 1, pp. 45–54, 2015.
- [76] M. Creze, K. Nyangoh Timoh, O. Gagey, L. Rocher, M.-F. Bellin, and M. Soubeyrand, “Feasibility assessment of shear wave elastography to lumbar back muscles: a radioanatomic study,” *Clinical Anatomy*, vol. 30, no. 6, pp. 774–780, 2017.
- [77] D. T. Cawley, M. Alexander, and S. Morris, “Multifidus innervation and muscle assessment post-spinal surgery,” *European Spine Journal*, vol. 23, no. 2, pp. 320–327, 2014.
- [78] O. Airaksinen, A. Herno, E. Kaukanen, T. Saari, T. Sihvonen, and O. Suomalainen, “Density of lumbar muscles 4 years after decompressive spinal surgery,” *European Spine Journal*, vol. 5, no. 3, pp. 193–197, 1996.
- [79] M. Jackson, M. Solomonow, B. Zhou, R. V. Baratta, and M. Harris, “Multifidus EMG and tension-relaxation recovery after prolonged static lumbar flexion,” *Spine (Phila Pa 1976)*, vol. 26, no. 7, pp. 715–723, 2001.
- [80] J. J. Hebert, J. M. Fritz, A. Thackeray, S. L. Koppenhaver, and D. Teyhen, “Early multimodal rehabilitation following lumbar disc surgery: a randomised clinical trial comparing the effects of two exercise programmes on clinical outcome and lumbar multifidus muscle function,” *British Journal of Sports Medicine*, vol. 49, no. 2, pp. 100–106, 2014.
- [81] M. D. Freeman, M. Woodham, A. W. Woodham, and J. W. Skeate, “Long-term lumbar multifidus muscle atrophy changes documented with magnetic resonance imaging: a case series,” *Journal of Radiology Case Reports*, vol. 8, no. 5, pp. 27–34, 2014.
- [82] I. Kliziene, S. Sipaviciene, S. Klizas, and D. Imbrasiene, “Effects of core stability exercises on multifidus muscles in healthy women and women with chronic low-back pain,” *Journal of Back and Musculoskeletal Rehabilitation*, vol. 28, no. 4, pp. 841–847, 2015.
- [83] L. Käser, A. F. Mannion, A. Rhyner, E. Weber, J. Dvorak, and M. Müntener, “Active therapy for chronic low back pain: part 2. Effects on paraspinal muscle cross-sectional area, fiber type size, and distribution,” *Spine (Phila Pa 1976)*, vol. 26, no. 8, pp. 909–919, 2001.
- [84] S. Konno, S. Kikuchi, and Y. Nagaosa, “The relationship between intramuscular pressure of the paraspinal muscles and low back pain,” *Spine (Phila Pa 1976)*, vol. 19, no. 19, pp. 2186–2188, 1994.
- [85] T. Kumamoto, T. Seko, R. Matsuda, S. Miura, T. Okumura, and S. Nitta, “Change in the circulation and activity of the lower erector spinae muscles after repeated trunk extension movement,” *Journal of Back and Musculoskeletal Rehabilitation*, vol. 32, no. 6, pp. 931–936, 2019.
- [86] W. J. Garcia, A. Johnson, D. Keldermans, and B. Tang, “Exercise and low back pain in the older adult: current recommendations,” *Journal of Allied Health*, vol. 48, no. 4, pp. 302–307, 2019.
- [87] S. K. Kim, I. Jung, and J. H. Kim, “Exercise reduces C-reactive protein and improves physical function in automotive workers with low back pain,” *Journal of Occupational Rehabilitation*, vol. 18, no. 2, pp. 218–222, 2008.

Research Article

Salvianolic Acid B Protects Intervertebral Discs from Oxidative Stress-Induced Degeneration via Activation of the JAK2/STAT3 Signaling Pathway

Shouqian Dai,¹ Ting Liang,¹ Xiu Shi,² Zongping Luo ¹ and Huilin Yang ¹

¹Department of Orthopedics, The First Affiliated Hospital of Soochow University, Orthopedics Institute of Soochow University, Suzhou, Jiangsu, China

²Department of Obstetrics and Gynecology, The First Affiliated Hospital, Soochow University, Suzhou, Jiangsu, China

Correspondence should be addressed to Zongping Luo; zongping_luo@yahoo.com and Huilin Yang; suzhouspine@163.com

Received 27 December 2020; Revised 15 January 2021; Accepted 23 January 2021; Published 13 February 2021

Academic Editor: Sidong Yang

Copyright © 2021 Shouqian Dai et al. This is an open access article distributed under the Creative Commons Attribution License, which permits unrestricted use, distribution, and reproduction in any medium, provided the original work is properly cited.

Objective. To evaluate the influence of salvianolic acid B (SAB), an antioxidant derived from Danshen, on intervertebral disc degeneration (IDD) and its possible molecular mechanisms. **Methods.** Sixty adult rats were randomly grouped (control, IDD, and SAB IDD groups). IDD was induced using needle puncture. The rats received daily administration of SAB (20 mg/kg) in the SAB IDD group while the other two groups received only distilled water. The extent of IDD was evaluated using MRI after 3 and 6 weeks and histology after 6 weeks. Oxidative stress was assessed using the ELISA method. In *in vitro* experiments, nucleus pulposus cells (NPCs) were treated with H₂O₂ (100 μM) or SAB+H₂O₂, and levels of oxidative stress were measured. Cell apoptosis was assessed by flow cytometry, expression levels of Bcl-2, Bax, and cleaved caspase-3 proteins. Cell proliferation rate was assessed by EdU analysis. Pathway involvement was determined by Western blotting while the influence of the pathway on NPCs was explored using the pathway inhibitor AG490. **Results.** The data demonstrate that SAB attenuated injury-induced IDD and oxidative stress, caused by activation of the JAK2/STAT3 signaling pathway *in vivo*. Oxidative stress induced by H₂O₂ was reversed by SAB *in vitro*. SAB reduced the increased cell apoptosis, cleaved caspase-3 expression, and caspase-3 activity induced by H₂O₂. Reduced cell proliferation and decreased Bcl-2/Bax ratio induced by H₂O₂ were rescued by SAB. Additionally, the JAK2/STAT3 pathway was activated by SAB, while AG490 counteracted this effect. **Conclusion.** The results suggest that SAB protects intervertebral discs from oxidative stress-induced degeneration by enhancing proliferation and attenuating apoptosis via activation of the JAK2/STAT3 signaling pathway.

1. Introduction

Over recent years, lower back pain has been recognized as a common disorder that primarily afflicts the elderly, contributing considerably to socioeconomic burden [1–3]. The intervertebral disc (IVD) is important for stabilization and biomechanical maintenance of the spinal column. IVD degeneration (IDD) is believed to be a principal cause of lower back pain, and more than eighty percent of adults have at some point suffered IDD [4]. Therefore, the search for treatments that would be effective for IDD has gained consid-

erable attention. Even now, the precise pathogenesis of IDD remains unknown, although the possible etiology includes genetic factors, trauma, infection, aging, smoking, and mechanical stress [5]. The characteristic changes in IDD are decreased intervertebral space, apoptosis of nucleus pulposus cells (NPCs), loss of nucleus pulposus (NP) collagen, and vertebral endplate calcification [6]. The central part of an adult IVD, the nucleus pulposus (NP), is primarily composed of chondrocyte-like NP cells (NPCs) that produce extracellular matrix molecules that stabilize the biomechanical equilibrium and structure of the IVD [7]. As IDD occurs and progresses,

the NPCs commonly become significantly functionally impaired due to either increased apoptosis or decreased proliferation [8]. Previous studies have demonstrated that oxidative stress may perform a crucial role in the pathology of IDD [9–11].

It has been reported that significant structural alterations in degenerated IVDs at least partly result from oxidative stress resulting from excessive accumulation of reactive oxygen species (ROS) [12]. In physiological conditions, the production and elimination of cellular ROS are in dynamic equilibrium. Oxidative stress occurs where this equilibrium is out of balance, for example, in the microenvironment of degenerated IVDs [13, 14]. A number of oxidative stress markers have been identified in human degenerated discs, including peroxynitrite, glutathione (GSH), superoxide dismutase 2 (SOD2), malondialdehyde (MDA), and advanced glycation end products (AGEs) [15–17]. Additionally, SOD2 activity in the serum of patients and rats with IDD has been found to be significantly reduced, while a number of markers such as MDA, peroxide, and NO are significantly increased [18]. The observations above demonstrate that ROS and oxidative stress may significantly influence the pathological development of IDD.

Previous studies have shown that the herbal drug Danshen has a number of pharmacological and clinical effects [19]. The constituents of Danshen are principally water-soluble phenolic acids and fat-soluble tanshinone compounds [20–22]. Salvianolic acid B (SAB) is the most abundant water-soluble compound extracted from Danshen. Previous studies have confirmed that SAB has antioxidative properties and eliminates superoxide anion radicals ($\cdot\text{O}_2^-$), thereby inhibiting hydrogen peroxide- (H_2O_2 -) induced apoptosis [23, 24]. It has also been reported that SAB can increase the proliferation of human umbilical vein endothelial cells [25]. Chang et al. reported that SAB was effective in scavenging excess production of ROS, and this antioxidant activity was stronger than even glutathione or vitamin E [26]. Hence, it can be deduced that SAB may help attenuate oxidative stress-induced IDD. However, few studies have been conducted in this field, and thus the precise influence of SAB on degenerated IVDs or NPCs, and its underlying mechanisms remain unresolved.

The Janus kinase 2 (JAK2)/signal transducer and activator of transcription 3 (STAT3) pathway is a common pathway of signal transduction for multiple cytokines [27–29] such as TNF- α , IL-6, and IL-1 β , which transmits signals from the cell membrane directly to the nucleus to initiate gene transcription [30], occurring in inflammation and oxidative stress. Additionally, the JAK2/STAT3 signaling pathway has been shown to regulate the catabolism of genes related to degenerated disc NPCs [31]. From this, we have reason to infer that the degeneration of IVDs and NPCs is closely associated with the JAK2/STAT3 signaling pathway. However, whether the JAK2/STAT3 pathway is involved in the influence of SAB on IDD remains unclear.

Therefore, the present study is aimed at evaluating the protective effects of SAB on IVD in SD rats with injury-induced IDD *in vivo* and by use of an *in vitro* model of H_2O_2 -induced IDD in NPCs. Furthermore, the signaling

pathway involved in the attenuation of IDD by SAB was investigated. This research may facilitate advances in the clinical use of SAB for treatment of degenerative disease.

2. Methods and Materials

2.1. Reagents. SAB was obtained from ChromaDex, Inc. (Irvine, CA, USA), dissolved in distilled water, and stored at -20°C prior to use. Assays to quantify GSH, SOD2, MDA, and ROS and caspase-3 activity kits were acquired from Beyotime Biotechnology Co. Ltd. (Shanghai, China). Dulbecco's modified Eagle medium (DMEM)/F12 medium and fetal bovine serum (FBS) were purchased from Invitrogen Inc. (MD, USA). All primary antibodies used in the study were obtained from Cell Signaling Technology, Inc. (MA, USA). The secondary antibodies were from Beyotime Biotechnology Co. Ltd. (Shanghai, China). Sigma-Aldrich Inc. (St. Louis, MO, USA) supplied all other reagents.

2.2. *In Vivo* Study

2.2.1. Animal Protocol. Sixty adult male Sprague-Dawley rats were purchased from the animal center at Soochow University (Suzhou, China). Animals were maintained under normal conditions and randomly allocated into three equal groups (control, IDD, and SAB IDD) prior to surgery. All rats received treatments, as appropriate, for two weeks and then were subjected to experimental surgery, as described below. All animal experiments were approved by the Animal Care and Experiment Committee of Soochow University (2019 Approval No. ECSU-2019000210).

2.2.2. IDD Model Induction. Percutaneous needle puncture has been shown to be an effective method of induction of disc degeneration [32]. After acclimatization, animals were anesthetized by inhalation of 2% fluothane in oxygen/nitrous oxide. The surgical procedure was performed on the vertebrae in the tail, as described previously [33]. In the IDD and SAB IDD groups, the Co8-9 discs were punctured using a 20-gauge needle. Full penetration and sham surgery were performed on rats in the control group. Following surgery, all rats in the SAB IDD group received SAB (20 mg/kg) by oral gavage once per day for six consecutive weeks, consistent with the dose used in a previous study [34]. Only distilled water was administered to rats in the other two groups. After 6 weeks, all rat tails were scanned by MRI under isoflurane anesthesia and then the Co8-9 discs were collected for subsequent experiments. All experimental steps complied with the Animal Research Reporting of *In Vivo* Experiments (ARRIVE) guidelines.

2.2.3. Magnetic Resonance Imaging (MRI) Examination. T2 mapping of MRI signal intensity is commonly used to measure the degree of IDD. The procedure was conducted as previously described, in a 1.5 T MRI scanner (GE, USA) [35]. Briefly, all rat IVDs were scanned at the 3- and 6-week time points. The T2 signal intensity of Co8-9 discs was recorded, and the ratio of T2 signal intensity of the injured to control discs was calculated then analyzed using the ImageJ software. Therefore, normalized disc intensity was presented as values between 0 and 1.

2.2.4. Histological Evaluation. All target IVDs collected were fixed in 10% formalin and embedded in paraffin. Then, 5 μm serial sections were prepared from the midsagittal region. Hematoxylin and eosin (H&E), Safranin-O Fast green, and alcian blue staining were used to identify histological changes in the IVDs and assessed using a previously described grading scale [33], providing scores from 5 to 15 points, representing IVDs that were normal to severely degenerated [33].

2.2.5. Biochemical Analysis. The collected Co8-9 discs were digested by papain at 65°C for 1 hour then centrifuged for 10 min. GSH concentration was then measured using a glutathione assay kit, in accordance with standard experimental procedures. A lipid peroxidation MDA assay kit was used to calculate MDA concentration. SOD2 levels were measured using an ELISA, in accordance with standard protocols.

2.2.6. Western Blotting. Expression levels of JAK2, p-JAK2, STAT3, and p-STAT3 in the discs were tested using routine Western blotting analysis. After blocking in 5% nonfat milk, the membranes were incubated with the following anti-rat primary antibodies at 4°C overnight: JAK2 (1:1000), p-JAK2 (1:1000), STAT3 (1:1000), p-STAT3 (1:1000), and GAPDH (1:2000), after which they were incubated with an HRP-conjugated secondary antibody at 37°C for one hour. Finally, the relative optical densities of all bands were normalized to GAPDH.

2.3. In Vitro Study

2.3.1. NPC Isolation and Culture. Normal IVDs were obtained from rat tails and cut into small pieces. Firstly, the coccygeal spinal columns (Co6-Co10) of rats were separated and the NP of each disc collected under aseptic conditions. NPCs were obtained using a dissecting microscope in accordance with methods reported previously [36]. The NPCs were then cultured in DMEM/F12 medium supplemented with 10% FBS and 1% penicillin/streptomycin in a conventional culture environment. After cell cultures were confluent, the NPCs were subcultured and cells from the second passage were used in the *in vitro* studies. All protocols were conducted in accordance with the relevant guidelines of the Ethics Committee.

2.3.2. Cell Treatment. As previously described, H_2O_2 (100 μM) was used to induce oxidative damage [37]. Untreated NPCs were used as controls. An MTT assay was performed using different concentrations of SAB (0.001, 0.01, 0.1, 1, 10, and 100 nM) to determine the concentration most appropriate for use in the following experiments, as previously described [38]. To evaluate the effects of SAB on apoptosis, proliferation, and oxidative stress, NPCs were randomized into three groups: control, H_2O_2 , and SAB+ H_2O_2 groups (1 nM SAB for 24h, then 100 μM H_2O_2 for 24h). To determine the signaling pathway targeted by SAB, the NPCs were divided into four groups: control, H_2O_2 , SAB+ H_2O_2 , and AG490+SAB+ H_2O_2 (1 nM SAB for 24h, 40 μM AG490 for 24h, and then 100 μM H_2O_2 for 24h).

2.3.3. Identification of NPCs. Immunocytochemistry and immunofluorescence were used to identify the NPCs obtained from IVD tissue. NPCs were fixed in 4% paraformaldehyde for 20 min at 37°C, permeabilized in 0.2% Triton X-100, and blocked using goat serum. The NPCs were incubated with primary antibodies against collagen II and cytokeratin 19 at 4°C overnight. The NPCs were then incubated with an HRP-conjugated (for immunocytochemistry) or fluorescein isothiocyanate- (FITC-) labeled (for immunofluorescence) secondary antibody. Images were acquired using light or fluorescence microscopy.

2.3.4. Intracellular ROS Measurement. Briefly, after the treatment appropriate for their grouping, NPCs were incubated with DCFH-DA for half an hour then washed three times. ROS concentration of the NPCs was determined using a ROS assay kit in accordance with the manufacturer's instructions. Finally, ROS concentration, presented as relative fluorescence units (RFU), was calculated from fluorescence intensity at wavelengths of 490/585 nm.

2.3.5. Measurement of GSH, SOD2, and MDA. Intracellular levels of GSH, SOD2, and MDA, which reflect oxidation state, were measured using the corresponding assay kit (Beyotime Biotechnology Co. Ltd., Shanghai, China) in accordance with the manufacturer's instructions. The NPCs were first digested with 0.25% trypsin and centrifuged for 15 minutes at 4°C at 900 g. The sample supernatants and standards were prepared in cuvettes, and the OD values at 530 nm were recorded. GSH, SOD2, and MDA concentrations were obtained by reference to the standard curve. The data are presented as means \pm SD of three replicate experiments.

2.3.6. Flow Cytometry. The rate of apoptosis of NPCs was determined using a classic Annexin V-FITC/PI staining kit. Briefly, NPCs were collected and washed with PBS three times. NPCs were then resuspended and incubated with Annexin V-FITC and propidium iodide (PI) at 37°C in a dark room for 20 minutes. Finally, cell apoptosis was determined using a flow cytometer (BD Co., USA). Cells staining positive for Annexin V and negative for PI were considered apoptotic NPCs.

2.3.7. Western Blotting. The expression levels of Bcl-2, Bax, cleaved caspase-3, JAK2, p-JAK2, STAT3, and p-STAT3 in NPCs were measured using Western blotting, as described in the protocol above (Section 2.2.6). All primary antibodies were diluted 1:1000. Relative expression levels were normalized to GAPDH.

2.3.8. Measurement of Caspase-3 Activity. Caspase-3 activity was evaluated using an activity assay kit in accordance with standard protocols. Briefly, NPCs in culture medium were collected, lysed in RIPA lysis buffer, and then mixed with the appropriate reaction reagents at room temperature. Optical density (OD) was measured at a wavelength of 405 nm, and caspase-3 activity was calculated by reference to a standard curve then normalized to total protein concentration.

2.3.9. NPC Proliferation Assay. Cell proliferation in different groups was measured by staining with the thymidine analog 5-ethynyl-2-deoxyuridine (EdU). Briefly, NPCs (1×10^6) were seeded in each well of 6-well plates then treated with EdU (10 μ M) conjugated with Alexa-Fluor 594 (Alexa-594, Invitrogen) at 37°C in a dark room for 30 minutes. Cells were then counterstained with DAPI then mounted. Images were acquired using a Leica fluorescence microscope. The ratio of EdU-positive cells/total cells was obtained, and the rate of cell proliferation in the different groups compared.

2.4. Statistical Analyses. All data are presented as means \pm SD. One-way analysis of variance (ANOVA) was used to compare multiple groups after verification of normality with post hoc comparisons using a least-squares difference (LSD) method. Statistical analyses were performed using the SPSS v20 statistical software (SPSS Inc., Chicago, IL, USA). *P* values <0.05 were considered statistically significant.

3. Results

3.1. SAB Attenuates Injury-Induced IDD and Oxidative Stress and Activates the JAK2/STAT3 Signaling Pathway In Vivo. T2-weighted signal intensities of the MRI examination of Co8-9 IVDs were markedly lower in the IDD group than that of the control group after both 3 and 6 weeks. However, treatment with SAB in the SAB IDD group clearly reversed this decrease (Figures 1(a) and 1(b)). Histological staining indicated that the IVD in the control group had a normal structure but the border between the annulus fibrosus (AF) and nucleus pulposus (NP) in the IDD group was clearly disrupted. NPCs had become separated by an extracellular proteoglycan matrix, and the NP had almost disappeared. The AF became disorganized due to inward bulging of the inner annulus. However, SAB significantly reduced the injury induced by IDD and partially reestablished the structure of the IVD (Figures 1(c) and 1(d)).

Figures 2(a) and 2(b) demonstrate that GSH and SOD2 levels in the IVD of the IDD group decreased markedly compared with the control group, and SAB medication significantly reversed this change. Figure 2(c) shows that SAB treatment significantly decreased the levels of MDA that had been induced by disc injury in the IDD group. Western blotting demonstrated that the phosphorylation levels of JAK2 and STAT3 in the IDD group were significantly lower than in the control group. However, SAB clearly upregulated the expression levels of p-JAK2 and p-STAT3 in rats in the IDD group (Figures 2(d)–2(f)). These results suggest that SAB inhibits disc degeneration and oxidative stress *in vivo*, probably via the JAK2/STAT3 signaling pathway.

3.2. Viability Assays for SAB-Treated NPCs and Cell Identification. MTT assays were used to investigate the viability of NPCs incubated with different concentrations of SAB (0.001, 0.01, 0.1, 1, 10, and 100 nM). The data indicate that cell viability in the 0.1, 1, and 10 nM groups was clearly greater than other concentrations, 1 nM being the most significant (Figure 3(a)). Thus, 1 nM SAB was selected for subsequent experiments.

Normal NPCs exhibited an appearance similar to chondrocytes under phase-contrast microscopy (Figure 3(b)). Immunocytochemical staining indicated that collagen II was expressed within the cytoplasm (Figure 3(c)) while immunofluorescence demonstrated the expression of the molecular marker cytokeratin 19 in the NPCs (Figure 3(d)).

3.3. SAB Inhibits H₂O₂-Induced Oxidative Stress and Apoptosis In Vitro. ROS, GSH, SOD2, and MDA levels were assessed to reflect the degree of oxidative stress. Figures 4(a)–4(d) demonstrate that in the H₂O₂ group, ROS and MDA levels were clearly less, and GSH and SOD2 levels significantly higher than those of the control group. In the SAB group, however, ROS, GSH, SOD2, and MDA levels were restored, indicating that SAB was able to inhibit the antioxidant system *in vitro*.

Apoptosis of NPCs was evaluated by flow cytometry, Western blotting, and ELISA. The flow cytometry results indicate that NPC apoptosis in the H₂O₂ group was significantly higher than in the control group, an increase that was reversed by SAB (Figures 4(e) and 4(f)). Similar changes were also observed by Western blot analysis, where the ratio of Bcl-2/Bax increased and cleaved caspase-3 decreased in the SAB H₂O₂ group (Figures 4(g)–4(j)). Therefore, we propose that SAB inhibited H₂O₂-induced NPC apoptosis.

3.4. SAB Promotes NPC Proliferation and Activates the JAK2/STAT3 Signaling Pathway In Vitro. The EdU assay demonstrated that SAB clearly increased the proliferation of NPCs that had been reduced by H₂O₂ (Figures 5(a) and 5(b)). Western blotting demonstrated that treatment with SAB significantly increased the expression levels of p-JAK2 and p-STAT3, which were markedly lower in the H₂O₂ group (Figures 5(c)–5(e)). These data indicate that SAB was able to inhibit H₂O₂-induced oxidative stress and apoptosis, promote cell proliferation, and activate the JAK2/STAT3 pathway *in vitro*.

3.5. SAB Inhibits H₂O₂-Induced Disc Degeneration via the JAK2/STAT3 Signaling Pathway. To investigate whether SAB influences oxidative stress, apoptosis, and proliferation of NPCs through the JAK2/STAT3 signaling pathway, the JAK2 antagonist AG490 was utilized. The data indicate that SAB inhibited H₂O₂-induced oxidative stress and apoptosis in NPCs. However, this inhibitory behavior was markedly neutralized by the addition of AG490 (Figures 6(a)–6(c)). In addition, treatment with SAB also rescued changes in expression levels of Bcl-2, Bax, and cleaved caspase-3, and this alteration was abrogated by AG490 (Figures 6(d)–6(f)). Similarly, SAB increased H₂O₂-reduced cell proliferation, and this effect was also abrogated by AG490 (Figures 6(g) and 6(h)). Taken together, we conclude that SAB inhibits disc degeneration via the JAK2/STAT3 signaling pathway (Figure 7).

4. Discussion

In the present study, we investigated the effects of SAB on IDD. The results demonstrate that SAB reduced IVD degeneration *in vivo*, inhibited oxidative stress and apoptosis of

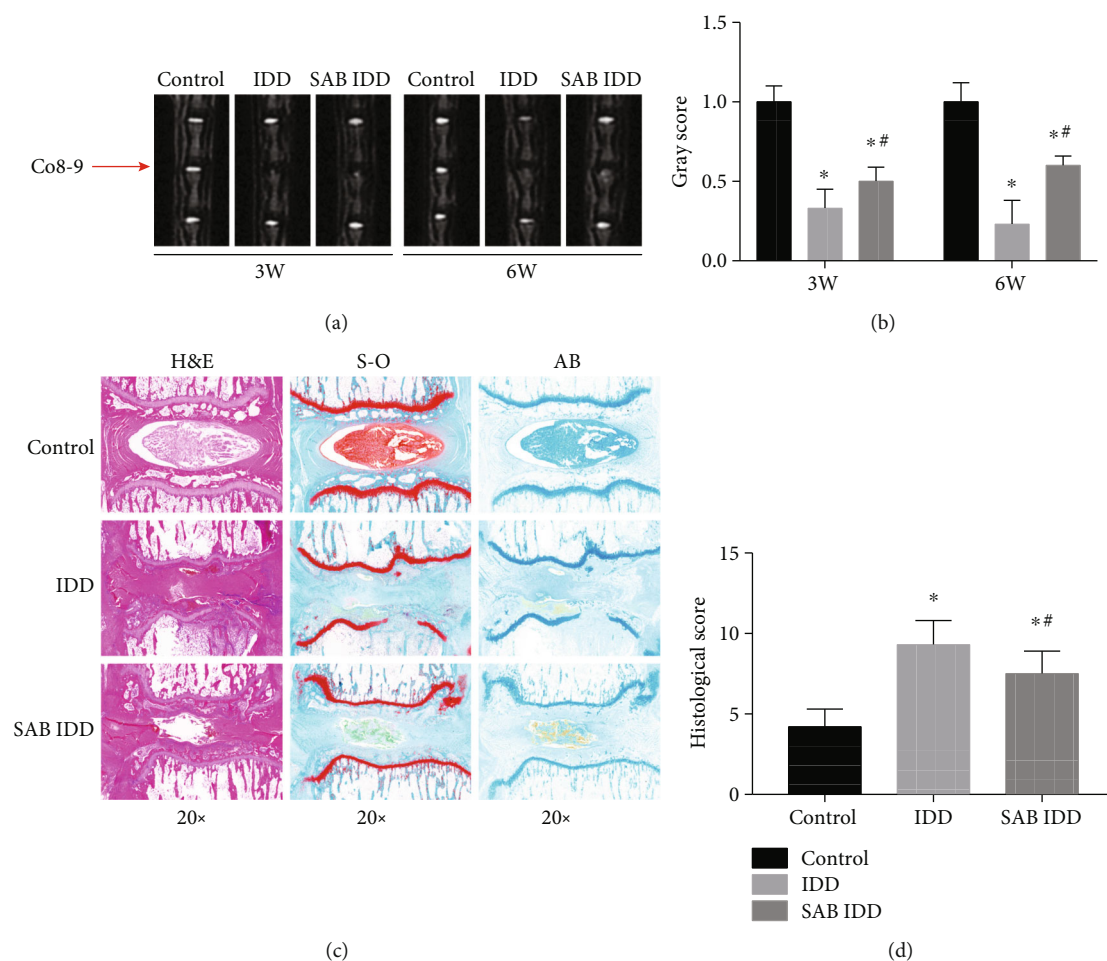


FIGURE 1: SAB reversed the reduced T2-weighted MR signal intensity induced by injury to IVDs and rescued the consequent disc degeneration *in vivo*. (a) MRI was used to detect changes in MR signal intensity of the Co8-9 discs in each group after 3 and 6 weeks. (b) Quantitative analysis demonstrated that a significant decrease of T2 signal intensity was found in injured IVDs. This decrease could be both reversed by treatment with SAB. (c) H&E staining displayed representative histopathological changes to IVDs in each group. IVDs in the control group exhibited a normal structure. In the IDD group, the border between the AF and NP was clearly disrupted, the NPCs becoming separated by extracellular proteoglycan matrix and the NP having almost disappeared. In the SAB IDD group, the characteristics of degeneration were largely reversed by treatment with SAB. (d) Induction of IDD resulted in significantly higher histological scores compared with the control group. SAB treatment significantly reduced the increased histological score. * $P < 0.05$ compared with the control group; # $P < 0.05$ compared with the IDD group. SAB: salvianolic acid B; IDD: intervertebral disc degeneration; IVD: intervertebral disc; NP: nucleus pulposus; AF: annulus fibrosus; H&E: hematoxylin and eosin; S-O: Safranin-O Fast green; AB: alcian blue.

NPCs, and promoted cell proliferation in an *in vitro* model of IDD. Further mechanistic investigation indicated that the JAK2/STAT3 signaling pathway was involved in the influence of SAB on IDD. The results demonstrate that SAB may represent a potential treatment for degenerative disc disease.

Disc degeneration is an important cause of lower back pain and disability [2]. Few effective therapies are available to ease or reverse the course of IDD. Therefore, the present study explored a strategy to prevent the progression of IDD. SAB, a natural polyphenolic ingredient rich in Danshen, has multiple pharmacological properties, such as being an antioxidant and anti-inflammatory agent [39, 40]. It has recently been reported that SAB combined with mesenchymal stem cells is able to repair degenerated IVDs more effectively than stem cells alone [41]. However, whether SAB can inhibit the progression of IDD remains controversial. There-

fore, the present study first examined the influence of SAB on injury-induced IDD in rats. The data indicate that needle puncture resulted in decreased T2-weighted signal intensity from the IVDs and altered disc morphology. Treatment with SAB significantly attenuated injury-induced IDD and restored changes to IVD structure.

It has previously been demonstrated that SAB can effectively protect the heart from ischemia-reperfusion injury [42]. SAB both increased and decreased cell viability, depending on the concentration. It has been reported that SAB promotes cell growth and inhibits the dedifferentiation of articular chondrocytes [43]. According to the MTT assay results, a SAB concentration of 1 nM most effectively promoted NPC viability. Similar results were also observed in previous studies involving different cell types [42]. We, therefore, used SAB at a concentration of 1 nM for subsequent *in vitro* experiments. Our findings demonstrate that H₂O₂

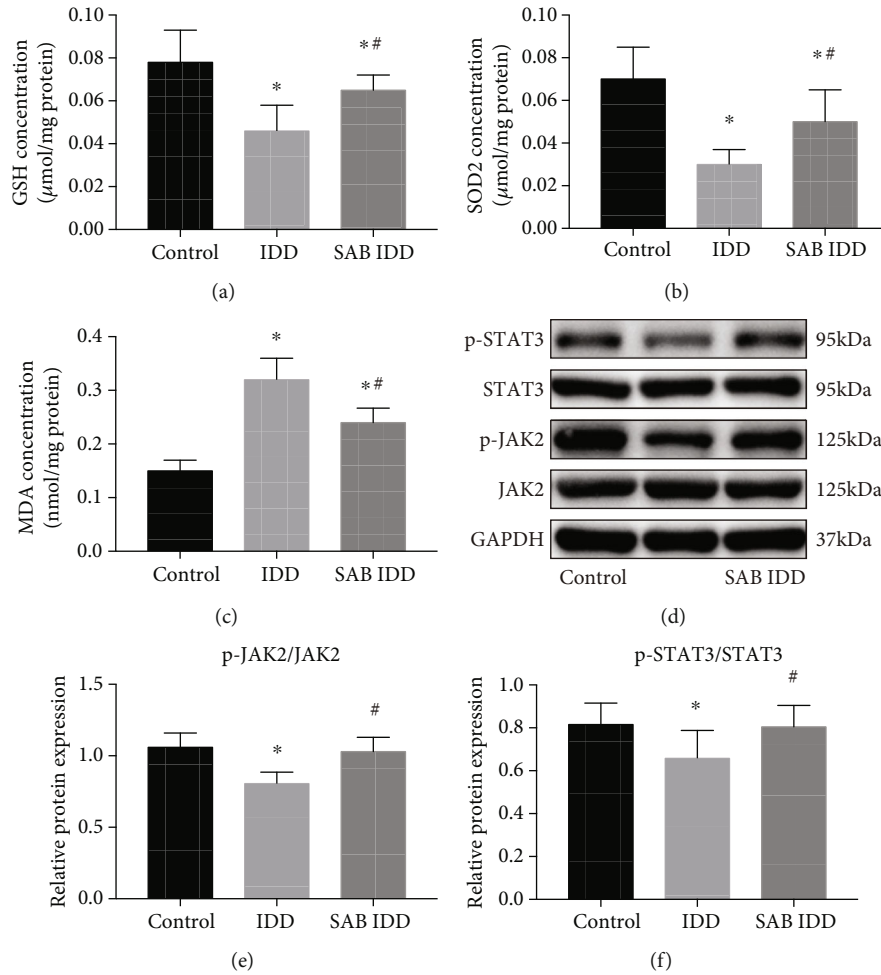


FIGURE 2: SAB reversed the effects on the antioxidant system induced by puncture injury *in vivo* that activated the JAK2/STAT3 signaling pathway. Animals were divided into three groups: control group, IDD group, or SAB group. Concentrations of (a) GSH, (b) SOD2, (c) and MDA were measured by assay kits. (d) Expression levels of phosphorylated and total JAK2 and STAT3 in IVDs were measured by Western blotting, and the relative ratios of (e) p-JAK2/JAK2 and (d) p-STAT3/STAT3 were calculated from gray-level values. * $P < 0.05$ compared with the control group; # $P < 0.05$ compared with the IDD group. SAB: salvianolic acid B; GSH: glutathione; SOD2: superoxide dismutase 2; MDA: malondialdehyde; GAPDH: glyceraldehyde-3-phosphate dehydrogenase; JAK2: Janus kinase 2; STAT3: signal transducer and activator of transcription 3.

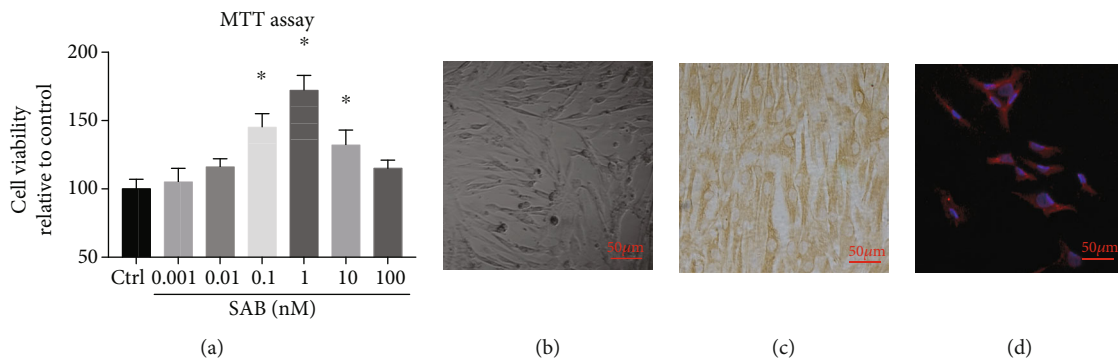


FIGURE 3: Cell viability in NPCs treated with SAB and identification of NPCs. (a) MTT assay of NPCs treated with different concentrations of SAB. (b) Morphology of NPCs by phase-contrast microscopy. (c) Immunocytochemistry showing the expression of collagen II in NPCs. (d) Immunofluorescence demonstrating the expression of cytokeratin 19 in NPCs. Scale bars = 50 μm . * $P < 0.05$ compared with the control group. SAB: salvianolic acid B; NPCs: nucleus pulposus cells.

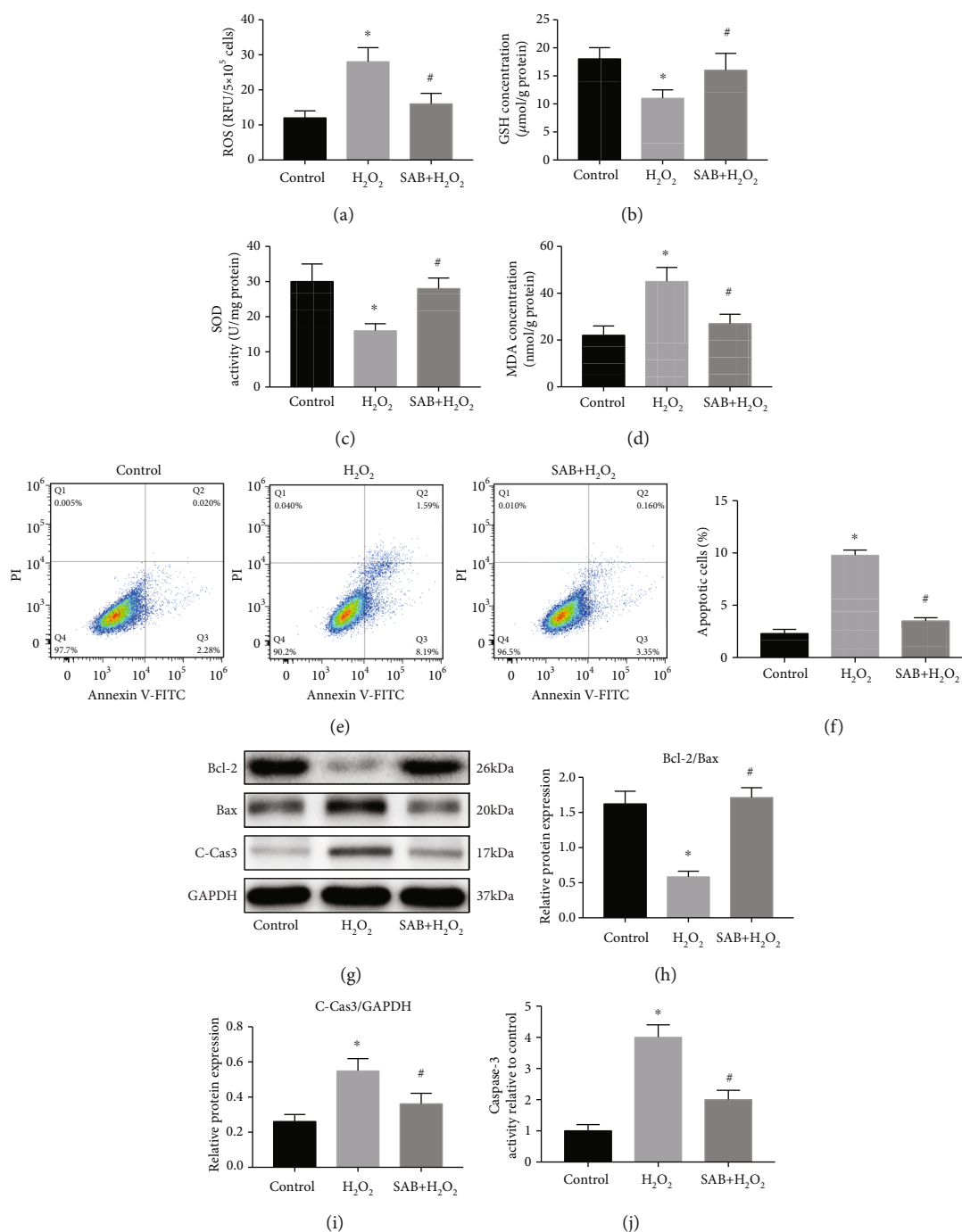


FIGURE 4: SAB attenuated H₂O₂-induced oxidative stress and apoptosis of NPCs *in vitro*. (a) H₂O₂-induced production of ROS was decreased by treatment with SAB. (b–d) Increased oxidative stress (decreased GSH and SOD2, and increased MDA) in the H₂O₂ group was reversed by SAB. (e, f) Flow cytometry assay demonstrated that SAB decreased H₂O₂-induced NPC apoptosis. (g–i) Western blotting showed an elevated ratio of Bcl-2/Bax and decreased level of cleaved caspase-3 in the SAB group compared with the H₂O₂ group. (j) Increased caspase-3 activity in the H₂O₂ group was inhibited by treatment with SAB. **P* < 0.05 compared with the control group; #*P* < 0.05 compared with the H₂O₂ group. SAB: salivianolic acid B; ROS: reactive oxygen species; GSH: glutathione; SOD2: superoxide dismutase; MDA: malondialdehyde; NPCs: nucleus pulposus cells; GAPDH: glyceraldehyde-3-phosphate dehydrogenase; C-Cas3: cleaved caspase-3.

significantly inhibited the proliferation of NPCs while treatment with SAB clearly rescued that reduction in cell proliferation. This indicates that SAB can attenuate disc degeneration, at least partly through the promotion of NPC proliferation.

Oxidative stress has been reported to play a critical role in a number of physiological and pathological processes, activating a variety of signaling pathways, resulting in cell apoptosis or hyperplasia [44]. Oxidative stress that induces excessive ROS production can injure DNA and cells, while

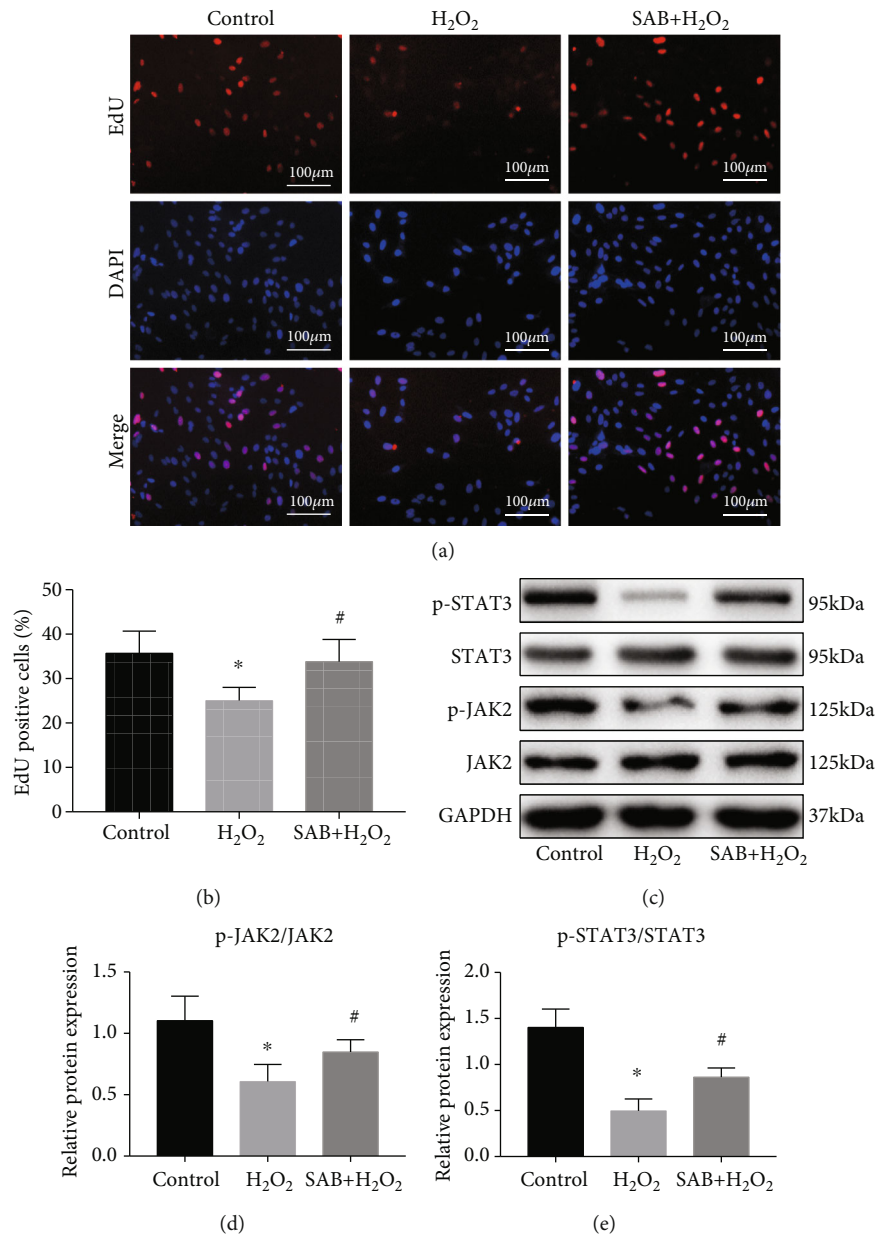


FIGURE 5: SAB promoted proliferation of NPCs reduced by H₂O₂ *in vitro* via activation of the JAK2/STAT3 signaling pathway. (a, b) EdU assay showed that H₂O₂-induced downregulation of NPC proliferation was reversed by treatment with SAB. (c) JAK2 and p-JAK2 and STAT3 and p-STAT3 were investigated by Western blotting. Expression levels of (d) p-JAK2/JAK2 and (e) p-STAT3/STAT3 increased by SAB in H₂O₂-injured NPCs. Scale bars = 100 μm. **P* < 0.05 compared with the control group; #*P* < 0.05 compared with the H₂O₂ group. SAB: salvianolic acid B; NPCs: nucleus pulposus cells; GAPDH: glyceraldehyde-3-phosphate dehydrogenase; JAK2: Janus kinase 2; STAT3: signal transducer and activator of transcription 3.

ROS scavengers will inhibit the cell apoptosis resulting from a variety of causes [45, 46]. Many previous studies suggest that oxidative stress plays a crucial role in the pathology of IDD [9, 10, 47], and oxidative stress-associated markers are significantly increased in degenerated human IVDs [15–17]. Cell apoptosis and injury can be markedly inhibited by antioxidants via radical-scavenging mechanisms [48]. Further studies have shown that the antioxidant capacity and scavenging activity of SAB were both greater than vitamin C [49]. The quantity of ROS production in microglial cells induced by lipopolysaccharide (LPS) was shown to be inhibited

by SAB in a dose-dependent manner [50], suggesting that SAB is able to prevent oxidative stress. Our data demonstrate that the antioxidant system was weakened by injury or H₂O₂, while the situation could be rescued by treatment with SAB both *in vivo* and *in vitro*. The results of the present study were also consistent with other previous reports [51, 52]. Thus, SAB provides a protective effect against oxidative stress by regulating the antioxidant system.

It was demonstrated many years ago that apoptosis participates in IDD, large numbers of IVD cells undergoing programmed cell death [53]. Excessive apoptosis of NPCs

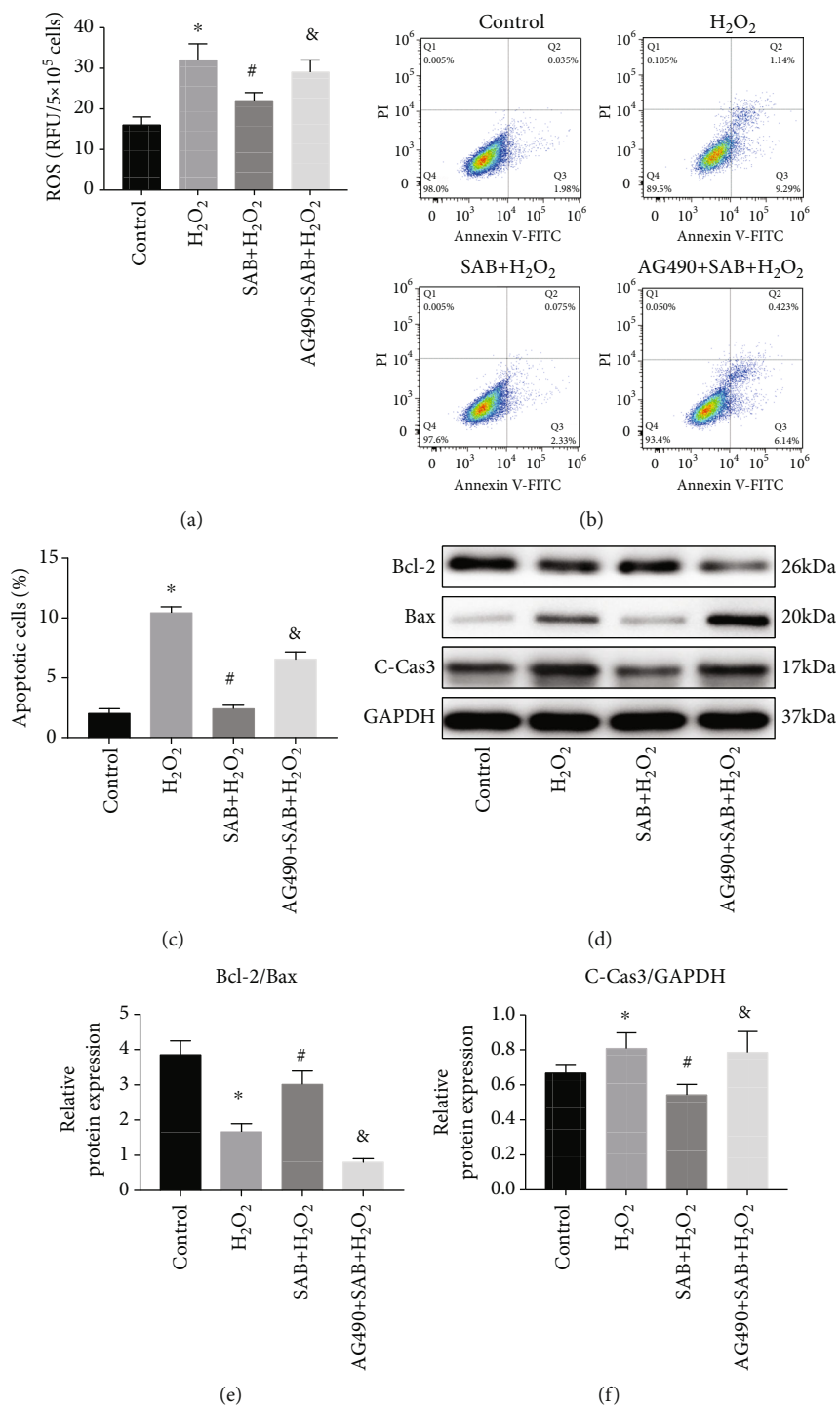


FIGURE 6: Continued.

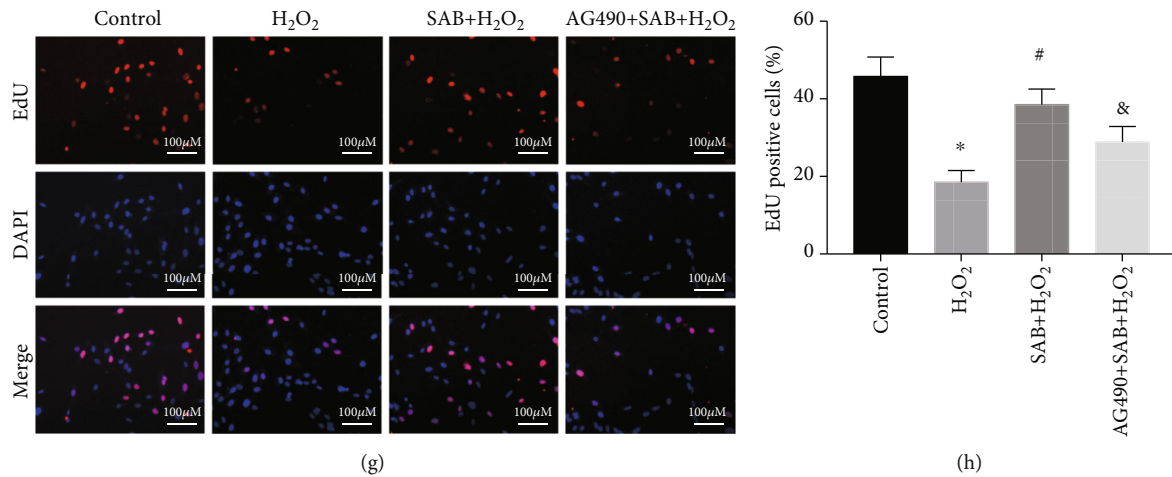


FIGURE 6: SAB reduced H₂O₂-induced ROS production, ameliorated H₂O₂-induced NPC apoptosis, and promoted H₂O₂-reduced proliferation of NPCs via the JAK2/STAT3 pathway. (a) Inhibitory effects of SAB on H₂O₂-induced ROS production were abrogated by AG490. (b, c) Flow cytometry demonstrated that the inhibitory effects of SAB on H₂O₂-induced NPCs apoptosis were abrogated by AG490. (d) Apoptosis-associated proteins assessed by Western blotting. Effects of SAB on H₂O₂-induced (e) Bcl-2/Bax and (f) cleaved caspase-3 were abrogated by AG490. (g, h) EdU assay demonstrated that the effects of SAB on NPC proliferation were downregulated by AG490 treatment. Scale bars = 100 μm. **P* < 0.05 compared with the control group; #*P* < 0.05 compared with the H₂O₂ group; &*P* < 0.05 compared with the SAB+H₂O₂ group. SAB: salvianolic acid B; NPCs: nucleus pulposus cells; ROS: reactive oxygen species; C-Cas3: cleaved caspase-3; GAPDH: glyceraldehyde-3-phosphate dehydrogenase.

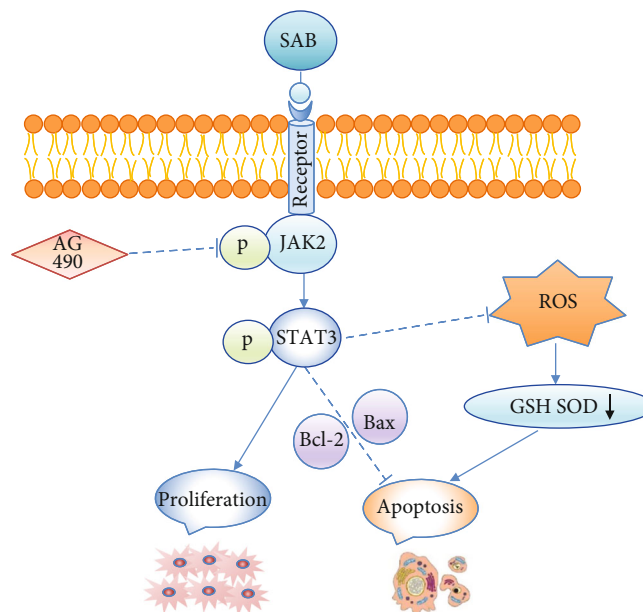


FIGURE 7: Model of involvement of SAB in enhancing proliferation and attenuating oxidative stress and apoptosis through activation of the JAK2/STAT3 signaling pathway. SAB: salvianolic acid B; ROS: reactive oxygen species; JAK2: Janus kinase 2; STAT3: signal transducer and activator of transcription 3; GSH: glutathione; SOD2: superoxide dismutase.

reflects evident cellular and biochemical changes which occur during IDD [54, 55]. It has been reported in previous studies that external stimuli result in oxidative damage and increased apoptosis of NPCs [56–58]. H₂O₂ is commonly used to induce cell injury in *in vitro* experiments [59]. Therefore, we induced oxidative damage using H₂O₂ and investigated whether SAB can influence the apoptosis induced in NPCs by oxidative stress. In the present study, oxidative damage

induced by 100 μM H₂O₂ resulted in significantly increased cell apoptosis. Notably, SAB treatment suppressed H₂O₂-induced NPC apoptosis, promoted Bcl-2 expression, and inhibited the expression of Bax, thus rescuing the Bcl-2/Bax protein ratio in the SAB+H₂O₂ group. Additionally, *in vitro* cleaved caspase-3 protein expression and caspase-3 activity were decreased substantially by SAB. This suggests that SAB has the potential to treat IDD by preventing NPC

apoptosis in conditions of oxidative stress. A previous study reported that SAB protected against dopamine-induced apoptosis in SH-SY5Y cells [60]. This protective effect of SAB appears to be due to its antioxidative potential. Additionally, another study demonstrated the protective effect of SAB against ox-LDL-induced HUVEC injury and apoptosis [61]. Finally, it was demonstrated that SAB protected vascular endothelial cells against oxidative stress-induced injury [28]. These findings further support the present observations.

Based on the previous findings, the underlying molecular mechanism and pathways of the IDD-attenuating properties of SAB were further explored. In the present study, the expression levels of p-JAK2 and p-STAT3 proteins in the SAB group were higher than those in the corresponding model group. However, after the addition of AG490, the p-JAK2 and p-STAT3 protein levels were clearly reduced. These findings demonstrate that the JAK2/STAT3 pathway can be activated by SAB, and treatment with the JAK2 antagonist AG490 significantly abrogated inhibition of apoptosis and promotion of proliferation by SAB. According to Liu et al. [62], SAB is able to maintain stem cell pluripotency via the JAK2/STAT3 signaling pathway. Liu et al. demonstrated that articular cartilage degeneration in osteoarthritis can be rescued by treatment with Danshen (that contains SAB), both *in vivo* and *in vitro* via activation of the JAK2/STAT3 pathway [62]. Furthermore, SMND-309, a novel derivative of SAB, has been shown to protect rat brains from ischemia and reperfusion damage via the JAK2/STAT3 signaling pathway. However, it should also be noted that the JAK2/STAT3 signaling pathway is probably not the only signaling pathway by which SAB attenuates IDD. It has previously been shown that SAB maintained stem cell pluripotency and promoted cell proliferation via activation of the JAK2/STAT3 pathway, in addition to the epidermal growth factor receptor-(EGFR-) extracellular signal-regulated kinase 1/2 (ERK1/2) pathways [62]. However, further evidence is required. The JAK2-STAT3 signaling pathway consists of three main components, namely, tyrosine kinase associated receptor (TKAR), JAK2, and STAT3. The receptors of multiple cytokines such as interleukins, growth hormones, epidermal growth factor, platelet-derived growth factor, and interferon are present on cell membranes. The binding of such a ligand to its corresponding receptor can activate JAK2, STAT3, and other target proteins that initiate the transcription of target genes representing the transmission of a biological signal from the extracellular environment to the intracellular biochemical systems. As a water-soluble substance, we speculate that SAB may also initiate a signaling cascade to achieve its multiple biological functions through combining with the cell membrane receptor, TKAR. However, reports of such aspects have not so far been found. Therefore, we will focus on the SAB receptor and its target genes in subsequent experiments to fully elucidate the complete signaling pathway. Together with the aforementioned findings, the present study demonstrates that SAB attenuates NPC apoptosis induced by oxidative damage and promotes cell proliferation via regulation of the JAK2/STAT3 signaling pathway.

However, there remain some limitations to the study. Firstly, we recognize that the protective effects of SAB on IDD require additional confirmation, especially in high-level animals or even humans before it can be used clinically. Secondly, the optimal therapeutic dose requires additional study, if possible. Thirdly, to further illustrate the molecular mechanism by which SAB inhibits IDD, additional research is required.

In conclusion, the results of the research suggest that SAB can reduce IVD degeneration *in vivo*, inhibit oxidative stress and apoptosis of NPCs, and promote cell proliferation in an IDD model *in vitro*. Additional study indicated that activation of the JAK2/STAT3 pathway is involved in the pathology of IDD. Taken together, it can be concluded that SAB ameliorates IDD by activating the JAK2/STAT3 signaling pathway. The results suggest that SAB may represent a potential treatment for disc degeneration.

Data Availability

The data used to support the findings of this study are available from the corresponding author upon request.

Conflicts of Interest

The authors declare that they have no conflicts of interest.

Authors' Contributions

Shouqian Dai, Ting Liang, and Xiu Shi contributed equally to this work.

References

- [1] T. Pulickal, J. Boos, M. Konieczny et al., "MRI identifies biochemical alterations of intervertebral discs in patients with low back pain and radiculopathy," *European Radiology*, vol. 29, no. 12, pp. 6443–6446, 2019.
- [2] V. K. Podichetty, "The aging spine: the role of inflammatory mediators in intervertebral disc degeneration," *Cellular and Molecular Biology*, vol. 53, no. 5, pp. 4–18, 2007.
- [3] C. Speed, "Low back pain," *BMJ*, vol. 328, no. 7448, pp. 1119–1121, 2004.
- [4] G. Waddell, "Low back pain: a twentieth century health care enigma," *Spine*, vol. 21, no. 24, pp. 2820–2825, 1996.
- [5] N. V. Vo, R. A. Hartman, P. R. Patil et al., "Molecular mechanisms of biological aging in intervertebral discs," *Journal of Orthopaedic Research*, vol. 34, no. 8, pp. 1289–1306, 2016.
- [6] C. L. Le Maitre, A. J. Freemont, and J. A. Hoyland, "The role of interleukin-1 in the pathogenesis of human intervertebral disc degeneration," *Arthritis Research & Therapy*, vol. 7, no. 4, pp. R732–R745, 2005.
- [7] C. J. Hunter, J. R. Matyas, and N. A. Duncan, "Cytomorphology of notochordal and chondrocytic cells from the nucleus pulposus: a species comparison," *Journal of Anatomy*, vol. 205, no. 5, pp. 357–362, 2004.
- [8] H. E. Gruber and E. N. Hanley Jr., "Analysis of aging and degeneration of the human intervertebral disc. Comparison of surgical specimens with normal controls," *Spine*, vol. 23, no. 7, pp. 751–757, 1998.

- [9] S. Suzuki, N. Fujita, N. Hosogane et al., "Excessive reactive oxygen species are therapeutic targets for intervertebral disc degeneration," *Arthritis Research & Therapy*, vol. 17, article 316, 2015.
- [10] A. Dimozi, E. Mavrogonatou, A. Sklirou, and D. Kletsas, "Oxidative stress inhibits the proliferation, induces premature senescence and promotes a catabolic phenotype in human nucleus pulposus intervertebral disc cells," *European Cells and Materials*, vol. 30, pp. 89–102, 2015.
- [11] K. Schroder, "NADPH oxidases in bone homeostasis and osteoporosis," *Free Radical Biology and Medicine*, vol. 132, pp. 67–72, 2019.
- [12] D. Harman, "Aging: a theory based on free radical and radiation chemistry," *Journal of gerontology*, vol. 11, no. 3, pp. 298–300, 1956.
- [13] T. Finkel and N. J. Holbrook, "Oxidants, oxidative stress and the biology of ageing," *Nature*, vol. 408, no. 6809, pp. 239–247, 2000.
- [14] H. Sies, "Oxidative stress: a concept in redox biology and medicine," *Redox Biology*, vol. 4, pp. 180–183, 2015.
- [15] A. G. Nerlich, B. E. Bachmeier, E. Schleicher, H. Rohrbach, G. Paesold, and N. Boos, "Immunomorphological analysis of RAGE receptor expression and NF- κ B activation in tissue samples from normal and degenerated intervertebral discs of various ages," *Annals of the New York Academy of Sciences*, vol. 1096, pp. 239–248, 2007.
- [16] S. S. Sivan, E. Tsitron, E. Wachtel et al., "Age-related accumulation of pentosidine in aggrecan and collagen from normal and degenerate human intervertebral discs," *Biochemical Journal*, vol. 399, no. 1, pp. 29–35, 2006.
- [17] L. Poveda, M. Hottiger, N. Boos, and K. Wuertz, "Peroxynitrite induces gene expression in intervertebral disc cells," *Spine*, vol. 34, no. 11, pp. 1127–1133, 2009.
- [18] O. S. Leon Fernandez, M. Pantoja, M. T. Diaz Soto et al., "Ozone oxidative post-conditioning reduces oxidative protein damage in patients with disc hernia," *Neurological Research*, vol. 34, no. 1, pp. 59–67, 2012.
- [19] C. To, "Cardiovascular effects of Danshen," *International Journal of Cardiology*, vol. 121, no. 1, pp. 9–22, 2007.
- [20] M. Zeng, L. Pan, S. Qi et al., "Systematic review of recent advances in pharmacokinetics of four classical Chinese medicines used for the treatment of cerebrovascular disease," *Fito-terapia*, vol. 88, pp. 50–75, 2013.
- [21] H. Luo, W. Kong, Y. Hu et al., "Quality evaluation of *Salvia miltiorrhiza* Bge. by ultra high performance liquid chromatography with photodiode array detection and chemical fingerprinting coupled with chemometric analysis," *Journal of Separation Science*, vol. 38, no. 9, pp. 1544–1551, 2015.
- [22] M. Li, F. Wang, Y. Huang et al., "Systemic exposure to and disposition of catechols derived from *Salvia miltiorrhiza* roots (Danshen) after intravenous dosing DanHong injection in human subjects, rats, and dogs," *Drug Metabolism and Disposition*, vol. 43, no. 5, pp. 679–690, 2015.
- [23] Q. Song, X. Han, Y. Xue et al., "Effects of salvanolic acid B on L-type calcium channels and myocardial contractility in isolated rat ventricular myocytes and hERG K⁺ channels expressed in HEK293 cells," *Naunyn-Schmiedeberg's Archives of Pharmacology*, vol. 390, no. 8, pp. 791–799, 2017.
- [24] J. Y. Zhang, B. Zhang, M. Wang et al., "Calcium homeostasis and endoplasmic reticulum stress are involved in Salvanolic acid B-offered protection against cardiac toxicity of arsenic trioxide," *Oncotarget*, vol. 8, no. 57, pp. 97384–97393, 2017.
- [25] T. M. Chang, G. Y. Shi, H. L. Wu et al., "Effects of salvanolic acid B on protein expression in human umbilical vein endothelial cells," *Evidence-Based Complementary and Alternative Medicine*, vol. 2011, Article ID 213050, 9 pages, 2011.
- [26] C. C. Chang, Y. C. Chang, W. L. Hu, and Y. C. Hung, "Oxidative stress and salvia miltiorrhiza in aging-associated cardiovascular diseases," *Oxidative Medicine and Cellular Longevity*, vol. 2016, Article ID 4797102, 11 pages, 2016.
- [27] M. S. Kim, W. S. Lee, J. Jeong, S. J. Kim, and W. Jin, "Induction of metastatic potential by TrkB via activation of IL6/JAK2/STAT3 and PI3K/AKT signaling in breast cancer," *Oncotarget*, vol. 6, no. 37, pp. 40158–40171, 2015.
- [28] H. Zhao, Y. Guo, S. Li et al., "A novel anti-cancer agent Icaritin suppresses hepatocellular carcinoma initiation and malignant growth through the IL-6/Jak2/Stat3 pathway," *Oncotarget*, vol. 6, no. 31, pp. 31927–31943, 2015.
- [29] S. Zhu, Z. Wang, Z. Li et al., "Icaritin suppresses multiple myeloma, by inhibiting IL-6/JAK2/STAT3," *Oncotarget*, vol. 6, no. 12, pp. 10460–10472, 2015.
- [30] J. S. Fridman, P. A. Scherle, R. Collins et al., "Selective inhibition of JAK1 and JAK2 is efficacious in rodent models of arthritis: preclinical characterization of INCB028050," *The Journal of Immunology*, vol. 184, no. 9, pp. 5298–5307, 2010.
- [31] D. Miao and L. Zhang, "Leptin modulates the expression of catabolic genes in rat nucleus pulposus cells through the mitogen-activated protein kinase and Janus kinase 2/signal transducer and activator of transcription 3 pathways," *Molecular Medicine Reports*, vol. 12, no. 2, pp. 1761–1768, 2015.
- [32] L. Kang, Q. Xiang, S. Zhan et al., "Restoration of autophagic flux rescues oxidative damage and mitochondrial dysfunction to protect against intervertebral disc degeneration," *Oxidative Medicine and Cellular Longevity*, vol. 2019, Article ID 7810320, 27 pages, 2019.
- [33] B. Han, K. Zhu, F. C. Li et al., "A simple disc degeneration model induced by percutaneous needle puncture in the rat tail," *Spine*, vol. 33, no. 18, pp. 1925–1934, 2008.
- [34] X. Ma, W. Xu, Z. Zhang et al., "Salvanolic acid B ameliorates cognitive deficits through IGF-1/Akt pathway in rats with vascular dementia," *Cellular Physiology and Biochemistry*, vol. 43, no. 4, pp. 1381–1391, 2017.
- [35] R. C. Lawrence, C. G. Helmick, F. C. Arnett et al., "Estimates of the prevalence of arthritis and selected musculoskeletal disorders in the United States," *Arthritis & Rheumatism*, vol. 41, no. 5, pp. 778–799, 1998.
- [36] M. V. Risbud, J. Fertala, E. J. Vresilovic, T. J. Albert, and I. M. Shapiro, "Nucleus pulposus cells upregulate PI3K/Akt and MEK/ERK signaling pathways under hypoxic conditions and resist apoptosis induced by serum withdrawal," *Spine*, vol. 30, no. 8, pp. 882–889, 2005.
- [37] B. Zhang, L. Xu, N. Zhuo, and J. Shen, "Resveratrol protects against mitochondrial dysfunction through autophagy activation in human nucleus pulposus cells," *Biochemical and Biophysical Research Communications*, vol. 493, no. 1, pp. 373–381, 2017.
- [38] S. P. Liu, H. J. Harn, Y. J. Chien et al., "n-Butylidenephthalide (BP) maintains stem cell pluripotency by activating Jak2/Stat3 pathway and increases the efficiency of iPS cells generation," *PLoS One*, vol. 7, no. 9, article e44024, 2012.
- [39] M. Huang, P. Wang, S. Xu et al., "Biological activities of salvanolic acid B from *Salvia miltiorrhiza* on type 2 diabetes

- induced by high-fat diet and streptozotocin,” *Pharmaceutical Biology*, vol. 53, no. 7, pp. 1058–1065, 2015.
- [40] J. Q. Zhang, X. H. Wu, Y. Feng et al., “Salvianolic acid B ameliorates depressive-like behaviors in chronic mild stressed mice: involvement of the neuroinflammatory pathway,” *Acta Pharmacologica Sinica*, vol. 37, no. 9, pp. 1141–1153, 2016.
- [41] H. S. Yan, C. Hang, S. W. Chen, K. K. Wang, and P. Bo, “Salvianolic acid B combined with mesenchymal stem cells contributes to nucleus pulposus regeneration,” *Connective Tissue Research*, vol. 61, no. 5, pp. 435–444, 2020.
- [42] L. X. Feng, C. J. Jing, K. L. Tang et al., “Clarifying the signal network of salvianolic acid B using proteomic assay and bioinformatic analysis,” *Proteomics*, vol. 11, no. 8, pp. 1473–1485, 2011.
- [43] X. Yang, S. Liu, S. Li et al., “Salvianolic acid B regulates gene expression and promotes cell viability in chondrocytes,” *Journal of Cellular and Molecular Medicine*, vol. 21, no. 9, pp. 1835–1847, 2017.
- [44] S. Ogura and T. Shimomura, “Oxidative stress and organ damages,” *Current Hypertension Reports*, vol. 16, no. 8, article 452, 2014.
- [45] P. Li, Q. L. Zhao, L. H. Wu et al., “Isofraxidin, a potent reactive oxygen species (ROS) scavenger, protects human leukemia cells from radiation-induced apoptosis via ROS/mitochondria pathway in p53-independent manner,” *Apoptosis*, vol. 19, no. 6, pp. 1043–1053, 2014.
- [46] X. Zhang, Y. Chen, G. Cai, X. Li, and D. Wang, “Carnosic acid induces apoptosis of hepatocellular carcinoma cells via ROS-mediated mitochondrial pathway,” *Chemico-Biological Interactions*, vol. 277, pp. 91–100, 2017.
- [47] L. A. Nasto, A. R. Robinson, K. Ngo et al., “Mitochondrial-derived reactive oxygen species (ROS) play a causal role in aging-related intervertebral disc degeneration,” *Journal of Orthopaedic Research*, vol. 31, no. 7, pp. 1150–1157, 2013.
- [48] N. Dilsiz, A. Sahaboglu, M. Z. Yildiz, and A. Reichenbach, “Protective effects of various antioxidants during ischemia-reperfusion in the rat retina,” *Graefes Archive for Clinical and Experimental Ophthalmology*, vol. 244, no. 5, pp. 627–633, 2006.
- [49] Y. Sun, H. Zhu, J. Wang, Z. Liu, and J. Bi, “Isolation and purification of salvianolic acid A and salvianolic acid B from *Salvia miltiorrhiza* by high-speed counter-current chromatography and comparison of their antioxidant activity,” *Journal of Chromatography B*, vol. 877, no. 8-9, pp. 733–737, 2009.
- [50] S. X. Wang, L. M. Hu, X. M. Gao, H. Guo, and G. W. Fan, “Anti-inflammatory activity of salvianolic acid B in microglia contributes to its neuroprotective effect,” *Neurochemical Research*, vol. 35, no. 7, pp. 1029–1037, 2010.
- [51] S. Gao, S. Li, Q. Li et al., “Protective effects of salvianolic acid B against hydrogen peroxide-induced apoptosis of human umbilical vein endothelial cells and underlying mechanisms,” *International Journal of Molecular Medicine*, vol. 44, no. 2, pp. 457–468, 2019.
- [52] D. H. Zhao, Y. J. Wu, S. T. Liu, and R. Y. Liu, “Salvianolic acid B attenuates lipopolysaccharide-induced acute lung injury in rats through inhibition of apoptosis, oxidative stress and inflammation,” *Experimental and Therapeutic Medicine*, vol. 14, no. 1, pp. 759–764, 2017.
- [53] S. Yang, F. Zhang, J. Ma, and W. Ding, “Intervertebral disc ageing and degeneration: the antiapoptotic effect of oestrogen,” *Ageing Research Reviews*, vol. 57, article 100978, 2020.
- [54] H. E. Gruber and E. N. Hanley Jr., “Biologic strategies for the therapy of intervertebral disc degeneration,” *Expert Opinion on Biological Therapy*, vol. 3, no. 8, pp. 1209–1214, 2003.
- [55] D. Wang, Z. Hu, J. Hao et al., “SIRT1 inhibits apoptosis of degenerative human disc nucleus pulposus cells through activation of Akt pathway,” *Age*, vol. 35, no. 5, pp. 1741–1753, 2013.
- [56] F. Zhang, X. Zhao, H. Shen, and C. Zhang, “Molecular mechanisms of cell death in intervertebral disc degeneration (Review),” *International Journal of Molecular Medicine*, vol. 37, no. 6, pp. 1439–1448, 2016.
- [57] F. Ding, Z. W. Shao, and L. M. Xiong, “Cell death in intervertebral disc degeneration,” *Apoptosis*, vol. 18, no. 7, pp. 777–785, 2013.
- [58] C. Q. Zhao, L. S. Jiang, and L. Y. Dai, “Programmed cell death in intervertebral disc degeneration,” *Apoptosis*, vol. 11, no. 12, pp. 2079–2088, 2006.
- [59] L. Xue, Z. Wu, X. P. Ji, X. Q. Gao, and Y. H. Guo, “Effect and mechanism of salvianolic acid B on the myocardial ischemia-reperfusion injury in rats,” *Asian Pacific Journal of Tropical Medicine*, vol. 7, no. 4, pp. 280–284, 2014.
- [60] L. L. Tian, X. J. Wang, Y. N. Sun et al., “Salvianolic acid B, an antioxidant from *Salvia miltiorrhiza*, prevents 6-hydroxydopamine induced apoptosis in SH-SY5Y cells,” *The International Journal of Biochemistry & Cell Biology*, vol. 40, no. 3, pp. 409–422, 2008.
- [61] H. M. Chen, H. Luo, W. B. Zeng et al., “Salvianolic acid B attenuates oxidized low-density lipoprotein-induced endothelial cell apoptosis through inhibition of oxidative stress, p53, and caspase-3 pathways,” *Chinese Journal of Integrative Medicine*, 2017.
- [62] C. H. Liu, W. C. Shyu, R. H. Fu et al., “Salvianolic acid B maintained stem cell pluripotency and increased proliferation rate by activating Jak2–Stat3 combined with EGFR–Erk1/2 pathways,” *Cell Transplant*, vol. 23, no. 4-5, pp. 657–668, 2014.

Research Article

Mechanosensitive Ion Channel Piezo1 Activated by Matrix Stiffness Regulates Oxidative Stress-Induced Senescence and Apoptosis in Human Intervertebral Disc Degeneration

Bingjin Wang , Wencan Ke, Kun Wang, Gaocai Li, Liang Ma, Saideng Lu, Qian Xiang , Zhiwei Liao, Rongjin Luo, Yu Song, Wenbin Hua, Xinghuo Wu, Yukun Zhang , Xianlin Zeng , and Cao Yang 

Department of Orthopaedics, Union Hospital, Tongji Medical College, Huazhong University of Science and Technology, Wuhan 430022, China

Correspondence should be addressed to Xianlin Zeng; 2010xh0875@hust.edu.cn and Cao Yang; caoyangunion@hust.edu.cn

Received 31 October 2020; Revised 10 January 2021; Accepted 16 January 2021; Published 10 February 2021

Academic Editor: Wenyuan Ding

Copyright © 2021 Bingjin Wang et al. This is an open access article distributed under the Creative Commons Attribution License, which permits unrestricted use, distribution, and reproduction in any medium, provided the original work is properly cited.

Mechanical stimulation plays a crucial part in the development of intervertebral disc degeneration (IDD). Extracellular matrix (ECM) stiffness, which is a crucial mechanical microenvironment of the nucleus pulposus (NP) tissue, contributes to the pathogenesis of IDD. The mechanosensitive ion channel Piezo1 mediates mechanical transduction. This study purposed to investigate the function of Piezo1 in human NP cells under ECM stiffness. The expression of Piezo1 and the ECM elasticity modulus increased in degenerative NP tissues. Stiff ECM activated the Piezo1 channel and increased intracellular Ca^{2+} levels. Moreover, the activation of Piezo1 increased intracellular reactive oxygen species (ROS) levels and the expression of GRP78 and CHOP, which contribute to oxidative stress and endoplasmic reticulum (ER) stress. Furthermore, stiff ECM aggravated oxidative stress-induced senescence and apoptosis in human NP cells. Piezo1 inhibition alleviated oxidative stress-induced senescence and apoptosis, caused by the increase in ECM stiffness. Finally, Piezo1 silencing ameliorated IDD in an in vivo rat model and decreased the elasticity modulus of rat NP tissues. In conclusion, we identified the mechanosensitive ion channel Piezo1 in human NP cells as a mechanical transduction mediator for stiff ECM stimulation. Our results provide novel insights into the mechanism of mechanical transduction in NP cells, with potential for treating IDD.

1. Introduction

Low back pain (LBP) caused by the intervertebral disc (IVD) degeneration (IDD) significantly influences the living quality in patients and causes a large financial burden. Weight-bearing and repeated bending are high-risk factors for IDD [1]. During repeated mechanical stimulation, the excessive mechanical load on nucleus pulposus (NP) cells, as keys to the development of degenerative disc diseases, exacerbates IDD progression [2, 3]. However, until recently, detailed pathogenesis and effective treatment of disc degeneration after excessive mechanical load are still not fully elucidated.

Mechanical loading is not only the physiological function of human NP tissues but also an important characteristic of the NP tissue mechanical microenvironment. Pressure and

extracellular matrix (ECM) stiffness are the main mechanical microenvironment in the NP tissue. With changes in the body position and weight bearing, the pressure in the NP tissue can fluctuate greatly, which influences the balance of the mechanical microenvironment of the NP tissue [1]. Compression stress can result in the accelerated functional transition of NP cells and ECM remodeling during the progression of IVD [4].

Among mechanical stimulations, matrix stiffness can profoundly control cell behavior, including proliferation, apoptosis, and differentiation [5–7]. The mechanical properties of ECM in the NP tissue are closely related to IDD, and ECM stiffness increases with increasing age and grade of the degeneration [8]. Matrix stiffness is closely related to NP cell shape, which is crucial in the NP cell phenotype,

and ECM stiffness (0.3 kPa) can regulate the inhibition of F-actin polymerization, cell shape, clustered morphology, and subsequent transcriptional inactivation, which is involved in maintaining the healthy NP cell phenotype [9]. Moreover, substrate stiffness can regulate growth, apoptosis, and ECM metabolism of the annulus fibrosus cells [7]. Although the imbalance of the mechanical microenvironment caused by ECM stiffness is the principal factor that accelerates IDD, the detailed mechanisms of mechanical transductions, which respond to the conversion of mechanical signals into chemical signals, remain unclear.

Previous studies have confirmed that oxidative stress can result in increased concentrations of reactive oxygen species (ROS) and lead to IDD [10, 11]. The increase of ROS has close related to cell senescence and apoptosis. Oxidative stress-induced senescence and apoptosis have been identified as major risk factors of IDD [12–15]. Mechanical compression can increase ROS generation and aggravate NP cell senescence [3]. However, the mechanosignaling pathways underlying mechanical transductions remain elusive.

The mechanosensitive Piezo1 channel is a Ca^{2+} ion channel that responds to mechanical stimulations [16–18]. Piezo1 mediates mechanical transduction in basic life functions, such as vascular development, blood pressure regulation, bone formation, and innate immunity [19–22]. Piezo1 can sense shear stress, mediate neuronal sensing of blood pressure, and play a crucial role in maintaining blood pressure homeostasis [19]. Piezo1 is required for bone formation and can sense and respond to changes in fluid shear stress and microgravity and alter bone formation by affecting bone mass and strength [21, 23]. Moreover, inhibiting Piezo1 allows oligodendrocyte progenitor cells to maintain the activity in stiff tissues caused by aging [24]. In NP cells, Piezo1 can sense abnormal mechanical stretch stress and is involved in regulating NLRP3 inflammasome assembly and NP cell apoptosis [25, 26]. Thus, Piezo1 may play important roles in IDD. The potential roles of Piezo1 activated by stiff ECM and the mechanism of mechanical transduction require further study.

In the present study, we aimed to observe the effect of IDD on ECM stiffness of NP tissues and expression of Piezo1 and provide novel insights into the underlying mechanism of mechanical transduction in NP cell for treating IDD.

2. Material and Methods

2.1. Patient Tissue Samples. Lumbar NP samples were obtained from 18 patients (ten men and eight women; age range: 21–65 years) with lumbar disc herniation and ten patients (four men and six women; age range: 15–25 years) with idiopathic scoliosis. The study protocol was approved by the Ethics Committee of Tongji Medical College, Huazhong University of Science and Technology (no. S214). Written informed consent was obtained from all patients.

2.2. ECM Stiffness. The degree of IDD was estimated before spinal surgery by three experienced spine surgeons using the Pfirrmann magnetic resonance imaging (MRI) grade system (grades I–V) [27]. NP specimens were collected from 18

patients with lumbar disc herniation (grades II–III, 11 patients; grades IV–V, seven patients) and ten patients with idiopathic scoliosis (grade I, six patients; grades II–III, four patients). An atomic force microscope (AFM) (INNOVA, Bruker Nano, Inc, USA) was used to test ECM stiffness of one 20 μm -thick slice at the center of the human or rat disc. The elastic modulus was calculated as described in previous studies [28, 29].

2.3. Isolation and Culture of NP Cells. Three lumbar NP specimens from patients with idiopathic scoliosis were used for NP cell isolation, as described in a previous study [11]. NP cells were plated and cultured at 37°C and 5% CO_2 in Dulbecco's Modified Eagle's Medium/F12 (Gibco, Grand Island, NY, USA) containing 15% fetal bovine serum (Gibco) and 1% penicillin/streptomycin (Invitrogen, Carlsbad, CA, USA). The passage cells were seeded into hydrogels bound to polystyrene plates (Matrigen, Brea, CA) with different stiffnesses (soft: 1 kPa, stiff: 25 kPa) for subsequent experiments. The culture medium was changed every three days.

2.4. Immunohistochemistry. Human NP specimens were fixed with formaldehyde, embedded in paraffin, and sliced into 4 μm sections. Subsequently, the sections were incubated with the antibody against Piezo1 (No. NBP1-78537, Novus, Littleton, CO, USA). The Dako REAL™ En-Vision™ Detection System, Peroxidase/DAB+, Rabbit/Mouse (Dako Cytomation, Glostrup, Denmark), was used to stain the sections according to the manufacturer's instructions. The sections were imaged and analyzed via microscopy (Olympus, Tokyo, Japan).

2.5. Quantitative Reverse Transcription PCR (qRT-PCR). Total RNA from human NP cells in different groups was extracted using TRIzol reagent (Invitrogen, Carlsbad, CA, USA). qRT-PCR was performed according to the manufacturer's instructions. PrimeScript™ 1st RT Master Mix (TaKaRa Biotechnology, Otsu, Japan) was used to synthesize cDNA from total RNA. qRT-PCR was performed using SYBR Prime-Script RT-PCR Kit (TaKaRa Biotechnology, Otsu, Japan) on the CFX connect™ Real-time system (Bio-Rad, USA). The primers of Piezo1 used for qRT-PCR were forward, 5'-ACTT TCTGGTGACCCTGCAC-3', reverse, 5'-GGCAGGTACAG CCACTTGAT-3'. The relative RNA expression levels were normalized to GAPDH (forward, 5'-TCAAGAAGGTGGTG AAGCAGG-3', reverse, 5'-TCAAAGGTGGAGGAGTGGG T-3'). The test was performed in triple replication. The relative Piezo1 expression level was analyzed using the $2^{-\Delta\Delta\text{Ct}}$ method.

2.6. Western Blotting Analysis. Total protein was extracted from human NP cells using radioimmunoprecipitation assay (RIPA) (Beyotime, Shanghai, China) buffer with 1 mmol/L phenylmethanesulfonyl fluoride (PMSF), and total protein concentrations were measured using BCA protein assay kit (Beyotime, Shanghai, China) according to the manufacturer's instructions. The proteins were denatured by heat and stored at -80°C if necessary. Proteins (30 μg) from each sample were separated using surePAGE™ prefabricated gels (4–20%, Genscript, Nanjing, China) and transferred onto polyvinylidene fluoride (PVDF) membrane (Bio-Rad,

Hercules, CA, USA). The membranes were blocked with 5% skimmed milk in Tris-HCl buffer saline containing 0.1% Tween-20 (TBST) and incubated overnight at 4°C with primary antibodies, including Piezo1 (No. NBP1-78537, Novus), GRP78 (No. 11587-1-AP, Proteintech, IL, USA), C/EBP homologous protein (CHOP) (No. 15204-1-AP, Proteintech), cleaved caspase-3 (No. 9664; Cell Signaling Technology, Danvers, MA, USA), Bax (No. 50599-2-Ig, Proteintech), Bcl-2 (No. 12789-1-AP, Proteintech), p53 (No. ab26, Abcam, Cambridge, UK), and p16 (No. ab51243, Abcam), and GAPDH (No. 10494-1-AP, Proteintech) was used as the internal reference protein. After incubation with appropriate HRP-conjugated anti-rabbit or anti-mouse secondary antibodies (Proteintech) (room temperature, 1 h), the protein bands were visualized using an enhanced chemiluminescence reagents (Thermo Fisher Scientific, Waltham, MA, USA) and detected using the ChemiDoc-It 610 imaging system (UVP, upland, CA, USA).

2.7. RNA Interference. Piezo1 silencing was achieved via Piezo1-targeting siRNA (Piezo1: stB0009164A) and the corresponding negative controls (RiboBio, Guangzhou, China). Cell transfections were performed using Lipofectamine 2000 (Invitrogen), according to the manufacturer's protocol.

2.8. Determining Calcium Levels. Intracellular Ca^{2+} levels were detected using the specific Ca^{2+} -sensitive fluorescent indicator Fura-4-AM (MedChemExpress, Monmouth Junction, NJ, USA) according to the manufacturer's instructions. Briefly, after the cells were cultured and treated with stimulation or corresponding reagent, NP cells were incubated with 5 μ M Fura-4-AM for 30 min at 37°C in the dark, and intracellular Ca^{2+} levels were calculated by analyzing fluorescence images collected via fluorescence microscopy (Olympus).

2.9. Flow Cytometry. The apoptosis rate in human NP cells was assessed using an Annexin V-FITC/PI Apoptosis Detection Kit (Yeasen Biotech, Shanghai, China) following the manufacturer's protocols. Fluorescence emission peaks were analyzed using a flow cytometer (BD FACSCalibur; BD Biosciences, San Jose, USA).

2.10. ROS Measurement. Intracellular total ROS levels were measured using 2',7'-dichlorofluorescein diacetate (DCFH-DA, S0033; Beyotime, Shanghai, China) according to the manufacturer's instructions. Subsequently, fluorescence emission peaks were detected using BD FACSCalibur (BD Biosciences).

2.11. Senescence-Associated β -Galactosidase (SA- β -Gal) Staining. SA- β -gal staining was performed using the SA- β -gal staining kit (Beyotime, Shanghai, China) following the manufacturer's instructions. Briefly, human NP cells were cultured in polystyrene plates with different stiffnesses (soft: 1 kPa, stiff: 25 kPa) for 24 h. Cells were washed with phosphate buffer saline (PBS) and fixed with 4% paraformaldehyde (15 min, room temperature), then incubated with fresh SA- β -gal staining solution at 37°C overnight (no CO_2). The senescent NP cells with positive staining were imaged using a light microscope (Olympus). Five fields at

least were selected for analyzation. The average percentage of SA- β -Gal-positive cells was analyzed.

2.12. Immunofluorescence. Immunofluorescence staining was implemented as described in a previous study [30]. Human NP cells in different groups were rinsed with PBS, fixed with 4% paraformaldehyde, and incubated with a primary antibody against Piezo1 (1:50, Novus) overnight at 4°C. After the cells were washed three times and incubated with a goat anti-mouse antibody (1:100; Abcam), nuclei were stained with DAPI (4,6-diamidino-2-phenylindole). The samples were imaged using a fluorescence microscope (Olympus).

2.13. The Rat IDD Model. Sprague-Dawley rats (three months old) were provided by the Laboratory Animal Center of Huazhong University of Science and Technology (Wuhan, China). All experimental protocols were approved by the Animal Experimentation Committee of Huazhong University of Science and Technology (No. S2394). The surgical procedure for constructing rat IDD models was previously described [11, 31]. The rat disc levels Co6/7, Co7/8, and Co8/9 were located, and the annulus fibrosus layer was punctured using a needle (27G) parallel to the end plates, after anesthesia with 2% (weight in volume) pentobarbital (40 mg/kg). Three groups, including Con+siNC, IDD + siNC, and IDD + siPiezo1, were prepared to evaluate the effect of Piezo1 on NP cells and IDD and the potential therapeutic effect of siRNA transfection in vivo. Precisely, 2 μ l of the siRNA solution was slowly injected into the target level, and each needle was kept in the disc for 10 s. Free unrestricted weight bearing activity of all animals was permitted.

2.14. Magnetic Resonance Imaging. Magnetic resonance imaging (MRI) of all rat tails was examined at 4 weeks after surgery and treatment. The T2 weighted images were obtained by using a BioSpec MRI (7.0 T/20 cm; Bruker, Billerica, MA, USA). According to the images, the Pfirrmann grades were used to evaluate the degenerative degree of the rat tails [27]. Subsequent immunohistochemical staining and histological assessment were performed on the discs after the magnetic resonance examination.

2.15. Immunohistochemical Staining and Histological Assessment in Animal Models. Rats were euthanized 4 weeks postsurgery. Rat IDD specimens were harvested, fixed with formaldehyde, decalcified, and embedded in paraffin. Subsequently, the specimens were sliced into 4 μ m sections. Then, the sections were stained with hematoxylin and eosin (HE), as well as Safranin-O (SO). The histopathological assessment was performed as previously described [32]. In addition, the immunohistochemical experiments were performed as described in previous studies [33]. Subsequently, the sections were incubated with primary antibodies against cleaved caspase-3 (Cell Signaling Technology) and p16 (Abcam) overnight at 4°C, and then the sections were incubated with appropriate secondary antibodies and counterstained with hematoxylin. The sections were imaged and analyzed via the digital pathology section scanning system (S360, Hamamatsu, Japan). The histologic grading scale includes the morphology (the shape and the constitution) and

cellularity (the rate of stellar shaped cells and the location of proteoglycan matrix) of the NP tissue, the morphology (collagen lamellae and fibers) and cellularity (the proportion of fibroblasts and chondrocytes) of the anular fibrosus, and continuity of the endplates. The histological score of 5 is classified as normal intervertebral disc, 6 to 11 are classified as moderate IDD, and 12 to 14 are classified as severe IDD.

2.16. Statistical Analysis. Data are presented as the mean \pm standard deviation (SD) of at least three independent experiments. Statistical analyses were performed using GraphPad Prism 8 software (La Jolla, CA, USA). The differences between groups were determined by Student's *t*-test or one-way ANOVA. *P* < 0.05 was considered statistically significant.

3. Results

3.1. Piezo1 Was Upregulated and ECM Stiffness Increased in Degenerative NP Tissues. The Piezo1 mRNA expression increased significantly in human NP tissue specimens with IDD contrasted to that in specimens with idiopathic scoliosis (Figure 1(a)). In addition, immunohistochemistry indicated that the percentage of Piezo1 positive cells increased in the grade IV-V group (Figures 1(b) and 1(c)). Furthermore, the elasticity modulus (~23 kPa) in the IDD group significantly increased, and the elasticity modulus in the grade I group was approximately 2 kPa (Figure 1(d)).

3.2. The Piezo1 Expression in NP Cells Was Upregulated in Response to Stiff ECM. According to the elasticity modulus measured in human NP tissues, NP cells were cultured in polystyrene plates with different stiffnesses (soft: 1 kPa, stiff: 25 kPa) for 6, 12, 24, and 48 h. The Piezo1 mRNA expression was assessed using qRT-PCR. As shown in Figure 2(a), there was a most significant difference in the Piezo1 expression after 24 h of treatment. Furthermore, immunofluorescence showed that the Piezo1 expression increased in stiff substrate (Figure 2(b)). NP cells on the soft substrate showed a round morphology, while elongated and spindle-shaped NP cells were present on the stiff substrate (Figure 2(b)). Additionally, western blotting, qRT-PCR, and corresponding qualification revealed that stiff substrate significantly increased the expression of Piezo1 at protein and mRNA levels (Figures 2(c)–2(e)). Stiff substrate not only increased the expression of Piezo1 but also activated the Piezo1 channel and increased intracellular Ca²⁺ levels (Figure 2(f)).

3.3. Stiff ECM Triggered the Increase of ROS and the Activation of Endoplasmic Reticulum Stress (ER) in Human NP Cells. To investigate whether stiff ECM triggered an increase in ROS and the activation of endoplasmic reticulum stress in human NP cells, the ROS levels in human NP cells were measured after treatment with different levels of stiffness. As shown in Figures 2(g) and 2(h), stiff substrate significantly increased the ROS level. Western blotting and relative quantitative analysis indicated that the protein levels of GPR78 and CHOP were increased in the stiff substrate group contrasted to those in the soft substrate group (Figures 2(i) and 2(j)).

3.4. Piezo1 Knockdown Attenuated Stiff ECM-Induced Increase in ROS and Activation of ER Stress. The effect of Piezo1 on ROS levels and the activation of ER stress were verified via Piezo1 knockdown using siRNA. As shown in Figures 3(a) and 3(b), ROS levels increased in the stiff substrate group, but decreased significantly after Piezo1 was knocked down. These results showed that stiff substrates activated Piezo1 and exacerbated oxidative stress, and clarified Piezo1 plays an important role in ECM stiff-induced oxidative stress through Piezo1 silencing in human NP cells. Moreover, human NP cells transfected with siPiezo1 were treated with the stiff substrate. Western blotting and relative quantitative analysis indicated that GPR78 and CHOP expressions increased in the stiff substrate group. However, Piezo1 knockdown significantly decreased the expression of GPR78 and CHOP, which indicated that treatment with siPiezo1 attenuated stiff ECM-induced ER stress (Figures 3(c) and 3(d)).

3.5. Piezo1 Knockdown Attenuated NP Cell Senescence and Apoptosis Induced by Stiff ECM. The activation of oxidative stress can aggravate senescence and apoptosis in human NP cells. To investigate the effects of the stiff substrate, human NP cells were cultured under the stimulation of stiff ECM for 24 h. The results demonstrated that the expression of cleaved caspase-3, Bax, p53, and p16 increased, and that of Bcl-2 decreased significantly in the stiff substrate group (Figures 3(e) and 3(f)). As shown in Figures 3(i) and 3(j), compared with that in the soft substrate group, the average percentage of SA- β -Gal-positive cells increased in the stiff substrate group. In addition, flow cytometry showed that stiff substrate increased the apoptosis rate in human NP cells (Figures 3(g) and 3(h)). These results indicated that stiff substrates aggravated NP cell senescence and apoptosis. The effect of Piezo1 on stiff ECM-induced NP cell senescence and apoptosis was confirmed using siPiezo1. Piezo1 knockdown in NP cells on stiff substrates downregulated the expression of cleaved caspase-3, Bax, p53, and p16 and upregulated that of Bcl-2 (Figures 3(e) and 3(f)). The results of SA- β -gal staining indicated that siPiezo1 significantly decreased the average percentage of SA- β -gal-positive cells (Figures 3(i) and 3(j)). Moreover, Piezo1 knockdown attenuated stiff substrate-induced apoptosis, manifested by a decrease in the apoptosis rate (Figures 3(g) and 3(h)).

3.6. siPiezo1 Partially Attenuated IDD Progression and Decreased ECM Stiffness In Vivo. To investigate the potential role of Piezo1 in IDD, IDD animal models were established using a disc puncture procedure in Sprague–Dawley rats. The representative T2 weighted MR images and Pfirrmann grades showed that the degeneration degree in the IDD + siNC group was severer than those in the Con+siNC group, the T2 weighted signal intensity was stronger than that in the IDD + siNC group, and the Pfirrmann scores in the IDD + siPiezo1 group were lower than those in the IDD + siNC group (Figures 4(a) and 4(b)). As shown in Figure 4(c), the NP tissue was oval-shaped and occupied a large volume of the whole disc in the Con+siNC group, detected using HE staining. In addition, high glycosaminoglycan content was

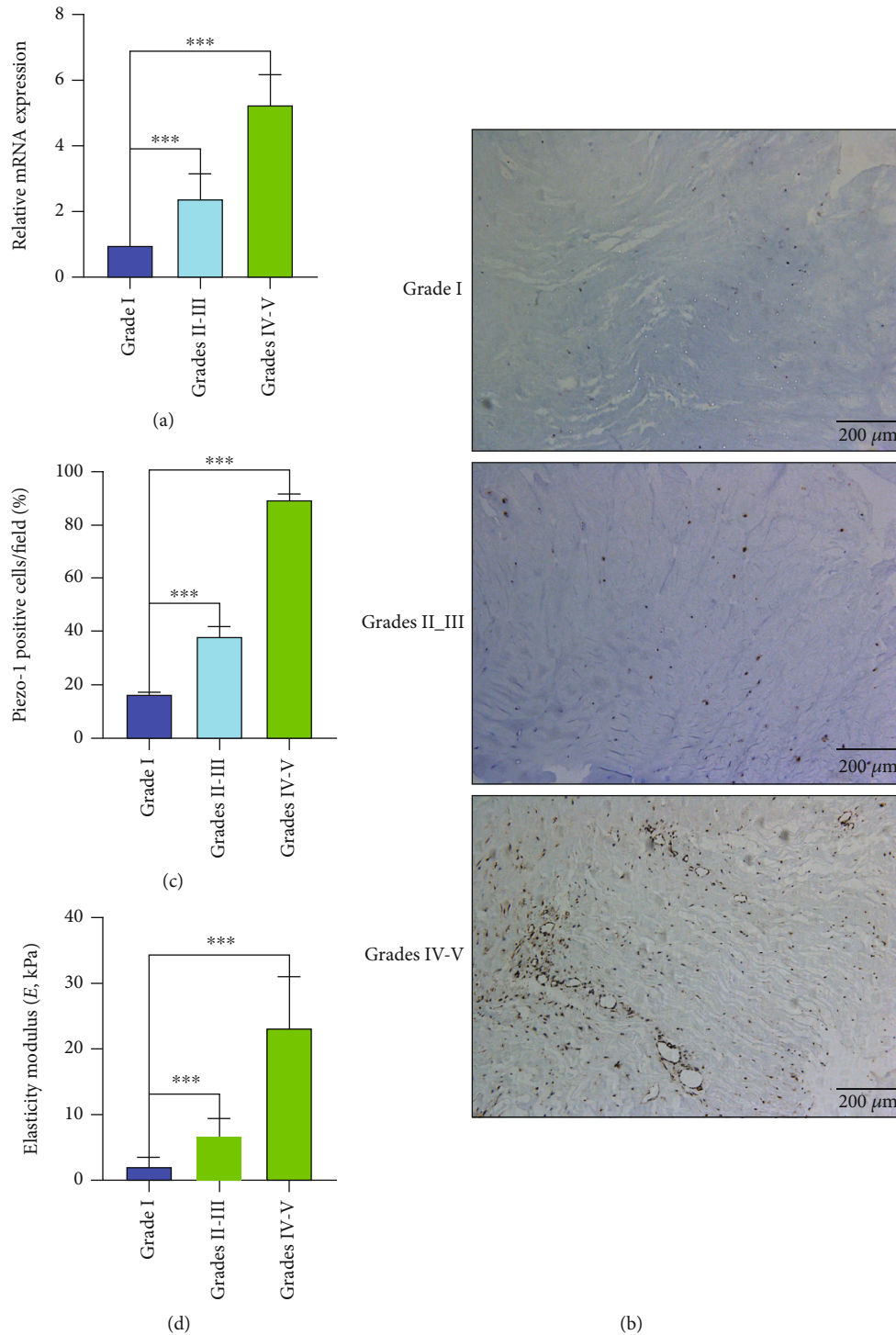


FIGURE 1: The Piezo1 expression and ECM stiffness in degenerative NP tissues. (a) The Piezo1 mRNA expression in human NP tissue specimens with different Pfirrmann grades was determined by qRT-PCR. (b) Immunohistochemistry analysis of Piezo1 in human NP tissue specimens with different Pfirrmann grades. (c) Piezo1-positive cells are presented as mean \pm SD from three independent experiments. (d) The elasticity modulus of human NP tissue specimens with different Pfirrmann grades were measured via atomic force microscope (AFM) (** $P < 0.001$, scale bar: 200 μ m).

confirmed in NP tissues as shown using SO staining in the Con+siNC group (Figure 4(d)). HE staining indicated the destruction of disc morphology, disruption of annulus fibrosus, increased tissue fibrillation, and lower glycosaminoglycan

content in the NP tissue in the IDD+siNC group (Figures 4(c) and 4(d)). Conversely, siPiezo1 ameliorated the changes in IDD compared to the IDD + siNC group, as clarified by the moderate boundary of the nucleus pulposus and

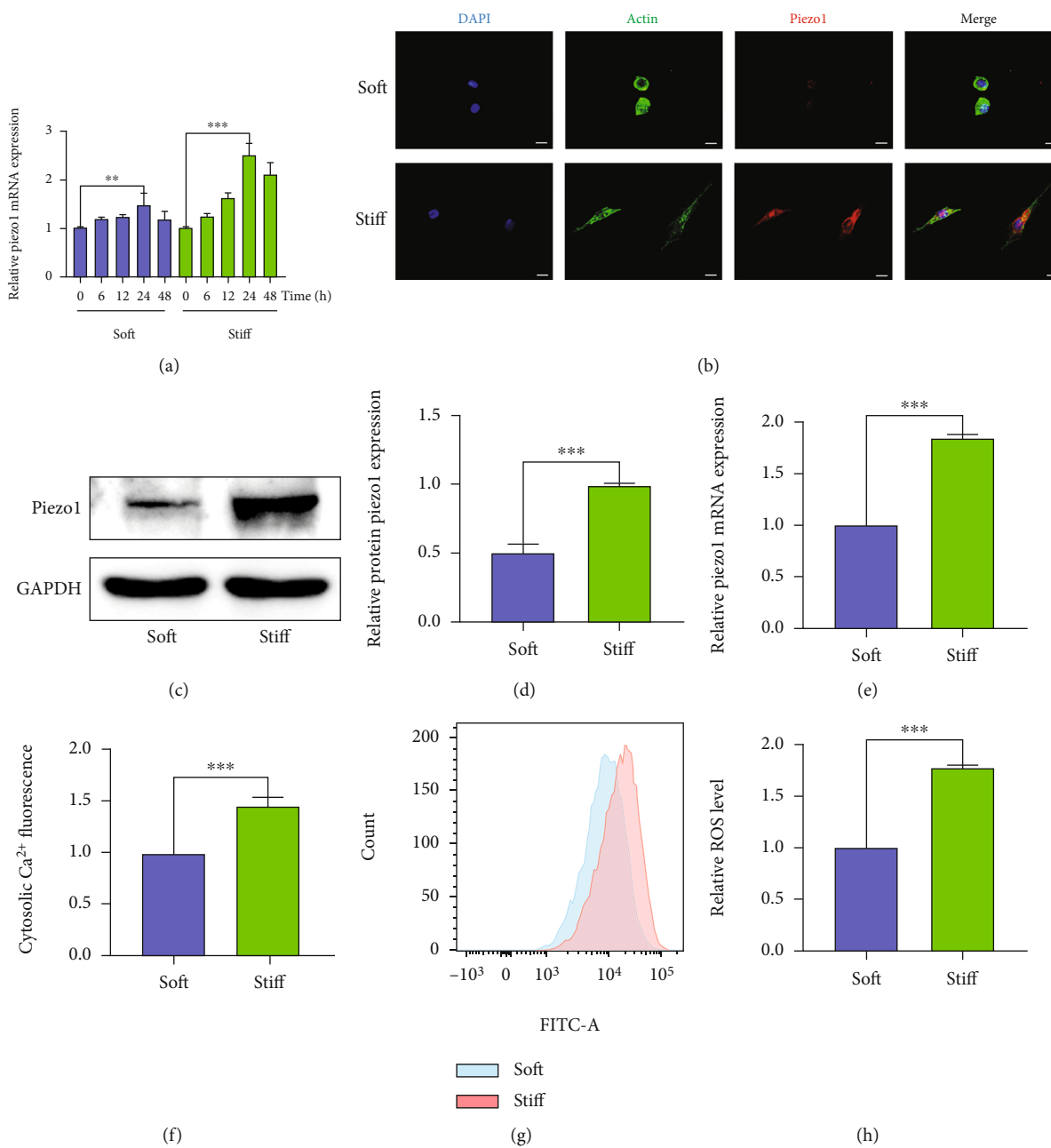


FIGURE 2: Continued.

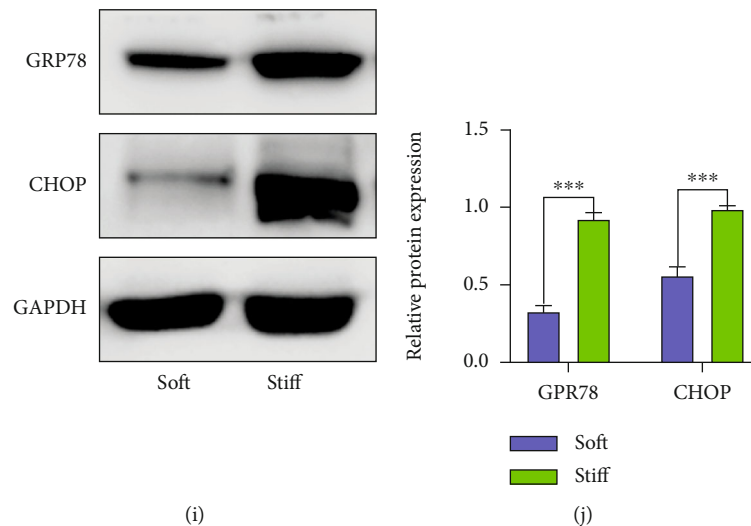


FIGURE 2: Stiff ECM induces the Piezo1 expression and activates oxidative stress and ER stress. (a) Piezo1 mRNA expression levels were analyzed by qRT-PCR in human NP cells cultured in polystyrene plates with different stiffnesses (soft: 1 kPa, stiff: 25 kPa) for 6, 12, 24, and 48 h. (b) The Piezo1 expression and cell morphology after 24 h of treatment were evaluated using immunofluorescence. Cytoskeleton was stained by phalloidin, and Cell nuclei are stained by DAPI. (c, d) The Piezo1 protein level was measured by western blotting. (e) Piezo1 mRNA expression levels were analyzed by qRT-PCR. (f) Intracellular Ca^{2+} levels measured using the specific Ca^{2+} -sensitive fluorescent indicator Fura-4-AM and analyzed via fluorescence microscopy. (g, h) The ROS levels were measured using DCFH-DA and analyzed using a flow cytometer. (i, j) GRP78 and CHOP protein levels were evaluated by western blotting. Data are presented as mean \pm SD (** $P < 0.01$, *** $P < 0.001$, magnification: $\times 400$, scale bar: $50 \mu\text{m}$).

annulus fibrosus and the disc height, although there was still a partial degenerative phenotype (Figures 4(c) and 4(d)). Moreover, histologic scores increased in the IDD + siNC group, but significantly decreased in the IDD + siPiezo1 group (Figure 4(e)). As shown in Figure 4(f), IDD increased the ECM elasticity modulus of the rat NP tissue, compared with that in the control group, and the ECM elasticity modulus in the IDD + siPiezo1 group decreased in vivo as expected. Moreover, immunohistochemical experiments of cleaved caspase-3 and P16 indicated that IDD increased the expression of apoptosis and senescence-related indicators, and siPiezo1 attenuated NP cell apoptosis and senescence in vivo (Figures 4(g) and 4(h)).

4. Discussion

Piezo1, a mechanosensitive ion channel, responds several kinds of mechanical stimulations [21–24]. Extracellular mechanical stimulations are able to activate the open of the Piezo1 channel and regulate the Ca^{2+} influx [16]. ECM stiffness, as one of the mechanical stimulations, may be a crucial regulator of NP cell phenotype, metabolism, and morphology [34]. However, the function of Piezo1 in human NP cells under the ECM stiffness stimulation is still unknown. In this study, the expression and function of Piezo1 in IDD progression were investigated. We demonstrated that the expression of Piezo1 and the ECM elasticity modulus increased in degenerative NP tissues. In addition, the results showed that Piezo1 activated due to matrix stiffness regulated oxidative stress-induced senescence and apoptosis in human IDD. Here, we identified the mechanosensitive ion channel Piezo1

in human NP cells as a mechanical transduction mediator for stiff ECM stimulation (Figure 5).

Piezo1 can be activated by mechanical stretch stimulation in NP cells, and the increase in intracellular Ca^{2+} levels involved in the activation of NLRP3 inflammasome [25]. The expression of Piezo1 is also upregulated under the stimulation of mechanical stretch stress or shear stress [23, 26]. Moreover, intracellular Ca^{2+} elevation disturbs intracellular Ca^{2+} homeostasis, which is closely related to ER stress [35, 36]. The ER stress leads to subsequent cell apoptosis. In chondrocytes, Piezo1, activated by mechanical stretch, plays an important role in ER stress-induced apoptosis [37]. Excessive ER stress can upregulate the expression of GRP78 and CHOP as ER stress markers [36, 38]. Moreover, previous studies have reported that excessive ROS can result in oxidative stress [39]. Similar with previous study, the elasticity modulus increased along with the increase of IDD degree in the present study [8]. The elasticity modulus in the NP tissue with Pfirrmann grades IV-V was about 23 kPa, so 25 kPa was selected as the stiffness of stiff substrate. The results indicated that Piezo1 was activated by stiff ECM, which resulted in intracellular Ca^{2+} elevation and increase in ROS levels, which activated ER stress and oxidative stress. The potential mechanism might be that the stiff ECM regulated NP cell morphology and changed the traction force in the cytomembrane. Previous studies had reported that extracellular mechanical stimuli regulated the traction forces, which activated the Piezo1 channel in the membrane subsequently [40]. In human NP cells, the activation of Piezo1 led to impaired intracellular Ca^{2+} homeostasis and increased ROS levels. Our previous study indicated that intracellular Ca^{2+}

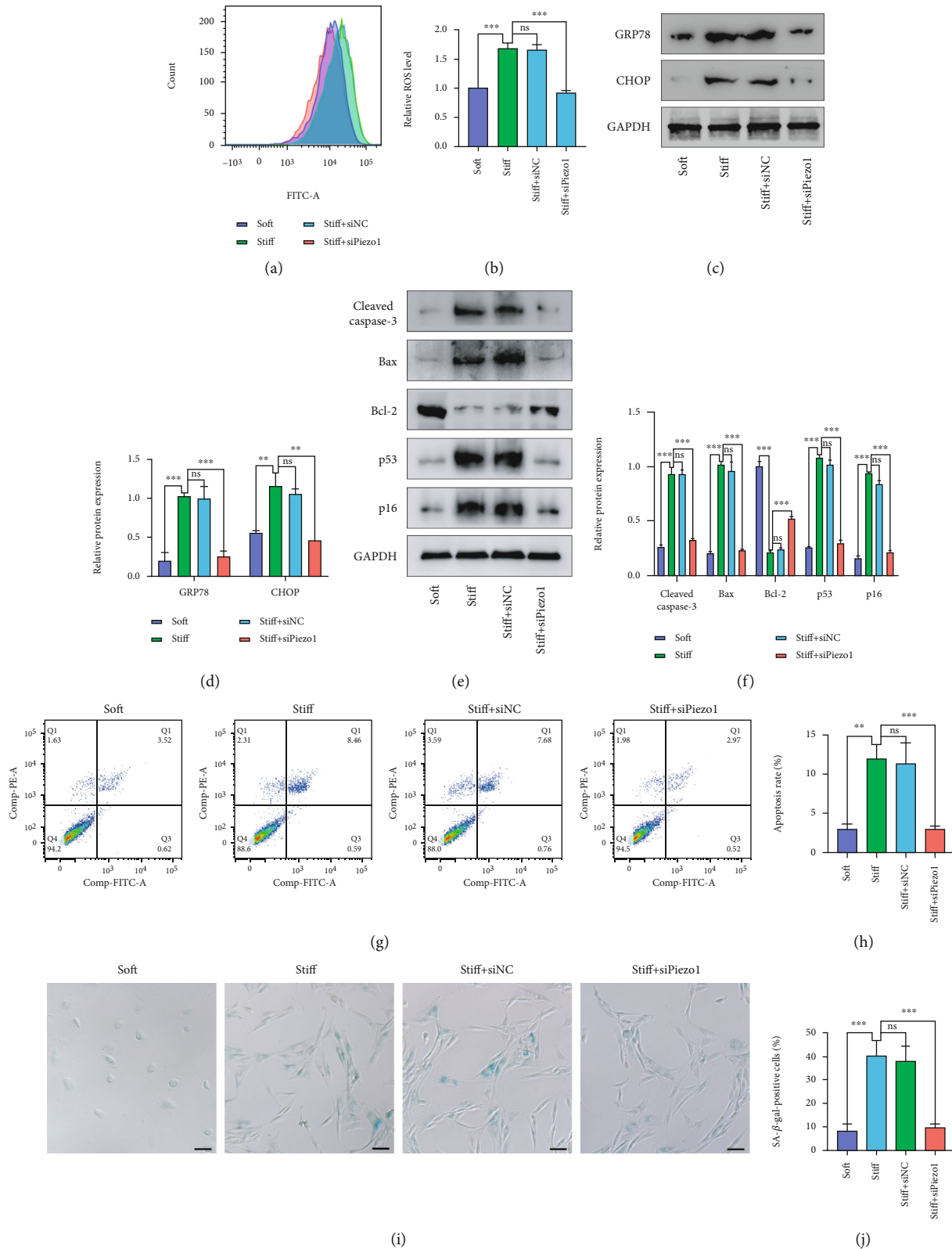


FIGURE 3: Piezo1 knockdown attenuates stiff ECM-induced oxidative stress and ER stress and oxidative stress-induced NP cell senescence and apoptosis. (a, b) The ROS levels were measured using DCFH-DA and analyzed using a flow cytometer. (c, d) GRP78 and CHOP protein levels were evaluated by western blotting. (e, f) The protein levels of cleaved caspase-3, Bax, Bcl-2, p53, and p16 were evaluated by western blotting. (g, h) Flow cytometry was performed to analyze the apoptosis rate in NP cells. (i, j) SA- β -gal staining of human NP cells and the average percentage of SA- β -gal-positive cells in different groups, scale bar: 100 μ m. Data are presented as mean \pm SD (ns: not significant; ** P < 0.01, *** P < 0.001).

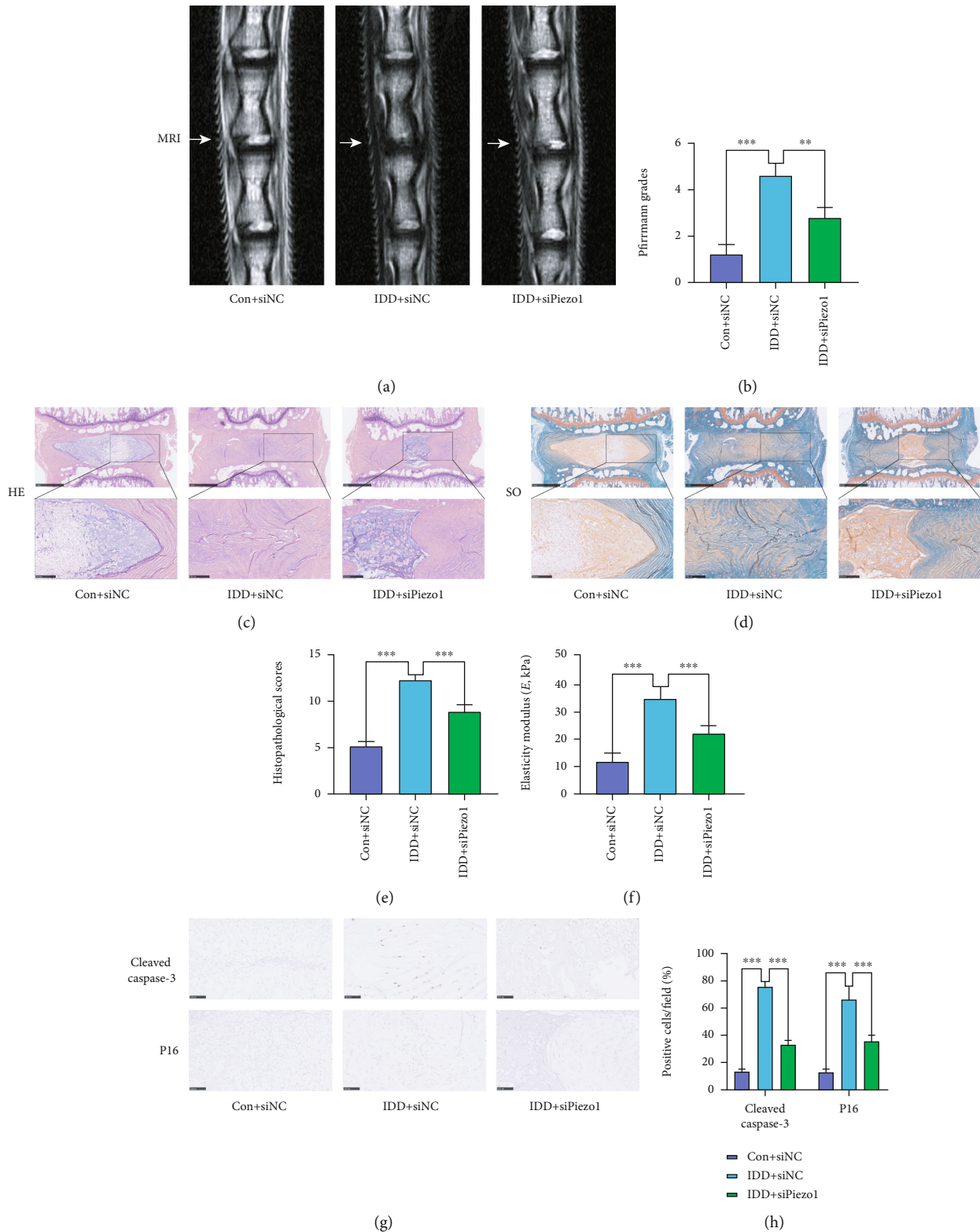


FIGURE 4: siPiezo1 partially ameliorates IDD and decreases ECM stiffness in vivo. (a) The representative T2 weighted MR images of rat tails after surgery and treatment. (b) Pfirrmann grades of different experimental groups at 4 weeks after surgery. (c) Representative HE staining images of disc specimens from different experimental groups, scale bar: 1 mm and 250 μm. (d) Representative SO staining images of disc specimens from different experimental groups, scale bar: 1 mm and 250 μm. (e) Histological scores in different experimental groups. (f) The elasticity modulus of rat NP tissue specimens from different experimental groups was measured via atomic force microscope (AFM). (g) Immunohistochemical experiments of apoptosis indicator (cleaved caspase-3) and senescence marker (P16). (h) Average percentages of cleaved caspase-3 and P16-positive cells in different groups, scale bar: 100 μm. Data are presented as mean ± SD (***) $P < 0.001$.

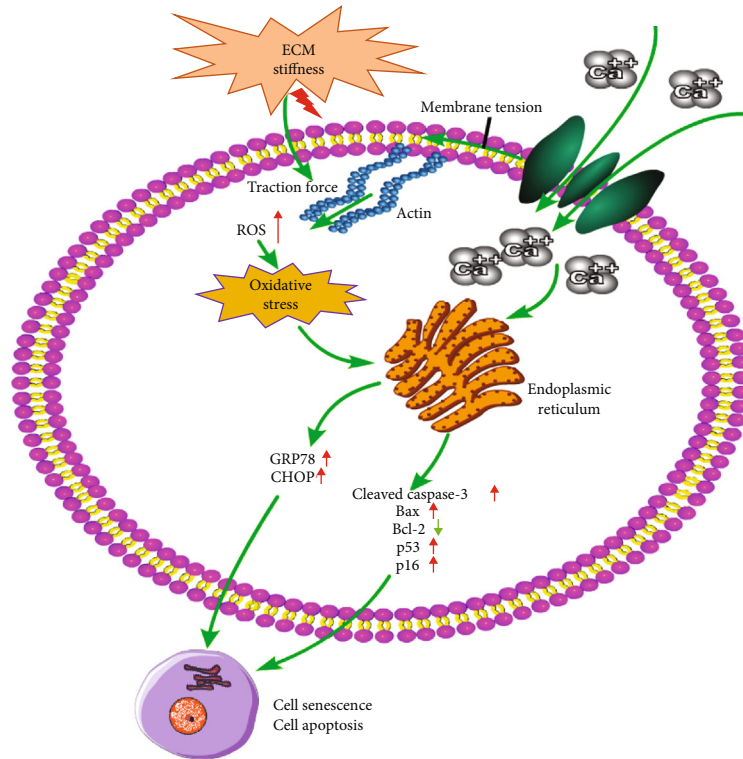


FIGURE 5: Schematic illustration of Piezo1 in human NP cells as a mechanical transduction mediator for stiff ECM stimulation. Piezo1, activated by matrix stiffness, increases intracellular Ca^{2+} levels and regulates ER stress and oxidative stress-induced apoptosis and senescence in human NP cells.

homeostasis impaired influenced the ER stress, and the intracellular ROS level had closely related to oxidative stress [36, 41]. Therefore, stiff ECM regulated ER stress and oxidative stress via the activation of the Piezo1 channel.

Oxidative stress involves in the regulation of apoptosis, senescence, ER stress, and autophagy [36, 41, 42]. Downregulation of Bcl-2, along with upregulation of Bax and cleaved caspase-3 in NP cells, is related to an increase of cell apoptosis [43, 44]. In the present study, stiff ECM decreased the expression of Bcl-2 and increased the expression of Bax and cleaved caspase-3, which indicated that stiff ECM increased the apoptosis of NP cells. Therefore, the apoptosis might be induced by the activation of ER stress and oxidative stress. The upregulation of p53 and p16 as senescence markers is common in IDD [45]. Mechanical stress can induce and promote rat NP cell senescence [46]. In our study, stiff ECM, as a mechanical stimulation, upregulated the expression of p53 and p16 in NP cells, which demonstrated that stiff ECM aggravated the senescence of NP cells. Accumulating studies have reported that excessive ROS accumulation is related to oxidative stress, and cellular senescence occurs under activation of oxidative stress; thus, excessive ROS accumulation contributes to cellular senescence [39, 47, 48]. In human NP cells, cellular senescence could be also due to excessive ROS accumulation and subsequent oxidative stress. Moreover, oxidative stress-induced apoptosis and senescence contribute to IDD progression [14]. The present results indicated that stiff ECM increases intracellular ROS, activates oxidative

stress, and aggravates oxidative stress-induced apoptosis and senescence. The inhibition of Piezo1 attenuated oxidative stress-induced apoptosis and senescence, which indicated that stiff ECM increased oxidative stress-induced apoptosis and senescence via activation of Piezo1.

Piezo1 plays a crucial role in mechanical transduction, and its inhibition can reduce chondrocyte death after mechanical injury [49]. Piezo1 knockdown attenuates mechanical stretch stress-induced apoptosis in NP cells [26]. To the best of related knowledge, the relation between Piezo1 activated by ECM stiffness and oxidative stress or ER stress has not been investigated. In this study, Piezo1 inhibition decreased ROS levels and the expression of GRP78 and CHOP. The oxidative stress and ER stress activated by stiff ECM were inhibited by siPiezo1 in human NP cells. Moreover, Piezo1 knockdown alleviated oxidative stress-induced apoptosis and senescence. Finally, Piezo1 silencing ameliorated IDD in an in vivo rat model and decreased the elasticity modulus of rat NP tissues.

There are some limitations in the present study. First, similar with the animal models in previous studies [11, 31, 44, 50], a simple and effective rat acupuncture model is established to investigate the mechanism of mechanical stimulation in IDD and the potential therapeutic effects of Piezo1 inhibition. However, except for the stimulation of ECM stiffness, the acupuncture of rat tails also causes the biomechanical instability of intervertebral disc. The pathological mechanism of IDD may be related to interactive or

associated effect of different biomechanical stimulations. The interactive relationship of different biomechanical stimulations in IDD should be investigated. Second, the mutation of the mechanosensitive cation channels Piezo2 may be responsible for symptoms of scoliosis. The NP tissues of Pfirrmann grade I were obtained from the patients with idiopathic scoliosis, but the potential genic changes were possible to influence our results about Piezo1. Further studies about the potential influences of Piezo on scoliosis should be conducted. Third, although the current work reveals the mechanism of IDD from a new perspective of biomechanics and oxidative stress according to the results in vitro and in vivo, the particular changing process of oxidative stress and ECM stiffness remains unclear. The histological evaluation in vivo at different time points is needed in further investigations.

5. Conclusion

The present results indicate that Piezo1 activation under stiff ECM is the mechanism underlying oxidative stress-induced apoptosis and senescence in IDD, leading to pathologic progression of IVD. Central to this mechanical signal transduction is the activation of Piezo1. We identified the mechanosensitive ion channel Piezo1 in human NP cells as a mechanical transduction mediator for stiff ECM stimulation. Our results provide novel insights into the mechanism of mechanical transduction in NP cells, with therapeutic potential for treating IDD.

Data Availability

The data are included in the article to support the findings of this study.

Conflicts of Interest

The authors declare that there is no conflict of interest regarding the publication of this paper.

Authors' Contributions

Bingjin Wang, Wencan Ke, and Kun Wang contributed equally to this work.

Acknowledgments

This study was supported by the National Key R&D Program of China (2018YFB1105700), the National Natural Science Foundation of China (81772401 and 82072505), the Fundamental Research Funds for the Central Universities (2019kfyXMBZ063), and the Application Foundation and Advanced Program of Wuhan Science and Technology Bureau (2019020701011457).

References


- [1] P. P. Vergroesen, I. Kingma, K. S. Emanuel et al., "Mechanics and biology in intervertebral disc degeneration: a vicious circle," *Osteoarthritis and Cartilage*, vol. 23, no. 7, pp. 1057–1070, 2015.
- [2] P. Li, R. Zhang, L. Wang et al., "Long-term load duration induces N-cadherin down-regulation and loss of cell phenotype of nucleus pulposus cells in a disc bioreactor culture," *Bio-science Reports*, vol. 37, no. 2, article BSR20160582, 2017.
- [3] P. Li, G. Hou, R. Zhang et al., "High-magnitude compression accelerates the premature senescence of nucleus pulposus cells via the p38 MAPK-ROS pathway," *Arthritis Research & Therapy*, vol. 19, no. 1, p. 209, 2017.
- [4] Q. Bian, L. Ma, A. Jain et al., "Mechanosignaling activation of TGF β maintains intervertebral disc homeostasis," *Bone Research*, vol. 5, no. 1, p. 17008, 2017.
- [5] C. Xue, Q. Huang, T. Zhang et al., "Matrix stiffness regulates arteriovenous differentiation of endothelial progenitor cells during vasculogenesis in nude mice," *Cell Proliferation*, vol. 52, no. 2, article e12557, 2018.
- [6] N. D. Leipzig and M. S. Shoichet, "The effect of substrate stiffness on adult neural stem cell behavior," *Biomaterials*, vol. 30, no. 36, pp. 6867–6878, 2009.
- [7] Y. H. Zhang, C. Q. Zhao, L. S. Jiang, and L. Y. Dai, "Substrate stiffness regulates apoptosis and the mRNA expression of extracellular matrix regulatory genes in the rat annular cells," *Matrix Biology*, vol. 30, no. 2, pp. 135–144, 2011.
- [8] J. Iatridis, L. Setton, M. Weidenbaum, and V. Mow, "Alterations in the mechanical behavior of the human lumbar nucleus pulposus with degeneration and aging," *Journal of Orthopaedic Research: Official Publication of the Orthopaedic Research Society*, vol. 15, no. 2, pp. 318–322, 1997.
- [9] B. V. Fearing, L. Jing, M. N. Barcellona et al., "Mechanosensitive transcriptional coactivators MRTF-A and YAP/TAZ regulate nucleus pulposus cell phenotype through cell shape," *The FASEB Journal*, vol. 33, no. 12, pp. 14022–14035, 2019.
- [10] C. Feng, M. Yang, M. Lan et al., "ROS: crucial intermediators in the pathogenesis of intervertebral disc degeneration," *Oxidative Medicine and Cellular Longevity*, vol. 2017, Article ID 5601593, 12 pages, 2017.
- [11] Y. Song, S. Li, W. Geng et al., "Sirtuin 3-dependent mitochondrial redox homeostasis protects against AGEs-induced intervertebral disc degeneration," *Redox Biology*, vol. 19, pp. 339–353, 2018.
- [12] P. Patil, M. Falabella, A. Saeed et al., "Oxidative stress-induced senescence markedly increases disc cell bioenergetics," *Mechanisms of Ageing and Development*, vol. 180, pp. 97–106, 2019.
- [13] H. Che, J. Li, Y. Li et al., "p16 deficiency attenuates intervertebral disc degeneration by adjusting oxidative stress and nucleus pulposus cell cycle," *Elife*, vol. 9, 2020.
- [14] L. Kang, S. Liu, J. Li, Y. Tian, Y. Xue, and X. Liu, "Parkin and Nrf2 prevent oxidative stress-induced apoptosis in intervertebral endplate chondrocytes via inducing mitophagy and anti-oxidant defenses," *Life Sciences*, vol. 243, p. 117244, 2020.
- [15] Y. Zhang, B. Yang, J. Wang et al., "Cell senescence: a non-negligible cell state under survival stress in pathology of intervertebral disc degeneration," *Oxidative Medicine and Cellular Longevity*, vol. 2020, Article ID 9503562, 12 pages, 2020.
- [16] B. Coste, B. Xiao, J. S. Santos et al., "Piezo proteins are pore-forming subunits of mechanically activated channels," *Nature*, vol. 483, no. 7388, pp. 176–181, 2012.

- [17] B. Coste, J. Mathur, M. Schmidt et al., "Piezo1 and Piezo2 are essential components of distinct mechanically activated cation channels," *Science*, vol. 330, no. 6000, pp. 55–60, 2010.
- [18] K. Saotome, S. E. Murthy, J. M. Kefauver, T. Whitwam, A. Papatoutian, and A. B. Ward, "Structure of the mechanically activated ion channel Piezo1," *Nature*, vol. 554, no. 7693, pp. 481–486, 2018.
- [19] W. Z. Zeng, K. L. Marshall, S. Min et al., "PIEZOs mediate neuronal sensing of blood pressure and the baroreceptor reflex," *Science*, vol. 362, no. 6413, pp. 464–467, 2018.
- [20] D. Douguet, A. Patel, A. Xu, P. M. Vanhoutte, and E. Honore, "Piezo ion channels in cardiovascular mechanobiology," *Trends in Pharmacological Sciences*, vol. 40, no. 12, pp. 956–970, 2019.
- [21] W. Sun, S. Chi, Y. Li et al., "The mechanosensitive Piezo1 channel is required for bone formation," *Elife*, vol. 8, article e47454, 2019.
- [22] A. G. Solis, P. Bielecki, H. R. Steach et al., "Mechanosensation of cyclical force by PIEZO1 is essential for innate immunity," *Nature*, vol. 573, no. 7772, pp. 69–74, 2019.
- [23] X. Li, L. Han, I. Nookaew et al., "Stimulation of Piezo1 by mechanical signals promotes bone anabolism," *Elife*, vol. 8, article e49631, 2019.
- [24] M. Segel, B. Neumann, M. F. E. Hill et al., "Niche stiffness underlies the ageing of central nervous system progenitor cells," *Nature*, vol. 573, no. 7772, pp. 130–134, 2019.
- [25] Y. Sun, P. Leng, M. Song et al., "Piezo1 activates the NLRP3 inflammasome in nucleus pulposus cell-mediated by Ca^{2+} /NF- κ B pathway," *International Immunopharmacology*, vol. 85, article 106681, 2020.
- [26] Q. Yang, Y. Zhou, J. Wang, W. Fu, and X. Li, "Study on the mechanism of excessive apoptosis of nucleus pulposus cells induced by shRNA-Piezo1 under abnormal mechanical stretch stress," *Journal of Cellular Biochemistry*, vol. 120, no. 3, pp. 3989–3997, 2018.
- [27] C. Pfirrmann, A. Metzendorf, M. Zanetti, J. Hodler, and N. Boos, "Magnetic resonance classification of lumbar intervertebral disc degeneration," *Spine*, vol. 26, no. 17, pp. 1873–1878, 2001.
- [28] T. Liang, D. Y. Zhong, Y. J. Che et al., "Nano and micro biomechanical analyses of the nucleus pulposus after *in situ* immobilization in rats," *Micron*, vol. 130, p. 102824, 2020.
- [29] M. Loparic, D. Wirz, A. U. Daniels et al., "Micro- and nanomechanical analysis of articular cartilage by indentation-type atomic force microscopy: validation with a gel-microfiber composite," *Biophysical Journal*, vol. 98, no. 11, pp. 2731–2740, 2010.
- [30] S. Zhan, K. Wang, Q. Xiang et al., "lncRNA HOTAIR upregulates autophagy to promote apoptosis and senescence of nucleus pulposus cells," *Journal of Cellular Physiology*, vol. 235, no. 3, pp. 2195–2208, 2020.
- [31] D. Chen, D. Xia, Z. Pan et al., "Metformin protects against apoptosis and senescence in nucleus pulposus cells and ameliorates disc degeneration *in vivo*," *Cell Death & Disease*, vol. 7, no. 10, article e2441, 2016.
- [32] H. J. Mao, Q. X. Chen, B. Han et al., "The effect of injection volume on disc degeneration in a rat tail model," *Spine (Phila Pa 1976)*, vol. 36, no. 16, pp. E1062–E1069, 2011.
- [33] Z. Liao, R. Luo, G. Li et al., "Exosomes from mesenchymal stem cells modulate endoplasmic reticulum stress to protect against nucleus pulposus cell death and ameliorate intervertebral disc degeneration *in vivo*," *Theranostics*, vol. 9, no. 14, pp. 4084–4100, 2019.
- [34] P. Y. Hwang, J. Chen, L. Jing, B. D. Hoffman, and L. A. Setton, "The role of extracellular matrix elasticity and composition in regulating the nucleus pulposus cell phenotype in the intervertebral disc: a narrative review," *Journal of Biomechanical Engineering*, vol. 136, no. 2, article 021010, 2014.
- [35] A. Ruiz, C. Matute, and E. Alberdi, "Intracellular Ca^{2+} release through ryanodine receptors contributes to AMPA receptor-mediated mitochondrial dysfunction and ER stress in oligodendrocytes," *Cell Death & Disease*, vol. 1, no. 7, article e54, 2010.
- [36] R. Luo, Y. Song, Z. Liao et al., "Impaired calcium homeostasis via advanced glycation end products promotes apoptosis through endoplasmic reticulum stress in human nucleus pulposus cells and exacerbates intervertebral disc degeneration in rats," *The FEBS Journal*, vol. 286, no. 21, pp. 4356–4373, 2019.
- [37] X. F. Li, Z. Zhang, Z. K. Chen, Z. W. Cui, and H. N. Zhang, "Piezo1 protein induces the apoptosis of human osteoarthritis-derived chondrocytes by activating caspase-12, the signaling marker of ER stress," *International Journal of Molecular Medicine*, vol. 40, no. 3, pp. 845–853, 2017.
- [38] R. Iurlaro and C. Munoz-Pinedo, "Cell death induced by endoplasmic reticulum stress," *The FEBS Journal*, vol. 283, no. 14, pp. 2640–2652, 2016.
- [39] A. Belenguer-Varea, F. J. Tarazona-Santabalbina, J. A. Avellana-Zaragoza, M. Martinez-Reig, C. Mas-Bargues, and M. Inglés, "Oxidative stress and exceptional human longevity: systematic review," *Free Radical Biology and Medicine*, vol. 149, pp. 51–63, 2020.
- [40] K. L. Ellefsen, J. R. Holt, A. C. Chang et al., "Myosin-II mediated traction forces evoke localized Piezo1-dependent Ca^{2+} flickers," *Communications Biology*, vol. 2, no. 1, p. 298, 2019.
- [41] R. Luo, Z. Liao, Y. Song et al., "Berberine ameliorates oxidative stress-induced apoptosis by modulating ER stress and autophagy in human nucleus pulposus cells," *Life Sciences*, vol. 228, pp. 85–97, 2019.
- [42] J. Y. Tang, F. Ou-Yang, M. F. Hou et al., "Oxidative stress-modulating drugs have preferential anticancer effects - involving the regulation of apoptosis, DNA damage, endoplasmic reticulum stress, autophagy, metabolism, and migration," *Seminars in Cancer Biology*, vol. 58, pp. 109–117, 2019.
- [43] H. Sudo and A. Minami, "Regulation of apoptosis in nucleus pulposus cells by optimized exogenous Bcl-2 overexpression," *Journal of Orthopaedic Research*, vol. 28, no. 12, pp. 1608–1613, 2010.
- [44] S. Zhan, K. Wang, Y. Song et al., "Long non-coding RNA HOTAIR modulates intervertebral disc degenerative changes via Wnt/ β -catenin pathway," *Arthritis Research & Therapy*, vol. 21, no. 1, p. 201, 2019.
- [45] P. Li, Y. Gan, Y. Xu et al., "17beta-estradiol attenuates TNF- α -Induced premature senescence of nucleus pulposus cells through regulating the ROS/NF- κ B pathway," *International Journal of Biological Sciences*, vol. 13, no. 2, pp. 145–156, 2017.
- [46] Q. Xing, Q. Liang, Q. Bian et al., "Leg amputation accelerates senescence of rat lumbar intervertebral discs," *Spine*, vol. 35, no. 23, pp. E1253–E1261, 2010.
- [47] R. Colavitti and T. Finkel, "Reactive oxygen species as mediators of cellular senescence," *IUBMB Life*, vol. 57, no. 4–5, pp. 277–281, 2005.

- [48] S. Yang, F. Zhang, J. Ma, and W. Ding, "Intervertebral disc ageing and degeneration: The antiapoptotic effect of oestrogen," *Ageing Research Reviews*, vol. 57, p. 100978, 2020.
- [49] W. Lee, H. A. Leddy, Y. Chen et al., "Synergy between Piezo1 and Piezo2 channels confers high-strain mechanosensitivity to articular cartilage," *Proceedings of the National Academy of Sciences of the United States of America*, vol. 111, no. 47, pp. E5114–E5122, 2014.
- [50] J. Ge, Q. Zhou, X. Cheng et al., "The protein tyrosine kinase inhibitor, genistein, delays intervertebral disc degeneration in rats by inhibiting the p38 pathway-mediated inflammatory response," *Aging*, vol. 12, no. 3, pp. 2246–2260, 2020.

Research Article

Ferroportin-Dependent Iron Homeostasis Protects against Oxidative Stress-Induced Nucleus Pulposus Cell Ferroptosis and Ameliorates Intervertebral Disc Degeneration *In Vivo*

Saideng Lu,¹ Yu Song,¹ Rongjin Luo,¹ Shuai Li,¹ Gaocai Li,¹ Kun Wang,¹ Zhiwei Liao,¹ Bingjin Wang,¹ Wencan Ke,¹ Qian Xiang ¹, Chao Chen,¹ Xinghuo Wu,¹ Yukun Zhang,¹ Li Ling ², and Cao Yang ¹

¹Department of Orthopaedics, Union Hospital, Tongji Medical College, Huazhong University of Science and Technology, Wuhan 430022, China

²Department of Health Management Center, Union Hospital, Tongji Medical College, Huazhong University of Science and Technology, Wuhan 430022, China

Correspondence should be addressed to Li Ling; 1580209179@qq.com and Cao Yang; caoyangunion@hust.edu.cn

Received 5 November 2020; Revised 19 January 2021; Accepted 21 January 2021; Published 10 February 2021

Academic Editor: Sidong Yang

Copyright © 2021 Saideng Lu et al. This is an open access article distributed under the Creative Commons Attribution License, which permits unrestricted use, distribution, and reproduction in any medium, provided the original work is properly cited.

Ferroptosis is a specialized form of regulated cell death that is characterized by iron-dependent lethal lipid peroxidation, a process associated with multiple diseases. However, its role in the pathogenesis of intervertebral disc degeneration (IVDD) is rarely investigated. This study is aimed at investigating the role of ferroptosis in oxidative stress- (OS-) induced nucleus pulposus cell (NPC) decline and the pathogenesis of IVDD and determine the underlying regulatory mechanisms. We used tert-butyl hydroperoxide (TBHP) to simulate OS conditions around human NPCs. Flow cytometry and transmission electron microscopy were used to identify ferroptosis, while iron assay kit, Perl's staining, and western blotting were performed to assay the intracellular iron levels. A ferroportin- (FPN-) lentivirus and FPN-siRNA were constructed and used to explore the relationship between FPN, intracellular iron homeostasis, and ferroptosis. Furthermore, hinokitiol, a bioactive compound known to specifically resist OS and restore FPN function, was evaluated for its therapeutic role in IVDD both *in vitro* and *in vivo*. The results indicated that intercellular iron overload plays an essential role in TBHP-induced ferroptosis of human NPCs. Mechanistically, FPN dysregulation is responsible for intercellular iron overload under OS. The increase in nuclear translocation of metal-regulatory transcription factor 1 (MTF1) restored the function of FPN, abolished the intercellular iron overload, and protected cells against ferroptosis. Additionally, hinokitiol enhanced the nuclear translocation of MTF1 by suppressing the JNK pathway and ameliorated the progression of IVDD *in vivo*. Taken together, our results demonstrate that ferroptosis and FPN dysfunction are involved in the NPC depletion and the pathogenesis of IVDD under OS. To the best of our knowledge, this is the first study to demonstrate the protective role of FPN in ferroptosis of NPCs, suggesting its potential used as a novel therapeutic target against IVDD.

1. Introduction

Intervertebral disc degeneration (IVDD) is a leading cause of low back pain [1], which approximately 80–90% of the global population suffer from, causing immense health and economic burdens [2]. The intervertebral disc (IVD) comprises an inner aggrecan-rich, gel-like nucleus pulposus (NP) and an outer collagen I-rich fibrocartilaginous annu-

lus fibrosus, bordered superiorly and inferiorly by hyaline cartilaginous endplates [3]. Located in the inner disc, NP cells (NPCs) constitute the largest proportion of the cell types found in the NP and are responsible for the synthesis and secretion of the extracellular matrix (ECM) which, in turn, maintains the multiple biological functions of the spine. The depletion of NPCs and the subsequent degradation of the ECM are the primary etiology of IVDD [4].

Therefore, exploring the mechanisms underlying the depletion of NPCs is considered important. IVDD is a complicated process that involves tissue damage caused by age-related changes as well as multiple stress factors [5]. Studies have increasingly implicated oxidative stress (OS) in the initiation and progression of IVDD [5–7]. In addition, reactive oxygen species (ROS) are reportedly involved in the apoptosis, autophagy, and senescence of NPCs, which alter cellular phenotypes and contribute to disc degeneration [2, 8–11]. However, these mechanisms do not fully explain the decline of NPCs or the unsatisfactory performance of current IVDD treatment strategies.

The term ferroptosis, coined in 2012, describes a form of regulated cell death induced by the small molecule erastin, which inhibits the cystine-glutamate antiporter and causes the depletion of glutathione. Ferroptosis is characterized by iron-dependent excessive accumulation of lipid hydroperoxides, which is distinct from necrosis, apoptosis, and autophagy based on biochemical, morphological, and genetic criteria [12]. The main morphological characteristics seen under transmission electron microscopy (TEM) signifying ferroptosis include dense, smaller mitochondria with vestigial cristae and increased membrane density [12]. Ferroptosis could be effectively prevented via specific ferroptosis inhibitors as well as iron chelators, which blocks pathological cell death process in the kidney, cerebrum, and other organs [13]. Ferroptosis is involved in pathological cell death associated with ischemia-reperfusion injury, stroke, carcinogenesis, kidney injury, and degenerative diseases such as Parkinson's, Huntington's, and Alzheimer's diseases [14]. Additionally, some studies found that ferroptosis may also play an important role in IVDD [15, 16].

Ferroportin (FPN), a multitransmembrane protein, is the only known mammalian iron exporter that transports iron from the cytoplasm to the extracellular space [17]. FPN is highly expressed in hepatocytes, macrophages, and duodenal enterocytes, which are responsible for iron acquisition [17]. FPN plays an important role in maintaining cellular iron homeostasis and systemic iron homeostasis. Additionally, altering the FPN expression could cause iron overload or iron deficiency [18]. Ward and Kaplan reported that knocking out FPN expression caused a reduction in the cycling of iron in red blood cell hemoglobin and reduced absorption of dietary iron, which resulted in iron deficiency [19]. Ma et al. demonstrated that intracellular iron accumulation in breast cancer cells, which involves a lack of FPN, contributes to ferroptosis via increasing lipid ROS production by way of Fenton's reaction [20]. In addition to being expressed in the liver, spleen, and duodenum, FPN is also found in the NP tissue of the human IVD in which its role remains undefined.

Metal-regulatory transcription factor 1 (MTF1) is responsible for regulating various metals at the cellular level, especially iron and zinc [21]. When required, MTF1 translocates from the cytosol into the nucleus and binds to the promoters of target genes to activate transcription [21]. Hinokitiol (4-isopropyl-tropolone) is a bioactive aromatic tropolone first isolated from the heart wood of *Chymacyparis taiwanensis*. As a component of essential oils, hinokitiol has been shown to resist OS and restore FPN function [22, 23],

inhibit the activation of JNK, and increase the nuclear translocation of MTF1, which leads to an increase in copper-inducible metallothionein-I transcription [22, 24, 25].

In the current study, OS was induced in NPCs via exposure to tert-butyl hydroperoxide (TBHP). The results indicated that ferroptosis was involved in TBHP-induced human NPC death and IVDD. TBHP aggravated ferroptosis in NPCs by suppressing FPN expression via MTF1. Suppression of the JNK pathway using hinokitiol reversed the ferroptosis induced by the TBHP treatment. We explored the ferroptotic mechanism underlying OS-induced IVDD with the expectation of detecting potential treatment strategies for IVDD.

2. Materials and Methods

2.1. Isolation and Culture of Human NPCs. All experimental were approved by the Ethics Committee of Tongji Medical College, Huazhong University of Science and Technology (No. S214). Having obtained informed consent from all patients, normal NP tissues were acquired from 7 males and 6 females ($n = 13$), aged 11–24 years with a mean age of 15.8 years, who had undergone surgery for idiopathic scoliosis. Degenerative NP tissues were obtained from 6 males and 7 females ($n = 13$), aged 28–65 years with a mean age of 45.2 years, who underwent disc excision surgery for lumbar disc herniation. The degenerative grade of NP tissue samples was classified according to Pfirrmann grades using magnetic resonance images as previously described [7].

Human NPCs were isolated as described previously [26]. Briefly, NP tissues were sectioned into fragments and enzymatically digested with 0.25 mg/ml type II collagenase (Invitrogen) for 6 h. After being washed in PBS and centrifuged, the isolated NPCs were cultured in Dulbecco's modified Eagle medium (DMEM)/F12 (Gibco) containing 15% fetal bovine serum (Gibco) and 1% penicillin-streptomycin (Invitrogen). After identification using NPC markers (CD24, KRT18, Abcam), the second-passage cells were used for subsequent experiments. In our experiments *in vitro*, NPCs were exposed to 25, 50, and 100 μM of TBHP (Sigma) for 6 h or 12 h. For the purpose of inhibiting ferroptosis, NPCs were treated with medium containing ferrostatin-1 5 μM (HY-100579, MedChemExpress), liproxstatin-1 5 μM (HY-12726, MedChemExpress), deferoxamine 100 μM (HY-B0988, MedChemExpress), hinokitiol 8 μM (HY-B2230, MedChemExpress), or SP600125 20 μM , a specific inhibitor of JNK (HY-12041, MedChemExpress), and harvested for subsequent analysis.

2.2. Measurement of Cell Viability and Proliferation. Cell viability was performed using the Cell Counting Kit-8 (CCK-8) (C0037, Beyotime, Shanghai, China) according to the manufacturer's instructions. The absorbance was measured at 450 nm using a spectrophotometer (BioTek, Winooski, VT, USA). NPC proliferation was detected via the incorporation of EdU (5-ethynyl-2'-deoxyuridine) (C0078S; Beyotime, Shanghai, China) according to the manufacturer's instructions, and fluorescence images were acquired using a fluorescence microscope (Olympus, BX53, Melville, NY, USA).

2.3. Lipid ROS Analysis. Lipid ROS levels were assayed using C11-BODIPY 581/591 (Thermo Fisher, D3861) according to the manufacturer's instructions. Briefly, cells were treated with the intended compounds and 10 μ M C11-BODIPY 581/591, following which the preparation was incubated at 37°C for 30 min. Next, cells were washed thrice with PBS before being trypsinized and resuspended in fresh PBS. Fluorescence emission peaks were analyzed using a flow cytometer (BD Biosciences, San Jose, CA, USA). The peak from ~590 nm to ~510 nm is proportional to lipid ROS generation.

2.4. TEM. Cells were fixed in 2.5% glutaraldehyde (Sigma-Aldrich, USA) for 1 h, followed by fixation in 2% osmium tetroxide for 3 h. After washing, cells were stained with 0.5% uranyl acetate for 12 h. Following dehydration and polymerization, samples were cut into 70–90 nm ultrathin sections with an ultramicrotome (EM UC7, Leica) and observed using a transmission electron microscope (FEL, USA).

2.5. Measurement of Labile Iron Levels. Iron concentrations were measured using an iron assay kit (ab83366, Abcam, Cambridge, MA) following the manufacturer's instructions. After being treated with various compounds, cells were collected, homogenized in 5x volume of iron assay buffer on ice, and centrifuged (13,000 \times g, 10 min) at 4°C. The supernatant was collected and 5 μ l of iron reducer was added to each sample and incubated for 30 min at 37°C. Next, 100 μ l of iron probe was added to each sample and incubated for 60 min at 37°C away from light. Absorbance was measured at 593 nm using a microplate reader (Thermo Fisher Scientific).

2.6. Perl's Prussian Blue Stain. The iron content in tissue sections was determined using an iron stain kit (ab150674; Cambridge, UK). Histological sections were deparaffinized and rehydrated. Next, the iron stain solution was produced by combining equal volumes of potassium ferrocyanide and hydrochloric acid solutions. Slides containing tissue sections were incubated in the solution for 3 min, washed with distilled water, stained using Abcam nuclear fast red solution for 5 min, and then washed with distilled water. Finally, the sections were dehydrated in 95% ethanol, followed by absolute ethanol. The final blue stain directly correlates with nonchelated iron in the human NP tissue.

2.7. Western Blotting Analysis. Total proteins, cytoplasmic proteins, and nuclear proteins were extracted from cultured cells using the corresponding kits (Beyotime, Shanghai, China) according to the manufacturer's instructions. The protein samples were incubated with the following primary antibodies: TFRC (1:500), FTL (1:500), DMT1 (1:1000), MTF1 (1:500), JNK (1:1000), beta-actin (1:5000), GAPDH (1:1000), and Histone 3 (1:1000) (all obtained from Proteintech), FPN (1:1000; Novus Biologicals), and Phospho-JNK (1:1000; Cell Signaling Technology). This was followed by incubation with a horseradish peroxidase- (HRP-) conjugated secondary antibody (1:2000; Abcam). Beta-actin, GAPDH, and Histone 3 were used for normalization.

2.8. Quantitative Reverse Transcription Polymerase Chain Reaction (RT-qPCR). TRIzol reagent (Invitrogen) was used to extract total RNA from cultured cells according to the manufacturer's instructions. The following primers were used: Homo FPN (F: 5'-TCTTTGCTTGC GGTCCTGAT-3', R: 5'-GAGCAAACACCCAGCCATT-3'); Homo TFRC (F: 5'-AAATGCCCTCTCTGGTGACG-3', R: 5'-AGCACGATCAGCACAAGTCT-3'); Homo DMT1 (F: 5'-AAAAGCGCAGACTGGATGGA-3', R: 5'-CGATGGTAAGGGGAGGAGGC-3'); and Homo GAPDH (F: 5'-GGAGTCCACTGGCGTCTTCA-3', R: 5'-GTCATGAGT CCTTCCACGATACC-3'). GAPDH was used for normalization.

2.9. RNA Interference. Knockdown of FPN in human NPCs was achieved via transfection of FPN-siRNA (siFPN) (Ribo-Bio Co., Guangzhou, China) using Lipofectamine 2000 (Invitrogen) according to the manufacturer's instructions. After verifying high silencing efficiency, the NPCs were used as the treatment group.

2.10. Plasmids and Transfection. Overexpression of FPN or MTF1 in human NPCs was conducted via transfection of lentiviral plasmid generating Lenti-FPN and Lenti-MTF1, respectively, (GeneChem, Shanghai, China) according to the manufacturer's instructions.

2.11. Surgical Procedure. All procedures involving animal were conducted in accordance with the National Institutes of Health guidelines for the care and use of laboratory animals and were approved by the ethical standards of the Animal Experimentation Committee of Huazhong University of Science and Technology. A simple annulus fibrosus puncture rat model was developed as previously described [27, 28]. Briefly, 40 Sprague-Dawley rats (3 months old) were randomly divided into five groups ($n = 8$ for each group), which were obtained from the Laboratory Animal Center of Huazhong University of Science and Technology (Wuhan, China). After the rats were weighed and anesthetized with 2% (w/v) pentobarbital (40 mg/kg), the experimental level (Co7/8) was located by digital palpation on the coccygeal vertebrae and confirmed by counting the vertebrae from the sacral region in a trial radiograph. The tail skin was sterilized, and the tail vertebral disc of Co7/8 was punctured through the tail skin, parallel to the end plates with a 27-gauge sterile needle from the lateral side of the tail and was held with a 4 mm depth for 30 s. After surgery, DFO, Fer-1, or hinokitiol was diluted with normal saline and injected intraperitoneally for 8 weeks at a dose of 200 mg/kg/d, 150 mg/kg/d, or 150 mg/kg/d, respectively. The degeneration group was administered an equal amount of normal saline daily until the rats were killed. All animals were allowed free unrestricted weight bearing and activity.

2.12. Immunofluorescence Analysis. Immunofluorescence analysis was performed as previously described [29]. First, cells were fixed with 4% paraformaldehyde for 20 min, permeabilized in PBS containing 0.1% Triton X-100 for 3 min, saturated in PBS containing 3% bovine serum albumin

for 1 h, and incubated with anti-MTF1 (1 : 50, Santa Cruz Biotechnology) overnight at 4°C. Subsequently, the cells were incubated with goat anti-mouse antibodies for 1 h. Nuclei were then costained with DAPI (4, 6-diamidino-2-phenylindole) for 5 min, and the results were visualized using an Olympus fluorescence microscope (Olympus, NY, USA).

2.13. Histological and Immunohistological Analyses in Human NP Tissues and Animal Models. NP tissue was fixed in 10% formaldehyde for 24 h, embedded in paraffin, and sliced into 4 μ m sections. For histological analysis, the sections were deparaffinized, rehydrated, and stained with hematoxylin and eosin (HE) and safranin-O (SO). Immunohistochemistry was conducted as previously described [30]. Sections were incubated with primary antibody (diluted 1 : 200) against FPN (NBP1-21502, Novus Biologicals), FTL (10727-1-AP, Proteintech), and MTF1 (25383-1-AP, Proteintech). Next, the sections were incubated with secondary antibody (Santa Cruz Biotechnology). For the negative control, the primary antibodies were replaced with buffer. Finally, three fields of each slide were randomly chosen for microscopic observation using microscopy (Olympus, Tokyo, Japan).

2.14. Statistical Analysis. Data are expressed as the mean \pm SD of at least three independent experiments. Statistical analyses were performed using GraphPad Prism 7 software (La Jolla, CA, USA). Significance of difference was determined by unpaired *t*-test or one-way ANOVA. Significance was defined as $p < 0.05$.

3. Results

3.1. Ferroptosis Was Involved in TBHP-Induced Cell Viability Decline and ROS Accumulation in Human NPCs. Previous studies have demonstrated that peroxide-induced cell death is involved in ferroptosis [31] and that the trigger of ferroptosis requires continuous formation of iron-dependent ROS over an extended period [12]. Therefore, we simulated OS conditions around human NPCs using various concentrations of TBHP for 6 h or 12 h. Cell viability was examined via EdU and CCK-8 assays to observe the impact of TBHP on human NPCs. As the TBHP concentration increased over a period of 6 h or 12 h, the viability of NPCs gradually decreased (Figures 1(a) and 1(b)). However, TBHP-induced decline in the viability of NPCs was significantly rescued by the iron chelator deferoxamine (DFO) and ferroptosis inhibitors ferrostatin-1 (Fer-1) or liproxstatin-1 (Lip-1) [12] (Figures 1(c) and 1(d)). According to previous reports, lipid ROS accumulation is a hallmark of ferroptosis [12]. To verify this, lipid ROS were assessed using flow cytometry via the fluorescent probe, C11-BODIPY. The data indicated that treatment of NPCs with TBHP caused a dose-dependent and time-dependent increase in lipid ROS (Figures 1(e) and 1(f)). Similarly, lipid ROS accumulation was also suppressed by cotreatment with Fer-1, Lip-1, and DFO (Figures 1(g) and 1(h)). In addition, TEM observations indicated that TBHP-treated human NPCs contained smaller mitochondria with increased membrane density compared to

the control group, a morphological characteristic of ferroptosis that is distinct from necrosis, apoptosis, and autophagy [12] (Figure 1(i)). These results suggested that ferroptosis was involved in TBHP-induced cell death in human NPCs, which was significantly alleviated by treatment with ferroptosis inhibitors and iron chelators.

3.2. Ferroptosis in Human NPCs Was Associated with FPN-Dependent Increase in Intracellular Iron Levels. Ferroptosis is an iron-dependent regulated cell death, and cellular iron is required for ferroptotic ROS accumulation [12]. To test the hypothesis that TBHP promotes ferroptotic ROS accumulation through an increase in intracellular iron levels, we determined the levels of labile iron pools (LIP) in human NPCs during exposure to different concentrations of TBHP. LIP can be measured indirectly by monitoring changes in cellular ferritin expression [32]. Western blotting results showed that TBHP treatment resulted in a significant increase in intracellular iron levels compared to that of the control, as indicated by the levels of ferritin light chain (FTL) in human NPCs (Figure 2(a)). To further verify the change in LIP, we directly measured LIP in human NPCs using an iron assay kit (Figure 2(b)), which showed that TBHP treatment led to a dose-dependent increase in intracellular LIP. Immunohistochemistry and Perl's staining of human NP tissues showed that iron in the IVDD group was increased compared to the control group (Figure 2(c)). These results suggested that intercellular iron overload plays an essential role in TBHP-induced ferroptosis of NPCs and IVDD.

Considering that the divalent metal transporter 1 (DMT1), transferrin receptor (TFRC), and FPN are mainly responsible for regulating the intercellular iron levels, we measured the corresponding mRNA and protein expression levels using RT-qPCR and western blotting, respectively. The results showed that FPN, but not TFRC or DMT1, was significantly downregulated in human NPCs treated with TBHP (Figures 2(d) and 2(e)), suggesting that it is FPN that mainly accounts for intercellular iron overload in human NPCs. In addition, we assessed the FPN level in human NP tissue specimens. Immunohistochemistry showed the expression of FPN decreased in the IVDD group compared to the control group (Figure 2(f)). These results demonstrated that FPN was downregulated in TBHP-induced human NPCs as well as human NP tissue of IVDD.

3.3. FPN Protected against TBHP-Induced Intercellular Iron Overload and Ferroptosis in Human NPCs. To further determine the role of FPN in generating intercellular iron overload and ferroptosis in human NPCs, we knocked down FPN using siFPN and overexpressed FPN by transfecting a lentiviral plasmid (Lenti-FPN) in control NPCs and TBHP-induced NPCs. Western blotting results showed the knock-down of FPN was efficient, and it increased intercellular iron levels in both control NPCs and TBHP-induced NPCs, indicated in ferritin and LIP (Figures 3(a) and 3(b)). FPN knock-down not only partially mimicked the effect of ferroptosis in control NPCs but also aggravated this effect in TBHP-induced NPCs (Figures 3(c)–3(e)). In addition, the results

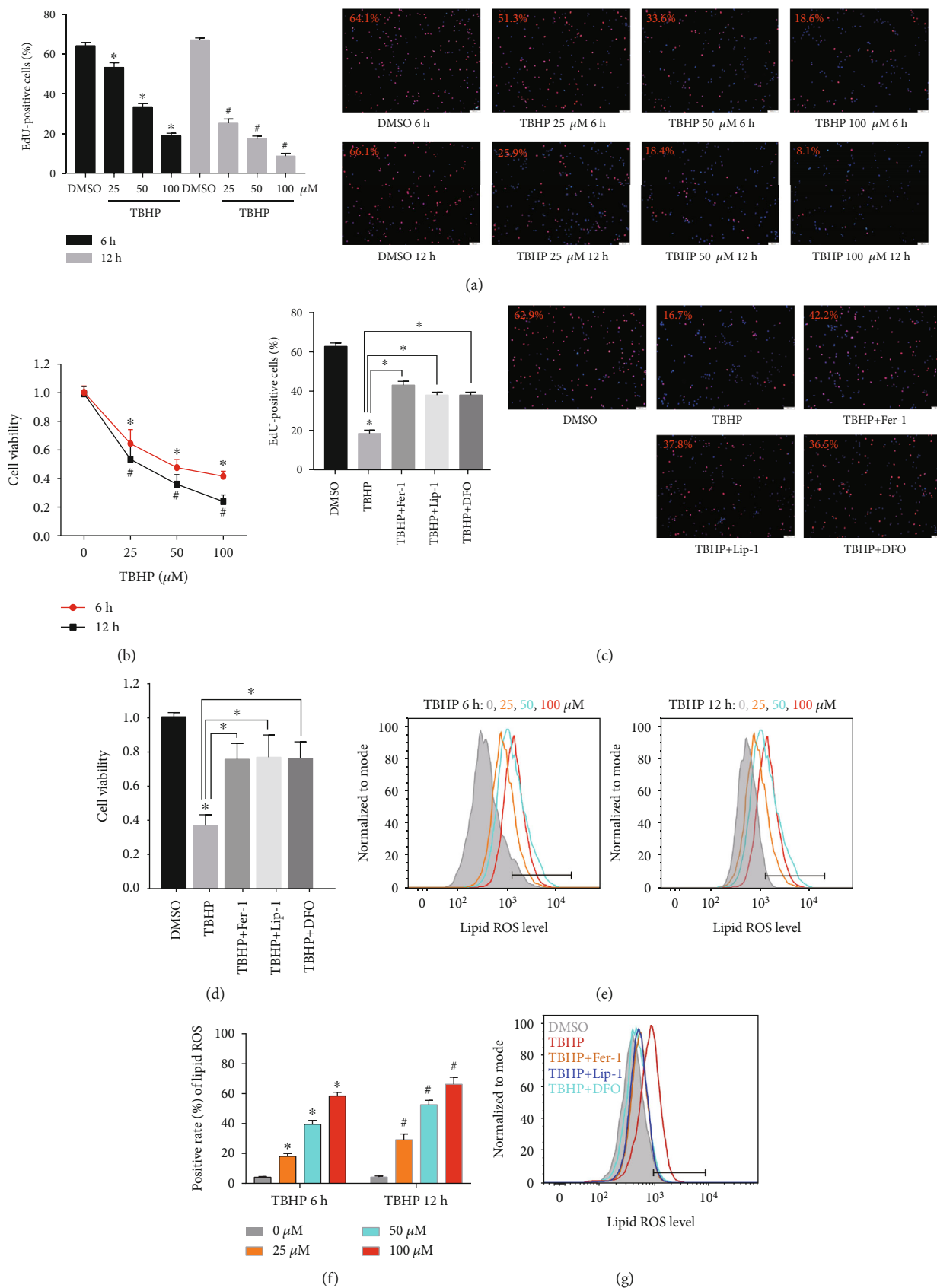


FIGURE 1: Continued.

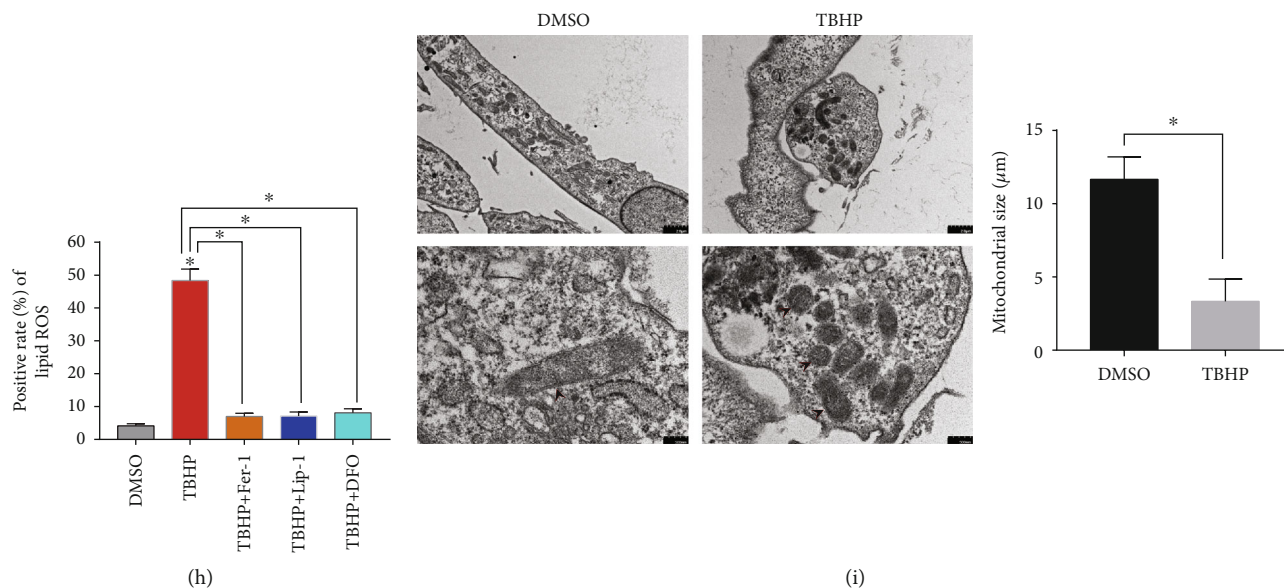


FIGURE 1: TBHP treatment induced cell viability decline, ROS accumulation, and ferroptosis in human NPCs. (a, b, e, f) The human NPCs were treated with TBHP (25–100 μM) or DMSO for 6 h or 12 h. The quantitative values are expressed as mean \pm SD ($n = 3$); $*p < 0.05$ versus DMSO (6 h), $*p < 0.05$ versus DMSO (12 h). (a) Cell proliferation was detected using EdU staining under fluorescence microscope and the positive cells were quantitated. (b) Cell viability was examined by the absorbance of CCK-8. (c, d, g, h) The human NPCs were treated with DMSO, TBHP (50 μM), Fer-1 (5 μM), Lip-1 (5 μM), or DFO (100 μM) for 12 h. The quantitative values are expressed as mean \pm SD ($n = 3$); $*p < 0.05$, TBHP versus DMSO; $*p < 0.05$, TBHP+ Fer-1/Lip-1/DFO versus TBHP. (c) Cell proliferation was detected using EdU staining under fluorescence microscope, and the positive cells were quantitated. (d) Cell viability was examined by the absorbance of CCK-8. (e–h) Lipid ROS levels were assayed using C11-BODIPY 581/591 by flow cytometry. (i) Observation of human NPC morphologic change after treatment with TBHP by TEM. The quantification of mitochondrial size is expressed as mean \pm SD ($n = 3$); $*p < 0.05$ TBHP versus DMSO.

showed that Lenti-FPN infection significantly increased the expression of FPN and alleviated intercellular iron overload in TBHP-induced NPCs (Figures 3(f) and 3(g)). Lenti-FPN infection also alleviated ferroptosis in TBHP-induced NPCs (Figures 3(h)–3(j)). These data showed the intercellular iron overload and ferroptosis in TBHP-induced NPCs was associated with FPN dysfunction. FPN played a critical role in maintaining iron homeostasis and suppressing ferroptosis in human NPCs.

3.4. Suppression of MTF1 Downregulated FPN and Aggravated Ferroptosis in Human NPCs. Next, we aimed to identify the regulator responsible for the decrease of FPN during TBHP treatment. Based on a literature search, MTF1 could regulate the genetic expression of FPN at the transcriptional level [21, 33, 34]. Western blotting results showed that TBHP treatment significantly reduced the nuclear fractions of MTF1 protein, but not of Histone 3 (nuclear loading control) (Figure 4(a)). Suppression of MTF1 nuclear translocation by TBHP treatment was further validated using an immunofluorescence assay (Figure 4(b)). In addition, immunohistochemistry showed decreased nuclear localization of MTF1 in the IVDD group compared to the control group (Figure 4(c)). To further confirm the role of MTF1 in the suppression of FPN, we overexpressed MTF1 by transfecting a lentiviral plasmid (Lenti-MTF1). Subsequent western blotting results indicated that Lenti-MTF1 infection upregulated MTF1 nuclear translocation, increased

FPN protein levels, and decreased FTL protein levels and LIP in human NPCs (Figures 4(d)–4(f)). Consistently, overexpression of MTF1 also alleviated the ferroptosis phenotypes under TBHP treatment (Figures 4(f)–4(i)). To further confirm the essential role of FPN in MTF1 overexpression, we initiated FPN knockdown in Lenti-MTF1-infected NPCs. FPN knockdown significantly inhibited the protective effect of ferroptosis phenotypes in Lenti-MTF1-infected NPCs (Figures 4(f)–4(i)). These data indicated that TBHP treatment reduced the nuclear translocation of MTF1 in human NPCs, which resulted in the decreased expression of FPN and ferroptosis of NPCs.

3.5. Administering Hinokitiol Restored FPN Function and Suppressed TBHP-Induced Ferroptosis by Regulating the JNK/MTF1 Pathway. A 12 h treatment with $>10 \mu\text{M}$ hinokitiol was cytotoxic to human NPCs, whereas doses with $<8 \mu\text{M}$ hinokitiol did not cause cytotoxicity (Figure 5(a)). Thus, we selected 8 μM hinokitiol for the current study to determine its therapeutic role in protecting against ferroptosis of NPCs *in vitro*. Western blotting indicated that hinokitiol significantly suppressed activation of the JNK pathway by decreasing the phosphorylation level of JNK in a manner consistent with SP600125 (a specific inhibitor of JNK) (Figure 5(b)). We next investigated whether hinokitiol and SP600125 affected the nuclear translocation of MTF1 in human NPCs. MTF1 was found in both the cytosol and the nuclei of control NPCs using immunofluorescence assay

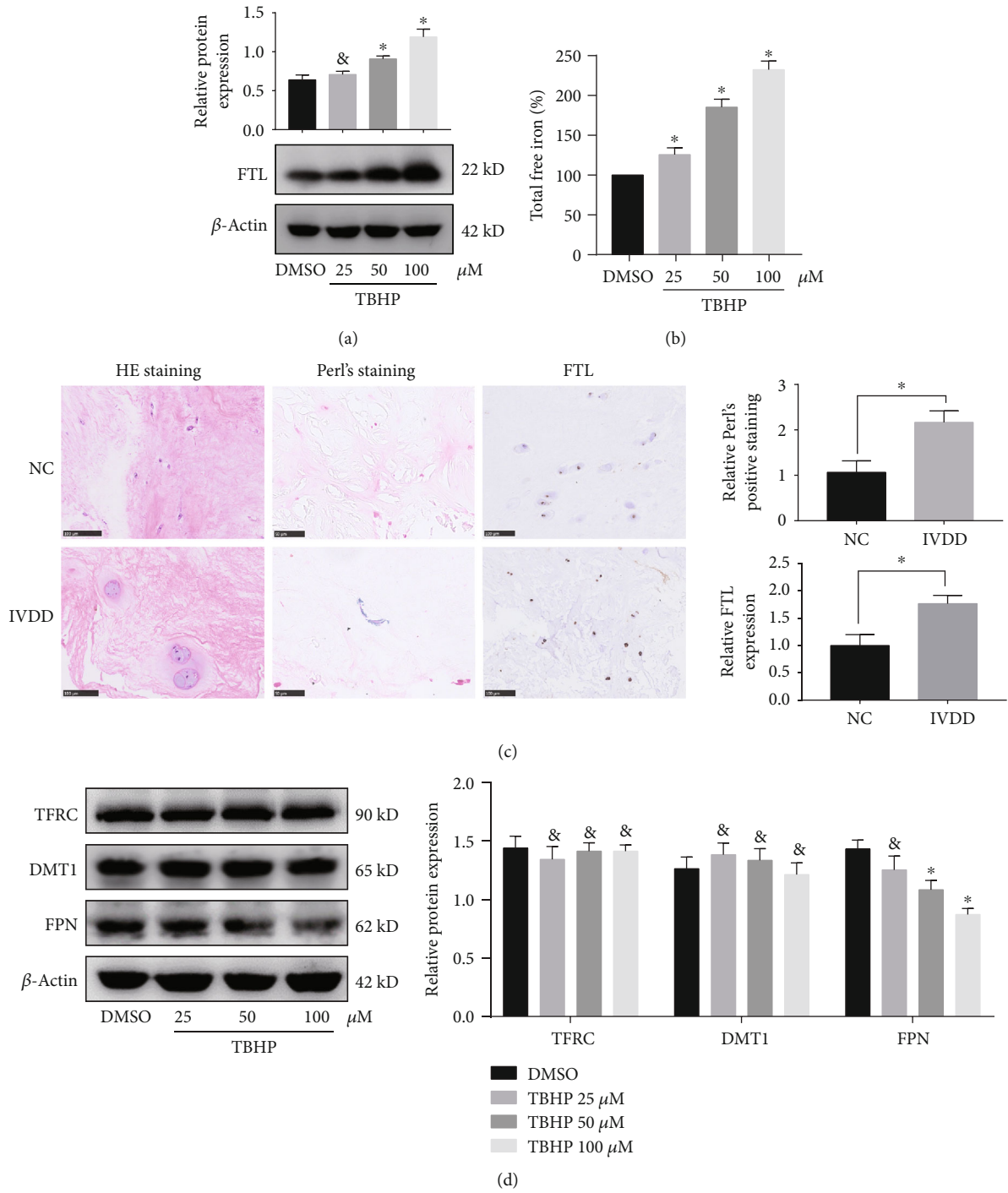


FIGURE 2: Continued.

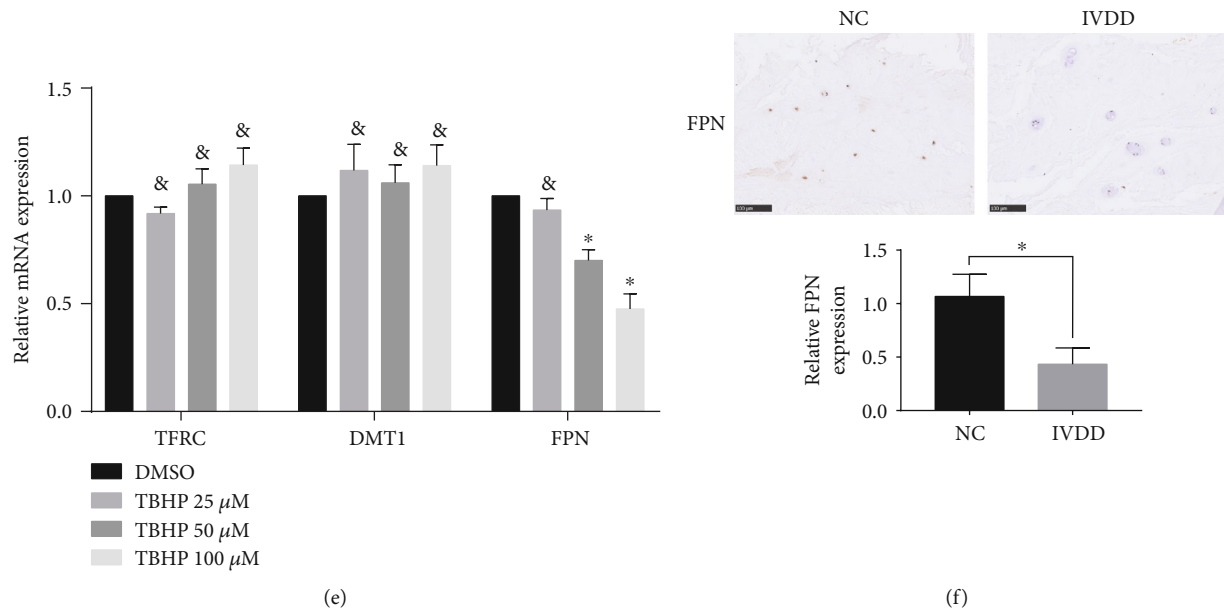


FIGURE 2: Ferroptosis in human NPCs was associated with intracellular iron overload and FPN dysfunction. (a, b, d, e) The human NPCs were treated with DMSO or TBHP (25–100 μ M) for 12 h. The quantitative values are expressed as mean \pm SD ($n = 3$); * $p < 0.05$ versus DMSO. &No significance versus DMSO. (a) FTL protein levels in human NPCs were determined using western blotting, which was normalized to β -actin. (b) Intracellular total free iron levels in human NPCs were assayed using iron assay kit. (c) Representative images of Perl's staining and FTL expression were performed in human NP tissues from the control (NC) group and IVDD group. Data are expressed as mean \pm SD ($n = 3$); * $p < 0.05$, the IVDD group versus the control (NC) group. (d) TFRC, DMT1, and FPN protein levels in human NPCs were determined using western blotting, which was normalized to β -actin. (e) TFRC, DMT1, and FPN mRNA levels in human NPCs were determined by RT-qPCR, which was normalized to β -actin. (f) Representative images of FPN were performed in human NP tissues from the control (NC) group and IVDD group using immunohistochemistry analysis. Data are expressed as mean \pm SD ($n = 3$); * $p < 0.05$, the IVDD group versus the control (NC) group.

(Figure 5(c)). Additionally, hinokitiol and SP600125 significantly rescued TBHP-induced suppression of MTF1 nuclear localization (Figure 5(c)). Furthermore, hinokitiol upregulated the expression of FPN in TBHP-treated NPCs, and SP600125 consistently exerted a protective effect (Figure 5(b)). Finally, hinokitiol and SP600125 also alleviated the ferroptosis phenotypes under TBHP treatment (Figures 5(d)–5(g)). Together, these data indicated that hinokitiol increased the nuclear translocation of MTF1 by suppressing the JNK pathway in TBHP-induced human NPCs, which resulted in an increase in FPN expression, a decline in intercellular iron levels, and the prevention of ferroptosis.

3.6. Suppressing Ferroptosis and Administering Hinokitiol Ameliorated the Intervertebral Disc Degeneration In Vivo. To further investigate the relationship between ferroptosis and IVDD and the therapeutic efficacy of hinokitiol *in vivo*, we constructed a tail disc percutaneous needle puncture animal model of IVDD using Sprague–Dawley rats as previously described [27, 28]. After 8 weeks of model operation, the midsagittal sections of IVD specimens from the animal models were subjected to histopathologic analysis and scoring. HE staining and SO staining showed that the structure of IVD degenerated in the saline group, DFO group, Fer-1 group, and hinokitiol group (Figures 6(a)–6(c)) and the degree of disc degeneration in the DFO group, Fer-1 group, and hinokitiol group was lesser than that in the saline group

(Figures 6(a)–6(c)). Immunohistochemistry showed that FTL was increased in the saline group compared with the control group. Treatment with hinokitiol significantly alleviated the increase of FTL (Figure 6(d)). In addition, the nuclear translocation of MTF1 and the expression of FPN decreased in the saline group compared with the control group and were increased significantly when rats were treated with hinokitiol (Figure 6(d)). Taken together, these results revealed that ferroptosis and FPN dysfunction were involved in the pathogenesis of IVDD *in vivo*. Administration of hinokitiol may ameliorate IVDD progression through increasing the nuclear translocation of MTF1 and restoring the function of FPN *in vivo*.

4. Discussion

Lower back pain has a negative impact on quality of life, with IVDD being its major cause. Although much effort has been made to diagnose lower back pain disorders in advance [35, 36], the available treatment is limited to muscle relaxants or nonsteroidal anti-inflammatory drugs to relieve symptoms [37, 38]. However, these drugs are unable to effectively alleviate IVDD or prevent its progression. The current study demonstrated the involvement of ferroptosis in the pathogenesis of IVDD. The decreased expression of FPN resulted in intercellular iron overload and ferroptosis in human NPCs (Figure 7). In addition, hinokitiol effectively suppressed

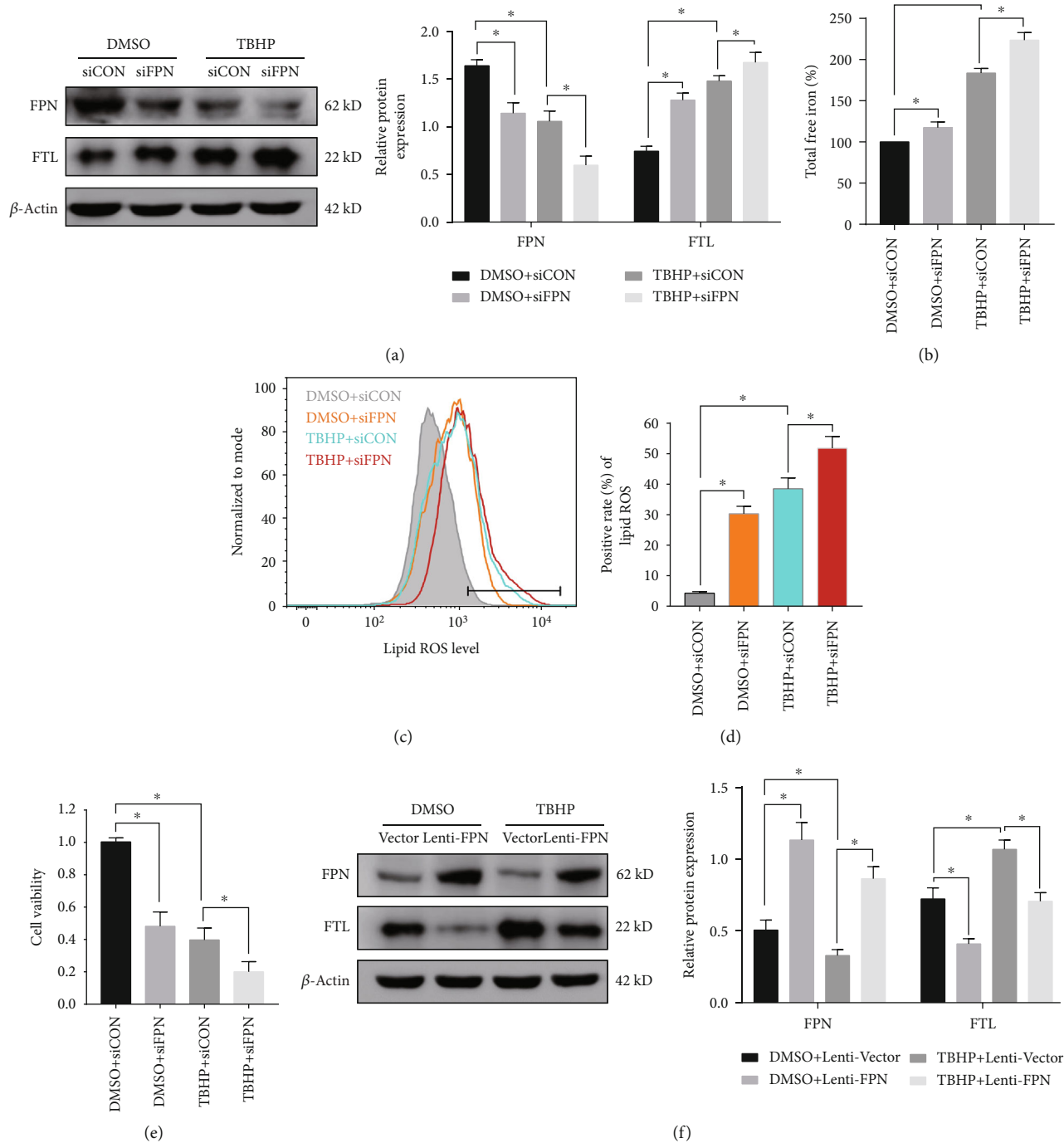


FIGURE 3: Continued.

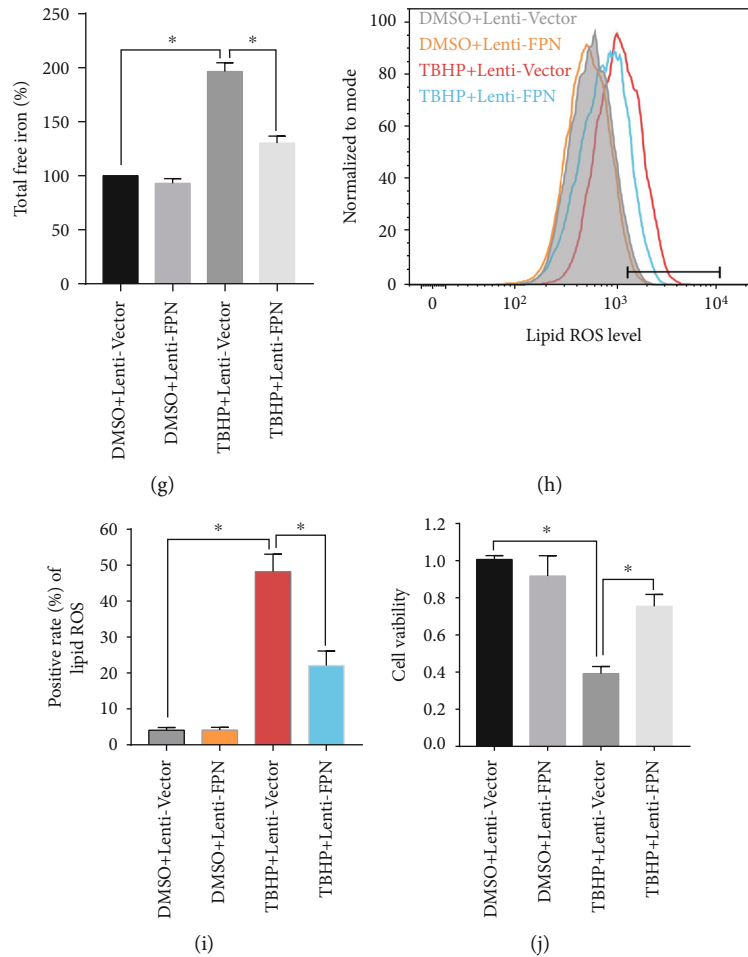


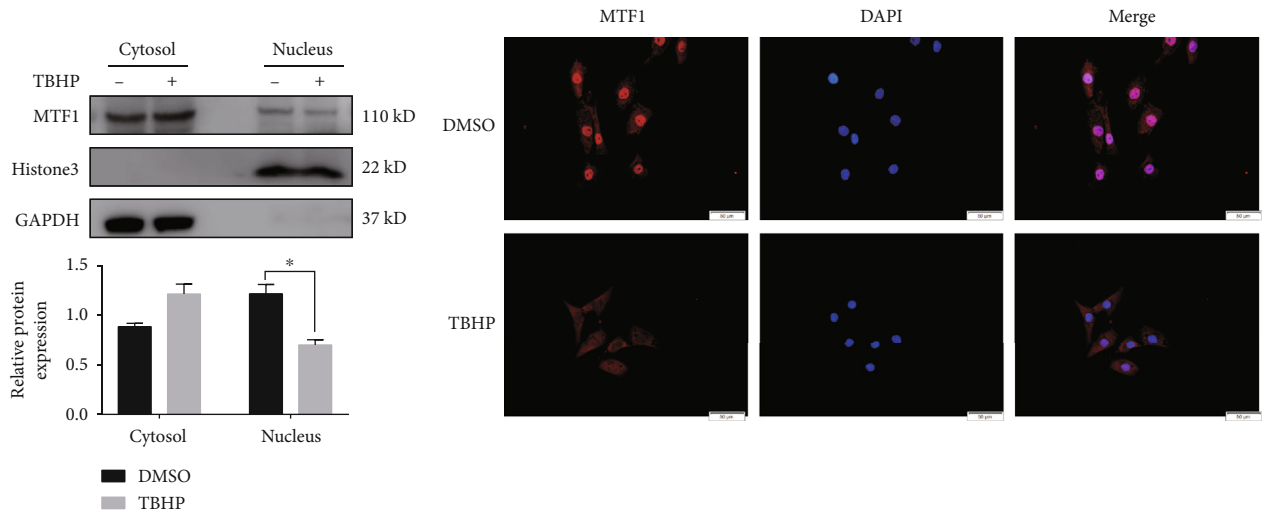
FIGURE 3: FPN protected human NPCs against intercellular iron overload and ferroptosis induced by TBHP treatment. (a–e) Scrambled siRNA (siCON) or FPN siRNA (siFPN) transfection was performed before DMSO or TBHP treatment (50 μ M) for 12 h. The quantitative values are expressed as mean \pm SD ($n = 3$); * $p < 0.05$. (a) Representative western blotting assay and quantitation of the level of FPN and FTL protein, which was normalized to β -actin. (b) Intracellular total free iron levels in human NPCs were assayed using iron assay kit. (c, d) Lipid ROS levels were assayed using C11-BODIPY 581/591 using flow cytometry. (e) Cell viability was examined by the absorbance of CCK-8. (f–j) Lenti-Vector or Lenti-FPN infection was performed before DMSO or TBHP treatment (50 μ M) for 12 h. The quantitative values are expressed as mean \pm SD ($n = 3$); * $p < 0.05$. (f) Representative western blotting assay and quantitation of the level of FPN and FTL protein, which was normalized to β -actin. (g) Intracellular total free iron levels in human NPCs were assayed using iron assay kit. (h, i) Lipid ROS levels were assayed using C11-BODIPY 581/591 by flow cytometry. (j) Cell viability was examined by the absorbance of CCK-8.

ferroptosis and ameliorated IVDD via restoring the function of FPN both *in vitro* and *in vivo*.

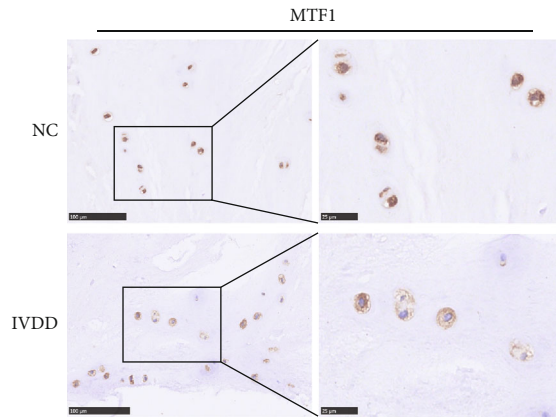
OS is a common pathological phenomenon involved in various diseases, including diabetes, nonalcoholic fatty liver disease, and Alzheimer's disease [39]. The levels of ROS in the IVD increase significantly with the progression of IVDD. NPCs, the most important functional cells in the IVD, can utilize aerobic metabolism to produce ROS. OS mediated by excessive ROS accelerates the process of IVDD by multiple biological mechanisms [40]. He et al. studied that rat NPCs lose their ability to proliferate and become senescent, when exposed to sublethal hydroperoxide [40]. Yu et al. identified advanced glycation end products associated with IVDD that created OS and promoted mitochondrial dysfunction and apoptosis of NPCs [7]. Jiang et al. investigated autophagy and apoptosis as well as their interactions in NPCs under OS

[9]. Other studies have determined that the expression of collagen type II and aggrecan was downregulated in hydroperoxide-induced NPCs [41]. However, these do not fully explain the decrease in NPCs and ECM degradation, as seen by the failure of drugs targeting these mechanisms to fully treat IVDD. Further research is needed to explore the mechanisms underlying IVDD.

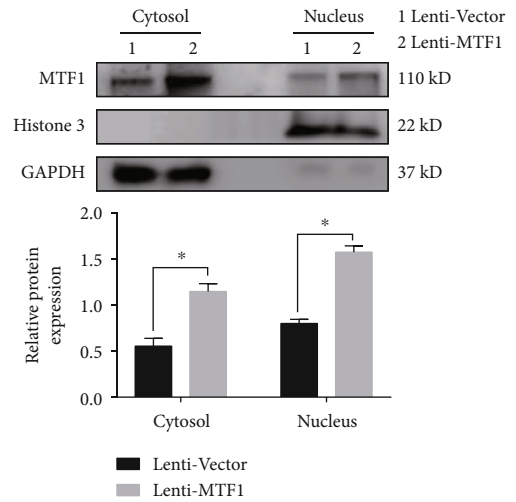
Ferroptosis, an iron-dependent regulated cell death, was first identified while investigating cell death induced by the small molecule erastin, which inhibits the function of cystine-glutamate antiporter. Initial studies indicated that ferroptosis was biochemically, morphologically, and genetically distinct from necrosis, apoptosis, and autophagy [12]. However, recent studies have revealed that ferroptosis also is an autophagic process, which includes SQSTM1-mediated clathrin-mediated autophagy, ROS-mediated autophagy, NCOA4-



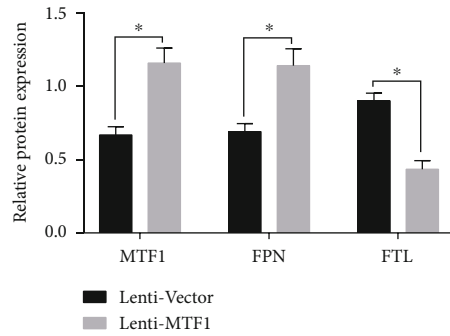
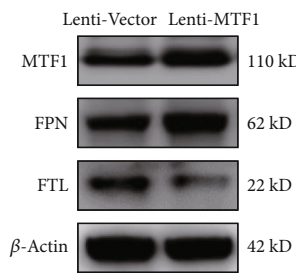
(a)



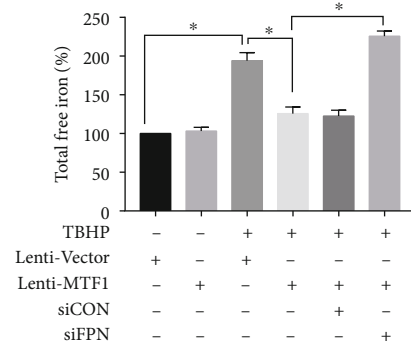
(b)



(c)



(e)



(f)

FIGURE 4: Continued.

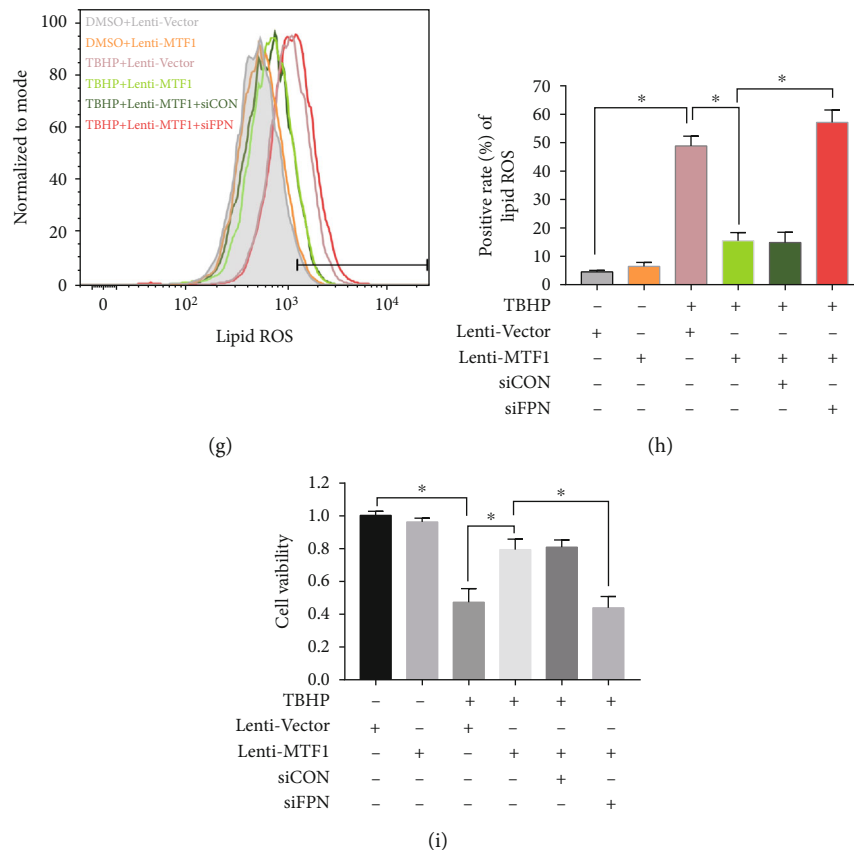


FIGURE 4: TBHP treatment aggravated FPN downregulation in human NPCs by MTF1 suppression. (a, b) The human NPCs were treated with DMSO or TBHP (50 μ M) for 12 h. The quantitative values are expressed as mean \pm SD ($n = 3$); * $p < 0.05$. (a) MTF1 protein levels in cytosolic and nuclear fractions of human NPCs were determined using western blotting, which was, respectively, normalized to GADPH and Histone 3. (b) The human NPCs were fixed and stained with DAPI (nuclear) and MTF1 antibody. Representative images were shown to visualize the subcellular locations of MTF1. (c) The subcellular localization of MTF1 was performed in human NP tissues from the control (NC) groups and IVDD groups by immunohistochemistry analysis. (d, e) Lenti-Vector or Lenti-MTF1 infection was performed in human NPCs. The quantitative values are expressed as mean \pm SD ($n = 3$); * $p < 0.05$. (d) MTF1 protein levels in cytosolic and nuclear fractions of human NPCs were determined using western blotting, which was, respectively, normalized to GADPH and Histone 3. (e) Representative western blotting assay and quantitation of the level of MTF1, FPN, and FTL proteins, which was normalized to β -actin. (f–i) Lenti-Vector or Lenti-MTF1 infection and scrambled siRNA (siCON) or FPN siRNA (siFPN) transfection were performed before DMSO or TBHP treatment (50 μ M) for 12 h. Data are expressed as mean \pm SD ($n = 3$); * $p < 0.05$. (f) Intracellular total free iron levels in human NPCs were assayed using iron assay kit. (g, h) Lipid ROS levels were assayed using C11-BODIPY 581/591 using flow cytometry. (i) Cell viability was examined by the absorbance of CCK-8.

mediated ferroptinophagy, and degradation of GPX4 by chaperone-mediated autophagy [42–45]. Previous studies have reported that homocysteine promoted rat NPC death by ferroptosis, which was mediated by the upregulated methylation of GPX4 [15]. The current study used TBHP to simulate OS conditions. Lipid ROS, which are the hallmark of ferroptosis, significantly increased in TBHP-induced NPCs compared to that in noninduced cells. TEM showed that the distinctive morphological characteristics of ferroptosis were evident in TBHP-induced NPCs. TBHP-induced cell death was significantly declined when cells were coincubated with ferroptosis inhibitors and iron chelators. Additionally, ferroptosis inhibitors and iron chelators also ameliorated IVDD progression *in vivo*. This confirms the involvement of ferroptosis in TBHP-induced decline of NPCs and IVDD pathogenesis.

The sensitivity to ferroptosis is tightly linked to various biological processes, including lipid metabolism, iron metabolism, amino acid and glutathione metabolism, and the biosynthesis of GPX4, p53, coenzyme Q10, ferroptosis-suppressor-protein 1 (FSP1), and NADPH [14, 46–48]. Iron, a constituent of iron-sulfur proteins and hemoproteins, is required for the accumulation of lipid peroxides in the development of ferroptosis [49]. The export, import, storage, and turnover of iron impact ferroptosis sensitivity [14]. FPN is responsible for iron homeostasis at both systemic levels and cellular levels [50]. A previous study has reported that siramesine in combination with lapatinib induced ferroptosis via increased transferrin expression and decreased FPN expression, resulting in intercellular iron overload [20]. However, the role of FPN in human NPCs remains to be determined. The current study found that the expression

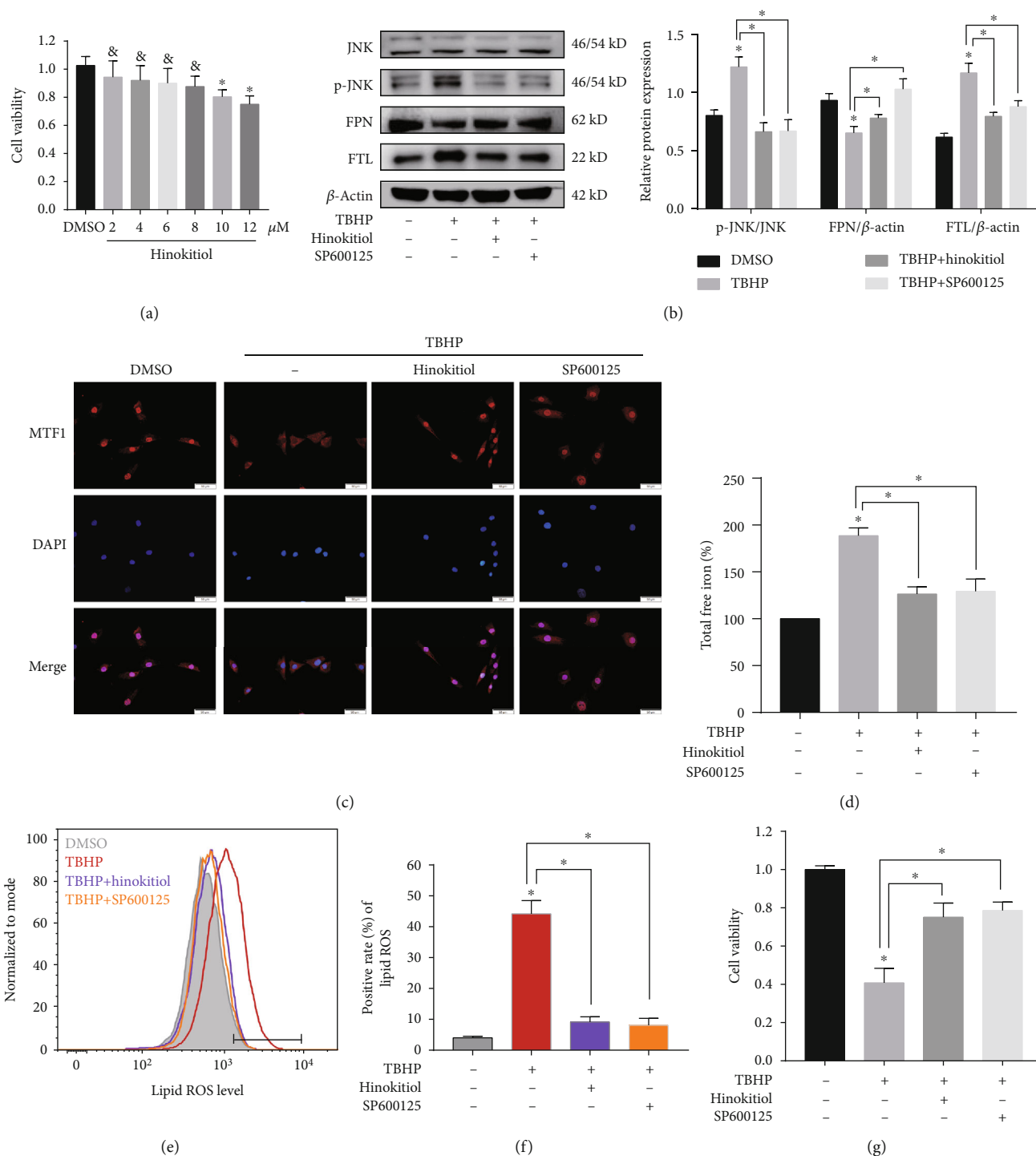
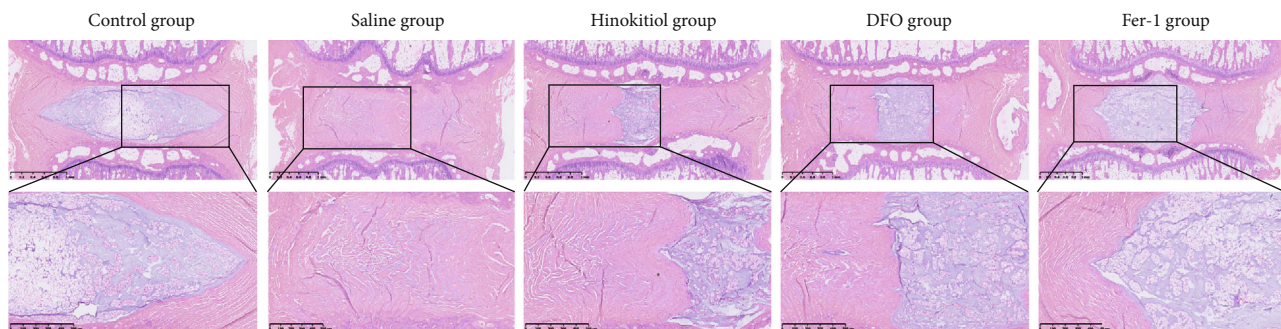
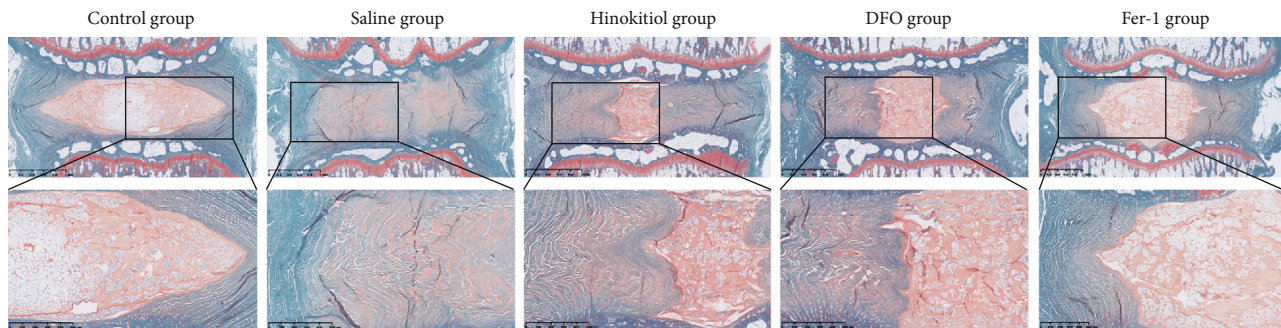


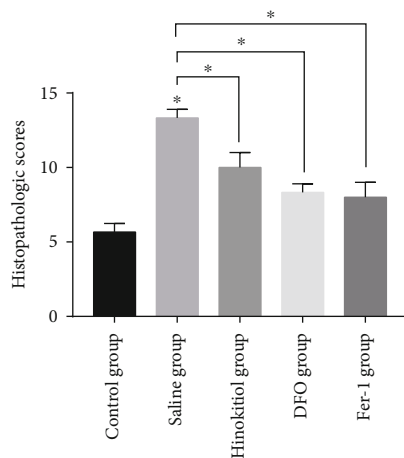
FIGURE 5: Hinokitiol restored FPN function and suppressed TBHP-induced ferroptosis by regulating the JNK/MTF1 pathway. (a) After treatment with various concentrations (2–12 μM) of hinokitiol or DMSO, cell viability was examined by the absorbance of CCK-8 in human NPCs. The quantitative values are expressed as mean \pm SD ($n = 3$); * $p < 0.05$ versus DMSO. &No significance versus DMSO. (b–g) The human NPCs were treated with DMSO, TBHP (50 μM), hinokitiol (8 μM), or SP600125 (20 μM) for 12 h. Data are expressed as mean \pm SD ($n = 3$); * $p < 0.05$ TBHP versus DMSO, * $p < 0.05$ TBHP+hinokitiol/SP600125 versus TBHP. (b) Representative western blotting assay and quantitation of the level of p-JNK, FPN, and FTL proteins. P-JNK was normalized to JNK, while FPN and FTL were normalized to β -actin. (c) The human NPCs were fixed and stained with DAPI (nuclear) and MTF1 antibody. Representative images are shown to visualize the subcellular locations of MTF1. (d) Intracellular total free iron levels in human NPCs were assayed using iron assay kit. (e, f) Lipid ROS levels were assayed using C11-BODIPY 581/591 by flow cytometry. (g) Cell viability was examined by the absorbance of CCK-8.



(a)

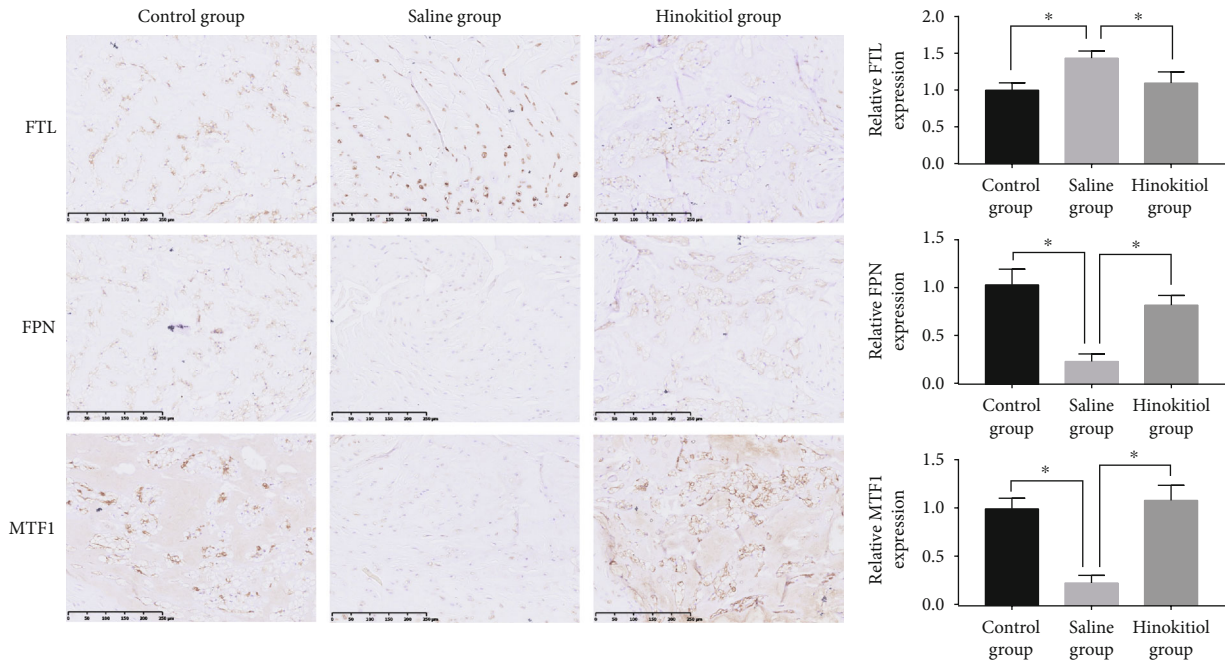


(b)



(c)

FIGURE 6: Continued.



(d)

FIGURE 6: Ferroptosis occurred during IVDD, while administration of hinokitiol reduced the degree of disc degeneration *in vivo*. (a, b) Representative HE and SO staining images of the midsagittal sections of IVD specimens. (c) Histologic scores of the midsagittal sections of IVD specimens. Data are expressed as mean \pm SD ($n = 3$); $*p < 0.05$, the saline group versus the control group; $*p < 0.05$, the DFO group/Fer-1 group/hinokitiol group versus the saline group. The interobserver error of each group is, respectively, 0.05 (control group), 0.02 (saline group), 0.05 (hinokitiol group), 0.03 (DFO group), and 0.07 (Fer-1 group). (d) Immunohistochemical staining for FTH, FPN, and MTF1 expressions in the rats' NP samples. Data are expressed as mean \pm SD ($n = 3$); $*p < 0.05$, the saline group versus the control group; $*p < 0.05$, the hinokitiol group versus the saline group.

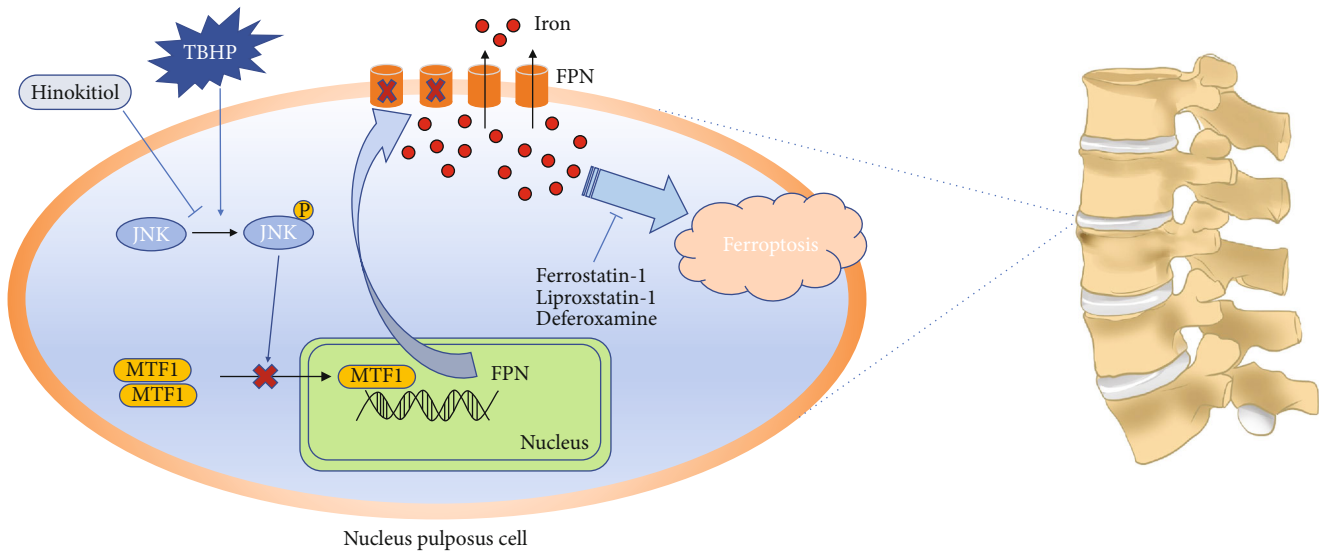


FIGURE 7: Schematic model illustrating the signaling pathway by JNK/MTF1/FPN to mediate TBHP-induced and hinokitiol-protective effect on human NPC ferroptosis.

level of FPN was reduced in TBHP-induced NPCs, degenerative human NP tissues, and degenerative rats' NP samples. Importantly, we further confirmed that the reduced expression of FPN resulted in intracellular iron overload, which contributed to the development of ferroptosis.

FPN plays a critical role in iron homeostasis, and alterations in FPN may result in either iron overload or deficiency. The regulation of FPN expression is complex, with important layers of control at the transcriptional level via the regulation of levels and splice variants of mRNA, at the

posttranscriptional level via an iron-regulatory element in the 5'-untranslated region of FPN mRNA and at the post-translational level via direct interaction between FPN and hepcidin, a peptide hormone. These different regulatory mechanisms could influence FPN activity at its various sites of expression [19]. Previous studies have demonstrated that, at the transcriptional level, MTF1 can induce FPN transcription by translocating into the nucleus and binding to the FPN1 promoter in response to stress situations such as OS and heavy metal loading [33, 34]. We demonstrated that the nuclear translocation of MTF1 decreased in TBHP-induced NPCs, degenerative human NP tissues, and degenerative rats' NP samples. TBHP suppressed the nuclear translocation of MTF1, which resulted in the reduced expression of FPN, intracellular iron overload, and ferroptosis of NPCs.

Hinokitiol, a natural tropolone derivative, exhibits multiple biological activities such as antibacterial, antifungal, antiviral, anti-inflammatory, and anticancer. This compound has been used to treat decubitus ulcers, pulmonary tuberculosis, and lung gangrene in clinical practice [22, 51]. Hinokitiol inhibits platelet activation by suppressing the formation of hydroxyl radicals and attenuating the activation of Akt and MAPKs during antithrombotic activity *in vivo* [52]. Inhibition of JNK1/2 phosphorylation by hinokitiol suppressed mouse melanoma cell migration [22]. The current study demonstrated that hinokitiol increases nuclear translocation of MTF1, restores the function of FPN, and alleviates TBHP-induced NPC ferroptosis by suppressing the JNK pathway (Figure 7). Also, hinokitiol ameliorated IVDD progression *in vivo*. Our study has some limitations. Although our study found that TBHP attenuated ferroptosis in human NPCs by reducing FPN via MTF1, further investigation is warranted to elucidate the mechanisms underlying TBHP and MTF1 interaction. Furthermore, only a ferroptosis-associated decrease in human NPCs subjected to OS was investigated in our study. Additional investigations are warranted to confirm the universality of ferroptosis in IVDD via the simulation of other stress factors, such as inflammation, hypoxia, and compression.

5. Conclusions

To the best of our knowledge, the current study is the first to demonstrate the protective role of FPN in ferroptosis of human NPCs and the pathogenesis of IVDD. Furthermore, we revealed that TBHP downregulated FPN expression by reducing the nuclear translocation of MTF1, which causes intracellular iron overload and ferroptosis in human NPCs. Moreover, hinokitiol alleviated TBHP-induced OS and ferroptosis of NPCs by restoring the FPN function. Therefore, we inferred that repairing FPN function and inhibiting ferroptosis in human NPCs may be potentially effective therapeutic targets against OS-associated IVDD.

Abbreviations

CCK-8:	Cell counting kit-8
DFO:	Deferoxamine
DMT1:	Divalent metal transporter 1

ECM:	Extracellular matrix
Fer-1:	Ferrostatin-1
FPN:	Ferroportin
FSP1:	Ferroptosis-suppressor-protein 1
FTL:	Ferritin light chain
GAPDH:	Glyceraldehyde-3-phosphate dehydrogenase
IVD:	Intervertebral disc
IVDD:	Intervertebral disc degeneration
JNK:	c-Jun N-terminal kinase 1
Lip-1:	Liproxstatin-1
LIP:	Labile iron pools
MTF1:	Metal-regulatory transcription factor 1
NP:	Nucleus pulposus
NPCs:	Nucleus pulposus cells
OS:	Oxidative stress
ROS:	Reactive oxygen species
TBHP:	tert-Butyl hydroperoxide
TEM:	Transmission electron microscopy
TFRC:	Transferrin receptor
RT-qPCR:	Quantitative reverse transcription polymerase chain reaction.

Data Availability

The data used to support the findings of this study are included within the article.

Conflicts of Interest

The authors declare that there is no conflict of interest regarding the publication of this paper.

Authors' Contributions

Saideng Lu, Yu Song, Rongjin Luo, and Shuai Li contributed equally to the study.

Acknowledgments

This study was supported by the National Natural Science Foundation of China (Grant Nos. 81772401 and 81803917), the National Key Research and Development Program of China (2018YFB1105700), the Application Foundation and Advanced Program of Wuhan Science and Technology Bureau (2019020701011457), and the Fundamental Research Funds for the Central Universities (2019kfyXMBZ063).

References

- [1] P. Priyadarshani, Y. Li, and L. Yao, "Advances in biological therapy for nucleus pulposus regeneration," *Osteoarthritis and Cartilage*, vol. 24, no. 2, pp. 206–212, 2016.
- [2] H. Che, J. Li, Y. Li et al., "p16 deficiency attenuates intervertebral disc degeneration by adjusting oxidative stress and nucleus pulposus cell cycle," *eLife*, vol. 9, 2020.
- [3] H. Choi, C. Merceron, L. Mangiavini et al., "Hypoxia promotes noncanonical autophagy in nucleus pulposus cells independent of MTOR and HIF1A signaling," *Autophagy*, vol. 12, no. 9, pp. 1631–1646, 2016.

- [4] P. P. Vergroesen, I. Kingma, K. S. Emanuel et al., "Mechanics and biology in intervertebral disc degeneration: a vicious circle," *Osteoarthritis and Cartilage*, vol. 23, no. 7, pp. 1057–1070, 2015.
- [5] F. Wang, F. Cai, R. Shi, X. H. Wang, and X. T. Wu, "Aging and age related stresses: a senescence mechanism of intervertebral disc degeneration," *Osteoarthritis and Cartilage*, vol. 24, no. 3, pp. 398–408, 2016.
- [6] C. Feng, M. Yang, M. Lan et al., "ROS: crucial Intermediators in the pathogenesis of intervertebral disc degeneration," *Oxidative Medicine and Cellular Longevity*, vol. 2017, Article ID 5601593, 12 pages, 2017.
- [7] Y. Song, S. Li, W. Geng et al., "Sirtuin 3-dependent mitochondrial redox homeostasis protects against AGEs- induced intervertebral disc degeneration," *Redox Biology*, vol. 19, pp. 339–353, 2018.
- [8] A. Larrañaga, I. L. M. Isa, V. Patil et al., "Antioxidant functionalized polymer capsules to prevent oxidative stress," *Acta Biomaterialia*, vol. 67, pp. 21–31, 2018.
- [9] J. W. Chen, B. B. Ni, B. Li, Y. H. Yang, S. D. Jiang, and L. S. Jiang, "The responses of autophagy and apoptosis to oxidative stress in nucleus pulposus cells: implications for disc degeneration," *Cellular Physiology and Biochemistry*, vol. 34, no. 4, pp. 1175–1189, 2014.
- [10] Y. H. Cheng, S. H. Yang, C. C. Liu, A. Gefen, and F. H. Lin, "Thermosensitive hydrogel made of ferulic acid-gelatin and chitosan glycerophosphate," *Carbohydrate Polymers*, vol. 92, no. 2, pp. 1512–1519, 2013.
- [11] S. Yang, F. Zhang, J. Ma, and W. Ding, "Intervertebral disc ageing and degeneration: the antiapoptotic effect of oestrogen," *Ageing Research Reviews*, vol. 57, article 100978, 2020.
- [12] S. J. Dixon, K. M. Lemberg, M. R. Lamprecht et al., "Ferroptosis: an iron-dependent form of nonapoptotic cell death," *Cell*, vol. 149, no. 5, pp. 1060–1072, 2012.
- [13] J. Y. Cao and S. J. Dixon, "Mechanisms of ferroptosis," *Cellular and Molecular Life Sciences*, vol. 73, no. 11–12, pp. 2195–2209, 2016.
- [14] B. R. Stockwell, J. P. Friedmann Angeli, H. Bayir et al., "Ferroptosis: a regulated cell death nexus linking metabolism, redox biology, and disease," *Cell*, vol. 171, no. 2, pp. 273–285, 2017.
- [15] X. Zhang, Z. Huang, Z. Xie et al., "Homocysteine induces oxidative stress and ferroptosis of nucleus pulposus via enhancing methylation of GPX4," *Free Radical Biology & Medicine*, vol. 160, pp. 552–565, 2020.
- [16] R. Z. Yang, W. N. Xu, H. L. Zheng et al., "Involvement of oxidative stress-induced annulus fibrosus cell and nucleus pulposus cell ferroptosis in intervertebral disc degeneration pathogenesis," *Journal of Cellular Physiology*, pp. 1–15, 2020.
- [17] H. Drakesmith, E. Nemeth, and T. Ganz, "Ironing out ferroportin," *Cell Metabolism*, vol. 22, no. 5, pp. 777–787, 2015.
- [18] M. W. Hentze, M. U. Muckenthaler, B. Galy, and C. Camaschella, "Two to tango: regulation of mammalian iron metabolism," *Cell*, vol. 142, no. 1, pp. 24–38, 2010.
- [19] D. M. Ward and J. Kaplan, "Ferroportin-mediated iron transport: expression and regulation," *Biochimica et Biophysica Acta*, vol. 1823, no. 9, pp. 1426–1433, 2012.
- [20] S. Ma, E. S. Henson, Y. Chen, and S. B. Gibson, "Ferroptosis is induced following siramesine and lapatinib treatment of breast cancer cells," *Cell Death & Disease*, vol. 7, no. 7, article e2307, 2016.
- [21] J. C. Rutherford and A. J. Bird, "Metal-responsive transcription factors that regulate iron, zinc, and copper homeostasis in eukaryotic cells," *Eukaryotic Cell*, vol. 3, no. 1, pp. 1–13, 2004.
- [22] C. H. Huang, S. H. Lu, C. C. Chang, P. A. Thomas, T. Jayakumar, and J. R. Sheu, "Hinokitiol, a tropolone derivative, inhibits mouse melanoma (B16-F10) cell migration and in vivo tumor formation," *European Journal of Pharmacology*, vol. 746, pp. 148–157, 2015.
- [23] A. S. Grillo, A. M. SantaMaria, M. D. Kafina et al., "Restored iron transport by a small molecule promotes absorption and hemoglobinization in animals," *Science*, vol. 356, no. 6338, pp. 608–616, 2017.
- [24] P. S. Yang, M. J. Wang, T. Jayakumar et al., "Antiproliferative activity of hinokitiol, a tropolone derivative, is mediated via the inductions of p-JNK and p-PLC γ 1 signaling in PDGF-BB-stimulated vascular smooth muscle cells," *Molecules*, vol. 20, no. 5, pp. 8198–8212, 2015.
- [25] M. D. Mattie and J. H. Freedman, "Copper-inducible transcription: regulation by metal- and oxidative stress-responsive pathways," *American Journal of Physiology-Cell Physiology*, vol. 286, no. 2, pp. C293–C301, 2004.
- [26] R. Luo, Z. Liao, Y. Song et al., "Berberine ameliorates oxidative stress-induced apoptosis by modulating ER stress and autophagy in human nucleus pulposus cells," *Life Sciences*, vol. 228, pp. 85–97, 2019.
- [27] H. J. Mao, Q. X. Chen, B. Han et al., "The effect of injection volume on disc degeneration in a rat tail model," *Spine*, vol. 36, no. 16, pp. E1062–E1069, 2011.
- [28] B. Han, K. Zhu, F. C. Li et al., "A simple disc degeneration model induced by percutaneous needle puncture in the rat tail," *Spine*, vol. 33, no. 18, pp. 1925–1934, 2008.
- [29] G. Li, Y. Song, Z. Liao et al., "Bone-derived mesenchymal stem cells alleviate compression-induced apoptosis of nucleus pulposus cells by N6 methyladenosine of autophagy," *Cell Death & Disease*, vol. 11, no. 2, 2020.
- [30] S. Zhan, K. Wang, Y. Song et al., "Long non-coding RNA HOTAIR modulates intervertebral disc degenerative changes via Wnt/ β -catenin pathway," *Arthritis Research & Therapy*, vol. 21, no. 1, 2019.
- [31] I. Ingold, C. Berndt, S. Schmitt et al., "Selenium utilization by GPX4 is required to prevent hydroperoxide-induced ferroptosis," *Cell*, vol. 172, no. 3, pp. 409–422.e21, 2018.
- [32] Z. K. Pinnix, L. D. Miller, W. Wang et al., "Ferroportin and iron regulation in breast cancer progression and prognosis," *Science translational medicine*, vol. 2, no. 43, article 43ra56, 2010.
- [33] P. H. Chen, J. Wu, C. C. Ding et al., "Kinome screen of ferroptosis reveals a novel role of ATM in regulating iron metabolism," *Cell Death and Differentiation*, vol. 27, no. 3, pp. 1008–1022, 2020.
- [34] M. B. Troadec, D. M. Ward, E. Lo, J. Kaplan, and I. de Domenico, "Induction of FPN1 transcription by MTF-1 reveals a role for ferroportin in transition metal efflux," *Blood*, vol. 116, no. 22, pp. 4657–4664, 2010.
- [35] H. J. Wilke, J. Urban, and M. Kumin, "The benefits of multidisciplinary research on intervertebral disc degeneration," *European Spine Journal*, vol. 23, Supplement 3, pp. 303–304, 2014.
- [36] A. Lazary, Z. Szoverfi, J. Szita, A. Somhegyi, M. Kumin, and P. P. Varga, "Primary prevention of disc degeneration-related symptoms," *European Spine Journal*, vol. 23, Supplement 3, pp. 385–393, 2014.

- [37] H. C. Wenger and A. S. Cifu, "Treatment of low back pain," *Journal of the American Medical Association*, vol. 318, no. 8, pp. 743-744, 2017.
- [38] C. Maher, M. Underwood, and R. Buchbinder, "Non-specific low back pain," *The Lancet*, vol. 389, no. 10070, pp. 736-747, 2017.
- [39] S. S. Cao and R. J. Kaufman, "Endoplasmic reticulum stress and oxidative stress in cell fate decision and human disease," *Antioxidants & Redox Signaling*, vol. 21, no. 3, pp. 396-413, 2014.
- [40] G. Z. Zhang, Y. J. Deng, Q. Q. Xie et al., "Sirtuins and intervertebral disc degeneration: roles in inflammation, oxidative stress, and mitochondrial function," *Clinica Chimica Acta*, vol. 508, pp. 33-42, 2020.
- [41] S. M. Rider, S. Mizuno, and J. D. Kang, "Molecular mechanisms of intervertebral disc degeneration," *Spine surgery and related research*, vol. 3, no. 1, pp. 1-11, 2018.
- [42] M. Yang, P. Chen, J. Liu et al., "CLOCKophagy is a novel selective autophagy process favoring ferroptosis," *Science advances*, vol. 5, no. 7, article eaaw2238, 2019.
- [43] E. Park and S. W. Chung, "ROS-mediated autophagy increases intracellular iron levels and ferroptosis by ferritin and transferrin receptor regulation," *Cell Death & Disease*, vol. 10, no. 11, 2019.
- [44] M. Gao, P. Monian, Q. Pan, W. Zhang, J. Xiang, and X. Jiang, "Ferroptosis is an autophagic cell death process," *Cell Research*, vol. 26, no. 9, pp. 1021-1032, 2016.
- [45] Z. Wu, Y. Geng, X. Lu et al., "Chaperone-mediated autophagy is involved in the execution of ferroptosis," *Proceedings of the National Academy of Sciences of the United States of America*, vol. 116, no. 8, pp. 2996-3005, 2019.
- [46] S. Doll, F. P. Freitas, R. Shah et al., "FSP1 is a glutathione-independent ferroptosis suppressor," *Nature*, vol. 575, no. 7784, pp. 693-698, 2019.
- [47] K. Bersuker, J. M. Hendricks, Z. Li et al., "The CoQ oxidoreductase FSP1 acts parallel to GPX4 to inhibit ferroptosis," *Nature*, vol. 575, no. 7784, pp. 688-692, 2019.
- [48] L. Jiang, N. Kon, T. Li et al., "Ferroptosis as a p53-mediated activity during tumour suppression," *Nature*, vol. 520, no. 7545, pp. 57-62, 2015.
- [49] S. Lakhali-Littleton, M. Wolna, C. A. Carr et al., "Cardiac ferroportin regulates cellular iron homeostasis and is important for cardiac function," *Proceedings of the National Academy of Sciences of the United States of America*, vol. 112, no. 10, pp. 3164-3169, 2015.
- [50] S. Lakhali-Littleton, A. Crosby, M. C. Frise et al., "Intracellular iron deficiency in pulmonary arterial smooth muscle cells induces pulmonary arterial hypertension in mice," *Proceedings of the National Academy of Sciences of the United States of America*, vol. 116, no. 26, pp. 13122-13130, 2019.
- [51] G. Zhang, J. He, X. Ye et al., " β -Thujaplicin induces autophagic cell death, apoptosis, and cell cycle arrest through ROS-mediated Akt and p38/ERK MAPK signaling in human hepatocellular carcinoma," *Cell death & disease*, vol. 10, no. 4, 2019.
- [52] K. H. Lin, J. R. Kuo, W. J. Lu et al., "Hinokitiol inhibits platelet activation ex vivo and thrombus formation in vivo," *Biochemical Pharmacology*, vol. 85, no. 10, pp. 1478-1485, 2013.

Research Article

Long Noncoding RNA ANPODRT Overexpression Protects Nucleus Pulposus Cells from Oxidative Stress and Apoptosis by Activating Keap1-Nrf2 Signaling

Liang Kang,^{1,2} Yueyang Tian,^{1,2} Xing Guo,^{1,2} Xu Chu,^{1,2} and Yuan Xue ^{1,2}

¹Department of Orthopedics, Tianjin Medical University General Hospital, Tianjin 300052, China

²Tianjin Key Laboratory of Spine and Spinal Cord Injury, Tianjin 300052, China

Correspondence should be addressed to Yuan Xue; xueyuanzy@tmu.edu.cn

Received 9 October 2020; Revised 21 December 2020; Accepted 12 January 2021; Published 2 February 2021

Academic Editor: Sidong Yang

Copyright © 2021 Liang Kang et al. This is an open access article distributed under the Creative Commons Attribution License, which permits unrestricted use, distribution, and reproduction in any medium, provided the original work is properly cited.

Oxidative stress and subsequent nucleus pulposus (NP) cell apoptosis are important contributors to the development of intervertebral disc degeneration (IDD). Emerging evidences show that long noncoding RNAs (lncRNAs) play a role in the pathogenesis of IDD. In this study, we investigated the role of lncRNA ANPODRT (anti-NP cell oxidative damage-related transcript) in oxidative stress and apoptosis in human NP cells. We found that ANPODRT was downregulated in degenerative NP tissues and in NP cells treated with tert-butyl hydroperoxide (TBHP, the oxidative stress inducer). ANPODRT overexpression alleviated oxidative stress and apoptosis in NP cells exposed to TBHP, while ANPODRT knockdown exerted opposing effects. Mechanistically, ANPODRT facilitated nuclear factor E2-related factor 2 (Nrf2) accumulation and nuclear translocation and activated its target genes by disrupting the kelch-like ECH-associated protein 1- (Keap1-) Nrf2 association in NP cells. Nrf2 knockdown abolished the antioxidative stress and antiapoptotic effects of ANPODRT in NP cells treated with TBHP. Collectively, our findings suggest that ANPODRT protects NP cells from oxidative stress and apoptosis, at least partially, by activating Nrf2 signaling, implying that ANPODRT may be a potential therapeutic target for IDD.

1. Introduction

Low back pain (LBP), one of the most common health issues, is a leading cause of disability worldwide and results in an enormous global economic and public health burden [1]. Intervertebral disc (IVD) degeneration (IDD) and secondary pathomorphological changes in spine structure are widely acknowledged as the major causes of LBP [2, 3]. The IVD consists of three interrelated structures: the nucleus pulposus (NP), the annulus fibrosus, and the cartilaginous endplates. The centrally situated NP allows the IVD to maintain a high water content and withstand different patterns of mechanical stress [4]. Excessive NP cell apoptosis disrupts normal metabolic activity within the NP, thus disrupting the normal IVD structure and physiological function, which is a key contributor to IDD initiation and progression [5, 6].

Oxidative stress results from an imbalance between the production of reactive oxygen species (ROS) and scavenging

capacity of the antioxidant system [7]. Oxidative stress leads to the damage of nucleic acids, lipids, and proteins through the production of high levels of ROS, which leads to cytotoxicity. Recent studies have verified the presence of oxidative stress and increased concentrations of oxidation products in degenerated discs [8, 9]. Furthermore, oxidative stress and its induced mitochondrial pathway play an important role in NP cell apoptosis and IDD [10–13]. We and others have previously reported that amelioration of oxidative stress and subsequent NP cell apoptosis has a therapeutic effect on IDD progression [14–16]. Therefore, an understanding of the underlying pathway regulating oxidative stress and subsequent NP cell apoptosis would significantly benefit IDD treatment.

Antioxidant system plays an important role in the occurrence of oxidative stress. The Keap1-Nrf2 signaling cascade is considered a central hub that neutralizes ROS and restores cellular redox balance [17–20]. Under resting conditions,

Nrf2 activity is tightly restricted through its interaction with Keap1 in the cytoplasm. Keap1 reportedly serves as a substrate scaffold for Cul3-containing E3 ubiquitin ligase, which can induce ubiquitin-proteasome degradation of Nrf2 [17]. Upon dissociation from Keap1, Nrf2 is translocated into the nucleus, where it initiates the transcription of a battery of antioxidative and cellular defense targets to counteract oxidative stress and modulate redox balance [20]. In a mouse model of IDD, degenerative changes in IVDs in Nrf2-knockout mice were more severe than those in wild-type mice [3]. We previously reported that the activation of the Nrf2 cascade is an effective strategy to protect human disc cells from oxidative damage and prevent IDD progression [14, 15]. Therefore, Nrf2 signal plays an important role in IDD characterized by oxidative stress.

Long noncoding RNAs (lncRNAs) are a large and diverse class of ncRNAs whose transcripts are >200 nt with limited or no protein-coding capacity. Increasing evidence indicates that lncRNAs are implicated in almost all physiological and pathological processes, including IDD [21, 22]. Numerous lncRNAs are dysregulated in IDD. LncRNAs are reportedly upregulated in IDD include RP11-296A18.3 [23], TUG1 [24], HCG18 [25], SNHG1 [26], and NEAT1 [27]. LncRNAs reportedly downregulated in IDD include linc-ADAMTS5 [22], MALAT1 [28], and MAGI2-AS3 [29]. In addition, SNHG6 functions as a promoter of NP cell apoptosis by regulating miR-101-3p [30]. NEAT1 downregulation suppressed advanced glycation end product-induced apoptosis in NP cells [31]. Although several lncRNAs have been studied in IDD, >58,000 lncRNAs have been identified in human cells, compared to 21,000 protein-coding genes in human cells [32]. Therefore, other lncRNAs potentially play a vital role in IDD development, which requires further investigation.

Many lncRNAs dysregulated in IDD have been previously identified through a lncRNA microarray analysis [33]. Among these differentially expressed lncRNAs, lncRNA AC068196.1 was significantly downregulated in IDD. We named lncRNA AC068196.1 as anti-NP cell oxidative damage-related transcript (ANPODRT). This study investigated the role of ANPODRT in oxidative stress and apoptosis in human NP cells. We showed that ANPODRT alleviates oxidative stress and apoptosis in human NP cells, and the activation of the Keap1-Nrf2 signaling cascade is involved in this process. Our results provide novel insights into the mechanism of oxidative stress and apoptosis in NP cells, with therapeutic implications for treating IDD.

2. Material and Methods

2.1. Tissue Specimens and Cell Culture. This study was approved by the Ethics Committee of Tianjin Medical University General Hospital, and written informed consent was obtained from each donor. Nucleus pulposus specimens were collected from 16 IDD patients (3 males and 2 females, grade II; 2 males and 1 female, grade III; 2 males and 2 females, grade IV; 1 male and 3 females, grade V). Nucleus pulposus cell isolation and culture were carried out as previously described [34]. Five human NP tissues (grade II) were used

for NP cell isolation. Briefly, the NP tissue samples were separated, cut into small pieces, and treated with 0.25% trypsin (Gibco) for 30 min and then 0.2% type II collagenase (Invitrogen) for 4 h at 37°C. After isolation, the NP cells were resuspended in DMEM/F12 containing 15% fetal bovine serum (FBS, Gibco) and 1% penicillin-streptomycin and incubated at 37°C in a humidified 5% CO₂ atmosphere. The culture medium was replaced every three days. When the NP cells grew to 80% confluence, they were detached by trypsinization and passed for expansion. Fluorescently labeled antibodies against NP cell markers (CD24 and KRT18) were used to identify the phenotype of NP cells, as described previously [35]. Cells from the second passage were used in subsequent experiments.

2.2. Cell Transfection. The siRNA targeting ANPODRT, Keap1, Nrf2, and appropriate negative controls were obtained from RiboBio. The overexpression plasmids containing ANPODRT and the matched negative control plasmid were obtained from GeneChem. Cell transfections were performed with lipofectamine 2000 (Invitrogen) based on provided instructions.

2.3. Cell Viability Assay. According to the manufacturer's instructions, the viability of human NP cells was assessed using a cell counting kit (CCK-8; Dojindo). Briefly, the cells were seeded in 96-well plates and exposed to corresponding treatments. Subsequently, the cells were incubated with 10 μ L CCK-8 solution at 37°C for 2 hours. The absorbance at 450 nm was measured using a spectrophotometer (BioTek).

2.4. Measurement of ROS and Malondialdehyde (MDA) Level. After corresponding treatment, the ROS and MDA level in human NP cells were measured using kit for ROS (Beyotime) and MDA (Beyotime), respectively, as per manufacturer instructions.

2.5. Flow Cytometry. Apoptosis levels in human NP cells from each treatment group were assessed using an Annexin V-APC/7-AAD Apoptosis Detection Kit (Yeasten) as previously described. After labelling, samples were examined using a FACSCalibur flow cytometer (BD Biosciences).

2.6. Western Blotting and Coimmunoprecipitation (Co-IP). After cell treatments, protein samples from NP cells were extracted using commercial kits (Beyotime) according to the manufacturer's instructions. Protein concentrations were determined with a BCA Protein Assay Kit (Beyotime). Equal amounts of protein from each sample were separated using SDS-PAGE and transferred to PVDF membranes. The membranes were blocked with 7.5% nonfat milk for 1 hour and then incubated at 4°C overnight with the following primary antibodies: cytochrome c, cleaved caspase-3, Nrf2, and Keap1. GAPDH and LaminB were used as internal controls. The membranes were subsequently incubated with the respective secondary antibodies at room temperature for 1 hour. Protein bands were visualized by the enhanced chemiluminescence method (Amersham Biosciences) according to

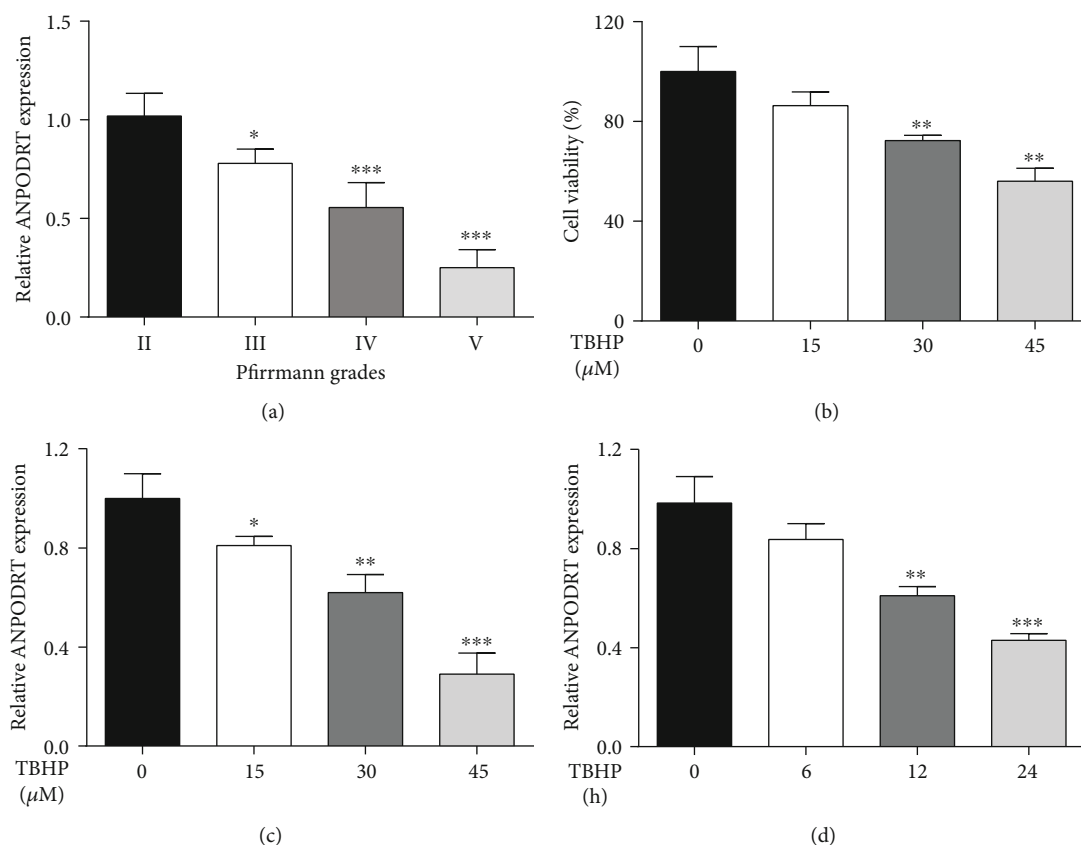


FIGURE 1: ANPODRT was downregulated in degenerative NP tissues and TBHP-stimulated NP cells. (a) The expression of ANPODRT from NP tissues of different degrees of IDD patients was analyzed by qRT-PCR. * $p < 0.05$ and *** $p < 0.001$ versus Pfirrmann grade II group. (b) CCK-8 assay was used to determine the cytotoxic effects of TBHP on human NP cells by treating the cells with various concentrations of TBHP for durations of 24 h. (c) The expression of ANPODRT in human NP cells that treated with different TBHP concentrations for 24 h. (d) The expression of ANPODRT in human NP cells that treated with 45 μM TBHP for different time. Data are represented as the mean \pm SD. * $p < 0.05$, ** $p < 0.01$, and *** $p < 0.001$ versus control group.

the manufacturer's instructions. Band intensities were quantified using the ImageJ software (NIH).

For Co-IP analysis, anti-Keap1 or control IgG was used as the primary antibody, and then the antibody-protein complex was following incubated with Protein A/G PLUS-Agarose. The agarose-antibody-protein complex was collected and then analyzed by Western blotting.

2.7. RNA Extraction and Quantitative Real-Time PCR (qRT-PCR). After treatments of human NP cells in the different groups, total RNA was extracted using a TRIzol reagent (Invitrogen, Carlsbad, CA, USA) and reverse-transcribed using a Transcriptor First Strand cDNA Synthesis Kit (Takara Biotechnology, Otsu, Japan). qRT-PCR was conducted using SYBR Green Kit Master Mix (Applied Biosystems, Foster City, CA, USA), and the products were analyzed using an ABI 7500 Sequencing Detection System, according to the manufacturer's instructions. GAPDH was used as an internal control.

2.8. Statistical Analysis. Data are presented as the mean \pm standard deviation (SD) of at least three independent experiments and were analyzed using the SPSS version 18.0 soft-

ware (SPSS Inc, Chicago, IL, USA). Differences between groups were evaluated using Student's t -test or one-way analysis of variance (ANOVA) followed by Tukey's test. $p < 0.05$ was considered statistically significant.

3. Results

3.1. ANPODRT Was Downregulated in Degenerative NP Tissues and TBHP-Stimulated NP Cells. ANPODRT is significantly downregulated in degenerative NP tissues. To investigate the association between ANPODRT and IDD, NP tissues of patients with different degrees of degeneration were harvested to determine the ANPODRT expression levels through qRT-PCR. As shown in Figure 1(a), in this study, ANPODRT was downregulated in NP tissues with the degree of disc degeneration. Since oxidative stress is an essential contributor to IDD pathophysiology, TBHP, an exogenous ROS donor, was applied to establish an IDD model in vitro. The CCK-8 assay revealed that TBHP inhibited NP cell viability (Figure 1(b)). Notably, TBHP treatment downregulated ANPODRT in a dose- and time-dependent manner in human NP cells (Figures 1(c) and 1(d)). These results indicate that ANPODRT is potentially associated with IDD.

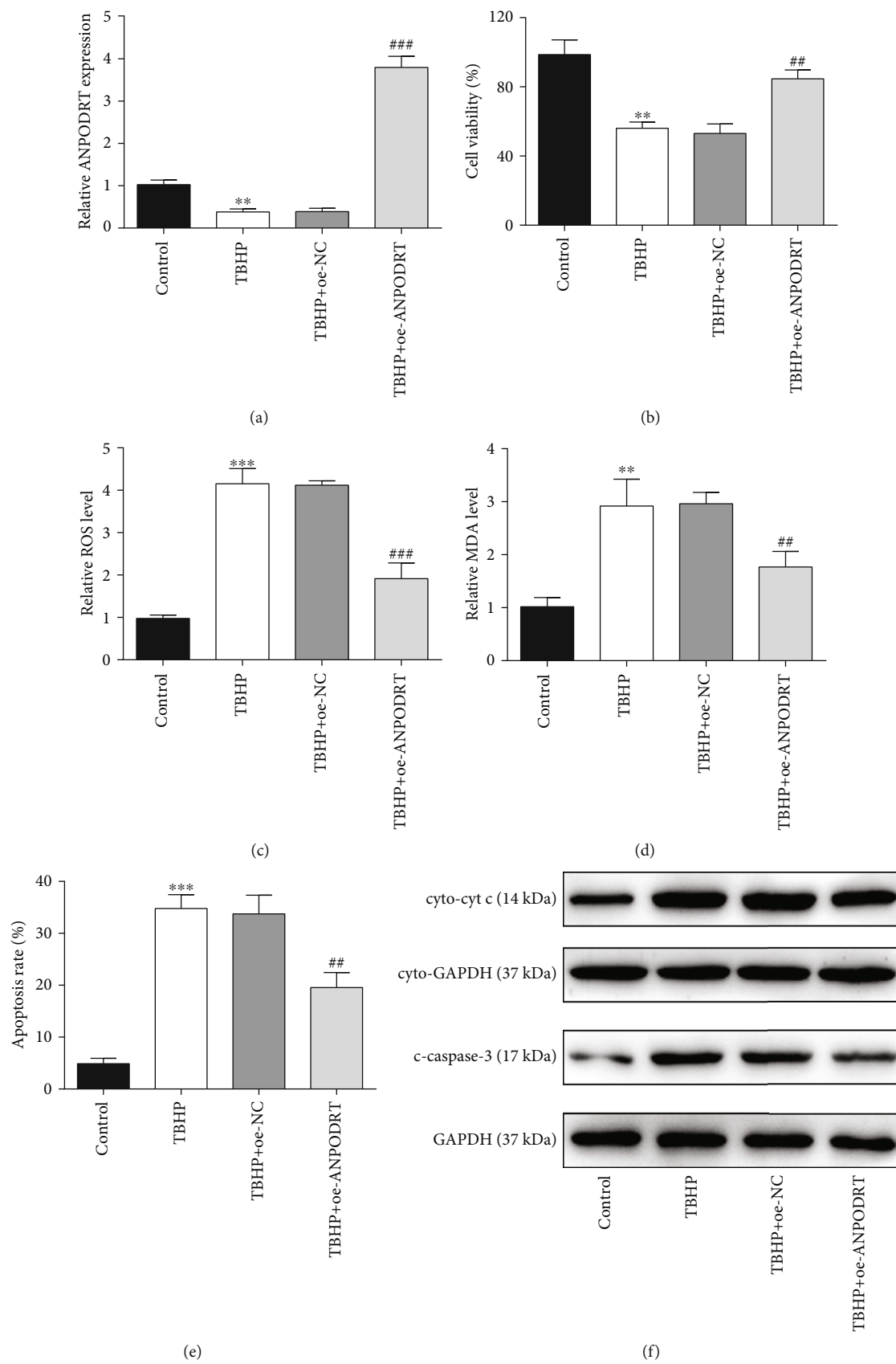


FIGURE 2: Continued.

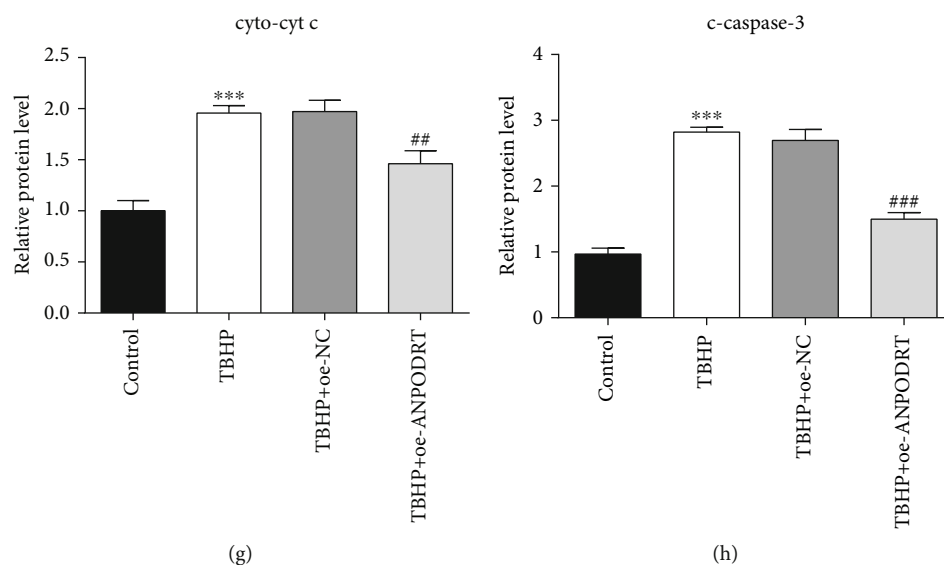


FIGURE 2: ANPODRT overexpression attenuates TBHP-induced oxidative stress and apoptosis in human NP cells. Human NP cells were transfected with ANPODRT overexpression vector (oe-ANPODRT) or negative control (oe-NC) and then exposed to TBHP. (a) The expression of ANPODRT in human NP cells was detected by qRT-PCR. (b) Cell viability of human NP cells was detected by CCK-8 assay. (c) Intracellular ROS production and (d) MDA level in the human NP cells. (e) Annexin V-APC/7-AAD staining results showing the rate of apoptosis in human NP cells. (f–h) The protein levels of cytoplasmic cytochrome c (cyto-cyt c) and cleaved caspase-3 (c-caspase-3) in the human NP cells were measured by Western blotting. Data are represented as the mean \pm SD. ** $p < 0.01$ and *** $p < 0.001$ versus control group; ## $p < 0.01$ and ### $p < 0.001$ versus TBHP+oe-NC group.

3.2. ANPODRT Overexpression Attenuates TBHP-Induced Oxidative Stress and Apoptosis in Human NP Cells. To determine whether ANPODRT plays a role in the TBHP-induced IDD model in vitro, we used an ANPODRT expression vector to overexpress ANPODRT in TBHP-treated human NP cells. qRT-PCR confirmed the overexpression efficiency (Figure 2(a)). Oxidative stress and its induced mitochondrial pathway-mediated apoptosis of NP cells play an important role in IDD pathogenesis. Therefore, indicators of oxidative stress and mitochondrial apoptotic pathway were subsequently assessed. The CCK-8 assay revealed that ANPODRT overexpression inhibited the reduction in NP cell viability induced by TBHP (Figure 2(b)). Furthermore, ROS and MDA levels were determined to evaluate oxidative stress levels in human NP cells. As shown in Figures 2(c) and 2(d), TBHP treatment elevated the ROS and MDA levels, which was suppressed by ANPODRT overexpression. Moreover, flow cytometry revealed that ANPODRT overexpression alleviated the TBHP-induced increase in NP cell apoptosis (Figure 2(e)). Mitochondrial cytochrome c (cyt c) release and caspase-3 activation induced by cyt c are important features of mitochondrial pathway-mediated apoptosis. We found that protein levels of cytoplasmic cyt c and cleaved caspase-3 were significantly increased in human NP cells treated with TBHP, and these TBHP-induced alterations were prevented through ANPODRT overexpression (Figures 2(f)–2(h)).

3.3. ANPODRT Knockdown Aggravates TBHP-Induced Human NP Cell Injury. To investigate the role of ANPODRT in the TBHP-induced IDD model in vitro, ANPODRT expression was knocked down using siRNA in TBHP-treated human

NP cells. As shown in Figure 3(a), qRT-PCR analysis revealed that ANPODRT downregulation induced by TBHP in human NP cells was aggravated through transfection with si-ANPODRT. Functional studies revealed that contrary to ANPODRT overexpression, ANPODRT knockdown further exacerbated TBHP-induced oxidative stress and apoptosis in human NP cells, as manifested by a reduction in cell viability (Figure 3(b)) and an increase in ROS accumulation (Figure 3(c)), MDA production (Figure 3(d)), apoptosis rate (Figure 3(e)), cytoplasmic cyt c level (Figures 3(f) and 3(g)), and cleaved caspase-3 level (Figures 3(f) and 3(h)).

3.4. ANPODRT Activates Nrf2 Signaling in Human NP Cells. Nrf2 is a key regulator of the cellular antioxidative defense system. The activation of Nrf2 signaling can efficiently protect human intervertebral disc cells from oxidative stress. To further investigate the mechanism underlying ANPODRT-mediated inhibition of oxidative injury in human NP cells, we examined whether ANPODRT expression affects Nrf2 signaling. Our results show that ANPODRT overexpression significantly increased the protein level of Nrf2 in human NP cells. In contrast, ANPODRT knockdown markedly downregulated Nrf2 protein (Figures 4(a)–4(d)). Remarkably, Nrf2 mRNA levels were not altered through ANPODRT overexpression or knockdown (Figures 4(e) and 4(f)). These results indicate that ANPODRT positively regulated Nrf2 accumulation, which was not observed at the transcriptional level. Furthermore, we investigated the regulation of ANPODRT on the intracellular distribution of Nrf2 protein. As shown in Figures 4(g)–4(j), ANPODRT overexpression increased Nrf2 nuclear translocation, while ANPODRT knockdown decreased it. Nuclear Nrf2 can bind to the

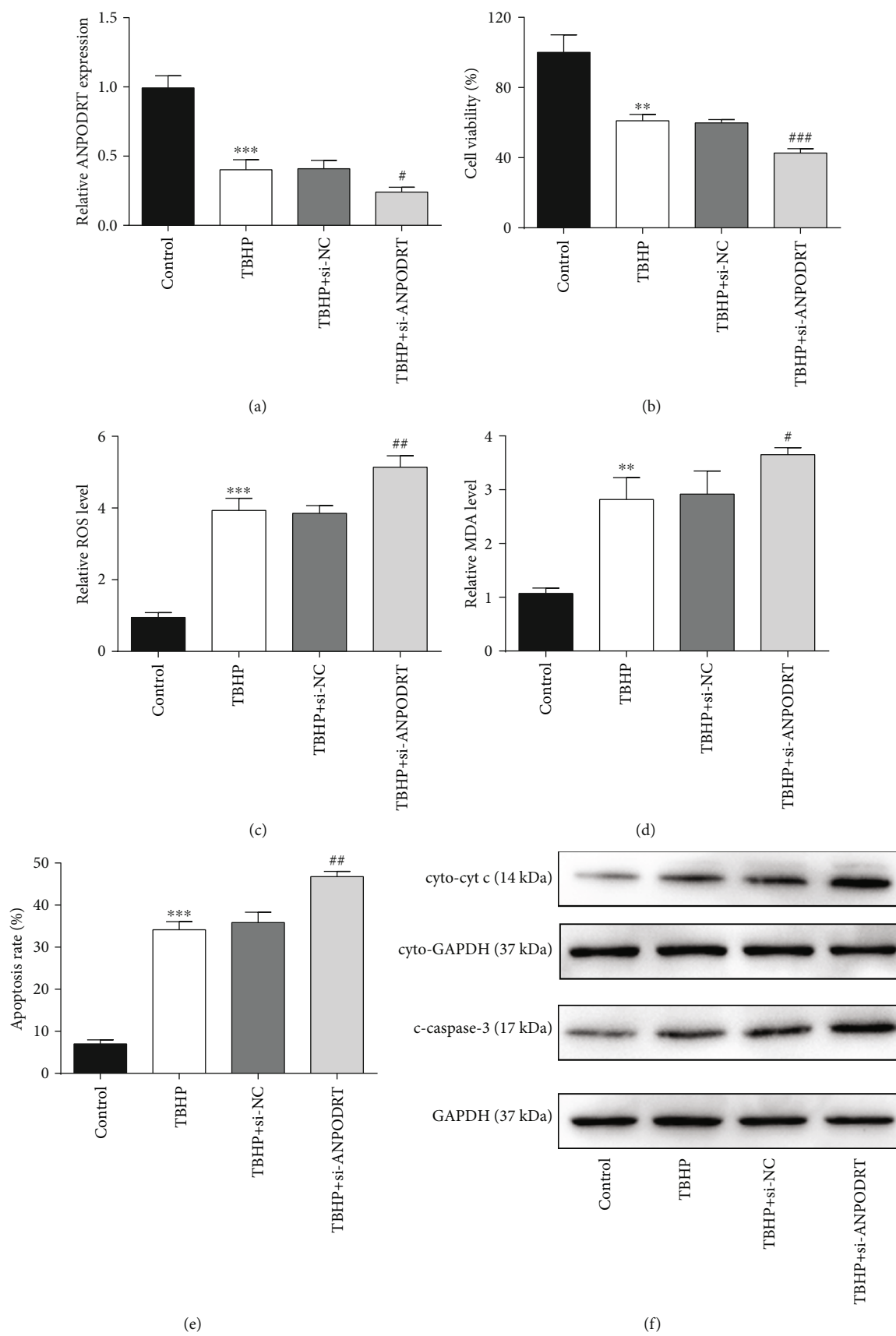


FIGURE 3: Continued.

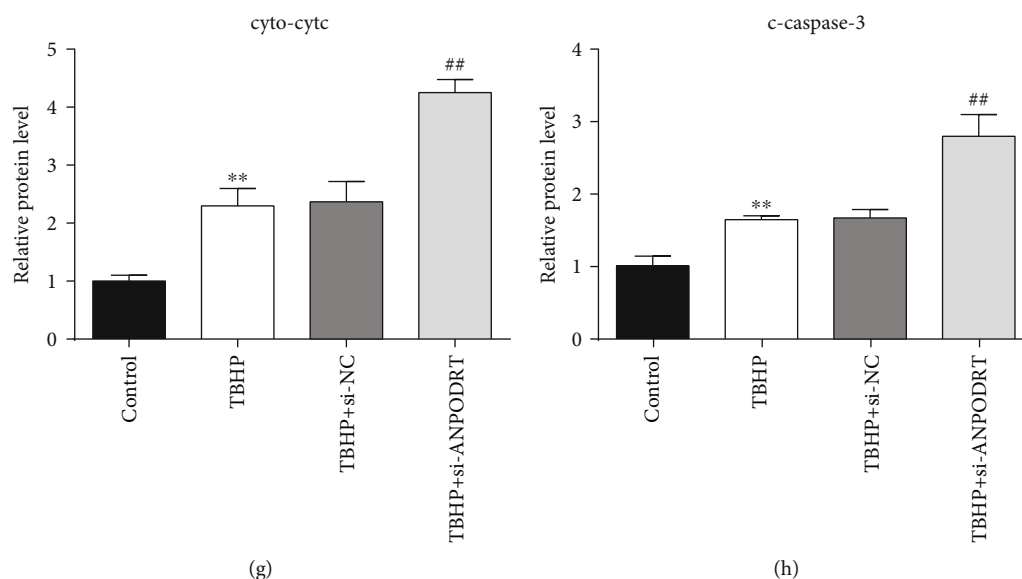


FIGURE 3: ANPODRT knockdown aggravates TBHP-induced human NP cell injury. Human NP cells were transfected with short interfering RNA (siRNA) against ANPODRT (si-ANPODRT) or negative control (si-NC) and then exposed to TBHP. (a) The expression of ANPODRT in human NP cells was detected by qRT-PCR. (b) Cell viability of human NP cells was detected by CCK-8 assay. (c) Intracellular ROS production and (d) MDA level in the human NP cells. (e) Annexin V-APC/7-AAD staining results showing the rate of apoptosis in human NP cells. (f–h) The protein levels of cytoplasmic cytochrome c (cyto-cyt c) and cleaved caspase-3 (c-caspase-3) in the human NP cells were measured by Western blotting. Data are represented as the mean \pm SD. ** $p < 0.01$ and *** $p < 0.001$ versus control group; # $p < 0.05$, ## $p < 0.01$, and ### $p < 0.001$ versus TBHP+si-NC group.

antioxidant response element and then activate its target genes to counteract oxidative stress and modulate redox status balance. To evaluate the transcriptional activity of Nrf2, mRNA expression of well-established Nrf2-dependent genes, including HO1 and NQO1, were detected through qRT-PCR. We found that HO1 and NQO1 mRNA levels were increased after ANPODRT overexpression in human NP cells, while those of HO1 and NQO1 were decreased after ANPODRT knockdown (Figures 4(k)–4(n)). Collectively, these results suggest that ANPODRT promotes accumulation, nuclear translocation, and Nrf2 activation in human NP cells.

3.5. ANPODRT Disrupts the Keap1-Nrf2 Complex Formation in Human NP Cells. Furthermore, we investigated how ANPODRT regulates Nrf2 signaling in human NP cells. Nrf2 can not only be captured by Keap1, but also undergo Keap1-mediated ubiquitination and subsequent proteasomal degradation. Consequently, the proteasome inhibitor MG132 increased Nrf2 protein levels (Figures 5(a)–5(d)). Notably, MG132 also abolished the regulation of ANPODRT overexpression or knockdown on Nrf2 expression (Figures 5(a)–5(d)). The present data indicate that proteasomal Nrf2 degradation is involved in Nrf2 regulation by ANPODRT. Furthermore, Nrf2 degradation may be induced in a Keap1-independent manner. Therefore, we investigated whether Keap1 is involved in ANPODRT-induced Nrf2 accumulation in human NP cells. These results indicate that in Keap1-knockdown human NP cells, ANPODRT overexpression and knockdown were both ineffective in regulating Nrf2 accumulation (Figures 5(e)–5(h)) and Nrf2-dependent gene (HO1 and NQO1) expression (Figures 5(i) and 5(j)), suggesting that ANPODRT regulates Nrf2 accumulation primarily by inter-

fering with Keap1. Nonetheless, Keap1 expression was not affected through ANPODRT expression (Figures 5(k)–5(n)). Therefore, we speculated that ANPODRT potentially disrupts the Keap1-Nrf2 association. To investigate this possibility, we analyzed the association between Keap1 and Nrf2 in human NP cells after ANPODRT overexpression or knockdown. Co-IP assays revealed that ANPODRT overexpression reduced the association between Keap1 and Nrf2 in human NP cells (Figure 5(o)). In contrast, the association between Keap1 and Nrf2 was increased upon ANPODRT knockdown (Figure 5(p)). Together, these findings suggest that ANPODRT induces the dissociation of the Keap1-Nrf2 complex, thus activating the Nrf2 cascade in human NP cells.

3.6. Nrf2 Activation Is Required for ANPODRT-Induced Human NP Cell Protection against Oxidative Injury. The present results show that ANPODRT overexpression activates the Nrf2 cascade and protects human NP cells from oxidative injury. To confirm whether Nrf2 mediates the protective effects of ANPODRT, rescue experiments were performed through siRNA-mediated Nrf2 silencing. Western blotting confirmed the Nrf2 knockdown efficiency (Figures 6(a) and 6(b)). Importantly, the protection of ANPODRT overexpression against TBHP-induced oxidative stress and apoptosis in human NP cells was reversed through Nrf2 knockdown, as indicated through the results of ROS levels (Figure 6(c)), MDA production (Figure 6(d)), apoptosis rate (Figure 6(e)), cytoplasmic cyt c levels (Figures 6(f) and 6(g)), and cleaved caspase-3 levels (Figures 6(f) and 6(h)). Together, these results indicate that the effects of ANPODRT overexpression-induced antioxidative injury

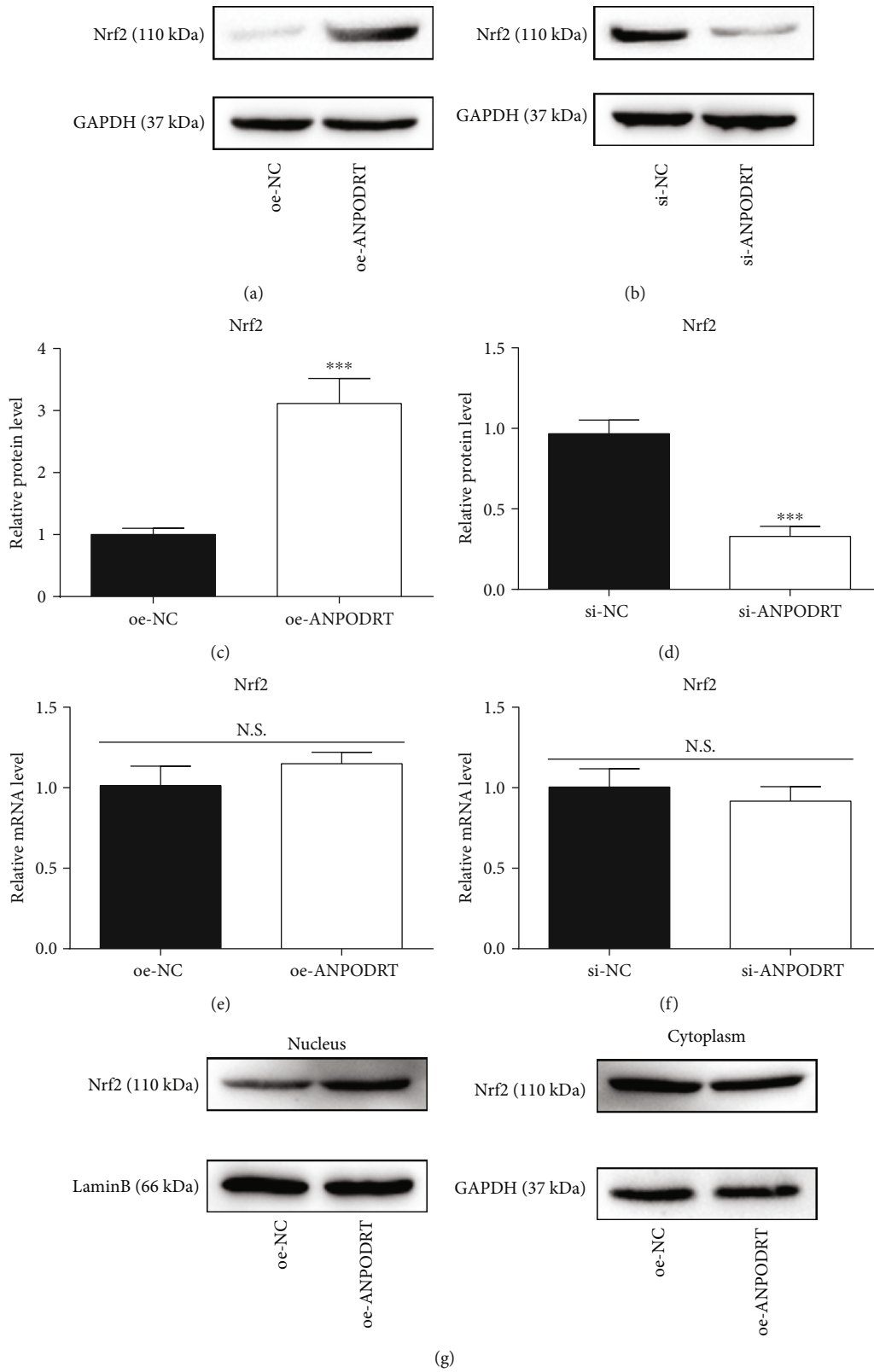


FIGURE 4: Continued.

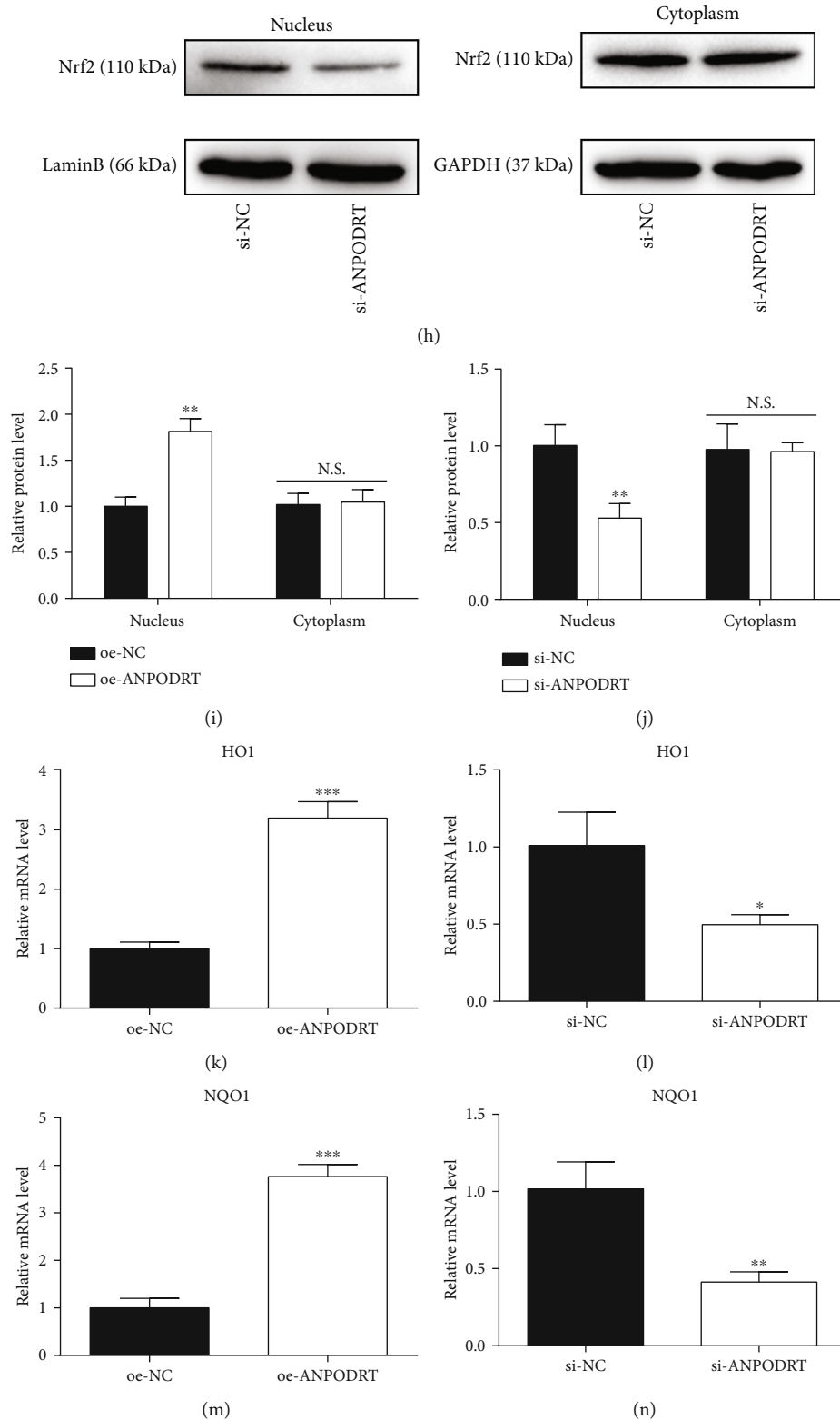


FIGURE 4: ANPODRT activates Nrf2 signaling in human NP cells. (a–d) The protein expression of Nrf2 in human NP cells transfected with oe-ANPODRT, si-ANPODRT, or negative control was measured by Western blotting. (e, f) The mRNA expression of Nrf2 in human NP cells transfected with oe-ANPODRT, si-ANPODRT, or negative control was measured by qRT-PCR. (g–j) The protein expression of nucleus Nrf2 and cytoplasm Nrf2 was measured by Western blotting. (k–n) The mRNA expression of HO1 and NQO1 in human NP cells transfected with oe-ANPODRT, si-ANPODRT, or negative control was measured by qRT-PCR. Data are represented as the mean \pm SD. * $p < 0.05$, ** $p < 0.01$, and *** $p < 0.001$ versus si-NC/oe-NC group; N.S.: not significant.

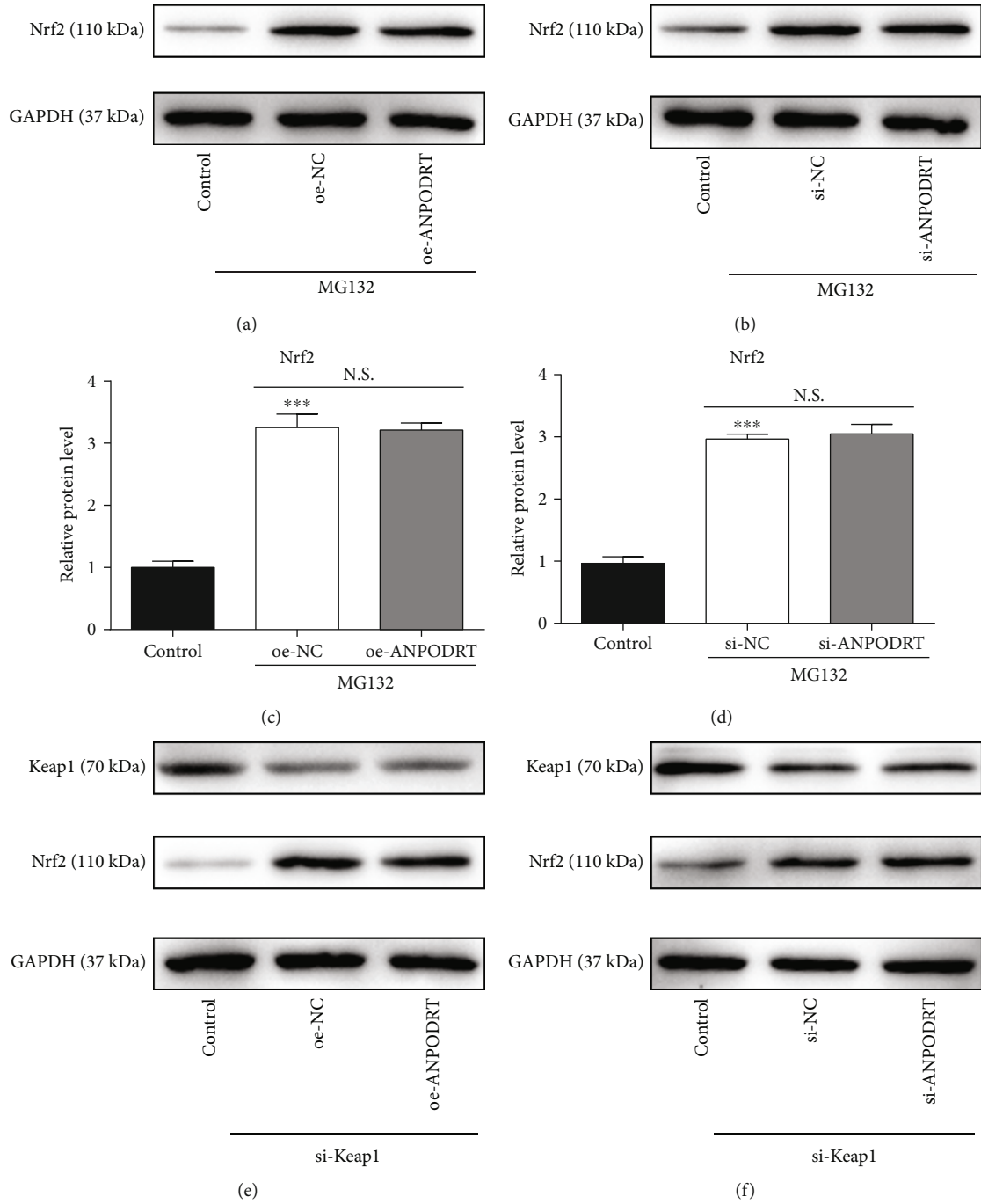


FIGURE 5: Continued.

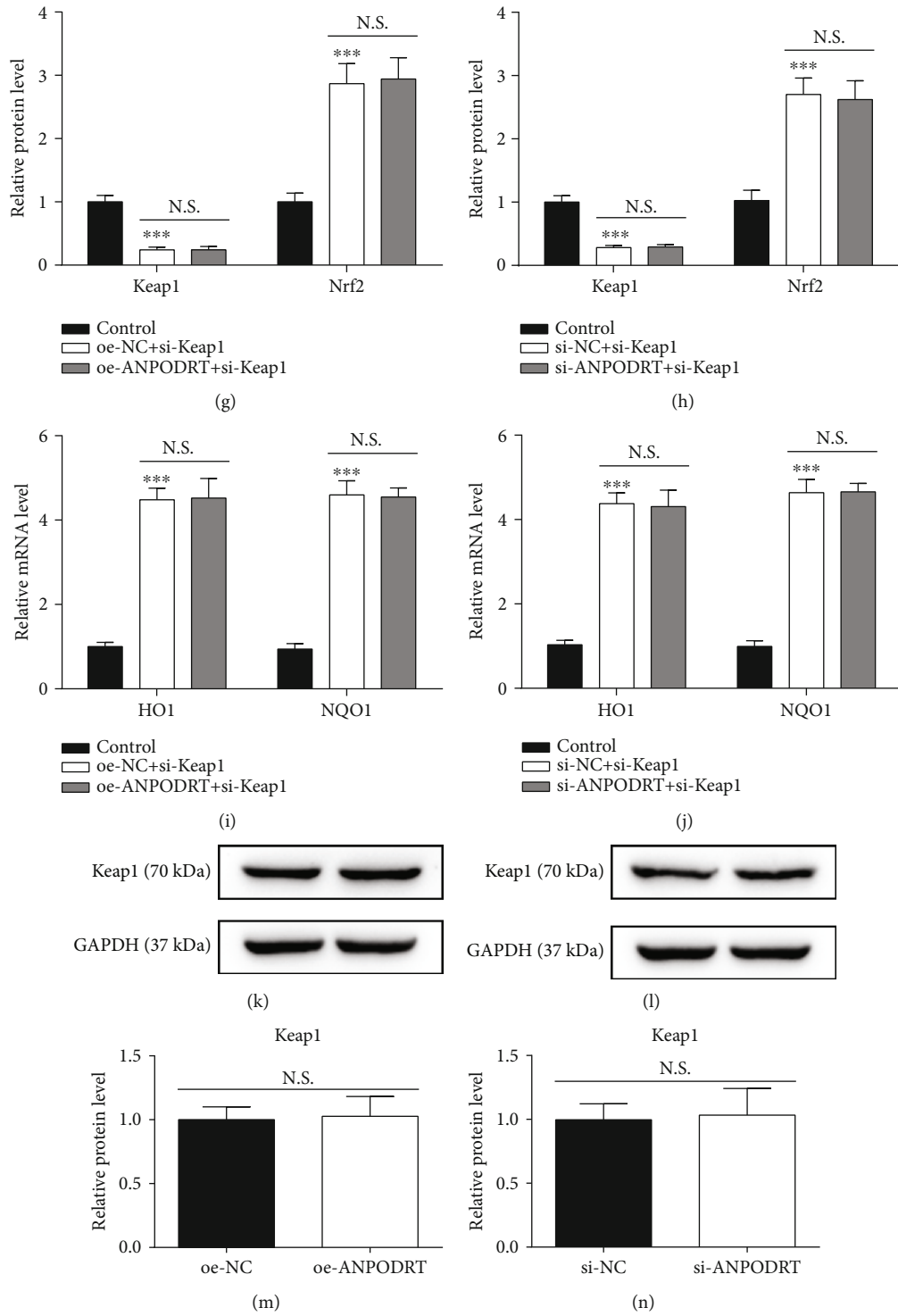


FIGURE 5: Continued.

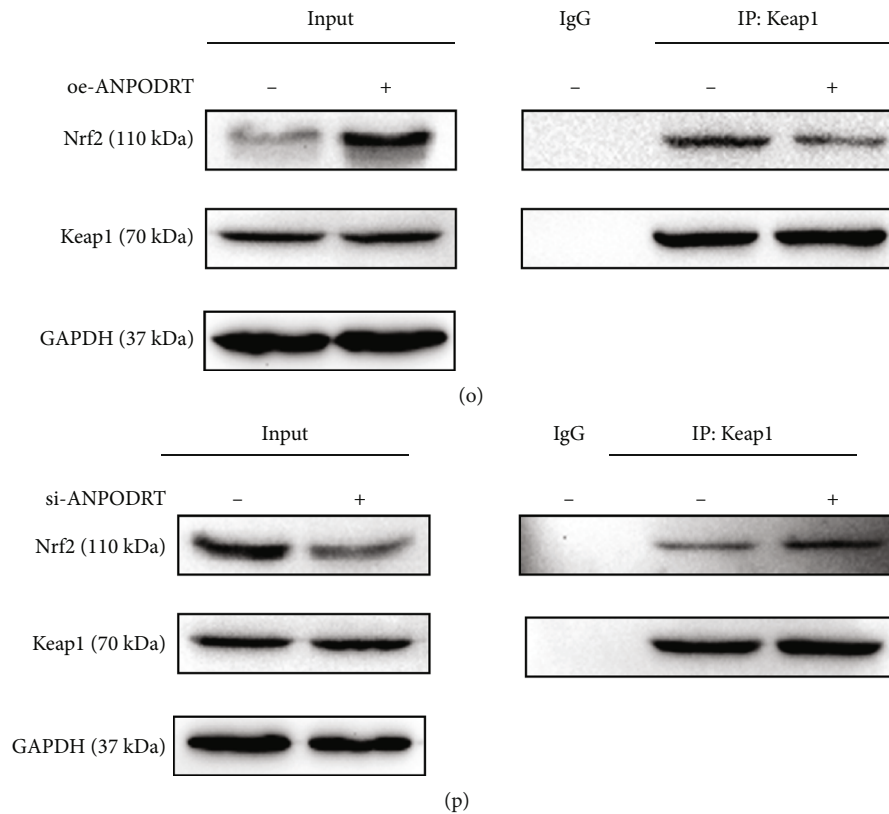


FIGURE 5: ANPODRT disrupts the Keap1-Nrf2 complex formation in human NP cells. (a–d) Human NP cells were transfected with oe-ANPODRT, si-ANPODRT, or negative control followed by MG132 treatment. The protein level of Nrf2 in human NP cells was measured. (e–h) The protein level of Keap1 and Nrf2 in human NP cells transfected using oe-ANPODRT/si-ANPODRT and si-Keap1. (i, j) The mRNA level of HO1 and NQO1 in human NP cells transfected using oe-ANPODRT/si-ANPODRT and si-Keap1. (k–n) The protein level of Keap1 in human NP cells transfected with oe-ANPODRT, si-ANPODRT, or negative control. (o, p) After oe-ANPODRT/si-ANPODRT transfection, the interaction between Keap1 and Nrf2 was determined by Co-IP assay. Data are represented as the mean \pm SD. *** $p < 0.001$ versus control group; N.S.: not significant.

depend on the activation of the Nrf2 cascade in human NP cells.

4. Discussion

Although numerous studies have reported the important roles and clinical significance of lncRNAs in various diseases, the functional roles of most of these molecules are unknown, particularly in the context of IDD [36–38]. In this study, we investigated the expression and function of ANPODRT in IDD. We observed a decreasing trend for ANPODRT expression during IDD pathogenesis, and the well-recognized oxidative stress inducer TBHP downregulated ANPODRT in human NP cells in a dose- and time-dependent manner. Gain-of-function and loss-of-function assays indicated that ANPODRT overexpression suppressed oxidative stress and apoptosis in TBHP-treated human NP cells, while ANPODRT knockdown exerted opposing effects. Mechanistically, these results show that ANPODRT disrupted the Keap1-Nrf2 association, inducing Nrf2 accumulation and nuclear translocation and the expression of Nrf2 target genes in human NP cells. Nrf2 knockdown abolished lncRNA-induced antioxidative stress and antiapoptotic effects in TBHP-treated human NP cells. These data indicate that

ANPODRT inhibits oxidative stress and apoptosis in human NP cells, thus highlighting it as a potential target for IDD treatment.

Accumulating evidence indicates that degenerated IVDs exhibit increased ROS levels, which contributes to IDD pathogenesis. Furthermore, TBHP has several advantages over H_2O_2 , such as high stability and gradual release. Accordingly, previous reports support the in vitro TBHP-induced IDD model used herein [39, 40]. Apoptosis can be initiated by the extrinsic death receptor pathway and the intrinsic mitochondrial apoptosis pathway. The latter has been confirmed to be deeply involved in the increased NP cell death in IDD pathogenesis [16, 39]. Oxidative stress-induced dysfunctional mitochondria can release proapoptotic proteins to form the apoptosome and activate caspase cascades for NP cell apoptosis. Cytoplasmic translocation of mitochondrial cyt c and caspase-3 activation induced by cyt c are characteristics of NP cell apoptosis through the mitochondrial pathway [41]. Several lncRNAs reportedly participate in oxidative stress and the mitochondrial apoptosis pathway. For example, Niu et al. reported that lncRNA Oip5-as1 suppresses microRNA-29a, thus activating the SIRT1/AMPK/PGC1 α pathway, which attenuates oxidative stress and mitochondria-mediated apoptosis

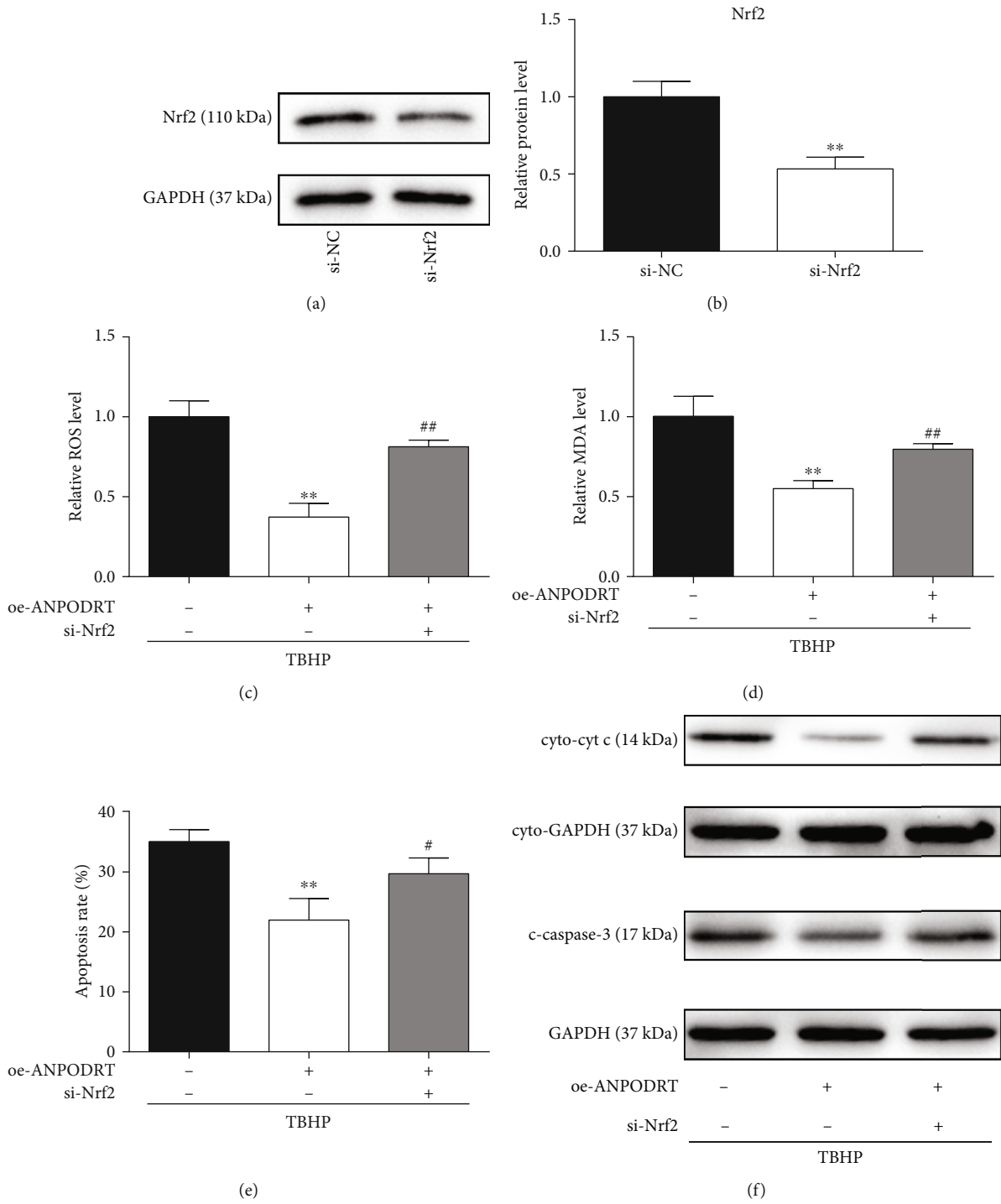


FIGURE 6: Continued.

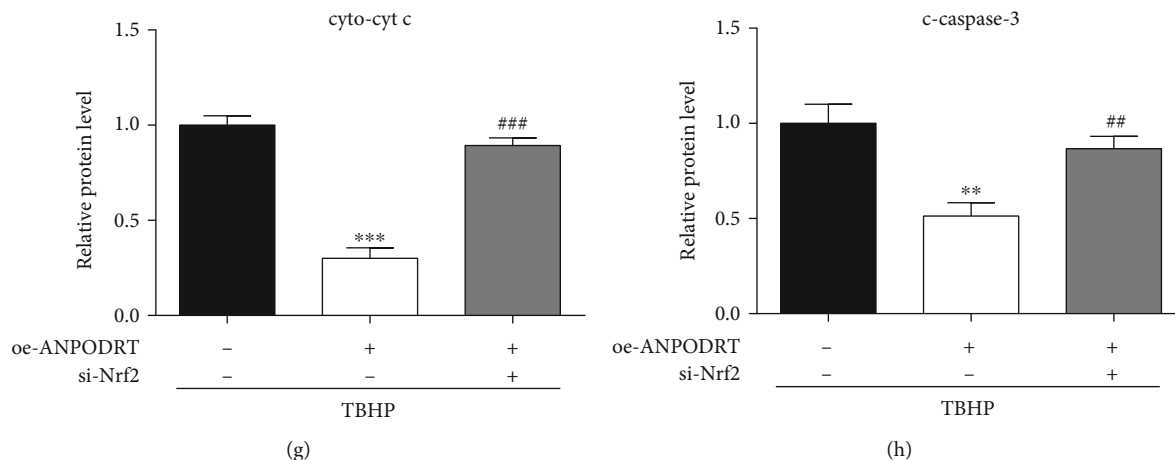


FIGURE 6: Nrf2 activation is required for ANPODRT-induced human NP cell protection against oxidative injury. (a, b) The protein level of Nrf2 in human NP cells transfected with si-Nrf2 or negative control. $**p < 0.01$ versus si-NC group. (c–h) Human NP cells were transfected with oe-ANPODRT and si-Nrf2 followed by TBHP treatment. (c) Intracellular ROS production and (d) MDA level in the human NP cells. (e) Annexin V-APC/7-AAD staining results showing the rate of apoptosis in human NP cells. (f–h) The protein levels of cytoplasmic cytochrome c (cyto-cyt c) and cleaved caspase-3 (c-caspase-3) in the human NP cells were measured by Western blotting. Data are represented as the mean \pm SD. $**p < 0.01$ and $***p < 0.001$ versus TBHP treatment only group; $\#p < 0.05$, $\##p < 0.01$, and $\###p < 0.001$ versus TBHP+oe-ANPODRT group.

during myocardial ischemia/reperfusion injury [42]. Li et al. reported that lncRNA H19 overexpression attenuates H_2O_2 -induced cardiomyocyte injury by suppressing micro-RNA-877-3p/Bcl-2 pathway-mediated mitochondrial apoptosis [43]. However, the role of ANPODRT in oxidative stress and its induction of the mitochondrial apoptosis pathway in human NP cells remain unknown. Therefore, we performed a functional analysis of ANPODRT to determine whether it is involved in oxidative stress and human NP cell apoptosis during IDD. The present results show that ANPODRT was downregulated during IDD pathogenesis, and oxidative stress induced by TBHP downregulated ANPODRT. Notably, ANPODRT overexpression attenuated the accumulation of ROS and MDA, suppressed the upregulation of cytoplasmic-cyto-c and cleaved caspase-3, and inhibited the elevation of the apoptotic rate in human NP cells stimulated with TBHP. These effects were reversed through ANPODRT inhibition. These findings suggest that ANPODRT inhibits oxidative stress and apoptosis in human NP cells.

Mechanistically, considering that ANPODRT inhibits oxidative stress in human NP cells and that the Keap1-Nrf2 complex is an important regulator of oxidative stress, we investigated whether the Keap1-Nrf2 complex is involved in the ANPODRT-mediated protective effects in TBHP-treated human NP cells. Lv et al. reported that eriodictyol-induced retinal ganglion cell protection against high glucose-induced oxidative stress and apoptosis is associated with the activation of Nrf2 signaling [44]. Moreover, along with direct Nrf2 activation, the disruption of the Keap1-Nrf2 interaction has been widely studied. Certain internal disruptors including p62 [45], iASPP [17], and lncRNA-Sox2OT [46] reportedly interfere with the Keap1-Nrf2 complex, thus decreasing the Keap1-Nrf2 interaction and subsequently activating Nrf2 signaling, ultimately affecting the antioxidative status of the cell. Lu et al. reported that

CPUY192018, a potent inhibitor of the Keap1-Nrf2 interaction, alleviates renal inflammation in mice by restricting oxidative stress and NF- κ B activation [19]. The present results show that ANPODRT induced Keap1-Nrf2 disassociation, leading to Nrf2 protein accumulation and nuclear translocation and the expression of Nrf2 targets, including HO1 and NQO1, in human NP cells. Furthermore, Nrf2 knockdown almost obliterated ANPODRT-induced protection of human NP cells against oxidative stress and apoptosis. These results suggest that Nrf2 activation is required for ANPODRT-induced cytoprotective effects in TBHP-treated human NP cells.

There are several difficulties in isolating and culturing NP cells. For the isolation of NP cells, because excessive enzyme digestion will destroy the cells, we cut the NP tissue into small pieces as much as possible, so that the tissue can be in better contact with the enzyme, thus shortening the enzyme digestion time. In the process of primary cell culture, we use penicillin and streptomycin to solve the problem that primary cell culture is easy to be contaminated.

3D culture and hypoxic environment are two aspects that cannot be ignored in the study of IDD. The physiological properties of the intervertebral disc are linked to the structure of its extracellular matrix (ECM) [5]. The ECM in healthy intervertebral disc is a 3D network of natural nanoscale fibers. NP cells in vivo are surrounded by ECM. NP cells can easily lose their phenotype characteristics in monolayer growth [47]. In addition, there are steep gradients in oxygen concentrations across the avascular intervertebral disc, with O_2 falling to as low as 1% in the center of a large disc [48]. A low oxygen tension environment plays a vital role in maintaining intervertebral disc physiological function, including matrix synthesis and even cell metabolism [49]. Studies have shown that a physiological oxygen of 1% appears to promote the best NP phenotype for bovine intervertebral disc cells in alginate [48]. In addition, Pei et al. have reported that low

oxygen tension (5%) enhanced the ECM synthesis of porcine NP cells in a pellet culture system [50]. Therefore, the application of 3D culture in hypoxia can better reflect the actual environment of intervertebral disc. The role of lncRNA in IDD needs more investigations in 3D culture under hypoxia in the future.

Another limitation of this study was that our experiments were performed *in vitro*, and *in vitro* results may not directly reflect the clinical settings. Thus, *in vivo* experiments are needed to confirm the role of ANPODRT in IDD and to increase our understanding of the molecular mechanisms underlying this effect.

In summary, this study shows that ANPODRT protects human NP cells from oxidative stress and apoptosis, at least partially, by interfering with Keap1-Nrf2 association and activating Nrf2-mediated antioxidant system. Our findings further the current understanding of the pathomechanism of IDD and suggest that ANPODRT is a potentially promising therapeutic target for IDD.

Abbreviations

LBP:	Low back pain
IDD:	Intervertebral disc degeneration
NP:	Nucleus pulposus
ROS:	Reactive oxygen species
lncRNAs:	Long noncoding RNAs
MDA:	Malondialdehyde
Nrf2:	Nuclear factor E2-related factor 2
Keap1:	Kelch-like ECH-associated protein 1
TBHP:	Tert-butyl hydroperoxide.

Data Availability

The data used to support the findings of this study are included within the article.

Conflicts of Interest

These authors have no conflict of interest to declare.

Authors' Contributions

Liang Kang, Yueyang Tian, and Xing Guo contributed equally to this work.

Acknowledgments

This work was supported by the Key Program of Tianjin Natural Science Foundation (No. 20JCZDJC00310).

References

- [1] T. Vos, A. A. Abajobir, K. H. Abate et al., "Global, regional, and national incidence, prevalence, and years lived with disability for 328 diseases and injuries for 195 countries, 1990-2016: a systematic analysis for the Global Burden of Disease Study 2016," *The Lancet*, vol. 390, no. 2017, pp. 1211-1259, 2017.
- [2] T. Kadow, G. Sowa, N. Vo, and J. D. Kang, "Molecular basis of intervertebral disc degeneration and herniations: what are the important translational questions?," *Clinical Orthopaedics and Related Research*, vol. 473, no. 6, pp. 1903-1912, 2015.
- [3] Z. Tang, B. Hu, F. Zang, J. Wang, X. Zhang, and H. Chen, "Nrf2 drives oxidative stress-induced autophagy in nucleus pulposus cells via a Keap1/Nrf2/p62 feedback loop to protect intervertebral disc from degeneration," *Cell Death & Disease*, vol. 10, no. 7, p. 510, 2019.
- [4] C. K. Kepler, R. K. Ponnappan, C. A. Tannoury, M. V. Risbud, and D. G. Anderson, "The molecular basis of intervertebral disc degeneration," *The spine journal : official journal of the North American Spine Society*, vol. 13, no. 3, pp. 318-330, 2013.
- [5] Y. Wang, M. Che, J. Xin, Z. Zheng, J. Li, and S. Zhang, "The role of IL-1 β and TNF- α in intervertebral disc degeneration," *Biomedicine & Pharmacotherapy*, vol. 131, p. 110660, 2020.
- [6] S. Yang, F. Zhang, J. Ma, and W. Ding, "Intervertebral disc ageing and degeneration: the antiapoptotic effect of oestrogen," *Ageing Research Reviews*, vol. 57, p. 100978, 2020.
- [7] J. Liang, M. Wu, C. Chen, M. Mai, J. Huang, and P. Zhu, "Roles of reactive oxygen species in cardiac differentiation, reprogramming, and regenerative therapies," *Oxidative Medicine and Cellular Longevity*, vol. 2020, Article ID 2102841, 2020.
- [8] C. Feng, M. Yang, M. Lan et al., "ROS: crucial intermediators in the pathogenesis of intervertebral disc degeneration," *Oxidative Medicine and Cellular Longevity*, vol. 2017, Article ID 5601593, 2017.
- [9] B. Scharf, C. C. Clement, S. Yodmuang et al., "Age-related carbonylation of fibrocartilage structural proteins drives tissue degenerative modification," *Chemistry & Biology*, vol. 20, no. 7, pp. 922-934, 2013.
- [10] S. Chen, X. Lv, B. Hu et al., "Critical contribution of RIPK1 mediated mitochondrial dysfunction and oxidative stress to compression-induced rat nucleus pulposus cells necroptosis and apoptosis," *Apoptosis : an international journal on programmed cell death*, vol. 23, no. 5-6, pp. 299-313, 2018.
- [11] F. Ding, Z. W. Shao, S. H. Yang, Q. Wu, F. Gao, and L. M. Xiong, "Role of mitochondrial pathway in compression-induced apoptosis of nucleus pulposus cells," *Apoptosis : an international journal on programmed cell death*, vol. 17, no. 6, pp. 579-590, 2012.
- [12] L. Yang, L. Zhu, W. Dong et al., "Reactive oxygen species-mediated mitochondrial dysfunction plays a critical role in high glucose-induced nucleus pulposus cell injury," *International Orthopaedics*, vol. 38, pp. 205-206, 2013.
- [13] D. Xu, H. Jin, J. Wen et al., "Hydrogen sulfide protects against endoplasmic reticulum stress and mitochondrial injury in nucleus pulposus cells and ameliorates intervertebral disc degeneration," *Pharmacological Research*, vol. 117, pp. 357-369, 2017.
- [14] L. Kang, S. Liu, J. Li, Y. Tian, Y. Xue, and X. Liu, "Parkin and Nrf2 prevent oxidative stress-induced apoptosis in intervertebral endplate chondrocytes via inducing mitophagy and antioxidant defenses," *Life Sciences*, vol. 243, p. 117244, 2020.
- [15] L. Kang, S. Liu, J. Li, Y. Tian, Y. Xue, and X. Liu, "The mitochondria-targeted anti-oxidant MitoQ protects against intervertebral disc degeneration by ameliorating mitochondrial dysfunction and redox imbalance," *Cell Proliferation*, vol. 53, no. 3, 2020.

- [16] W. Xu, H. Zheng, R. Yang et al., "Mitochondrial NDUFA4L2 attenuates the apoptosis of nucleus pulposus cells induced by oxidative stress via the inhibition of mitophagy," *Experimental & Molecular Medicine*, vol. 51, no. 11, pp. 1–16, 2019.
- [17] W. Ge, K. Zhao, X. Wang et al., "iASPP is an antioxidative factor and drives cancer growth and drug resistance by competing with Nrf2 for Keap1 binding," *Cancer cell*, vol. 32, pp. 561–573.e566, 2017.
- [18] Q. Hui, M. Karlstetter, Z. Xu et al., "Inhibition of the Keap1-Nrf2 protein-protein interaction protects retinal cells and ameliorates retinal ischemia-reperfusion injury," *Free Radical Biology & Medicine*, vol. 146, pp. 181–188, 2020.
- [19] M.-C. Lu, J. Zhao, Y.-T. Liu et al., "CPUY192018, a potent inhibitor of the Keap1-Nrf2 protein-protein interaction, alleviates renal inflammation in mice by restricting oxidative stress and NF- κ B activation," *Redox Biology*, vol. 26, 2019.
- [20] L. Tian, Y. Lu, T. Yang et al., "aPKC ζ promotes gallbladder cancer tumorigenesis and gemcitabine resistance by competing with Nrf2 for binding to Keap1," *Redox Biology*, vol. 22, p. 101149, 2019.
- [21] Z. Li, X. Li, X. Chen et al., "Emerging roles of long non-coding RNAs in neuropathic pain," *Cell Proliferation*, vol. 52, no. 1, article e12528, 2019.
- [22] K. Wang, Y. Song, W. Liu et al., "The noncoding RNA linc-ADAMTS5 cooperates with RREB1 to protect from intervertebral disc degeneration through inhibiting ADAMTS5 expression," *Clinical Science*, vol. 131, no. 2017, pp. 965–979, 1979.
- [23] X. Wang, G. Lv, J. Li, B. Wang, Q. Zhang, and C. Lu, "LncRNA-RP11-296A18.3/miR-138/HIF1A pathway regulates the proliferation ECM synthesis of human nucleus pulposus cells (HNPCs)," *Journal of Cellular Biochemistry*, vol. 118, no. 12, pp. 4862–4871, 2017.
- [24] J. Chen, Y.-S. Jia, G.-Z. Liu et al., "Role of LncRNA TUG1 in intervertebral disc degeneration and nucleus pulposus cells via regulating Wnt/ β -catenin signaling pathway," *Biochemical and Biophysical Research Communications*, vol. 491, no. 3, pp. 668–674, 2017.
- [25] Y. Xi, T. Jiang, W. Wang et al., "Long non-coding HCG18 promotes intervertebral disc degeneration by sponging miR-146a-5p and regulating TRAF6 expression," *Scientific Reports*, vol. 7, no. 1, p. 13234, 2017.
- [26] H. Tan, L. Zhao, R. Song, Y. Liu, and L. Wang, "The long non-coding RNA SNHG1 promotes nucleus pulposus cell proliferation through regulating miR-326 and CCND1," *American Journal of Physiology. Cell Physiology*, vol. 315, no. 1, pp. C21–C27, 2018.
- [27] Z. Ruan, H. Ma, J. Li, H. Liu, H. Jia, and F. Li, "The long non-coding RNA NEAT1 contributes to extracellular matrix degradation in degenerative human nucleus pulposus cells," *Experimental biology and medicine*, vol. 243, no. 7, pp. 595–600, 2018.
- [28] H. Zheng, T. Wang, X. Li et al., "LncRNA MALAT1 exhibits positive effects on nucleus pulposus cell biology in vivo and in vitro by sponging miR-503," *BMC molecular and cell biology*, vol. 21, no. 1, p. 23, 2020.
- [29] S. Cui, Z. Liu, B. Tang, Z. Wang, and B. Li, "LncRNA MAGI2-AS3 is down-regulated in intervertebral disc degeneration and participates in the regulation of FasL expression in nucleus pulposus cells," *BMC Musculoskeletal Disorders*, vol. 21, no. 1, p. 149, 2020.
- [30] Z. Gao, Y. Lin, Z. Wu et al., "LncRNA SNHG6 can regulate the proliferation and apoptosis of rat degenerate nucleus pulposus cells via regulating the expression of miR-101-3p," *European Review for Medical and Pharmacological Sciences*, vol. 24, no. 16, pp. 8251–8262, 2020.
- [31] N. Tang, Y. Dong, J. Liu, and H. Zhao, "Silencing of long non-coding RNA NEAT1 upregulates miR-195a to attenuate intervertebral disk degeneration via the BAX/BAK pathway," *Frontiers in Molecular Biosciences*, vol. 7, p. 147, 2020.
- [32] M. K. Iyer, Y. S. Niknafs, R. Malik et al., "The landscape of long noncoding RNAs in the human transcriptome," *Nature Genetics*, vol. 47, no. 3, pp. 199–208, 2015.
- [33] P.-H. Lan, Z.-H. Liu, Y.-J. Pei et al., "Landscape of RNAs in human lumbar disc degeneration," *Oncotarget*, vol. 7, no. 39, pp. 63166–63176, 2016.
- [34] X. Cheng, L. Zhang, K. Zhang et al., "Circular RNA VMA21 protects against intervertebral disc degeneration through targeting miR-200c and X linked inhibitor-of-apoptosis protein," *Annals of the Rheumatic Diseases*, vol. 77, no. 5, pp. 770–779, 2018.
- [35] Y. Song, S. Li, W. Geng et al., "Sirtuin 3-dependent mitochondrial redox homeostasis protects against AGEs-induced intervertebral disc degeneration," *Redox Biology*, vol. 19, pp. 339–353, 2018.
- [36] A. He, S. He, X. Li, and L. Zhou, "ZFAS1: A novel vital oncogenic lncRNA in multiple human cancers," *Cell Proliferation*, vol. 52, no. 1, article e12513, 2019.
- [37] Z. Huang, J. Zhou, Y. Peng et al., "The role of long noncoding RNAs in hepatocellular carcinoma," *Molecular Cancer*, vol. 19, no. 1, p. 77, 2020.
- [38] K. T. Jin, J. Y. Yao, X. L. Fang, H. di, and Y. Y. Ma, "Roles of lncRNAs in cancer: focusing on angiogenesis," *Life Sciences*, vol. 252, p. 117647, 2020.
- [39] L. Kang, Q. Xiang, S. Zhan et al., "Restoration of autophagic flux rescues oxidative damage and mitochondrial dysfunction to protect against intervertebral disc degeneration," *Oxidative Medicine and Cellular Longevity*, vol. 2019, Article ID 7810320, 2019.
- [40] Y. Chen, J. Lin, J. Chen et al., "Mfn2 is involved in intervertebral disc degeneration through autophagy modulation," *Osteoarthritis and Cartilage*, vol. 28, no. 3, pp. 363–374, 2020.
- [41] M. L.-H. Huang, S. Chiang, D. S. Kalinowski, D.-H. Bae, S. Sahni, and D. R. Richardson, "The role of the antioxidant response in mitochondrial dysfunction in degenerative diseases: cross-talk between antioxidant defense, autophagy, and apoptosis," *Oxidative Medicine and Cellular Longevity*, vol. 2019, Article ID 6392763, 2019.
- [42] X. Niu, S. Pu, C. Ling et al., "LncRNA Oip5-as1 attenuates myocardial ischaemia/reperfusion injury by sponging miR-29a to activate the SIRT1/AMPK/PGC1 α pathway," *Cell Proliferation*, vol. 53, no. 6, article e12818, 2020.
- [43] X. Li, S. Luo, J. Zhang et al., "LncRNA H19 alleviated myocardial I/RI via suppressing miR-877-3p/Bcl-2-mediated mitochondrial apoptosis," *Molecular Therapy - Nucleic Acids*, vol. 17, pp. 297–309, 2019.
- [44] P. Lv, J. Yu, X. Xu, T. Lu, and F. Xu, "Eriodictyol inhibits high glucose-induced oxidative stress and inflammation in retinal ganglial cells," *Journal of Cellular Biochemistry*, vol. 120, no. 4, pp. 5644–5651, 2019.
- [45] M. Komatsu, H. Kurokawa, S. Waguri et al., "The selective autophagy substrate p62 activates the stress responsive

- transcription factor Nrf2 through inactivation of Keap1,” *Nature Cell Biology*, vol. 12, no. 3, pp. 213–223, 2010.
- [46] C.-P. Li, S.-H. Wang, W.-Q. Wang, S.-G. Song, and X.-M. Liu, “Long noncoding RNA-Sox2OT knockdown alleviates diabetes mellitus-induced retinal ganglion cell (RGC) injury,” *Cellular and Molecular Neurobiology*, vol. 37, no. 2, pp. 361–369, 2017.
- [47] H. A. Horner, S. Roberts, R. C. Bielby, J. Menage, H. Evans, and J. P. G. Urban, “Cells from different regions of the intervertebral disc: effect of culture system on matrix expression and cell phenotype,” *Spine*, vol. 27, no. 10, pp. 1018–1028, 2002.
- [48] F. Mwale, I. Ciobanu, D. Giannitsios, P. Roughley, T. Steffen, and J. Antoniou, “Effect of oxygen levels on proteoglycan synthesis by intervertebral disc cells,” *Spine*, vol. 36, no. 2, pp. E131–E138, 2011.
- [49] G. Feng, L. Li, Y. Hong et al., “Hypoxia promotes nucleus pulposus phenotype in 3D scaffolds in vitro and in vivo: laboratory investigation,” *Journal of Neurosurgery. Spine*, vol. 21, no. 2, pp. 303–309, 2014.
- [50] M. Pei, M. Shoukry, J. Li, S. D. Daffner, J. C. France, and S. E. Emery, “Modulation of in vitro microenvironment facilitates synovium-derived stem cell-based nucleus pulposus tissue regeneration,” *Spine*, vol. 37, no. 18, pp. 1538–1547, 2012.

Research Article

Tea Polyphenol Attenuates Oxidative Stress-Induced Degeneration of Intervertebral Discs by Regulating the Keap1/Nrf2/ARE Pathway

Dawei Song, Jun Ge, Yingjie Wang, Qi Yan, Cenhao Wu, Hao Yu, Ming Yang, Huilin Yang , and Jun Zou 

Department of Orthopaedic Surgery, The First Affiliated Hospital of Soochow University, Suzhou, Jiangsu 215006, China

Correspondence should be addressed to Huilin Yang; hlyang@suda.edu.cn and Jun Zou; jzou@suda.edu.cn

Received 13 November 2020; Revised 5 December 2020; Accepted 26 December 2020; Published 9 January 2021

Academic Editor: Sidong Yang

Copyright © 2021 Dawei Song et al. This is an open access article distributed under the Creative Commons Attribution License, which permits unrestricted use, distribution, and reproduction in any medium, provided the original work is properly cited.

Objective. Intervertebral disc degeneration (IDD) and low back pain caused by IDD have attracted public attention owing to their extremely high incidence and disability rate. Oxidative stress is a major cause of IDD. Tea polyphenols (TP) are natural-derived antioxidants extracted from tea leaves. This study explored the protective role of TP on the nucleus pulposus cells (NPCs) of intervertebral discs and their underlying mechanism. **Methods.** An *in vitro* model of H₂O₂-induced degeneration of NPCs was established. RT-qPCR and western blotting were used to detect the mRNA and protein expression of the targets. An *in vivo* model of IDD was established via acupuncture of the intervertebral disc. Radiological imaging and histological staining were performed to evaluate the protective role of TP. **Results.** H₂O₂ contributed to NPC degeneration by inducing high levels of oxidative stress. TP treatment effectively increased the expression of nucleus pulposus matrix-associated genes and reduced the expression of degeneration factors. Further mechanistic studies showed that TP delayed H₂O₂-mediated NPC degeneration by activating the Keap1/Nrf2/ARE pathway. *In vivo* experiments showed that TP delayed the degeneration of NPCs in rats through the Keap1/Nrf2/ARE pathway. **Conclusion.** Our study confirmed that TP activates the Keap1/Nrf2/ARE pathway to exert an antioxidative stress role, ultimately delaying the degeneration of intervertebral discs.

1. Introduction

Chronic low back pain induced by intervertebral disc degeneration (IDD) is limited to symptomatic treatment such as conservative medication or surgical intervention [1]. Commonly used drugs include nonsteroidal anti-inflammatory drugs, skeletal muscle relaxants, and opioids. However, drug treatment only temporarily relieves the symptoms and cannot fundamentally reverse the progression of disc degeneration in patients. Surgical removal of the intervertebral disc is usually used for patients with severe symptoms. Although effectively alleviating pain, surgical intervention is risky and expensive [2]. Moreover, surgical operation destroys the normal physiological structure of the spine and causes degeneration of adjacent segments, which cannot fundamentally reduce the incidence of disc degeneration. Neither pharmaceutical nor surgical treatments can delay IDD progression.

Therefore, it is clinically meaningful to elucidate the pathogenesis of IDD and develop a novel therapy to prevent disc degeneration.

It is well known that a variety of factors contribute to IDD, including inflammation and biomechanical stimulation. Recent studies have shown that oxidative stress plays an important role in the pathological mechanism of diverse diseases, including the degeneration of intervertebral discs [3, 4]. Mitochondrial dysfunction induced by oxidative stress is related to the pathogenesis of disc degeneration [5, 6] because mitochondria are the main source of reactive oxygen species (ROS) in cells. On the one hand, a large amount of ROS is produced during oxidative stress; on the other hand, the scavenging function of ROS in the body's antioxidant system is attenuated, disrupting the dynamic balance between ROS production and elimination [7]. ROS are an important mediator of the cell signaling network in the intervertebral

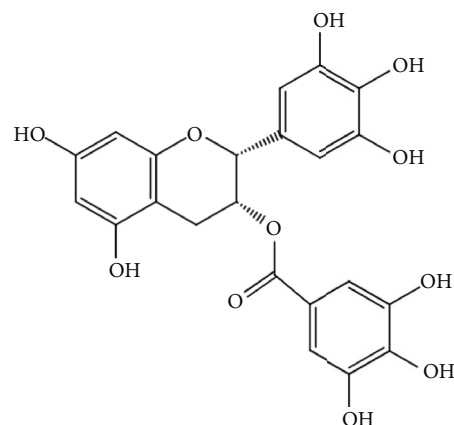
disc cells, regulating matrix metabolism, proinflammatory reactions, apoptotic cell death, autophagy, and aging [8]. Oxidative stress not only enhances the peripheral matrix degradation and inflammatory response in intervertebral disc cells but also attenuates cell number and cellular function in the intervertebral disc microenvironment [9]. In addition, ROS also modify the peripheral matrix protein, accelerate the oxidative damage of the extracellular matrix, and damage the mechanical function of the intervertebral disc [8]. Therefore, targeting oxidative stress may provide a new perspective for IDD treatment. A variety of antioxidants are considered effective drugs for the treatment of IDD [10, 11].

Given their plant origin, tea polyphenols (TP) extracted from tea leaves are a safer antioxidant than synthetic counterparts. TP are considered to be chain-breaking antioxidants, based on their potential for hydrogen atom transfer or single electron transfer reactions (SETs). Many studies have confirmed the antioxidant effects of TP, including prevention of oxidative stress and regulation of carcinogen metabolism [12]. In kidney diseases, damage, and toxic situations, e.g., excessive arginine supply, strong oxidative radicals, renal toxin, and diabetic nephropathy, TP play a beneficial role against pathological reactions related to oxidative stress [13]; TP also enhance the antioxidant activity of liver cells, making them a potential treatment of liver cancer [14]. Breast cancer cells pretreated with TP become more sensitive to methotrexate because of the reduction of intracellular ROS. TP also improve the cognitive impairment caused by chronic cerebral hypoperfusion by regulating oxidative stress reactions [15].

There is limited research on the effect of TP on the intervertebral disc, especially in the nucleus pulposus tissues. Given the unique antioxidative stress properties of TP, our study was aimed at exploring their protective roles in the nucleus pulposus cells (NPCs) from the intervertebral disc. The study verified the effect of TP on the nucleus pulposus using *in vitro* and *in vivo* assays.

2. Materials and Methods

2.1. Cell Line, Reagents, and Instruments. Fetal bovine serum, Dulbecco's modification of Eagle's medium (DMEM), Trizol reagent, a reverse transcription kit, and a SYBR Green Real-Time PCR Master Mix kit were purchased from Thermo Fisher Scientific (San Jose, CA, USA). RAPI protein lysates and a BCA kit were purchased from Invitrogen (Carlsbad, CA, USA). Primary antibodies against collagen II, aggrecan, SOX-9, collagen X, MMP3, iNOS, NOX4, SOD2, LDH, T-AOC, NRF2, KEAP1, and ARE as well as the corresponding secondary antibodies were purchased from Wuhan Amictech Technology Co., Ltd. (Wuhan, Hubei, China). A CCK-8 kit was purchased from Shanghai Yisheng Biotechnology Co., Ltd. (Shanghai, China). A microplate reader, a fluorescence quantitative PCR amplifier, and an electrophoresis and gel imaging system were purchased from Thermo Fisher Scientific (San Jose, CA, USA); an ultracentrifuge and electrophoresis tank were purchased from Beijing Liuyi Biotechnology Co., Ltd. (Beijing, China). TP (epigallocatechin-3-gallate



SCHEME 1: Chemical formula of the tea polyphenols.

(EGCG) Scheme 1) was purchased from Hangzhou Yibeiijia Tea Technology Co. Ltd.

2.2. Cell Culturing. Cells (nucleus pulposus cell lines, Crisprbio, Beijing, China) were cultured in DMEM containing 10% fetal bovine serum, 100 U/mL penicillin, and 0.1 mg/mL streptomycin at 37°C with 5% CO₂. NPCs in the log phase were digested with trypsin, seeded in a 6-well plate (10⁴ cells/well), and incubated at 37°C for 24 h for later use.

2.3. NPC Viability Assay. NPC cells were seeded in a 96-well plate at a density of 5 × 10³ cells/well and cultured at 37°C in an incubator for 24 h. CCK-8 solution (10 μL) was then added to each well. After incubation at 37°C for 2 h, optical absorbance was detected on a microplate reader, with at least three replicates.

2.4. Quantitative Real-Time PCR (RT-qPCR). Total RNA was extracted from tissues and cells using Trizol reagent. The RNA concentration was measured using agarose gel electrophoresis and reverse transcribed into cDNA. The mRNA levels of collagen II, aggrecan, SOX-9, collagen X, MMP3, iNOS, NOX4, SOD2, LDH, T-AOC, NRF2, KEAP1, and ARE were detected using a SYBR Green kit, and U6 served as an internal reference. Primers for gene amplification were designed using the Primer Premier 5.0 software. PCR reactions were performed at 95°C for 5 min, followed by denaturation at 94°C for 30 s and annealing at 60°C for 30 s, with a total of 45 cycles, in a final volume of 20 μL, including 2 μL cDNA, 10 μL SYBR Green Mix, 0.5 μL upstream and 0.5 μL downstream primers (10 μmol/L each), and 7 μL dH₂O. Relative gene levels were calculated by the 2-ΔΔCt method. The experiment was repeated three times independently. Prime sequence could be found in Table 1.

2.5. Western Blotting. Total proteins were extracted with RIPA lysis buffer, and their concentration and purity were measured with a BCA kit. Proteins were subjected to 10% SDS-PAGE at 80-120 V and transferred to polyvinylidene fluoride (PVDF) membranes at 100 mV for 1 h. The membranes were blocked in 5% skimmed milk powder for 1 h and incubated with the primary antibody (1:1,000) overnight at 4°C. The next day, the membranes were washed three

TABLE 1: Prime sequence.

iNOS	F: 5'-GATCA ATAAC CTGAA GCCCG-3' R: 5'-GCCCT TTTT GCTCC ATAGG-3'
NOX4	F: 5'-GAACCTCAACTGCAGCCTGATC-3' R: 5'-CTGTCAACAATCTTCTTCTCTC-3'
SOD2	F: 5'-CTGGCCAAGGGAGATGTTAC-3' R: 5'-AAAGACCCAAAGTCACGCTT-3'
LDH	F: 5'-TCATTCTGCCATAGTCCA-3' R: 5'-CAATTACACGAGTTACAGGTA-3'
T-AOC	F: 5'-CCAGGTGGCAGCCGACAATG-3' R: 5'-ACGAAGACGAGGACGAGGATGG-3'
Collagen 2	F: 5'-TGAAGACCCAGACTGCCTCAA-3' R: 5'-CGAGGTCAGCTGGGCAGAT-3'
Aggrecan	F: 5'-GGCATCGTGTTCATTAC-3' R: 5'-TCTCCATAGCAGCCTTCC-3'
SOX-9	F: 5'-ATCTGAAGAAGGAGAGCGAG-3' R: 5'-TCAGAAGTCTCCAGAGCTTG-3'
Collagen X	F: 5'-AGTGTCTTACGCTGAACG-3' R: 5'-TGCTCTCTTACTGCT-3'
MMP-3	F: 5'-TATGGATCCCCCTGACTCCCCTGAG-3' R: 5'-ATGGAATTCAGGTTCAAGCTTCTGAGG-3'
NRF2	F: 5'-ACTCCGCATTTCACTAAACACAAG-3' R: 5'-CTGAGGCCAAGTAGTGTGTCTCCA-3'
KEAP1	F: 5'-CATCGGCATCGCCAACTTC-3' R: 5'-ACCAGTTGGCAGTGGGACAG-3'
ARE	F: 5'-TCAGCAGCCACCACCTCTAC-3' R: 5'-AGTCACTACAGAGCCGCATCC-3'

times with Tris-Buffered Saline Tween-20 (TBST) for 5 min and incubated with the secondary antibody (1:5,000) at room temperature for 1 h. After washing the membranes three times with TBST, protein signals were developed using an ECL kit; the images were captured using a gel imaging system and quantitatively analyzed using ImageJ software. The experiment was repeated three times independently.

2.6. Animal Model. In total, 18 specific pathogen-free (SPF) male rats, weighing 400 ± 20 g, were purchased from Nanjing Pengsheng Biotechnology Development Co., Ltd. (Nanjing, Jiangsu, China). MRI and X-ray examination confirmed no congenital caudal disc deformity or degeneration. The rats were randomly divided into three groups using the digital table method: the degeneration group (normal saline group), the TP group (100 nM), and the TP+NRF2 siRNA group, with six rats in each group. The rats were weighed and intraperitoneally injected with ketamine hydrochloride (50 mg/kg) and piperazine hydrochloride (5 mg/kg). After anesthesia, the rats were fixed and disinfected, and the co8/9 vertebral space was penetrated to the opposite side completely and rotated 360° for 30 s using an 18G needle with X-ray guidance. Immediately, $2 \mu\text{L}$ TP saline (100 μM), TP (100 μM)+Nrf2 siRNA (100 μM , Santa Cruz Biotech, Santa Cruz, CA) saline, and an equal amount of normal saline were

injected into the intervertebral discs. Following surgery, rats had free access to food and water, and urinary retention and infection were closely monitored. All the experiments, conducted at the First Affiliated Hospital of Soochow University, were approved by the Ethics Committee and strictly abide by the "Declaration of Helsinki" (1964) and "Guidelines for Ethical Review of Laboratory Animal Welfare" (GB/T 35892-2018, China).

2.7. MRI Scan. The tails of the rats were exposed to MRI scans at weeks 1, 2, and 4 after surgery. First, rats were anesthetized by intraperitoneal injection with ketamine hydrochloride (50 mg/kg) and piperazine hydrochloride (5 mg/kg). The intervertebral disc signal was then obtained on a 1.5 T magnetic resonance scanner (Philips Eclipse, Cleveland, OH, USA), with the following parameters of the T2-weighted sagittal plane: TR/TE, 3,500/102 ms; FOV, 15.0; thickness, 3 mm; and interval, 0 mm. The degree of disc degeneration was assessed by signal intensity on a T2-weighted image (T2WI) of the intervertebral disc. The degree of IDD was evaluated based on T2WI signal intensity, including quantitative analysis of T2 phase signal using ImageJ, and disc grading by the modified Pfirrmann system (Table 2). The grading was performed independently by two experienced spinal surgeons. When the grades diverged, a third and more senior spinal surgeon was asked to evaluate the results, and three spinal surgeons negotiated and gave the final decision.

2.8. Histology. Following radiological examination, the rats were euthanized. The Co8/9 intervertebral discs were removed, fixed with 10% neutral formaldehyde at room temperature for 24 h, decalcified with 15% EDTA for 4 weeks, embedded, and sectioned. The sections were deparaffinized twice in xylene for 5 min, dehydrated in graded ethanol (75%, 1 min; 80%, 1 min; 95%, 1 min; and 100%, 2 min), and stained with hematoxylin for 5 min and with eosin for 2 min. Morphological changes of discs were observed under a light microscope and scored according to the classification criteria described in Table 3.

2.9. Immunohistochemical Staining. Immunohistochemistry was used to detect the expression of type II collagen, type X collagen, and SOD2. The sections were deparaffinized with xylene, dehydrated with graded ethanol, and incubated at 37°C with 3% H_2O_2 for 10 min. After being washed three times in PBS, the sections were boiled in 0.01 M citrate buffer (95°C , 15-20 min) and blocked in goat serum at 37°C for 10 min. The sections were then incubated with the primary antibody at 4°C overnight and the biotin-labeled secondary antibody (BioWorld, Visalia, CA, USA) at 37°C for 30 min. The sections were counterstained with hematoxylin and observed under a light microscope.

2.10. Statistical Analysis. The SPSS 18.0 software was used for statistical analysis. Differences between the two groups were analyzed using the *t*-test, and differences between multiple groups were analyzed using one-way analysis of variance. GraphPad Prism 8.2 was used to draw relevant figures. Values of $P < 0.05$ indicated statistical significance.

TABLE 2: Pfirrmann system.

Grade	Structure	Signal	Pfirrmann system	
			Disc height	Distinction between nucleus and anulus
I	Homogeneous	Bright hyperintense white signal intensity	Normal	Clear
II	Inhomogeneous	Hyperintense white signal	Normal	Clear, with or without horizontal gray bands
III	Inhomogeneous	Intermediate gray signal intensity	Normal or slightly decreased	Unclear
IV	Inhomogeneous	Hypointense dark gray signal intensity	Normal or moderately decreased	Lost
V	Inhomogeneous	Hypointense black signal intensity	Collapsed	Lost

TABLE 3: Grading for morphology.

		Morphology change under optical microscope	Grade
I	Annulus fibrosus (AF)	Normal texture and free of damage and distortion	1
		The damaged and distortion area is less than 30%	2
		The damaged and distortion area is more than 30%	3
II	Boundary between AF and NP	Normal	1
		Micro disrupted	2
		Medium or severe disrupted	3
III	NP cells	Normal cells with large amounts of vacuoles	1
		Cells and vacuoles decreased slightly	2
		Cells decreased moderately or severely without vacuoles	3
IV	NP matrix	Normal gel appearance	1
		Slightly congealed	2
		Moderate or severe condensation	3

3. Results

3.1. H_2O_2 -Induced NPC Degeneration. A CCK-8 assay revealed that H_2O_2 at $100 \mu M$ had no obvious effects on NPC viability, whereas higher doses of gradually decreased it (Figure 1(a), $P < 0.05$). Thus, H_2O_2 at $100 \mu M$ was chosen for further study. RT-qPCR results showed that mRNA levels of collagen II, aggrecan, and SOX-9 were significantly decreased (Figures 1(b)–1(d)), whereas collagen X and MMP3 levels were elevated (Figures 1(e) and 1(f)), following treatment with H_2O_2 at $100 \mu M$ or higher doses ($P < 0.05$). Western blotting identified a decrease in the protein expression of collagen II in NPCs treated with H_2O_2 at $100 \mu M$ or higher (Figures 1(g) and 1(h), $P < 0.05$).

3.2. H_2O_2 Induces NPC Degeneration via High Oxidative Stress. The RT-qPCR data unveiled that mRNA levels of iNOS, NOX4, SOD2, LDH, and T-AOC were significantly increased in NPCs exposed to $100 \mu M$ H_2O_2 (Figures 2(a)–2(e), $P < 0.05$). In addition, western blotting showed that SOD2 protein levels were dramatically elevated following treatment with $100 \mu M$ H_2O_2 (Figures 2(f) and 2(g), $P < 0.05$).

3.3. TP Delays H_2O_2 -Induced NPC Degeneration. Data from the CCK-8 assay suggested that TP at low doses had no obvious effects on H_2O_2 -treated NPCs. However, TP

($>50 \mu g/mL$) clearly promoted H_2O_2 -treated NPC cell viability (Figures 3(a), $P < 0.05$). RT-qPCR assay showed that treatment with TP significantly elevated mRNA levels of collagen II, aggrecan, and SOX-9 and decreased the levels of collagen X and MMP3 in $100 \mu M$ H_2O_2 treated NPCs (Figures 3(b)–3(f), $P < 0.05$). Moreover, western blotting analysis showed that TP could increase protein expression of collagen II in NPCs treated with H_2O_2 ($100 \mu M$) (Figures 3(g) and 3(h), $P < 0.05$).

3.4. TP Effectively Reduces H_2O_2 -Mediated High Oxidative Stress in NPCs. RT-qPCR results showed that TP ($100 \mu g/mL$) significantly inhibited the mRNA expression of iNOS, NOX4, SOD2, LDH, and T-AOC in NPCs treated with $100 \mu M$ H_2O_2 (Figures 4(a)–4(e), $P < 0.05$). In addition, TP ($100 \mu g/mL$) treatment significantly suppressed protein expression of SOD2 in NPCs treated with $100 \mu M$ H_2O_2 (Figures 4(g) and 4(h)).

3.5. TP Activates the Keap1/Nrf2/ARE Pathway to Delay H_2O_2 -Induced NPC Degeneration. RT-qPCR and western blotting showed that TP ($100 \mu g/mL$) increased the mRNA and protein levels of NRF2, KEAP1, and ARE ($P < 0.05$), similar to the effects of dimethylformamide (DMF), an activator of the Keap1/Nrf2/ARE pathway (Figures 5(a)–5(c)). H_2O_2 treatment alone slightly promoted the expression of NRF2, KEAP1, and ARE. Combined treatment with TP

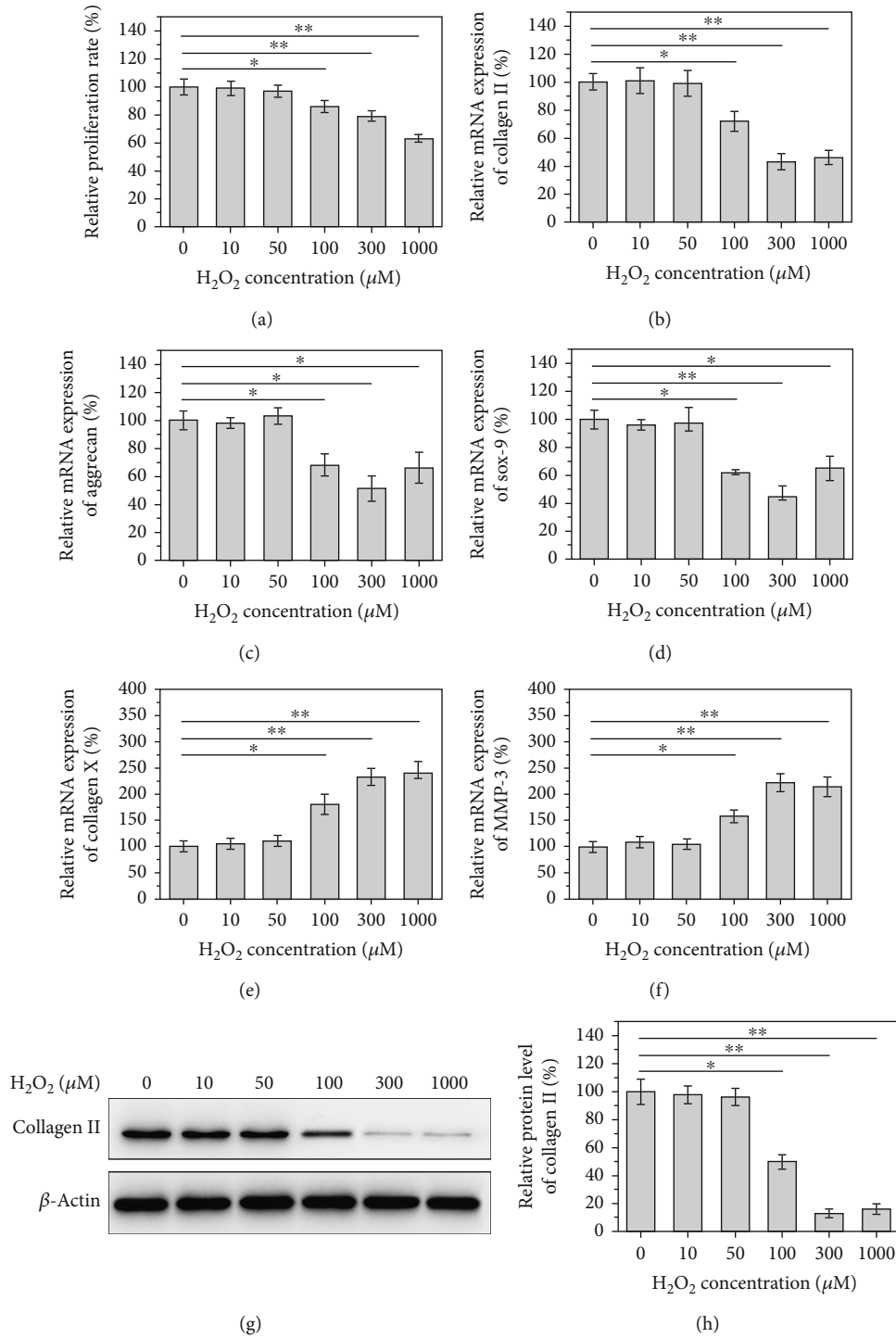


FIGURE 1: 100 μM H₂O₂ induces the degeneration of nucleus pulposus cells. When the concentration of H₂O₂ was more than 100 μM, (a) the proliferation rate of cells decreased significantly. The relative mRNA expression of (b) collagen II, (c) aggrecan, and (d) Sox-9 decreased significantly, while that of (e) collagen X and (f) MMP-3 increased significantly. (g, h) And the relative protein level of collagen II decreased significantly ($P < 0.05$).

(100 μg/mL) and H₂O₂ significantly promoted the mRNA and protein levels of NRF2, KEAP1, and ARE ($P < 0.05$). Moreover, DMF (30 μg/mL) combined with TP (100 μg/mL) further increased the mRNA and protein expression of NRF2, KEAP1, and ARE in NPCs treated with 100 μM H₂O₂ ($P < 0.05$) (Figures 5(d)–5(g)).

3.6. TP Delays NPC Degeneration via the Keap1/Nrf2/ARE Pathway In Vivo

3.6.1. MRI Examination and Pfirrmann Grading. MRI examination showed that TP treatment improved disc degeneration. Although rats in the saline degeneration group maintained the

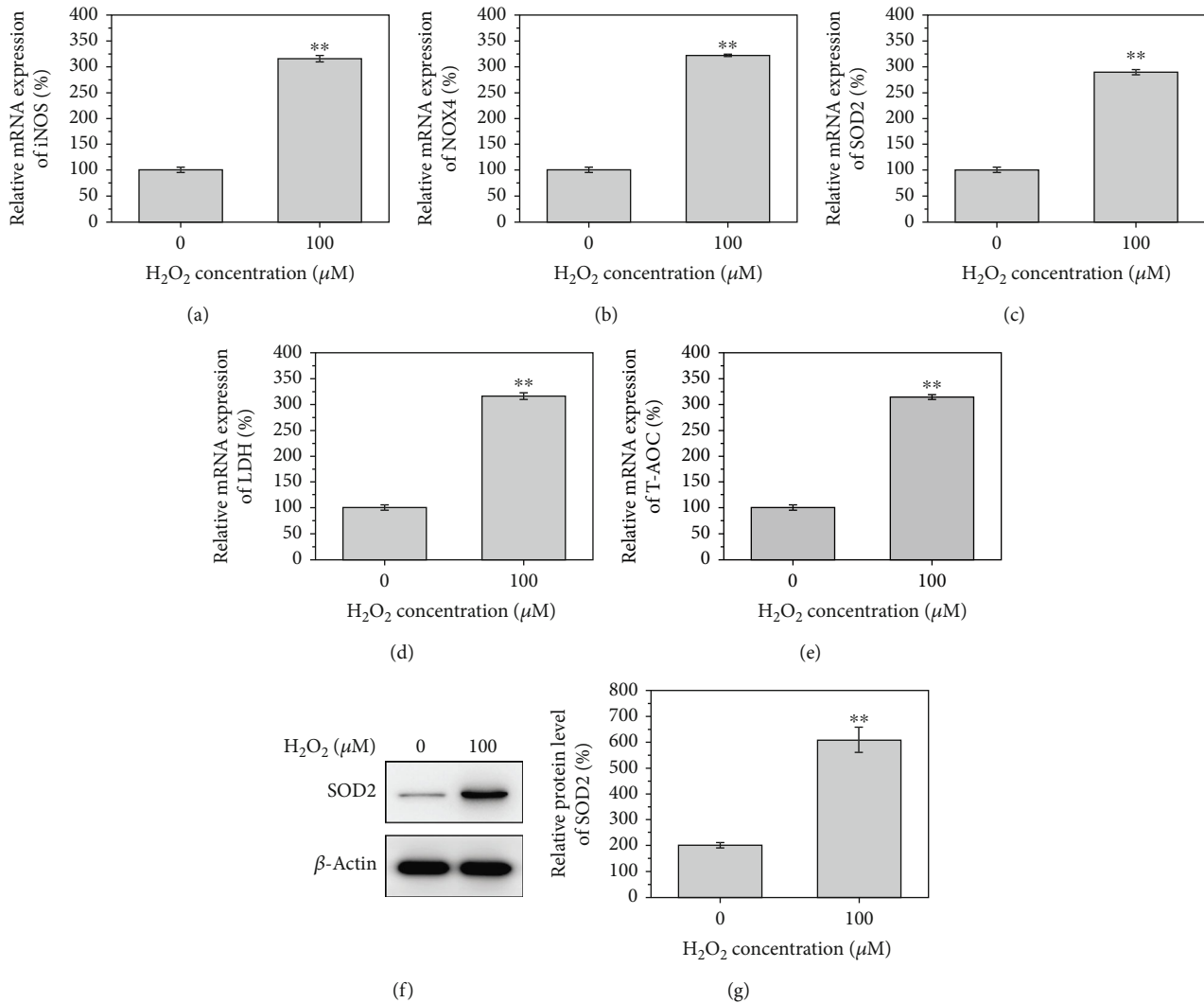


FIGURE 2: 100 μM H_2O_2 caused oxidative stress in nucleus pulposus cells. (a–e) The relative mRNA of iNOS, NOX4, SOD2, LDH, and T-AOC significantly increased after the treatment of 100 μM H_2O_2 . (f, g) The relative protein level of SOD2 increased significantly after the treatment of 100 μM H_2O_2 .

original height of the intervertebral space in the first week, the disc signal significantly decreased; however, TP-treated rats showed a high disc signal level in the first week. Although the signal was somewhat indistinct and dispersed compared to the signal observed in the control group, the overall situation was better than that of the degeneration group (saline). In the MRIs performed at the second and fourth weeks, it was observed that the discs in the degeneration group became “dark discs” with an obvious decreased height of the intervertebral space. Conversely, the discs in the TP group showed an obvious improvement and retained high signals; the signal of the disc did not go dark sharply, although the height of the intervertebral space continued to decrease. The addition of NRF2 siRNA to the TP solution decreased NRF2 mRNA levels, which accelerated the degeneration of the intervertebral disc (Figure 6(a)).

Quantitative and qualitative analyses further confirmed these results. Gray value analysis showed that TP effectively reduced the gray levels of the intervertebral disc signal, resulting in a high signal state ($P < 0.05$). The Pfirrmann

scores revealed significant differences between the TP and degeneration groups in the first week ($P < 0.05$). At the fourth week, such differences became more obvious among the TP, degeneration, and TP+Nrf2 siRNA groups ($P < 0.05$). Compared with the degeneration group, TP treatment alleviated disc degeneration *in vivo* (Figure 6(b)).

3.7. HE Staining and Histology Analysis. After four weeks of treatment, HE staining in the degeneration group showed that the volume of the intervertebral nucleus pulposus and the number of cartilage cells were reduced. In some sections, the nucleus pulposus tissue completely disappeared, and the fibrous annulus appeared to be twisted and damaged. Similar results were observed in the TP+NRF2 siRNA group. However, treatment with TP for four weeks significantly alleviated disc degeneration, as evidenced by regularly arranged cartilage cells and fibrous annulus in the nucleus pulposus (Figure 5(c)).

We proposed a scoring system for the quantitative assessment of disc degeneration (Table 2). No significant

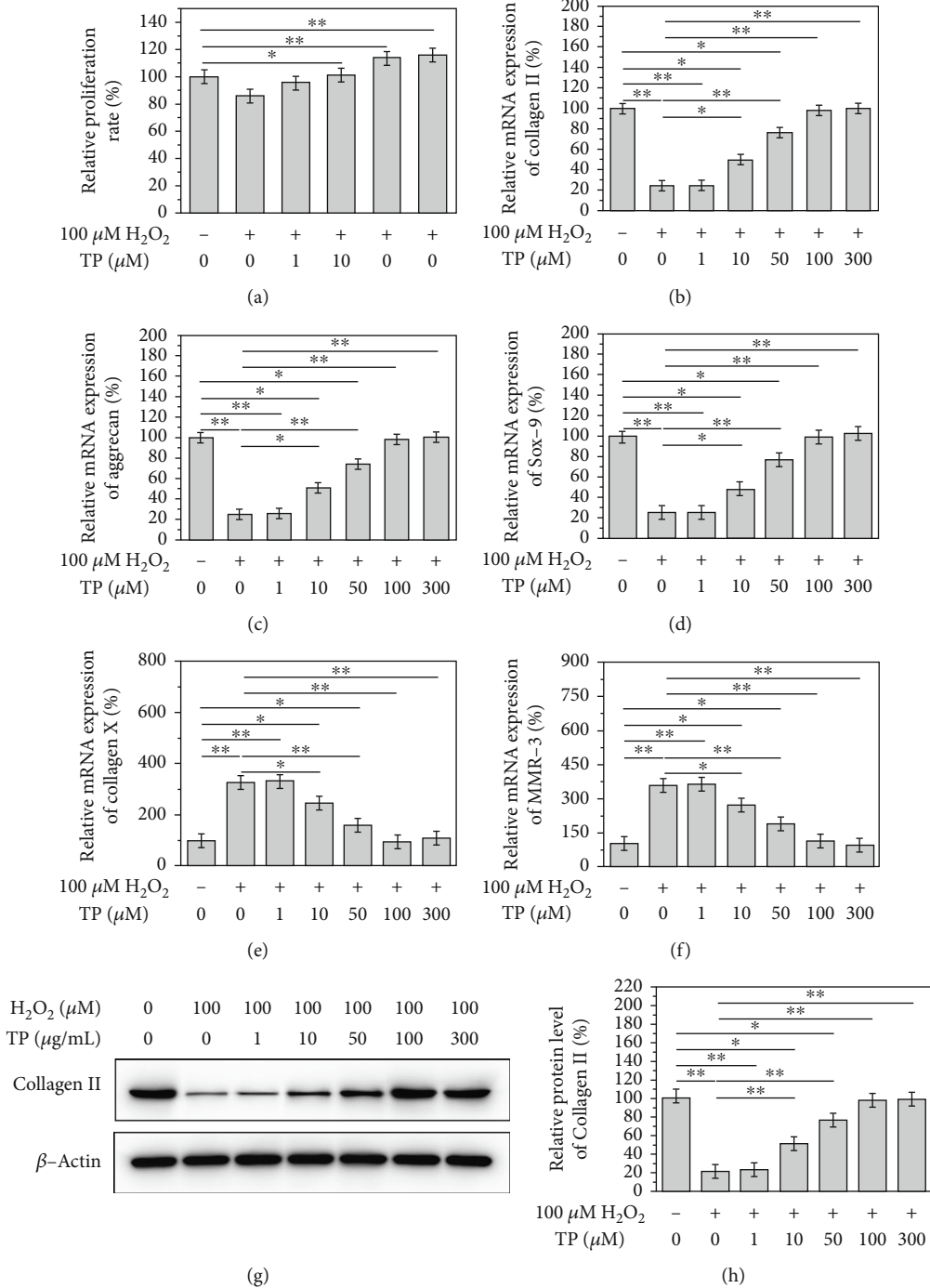


FIGURE 3: TP alleviated the degeneration of nucleus pulposus cells caused by H₂O₂ in a dose-dependent manner. After the treatment of TP, (a) the proliferation rate of cells came back to normal. The relative mRNA expression of (b) collagen II, (c) aggrecan, and (d) Sox-9 increased significantly, while that of (e) collagen X and (f) MMP-3 decreased significantly. (g, h) And the relative protein level of collagen II increased significantly ($P < 0.05$).

differences in the histological scores were observed between the TP+NRF2 siRNA and degeneration groups ($P > 0.05$), but significant differences were detected between the TP group and the degeneration and TP+NRF2 siRNA groups. Both radiological and histological results provided evidence that TP treatment could delay the progression of IDD (Figure 6(d)).

3.8. Immunohistochemistry. Type II collagen and aggrecan expression was positive in NPCs treated with TP (yellow), but negative in TP+NRF2 siRNA and degeneration groups (blue) (Figures 6(e) and 6(f)). The expression of type X collagen, an indicator of nucleus pulposus degeneration, was markedly different in the three groups. These findings suggest that TP treatment alleviated the degeneration of NPCs

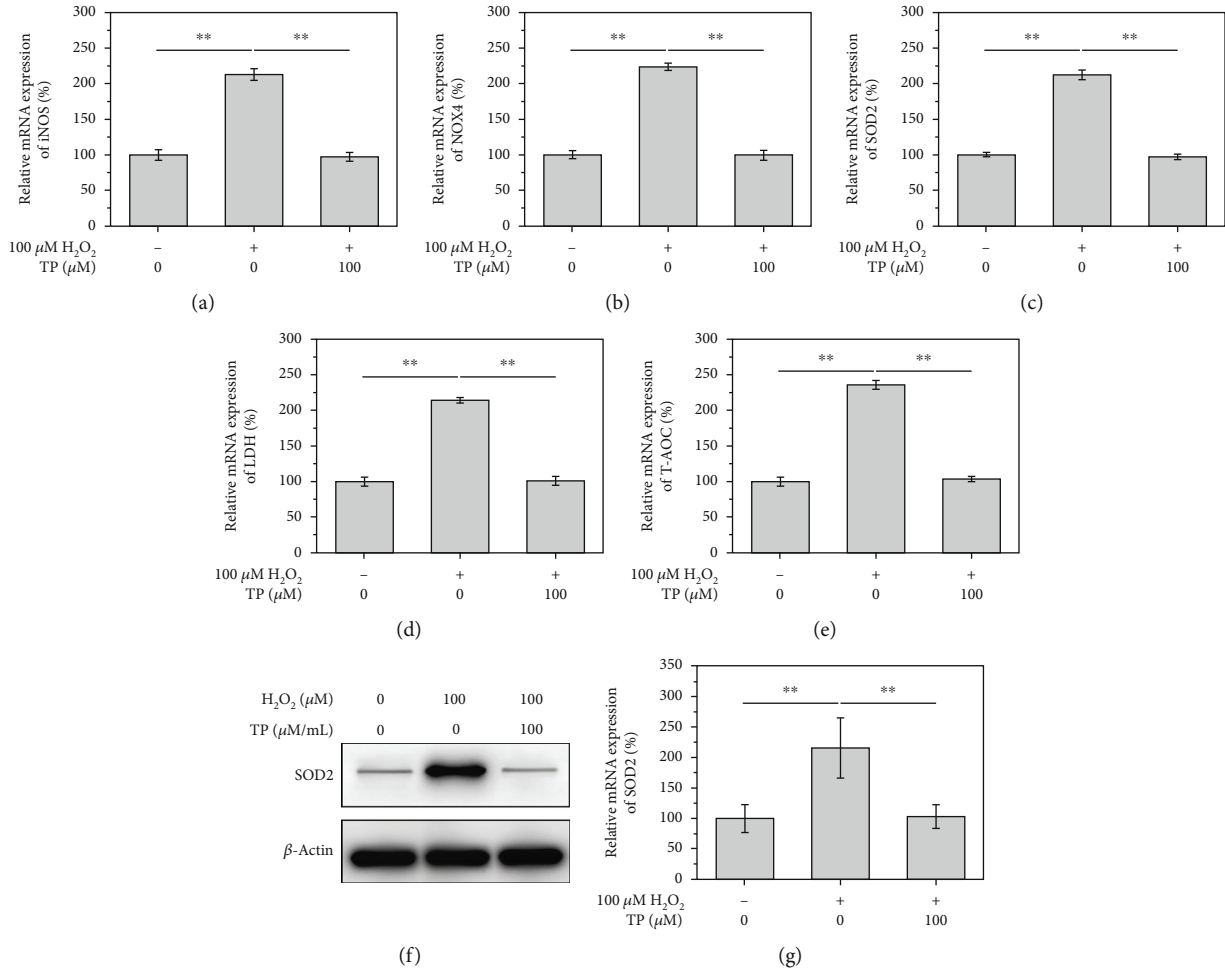


FIGURE 4: TP alleviated the oxidative stress in nucleus pulposus cells caused by H₂O₂. (a–e) The relative mRNA of iNOS, NOX4, SOD2, LDH, and T-AOC came back to normal after the treatment of both H₂O₂ and TP. (f, g) The relative protein level of SOD2 came back to normal after the treatment of both H₂O₂ and TP.

compared to the saline degeneration and TP+NRF2 siRNA groups (Figure 6(g)).

SOD2, an indicator of oxidative stress, was strongly detected in the nucleus pulposus tissue in the degeneration and TP+NRF2 siRNA groups (yellow or brown), indicating an intense oxidative stress. However, staining of SOD2 was weaker in the TP group, suggesting that TP treatment suppressed oxidative stress in rats through the Keap1/Nrf2/ARE pathway, thereby delaying the degeneration of NPCs (Figure 6(h)).

4. Discussion

In the present study, we established an *in vitro* model for oxidative stress analysis in NPCs. Many studies have suggested that H₂O₂ could induce oxidative stress injury, inflammatory response, apoptosis, matrix reduction, and, finally, degeneration of NPCs [16–18]. Consistently, our study identified the degenerative role of H₂O₂ and established an *in vitro* model for oxidative stress analysis in NPCs. Data from the CCK-8 assay showed that H₂O₂ 100 μM had no obvious effects on cell viability, whereas higher doses could suppress it. Thus, H₂O₂ at 100 μM was chosen for further study. We found that

H₂O₂ decreased the mRNA levels of type II collagen, aggrecan, and SOX-9 and increased type X collagen and MMP3. Moreover, H₂O₂ at 100 μM dramatically suppressed the protein expression of type II collagen.

Type II collagen, an important component of the extracellular matrix of the nucleus pulposus, is mainly expressed in cartilage and cartilage-derived NPCs. Studies have shown that type II collagen is essential for the removal of the spinal cord and the formation of intervertebral discs [19]. Aggrecan, another important component of the extracellular matrix, has unique water-retaining and microstructural properties and serves a vital role in the intervertebral disc response to various loads [20]. The degradation and decreased synthesis of aggrecan could lead to a reduction in intervertebral disc function. SOX-9 is also a protective factor for intervertebral discs, which has the effect of regulating the expression of type II collagen [21]. When the intervertebral disc degenerates, the content of proteoglycan and type II collagen in the extracellular matrix decreases, with decreased water retention capacity and stress load capacity. The abovementioned three factors are all cartilage-specific genes. The reduction of type II collagen, aggrecan, and SOX-9 in NPCs is usually related to a severe disc degeneration [22]. Type X collagen indicates

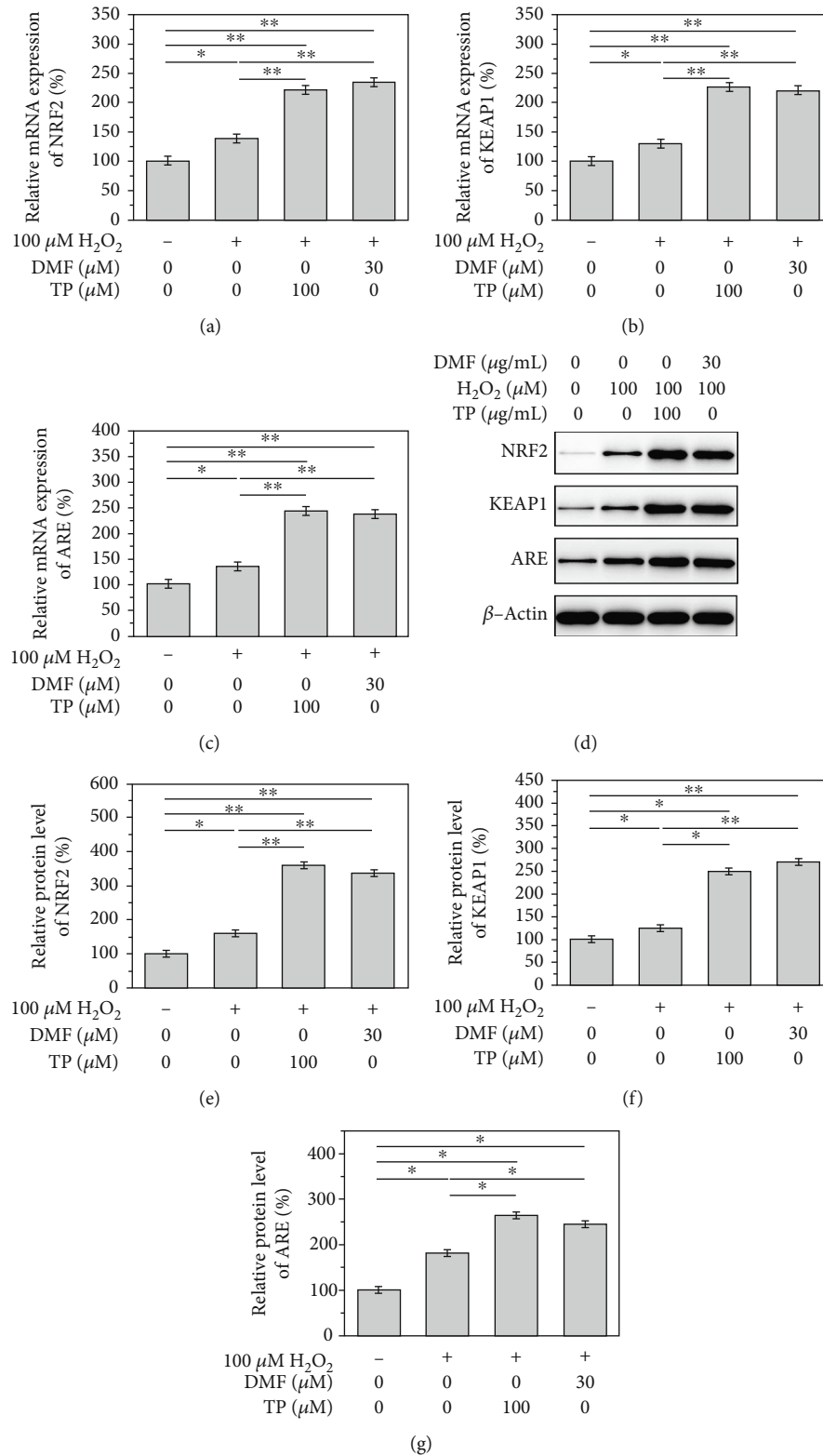


FIGURE 5: TP exerts its function via the Nrf2/KEAP1/ARE pathway. After the TP treatment, the relative mRNA expression of (a) Nrf2, (b) KEAP1, and (c) ARE significantly increased, (d–g) so does the protein level of Nrf2, KEAP1, and ARE ($P < 0.05$).

IDD, and it is a short-chain nonfibrous gel with a network structure. In adult intervertebral discs, type X collagen is highly expressed in the extracellular matrix of the intervertebral disc during the advanced stage of IDD [23, 24]. Type X

collagen cross-links with type II collagen fibers, affecting the structure of the intervertebral disc and reducing its load strength. As a substance that destroys articular cartilage and intervertebral disc matrix, MMP3 is involved in disc

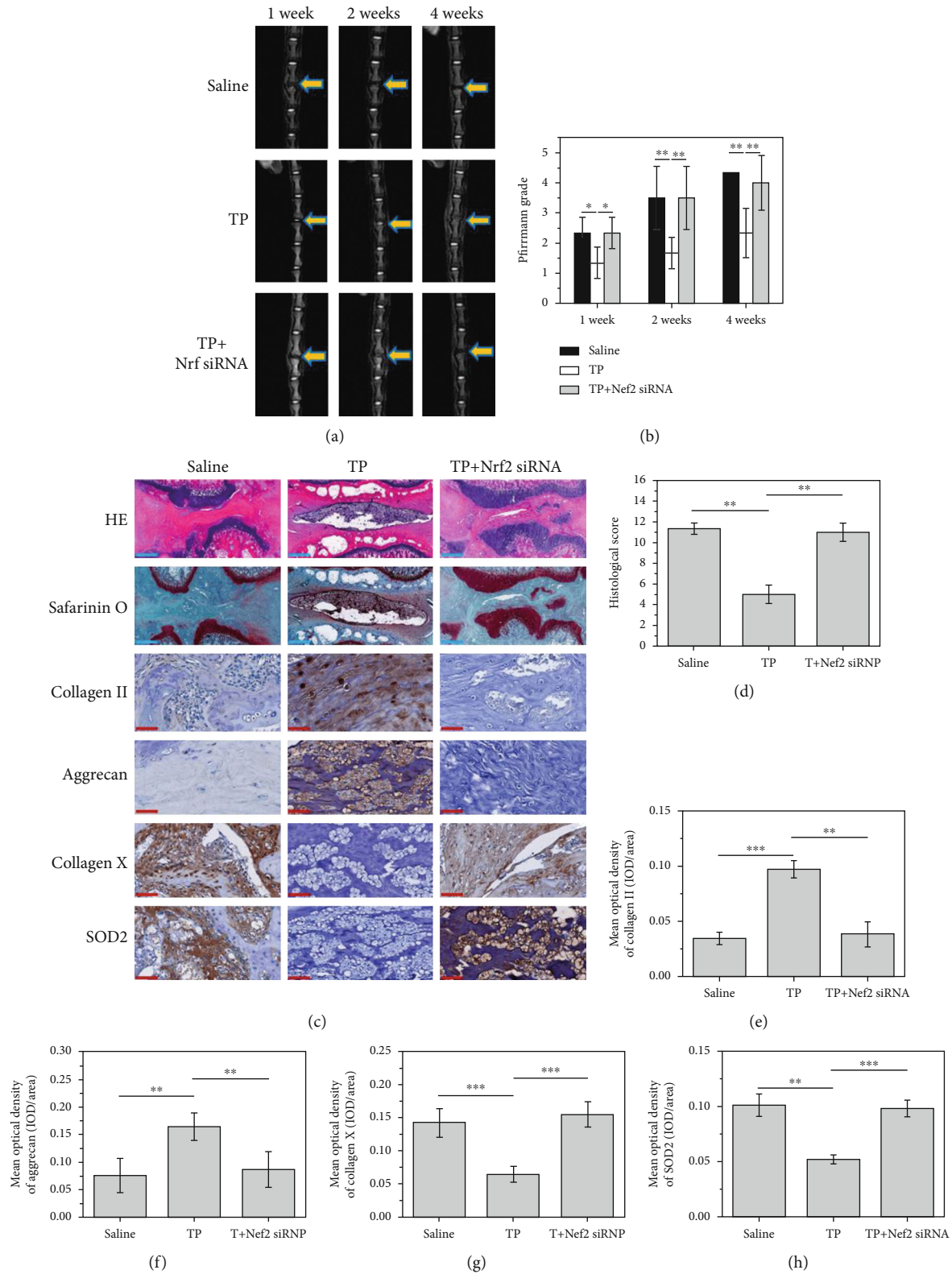


FIGURE 6: TP delays the intervertebral disc degeneration in vivo via the Nrf2/KEAP/ARE pathway. (a) MRI test of rat caudal discs reveals the protective role of TP in intervertebral disc degeneration. (b) Pfirrmann grade showed the significant protective role of TP. (c) Histological analysis of caudal discs. (d) Histological grading test. (e-h) Mean optical density of collagen II, aggrecan, collagen X, and SOD2 ($P < 0.05$). Blue scale bar = 500 μm ; red scale bar = 50 μm .

degeneration, especially during the matrix degradation stage [25]. Therefore, type X collagen and MMP3 are highly expressed in degenerated NPCs. These results showed that 100 μ M H₂O₂ inhibited the expression of type II collagen, aggrecan, and SOX-9; increased type X collagen and MMP3; and accelerated the protein degradation of type II collagen, eventually causing degeneration of NPCs of intervertebral discs.

In the present study, we found that TP effectively reversed H₂O₂-induced downregulation of cartilage-specific genes. In addition, TP significantly reduced type X collagen and MMP3, indicators of IDD, which suggests that TP exhibits a protective role in NPCs. Western blotting results indicated that TP effectively increased the protein expression of type 2 collagen, whereas immunofluorescence staining showed that TP effectively reduced the expression of MMP3. This may be because of the fact that TP could increase the expression of type 2 collagen and suppress MMP3, thereby improving the microenvironment of NPCs and reducing type 2 collagen degradation. The protective effect of TP is concentration- and time-dependent at a certain concentration; that is, the protective effect of TP is more obvious at a larger dose in a longer intervention period. Furthermore, we explored the molecular mechanism by which TP protects degenerated NPCs. Previous studies have suggested that the prevention of DNA damage is associated with the anticancer role of tea and TP [12]. A recent study showed that TP attenuates oxidative stress induced by H₂O₂ and continuous darkness by regulating the Keap1/Nrf2 signaling pathway in HepG2 cells and mouse liver [26].

The Keap1/Nrf2/ARE pathway is critical for the defense against oxidative stress. Nrf2, a Cap'N'Collar family member, is widely expressed in human tissues and organs [27]. With a leucine zipper structure, Nrf2 activates ARE and initiates a variety of antioxidant reactions, thereby regulating the body's defense system against oxidative stress. Kelch-like ECH associating protein1 (Keap1) is the receptor of Nrf2 and affects its expression. Under physiological conditions, Nrf2 is located in the cytoplasm and binds to Keap1 in a resting state [28]. The Nrf2-Keap1 complex is rapidly degraded through the ubiquitin proteasome pathway. Upon oxidative stress stimulation, Nrf2 quickly disassociates from Keap1, translocates into the nucleus, binds to small Maf proteins to form heterodimers, and interacts with ARE in the target genes, thereby regulating the transcription and translation of antioxidant genes [29].

The activation of Nrf2 is regulated at multiple levels, mainly involving the interaction between Nrf2 and Keap1 as well as the mechanism mediating the stability of Nrf2. There are two mechanisms for the dissociation of Nrf2 from Keap1: the direct attack of nucleophiles or ROS and the indirect effect of phosphorylated Keap1.

In our study, there is evidence that H₂O₂-treated NPCs were attacked by ROS, leading to the disassociation of Nrf2 from Keap1. Elevated expression of Nrf2 increased the expression of ARE elements. TP exhibited a protective role in NPCs, increasing the expression of Nrf2 and downstream targets. These findings imply that TP may activate the Keap1/Nrf2/ARE pathway and protect NPCs against oxidative stress injury.

To test our hypothesis, we used DMF, the activator of the Keap1/Nrf2/ARE pathway, and observed that it exhibited a similar effect to that of TP. In addition, combined treatment with TP and DMF further increased the expression of Nrf2 and ARE. Collectively, these results suggest that TP activates the Keap1/Nrf2/ARE pathway to protect NPCs against H₂O₂.

The *in vivo* experiments also confirmed our hypothesis. The discs of rats were injected with TP (100 nM), TP+Nrf2 siRNA, and normal saline. Rats injected with normal saline exhibited obvious degenerated dark discs and low signal intensity. The likely causes are puncture-induced stress imbalance, oxidative stress injury, loss of proteoglycan, and type II collagen. In the normal saline group, the cartilage-like cells in the nucleus pulposus disappeared and the fibrous annulus was damaged. Treatment with TP at 100 nM greatly improved the degeneration of intervertebral discs in the first two weeks. Compared with the normal saline group, the T2-weighted image showed high signal intensity, indicating that the core components of the intervertebral discs were not destroyed. At week 4, the intervertebral disc signal of the rat also began to decrease, and the height of the intervertebral space narrowed, suggesting the degeneration of the nucleus pulposus. Histological analysis data, consistent with radiological results, suggested that the degeneration of intervertebral discs was alleviated in the TP group compared to that in the normal control *in vivo*. The addition of TP and Nrf2 siRNA produced similar effects on disc degeneration to the normal saline group, which was slower than in the control but faster than in the TP group. Immunohistochemical staining showed that TP significantly reduced the expression of oxidative stress factors in the tissues, whereas Nrf2 siRNA cotreatment and the degeneration groups showed a higher expression of SOD2. In summary, *in vivo* experiments showed that TP activated the Keap1/Nrf2/ARE pathway to exert its antioxidative stress function and ultimately delay the degeneration of intervertebral discs.

There were some limitations to this study. First, the long-term efficacy and safety of TP should be evaluated in the future. Second, this study mainly focused on the role of TP in signal transduction. The specific effect of TP on Nrf2 protein and the other key proteins in the pathway has not been determined. Besides, mitochondrial dysfunction is an important mechanism of oxidative stress damage in NPCs and should be further explored.

In summary, we have demonstrated that TP, a plant-derived natural antioxidant agent, plays an important role in activating the Keap1/Nrf2/ARE pathway and delaying disc degeneration. TP effectively increases the expression of NRF2 and its downstream targets, thereby inhibiting the degeneration of intervertebral discs. These findings reveal the protective function of TP via the Keap1/Nrf2/ARE pathway in intervertebral disc degeneration and deepen our understanding of IDD treatment and prevention.

Data Availability

The datasets generated during and/or analyzed during the current study are available from the corresponding author on reasonable request.

Conflicts of Interest

The authors declare that they have no competing interests.

Authors' Contributions

Dawei Song and Jun Ge contributed equally to the work.

Acknowledgments

This study was supported by the National Natural Science Foundation of China (81472132, 81572183, 81672220, and 91849114).

References

- [1] K. Wang, W. Liu, Y. Song et al., "The role of angiotensin-2 in nucleus pulposus cells during human intervertebral disc degeneration," *Laboratory Investigation*, vol. 97, no. 8, pp. 971–982, 2017.
- [2] J. W. Frymoyer and W. L. Cats-Baril, "An overview of the incidences and costs of low back pain," *Orthopedic Clinics of North America*, vol. 22, no. 2, pp. 263–271, 1991.
- [3] Y. Han, X. Li, M. Yan et al., "Oxidative damage induces apoptosis and promotes calcification in disc cartilage endplate cell through ROS/MAPK/NF- κ B pathway: Implications for disc degeneration," *Biochemical and Biophysical Research Communications*, vol. 516, no. 3, pp. 1026–1032, 2019.
- [4] H. Che, J. Li, Y. Li et al., "p16 deficiency attenuates intervertebral disc degeneration by adjusting oxidative stress and nucleus pulposus cell cycle," *eLife*, vol. 9, no. 3, 2020.
- [5] J. Wang, M. Nisar, C. Huang et al., "Small molecule natural compound agonist of SIRT3 as a therapeutic target for the treatment of intervertebral disc degeneration," *Experimental & Molecular Medicine*, vol. 50, no. 11, pp. 1–14, 2018.
- [6] L. A. Nasto, A. R. Robinson, K. Ngo et al., "Mitochondrial-derived reactive oxygen species (ROS) play a causal role in aging-related intervertebral disc degeneration," *Journal of Orthopaedic Research*, vol. 31, no. 7, pp. 1150–1157, 2013.
- [7] I. Peluso, G. Morabito, L. Urban, F. Ioannone, and M. Serafi, "Oxidative Stress in Atherosclerosis Development: The Central Role of LDL and Oxidative Burst," *Endocrine, Metabolic & Immune Disorders-Drug Targets*, vol. 12, no. 4, pp. 351–360, 2012.
- [8] C. Feng, M. Yang, M. Lan et al., "ROS: Crucial Intermediators in the Pathogenesis of Intervertebral Disc Degeneration," *Oxidative Medicine and Cellular Longevity*, vol. 2017, Article ID 5601593, 12 pages, 2017.
- [9] S. Suzuki, N. Fujita, N. Hosogane et al., "Excessive reactive oxygen species are therapeutic targets for intervertebral disc degeneration," *Arthritis Research & Therapy*, vol. 17, no. 1, 2015.
- [10] X. Yang, L. Jin, L. Yao, F. H. Shen, A. Shimer, and X. Li, "Antioxidative nanofullerol prevents intervertebral disk degeneration," *International Journal of Nanomedicine*, vol. 9, p. 2419, 2014.
- [11] K. Wang, S. Hu, B. Wang, J. Wang, X. Wang, and C. Xu, "Genistein protects intervertebral discs from degeneration via Nrf2-mediated antioxidant defense system: An in vitro and in vivo study," *Journal of Cellular Physiology*, vol. 234, no. 9, pp. 16348–16356, 2019.
- [12] C. S. Yang, J. D. Lambert, and S. Sang, "Antioxidative and anti-carcinogenic activities of tea polyphenols," *Archives of Toxicology*, vol. 83, no. 1, pp. 11–21, 2009.
- [13] T. Yokozawa, J. S. Noh, and C. H. Park, "Green Tea Polyphenols for the Protection against Renal Damage Caused by Oxidative Stress," *Evidence-Based Complementary and Alternative Medicine*, vol. 2012, Article ID 845917, 12 pages, 2012.
- [14] Y. A. S. U. T. A. K. A. BABA, J. U. N.-I. C. H. I. R. O. SONODA, S. A. D. A. O. HAYASHI et al., "Reduction of oxidative stress in liver cancer patients by oral green tea polyphenol tablets during hepatic arterial infusion chemotherapy," *Experimental Therapeutic Medicine*, vol. 4, no. 3, pp. 452–458, 2012.
- [15] Y. Xu, J.-j. Zhang, L. Xiong, L. Zhang, D. Sun, and H. Liu, "Green tea polyphenols inhibit cognitive impairment induced by chronic cerebral hypoperfusion via modulating oxidative stress," *The Journal of Nutritional Biochemistry*, vol. 21, no. 8, pp. 741–748, 2010.
- [16] X. Deng, S. Chen, D. Zheng, Z. Shao, H. Liang, and H. Hu, "Icariin Prevents H₂O₂-Induced Apoptosis via the PI3K/Akt Pathway in Rat Nucleus Pulposus Intervertebral Disc Cells," *Evidence-Based Complementary and Alternative Medicine*, vol. 2017, Article ID 2694261, 10 pages, 2017.
- [17] L. Yang, Z. Rong, M. Zeng et al., "Pyrroloquinoline quinone protects nucleus pulposus cells from hydrogen peroxide-induced apoptosis by inhibiting the mitochondria-mediated pathway," *European Spine Journal*, vol. 24, no. 8, pp. 1702–1710, 2015.
- [18] Y.-H. Cheng, S.-H. Yang, K.-C. Yang, M.-P. Chen, and F.-H. Lin, "The effects of ferulic acid on nucleus pulposus cells under hydrogen peroxide-induced oxidative stress," *Process Biochemistry*, vol. 46, no. 8, pp. 1670–1677, 2011.
- [19] A. Aszodi, D. Chan, E. Hunziker, J. F. Bateman, and R. Fässler, "Collagen II Is Essential for the Removal of the Notochord and the Formation of Intervertebral Discs," *Journal of Cell Biology*, vol. 143, no. 5, pp. 1399–1412, 1998.
- [20] T. Hassan, O. U. Çolak, and P. M. Clayton, "Uniaxial Strain and Stress-Controlled Cyclic Responses of Ultrahigh Molecular Weight Polyethylene: experiments and Model simulations," *Journal of Engineering Materials and Technology*, vol. 133, no. 2, 2011.
- [21] R. Paul, R. C. Haydon, H. Cheng et al., "Potential use of Sox9 gene therapy for intervertebral degenerative disc disease," *Spine*, vol. 28, no. 8, pp. 755–763, 2003.
- [22] I. Takahashi, G. H. Nuckolls, K. Takahashi et al., "Compressive force promotes sox9, type II collagen and aggrecan and inhibits IL-1 β expression resulting in chondrogenesis in mouse embryonic limb bud mesenchymal cells," *Journal of Cell Science*, vol. 111 (Part 14), pp. 2067–2076, 1998.
- [23] N. Boos, A. G. Nerlich, I. Wiest, K. von der Mark, and M. Aebi, "Immunolocalization of type X collagen in human lumbar intervertebral discs during ageing and degeneration," *Histochemistry Cell Biology*, vol. 108, no. 6, pp. 471–480, 1997.
- [24] T. Aigner, K.-R. Greskötter, J. C. T. Fairbank, K. von der Mark, and J. P. G. Urban, "Variation with Age in the Pattern of Type X Collagen Expression in Normal and Scoliotic Human Intervertebral Discs," *Calcified Tissue International*, vol. 63, no. 3, pp. 263–268, 1998.
- [25] O. Nemoto, M. Yamagishi, H. Yamada, T. Kikuchi, and H. Takaiishi, "Matrix Metalloproteinase-3 Production by Human Degenerated Intervertebral Disc," *Journal of SPINAL DISORDERS*, vol. 10, no. 6, p. 498, 1997.

- [26] G. Qi, Y. Mi, R. Fan et al., "Tea polyphenols ameliorate hydrogen peroxide- and constant darkness-triggered oxidative stress via modulating the Keap1/Nrf2 transcriptional signaling pathway in HepG2 cells and mice liver," *RSC Advances*, vol. 7, no. 51, pp. 32198–32208, 2017.
- [27] H.-Y. Cho, S. P. Reddy, and S. R. Kleeberger, "Nrf2 Defends the Lung from Oxidative Stress," *Antioxidants & Redox Signaling*, vol. 8, no. 1-2, pp. 76–87, 2006.
- [28] M.-I. Kang, A. Kobayashi, N. Wakabayashi, S.-G. Kim, and M. Yamamoto, "Scaffolding of Keap1 to the actin cytoskeleton controls the function of Nrf2 as key regulator of cytoprotective phase 2 genes," *Proceedings of the National Academy of Sciences*, vol. 101, no. 7, pp. 2046–2051, 2004.
- [29] S. Magesh, Y. Chen, and L. Hu, "Small molecule modulators of Keap1-Nrf2-ARE pathway as potential preventive and therapeutic agents," *Medicinal Research Reviews*, vol. 32, no. 4, pp. 687–726, 2012.

Research Article

Danshen Attenuates Intervertebral Disc Degeneration via Antioxidation in SD Rats

Rongqing Qin ^{1,2}, Shouqian Dai ³, Xing Zhang ^{1,2}, Hongpeng Liu,^{1,2} Bing Zhou,^{1,2} Pin Zhou,⁴ and Chuanliang Hu^{1,2}

¹Department of Spinal Surgery, Gaoyou Hospital Affiliated Soochow University, Gaoyou, Jiangsu 225600, China

²Department of Orthopedics, Gaoyou People's Hospital, Gaoyou, Jiangsu 225600, China

³Orthopedic Institute, Department of Orthopedics, The First Affiliated Hospital of Soochow University, Suzhou, Jiangsu 215007, China

⁴Department of Orthopedics, Gaoyou Hospital of Integrated Traditional Chinese and Western Medicine, Gaoyou, Jiangsu 225600, China

Correspondence should be addressed to Xing Zhang; bshzx1978@163.com

Received 31 October 2020; Revised 7 December 2020; Accepted 9 December 2020; Published 23 December 2020

Academic Editor: Sidong Yang

Copyright © 2020 Rongqing Qin et al. This is an open access article distributed under the Creative Commons Attribution License, which permits unrestricted use, distribution, and reproduction in any medium, provided the original work is properly cited.

Objective. To investigate the effects of Danshen on the imaging and histological parameters, expression levels of ECM-associated proteins and inflammatory factors, and antioxidative activity in the degenerated intervertebral disc (IVD) of SD rats. **Methods.** Sixty male rats were randomly divided into three groups (control, IDD, and Danshen IDD). Percutaneous needle puncture in Co8-9 intervertebral disc was conducted in all rats of the IDD and Danshen IDD groups to induce intervertebral disc degeneration (IDD). After operation, animals of the Danshen IDD group were administrated with Danshen granules (3 g/kg body weight) by gavage once a day. Four weeks later, the coccygeal vertebrae were harvested and used for imaging (disc height and MR signal), histological, immunohistochemical, and biochemical [water content, glycosaminoglycans (GAG), superoxide dismutase (SOD2), glutathione (GSH), and malondialdehyde (MDA)] analyses. **Results.** The puncture induced significant decreased IVD space and MR T2 signal at both 2 and 4 weeks, which were attenuated by Danshen treatment. The disc degeneration in the IDD group (HE and Safranin O-Fast Green histological staining was markedly more serious compared with that in the control group. Four weeks of Danshen treatment significantly alleviated this degeneration compared with the IDD group. Needle puncture resulted in the upregulation of IL-1 β and TNF- α , MMP-3, and downregulation of COL2 and aggrecan in the IDD group. However, this change was significantly weakened by Danshen treatment. Significantly lower water and GAG content, as well as the SOD2 and GSH levels, in the IDD group were found compared with those in the control group. However, the above parameters of the Danshen IDD group were significantly higher than those of the IDD group. Danshen treatment significantly decreased the content of MDA which was increased by needle puncture in the IDD group. **Conclusion.** Danshen can attenuate intervertebral disc degeneration in SD rats by suppressing the oxidation reaction.

1. Introduction

With the aging of society, low back pain has become a common disease that plagues the physical and mental health of middle-aged and elderly people [1]. Intervertebral disc degeneration (IDD) is believed to be one of the main causes of low back pain and its etiology is complex and multifactorial, including aging, mechanical stress, smoking, infection, trauma, and genetics [2]. Intervertebral disc (IVD) primarily

contains three parts: nucleus pulposus (NP), annulus fibrosus (AF), and cartilage endplate (EP). Structural or functional abnormalities of any component can finally result in IDD. The degenerated IVD shows a reduction in intervertebral height, the appearance of annulus fissures, the dysfunction of NPCs, the loss of ECM and water, and the calcification of the vertebral endplates, as well as increased production of inflammatory factors such as interleukin-1 β (IL-1 β) and tumor necrosis factor- α (TNF- α) [3]. At present, the specific

mechanism of IDD is still not clear. However, increasing evidences demonstrate that oxidative stress might play a crucial role in the occurrence and development of IDD [4–6].

According to the free radical theory of aging, the decline of tissue and organ function is closely related to the oxidative stress caused by reactive oxide species (ROS) [7]. Excessive ROS can inhibit normal cellular activity by destroying cell lipid, protein, and DNA content [8]. It has been reported that malondialdehyde (MDA) and the peroxidation product of polyunsaturated fatty acid residues accumulate in degenerated IVDs of rats [9]. In short, in the process of IDD, systemic and local oxidative stress increases significantly, indicating that oxidative stress may play a crucial role in the pathological development of IDD. MDA, SOD2, and glutathione (GSH) are indicators commonly used to evaluate the oxidative stress of the body, and their levels can reflect the severity of the oxidative stress damage. As the final decomposition product of cell membrane lipid peroxidation, MDA can destroy the structure and function of cell membrane, finally inducing cell senescence or death [10, 11]. SOD2 is an important antioxidant enzyme, which is widely distributed in various organisms and has the function of resisting oxidative stress. GSH is an important antioxidant, which is essential in the regulation of protein disulfide bonds and the treatment of electrophiles and oxidants. The determination of the GSH concentration is indispensable in many studies on oxidative stress [12, 13].

The common treatments of IDD contain conservative treatment and surgical treatment. Bed rest, nonsteroidal anti-inflammatory drugs, analgesia, and physical therapy are common conservative treatments, which can relieve pain to a certain extent, but cannot prevent the pathological progression of IDD. When conservative treatment fails, surgical treatment becomes the first choice. However, surgical treatment is expensive and traumatic, and some patients still have poor recovery after surgery.

Danshen (*Salvia miltiorrhiza*), a traditional Chinese medicine, can promote blood circulation and remove blood stasis. Danshen has a wide range of pharmacological effects and is primarily used clinically for the treatment of irregular menstruation, palpitations, insomnia, and various cardiovascular diseases, especially angina pectoris and myocardial infarction [14]. In recent years, a number of researches have confirmed the effects of Danshen on improving microcirculation, anticoagulant, antithrombotic, antihypertensive, and antioxidant [15], which has broad application prospects. Although the specific antioxidant mechanism is unknown, Danshen has been proved to act as a ROS inhibitor [16, 17]. Zhang et al. [18] found that Danshen has a significant protective effect on H₂O₂-induced H9c2 cardiomyocyte apoptosis at low concentrations. Comparative studies with vitamin C show that Danshen can scavenge more than 90% of free radicals and can be used to prevent cell damage caused by free radicals and intracellular ROS [19]. To sum up, Danshen has been proved to be functional in different cell types via the antioxidation process as an adjuvant treatment and the use of Danshen to potentially alleviate disorders has been investigated.

However, whether Danshen can inhibit the development of IDD via antioxidation remains unknown. Therefore, we hypothesized that Danshen can alleviate intervertebral disc degeneration through its antioxidant effect. This study is aimed at exploring the effects of Danshen on the imaging and histological parameters, water and GAG content, expression levels of ECM-associated proteins, and inflammatory factors, as well as SOD2, GSH, and MDA level of degenerated IVDs in a percutaneous puncture SD model.

2. Methods and Materials

2.1. Animals. Sixty 12-week-old Sprague Dawley rats (30 males and 30 females) were used. All animal experiments were approved by the Animal Care and Experiment Committee of Soochow University. All rats were group housed under a 12 h light/dark cycle and had free access to a standard diet and sterile water.

2.2. IDD Model and Experimental Design. All 60 animals were randomly divided into three groups (control, IDD, and Danshen IDD group), with 20 animals in each group. After one week of acclimatization, all rats were anesthetized by inhalation of 2% fluothane in oxygen/nitrous oxide. The needle puncture model was performed in the Co8-9 IVD of all rats in IDD and Danshen IDD groups for inducing the IDD model as previously described [20, 21]. The Co8-9 tail IVD was punctured using a 20-gauge needle with full penetration. Penicillin was injected into the operational animals to prevent postoperative infection. All procedures were approved by our animal welfare committee. Danshen granules were purchased from Shanghai First Biochemical Pharmaceutical Co., Ltd. (Shanghai, China). After surgery, the rats in the Danshen IDD group were administrated with a certain amount of Danshen granules (3 g/kg body weight dissolved in distilled water) by gavage once a day over a 4-week period according to the dose used in previous reports [22]. The rats in the control and IDD groups were treated with only distilled water. All steps of this study complied with the Animal Research Reporting In Vivo Experiments (ARRIVE) Guidelines for reporting animal research.

2.3. Tissue Preparation. All animals in three groups were euthanized by an excess of isoflurane (RWD Life Science Co., Shenzhen, China) four weeks after the operation. The whole discs of the punctured segments (Co8-9) in all rats were surgically removed and dissected. Ten discs from each group were fixed for 48 h in 4% paraformaldehyde (Beyotime Bio-Technology Co. Ltd., Shanghai, China) at 4°C then decalcified in 10% EDTA (Biosharp, Hefei, China) in 0.01 M PBS for 1 month at 4°C. The decalcified specimens were then embedded (Leica, Richmond, USA) in paraffin for further histological staining and immunohistochemistry. The remaining ten discs of each group were removed in liquid nitrogen after being harvested and stored at -80°C for western blot analysis and biochemical analysis. Histopathology, histological score, water and GAG content, expression levels of ECM-associated proteins and inflammatory factors, and GSH, MDA, and SOD2 concentration of the IVD were evaluated.

2.4. Radiographic Analysis and Magnetic Resonance Imaging (MRI) Examination. At two and four weeks after the needle puncture, all rats underwent X-ray radiography and MRI scans under isoflurane anesthesia. Radiographic images were taken with a digital X-ray machine (SHI- MADZU, Japan), and images were stored in a digital form. Based on the previously reported method [23], the disc height index (DHI) was calculated by averaging the measurements obtained from the anterior, middle, and posterior portions of the disc height and dividing them by the average height of the adjacent vertebral body using the image analysis program ImageJ. Changes in the DHI (representing the disc space) of IVD were presented as %DHI and normalized to DHI of preoperative IVD ($\%DHI = (DHI_{\text{postlesion}}/DHI_{\text{prelesion}}) * 100$).

T2 mapping magnetic resonance imaging (MRI) sequence is usually used to reflect the water proton molecule movements in the extracellular matrix of collagen and proteoglycan [24]. At the termination of the study, the IVDs of all rat coccygeal vertebrae were scanned in a 1.5 T MRI scanner (GE, USA). The T2 signal intensities were calculated using image analysis program ImageJ to indirectly measure the extent of disc hydration. The mean T2 signal intensity in the control IVD was set as reference for that of the punctured disc in each rat. Therefore, the normalized disc intensity was presented from 0 to 1.

2.5. Histological Evaluation. For histological analysis, 5 μm serial sections were prepared from the midsagittal region. The histological slices were stained with hematoxylin and eosin (H&E), Safranin O-Fast Green, and Alcian blue according to the standard procedures to reveal histological changes in the IVD tissues of different groups. Histological evaluation of IVD was performed based on a grading system reported by Han et al. [20]. The grading system was calculated based on the cellularity and morphology of the annulus fibrosus (AF), nucleus pulposus (NP), and the border between the AF and NP using a scale with five categories of IDD changes with scores ranging from 5 points (representing a normal disc) to 15 points (representing a severely degenerated disc) [20].

2.6. Immunohistochemical Analysis. Immunohistochemical analysis was conducted on decalcified sections of Co8-9 IVD under standard procedures [25]. ECM-associated proteins collagen II (COL2), aggrecan, and matrix metalloproteinase-3 (MMP-3) and inflammatory factors IL-1 β and TNF- α in the IVDs were semiquantitatively analyzed. The sections were incubated with rabbit primary antibodies (COL2 1:100, aggrecan 1:100, MMP-3 1:100, IL-1 β 1:200, and TNF- α 1:200; Abcam, England) or control rabbit IgG (1:100 in 5% BSA) overnight at 4°C and goat anti-rabbit secondary antibody (Cell Signaling Technology, USA, dilution 1:400). After being visualized by diaminobenzidine-based peroxidase (DAB) substrate, the images were acquired using an Olympus light microscope (Japan) at 40x magnification. Immunohistochemical staining results were further analyzed using a semi-quantitative method, as previously described [25]. Each slice was observed in ten vision fields. The number of stained positive cells and their staining intensity were used for scoring, and the two scores (range: 0–12) were multiplied to obtain

protein expression intensity. All sections were analyzed by two independent observers blinded to the experimental details. There was no significant difference within intraobserver and interobserver measurements.

2.7. Western Blot Analysis. The expression levels of COL2, aggrecan, and MMP-3 in each IVD were examined by a Western blot method. The concentration of isolated proteins was analyzed by a BCA Assay kit (Beyotime BioTechnology Co. Ltd., Shanghai, China). Equal quantities of protein from each sample were subsequently separated by gel electrophoresis and transferred onto polyvinylidene difluoride membranes. After blocking with 5% nonfat milk in Tris-buffered saline (TBS) containing 0.1% Tween-20 (TBST) for 1 h, the membrane was incubated with anti-rat primary antibodies in 5% nonfat milk diluted in TBST at 4°C overnight: COL2 (1:1000), aggrecan (1:1000), MMP-3 (1:1000), and GAPDH (1:2000). Then, the membranes were incubated with the HRP-conjugated secondary antibodies for 1 hour at 37°C. The membrane bands were detected by an enhanced chemiluminescent system, and the intensity of bands was analyzed by ImageJ software (NIH, USA). Finally, the relative optical densities of all bands were normalized to GAPDH.

2.8. Biochemical Analysis. After being removed from the liquid nitrogen, all tail discs were immediately dissected from their surrounding soft tissues carefully. Wet weight (WW) of the IVD tissue was immediately obtained after dissection. Then, the tissues were dehydrated at 60°C for one day and tissue dry weight (DW) was obtained, as described previously [20]. Thus, the water content of each disc was shown as follows: $\%H_2O = 100 * (WW - DW)/WW$. Next, the discs in each group were digested by papain (Beyotime BioTechnology Co. Ltd., Shanghai, China) in 1.5 mL of 20 mM sodium phosphate buffer at 65°C for 1 hour. The GAG concentration of IVD was measured based on the previously described method [26]. The DW protein content of each IVD was used to standardize the GAG content. The GSH content was measured using the Glutathione Assay Kit purchased from Beyotime BioTechnology Co. Ltd. according to the standard experimental procedure. The GSH concentration was assayed based on the standard curve of GSH. Lipid Peroxidation MDA Assay Kit (Beyotime BioTechnology Co. Ltd., Shanghai, China) was used to calculate the MDA content in IVDs of all animals. The sandwich ELISA method was employed to detect the SOD2 using Superoxide Dismutase Assay Kit (Beyotime BioTechnology Co. Ltd., Shanghai, China), and SOD2 levels were measured by comparing the standard curve in photometry according to the manufacturer's protocol.

2.9. Statistical Analyses. Experimental data were expressed as the means \pm standard deviation (SD). All experiments were repeated at least three times. Differences among groups were assessed using one-way ANOVA after verification of normality. Post hoc comparisons between two groups were tested using a least square difference (LSD) method. Statistical analysis was performed using SPSS v17.0 software (SPSS Inc., Chicago, IL, USA). *P* values < 0.05 were considered statistically significant.

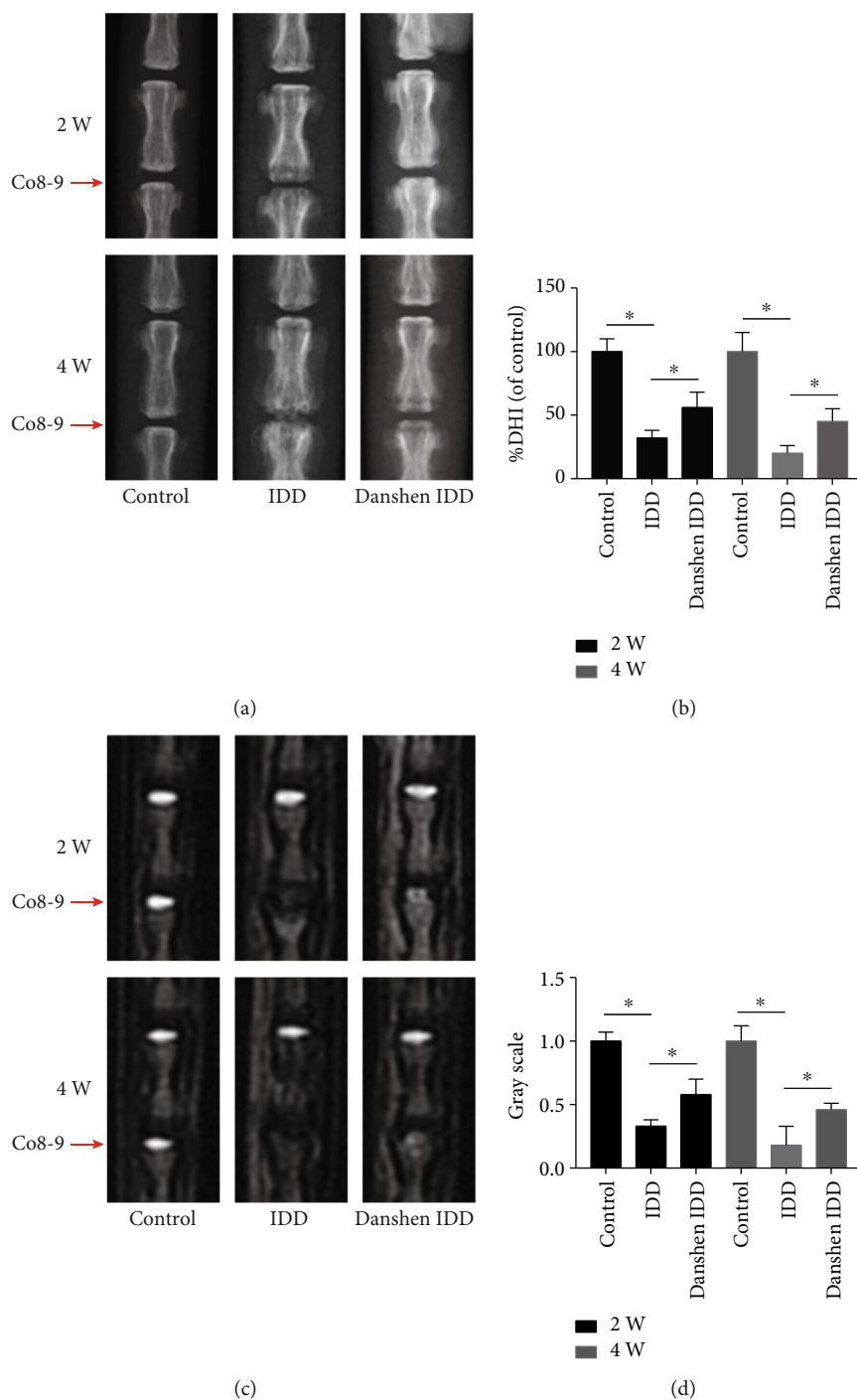


FIGURE 1: Imaging characteristics of IVDs in each group after 2 and 4 weeks. (a) Representative radiographs (X-ray) of the Co8-9 discs in the control group, IDD group, and Danshen IDD group. (b) Analysis of disc height index (DHI) based on X-ray film. A significant decrease of %DHI was observed in the IDD group. However, this reduction of disc space was significantly alleviated in the Danshen IDD group. (c) Representative images of T2-weighted MRI in Co8-9 discs. (d) Analysis of signal intensity based on MRI. Punctured discs in the IDD group showed a significant decrease of MRI signal intensity. However, the signal intensity in the Danshen IDD group was significantly higher compared to that in the IDD group. The values are expressed as the mean \pm SD. * $P < 0.05$. IDD: intervertebral disc degeneration.

3. Results

3.1. Radiographic Assessment and MRI Examination. Radiographic assessment of the IVD height was performed at the 2- and 4-week time point using the calculated DHI by averag-

ing measures before and after disc injury. Changes of IVD space at Co8-9 and the representative images of disc X-ray in the three groups are shown in Figure 1(a). At 2 weeks after puncture, the IVDs in the IDD group indicated obvious signs of disc degeneration including significantly decreased IVD

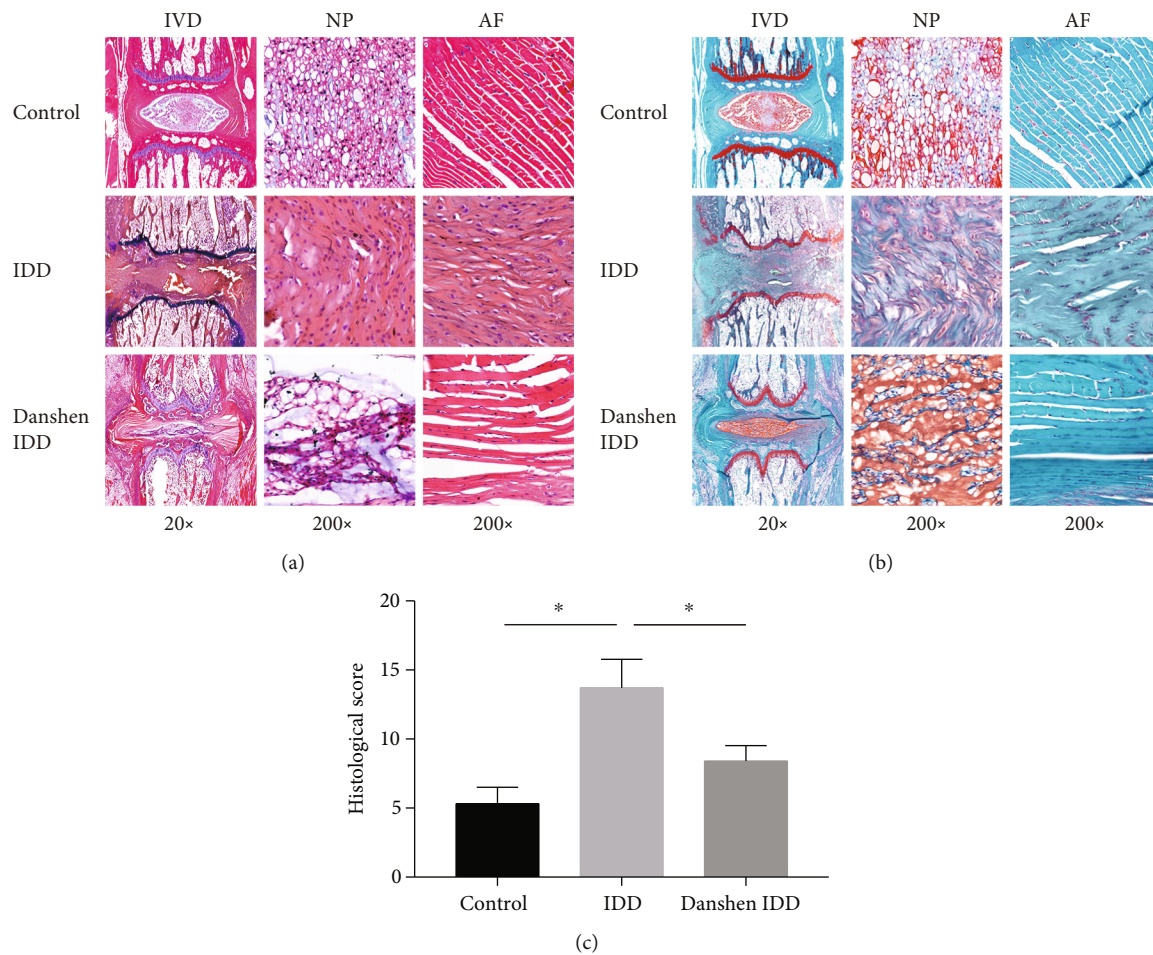


FIGURE 2: Histological analysis of IDD. (a) Representative histological appearance of IVDs stained with H&E. The control IVD presents a rounded nucleus pulposus, well-organized collagen lamellas, and a well-defined border between the annulus fibrosus (AF) and nucleus pulposus (NP). NP cells were stellar shaped and evenly distributed in the NP. In the IDD group, the size of the NP decreased and the border between the AF and NP became interrupted. The NP cells became large, rounded, clustered, and separated by dense areas of proteoglycan matrix. The annular collagen layers became disorganized with inward bulging of the inner annulus. The degenerated characteristics of rat IVD was alleviated by four weeks of Danshen treatment. (b) Representative histological appearance of IVDs stained with Safranin O-Green. (c) Analysis of the extent of IDD based on histological staining. Significantly higher histological scores were found four weeks after IDD induction. The histological score of the Danshen IDD group was significantly decreased than that of the IDD group. The values are expressed as the mean \pm SD. * $P < 0.05$. IDD: intervertebral disc degeneration; IVD: intervertebral disc; NP: nucleus pulposus; AF: annulus fibrosus.

space and tissue swelling. In the Danshen IDD group, tissue swelling and height loss of the IVD were significantly alleviated compared to those in the IDD group. This finding indicated that Danshen treatment can protect the IVD from degeneration, which was further verified by the 4-week results and the subsequent MRI examination.

The T2-weighted MR signal intensity of IVDs can indicate the degeneration of the discs. Figure 1(c) shows the representative images of tail disc in the three groups. Punctured Co8-9 IVDs in the IDD group showed a significant decrease of the T2-weighted signal in comparison with those in the control group at 2 weeks. The T2-weighted signal intensity in the Danshen IDD group was significantly higher than that of IDD group after 2-week Danshen treatment. Similar results were also found in the three groups at 4 weeks after puncture.

3.2. Histology. The HE and Safranin O-Fast Green staining results of rat tail IVD and representative histological appearance of three groups are shown in Figure 2. In the control group, tail discs contained a rounded NP, well-organized collagen lamellas, and a clear boundary between the AF and NP. Nuclear cells were stellar shaped and evenly distributed in the NP. Annular cells were mostly fibroblastic and located between well-organized collagen layers. However, in the IDD group, the discs demonstrated a typical disc degeneration features including the decreased size of the NP and the interrupted border between the NP and AF. The nuclear cells turned large and round and gathered to form clusters, sometimes separated by proteoglycan matrix. Inward bulging of the inner annulus appeared in disorganized collagen layers of AF. In the Danshen IDD group, the degenerated characteristics of

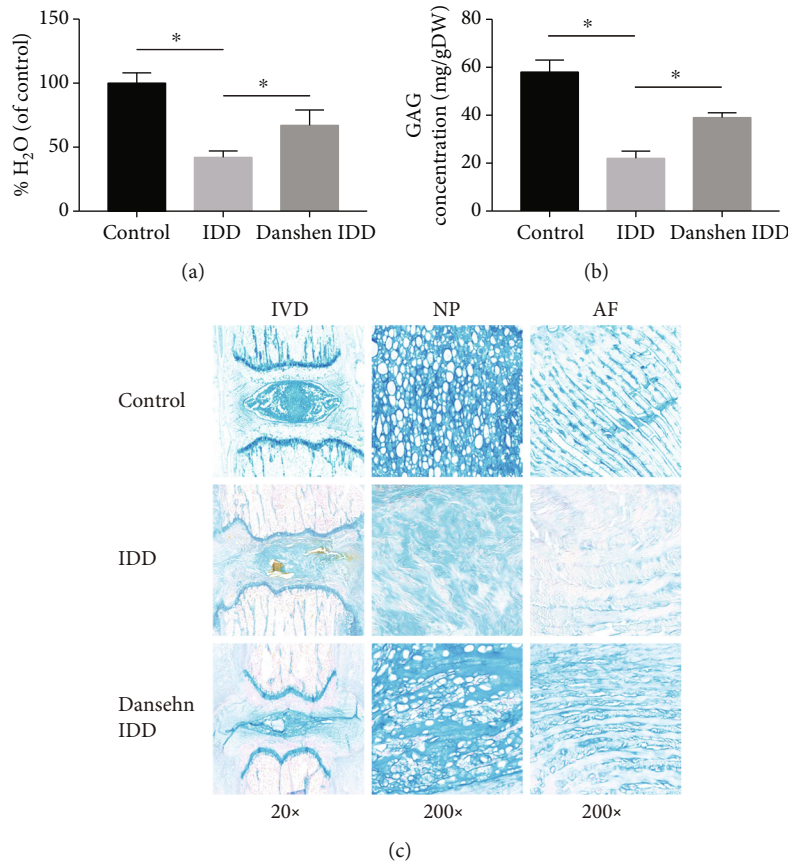


FIGURE 3: Analysis of water and GAG content of each group. (a) Water content of each group. (b) GAG content of each group. Significant decrease in water (a) and GAG (b) content in the IDD group was observed. However, this decrease was significantly alleviated by Danshen treatment in the Danshen IDD group. (c) Representative staining of Alcian blue staining of each group. The blue dye is proportional to the GAG content. The values are expressed as the mean \pm SD. * $P < 0.05$. IDD: intervertebral disc degeneration; IVD: intervertebral disc; NP: nucleus pulposus; AF: annulus fibrosus.

rat IVD were alleviated by four weeks of Danshen treatment, including the appearance of partly preserved NP and regular arrangement of AF. (Figures 2(a) and 2(b)).

The histological evaluation of IVD is shown in Figure 2(c). Histology was shown significantly different in three groups ($P < 0.001$). The scores of IVD histological staining of both the IDD and the Danshen IDD groups were significantly higher than that of the control group ($P < 0.001$). However, the histological score of the Danshen IDD group was significantly lower in comparison with that of the IDD group ($P < 0.001$). Therefore, Danshen could significantly protect the structural integrity of rat IVD and delay IDD.

3.3. Water and GAG Content of IVD. The reduction of water content in the IVD is one of the typical signs of IDD. Our data demonstrated that disc needle puncture induced a significant decrease of the water content in the IDD group (Figure 3(a)). However, the water content of IVD in the Danshen IDD group was significantly higher compared with that in the IDD group with four weeks of Danshen treatment.

The GAG content in IVD can reflect its proteoglycan content. Interestingly, a similar pattern as water content was found in the amount of GAG in all tail IVDs in the three

groups (Figure 3(b)). The GAG content of IVD in the IDD group was significantly decreased after four weeks of needle puncture. The GAG concentration in the Danshen IDD group was significantly higher than that of the IDD group with four weeks of Danshen treatment. Alcian blue is a commonly used dye for presenting GAG in tissue sections. In order to visualize the different contents of proteoglycan components of disc ECM, Alcian blue staining was performed, and the representative images are shown in Figure 3(c). The darkest blue staining was found in the IVD in the control group. Staining of the IDD group was shown to be lighter than that of the Danshen IDD group. These findings were consistent with that in quantitative analysis.

3.4. Expression Levels of COL2, Aggrecan, and MMP-3. In order to investigate the ECM remodeling of IVD, the immunohistochemical staining and western blot analysis of COL2, aggrecan, and MMP-3 were conducted. In the IDD group, the needle puncture resulted in the ECM remodeling by suppressing the production of COL2 and aggrecan and activating MMP-3, which were both shown in immunohistochemical analysis and western blot (Figures 4 and 5). After 4 weeks of Danshen treatment, the decreased expressions of

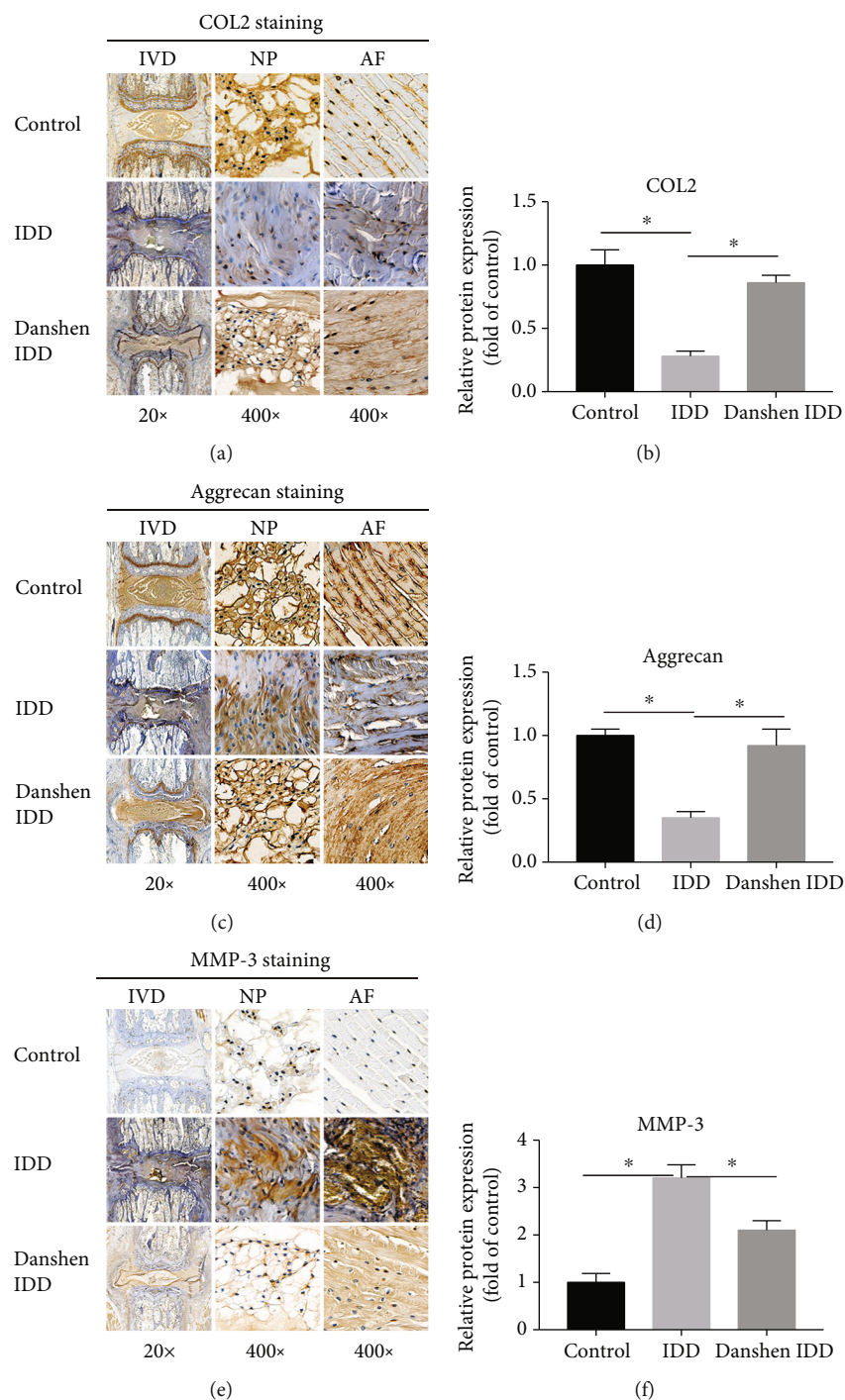


FIGURE 4: Immunohistochemical analysis of COL2, aggrecan, and MMP-3. (a) Representative images of COL2 staining. (b) Semi-quantitative analysis of COL2. (c) Representative images of aggrecan staining. (d) Semi-quantitative analysis of aggrecan. (e) Representative images of MMP-3 staining. (f) Semi-quantitative analysis of MMP-3. Significant decrease in COL2 and aggrecan levels and increase in MMP-3 level in the IDD group was observed. However, this change was significantly alleviated by Danshen treatment. The values are expressed as the mean \pm SD. * $P < 0.05$. IDD: intervertebral disc degeneration; IVD: intervertebral disc; NP: nucleus pulposus; AF: annulus fibrosus; COL2: collagen II; MMP-3: matrix metalloproteinase-3.

COL2 and aggrecan were significantly restored and the increased MMP-3 level was concomitantly weakened in the Danshen IDD group. These results indicated that Danshen can protect the IVD from degeneration by regulating the components of NP ECM.

3.5. Immunohistochemical Staining of IL-1 β and TNF- α . The expressions of inflammatory factors IL-1 β and TNF- α in the IVDs were explored and are shown in Figure 6. The light yellow-stained IL-1 β and TNF- α in the control group represented the low expression level of proteins, while

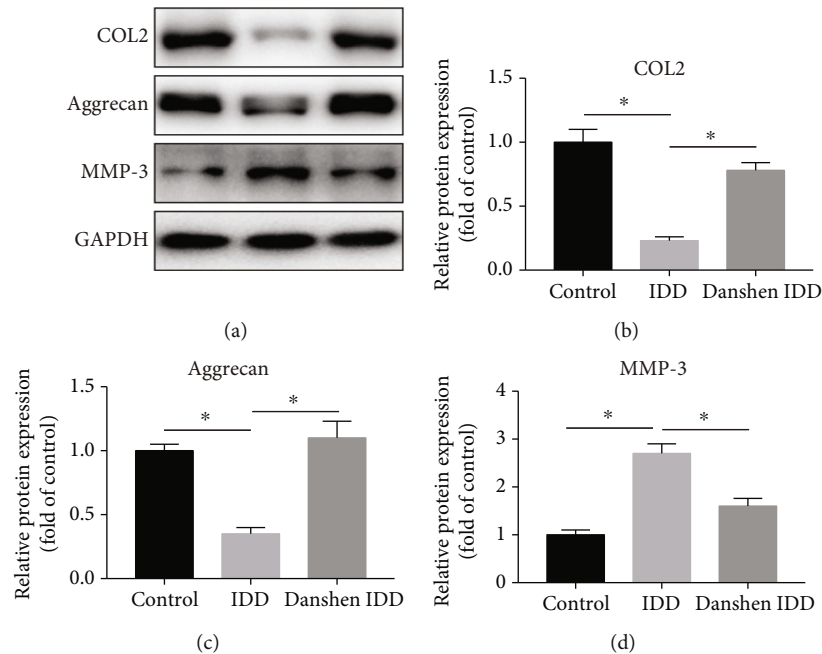


FIGURE 5: Western blot analysis of COL2, aggrecan, and MMP-3 in each group. (a) Protein expression levels of COL2, aggrecan, and MMP-3. (b) Semiquantitative analysis of COL2. (c) Semiquantitative analysis of aggrecan. (d) Semiquantitative analysis of MMP-3. The relative ratio of target proteins and GAPDH was calculated based on their gray values. Significant decrease in COL2 and aggrecan levels and increase in MMP-3 level in the IDD group were observed. However, this change was significantly alleviated by Danshen treatment. The values are expressed as the mean \pm SD. * $P < 0.05$. IDD: intervertebral disc degeneration; COL2: collagen II; MMP-3: matrix metalloproteinase-3; GAPDH: glyceraldehyde-3-phosphate dehydrogenase.

brown-stained sections in the IDD group represented the high expressions levels. It appeared that these proteins were primarily distributed within the ECM of NP. Semiquantitative analysis showed that production of IL-1 β and TNF- α in the IDD group was significantly promoted, which indicated that inflammatory response was activated during the IDD process. After Danshen treatment, the expression levels of IL-1 β and TNF- α were significantly inhibited compared to the IDD group. This data indicated that Danshen can inhibit the inflammation during the IDD process.

3.6. GSH, SOD2, and MDA Concentrations of IVD. Figure 7(a) shows that the GSH contents of IVD in the three groups were significantly different. The GSH level in IVD in the IDD group ($0.041 \pm 0.013 \mu\text{mol}/\text{mg}$ protein) was significantly lower compared to that in the control group ($0.082 \pm 0.024 \mu\text{mol}/\text{mg}$ protein, $P < 0.001$). However, the GSH concentration of IVD in the IDD Danshen group ($0.059 \pm 0.015 \mu\text{mol}/\text{mg}$ protein) was significantly higher than that of the IDD group after four weeks of Danshen medication ($P < 0.001$).

A similar pattern was also found in the SOD2 concentration of all tail IVDs in the three groups (Figure 7(b)). After four weeks of needle puncture, the SOD2 concentration of IVD in the IDD group was significantly decreased ($P < 0.001$). After four weeks of Danshen treatment, the SOD2 concentration in the Danshen IDD group ($0.064 \pm 0.011 \mu\text{mol}/\text{mg}$ protein) was markedly higher compared to that in the IDD group ($0.043 \pm 0.014 \mu\text{mol}/\text{mg}$ protein, $P < 0.001$).

MDA concentrations of tail IVD in the three groups were significantly different as shown in Figure 7(c). The MDA level in IVD in the IDD group ($0.233 \pm 0.042 \text{ nmol}/\text{mg}$ protein) was significantly higher compared to that in the control group ($0.109 \pm 0.018 \text{ nmol}/\text{mg}$ protein, $P < 0.001$). The MDA concentration of IVD in the IDD Danshen group ($0.165 \pm 0.035 \text{ nmol}/\text{mg}$ protein) was markedly decreased compared to that in the IDD group ($P < 0.001$).

4. Discussion

At present, the most popular method is IVD injury in which the damage of AF, NP, or endplate through surgical approach leads to corresponding pathological changes and causes IDD finally [27]. Needle puncture is the most common way of damage models due to its reproducibility and the short period resulting in degenerative changes [28]. The rodents are proposed as an ideal model for IDD research because of easily degenerated tail discs of puncture [20]. In our research, the IDD model was induced by needle puncture with full penetration and the characteristic changes of IDD were shown, which demonstrated that the needle puncture model was quite effective.

In our in vivo research, a relative index %DHI (representing the IVD height) and MRI T2 signal strength were used to reflect the imaging alterations of IVDs. In the IDD group, significantly narrowed IVD space and tissue swelling was found at both 2 and 4 weeks, and the MR T2 signal of IVDs was obviously decreased and almost black. However, this IVD height and signal decrease were significantly attenuated by

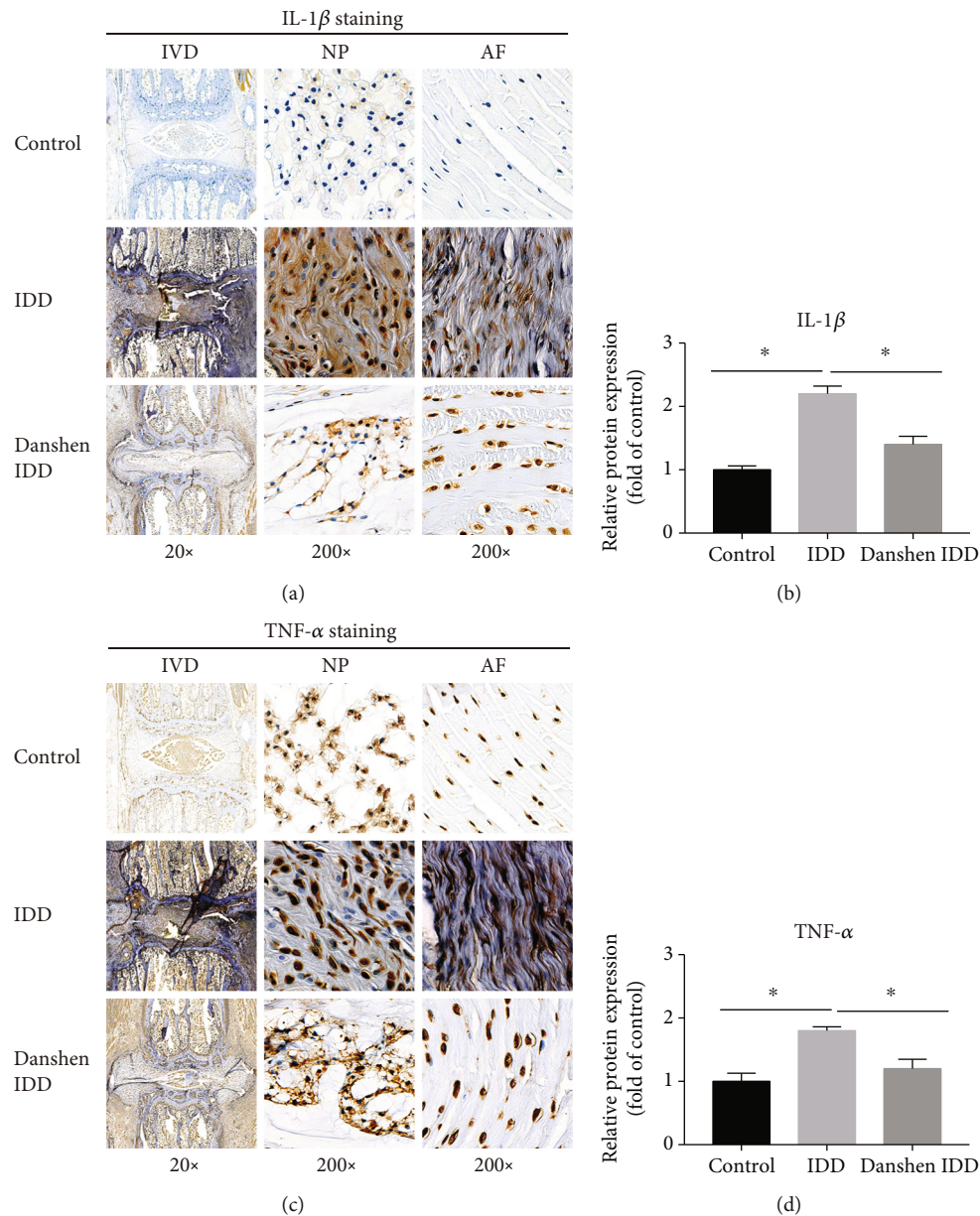


FIGURE 6: Immunohistochemical analysis of IL-1 β and TNF- α . (a) Representative images of IL-1 β staining. (b) Semiquantitative analysis of IL-1 β . (c) Representative images of TNF- α staining. (d) Semiquantitative analysis of TNF- α . Significant increase in IL-1 β and TNF- α level in the IDD group was observed. However, this increase was significantly downregulated by Danshen treatment. The values are expressed as the mean \pm SD. * P < 0.05. IDD: intervertebral disc degeneration; IVD: intervertebral disc; NP: nucleus pulposus; AF: annulus fibrosus; COL2: collagen II; MMP-3: matrix metalloproteinase-3; IL-1 β : interleukin-1 β ; TNF- α : tumor necrosis factor- α .

the Danshen treatment at both two time points. These findings indicated that Danshen could inhibit the change of disc height and MRI signal induced by disc injury, which was confirmed by the subsequent histological staining and protein expression analysis.

The HE and Safranin O-Fast Green histological staining and histological scores were used to assess the extent of tail disc degeneration in the three experimental groups. In the IDD group, needle puncture led to histological changes including the decreased NP size and the interrupted border between NP and AF, as well as nuclear cells gathering to form clusters and inward bulging of the inner annulus in disorga-

nized collagen layers of AF. These altered morphological features were consistent with many of reports in rats [20, 29, 30] and human degenerative IVDs [23, 31]. Additionally, the histological score of the Danshen IDD group was lower than that of the IDD group, which demonstrates that Danshen treatment could prevent disc degeneration in rats.

Under physiological conditions, adequate GAG is crucial for the spine to withstand pressure and can help to expand discs and keep the separation of vertebrae [32]. The changes of water and GAG content in the IVDs may affect disc functions and be directly involved in IDD. In our research, the water and GAG content in the IDD disc was markedly

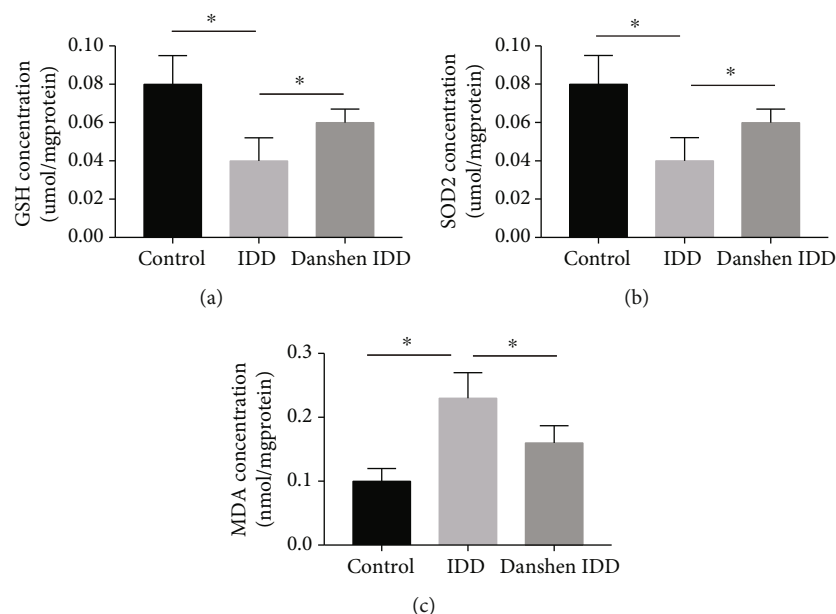


FIGURE 7: GSH, SOD2 and MDA content in tail IVDs of each group. Significant decrease in GSH (a) and SOD2 (b) content in IDD group was observed compared with the control group and this decrease was significantly alleviated by Danshen treatment. Significant increase in MDA (c) content in IDD group was observed compared with the control group. However, this increase was significantly alleviated by Danshen treatment in the Danshen IDD group. The values are expressed as mean \pm SD. * $P < 0.05$. IDD: intervertebral disc degeneration; GSH: glutathione; SOD2: superoxide dismutase; MDA: malondialdehyde.

lowered than that of the control IVD. Similar results were previously reported in which total GAG reduction of IVDs appeared at as early as the initial stage of IDD [33, 34]. After four weeks of Danshen treatment, the water and GAG content significantly increased, which was consistent with the recovery of MRI T2 signal in the Danshen IDD group. Our data suggested that Danshen might help to protect water and GAG from loss and to slow down the occurrence of IDD.

COL2 and aggrecan are two main components of the ECM and can keep the fluids within the IVDs and preserve the resilience and volume of NP. The MMP family, especially MMP-3, is the main catabolic enzyme that is responsible for the ECM degradation. The abnormal reduction of COL2 and aggrecan or increase of MMP-3 may result in the failure of the NP structure and ultimately the onset of IDD. In our study, needle puncture downregulated the expressions of COL2 and aggrecan and upregulated the MMP-3 level. This catabolic change was significantly inhibited by Danshen treatment. In addition, inflammation plays crucial roles in the initiation and progression of IDD. The inflammatory factors IL-1 β and TNF- α were reported to be involved in many pathological processes, including oxidative stress, autophagy, ECM destruction, and cell apoptosis [35–37]. We found that IL-1 β and TNF- α were both more expressed in IVD tissues of the punctured rats compared with the control rats. However, this increase of inflammatory factors was greatly suppressed by Danshen in contrast to the IDD group, indicating the potent anti-inflammatory effect of Danshen. Taken together, our study demonstrated that Danshen was effective in protecting the structure integrity of the NP and inhibiting inflammation, which in turn delayed the IDD process.

It has been reported that redox imbalance can lead to damage to cells and tissues via oxidative stress [38]. Previous researches demonstrated that oxidative stress was closely related to histological changes of IVD and development of IDD [5, 39] and treatments that target oxidative stress may alleviate the progression of IDD [4]. Recent studies have found that Danshen could prevent the onset of oxidative stress in the aorta and eyes of diabetic rats [22], suggesting that Danshen could have a negative effect on oxidative stress. For further investigating the specific mechanism of Danshen attenuating IDD, the GSH, SOD2, and MDA (primary biomarkers of oxidative stress) contents of IVD tissues were measured. Our study showed that the GSH and SOD2 concentrations of rat IVDs in the IDD group were significantly lower compared with those in the control group. Our finding was similar to other research in which the activity of antioxidant materials decreased in age-related degenerated IVDs in Wistar rats [39]. The reduction in GSH and SOD2 content of degenerated IDD means an increase in consumption or decrease in production of the antioxidant substances. Additionally, increased intracellular ROS levels and oxidative stress under IVD injury by needle puncture have been previously reported [4]. Combining previous results and our findings, we believe that the decreased concentrations of GSH and SOD2 in the degenerated IVDs of rats are probably due to increased consumption of GSH and SOD2 in order to fight with the excessive ROS from IVD injury. However, Danshen treatment significantly increased the GSH and SOD2 content of IVDs in the Danshen IDD group. Similar findings have been reported that 4-week Danshen treatment significantly raised GSH content in articular cartilage and synovium tissues of osteoarthritis rabbits [40]. These results

demonstrated that Danshen could either induce GSH and SOD2 synthesis or directly scavenge excessive ROS generated during disc injury. MDA, a degradation product of peroxidized polyunsaturated fatty acids, is a common marker of oxidative stress [41, 42]. Previous studies showed that the MDA level in patients with lumbar IDD was markedly increased compared to that in the control group [9] and that serum and intervertebral MDA levels gradually increased with age in rats [39]. Similar results were also found in our research that MDA content in IVDs of the IDD group was statistically higher than that of the control group. However, Danshen treatment markedly downregulate the level of MDA in IVDs of the Danshen group. Taken together, our data indicated that lipid peroxidation occurred during IDD and Danshen can inhibit lipid peroxidation in the discs of rat tails.

There are some limitations that should be considered in our research. First, the pathogenesis environment of rat IVDs is not the same as human's and it is better to include human IVDs in the future. Second, only one time point (four weeks) was used to explore the effect of Danshen on IVDs and dynamic observation of this effect may be more convincing. Third, the precise mechanism of Danshen inhibiting oxidative stress is still unclear and needs further studies.

In conclusion, the present study indicated that Danshen could attenuate intervertebral disc degeneration and inhibit inflammation via antioxidation in puncture-induced SD rats. It has been suggested that the use of Danshen may have broad prospects in the medical treatment of intervertebral disc degeneration.

Data Availability

The data used to support the findings of this study are available from the corresponding author upon request.

Conflicts of Interest

The authors declare that they have no conflicts of interest.

Authors' Contributions

Rongqing Qin and Shouqian Dai contributed equally to this work.

References

- [1] T. Pulickal, J. Boos, M. Konieczny et al., "MRI identifies biochemical alterations of intervertebral discs in patients with low back pain and radiculopathy," *European Radiology*, vol. 29, no. 12, pp. 6443–6446, 2019.
- [2] N. V. Vo, R. A. Hartman, P. R. Patil et al., "Molecular mechanisms of biological aging in intervertebral discs," *Journal of Orthopaedic Research*, vol. 34, no. 8, pp. 1289–1306, 2016.
- [3] C. L. Le Maitre, A. J. Freemont, and J. A. Hoyland, "The role of interleukin-1 in the pathogenesis of human intervertebral disc degeneration," *Arthritis Research & Therapy*, vol. 7, no. 4, pp. R732–R745, 2005.
- [4] S. Suzuki, N. Fujita, N. Hosogane et al., "Excessive reactive oxygen species are therapeutic targets for intervertebral disc degeneration," *Arthritis Research & Therapy*, vol. 17, no. 1, p. 316, 2015.
- [5] A. Dimozi, E. Mavrogenatou, A. Sklirou, and D. Kletsas, "Oxidative stress inhibits the proliferation, induces premature senescence and promotes a catabolic phenotype in human nucleus pulposus intervertebral disc cells," *European Cells & Materials*, vol. 30, pp. 89–103, 2015, discussion 103.
- [6] K. Schroder, "NADPH oxidases in bone homeostasis and osteoporosis," *Free Radical Biology & Medicine*, vol. 132, pp. 67–72, 2019.
- [7] T. E. S. Kauppila, J. H. K. Kauppila, and N. G. Larsson, "Mammalian mitochondria and aging: an update," *Cell Metabolism*, vol. 25, no. 1, pp. 57–71, 2017.
- [8] K. Yudoh, N. van Trieu, H. Nakamura, K. Hongo-Masuko, T. Kato, and K. Nishioka, "Potential involvement of oxidative stress in cartilage senescence and development of osteoarthritis: oxidative stress induces chondrocyte telomere instability and downregulation of chondrocyte function," *Arthritis Research & Therapy*, vol. 7, no. 2, pp. R380–R391, 2005.
- [9] S. D. Bakirezer, C. K. Yaltirik, A. H. Kaya et al., "The evaluation of glutathione reductase and malondialdehyde levels in patients with lumbar disc degeneration disease," *In Vivo*, vol. 33, no. 3, pp. 811–814, 2019.
- [10] K. H. Mahdieh, A. Beitollah, E. S. Bina, M. Aida, M. Abdolvahab, and V. A. Mansour, "Effects of sesame seed supplementation on lipid profile and oxidative stress biomarkers in patients with knee osteoarthritis," *Health Promotion Perspective*, vol. 4, no. 1, pp. 90–97, 2014.
- [11] T. Suantawee, S. Tantavisut, S. Adisakwattana et al., "Oxidative stress, vitamin E, and antioxidant capacity in knee osteoarthritis," *Journal of Clinical and Diagnostic Research*, vol. 7, no. 9, pp. 1855–1859, 2013.
- [12] C. Anghong, N. P. Morales, W. Sutipornpalangkul, A. Khadsongkram, P. Pinsornsak, and B. Pongcharoen, "Can levels of antioxidants in synovial fluid predict the severity of primary knee osteoarthritis: a preliminary study," *Springerplus*, vol. 2, no. 1, p. 652, 2013.
- [13] K. M. Surapaneni and G. Venkataramana, "Status of lipid peroxidation, glutathione, ascorbic acid, vitamin E and antioxidant enzymes in patients with osteoarthritis," *Indian Journal of Medical Sciences*, vol. 61, no. 1, pp. 9–14, 2007.
- [14] T. O. Cheng, "Cardiovascular effects of Danshen," *International Journal of Cardiology*, vol. 121, no. 1, pp. 9–22, 2007.
- [15] C. Y. Su, Q. L. Ming, K. Rahman, T. Han, and L. P. Qin, "Salvia miltiorrhiza: Traditional medicinal uses, chemistry, and pharmacology," *Chinese Journal of Natural Medicines*, vol. 13, no. 3, pp. 163–182, 2015.
- [16] X. Liu, R. Chen, Y. Shang, B. Jiao, and C. Huang, "Superoxide radicals scavenging and xanthine oxidase inhibitory activity of magnesium lithospermate B from Salvia miltiorrhiza," *Journal of Enzyme Inhibition and Medicinal Chemistry*, vol. 24, no. 3, pp. 663–668, 2009.
- [17] L. L. Tian, X. J. Wang, Y. N. Sun et al., "Salvianolic acid B, an antioxidant from Salvia miltiorrhiza, prevents 6-hydroxydopamine induced apoptosis in SH-SY5Y cells," *The International Journal of Biochemistry & Cell Biology*, vol. 40, no. 3, pp. 409–422, 2008.
- [18] J. Zhang, Q. Jin, Y. Deng, J. Hou, W. Wu, and D. Guo, "New depsides from the roots of Salvia miltiorrhiza and their radical-scavenging capacity and protective effects against H₂O₂-induced H9c2 cells," *Fitoterapia*, vol. 121, pp. 46–52, 2017.

- [19] X. Wang, A. Gao, Y. Jiao, Y. Zhao, and X. Yang, "Antitumor effect and molecular mechanism of antioxidant polysaccharides from *Salvia miltiorrhiza* Bunge in human colorectal carcinoma LoVo cells," *International Journal of Biological Macromolecules*, vol. 108, pp. 625–634, 2018.
- [20] B. Han, K. Zhu, F. C. Li et al., "A simple disc degeneration model induced by percutaneous needle puncture in the rat tail," *Spine*, vol. 33, no. 18, pp. 1925–1934, 2008.
- [21] A. C. Issy, V. Castania, M. Castania et al., "Experimental model of intervertebral disc degeneration by needle puncture in Wistar rats," *Brazilian Journal of Medical and Biological Research*, vol. 46, no. 3, pp. 235–244, 2013.
- [22] K. K. Yue, K. W. Lee, K. K. C. Chan, K. S. Y. Leung, A. W. N. Leung, and C. H. K. Cheng, "Danshen prevents the occurrence of oxidative stress in the eye and aorta of diabetic rats without affecting the hyperglycemic state," *Journal of Ethnopharmacology*, vol. 106, no. 1, pp. 136–141, 2006.
- [23] K. Masuda, Y. Aota, C. Muehleman et al., "A novel rabbit model of mild, reproducible disc degeneration by an annulus needle puncture: correlation between the degree of disc injury and radiological and histological appearances of disc degeneration," *Spine*, vol. 30, no. 1, pp. 5–14, 2005.
- [24] R. C. Lawrence, C. G. Helmick, F. C. Arnett et al., "Estimates of the prevalence of arthritis and selected musculoskeletal disorders in the United States," *Arthritis and Rheumatism*, vol. 41, no. 5, pp. 778–799, 1998.
- [25] J. J. Chen, J. F. Huang, W. X. du, and P. J. Tong, "Expression and significance of MMP3 in synovium of knee joint at different stage in osteoarthritis patients," *Asian Pacific Journal of Tropical Medicine*, vol. 7, no. 4, pp. 297–300, 2014.
- [26] R. W. Farndale, D. J. Buttle, and A. J. Barrett, "Improved quantitation and discrimination of sulphated glycosaminoglycans by use of dimethylmethylene blue," *Biochimica et Biophysica Acta*, vol. 883, no. 2, pp. 173–177, 1986.
- [27] F. Sun, J. N. Qu, and Y. G. Zhang, "Animal models of disc degeneration and major genetic strategies," *Pain Physician*, vol. 16, no. 3, pp. E267–E275, 2013.
- [28] G. Keorochana, J. S. Johnson, C. E. Taghavi et al., "The effect of needle size inducing degeneration in the rat caudal disc: evaluation using radiograph, magnetic resonance imaging, histology, and immunohistochemistry," *The Spine Journal*, vol. 10, no. 11, pp. 1014–1023, 2010.
- [29] H. Zhang, F. la Marca, S. J. Hollister, S. A. Goldstein, and C. Y. Lin, "Developing consistently reproducible intervertebral disc degeneration at rat caudal spine by using needle puncture," *Journal of Neurosurgery. Spine*, vol. 10, no. 6, pp. 522–530, 2009.
- [30] H. Zhang, S. Yang, L. Wang et al., "Time course investigation of intervertebral disc degeneration produced by needle-stab injury of the rat caudal spine: laboratory investigation," *Journal of Neurosurgery. Spine*, vol. 15, no. 4, pp. 404–413, 2011.
- [31] S. Sobajima, J. F. Kempel, J. S. Kim et al., "A slowly progressive and reproducible animal model of intervertebral disc degeneration characterized by MRI, X-ray, and histology," *Spine*, vol. 30, no. 1, pp. 15–24, 2005.
- [32] P. J. Roughley, "Biology of intervertebral disc aging and degeneration: involvement of the extracellular matrix," *Spine*, vol. 29, no. 23, pp. 2691–2699, 2004.
- [33] F. Wei, R. Zhong, Z. Zhou et al., "In vivo experimental intervertebral disc degeneration induced by bleomycin in the rhesus monkey," *BMC Musculoskeletal Disorders*, vol. 15, no. 1, p. 340, 2014.
- [34] D. G. Anderson and C. Tannoury, "Molecular pathogenic factors in symptomatic disc degeneration," *The Spine Journal*, vol. 5, no. 6, pp. S260–S266, 2005.
- [35] W. Yang, X. H. Yu, C. Wang et al., "Interleukin-1 β in intervertebral disc degeneration," *Clinica Chimica Acta*, vol. 450, pp. 262–272, 2015.
- [36] C. A. Séguin, M. Bojarski, R. M. Pilliar, P. J. Roughley, and R. A. Kandel, "Differential regulation of matrix degrading enzymes in a TNF α -induced model of nucleus pulposus tissue degeneration," *Matrix Biology*, vol. 25, no. 7, pp. 409–418, 2006.
- [37] S. Yang, F. Zhang, J. Ma, and W. Ding, "Intervertebral disc ageing and degeneration: the antiapoptotic effect of oestrogen," *Ageing Research Reviews*, vol. 57, p. 100978, 2020.
- [38] H. Sies, "Oxidative stress: oxidants and antioxidants," *Experimental Physiology*, vol. 82, no. 2, pp. 291–295, 1997.
- [39] G. Hou, H. Lu, M. Chen, H. Yao, and H. Zhao, "Oxidative stress participates in age-related changes in rat lumbar intervertebral discs," *Archives of Gerontology and Geriatrics*, vol. 59, no. 3, pp. 665–669, 2014.
- [40] B. Bai and Y. Li, "Danshen prevents articular cartilage degeneration via antioxidation in rabbits with osteoarthritis," *Osteoarthritis and Cartilage*, vol. 24, no. 3, pp. 514–520, 2016.
- [41] H. Z. Pan, H. Zhang, D. Chang, H. Li, and H. Sui, "The change of oxidative stress products in diabetes mellitus and diabetic retinopathy," *The British Journal of Ophthalmology*, vol. 92, no. 4, pp. 548–551, 2008.
- [42] H. Z. Pan, L. Zhang, M. Y. Guo et al., "The oxidative stress status in diabetes mellitus and diabetic nephropathy," *Acta Diabetologica*, vol. 47, Suppl 1, pp. 71–76, 2010.

Research Article

Allicin Attenuated Advanced Oxidation Protein Product-Induced Oxidative Stress and Mitochondrial Apoptosis in Human Nucleus Pulposus Cells

Qian Xiang, Zhangrong Cheng, Juntan Wang, Xiaobo Feng, Wenbin Hua, Rongjin Luo, Bingjin Wang, Zhiwei Liao, Liang Ma, Gaocai Li, Saideng Lu, Kun Wang, Yu Song, Shuai Li, Xinghuo Wu, Cao Yang, and Yukun Zhang 

Department of Orthopaedics, Union Hospital, Tongji Medical College, Huazhong University of Science and Technology, Wuhan 430022, China

Correspondence should be addressed to Yukun Zhang; zhangyukuncom@126.com

Received 4 October 2020; Revised 30 November 2020; Accepted 2 December 2020; Published 16 December 2020

Academic Editor: Sidong Yang

Copyright © 2020 Qian Xiang et al. This is an open access article distributed under the Creative Commons Attribution License, which permits unrestricted use, distribution, and reproduction in any medium, provided the original work is properly cited.

Intervertebral disc degeneration (IDD) is one of the most common chronic degenerative musculoskeletal disorders. Oxidative stress-induced apoptosis of the nucleus pulposus (NP) cells plays a key role during IDD progression. Advanced oxidation protein products (AOPP), novel biomarkers of oxidative stress, have been reported to function in various diseases due to their potential for disrupting the redox balance. The current study is aimed at investigating the function of AOPP in the oxidative stress-induced apoptosis of human NP cells and the alleviative effects of allicin during this process which was known for its antioxidant properties. AOPP were demonstrated to hamper the viability and proliferation of NP cells in a time- and concentration-dependent manner and cause cell apoptosis markedly. High levels of reactive oxygen species (ROS) and lipid peroxidation product malondialdehyde (MDA) were detected in NP cells after AOPP stimulation, which resulted in depolarized mitochondrial transmembrane potential (MTP). Correspondingly, higher levels of AOPP were discovered in the human degenerative intervertebral discs (IVD). It was also found that allicin could protect NP cells against AOPP-mediated oxidative stress and mitochondrial dysfunction via suppressing the p38-MAPK pathway. These results disclosed a significant role of AOPP in the oxidative stress-induced apoptosis of NP cells, which could be involved in the primary pathogenesis of IDD. It was also revealed that allicin could be a promising therapeutic approach against AOPP-mediated oxidative stress during IDD progression.

1. Introduction

Low back pain (LBP) has become an increasingly common disorder in contemporary times, lowering patients' quality of life and burthening cosmopolitan healthcare system and society economically [1, 2]. One of the leading causes of LBP is intervertebral disc degeneration (IDD) [3]. The intervertebral disc, the largest avascular organ in the human body, comprises a centric nucleus pulposus (NP) and an ambient annulus fibrosus [4]. Many previous studies demonstrate that the main pathological changes in degenerated discs include excess apoptosis of NP cells and degradation of the extracellular matrix (ECM) [5, 6]. Apoptosis is a highly conserved

cellular function to remove excrescent and volatile cells in different pathophysiological processes, and plays a vital role in sustaining healthy function of tissues and organs; however, superfluous apoptosis of NP cells is the primary cause of IDD [7–9]. Recent studies have shown that excess apoptosis of NP cells is largely promoted by an imbalance of the cellular redox system in the disc microenvironment, while interventions targeting oxidative stress markedly protect NP cells from apoptosis [10, 11].

Once cellular redox homeostasis is disrupted, proteins in this environment are prone to be damaged under oxidative stress [12–14]. Advanced oxidation protein products (AOPP), which are important derivatives of such damaged

proteins, mainly originate from oxidatively modified albumin and have been identified recently as circulating plasma biomarkers of oxidation stress [15]. Indeed, AOPP accumulate in the serum of patients with various chronic diseases, such as inflammatory bowel disease, diabetes, and chronic kidney disease [16]. A previous study revealed that reactive oxygen species (ROS), which are potent oxidants, can be generated by AOPP through a NADPH oxidase-dependent pathway [17]. Research on diabetic nephropathy also showed that the accumulation of AOPP can induce oxidative stress and mitochondrial injury [18]. Other studies demonstrated that AOPP can act as potent inducers of apoptosis [19, 20]. Recently, abnormal accumulation of AOPP was found in the articular cartilage of rodent osteoarthritis (OA) models and had an endogenous pathogenic role in OA progression [21]. In addition, a prior study showed that AOPP participated in age-related changes in rat lumbar IVDs [22]. Considering that IVD cells and chondrocytes share phenotypic and morphological similarities, it is important to investigate how AOPP work in IDD progression, which remains unclear thus far [23].

Many constituents of medicinal herbs, including allicin, have various benefits [24]. Allicin, one of the organosulfur compounds extracted from the garlic bulb, shows potent effects on eliminating free radicals, abating oxidative stress, and protecting mitochondrial functions [25–28]. Recent studies have also demonstrated that allicin exerts extensive therapeutic effects in various diseases, such as cardiovascular and chronic kidney disease, because of its antioxidant properties, while its influence on IDD is still unknown [28–30].

Based on the above findings, we hypothesized that the accumulation of AOPP in the disc microenvironment might contribute to oxidative stress in NP cells, which further erode mitochondrial functions and promote apoptosis. The present study was undertaken to explore the role of AOPP in oxidative stress and apoptosis of human NP cells and to determine the effect of allicin on these AOPP-mediated processes. We exposed NP cells *in vitro* to different levels of AOPP or allicin and gathered experimental data on multiple aspects, such as cell proliferation, apoptosis, oxidative stress, and changes in the mitochondrial membrane. In addition, as an important avenue for cell demise, the activation of MAPK pathways was reported to be crucially involved in ROS-triggered apoptosis [31, 32]. Considering the role of ROS as a pathogenic intermediary of AOPP-initiated diseases, thus, we detected the expression of key proteins in MAPK signaling pathways potentially mediating the effects of AOPP on NP cells [17]. We aimed to provide a general overview of the molecular mechanisms by which AOPP affected human NP cells and inform possible therapeutic strategies. Our research is aimed at helping to better understand the pathogenesis of IDD and providing a promising therapeutic approach to retard its progression.

2. Material and Methods

2.1. Collection of NP Tissue and Ethics Statement. To separate NP cells, the healthy NP specimens (Pfirrmann I or II) of human IVD were obtained from deformity correction sur-

gery for 6 patients (3 females and 3 males; average age: 18.3 years; age range: 16–20 years) with idiopathic scoliosis. To compare AOPP levels, the degenerative NP tissues (Pfirrmann IV or V) were acquired from spinal decompression surgery for 3 patients (2 females and 1 male; average age 63.4 years; age range: 63–65 years) with spinal stenosis, and the healthy tissues were collected from deformity correction surgery for 3 patients (2 males and 1 female; average age 25 years; age range: 24–26 years) with idiopathic scoliosis. In brief, after being excised intraoperatively, the healthy tissues used for separating cells were instantly put into a chilled vessel with Hank's balanced salt solution, and the other healthy or degenerative tissues used for AOPP testing were snap-frozen. All samples were then transported to the laboratory for the further handling according to their intended use or cryopreserved in liquid nitrogen. Each donor was informed of the experimental usage of the NP tissue, and their approvals were acquired. Our research protocol was approved by the Clinical Research Ethics Committee of Tongji Medical College, Huazhong University of Science and Technology. All methods were applied in strict adherence with the approved guidelines.

2.2. Separation and Culture of NP Cells. Briefly, the fresh tissue was chopped into small pieces (1 mm³ or so) and digested at 37°C using 0.25% trypsin (Gibco, UK) for 30 min before 0.2% collagenase-type 2 (Gibco, UK) for 4 h in a humid environment with 5% CO₂. The suspension was centrifuged after the pieces were filtered and washed using phosphate buffered saline (PBS). Next, the cultivation of separate cells was conducted in Dulbecco's modified Eagle' medium (DMEM) comprising nutrient admixture F12 (Gibco, USA) and 15% fetal bovine serum (FBS; Gibco, USA) and streptomycin (100 µg/ml; Gibco, USA) as well as penicillin (100 units/ml; Gibco, USA). The culture medium was renewed every three days until cell passaging was performed at 80% confluence. Fluorescently labeled antibodies against NP cell markers (CD24, ab31622; KRT18, ab215839; Abcam, UK) were used to identify the phenotype of NP cells, as described previously [33]. Cells at the second passage were utilized in the subsequent experiments.

2.3. AOPP Preparation and Assessment. Human serum albumin (HSA) solution (30 mg/ml) was incubated with 100 mM HOCl in PBS (pH = 7.4) at ordinary temperature for 30 min. An equimolar concentration of thiosulfate was used to discontinue the reaction and block excess HOCl before the solution was dialyzed for 24 h at 4°C. AOPP-HSA were assessed according to previous description [34]. In short, the samples and 160 µL citric acid (0.20 mol/L) were added into a 96-well microplate. Then, the calibrated chloramine-T model compound, 10 ml potassium iodide (KI, 1.16 mol/L in PBS), and 10 µL citric acid (0.20 mol/L) were successively pipetted into the plate. Next, the absorbance was read on a spectrophotometer (Waltham, MA, USA) at 340 nm. The level of AOPP was expressed as µMol/ml of chloramine-T equivalents.

2.4. Protocols of NP Cell Culture and Treatment. To evaluate the impact of AOPP, the NP cells were either cotreated with

incremental concentrations of AOPP (0, 100, 200, and 400 $\mu\text{g/ml}$) for 24 h, or with 400 $\mu\text{g/ml}$ AOPP for different time points (0, 2, 6, 12, and 24 h). Allicin (purity > 98%) was bought from MedChemExpress (Shanghai, China). The cells were cotreated with incremental levels of allicin (0, 5, 10, 20, and 40 μM) for 24 h to explore the effect of allicin on them. Then, to evaluate the possible protective role of allicin against AOPP-induced unfavorable influences including restrained viability and proliferation, apoptosis, oxidative stress, and mitochondrial dysfunction, the cells were pretreated with incremental concentrations (0, 5, 10, and 20 μM) of allicin for 2 h and then with AOPP (400 $\mu\text{g/ml}$) for 24 h. To examine whether MAPK pathways were activated in AOPP-induced oxidative damage, NP cells were treated with 400 $\mu\text{g/ml}$ AOPP. To explore the signaling pathway through which allicin mitigated AOPP-induced oxidative stress and apoptosis of NP cells, the cells in the experimental groups were pretreated with different concentrations of allicin (0, 5, 10, and 20 μM) for 2 h, and then cotreated with AOPP (400 $\mu\text{g/ml}$) for 24 h. To validate the MAPK pathway underlying the protective effects of allicin against AOPP, the NP cells were treated, respectively, with allicin (10 μM), p38-MAPK inhibitor SB202190 (10 μM), JNK inhibitor SP600125 (10 μM), and ERK inhibitor SCH772984 (10 μM) for 2 h, and then with AOPP (400 $\mu\text{g/ml}$) for 24 h. To examine whether the p38-MAPK agonist can block the positive effects of allicin, the human NP cells were pretreated with allicin (10 μM) or allicin (10 μM) in combination with p38-MAPK activator Dehydrocorydaline chloride (Dc, 500 nM) for 2 h, then treated with AOPP (400 $\mu\text{g/ml}$) for 24 h.

2.5. Appraisals of NP Cell Viability and Proliferation. The viability of human NP cells treated with allicin or AOPP was evaluated employing CCK-8 assay (Dojindo, Japan). Briefly, suspended human NP cells were pipetted into a 96-well plate for 24 h incubation, and then the cells were cotreated with incremental concentrations of allicin or AOPP for different time periods. Afterward, NP cells in each well were appended with 10 μL solution of CCK-8 and then were cultured in the fresh medium at 37°C for 4 h. Eventually, the absorbance at 450 nm was gauged employing a spectrophotometer (BioTek, Winooski, USA).

The evaluation of NP cell proliferation was performed with a BeyoClickEdU-488 Cell Proliferation kit (Beyotime, Shanghai, China). The procedures were mainly in accord with instructions of the manufacturer. The images were acquired employing fluorescent microscopy (Olympus IX71, Japan).

2.6. Flow Cytometry for Analyzing Apoptosis, ROS, and MTP. Human NP cells were harvested after being treated in each group. An Annexin V-FITC Apoptosis Detection Kit (KeyGEN, China) was utilized to estimate the apoptotic levels of NP cells. The alterations of MTP were measured utilizing the cationic fluorescent indicator JC-1 (Beyotime). The ROS levels of cells were detected using the fluorescent dye dihydroethidium (DHE, Beyotime). The fluorescence intensity emitted by DHE was measured by flow cytometry, and

ROS levels were expressed as mean fluorescence intensity for comparison. The final ROS level of each experimental group was expressed as a ratio relative to that of control group. All the above procedures were in accordance with previous descriptions [35]. Analysis of the sample was by dint of a FACSCalibur flow cytometer (BD Biosciences).

2.7. Lipid Peroxidation Detection. A malondialdehyde (MDA) Assay Kit (Beyotime, China) was used to detect the cellular lipid peroxidation. MDA is considered as a distinctive peroxidative product of lipid. Briefly speaking, NP cells were dissolved in MDA standards before blending with the working solution of thiobarbituric acid (TBA), in accordance with instructions. The absorbance of the MDA-TBA compound was gauged at 532 nm by using an automatic microplate reader (Multiskan MK3, Thermo Scientific, USA). The level of cellular MDA was reckoned on the basis of the standard curve.

2.8. Immunofluorescence Staining. Immunofluorescence staining was done to NP cells according to previous descriptions [36]. Primary antibodies aiming at cleaved caspase-3 (1:400; #9579, Cell Signaling Technology) were first used to incubate with NP cells at 4°C for all night. In the second day, a continued incubation with the secondary antibodies Cy3 conjugated goat anti-rabbit IgG (1:200; BA1032, Boster Biological Technology) lasted for 2 h. DAPI (Beyotime) was used to stain the nuclei. Images of fluorescence were obtained via immunofluorescent microscopy (Olympus IX71, Japan) as well as confocal laser-scanning microscopy (LSM780, ZEISS, Germany). The immunofluorescence intensity values were determined using the ImageJ image analysis software (NIH). For the stained sample from each group, the mean immunofluorescence was determined by analyzing the fluorescence intensity values of three randomly selected images under the same magnification ($\times 400$). In order to compare the fluorescence intensity between groups, all the image analyses were performed using the same protocol. The final fluorescence intensity of each experiment group was expressed as a ratio relative to that of control group.

2.9. Western Blotting. The total and cytoplasmic, as well as mitochondrial proteins from elaborately treated NP cells were extracted employing the commercial kits, following the merchant guide (Beyotime, China). Levels of these proteins were then gauged employing an Enhanced BCA Protein Assay Kit (Beyotime, China). 10–12% SDS-PAGE gels were used to separate these proteins, which were then transferred to polyvinylidene fluoride (PVDF) membranes (Millipore, USA). The PVDF membranes were previously blocked before an overnight incubation at 4°C with primary antibodies (1:500–1:1000) and then with horseradish peroxidase-(HRP-) conjugated secondary antibodies (1:2000; Abcam). Enhanced chemiluminescence reagents (Amersham, Piscataway, USA) were utilized to examine the expressed proteins. Primary antibodies against the following molecules were used: Bax (ab32503, Abcam), cytochrome-c (ab133504, Abcam), cleaved caspase-3 (#9579, Cell signaling Technology), Bcl-2 (ab196495, Abcam), VDAC1 (sc-32063, Santa

Cruz Bio-technology), cleaved caspase-9 (#9505, Cell Signaling Technology), GAPDH (#5174, Cell Signaling Technology), MAPK Family Antibody Sampler Kit (#8690, #4695, and #9252; Cell Signaling Technology), and Phospho-MAPK Family Antibody Sampler Kit (#4511, #4370, and #4668; Cell Signaling Technology).

2.10. Enzyme-Linked Immunosorbent Assay (ELISA) for AOPP Testing. After being weighted, the NP tissues were cut into pieces, mixed with PBS solution (9 ml per gram), and fully ground. Then, the sample was centrifuged (C2500-R-230V, Labnet, USA) at $1000 \times g$ for 20 min. The supernatant was collected and tested with ELISA Kit for AOPP (Cloud-Clone Corp, USA) according to the manual. The optical density (O.D. value) of each well was measured at 450 nm using a microplate reader (Multiskan MK3, Thermo scientific). The concentrations of AOPP were calculated from the standard curve according to the manufacturer's instructions.

2.11. Data Analysis. All experiments were independently replicated at least three times. The analysis of data was finished with the SPSS v.18.0 software (USA). The data from all groups were presented as means \pm SD (standard deviation). Contrastive analysis of means between groups was evaluated using Student's *t*-test or one-way analysis of variance (ANOVA) with post hoc analysis using the Tukey's test. Graphic analysis of the data was conducted using GraphPad Prism 7.0 (GraphPad Software, California, USA). $p < 0.05$ was the prerequisite to conclude that differences among statistics were meaningful.

3. Results

3.1. AOPP Inhibited NP Cell Viability and Proliferation and Were Accumulated in the Degenerative IVD. To explore the impact of AOPP on the viability and proliferation of NP cells in vitro, a group of human NP cells were treated with incremental concentrations of AOPP (0, 100, 200, and 400 $\mu\text{g/ml}$) made from human serum albumin (HSA) for 24 h, and then another contrastive group was treated with a high level of AOPP (400 $\mu\text{g/ml}$) for different times (0, 2, 6, 12, and 24 h). Compared with the control, the AOPP-treated groups showed suppressed cell viability and proliferation, detected by CCK-8 kit and EdU staining, respectively. Notably, this visualized inhibition was both dose-dependent and time-dependent as depicted (Figures 1(a)–1(d)). Moreover, to explore the clinical relevance of the current study, we compared the levels of AOPP between the control human IVD tissues (Pfirrmann I or II) and the degenerative IVD tissues (Pfirrmann IV or V). Results showed that the levels of AOPP in degenerative tissues were significantly higher than that of control tissues (Figure S1(c)).

3.2. Effect of Allicin on NP Cell Viability and Proliferation. To explore the cytotoxic effect of allicin on NP cells, incremental concentrations of allicin (0, 5, 10, 20, and 40 μM) were separately appended to independent groups for 24 h. The CCK-8 assay and EdU staining showed that incubation with $<40 \mu\text{M}$ allicin enhanced the cell viability and proliferation, which

reached the highest level when the allicin was around 10 μM . However, the concentration growing from a critical value between 20 μM and 40 μM showed inhibition to cell viability and proliferation as presented in the figure (Figures 2(a) and 2(b)).

3.3. Allicin Improved the Viability and Proliferation of AOPP-Stimulated NP Cells. Considering the critical value of the beneficial dosage, we used 0, 5, 10, and 20 μM allicin to pretreat the NP cells for 2 h, which were then cotreated with AOPP-HSA for 24 h. Unsurprisingly, allicin pretreatment attenuated the impaired viability and proliferation of NP cells under AOPP challenge, which were measured employing CCK-8 and EdU staining. In addition, the most beneficial concentration of allicin was around 10 μM (Figures 2(c) and 2(d)).

3.4. Allicin Protected NP Cells from AOPP-Induced Apoptosis. Apoptosis of NP cells was detected employing the Annexin V-FITC Apoptosis Detection Kit (KeyGEN, China). After treated by 400 $\mu\text{g/ml}$ AOPP for 24 h, the NP cells exhibited a high apoptosis rate ($>30\%$) compared with that ($<10\%$) of the control group (Figure 3(a)). However, when pretreated with different levels of allicin (5, 10, and 20 μM), 10 and 20 μM allicin pretreatment groups showed reduced apoptosis rate compared with the AOPP alone treatment group. It was of note that 10 μM seemed to be the best protective concentration of allicin against AOPP-induced apoptosis (Figure 3(a)). Also, apoptosis-associated proteins were measured by using Western blotting. As expected, common proapoptotic proteins including Bax, cleaved caspase-3, cytoplasmic cytochrome-c, and cleaved caspase-9 were highly promoted in the AOPP-treated group, while that in allicin-pretreated groups were relatively abated, especially in the 10 μM allicin group. Correspondingly, antiapoptotic Bcl-2 and mitochondrial cytochrome-c were lowered in the group only treated with high levels of AOPP, while that were raised in allicin-pretreated groups, particularly in the 10 μM allicin group. To detect cleaved caspase-3, another assay, immunofluorescence staining, was also employed to appraise the apoptotic differences among groups. Results showed that cleaved caspase-3 was highly expressed in AOPP group compared with allicin groups, where the level of cleaved caspase-3 dropped to varying degrees. In summary, these results indicated that allicin worked in resisting AOPP-induced apoptosis to protect NP cells.

3.5. Allicin Protected NP Cells from Oxidative Stress and Mitochondrial Dysfunction Induced by AOPP. Next, we explored the mechanisms behind AOPP-induced apoptosis and how allicin antagonized it. AOPP have been reported to cause mitochondrial dysfunction through a ROS-dependent way, which might expound the apoptosis phenomenon of NP cells [37]. Here, the dihydroethidium-(DHE-) dyed products of ROS were detected by flow cytometry. The results showed that AOPP evidently increased ROS levels in NP cells, while allicin pretreatment partially restrained this effect (Figures 4(a)–4(c)). Moreover, we detected the level of MDA, a characteristic peroxidative

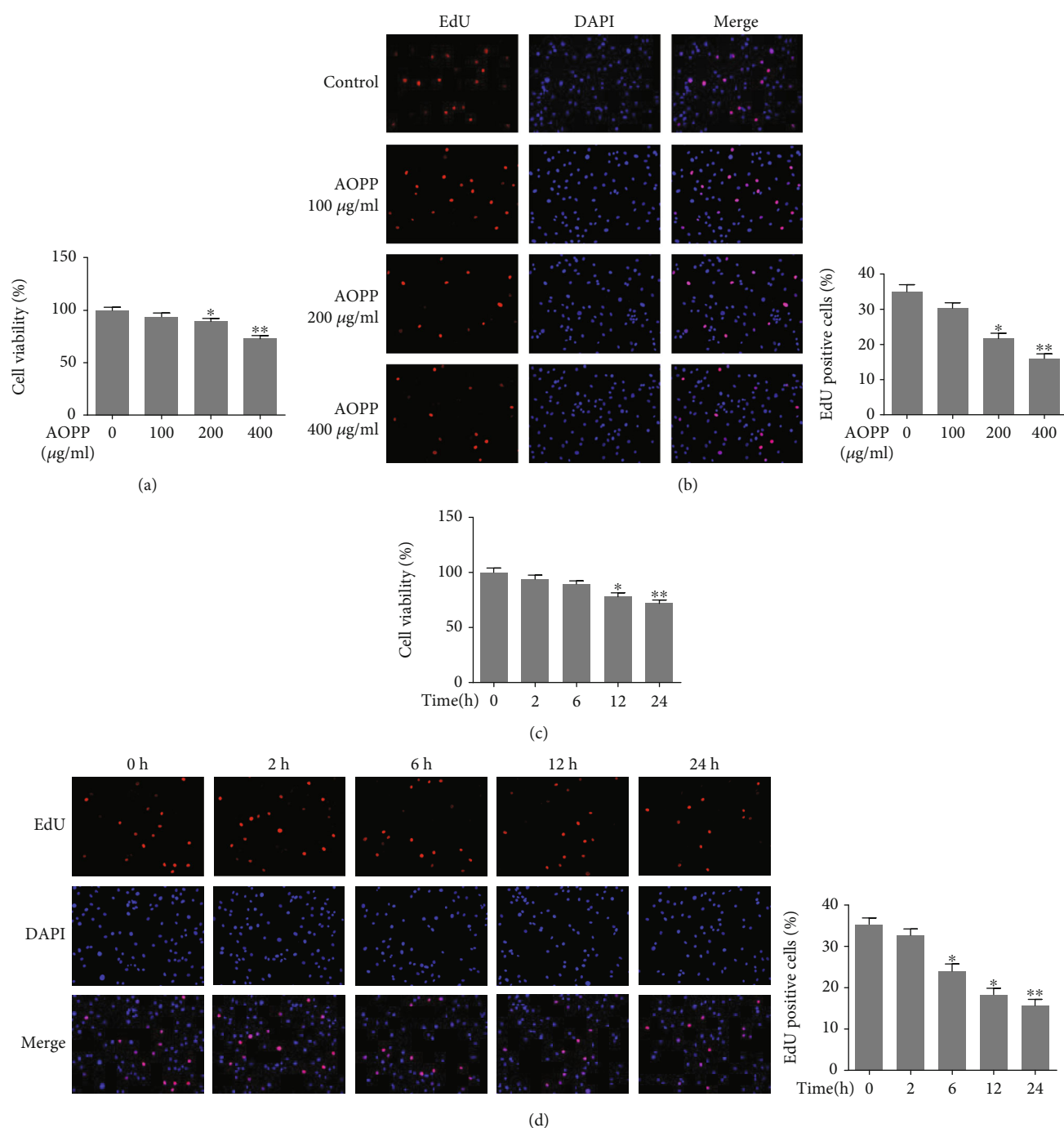


FIGURE 1: AOPP treatment inhibited human NP cell viability and proliferation in a dose- and time-dependent manner. (a) The human NP cells were treated with AOPP (0, 100, 200, and 400 µg/ml) for 24 h, and 0 µg/ml group served as a control. The cell viability of each group was detected by a CCK-8 assay. (b) The human NP cells were treated with AOPP (0-400 µg/ml) for 24 h, and 0 µg/ml group served as a control. The cell proliferation was determined using EdU staining combined with DAPI staining for the nuclei under fluorescence microscope, with the EdU positive cells quantitated. Original magnification: $\times 200$. (c) The human NP cells were treated with 400 µg/ml AOPP for 0 h, 2 h, 6 h, 12 h, and 24 h, and 0 h group served as a control. The cell viability of each group was detected by a CCK-8 assay. (d) The human NP cells were treated with 400 µg/ml AOPP for 0 h, 2 h, 6 h, 12 h, and 24 h, and 0 h group served as a control. The cell proliferation was determined using EdU staining combined with DAPI staining for the nuclei under fluorescence microscope, with the EdU positive cells quantitated. Original magnification: $\times 200$. Data were represented as mean \pm SD. * $p < 0.05$ and ** $p < 0.01$ versus the control group, $n = 3$.

product of lipid. We found that the AOPP challenge promoted the MDA generation, which was inhibited partially by allicin pretreatment (Figure 4(d)). To appraise the func-

tion of mitochondria under oxidative stress, we turned our attention to the MTP, whose depolarization proved the key event of intrinsic apoptosis. JC-1 assay indicated that the

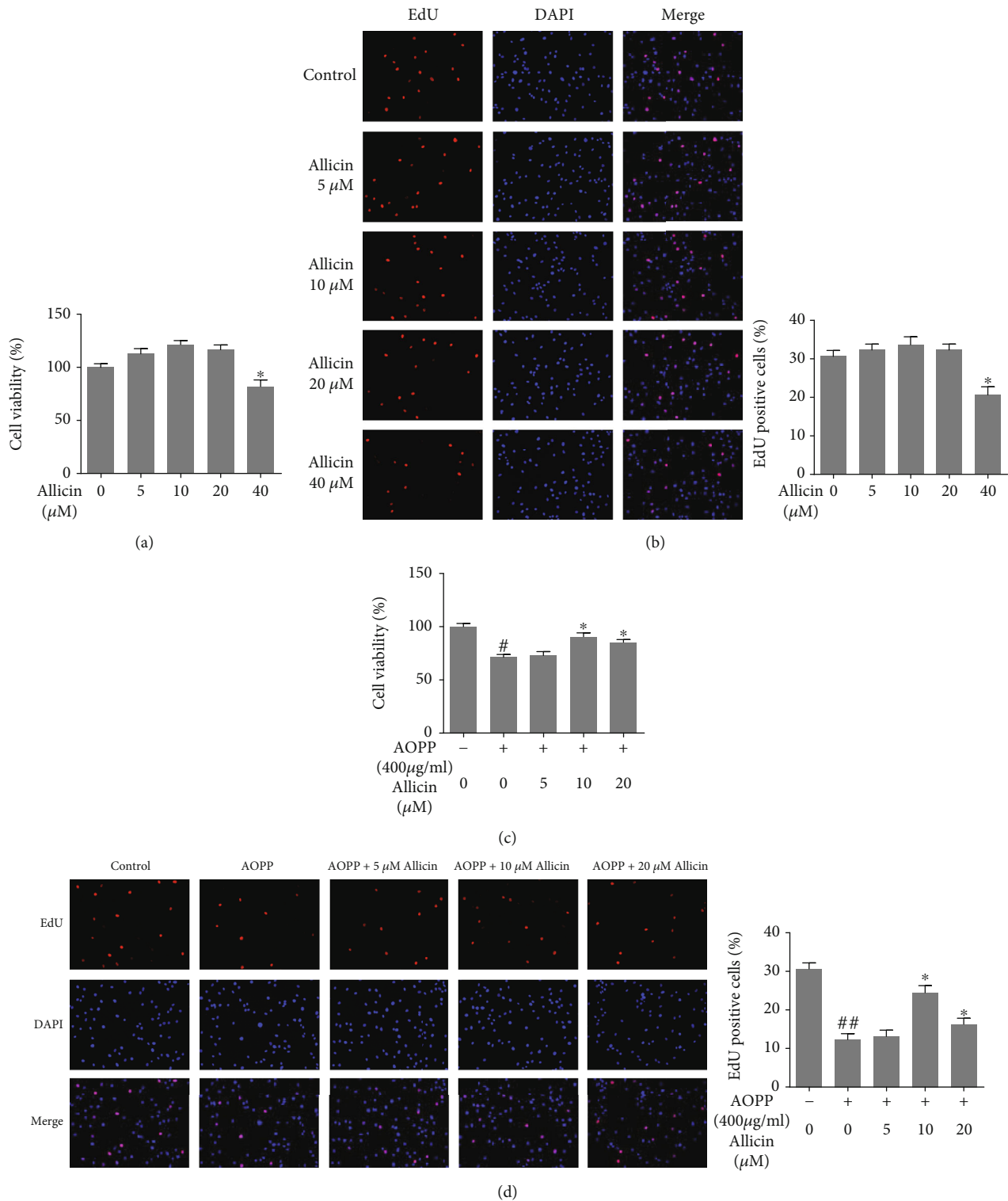
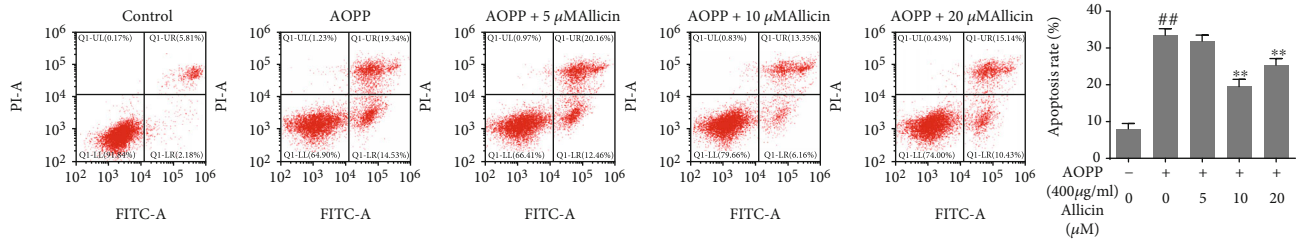
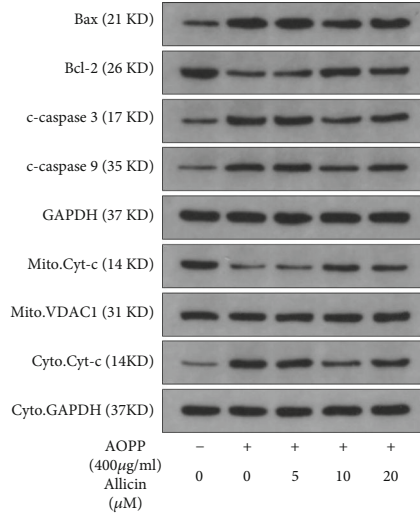


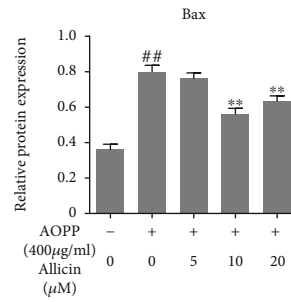
FIGURE 2: Effects of allicin on the human NP cell viability and proliferation. (a) The human NP cells were treated with allicin (0, 5, 10, 20, and 40 μM) for 24 h, and 0 μM group served as a control. The cell viability of each group was detected by a CCK-8 assay. * $p < 0.05$ versus the control group, $n = 3$. (b) The human NP cells were treated with allicin (0–40 μM) for 24 h, and 0 μM group served as a control. The cell proliferation was determined using EdU staining combined with DAPI staining for the nuclei under fluorescence microscope, with the EdU positive cells quantitated. Original magnification: $\times 200$. * $p < 0.05$ versus the control group, $n = 3$. (c) The human NP cells pretreated by allicin (0, 5, 10, and 20 μM) were treated with 400 $\mu\text{g/ml}$ AOPP, and the cell viability of each group was examined by the CCK-8 assay. # $p < 0.05$ versus the control group, * $p < 0.05$ versus the AOPP alone treatment group, $n = 3$. (d) The cell proliferation of each group was determined using EdU staining under fluorescence microscope, with the EdU positive cells quantitated. Original magnification: $\times 200$. Data were represented as mean \pm SD. ## $p < 0.01$ versus the control group, * $p < 0.05$ versus the AOPP alone treatment group, $n = 3$.



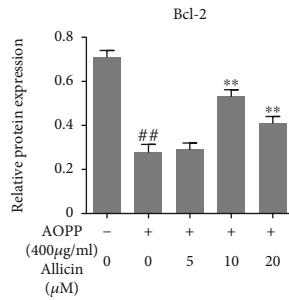
(a)



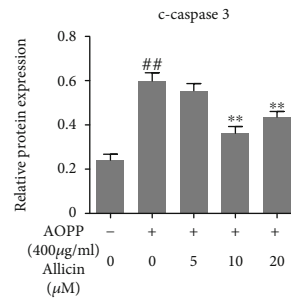
(b)



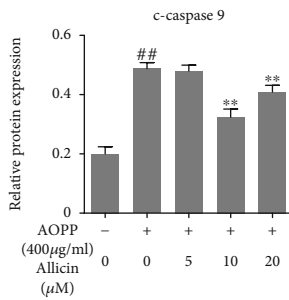
(c)



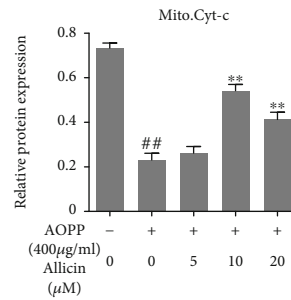
(d)



(e)



(f)



(g)

FIGURE 3: Continued.

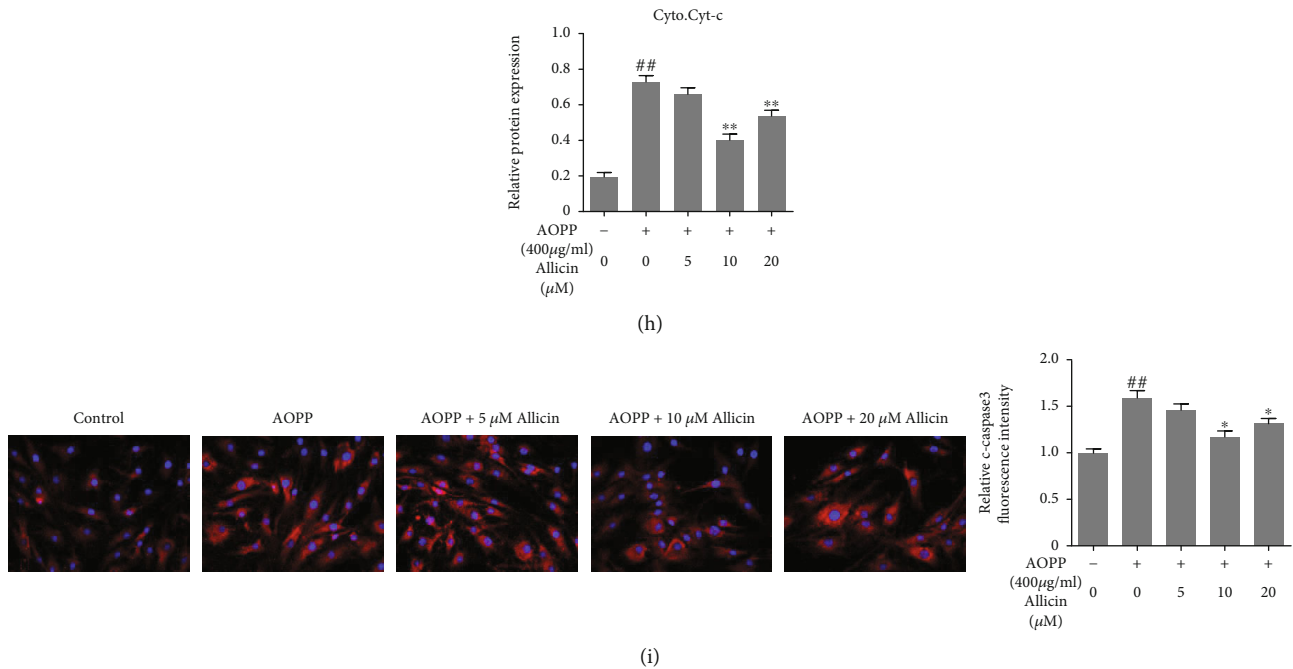


FIGURE 3: Allicin treatment alleviated AOPP-induced human NP cell apoptosis. (a) The human NP cells were pretreated with various concentrations of allicin (0, 5, 10, and 20 μM) for 2 h, followed by stimulation with 400 $\mu\text{g}/\text{ml}$ AOPP for 24 h. And the rate of cell apoptosis was detected by flow cytometry with Annexin V-FITC/PI dual staining. The proportion of apoptotic cells in the first and fourth quadrant was measured for analysis. (b–h) The protein levels of Bax, Bcl-2, c-caspase 3, c-caspase 9, mitochondrial Cyt-c, and cytoplasmic Cyt-c were determined using Western blotting analysis (b) and quantified in (c–h). (i) Representative images of immunofluorescence staining for cleaved caspase-3 in each group, with the relative fluorescence intensity quantified. Original magnification: $\times 400$. Data were represented as mean \pm SD. ^{##} $p < 0.01$ versus the control group; ^{*} $p < 0.05$ and ^{**} $p < 0.01$ versus the AOPP alone treatment group, $n = 3$.

MTP was decreased markedly due to AOPP stimulation, while allicin pretreatment could attenuate this damage to some extent (Figure 4(e)). In summary, allicin pretreatment attenuated oxidative stress and mitochondrial dysfunction induced by AOPP in NP cells.

3.6. Allicin Protected against AOPP Mediated Oxidative Stress and Mitochondrial Apoptosis via Suppressing the p38-MAPK Pathway. Activation of MAPK pathways constitutes a key component in oxidative stress-associated apoptosis [38]. To ascertain the signaling pathway underlying apoptosis of NP cells stimulated by AOPP, Western blotting was performed to appraise the levels of MAPK subfamilies: p38, p-p38, ERK, p-ERK, JNK, and p-JNK. The results showed that AOPP treatment markedly increased the expression of all the above proteins associated with MAPK pathways (Figures 5(a)–5(d)). Therefore, MAPK signaling pathways might play an important role in AOPP-induced apoptosis of human NP cells. Next, we detected the levels of activated MAPK pathways in allicin-pretreated groups. Unsurprisingly, allicin pretreatment suppressed the activation of these MAPK pathways, with the best performance in 10 μM allicin group. Then, the p38 inhibitor SB202190, the JNK inhibitor SP600125, and the ERK inhibitor SCH772984 were used to validate the activation of MAPK pathways. NP cells were pretreated, respectively, with allicin (10 μM), SB202190 (10 μM), SP600125 (10 μM), and SCH772984 (10 μM) for 2 h, before being treated with AOPP for 24 h. Compared with AOPP-treated group, in SB202190-treated group, we observed pro-

moted proliferation, decreased level of ROS, downregulated cleaved caspase-3, and partial recovery of MTP, and these effects resembled the allicin-treated group (Figures 6(a)–6(d)). The inhibited expression of p38 or p-p38 in SB202190-treated group was corroborated by Western blot (Figure S1(a), (b)). However, parts of such protective effects were not found in SP600125- or SCH772984-treated groups, where the cell viability, apoptosis rate, and relative ROS levels of NP cells resembled that of the AOPP alone treatment group (Figure S2). In summary, AOPP induced oxidative stress and activated mitochondrial apoptosis in NP cells via activation of p38-MAPK pathway, while allicin could exert protective effects against AOPP by inhibition of such signaling pathway.

3.7. p38-MAPK Agonist Could Block the Effects of Allicin on AOPP-Induced Oxidative Stress and Mitochondrial Apoptosis. To further examine whether inhibited p38-MAPK pathway actually functioned in allicin-mediated protection against AOPP-induced oxidative stress and mitochondrial apoptosis, the p38-MAPK activator Dehydrocorydaline chloride (Dc) was used. The human NP cells were pretreated with allicin (10 μM) or allicin (10 μM) in combination with Dc (500 nM) for 2 h, and then treated with AOPP (400 $\mu\text{g}/\text{ml}$) for 24 h. The restrained cell proliferation, promoted apoptosis, ROS generation, and decrease of MTP induced by AOPP were mitigated to varying degrees in allicin pretreatment group, while these protective effects of allicin were markedly blocked by p38-MAPK agonist Dc

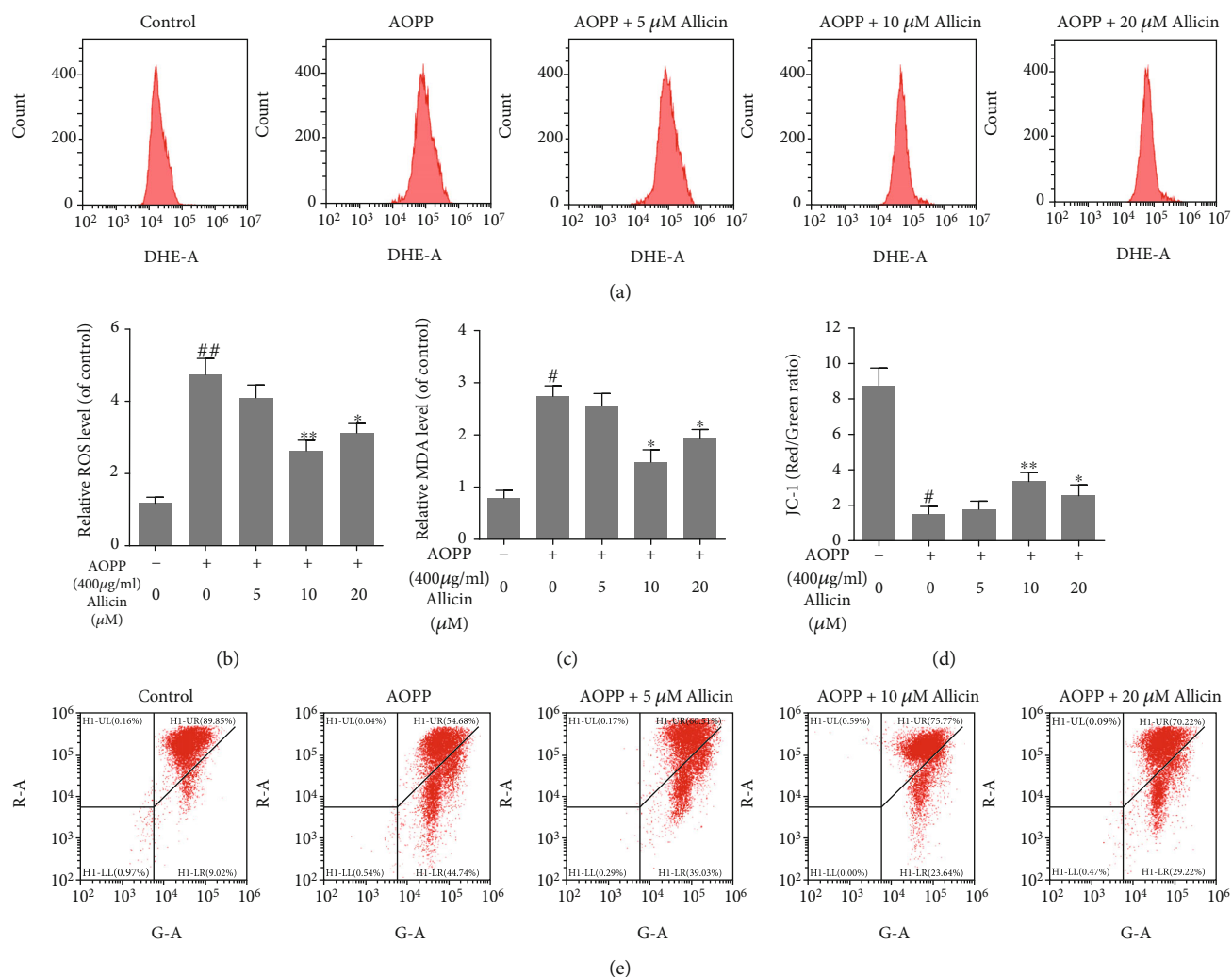


FIGURE 4: Allicin treatment inhibited AOPP-induced oxidative stress and mitochondrial dysfunction of human NP cells. (a, b) The human NP cells were pretreated with different concentrations of allicin (0, 5, 10, and 20 μ M) for 2 h, before treatment with 400 μ g/ml AOPP for 24 h. The intracellular ROS levels of the NP cells for each group were detected by ROS-specific fluorescent probe DHE and measured by subsequent flow cytometry analysis. Representative peak charts of flow cytometry and relative quantitative analysis were shown. (c) The intracellular MDA levels (as a marker of lipid peroxidation) of human NP cells were examined by a commercial kit. (d, e) The mitochondrial membrane potential of human NP cells in each group was examined by JC-1 staining and measured by subsequent flow cytometry analysis. The quantitative analysis of the ratio of red fluorescence (y axis) to green fluorescence (x axis) and representative scatter plots of flow cytometry were shown. Data were represented as mean \pm SD. [#] p < 0.05 and ^{##} p < 0.01 versus the control group; ^{*} p < 0.05 and ^{**} p < 0.01 versus the AOPP alone treatment group, n = 3.

(Figure 7). In short, inhibition of the p38-MAPK pathway was an important avenue mediating the effect of allicin on AOPP-induced oxidative stress and mitochondrial apoptosis.

4. Discussion

LBP is a cosmopolitan problem that has become not only a medical issue, but also a socioeconomic burden in contemporary society [39]. IDD is the main contributor to LBP [40]. Although many efforts have been made to alleviate the symptoms of IDD, valid pharmacotherapy to inhibit IDD progression is still missing, possibly due to an insufficient understanding of its etiology [17, 41]. As a joint outcome of various initiators, abnormal apoptosis of NP cells has been

widely detected in degenerative discs and is considered one of the most common pathogenetic mechanisms of IDD [9]. In fact, the extent of apoptosis of cells in regressive disc specimens is 53%~73%, as reported previously [42].

Apoptotic pathways include the death receptor (also called the extrinsic) pathway and the mitochondrial (also called the intrinsic) pathway [43]. Cytochrome-c release, apoptotic body formation, and activating the caspase cascade are necessary components of the mitochondrial apoptotic pathway, which can be initiated by diverse factors including intracellular oxidative stress [44]. A newly described marker of oxidative stress in the serum is represented by AOPP, a group of protein products that contain dityrosine residues and are produced by oxidants, such as hypochlorous acid

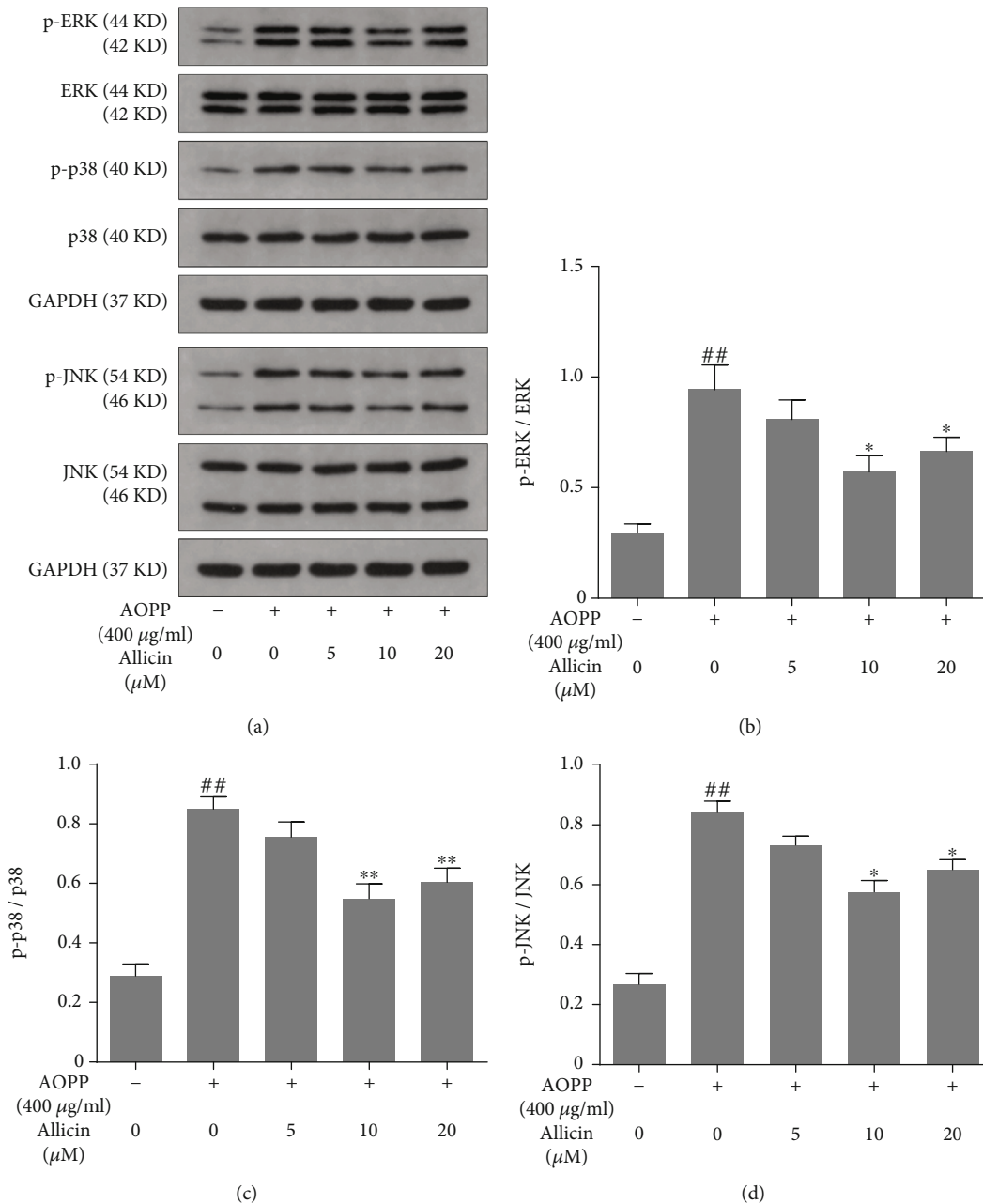


FIGURE 5: Effects of allicin on AOPP-induced MAPK pathway activation. (a) The human NP cells were pretreated with various concentrations of allicin (0, 5, 10, and 20 μM) for 2 h, followed by stimulation with 400 μg/ml AOPP for 24 h. The protein levels of ERK, phosphorylated ERK, p38, phosphorylated p38, JNK, and phosphorylated JNK were determined using Western blotting analysis. (b–d) Immunoblot bands corresponded to (b) p-ERK, (c) p-p38, and (d) p-JNK were quantified by densitometric analysis and normalized to their corresponding total kinase. Data were represented as mean ± SD. ^{##} $p < 0.01$ versus the control group; ^{*} $p < 0.05$ and ^{**} $p < 0.01$ versus the AOPP alone treatment group, $n = 3$.

and chloramines secreted by activated neutrophils [45, 46]. However, recent studies have shown that AOPP are not only biomarkers of oxidative stress, but also a new type of oxidative pathogenic mediator [17]. To date, AOPP have been reported to be involved in several diseases, including progressive nephropathies and neuroinflammation, via a redox-dependent way [47, 48]. For example, a previous study showed that extracellular accumulation of AOPP triggered the production of ROS and induced apoptosis of dorsal root

ganglion neurons [49]. However, it has not yet been elucidated whether the accumulation of AOPP can lead to apoptosis of human NP cells, which plays a key role in the pathogenesis of IDD. In the present study, we found disparities of the AOPP levels in between healthy (Pfirrmann I or II) and degenerated (Pfirrmann IV or V) human NP tissues. The levels of AOPP in the degenerated specimens were much higher than that in the healthy samples, which might suggest a pathogenic function of AOPP in IDD progression.

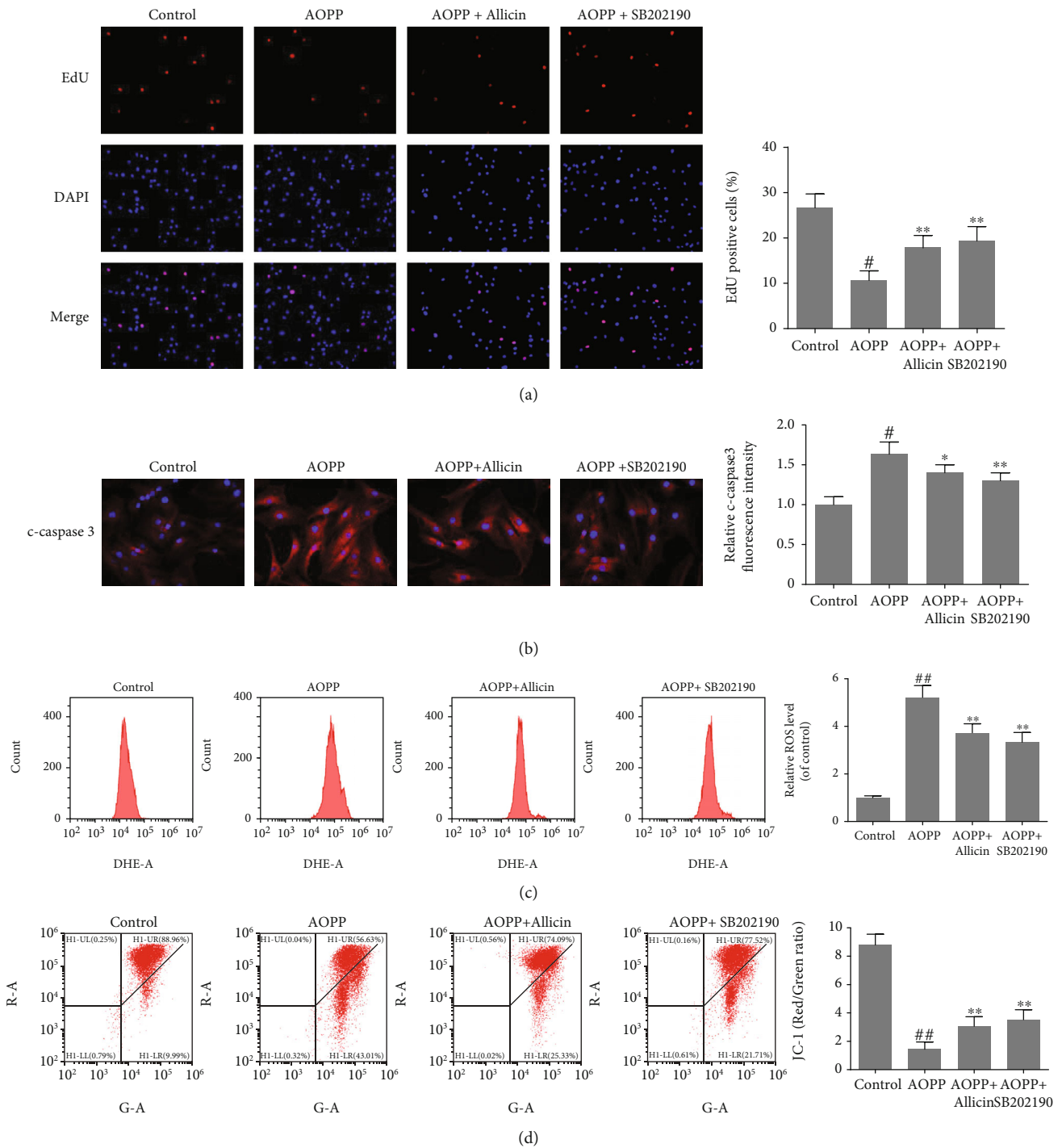


FIGURE 6: Allicin alleviated AOPP-induced oxidative stress and mitochondrial dysfunction via p38-MAPK pathway in human NP cells. (a) The human NP cells were pretreated with allicin (10 μ M) or p38-MAPK inhibitor SB202190 (10 μ M) for 2 h, then treated with AOPP (400 μ g/ml) for 24 h. The cell proliferation was determined using EdU staining combined with DAPI staining for the nuclei under fluorescence microscope, with the EdU positive cells quantitated. Original magnification: \times 200. (b) Representative images of immunofluorescence staining for cleaved caspase-3 in each group, with the relative fluorescence intensity quantified. Original magnification: \times 400. (c) The intracellular ROS levels of the NP cells for each group were detected by ROS-specific fluorescent probe DHE and measured by subsequent flow cytometry analysis. (d) The mitochondrial membrane potential of human NP cells in each group was examined by JC-1 staining and measured by subsequent flow cytometry analysis. Representative scatter plots of flow cytometry and the quantitative analysis of red fluorescence to green fluorescence ratio were shown. Data were represented as mean \pm SD. [#] $p < 0.05$ and ^{##} $p < 0.01$ versus the control group; ^{*} $p < 0.05$ and ^{**} $p < 0.01$ versus the AOPP alone treatment group, $n = 3$.

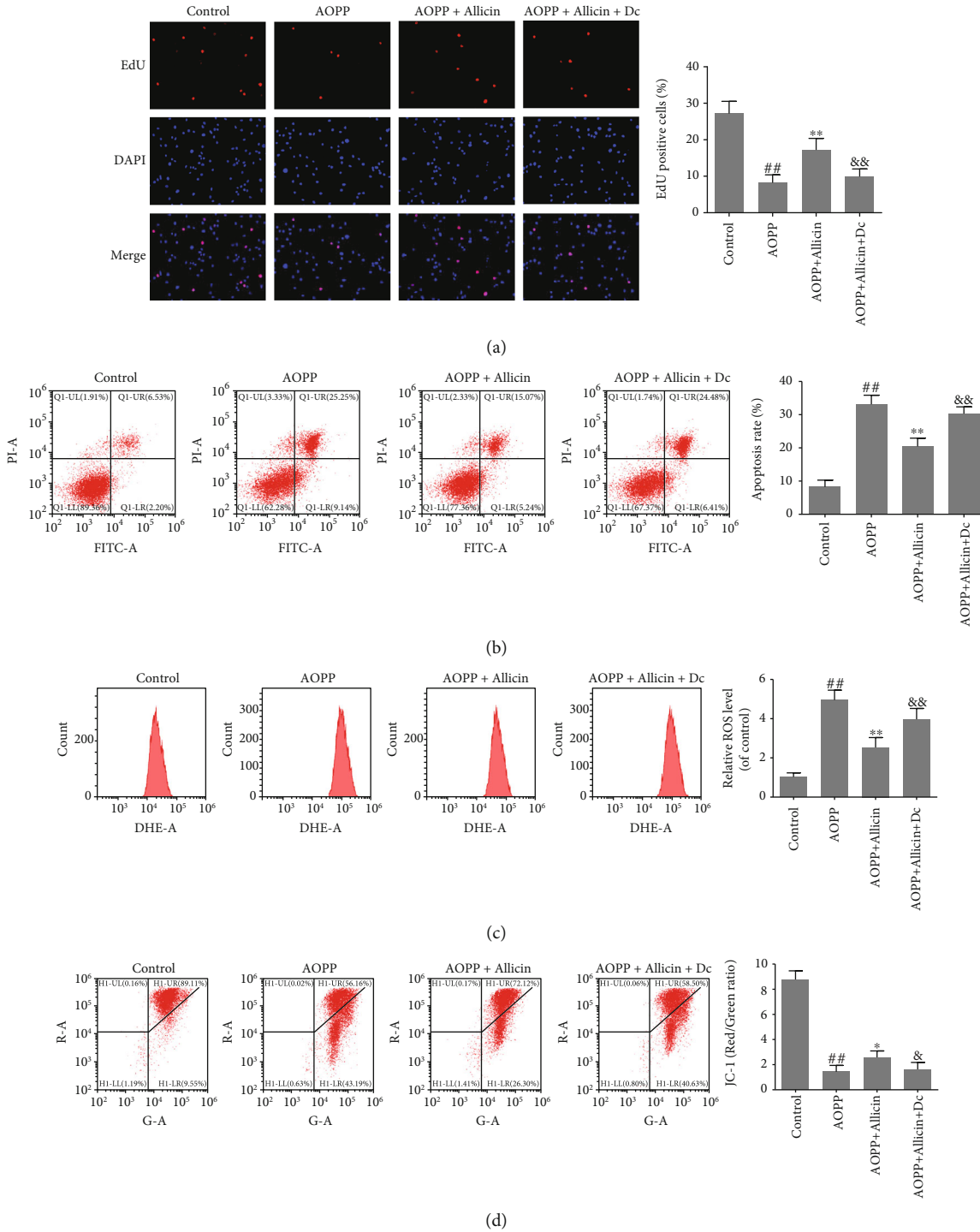


FIGURE 7: Allicin alleviated AOPP-induced oxidative stress and mitochondrial dysfunction via p38-MAPK pathway in human NP cells. (a) The human NP cells were pretreated with allicin (10 μ M) or allicin (10 μ M) in combination with p38-MAPK activator Dehydrocorydaline chloride (Dc, 500 nM) for 2 h, then treated with AOPP (400 μ g/ml) for 24 h. The cell proliferation was determined by EdU staining combined with DAPI staining for the nuclei under fluorescence microscope, with the EdU positive cells quantitated. Original magnification: $\times 200$. (b) The cell apoptosis rate was detected by flow cytometry with Annexin V-FITC/PI dual staining. The proportion of apoptotic cells in the first and fourth quadrant was measured for analysis. (c) The intracellular ROS levels for each group were detected by ROS-specific fluorescent probe DHE and measured by subsequent flow cytometry analysis. (d) The mitochondrial membrane potential of human NP cells in each group was examined by JC-1 staining and measured by subsequent flow cytometry analysis. Data were represented as mean \pm SD. ## $p < 0.01$ versus the control group, * $p < 0.05$ and ** $p < 0.01$ versus the AOPP alone treatment group, and &# $p < 0.05$ and && $p < 0.01$ versus the AOPP+allicin treatment group, $n = 3$.

To explore the effects of AOPP on IDD, we separated NP cells from the healthy samples for further research. For the human NP cell isolation, since excessive time of digestion may be harmful to the cell viability, we chopped the NP tissue into small pieces to digest faster [50, 51]. In addition, a noteworthy difficulty for us in primarily culturing human NP cells was contamination, and the combined use of penicillin and streptomycin effectively prevented microbial contamination in the cell culture. Next, we exposed well-grown human NP cells of second passage to different levels of AOPP and assessed cell viability, proliferation, and apoptosis using the CCK-8 assay, EDU staining, and flow cytometry, respectively. The results showed that AOPP restrained the activity and proliferation of NP cells in both concentration- and time-dependent manners and promoted cell apoptosis.

After treating NP cells with AOPP, we detected the overexpression of proapoptotic proteins, including Bax, cytochrome-c, cleaved caspase-9, and cleaved caspase-3, while the level of the antiapoptotic protein, Bcl-2, was downregulated. This might be related to impaired mitochondrial function. Moreover, previous research found that AOPP could augment the level of ROS by activating NADPH oxidase, thus inducing preosteoblast apoptosis [19]. A leading source of cellular oxidative stress, ROS, is mainly derived from mitochondria, being generated in the electron transport chain [52, 53]. Previous studies indicated that excess ROS increased the Bax/Bcl-2 ratio and damaged key intracellular targets, such as the mitochondrial membrane, thereby promoting apoptosis through the mitochondrial apoptotic pathway [52, 54, 55]. In the prophase of mitochondrial apoptosis, the mitochondrial membrane is oxidatively damaged after attack by ROS, resulting in enhanced mitochondrial outer membrane permeability and a decreased MTP [56–58]. Moreover, ROS overproduction also increases Bax/Bcl-2 ratio, which can further impair the mitochondrial membrane and decrease the MTP [55]. Depolarization of the MTP, as a characteristic change in the forefront of apoptosis, contributes to the release of apoptosis-inducing factor and cytochrome-c from mitochondria, which in turn triggers the activation of caspase-9 and caspase-3, and the subsequent cascade of caspases, leading to the irreversible process of apoptosis [57, 59–62]. Therefore, our results indicated that AOPP might trigger the mitochondrial apoptosis pathway.

To further explore the mechanism underlying apoptosis, we first measured the intracellular levels of two main indicators of oxidative stress after treatment of NP cells with AOPP: ROS and malondialdehyde (MDA), a specific marker for lipid oxidation. As expected, the levels of both compounds were elevated, demonstrating the existence of AOPP-induced oxidative stress in NP cells. Then, we measured the MTP using the cationic fluorescent indicator, JC-1. The results showed depolarization of the MTP, suggesting mitochondrial dysfunction. A recent study targeting human chondrocytes revealed that AOPP could cause mitochondrial dysfunction in a ROS-dependent manner and induce apoptosis, in line with our findings [37].

As a natural compound extracted from garlic bulbs, allicin has been shown to exert potent antioxidant properties and is thus used as an antioxidant agent for the treatment

of many diseases [63]. Previous studies have shown that allicin can reduce ROS levels, abate lipid peroxidation, and protect cells from apoptosis [28, 30, 64, 65]. Considering the prominent antioxidant properties of allicin, we conjectured that it could antagonize AOPP-induced oxidative injury to NP cells and inhibit apoptosis. Therefore, we used AOPP as an oxidative source and explored the function of allicin. NP cells were pretreated with different levels of allicin before exposure to high concentrations of AOPP (400 $\mu\text{g/ml}$). Compared with the AOPP alone treatment group, allicin-pretreated NP cells exhibited less apoptosis and a lower Bax/Bcl-2 ratio, as well as reduced expression of apoptosis-related proteins including cleaved caspase-3 and -9 and cytochrome-c, demonstrating that allicin could mitigate AOPP-induced apoptosis of NP cells.

We also measured the intracellular levels of ROS and MDA, which were decreased in allicin-pretreated groups compared with the AOPP alone treatment group. This supported the antioxidative capability of allicin. In addition, by measuring MTP, we showed that AOPP-induced mitochondrial damage in NP cells was attenuated in the allicin-pretreated groups. Overall, our results showed that allicin could mitigate AOPP-induced oxidative stress and activation of the mitochondrial apoptosis pathway through its antioxidative properties in human NP cells, consistent with the results of Hong et al. [66] who discovered that allicin abated acrylamide-induced oxidative stress in BRL-3A cells. However, it is possible that these results do not represent the intracorporal effect of allicin, whose elucidation requires further experiments.

Mitogen-activated protein kinase (MAPK) signaling pathways are important avenues for apoptosis. MAPK is comprised of three chief subgroups: p38-MAPK, extracellular signal-regulated kinase (ERK), and c-Jun N-terminal kinase (JNK) [67]. Previous studies have shown that the MAPK pathway is significantly involved in cell proliferation, differentiation, and apoptosis and can be activated by various inflammatory cytokines and cellular stressors, such as ultraviolet rays, DNA damage, and oxidative stress [68, 69]. In particular, ROS engendered by NADPH oxidase are potent MAPK activators [70, 71]. Therefore, we choose to assess these primary members of the MAPK family to ascertain the signaling pathway underlying AOPP-induced apoptosis in NP cells and the protective role of allicin. The NP cells were treated with high levels of AOPP (400 $\mu\text{g/ml}$) before determining the levels of p38, ERK, JNK, and their phosphorylation forms. All three MAPK subfamilies were significantly activated by AOPP administration. According to previous studies, it is of note that p38-MAPK signaling pathway could also be activated in a time-dependent manner by various factors, such as LPS, TNF- α , and IL-1 β [72, 73]. A similar assay was performed following treatment with different concentrations of allicin for 2 h, and then with the highest level of AOPP (400 $\mu\text{g/ml}$) for 24 h. Notably, we observed concentration-dependent inhibition of all the three MAPK pathways in the allicin-pretreated groups. Afterwards, p38 inhibitor SB202190, JNK inhibitor SP600125, and ERK inhibitor SCH772984 were used to validate the pathway involved in AOPP-induced apoptosis of NP cells and in the

antagonistic effect of allicin against AOPP. It was of note that though all MAPK subfamilies were activated, the protective function against AOPP was found only when the p38, but not the JNK or ERK, was inhibited. The extent of apoptosis and the levels of ROS of the SB202190-treated group were significantly lower than that of the AOPP alone treatment group and were similar with that of allicin-treated group. Correspondingly, our results of Western blotting showed that the expression of p38 or p-p38 was decreased by allicin pretreatment. Next, we used the p38-MAPK activator Dc to further validate the role of inhibited p38-MAPK pathway in allicin-mediated protection against AOPP-induced oxidative stress and mitochondrial apoptosis. In the case of levels of apoptosis, MTP, ROS, and cell proliferation, the allicin and Dc combined pretreatment group was much closer to AOPP alone treatment group than the allicin alone pretreatment group, suggesting that the anti-AOPP effects of allicin were blocked by Dc. In summary, our experimental results revealed that allicin could mitigate AOPP-induced oxidative stress and mitochondrial apoptosis in NP cells by inhibiting activation of the p38-MAPK pathway.

In conclusion, our findings provide new insights into the etiology of apoptosis in NP cells and, more importantly, suggest that allicin may be a novel remedy to mitigate the progression of IDD. However, there are a few limitations to our study. Because all our observations were based on in vitro experiments, further research is required to validate these findings in vivo. In addition, because the use of allicin as a multifunctional medicine has a long history, its protective role in NP cells may also involve other mechanisms. Indeed, a prior study showed that allicin could mitigate the dexamethasone-induced abnormal expression of cytochrome-c, c-caspase 3, c-caspase 9, Bax, and Bcl-2 through activating the PI3K/AKT pathway, and thus rescued apoptosis of osteoblasts induced by dexamethasone in rats [74]. Another study revealed that allicin attenuated age-related cognitive dysfunction through activating Nrf2 antioxidant signaling pathways [75]. Therefore, further investigations focusing on molecular mechanisms are required to shed light on the anti-apoptotic function of allicin against AOPP in NP cells.

Recently, the comparability between 3D culture in hypoxia and IVD microenvironment aroused our interest. The NP cells mainly obtain oxygen and nutrients through the osmosis of the cartilage endplate (CEP). During IDD, unexplained calcification of the CEP usually blocks this effect and helps to form hypoxic areas. Therefore, NP cells in IDD are likely to be hypoxic. In a 2D monolayer, all cells are exposed to the gas phase, but the internal area of the 3D culture is usually limited by diffusion, leading to hypoxia and necrosis [76]. Similarly, the distribution of NP cells is also 3D due to the thickness of IVD, which means that the internal cells are more prone to be anoxic than the cells close to the CEP. Therefore, 3D culture in hypoxia can better mimic the microenvironment in native IVDs. In addition, studies have shown that hypoxia can also influence intracellular oxidative stress. For example, exposure to hypoxia could restrict the generation of ROS in NP cells and inhibit apoptosis [77–79]. It can be inferred that hypoxia, a nonignorable variable in the human IVD, might have an impact on our

research and change the existing experimental results of AOPP. Hence, applying 3D culture in hypoxia might better reflect the actual level of oxidative stress and apoptosis induced by AOPP in human NP cells. It is also helpful to better determine the pharmacodynamic curve of allicin for that the antioxidative function of allicin might be attenuated by hypoxia. Therefore, we are very interested in 3D culture under hypoxic conditions and hope to determine the effects of AOPP on NP cells in this context, which inspired our follow-up research. At the same time, more investigations in the future are needed to uncover the role of oxidative stress in IDD by using 3D culture in hypoxia.

Abbreviations

AOPP:	Advanced oxidation protein products
LBP:	Low back pain
IVD:	Intervertebral disc
IDD:	Intervertebral disc degeneration
NP:	Nucleus pulposus
ECM:	Extracellular matrix
AF:	Annulus fibrosus
MAPK:	Mitogen-activated protein kinase
ERK:	Extracellular signal-regulated kinase
JNK:	c-Jun N-terminal kinase
ROS:	Reactive oxygen species
DHE:	Dihydroethidium
MDA:	Malondialdehyde
MTP:	Mitochondrial transmembrane potential.

Data Availability

The data used to support the findings of this study were included within the article.

Conflicts of Interest

The authors reported no conflict of interest.

Authors' Contributions

Qian Xiang, Zhangrong Cheng, and Juntan Wang contributed equally to this work.

Acknowledgments

This study was supported by the grants from the National Natural Science Foundation of China (81772391, 81974348, and 81902260).

Supplementary Materials

Supplementary Figure S1: allicin alleviated AOPP-induced oxidative stress and mitochondrial dysfunction via p38-MAPK pathway. Supplementary Figure S2: allicin alleviated AOPP-induced oxidative stress and mitochondrial dysfunction via p38-MAPK pathway. Supplementary Figure S3: the schematic diagram illustrating that allicin attenuated AOPP-induced oxidative stress and mitochondrial apoptosis in human NP cells. (*Supplementary Materials*)

References

- [1] T. Vos, A. A. Abajobir, K. H. Abate et al., "Global, regional, and national incidence, prevalence, and years lived with disability for 328 diseases and injuries for 195 countries, 1990–2016: a systematic analysis for the Global Burden of Disease Study 2016," *The Lancet*, vol. 390, no. 10100, pp. 1211–1259, 2017.
- [2] R. Buchbinder, M. van Tulder, B. Öberg et al., "Low back pain: a call for action," *Lancet*, vol. 391, no. 10137, pp. 2384–2388, 2018.
- [3] S. Yang, F. Zhang, J. Ma, and W. Ding, "Intervertebral disc ageing and degeneration: the antiapoptotic effect of oestrogen," *Ageing Research Reviews*, vol. 57, article 100978, 2020.
- [4] D. Sakai and S. Grad, "Advancing the cellular and molecular therapy for intervertebral disc disease," *Advanced Drug Delivery Reviews*, vol. 84, pp. 159–171, 2015.
- [5] C. Q. Zhao, L. M. Wang, L. S. Jiang, and L. Y. Dai, "The cell biology of intervertebral disc aging and degeneration," *Ageing Research Reviews*, vol. 6, no. 3, pp. 247–261, 2007.
- [6] X. Wu, Z. Liao, K. Wang et al., "Targeting the IL-1 β /IL-1Ra pathways for the aggregation of human islet amyloid polypeptide in an ex vivo organ culture system of the intervertebral disc," *Experimental & Molecular Medicine*, vol. 51, no. 9, pp. 1–16, 2019.
- [7] A. Slinsky, D. Barnes, and J. M. Pipas, "Simian virus 40 large T antigen J domain and Rb-binding motif are sufficient to block apoptosis induced by growth factor withdrawal in a neural stem cell line," *Journal of Virology*, vol. 73, no. 8, pp. 6791–6799, 1999.
- [8] Z. Zhai, N. Ha, F. Papagiannouli et al., "Antagonistic regulation of apoptosis and differentiation by the cut transcription factor represents a tumor-suppressing mechanism in *Drosophila*," *PLoS Genetics*, vol. 8, no. 3, article e1002582, 2012.
- [9] Z. Gao, Y. Lin, P. Zhang et al., "Sinomenine ameliorates intervertebral disc degeneration via inhibition of apoptosis and autophagy in vitro and in vivo," *American Journal of Translational Research*, vol. 11, no. 9, pp. 5956–5966, 2019.
- [10] Y. H. Cheng, S. H. Yang, C. C. Liu, A. Gefen, and F. H. Lin, "Thermosensitive hydrogel made of ferulic acid-gelatin and chitosan glycerophosphate," *Carbohydrate Polymers*, vol. 92, no. 2, pp. 1512–1519, 2013.
- [11] R. Luo, Z. Liao, Y. Song et al., "Berberine ameliorates oxidative stress-induced apoptosis by modulating ER stress and autophagy in human nucleus pulposus cells," *Life Sciences*, vol. 228, pp. 85–97, 2019.
- [12] Z. Zhang, L. Rong, and Y. P. Li, "Flaviviridae viruses and oxidative stress: implications for viral pathogenesis," *Oxidative Medicine and Cellular Longevity*, vol. 2019, Article ID 1409582, 17 pages, 2019.
- [13] E. Chierito, A. Simon, F. Castoldi et al., "Mechanical stretch of high magnitude provokes axonal injury, elongation of paranodal junctions, and signaling alterations in oligodendrocytes," *Molecular Neurobiology*, vol. 56, no. 6, pp. 4231–4248, 2019.
- [14] M. L. Stama, E. Lacivita, L. N. Kirpotina et al., "Functional N-formyl peptide receptor 2 (FPR2) antagonists based on the ureidopropanamide scaffold have potential to protect against inflammation-associated oxidative stress," *ChemMedChem*, vol. 12, no. 22, pp. 1839–1847, 2017.
- [15] V. Witko-Sarsat, M. Friedlander, C. Capeillère-Blandin et al., "Advanced oxidation protein products as a novel marker of oxidative stress in uremia," *Kidney International*, vol. 49, no. 5, pp. 1304–1313, 1996.
- [16] F. Xie, S. Sun, A. Xu et al., "Advanced oxidation protein products induce intestine epithelial cell death through a redox-dependent, c-jun N-terminal kinase and poly (ADP-ribose) polymerase-1-mediated pathway," *Cell Death & Disease*, vol. 5, no. 1, p. e1006, 2014.
- [17] S. Sun, F. Xie, X. Xu et al., "Advanced oxidation protein products induce S-phase arrest of hepatocytes via the ROS-dependent, β -catenin-CDK2-mediated pathway," *Redox Biology*, vol. 14, pp. 338–353, 2018.
- [18] R. Qi and C. Yang, "Renal tubular epithelial cells: the neglected mediator of tubulointerstitial fibrosis after injury," *Cell Death & Disease*, vol. 9, no. 11, 2018.
- [19] S. Y. Zhu, J. S. Zhuang, Q. Wu et al., "Advanced oxidation protein products induce pre-osteoblast apoptosis through a nicotinamide adenine dinucleotide phosphate oxidase-dependent, mitogen-activated protein kinases-mediated intrinsic apoptosis pathway," *Aging Cell*, vol. 17, no. 4, article e12764, 2018.
- [20] L. L. Zhou, W. Cao, C. Xie et al., "The receptor of advanced glycation end products plays a central role in advanced oxidation protein products-induced podocyte apoptosis," *Kidney International*, vol. 82, no. 7, pp. 759–770, 2012.
- [21] C. R. Liao, S. N. Wang, S. Y. Zhu et al., "Advanced oxidation protein products increase TNF- α and IL-1 β expression in chondrocytes via NADPH oxidase 4 and accelerate cartilage degeneration in osteoarthritis progression," *Redox Biology*, vol. 28, article 101306, 2020.
- [22] G. Hou, H. Lu, M. Chen, H. Yao, and H. Zhao, "Oxidative stress participates in age-related changes in rat lumbar intervertebral discs," *Archives of Gerontology and Geriatrics*, vol. 59, no. 3, pp. 665–669, 2014.
- [23] A. Tekari, S. C. W. Chan, D. Sakai, S. Grad, and B. Gantenbein, "Angiopoietin-1 receptor Tie2 distinguishes multipotent differentiation capability in bovine coccygeal nucleus pulposus cells," *Stem Cell Research & Therapy*, vol. 7, no. 1, 2016.
- [24] M. A. Dkhil, D. Delic, H. A. El Enshasy, and A. E. Abdel Monem, "Medicinal plants in therapy: antioxidant activities," *Oxidative Medicine and Cellular Longevity*, vol. 2016, Article ID 7468524, 2016.
- [25] S. Hayat, Z. Cheng, H. Ahmad, M. Ali, X. Chen, and M. Wang, "Garlic, from remedy to stimulant: evaluation of antifungal potential reveals diversity in phytoalexin allicin content among garlic cultivars; allicin containing aqueous garlic extracts trigger antioxidants in cucumber," *Frontiers in Plant Science*, vol. 7, 2016.
- [26] L. Wang, H. Jiao, J. Zhao, X. Wang, S. Sun, and H. Lin, "Allicin alleviates reticuloendotheliosis virus-induced immunosuppression via ERK/mitogen-activated protein kinase pathway in specific pathogen-free chickens," *Frontiers in Immunology*, vol. 8, 2017.
- [27] R. T. M. Alam, E. M. Fawzi, M. I. Alkhalaf, W. S. Alansari, L. Aleya, and M. M. Abdel-Daim, "Anti-inflammatory, Immunomodulatory, and antioxidant activities of allicin, norfloxacin, or their combination against *Pasteurella multocida* infection in male New Zealand rabbits," *Oxidative Medicine and Cellular Longevity*, vol. 2018, Article ID 1780956, 10 pages, 2018.
- [28] M. Zhang, H. Pan, Y. Xu, X. Wang, Z. Qiu, and L. Jiang, "Allicin decreases lipopolysaccharide-induced oxidative stress and inflammation in human umbilical vein endothelial cells through suppression of mitochondrial dysfunction and

- activation of Nrf2,” *Cellular Physiology and Biochemistry*, vol. 41, no. 6, pp. 2255–2267, 2017.
- [29] C. Liu, F. Cao, Q. Z. Tang et al., “Allicin protects against cardiac hypertrophy and fibrosis via attenuating reactive oxygen species-dependent signaling pathways,” *The Journal of Nutritional Biochemistry*, vol. 21, no. 12, pp. 1238–1250, 2010.
- [30] M. M. Abdel-Daim, O. E. Kilany, H. A. Khalifa, and A. A. M. Ahmed, “Allicin ameliorates doxorubicin-induced cardiotoxicity in rats via suppression of oxidative stress, inflammation and apoptosis,” *Cancer Chemotherapy and Pharmacology*, vol. 80, no. 4, pp. 745–753, 2017.
- [31] M. L. Circu and T. Y. Aw, “Reactive oxygen species, cellular redox systems, and apoptosis,” *Free Radical Biology & Medicine*, vol. 48, no. 6, pp. 749–762, 2010.
- [32] L. Shi, H. Qin, X. Jin et al., “The natural phenolic piperobtusin A induces apoptosis of lymphoma U937 cells via the Caspase dependent and p38 MAPK signaling pathways,” *Biomedicine & Pharmacotherapy*, vol. 102, pp. 772–781, 2018.
- [33] Y. Song, S. Li, W. Geng et al., “Sirtuin 3-dependent mitochondrial redox homeostasis protects against AGEs-induced intervertebral disc degeneration,” *Redox Biology*, vol. 19, pp. 339–353, 2018.
- [34] M. Hanasand, R. Omdal, K. B. Norheim, L. G. Gøransson, C. Brede, and G. Jonsson, “Improved detection of advanced oxidation protein products in plasma,” *Clinica Chimica Acta*, vol. 413, no. 9–10, pp. 901–906, 2012.
- [35] X. Zhang, Y. Kang, T. Huo et al., “GL-V9 induced upregulation and mitochondrial localization of NAG-1 associates with ROS generation and cell death in hepatocellular carcinoma cells,” *Free Radical Biology & Medicine*, vol. 112, pp. 49–59, 2017.
- [36] J. Wang, M. Nisar, C. Huang et al., “Small molecule natural compound agonist of SIRT3 as a therapeutic target for the treatment of intervertebral disc degeneration,” *Experimental & Molecular Medicine*, vol. 50, no. 11, pp. 1–14, 2018.
- [37] W. Ye, S. Zhu, C. Liao et al., “Advanced oxidation protein products induce apoptosis of human chondrocyte through reactive oxygen species-mediated mitochondrial dysfunction and endoplasmic reticulum stress pathways,” *Fundamental & Clinical Pharmacology*, vol. 31, no. 1, pp. 64–74, 2017.
- [38] K. Wang, B. Chen, T. Yin et al., “N-Methylparoxetine Blocked autophagic flux and induced apoptosis by activating ROS-MAPK pathway in non-small cell lung Cancer Cells,” *International Journal of Molecular Sciences*, vol. 20, no. 14, p. 3415, 2019.
- [39] D. Lin, P. Alberton, M. Delgado Caceres et al., “Loss of tenomodulin expression is a risk factor for age-related intervertebral disc degeneration,” *Aging Cell*, vol. 19, no. 3, p. e13091, 2020.
- [40] J. N. Katz, “Lumbar disc disorders and low-back pain: socioeconomic factors and consequences,” *The Journal of Bone and Joint Surgery. American*, vol. 88, Supplement 2, p. 21, 2006.
- [41] P. H. Wu, H. S. Kim, and I. T. Jang, “Intervertebral disc diseases PART 2: a review of the current diagnostic and treatment strategies for intervertebral disc disease,” *International Journal of Molecular Sciences*, vol. 21, no. 6, p. 2135, 2020.
- [42] J. W. Chen, B. B. Ni, B. Li, Y. H. Yang, S. D. Jiang, and L. S. Jiang, “The responses of autophagy and apoptosis to oxidative stress in nucleus pulposus cells: implications for disc degeneration,” *Cellular Physiology and Biochemistry*, vol. 34, no. 4, pp. 1175–1189, 2014.
- [43] S. Nagata, “Apoptosis by death factor,” *Cell*, vol. 88, no. 3, pp. 355–365, 1997.
- [44] S. Deegan, S. Saveljeva, S. E. Logue et al., “Deficiency in the mitochondrial apoptotic pathway reveals the toxic potential of autophagy under ER stress conditions,” *Autophagy*, vol. 10, no. 11, pp. 1921–1936, 2014.
- [45] C. Capeillère-Blandin, V. Gausson, B. Descamps-Latscha, and V. Witko-Sarsat, “Biochemical and spectrophotometric significance of advanced oxidized protein products,” *Biochimica et Biophysica Acta*, vol. 1689, no. 2, pp. 91–102, 2004.
- [46] I. Sadowska-Bartosz, S. Galiniak, G. Bartosz, and M. Rachel, “Oxidative modification of proteins in pediatric cystic fibrosis with bacterial infections,” *Oxidative Medicine and Cellular Longevity*, vol. 2014, Article ID 389629, 10 pages, 2014.
- [47] W. Cao, F. F. Hou, and J. Nie, “AOPPs and the progression of kidney disease,” *Kidney International. Supplement*, vol. 4, no. 1, pp. 102–106, 2014.
- [48] Z. Liu, X. Yao, W. Jiang et al., “Advanced oxidation protein products induce microglia-mediated neuroinflammation via MAPKs-NF- κ B signaling pathway and pyroptosis after secondary spinal cord injury,” *Journal of Neuroinflammation*, vol. 17, no. 1, 2020.
- [49] R. Ding, B. Sun, Z. Liu et al., “Advanced oxidative protein products cause pain hypersensitivity in rats by inducing dorsal root ganglion neurons apoptosis via NADPH oxidase 4/c-Jun N-terminal kinase pathways,” *Frontiers in Molecular Neuroscience*, vol. 10, 2017.
- [50] X. Feng, L. Liu, B. Q. Yu, J. M. Huang, L. D. Gu, and D. F. Xu, “Effect of optimized collagenase digestion on isolated and cultured nucleus pulposus cells in degenerated intervertebral discs,” *Medicine*, vol. 97, no. 44, article e12977, 2018.
- [51] Q. Xiang, L. Kang, J. Wang et al., “CircRNA-CIDN mitigated compression loading-induced damage in human nucleus pulposus cells via miR-34a-5p/SIRT1 axis,” *eBioMedicine*, vol. 53, article 102679, 2020.
- [52] M. Schieber and N. S. Chandel, “ROS function in redox signaling and oxidative stress,” *Current Biology*, vol. 24, no. 10, pp. R453–R462, 2014.
- [53] D. B. Zorov, M. Juhaszova, and S. J. Sollott, “Mitochondrial reactive oxygen species (ROS) and ROS-induced ROS release,” *Physiological Reviews*, vol. 94, no. 3, pp. 909–950, 2014.
- [54] D. Trachootham, J. Alexandre, and P. Huang, “Targeting cancer cells by ROS-mediated mechanisms: a radical therapeutic approach?,” *Nature Reviews. Drug Discovery*, vol. 8, no. 7, pp. 579–591, 2009.
- [55] B. Zhang, X. Zhang, C. Zhang, Q. Shen, G. Sun, and X. Sun, “Notoginsenoside R1 protects db/db mice against diabetic nephropathy via upregulation of Nrf2-mediated HO-1 expression,” *Molecules*, vol. 24, no. 2, p. 247, 2019.
- [56] K. J. Kinghorn, J. I. Castillo-Quan, F. Bartolome et al., “Loss of PLA2G6 leads to elevated mitochondrial lipid peroxidation and mitochondrial dysfunction,” *Brain*, vol. 138, no. 7, pp. 1801–1816, 2015.
- [57] J. D. Ly, D. R. Grubb, and A. Lawen, “The mitochondrial membrane potential ($\Delta\psi(m)$) in apoptosis; an update,” *Apoptosis*, vol. 8, no. 2, pp. 115–128, 2003.
- [58] Y. Tan, Y. Jin, Q. Wang, J. Huang, X. Wu, and Z. Ren, “Perilipin 5 protects against cellular oxidative stress by enhancing mitochondrial function in HepG2 cells,” *Cells*, vol. 8, no. 10, p. 1241, 2019.
- [59] N. Zamzami, P. Marchetti, M. Castedo et al., “Sequential reduction of mitochondrial transmembrane potential and

- generation of reactive oxygen species in early programmed cell death." *The Journal of Experimental Medicine*, vol. 182, no. 2, pp. 367–377, 1995.
- [60] M. C. Maiuri, E. Zalckvar, A. Kimchi, and G. Kroemer, "Self-eating and self-killing: crosstalk between autophagy and apoptosis," *Nature Reviews. Molecular Cell Biology*, vol. 8, no. 9, pp. 741–752, 2007.
- [61] D. R. Green and G. Kroemer, "The pathophysiology of mitochondrial cell death," *Science*, vol. 305, no. 5684, pp. 626–629, 2004.
- [62] W. Hu and J. J. Kavanagh, "Anticancer therapy targeting the apoptotic pathway," *The Lancet Oncology*, vol. 4, no. 12, pp. 721–729, 2003.
- [63] J. Borlinghaus, F. Albrecht, M. C. Gruhlke, I. D. Nwachukwu, and A. J. Slusarenko, "Allicin: chemistry and biological properties," *Molecules*, vol. 19, no. 8, pp. 12591–12618, 2014.
- [64] S. Chen, Y. Tang, Y. Qian et al., "Allicin prevents H₂O₂-induced apoptosis of HUVECs by inhibiting an oxidative stress pathway," *BMC Complementary and Alternative Medicine*, vol. 14, no. 1, 2014.
- [65] J. Y. Chan, A. C. Yuen, R. Y. Chan, and S. W. Chan, "A review of the cardiovascular benefits and antioxidant properties of allicin," *Phytotherapy Research*, vol. 27, no. 5, pp. 637–646, 2013.
- [66] Y. Hong, B. Nan, X. Wu, H. Yan, and Y. Yuan, "Allicin alleviates acrylamide-induced oxidative stress in BRL-3A cells," *Life Sciences*, vol. 231, article 116550, 2019.
- [67] J. Yue and J. M. López, "Understanding MAPK signaling pathways in apoptosis," *International Journal of Molecular Sciences*, vol. 21, no. 7, p. 2346, 2020.
- [68] Q. Liu, B. Tao, G. Liu et al., "Thromboxane A₂ receptor inhibition suppresses multiple myeloma cell proliferation by inducing p38/c-Jun N-terminal kinase (JNK) mitogen-activated protein kinase (MAPK)-mediated G₂/M progression delay and cell apoptosis," *The Journal of Biological Chemistry*, vol. 291, no. 9, pp. 4779–4792, 2016.
- [69] J. D. Ashwell, "The many paths to p38 mitogen-activated protein kinase activation in the immune system," *Nature Reviews. Immunology*, vol. 6, no. 7, pp. 532–540, 2006.
- [70] Y. Son, Y. K. Cheong, N. H. Kim, H. T. Chung, D. G. Kang, and H. O. Pae, "Mitogen-activated protein kinases and reactive oxygen species: how can ROS activate MAPK pathways?," *Journal of Signal Transduction*, vol. 2011, Article ID 792639, 6 pages, 2011.
- [71] K. W. Zeng, F. J. Song, Y. H. Wang et al., "Induction of hepatoma carcinoma cell apoptosis through activation of the JNK-nicotinamide adenine dinucleotide phosphate (NADPH) oxidase-ROS self-driven death signal circuit," *Cancer Letters*, vol. 353, no. 2, pp. 220–231, 2014.
- [72] L. Li, J. Hu, T. He et al., "P38/MAPK contributes to endothelial barrier dysfunction via MAP4 phosphorylation-dependent microtubule disassembly in inflammation-induced acute lung injury," *Scientific Reports*, vol. 5, no. 1, 2015.
- [73] N. Tang, Y. P. Zhang, W. Ying, and X. X. Yao, "Interleukin-1 β upregulates matrix metalloproteinase-13 gene expression via c-Jun N-terminal kinase and p38 MAPK pathways in rat hepatic stellate cells," *Molecular Medicine Reports*, vol. 8, no. 6, pp. 1861–1865, 2013.
- [74] J. Zhan, Z. Yan, M. Zhao et al., "Allicin inhibits osteoblast apoptosis and steroid-induced necrosis of femoral head progression by activating the PI3K/AKT pathway," *Food & Function*, vol. 11, no. 9, pp. 7830–7841, 2020.
- [75] X. H. Li, C. Y. Li, J. M. Lu, R. B. Tian, and J. Wei, "Allicin ameliorates cognitive deficits ageing-induced learning and memory deficits through enhancing of Nrf2 antioxidant signaling pathways," *Neuroscience Letters*, vol. 514, no. 1, pp. 46–50, 2012.
- [76] K. M. McMahon, M. Volpato, H. Y. Chi et al., "Characterization of changes in the proteome in different regions of 3D multicell tumor spheroids," *Journal of Proteome Research*, vol. 11, no. 5, pp. 2863–2875, 2012.
- [77] J. W. Chen, B. B. Ni, X. F. Zheng, B. Li, S. D. Jiang, and L. S. Jiang, "Hypoxia facilitates the survival of nucleus pulposus cells in serum deprivation by down-regulating excessive autophagy through restricting ROS generation," *The International Journal of Biochemistry & Cell Biology*, vol. 59, pp. 1–10, 2015.
- [78] L. B. Jiang, L. Cao, Y. Q. Ma et al., "TIGAR mediates the inhibitory role of hypoxia on ROS production and apoptosis in rat nucleus pulposus cells," *Osteoarthritis and Cartilage*, vol. 26, no. 1, pp. 138–148, 2018.
- [79] H. J. Kim, H. R. Lee, H. Kim, and S. H. Do, "Hypoxia helps maintain nucleus pulposus homeostasis by balancing autophagy and apoptosis," *Oxidative Medicine and Cellular Longevity*, vol. 2020, Article ID 5915481, 13 pages, 2020.

Research Article

Overexpression of LMP-1 Decreases Apoptosis in Human Nucleus Pulposus Cells via Suppressing the NF- κ B Signaling Pathway

Yuan Liu ¹, Wei Zhou ², Fei-Fan Chen ¹, Fei Xiao ¹, Hai-Yang Zhu ¹, Yun Zhou,¹
and Guan-Cheng Guo ¹

¹Department of Emergency, The First Affiliated Hospital of Zhengzhou University, 1 Jianshe Road, Zhengzhou City, Henan 450052, China

²Department of Orthopedics, The First Affiliated Hospital of Zhengzhou University, 1 Jianshe Road, Zhengzhou City, Henan 450052, China

Correspondence should be addressed to Yuan Liu; yuan_friend_kang@163.com
and Guan-Cheng Guo; guoquanchengzdyfy@163.com

Received 1 August 2020; Revised 15 November 2020; Accepted 25 November 2020; Published 14 December 2020

Academic Editor: Ji Tu

Copyright © 2020 Yuan Liu et al. This is an open access article distributed under the Creative Commons Attribution License, which permits unrestricted use, distribution, and reproduction in any medium, provided the original work is properly cited.

Intervertebral disc degeneration (IDD) is a prevalent disease characterized by low back pain. Increasing extracellular matrix (ECM) synthesis and decreasing nucleus pulposus cell (NPC) apoptosis are promising strategies to recover degenerated NP. LIM mineralization protein- (LMP-) 1 has anti-inflammatory potential and is a promising gene target for the treatment of NP degeneration. In this study, we measured the expression of LMP-1 in the NP of patients. Then, we constructed LMP-1-overexpressing NPCs using lentiviral vectors and investigated the effects of LMP-1 on cell proliferation, apoptosis, and ECM synthesis in NPCs. The results showed that LMP-1 was highly expressed in the NP of patients. LMP-1 overexpression significantly increased proliferation and decreased apoptosis in NPCs. The expression of collagen II and sulfated glycosaminoglycan (sGAG) in NPCs was also upregulated after LMP-1 was overexpressed. Moreover, we demonstrated that LMP-1 decreased apoptosis of NPCs by inhibiting NF- κ B signaling activation. These findings suggest that LMP-1 plays an essential role in mediating apoptosis in NPCs by regulating NF- κ B signaling and can be used as a gene target for the treatment of IDD.

1. Introduction

Intervertebral disc degeneration (IDD) increases the risk of low back pain and gives risk to a large economic burden [1]. In addition, IDD can result in secondary spinal deformity and spinal canal stenosis [2]. Intervertebral discs (IVDs) are cartilaginous, articulating structures that allow movement of the vertebral column. IVDs form a very complex system, with an outer anulus fibrosus surrounding a central nucleus pulposus (NP) and cartilaginous endplates located between the IVDs and the adjacent vertebral column [3]. Although NP cell (NPC) dysfunction and the consequent extracellular matrix (ECM) degradation are thought to be the cause of IDD, the pathogenesis of IDD is still unknown [4].

The acidic environment in the NP, which is caused by the accumulation of cell waste products and degraded matrix molecules, affects the function and viability of NPCs [5]. Inflammation plays an important role in IDD, and the inflammatory response is related to the apoptosis and dysfunction of NPCs [6]. The acidic environment increases the mRNA expression levels of inflammatory and catabolic genes in NPCs and leads to inflammation, matrix degradation, oxidative stress responses, and apoptosis during IDD [7, 8]. Anti-inflammatory therapy is a promising method for treating and mitigating IDD. Phytochemicals extracted from medicinal plants and small molecules are widely used for IDD treatment for their anti-inflammatory and antioxidative properties [9–11]. However, these drugs can only partly

alleviate the inflammatory response in the NP and have low efficiency for treating NP degeneration.

Genetic engineering is highly efficient in modulating the function and viability of cells [12]. With genetic engineering, we can improve the viability and ECM synthesis function of NPCs to regenerate degenerated NP. LIM mineralization protein- (LMP-) 1 is an intracellular regulator of bone formation [13]. A study has demonstrated that LMP-1 can significantly inhibit lipopolysaccharide- (LPS-) induced nitric oxide production in preosteoclasts [14]. In addition, LMP-1 can maintain ECM production in the NP and inhibit matrix metalloproteinase expression [15, 16]. We think LMP-1 may be a promising gene target for the treatment of NP degeneration. Therefore, the effects of LMP-1 in NPCs should be further studied. We hypothesize that LMP-1 could increase the survival, decrease the apoptosis, and improve the ECM synthesis function of NPCs.

The nuclear factor kappa B (NF- κ B) signaling pathway is important in controlling the inflammatory response [17, 18]. NF- κ B induces the expression of various proinflammatory genes, and deregulated NF- κ B activation contributes to the pathogenic processes of various inflammatory diseases [19]. NF- κ B signaling mediates catabolic and inflammatory responses to inflammatory and mechanical stimulation in IVDs [18]. The downregulation of matrix metalloproteinase expression is related to NF- κ B inhibition [15]. Moreover, LMP-1 inhibits LPS-induced nitric oxide production by suppressing the transcriptional activity of NF- κ B [14]. Therefore, we think that there may be a relationship between LMP-1 and NF- κ B signaling.

In this study, we aimed to demonstrate the effects of LMP-1 on the proliferation, apoptosis, and ECM synthesis of NPCs. We further studied the interaction between LMP-1 and NF- κ B signaling to investigate the underlying mechanisms of cell survival induced by LMP-1. We hope our study will provide new ideas in searching for novel strategies for IDD treatment.

2. Materials and Methods

2.1. Tissue Source. The degenerative NP samples were donated by twenty patients (fifteen patients were 20 to 30 years old, and the other five were 50 to 60 years old). Four 20- to 30-year-old patients suffered burst thoracolumbar fracture and without a previously documented clinical history of IDD donated normal NP samples. The study was approved by the Ethics Committee of The First Affiliated Hospital of Zhengzhou University, and informed consent was obtained from all the patients involved in our study. A magnetic resonance imaging (MRI) scan of the NP was performed for all degenerative patients, and the disc degeneration grade was evaluated according to the Pfirrmann classification [20]. Degenerative NP sample with a Pfirrmann classification at most grade III was involved in our study. Nucleotomy and intervertebral fusion surgery were performed under sterile conditions to obtain the NP samples, and all NP samples used for subsequent experiments were processed within 1 hour after being harvested.

2.2. NPC Isolation and Cultivation. NP samples donated from ten 20- to 30-year-old patients were used to isolate NPCs. The isolation of NPCs was described previously [21]. Briefly, the tissues were washed three times with phosphate-buffered saline (PBS) and cut into small pieces. Next, 0.2% collagenase II (Gibco, Shanghai, China) and 2 U/mL hyaluronidase (Gibco) were used to enzymatically dissociate the tissues for 4 hours at 37°C with gentle shaking. Then, the digested tissues were passed through a 100 μ m mesh filter to remove debris and centrifuged at 1000 rpm for 5 min. The isolated cells were cultured in Dulbecco's modified Eagle's medium (DMEM) supplemented with 10% fetal bovine serum (FBS), 2 mM L-glutamine and antibiotics (1% penicillin-streptomycin) in a humidified incubator at 37°C with 5% CO₂. The complete medium was changed every three days, and cells were harvested with 0.25% trypsin-ethylene diamine tetraacetic acid (EDTA) at confluence 80%. Cells at passage 2 were used for subsequent experiments. NPCs after infection were cultured in an acidic environment with a pH level of 6.8, which was adjusted with sterilized HCl (1 M), to represent mildly degenerated IVD conditions.

2.2.1. Flow Cytometry. After detachment in 0.25% trypsin, the cells were incubated with fluorescein isothiocyanate-(FITC-) conjugated primary antibody (CD45, CD73, and CD90; eBioscience, Shanghai, China) at 4°C for 45 min in the dark. After washing with PBS three times, cells were centrifuged and resuspended in 100 μ L PBS and were detected using a flow cytometer (FACScan, BD Biosciences, San Jose, CA, USA) equipped with the CellQuest software (BD Biosciences). For Annexin V-FITC/propidium iodide (PI) staining, cells were resuspended in 500 μ L binding buffer and treated with 5 μ L Annexin V-FITC and 5 μ L PI (BD Biosciences). After incubated for 15 mins at room temperature, the mixture was detected using a flow cytometer (FACScan).

2.3. Lentiviral Packaging and Cell Infection. Particles from lentiviruses overexpressing LMP-1 (LV-LMP-1, pLV[Exp]-EGFP:T2A:Puro-EF1A > hLMP-1[NM_005451.5]) and lentiviral GFP (LV-control, pLV[Exp]-EGFP:T2A:Puro-Null) were prepared by Cyagen Biosciences. For infections, 40-60% confluent NPCs were incubated with lentiviral particles and polybrene (5 μ g/mL) in medium at a multiplicity of infection of 50 for 12 hours before changing the medium. Three days later, the transfected cells were passaged for use in subsequent experiments. The expression of LMP-1 was determined by real-time quantitative polymerase chain reaction (RT-qPCR) and Western blotting analyses.

2.4. Small Interfering RNA Transfection. Double-stranded small interfering RNA (siRNA) for human LMP-1 gene silencing was designed and chemically synthesized by Sangon Biotech (Shanghai, China). NPCs were transfected with siRNA (50 nM) using Lipofectamine 2000™ transfection reagent (Invitrogen, Shanghai, China) and Opti-MEM (Gibco, Shanghai, China) according to the manufacturer's instructions. After 48 hours of incubation, NPCs with low

TABLE 1: Primers used in quantitative RT-PCR.

Gene	Forward primer (5' to 3')	Reverse primer (5' to 3')
<i>18s</i>	ATCCTCAGTGAGTTCTCCCG	CTTTGCCATCACTGCCATTA
<i>LMP-1</i>	CAGCAGAATGGACAGCCGC	GTCTTGCATGAACTCGGTGC
<i>Acan</i>	AGAATCAAGTGGAGCCGTGT	GGTAGTTGGGCAGTGAGACC
<i>SOX9</i>	AGCGAACGCACATCAAGAC	CTGTAGGCGATCTGTTGGGG
<i>Col2</i>	CATCCCACCCTCTCACAGTT	ACCAGTTAGTTTCTGCCTCTG
<i>Col1</i>	AGTCTGTCTGCGTCCTCTG	TGTTTGGGTCATTTCCACAT

expression of LMP-1 were selected for subsequent experiments.

2.5. Cell Proliferation. Cell proliferation of NPCs was assessed with a cell counting kit-8 (CCK8, Dojindo, Dalian, China). In brief, NPC cells were seeded into a 96-well plate (5000/well). At each time point, the medium was removed, and the cells were treated with 10% CCK8 in 100 μ L DMEM for 3 hours at 37°C. The absorbance of the wells was then measured at 450 nm using a microplate reader (Bio-Rad, Hercules, CA, USA).

2.6. RNA Isolation and RT-qPCR. Total RNA was extracted using an RNAiso reagent (Takara, Shanghai, China) and quantified by measuring the absorbance at 260 nm. Next, 500 ng of RNA was reverse-transcribed to complementary DNA using PrimeScript™ RT Master Mix (Takara). All gene transcripts were quantified by RT-qPCR using Power SYBR Green PCR Master Mix (Takara) on an ABI StepOnePlus System (Applied Biosystems, Warrington, UK). The cycle conditions were as follows: 95°C for 30 s, followed by 40 cycles at 95°C for 5 s and 60°C for 30 s. GAPDH was used as a housekeeping gene, and the data was analyzed using the $2^{-\Delta\Delta CT}$ method. The primer sequences used in this study were synthesized by Sangon Biotech (Table 1).

2.7. Western Blotting Analyses. Protein was extracted from tissue and cell samples by RIPA buffer supplemented with a proteasome inhibitor (Beyotime, China). After sodium dodecyl sulfate-polyacrylamide gel electrophoresis, the proteins were transferred to a polyvinylidene fluoride membrane (Millipore, Shanghai, China) by electroblotting. The membrane was blocked for 2 hours at room temperature in 5% nonfat milk and incubated with primary antibodies specific to LMP-1 (1:2000, Abcam, Shanghai, China), caspase-3 (1:1000, Cell Signaling Technology, Shanghai, China), cleaved-caspase-3 (1:1000, Cell Signaling Technology), Bcl-2 (1:1000, Cell Signaling Technology), Bax (1:1000, Cell Signaling Technology), aggrecan (1:1000, Abcam), SOX9 (1:1000, Abcam), collagen II (1:1000, Abcam), collagen I (1:1000, Abcam), p65 (1:1000, Cell Signaling Technology), phosphor-p65 (1:1000, Cell Signaling Technology), I κ B α (1:1000, Cell Signaling Technology), phosphor-I κ B α (1:1000, Cell Signaling Technology), or GAPDH (1:2000, Cell Signaling Technology) overnight at 4°C. After washing with TBST three times (5 min each), the membranes were incubated with specific horseradish peroxidase-conjugated

secondary antibodies (Beyotime) for 1 hour at room temperature. After washing with TBST three times (5 min each), the blots were then developed using enhanced chemiluminescence (Millipore). Signal intensity was measured using the Bio-Rad XRS chemiluminescence detection system (Bio-Rad).

2.8. Fluorescence Analysis. Each group of NPCs was cultured in 12-well plates. After fixation with 4% paraformaldehyde for 10 min at room temperature, the cells were incubated with 3% H₂O₂ and 0.1% Triton X-100 for 10 min and washed three times with PBS. The terminal deoxynucleotidyl transferase dUTP nick end labeling (TUNEL) method was used for measuring apoptotic DNA fragmentation, and cells were stained with an *in situ* cell death detection kit (Roche Life Science, Shanghai, China) according to the manufacturer's instructions. Nuclei were stained with 4',6-diamidino-2-phenylindole (DAPI, Sigma-Aldrich, Shanghai, China) for 5 min. For immunofluorescence staining, cells were incubated with anticollagen II (1:200, Abcam) and antiaggrecan (1:200, Abcam) antibodies overnight and then incubated with an Alexa Fluor 555-labeled secondary antibody for 1 hour at room temperature in the dark. Nuclei were stained with DAPI for 5 min. The samples were then observed under a fluorescence microscope (Leica, Wetzlar, Germany).

2.9. Alcian Blue Staining. Each group of NPCs was cultured in 6-well plates. After cultivation for 14 days, the cells were fixed with 4% paraformaldehyde for 10 min at room temperature and subsequently washed three times with distilled water. The cells were then incubated with Alcian blue staining solution (Sigma-Aldrich) for 30 min at room temperature, followed by washing three times with distilled water. Three fields of each well were chosen randomly for microscopic observation using an inverted microscope (Leica).

2.9.1. Detection of Cellular ROS. Each group of NPCs was cultured in 12-well plates. After treatment, cells were rinsed and incubated with 5 μ M DCFH-DA (Sigma-Aldrich) in the dark at 37°C for 30 minutes, and then, fluorescence was detected using a fluorescence microscope (Leica).

2.10. Microarray Analysis. Total RNA of cells was extracted using Trizol reagent (Takara) and quantified using a Nanodrop ND-2000 (Thermo Scientific, Shanghai, China). Total RNA was purified with a QIAGEN RNeasy Kit (QIAGEN,

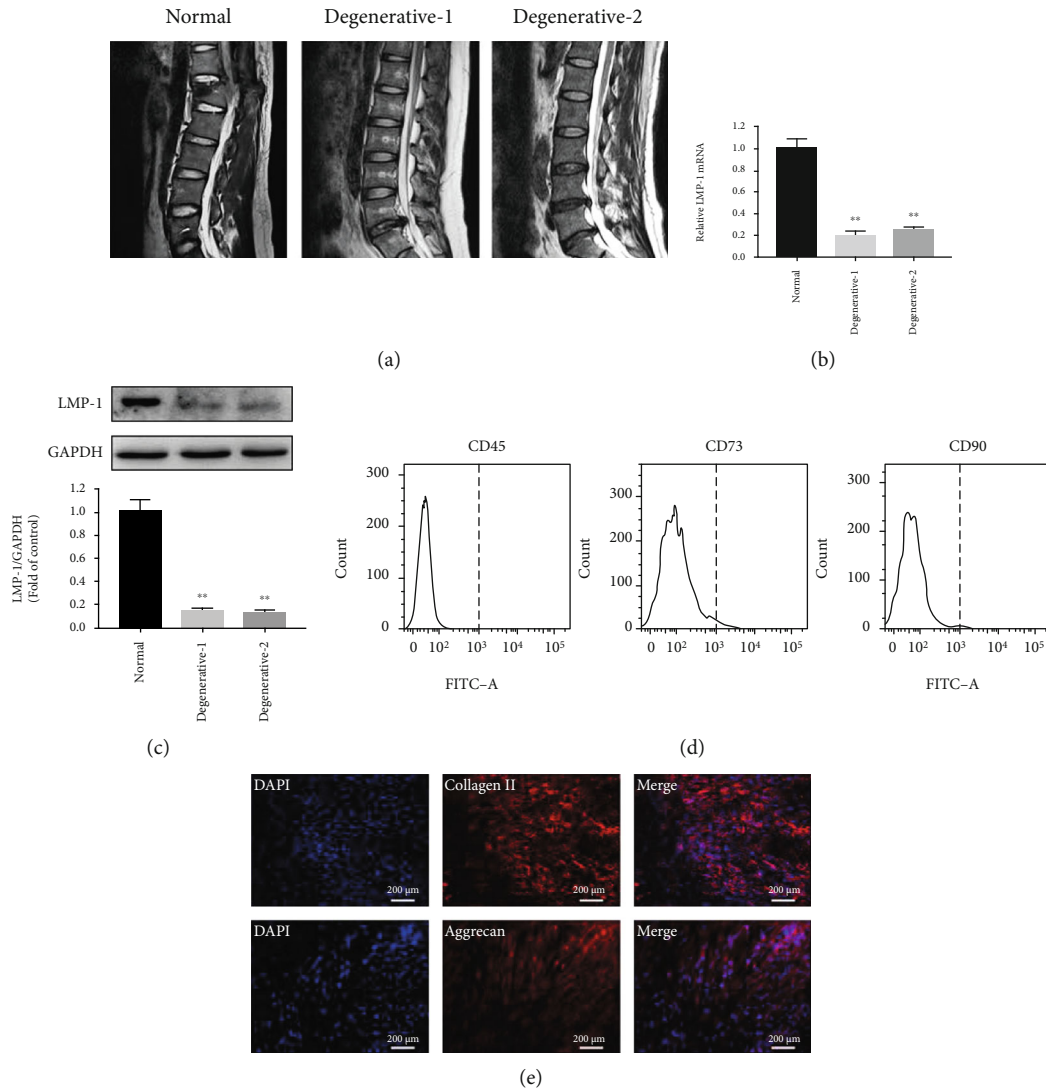


FIGURE 1: Low LMP-1 expression in NP of patients with disc degeneration. (a) Representative T2 signal MRI images of each group. (b) Gene expression levels of LMP-1 in the NP of IDD patients were measured and normalized to 18 s and to the normal group. (c) The protein expression of LMP-1 in each group was measured by western blotting analysis and quantified. (d) CD45, CD73, and CD90 of the isolated cells were detected by flow cytometry. (e) The expression of collagen II and aggrecan of the isolated cells was measured by immunofluorescence staining. The degenerative-1 group represented patients aged from 20 to 30 years old, and the degenerative-2 group represented patients aged from 50 to 60 years old. Data represent mean \pm SD; ** $p < 0.01$ vs. the normal group.

Shanghai, China) and amplified and labeled with Cy-3. After RNA was hybridized at 65°C for 17 h, array images were acquired using Agilent Scanner G5761A (Agilent Technologies) and analyzed using the Agilent Feature Extraction software (version 12.0.1.1). GeneSpring v14.8 software package (Agilent Technologies) was used to perform quantile normalization and subsequent data processing. miRNAs that at least three out of the six samples have flags in detected were chosen for further data analysis. Differentially expressed miRNAs with statistical significance ($p < 0.01$) were identified and conducted by hierarchical cluster analysis. Gene ontology (GO) and Kyoto Encyclopedia of Genes and Genomes (KEGG) enrichment analysis were used to express and indicate the biological function of the differentially expressed miRNAs.

2.11. Animal Experiments. Male Sprague Dawley (SD) rats weighting 250 g were used in animal experiments. All animals were obtained from the Animal Center of Zhengzhou University, and all procedures were approved by the Ethics Committee of The First Affiliated Hospital of Zhengzhou University. All animals were anesthetized with 1% sodium pentobarbital (Sigma-Aldrich). Rat tail disc degeneration model was fabricated by needle puncture of a 20-G sterile needle in the disc of coccygeal vertebrae (Co) 7/Co8 and Co8/Co9 ([22]). After the model were successfully established, a suspension of 1×10^8 TU/mL LV-LMP-1-control or LV-LMP-1-OE (Cyagen Biosciences) was injected into rats in the LMP-1 ctrl and LMP-1 OE groups. The rats with needle puncture and PBS injection were regarded as the degeneration group, and the rats without needle puncture

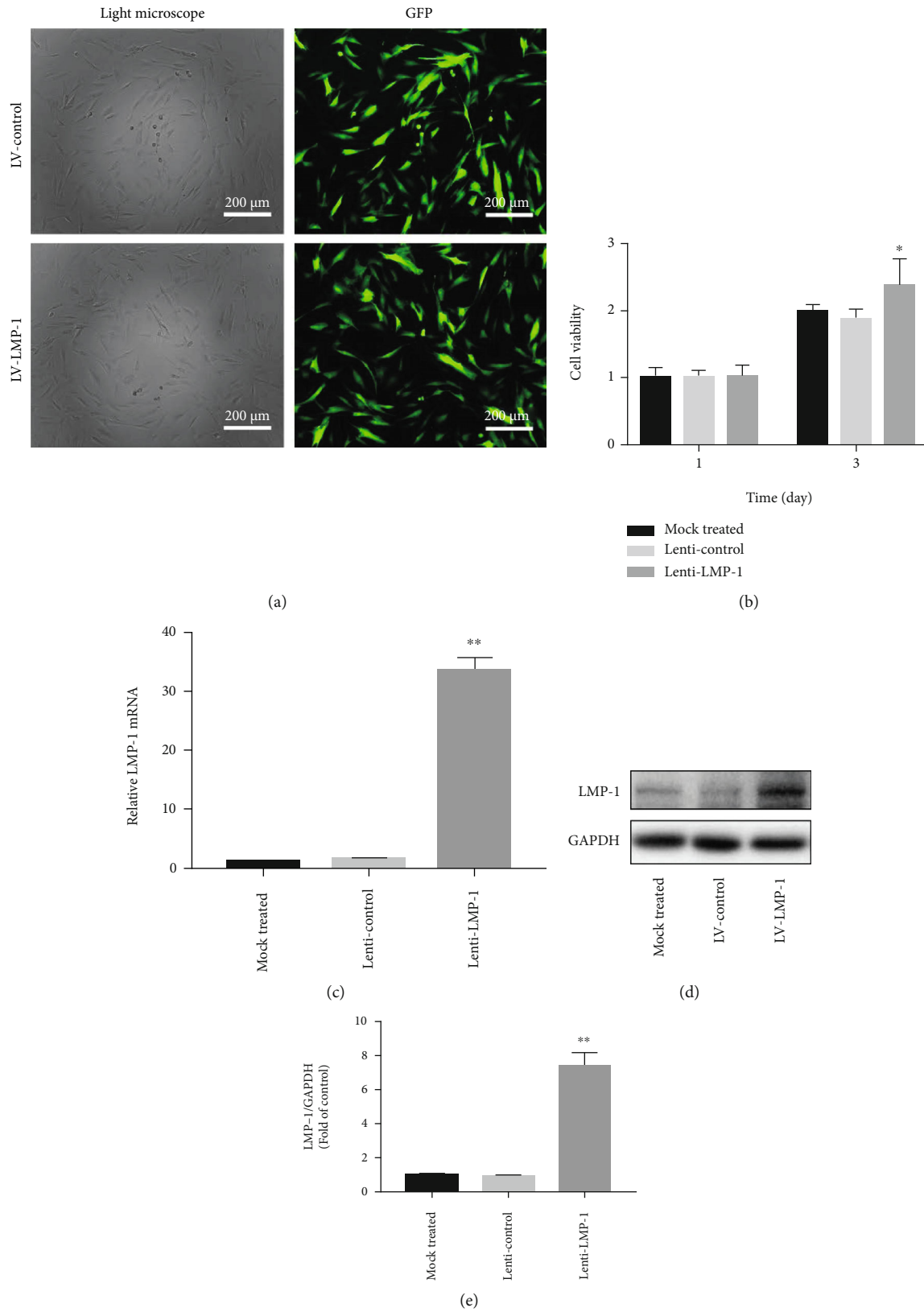


FIGURE 2: The construction of LMP-1 overexpression and lenti-control NPCs. (a) NPCs after lentiviral transfection and puromycin screening were observed under a normal microscope and a fluorescence microscope. (b) Cell viability was measured by CCK-8 on days 1 and 3. (c) The gene expression level of LMP-1 was determined by RT-qPCR and normalized to 18 s. (d) The protein expression of LMP-1 in each group was determined by western blotting analysis. (e) The protein expression of LMP-1 was quantified. Data represent mean \pm SD; * $p < 0.05$, ** $p < 0.01$ vs. the mock treated group. Scale bar = 200 μm .

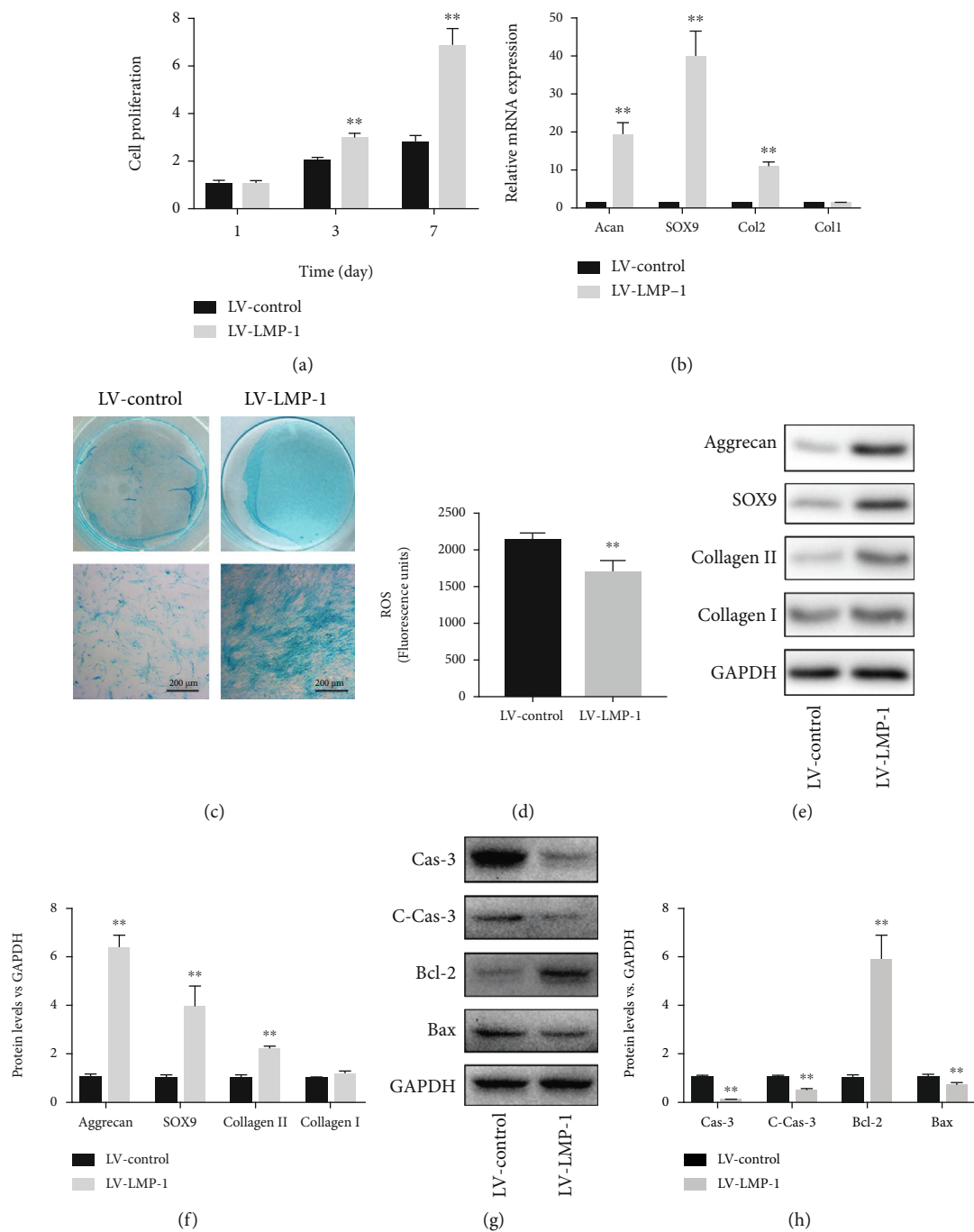


FIGURE 3: Continued.

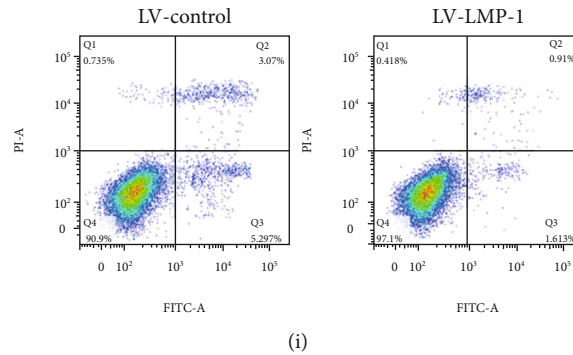


FIGURE 3: LMP-1 overexpression mediated proliferation, ECM synthesis, and apoptosis of NPCs. (a) Cell proliferation of the LV-control and LV-LMP-1 groups was measured on days 1, 3, and 7. (b) Gene expression levels of Acan, SOX9, Col2, and Col1 of NPCs in each group were measured on day 14 and normalized to 18 s. (c) sGAG synthesis by NPCs was observed by Alcian blue staining on days 14. (d) Measurement of intracellular ROS generation in the LV-control and LV-LMP-1 groups using a DCFH-DA probe by fluorometry. (e) The protein expression levels of aggrecan, SOX9, collagen II, and collagen I of NPCs in each group were measured and (f) quantified on day 14. (g) The protein expression levels of caspase-3, cleaved-caspase-3, Bcl-2, and Bax of NPCs in each group were measured and (h) quantified on day 3. (i) Cell apoptosis of each group was detected by PI/Annexin V assays. Data represent mean \pm SD; ** $p < 0.01$ vs. the LV-control group. Scale bar = 200 μ m.

and injection were regarded as the control group. 3 μ L of liquid using a microsyringe with a 31-G needle was injected. The follow-up experiments were conducted 4 weeks after transfection.

2.12. Histological and Biochemical Analysis. Four weeks after the injection, all rats were sacrificed, and the IVD tissues were collected and fixed with 4% paraformaldehyde for 2 days. Then, the tissues were decalcified, embedded in paraffin, and sectioned at a thickness of 4 μ m using a microtome. For histological analysis, hematoxylin and eosin (H&E) and Safranin O-fast green were performed separately on tissue sections. For biochemical analysis, NP tissues of IVDs were lyophilized, and the dry weight was recorded. The contents of sulfate glycosaminoglycans (sGAG) were detected using the Blyscan assay (Biocolor, Beijing, China), and the contents of collagen were detected using the hydroxyproline assay kit (Jiancheng Bioengineering Institute, Nanjing, China) and normalized with dry weight.

2.13. Statistical Analysis. Statistical analyses were performed using SPSS 19.0 (IBM, Armonk, NY, USA). The data are presented as the means \pm standard deviation. Statistical significance was determined using a two-tailed Student's *t*-test when comparing two groups and one-way ANOVA followed by Bonferroni's post hoc test when comparing more than two groups. A value of $p < 0.05$ was considered to be a statistically significant difference. All experiments were performed at least in triplicate.

3. Results

3.1. Low LMP-1 Expression in the NP of Patients with Disc Degeneration. The representative MRI images of the three groups were showed in Figure 1(a). The gene and protein expression levels of LMP-1 were significantly lower in degenerated NP than in normal NP. No significant difference was observed between the two different-age degenerative groups

(Figures 1(b) and 1(c)). CD45, CD73, and CD90 were not detected on the surface of cells (Figure 1(d)). We also detected the expression of collagen II and aggrecan of the isolated cells by immunofluorescence staining and demonstrated that both collagen II and aggrecan were expressed in the cells (Figure 1(e)).

3.2. LMP-1 Overexpression Mediated Proliferation, ECM Synthesis, and Apoptosis of NPCs. We used a lentiviral vector system to efficiently increase the gene expression of LMP-1 in degenerated human NPCs. The efficiency of LMP-1 overexpression was quantified by evaluating the ratio of green fluorescent protein- (GFP-) positive cells to the total number of cells (Figure 2(a)). The viability of NPCs was determined on days 1 and 3 and was not decreased by the operation of transfection (Figure 2(b)). The gene and protein expression levels of LMP-1 were significantly higher in the LV-LMP-1 group than in the nontransfected and LV-control groups (Figures 2(c)–2(e)). The proliferation of NPCs was significantly increased after LMP-1 overexpression at different time points (3 and 7 days) (Figure 3(a)). Acan, SOX9, col2, and col1 are gene markers that indicate ECM synthesis in NPCs. After LMP-1 was overexpressed, the gene expression of Acan (19.25-fold), SOX9 (40.24-fold), and col2 (10.71-fold) was significantly increased (Figure 3(b)). Sulfated glycosaminoglycan (sGAG) deposition of NPCs was observed by Alcian blue staining. Larger areas and deeper staining of Alcian blue were observed in the LV-LMP-1 group compared with those in the LV-control group (Figure 3(c)). The ROS generation was also decreased by LMP-1 overexpression (Figure 3(d)). The protein expression of aggrecan, SOX9, and collagen II was also significantly higher in the LV-LMP-1 group than in the LV-control group. No significant differences were observed in the gene and protein expression levels of collagen I between the two groups (Figures 3(e) and 3(f)). The protein expression of caspase-3, cleaved-caspase-3, and Bax was decreased, while the expression of Bcl-2 was increased after LMP-1 was overexpressed (Figures 3(g) and 3(h)). According

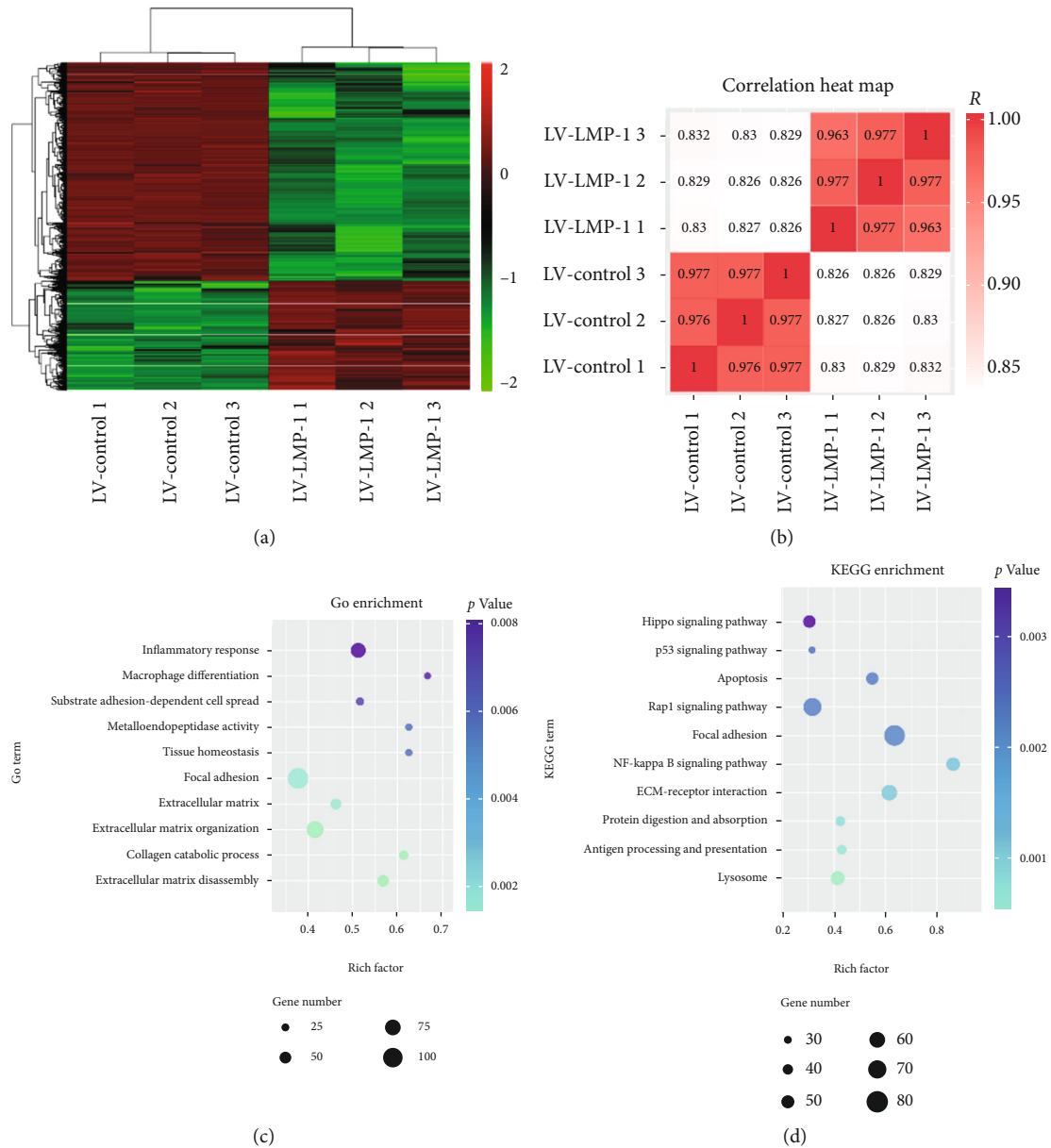


FIGURE 4: The activation of NF- κ B signaling pathway was mediated by LMP-1. (a) The heat map showed differentially expressed miRNAs between the LV-control and LV-LMP-1 groups. (b) Pearson correlation between each sample was expressed by heat map. (c) GO terms with significant p values for biological processes, molecular function, and cellular component. (d) KEGG terms with significant p values were analyzed.

to the flow cytometry results, cell apoptosis was significantly decreased in the LV-LMP-1 group compared with the LV-control group (Figure 3(i)).

3.3. The Activation of NF- κ B Signaling Pathway Was Inhibited by LMP-1. We performed miRNA microarray analysis to search differentially activated signaling pathways between the LV-control and LV-LMP-1 groups. Only miRNAs with a mean fold change > 5 or < 0.2 and a p value < 0.01 were selected for further analysis. Differentially expressed miRNAs and Pearson correlation between samples were presented by heat map (Figures 4(a) and 4(b)). Our results also showed that the GO terms with the most significant p values were related to ECM, ECM organization, ECM

disassembly, and collagen catabolic process, as well as inflammatory response (Figure 4(c)). We further analyzed the potential signaling pathway regulated by LMP-1 and found that NF- κ B signaling pathway was significantly related to LMP-1, which indicated that LMP-1 may affect the inflammatory response in NPCs by mediating the activation of NF- κ B signaling pathway (Figure 4(d)).

3.4. LMP-1 Overexpression Inhibited the Activation of NF- κ B Signaling Pathway. To determine whether the NF- κ B signaling pathway was mediated by LMP-1, we performed Western blotting analyses and quantified the resulting data. The protein expression of total p65 and $\text{I}\kappa\text{B}\alpha$ was not significantly influenced by LMP-1 overexpression. However, the

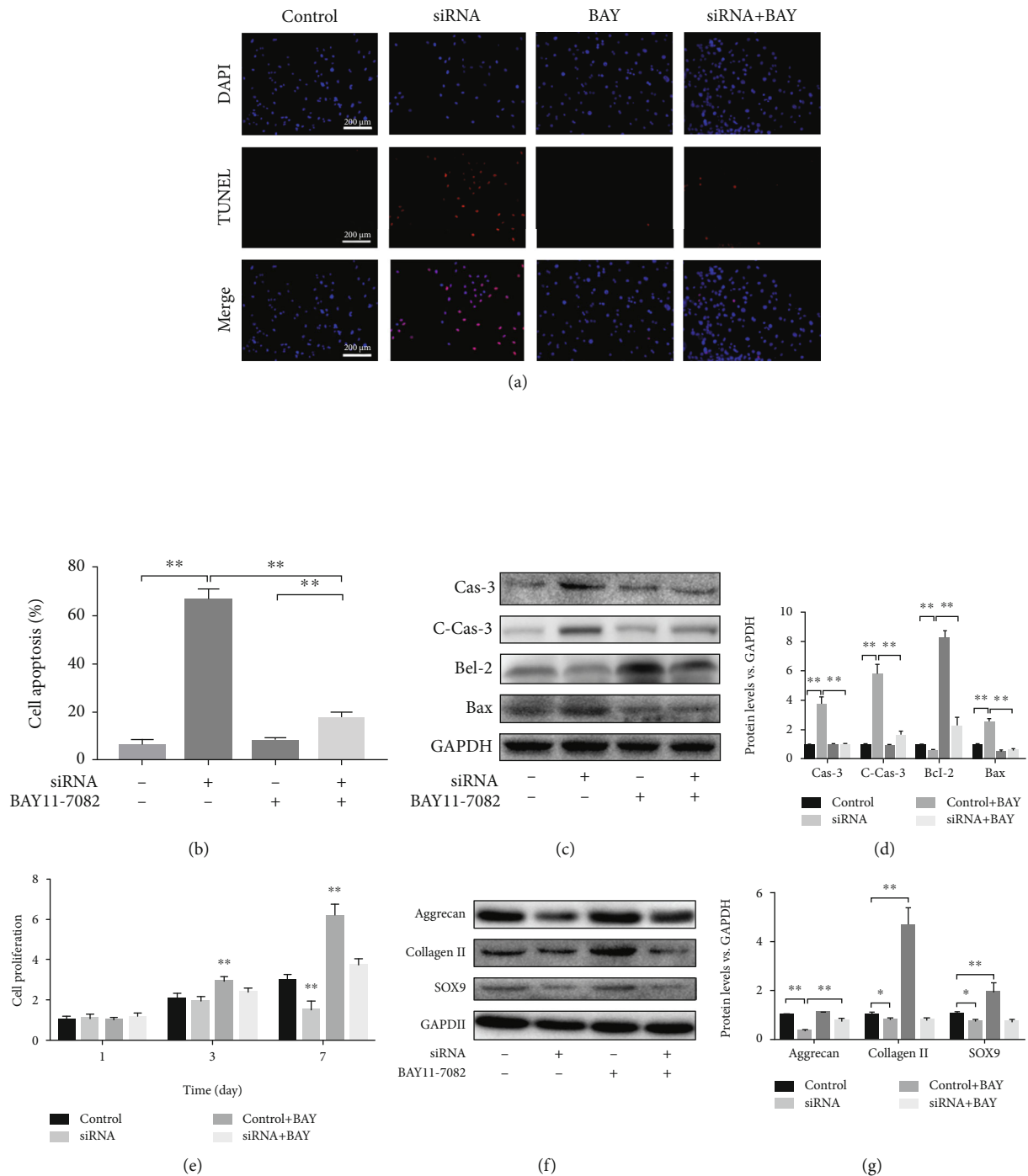


FIGURE 6: LMP-1 silencing increased apoptosis of NPCs by activating the NF- κ B signaling pathway. (a) TUNEL method was performed to measure apoptosis of NPCs (red), and the results were observed by fluorescence. Nuclei (blue) were stained by DAPI. (b) Cell apoptosis was quantified according to the results of TUNEL. ** $p < 0.01$. (c) The protein expression levels of caspase-3, cleaved-caspase-3, Bcl-2, and Bax of NPCs were measured by western blotting analysis on day 3. (d) The protein expression levels of caspase-3, cleaved-caspase-3, Bcl-2, and Bax of NPCs were quantified. ** $p < 0.01$. (e) Cell proliferation on each group was measured by CCK-8 assay on days 1, 3, and 7. ** $p < 0.01$ vs. the control group. (f) The protein expression levels of aggrecan, SOX9, and collagen II of NPCs in each group were measured on day 14 by western blotting analysis. (g) The protein expression levels of aggrecan, SOX9, and collagen II of NPCs were quantified. * $p < 0.05$, ** $p < 0.01$. BAY11-7082 was used as a specific inhibitor of the NF- κ B signaling pathway. Data represent mean \pm SD; scale bar = 200 μ m.

showed the highest contents of sGAG and hydroxyproline among all groups, but no significant difference was observed between the control and LMP-1 OE groups. Both control and

LMP-1 groups showed higher contents of sGAG and hydroxyproline compared with those of the degeneration and LMP-1 ctrl groups (Figures 7(b) and 7(c)).

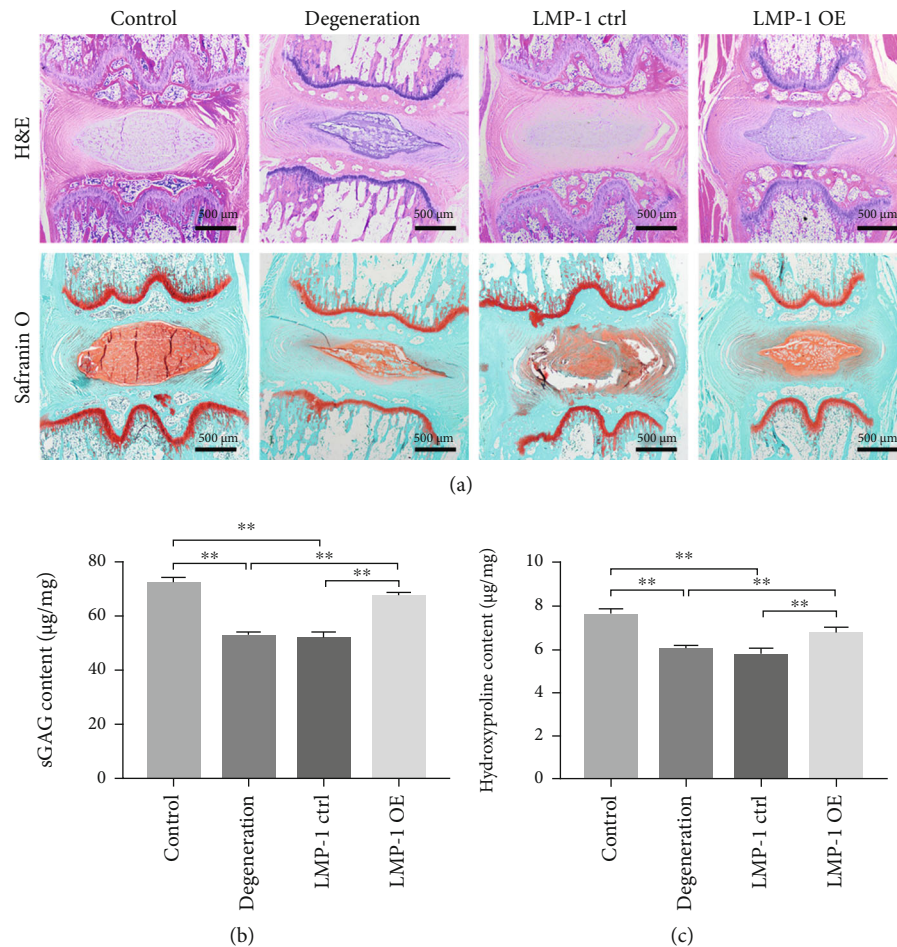


FIGURE 7: LMP-1 overexpression prevented the degeneration of IVDs. (a) Representative H&E and Safranin O staining of discs from different groups were observed. All samples were harvested at 4 weeks after injection. The contents of (b) sGAG and (c) hydroxyproline in each group at 4 weeks after injection were quantified. Data represent mean \pm SEM; ** $p < 0.01$. Scale bar = 500 μ m.

4. Discussion

IVD degeneration is a major public health issue that is caused by NPC dysfunction and apoptosis NPCs [23]. LMP-1 induces antioxidant stress and can maintain ECM production in NPCs [14, 15]. Significantly different expression levels of LMP-1 were observed in healthy and degenerative NP patients. Therefore, the expressions of LMP-1 and NP degeneration are related. In addition, restoring the expression of LMP-1 in degenerative NPCs may decrease apoptosis and improve the ECM synthesis function of NPCs.

A previous study reported that LMP-1 can inhibit cell proliferation and induce apoptosis in osteosarcoma cells [24]. However, Liu et al. showed that LMP-1 has an anti-inflammatory effect and promotes the survival of preosteoclasts [14]. We think this is because the different cell types lead to different effects of LMP-1. The effects of LMP-1 in NPCs have not yet been studied. In this study, we first investigate the role of LMP-1 in the senescence of NP, and no significant difference was observed between patients of different ages. However, we demonstrated the effects of LMP-1 in promoting proliferation and inhibiting apoptosis and intracellular ROS generation in NPCs. The microenvironment of

degenerated discs is characterized by an acidic pH, hypoxia, limited nutrition, high osmolarity, and so on [25]. It is difficult to completely simulate the microenvironment of degenerated IVD. Acidic pH is important in inducing IDD for it can induce inflammatory, matrix degradation, oxidative stress responses, and apoptosis of NPCs [8]. Therefore, we used an acidic environment to simulate NP degeneration, and our results showed that LMP-1 was beneficial for the survival of NPCs in acidic environments. Overexpression of LMP-1 increases cell proliferation and decreases apoptosis in NPCs. Our *in vivo* study also showed that LMP-1 overexpression increased ECM content in NP and hindered the degeneration of IVD.

The molecular mechanism of LMP-1 inhibition of NPC apoptosis is also not yet clear. We used microarray analysis to detect the different biological functions before and after the transfection of LMP-1. Our results demonstrated that ECM synthesis function of NPCs was significantly regulated by LMP-1. In addition, inflammatory response in NPCs was also mediated by LMP-1. We also performed KEGG enrichment to explore potential signaling pathways regulated by LMP-1. NF- κ B signaling showed a high rich factor and low p value in KEGG enrichment. Studies have reported that

NF- κ B signaling is involved in the inflammatory effect and cell apoptosis [26, 27]. p65 and I κ B α are two key elements in NF- κ B signaling [28]. In our study, the phosphorylation of p65 and I κ B α was decreased after LMP-1 was overexpressed and increased after LMP-1 was silenced. In addition, BAY11-7082 decreased the phosphorylation of p65 and I κ B α . Bcl-2 is known as an antiapoptosis protein related to mitochondria, while Bax and caspase 3 are apoptosis-related proteins [29–31]. LMP-1 overexpression decreased the expression of caspase-3 and Bax but increased the expression of Bcl-2. However, LMP-1 silencing yielded the opposite results. Expression of caspase-3, cleaved-caspase-3, and Bax was increased, and Bcl-2 was downregulated. These results indicated that LMP-1 can inhibit the activation of NF- κ B signaling and consequently inhibit the apoptosis of NPCs. Previous studies have already demonstrated that NF- κ B signaling regulates oxidative stress of NPCs by increasing ROS generation [32]. Therefore, we think that the decreased ROS generation of NPCs induced by LMP-1 overexpression was mediated by the inhibition of the NF- κ B signaling pathway.

Our GO enrichment results showed the anabolism and catabolism of ECM were significantly influenced by LMP-1. In this study, we demonstrated the positive effects of LMP-1 in ECM metabolism. We showed that the gene and protein expression levels of aggrecan, SOX9, and collagen II were improved after LMP-1 was overexpressed. Significant sGAG deposition could be observed by Alcian blue staining in the LMP-1 overexpression group. Other researchers have also showed similar conclusions with us that LMP-1 can maintain ECM production in the NP and inhibit matrix metalloproteinase expression [15, 16]. There is a degenerative circle in IDD. Apoptosis and dysfunction in NPCs lead to the loss of collagen II and sGAG in the NP, and the shift in ECM composition changes the biomechanical behavior of IVDs, which further alters the function of NPCs [33]. Therefore, increasing the content of collagen II and sGAG in the NP contributes to breaking the vicious cycle in IDD and is beneficial for NP regeneration.

5. Conclusions

In this study, we demonstrated that the expression level of LMP-1 is clinically related to IDD. We aimed to discover the effects of LMP-1 on the proliferation, apoptosis, and ECM synthesis function of NPCs and found that LMP-1 increases proliferation and ECM synthesis function in NPCs and decreases apoptosis in NPCs. We also investigated the molecular mechanism of LMP-1-mediated apoptosis in NPCs and found that the NF- κ B signaling pathway was inhibited by LMP-1. In addition, our animal experiments demonstrated that LMP-1 overexpression has the ability of preventing the degeneration of IVDs. As a result, we think LMP-1 can be used as a target for slowing the degenerative process and inducing regeneration in IDD. More studies should be carried out to demonstrate the regenerative effects of LMP-1 in vivo before clinical application. Our findings provide a new target for protecting against IDD and inducing regeneration.

Data Availability

The data used to support the findings of this study are available from the corresponding author upon request.

Conflicts of Interest

The authors declare that they have no conflicts of interest.

Authors' Contributions

Yuan Liu, Wei Zhou, and Fei-Fan Chen contributed equally to this work.

Acknowledgments

This study was partly supported by grants from the Joint Construction Project of Henan Medical Science and Technology Research Plan (LHGJ20190172).

References

- [1] A. J. Freemont, "The cellular pathobiology of the degenerate intervertebral disc and discogenic back pain," *Rheumatology (Oxford)*, vol. 48, no. 1, pp. 5–10, 2009.
- [2] D. Sakai, "Future perspectives of cell-based therapy for intervertebral disc disease," *European Spine Journal*, vol. 17, Suppl 4, pp. 452–458, 2008.
- [3] S. Roberts, H. Evans, J. Trivedi, and J. Menage, "Histology and pathology of the human intervertebral disc," *The Journal of Bone and Joint Surgery. American Volume*, vol. 88, Supplement 2, pp. 10–14, 2006.
- [4] J. Antoniou, T. Steffen, F. Nelson et al., "The human lumbar intervertebral disc: evidence for changes in the biosynthesis and denaturation of the extracellular matrix with growth, maturation, ageing, and degeneration," *The Journal of Clinical Investigation*, vol. 98, no. 4, pp. 996–1003, 1996.
- [5] J. P. G. Urban, S. Smith, and J. C. T. Fairbank, "Nutrition of the intervertebral disc," *Spine*, vol. 29, no. 23, pp. 2700–2709, 2004.
- [6] J. G. Burke, R. W. G. Watson, D. McCormack, F. E. Dowling, M. G. Walsh, and J. M. Fitzpatrick, "Intervertebral discs which cause low back pain secrete high levels of proinflammatory mediators," *Journal of Bone and Joint Surgery. British*, vol. 84-B, no. 2, pp. 196–201, 2002.
- [7] W. Yang, X. H. Yu, C. Wang et al., "Interleukin-1 β in intervertebral disk degeneration," *Clinica Chimica Acta*, vol. 450, pp. 262–272, 2015.
- [8] L. Quero, M. Klawitter, A. Schmaus et al., "Hyaluronic acid fragments enhance the inflammatory and catabolic response in human intervertebral disc cells through modulation of toll-like receptor 2 signalling pathways," *Arthritis Research & Therapy*, vol. 15, no. 4, p. R94, 2013.
- [9] H. Huang, S. Cheng, T. Zheng et al., "Vitamin D retards intervertebral disc degeneration through inactivation of the NF- κ B pathway in mice," *American Journal of Translational Research*, vol. 11, no. 4, pp. 2496–2506, 2019.
- [10] X. Su, B. Liu, F. Gong et al., "Isofraxidin attenuates IL-1 β -induced inflammatory response in human nucleus pulposus cells," *Journal of Cellular Biochemistry*, vol. 120, no. 8, pp. 13302–13309, 2019.

- [11] H. Jin, Q. Wang, J. Wu et al., “Baicalein inhibits the IL-1 β -induced inflammatory response in nucleus pulposus cells and attenuates disc degeneration in vivo,” *Inflammation*, vol. 42, no. 3, pp. 1032–1044, 2019.
- [12] A. Nowakowski, P. Walczak, B. Lukomska, and M. Janowski, “Genetic engineering of mesenchymal stem cells to induce their migration and survival,” *Stem Cells International*, vol. 2016, Article ID 4956063, 9 pages, 2016.
- [13] S. D. Boden, Y. Liu, G. A. Hair et al., “LMP-1, a LIM-domain protein, mediates BMP-6 effects on bone formation,” *Endocrinology*, vol. 139, no. 12, pp. 5125–5134, 1998.
- [14] H. Liu, M. Bargouti, S. Zughaier et al., “Osteoinductive LIM mineralization protein-1 suppresses activation of NF- κ B and selectively regulates MAPK pathways in pre-osteoclasts,” *Bone*, vol. 46, no. 5, pp. 1328–1335, 2010.
- [15] H. Liu, H. Pan, H. Yang et al., “LIM mineralization protein-1 suppresses TNF- α induced intervertebral disc degeneration by maintaining nucleus pulposus extracellular matrix production and inhibiting matrix metalloproteinases expression,” *Journal of Orthopaedic Research*, vol. 33, no. 3, pp. 294–303, 2015.
- [16] S. T. Yoon, J. S. Park, K. S. Kim et al., “ISSLS prize winner: LMP-1 upregulates intervertebral disc cell production of proteoglycans and BMPs in vitro and in vivo,” *Spine (Phila Pa 1976)*, vol. 29, no. 23, pp. 2603–2611, 2004.
- [17] M. Jarosz, M. Olbert, G. Wyszogrodzka, K. Młyniec, and T. Librowski, “Antioxidant and anti-inflammatory effects of zinc. Zinc-dependent NF- κ B signaling,” *Inflammopharmacology*, vol. 25, no. 1, pp. 11–24, 2017.
- [18] R. Tisherman, P. Coelho, D. Phillibert et al., “NF- κ B signaling pathway in controlling intervertebral disk cell response to inflammatory and mechanical stressors,” *Physical Therapy*, vol. 96, no. 5, pp. 704–711, 2016.
- [19] T. Liu, L. Zhang, D. Joo, and S. C. Sun, “NF- κ B signaling in inflammation,” *Signal Transduction and Targeted Therapy*, vol. 2, no. 1, 2017.
- [20] C. W. A. Pfirrmann, A. Metzdorf, M. Zanetti, J. Hodler, and N. Boos, “Magnetic resonance classification of lumbar intervertebral disc degeneration,” *Spine*, vol. 26, no. 17, pp. 1873–1878, 2001.
- [21] X. Cheng, G. Zhang, L. Zhang et al., “Mesenchymal stem cells deliver exogenous miR-21 via exosomes to inhibit nucleus pulposus cell apoptosis and reduce intervertebral disc degeneration,” *Journal of Cellular and Molecular Medicine*, vol. 22, no. 1, pp. 261–276, 2018.
- [22] K. Masuda, Y. Aota, C. Muehleman et al., “A novel rabbit model of mild, reproducible disc degeneration by an annulus needle puncture: correlation between the degree of disc injury and radiological and histological appearances of disc degeneration,” *Spine (Phila Pa 1976)*, vol. 30, no. 1, pp. 5–14, 2005.
- [23] J. Chen, W. Yan, and L. A. Setton, “Molecular phenotypes of notochordal cells purified from immature nucleus pulposus,” *European Spine Journal*, vol. 15, Supplement 3, pp. 303–311, 2006.
- [24] H. Liu, L. Huang, Z. Zhang et al., “LIM mineralization protein-1 inhibits the malignant phenotypes of human osteosarcoma cells,” *International Journal of Molecular Sciences*, vol. 15, no. 4, pp. 7037–7048, 2014.
- [25] Y.-C. Huang, V. Y. L. Leung, W. W. Lu, and K. D. K. Luk, “The effects of microenvironment in mesenchymal stem cell-based regeneration of intervertebral disc,” *The Spine Journal*, vol. 13, no. 3, pp. 352–362, 2013.
- [26] S. Xu, J. Li, M. Zhai et al., “1,25-(OH)₂D₃ protects Schwann cells against advanced glycation end products-induced apoptosis through PKA-NF- κ B pathway,” *Life Sciences*, vol. 225, pp. 107–116, 2019.
- [27] K. Ishii and T. Kato, “Increase of dopamine turnover in bilateral striata after unilateral injection of haloperidol into substantia nigra of unrestrained rats,” *Brain Research*, vol. 359, no. 1-2, pp. 260–266, 1985.
- [28] A. Kauppinen, T. Suuronen, J. Ojala, K. Kaarniranta, and A. Salminen, “Antagonistic crosstalk between NF- κ B and SIRT1 in the regulation of inflammation and metabolic disorders,” *Cellular Signalling*, vol. 25, no. 10, pp. 1939–1948, 2013.
- [29] A. Ashkenazi, W. J. Fairbrother, J. D. Levenson, and A. J. Souers, “From basic apoptosis discoveries to advanced selective BCL-2 family inhibitors,” *Nature Reviews. Drug Discovery*, vol. 16, no. 4, pp. 273–284, 2017.
- [30] S. Matsuyama, J. Palmer, A. Bates et al., “Bax-induced apoptosis shortens the life span of DNA repair defect Ku70-knockout mice by inducing emphysema,” *Experimental Biology and Medicine (Maywood, N.J.)*, vol. 241, no. 12, pp. 1265–1271, 2016.
- [31] B. Khalilzadeh, N. Shadjou, G. S. Kanberoglu et al., “Advances in nanomaterial based optical biosensing and bioimaging of apoptosis via caspase-3 activity: a review,” *Mikrochimica Acta*, vol. 185, no. 9, 2018.
- [32] J. Chen, G. Z. Liu, Q. Sun et al., “Protective effects of ginsenoside Rg3 on TNF- α -induced human nucleus pulposus cells through inhibiting NF- κ B signaling pathway,” *Life Sciences*, vol. 216, pp. 1–9, 2019.
- [33] P.-P. A. Vergroesen, I. Kingma, K. S. Emanuel et al., “Mechanics and biology in intervertebral disc degeneration: a vicious circle,” *Osteoarthritis and Cartilage*, vol. 23, no. 7, pp. 1057–1070, 2015.

Research Article

Exosomes Derived from Human Urine-Derived Stem Cells Inhibit Intervertebral Disc Degeneration by Ameliorating Endoplasmic Reticulum Stress

HongFei Xiang ¹, WeiLiang Su ¹, XiaoLin Wu ¹, WuJun Chen ², WenBin Cong ³,
Shuai Yang ¹, Chang Liu ¹, ChenSheng Qiu ⁴, Shang-You Yang ⁵, Yan Wang ¹,
GuoQing Zhang ¹, Zhu Guo ¹, DongMing Xing ^{2,6} and BoHua Chen ¹

¹Department of Orthopedics, The Affiliated Hospital of Qingdao University, Qingdao, China 266003

²Cancer Institute, The Qingdao University, Qingdao, China 266003

³Radiology Department, The Affiliated Hospital of Qingdao University, Qingdao, China 266003

⁴Department of Orthopedics, Qingdao Municipal Hospital, Qingdao, Shandong 266011, China

⁵University of Kansas, School of Medicine-Wichita, 929 N St. Francis Street, Wichita, KS, USA 67230

⁶School of Life Sciences, Tsinghua University, Beijing, China 100084

Correspondence should be addressed to Zhu Guo; guozhugz@126.com, DongMing Xing; xdm_tsinghua@163.com, and BoHua Chen; bhchen@hotmail.com

Received 9 October 2020; Revised 14 November 2020; Accepted 18 November 2020; Published 7 December 2020

Academic Editor: Wenyan Ding

Copyright © 2020 HongFei Xiang et al. This is an open access article distributed under the Creative Commons Attribution License, which permits unrestricted use, distribution, and reproduction in any medium, provided the original work is properly cited.

Objective. This study is aimed at determining the effects of human urine-derived stem cell-derived exosomes (USCs-exos) on pressure-induced nucleus pulposus cell (NPC) apoptosis and intervertebral disc degeneration (IDD) and on the ERK and AKT signaling pathways. **Methods.** The NPCs were obtained from patients with herniated lumbar discs. Western blot analysis (WB) and quantitative real-time polymerase chain reaction (qRT-PCR) were used to determine endoplasmic reticulum (ER) stress levels of NPCs under stress. Human USCs were identified using an inverted microscope, three-line differentiation experiments, and flow cytometry. A transmission microscope, nanoparticle size analysis, and WB procedures were used to identify the extracted exosomes and observe NPC uptake. A control group, a 48 h group, and a USCs-exos group were established. The control group was untreated, and the 48 h group was pressure-trained for 48 h, while the USCs-exos group was pressure-trained for 48 h and treated with USCs-exos. WB, qRT-PCR, and terminal deoxynucleotidyl transferase dUTP nick end labeling (TUNEL) analysis were used to determine the ER stress levels in stress conditions and after exosomal treatment. The AKT and ERK pathways were partially detected. Magnetic Resonance Imaging (MRI) and computed tomography (CT) were used to evaluate cell degeneration while exosomal effects on the intervertebral disc (IVD) tissue were determined by hematoxylin and eosin (HE) staining, Safranin O-fast green staining, immunohistochemical staining (IHC), nuclear magnetic resonance (NMR), spectrometric detection, and total correlation spectroscopy (TOCSY). IVD metabolites were also identified and quantified. **Results.** After pressure culture, ER stress markers (GRP78 and C/EBP homologous protein (CHOP)) in the NPCs were significantly elevated with time ($p < 0.05$). Human USCs are short and spindle-shaped. They can successfully undergo osteogenic, adipogenic, and chondrogenic differentiation. In this study, these stem cells were found to be positive for CD29, CD44, and CD73. The exosomes were centrally located with a diameter of 50-100 nm. CD63 and Tsg101 were highly expressed while the expression of Calnexin was suppressed. The exosomes can be ingested by NPCs. USCs-exos significantly improved ER stress responses and inhibited excessive activation of the unfolded protein response (UPR) as well as cell apoptosis and disc degeneration through the AKT and ERK signaling pathways ($p < 0.05$). **Conclusion.** Through the AKT and ERK signaling pathways, USCs-exos significantly inhibit ER stress-induced cell apoptosis and IDD under pressure conditions. It is, therefore, a viable therapeutic strategy.

1. Introduction

Lower back pain (LBP) is a common condition that affects the quality of life and results in a heavy financial burden [1]. The IDD is the main cause of LBP [2]. The IVD is a cartilage tissue composed of the central colloidal nucleus pulposus (NP), peripheral fibrous annulus (AF), and the upper and lower endplates [3]. During the IDD process, the NP area first exhibits degenerative changes. The apoptosis of NP cells is one of the most common manifestations of IDD [4–6]. Apoptosis refers to programmed cell death that is triggered by the activation of caspase [7]. Studies on IVD degeneration have focused on NPC apoptosis. Gruber and Hanley [8] were the first to identify apoptotic cells in the degenerated IVD. Later, Rannou et al. [9] proved that IDD is positively correlated with NP cell apoptosis. Therefore, the decrease in the number of cells in the nucleus pulposus area during IDD is the apoptosis of NPCs.

The biochemical cascade involved in IDD pathogenesis is extremely complex. IDD is associated with a decrease in proteoglycan content of NPCs, which leads to biomechanical changes [10]. However, the relationship between mechanical load and IDD onset has not been established. As it is subjected to mechanical stresses of different intensities in daily work and life, the IVD tissue plays an important role in spinal biomechanics [11]. Wilke et al. [12] measured the pressure on the L4/5 discs of healthy people. They found that the pressure is 0.1 MPa during sleep and 0.3–2.3 MPa during daily activities (it is 0.3–0.83 MPa when sitting, 0.5–1.1 MPa when standing, and 1.1–2.3 MPa when carrying a load). Zhang et al. [13] utilized 0.8 MPa to simulate IVD force during activity. And they found that it caused apoptosis in NPCs. Studies have documented that mechanical load is an important factor in IDD pathogenesis. Excessive mechanical pressure promotes cell apoptosis, increases the secretion of extracellular matrix-degrading enzymes, and suppresses the enzymes associated with the synthesis of the extracellular matrix, which ultimately lead to IDD [14, 15]. Therefore, studies should be aimed at elucidating the relationship between mechanical load and NPC apoptosis during IDD.

As an important organelle in eukaryotic cells, the ER is involved in the regulation of basic cellular processes, including folding transmembrane and secreted proteins, lipid synthesis, drug detoxification, Ca^{2+} storage, and signal transduction [16]. However, various factors such as inhibition of protein glycosylation, Ca^{2+} depletion, redox state changes, and the expression of misfolded proteins suppress ER functions. These dysfunctions may cause protein toxicity in the ER, collectively referred to as ER stress, which leads to the activation of the UPR [17, 18]. A certain degree of UPR protects cells from external stimuli and reestablishes cell homeostasis. However, under long-term or excessive pressure, UPR cannot restore protein homeostasis and cell homeostasis. Instead, cell death occurs through the ER stress-induced apoptosis mechanism [19–21]. Proper biomechanical loading plays an active role in the structure and function of articular cartilage [22]. However, continuous abnormal biomechanical stimulation leads to the accumulation of misfolded proteins in the ER lumen [23], causing ER stress [24].

Paracrine factors of mesenchymal stem cells (MSCs) play an important role in maintaining NP cell proliferation and inhibiting their apoptosis [25, 26]. MSCs secrete specific types of extracellular vesicles, such as exosomes, to achieve their therapeutic paracrine effect [27]. Exosomes are cell-secreted extracellular vesicles with a diameter of about 30–100 nm [28]. They provide a high number of biologically active substances, such as lipids, nucleic acids, and proteins, to recipient cells through membrane fusion. They are also involved in material and information exchange between cells [29]. However, MSC sources in the body are limited, and it causes certain trauma to the body when extracted, which limits its application. Human USCs exhibit a multidirectional differentiation potential. These cells have a wide range of sources from which they can be easily obtained in a safe and noninvasive manner. In addition, they are better sources of exosomes [30–32]. However, the specific mechanism by which exosomes promote the proliferation of NPCs and reduce their apoptosis has not been established.

In this study, we determined the expression levels of ER stress markers and UPR-related genes in NPCs under normal and stress conditions. The findings of this study provide new avenues for exploring the relationship between IDD and ER stress to inform the development of therapeutic options.

2. Materials and Methods

2.1. Isolation and Culture of NPCs. This study was approved by the Ethical Committee of the Affiliated Hospital of Qingdao University (approval number: QDFY-19-012-03). Patients or their guardians were required to sign informed consent before being enrolled in the study. The IVD tissues were obtained from patients with lumbar degenerative diseases who had been subjected to posterior foraminal lumbar intervertebral surgery. The AF and cartilaginous endplate (CEP) in the specimen were carefully removed under a microscope. After being washed 3 times with phosphate-buffered saline (PBS), the nucleus pulposus tissue was sliced to 1 mm^3 and digested in 0.2% type II collagenase (Gibco) for 3 h. A $75\text{ }\mu\text{m}$ filter was then used to remove tissue residues before the obtained cells were centrifuged at 800 r/min for 5–10 minutes. The cells were resuspended in Dulbecco's modified Eagle medium/F-12 (DMEM/F-12) medium (Gibco, Grand Island, NY, USA) supplemented with 10% fetal bovine serum (Gibco) and 1% penicillin-streptomycin. They were incubated at 37°C in a 5% CO_2 environment.

2.2. USC Extraction. A 200 ml fresh sterile urine sample from 6 healthy male adults (average age 25.5 ± 1.26) was obtained in aseptic conditions. The urine sample was centrifuged at 400 g for 10 minutes, the supernatant was discarded, and the cell pellet was resuspended in PBS. It was centrifuged again at 200 g for 10 minutes, and the supernatant was carefully aspirated. The cell pellet was resuspended in 4 ml mixture of 10% fetal bovine serum (FBS) (Gibco, Australia), 1% penicillin-streptomycin, and REGM SingleQuot growth factor additive (Lonza, Basel, Switzerland) DMEM/F-12 medium (HyClone, Utah, USA). They were then inoculated in a 12-well plate that had been precoated with gelatin and

incubated at 37°C in 5% CO₂. The medium was changed every two days until a cell colony was formed. The colony was then transferred to RE/MC medium to continue the culture. The RE cell proliferation medium was made of 500 ml of RE cell basal medium with REGM SingleQuot kit components. The MC Proliferation Medium was a DMEM/F-12 medium supplemented with 10% FBS, 1% GlutaMAX (Gibco, Japan), 1% NEAA (Gibco, Grand Island, USA), 1% pen/strep (Gibco, Grand Island, USA), 5 ng/ml bFGF (PeproTech, Rocky Hill, USA), 5 ng/ml PDGF-AB (PeproTech, Rocky Hill, USA), and 5 ng/ml EGF (PeproTech, Rocky Hill, USA). The RE/MC medium was a 1 : 1 mixture of RE multiplication medium and MC multiplication medium. The passage was performed when the cell density reached 70%-80%. The P2-4 cells were obtained for subsequent experiments.

2.3. Flow Cytometry and Identification of USC Surface Markers. After digestion with trypsin, P3 generation USCs with good growth characteristics were obtained and washed 3 times using PBS after centrifugation. A cell suspension with a final concentration of 1×10^6 cells/ml was made. A 100 μ l cell suspension was pipetted and mixed with 10 μ l of CD29, CD44, and CD73 (Santa Cruz Biotechnology, USA) monoclonal antibody working solution. They were incubated in the dark for 1 h at room temperature. The cells were washed 3 times and analyzed by flow cytometry.

2.4. Three-Line Differentiation of USCs. To evaluate the differentiation potential of human USCs, they were induced to differentiate into osteogenic, adipogenic, and chondrogenic cells according to the osteogenesis, adipogenesis, and chondrogenesis differentiation culture kit (Cyagen Biosciences, Guangzhou, China) instructions. USCs were seeded into a 6-well plate. When the cell fusion rate was 80%, differentiation was induced. Upon the induction of osteogenic differentiation, osteogenic differentiation medium (Cyagen, Guangzhou, China) was added and replaced every 3 days. After 21 days of induction, the cells were fixed in 4% paraformaldehyde and stained with Alizarin Red for observation. The osteogenic differentiation complete medium kit contains 175 ml basal medium, 20 ml serum, 2 ml penicillin-streptomycin, 2 ml glutamine, 2 ml beta-glycerophosphate sodium, 400 μ l ascorbic acid, and 20 μ l dexamethasone. To induce differentiation by adipogenesis, the adipogenic differentiation medium A (Cyagen, Guangzhou, China) was added; 3 days later, it was changed to adipogenic differentiation medium B (Cyagen, Guangzhou, China); 24 h later, it was again changed to medium A. Medium alterations were made for a total of 3 times. The cells were finally fixed with 4% paraformaldehyde and observed after staining with Oil Red O. The adipogenic differentiation medium A kit contains 175 ml basal medium, 20 ml fetal bovine serum, 2 ml penicillin-streptomycin, 2 ml glutamine, 400 μ l insulin, 200 μ l 3-isobutyl-1-methylxanthine (IBMX), 200 μ l dexamethasone, and 200 μ l rosiglitazone. The adipogenic differentiation medium B kit contains 175 ml basal medium, 20 ml fetal bovine serum, 2 ml penicillin-streptomycin, 2 ml glutamine, and 400 μ l insulin. Upon the induction of chondrogenesis, cell counting was done. Approximately 2.5×10^5 of USCs were centrifuged

at 150 g in a 15 ml centrifuge tube for 5 minutes, and the supernatant was discarded. Chondrogenic differentiation medium (0.5 ml) was added to the cells and cultured. The medium was changed every 3 days. The cells were then fixed in 4% paraformaldehyde for 21 days and sliced after embedding in paraffin. They were finally stained with Alcian Blue for observation. The chondrogenic differentiation medium kit contains 194 ml of basic medium, 600 μ l ascorbic acid, 20 μ l dexamethasone, 2 ml ITS supplement (ITS+supplement), 200 μ l sodium pyruvate, 200 μ l proline, and 2 ml transforming growth factor- β 3 (TGF- β 3).

2.5. Extraction and Identification of Exosomes. After the cells had grown to a 70-75% confluence, the medium was aspirated. The cells were washed 3 times using PBS. Serum-free medium was added to the cells and cultured for 48 h. The culture medium was then centrifuged at 500 g for 10 min at 4°C to remove residual cells, centrifuged at 2000 g for 20 min at 4°C to remove cell debris, and centrifuged at 10000 g for 30 min at 4°C to further remove impurities. The supernatant was obtained and filtered using a 0.22 μ m filter membrane to remove oversized particles. The supernatant was then ultracentrifuged at 100000 g at 4°C for 2 h. The resulting pellet was resuspended in PBS. A transmission electron microscope (TEM) (JEM-1200EX, Japan) was then used to observe the morphology of exosomes while the NanoSight detector (Malvern, England) as well as the NTA detection and analysis software was used to analyze the number and size distribution of the exosomes. Western blot was used to detect exosomal markers (CD63, TSG101, and Calnexin).

2.6. Uptake of Exosomes by NPCs. The PKH26 fluorescent dye kit (Sigma-Aldrich) was used to label exosomes according to the manufacturer's instructions. Excess dye was neutralized with an equal volume of PBS containing 5% BSA. The labeled cells were then centrifuged at 4°C and 100000 g for 70 minutes. The supernatant was removed, and the labeled cells were resuspended in 50 μ l PBS. The prepared exosomes of labeled USCs were added to NPCs, incubated for 12 h in the dark, fixed in 4% paraformaldehyde for 20 minutes, stained with DAPI, and mounted with glycerol to observe their uptake using a laser confocal microscope. The Leica Application Suite Advanced Fluorescence software was used to analyze the obtained image.

2.7. Construction of Pneumatic Pressure Model. The NPCs were introduced into a pneumatic pressure device assembled by our research group to simulate pressure-associated IVD tissue damage. The device is composed of a cell culture apparatus and a high-pressure gas scheme. About two liters of double-distilled water was added to the cell culture device to a level that did not exceed the cell placement equipment. After placing the cell culture plate in the corresponding position, the equipment was turned off. To obtain 1.0 MPa, a high-pressure gas device was used to fill the cell culture environment with a mixed gas containing 90% N₂, 5% CO₂, and 5% O₂. The temperature of the cell culture device was set to 37°C. After 48 hours of culture, the cells were obtained for Western blotting and other experiments.

2.8. Western Blot Analysis. The obtained cells were lysed in radioimmunoprecipitation assay (RIPA) lysis buffer (Solarbio, Beijing, China) containing 1 mM phenylmethane-sulfonyl fluoride (PMSF) and protease inhibitors to extract proteins. The concentration of the extracted protein was determined using a bicinchoninic acid (BCA) kit (Solarbio, Beijing, China). The protein and the loading buffer were then mixed at a ratio of 4:1 (V/V), boiled for 10 minutes, separated by sodium dodecyl sulfate-polyacrylamide gel electrophoresis (SDS-PAGE), and transferred to a polyvinylidene fluoride (PVDF) membrane. The PVDF membrane was sealed with 5% skimmed milk powder at room temperature. The membrane was then incubated overnight at 4°C with primary antibodies (CD63, TSG101, Calnexin, GRP78, CHOP, GRP94, caspase-3, caspase-12, p-PERK, PERK, ATF6, p-IRE1 α , IRE1 α , XBP1, ATF4, ERK, p-ERK, AKT, p-AKT, and β -actin) (Santa Cruz Biotechnology, USA). After overnight incubation, the membrane was incubated with a horseradish peroxidase- (HRP-) labeled secondary antibody (ABclonal, Wuhan, China) for 1 h. An ECL kit (Thermo Fisher Scientific, Rockville, MD, USA) was then used for luminescence observation. The obtained images were analyzed using Image Lab software (Bio-Rad, Hercules, CA, USA).

2.9. Quantitative Real-Time Polymerase Chain Reaction (qRT-PCR). Total RNA was extracted from the cultured cells using a TRIzol reagent (Invitrogen, Carlsbad, CA, USA). Reverse transcription and gene amplification procedures were done according to the kit manufacturer's instructions (TransGen Biotech, Beijing, China). GAPDH was set as an internal reference. The primer sequences used in this study are presented in Table 1. The obtained data was analyzed using the 2- $\Delta\Delta$ Ct algorithm.

2.10. Terminal Deoxynucleotidyl Transferase dUTP Nick End Labeling (TUNEL) Staining. TUNEL staining was used to detect cell apoptosis. Cells were fixed in 4% paraformaldehyde for 1 h at room temperature. They were then incubated with 0.5% TritonX-100 in PBS for 5 minutes. After washing using PBS, they were incubated for 60 minutes as described by the apoptosis detection kit (Roche, Basel, Switzerland). The cells were finally stained with 0.1 g/ml DAPI and mounted with glycerol to observe apoptosis using a laser confocal microscope.

2.11. Rat Tail Degeneration Experiment. Twenty 3-month-old SD rats were purchased for the in vivo experiments. Five rats were randomly selected and assigned to the normal control group, without any treatment; the remaining 15 rats were all treated as the experimental group. The rats were anesthetized with 2% pentobarbital, and the three IVDs (Co4/5, Co5/6, and Co6/7) of each rat were determined on the tail vertebrae by palpation. A 21 G needle was used to puncture the IVDs of Co4/5 and Co5/6, respectively. The Co4/5 was injected with USC-exos (100 μ g/ml). The injection was done every 2 weeks. The condition of the IVD was observed in the 4th and 8th weeks using CT and MRI scans. Then, the degeneration of the IVD was evaluated according to the signal changes in MRI images. After the 8th week, the rats were

TABLE 1: Primer sequences for quantitative real-time PCR.

Gene name	Primer sequences (5'-3')
CHOP	Forward (F) 5'-CTTCTCTGGCTTGCTGACT-3'
	Reverse (R) 5'-TCTGTTTCCGTTTCTGGTT-3'
GRP78	Forward (F) 5'-TCCTATGTCGCCTTCACTCC-3'
	Reverse (R) 5'-ATGTCTTTGTTTGCCACCT-3'
ATF4	Forward (F) 5'-TGAAGGAGATAGGAAGCCAGA-3'
	Reverse (R) 5'-GCAGACCCACAGAGAACACC-3'
XBP1	Forward (F) 5'-ATGGATTCTGGCGGTATTGA-3'
	Reverse (R) 5'-AAAGGGAGGCTGGTAAGGAA-3'
GAPDH	Forward (F) 5'-CGACCACTTTGTCAAGCTCA-3'
	Reverse (R) 5'-AGGGGAGATTCACTGTGGTG-3'

sacrificed and the IVD samples were obtained. This experimental protocol was approved by the Animal Experiment Committee of Qingdao University, China.

2.12. Safranin O-Fast Green Cartilage Stain. The IVD tissue samples were fixed with paraformaldehyde, decalcified, dehydrated, and then embedded in paraffin. The Safranin O-Fast Green Cartilage Staining Kit (Solarbio, Beijing, China) was used for staining according to the manufacturer's instructions. The tissue samples were deparaffinized in water, introduced in freshly prepared Weigert dye solution for 3-5 minutes, and washed with water. They were differentiated in acidic differentiation solution for 15 seconds, washed with distilled water for 10 minutes, immersed in the fast green staining solution for 5 minutes, and quickly washed using a weak acid solution for 10-15 seconds to remove the excess fast green. The samples were then introduced into Safranin O stain for 5 min, dehydrated using 95% ethanol and absolute ethanol, and made transparent using xylene. They were observed after sealing using an optical resin.

2.13. Hematoxylin-Eosin (HE) Staining. The samples were decalcified and fixed in formaldehyde, dehydrated, embedded in paraffin, and sectioned. HE staining was performed using the Hematoxylin and Eosin (HE) Staining Kit (Solarbio, Beijing, China) according to the manufacturer's instructions. Briefly, paraffin sections were deparaffinized, hydrated, stained using the hematoxylin staining solution for 5-20 minutes, and introduced into the differentiation solution for 30 seconds. The sections were washed with warm water at 37°C, introduced in eosin dye solution, washed, soaked again, dehydrated, made transparent using xylene, mounted, sealed with neutral gum, and observed under a microscope.

2.14. Immunohistochemical Analysis (IHC). The rats were euthanized, and their IVDs were obtained, decalcified, fixed in formaldehyde, dehydrated, and embedded in paraffin. The sections were dewaxed, hydrated, incubated at room temperature with 3% hydrogen peroxide for 10 minutes, and then twice soaked in PBS for 5 minutes each time for

antigen repair. The sections were then blocked using PBS supplemented with 5% goat serum for 1 h. Caspase-3 primary antibody (Santa Cruz Biotechnology, USA) was then added and incubated overnight at 4°C. After overnight incubation, the sections were rinsed with PBS 3 times; 5 minutes later, a horseradish peroxidase-labeled secondary antibody was added and incubated at 37°C for 30 minutes. The sections were thrice rinsed using PBS for 5 minutes each time. Approximately 5 ml of diaminobenzidine (DAB) was added for 3–15 minutes to induce color development. Tap water was then used to fully rinse after which the sections were counterstained, dehydrated, made transparent using xylene, covered with neutral resin, and observed under a microscope.

2.15. Nuclear Magnetic Resonance Spectroscopy and TOCSY Spectra Identification of Metabolites in IVD. Fresh IVD tissue was ground and lysed in RIPA lysis buffer (Solarbio, Beijing, China) containing 1 mM phenylmethanesulfonyl fluoride (PMSF) and protease inhibitors to obtain protein. The concentration of the extracted protein was detected using a BCA kit (Solarbio, Beijing, China) according to the manufacturer's instructions. Five hundred microliter of D₂O and 100 μ l of 10% 3-(trimethylsilyl) propionic acid sodium salt (TSP) were then added to the protein. They were mixed and centrifuged at 14,000 g for 15 minutes (to remove the precipitated particles of the tissue in the solution). 550 μ l of the supernatant was obtained and used to detect the protein and metabolite solution using the 600 MHz NMR (Bruker, Germany) equipment according to the manufacturer's instructions. The characteristic TOCSY, two-dimensional spectrum of the tissue metabolites and protein solution, was obtained and analyzed using the MestReNova (Mestrelab Research Co. Ltd., USA) software in order to identify the main differences in the metabolite and protein residues.

2.16. Statistical Analysis. The experiments were done in triplicates. Continuous data is expressed as the mean \pm standard deviation (SD) while the nonparametric data is expressed in the median and interquartile range. One-way analysis of variance (ANOVA) was used to compare the statistical differences among groups while the parallel group parameters were compared by a *t*-test. *p* < 0.05 was set as the threshold for statistical significance. Statistical analysis was done using SPSS 20.0 software (SPSS, Chicago, IL, USA), while the GraphPad Prism 8 (GraphPad Software, USA) software was used to draw statistical graphs.

3. Results

3.1. Expression of ER Stress Markers in NPCs after Pressure Culture. Endoplasmic reticulum stress is associated with the pathogenesis of IDD. Severe ER stress induces excessive apoptosis of NP cells [33, 34]. In this study, protein was extracted from the pressure-cultured NPCs. The ER stress marker GRP78 and the downstream protein CHOP were detected by Western blot (Figures 1(a)–1(c)). The expression levels of GRP78 and CHOP were also determined by qRT-PCR at different times of pressure culture (*n* = 3). The gene and protein expressions of GRP78 and CHOP were positively corre-

lated with the time of pressurized culture (Figures 1(d) and 1(e)). These findings indicate that external pressure stimulation induced ER stress, which caused NPC apoptosis thereby leading to the occurrence or acceleration of IDD.

3.2. Identification of USCs-Exos and NP Cell Uptake. Human USCs were extracted from the urine of healthy adults. Under a light microscope, human USCs exhibit a short fusiform or spindle-shaped appearance (Figure 2(a)). Their differentiation into three cell lines was induced by osteogenic, cartilage, and adipogenic media (Figure 2(b)). Flow cytometry showed that the USC surface markers CD29, CD44, and CD73 were positive (Figure 2(c)). USCs exhibit a variety of biological characteristics such as clonogenicity, expression of specific cell surface markers, and pluripotent differentiation abilities that correspond to those of the adult MSCs [28, 35–37]. The positive CD29, CD44, and CD73 findings were consistent with previous studies. The shape of USCs-exos was similar to a circular sacculus with a depressed center with a diameter in the range of 50–100 nm (Figure 2(d)). Nanoparticle size analysis revealed that the USCs-exos exhibited a particle size range of 50–100 nm (Figure 2(e)). The USC exosomal marker proteins (CD63 and Tsg101) were highly expressed, while the negative protein Calnexin was suppressed (Figure 2(f)). The exosomes were labeled with PKH26 and incubated with NP cells to confirm that they could be taken up by NPCs. Fluorescently labeled exosomes were observed in the cytoplasm of NPCs, indicating that the exosomes had been taken up by NPCs (Figure 2(g)).

3.3. USCs-Exos Inhibit Pressure-Induced ER Stress and Suppress NPC Apoptosis. Pressure stimulation causes cell apoptosis [38, 39]. Stem cell exosomes exhibit an antiapoptotic effect under a variety of conditions [25, 27]. Figures 3(a)–3(c) show the expression levels of ER stress marker proteins (GRP78 and GRP94) and their relative protein expression levels. Severe ER stress causes cell apoptosis; therefore, the expression of caspase-3 and caspase-12 between the groups was compared (Figures 3(d)–3(f)). It was revealed that the apoptotic rate increased under pressure culture conditions while treatment with USCs-exos decreased the apoptotic rate (Figures 3(g) and 3(h)). The above results indicate that pressure elevates the ER stress of NPCs, while USCs-exos inhibit the occurrence of ER stress and, therefore, reduce cell apoptosis, which may exert a protective effect on the IVD tissue.

3.4. USCs-Exos Inhibit the Activation of UPR Caused by ER Stress in Human NPCs under Pressure Culture Conditions. It has been documented that severe or prolonged ER stress may overactivate UPR, excessive protein degradation, and eventually apoptosis [40]. The role of USCs-exos in stress-induced ER stress was determined by evaluating the expression levels of three transmembrane proteins (protein kinase-like endoplasmic reticulum kinase (PERK), inositol-requiring protein 1 α (IRE1 α), and activating transcription factor (ATF6)) in the classic branch of UPR (Figure 4(a)). Pressure culture enhanced the expression levels of ATF6, phosphorylated IRE1 α (p-IRE1 α), and phosphorylated PERK (p-PERK) in NPCs, indicating that UPR was activated

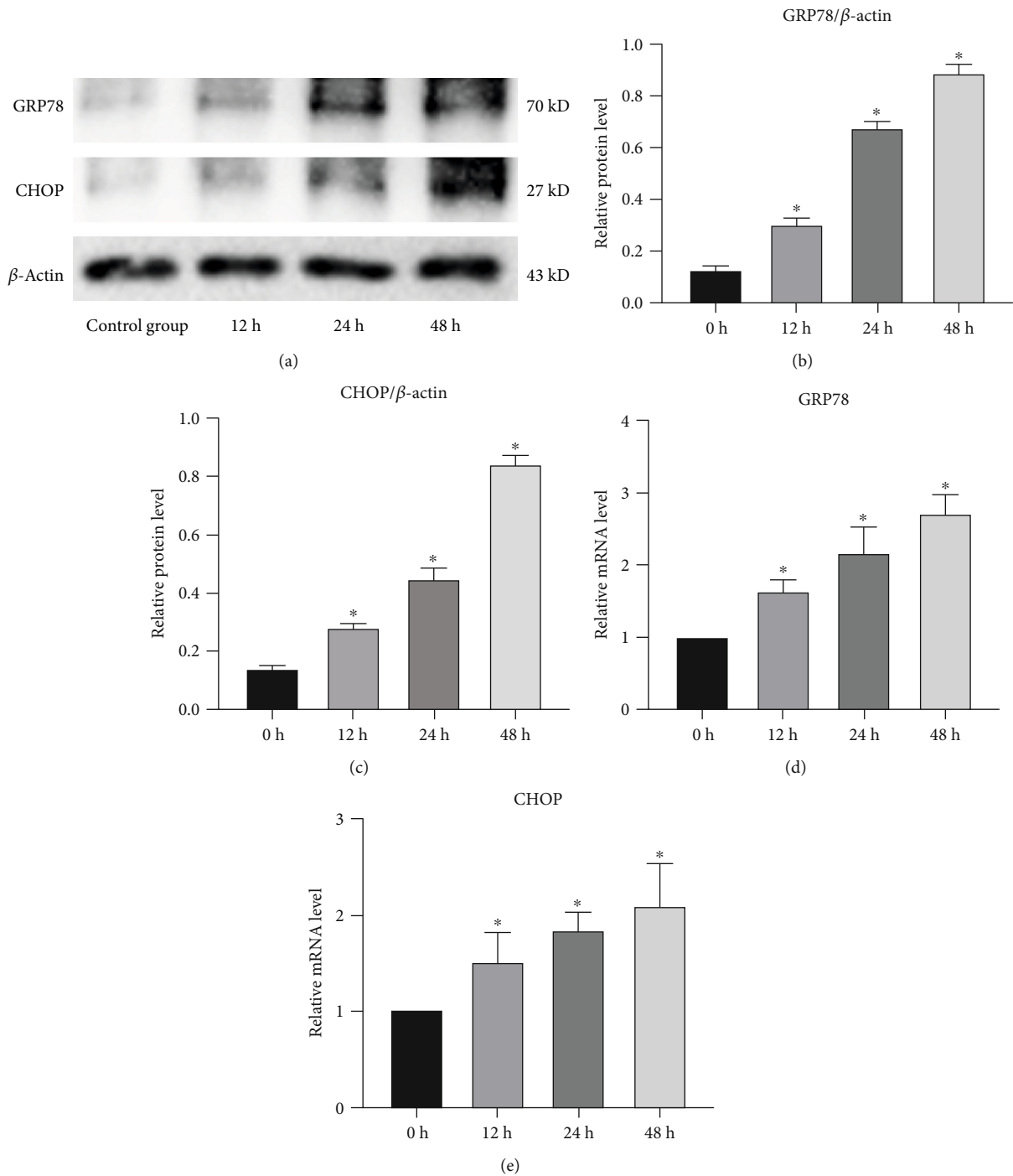
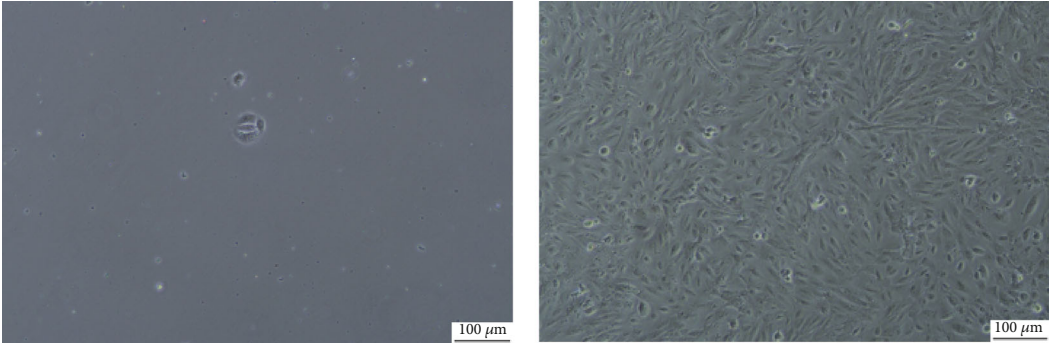


FIGURE 1: Endoplasmic reticulum stress level after stress culture of human NPCs. (a–c) Analysis of the protein levels of GRP78 and CHOP by Western blot (a), and based on this, the gray values of relative protein expression are compared (b, c). β -Actin was used as an internal control. *Compared to the control group, $p < 0.05$. (d, e) The mRNA levels of GRP78 and CHOP in NPCs after pressure culture. *Compared to the NC group, $p < 0.05$.

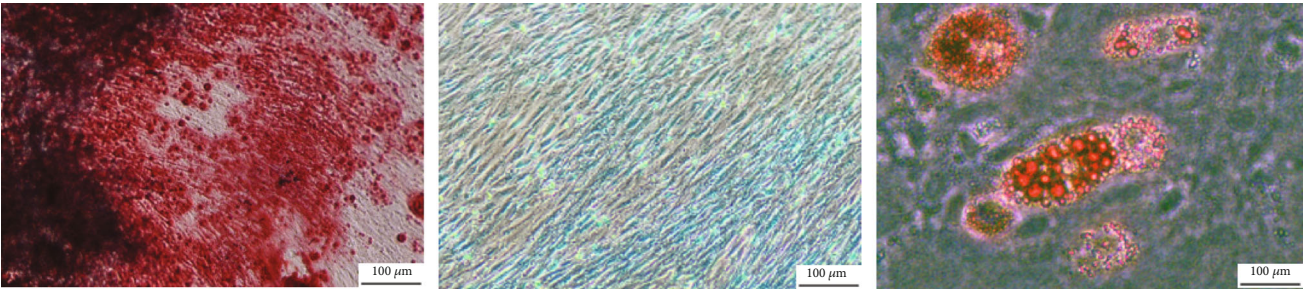
(Figure 4(a)). Furthermore, transcription of the downstream genes of UPR gene activating transcription factor 4 (ATF4) and X-box binding protein 1 (XBP1) was also elevated (Figures 4(h) and 4(i)). After stress culture, CHOP was found to be activated at the RNA and protein levels as an apoptotic mediator of ER stress (Figure 4(j)). Compared to the control group, the expression levels of ATF4, XBP1, and CHOP in

the exosomal group were significantly suppressed. The above results indicate that USC-exos regulate UPR activation by regulating the ER stress of NPCs under pressure.

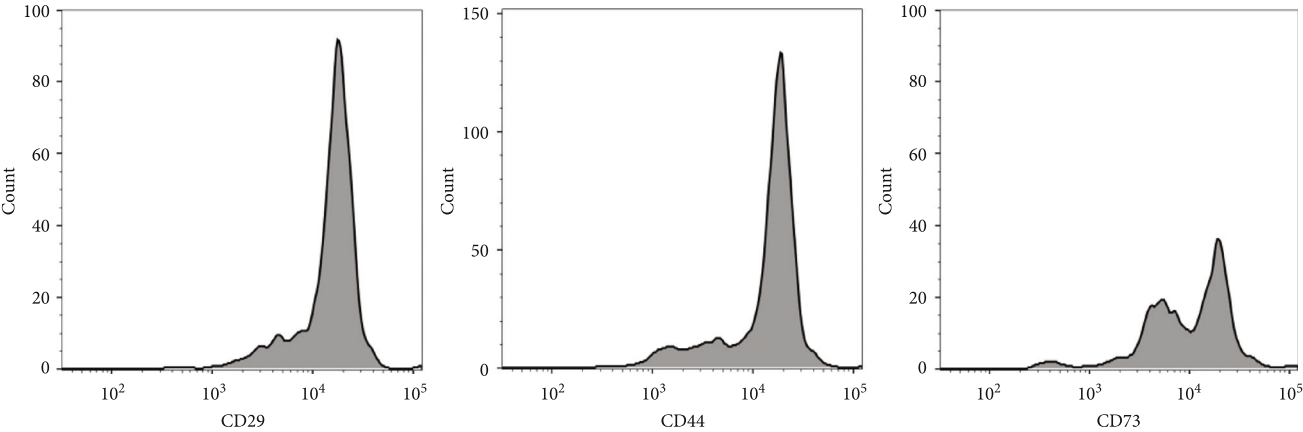
3.5. USC-Exos Inhibit Stress-Induced ER Stress-Related Apoptosis through the AKT and ERK Pathways. The uptake of exosomes by cells activates the AKT and ERK pathways



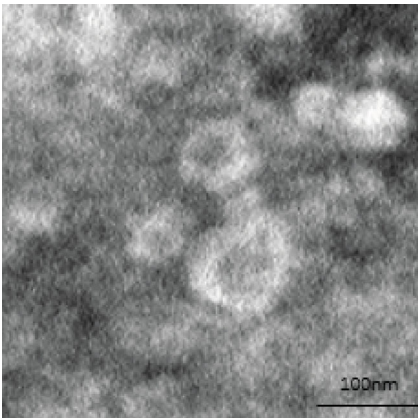
(a)



(b)

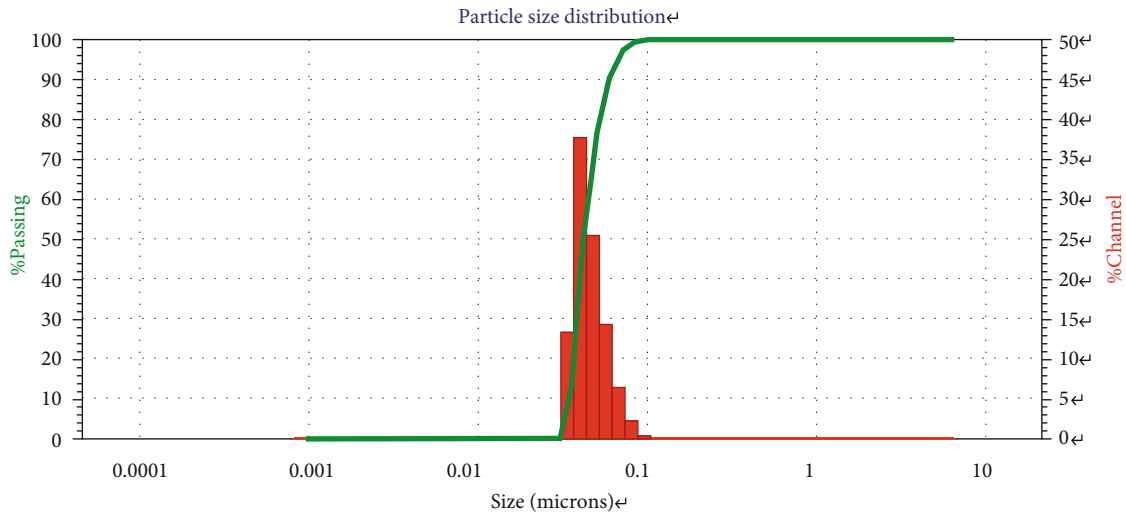


(c)

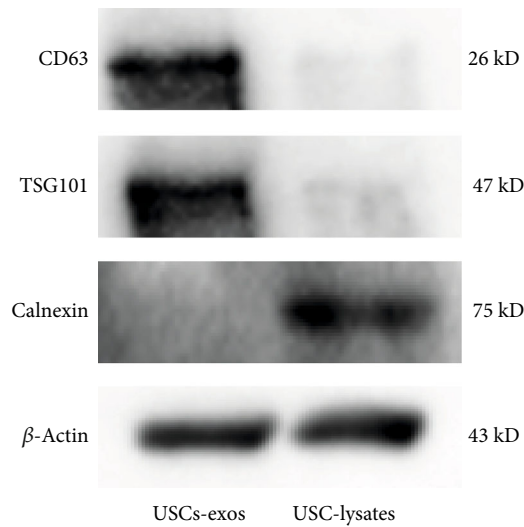


(d)

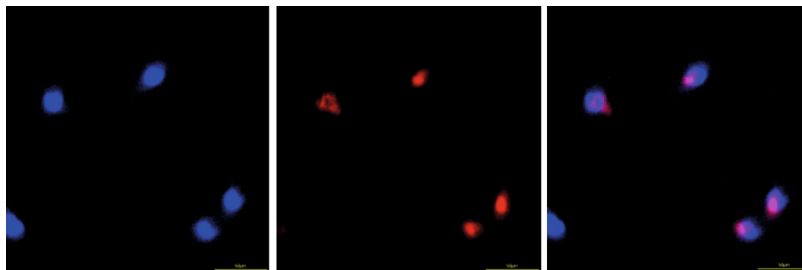
FIGURE 2: Continued.



(e)



(f)



(g)

FIGURE 2: Identification of human USC exosomes (USCs-exos). (a) Human USCs exhibit a short fusiform or spindle-shaped appearance, with sporadic cells appearing on day three (left picture) and large numbers of cells appearing at day seven (right picture). (b) Osteogenic, adipogenic, and chondrogenic differentiation capabilities of USCs were determined by Alizarin Red, Oil Red O, and Alcian Blue staining. (c) USC surface markers (CD29, CD44, and CD73) were detected by flow cytometry. (d) A typical image of USCs-exos morphology as obtained by a transmission electron microscope (TEM). (e) Particle size distribution of USCs-exos as determined by the nanoparticle size analysis. (f) The protein marker of USCs-exos as detected in exosomes and USCs by Western blot analysis. (g) Exosomes taken by NP cells incubated with PKH26-labeled USCs-exos for 12 hours, and NP cell nuclei were stained with DAPI.

[41, 42]. In this study, we found that after pressure incubation, the phosphorylation levels of AKT and ERK in the USCs-exos (100 $\mu\text{g}/\text{ml}$) group were significantly elevated

when compared to the control group (Figures 5(a)–5(c)). Figures 5(d)–5(g) show the expression levels of CHOP and the activation of caspase-3 as well as caspase-12. It was

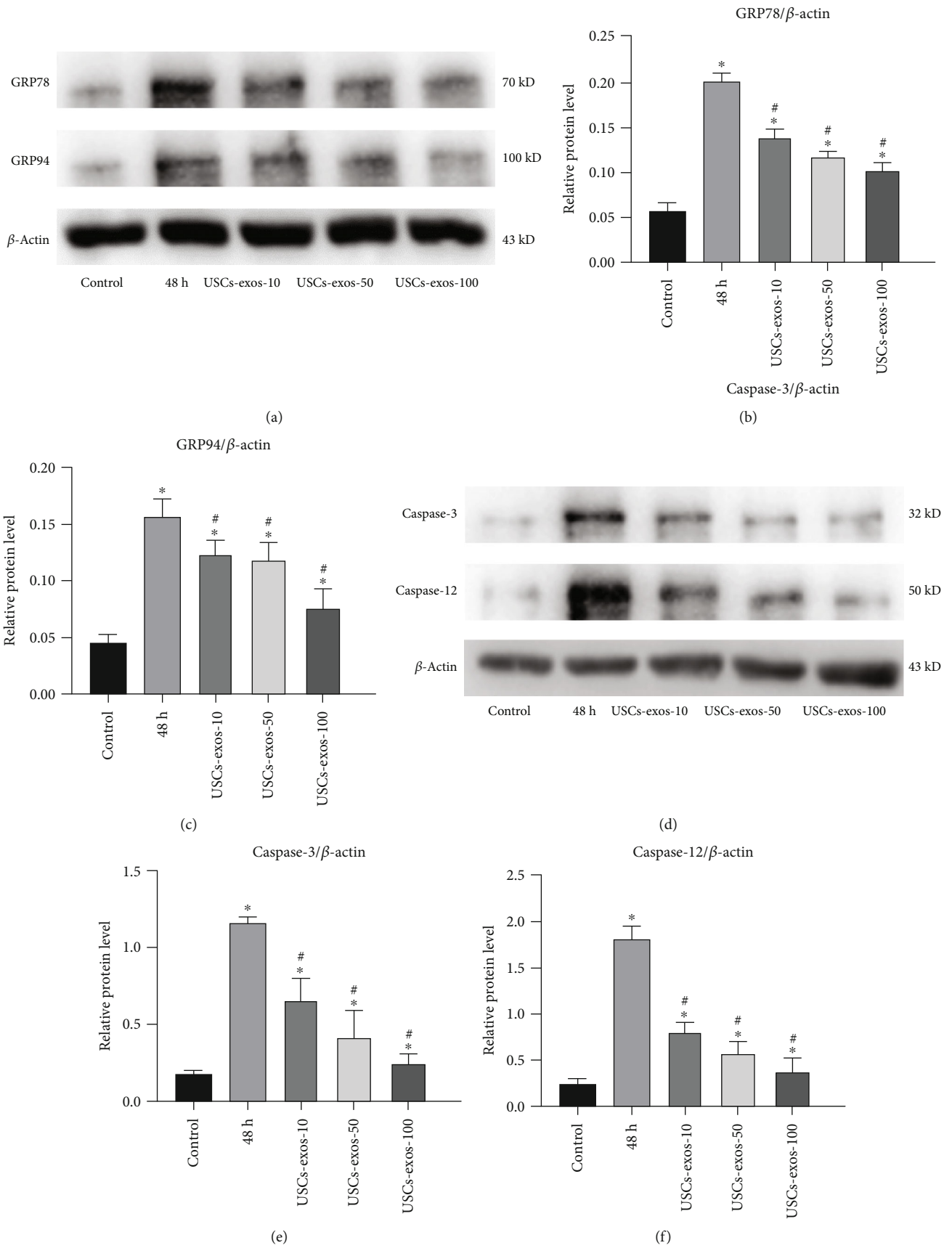


FIGURE 3: Continued.

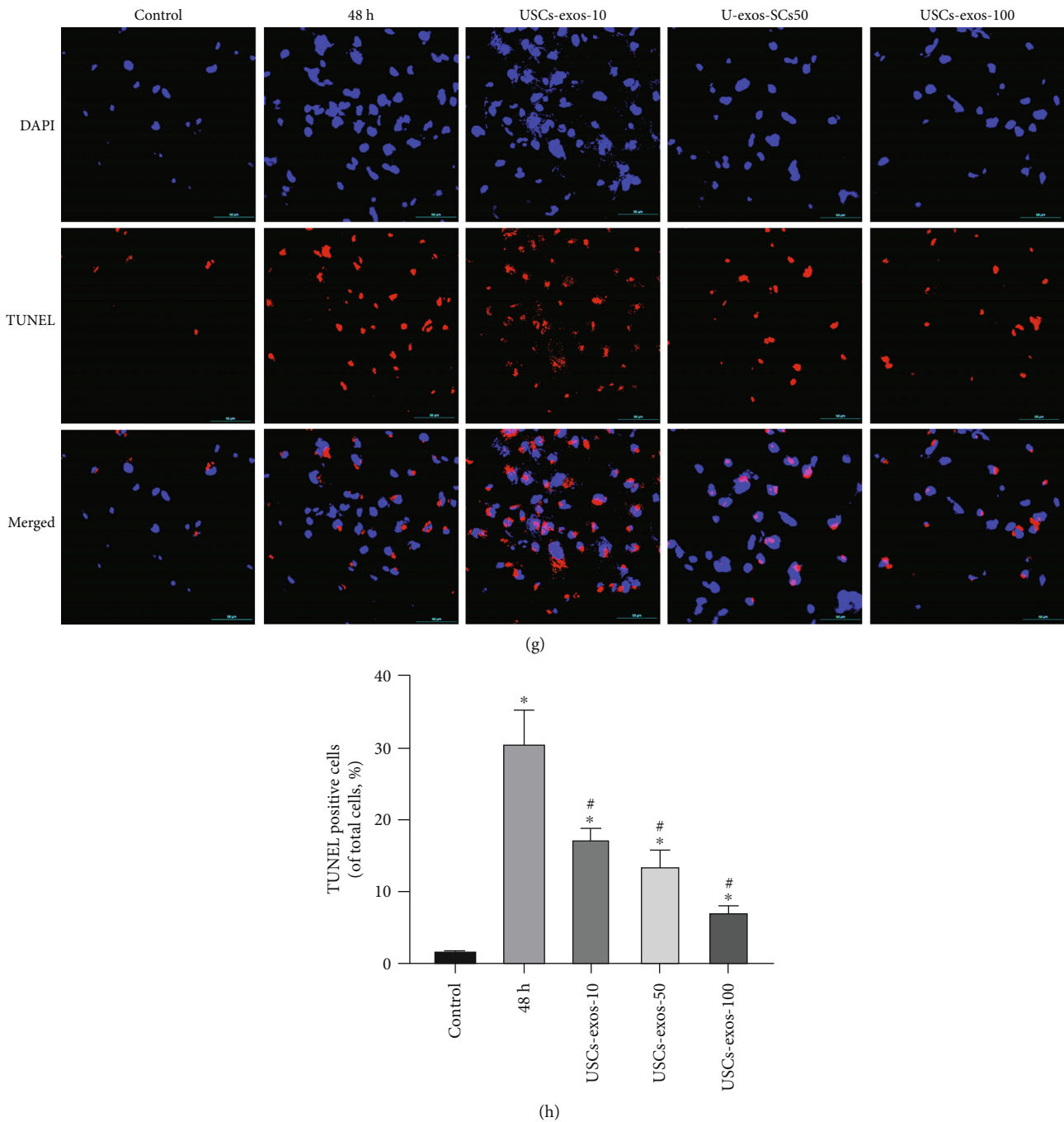
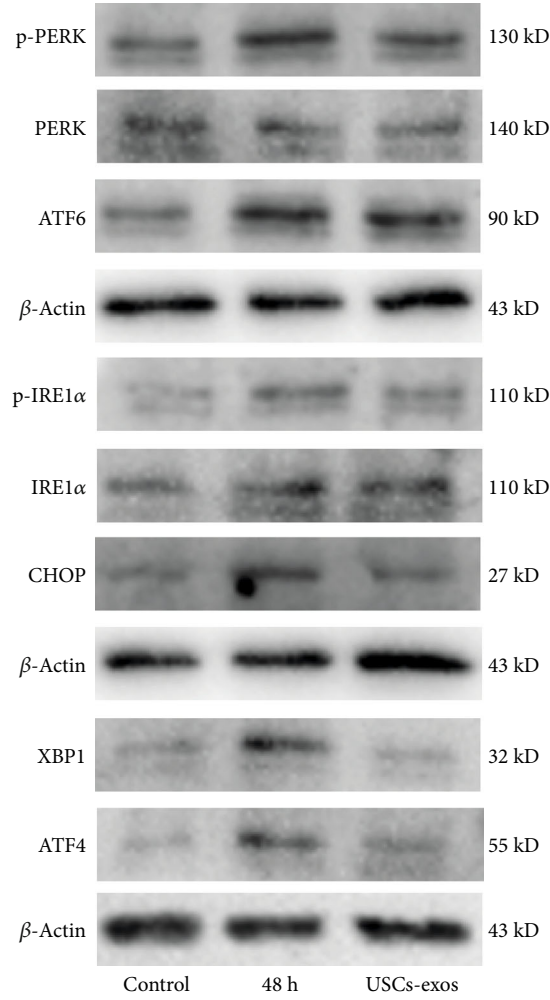


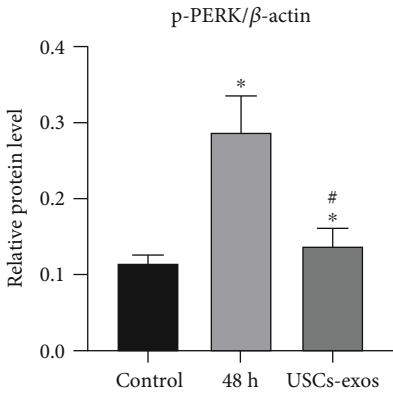
FIGURE 3: Under stress conditions, USCs-exos suppressed the expression of GRP78 and GRP94. Except the control group, NP cells were cultured for 48 h under pressure. USCs-exos-10, 50, and 100 indicated that 10, 50, or 100 $\mu\text{g/ml}$ exosomes were added to each response group. (a) Protein levels of GRP78 and GRP94 were measured by Western blot analysis, and their relative quantities were calculated (b, c) using β -actin as an internal reference. (d) Western blot analysis was used to detect the expression levels of caspase-3 and caspase-12, and their relative quantities (e, f) were calculated using β -actin as an internal reference. (g) Fluorescence images of TUNEL analysis in different groups. The nucleus was stained with DAPI. (h) The proportion of apoptotic cells according to TUNEL staining. Data are expressed as the mean \pm SD. * Compared to the control group, $p < 0.05$; # compared to the 48 h group, $p < 0.05$.

observed that under pressure, the phosphorylation levels of AKT and ERK decreased. This was attributed to the expression of CHOP and the activation of caspase protein. Treatment of the pressure-cultured cells with USCs-exos significantly activated the AKT and ERK signaling pathways,

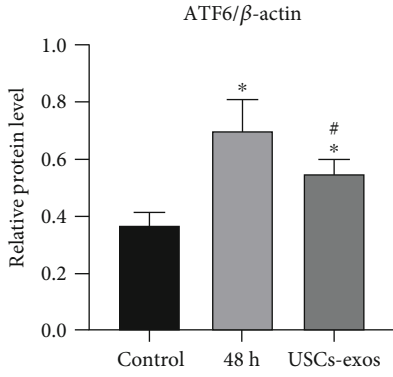
thereby suppressing CHOP expression while downregulating caspase-3 and caspase-12 activation. When the NPCs were treated with AKT signal inhibitor (LY294002) or ERK signal inhibitor (PD98059), the protective effect of USCs-exos was reduced. These experiments imply that USCs-exos partially



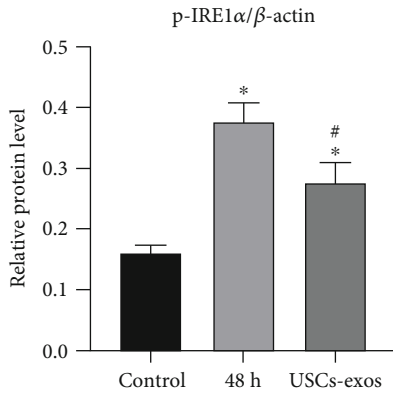
(a)



(b)



(c)



(d)

FIGURE 4: Continued.

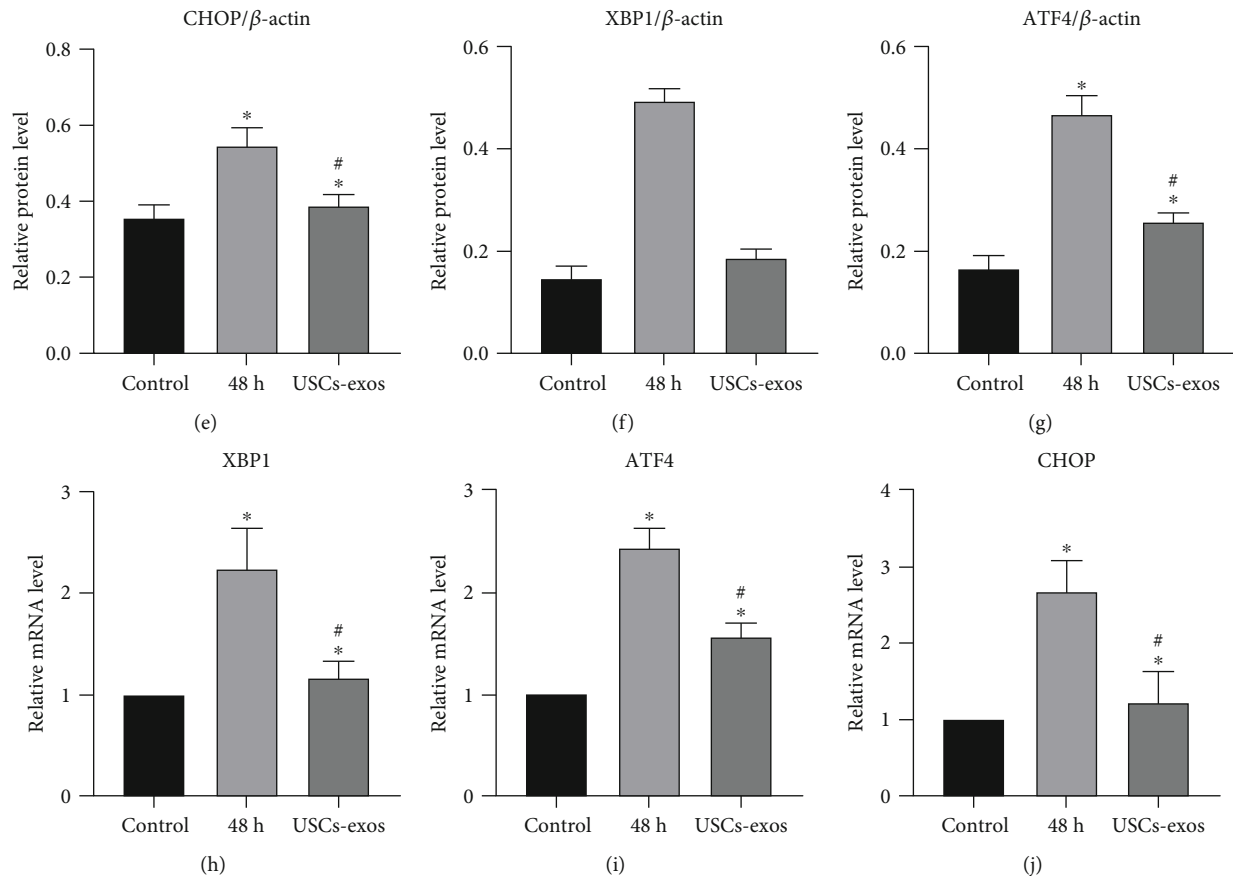


FIGURE 4: USC-exos enhance the activation of UPR and related proteins under stress conditions. The USC-exos group was treated with USC-exos (100 $\mu\text{g}/\text{ml}$). (a–g) Protein expression levels of p-PERK, PERK, ATF6, p-IRE1 α , IRE1 α , XBP1, ATF4, and CHOP as determined by Western blot analysis and calculation of their relative quantities (b–g) using β -actin as an internal reference. (h–j) The transcription levels of XBP1 (h), ATF4 (i), and CHOP (j) as determined by qRT-PCR. The data are expressed as the mean \pm SD. * Compared to the control group, $p < 0.05$; # compared to the 48 h group, $p < 0.05$.

activate AKT and ERK signal transduction pathways in human NPCs to inhibit the related ER stress-induced apoptosis.

3.6. USC-Exos Inhibit ER Stress-Related Apoptosis and Suppress IVD Degeneration. Figures 6(d) and 6(e) show the MRI and CT scans of the rat models at 0, 4, and 8 weeks after the puncture to measure the disc height and degeneration grade. The USC-exos were shown to delay disc degeneration by reducing apoptosis (Figures 6(a)–6(c)). In addition, the characteristic TOCSY two-dimensional spectra of the metabolites and protein solutions of IVD tissues also showed obvious changes (Figure 6(f)). Compared to the simple puncture, the CHOP amino acid residue leucine (Leu) in the IVDs punctured and treated with USC-exos was significantly reduced; the quantity of aspartic acid (Asp), the amino acid residue of caspase-3, in the IVD of the injected exosomes was significantly lower than that of the pure puncture segment; after injection of the exosomes, the anaerobic glycolysis product, lactic acid (Lac), was significantly decreased. The HE and Safranin O-fast green staining of cross-section of IVD tissue showed (Figure 6(g)) that the IVD with a simple puncture was more disordered and looser than the annulus fibrosus injected with USC-exos. Moreover, it contained a

lot of inflammatory cells and scars with degenerating nucleus pulposus tissue protruding into the annulus. In short, the degeneration degree was significantly higher. And on the longitudinal section of the IVD tissue (Figure 6(h)), Masson staining showed that the fibrous tissue content of the IVD in the simple puncture group was significantly higher than that of the USC-exos group, while the nucleus pulposus tissue content was significantly lower than that of the USC-exos group. Similar results were observed with HE staining and Safranin O-fast green staining. These findings were confirmed by the immunohistochemical staining procedure. Compared to the simple puncture group, caspase-3 expression, which is associated with apoptosis, was significantly suppressed after treatment with USC-exos (Figure 6(h)).

Therefore, the *in vivo* study revealed that USC-exos inhibit IDD by inhibiting ER stress-associated cell apoptosis.

4. Discussion

Studies have established that paracrine plays an important role in stem cell-associated inhibition of IDD [43, 44]. Exosomes are the key bioactive paracrine components of stem cells and can replace stem cell transplant-based therapies. Excess stress due to mechanical loads and ER stress is

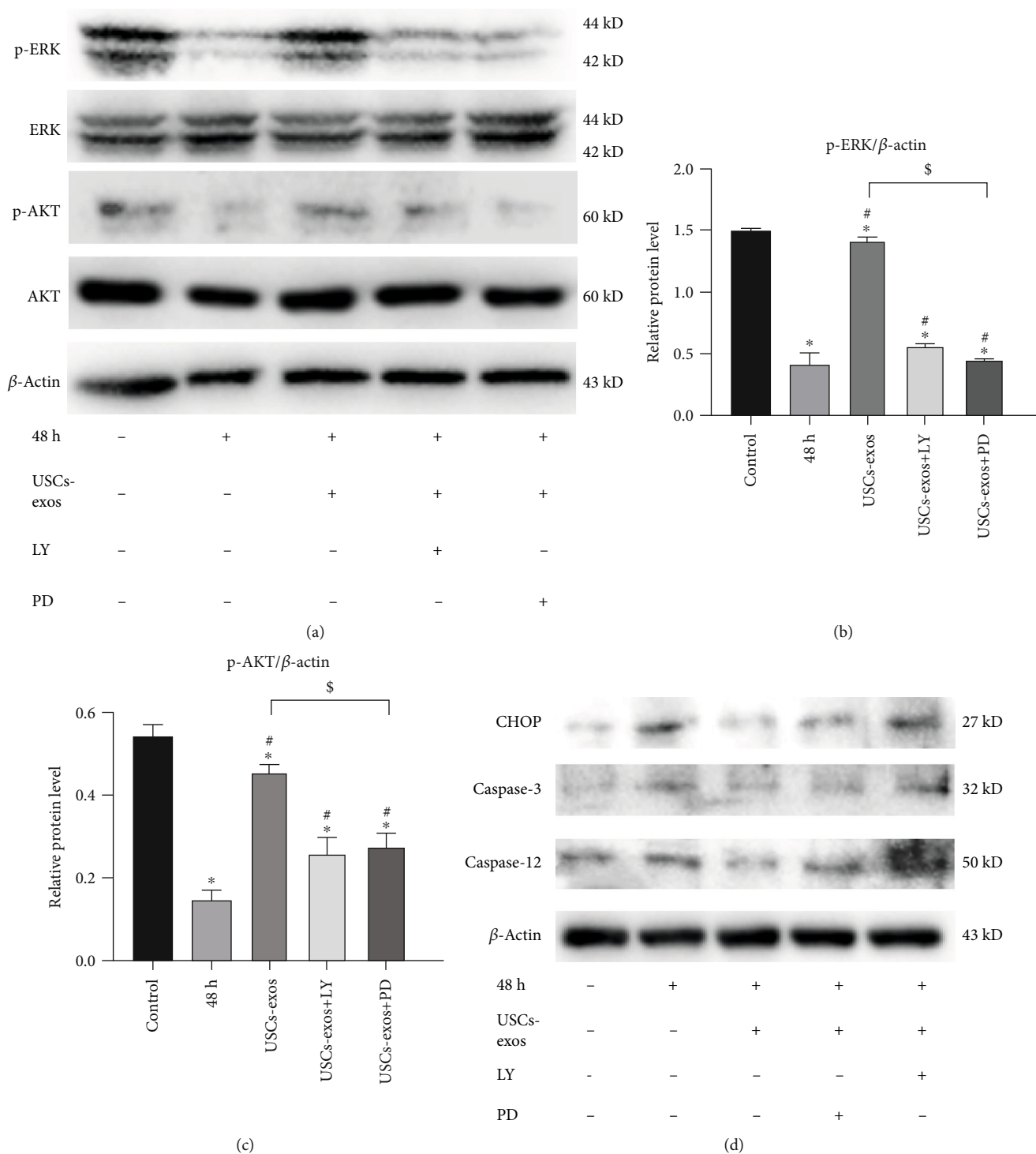


FIGURE 5: Continued.

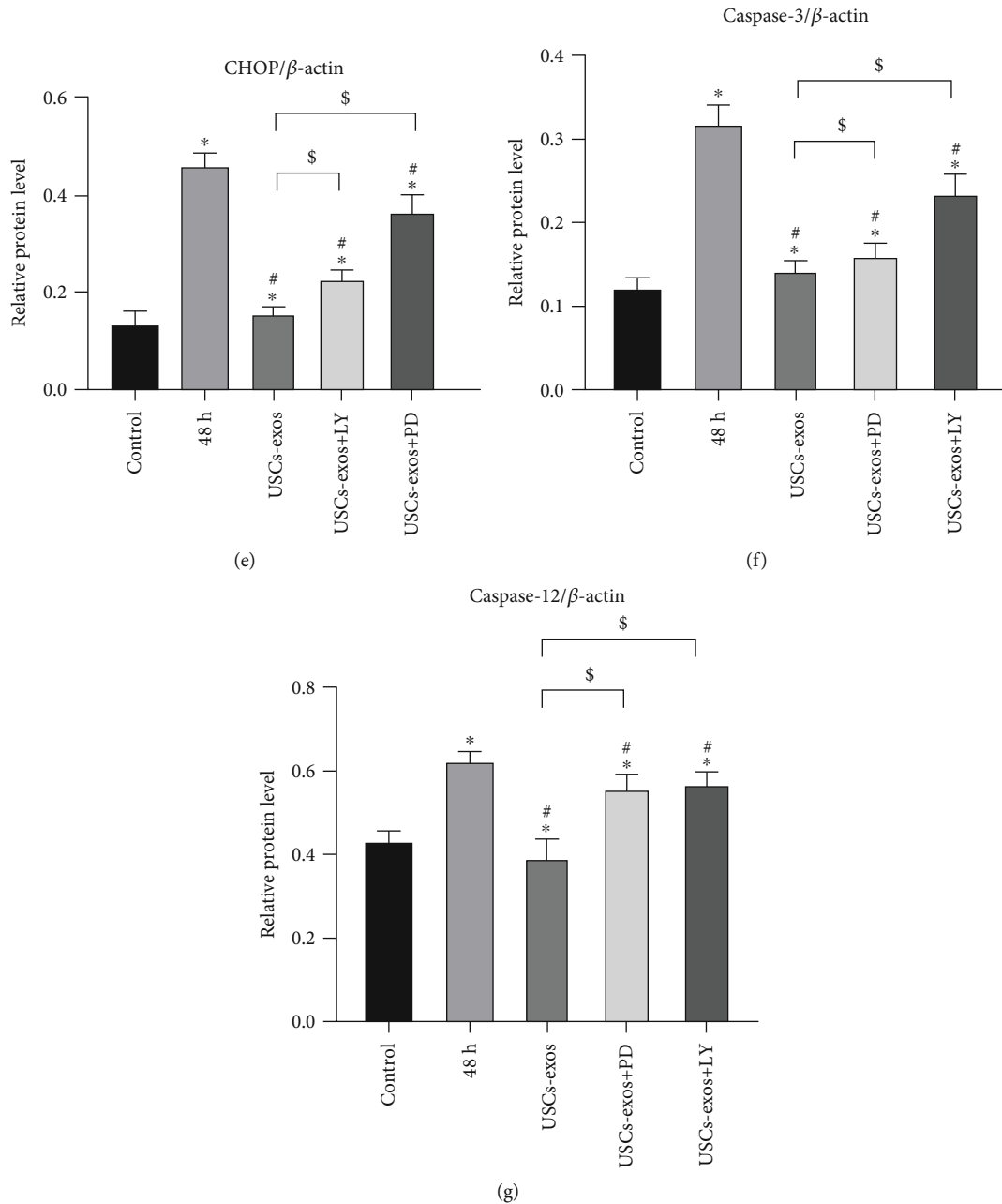


FIGURE 5: USC-exos regulate ER stress under stress-induced conditions by activating the AKT and ERK signaling pathways in NPCs. In the USC-exos group, USC-exos (100 μ g/ml) was added for intervention under pressure. (a–c) Protein levels of AKT, p-AKT, ERK, and p-ERK were evaluated by Western blotting, and their relative quantities were calculated (b, c) using β -actin as the internal reference. LY294002 (LY) is an inhibitor of PI3K/AKT. PD98059 (PD) is an inhibitor of ERK1/2 phosphorylation. (d–g) The protein levels of CHOP, caspase-12, and caspase-3 were measured by Western blotting and statistically analyzed (e–g) using β -actin as an internal control. The data are expressed as the mean \pm SD. *Compared to the control group, $p < 0.05$; # compared to the 48 h group, $p < 0.05$; \$ compared to USC-exos group, $p < 0.05$.

involved in IDD pathogenesis. Abnormal mechanical load-associated pressures can lead to the apoptosis of NPCs [13, 39]. Long-term abnormal pressure enhances ER stress, which leads to cell apoptosis. The earliest response to ER stress is UPR. Long-term excessive stress leads to a transition from adaptive to proapoptotic responses, which cause pathological conditions [45]. The activation of UPR triggers a series of downstream cascade reactions, including ATF4 and XBP1, which enhance the overexpression of CHOP [46–49].

Overexpressed CHOP activates caspase-3 and elevates the apoptotic rate [50].

In this study, USC-exos were shown to inhibit NPCs ER stress-induced cell apoptosis in a dose-dependent manner. The antiapoptotic effect of USC-exos is realized through the inhibition of ER stress and the activation of the AKT and ERK signaling pathways. After prolonged stress stimulation, NPCs exhibit excess ER stress that leads to UPR accumulation. UPR accumulation elevates the secretion of

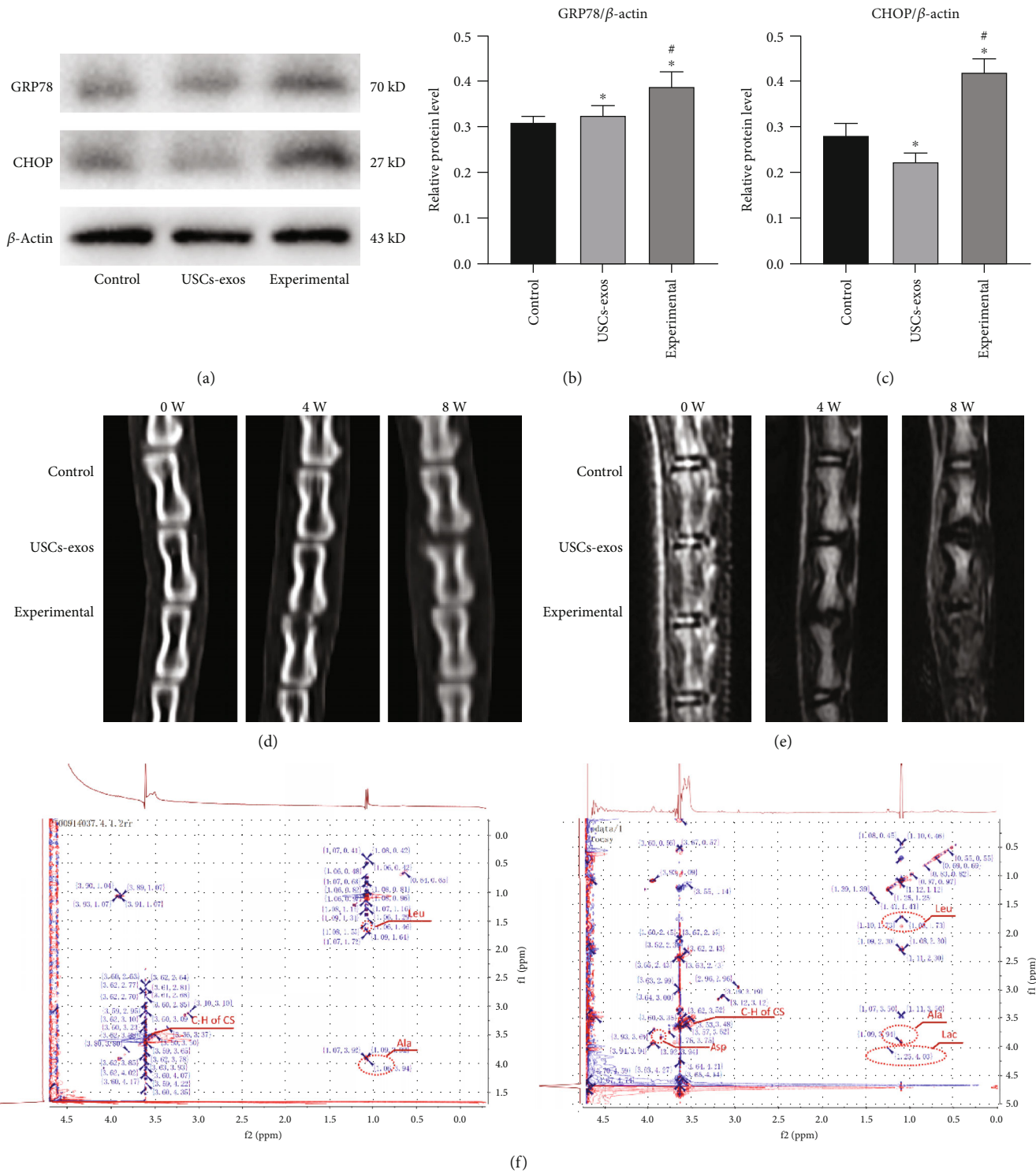


FIGURE 6: Continued.

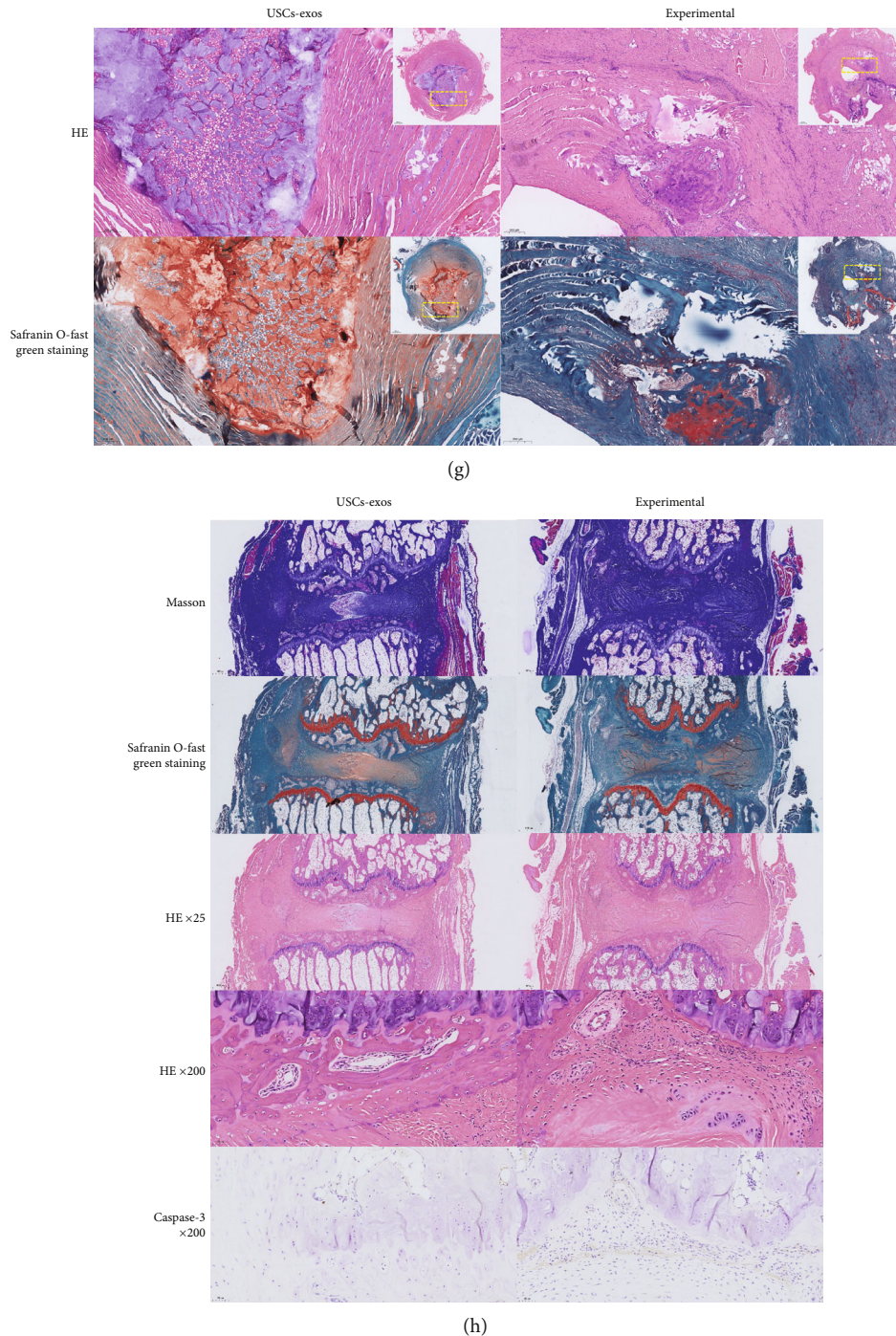


FIGURE 6: USC-exos inhibits ER stress-associated cell apoptosis and delays IDD in vivo. (a–c) The expression levels of GRP78 and CHOP in rat degeneration models as determined by Western blotting, and their relative quantities (b, c). (d) CT scans of the three adjacent IVDs of the rat's tail vertebra at 0, 4, and 8 weeks. The height of the intervertebral space in the experimental group was significantly lower than that of the USC-exos group and the control group. (e) T2W1-weighted images of the MRI scans performed on the rat's tail at 0, 4, and 8 weeks. The degeneration of the experimental group was significantly stronger than that of the USC-exos group and control group. (f) In the NMR detection, compared to the simple puncture, the CHOP amino acid residue leucine (Leu) in the IVDs punctured and injected with USC-exos was significantly suppressed; caspase-3 amino acid residue aspartic acid. The content of the injected exosomes in the IVD is significantly lower than that of the pure puncture segment; lactic acid (Lac) levels were also significantly low. (g) The HE and Safranin O-fast green staining of the IVD revealed that the IVD with simple puncture was more disordered and looser than the annulus fibrosus injected with USC-exos and contained a large number of inflammatory cells and scars. The degenerated nucleus pulposus tissue protrudes into the annulus fibrosus. (h) Masson staining, Safranin O-fast green staining, and HE staining all showed that the degree of degeneration of the IVD tissue of injected USC-exos was less, and IHC showed that the expression of caspase-3 was lower. *Compared to the control group, $p < 0.05$; # compared to the USC-exos group, $p < 0.05$.

CHOP protein that cleaves caspase-12 and caspase-3. In addition, a modified gas pressurization device was used to cultivate NPCs. As the pressurization time increased, the expression levels of GRP78 and CHOP increased. Furthermore, the expression levels of caspase-12 and caspase-3 were also elevated. Treatment of NPCs using USCs-exos revealed that as the exos concentration increased, the expression levels of CHOP, caspase-3, and caspase-12 decreased. This indicates that USCs-exos inhibited NPC apoptosis by inhibiting ER stress in a dose-dependent manner. Therefore, we hypothesized that stress stimulation promotes IDD progression through ER stress. Inhibiting ER stress may, therefore, be an effective way of delaying or reversing IDD.

Stem cells are considered to be ideal for IVD regeneration because they can prevent IVD cells from aging and apoptosis [51]. Studies have found that exosomes can be used among different individuals or species and are, therefore, viable alternatives to stem cell transplantation therapy [29, 52, 53]. The effects of MSCs-exos on immune regulation, wound healing, inflammation, and regulation of apoptosis have been documented [41, 42, 54, 55]. However, the sources of MSCs are limited. The acquisition procedures of these MSCs cause trauma to the body and are expensive, thereby limiting their use [56, 57]. Compared to the other types of stem cells, human USCs are obtained from noninvasive sources and their acquisition procedures do not violate ethics, avoid immune rejection when used in autologous therapy, have a low cost of culture, and have a faster proliferative rate [32, 58]. The human USCs can differentiate into the mesoderm cell lineage, including muscle cells, adipocytes, bone cells, chondrocytes, and endothelial cells [30]. Compared to the use of MSCs in IDD therapy, USCs are a more ideal choice. When cells were treated with AKT antagonists or ERK antagonists, the antiapoptotic effect of USCs-exos was reduced. This shows that under severe ER stress, USCs-exos inhibit CHOP expression to reduce the activation of its lower-level caspase. USCs-exos inhibit excess ER stress by activating the AKT and ERK signaling pathways, suppressing UPR activation, and inhibiting CHOP expression and accumulation. These effects inhibit NPC apoptosis.

Extracellular vesicles (EVs) are membrane organelles of different sizes that are actively secreted by living cells. According to their secretion manner, they can be classified into three subgroups: apoptotic bodies, microvesicles, and exosomes [59]. Exosomes have a unique double-layer membrane structure, which makes it difficult for the substances they contain to be degraded by various enzymes in body fluids. Exosomes can be extracted and identified through their unique shape, size, and density range, as well as specific molecular markers on their surfaces. The process of IDD is associated with changes in various signal transduction mechanisms such as Wnt/ β -catenin, MAPK, NF- κ B, Notch, and PI3K/Akt. These cell signaling pathways cross-influence each other to form a very complex signaling pathway network, which regulates IDD. The IDD process is accompanied by NPC apoptosis. However, the activation of the ERK signaling pathway in PI3K/Akt and MAPK inhibits cell apoptosis, promotes cell proliferation, and delays IDD. Yang et al. [60] found that estrogen can reduce the expression of caspase-3

by activating the PI3K/Akt pathway, thereby reducing the apoptosis of NPCs. Shabbir et al. [61] reported that exosomes from human bone marrow-derived MSCs can activate signal transduction pathways including Akt, Erk1/2, and STAT3 in fibroblasts. Zhang et al. [55] documented that human UCB-derived MSCs shuttle the Wnt4 protein, which induces β -catenin nuclear translocation and enhances epidermal cell activity. Exosomes in plasma activate the AKT and ERK pathways to promote angiogenesis and increase the expression of antiapoptotic proteins [42]. The proteins contained in exosomes have also been found to mediate the activation of AKT and ERK signals [62]. AKT and ERK signal transduction pathways are involved in the regulation of cell proliferation and migration, as well as protein synthesis, apoptosis, and metabolism [62–64]. Xu et al. found that inhibition of the AKT and ERK signaling pathways enhances ER stress and mitochondrial dysfunction-associated apoptosis [34]. We hypothesized that USCs-exos inhibit ER stress-induced apoptosis by activating the AKT and ERK signaling pathways. Elevated CHOP expression levels suppressed AKT and ERK phosphorylation. However, treatment with USCs-exos activated the AKT and ERK signaling pathways to a certain extent, thereby reducing the apoptotic rate of human NP cells. Moreover, the PI3K/AKT inhibitor (LY294002) and the ERK inhibitor (PD98059) suppressed the antiapoptotic effect of exosomes. Therefore, USCs-exos inhibit ER stress with CHOP as a downstream product.

The *in vivo* experiment revealed that the 21 G puncture needle can effectively cause IDD. However, the IDD degree was lower in the USCs-exos-treated group when compared to the untreated group. These findings imply that exosomes can effectively delay IDD *in vivo*. *In vivo* studies have shown that USCs-exos slow down IDD by suppressing NPC apoptosis, which is consistent with the *in vitro* experiment results. The expression of GRP78 and CHOP in the degenerated IVD tissue was significantly elevated, indicating that IDD is closely correlated with ER stress. In addition, the increase in pressure culture time elevated the expression levels of GRP78 and CHOP in NPCs, indicating an increase in ER stress. Equally, USCs-exos intervention suppressed the expression of GRP78, CHOP, caspase-3, and caspase-12. The injection of USCs-exos into the IVD of rats can reduce GRP78 and CHOP expression levels, indicating that exos inhibit ER stress-induced IDD. Metabolomics revealed that compared to the IVDs treated with USCs-exos, the levels of leucine (Leu), aspartic acid (Asp), and lactic acid in the purely degenerated tissue were significantly higher while the alterations in alanine (Ala) levels were small and transient. Leucine was attributed to be the amino acid residue of CHOP and aspartic acid as the amino acid residue of caspase-3, while lactic acid was the product of anaerobic glycolysis caused by ER stress. Treatment with USCs-exos caused these alterations.

The lack of nutrients in the IDD microenvironment enhances the degeneration process [65, 66]. Sufficient amounts of nutrients are required for cell survival and function. Due to the avascular nature of IVD [67–69], important nutrients (such as glucose and oxygen) can only be transferred from the capillaries of the endplate or the edge of AF to the area of the nucleus pulposus through the extracellular

matrix (ECM). This translocation sharply reduces nutrient concentration in the NPCs [70–72], making it extremely difficult to maintain a healthy state of IVD. The hypoxic environment may be a normal condition of IVD cells, and the increase in oxygen concentration after IVD degeneration may be considered a pathological condition [73]. During degeneration, there is tissue angiogenesis that leads to more blood supply [74]. Studies have also reported that hypoxia promotes ECM synthesis in mammalian IVD cells [75–77]; therefore, it is essential for maintaining the normal IVD physiological structure and function. Moreover, as cells adapt, changes in oxygen concentration activate or inhibit the expression of multiple genes such as the hypoxia-inducible factor-1 (HIF-1) [78]. Hypoxia-inducible factor (HIF) is a transcription factor that responds to hypoxic tension and is one of the most important factors that directly mediate cell response to hypoxia. HIF-1 is involved in the homeostasis of NP, energy metabolism, and extracellular matrix (ECM) metabolism of NPC [79, 80]. Schipani et al. [81] reported that HIF-1 plays an important role in avascular tissue survival and increases the enzyme activity of glycolysis and metabolism under hypoxic conditions. Meng et al. [82] documented that HIF-1 knockout causes IDD. Furthermore, the interactions between HIF-1 α and the intracellular domain of Notch protein (Notch-ICD) inhibit the differentiation of myoblasts and neural precursor cells. Hypoxia elevates the expression levels of known Notch target genes, such as Hes1 and Hey1 [83]. The Notch pathway may be involved in signal transduction during the normal functioning of IVD. IVD is a relatively complex structure in the human body. Only by using a three-dimensional (3D) structure can its in vitro growth be simulated. Rastogi et al. [84] found that the 3D structure can better maintain the IVD cell phenotype when compared to the 2D monolayer structure. Gantenbein et al. [85] also showed that 3D salt culture partially prevented the rapid loss of cell components for up to 34 days. Utilization of 3D structures in studies may change the cell's perception of physical, spatial, and biochemical factors [86]. It can also affect cell responses to inflammation and hypoxic stimulation. Studies have also shown that the 3D structure exhibits an immunomodulatory effect on the expression of catabolic genes in inflammatory and hypoxic environments [87]. The functional mechanisms of HIF-1 could be attributed to the signal transduction role of the Notch pathway. The specific mechanism has not yet been established.

Exosomes have the potential to treat IDD. MSCs-exos promote NPC proliferation and enhance the secretion of the extracellular matrix [27]. Lu et al. found that MSCs-exos inhibit NPC apoptosis by targeting the transfer of exosomal microRNA that activates the PI3K/AKT pathway [26]. Liao et al. [88] incubated MSCs-exos with NPCs induced by advanced glycation end products and confirmed that the levels of apoptosis-related markers (caspase-3 and caspase-12) were significantly suppressed. In this experiment, USC-exos were used to intervene NPC apoptosis. The findings were consistent with the results of previous studies. Although this study revealed that USC-exos inhibit ER stress-induced apoptosis by activating the AKT and ERK signal transduction pathways, the specific signal molecules

involved have not been established. This study was limited by the parallel verification of the effectiveness of metabolomics and proteomics.

In conclusion, USC-exos inhibited ER stress-induced apoptosis of NPCs in vivo and in vitro. Moreover, the unique advantages of USCs and their exosomes enhance their consideration as therapeutic options for IDD.

Data Availability

All the data and material can be available from HongFei Xiang, WeiLiang Su, XiaoLin Wu, Zhu Guo, DongMing Xing, and BoHua Chen for reasonable request.

Ethical Approval

This study was approved by the ethical committee of the Affiliated Hospital of Qingdao University. The data of study participants was coded for confidentiality and compliance with the Declaration of Helsinki.

Consent

The study participants were required to give written informed consent.

Conflicts of Interest

The authors declare that they have no conflict of interest.

Authors' Contributions

HongFei Xiang, WeiLiang Su, BoHua Chen, and Zhu Guo designed the study; WeiLiang Su, HongFei Xiang, Zhu Guo, Chang Liu, Shuai Yang, WenBin Cong, XiaoLin Wu, WuJun Chen, DongMing Xing, Yan Wang, GuoQing Zhang, Shang-You Yang, and ChenSheng Qiu enrolled the study participants and collected data; WeiLiang Su and Zhu Guo analyzed the data; WeiLiang Su, BoHua Chen, and Zhu Guo interpreted the data and wrote the manuscript. All authors reviewed and approved the manuscript. HongFei Xiang, WeiLiang Su, and XiaoLin Wu contributed contributed equally to this work.

Acknowledgments

This study was funded by the National Natural Science Foundation of China (81802190 and 81772412), Shandong Provincial Science Foundation, China (ZR2019BH084), Young Taishan Scholars Program (tsqn201909190), Qingdao Basic Applied Research Project (19-6-2-51-cg), and National Key Research and Development Project (2019YFC0121404).

References

- [1] G. J. Macfarlane, E. Thomas, P. R. Croft, A. C. Papageorgiou, M. I. V. Jayson, and A. J. Silman, "Predictors of early improvement in low back pain amongst consulters to general practice: the influence of pre-morbid and episode-related factors," *Pain*, vol. 80, no. 1, pp. 113–119, 1999.

- [2] J. Fu, W. Yu, and D. Jiang, "Acidic pH promotes nucleus pulposus cell senescence through activating the p38 MAPK pathway," *Bioscience Reports*, vol. 38, no. 6, 2018.
- [3] B. A. Frost, S. Camarero-Espinosa, and E. J. Foster, "Materials for the spine: anatomy, problems, and solutions," *Materials*, vol. 12, no. 2, p. 253, 2019.
- [4] F. ZHANG, X. ZHAO, H. SHEN, and C. ZHANG, "Molecular mechanisms of cell death in intervertebral disc degeneration (review)," *International Journal of Molecular Medicine*, vol. 37, no. 6, pp. 1439–1448, 2016.
- [5] F. Ding, Z. W. Shao, and L. M. Xiong, "Cell death in intervertebral disc degeneration," *Apoptosis*, vol. 18, no. 7, pp. 777–785, 2013.
- [6] C. Q. Zhao, L. S. Jiang, and L. Y. Dai, "Programmed cell death in intervertebral disc degeneration," *Apoptosis*, vol. 11, no. 12, pp. 2079–2088, 2006.
- [7] J.-B. Park, I.-C. Park, S.-J. Park, H.-O. Jin, J.-K. Lee, and K. D. Riew, "Anti-apoptotic effects of caspase inhibitors on rat intervertebral disc cells," *The Journal of Bone and Joint Surgery. American Volume*, vol. 88, no. 4, pp. 771–779, 2006.
- [8] H. E. Gruber and E. J. Hanley, "Analysis of aging and degeneration of the human intervertebral disc," *Spine*, vol. 23, no. 7, pp. 751–757, 1998.
- [9] F. Rannou, T. S. Lee, R. H. Zhou et al., "Intervertebral disc degeneration: the role of the mitochondrial pathway in annulus fibrosus cell apoptosis induced by overload," *The American Journal of Pathology*, vol. 164, no. 3, pp. 915–924, 2004.
- [10] C. K. Kepler, R. K. Ponnappan, C. A. Tannoury, M. V. Risbud, and D. G. Anderson, "The molecular basis of intervertebral disc degeneration," *Spine Journal*, vol. 15, no. 3, pp. 318–330, 2012.
- [11] L. A. Setton and J. Chen, "Mechanobiology of the intervertebral disc and relevance to disc degeneration," *The Journal of Bone and Joint Surgery (American)*, vol. 88, Supplement 2, pp. 52–57, 2006.
- [12] H. J. Wilke, P. Neef, M. Caimi, T. Hoogland, and L. E. Claes, "New in vivo measurements of pressures in the intervertebral disc in daily life," *Spine*, vol. 24, no. 8, pp. 755–762, 1999.
- [13] K. Zhang, C. Xue, N. Lu et al., "Mechanical loading mediates human nucleus pulposus cell viability and extracellular matrix metabolism by activating of NF- κ B," *Experimental and Therapeutic Medicine*, vol. 18, no. 3, pp. 1587–1594, 2019.
- [14] R. Gawri, D. H. Rosenzweig, E. Krock et al., "High mechanical strain of primary intervertebral disc cells promotes secretion of inflammatory factors associated with disc degeneration and pain," *Arthritis Research & Therapy*, vol. 16, no. 1, p. R21, 2014.
- [15] C. Wang, S. Gonzales, H. Levene, W. Gu, and C. Y. C. Huang, "Energy metabolism of intervertebral disc under mechanical loading," *Journal of Orthopaedic Research*, vol. 31, no. 11, pp. 1733–1738, 2013.
- [16] T. Verfaillie, A. D. Garg, and P. Agostinis, "Targeting ER stress induced apoptosis and inflammation in cancer," *Cancer Letters*, vol. 332, no. 2, pp. 249–264, 2013.
- [17] Y. Cao, J. Long, L. Liu et al., "A review of endoplasmic reticulum (ER) stress and nanoparticle (NP) exposure," *Life Sciences*, vol. 186, pp. 33–42, 2017.
- [18] R. Sano and J. C. Reed, "ER stress-induced cell death mechanisms," *Biochimica et Biophysica Acta*, vol. 1833, no. 12, pp. 3460–3470, 2013.
- [19] I. Kim, W. Xu, and J. C. Reed, "Cell death and endoplasmic reticulum stress: disease relevance and therapeutic opportunities," *Nature Reviews. Drug Discovery*, vol. 7, no. 12, pp. 1013–1030, 2008.
- [20] R. Jäger, M. J. Bertrand, A. M. Gorman, P. Vandennebeele, and A. Samali, "The unfolded protein response at the crossroads of cellular life and death during endoplasmic reticulum stress," *Biology of the Cell*, vol. 104, no. 5, pp. 259–270, 2012.
- [21] I. Tabas and D. Ron, "Integrating the mechanisms of apoptosis induced by endoplasmic reticulum stress," *Nature Cell Biology*, vol. 13, no. 3, pp. 184–190, 2011.
- [22] M. A. Hunt, J. M. Charlton, and J. F. Esculier, "Osteoarthritis year in review 2019: mechanics," *Osteoarthritis and Cartilage*, vol. 28, no. 3, pp. 267–274, 2020.
- [23] H. Yang, Y. Wen, M. Zhang et al., "MTORC1 coordinates the autophagy and apoptosis signaling in articular chondrocytes in osteoarthritic temporomandibular joint," *Autophagy*, vol. 16, no. 2, pp. 271–288, 2020.
- [24] M. Wang and R. J. Kaufman, "Protein misfolding in the endoplasmic reticulum as a conduit to human disease," *Nature*, vol. 529, no. 7586, pp. 326–335, 2016.
- [25] X. Cheng, G. Zhang, L. Zhang et al., "Mesenchymal stem cells deliver exogenous miR-21 via exosomes to inhibit nucleus pulposus cell apoptosis and reduce intervertebral disc degeneration," *Journal of Cellular and Molecular Medicine*, vol. 22, no. 1, pp. 261–276, 2018.
- [26] K. Lu, H.-y. Li, K. Yang et al., "Exosomes as potential alternatives to stem cell therapy for intervertebral disc degeneration: in-vitro study on exosomes in interaction of nucleus pulposus cells and bone marrow mesenchymal stem cells," *Stem Cell Research & Therapy*, vol. 8, no. 1, p. 108, 2017.
- [27] S. Rani, A. E. Ryan, M. D. Griffin, and T. Ritter, "Mesenchymal stem cell-derived extracellular vesicles: toward cell-free therapeutic applications," *Molecular Therapy*, vol. 23, no. 5, pp. 812–823, 2015.
- [28] S. Kourembanas, "Exosomes: vehicles of intercellular signaling, biomarkers, and vectors of cell therapy," *Annual Review of Physiology*, vol. 77, no. 1, pp. 13–27, 2015.
- [29] W. S. Toh, R. C. Lai, J. Hui, and S. K. Lim, "MSC exosome as a cell-free MSC therapy for cartilage regeneration: implications for osteoarthritis treatment," *Seminars in Cell & Developmental Biology*, vol. 67, pp. 56–64, 2017.
- [30] Y. Zhang, E. McNeill, H. Tian et al., "Urine derived cells are a potential source for urological tissue reconstruction," *Journal of Urology*, vol. 180, no. 5, pp. 2226–2233, 2008.
- [31] X. Ji, M. Wang, F. Chen, and J. Zhou, "Urine-derived stem cells: the present and the future," *Stem Cells International*, vol. 2017, Article ID 4378947, 8 pages, 2017.
- [32] N. P. A. Manaph, M. Al-Hawwas, L. Bobrovskaya, P. T. Coates, and X.-F. Zhou, "Urine-derived cells for human cell therapy," *Stem Cell Research & Therapy*, vol. 9, no. 1, p. 189, 2018.
- [33] T. Fujii, N. Fujita, S. Suzuki et al., "The unfolded protein response mediated by PERK is casually related to the pathogenesis of intervertebral disc degeneration," *Journal of Orthopaedic Research*, vol. 36, no. 5, pp. 1334–1345, 2018.
- [34] D. Xu, H. Jin, J. Wen et al., "Hydrogen sulfide protects against endoplasmic reticulum stress and mitochondrial injury in nucleus pulposus cells and ameliorates intervertebral disc degeneration," *Pharmacological Research*, vol. 117, pp. 357–369, 2017.

- [35] C. Benda, T. Zhou, X. Wang et al., "Urine as a source of stem cells," *Advances in Biochemical Engineering/Biotechnology*, vol. 129, pp. 19–32, 2012.
- [36] S. E. Tayhan, G. Tezcan Keles, I. Topcu, E. Mir, and S. Ismet Deliloglu Gurhan, "Isolation and in vitro cultivation of human urine-derived cells: an alternative stem cell source," *Turkish Journal of Urology*, vol. 43, no. 3, pp. 345–349, 2017.
- [37] D. Zhang, G. Wei, P. Li, X. Zhou, and Y. Zhang, "Urine-derived stem cells: a novel and versatile progenitor source for cell-based therapy and regenerative medicine," *Genes & Diseases*, vol. 1, no. 1, pp. 8–17, 2014.
- [38] H. Liu, W. Wang, X. Li et al., "The high hydrostatic pressure induces apoptosis of retinal ganglion cells via regulation of the NGF plays signalling pathway," *Molecular Medicine Reports*, vol. 12, no. 6, pp. 5321–5334, 2019.
- [39] Z. Li, Z. Shao, S. Chen et al., "TIGAR impedes compression-induced intervertebral disc degeneration by suppressing nucleus pulposus cell apoptosis and autophagy," *Journal of Cellular Physiology*, vol. 235, no. 2, pp. 1780–1794, 2019.
- [40] I. Hirsch, M. Weiwad, E. Prell, and D. M. Ferrari, "ERp29 deficiency affects sensitivity to apoptosis via impairment of the ATF6-CHOP pathway of stress response," *Apoptosis*, vol. 19, no. 5, pp. 801–815, 2014.
- [41] S. C. Guo, S. C. Tao, W. J. Yin, X. Qi, T. Yuan, and C. Q. Zhang, "Exosomes derived from platelet-rich plasma promote the re-epithelization of chronic cutaneous wounds via activation of YAP in a diabetic rat model," *Theranostics*, vol. 7, no. 1, pp. 81–96, 2017.
- [42] S. C. Tao, T. Yuan, B. Y. Rui, Z. Z. Zhu, S. C. Guo, and C. Q. Zhang, "Exosomes derived from human platelet-rich plasma prevent apoptosis induced by glucocorticoid-associated endoplasmic reticulum stress in rat osteonecrosis of the femoral head via the Akt/Bad/Bcl-2 signal pathway," *Theranostics*, vol. 7, no. 3, pp. 733–750, 2017.
- [43] F. Yang, V. Y. Leung, K. D. Luk, D. Chan, and K. M. C. Cheung, "Mesenchymal stem cells arrest intervertebral disc degeneration through chondrocytic differentiation and stimulation of endogenous cells," *Molecular Therapy*, vol. 17, no. 11, pp. 1959–1966, 2009.
- [44] V. Y. Leung, D. M. Aladin, F. Lv et al., "Mesenchymal stem cells reduce intervertebral disc fibrosis and facilitate repair," *Stem Cells*, vol. 32, no. 8, pp. 2164–2177, 2014.
- [45] F. Engin, T. Nguyen, A. Yermalovich, and G. S. Hotamisligil, "Aberrant islet unfolded protein response in type 2 diabetes," *Scientific Reports*, vol. 4, p. 4054, 2015.
- [46] R. Guo, W. Liu, B. Liu, B. Zhang, W. Li, and Y. Xu, "SIRT1 suppresses cardiomyocyte apoptosis in diabetic cardiomyopathy: an insight into endoplasmic reticulum stress response mechanism," *International Journal of Cardiology*, vol. 191, pp. 36–45, 2015.
- [47] C. E. Senkal, S. Ponnusamy, J. Bielawski, Y. A. Hannun, and B. Ogretmen, "Antiapoptotic roles of ceramide-synthase-6-generated C16-ceramide via selective regulation of the ATF6/CHOP arm of ER-stress-response pathways," *The FASEB Journal*, vol. 24, no. 1, pp. 296–308, 2009.
- [48] Z. Xu, Y. Bu, N. Chitnis, C. Koumenis, S. Y. Fuchs, and J. A. Diehl, "miR-216b regulation of c-Jun mediates GADD153/CHOP-dependent apoptosis," *Nature Communications*, vol. 7, no. 1, p. 11422, 2016.
- [49] E. Segezdi, S. E. Logue, A. M. Gorman, and A. Samali, "Mediators of endoplasmic reticulum stress-induced apoptosis," *EMBO Reports*, vol. 7, no. 9, pp. 880–885, 2006.
- [50] X. Ding, M. Ma, J. Teng, F. Shao, E. Wu, and X. Wang, "Numb protects human renal tubular epithelial cells from bovine serum albumin-induced apoptosis through antagonizing CHOP/PERK pathway," *Journal of Cellular Biochemistry*, vol. 117, no. 1, pp. 163–171, 2016.
- [51] S. M. Richardson, G. Kalamegam, P. N. Pushparaj et al., "Mesenchymal stem cells in regenerative medicine: focus on articular cartilage and intervertebral disc regeneration," *Methods*, vol. 99, pp. 69–80, 2016.
- [52] J. Meldolesi, "Exosomes and ectosomes in intercellular communication," *Current Biology*, vol. 28, no. 8, pp. R435–R444, 2018.
- [53] A. Monsel, Y. G. Zhu, S. Gennai et al., "Therapeutic effects of human mesenchymal stem cell-derived microvesicles in severe pneumonia in mice," *American Journal of Respiratory and Critical Care Medicine*, vol. 192, no. 3, pp. 324–336, 2015.
- [54] S. Cosenza, K. Toupet, M. Maumus et al., "Mesenchymal stem cells-derived exosomes are more immunosuppressive than microparticles in inflammatory arthritis," *Theranostics*, vol. 8, no. 5, pp. 1399–1410, 2018.
- [55] B. Zhang, M. Wang, A. Gong et al., "HucMSC-exosome mediated-Wnt4 signaling is required for cutaneous wound healing," *Stem Cells*, vol. 33, no. 7, pp. 2158–2168, 2015.
- [56] M. A. Javaid, "Mesenchymal stem cell-based bone tissue engineering," *International Dental Journal of Students Research*, vol. 1, no. 3, pp. 24–35, 2012.
- [57] D. Sakai and G. B. Andersson, "Stem cell therapy for intervertebral disc regeneration: obstacles and solutions," *Nature Reviews Rheumatology*, vol. 11, no. 4, pp. 243–256, 2015.
- [58] D. Qin, T. Long, J. Deng, and Y. Zhang, "Urine-derived stem cells for potential use in bladder repair," *Stem Cell Research & Therapy*, vol. 5, no. 3, p. 69, 2014.
- [59] R. Crescitelli, C. Lässer, T. G. Szabó et al., "Distinct RNA profiles in subpopulations of extracellular vesicles: apoptotic bodies, microvesicles and exosomes," *Journal of Extracellular Vesicles*, vol. 2, no. 1, 2013.
- [60] S. Yang, F. Zhang, J. Ma, and W. Ding, "Intervertebral disc ageing and degeneration: the antiapoptotic effect of oestrogen," *Ageing Research Reviews*, vol. 57, p. 100978, 2020.
- [61] A. Shabbir, A. Cox, L. Rodriguez-Menocal, M. Salgado, and E. V. Badiavas, "Mesenchymal stem cell exosomes induce proliferation and migration of normal and chronic wound fibroblasts, and enhance angiogenesis in vitro," *Stem Cells and Development*, vol. 24, no. 14, pp. 1635–1647, 2015.
- [62] M. Xiao, Y. Tang, W. W. Chen et al., "Tubb3 regulation by the Erk and Akt signaling pathways: a mechanism involved in the effect of arginine ADP-ribosyltransferase 1 (Art1) on apoptosis of colon carcinoma CT26 cells," *Tumour Biology*, vol. 37, no. 2, pp. 2353–2363, 2016.
- [63] S. Zhang, S. J. Chuah, R. C. Lai, J. H. P. Hui, S. K. Lim, and W. S. Toh, "MSC exosomes mediate cartilage repair by enhancing proliferation, attenuating apoptosis and modulating immune reactivity," *Biomaterials*, vol. 156, pp. 16–27, 2018.
- [64] J. Zhu, J. Yao, R. Huang, Y. Wang, M. Jia, and Y. Huang, "Ghrelin promotes human non-small cell lung cancer A549 cell proliferation through PI3K/Akt/mTOR/P70S6K and ERK signaling pathways," *Biochemical and Biophysical Research Communications*, vol. 498, no. 3, pp. 616–620, 2018.
- [65] Y. C. Huang, J. P. Urban, and K. D. Luk, "Intervertebral disc regeneration: do nutrients lead the way?," *Nature Reviews Rheumatology*, vol. 10, no. 9, pp. 561–566, 2014.

- [66] M. V. Risbud, E. Schipani, and I. M. Shapiro, "Hypoxic regulation of nucleus pulposus cell survival: from niche to notch," *The American Journal of Pathology*, vol. 176, no. 4, pp. 1577–1583, 2010.
- [67] S. R. Bibby, D. A. Jones, R. M. Ripley, and J. P. G. Urban, "Metabolism of the intervertebral disc: effects of low levels of oxygen, glucose, and pH on rates of energy metabolism of bovine nucleus pulposus cells," *Spine*, vol. 30, no. 5, pp. 487–496, 2005.
- [68] J. P. Urban, S. Smith, and J. C. Fairbank, "Nutrition of the intervertebral disc," *Spine*, vol. 29, no. 23, pp. 2700–2709, 2004.
- [69] S. Holm, A. Maroudas, J. P. G. Urban, G. Selstam, and A. Nachemson, "Nutrition of the intervertebral disc: solute transport and metabolism," *Connective Tissue Research*, vol. 8, no. 2, pp. 101–119, 2009.
- [70] E. M. Bartels, J. C. Fairbank, C. P. Winlove, and J. P. G. Urban, "Oxygen and lactate concentrations measured in vivo in the intervertebral discs of patients with scoliosis and back pain," *Spine*, vol. 23, no. 1, pp. 1–7, 1998, 8.
- [71] J. P. Urban and S. Roberts, "Degeneration of the intervertebral disc," *Arthritis Research & Therapy*, vol. 5, no. 3, pp. 120–130, 2003.
- [72] H. Ishihara and J. P. Urban, "Effects of low oxygen concentrations and metabolic inhibitors on proteoglycan and protein synthesis rates in the intervertebral disc," *Journal of Orthopaedic Research*, vol. 17, no. 6, pp. 829–835, 1999.
- [73] W. K. Kwon, H. J. Moon, T. H. Kwon, Y. K. Park, and J. H. Kim, "The role of hypoxia in angiogenesis and extracellular matrix regulation of intervertebral disc cells during inflammatory reactions," *Neurosurgery*, vol. 81, no. 5, pp. 867–875, 2017.
- [74] L. I. Kauppila, "Ingrowth of blood vessels in disc degeneration. Angiographic and histological studies of cadaveric spines," *The Journal of Bone and Joint Surgery. American Volume*, vol. 77, no. 1, pp. 26–31, 1995.
- [75] F. Mwale, I. Ciobanu, D. Giannitsios, P. Roughley, T. Steffen, and J. Antoniou, "Effect of oxygen levels on proteoglycan synthesis by intervertebral disc cells," *Spine*, vol. 36, no. 2, pp. E131–E138, 2011.
- [76] A. Agrawal, A. Guttapalli, S. Narayan, T. J. Albert, I. M. Shapiro, and M. V. Risbud, "Normoxic stabilization of HIF-1 α drives glycolytic metabolism and regulates aggrecan gene expression in nucleus pulposus cells of the rat intervertebral disk," *American Journal of Physiology. Cell Physiology*, vol. 293, no. 2, pp. C621–C631, 2007.
- [77] Biomedical Laboratories, Swiss Paraplegic Research, G A Zaech Strasse 4, CH 6207 Nottwil, Switzerland, A. Bertolo, L. Ettinger et al., "The in vitro effects of dexamethasone, insulin and triiodothyronine on degenerative human intervertebral disc cells under normoxic and hypoxic conditions," *European Cells & Materials*, vol. 21, pp. 221–229, 2011.
- [78] W. J. Wu, X. K. Zhang, X. F. Zheng, Y. H. Yang, S. D. Jiang, and L. S. Jiang, "SHH-dependent knockout of HIF-1 α accelerates the degenerative process in mouse intervertebral disc," *International Journal of Immunopathology and Pharmacology*, vol. 26, no. 3, pp. 601–609, 2013.
- [79] C. M. Tran, N. Fujita, B. L. Huang et al., "Hypoxia-inducible factor (HIF)-1 α and CCN2 form a regulatory circuit in hypoxic nucleus pulposus cells," *The Journal of Biological Chemistry*, vol. 288, no. 18, pp. 12654–12666, 2013.
- [80] N. Fujita, Y. Hirose, C. M. Tran et al., "HIF-1-PHD2 axis controls expression of syndecan 4 in nucleus pulposus cells," *The FASEB Journal*, vol. 28, no. 6, pp. 2455–2465, 2014.
- [81] E. Schipani, H. E. Ryan, S. Didrickson, T. Kobayashi, M. Knight, and R. S. Johnson, "Hypoxia in cartilage: HIF-1 α is essential for chondrocyte growth arrest and survival," *Genes & Development*, vol. 15, no. 21, pp. 2865–2876, 2001.
- [82] X. Meng, L. Zhuang, J. Wang et al., "Hypoxia-inducible factor (HIF)-1 α knockout accelerates intervertebral disc degeneration in mice," *International Journal of Clinical and Experimental Pathology*, vol. 11, no. 2, pp. 548–557, 2018.
- [83] M. V. Gustafsson, X. Zheng, T. Pereira et al., "Hypoxia requires notch signaling to maintain the undifferentiated cell state," *Developmental Cell*, vol. 9, no. 5, pp. 617–628, 2005.
- [84] A. Rastogi, P. Thakore, A. Leung et al., "Environmental regulation of notochordal gene expression in nucleus pulposus cells," *Journal of Cellular Physiology*, vol. 220, no. 3, pp. 698–705, 2009.
- [85] B. Gantenbein, E. Calandriello, K. Wuertz-Kozak, L. M. Benneker, M. J. B. Keel, and S. C. W. Chan, "Activation of intervertebral disc cells by co-culture with notochordal cells, conditioned medium and hypoxia," *BMC Musculoskeletal Disorders*, vol. 15, no. 1, p. 422, 2014.
- [86] E. R. Shamir and A. J. Ewald, "Three-dimensional organotypic culture: experimental models of mammalian biology and disease," *Nature Reviews. Molecular Cell Biology*, vol. 15, no. 10, pp. 647–664, 2014.
- [87] A. Ouyang, A. E. Cerchiarri, X. Tang et al., "Effects of cell type and configuration on anabolic and catabolic activity in 3D co-culture of mesenchymal stem cells and nucleus pulposus cells," *Journal of Orthopaedic Research*, vol. 35, no. 1, pp. 61–73, 2017.
- [88] Z. Liao, R. Luo, G. Li et al., "Exosomes from mesenchymal stem cells modulate endoplasmic reticulum stress to protect against nucleus pulposus cell death and ameliorate intervertebral disc degeneration in vivo," *Theranostics*, vol. 9, no. 14, pp. 4084–4100, 2019.

Review Article

Mitochondrial Dysfunction in Intervertebral Disc Degeneration: From Pathogenesis to Therapeutic Target

Danni Li,¹ Fenghua Tao,² and Lin Jin ²

¹Department of Anesthesiology, Renmin Hospital of Wuhan University, Wuhan 430060, China

²Department of Orthopedics, Renmin Hospital of Wuhan University, Wuhan 430060, China

Correspondence should be addressed to Lin Jin; jinlin2010@whu.edu.cn

Received 5 September 2020; Revised 16 November 2020; Accepted 17 November 2020; Published 27 November 2020

Academic Editor: Sidong Yang

Copyright © 2020 Danni Li et al. This is an open access article distributed under the Creative Commons Attribution License, which permits unrestricted use, distribution, and reproduction in any medium, provided the original work is properly cited.

Mitochondria are cytosolic organelles essential for cellular function and survival. The function of mitochondria is maintained by mitochondrial quality control systems including mitochondrial fission and fusion to adapt the altered environment and mitophagy for removal of damaged mitochondria. Mitochondrial dysfunction is closely involved in aging-related diseases. Intervertebral disc (IVD) degeneration, an aging-associated process, is the major contributor to low back pain. Growing evidence has suggested that the mitochondrial function in IVD cells is severely compromised during the degenerative process of IVD, and dysfunctional mitochondria along with impaired mitochondrial dynamics and mitophagy cause a series of cascade reactions that have been implicated in increased oxidative stress, senescence, matrix catabolism, and apoptosis of IVD cells, thereby contributing to the degeneration of IVD. Accordingly, therapies that target mitochondrial dysfunction and related mechanisms, such as ROS generation, mitophagy, and specific molecules and signaling, hold great promise. The present review summarizes the current state of the role of mitochondrial dysfunction in the pathophysiology of IVD degeneration and potential therapeutic strategies that could be developed.

1. Introduction

The intervertebral disc (IVD) is a fibrocartilaginous tissue interspersing and connecting adjacent vertebrae, which serves to absorb and transmit mechanical loading from the spine and permits movement of the spine [1]. The IVD consists of three components. The central gelatinous nucleus pulposus (NP) primarily contains NP cells, type II collagen, and proteoglycan. The outer annulus fibrosus (AF) is mainly composed of AF cells and type I collagen fibers. The cartilaginous endplate (CEP) is a hyaline cartilaginous tissue that joins IVD with the adjacent bony vertebrae [2]. NP cells act a critical role in producing extracellular matrix (ECM) components including type II collagen and proteoglycan, maintaining the integrity and homeostasis of IVD [3].

Low back pain (LBP) is globally prevalent and more than 80% of people will suffer from LBP during their lifetime [4, 5]. It is also the main cause of disability, causing heavy socioeconomic cost each year worldwide [4, 6]. Degeneration of the IVD characterized by advanced signs of aging and pro-

gressive structural destruction is widely recognized as a major contributor to LBP [7]. Although factors including obesity, genetic, trauma, and lifestyle (e.g., sedentary work and the lack of sports activities) are associated with the development of IVD degeneration [8, 9], the exact cellular and molecular mechanisms underlying IVD degeneration are complex and multifactorial. From past decades, extensive evidence has suggested that oxidative stress, apoptosis, and metabolic dysregulation of disc-resident cells, especially in NP cells, are closely involved in the pathogenesis of IVD degeneration [10]. Therefore, some intracellular regulatory approaches that control these cellular processes are extremely important and receive considerable attention.

Mitochondria are the double membrane, cytoplasmic organelles with their own genome, the mitochondrial DNA (mtDNA). Mitochondria play a crucial role in energy production, mainly through the mechanism of oxidative phosphorylation [2]. In addition, these organelles contribute to key biochemical processes including the generation of reactive oxygen species (ROS) [11] and the regulation of calcium

homeostasis [12], which affect cell metabolism, function, and survival. The mitochondrial quality control system, including mitochondrial fission and fusion, and selective self-clearance mechanism termed mitophagy, enables them to modify their shape, size, quality, and quantity in response to the cellular needs and various stresses, thereby maintaining mitochondrial and cellular homeostasis [13, 14]. Given its essential roles in cellular processes, it is not surprising that dysfunction or impairment of mitochondria will be implicated in a series of pathological processes, such as oxidative stress, senescence, apoptosis, and ECM degradation, consequently causing detrimental effects on cell function and survival. As we know, a wide range of diseases covering metabolic disorders, cancer, and inflammatory diseases, particularly in degenerative diseases, is characterized by the involvement of mitochondrial dysfunction [15–18].

In recent years, the role of mitochondria in IVD degeneration is widely studied, and these studies have yielded a more comprehensive understanding of the pathophysiology of IVD degeneration and provided some promising therapeutic approaches for the treatment of IVD degeneration, which we aim to summarize and discuss in this review.

2. Mitochondrial Function and Homeostasis

As energy factories in mammal cells, mitochondria are responsible for producing energy. Additionally, these organelles are vital regulators of redox state and calcium balance. A quality control machinery of mitochondria, referring to mitochondrial dynamics and mitophagy, serves for the maintenance of mitochondrial homeostasis to fulfill their function. These processes proceed properly under the physiological conditions, whereas aberrant stresses or stimulus will cause mitochondrial dysfunction, subsequently leading to a series of cascade reactions (Figure 1).

2.1. Energy Metabolism, Redox, and Calcium Regulation. In mammal cells, mitochondria are the sites of the tricarboxylic acid (TCA) cycle and oxidative phosphorylation (OXPHOS). These “factories” produce energy using the electrochemical gradient generated across the inner of two membranes by the electron transport chain (ETC) [19]. There exists a special mitochondrial membrane system to perform productive work of energy. Inner mitochondrial membrane (IMM) surrounds the mitochondrial matrix and takes in the electrons produced by the TCA cycle through ETC. The ETC, located at IMM, contains a number of proteins, for example, complex I-IV, that perform the transfer and incremental release of energy from the electrons in order to pump protons (H^+) into the intermembrane space and establish the electrochemical gradient. This mitochondrial membrane potential ($\Delta\psi_m$) drives the process of OXPHOS, providing energy by converting ADP to ATP [20]. Although residing in a low oxygen tension environment, IVD cells are not entirely anaerobic and still carry out oxidative metabolism [21, 22].

Mitochondria continuously metabolize oxygen and meantime generate ROS. During the transportation of electrons, a small part of electrons will leak and reduce oxygen to superoxide anion (O_2^-), termed “primary” ROS [23]. The

O_2^- could be further converted to the “secondary” ROS including hydrogen peroxide (H_2O_2) and hydroxyl radical (OH^-) via enzymatic and nonenzymatic mechanisms. The mitochondrial-dependent ROS (mtROS) generation has been found in multiple disc-resident cells including NP cells of humans and rats and AF cells of humans and rats [24–27]. A proper level of ROS is fundamental to organismal physiology and adaptive responses [28], which relies on a balance between ROS generation and ROS scavenge by nonenzymatic and enzymatic antioxidants. The interruption of this balance will induce oxidative stress that is detrimental to the mitochondrial function and cells [29].

Mitochondria also play a vital role in regulating cellular calcium (Ca^{2+}) homeostasis. The cytosolic Ca^{2+} is taken into mitochondria by energy-driven uniporters, while the efflux of Ca^{2+} from the mitochondria is mediated by ion gradient-driven antiporters [30]. The mitochondrial permeability transition pore (mPTP) is a high-conductance, voltage- and Ca^{2+} -sensitive channel, whose opening can be transient to physiologically allow quick release of Ca^{2+} and/or metabolite exchange between the mitochondrial matrix and the cytosol [31]. However, mitochondrial Ca^{2+} overload, especially when combined with oxidative stress and/or ATP depletion, will trigger a drastic efflux of Ca^{2+} through the prolonged opening of mPTP, consequently causing dissipation of the $\Delta\psi_m$, respiratory chain uncoupling, cessation of ATP synthesis, ROS generation, and eventually mitochondrial swelling, rupture, and cell death [31].

2.2. Mitochondrial Dynamics and Mitophagy. Mitochondria are dynamic organelles, continually undergoing fission and fusion for regulating their number, size, and distribution [32]. Mitochondrial fission is a multistep process allowing the division of one mitochondrion in two mitochondria that are controlled by proteins such as dynamin-related protein 1 (DRP1), mitochondrial fission factor (Mff), and fission 1 (Fis1) [33]. Mitochondrial fusion is the combination of two mitochondria with the outer mitochondrial membrane (OMM) fusion mediated by mitofusins (MFN1 and MFN2) followed by IMM fusion, determined by optic atrophy 1 (OPA1) [34]. These balanced dynamic transitions are required not only to ensure mitochondrial function but also to respond to meet cellular metabolic demands and adapt the nutrient condition [13]. In addition, mitochondrial dynamics is engaged in repairing damaged mitochondria [35]. If these processes fail to restore mitochondria in a healthy state, the damaged mitochondria will be eliminated by a selective autophagy mechanism termed mitophagy.

Mitophagy is involved in the basal mitochondrial turnover and quality control via the clearance of long-lived or damaged mitochondria [36]. Different stimulus and conditions induce mitophagy in distinct mechanisms. Generally, mitophagy can be divided into Parkin RBR E3 ubiquitin-protein ligase- (Parkin-) dependent and Parkin-independent pathways. When mitochondria are depolarized under various cellular stress, the PINK1 accumulates on OMM and subsequently recruits and activates Parkin [37]. The Parkin polyubiquitylates multiple OMM proteins, which will be recognized by LC3 adaptors, such as P62 and NDP52

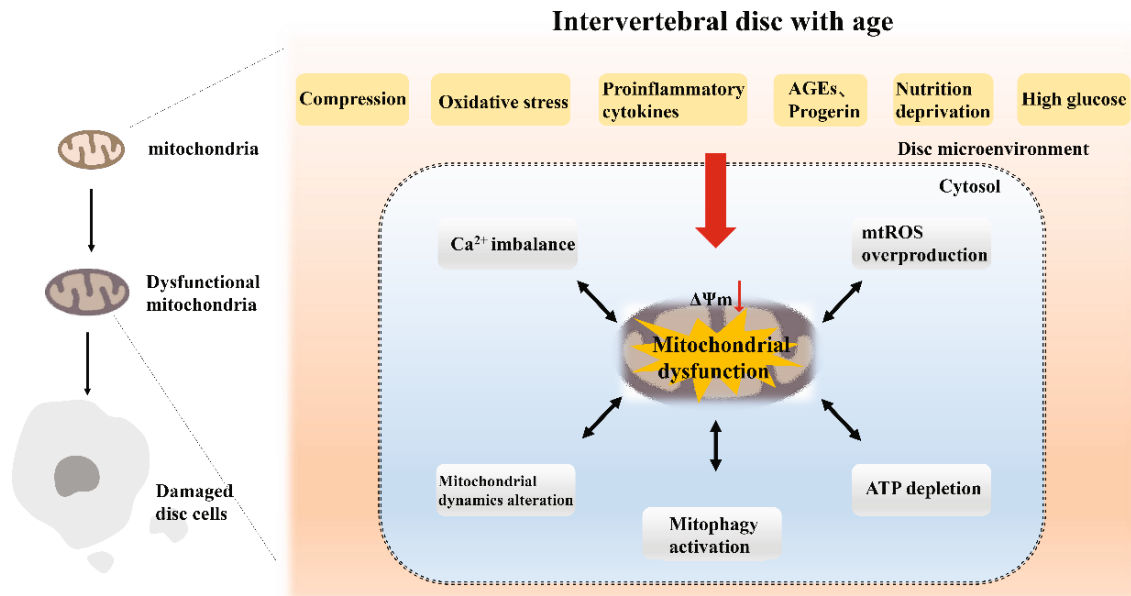


FIGURE 1: The occurrence of mitochondrial dysfunction in IVD cells. Mitochondrial dysfunction in IVD cells primarily originates from the effects of aberrant microenvironment within the disc including mechanical compression, proinflammatory cytokines, oxidative stress, nutrition deprivation, and high glucose. These pathological conditions induce ATP depletion, mtROS overproduction, Ca²⁺ imbalance, loss of $\Delta\psi_m$, and impairment of mitochondrial quality control, involved in multiple cellular events.

on phagophore [37]. Damaged mitochondria are engulfed by autophagosomes to form mitophagosomes, followed by the fusion with lysosomes for hydrolytic degradation [38]. With regard to Parkin-independent pathways, BNIP3, NIX, and FUNDC could directly bind the LC3 molecules decorating the autophagosome [39]. In addition, the mechanisms of mitophagy and mitochondrial dynamics are tightly related. For example, the Parkin-mediated ubiquitylation of MFN is able to promote mitochondria accessible for degradation and prevents fusion of damaged mitochondria. The dephosphorylation of FUNDC1 could enhance mitochondrial fission by the disassembly of OPA1 and increasing the interaction with DRP1 on the mitochondrial surface [39]. In physiological conditions, mitochondrial homeostasis could be achieved through these interactive processes. However, mitochondrial fusion and fission and mitophagy could be strongly dysregulated by various pathological stresses, such as $\Delta\psi_m$ collapse, oxidative stress, and nutrition deprivation, causing or accelerating mitochondrial dysfunction [40].

3. The Roles of Mitochondrial Dysfunction in IVD Degeneration

It has been shown an abnormal mitochondrial morphology with dark color, small cristae, and dense inclusion bodies, decreased mitochondrial mass, and reinforced mitochondrial respiration in human AF cells from degenerative discs [24]. The reduced mitochondrial respiration, $\Delta\psi_m$, and mitochondrial number were also found in NP and AF cells from aged rabbits compared with that from young rabbits [41]. These findings confirm the association between mitochondrial dysfunction and IVD degeneration. Importantly, the current evidence indicates that the pathophysiological char-

acteristics of IVD degeneration primarily include oxidative stress, senescence and death of disc cell, and ECM degradation, all of which could be, at least partly, attributed to mitochondrial dysfunction. We will focus on the roles of mitochondrial dysfunction in the pathogenesis of IVD degeneration through these pathological processes (Figure 2).

3.1. Mitochondrial Dysfunction and Oxidative Stress. The accumulated evidence has shown that oxidative stress as a cause and/or consequence of mitochondrial dysfunction is one of the main drivers of aging and aging-related diseases [42]. Excessive ROS production has also been found in degenerative discs [43]. During the development of IVD degeneration, there exist various exogenous stimuli, such as mechanical loading, proinflammatory cytokines, high oxygen tension, and glucose stress in the microenvironment of IVD, inducing overproduction of ROS in disc cells [44]. Interestingly, mitochondrial dysfunction plays a core role in all of these processes. The compression, a type of mechanical stresses, is commonly used to mimic the pathological condition of IVD degeneration. This stress promoted excessive mitochondrial ROS production accompanied by increased mPTP opening and decreased $\Delta\psi_m$ in NP cells [25, 45]. In addition to the mechanical stress, proinflammatory cytokines, including interleukin- (IL-) 1 β and tumor necrosis factor- α (TNF- α), increased in degenerative intervertebral disc, are also considered as critical contributors in the process of IVD degeneration [46, 47]. At the cellular level, these inflammatory mediators can trigger sustained mPTP opening, negatively alter mitochondrial membrane potential and ATP content, and cause aberrant mitochondrial fragmentation and swelling in NP cells, leading to mitochondrial dysfunction and ROS overproduction [46, 48, 49]. Previous

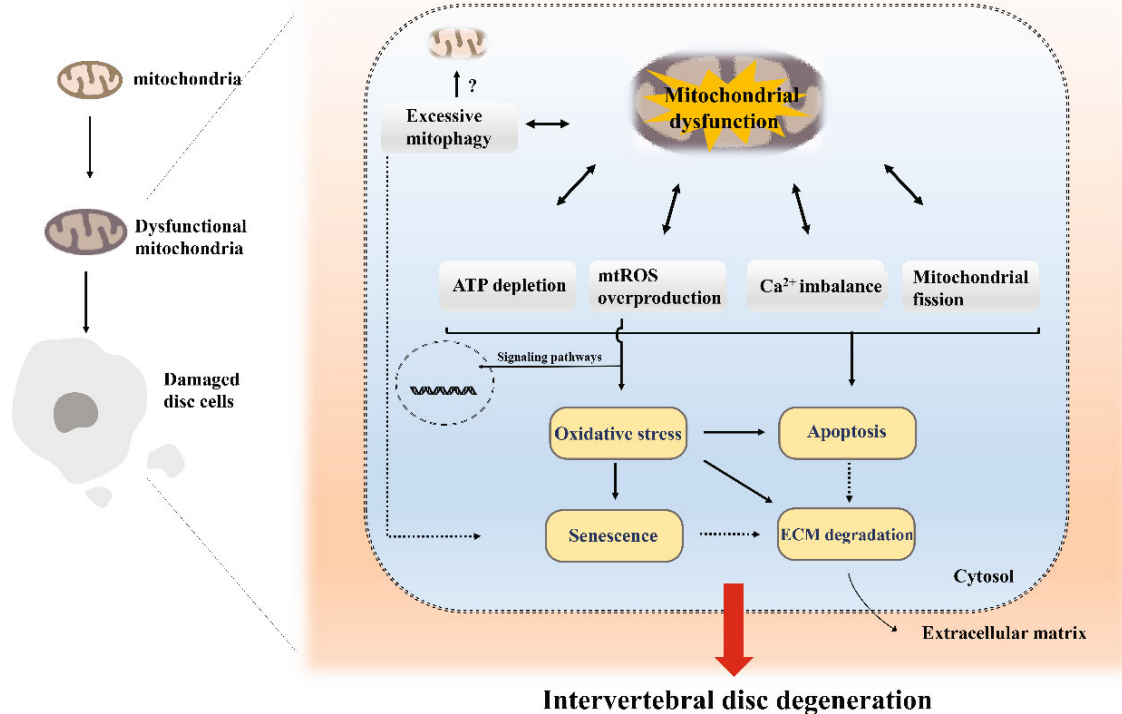


FIGURE 2: The role of mitochondrial dysfunction in the pathogenesis of IVD degeneration. The dysfunctional mitochondria could cause a series of cascade reactions, leading to increased oxidative stress, senescence, apoptosis, and ECM catabolism of disc cells, involved in the pathology of IVD degeneration.

studies have reported a higher incidence of degenerative disc diseases in patients with diabetes mellitus (DM) than in non-diabetic patients, and the accumulation of advanced glycation end products (AGEs) was potentially involved in DM and other age-related diseases [50, 51]. Some researchers work on this topic and found that high glucose could also disrupt $\Delta\psi_m$ and enhance ROS generation in rat NP cells, AF cells, and CEP cells [27, 52–54]. In addition, it was reported that the accumulation of AGEs in NP tissues could induce mitochondrial dysfunction and an oxidative microenvironment, which was also closely correlated to IVD degeneration [55, 56]. The above studies suggest the pathological stimulus and stresses in the microenvironment of IVD contribute to mitochondrion dysfunction and oxidative stress, implicated in the pathogenesis of IVD degeneration.

Mitochondria are not only the main cellular source of ROS; they are also susceptible to oxidative injury [57]. When stimulated by exogenous ROS, hydrogen peroxide, mitochondria in disc cells lose their ATP content, transmembrane potential, which induce the release of mtROS [58–60]. The ROS-induced mitochondrial dysfunction is able to further promote ROS generation, resulting in a feed-forward vicious cycle between ROS and mitochondria that causes a series of signaling cascades and oxidative damage [61].

3.2. Mitochondrial Dysfunction and Senescence. Cellular senescence is a permanent state of growth arrest characterized by the chronic elevated secretion of proinflammatory cytokines and matrix proteases, namely, senescence-

associated secretory phenotype (SASP) [62]. Senescent cells have been found to be increased with age and degeneration of human IVD [63, 64]. Interestingly, senescence of IVD cells is one of the cascade events of mitochondrial dysfunction [65]. As reported, the mitochondria's role in senescent process was closely associated with overproduction of ROS that initials the related signaling networks to facilitate the senescent phenotype [66]. Specifically, a severe ROS production induced by H₂O₂ further activates the ATM-Chk2-p53-p21-Rb pathway to enhance DNA damage and the accumulation of senescence-associated β -galactosidase, driving senescence of human NP cells [58, 67]. In addition to NP cells, mitochondrial ROS-induced senescence was also found in human CEP cells, mediated by the p53-p21-Rb pathway [68]. Not only that, the impaired mitochondrial function and ROS generation is also involved in the senescence of IVD cells under other pathological conditions including pro-inflammatory cytokines, mechanical compression, aging-related proteins, and high glucose [27, 48, 69, 70]. It was reported that the aberrant mitophagy caused by continuous compression could accelerate the senescence of NP cells, which we will discuss later [70]. Taking together, mitochondrial dysfunction is a major cause of cell senescence, and maintenance or recovery of mitochondrial function in IVD cells is important to mitigate cell senescence.

3.3. Mitochondrial Dysfunction and Apoptosis. The loss of IVD cells in the form of apoptosis is a key factor of IVD degeneration [71–73]. Mitochondrial-dependent apoptosis

is one of the apoptotic pathways and most studied in the progression of IVD degeneration [74]. This apoptotic pathway requires mitochondrial outer membrane permeabilization (MOMP) driven by effector proapoptotic members of the B cell lymphoma 2 (BCL-2) family of proteins for the release of cytochrome c into the cytosol and further activating caspase (caspase3, 9) that leads to cell death [75]. The initiation of the above process heavily relies on the alteration of mitochondrial function, including elevated ROS production, the opening of mPTP, and mitochondrial fission, which have been confirmed in the apoptotic process of IVD cells induced by various pathological conditions. For example, H₂O₂ induced mitochondrial-dependent apoptosis through inhibiting the activity of complex III, decreasing the ATP levels and $\Delta\psi_m$ in AF cells [76]. IL-1 β reduced Bcl-2/Bax ratio and enhanced cytochrome c released from the mitochondria to the cytosol, which proved mitochondrial-mediated apoptosis was induced in NP cells. The similar apoptotic process in disc cells was also found under the conditions of nutrient deprivation [77, 78], high glucose [52], and AGE accumulation [79]. In addition, compression elicited a time-dependent mitochondrial dysfunction, evident by $\Delta\psi_m$ loss, mPTP opening, ATP depletion, and elevated mtROS, eventually leading to apoptosis [25] together with necroptosis in NP cells [80]. Chen et al. found that RIPK1 mediated this process of cell death during compression injury [80]. In short, these important pathogenic factors share similar mitochondrial-dependent apoptotic mechanism, further confirming the core role of mitochondrial dysfunction in cell apoptosis and IVD degeneration. It should be noted that some molecules have recently been demonstrated to involve in mitochondrial-dependent apoptosis in disc cells. Islet amyloid polypeptide (IAPP) is a polypeptide mainly participating in the regulation of glucose metabolism [81]; its expression was considerably decreased with the progression of IVD degeneration, and downregulated IAPP has a detrimental effect on AF cell survival through increasing cellular Ca²⁺ concentration, ROS, and apoptosis [82]. Acid-sensing ion channel 1a, a receptor of protons, also functions in CEP cells, allowing the influx of Ca²⁺ and triggering Ca²⁺-mediated apoptotic signals [83]. These molecules give a novel and wide insight into the mitochondrial pathway of apoptosis in degenerative disc cells.

3.4. Mitochondrial Dysfunction and ECM Metabolism. ECM degradation is a hallmark of IVD degeneration. The degeneration, driven by increased proteolysis of matrix components including aggrecan and type II collagen mediated by catabolic enzymes, like matrix metalloproteinases (MMPs) and a disintegrin and metalloproteinase with thrombospondin motifs (ADAMTS), is closely correlated to mitochondrial dysfunction in IVD cells [84]. On the one hand, anabolism of ECM requires ATP for providing energy [85] while mitochondrial dysfunction, showing ATP depletion, indeed reduces the anabolic process in IVD cells [69, 86]. On the other hand, the mitochondrial-mediated ROS generation could significantly interrupt the metabolism of ECM. A number of studies showed reduced expression of aggrecan and type II collagen while increased expression of MMP13

in human and rat disc cells exposed to exogenous H₂O₂ [67, 87, 88]. Moreover, the ROS accumulation induced by mechanical compression and proinflammatory cytokines is associated with matrix degradation [48, 89]. The excessive ROS not only is able to directly cause the oxidative damage of anabolic-related DNA and proteins but also acts as signaling messengers of NF- κ B, nuclear factor, erythroid 2-like 2 (Nrf2)/HO-1, AKT, and mitogen-activated protein kinase (MAPK) pathways that affect the expression of ECM metabolic markers [67]. However, some pathological factors, especially for proinflammatory cytokines, could directly regulate the above signaling pathways, contributing to the inflammation-mediated ECM degradation in human and rat disc cells [90–92]. Taken all the results into account, although the molecular mechanism of ECM degradation is complicated, mitochondria, as a hub of multiple signal transduction, play a crucial role in this process. Impaired mitochondria are prone to drive the cascade reactions to promote matrix degradation and structure loss in IVD.

3.5. The Roles of Mitochondrial Energy Metabolism in IVD Degeneration. Maintenance of the ECM in the IVD is a high energy demanding process that requires glucose and oxygen consumption to produce ATP [22]. However, ATP content has been found decreased in degenerative disc under some pathological conditions [69, 76], and age-related decline in disc cellular bioenergetics has been considered as a contributor to the matrix degradation [93]. The previous study revealed a profound increase in glycolysis, altered mitochondrial morphology, and lower membrane potential but no change in mitochondrial respiration in AF cells from older rabbits [41]. In contrast, NP cells from older rabbits showed a significant decrease in OXPHOS without a concomitant increase in glycolysis, and it also exhibited a significant loss in maximum respiratory capacity and bioenergetic reserve [41], which may cause protein damage and cell death [94]. These limited mitochondrial capacities could hamper matrix repair or cellular stress responses. On the other hand, exogenous ATP could significantly promote ECM deposition and corresponding gene expression (aggrecan and type II collagen) in NP cells and AF cells in three-dimensional agarose culture [85].

These findings indicate that normal metabolism of energy is essential for ECM homeostasis, while age-related disc cell mitochondrial and bioenergetic changes might contribute to the loss of matrix homeostasis that underlay disc degeneration. However, it is important to note that the results of cell culture should be confirmed in vivo.

3.6. The Roles of Mitochondrial Dynamics and Mitophagy in IVD Degeneration. The recent evidence revealed that imbalanced mitochondrial dynamics and mitophagy are implicated in various age-related diseases including Alzheimer's disease, osteoarthritis, and IVD degeneration [45, 95–97]. Disturbed mitochondrial dynamics occurs in response to abnormal stresses and directly impacts mitochondrial function in disc cells. Recent studies have demonstrated that oxidative stress enhanced mitochondrial fission events and, meantime, impaired fusion events [59]. Additionally,

compared to control cells, Mff and Fis1 protein levels were significantly upregulated, while MFN1, MFN2, and OPA1 protein levels were reduced in compression-treated NP cells [45]. Furthermore, blocking mitochondrial fission by mitochondrial division inhibitor 1 (mdivi-1) inhibited the elevated mitochondrial impairment, ROS generation, and apoptosis induced by compression treatment [45]. Mitochondrial fission also mediates programmed necrosis of NP cells. mdivi-1 and knockdown of DRP1 prevented the compression-induced programmed necrosis of NP cells by enhancing mitochondrial translocation of p53 and nuclear translocation of apoptosis-inducing factor (AIF) [98]. MitoQ is a mitochondrial-targeted antioxidant that can rescue the oxidative damage and imbalance between mitochondrial fission and fusion induced by compression in human NP cells, while the beneficial effects of MitoQ could be partially repressed by an agonist of mitochondrial fission, FCCP [45]. Actually, mitochondrial fusion is also indispensable for autophagic flux and mitochondrial function in NP cells. Chen et al. found that MFN2 deficiency contributed to IVD degeneration due to its impairment on mitochondrial function and mitophagy. Furthermore, overexpression of MFN2 can attenuate oxidative damage of NP cells and the development of IVD degeneration in rats through the activation of PINK1/Parkin-mediated mitophagy [99]. Collectively, these studies demonstrate the importance of balanced mitochondrial dynamics in the maintenance of mitochondrial homeostasis and NP cell survival. The active mitochondrial fission promotes the separation of dysfunctional and even healthy mitochondria for their degradation through mitophagy. Several studies have shown that mitophagy is activated in degenerative disc cells [26, 83, 84]. Given that the initiation of mitophagy is commonly caused by loss of $\Delta\psi_m$, hypoxia condition, and overproduced ROS, it is not surprising that pathological factors, including oxidative stress, mechanical compression, and TNF- α , are prone to induce mitophagy in disc cells [49, 70, 100]. So here comes the question, what is the role of mitophagy in mitochondrial dysfunction and the progression of IVD degeneration. On the one hand, mitophagy is considered a protective mechanism owing to its clearance of damaged mitochondria. Several laboratories revealed that inhibition of PINK1-Parkin-mediated mitophagy aggravated TNF- α or oxidative stress-stimulated mitochondrial dysfunction and apoptosis of disc cells, whereas the activated mitophagy induced by its activators such as melatonin and urolithin A could protect disc cells from apoptosis and retard IVD degeneration in vivo [88, 101]. On the other hand, it was reported that suppression of PINK1/Parkin-mediated mitophagy by a mitophagy inhibitor, cyclosporin A (CsA), or PINK1 knockdown attenuated the compression-induced senescence of NP cells [70]. Moreover, CsA exerted a protective role in oxidative stress-induced apoptosis of NP cells [102]. These results indicate continuous pathological stress might induce inordinate mitophagy with an excessive clearance of mitochondria which accelerates the damage of NP cells. Taken together, the role of mitophagy in cell survival and function is possibly dependent on the mitophagy level under the pathological conditions. The differential roles of mitophagy in degenerative disc cells and in vivo studies need further investigation.

4. Therapeutic Strategies to Target Mitochondrial Dysfunction

The emerging evidence implies that mitochondrial dysfunction plays a central role in the pathophysiology of IVD degeneration. The involvement of mitochondrial dysfunction in IVD degeneration also represents an attractive target for its therapies. Accordingly, following strategies focusing on the improvement of mitochondrial function, attenuation of mitochondrial dysfunction, and the elimination of damaged mitochondria might be beneficial for the IVD degeneration (Figure 3).

4.1. Targeting ROS. Numerous studies have shown that a wide range of antioxidants exerts a significant protective role in degenerative IVD cells and animal models. N-acetylcysteine (NAC) is a well-known ROS scavenger that can, directly and indirectly, enter the cell and react with glutamic acid and glycine to generate intracellular glutathione [103]. It has been widely reported that NAC attenuates premature senescence, autophagy, and apoptosis in disc cells by decreasing the level of mtROS [67, 104, 105]. Moreover, the oral administration of NAC suppresses oxidative stress, inflammation, and matrix catabolism in rat discs to mitigate IVD degeneration [105]. Hydrogen sulfide (H₂S), a gaseous signaling messenger, has attracted attention for its biological functions [106]. Several studies have shown that H₂S can readily scavenge ROS at higher rates than other classic antioxidants [107], and exogenous H₂S has demonstrated profound antioxidant and cytoprotective capabilities in physiologic systems exposed to ROS [108]. H₂S also plays a protective role in degenerative NP cells and in the rat model of IVD degeneration induced by needle puncture, and the underlying mechanism involves inhibitory effect of H₂S on mitochondrial dysfunction and endoplasmic reticulum stress in IL-1 β -induced NP cells [46]. Considering the powerful antioxidative property of H₂S, it is likely that H₂S could repress the generation of ROS to protect against IVD degeneration.

In addition, some natural compounds with antioxidative properties have been demonstrated to be beneficial for mitochondrial function of IVD cells and IVD degeneration. Kinsenoside (3-(R)-3- β -D-glucopyranosyloxybutanolide) is a bioactive monomer extracted from the *Anoectochilus roxburghii* [109]. This compound exerts its therapeutic potential through alleviating IVD degeneration in a puncture-induced model and protecting NP cells against mitochondrial dysfunction, senescence, and apoptosis under oxidative stress in an Nrf2-dependent way [110]. In line with kinsenoside, other natural compounds, such as epigallocatechin 3-gallate (EGCG), resveratrol, icariin, and polydatin, also have shown promising effects at cellular levels and/or animal models of this disease [58, 111–113]. These agents propose more choices for new drug development. Recently, antioxidant compounds incorporating ubiquinone (MitoQ) or TEMPO (Mito-TEMPO) specifically targeted to mitochondria have been successively used against mitochondrial dysfunction [114]. MitoQ consists of coenzyme Q10 and a TPP cation that can easily accumulate in the mitochondria,

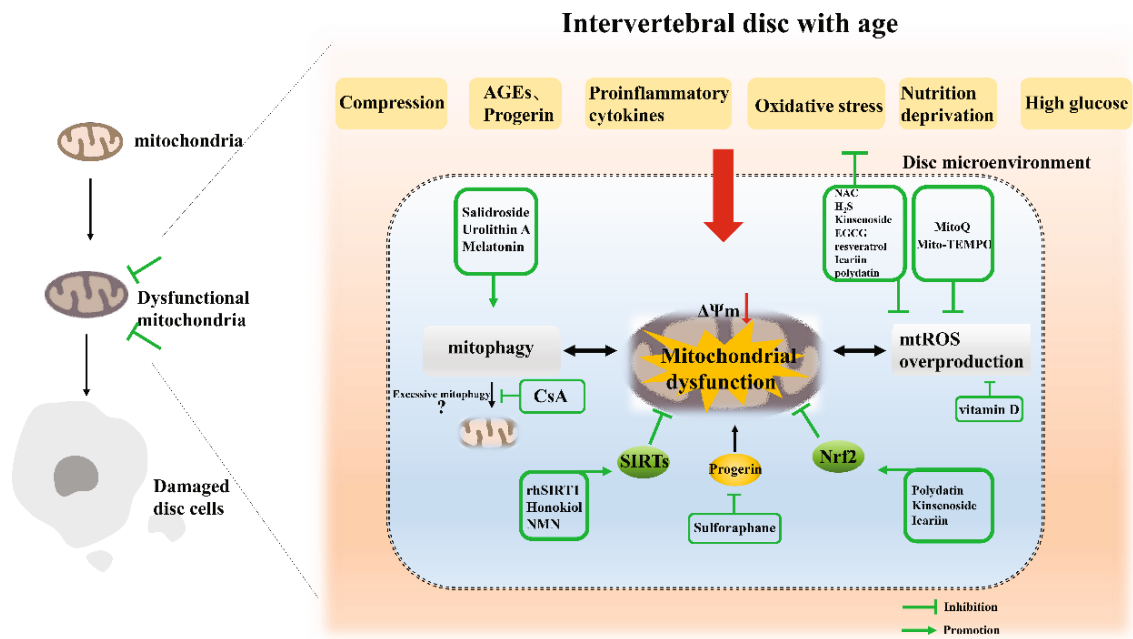


FIGURE 3: The therapies that target mitochondrial dysfunction. According to the role of mitochondrial dysfunction in IVD degeneration, multiple therapeutic agents that function on the improvement of mitochondrial function, attenuation of mitochondrial dysfunction, and the elimination of damaged mitochondria might be beneficial for the IVD degeneration.

thereby making it more powerful in preventing mitochondrial oxidative damage than untargeted antioxidants [115]. Actually, MitoQ restores mitochondrial function, eradicates oxidative insults, and promotes the survival of human NP cells under pathological condition [45], suggesting that MitoQ might serve as an effective therapeutic agent for IVD degeneration. Like MitoQ, Mito-TEMPO is also a mitochondrial-targeted antioxidant and protects NP cells against oxidative damage [60]. MitoVitE is another mitochondrial-targeted antioxidant. However, there is no evidence about its effects on degenerative IVD. Given its dramatic properties of antioxidation and antiapoptosis in multiple age-related diseases [116, 117], MitoVitE also deserves to be further studied and developed as a potential drug in IVD degeneration.

4.2. Targeting Mitophagy. Regulating mitophagy presents as an effective approach due to the involvement of impaired mitophagy in the development of IVD degeneration. Increasing Parkin-mediated mitophagy by using salidroside has been shown to eliminate impaired mitochondria and promote the survival of NP cells under TNF- α treatment. Salidroside also ameliorated the apoptosis of NP cells and the progression of IVD degeneration [49]. Urolithin A and melatonin have been widely studied in various diseases owing to their dramatic role in inducing mitophagy [118, 119]. Therefore, it is not surprising that both compounds could effectively alleviate cellular oxidative damage and the progression of puncture-induced IVD degeneration in rats [88, 101]. These evidences indicate Parkin-mediated mitophagy as a potential therapeutic target for IVD degeneration.

As mentioned above, there might exist dual roles of mitophagy with the development of IVD degeneration. Several

groups have found that the suppression of excessive mitophagy displays a positive effect in preclinical experiments. Xu et al. found that oxidative stress induced apoptotic cell death via mitophagy while inhibiting mitophagy by CsA protected AF cells against apoptosis [102]. And they further found that repression of mitophagy could also alleviate the apoptosis of NP cells [120]. In addition, another study reported that CSA and PINK1 knockdown inhibited PINK1/Parkin-mediated mitophagy, thereby rescuing the senescence of NP cells under the treatment of compression [70]. These results imply that the excessive mitophagy in disc cells is deleterious and might be a target for therapeutic intervention. However, the changing roles of mitophagy during the development of IVD degeneration are not fully clarified. For better therapeutic applications that target mitophagy, it is necessary to elaborate the definite role of mitophagy in IVD at different pathophysiological stages and proper time window of therapeutic intervention in further studies.

4.3. Targeting Molecules and Signaling. Mitochondrial homeostasis is precisely regulated by signaling networks, among which some molecules present therapeutic potential as pharmacologic targets. As previously described, the level of progerin is elevated in degenerated human NP tissues and the accumulated progerin is involved in the pathogenesis of IVD degeneration. Sulfaphane was demonstrated to show a remarkable ability to modulate the progerin level and mitochondrial homeostasis, and consequently, this compound alleviated progerin-induced IVD degeneration [69]. Previous studies have exhibited that vitamin D via its receptor (VDR) can effectively scavenge free radicals to protect cell mitochondria [121]. A recent study showed that the expression level of VDR was significantly reduced in the disc of

aged rats and severe degenerative discs. However, activation of VDR by 1,25(OH)₂D₃ successfully preserved mitochondrial function and ameliorated oxidative stress-induced apoptosis of AF cells, providing a novel insight into the treatment of IVD degeneration [76].

Growing shreds of evidence have demonstrated that sirtuins (SIRT) are essential for every aspect of mitochondrial biology, including energy metabolism, ROS detoxification, mitochondrial dynamics, and mitophagy [122]. Miyazaki et al. reported that administration of recombinant human SIRT1 (rhSIRT1) exhibited a protective effect on nutrient deprivation-induced mitochondrial-dependent apoptosis in human NP cells, suggesting that rhSIRT1 may be a potent treatment agent for IVD diseases [77]. In addition, activated SIRT3 through adenosine monophosphate-activated protein kinase (AMPK) and peroxisome proliferator-activated receptor- γ coactivator 1 α (PGC-1 α) pathway enhances mitochondrial function, mitochondrial antioxidant capacity, and mitochondrial dynamics, thereby attenuating AGEs or oxidative stress-induced apoptosis and senescence of NP cells and IVD degeneration in vivo [59, 79]. It is noteworthy that these functions of SIRT3 can be promoted by honokiol and nicotinamide mononucleotide (NMN) [59, 79], which provide available activators of SIRT3 and make SIRT3 possible to delay IVD degeneration as a target. Nrf2 is a master transcription factor that regulates cellular redox state and mitochondrial function [123]. In a mouse model of IVD degeneration, the Nrf2-knockout mice showed more severe degenerative changes in IVD than those in wild-type mice [124], and knockdown of Nrf2 accelerated H₂O₂-induced damage of mitochondria and CEP cell [60]. Furthermore, some phytochemicals including polydatin, kinsenoside, and icariin were proved to protect IVD cells from mitochondrial dysfunction and apoptosis through activating Nrf2 signaling [48, 110, 113]. These findings confirm the essential role of Nrf2 signaling in cellular homeostasis of the disc and highlight it as an effective therapeutic target in the management of IVD degeneration.

5. Conclusion

Mitochondrial functions, mainly including energy metabolism, redox, and calcium regulation, are altered in the degenerative disc. Mitochondrial dysfunction in IVD cells primarily originates from the effects of aberrant microenvironment within the disc including mechanical compression, proinflammatory cytokines, oxidative stress, nutrition deprivation, and high glucose. The dysfunctional mitochondria along with impaired mitochondrial quality control are prone to cause a series of cascade reactions, leading to ROS overproduction, senescence, apoptosis, and ECM catabolism of disc cells, involved in the pathology of IVD degeneration. Based on this, the therapies that target the mtROS, mitophagy, and relative molecules and signaling are promising for IVD degeneration, which extensive evidence has been demonstrated in preclinical experiments. However, these therapeutic approaches were studied in a certain *in vitro* condition or animal model of IVD degeneration that cannot completely represent the pathophysiology of IVD degenera-

tion in humans. Moreover, some topics, such as the role of mitophagy in the degenerative disc, are still controversial. For the earlier and better clinical intervention by targeting mitochondrial dysfunction, it will be necessary to verify these therapeutic approaches in more animal models and clinical studies.

Abbreviations

IVD:	Intervertebral disc
NP:	Nucleus pulposus
GAGs:	Glycosaminoglycans
AF:	Annulus fibrosus
CEP:	Cartilaginous endplates
ECM:	Extracellular matrix
LBP:	Lower back pain
MMP:	Mitochondrial transmembrane potential
mtDNA:	Mitochondrial DNA
ROS:	Reactive oxygen species
TCA:	Tricarboxylic acid
OXPPOS:	Oxidative phosphorylation
ETC:	Electron transport chain
IMM:	Inner mitochondrial membrane
$\Delta\psi_m$:	Mitochondrial membrane potential
O ₂ ⁻ :	Superoxide anion
H ₂ O ₂ :	Hydrogen peroxide
OH ⁻ :	Hydroxyl radical
mtROS:	Mitochondrial-dependent ROS
Ca ²⁺ :	Calcium
mPTP:	Mitochondrial permeability transition pore
DRP1:	Dynamin-related protein 1
Mff:	Mitochondrial fission factor
Fis1:	Fission 1
OMM:	Outer mitochondrial membrane
MFN1:	Mitofusin 1
MFN2:	Mitofusin 2
OPA1:	Optic atrophy 1
mdivi-1:	Mitochondrial division inhibitor 1
Parkin:	Parkin RBR E3 ubiquitin-protein ligase
IL-1 β :	Interleukin-1 β
TNF- α :	Tumor necrosis factor-alpha
DM:	Diabetes mellitus
AGEs:	Advanced glycation end products
SASP:	Senescence-associated secretory phenotype
MOMP:	Mitochondrial outer membrane permeabilization
BCL-2:	B cell lymphoma 2
MMPs:	Matrix metalloproteinases
ADAMTS:	A disintegrin and metalloproteinase with thrombospondin motifs
Nrf2:	Nuclear factor, erythroid 2-like 2
MAPKs:	Mitogen-activated protein kinases
AIF:	Apoptosis-inducing factor
CsA:	Cyclosporin A
NAC:	N-acetylcysteine
H ₂ S:	Hydrogen sulfide
EGCG:	Epigallocatechin 3-gallate
MitoQ:	Mitoquinone
VDR:	Vitamin D receptor

SIRT6:	Sirtuins
rhSIRT1:	Recombinant human SIRT1
AMPK:	Adenosine monophosphate-activated protein kinase
PGC-1 α :	Peroxisome proliferator-activated receptor- γ coactivator 1 α
NMN:	Nicotinamide mononucleotide.

Conflicts of Interest

The authors declare that there is no conflict of interest regarding the publication of this article.

Authors' Contributions

Lin Jin worked on design and conception of this review and drafted the paper. Danni Li and Fenghua Tao contributed to revise the paper. Danni Li worked on the visualization, and all authors approved the final version of the manuscript.

References

- [1] P. P. A. Vergroesen, I. Kingma, K. S. Emanuel et al., "Mechanics and biology in intervertebral disc degeneration: a vicious circle," *Osteoarthritis and Cartilage*, vol. 23, no. 7, pp. 1057–1070, 2015.
- [2] G. Fontana, E. See, and A. Pandit, "Current trends in biologics delivery to restore intervertebral disc anabolism," *Advanced Drug Delivery Reviews*, vol. 84, pp. 146–158, 2015.
- [3] M. V. Risbud, Z. R. Schoepflin, F. Mwale et al., "Defining the phenotype of young healthy nucleus pulposus cells: recommendations of the spine research interest group at the 2014 annual ORS meeting," *Journal of Orthopaedic Research*, vol. 33, no. 3, pp. 283–293, 2015.
- [4] C. Maher, M. Underwood, and R. Buchbinder, "Non-specific low back pain," *The Lancet*, vol. 389, no. 10070, pp. 736–747, 2017.
- [5] N. Henry, J. Clouet, J. Le Bideau, C. Le Visage, and J. Guicheux, "Innovative strategies for intervertebral disc regenerative medicine: from cell therapies to multiscale delivery systems," *Biotechnology Advances*, vol. 36, no. 1, pp. 281–294, 2018.
- [6] C. J. L. Murray, T. Vos, R. Lozano et al., "Disability-adjusted life years (DALYs) for 291 diseases and injuries in 21 regions, 1990–2010: a systematic analysis for the global burden of disease study 2010," *The Lancet*, vol. 380, no. 9859, pp. 2197–2223, 2012.
- [7] G. Livshits, M. Popham, I. Malkin et al., "Lumbar disc degeneration and genetic factors are the main risk factors for low back pain in women: the UK twin spine study," *Annals of the Rheumatic Diseases*, vol. 70, no. 10, pp. 1740–1745, 2011.
- [8] T. Oichi, Y. Taniguchi, Y. Oshima, S. Tanaka, and T. Saito, "Pathomechanism of intervertebral disc degeneration," *JOR Spine*, vol. 3, no. 1, article e1076, 2020.
- [9] A. Elfering, N. Semmer, D. Birkhofer, M. Zanetti, J. Hodler, and N. Boos, "Young Investigator Award 2001 Winner: risk factors for lumbar disc Degeneration," *Spine*, vol. 27, no. 2, pp. 125–134, 2002.
- [10] J. Clouet, C. Vinatier, C. Merceron et al., "The intervertebral disc: from pathophysiology to tissue engineering," *Joint, Bone, Spine*, vol. 76, no. 6, pp. 614–618, 2009.
- [11] G. S. Shadel and T. L. Horvath, "Mitochondrial ROS signaling in organismal homeostasis," *Cell*, vol. 163, no. 3, pp. 560–569, 2015.
- [12] M. Giacomello, I. Drago, P. Pizzo, and T. Pozzan, "Mitochondrial Ca²⁺ as a key regulator of cell life and death," *Cell Death & Differentiation*, vol. 14, no. 7, pp. 1267–1274, 2007.
- [13] R. J. Youle and A. M. van der Bliek, "Mitochondrial fission, fusion, and stress," *Science*, vol. 337, no. 6098, pp. 1062–1065, 2012.
- [14] S. Pickles, P. Vigié, and R. J. Youle, "Mitophagy and quality control mechanisms in mitochondrial maintenance," *Current Biology: CB*, vol. 28, no. 4, pp. R170–R185, 2018.
- [15] M. T. Lin and M. Flint Beal, "Mitochondrial dysfunction and oxidative stress in neurodegenerative diseases," *Nature*, vol. 443, no. 7113, pp. 787–795, 2006.
- [16] W.-X. Zong, J. D. Rabinowitz, and E. White, "Mitochondria and cancer," *Molecular Cell*, vol. 61, no. 5, pp. 667–676, 2016.
- [17] J. Chow, J. Rahman, J. C. Achermann, M. T. Dattani, and S. Rahman, "Mitochondrial disease and endocrine dysfunction," *Nature Reviews Endocrinology*, vol. 13, no. 2, pp. 92–104, 2017.
- [18] D. R. Green, L. Galluzzi, and G. Kroemer, "Mitochondria and the autophagy-inflammation-cell death axis in organismal aging," *Science (New York, N.Y.)*, vol. 333, no. 6046, pp. 1109–1112, 2011.
- [19] D. F. Wilson, "Oxidative phosphorylation: regulation and role in cellular and tissue metabolism," *The Journal of Physiology*, vol. 595, no. 23, pp. 7023–7038, 2017.
- [20] P. R. Rich and A. Maréchal, "The mitochondrial respiratory chain," *Essays in Biochemistry*, vol. 47, pp. 1–23, 2010.
- [21] S. R. S. Bibby, D. A. Jones, R. M. Ripley, and J. P. G. Urban, "Metabolism of the intervertebral disc: effects of low levels of oxygen, glucose, and pH on rates of energy metabolism of bovine nucleus pulposus cells," *Spine*, vol. 30, no. 5, pp. 487–496, 2005.
- [22] J. C. Salvatierra, T. Y. Yuan, H. Fernando et al., "Difference in energy metabolism of annulus fibrosus and nucleus pulposus cells of the intervertebral disc," *Cellular and Molecular Biomechanics*, vol. 4, no. 2, pp. 302–310, 2011.
- [23] W. Dröge, "Free radicals in the physiological control of cell function," *Physiological Reviews*, vol. 82, no. 1, pp. 47–95, 2002.
- [24] H. E. Gruber, J. A. Watts, F. E. Riley, F. Mary-Beth, H. James Norton, and E. N. Hanley Jr., "Mitochondrial bioenergetics, mass, and morphology are altered in cells of the degenerating human annulus," *Journal of Orthopaedic Research*, vol. 31, no. 8, pp. 1270–1275, 2013.
- [25] F. Ding, Z.-W. Shao, S.-H. Yang, Q. Wu, F. Gao, and L.-M. Xiong, "Role of mitochondrial pathway in compression-induced apoptosis of nucleus pulposus cells," *Apoptosis*, vol. 17, no. 6, pp. 579–590, 2012.
- [26] L. A. Nasto, A. R. Robinson, K. Ngo et al., "Mitochondrial-derived reactive oxygen species (ROS) play a causal role in aging-related intervertebral disc degeneration," *Journal of Orthopaedic Research*, vol. 31, no. 7, pp. 1150–1157, 2013.
- [27] J.-S. Park, J.-B. Park, I.-J. Park, and E.-Y. Park, "Accelerated premature stress-induced senescence of young annulus fibrosus cells of rats by high glucose-induced oxidative stress," *International Orthopaedics*, vol. 38, no. 6, pp. 1311–1320, 2014.

- [28] R. B. Hamanaka and N. S. Chandel, "Mitochondrial reactive oxygen species regulate cellular signaling and dictate biological outcomes," *Trends in Biochemical Sciences*, vol. 35, no. 9, pp. 505–513, 2010.
- [29] T. Finkel and N. J. Holbrook, "Oxidants, oxidative stress and the biology of ageing," *Nature*, vol. 408, no. 6809, pp. 239–247, 2000.
- [30] K. Kalani, S. F. Yan, and S. S. Du Yan, "Mitochondrial permeability transition pore: a potential drug target for neurodegeneration," *Drug Discovery Today*, vol. 23, no. 12, pp. 1983–1989, 2018.
- [31] A. P. Halestrap, "What is the mitochondrial permeability transition pore?," *Journal of Molecular and Cellular Cardiology*, vol. 46, no. 6, pp. 821–831, 2009.
- [32] L. Tilokani, S. Nagashima, V. Paupe, and J. Prudent, "Mitochondrial dynamics: overview of molecular mechanisms," *Essays in Biochemistry*, vol. 62, no. 3, pp. 341–360, 2018.
- [33] L. D. Osellame, A. P. Singh, D. A. Stroud et al., "Cooperative and independent roles of the Drp 1 adaptors Mff, MiD49 and MiD51 in mitochondrial fission," *Journal of Cell Science*, vol. 129, no. 11, pp. 2170–2181, 2016.
- [34] A. Santel and M. T. Fuller, "Control of mitochondrial morphology by a human mitofusin," *Journal of Cell Science*, vol. 114, no. 5, p. 867, 2001.
- [35] T. Wai and T. Langer, "Mitochondrial dynamics and metabolic regulation," *Trends in Endocrinology & Metabolism*, vol. 27, no. 2, pp. 105–117, 2016.
- [36] B. Bingol and M. Sheng, "Mechanisms of mitophagy: PINK1, Parkin, USP30 and beyond," *Free Radical Biology and Medicine*, vol. 100, pp. 210–222, 2016.
- [37] T. N. Nguyen, B. S. Padman, and M. Lazarou, "Deciphering the molecular signals of PINK1/parkin mitophagy," *Trends in Cell Biology*, vol. 26, no. 10, pp. 733–744, 2016.
- [38] T. Kanki, D. J. Klionsky, and K. Okamoto, "Mitochondria autophagy in yeast," *Antioxidants & Redox Signaling*, vol. 14, no. 10, pp. 1989–2001, 2011.
- [39] K. Palikaras, E. Lionaki, and N. Tavernarakis, "Mechanisms of mitophagy in cellular homeostasis, physiology and pathology," *Nature Cell Biology*, vol. 20, no. 9, pp. 1013–1022, 2018.
- [40] C. Guo, G. Kroemer, and O. Kepp, "Mitophagy: an emerging role in aging and age-associated diseases," *Frontiers in Cell and Developmental Biology*, vol. 8, p. 200, 2020.
- [41] R. Hartman, P. Patil, R. Tisherman et al., "Age-dependent changes in intervertebral disc cell mitochondria and bioenergetics," *European Cells and Materials*, vol. 36, pp. 171–183, 2018.
- [42] D. A. Pulliam, A. Bhattacharya, and H. Van Remmen, "Mitochondrial dysfunction in aging and longevity: a causal or protective role?," *Antioxidants & Redox Signaling*, vol. 19, no. 12, pp. 1373–1387, 2013.
- [43] K.-W. Kim, H.-N. Chung, K.-Y. Ha, J.-S. Lee, and Y.-Y. Kim, "Senescence mechanisms of nucleus pulposus chondrocytes in human intervertebral discs," *The Spine Journal*, vol. 9, no. 8, pp. 658–666, 2009.
- [44] C. Feng, M. Yang, M. Lan et al., "ROS: crucial intermediators in the pathogenesis of intervertebral disc degeneration," *Oxidative Medicine and Cellular Longevity*, vol. 2017, Article ID 5601593, 12 pages, 2017.
- [45] K. Liang, S. Liu, J. Li, Y. Tian, Y. Xue, and X. Liu, "The mitochondria-targeted anti-oxidant Mito Q protects against intervertebral disc degeneration by ameliorating mitochondrial dysfunction and redox imbalance," *Cell Proliferation*, vol. 53, no. 3, article e12779, 2020.
- [46] D. Xu, H. Jin, J. Wen et al., "Hydrogen sulfide protects against endoplasmic reticulum stress and mitochondrial injury in nucleus pulposus cells and ameliorates intervertebral disc degeneration," *Pharmacological Research*, vol. 117, pp. 357–369, 2017.
- [47] M. V. Risbud and I. M. Shapiro, "Role of cytokines in intervertebral disc degeneration: pain and disc content," *Nature Reviews Rheumatology*, vol. 10, no. 1, pp. 44–56, 2014.
- [48] J. Wang, C. Huang, Z. Lin et al., "Polydatin suppresses nucleus pulposus cell senescence, promotes matrix homeostasis and attenuates intervertebral disc degeneration in rats," *Journal of Cellular and Molecular Medicine*, vol. 22, no. 11, pp. 5720–5731, 2018.
- [49] Z. Zhang, T. Xu, J. Chen et al., "Parkin-mediated mitophagy as a potential therapeutic target for intervertebral disc degeneration," *Cell Death & Disease*, vol. 9, no. 10, p. 980, 2018.
- [50] M. Teraguchi, N. Yoshimura, H. Hashizume et al., "Progression, incidence, and risk factors for intervertebral disc degeneration in a longitudinal population-based cohort: the Wakayama spine study," *Osteoarthritis and Cartilage*, vol. 25, no. 7, pp. 1122–1131, 2017.
- [51] S.-Y. Goh and M. E. Cooper, "The role of advanced glycation end products in progression and complications of diabetes," *The Journal of Clinical Endocrinology & Metabolism*, vol. 93, no. 4, pp. 1143–1152, 2008.
- [52] Z. Jiang, W. Lu, Q. Zeng, D. Li, L. Ding, and W. Jingping, "High glucose-induced excessive reactive oxygen species promote apoptosis through mitochondrial damage in rat cartilage endplate cells," *Journal of Orthopaedic Research*, vol. 36, no. 9, pp. 2476–2483, 2018.
- [53] E.-Y. Park and J.-B. Park, "High glucose-induced oxidative stress promotes autophagy through mitochondrial damage in rat notochordal cells," *International Orthopaedics*, vol. 37, no. 12, pp. 2507–2514, 2013.
- [54] M.-B. Guo, D.-C. Wang, H.-F. Liu et al., "Lupeol against high-glucose-induced apoptosis via enhancing the anti-oxidative stress in rabbit nucleus pulposus cells," *European Spine Journal*, vol. 27, no. 10, pp. 2609–2620, 2018.
- [55] Y. Song, Y. Wang, Y. Zhang et al., "Advanced glycation end products regulate anabolic and catabolic activities via NLRP3-inflammasome activation in human nucleus pulposus cells," *Journal of Cellular and Molecular Medicine*, vol. 21, no. 7, pp. 1373–1387, 2017.
- [56] T.-T. Tsai, N. Y.-J. Ho, Y.-T. Lin et al., "Advanced glycation end products in degenerative nucleus pulposus with diabetes," *Journal of Orthopaedic Research*, vol. 32, no. 2, pp. 238–244, 2014.
- [57] H.-M. Ni, J. A. Williams, and W.-X. Ding, "Mitochondrial dynamics and mitochondrial quality control," *Redox Biology*, vol. 4, pp. 6–13, 2015.
- [58] O. Krupkova, J. Handa, M. Hlavna et al., "The natural polyphenol epigallocatechin gallate protects intervertebral disc cells from oxidative stress," *Oxidative Medicine and Cellular Longevity*, vol. 2016, Article ID 7031397, 17 pages, 2016.
- [59] J. Wang, M. Nisar, C. Huang et al., "Small molecule natural compound agonist of SIRT3 as a therapeutic target for the treatment of intervertebral disc degeneration," *Experimental & Molecular Medicine*, vol. 50, no. 11, pp. 1–14, 2018.

- [60] K. Liang, S. Liu, J. Li, Y. Tian, Y. Xue, and X. Liu, "Parkin and Nrf 2 prevent oxidative stress-induced apoptosis in intervertebral endplate chondrocytes via inducing mitophagy and anti-oxidant defenses," *Life Sciences*, vol. 243, p. 117244, 2020.
- [61] J. W. Chen, B. B. Ni, B. Li, Y. H. Yang, S. D. Jiang, and L. S. Jiang, "The responses of autophagy and apoptosis to oxidative stress in nucleus pulposus cells: implications for disc degeneration," *Cellular Physiology and Biochemistry*, vol. 34, no. 4, pp. 1175–1189, 2014.
- [62] C. D. Wiley and J. Campisi, "From ancient pathways to aging cells—connecting metabolism and cellular senescence," *Cell Metabolism*, vol. 23, no. 6, pp. 1013–1021, 2016.
- [63] L. Maitre, C. Lyn, A. J. Freemont, and J. A. Hoyland, "Accelerated cellular senescence in degenerate intervertebral discs: a possible role in the pathogenesis of intervertebral disc degeneration," *Arthritis Research & Therapy*, vol. 9, no. 3, p. R45, 2007.
- [64] H. E. Gruber, J. A. Ingram, D. E. Davis, and E. N. Hanley, "Increased cell senescence is associated with decreased cell proliferation in vivo in the degenerating human annulus," *The Spine Journal*, vol. 9, no. 3, pp. 210–215, 2009.
- [65] P. Patil, M. Falabella, A. Saeed et al., "Oxidative stress-induced senescence markedly increases disc cell bioenergetics," *Mechanisms of Ageing And Development*, vol. 180, pp. 97–106, 2019.
- [66] J. F. Passos, G. Nelson, C. Wang et al., "Feedback between P 21 and reactive oxygen production is necessary for cell senescence," *Molecular Systems Biology*, vol. 6, no. 1, p. 347, 2010.
- [67] A. Dimozi, E. Mavrogonatos, A. Sklirou, and D. Kletsas, "Oxidative stress inhibits the proliferation, induces premature senescence and promotes a catabolic phenotype in human nucleus pulposus intervertebral disc cells," *European Cells & Materials*, vol. 30, pp. 89–103, 2015.
- [68] N. Zhou, X. Lin, W. Dong et al., "SIRT1 alleviates senescence of degenerative human intervertebral disc cartilage endplate cells via the p53/p21 pathway," *Scientific Reports*, vol. 6, no. 1, p. 22628, 2016.
- [69] X. Xu, D. Wang, C. Zheng et al., "Progerin accumulation in nucleus pulposus cells impairs mitochondrial function and induces intervertebral disc degeneration and therapeutic effects of sulforaphane," *Theranostics*, vol. 9, no. 8, pp. 2252–2267, 2019.
- [70] D. Huang, Y. Peng, Z. Li et al., "Compression-induced senescence of nucleus pulposus cells by promoting mitophagy activation via the PINK1/PARKIN pathway," *Journal of Cellular and Molecular Medicine*, vol. 24, no. 10, pp. 5850–5864, 2020.
- [71] C.-Q. Zhao, Y.-H. Zhang, S.-D. Jiang, L.-S. Jiang, and L.-Y. Dai, "Both endoplasmic reticulum and mitochondria are involved in disc cell apoptosis and intervertebral disc degeneration in rats," *Age (Dordrecht, Netherlands)*, vol. 32, no. 2, pp. 161–177, 2010.
- [72] H. Sudo and A. Minami, "Caspase 3 as a therapeutic target for regulation of intervertebral disc degeneration in rabbits," *Arthritis and Rheumatism*, vol. 63, no. 6, pp. 1648–1657, 2011.
- [73] S. Yang, F. Zhang, J. Ma, and W. Ding, "Intervertebral disc ageing and degeneration: the antiapoptotic effect of oestrogen," *Ageing Research Reviews*, vol. 57, p. 100978, 2020.
- [74] H. Wang, H. Liu, Z.-M. Zheng et al., "Role of death receptor, mitochondrial and endoplasmic reticulum pathways in different stages of degenerative human lumbar disc," *Apoptosis*, vol. 16, no. 10, pp. 990–1003, 2011.
- [75] S. W. G. Tait and D. R. Green, "Mitochondria and cell death: outer membrane permeabilization and beyond," *Nature Reviews Molecular Cell Biology*, vol. 11, no. 9, pp. 621–632, 2010.
- [76] T. Tong, Z. Liu, H. Zhang et al., "Age-dependent expression of the vitamin D receptor and the protective effect of vitamin D receptor activation on H₂O₂-induced apoptosis in rat intervertebral disc cells," *The Journal of Steroid Biochemistry and Molecular Biology*, vol. 190, pp. 126–138, 2019.
- [77] S. Miyazaki, K. Kakutani, T. Yurube et al., "Recombinant human SIRT1 protects against nutrient deprivation-induced mitochondrial apoptosis through autophagy induction in human intervertebral disc nucleus pulposus cells," *Arthritis Research & Therapy*, vol. 17, no. 1, p. 253, 2015.
- [78] J. Liu, J. Wang, and Y. Zhou, "Upregulation of BNIP3 and translocation to mitochondria in nutrition deprivation induced apoptosis in nucleus pulposus cells," *Joint, Bone, Spine*, vol. 79, no. 2, pp. 186–191, 2012.
- [79] Y. Song, S. Li, W. Geng et al., "Sirtuin 3-dependent mitochondrial redox homeostasis protects against AGEs-induced intervertebral disc degeneration," *Redox Biology*, vol. 19, pp. 339–353, 2018.
- [80] S. Chen, X. Lv, B. Hu et al., "Critical contribution of RIPK1 mediated mitochondrial dysfunction and oxidative stress to compression-induced rat nucleus pulposus cells necroptosis and apoptosis," *Apoptosis*, vol. 23, no. 5–6, pp. 299–313, 2018.
- [81] J. Montane, A. Klimek-Abercrombie, K. J. Potter, C. Westwell-Roper, and C. Bruce Verchere, "Metabolic stress, IAPP and islet amyloid," *Diabetes, Obesity and Metabolism*, vol. 14, pp. 68–77, 2012.
- [82] X. Wu, K. Wang, W. Hua et al., "Down-regulation of islet amyloid polypeptide expression induces death of human annulus fibrosus cells via mitochondrial and death receptor pathways," *Biochimica et Biophysica Acta (BBA) - Molecular Basis of Disease*, vol. 1863, no. 6, pp. 1479–1491, 2017.
- [83] X. Li, F. R. Wu, R. S. Xu et al., "Acid-sensing ion channel 1A-mediated calcium influx regulates apoptosis of endplate chondrocytes in intervertebral discs," *Expert Opinion on Therapeutic Targets*, vol. 18, no. 1, pp. 1–14, 2014.
- [84] P. J. Roughley, "Biology of intervertebral disc aging and Degeneration," *Spine*, vol. 29, no. 23, pp. 2691–2699, 2004.
- [85] S. Gonzales, C. Wang, H. Levene, H. S. Cheung, and C.-Y. C. Huang, "ATP promotes extracellular matrix biosynthesis of intervertebral disc cells," *Cell and Tissue Research*, vol. 359, no. 2, pp. 635–642, 2015.
- [86] X. Yin, S. Gonzales, S. Sha, H. Levene, and C. Y. Huang, "The effect of adenosine on extracellular matrix production in porcine intervertebral disc cells," *Cells, Tissues, Organs*, vol. 206, no. 1–2, pp. 73–81, 2019.
- [87] L. Yang, Z. Rong, M. Zeng et al., "Pyrroloquinoline quinone protects nucleus pulposus cells from hydrogen peroxide-induced apoptosis by inhibiting the mitochondria-mediated pathway," *European Spine Journal*, vol. 24, no. 8, pp. 1702–1710, 2015.
- [88] Y. Chen, Y. Wu, H. Shi et al., "Melatonin ameliorates intervertebral disc degeneration via the potential mechanisms of mitophagy induction and apoptosis inhibition," *Journal of Cellular and Molecular Medicine*, vol. 23, no. 3, pp. 2136–2148, 2019.

- [89] H. Lin, X. Ma, B.-C. Wang et al., "Edaravone ameliorates compression-induced damage in rat nucleus pulposus cells," *Life Sciences*, vol. 189, pp. 76–83, 2017.
- [90] N. Fujita, S. S. Gogate, K. Chiba, Y. Toyama, I. M. Shapiro, and M. V. Risbud, "Prolyl hydroxylase 3 (PHD3) modulates catabolic effects of tumor necrosis factor- α (TNF- α) on cells of the nucleus pulposus through co-activation of nuclear factor κ B (NF- κ B)/p 65 signaling," *The Journal of Biological Chemistry*, vol. 287, no. 47, pp. 39942–39953, 2012.
- [91] A. Hiyama, K. Yokoyama, T. Nukaga, D. Sakai, and J. Mochida, "A complex interaction between Wnt signaling and TNF- α in nucleus pulposus cells," *Arthritis Research & Therapy*, vol. 15, no. 6, p. R189, 2013.
- [92] Y. Tian, W. Yuan, N. Fujita et al., "Inflammatory cytokines associated with degenerative disc disease control aggrecanase-1 (ADAMTS-4) expression in nucleus pulposus cells through MAPK and NF- κ B," *The American Journal of Pathology*, vol. 182, no. 6, pp. 2310–2321, 2013.
- [93] R. M. Mason and C. Sweeney, "The relationship between proteoglycan synthesis in swarm chondrocytes and pathways of cellular energy and UDP-sugar metabolism," *Carbohydrate Research*, vol. 255, pp. 255–270, 1994.
- [94] B. P. Dranka, B. G. Hill, and V. M. Darley-Usmar, "Mitochondrial reserve capacity in endothelial cells: the impact of nitric oxide and reactive oxygen species," *Free Radical Biology and Medicine*, vol. 48, no. 7, pp. 905–914, 2010.
- [95] P. H. Reddy, X. L. Yin, M. Manczak et al., "Mutant APP and amyloid beta-induced defective autophagy, mitophagy, mitochondrial structural and functional changes and synaptic damage in hippocampal neurons from Alzheimer's disease," *Human Molecular Genetics*, vol. 27, no. 14, pp. 2502–2516, 2018.
- [96] X. Yao, J. Zhang, X. Jing et al., "Fibroblast growth factor 18 exerts anti-osteoarthritic effects through PI3K-AKT signaling and mitochondrial fusion and fission," *Pharmacological Research*, vol. 139, pp. 314–324, 2019.
- [97] M. Y. Ansari, N. M. Khan, I. Ahmad, and T. M. Haqqi, "Parkin clearance of dysfunctional mitochondria regulates ROS levels and increases survival of human chondrocytes," *Osteoarthritis and Cartilage*, vol. 26, no. 8, pp. 1087–1097, 2018.
- [98] H. Lin, L. Zhao, X. Ma et al., "Drp 1 mediates compression-induced programmed necrosis of rat nucleus pulposus cells by promoting mitochondrial translocation of P 53 and nuclear translocation of AIF," *Biochemical and Biophysical Research Communications*, vol. 487, no. 1, pp. 181–188, 2017.
- [99] Y. Chen, J. Lin, J. Chen et al., "Mfn 2 is involved in intervertebral disc degeneration through autophagy modulation," *Osteoarthritis and Cartilage*, vol. 28, no. 3, pp. 363–374, 2020.
- [100] Y. Wang, J. Shen, Y. Chen et al., "PINK1 protects against oxidative stress induced senescence of human nucleus pulposus cells via regulating mitophagy," *Biochemical and Biophysical Research Communications*, vol. 504, no. 2, pp. 406–414, 2018.
- [101] J. Lin, J. Zhuge, X. Zheng et al., "Urolithin A-induced mitophagy suppresses apoptosis and attenuates intervertebral disc degeneration via the AMPK signaling pathway," *Free Radical Biology and Medicine*, vol. 150, pp. 109–119, 2020.
- [102] W.-N. Xu, H.-L. Zheng, R.-Z. Yang et al., "Mitochondrial NDUFA4L2 attenuates the apoptosis of nucleus pulposus cells induced by oxidative stress via the inhibition of mitophagy," *Experimental & Molecular Medicine*, vol. 51, no. 11, pp. 1–16, 2019.
- [103] R. Schreck, P. Rieber, and P. A. Baeuerle, "Reactive oxygen intermediates as apparently widely used messengers in the activation of the NF-kappa B transcription factor and HIV-1," *The EMBO Journal*, vol. 10, no. 8, pp. 2247–2258, 1991.
- [104] K. G. Ma, Z. W. Shao, S. H. Yang et al., "Autophagy is activated in compression-induced cell degeneration and is mediated by reactive oxygen species in nucleus pulposus cells exposed to compression," *Osteoarthritis and Cartilage*, vol. 21, no. 12, pp. 2030–2038, 2013.
- [105] S. Suzuki, N. Fujita, N. Hosogane et al., "Excessive reactive oxygen species are therapeutic targets for intervertebral disc degeneration," *Arthritis Research & Therapy*, vol. 17, no. 1, p. 316, 2015.
- [106] C. R. Powell, K. M. Dillon, and J. B. Matson, "A review of hydrogen sulfide (H₂S) donors: Chemistry and potential therapeutic applications," *Biochemical Pharmacology*, vol. 149, pp. 110–123, 2018.
- [107] R. Wedmann, S. Bertlein, I. Macinkovic et al., "Working with 'H₂S': Facts and apparent artifacts," *Nitric Oxide*, vol. 41, pp. 85–96, 2014.
- [108] B. Murphy, R. Bhattacharya, and P. Mukherjee, "Hydrogen sulfide signaling in mitochondria and disease," *FASEB Journal*, vol. 33, no. 12, pp. 13098–13125, 2019.
- [109] C.-x. Qi, Q. Zhou, Z. Yuan et al., "Kinsenoside: a promising bioactive compound from *Anoectochilus* species," *Current Medical Science*, vol. 38, no. 1, pp. 11–18, 2018.
- [110] Y. Wang, R. Zuo, Z. Wang et al., "Kinsenoside ameliorates intervertebral disc degeneration through the activation of AKT-ERK1/2-Nrf2 signaling pathway," *Aging*, vol. 11, no. 18, pp. 7961–7977, 2019.
- [111] B. Zhang, L. Xu, N. Zhuo, and J. Shen, "Resveratrol protects against mitochondrial dysfunction through autophagy activation in human nucleus pulposus cells," *Biochemical and Biophysical Research Communications*, vol. 493, no. 1, pp. 373–381, 2017.
- [112] X. Li, F. M. Phillips, H. S. An et al., "The action of resveratrol, a phytoestrogen found in grapes, on the intervertebral disc," *Spine*, vol. 33, no. 24, pp. 2586–2595, 2008.
- [113] W. Hua, S. Li, R. Luo et al., "Icariin protects human nucleus pulposus cells from hydrogen peroxide-induced mitochondria-mediated apoptosis by activating nuclear factor erythroid 2-related factor 2," *Biochimica et Biophysica Acta (BBA) - Molecular Basis of Disease*, vol. 1866, no. 1, p. 165575, 2020.
- [114] G. F. Kelso, C. M. Porteous, C. V. Coulter et al., "Selective targeting of a redox-active ubiquinone to mitochondria within cells: antioxidant and antiapoptotic properties," *Journal of Biological Chemistry*, vol. 276, no. 7, pp. 4588–4596, 2001.
- [115] S. Rodriguez-Cuenca, H. M. Cochemé, A. Logan et al., "Consequences of long-term oral administration of the mitochondria-targeted antioxidant MitoQ to wild-type mice," *Free Radical Biology and Medicine*, vol. 48, no. 1, pp. 161–172, 2010.
- [116] A. Dhanasekaran, S. Kotamraju, S. V. Kalivendi et al., "Supplementation of endothelial cells with mitochondria-targeted antioxidants inhibit peroxide-induced mitochondrial iron uptake, oxidative damage, and apoptosis," *Journal of Biological Chemistry*, vol. 279, no. 36, pp. 37575–37587, 2004.
- [117] R. A. J. Smith, C. M. Porteous, A. M. Gane, and M. P. Murphy, "Delivery of bioactive molecules to mitochondria in vivo," *Proceedings of the National Academy of Sciences of*

- the United States of America*, vol. 100, no. 9, pp. 5407–5412, 2003.
- [118] E. F. Fang, Y. Hou, K. Palikaras et al., “Mitophagy inhibits amyloid- β and tau pathology and reverses cognitive deficits in models of Alzheimer’s disease,” *Nature Neuroscience*, vol. 22, no. 3, pp. 401–412, 2019.
- [119] X. Onphachanh, H. J. Lee, J. R. Lim et al., “Enhancement of high glucose-induced PINK1 expression by melatonin stimulates neuronal cell survival: involvement of MT2/Akt/NF- κ B pathway,” *Journal of Pineal Research*, vol. 63, no. 2, article e12427, 2017.
- [120] W.-N. Xu, R.-Z. Yang, H.-L. Zheng et al., “PGC-1 α acts as a mediator of Sirtuin2 to protect annulus fibrosus from apoptosis induced by oxidative stress through restraining mitophagy,” *International Journal of Biological Macromolecules*, vol. 136, pp. 1007–1017, 2019.
- [121] C. Ricca, A. Aillon, L. Bergandi, D. Alotto, C. Castagnoli, and F. Silvagno, “Vitamin D receptor is necessary for mitochondrial function and cell health,” *International Journal of Molecular Sciences*, vol. 19, no. 6, p. 1672, 2018.
- [122] R. A. H. van de Ven, D. Santos, and M. C. Haigis, “Mitochondrial sirtuins and molecular mechanisms of aging,” *Trends in Molecular Medicine*, vol. 23, no. 4, pp. 320–331, 2017.
- [123] A. T. Dinkova-Kostova and A. Y. Abramov, “The emerging role of Nrf2 in mitochondrial function,” *Free Radical Biology and Medicine*, vol. 88, Part B, pp. 179–188, 2015.
- [124] Z. Tang, B. Hu, F. Zang, J. Wang, X. Zhang, and H. Chen, “Nrf2 drives oxidative stress-induced autophagy in nucleus pulposus cells via a Keap1/Nrf2/p62 feedback loop to protect intervertebral disc from degeneration,” *Cell Death & Disease*, vol. 10, no. 7, p. 510, 2019.

Review Article

Effect of Platelet-Rich Plasma on Intervertebral Disc Degeneration *In Vivo* and *In Vitro*: A Critical Review

Yvang Chang ^{1,2} Ming Yang ^{1,2} Song Ke ^{1,2} Yu Zhang ^{1,2} Gang Xu ^{1,2}
and Zhonghai Li ^{1,2}

¹Department of Orthopaedics, First Affiliated Hospital of Dalian Medical University, Dalian, China

²Key Laboratory of Molecular Mechanism for Repair and Remodeling of Orthopaedic Diseases, Liaoning Province, China

Correspondence should be addressed to Gang Xu; 526423695@163.com and Zhonghai Li; lizhonghaispine@126.com

Received 6 September 2020; Revised 2 November 2020; Accepted 4 November 2020; Published 23 November 2020

Academic Editor: Sidong Yang

Copyright © 2020 Yvang Chang et al. This is an open access article distributed under the Creative Commons Attribution License, which permits unrestricted use, distribution, and reproduction in any medium, provided the original work is properly cited.

Intervertebral disc degeneration (IDD) is a globally occurring disease that represents a significant cause of socioeconomic problems. Currently, the main method for treating IDD is surgery, including discectomy and vertebral fusion. Several *in vitro* experiments demonstrated that platelet-rich plasma (PRP) could stimulate cell proliferation and extracellular matrix regeneration. Additionally, *in vivo* experiments have proven that PRP injection could restore intervertebral disc height. Clinical studies demonstrated that PRP injection could significantly relieve patient pain. However, further studies are still required to clarify the roles of PRP in IDD prevention and treatment. This review is aimed at summarizing and critically analyzing the current evidence regarding IDD treatment with PRP.

1. Introduction

Intervertebral disc degeneration (IDD) is becoming a serious medical and social problem. The global prevalence of IDD exceeds 60% and is higher in men and older adults [1], which results in high costs for society. During progress of IDD, dehydration of the nucleus pulposus, annulus fibrosus tears, fracture of the cartilage endplate, and release of inflammatory factors occur. IDD then leads to lumbar disc herniation and discogenic pain, which cause low back pain, and may severely affect spinal extension and flexion. Because of the avascular tissue structure of the intervertebral disc (IVD) with a poor self-healing capacity, oral medication is generally ineffective. Current IDD treatment methods mainly include bed rest, physical therapy, epidural injections, surgical decompression, disc replacement, and disc fusion [2]. Additionally, bioactive agents have attracted considerable attention because of the limited damage caused in their application, in which

the basic principle of IDD treatment is to delay or even reverse the trend of IDD through the activity of the agents' components.

Many bioactive agents are currently applied to treat IDD, with most direct treatment strategies for reversing IDD involving the injection of active agents. Platelet-rich plasma (PRP) is particularly attractive because of the high concentration of platelets that releases a variety of multifunctional growth factors (GFs) when activated and has been widely used to repair various avascular tissues, including but not limited to bones, cartilages, muscles, and tendons, and may represent a new strategy for IDD biotherapy [3, 4].

2. IVD and IDD

Anatomically, the IVD comprises a central highly hydrated nucleus pulposus (NP), a peripheral thin layer of the annulus fibrosus (AF), and upper and lower cartilage endplates (CEPs) [5]. Histologically, the NP mainly comprises water

and a low density of notochord and NP cells and the extracellular matrix (ECM). The ECM mainly comprises collagen II (COL II), elastin, fibers, and numerous proteoglycans especially aggrecan (ACAN) with negative charge. Physiologically, the hydrated NP can absorb the compressive pressure of the spine. The AF mainly comprises COL I as a lamellar ring structure of approximately 15–25 layers outside the NP, and the outer AF layer comprises fibroblasts with a neurovascular distribution, in which the nerves comprise spinal sensory and postganglionic sympathetic fibers [6]. The CEPs are located at both sides of the IVD and comprise a layer of horizontal hyaline cartilage, where nutrients and oxygen enter the IVD by free diffusion.

IVD homeostasis is a complex pathway, in which the factors associated with IDD are mainly genetic and environmental. The genes associated with IDD mainly include three types: (1) genes affecting intervertebral disc structure (ACAN, COL, etc.), (2) genes of metabolic enzymes affecting IVD metabolism (including matrix metalloproteinases [MMPs], cyclooxygenase- [COX-] 2, and tissue inhibitor of matrix metalloproteinases), and (3) inflammation-related genes (including interleukin- [IL-] 1 and IL-6). Changes in expression of these genes may affect homeostasis of the IVD. Furthermore, environmental factors, including repeated mechanical stimulation, poor nutritional supply, deficiencies of oestrogen, and other definite risk factors including obesity, cigarette smoking, and atherosclerosis may affect homeostasis of IVD, which could contribute to IDD [7]. In the early stages of IDD, the content of ACAN and other proteoglycans initially falls. This decrease leads to NP dehydration and atrophy, which alters the NP biomechanics. In advanced cases, the AF will directly bear the longitudinal pressure. The structure of the AF means that it is more resistant to tension than compressive pressure, resulting in a decrease in intervertebral disc height. At the same time, anabolism and catabolic homeostasis of the matrix are disrupted. This process is accompanied by cellular senescence and morphological changes associated with the aging of cells, reduced secretion of matrix proteins, and possible secretion of inflammatory factors. This could then lead to an inflammatory reaction, which further exacerbates progression of IDD. MMP-1, MMP-3, and MMP-13, a disintegrin-like and metalloproteinase with thrombospondin motifs (ADAMTSs), and enzymes that promote catabolism are highly expressed in the degenerated disc. Additionally, COX-2, which may be the cause of pain, is highly expressed. Pigment accumulation in the NP makes it more difficult to distinguish it from the AF, and the NP cell density is simultaneously reduced. These degenerative changes directly lead to a weakening of the mechanical function of the IVD, which in turn leads to structural deformation, disc height loss of the IVD, segmental instability of the spine, and ultimately structural damages, including the AF tearing and NP protrusion, resulting in discogenic pain [8].

Reactive oxygen species (ROS) are a family of unstable and highly reactive molecules with or without free radicals. ROS are inevitably produced through the oxygen-using metabolic processes of IVD cells residing in an environment of

low oxygen tension. Excessive ROS cause oxidative stress, which activates various signaling pathways in disc cells, including the NF- κ B pathway, deteriorating the viability and function of disc cells [9]. Injury to IVDs can also cause inflammation-driven ROS production and result in neovascularization and exposure of the otherwise hypoxic resident cells to higher oxygen tension [10].

In summary, oxidative stress induces damage of micro-environmental homeostasis and promotes degradation of the matrix in IVDs. Consequently, a significant loss of elasticity and the normal structure and biomechanical properties of the disc matrix causes IDD.

3. PRP

PRP is an autologous blood concentrate that can release abundant α particles containing high concentrations of proliferation- and differentiation-promoting GFs and has been widely used in oral surgery and orthopedics [11]. Different equipment and preparation methods may lead to different cells and types of cytokines and their concentrations in PRP. Dohan Ehrenfest et al. [12] defined PRP in four categories according to the content of leukocytes and fibrin: pure PRP (P-PRP), leukocyte-rich PRP (L-PRP), leukocyte platelet-rich fibrin, and pure platelet-rich fibrin. Because PRP is one component of the autologous plasma, it has the following advantages: (1) in principle, immune rejection does not occur; (2) it avoids the spread of diseases; and (3) it can be readily prepared by centrifugation, which is much cheaper than recombinant GFs. Furthermore, the main components of PRP are GFs, inflammatory cells, and adhesion molecules. GFs mainly include platelet-derived growth factor, transforming growth factor- β (TGF- β), vascular endothelial growth factor (VEGF), and epithelial growth factor. The published experimental results have proven that PRP can promote angiogenesis, cell proliferation, and collagen synthesis, thereby repairing damaged tissues, including tendons, ligaments, cartilage, and other avascular tissue with a low self-healing ability. Notably, PRP may be effective in repairing a patient's atrophic multifidus and compressed nerve roots [13–15]. Inflammatory cells in PRP are mainly leukocytes, and L-PRP may promote regeneration of cartilage and has a strong bactericidal effect. Therefore, PRP has promising prospects in the treatment of osteoarthritis, especially via augmented anti-inflammatory effects, antioxidative chondrocyte proliferation, inhibited MMP-1 activity, and calcification of the matrix [15, 16]. Furthermore, studies have shown that adhesive proteins (fibrin, fibronectin, and vitronectin) in PRP, which can serve as a carrier for stem cells and as tissue-engineering scaffolds, play a role in promoting stem cell therapy with good prospects for application [17].

4. *In Vitro* Study of the PRP Repair Function

More than 10 years of research on PRP has gradually demonstrated its potential therapeutic effect for IDD. Many *in vitro* studies explored how PRP functioned. In 2006, Akeda et al. [18] applied PRP to intervening porcine

IVD cells (NP and AF cells) and reported that PRP soluble releasate had a mild stimulatory effect on IVD cell proliferation and increased the synthesis of proteoglycans and collagen, whereas platelet-poor plasma (PPP) had no effect. Additionally, PRP displayed stronger stimulative effects in the AF compared with the NP. Chen et al. [19] conducted research on the TGF- β 1 in PRP and designed a concentration gradient of TGF- β 1 in PRP to stimulate human NP (hNP) cells. The result showed that PRP enhanced matrix gene expression (COL II and ACAN) and proteoglycan accumulation compared with the PPP intervention group and the control group. Additionally, they demonstrated what the optimum PRP concentration was when it contained 1 ng/ml TGF- β 1. Furthermore, they proved that the PRP's regeneration effects were via the Smad2/3 pathway phosphorylation. Several years later, a further study of Chen et al. [20] considered the entire IVD *ex vivo*. Porcine IVDs were digested using chymopain. At 2 weeks after the administration of 10% porcine PRP, mesenchymal stem cells (MSCs), or 10% PRP and MSCs, decreased apoptosis was found and NP cell viability was promoted in this *ex vivo* IVD system. COL II and ACAN mRNA expression was significantly upregulated, and ECM synthesis was promoted. Additionally, they demonstrated that PRP could direct MSC differentiation into chondrocytes. Pirvu et al. [21] compared the effects of different PRP and platelet lysate (PL) concentrations on bovine AF cells. They confirmed that both PRP and PL were able to increase cell proliferation and glycosaminoglycan accumulation in monolayer culture systems and maintain the spherical shape of cells in whole-disc organ culture. When using PRP or PL for an *in vivo* defect site, PRP was better than PL for the formation of a stable biological sponge for absorbing and storing some small molecules that regulated tissue regeneration.

In 2016, Yang et al. [22] also considered TGF- β 1 and tested the effects of PRP originating from rabbits. They found that PRP stimulated COL II, ACAN, and Sox-9 gene expression, suppressed COL X gene expression, and displayed the ability to stimulate NP cell proliferation. Additionally, they found that 2.5% PRP was the optimum concentration for NP cell stimulation, which was inhibited by a TGF- β 1 inhibitor or a Smad2/3 signaling pathway inhibitor. Inhibiting TGF- β 1 signaling significantly prevented the NP cellular expression of Smad2/3 and matrix protein. Nikkhoo et al. [23] reported that with PRP, IDD was able to recover its mechanical properties. Studies have shown that PRP could promote the proliferation of bone marrow NP stem cells, producing an optimal effect when applied at 10%. PRP has the ability to induce undifferentiated MSCs to express chondrocyte phenotype markers, including COL II and ACAN, while reducing the expression of stem cell markers. It also plays an important role in the differentiation of adipose-derived stem cells into NP cells [24–27].

Some researchers studied another mechanism for the treatment of IDD with PRP, namely, the anti-inflammatory effect. In 2014, Kim et al. [28] used the combination of IL-1 β and tumor necrosis factor- (TNF-) α on immortalized hNP (ihNP) cells and demonstrated upregulated MMP-3

and COX-2 expression, whereas ACAN and COL II expression was suppressed. Subsequently, they applied PRP, whereby the NP cells recovered the downregulated COL II and ACAN gene expression, reduced the increased MMP-3 and COX-2 gene expression, and suppressed cytokine-induced proinflammatory degrading enzymes and mediators. In 2014, Liu et al. [29] used lipopolysaccharides to induce an inflammatory condition in ihNP cells. There were changes similar to IDD. Sox-9, COL II, and ACAN expression on culture with PRP in two dimensions were strongly upregulated, and the inflammatory factors, including IL-1 β , TNF- α , and MMP-3, were absent. In 2016, Cho et al. [30] applied TNF- α to treat porcine AF cells and found that MMP-1 was induced by TNF- α . Then, with cocultivation by PRP, they came to a conclusion that PRP upregulated COL II and ACAN gene expression and inhibited MMP-1 expression.

Other opinions have been presented regarding the effects of PRP. High leukocyte concentrations in L-PRP may increase the levels of proinflammatory factors (the major components were IL-1 β and TNF- α) and exacerbate the degradation of ECM. Yin et al. [31] also demonstrated that IL-1 β and TNF- α from L-PRP could activate the NF- κ B signaling pathway and promote prostaglandin E2 and nitric oxide production, resulting in inhibited tissue regeneration.

Wang et al. [24] demonstrated that L-PRP treatment of NP-derived stem cells significantly upregulated the expression of the inflammatory genes IL-1 β and TNF- α and promoted catabolism. The authors believed that leukocyte exclusion from PRP might effectively prevent the activation of the NF- κ B signaling pathway.

Jia et al. [25] used P-PRP or L-PRP to treat rabbit NP MSCs (NPMSCs) *in vitro*. The results showed that P-PRP decreased the expression of stem cell markers and stimulated differentiation into NP-like cells. Additionally, P-PRP had a dose effect on NPMSCs, with the maximum proliferation at 10%. Because L-PRP has significantly higher TNF- α and IL-1 β concentrations, it induced differentiation of NPMSCs, upregulated TNF- α and IL-1 β expression, enhanced activation of the NF- κ B pathway, and increased MMP-1 and MMP-13 expression. Inflammation and catabolic reactions resulted in reduced ECM production in differentiated NPMSCs while P-PRP did not activate the NF- κ B pathway.

Conversely, Mietsch et al. [32] put forward different views in 2013. They reported that while PRP administration had stimulatory effects on cell proliferation in cultured NPC and MSC cultures, gene expression of chondrogenic markers (ACAN, COL II, COL I, and Sox-9) was considerably lower compared with TGF- β 1, and matrix protein deposition was weaker. Therefore, they did not recommend PRP to be applied in hNP tissue-engineering because of a probable lack of an effective activator.

Hondke et al. [33] conducted a study on the proliferation, migration, and ECM formation of early AF cells having Pfirrmann grades 2–3 and advanced AF cells having Pfirrmann grades 4–5 from the degenerative tissue. They reported that 5% PRP was the optimum concentration for cell migration, while COL I expression was decreased at this PRP concentration. Therefore, these authors were unable to conclude

TABLE 1: In vitro effects of PRP on IVD cells.

(a)

Year	Study	System used to obtain PRP	Type of cells	Dose
2006	Akeda et al. [18]	SYMPHONY	Porcine IVD NP cell AF cell	10% PRP, 10% PPP
2006	Chen et al. [19]	Centrifuged	hNP	PRP (defined as TGF- β 1 equivalent)
2009	Chen et al. [20]	Centrifuged	Porcine IVD organ induced with chymopapain	10% porcine PRP
2013	Mietsch et al. [32]	Centrifugation and double filtration	hNP MSC	10% PRP MSC
2014	Kim et al. [28]	GPS III System	hNP	5%, 10% PRP
2014	Liu et al. [29]	Not declared	ihNP	PRP (defined as TGF- β 1 1 ng/ml equivalent)
2014	Pirvu et al. [21]	INTERCEPT Blood System	Bovine AF cells	25%–50% human PRP 25%–50% human platelet lysate
2016	Yang et al. [22]	Centrifuged	Rabbit NP cells	10%, 5%, 2.5%, and 1% volume fractions of PRP
2016	Cho et al. [30]	Centrifuged	Porcine AF cells with TNF- α	PRP of 1, 5, 10 \times 10 ⁷ platelets/ml
2018	Wang et al. [24]	Two-step centrifugation	Rabbit NP-derived stem cells	5%–20% rabbit P-PRP or L-PRP
2018	Jia et al. [25]	Two-step centrifugation	NPMSCs	10% P-PRP or 10% L-PRP
2018	Hondke et al. [33]	Not declared	hAF	PRP 5%

(b)

Time of analysis	Activator	Results
72 h	Thrombin+CaCl ₂	Cell proliferation \uparrow , PG and col synthesis \uparrow , PG accumulation \uparrow NP cell proliferation and aggregation \uparrow ; optimum at 1 ng TGF- β 1 concentration in PRP. Tissue construct \uparrow
7, 9 days	Thrombin	COL II, AGN, SOX-9 mRNA \uparrow , GAG accumulation \uparrow phosphorylation of Smad2/3 \uparrow , apoptosis \downarrow
4 weeks	Thrombin	NP regeneration \uparrow mRNA involved in chondrogenesis and matrix accumulation \uparrow
7 days, 4 weeks	Acetic acid	Cell proliferation \uparrow chondrogenic differentiation \downarrow
48 h	CaCl ₂	IL-1 β and TNF- α led matrix synthesis gene expression \downarrow ; PRP degradation expression of COX-2 and MMP-3 \downarrow
7 days, 4 weeks	None	The expression of chondrogenic markers \uparrow , inflammatory mediators ,matrix degrading enzymes in ihNP \downarrow
2, 4 days	Sonication	50% PL-DNA and GAG \uparrow . Matrix synthesis \uparrow of defect AF after PRP injection
1, 2, 3, 4, 5, 6, and 7 days	10% CaCl ₂ 100 U thrombin	mRNA of COL II, AGN, and SOX-9 \uparrow ; protein of COL X level TGF-b1/Smad2/3 \uparrow COLII and AGN \uparrow by 2.5% PRP
24 h	1N HCL	COL II and AGN mRNA \uparrow ,MMP1 mRNA, protein \downarrow
14 days	None	P-PRP: AGN, COL II \uparrow , IL-1 β , TNF- α , IL-6, IL-8, MMP-1, MMP-13 mRNA, IL-1 β , TNF- α production \downarrow
7 days	10% CaCl ₂	P-PRP: AGN, COL II \uparrow L-PRP: IL-1 β , TNF- α MMP1, MMP-13 mRNA \uparrow NF- κ B/p65 protein \uparrow
0, 7, 14, 21 days	Freezing and thawing	Stimulated migration and cell viability in early COL II mRNA \uparrow , COL1 and 3 mRNA \downarrow

Abbreviations: ACT: activation; NP: nucleus pulposus; AF: annulus fibrosus; AGN: aggrecan; COL II: type II collagen; COX-2: cyclooxygenase-2; GAG: glycosaminoglycan; IVD: intervertebral disc; MMP: metalloproteinase; MSC: mesenchymal stem cell; Sox-9:SRY-related high mobility group box gene-9; PG: proteoglycan; PRP: platelet-rich plasma; P-PRP: leukocyte-poor PRP; R-PRP: leukocyte-rich PRP; TNF: tumor necrosis factor.

whether an AF-like ECM could be formed after stimulation by PRP. In summary, 5% PRP has an optimal chemotactic effect, but COL I expression in AF cells is significantly decreased. The authors believed that PRP treatment inhibits matrix formation of the AF.

In conclusion, *in vitro*, PRP was effective in stimulating IVD cell proliferation and ECM metabolism. The anti-

apoptotic and anti-inflammatory effects of PRP might contribute to disc repair and symptom relief in IDD patients in an early stage. Some mechanisms for PRP treatment of IDD, including the Smad pathway, were proposed over time and a direction for future research is of PRP promotion of MSC differentiation into NP cells (Table 1).

TABLE 2: In vivo effects of PRP in IVD degeneration animal models.

(a)

Year	Study	Animal model	Dose	Size of sample	Time of analysis after injection
2007	Nagae et al. [35]	Rabbits, nucleotomy	20 μ l	36	2, 4, and 8 weeks
2009	Kazuhide et al. [34]	Rabbits, nucleotomy	20 μ l	128	2, 4, and 8 weeks
2009	Chen et al. [20]	Miniature porcine, chymopapain	No mention	14	4 and 8 weeks
2011	GB et al. [36]	Rats, needle puncture	100 μ l	18	2, 4, and 6 weeks
2012	Obata et al. [37]	Rabbits, needle puncture	20 μ l	12	8 weeks
2015	Gui et al. [38]	Rabbits, needle puncture	100 μ l	36	2 weeks
2016	Wang et al. [39]	Rabbits, needle puncture	200 μ l	40	1, 2, and 8 weeks
2016	Yang et al. [22]	Rabbits, needle puncture	15 μ l	24	0, 4, 8, and 12 weeks
2016	Hou et al. [40]	Rabbits	40 μ l	60	4 and 8 weeks

(b)

Injection site	Activator	Results
Lumbar	None	PRP+GHM group decreased IDD and increased PG; PRP+PBS group showed no differences
Lumbar	None	PRP+GHM had greater DHI, water content, AGN, and COL II mRNA \uparrow ; fewer apoptotic cells in NP
Thoracic lumbar	None	PRP promote DHI and osteogenic MSC differentiation
Lumbar	None	Preserved IVD fluid content, decreased IVD degeneration
Lumbar	Autologous serum and 2 % CaCl ₂	Increased cell proliferation, no statistical differences on MRI findings
Lumbar	0.06 ml thrombin	DHI maintained, NP signal intensity maintained; significantly low MRI grading
Lumbar	None	PRP moderate effect on MRI, DHI PRP +BMSC: well-preserved ECM, cell density, increased T2 signal intensity, MRI grading, and expression of COL II
Lumbar	100 U thrombin + 10% CaCl ₂	T2 signal intensity: PRP > control or PRP+TGF- β inhibitor; histology: PRP-less degeneration, strong COL II staining, and Smad2/3-pathway activated
Lumbar	Thrombin+CaCl ₂	COL II and PG staining and MRI grade PRP + BMP2 – BMSC > PRP + BMSC > PRP

Abbreviations: ACT: activation; AGN: aggrecan; BMSC: bone marrow-derived mesenchymal stem cell; BMP2: bone morphogenetic protein 2; COL II: type II collagen; ECM: extracellular matrix; GHM: gelatin hydrogel microsphere; IVD: intervertebral disc; MRI: magnetic resonance imaging; PG: proteoglycan; PRP: platelet-rich plasma; DHI: disc height index.

5. In Vivo Study on Animal Models Treated with PRP

To further explore the effect of PRP on IDD, numerous *in vivo* studies have been performed.

In 2009 and 2006, Kazuhide et al. and Nagae et al. [34, 35], respectively, used an IDD rabbit model with partial discectomy and found that PRP may inhibit IDD while PRP combined with gelatin gel microspheres could significantly inhibit IDD. Compared with the IDD control group, magnetic resonance imaging (MRI) showed a significant increase in intervertebral disc height on PRP application. Histological examination detected increased ACAN and COL II expression and decreased apoptosis of NP cells. Additionally, the gelatin gel microspheres served as a carrier for PRP, prolonging its action time and providing mechanical support, whereby PRP could fully exert its therapeutic effect.

In 2009, Chen et al. [20] injected PRP into a porcine disc degeneration model induced by chymopapain. After 2 months, COL II and ACAN mRNA expressions were upregulated, MSC differentiation and fewer apoptotic cells were

detected, and MRI showed recovery of the disc height index (DHI). GB et al. [36] demonstrated that no matter when PRP was injected in the IDD model, there was a protective effect on IDD. However, earlier administration in the IDD process may be more beneficial than PRP treatment of advanced degenerated discs.

Obata et al. [37] in 2012 found that the administration of active autologous PRP releasate could induce a remedial effect on a rabbit needle puncture model. Compared with the PPP and phosphate-buffered saline groups, autologous PRP induced restoration of the DHI, the mean T2 values in MRI were not significantly different, and the number of chondrocyte-like cells was significantly higher. Their results suggested that PRP injection treatment had the potential for clinical application in IDD. Gui et al. [38] conducted a preclinical study of autologous PRP activated by thrombin and found the same result. Two and four weeks after PRP application, they found an increased DHI and signal intensity and elevated proteoglycan and COL II expression compared with the control group, which suggested that PRP intervention may be able to effectively suppress the IDD process.

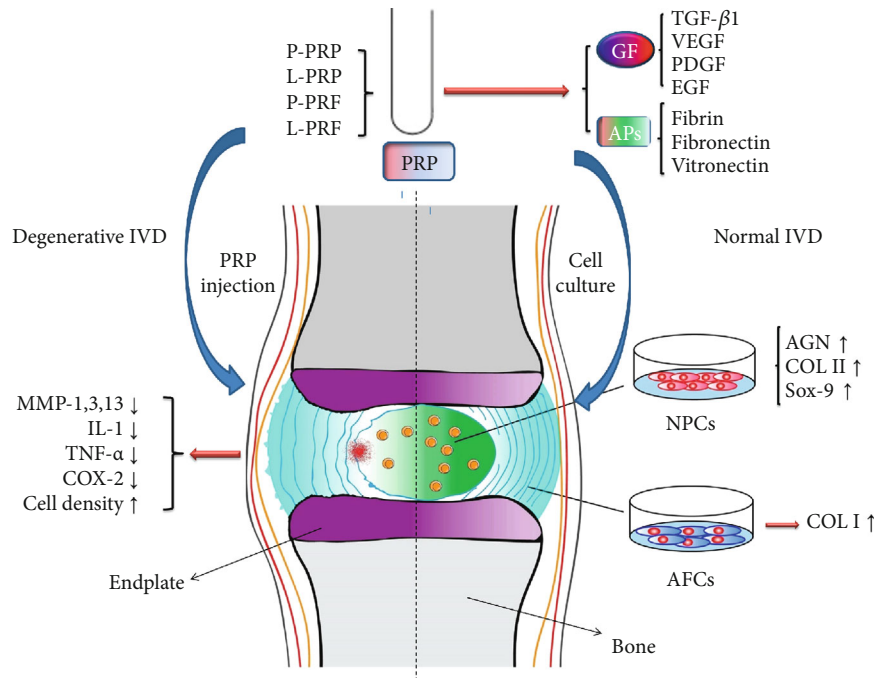


FIGURE 1: Mechanism of PRP on intervertebral disc cells and degenerated intervertebral disc. PRP: platelet-rich plasma; P-PRP: pure PRP; L-PRP: leukocyte platelet-rich PRP; P-PRF: pure platelet-rich fibrin; L-PRF: leukocyte platelet-rich fibrin; IVD: intervertebral disc; GFs: growth factors; APs: adhesive proteins; MMPs: matrix metalloproteinases; IL: interleukin; TNF: tumor necrosis factor; COX: cyclooxygenase; AGN: aggrecan; COL: collagen; Sox-9: SRY-related high-mobility group box-9; NPCs: nucleus pulposus cells; AFCs: annulus fibrosus cells.

Wang et al. [39] injected PRP with bone marrow-derived MSCs (BMSCs) in a rabbit AF puncture model and found that the ECM and cell densities were well preserved and increased T2 signal intensity on MRI grading, while a strong immunopositive staining for COL II showed a poor AF recovery. The MRI scores of the PRP group were similar to those of the PRP+BMSC group at 2 weeks, yet the efficacy of PRP+BMSC was diminished at 8 weeks. They hypothesized that the injected PRP was activated by the surrounding tissues and interacted with BMSCs to cure IDD.

In a rabbit study, Yang et al. [22] reported that MRI revealed a significant recovery of the signal intensity of T2 in the IVD of the PRP injection group compared with the very low signal intensity in the control group. In their histological study, the group of combining PRP and TGF-β1 inhibitor displayed significantly lower expression levels of Smad2/3 and COL II than the PRP group. Additionally, inhibiting the TGF-β1/Smad2/3 pathway could prevent the PRP-induced recovery by inactivating Smad2/3 and down-regulating the ECM. They concluded that the TGF-β1/Smad2/3 pathway might play a critical role in the ability of PRP to cure IDD.

Hou et al. [40] investigated the effects of the combined application of bone morphogenetic protein 2 (BMP2) and PRP to BMSCs. They reported that BMSCs transduced with BMP2 in PRP gel inhibited IDD with a relatively well-preserved NP structure and enhanced ECM accumulation in the NP. At 12 weeks after surgery, BMP2-transduced BMSCs could be detected.

The quantitative analysis by Li et al. [41] of previous studies showed that PRP treatment could restore the intervertebral disc height, reduce the degree of histological variation, and effectively increase the MRI T2 signal without a significant increase in COL II expression.

A consensus shows that the injection of PRP or its releasate is effective in enhancing ECM accumulation, retaining a high DHI, increasing the T2 signal intensity, and slowing the process of and even possibly reversing the effects of IDD. Therefore, the releasate may be a promising therapy for retarding IDD. More studies are currently focusing on combining either the PRP injection with other agents or the PRP activation pathways to determine how PRP is effective and to determine limitations as well as ways to optimize this potential treatment. *In vivo* animal studies alone are not sufficient to prove whether PRP injection can alleviate clinical symptoms (Table 2 and Figure 1).

6. Clinical Trials of PRP

The forms of PRP injections mainly include intradiscal and epidural, while intradiscal injection is considered first depending on the specific injection position. The following section will review recent studies on clinical PRP injection.

In 2011, Koji et al. [42] conducted the first preliminary clinical trial for the safety and efficacy of intradiscal injection therapy using PRP for IDD. They injected PRP activated by autologous serum and CaCl₂ in six patients who had suffered chronic low back pain for more than 3 months. After a 1-month follow-up, the scores of the

TABLE 3: Clinical studies of PRP for IDD.

(a)

Year	Study	Study design	Number of patients	Type of PRP	Activation
2011	Koji et al. [42]	Prospective preliminary trial	6	P-PRP releasate	CaCl ₂ +autoserum
2014	Bodor et al. [44]	Case series	35	P-PRP	None
2016	Navani and Hames [45]	Case series	6	L-PRP	None
2016	Levi et al. [46]	Prospective trial	22	L-PRP	None
2016	Tuakli-wosornu et al. [47]	Double-blind randomized	36 treatments and 22 controls	L-PRP	None
2017	Akeda et al. [43]	Prospective trial	14	P-PRP	CaCl ₂ +autoserum
2018	Lutz [48]	Single case report	1	L-PRP	None

(b)

Volume of whole blood	Volume of PRP injected	Number of injections during the study period	Study period	Pain scores evaluated in the study
200 ml	2 ml	Single	6 m	VAS RDQ
9 ml	2 ml	Single	2-10 m	NRS ODI
60 ml	1.5-3 ml	Single	24 w	VPS
30 or 60 ml	1.5 ml	Single, at one or multiple levels	6 m	VAS ODI
30 ml	1-2 ml	Single, at one or multiple levels	8 w	FRI, NRS, SF-36, and modified NASS
200 ml	2 ml	Single	10 m	VAS RDQ
Not mentioned	1.5 ml	Single	12 m	Improvement T2 nuclear signal intensity↑

Abbreviations: ACT: activation; BDI: Beck Depression Inventory; DPQ: Dallas Pain Questionnaire; FRI: functional rating index; L-PRP: leukocyte- and platelet-rich plasma; m: months; NRS: numerical rating scale; ODI: Oswestry Disability Index; P-PRP: leukocyte-poor PRP; PRP: platelet-rich plasma; RDQ: Roland-Morris Disability Questionnaire; SF: short form; SF-MPQ: short-form McGill Pain Questionnaire; vPS: verbal pain scale; w: weeks; VAS: visual analog scale; NASS: North American Spine Society.

verbal pain scale (VPS) and Roland-Morris Disability Questionnaire were significantly decreased. Additionally, at the 6-month follow-up, MRI did not show any significant change compared with before the injection. No adverse events were reported posttreatment. A few years later, they conducted another preliminary clinical trial including 14 patients with a mean follow-up period of 10 months [43]. In this study, they injected P-PRP isolated by the buffy coat method containing lower concentrations of proinflammatory cytokines (IL-1, TNF- α). The mean pain scores of patients before treatment were reduced by more than 70% at the first month. Except for two subjects with recurring low back pain, there were no adverse events. Akeda et al. showed the safety, feasibility, and efficacy of PRP in treatment of IDD.

Bodor et al. [44] injected PRP excluding leukocytes and erythrocytes into 47 thoracic or lumbar IVDs in 35 patients, and no activators were used for the PRP. The numerical rating scales (NRS) and the Oswestry Disability Index (ODI) scores were improved in 67% of the patients. Five patients were followed up for 10 months; these patients displayed substantial improvement in pain, enabling them to return to the normal physical activity. Despite 2 of 35 patients having vasovagal episodes, there were no complications or side effects related to this treatment.

In a case series study by Navani and Hames [45], six patients were given a single injection of autologous PRP.

During a 6-month follow-up period, 50% of the VPS scores of all the patients decreased by 3 months, and low pain levels were maintained until the 6-month follow-up. The short-form 36 health survey questionnaire was also improved in both the physical and mental scores with no adverse effects reported.

In 2016, Levi et al. [46] reported a prospective clinical trial of 22 patients investigating the effects of intradiscal L-PRP injections on discogenic back pain. After a 6-month follow-up period, 47% had a successful outcome defined as at least a 50% improvement in the VAS and at least a 30% improvement in the ODI. The authors speculated that the possible adverse effects from using the anesthetics and antibiotics before the 1.5 ml L-PRP injection and the PRP preparation method accounted for positive outcome being nonsignificant in this study.

None of the above studies included a randomized controlled trial (RCT). Tuakli et al. [47] conducted a double-blind RCT of intradiscal PRP therapy for discogenic low back pain (LBP). In total, 47 adults were included with chronic LBP (>6 months), and they were randomly assigned to the treatment group or the control group in a ratio of 2:1. The treatment group was given a single injection of L-PRP without an activator. At an 8-week follow-up, they demonstrated that in the treatment group compared with the control group, the NRS for pain, the functional rating index, and patient satisfaction (NASS outcome questionnaire) were significantly

improved. In total, 56% (15/27) of the participants were satisfied (NASS outcome questionnaire) with the treatment compared with only 18% (3/17) of the control participants (3 participants were lost to follow-up). However, the results were not compared after 8 weeks because of the lack of a follow-up of the control group. No complications were reported.

In 2017, Lutz [48] presented a single case report demonstrating the effect of intradiscal PRP injection on improving LBP and function. The patient was diagnosed with IDD and had received an ineffective caudal epidural steroid injection and physical therapy. The patient was given a single PRP injection and displayed considerable improvement in pain and motion after 6 weeks. At a 1-year follow-up, there was a remarkable improvement in the LBP, and the patient could return to athletic activities. Additionally, the patient's NP T2 signal intensity increased.

Comella et al. [49] injected PRP combined with stromal vascular fraction, which was enriched in GFs and stem cells extracted from autologous fat tissues. After 6 months of follow-up, the VAS, ODI, and BDI data displayed a positive trend, and a majority of the patients reported improvements in their Dallas Pain Questionnaire scores. No complications were reported.

In conclusion, the results of clinical application of PRP have been shown in many studies. Large-scale, double-blind randomized studies with well-controlled conditions of preparation and sufficient power, as well as effective analyses of PRP components, are required to establish an evidence-based and standardized treatment of IDD with PRP (Table 3).

7. Conclusion

In this review, we describe the effects of PRP with a focus on *in vitro* and *in vivo* (animal) studies, which revealed that PRP has significant biological effects in stimulating IVD cells to repair tissues and in intradiscal therapy from basic to clinical research for the treatment of discogenic LBP caused by IDD. The results are quite encouraging, and autologous PRP could be rapidly and readily prepared through a complete set of professional equipment.

The aforementioned experiments and clinical studies define PRP as a promising biological material. Furthermore, the three-dimensional network structure of the PRP gel is beneficial in nutrient acquisition of seed cells and metabolite circulation. PRP gel shows promise as a scaffold material for NP tissue engineering. The PRP gel is endowed with remarkable biomechanical properties and a three-dimensional network structure, which could be used alone as a growth factor source or as a tissue engineering scaffold material combined with seed cells for degenerative disc repair and tissue engineering in NP reconstruction. Although the results provided invaluable insights, they still require further research prior to application. (1) While the mechanism of TGF- β 1 is well-characterized, how it interacts with other growth factors remains unclear. (2) The action of multiple intradiscal injections may damage the AF, and repeated intradiscal injections

might cause an increase in the pressure of the IVD, which may accelerate the IDD process. (3) GFs (including VEGF) contained in PRP may further exacerbate the endogenous neurovasculature of IVD. (4) IDD is frequently associated with ossification of the CEPs with an accompanying decrease in oxygen and nutrients. Moreover, the regeneration of IVD cells is accompanied by various synthetic reactions of ACAN and COL II, which may accumulate lactic acid and accelerate the IDD process. (5) The indication for IDD treatment, the optimal PRP concentration and its composition, and how to evaluate the effect of IVD regeneration require investigation. (6) The role of PRP depends on the number of viable cells, but viable cells available in patients with advanced IDD are extremely limited. (7) The ideal amount of PRP injections and when and what timing clinicians should consider for application of PRP treatment remain unknown. (8) The potential adverse effects of PRP treatment are also unknown. Therefore, combining PRP therapy and stem cell implantation may provide new directions for IDD treatment strategy and IVD repair.

Data Availability

No data were used to support this study.

Disclosure

The funders had no role in the study design, data collection or analysis, decision to publish, or preparation of the manuscript.

Conflicts of Interest

The authors declare no conflict of interest.

Authors' Contributions

G.X. and Z.L. were responsible for the conceptualization; Z.L. was responsible for the methodology; Y.C. and Z.L. handled the formal analysis; Y.C., M.Y., Y.Z., and S.K. were responsible for the data curation; Y.C. was responsible for the original draft preparation (writing); G.X. and Z.L. handled the review and editing (writing); Z.L. handled the supervision; and Z.L. was in charge of project administration.

Acknowledgments

We would like to thank all the participants in the studies. We thank Robert Blakytyn, DPhil, from Liwen Bianji, Edanz Editing China (<http://www.liwenbianji.cn/ac>), for editing the English text of a draft of this manuscript. This review was supported by the Liaoning Revitalization Talents Program (XLYC1807131), the Natural Science Foundation of Liaoning Province (2019-BS-079), the Science and Technology Innovation Foundation of Dalian (2020JJ27SN070), and the Teaching Reform Research Project of Dalian Medical University (DYLX19010).




References

- [1] S. Gianola, G. Castellini, A. Andreano et al., “Effectiveness of treatments for acute and sub-acute mechanical non-specific low back pain: protocol for a systematic review and network meta-analysis,” *Systematic Reviews*, vol. 8, no. 1, 2019.
- [2] F. Lai, N. Kakudo, N. Morimoto et al., “Platelet-rich plasma enhances the proliferation of human adipose stem cells through multiple signaling pathways,” *Stem Cell Research & Therapy*, vol. 9, no. 1, 2018.
- [3] X. Xu, J. Hu, and H. Lu, “Histological observation of a gelatin sponge transplant loaded with bone marrow-derived mesenchymal stem cells combined with platelet-rich plasma in repairing an annulus defect,” *PLOS ONE*, vol. 12, no. 2, article e0171500, 2017.
- [4] S. Mohammed and J. Yu, “Platelet-rich plasma injections: an emerging therapy for chronic discogenic low back pain,” *Journal of Spine Surgery*, vol. 4, no. 1, pp. 115–122, 2018.
- [5] A. S. Ammar, Y. Osman, A. T. Hendam et al., “A method for reconstruction of severely damaged spinal cord using autologous hematopoietic stem cells and platelet-rich protein as a biological scaffold,” *Asian Journal of Neurosurgery*, vol. 12, no. 4, pp. 681–690, 2017.
- [6] S. Ohtori, G. Inoue, M. Miyagi, and K. Takahashi, “Pathomechanisms of discogenic low back pain in humans and animal models,” *The Spine Journal*, vol. 15, no. 6, pp. 1347–1355, 2015.
- [7] S. Yang, F. Zhang, J. Ma, and W. Ding, “Intervertebral disc ageing and degeneration: the antiapoptotic effect of oestrogen,” *Ageing Research Reviews*, vol. 57, article 100978, 2020.
- [8] X. Wu, Z. Liao, K. Wang et al., “Targeting the IL-1 β /IL-1Ra pathways for the aggregation of human islet amyloid polypeptide in an ex vivo organ culture system of the intervertebral disc,” *Experimental & Molecular Medicine*, vol. 51, no. 9, pp. 1–16, 2019.
- [9] Z. Zhou, Y. Wang, H. Liu et al., “PBN protects NP cells from AAPH-induced degenerative changes by inhibiting the ERK1/2 pathway,” *Connective Tissue Research*, pp. 1–10, 2020.
- [10] Z. Bai, W. Liu, D. He et al., “Protective effects of autophagy and NFE2L2 on reactive oxygen species-induced pyroptosis of human nucleus pulposus cells,” *Ageing*, vol. 12, no. 8, pp. 7534–7548, 2020.
- [11] K. Akeda, J. Yamada, E. T. Linn, A. Sudo, and K. Masuda, “Platelet-rich plasma in the management of chronic low back pain: a critical review,” *Journal of Pain Research*, vol. 12, pp. 753–767, 2019.
- [12] D. M. Dohan Ehrenfest, T. Bielecki, A. Mishra et al., “In search of a consensus terminology in the field of platelet concentrates for surgical use: platelet-rich plasma (PRP), platelet-rich fibrin (PRF), fibrin gel polymerization and leukocytes,” *Current Pharmaceutical Biotechnology*, vol. 13, no. 7, pp. 1131–1137, 2012.
- [13] R. Bhatia and G. Chopra, “Efficacy of platelet rich plasma via lumbar epidural route in chronic prolapsed intervertebral disc patients—a pilot study,” *Journal of Clinical and Diagnostic Research*, vol. 10, no. 9, pp. UC05–UC07, 2016.
- [14] M. Hussein and T. Hussein, “Effect of autologous platelet leukocyte rich plasma injections on atrophied lumbar multifidus muscle in low back pain patients with monosegmental degenerative disc disease,” *SICOT-J*, vol. 2, 2016.
- [15] A. Cieslik-Bielecka, P. Reichert, R. Skowronski, A. Krolkowska, and T. Bielecki, “A new aspect of in vitro anti-microbial leukocyte- and platelet-rich plasma activity based on flow cytometry assessment,” *Platelets*, vol. 30, no. 6, pp. 728–736, 2019.
- [16] Y. H. Wen, W. Y. Lin, C. J. Lin et al., “Sustained or higher levels of growth factors in platelet-rich plasma during 7-day storage,” *Clinica Chimica Acta*, vol. 483, pp. 89–93, 2018.
- [17] J. E. Fernández-Barbero, P. Galindo-Moreno, G. Ávila-Ortiz, O. Caba, E. Sánchez-Fernández, and H.-L. Wang, “Flow cytometric and morphological characterization of platelet-rich plasma gel,” *Clinical Oral Implants Research*, vol. 17, no. 6, pp. 687–693, 2006.
- [18] K. Akeda, H. S. An, M. Okuma et al., “Platelet-rich plasma stimulates porcine articular chondrocyte proliferation and matrix biosynthesis,” *Osteoarthritis and Cartilage*, vol. 14, no. 12, pp. 1272–1280, 2006.
- [19] W. H. Chen, W. C. Lo, J. J. Lee et al., “Tissue-engineered intervertebral disc and chondrogenesis using human nucleus pulposus regulated through TGF- β 1 in platelet-rich plasma,” *Journal of Cellular Physiology*, vol. 209, no. 3, pp. 744–754, 2006.
- [20] W.-H. Chen, H.-Y. Liu, W.-C. Lo et al., “Intervertebral disc regeneration in an ex vivo culture system using mesenchymal stem cells and platelet-rich plasma,” *Biomaterials*, vol. 30, no. 29, pp. 5523–5533, 2009.
- [21] T. N. Pirvu, J. E. Schroeder, M. Peroglio et al., “Platelet-rich plasma induces annulus fibrosus cell proliferation and matrix production,” *European Spine Journal*, vol. 23, no. 4, pp. 745–753, 2014.
- [22] H. Yang, C. Yuan, C. Wu et al., “The role of TGF- β 1/Smad2/3 pathway in platelet-rich plasma in retarding intervertebral disc degeneration,” *Journal of Cellular and Molecular Medicine*, vol. 20, no. 8, pp. 1542–1549, 2016.
- [23] M. Nikkhoo, J. L. Wang, M. Abdollahi, Y. C. Hsu, M. Parnianpour, and K. Khalaf, “A regenerative approach towards recovering the mechanical properties of degenerated intervertebral discs: Genipin and platelet-rich plasma therapies,” *Proceedings of the Institution of Mechanical Engineers, Part H: Journal of Engineering in Medicine*, vol. 231, no. 2, pp. 127–137, 2016.
- [24] S. Z. Wang, W. M. Fan, J. Jia, L. Y. Ma, J. B. Yu, and C. Wang, “Is exclusion of leukocytes from platelet-rich plasma (PRP) a better choice for early intervertebral disc regeneration?,” *Stem Cell Research & Therapy*, vol. 9, no. 1, 2018.
- [25] J. Jia, S. Z. Wang, L. Y. Ma, J. B. Yu, Y. D. Guo, and C. Wang, “The differential effects of leukocyte-containing and pure platelet-rich plasma on nucleus pulposus-derived mesenchymal stem cells: implications for the clinical treatment of intervertebral disc degeneration,” *Stem Cells International*, vol. 2018, Article ID 7162084, 12 pages, 2018.
- [26] E. Masoudi, J. Ribas, G. Kaushik, J. Leijten, and A. Khademhosseini, “Platelet-rich blood derivatives for stem cell-based tissue engineering and regeneration,” *Current Stem Cell Reports*, vol. 2, no. 1, pp. 33–42, 2016.
- [27] M. Angelone, V. Conti, C. Biacca et al., “The contribution of adipose tissue-derived mesenchymal stem cells and platelet-rich plasma to the treatment of chronic equine laminitis: a proof of concept,” *International Journal of Molecular Sciences*, vol. 18, no. 10, 2017.
- [28] H. J. Kim, J. S. Yeom, Y. G. Koh et al., “Anti-inflammatory effect of platelet-rich plasma on nucleus pulposus cells with response of TNF- α and IL-1,” *Journal of Orthopaedic Research*

- : *Official Publication of the Orthopaedic Research Society*, vol. 32, no. 4, pp. 551–556, 2014.
- [29] M. C. Liu, W. H. Chen, L. C. Wu et al., “Establishment of a promising human nucleus pulposus cell line for intervertebral disc tissue engineering,” *Tissue engineering. Part C: Methods*, vol. 20, no. 1, pp. 1–10, 2014.
- [30] H. Cho, D. C. Holt, R. Smith, S. J. Kim, R. J. Gardocki, and K. A. Hasty, “The effects of platelet-rich plasma on halting the progression in porcine intervertebral disc degeneration,” *Artificial Organs*, vol. 40, no. 2, pp. 190–195, 2016.
- [31] W. Yin, X. Qi, Y. Zhang et al., “Advantages of pure platelet-rich plasma compared with leukocyte- and platelet-rich plasma in promoting repair of bone defects,” *Journal of Translational Medicine*, vol. 14, no. 1, 2016.
- [32] A. Mietsch, C. Neidlinger-Wilke, H. Schrezenmeier et al., “Evaluation of platelet-rich plasma and hydrostatic pressure regarding cell differentiation in nucleus pulposus tissue engineering,” *Journal of Tissue Engineering and Regenerative Medicine*, vol. 7, no. 3, pp. 244–252, 2013.
- [33] S. Hondke, M. Cabraja, J. P. Krüger et al., “Proliferation, migration, and ECM formation potential of human annulus fibrosus cells is independent of degeneration status,” *Cartilage*, vol. 11, no. 2, pp. 192–202, 2018.
- [34] K. Sawamura, T. Ikeda, M. Nagae et al., “Characterization of in vivo effects of platelet-rich plasma and biodegradable gelatin hydrogel microspheres on degenerated intervertebral discs,” *Tissue Engineering Part A*, vol. 15, no. 12, pp. 3719–3727, 2009.
- [35] M. Nagae, T. Ikeda, Y. Mikami et al., “Intervertebral disc regeneration using platelet-rich plasma and biodegradable gelatin hydrogel microspheres,” *Tissue Engineering Part*, vol. 13, no. 1, pp. 147–158, 2007.
- [36] G. Gullung, W. Woodall, M. Tucci, J. James, D. Black, and R. McGuire, “Platelet-rich plasma effects on degenerative disc disease: analysis of histology and imaging in an animal model,” *Evidence-Based Spine-Care Journal*, vol. 2, no. 4, pp. 13–18, 2011.
- [37] S. Obata, K. Akeda, T. Imanishi et al., “Effect of autologous platelet-rich plasma-releasate on intervertebral disc degeneration in the rabbit anular puncture model: a preclinical study,” *Arthritis Research & Therapy*, vol. 14, no. 6, 2012.
- [38] K. Gui, W. Ren, Y. Yu, X. Li, J. Dong, and W. Yin, “Inhibitory effects of platelet-rich plasma on intervertebral disc degeneration: a preclinical study in a rabbit model,” *Medical Science Monitor*, vol. 21, pp. 1368–1375, 2015.
- [39] S. Z. Wang, J. Y. Jin, Y. D. Guo et al., “Intervertebral disc regeneration using platelet-rich plasma-containing bone marrow-derived mesenchymal stem cells: a preliminary investigation,” *Molecular Medicine Reports*, vol. 13, no. 4, pp. 3475–3481, 2016.
- [40] Y. Hou, G. Shi, J. Shi, G. Xu, Y. Guo, and P. Xu, “Study design: in vitro and in vivo assessment of bone morphogenic protein 2 combined with platelet-rich plasma on treatment of disc degeneration,” *International Orthopaedics*, vol. 40, no. 6, pp. 1143–1155, 2016.
- [41] P. Li, R. Zhang, and Q. Zhou, “Efficacy of platelet-rich plasma in retarding intervertebral disc degeneration: a meta-analysis of animal studies,” *BioMed Research International*, vol. 2017, Article ID 7919201, 10 pages, 2017.
- [42] K. Akeda, T. Imanishi, K. Ohishi et al., “Intradiscal injection of autologous serum isolated from platelet-rich-plasma for the treatment of discogenic low back pain: preliminary prospective clinical trial: GP141,” *Asian Spine Journal*, vol. 11, no. 3, pp. 380–389, 2017.
- [43] K. Akeda, K. Ohishi, K. Masuda et al., “Intradiscal injection of autologous platelet-rich plasma releasate to treat discogenic low back pain: a preliminary clinical trial,” *Asian Spine Journal*, vol. 11, no. 3, pp. 380–389, 2017.
- [44] M. Bodor, A. Toy, and D. Aufiero, “Disc Regeneration with Platelets and Growth Factors,” in *Platelet-Rich Plasma*, pp. 265–279, Springer, 2014.
- [45] A. Navani and A. Hames, “Platelet-rich plasma injections for lumbar discogenic pain: a preliminary assessment of structural and functional changes,” *Techniques in Regional Anesthesia and Pain Management*, vol. 19, no. 1-2, pp. 38–44, 2015.
- [46] D. Levi, S. Horn, S. Tyszko, J. Levin, C. Hecht-Leavitt, and E. Walko, “Intradiscal platelet-rich plasma injection for chronic discogenic low back pain: preliminary results from a prospective trial,” *Pain Medicine*, vol. 17, no. 6, pp. 1010–1022, 2015.
- [47] Y. A. Tuakli-Wosornu, A. Terry, K. Boachie-Adjei et al., “Lumbar Intradiscal Platelet-Rich Plasma (PRP) Injections: A Prospective, Double-Blind, Randomized Controlled Study,” *PM&R*, vol. 8, no. 1, pp. 1–10, 2016.
- [48] G. E. Lutz, “Increased nuclear T2 signal intensity and improved function and pain in a patient one year after an intradiscal platelet-rich plasma injection,” *Pain Medicine*, vol. 18, no. 6, pp. 1197–1199, 2017.
- [49] K. Comella, R. Silbert, and M. Parlo, “Effects of the intradiscal implantation of stromal vascular fraction plus platelet rich plasma in patients with degenerative disc disease,” *Journal of Translational Medicine*, vol. 15, no. 1, 2017.

Review Article

Cell Senescence: A Nonnegligible Cell State under Survival Stress in Pathology of Intervertebral Disc Degeneration

Yuang Zhang,^{1,2} Biao Yang,^{1,2} Jingkai Wang,^{1,2} Feng Cheng,^{1,2} Kesi Shi,^{1,2} Liwei Ying,^{1,2} Chenggui Wang,^{1,2} Kaishun Xia,^{1,2} Xianpeng Huang,^{1,2} Zhe Gong,^{1,2} Chao Yu,^{1,2} Fangcai Li ^{1,2}, Chengzhen Liang ^{1,2}, and Qixin Chen ^{1,2}

¹Department of Orthopedics Surgery, The Second Affiliated Hospital, Zhejiang University School of Medicine, 310009 Hangzhou, Zhejiang, China

²Zhejiang Key Laboratory of Bone and Joint Precision and Department of Orthopedics Research Institute of Zhejiang University, Hangzhou, Zhejiang 310009, China

Correspondence should be addressed to Fangcai Li; lifangcai@zju.edu.cn, Chengzhen Liang; liangchengzhen@zju.edu.cn, and Qixin Chen; zrcqx@zju.edu.cn

Received 3 July 2020; Revised 1 August 2020; Accepted 10 August 2020; Published 31 August 2020

Academic Editor: Wenyan Ding

Copyright © 2020 Yuang Zhang et al. This is an open access article distributed under the Creative Commons Attribution License, which permits unrestricted use, distribution, and reproduction in any medium, provided the original work is properly cited.

The intervertebral disc degeneration (IDD) with increasing aging mainly manifests as low back pain (LBP) accompanied with a loss of physical ability. These pathological processes can be preliminarily interpreted as a series of changes at cellular level. In addition to cell death, disc cells enter into the stagnation with dysfunction and deteriorate tissue microenvironment in degenerative discs, which is recognized as cell senescence. During aging, many intrinsic and extrinsic factors have been proved to have strong connections with these cellular senescence phenomena. Growing evidences of these connections require us to gather up critical cues from potential risk factors to pathogenesis and relative interventions for retarding cell senescence and attenuating degenerative changes. In this paper, we try to clarify another important cell state apart from cell death in IDD and discuss senescence-associated changes in cells and extracellular microenvironment. Then, we emphasize the role of oxidative stress and epigenomic perturbations in linking risk factors to cell senescence in the onset of IDD. Further, we summarize the current interventions targeting senescent cells that may exert the benefits of antidegeneration in IDD.

1. Introduction

A systematic analysis for the Global Burden of Disease Study 2017 showed that low back pain was the top cause of years lived with disability (YLD) counts from 1990 to 2017 [1]. Concerning the relation with potential loss of functional status in the work force, disc degenerative diseases, as the major cause of low back pain, have posed huge burden on the global health care systems and economies [2, 3]. Ascribed to the life-span extension and the growth of aging population worldwide, the incidence of IDD will progressively and steadily increase and exacerbate the problem above. Multiple studies support the notion that degenerative discs always accelerate cellular senescence which may precipitate the pathology of IDD [4]. Disc cells undergo not only apoptosis but also dys-

function in IDD in an age-related manner. The latter, an abnormal cell state, plays a crucial role in matrix homeostasis imbalance. New pharmacological strategies focus on the elimination or reverse of senescent cells in degenerative discs for the prevention and treatment of IDD [5, 6].

As a fundamental cause of aging, cell senescence has been proved in all major chronic diseases in the cardiovascular system, nervous system, and especially musculoskeletal system and in chronic tumor [7–10]. However, the initial factors triggering disc cell senescence are exceptionally complex. Among the perspectives proposed in recent years to explain the emerging senescent cells in degenerative discs, one states that inner age-related stress and external microenvironment-derived stimuli both act as a promoter of cellular senescence to accelerate IDD [11]. Since the IDD is involved in multiple

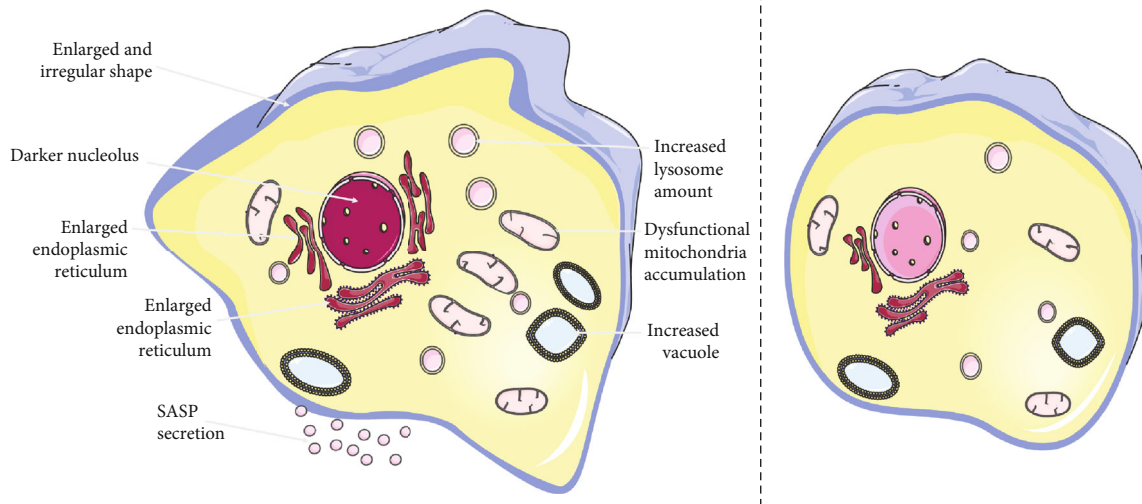


FIGURE 1: Morphological differences between senescent cells and normal cells. There are characteristic morphological alterations emerging in senescent cells compared with normal cells, such as increased but irregular cell size, darker nuclear chromatin, increased lysosome amount, dysfunctional mitochondrial accumulation, enlarged endoplasmic reticulum, increased vacuole, and secreting SASP. These features can be meaningful tools for identifying senescent cells and determining the senescent process.

risk factors, mechanisms underlying these stressors that induce adaptive cell state changes have not been fully clarified. Finding critical intermediators from intricate cues seems to be conducive to inhibit cell senescence at the beginning of IDD.

In this review, we introduce the features of cell senescence and emphasize that it occurs as a general stress response. And we illustrate the impact of senescence on IDD. The role of oxidative stress and epigenetics linking multiple risk factors to cell senescence is summarized. Finally, we discuss relative therapeutic strategies in IDD. Hopefully, the brief introduction could primarily establish a link between cellular survival stress and IDD from a perspective of cell senescence.

2. Cell Senescence

2.1. The Features of Cell Senescence. Cell senescence is characterized by a cell state of proliferating arrest and secreting senescence-associated secretory phenotype (SASP) [12]. Cell cycle arrest plays a bilateral role in pathophysiological processes. On the one hand, it inhibits cell division and blocks the tissue renewal. On the other hand, it also prevents a further proliferation of harmful cells undergoing senescence [13]. Underlying cell cycle arrest, various molecular signals and pathways organize a complex network to exert effects [14]. All of them eventually converge on the p53/p21/retinoblastoma (RB) and p16/RB pathways to prevent senescent cell proliferation [14, 15]. Telomere shortening and stressor induction lead to replicative-related senescence (RS) and stress-induced premature senescence (SIPS) with respective mechanisms [16]. Previous investigations proved that these two major senescence phenotypes were involved in most chronic diseases.

As another major characteristic of senescent cells, SASP contains secretions of proinflammatory factors, chemokines,

cytokines, protein enzymes, and other bioactive factors [17]. In mechanism, some certain pathways including nuclear factor kappa-B (NF- κ B), cyclic GMP-AMP synthase/stimulator of interferon genes (cGAS/STING), and mammalian target of rapamycin (mTOR) have been proved to control SASP [18, 19]. Meanwhile, epigenetic perturbations may regulate SASP at the transcriptional level [18]. This specific phenotype mediates cell-to-cell and cell-to-matrix signals to trigger immune-related clearance, inflammation formation, cell reprogramming, and microenvironment remodelling, which are involved in a series of diseases [17, 20–22]. Similar to senescence-associated markers like senescence-associated β -galactosidase (SA- β -gal), several major SASP components are used to indicate cell senescence [18, 23, 24]. However, the secretory factors are always variable due to their heterogeneity and nonspecificity. Therefore, increasing studies based on the diversity of SASP are carried out in recent years.

In addition to cell cycle arrest and SASP, there are multiple changes of cellular components and morphology emerging in senescent cells [18] (Figure 1). These traits can be meaningful tools for distinguishing senescent cells and determining senescence process [4, 25–27]. However, cellular senescence is actually weakly defined due to the diversity of senescent biomarker expression in various subtypes. Recently, Ogrodnik et al. proposed a new model coordinating cell expansion and cell cycle arrest to screen senescent cells, which provided us a novel idea [28]. Meanwhile, increasing senescence subtypes and hallmarks are found in different cell types [18]. Exploring novel biomarkers with specifically differential expression in various senescence types is of great significance, which has become the focus of current researches [29, 30]. Although the standard of identification is not fully unified, antagonizing the progression of cell senescence has been a potential strategy in approaches to blunt chronic diseases.

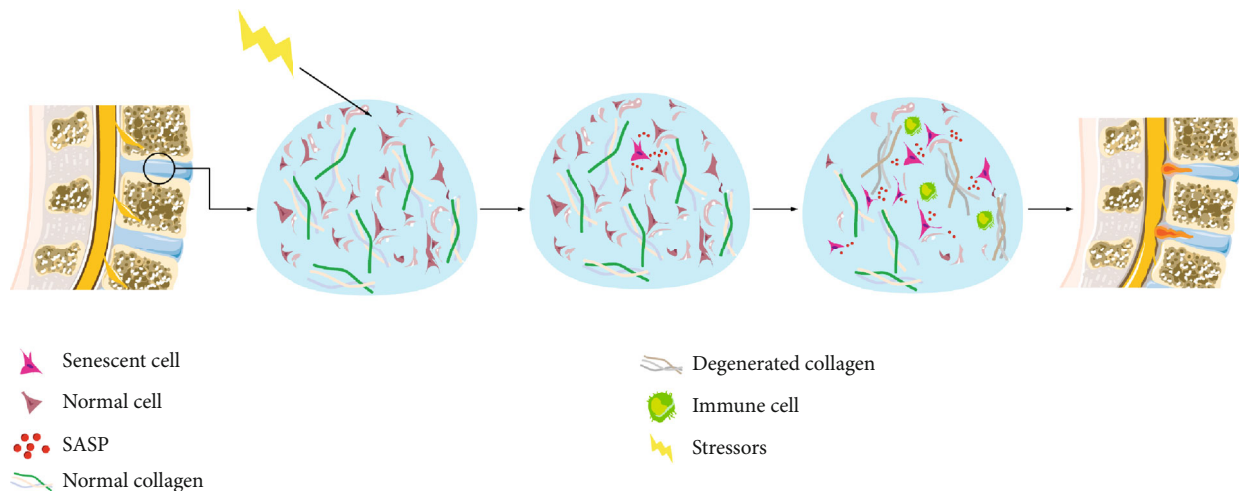


FIGURE 2: The role of cell senescence in the pathogenesis of IDD. Cell senescence occurs in response to intrinsic and extrinsic stressors in intervertebral discs. The primary senescent disc cells cause chronic inflammations, immune cell recruitment, and ECM degeneration through SASP. The deterioration of tissue microenvironment and persistent stress cause the accumulation of senescent cells which further accelerates tissue remodeling and eventually leads to IDD.

2.2. Cell Senescence Occurs under Various Stressors. Cell senescence has been proved in majority of cell types as a response to various stressors [31]. The telomere exhaustion was firstly proved to cause cell senescence during cell division [32]. In addition to deoxyribonucleic acid (DNA) replication-associated stress, cells also face many other stressors from the inner nucleus such as oncogene activation [33]. For instance, the expression of oncogenic *ras* transforms rodent cells to a permanent G1 arrest by upregulating p53 and p16 [33]. The cell cycle arrest prevents the original tumorigenesis. Moreover, under the stress of radiotherapy [34] or chemotherapy [35] without a fatal dose, cells suffer DNA damage and are driven into the premature senescence instead of apoptosis to seek survival. Moreover, under stressful microenvironment, epigenomic perturbations also regulate senescence process. The modification of global or local chromatin alters specific gene expression to trigger cellular senescence independent of the DNA damage response (DDR) [36].

Meanwhile, cells need to withstand stress from the extra nucleus. As a cellular response to tissue damage, cells at the damage site undergo transient senescence. Senescent fibroblasts and endothelial cells secrete platelet-derived growth factor AA (PDGF-AA) to induce myfibroblast differentiation at the site of injury, ensuring wound closure [37]. Interestingly, senescent cells provoke plasticity of neighboring cells to enter transient reprogramming, which enhances differential potential and is conducive to tissue repair [38, 39]. The different role of senescent cells exists under embryonic development pressure. A p21-mediated senescence is found in the apical ectodermal ridge (AER). Growth factors like fibroblast growth factors (FGFs) are secreted to drive limb patterning and optimize tissue remodeling, which is recognized as a programmed senescence [40, 41]. Cells also encounter the stress from intracellular bioenergetic metabolism due to increasing dysfunctional mitochondria during aging [42]. As a metabolically active cell state, mitochondrial

dysfunction-associated senescence (MiDAS) was proved to be implicated in this cell state transformation via adenosine 5'-monophosphate-activated protein kinase- (AMPK-) mediated p53 activation [42]. Despite the different stressors and complex signal pathways, the passive cell fate eventually arrives at the senescence outcome.

3. Cell Senescence Influences IDD

The intervertebral disc is composed of an inner highly hydrated colloid named the nucleus pulposus (NP) encircled by a dense fibrous ring, the annulus fibrosus (AF). The above parts are interfaced with the adjacent vertebrae through the vertebral endplates (EPs) [43]. There are specific features of oligocells and abundant matrix in intervertebral discs compared with other tissues like nervous or myocardial tissues [44]. Resident cells ensure long-term matrix renewal to maintain the balance of extracellular matrix (ECM) anabolism and catabolism with the huge survival burden during aging. Disc cells with slow turnover are suggested to be chronic senescence prone before apoptosis under cell replication and other stressors (Figure 2). A detrimental role of persistent senescent cells is predominant in chronic senescence processes like IDD [16, 33, 38]. Contrary to effective self-clearance of senescent cells in other tissues, the avascular nature of discs partly limits the immune-mediated clearance to cause the abnormal accumulation [11, 45]. Therefore, cell senescence in IDD results from not only the general aging process but also the structure and tissue specificity of discs.

3.1. Senescence Influences Functional Cells in IDD. As the functional cells in discs during intervertebral disc growth, NP, AF, and EP cells are in charge of ECM anabolic balance in separate regions, which play a key role in maintaining normal extracellular microenvironment [43]. These functional cells derived from degenerative discs all undergo the decline of proliferating potential, with high expressions of SA- β -gal

and p16 (Ink4a) as well as decreased telomere length [4, 46, 47]. Interestingly, these senescence-associated changes in EPs seem to appear later than in AF and NP [46]. Relatively rich nutrition as well as milder local mechanical stress may explain this temporal sequence [48]. Although the cellular turnover in discs is slow, cell division during an expected lifespan of several decades is sufficient for inducing telomere length erosion and DNA damage to cause replicative stress. Subsequent activation of the p53/p21/RB pathway drives functional cells into the senescent cell state of cell cycle arrest [49]. The increasing stagnation during aging depletes the reservoir of cell renewal to further decrease remaining functional cells in IDD. Recent study found that deleting cell cycle inhibition gene p16 of NP cells could significantly decrease the proportions of senescent cells and SASP in degenerative discs [50]. Interestingly, Novais et al. observed the opposite result. They found that deficiency of p16 (Ink4a) did not alter the disc cell viability and the percentage of senescent cells [51]. Probably because p16 (Ink4a) acted as a main trigger for SIPS, knocking out this gene failed to avoid the replicative stress during degeneration [52, 53]. Despite the impotent inhibition of age-dependent degeneration, significant changes in the content and constituent of ECM occurred indeed. Changing senescent cells via targeting cell cycle relative genes or molecules has been focused on increasingly for ameliorating IDD.

In addition to replicative stress, as shock absorbers, the NP always suffers more mechanical stress than other tissues [54]. The accumulation of senescent NP cells was observed in scaffold and organ cultures under high-magnitude compression, confirming that mechanical-related SIPS existed in IDD [55]. Selective elimination of senescent NP cells protects tail suspension- (TS-) induced IDD mice from disc degeneration. Similar relationship between mechanical stress and cell senescence is proved in AF and EP cells [46, 47]. Further investigation indicated that the increased oxidative stress acted as a causative intermedior during mechanical factor-associated SIPS in degenerated discs [50]. In fact, intervertebral discs also have to face systemic stress derived from other diseases or risk factors. A critical review analysis indicated that vertebral EP capillaries got significantly narrower to block the nutrition supplement in diabetic animals, which might partly accelerate the diabetic-related IDD [56]. In diabetic patients, dysfunctional endothelial cells could exhibit senescence-like cell state via thrombospondin 1-cluster of differentiation 47- (TSP1-CD47-) dependent signaling to impair microvessels [57]. Although similar research in IDD is not reported, an endothelial senescence-related microcirculatory disturbance may partly promote the degeneration of EPs or even the whole discs under systemic risk factors like diabetes and hyperlipidemia. Therefore, cellular senescence in degenerative discs cannot always be ascribed to DNA replication and cell division as many cases of IDD occur in the stressful environment. In fact, RS and SIPS jointly accelerate the emergence of senescent cells in IDD compared with age-matched normal discs [4, 58].

3.2. Senescence Influences Extracellular Microenvironment in IDD. In addition to the stagnation of cell proliferation, the

senescent disc cells also overexpress a range of bioactive components as fundamental features of SASP [12, 59–62]. SASP during IDD plays a crucial role in altering tissue microenvironment [12, 63]. Among them, proinflammatory factors such as interleukin-1 β (IL-1 β), interleukin-6 (IL-6), interleukin-8 (IL-8), and tumor necrosis factor- α (TNF- α) have been proved to be generally upregulated by senescent cells to trigger inflammatory cascades, which cause the chronic inflammation and accelerate IDD [51, 64]. Despite the low specificity, growing studies recognize them as indexes to cell senescence [18, 23, 24]. Apart from the inflammatory effect, some specific cytokines like IL-6 and IL-8 also provide intercellular dialogue to induce adjacent cells to be senescence or reprogramming prone [12, 21, 24, 39]. The persistent dedifferentiation of neighboring cells may inhibit the supplement for lost or damaged cells and disturb tissue rejuvenation [65]. Meanwhile, specific SASP like (C–C motif) ligand 2 (CCL-2), vascular endothelial growth factor (VEGF), transforming growth factor β (TGF- β), and chemokine (C–C motif) ligand 20 (CCL-20) are proved to induce adjacent normal cells to be “paracrine senescence” [63]. Although it has not been fully clarified in IDD, these cell-to-cell signals may partly promote the accumulation of dysfunctional disc cells.

As the fertile soil for NP cells, collagen matrix consisted of generous type II collagen and aggrecan provides nutrients for cell metabolism and maintains disc tensile stiffness [43]. Collagen falls into the stagnation period of renewal during the development of IDD. Che et al. observed that many matrix remodelling enzymes in SASP like matrix metalloproteinases (MMPs) family (MMP3, MMP9, MMP10, and MMP13) were secreted increasingly in senescent disc cells of TS mice [66]. MMPs degraded collagen II as well as ECM proteins like proteoglycan and aggrecan, decreasing hydration of NPs in IDD. In addition to MMPs, senescent disc cells also raise the level of a disintegrin and metalloproteinase with thrombospondin motifs (ADAMTS) family (ADAMTS-4, ADAMTS-5). The increased proteolytic enzymes cleave the aggrecan interglobular domain and drive the matrix PG loss in vitro compared to nonsenescent disc cells, where certain pathways like β -catenin may play a key role [62, 67, 68]. As a crucial regulator in joint development, β -catenin is proved to mediate cell senescence in cartilages and discs, indicating that analogical cartilaginous tissue may be comparable in senescence mechanism [68, 69]. The continuous secretion of catabolic enzymes produced by senescent cells severely perturbs the ECM homeostasis since disc cells are unable to act as the major producer of ECM. Notably, SASP in senescent disc cells may be a unique response of tissue to different stress like physical activities, and the specific disc structure for low pH, low oxygen tension, and cellular environment may further amplify this effect of SASP on ECM [12, 70].

4. The Underlying Pathogenesis of Cell Senescence in IDD

As a multifactor-induced degenerative disease, IDD is associated with many potential risk factors such as abnormal

mechanical loading, inappropriate exercise, obesity, and even specific diet style [55, 71, 72]. Growing studies indicate that oxidative stress (OS) and epigenomic perturbations may act as major mediators between these risk factors and cell senescence in IDD [73].

4.1. Oxidative Stress. Reactive oxygen species (ROS) production is inevitable due to the oxygen-utilizing metabolism of disc cells despite the hypoxic microenvironment in IDD [74]. Subsequent OS increases cellular survival stress which activates the DDR to trigger cell senescence and force the dysfunction of resident cells [45, 75]. Apart from the harsher microenvironment like insufficient nutrient supply and metabolite clearance during aging, exogenous stimuli exacerbate excessive ROS generation in disc cells [76]. These excessive oxidizing products drive disc cells into the state of SIPS in IDD [14]. Underlying the cellular transformation, diverse signaling pathways have been proved to participate in the senescence process (Figure 3). Considering the nonmitochondrial-dependent ROS productions like nicotinamide adenine dinucleotide phosphate (NADPH) oxidase and xanthine oxidase are scarcely reported in the discs, we focus on the role of mitochondrial-derived ROS in cell senescence during IDD [76, 77].

NP cells exhibit the stagnant state with senescence markers like high SA- β -gal activity by the accumulation of ROS in NP cells under various stimuli such as high-magnitude compression [4] and high glucose [58]. Indeed, the OS appears due to the imbalance between excessive ROS generation and impaired antioxidative molecules or enzymes disturbed by these stressors [78]. Recent studies significantly inhibited cell senescence through reversing this imbalance, emphasizing the role of OS in degenerative discs. The hydrogen peroxide (H_2O_2) was used to aggravate intracellular oxidative stress to provoke DNA damage and successfully induced cell cycle arrest as well as SASP of NP cells via the ataxia telangiectasia-mutated checkpoint kinase 2-p53-p21 (ATM-Chk2-p53-p21) pathway [58, 79]. This H_2O_2 -induced premature senescence could be partly reversed by the antioxidants like N-acetyl-L-cysteine [58]. Targeting the elimination of ROS components like H_2O_2 , hydroxyl ($\cdot OH$), and superoxide anion ($\cdot O_2^-$) becomes a potential therapeutic strategy. Recently, Larrañaga et al. constructed antioxidant polymer capsules, which can be engulfed by NP cells to scavenge intracellular ROS like H_2O_2 and $\cdot OH$. The decline of ROS level significantly attenuated the catabolic and proinflammatory cell phenotype [80]. In addition, the ROS-induced autophagy inhibition is also proved to cause oxidative stress in many cell types [81–83]. And by enhancing and restoring impaired autophagy during IDD, Kang et al. affirmed that excessive ROS production could be suppressed to protect the mitochondrial hemostasis and ameliorate NP cell senescence [84].

Mitochondria are not only the main source of excessive ROS production but also the major attacking target of ROS [37, 76, 85, 86]. Literature demonstrated that OS could be increased due to proinflammatory factors like TNF- α to induce mitochondrial dysfunction to aggravate the senescence in NP cells [87, 88]. Moreover, TNF- α -induced abnor-

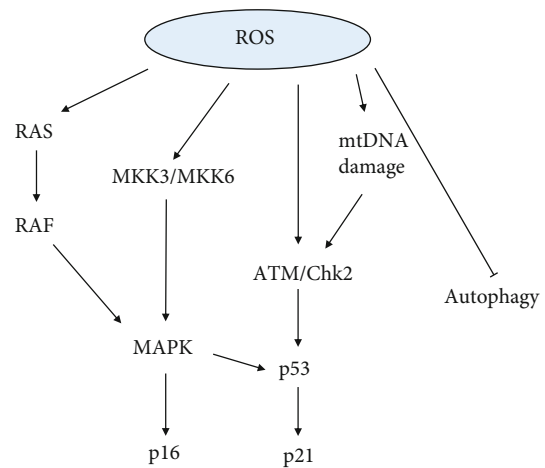


FIGURE 3: The signaling pathways between ROS and cell senescence.

mal OS can also disturb hypoxic conditions in senescent EPs, which transfer the cartilage endplate stem cell (CESC) differentiation from chondrogenesis to osteogenesis [89]. The ROS dysregulate respiratory enzyme activity and cause the respiratory chain defect in dysfunctional mitochondria, leaking extensive electrons to produce more ROS [76]. Lack of effective antioxidant mechanisms during senescence, a ROS-mediated positive feedback loop may act as a critical murderer to accelerate senescence. In turn, interventions targeting cellular senescence may attenuate the oxidative stress. For instance, Che et al. observed a reverse of senescent NP cells by p16 deletion in IDD, which was accompanied with a reduced oxidative stress [50]. A strong interaction between oxidative stress and disc cell senescence brings us more possibility for intervening IDD. Moreover, Wang et al. confirmed that ROS-mediated mitochondrial dysfunction could be inhibited by polydatin via activating the Nrf2/hemeoxygenase 1(HO-1) pathway to prevent senescence in rat NP cells [88], further testifying a significant effect of blocking this vicious circle. Although other pathways independent of ROS may also mediate the mitochondrial dysfunction to drive the senescent phenotype [85], maintaining a mitochondrial homeostasis should exert antioxidative benefits on preventing cell senescence.

4.2. Epigenomic Perturbations. Senescence phenotypes always appear in various forms no matter in different senescent cells or different senescence stages of the same cell [90]. Multiple stressors can be drivers of disc cell senescence through altering chromatin structural organization or gene expressions during aging, where epigenetic perturbations act as a critical link [91].

In recent years, increasing studies have focused on the role of epigenetics during IDD. As major protein components of chromatin, histone and related modifications participate in DNA damage-induced senescence. Under various stressors, the histone phosphorylation at the site of DNA damage initiates the first step of cascade reactions from DDR to the activation of p53/p21/Rb and eventually causes an irreversible cell cycle arrest [60, 92, 93]. The histone trimethylation also plays a critical role in the positive feedback

TABLE 1: Function characterization of epigenetic alterations in IDD in text.

Name	Type	Target	Expression	Functional role	Reference
/	Histone phosphorylation	Chk2	Up	Cell cycle arrest	[92, 93]
H3K27me3	Histone trimethylation	NOX4	Up	Oxidative stress	[94]
PARK2	DNA methylation	Parkin	Up	Mitophagy	[95, 96]
WNT5A	DNA methylation	Wnt- β	Up	Proinflammation	[98]
CARD14	DNA methylation	NF- κ B	Up	Proinflammation	[98]
EFHD2	DNA methylation	NF- κ B	Up	Proinflammation	[98]
RTKN2	DNA methylation	NF- κ B	Up	Proinflammation	[98]
MAPKAPK5	DNA methylation	MAPK	Up	Proinflammation	[98]
PRKCZ	DNA methylation	MAPK	Up	Proinflammation	[98]
miR-21	Noncoding RNA	PDCD4	Down	Proliferation	[100]
miR-146a	Noncoding RNA	TRAF6	Down	ECM degradation	[101]
miR-98	Noncoding RNA	IL-6/STAT3	Down	Inhibition of ECM degeneration and apoptosis	[102]
miR-494	Noncoding RNA	SOX9	Down	ECM degeneration and apoptosis	[103]
miR-132	Noncoding RNA	GDF5	Down	ECM degradation	[104]
SPARC	DNA methylation	SPARC	Down	ECM degradation	[106]

loop between enhancer of zeste homolog 2 (EZH2) and NADPH oxidase 4 (NOX4) to promote the NP cell senescence during IDD [94]. The latter of the loop has been proved as an important mediator of various stressors to induce OS-associated SIPS in degenerative discs [94]. Recently, Williams et al. observed a hypermethylation level at one cytosine guanine (CpG) site (cg15832436) of the parkinson protein 2 (PARK2) promoter in IDD [95]. The modification of PARK2 at transcriptional level may regulate mitochondrial-associated OS in degenerative NP and EP cells via parkin-mediated mitophagy [96, 97]. Therefore, epigenetic changes may affect cellular senescence via the regulation of OS at transcriptional level. In addition, the genome-wide analysis of DNA methylation profile indicated that DNA methylation profiles were significantly distinct between early and advanced stages of human IDD, especially in NP tissue [98]. The group further identified 220 differentially methylated loci comprising 187 individual genes. Among them, Wnt-5a, one of the representative ligands of the wntless/integration-1- (Wnt-) β -catenin pathway, was observed differentially methylated in advanced stage of IDD [98]. Notably, the Wnt- β -catenin pathway has been reported to be relative to promote disc cell senescence via a positive feedback loop of Wnt signaling and cytokines [60]. Moreover, they also found several hypermethylated genes that may play important roles in regulating catabolic molecules of IDD, such as caspase recruitment domain 14 (CARD14), EF-hand domain-containing protein D2 (EFHD2), rhotekin 2 (RTKN2), mitogen-activated protein kinase-activated protein kinase 5 (MAPKAPK5), and protein kinase C/ ζ (PRKCZ) associated with the MAPK pathway [98]. These mitogen-activated protein kinase (MAPK) and NF- κ B-associated genes may be involved in controlling SASP. The differential methylations dominantly exist in genes which are located upstream instead of directly regulating downstream target genes associated with proinflammatory cytokines and catabolic molecules [98]. However, considering a series of discoveries about DNA demethylation located in

promoter sites of catabolic enzyme MMPs in osteoarthritis (OA), further studies like ribonucleic acid (RNA) sequencing are needed to explore this possibility in IDD with more samples [99].

Based on previous literature, the overexpressions of many catabolic enzymes like MMPs and ADAMTS are recognized as characteristics of senescence-associated ECM remodelling in senescent discs during IDD [50, 62]. Many microRNAs have been proved to target these enzymes to modulate the ECM remodeling process through a specific pathway, respectively [100–102]. Notably, some of them such as microRNA-132 (miR-132) and microRNA-494 (miR-494) are reported to be upregulated by the methylation of CpG islands in the promoter region in degenerative human NP cells [103, 104]. Secreted protein acidic and rich in cysteine (SPARC) is widely accepted as another matricellular protein to regulate cell-matrix interactions and collagen fibrillogenesis in IDD [105]. And the hypermethylation of SPARC promoter is observed to decrease related gene expressions of degenerative discs in both humans and animal models, which may partly cause ECM remodeling in IDD [106].

Although the relationship between epigenetics and cell senescence in IDD has been primarily established, how various stressors trigger these epigenetic perturbations is still unclear. Further exploration for these epigenetic changes will provide us more potential biomarkers as well as therapeutic targets for the management of IDD (Table 1).

5. The Promising Therapy for IDD: Senotherapies

Optimizing disc health in an aging population requires maintaining normal renewal and proliferation as well as function of parenchymal cells [107]. Due to the key role that cell senescence plays in IDD, recent studies highlight the significance of developing senotherapeutic approaches that target senescent cells therapeutically to blunt or even reverse IDD.

There are several potential strategies for antisenescent cells including directly eliminating senescent cells, targeting SASP for reducing its adverse effects, and relieving senescence-associated growth arrest [108]. The first way seems to be the most direct and hitting home. Specifically, preventing accumulation of p16(Ink4a)-positive senescent cells in intervertebral discs has been proved to ameliorate matrix homeostasis and mitigate the progress of IDD [51, 109]. Furthermore, small molecules termed senolytics have emerged in recent years, and these selective eliminators of senescent cells are considered to exert great benefits on antiaging process [110]. Dasatinib and quercetin targeting ephrin (Eph) receptor tyrosine kinases and phosphatidylinositol 3-kinase/protein kinase B (PI3K/AKT) pathway modules, respectively, were the first molecules to be identified as senolytics in 2015 [5]. From then on, many drugs are found to be efficacious in animal models and human cells or tissues [73]. Some known antiaging compounds against other diseases exert new senotherapeutic activity on IDD. As an antidiabetic drug before, metformin confers antisenescence effect in NP cells and annulus fibrosus stem cells (AFSCs) which significantly ameliorate disc degeneration [111, 112]. Classic bisphosphonate antiosteoporosis (OP) drug has been demonstrated to benefit not only OA but also IDD [6]. The discs of rats treated with alendronate significantly retarded EP thickening and increased the aggrecan and type II collagen anabolism in discs [6]. Although the underlying mechanism has not been clarified, the analogical benefits in OP, OA, and IDD provide the possibility for preventing the whole musculoskeletal system aging and degeneration. Classic senotherapeutic drug repurposing emerges as an interesting aspect and may provide potential appealing therapeutic approaches for IDD [110]. Notably, whether the excellent result is a cause of antiaging effects or a consequence is worth considering because of the multifaceted effects of these compounds [12]. Despite their senotherapeutic effects, these drugs possess various disadvantages such as off-target effect and low potency. For example, the usage of dasatinib is reported to inhibit hypoxic pulmonary vasoconstriction to induce pulmonary hypertension independent of regular Src kinase and tyrosine kinase-induced mechanism [113]. As a broad-spectrum kinase inhibitor, it may target potential irrelevant kinases to cause nonessential damage [12]. Moreover, the avascular structures in intervertebral discs are not conducive to drug accumulation after systemic administration, which may further amplify the off-target effect and low potency. Therefore, delivering drugs directly to degenerative sites may partly avoid these deficiencies. In recent years, some drug delivery systems connected with antibodies against senescence-specific surface antigens are synthesized to solve the problem of targeted drug delivery. Qu et al. used the beta-2-microglobulin antibody (anti-B2MG) to successfully construct a nanoparticle tetrahedron which could recognize and selectively clear senescent cells [114]. Amor et al. screened a cell surface protein called the urokinase-type plasminogen activator receptor (uPAR) and constructed senolytic chimeric antigen receptor (CAR) T cells

to eliminate target cells in multiple senescence models, which emerged as a striking senolytic strategy [29]. Therefore, further screening and identifying senescence-specific surface antigens will provide more potential targets, which may facilitate the diagnosis and interventions of senescence [29, 115].

Another promising strategy is targeting the SASP for blocking the adverse effects of specific components like pro-inflammatory factors and matrix catabolic enzymes, without changing the inner antioncogenic pathways and cell cycle in senescent cells [108, 116]. This could be achieved by targeting signaling cascade upstream of the SASP of senescent disc cells, such as NF- κ B or p38 MAPK as well as related regulators [12, 87, 117]. For instance, depletion of ATM downregulates the expression of SASP factors like ADAMTS and MMPs and significantly attenuates age-associated IDD [118, 119]. However, the SASP expression on different cells, tissues, and organs is not always constant considering the diversity of senescence types [65]. Finding relative conserved molecular phenotypes existing in different senescence types will be meaningful for clarifying the mechanism underlying SASP and find potential targets [65]. Moreover, considering the self-clearing mechanism of senescent cells via SASP [120–122], it is essential to weigh the benefit between SASP-mediated immune clearance and inflammation damage in IDD and the conclusion is still not be casually established [12]. To avoid this dilemma, targeting specific proinflammation factors or proteins like TNF- α , MMP instead of the whole SASP is considered to be more promising for anti-IDD [43, 123]. Therefore, accurately identifying “the black sheep” of SASP and relative signal pathways in disc senescence may develop SASP-related interventions further.

The third approach, relieving senescence-associated growth arrest, could be realized through blocking the effect of cell cycle inhibitor like p16 and forkhead box O4 (FOXO4) or deleting relative genes [50]. Baar et al. synthesized a competitive inhibitor of FOXO4 to perturb the interaction between p53 and FOXO4 and successfully transferred the cell cycle from arrest to apoptosis [124]. However, this strategy needs to be treated with caution, considering that a potential excessive cell replication and proliferation may trigger tumorigenesis [108]. In contrast, reserving the senescent state instead of directly eliminating them seems to be more appealing because of the rare cell number in degenerative discs. There is no relative report in IDD, but Zhang et al. realized the reprogramming of senescent muscle stem cells via supplying cellular nicotinamide adenine dinucleotide (NAD⁺) and increased mouse lifespan [125]. Regardless of the difference of cell characteristics, restoring the function of senescent disc cells will greatly ameliorate the condition of oligocytes and cell dysfunction in degenerative discs.

6. Prospects of Cell Senescence in IDD

In this review, we demonstrated the pathogenesis of disc degenerative diseases from a perspective of cell senescence and highlighted the pivotal role of oxidative stress and epigenomic perturbations played. And we analyzed the potential of interventions targeting senescent cells and the SASP,

which seemed to be prospective strategies. Notably, there are some confusing questions to be answered: one unsolved is that most applications of current senescent animal models inevitably ignore the accumulation of time effect. And it is unconvincing to attribute the degeneration entirely to cell senescence, considering the real chronic degeneration process in our body. In addition, the heterogeneity of cell senescence in different cells or tissues has been proved, but little is known about that which may exist in the same cell types in intervertebral discs. Investigating every single senescent cell could be an interesting topic, which may help us further understand the detail of cell senescence in IDD. Finally, days are early to say whether changing the outcome of senescent cells can really ameliorate or even reverse the progression of disc degeneration, as many emerging strategies are only preliminarily proved in vitro. Cell senescence itself is a complex biological process that has not been fully clarified, and more problems could be readily solved when further cognition is established.

Conflicts of Interest

The authors declare no potential conflict of interest.

Acknowledgments

This paper was supported by grants from the Medical Science and Technology Project of Zhejiang Province of China (No. 2020385155), China Postdoctoral Science Foundation (2017M612011), Scientific Research Fund of Zhejiang Provincial Education Department (Nos. Y201941476 and Y201941491), Natural Science Foundation of Zhejiang Province (LQ18H060003 and LY19H060005), and the National Natural Science Foundation of China (No. 81972096, No. 81902238, and No. 81772379).

Supplementary Materials

The supplementary material is a summary list of abbreviations and their corresponding full names mentioned in this review. (*Supplementary Materials*)

References

- [1] GBD 2017 Disease and Injury Incidence and Prevalence Collaborators, "Global, regional, and national incidence, prevalence, and years lived with disability for 354 diseases and injuries for 195 countries and territories, 1990–2017: a systematic analysis for the global burden of disease study 2017," *The Lancet*, vol. 392, no. 10159, pp. 1789–1858, 2018.
- [2] C. Fitzmaurice and Global Burden of Disease Cancer Collaboration, "Global, regional, and national cancer incidence, mortality, years of life lost, years lived with disability, and disability-adjusted life-years for 29 cancer groups, 2006 to 2016: a systematic analysis for the Global Burden of Disease Study," *Journal of Clinical Oncology*, vol. 36, 15 Supplement, pp. 1568–1568, 2018.
- [3] M. Millicamps and L. S. Stone, "Delayed onset of persistent discogenic axial and radiating pain after a single-level lumbar intervertebral disc injury in mice," *Pain*, vol. 159, no. 9, pp. 1843–1855, 2018.
- [4] C. Le Maitre, A. Freemont, and J. Hoyland, "Accelerated cellular senescence in degenerate intervertebral discs: a possible role in the pathogenesis of intervertebral disc degeneration," *Arthritis Research & Therapy*, vol. 9, no. 3, article R45, 2007.
- [5] Y. Zhu, T. Tchkonina, T. Pirtskhalava et al., "The Achilles' heel of senescent cells: from transcriptome to senolytic drugs," *Aging Cell*, vol. 14, no. 4, pp. 644–658, 2015.
- [6] Y. Gologorsky and J. Chi, "Bisphosphonate therapy for degenerative disc disease?," *Neurosurgery*, vol. 73, no. 4, pp. N12–N13, 2013.
- [7] J. Wang, A. K. Uryga, J. Reinhold et al., "Vascular smooth muscle cell senescence promotes atherosclerosis and features of plaque vulnerability," *Circulation*, vol. 132, no. 20, pp. 1909–1919, 2015.
- [8] P. Zhang, Y. Kishimoto, I. Grammatikakis et al., "Senolytic therapy alleviates A β -associated oligodendrocyte progenitor cell senescence and cognitive deficits in an Alzheimer's disease model," *Nature Neuroscience*, vol. 22, no. 5, pp. 719–728, 2019.
- [9] S. Lee and C. A. Schmitt, "The dynamic nature of senescence in cancer," *Nature Cell Biology*, vol. 21, no. 1, pp. 94–101, 2019.
- [10] M. P. Baar, E. Perdiguero, P. Muñoz-Cánoves, and P. L. J. de Keizer, "Musculoskeletal senescence: a moving target ready to be eliminated," *Current Opinion in Pharmacology*, vol. 40, pp. 147–155, 2018.
- [11] F. Wang, F. Cai, R. Shi, X. H. Wang, and X. T. Wu, "Aging and age related stresses: a senescence mechanism of intervertebral disc degeneration," *Osteoarthritis and Cartilage*, vol. 24, no. 3, pp. 398–408, 2016.
- [12] B. G. Childs, M. Durik, D. J. Baker, and J. M. van Deursen, "Cellular senescence in aging and age-related disease: from mechanisms to therapy," *Nature Medicine*, vol. 21, no. 12, pp. 1424–1435, 2015.
- [13] C. Michaloglou, L. C. W. Vredeveld, M. S. Soengas et al., "BRAFE600-associated senescence-like cell cycle arrest of human naevi," *Nature*, vol. 436, no. 7051, pp. 720–724, 2005.
- [14] D. Muñoz-Espín and M. Serrano, "Cellular senescence: from physiology to pathology," *Nature Reviews Molecular Cell Biology*, vol. 15, no. 7, pp. 482–496, 2014.
- [15] A. Chicas, X. Wang, C. Zhang et al., "Dissecting the unique role of the retinoblastoma tumor suppressor during cellular senescence," *Cancer Cell*, vol. 17, no. 4, pp. 376–387, 2010.
- [16] A. Calcinotto, J. Kohli, E. Zagato, L. Pellegrini, M. Demaria, and A. Alimonti, "Cellular senescence: aging, cancer, and injury," *Physiological Reviews*, vol. 99, no. 2, pp. 1047–1078, 2019.
- [17] J. L. Kirkland and T. Tchkonina, "Cellular senescence: a translational perspective," *eBioMedicine*, vol. 21, pp. 21–28, 2017.
- [18] A. Hernandez-Segura, J. Nehme, and M. Demaria, "Hallmarks of cellular senescence," *Trends in Cell Biology*, vol. 28, no. 6, pp. 436–453, 2018.
- [19] S. G. Rao and J. G. Jackson, "SASP: tumor suppressor or promoter? Yes!," *Trends Cancer*, vol. 2, no. 11, pp. 676–687, 2016.
- [20] T. S. Chikenji, Y. Saito, N. Konari et al., "p16INK4A-expressing mesenchymal stromal cells restore the senescence-clearance-regeneration sequence that is impaired in chronic

- muscle inflammation,” *eBioMedicine*, vol. 44, pp. 86–97, 2019.
- [21] L. Mosteiro, C. Pantoja, A. de Martino, and M. Serrano, “Senescence promotes in vivo reprogramming through p16INK4a and IL-6,” *Aging Cell*, vol. 17, no. 2, 2018.
- [22] X. Zhou, F. Perez, K. Han, and D. A. Jurivich, “Clonal senescence alters endothelial ICAM-1 function,” *Mechanisms of Ageing and Development*, vol. 127, no. 10, pp. 779–785, 2006.
- [23] D. A. McCarthy, R. R. Clark, T. R. Bartling, M. Trebak, and J. A. Melendez, “Redox control of the senescence regulator interleukin-1 α and the secretory phenotype,” *The Journal of Biological Chemistry*, vol. 288, no. 45, pp. 32149–32159, 2013.
- [24] P. Ortiz-Montero, A. Londoño-Vallejo, and J. P. Vernot, “Senescence-associated IL-6 and IL-8 cytokines induce a self- and cross-reinforced senescence/inflammatory milieu strengthening tumorigenic capabilities in the MCF-7 breast cancer cell line,” *Cell Communication and Signaling: CCS*, vol. 15, no. 1, p. 17, 2017.
- [25] S. Roberts, E. H. Evans, D. Kletsas, D. C. Jaffray, and S. M. Eisenstein, “Senescence in human intervertebral discs,” *European Spine Journal*, vol. 15, no. S3, pp. 312–316, 2006.
- [26] H. E. Gruber, J. A. Ingram, H. J. Norton, and E. N. Hanley Jr., “Senescence in cells of the aging and degenerating intervertebral disc: immunolocalization of senescence-associated β -galactosidase in human and sand rat discs,” *Spine*, vol. 32, no. 3, pp. 321–327, 2007.
- [27] W. Erwin, D. Islam, R. D. Inman, M. G. Fehlings, and F. W. L. Tsui, “Notochordal cells protect nucleus pulposus cells from degradation and apoptosis: implications for the mechanisms of intervertebral disc degeneration,” *Arthritis Research & Therapy*, vol. 13, no. 6, p. R215, 2011.
- [28] M. Ogrodnik, H. Salmonowicz, D. Jurk, and J. F. Passos, “Expansion and cell-cycle arrest: common denominators of cellular senescence,” *Trends in Biochemical Sciences*, vol. 44, no. 12, pp. 996–1008, 2019.
- [29] C. Amor, J. Feucht, J. Leibold et al., “Senolytic CAR T cells reverse senescence-associated pathologies,” *Nature*, vol. 583, no. 7814, pp. 127–132, 2020.
- [30] G. Casella, R. Munk, K. M. Kim et al., “Transcriptome signature of cellular senescence,” *Nucleic Acids Research*, vol. 47, no. 14, pp. 7294–7305, 2019.
- [31] T. Tchkonja and J. L. Kirkland, “Aging, cell senescence, and chronic disease: emerging therapeutic strategies,” *JAMA*, vol. 320, no. 13, pp. 1319–1320, 2018.
- [32] J. Birch, P. J. Barnes, and J. F. Passos, “Mitochondria, telomeres and cell senescence: implications for lung ageing and disease,” *Pharmacology & Therapeutics*, vol. 183, pp. 34–49, 2018.
- [33] M. Serrano, A. W. Lin, M. E. McCurrach, D. Beach, and S. W. Lowe, “Oncogenic ras provokes premature cell senescence associated with accumulation of p53 and p16INK4a,” *Cell*, vol. 88, no. 5, pp. 593–602, 1997.
- [34] A. Chandra, A. B. Lagnado, J. N. Farr et al., “Targeted reduction of senescent cell burden alleviates focal radiotherapy-related bone loss,” *Journal of Bone and Mineral Research*, vol. 35, no. 6, pp. 1119–1131, 2020.
- [35] A. F. Phoa, A. Recasens, F. M. S. Gurgis et al., “MK2 inhibition induces p53-dependent senescence in glioblastoma cells,” *Cancers*, vol. 12, no. 3, p. 654, 2020.
- [36] P. P. Shah, G. Donahue, G. L. Otte et al., “Lamin B1 depletion in senescent cells triggers large-scale changes in gene expression and the chromatin landscape,” *Genes & Development*, vol. 27, no. 16, pp. 1787–1799, 2013.
- [37] M. Demaria, N. Ohtani, S. A. Youssef et al., “An essential role for senescent cells in optimal wound healing through secretion of PDGF-AA,” *Developmental Cell*, vol. 31, no. 6, pp. 722–733, 2014.
- [38] K. R. Jessen, R. Mirsky, and P. Arthur-Farraj, “The role of cell plasticity in tissue repair: adaptive cellular reprogramming,” *Developmental Cell*, vol. 34, no. 6, pp. 613–620, 2015.
- [39] L. Mosteiro, C. Pantoja, N. Alcazar et al., “Tissue damage and senescence provide critical signals for cellular reprogramming in vivo,” *Science*, vol. 354, no. 6315, article aaf4445, 2016.
- [40] M. Storer, A. Mas, A. Robert-Moreno et al., “Senescence is a developmental mechanism that contributes to embryonic growth and patterning,” *Cell*, vol. 155, no. 5, pp. 1119–1130, 2013.
- [41] D. Muñoz-Espín, M. Cañamero, A. Maraver et al., “Programmed cell senescence during mammalian embryonic development,” *Cell*, vol. 155, no. 5, pp. 1104–1118, 2013.
- [42] C. D. Wiley, M. C. Velarde, P. Lecot et al., “Mitochondrial dysfunction induces senescence with a distinct secretory phenotype,” *Cell Metabolism*, vol. 23, no. 2, pp. 303–314, 2016.
- [43] N. Henry, J. Clouet, J. le Bideau, C. le Visage, and J. Guicheux, “Innovative strategies for intervertebral disc regenerative medicine: from cell therapies to multiscale delivery systems,” *Biotechnology Advances*, vol. 36, no. 1, pp. 281–294, 2018.
- [44] L. J. Smith, N. L. Nerurkar, K. S. Choi, B. D. Harfe, and D. M. Elliott, “Degeneration and regeneration of the intervertebral disc: lessons from development,” *Disease Models & Mechanisms*, vol. 4, no. 1, pp. 31–41, 2011.
- [45] J. P. de Magalhães and J. F. Passos, “Stress, cell senescence and organismal ageing,” *Mechanisms of Ageing and Development*, vol. 170, pp. 2–9, 2018.
- [46] Q. J. Xing, Q. Q. Liang, Q. Bian et al., “Leg amputation accelerates senescence of rat lumbar intervertebral discs,” *Spine (Phila Pa 1976)*, vol. 35, no. 23, pp. E1253–E1261, 2010.
- [47] L. Zhao, B. Tian, Q. Xu, C. Zhang, L. Zhang, and H. Fang, “Extensive mechanical tension promotes annulus fibrosus cell senescence through suppressing cellular autophagy,” *BioScience Reports*, vol. 39, no. 4, 2019.
- [48] G. Fontana, E. See, and A. Pandit, “Current trends in biologics delivery to restore intervertebral disc anabolism,” *Advanced Drug Delivery Reviews*, vol. 84, pp. 146–158, 2015.
- [49] K. W. Kim, H. N. Chung, K. Y. Ha, J. S. Lee, and Y. Y. Kim, “Senescence mechanisms of nucleus pulposus chondrocytes in human intervertebral discs,” *The Spine Journal*, vol. 9, no. 8, pp. 658–666, 2009.
- [50] H. Che, J. Li, Y. Li et al., “p16 deficiency attenuates intervertebral disc degeneration by adjusting oxidative stress and nucleus pulposus cell cycle,” *eLife*, vol. 9, 2020.
- [51] E. J. Novais, B. O. Diekman, I. M. Shapiro, and M. V. Risbud, “p16Ink4a deletion in cells of the intervertebral disc affects their matrix homeostasis and senescence associated secretory phenotype without altering onset of senescence,” *Matrix Biology*, vol. 82, pp. 54–70, 2019.
- [52] J. Campisi, “Senescent cells, tumor suppression, and organismal aging: good citizens, bad neighbors,” *Cell*, vol. 120, no. 4, pp. 513–522, 2005.
- [53] U. Herbig and J. M. Sedivy, “Regulation of growth arrest in senescence: telomere damage is not the end of the story,”

- Mechanisms of Ageing and Development*, vol. 127, no. 1, pp. 16–24, 2006.
- [54] Z. Zhou, M. Gao, F. Wei et al., “Shock absorbing function study on denucleated intervertebral disc with or without hydrogel injection through static and dynamic biomechanical tests in vitro,” *BioMed Research International*, vol. 2014, Article ID 461724, 7 pages, 2014.
- [55] P. Li, G. Hou, R. Zhang et al., “High-magnitude compression accelerates the premature senescence of nucleus pulposus cells via the p38 MAPK-ROS pathway,” *Arthritis Research & Therapy*, vol. 19, no. 1, p. 209, 2017.
- [56] K. Alpantaki, A. Kampouroglou, C. Koutserimpas, G. Effraimidis, and A. Hadjipavlou, “Diabetes mellitus as a risk factor for intervertebral disc degeneration: a critical review,” *European Spine Journal*, vol. 28, no. 9, pp. 2129–2144, 2019.
- [57] M. Bitar, “Diabetes impairs angiogenesis and induces endothelial cell senescence by up-regulating thrombospondin-CD47-dependent signaling,” *International Journal of Molecular Sciences*, vol. 20, no. 3, p. 673, 2019.
- [58] A. Dimozi, E. Mavrogonatou, A. Sklirou, and D. Kleatsas, “Oxidative stress inhibits the proliferation, induces premature senescence and promotes a catabolic phenotype in human nucleus pulposus intervertebral disc cells,” *European Cells & Materials*, vol. 30, pp. 89–103, 2015.
- [59] S. W. Jeong, J. S. Lee, and K. W. Kim, “In vitro lifespan and senescence mechanisms of human nucleus pulposus chondrocytes,” *The Spine Journal*, vol. 14, no. 3, pp. 499–504, 2014.
- [60] C. Feng, H. Liu, M. Yang, Y. Zhang, B. Huang, and Y. Zhou, “Disc cell senescence in intervertebral disc degeneration: causes and molecular pathways,” *Cell Cycle*, vol. 15, no. 13, pp. 1674–1684, 2016.
- [61] J. P. Coppé, C. K. Patil, F. Rodier et al., “Senescence-associated secretory phenotypes reveal cell-nonautonomous functions of oncogenic RAS and the p53 tumor suppressor,” *PLoS Biology*, vol. 6, no. 12, pp. 2853–2868, 2008.
- [62] K. Ngo, P. Patil, S. J. McGowan et al., “Senescent intervertebral disc cells exhibit perturbed matrix homeostasis phenotype,” *Mechanisms of Ageing and Development*, vol. 166, pp. 16–23, 2017.
- [63] J. C. Acosta, A. Banito, T. Wuestefeld et al., “A complex secretory program orchestrated by the inflammasome controls paracrine senescence,” *Nature Cell Biology*, vol. 15, no. 8, pp. 978–990, 2013.
- [64] M. V. Risbud and I. M. Shapiro, “Role of cytokines in intervertebral disc degeneration: pain and disc content,” *Nature Reviews Rheumatology*, vol. 10, no. 1, pp. 44–56, 2014.
- [65] P. L. J. de Keizer, “The fountain of youth by targeting senescent cells?,” *Trends in Molecular Medicine*, vol. 23, no. 1, pp. 6–17, 2017.
- [66] J. M. van Deursen, “The role of senescent cells in ageing,” *Nature*, vol. 509, no. 7501, pp. 439–446, 2014.
- [67] X. Wang, M. Zou, J. Li et al., “LncRNA H19 targets miR-22 to modulate H₂O₂-induced deregulation in nucleus pulposus cell senescence, proliferation, and ECM synthesis through Wnt signaling,” *Journal of Cellular Biochemistry*, vol. 119, no. 6, pp. 4990–5002, 2018.
- [68] L. Ding, Z. Jiang, J. Wu et al., “ β -catenin signalling inhibits cartilage endplate chondrocyte homeostasis in vitro,” *Molecular Medicine Reports*, vol. 20, no. 1, pp. 567–572, 2019.
- [69] A. Hiyama, D. Sakai, F. Arai, D. Nakajima, K. Yokoyama, and J. Mochida, “Effects of a glycogen synthase kinase-3 β inhibitor (LiCl) on c-myc protein in intervertebral disc cells,” *Journal of Cellular Biochemistry*, vol. 112, no. 10, pp. 2974–2986, 2011.
- [70] J. Antoniou, T. Steffen, F. Nelson et al., “The human lumbar intervertebral disc: evidence for changes in the biosynthesis and denaturation of the extracellular matrix with growth, maturation, ageing, and degeneration,” *The Journal of Clinical Investigation*, vol. 98, no. 4, pp. 996–1003, 1996.
- [71] C. Ruiz-Fernández, V. Francisco, J. Pino et al., “Molecular relationships among obesity, inflammation and intervertebral disc degeneration: are adipokines the common link?,” *International Journal of Molecular Sciences*, vol. 20, no. 8, p. 2030, 2019.
- [72] D. Krishnamoorthy, R. C. Hoy, D. M. Natelson et al., “Dietary advanced glycation end-product consumption leads to mechanical stiffening of murine intervertebral discs,” *Disease Models & Mechanisms*, vol. 11, no. 12, article dmm036012, 2018.
- [73] J. Campisi, P. Kapahi, G. J. Lithgow, S. Melov, J. C. Newman, and E. Verdin, “From discoveries in ageing research to therapeutics for healthy ageing,” *Nature*, vol. 571, no. 7764, pp. 183–192, 2019.
- [74] D. C. Lee, C. S. Adams, T. J. Albert, I. M. Shapiro, S. M. Evans, and C. J. Koch, “In situ oxygen utilization in the rat intervertebral disc,” *Journal of Anatomy*, vol. 210, no. 3, pp. 294–303, 2007.
- [75] J. F. Passos, G. Nelson, C. Wang et al., “Feedback between p21 and reactive oxygen production is necessary for cell senescence,” *Molecular Systems Biology*, vol. 6, no. 1, p. 347, 2010.
- [76] C. Feng, M. Yang, M. Lan et al., “ROS: crucial intermediators in the pathogenesis of intervertebral disc degeneration,” *Oxidative Medicine and Cellular Longevity*, vol. 2017, Article ID 5601593, 12 pages, 2017.
- [77] Y. Lin, G. Tang, Y. Jiao et al., “*Propionibacterium acnes* induces intervertebral disc degeneration by promoting iNOS/NO and COX-2/PGE₂ activation via the ROS-dependent NF- κ B pathway,” *Oxidative Medicine and Cellular Longevity*, vol. 2018, Article ID 3692752, 12 pages, 2018.
- [78] D. P. Jones, “Radical-free biology of oxidative stress,” *American Journal of Physiology Cell Physiology*, vol. 295, no. 4, pp. C849–C868, 2008.
- [79] H. Liu, H. Kang, C. Song et al., “Urolithin A inhibits the catabolic effect of TNF α on nucleus pulposus cell and alleviates intervertebral disc degeneration in vivo,” *Frontiers in Pharmacology*, vol. 9, p. 1043, 2018.
- [80] A. Larrañaga, I. L. M. Isa, V. Patil et al., “Antioxidant functionalized polymer capsules to prevent oxidative stress,” *Acta Biomaterialia*, vol. 67, pp. 21–31, 2018.
- [81] J. J. Wu, C. Quijano, E. Chen et al., “Mitochondrial dysfunction and oxidative stress mediate the physiological impairment induced by the disruption of autophagy,” *Ageing*, vol. 1, no. 4, pp. 425–437, 2009.
- [82] T. Toshima, K. Shirabe, T. Fukuhara et al., “Suppression of autophagy during liver regeneration impairs energy charge and hepatocyte senescence in mice,” *Hepatology*, vol. 60, no. 1, pp. 290–300, 2014.
- [83] P. Davalli, T. Mitic, A. Caporali, A. Lauriola, and D. D’Arca, “ROS, cell senescence, and novel molecular mechanisms in

- aging and age-related diseases," *Oxidative Medicine and Cellular Longevity*, vol. 2016, Article ID 3565127, 18 pages, 2016.
- [84] L. Kang, Q. Xiang, S. Zhan et al., "Restoration of autophagic flux rescues oxidative damage and mitochondrial dysfunction to protect against intervertebral disc degeneration," *Oxidative Medicine and Cellular Longevity*, vol. 2019, Article ID 7810320, 27 pages, 2019.
- [85] P. Vasileiou, K. Evangelou, K. Vlasis et al., "Mitochondrial homeostasis and cellular senescence," *Cells*, vol. 8, no. 7, p. 686, 2019.
- [86] M. C. Marazita, A. Dugour, M. D. Marquioni-Ramella, J. M. Figueroa, and A. M. Suburo, "Oxidative stress-induced premature senescence dysregulates VEGF and CFH expression in retinal pigment epithelial cells: implications for age-related macular degeneration," *Redox Biology*, vol. 7, pp. 78–87, 2016.
- [87] P. Li, Y. Gan, Y. Xu et al., "17beta-estradiol attenuates TNF- α -induced premature senescence of nucleus pulposus cells through regulating the ROS/NF- κ B pathway," *International Journal of Biological Sciences*, vol. 13, no. 2, pp. 145–156, 2017.
- [88] J. Wang, C. Huang, Z. Lin et al., "Polydatin suppresses nucleus pulposus cell senescence, promotes matrix homeostasis and attenuates intervertebral disc degeneration in rats," *Journal of Cellular and Molecular Medicine*, vol. 22, no. 11, pp. 5720–5731, 2018.
- [89] R. Zuo, Y. Wang, J. Li et al., "Rapamycin induced autophagy inhibits inflammation-mediated endplate degeneration by enhancing Nrf 2/Keap 1 signaling of cartilage endplate stem cells," *Stem Cells*, vol. 37, no. 6, pp. 828–840, 2019.
- [90] L. Q. Cheng, Z. Q. Zhang, H. Z. Chen, and D. P. Liu, "Epigenetic regulation in cell senescence," *Journal of Molecular Medicine (Berlin, Germany)*, vol. 95, no. 12, pp. 1257–1268, 2017.
- [91] C. Li, Y. Chai, L. Wang et al., "Programmed cell senescence in skeleton during late puberty," *Nature Communications*, vol. 8, no. 1, p. 1312, 2017.
- [92] U. Herbig, W. A. Jobling, B. P. C. Chen, D. J. Chen, and J. M. Sedivy, "Telomere shortening triggers senescence of human cells through a pathway involving ATM, p53, and p21 (CIP1), but not p16 (INK4a)," *Molecular Cell*, vol. 14, no. 4, pp. 501–513, 2004.
- [93] V. Gire, P. Roux, D. Wynford-Thomas, J. M. Brondello, and V. Dulic, "DNA damage checkpoint kinase Chk 2 triggers replicative senescence," *The EMBO Journal*, vol. 23, no. 13, pp. 2554–2563, 2004.
- [94] C. Liu, L. Liu, M. Yang et al., "A positive feedback loop between EZH2 and NOX4 regulates nucleus pulposus cell senescence in age-related intervertebral disc degeneration," *Cell Division*, vol. 15, no. 1, p. 2, 2020.
- [95] F. M. K. Williams, A. T. Bansal, J. B. van Meurs et al., "Novel genetic variants associated with lumbar disc degeneration in northern Europeans: a meta-analysis of 4600 subjects," *Annals of the Rheumatic Diseases*, vol. 72, no. 7, pp. 1141–1148, 2013.
- [96] Z. Zhang, T. Xu, J. Chen et al., "Parkin-mediated mitophagy as a potential therapeutic target for intervertebral disc degeneration," *Cell Death & Disease*, vol. 9, no. 10, p. 980, 2018.
- [97] L. Kang, S. Liu, J. Li, Y. Tian, Y. Xue, and X. Liu, "Parkin and Nrf 2 prevent oxidative stress-induced apoptosis in intervertebral endplate chondrocytes via inducing mitophagy and anti-oxidant defenses," *Life Sciences*, vol. 243, p. 117244, 2020.
- [98] A. Ikuno, K. Akeda, S. I. Takebayashi, M. Shimaoka, K. Okumura, and A. Sudo, "Genome-wide analysis of DNA methylation profile identifies differentially methylated loci associated with human intervertebral disc degeneration," *PLoS One*, vol. 14, no. 9, article e0222188, 2019.
- [99] K. McCulloch, G. J. Litherland, and T. S. Rai, "Cellular senescence in osteoarthritis pathology," *Aging Cell*, vol. 16, no. 2, pp. 210–218, 2017.
- [100] B. Chen, S. G. Huang, L. Ju et al., "Effect of microRNA-21 on the proliferation of human degenerated nucleus pulposus by targeting programmed cell death 4," *Brazilian Journal of Medical and Biological Research*, vol. 49, no. 6, 2016.
- [101] S. X. Gu, X. Li, J. L. Hamilton et al., "MicroRNA-146a reduces IL-1 dependent inflammatory responses in the intervertebral disc," *Gene*, vol. 555, no. 2, pp. 80–87, 2015.
- [102] M. L. Ji, J. Lu, P. L. Shi et al., "Dysregulated miR-98 contributes to extracellular matrix degradation by targeting IL-6/STAT3 signaling pathway in human intervertebral disc degeneration," *Journal of Bone and Mineral Research*, vol. 31, no. 4, pp. 900–909, 2016.
- [103] L. Kang, C. Yang, Y. Song et al., "MicroRNA-494 promotes apoptosis and extracellular matrix degradation in degenerative human nucleus pulposus cells," *Oncotarget*, vol. 8, no. 17, pp. 27868–27881, 2017.
- [104] W. Liu, P. Xia, J. Feng et al., "MicroRNA-132 upregulation promotes matrix degradation in intervertebral disc degeneration," *Experimental Cell Research*, vol. 359, no. 1, pp. 39–49, 2017.
- [105] J. Bedore, A. Leask, and C. A. Séguin, "Targeting the extracellular matrix: matricellular proteins regulate cell-extracellular matrix communication within distinct niches of the intervertebral disc," *Matrix Biology*, vol. 37, pp. 124–130, 2014.
- [106] M. Tajerian, S. Alvarado, M. Millemcamps et al., "DNA methylation of SPARC and chronic low back pain," *Molecular Pain*, vol. 7, pp. 1744–8069, 2011.
- [107] S. Roberts, P. Colombier, A. Sowman et al., "Ageing in the musculoskeletal system," *Acta Orthopaedica*, vol. 87, Supplement 363, pp. 15–25, 2017.
- [108] T. Tchkonja, Y. Zhu, J. van Deursen, J. Campisi, and J. L. Kirkland, "Cellular senescence and the senescent secretory phenotype: therapeutic opportunities," *The Journal of Clinical Investigation*, vol. 123, no. 3, pp. 966–972, 2013.
- [109] P. Patil, Q. Dong, D. Wang et al., "Systemic clearance of p16INK4a-positive senescent cells mitigates age-associated intervertebral disc degeneration," *Aging Cell*, vol. 18, no. 3, article e12927, 2019.
- [110] V. Myrianthopoulos, "The emerging field of senotherapeutic drugs," *Future Medicinal Chemistry*, vol. 10, no. 20, pp. 2369–2372, 2018.
- [111] D. Chen, D. Xia, Z. Pan et al., "Metformin protects against apoptosis and senescence in nucleus pulposus cells and ameliorates disc degeneration in vivo," *Cell Death & Disease*, vol. 7, no. 10, article e2441, 2016.
- [112] Y. Han, F. Yuan, C. Deng et al., "Metformin decreases LPS-induced inflammatory response in rabbit annulus fibrosus stem/progenitor cells by blocking HMGB1 release," *Aging (Albany NY)*, vol. 11, no. 22, pp. 10252–10265, 2019.

- [113] N. Ö. Yurttaş and A. E. Eşkazan, “Dasatinib-induced pulmonary arterial hypertension,” *British Journal of Clinical Pharmacology*, vol. 84, no. 5, pp. 835–845, 2018.
- [114] A. Qu, X. Wu, S. Li et al., “An NIR-responsive DNA-mediated nanotetrahedron enhances the clearance of senescent cells,” *Advanced Materials*, vol. 32, no. 14, article 2000184, 2020.
- [115] M. Althubiti, L. Lezina, S. Carrera et al., “Characterization of novel markers of senescence and their prognostic potential in cancer,” *Cell Death & Disease*, vol. 5, no. 11, article e1528, 2014.
- [116] M. Amaya-Montoya, A. Pérez-Londoño, V. Guatibonza-García, A. Vargas-Villanueva, and C. O. Mendivil, “Cellular senescence as a therapeutic target for age-related diseases: a review,” *Advances in Therapy*, vol. 37, no. 4, pp. 1407–1424, 2020.
- [117] N. Malaquin, A. Martinez, and F. Rodier, “Keeping the senescence secretome under control: molecular reins on the senescence-associated secretory phenotype,” *Experimental Gerontology*, vol. 82, pp. 39–49, 2016.
- [118] Y. Han, C. M. Zhou, H. Shen et al., “Attenuation of ataxia telangiectasia mutated signalling mitigates age-associated intervertebral disc degeneration,” *Aging Cell*, vol. 19, no. 7, 2020.
- [119] J. Zhao, L. Zhang, A. Lu et al., “ATM is a key driver of NF- κ B-dependent DNA-damage-induced senescence, stem cell dysfunction and aging,” *Aging*, vol. 12, no. 6, pp. 4688–4710, 2020.
- [120] L. Hoenicke and L. Zender, “Immune surveillance of senescent cells—biological significance in cancer- and non-cancer pathologies,” *Carcinogenesis*, vol. 33, no. 6, pp. 1123–1126, 2012.
- [121] V. Krizhanovsky, M. Yon, R. A. Dickins et al., “Senescence of activated stellate cells limits liver fibrosis,” *Cell*, vol. 134, no. 4, pp. 657–667, 2008.
- [122] W. Xue, L. Zender, C. Miething et al., “Senescence and tumour clearance is triggered by p53 restoration in murine liver carcinomas,” *Nature*, vol. 445, no. 7128, pp. 656–660, 2007.
- [123] A. Freund, A. V. Orjalo, P. Y. Desprez, and J. Campisi, “Inflammatory networks during cellular senescence: causes and consequences,” *Trends in Molecular Medicine*, vol. 16, no. 5, pp. 238–246, 2010.
- [124] M. P. Baar, R. M. C. Brandt, D. A. Putavet et al., “Targeted apoptosis of senescent cells restores tissue homeostasis in response to chemotoxicity and aging,” *Cell*, vol. 169, no. 1, pp. 132–147.e16, 2017.
- [125] H. Zhang, D. Ryu, Y. Wu et al., “NAD⁺ repletion improves mitochondrial and stem cell function and enhances life span in mice,” *Science*, vol. 352, no. 6292, pp. 1436–1443, 2016.